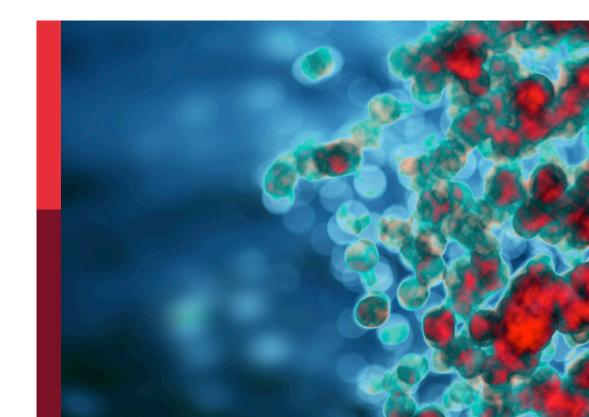
Combinational immunotherapy of cancer: Novel targets, mechanisms, and strategies

Edited by Xuyao Zhang, Xian Zeng, Yubin Li and Dianwen Ju

Published in Frontiers in Immunology Frontiers in Oncology





FRONTIERS EBOOK COPYRIGHT STATEMENT

The copyright in the text of individual articles in this ebook is the property of their respective authors or their respective institutions or funders. The copyright in graphics and images within each article may be subject to copyright of other parties. In both cases this is subject to a license granted to Frontiers.

The compilation of articles constituting this ebook is the property of Frontiers.

Each article within this ebook, and the ebook itself, are published under the most recent version of the Creative Commons CC-BY licence. The version current at the date of publication of this ebook is CC-BY 4.0. If the CC-BY licence is updated, the licence granted by Frontiers is automatically updated to the new version.

When exercising any right under the CC-BY licence, Frontiers must be attributed as the original publisher of the article or ebook, as applicable.

Authors have the responsibility of ensuring that any graphics or other materials which are the property of others may be included in the CC-BY licence, but this should be checked before relying on the CC-BY licence to reproduce those materials. Any copyright notices relating to those materials must be complied with.

Copyright and source

acknowledgement notices may not be removed and must be displayed in any copy, derivative work or partial copy which includes the elements in question.

All copyright, and all rights therein, are protected by national and international copyright laws. The above represents a summary only. For further information please read Frontiers' Conditions for Website Use and Copyright Statement, and the applicable CC-BY licence.

ISSN 1664-8714 ISBN 978-2-8325-3351-2 DOI 10.3389/978-2-8325-3351-2

About Frontiers

Frontiers is more than just an open access publisher of scholarly articles: it is a pioneering approach to the world of academia, radically improving the way scholarly research is managed. The grand vision of Frontiers is a world where all people have an equal opportunity to seek, share and generate knowledge. Frontiers provides immediate and permanent online open access to all its publications, but this alone is not enough to realize our grand goals.

Frontiers journal series

The Frontiers journal series is a multi-tier and interdisciplinary set of openaccess, online journals, promising a paradigm shift from the current review, selection and dissemination processes in academic publishing. All Frontiers journals are driven by researchers for researchers; therefore, they constitute a service to the scholarly community. At the same time, the *Frontiers journal series* operates on a revolutionary invention, the tiered publishing system, initially addressing specific communities of scholars, and gradually climbing up to broader public understanding, thus serving the interests of the lay society, too.

Dedication to quality

Each Frontiers article is a landmark of the highest quality, thanks to genuinely collaborative interactions between authors and review editors, who include some of the world's best academicians. Research must be certified by peers before entering a stream of knowledge that may eventually reach the public - and shape society; therefore, Frontiers only applies the most rigorous and unbiased reviews. Frontiers revolutionizes research publishing by freely delivering the most outstanding research, evaluated with no bias from both the academic and social point of view. By applying the most advanced information technologies, Frontiers is catapulting scholarly publishing into a new generation.

What are Frontiers Research Topics?

Frontiers Research Topics are very popular trademarks of the *Frontiers journals series*: they are collections of at least ten articles, all centered on a particular subject. With their unique mix of varied contributions from Original Research to Review Articles, Frontiers Research Topics unify the most influential researchers, the latest key findings and historical advances in a hot research area.

Find out more on how to host your own Frontiers Research Topic or contribute to one as an author by contacting the Frontiers editorial office: frontiersin.org/about/contact

Combinational immunotherapy of cancer: Novel targets, mechanisms, and strategies

Topic editors

Xuyao Zhang — Fudan University, China Xian Zeng — Fudan University, China Yubin Li — GlaxoSmithKline, United States Dianwen Ju — Fudan University, China

Citation

Zhang, X., Zeng, X., Li, Y., Ju, D., eds. (2023). *Combinational immunotherapy of cancer: Novel targets, mechanisms, and strategies*. Lausanne: Frontiers Media SA. doi: 10.3389/978-2-8325-3351-2

The authors declare that the research was conducted in the absence of any commercial or financial relationships that could be construed as a potential conflict of interest.

🐉 frontiers | Research Topics

Table of contents

80	Editoria	al: Co	ombinatio	onal i	mmunc	otherapy	of cancer:	novel
	targets	, meo	chanisms	, and	strateg	jies		
			-	-				

Yanyang Nan, Dianwen Ju and Xuyao Zhang

10 Roburic Acid Targets TNF to Inhibit the NF-κB Signaling Pathway and Suppress Human Colorectal Cancer Cell Growth

Huanhuan Xu, Titi Liu, Jin Li, Fei Chen, Jing Xu, Lihong Hu, Li Jiang, Zemin Xiang, Xuanjun Wang and Jun Sheng

26 Localized Intra-Cavitary Therapy to Drive Systemic Anti-Tumor Immunity

Vera S. Donnenberg, Patrick L. Wagner, James D. Luketich, David L. Bartlett and Albert D. Donnenberg

34 Advances of DNA Damage Repair-Related Drugs and Combination With Immunotherapy in Tumor Treatment Yumin Wang, Meihan Duan, Zhouying Peng, Ruohao Fan, Yuxiang He, Hua Zhang, Wei Xiong and Weihong Jiang

45 GPC2 Is a Potential Diagnostic, Immunological, and Prognostic Biomarker in Pan-Cancer

Guoming Chen, Dongqiang Luo, Nan Zhong, Danyun Li, Jiyuan Zheng, Hui Liao, Zhuoyao Li, Xiaoxiao Lin, Qiqi Chen, Cheng Zhang, Yuanjun Lu, Yau-Tuen Chan, Qing Ren, Ning Wang and Yibin Feng

59 The Heterogeneity of Immune Cell Infiltration Landscape and Its Immunotherapeutic Implications in Hepatocellular Carcinoma

Yuanyuan Guo, Jing Yang, Kaidi Ren, Xueke Tian, Hua Gao, Xin Tian, Xiaojian Zhang and Quancheng Kan

73 MAOI Antidepressants: Could They Be a Next-Generation ICB Therapy?

James Brown, Bo Li and Lili Yang

78 Real-World Data of Different Immune Checkpoint Inhibitors for Non-Small Cell Lung Cancer in China

Kang Miao, Xiaotong Zhang, Hanping Wang, Xiaoyan Si, Jun Ni, Wei Zhong, Jing Zhao, Yan Xu, Minjiang Chen, Ruili Pan, Mengzhao Wang and Li Zhang

87 The Therapeutic Effect and Clinical Outcome of Immune Checkpoint Inhibitors on Bone Metastasis in Advanced Non-Small-Cell Lung Cancer

> Yohei Asano, Norio Yamamoto, Satoru Demura, Katsuhiro Hayashi, Akihiko Takeuchi, Satoshi Kato, Shinji Miwa, Kentaro Igarashi, Takashi Higuchi, Hirotaka Yonezawa, Yoshihiro Araki, Sei Morinaga, Shiro Saito, Takashi Sone, Kazuo Kasahara and Hiroyuki Tsuchiya

96 Identification and Validation in a Novel Quantification System of Ferroptosis Patterns for the Prediction of Prognosis and Immunotherapy Response in Left- and Right-Sided Colon Cancer

> Heng-Chun Zhang, Shen-Hui Deng, Ya-Nan Pi, Jun-Nan Guo, Hua Xi, Xin Shi, Xue-Fei Yang, Bo-Miao Zhang, Wei-Nan Xue, Bin-Bin Cui and Yan-Long Liu

- 112 Case Report: Immune Checkpoint Inhibitors as a Single Agent in the Treatment of Metastatic Cervical Cancer Manasa Anipindi, Ryan J. Smith and Madiha Gilani
- 119 Identification of a Tumor Immunological Phenotype-Related Gene Signature for Predicting Prognosis, Immunotherapy Efficacy, and Drug Candidates in Hepatocellular Carcinoma Yuqin Tang, Chengbin Guo, Zhao Yang, Yumei Wang, Yongqiang Zhang and Dong Wang
- 139 Case Report: Fulminant Celiac Disease With Combination Immune Checkpoint Therapy

Ayo S. Falade, Kerry L. Reynolds, Leyre Zubiri, Vikram Deshpande, Florian J. Fintelmann, Michael Dougan and Meghan J. Mooradian

- 143 miR-582 Suppresses the Proliferation of B-Cell Precursor Acute Lymphoblastic Leukemia (BCP-ALL) Cells and Protects Them From Natural Killer Cell-Mediated Cytotoxicity Xinxin Li, Yufei Zhang, Fei He, Dan Gao, Bo Che, Xiuli Cao, Siyong Huang, Minhua Zheng and Hua Han
- 155 IL-27 Improves Prophylactic Protection Provided by a Dead Tumor Cell Vaccine in a Mouse Melanoma Model Kyle Seaver, Olena Kourko, Katrina Gee, Peter A. Greer and Sameh Basta
- 169 DNA Hypermethylation-Regulated CX3CL1 Reducing T Cell Infiltration Indicates Poor Prognosis in Wilms Tumour Tao Mi, Liming Jin, Zhaoxia Zhang, Jinkui Wang, Mujie Li, Chenghao Zhanghuang, Xiaojun Tan, Zhang Wang, Xiaomao Tian, Bin Xiang and Dawei He
- 180 Molecular Characteristics of T Cell-Mediated Tumor Killing in Hepatocellular Carcinoma

Wei-feng Hong, Mou-yuan Liu, Li Liang, Yang Zhang, Zong-juan Li, Keqi Han, Shi-suo Du, Yan-jie Chen and Li-heng Ma

194 Noncanonical PD-1/PD-L1 Axis in Relation to the Efficacy of Anti-PD Therapy

Yiru Long, Xiaolu Yu, Runqiu Chen, Yongliang Tong and Likun Gong

206 Changes in Neutrophil to Lymphocyte Ratio, Lymphocyte to Monocyte Ratio, and Platelet to Lymphocyte Ratio During Palliative Radiotherapy May Predict Efficacy of Immune Checkpoint Inhibitor as Re-Challenge Treatment in Advanced Gastric Cancer: A Case Report

Jianxin Chen, Xilin Wu, Shijian Zhu and Junhui Wang

212 Oncolytic Adenoviral Vector-Mediated Expression of an Anti-PD-L1-scFv Improves Anti-Tumoral Efficacy in a Melanoma Mouse Model

> Maria Vitale, Filippo Scialò, Margherita Passariello, Eleonora Leggiero, Anna D'Agostino, Lorella Tripodi, Laura Gentile, Andrea Bianco, Giuseppe Castaldo, Vincenzo Cerullo, Claudia De Lorenzo and Lucio Pastore

224 Potentialities and Challenges of mRNA Vaccine in Cancer Immunotherapy

Li-Juan Duan, Qian Wang, Cuilian Zhang, Dong-Xiao Yang and Xu-Yao Zhang

231 SQLE, A Key Enzyme in Cholesterol Metabolism, Correlates With Tumor Immune Infiltration and Immunotherapy Outcome of Pancreatic Adenocarcinoma

Weiqiang You, Jia Ke, Yufeng Chen, Zerong Cai, Ze-ping Huang, Peishan Hu and Xiaojian Wu

- 247 Combination of Radiofrequency Ablation With Resiquimod to Treat Hepatocellular Carcinoma Via Inflammation of Tumor Immune Microenvironment and Suppression of Angiogenesis Zhou Tian, Baojian Hong, Jianzhong Chen and Zhe Tang
- 260 Prognostic Significance and Immunological Role of FBXO5 in Human Cancers: A Systematic Pan-Cancer Analysis Peng Liu, Xiaojuan Wang, Lili Pan, Bing Han and Zhiying He
- 279 Identification of Ligand-Receptor Pairs Associated With Tumour Characteristics in Clear Cell Renal Cell Carcinoma Fahui Liu, Ping Wang, Wenjuan Sun, Yan Jiang and Qiming Gong
- 297 Immunotherapy for Pediatric Acute Lymphoblastic Leukemia: Recent Advances and Future Perspectives Meng Lv, Yan Liu, Wei Liu, Yabing Xing and Shengnan Zhang
- 310 A Whole Exon Screening-Based Score Model Predicts Prognosis and Immune Checkpoint Inhibitor Therapy Effects in Low-Grade Glioma

Cheng Luo, Songmao Wang, Wenjie Shan, Weijie Liao, Shikuan Zhang, Yanzhi Wang, Qilei Xin, Tingpeng Yang, Shaoliang Hu, Weidong Xie, Naihan Xu and Yaou Zhang

- 327 Advances in Immune Microenvironment and Immunotherapy of Isocitrate Dehydrogenase Mutated Glioma Dongming Yan, Weicheng Li, Qibing Liu and Kun Yang
- 336 Use of Single Cell Transcriptomic Techniques to Study the Role of High-Risk Human Papillomavirus Infection in Cervical Cancer

Lingzhang Meng, Shengcai Chen, Guiling Shi, Siyuan He, Zechen Wang, Jiajia Shen, Jiajia Wang, Suren Rao Sooranna, Jingjie Zhao and Jian Song 347 Different Immunoregulation Roles of Activin A Compared With TGF- β

Fanglin Li, Yiru Long, Xiaolu Yu, Yongliang Tong and Likun Gong

356 Development and Validation of a Novel Ferroptosis-Related LncRNA Signature for Predicting Prognosis and the Immune Landscape Features in Uveal Melanoma

Xiaochen Ma, Sejie Yu, Bin Zhao, Wei Bai, Yubo Cui, Jinglan Ni, Qinghua Lyu and Jun Zhao

372 Orelabrutinib Combined With Lenalidomide and Immunochemotherapy for Relapsed/Refractory Primary Central Nervous System Lymphoma: A Retrospective Analysis of Case Series

> Chuanwei Yang, Yong Cui, Xiaohui Ren, Ming Li, Kefu Yu, Shaoping Shen, Haihui Jiang, Mingxiao Li, Xiaokang Zhang, Xuzhe Zhao, Qinghui Zhu and Song Lin

382 Lighting a Fire: Gasdermin-Mediated Pyroptosis Remodels the Glioma Microenvironment and Promotes Immune Checkpoint Blockade Response

Yonghua Cai, Ke Li, Jie Lin, Xianqiu Liang, Wei Xu, Zhengming Zhan, Shuaishuai Xue, Yu Zeng, Peng Chai, Yangqi Mao, Zibin Song, Lei Han, Ye Song, Xian Zhang and Hai Wang

402 A Novel PD-L1-Containing MSLN Targeting Vaccine for Lung Cancer Immunotherapy

> Wuyi Zeng, Jiayi Pan, Zixuan Fang, Jiangtao Jia, Rong Zhang, Menghua He, Hanyu Zhong, Jiashan He, Xinyu Yang, Yi Shi, Bei Zhong, Jun Zeng, Bishi Fu, Maoping Huang and Hui Liu

- 412 Discovering Innate Driver Variants for Risk Assessment of Early Colorectal Cancer Metastasis Ruo-Fan Ding, Yun Zhang, Lv-Ying Wu, Pan You, Zan-Xi Fang, Zhi-Yuan Li, Zhong-Ying Zhang and Zhi-Liang Ji
- 425 The Effect of Hypoxia-Induced Exosomes on Anti-Tumor Immunity and Its Implication for Immunotherapy Wenwen Guo, Tianyun Qiao, Bingwei Dong, Tian Li, Qiang Liu and Xiaofeng Xu
- 434 IGFBP7 and the Tumor Immune Landscape: A Novel Target for Immunotherapy in Bladder Cancer Xianyanling Yi, Xiaonan Zheng, Hang Xu, Jin Li, Tianyi Zhang,

Peng Ge, Dazhou Liao, Hong Li, Xiaoyan Lyu and Jianzhong Ai

- 447 Risk of Adverse Events in Cancer Patients Receiving Nivolumab With Ipilimumab: A Meta-Analysis
 Xin Zhao, Fengwei Gao, Jie Yang, Hua Fan, Qingyun Xie, Kangyi Jiang, Jie Gong, Benjian Gao, Qian Yang and Zehua Lei
- 459 Emergence of the CD226 Axis in Cancer Immunotherapy Michael Conner, Ken W. Hance, Sapna Yadavilli, James Smothers and Jeremy D. Waight

478 Mapping the Tumor Microenvironment in TNBC and Deep Exploration for M1 Macrophages-Associated Prognostic Genes

Baojin Xu, Hefen Sun, Xiaoqing Song, Qiqi Liu and Wei Jin

- 492 Pan-Cancer and Single-Cell Analysis Reveals CENPL as a Cancer Prognosis and Immune Infiltration-Related Biomarker Ziyang Feng, Yu Chen, Changjing Cai, Jun Tan, Ping Liu, Yihong Chen, Hong Shen, Shan Zeng and Ying Han
- 506 Recent Progress and Future Perspectives of Immunotherapy in Advanced Gastric Cancer Xin Jin, Zhaorui Liu, Dongxiao Yang, Kai Yin and Xusheng Chang
- 513 Case Report: A Programmed Cell Death-1 Inhibitor-Related Abdominal Fibroinflammatory Reaction Affecting Multiple Organs in A Non-Small-Cell Lung Cancer Patient An-Tian Chen, Yue-Quan Shi, Bei Tan, Liang Zhu, Ya-Ping Luo, Wei Zhong, Meng-Zhao Wang and Yan Xu

Check for updates

OPEN ACCESS

EDITED AND REVIEWED BY Afsheen Raza, Abu Dhabi University, United Arab Emirates

*CORRESPONDENCE Xuyao Zhang Xuyaozhang@fudan.edu.cn

RECEIVED 30 June 2023 ACCEPTED 03 August 2023 PUBLISHED 11 August 2023

CITATION

Nan Y, Ju D and Zhang X (2023) Editorial: Combinational immunotherapy of cancer: novel targets, mechanisms, and strategies. *Front. Immunol.* 14:1250975. doi: 10.3389/fimmu.2023.1250975

COPYRIGHT

© 2023 Nan, Ju and Zhang. This is an openaccess article distributed under the terms of the Creative Commons Attribution License (CC BY). The use, distribution or reproduction in other forums is permitted, provided the original author(s) and the copyright owner(s) are credited and that the original publication in this journal is cited, in accordance with accepted academic practice. No use, distribution or reproduction is permitted which does not comply with these terms.

Editorial: Combinational immunotherapy of cancer: novel targets, mechanisms, and strategies

Yanyang Nan, Dianwen Ju and Xuyao Zhang*

Department of Biological Medicines & Shanghai Engineering Research Center of Immunotherapeutics, School of Pharmacy, Fudan University, Shanghai, China

KEYWORDS

cancer immunotherapy, combination therapy, novel targets, therapy strategies, immune checkpoint inhibitors

Editorial on the Research Topic

Combinational immunotherapy of cancer: novel targets, mechanisms, and strategies

Cancer immunotherapy, distinct from traditional cancer therapies, is achieving unprecedented success by harnessing the host's immune system to control tumor progression. Current clinical strategies for cancer immunotherapy include immune checkpoint inhibitor therapy, chimeric antigen receptor T-cell therapy, oncolytic virotherapy and tumor vaccines (1–4). Nevertheless, the effectiveness of immunotherapy varies significantly among patients, with only a minority experiencing long-term clinical benefits (5). This highlights the need to identify potential targets of tumor therapy and diversify our combinational immunotherapy strategies, as well as to unravel the underlying molecular events.

Because the critical for tumor markers, researchers are dedicating to uncover novel biomarkers that can be used to identify cancer in its early stages, and to predict the effectiveness of treatment and the chance of cancer recurrence. Chen et al. disclosed the potential role of Glypican 2 (GPC2) in multiple cancers via pan-cancer bioinformatical analysis. Their data identified that GPC2 expression in multiple cancer types was significantly higher than that in normal tissues. High diagnosis performance of GPC2 was discovered in 6 types of cancer, and immune-related genes were highly co-expressed with GPC2 in 33 tumors, illuminating GPC2 can be used as a promising diagnostic, prognostic, and immunological biomarker in tumor. Wu et al. demonstrated that Apolipoprotein E (ApoE), which was secreted from melanoma cells, has an immune suppressant effect by inducing the secretion of IL-10 from activated dendritic cells and further suppressing T-cell function partially via the lrp8 receptor pathway. Moreover, ApoE knockout induced significant tumor suppression and improved overall survival in mouse melanoma model, hence providing a potent strategy for cancer immunotherapy by targeting ApoE. Squalene epoxidase (SQLE) is a key enzyme in regulating cholesterol metabolism. You et al. disclosed the upregulated expression of SQLE in pancreatic adenocarcinoma (PAAD) patients with poor disease-free survival and overall survival. Comprehensive analyses of multiple bioinformatic databases and anti-PD-1 clinical trials showed that the expression of SQLE was strongly negatively correlated with checkpoint inhibitors, immune infiltrations, and immunotherapy outcome. This study provides a promising target to potentiate the efficiency of immunotherapy in PAAD.

Although inhibitors targeting immune checkpoints have demonstrated efficacy in specific patient subgroups, optimal use is encumbered by high rates of drug resistance. To further enhance the antitumor effects of the existing cancer immunotherapies, researchers have performed various explorations. Wang et al. took an in-depth look on the drug resistance mechanisms of colorectal cancer (CRC) during anti-PD-1 treatment. Innovatively, the authors revealed that proprotein convertase subtilisin/kexin type 9 (PCSK9), a lipid metabolism-related protein, was upregulated after anti-PD-1 treatment. Targeting PCSK9 with anti-PCSK9 antibody enhanced antitumor effect of anti-PD-1 monotherapy by increasing both the infiltration of CD8⁺T cells and release of inflammatory cytokines, as well as reducing the proportion of Treg cells in tumor microenvironment. This study proposed a novel combinational immunotherapy strategy to overcome anti-PD-1 resistance in CRC by simultaneously targeting PD-1 and PCSK9. Vitale et al. engineered a novel oncolytic adenovirus expressing an anti-PD-L1-scFv based on Ad5A24 adenovirus (Ad5A24-anti-PD-L1-scFv) to improve the antitumor activity of oncolytic virotherapy in melanoma. Ad5Δ24anti-PD-L1-scFv not only secreted anti-PD-L1-scFv blocking PD-1/ PD-L1 pathway, but also induced cytopathic and lytic effects in melanoma cells. Moreover, intra-tumor injection of Ad5/24-anti-PD-L1-scFv enhanced the infiltration of CD8⁺T cells and effectively inhibited tumor growth. Although tumor vaccines based on dendritic cells (DCs) play a key role in tumor immunotherapy, the poor immunogenicity and weak immune response rate still limit their efficacy (6). Zeng et al. constructed a novel DCs-based therapeutic vaccine titled MSLN-PDL1-GMCSF that could self-activate and induce anti-PD-L1 antibody while targeting MSLN. The MSLN-PDL1-GMCSF vaccine elicited a robust and specific immune response in lung cancer. Moreover, combining the vaccine with PD-1 blockade demonstrated a synergistic antitumor effect, presenting a promising and effective combination strategy for tumor immunotherapy. Zhou et al. summarized and reviewed the underlying resistance mechanisms of immune checkpoint blockade (ICB), particularly in relation to the biological function of CD8⁺ T cells, and compiled a comprehensive overview of the latest combination strategies to enhance the effectiveness of ICB treatments.

References

1. Morad G, Helmink BA, Sharma P, Wargo JA. Hallmarks of response, resistance, and toxicity to immune checkpoint blockade. *Cell* (2022) 185:576. doi: 10.1016/j.cell.2022.01.008

2. Hovhannisyan L, Riether C, Aebersold DM, Medová M, Zimmer Y. CAR T cellbased immunotherapy and radiation therapy: potential, promises and risks. *Mol Cancer* (2023) 22:82. doi: 10.1186/s12943-023-01775-1

3. Shalhout SZ, Miller DM, Emerick KS, Kaufman HL. Therapy with oncolytic viruses: progress and challenges. *Nat Rev Clin Oncol* (2023) 20:160–77. doi: 10.1038/s41571-022-00719-w

In summary, the articles included in the project "Combinational Immunotherapy of Cancer: Novel Targets, Mechanisms, and Strategies" not only describe potential targets to expand our toolbox for manipulating antitumor immunity, but also provide novel combinational strategies to enhance antitumor therapy responses. Persisting investigation of new targets and combinational strategies could result in a better understanding of antitumor treatments and provide valuable promises for tumor immunotherapy.

Author contributions

YN, and XZ drafted the manuscript. XZ and DJ contributed to the design and critical revision of the manuscript. All authors contributed to the article and approved the submitted version.

Funding

This research was funded by National Natural Science Foundation of China (32200745, and 82073752), Shanghai Sailing Program (21YF1401900), Scientific and Innovative Action Plan of Shanghai (20S11904700 and 20JC1411000).

Conflict of interest

The authors declare that the research was conducted in the absence of any commercial or financial relationships that could be construed as a potential conflict of interest.

Publisher's note

All claims expressed in this article are solely those of the authors and do not necessarily represent those of their affiliated organizations, or those of the publisher, the editors and the reviewers. Any product that may be evaluated in this article, or claim that may be made by its manufacturer, is not guaranteed or endorsed by the publisher.

4. Diao L, Liu M. Rethinking antigen source: Cancer vaccines based on whole tumor cell/tissue lysate or whole tumor cell. *Adv Sci (Weinh)* (2023) 10:e2300121. doi: 10.1002/advs.202300121

5. Hegde PS, Chen DS. Top 10 challenges in cancer immunotherapy. *Immunity* (2020) 52:17–35. doi: 10.1016/j.immuni.2019.12.011

6. Sadeghzadeh M, Bornehdeli S, Mohahammadrezakhani H, Abolghasemi M, Poursaei E, Asadi M, et al. Dendritic cell therapy in cancer treatment; the state-of-the-art. *Life Sci* (2020) 254:117580. doi: 10.1016/j.lfs.2020.117580





Roburic Acid Targets TNF to Inhibit the NF-kB Signaling Pathway and Suppress Human Colorectal Cancer Cell Growth

OPEN ACCESS

Edited by:

Yubin Li, University of Pennsylvania, United States

Reviewed by:

Xi Lou, University of Alabama at Birmingham, United States Na Wang, Johns Hopkins University, United States

*Correspondence:

Zemin Xiang xiangzmwdx@sohu.com Xuanjun Wang jwang@ynau.edu.cn Jun Sheng shengj@ynau.edu.cn

[†]These authors have contributed equally to this work

Specialty section:

This article was submitted to Cancer Immunity and Immunotherapy, a section of the journal Frontiers in Immunology

Received: 12 January 2022 Accepted: 24 January 2022 Published: 09 February 2022

Citation:

Xu H, Liu T, Li J, Chen F, Xu J, Hu L, Jiang L, Xiang Z, Wang X and Sheng J (2022) Roburic Acid Targets TNF to Inhibit the NF-κB Signaling Pathway and Suppress Human Colorectal Cancer Cell Growth. Front. Immunol. 13:853165. doi: 10.3389/fimmu.2022.853165 Huanhuan Xu^{1,2†}, Titi Liu^{1,2†}, Jin Li^{1,2}, Fei Chen^{1,2}, Jing Xu¹, Lihong Hu¹, Li Jiang¹, Zemin Xiang^{1,2*}, Xuanjun Wang^{1,2,3*} and Jun Sheng^{1,3*}

¹ Key Laboratory of Pu-er Tea Science, Ministry of Education, Yunnan Agricultural University, Kunming, China, ² College of Science, Yunnan Agricultural University, Kunming, China, ³ State Key Laboratory for Conservation and Utilization of Bio-Resources in Yunnan, Yunnan Agricultural University, Kunming, China

Tumor necrosis factor (TNF)-stimulated nuclear factor-kappa B (NF-KB) signaling plays very crucial roles in cancer development and progression, and represents a potential target for drug discovery. Roburic acid is a newly discovered tetracyclic triterpene acid isolated from oak galls and exhibits anti-inflammatory activity. However, whether roburic acid exerts antitumor effects through inhibition of TNF-induced NF-KB signaling remains unknown. Here, we demonstrated that roburic acid bound directly to TNF with high affinity $(K_{\rm D} = 7.066 \,\mu\text{M})$, blocked the interaction between TNF and its receptor (TNF-R1), and significantly inhibited TNF-induced NF-KB activation. Roburic acid exhibited antitumor activity in numerous cancer cells and could effectively induce G0/G1 cell cycle arrest and apoptosis in colorectal cancer cells. Importantly, roburic acid inhibited the TNF-induced phosphorylation of IKK α/β , IxB α , and p65, degradation of IxB α , nuclear translocation of p65, and NF-kB-target gene expression, including that of XIAP, Mcl-1, and Survivin, in colorectal cancer cells. Moreover, roburic acid suppressed tumor growth by blocking NF-κB signaling in a xenograft nude mouse model of colorectal cancer. Taken together, our findings showed that roburic acid directly binds to TNF with high affinity, thereby disrupting its interaction with TNF-R1 and leading to the inhibition of the NF-kB signaling pathway, both in vitro and in vivo. The results indicated that roburic acid is a novel TNF-targeting therapeutics agent in colorectal cancer as well as other cancer types.

Keywords: roburic acid, TNF, TNF-R1, NF-kB signaling, colorectal cancer

Abbreviations: BLI, biolayer interferometry; BSA, bovine serum albumin; DMSO, dimethyl sulfoxide; FBS, fetal bovine serum; IC_{50} , half-maximal inhibitory concentration; K_{D} , binding affinity; K_{off} , dissociation constant; K_{on} , association constant; MTT, 3-(4,5-dimethylthiazol-2-yl)-2,5-diphenyltetrazolium bromide; NF-κB, nuclear factor-kappa B; PARP, poly (ADP-ribose) polymerase; PBS, phosphate-buffered saline; PI, propidium iodide; PMSF, phenylmethylsulfonyl fluoride; P/S, penicillin-streptomycin solution; PVDF, polyvinylidene fluoride; RIPA, radioactive immunoprecipitation assay; SEM, standard error of the mean; SPR, surface plasmon resonance; SSA, super streptavidin; TNF, tumor necrosis factor; TNF-R1, TNF receptor 1.

INTRODUCTION

Colorectal cancer, a malignant disease of the digestive system, is the third most common cause of new cancer cases in both men and women and the second most frequent cause of cancer deaths (1, 2). Globally, approximately 1.4 million new cases of colorectal cancer are diagnosed and over 690,000 people die from this condition every year (3). The pathophysiology of colorectal cancer is very complex, and its development is a multistage process. Interactions between multiple genetic alterations, the host immune system, and environmental carcinogens have been implicated in the development of human colorectal cancer, which eventually leads to the uncontrolled growth of transformed cells and poor prognosis for patients (4, 5). Under normal conditions, surgical resection provides a possibility for cure in early-stage patients, whereas several anticancer drugs, such as oxaliplatin, 5-fluorouracil, and leucovorin, are recommended for treating advanced colorectal cancer (6, 7). However, current therapy regimens are not always effective at treating advanced colorectal cancer because of drug resistance and adverse side effects and toxicity (3). Consequently, there is an urgent need to identify potential therapeutic targets and discover drugs with greater specificity and less adverse effects from natural resources to treat colorectal cancer, as well as elucidate the underlying molecular mechanisms.

Considerable accumulated evidence has shown that chronic inflammation is closely associated with cancer development and progression (8). In particular, colorectal cancer patients exhibit extensive inflammatory infiltrates with high expression levels of cytokines in the tumor microenvironment (9). The proinflammatory cytokine tumor necrosis factor (TNF)induced nuclear factor-kappa B (NF-KB) signaling pathway is the most intensively investigated pathway in most cell types (10). It represents a canonical NF-KB activation pathway that links inflammation and immunity to cancer development and progression and promotes tumorigenesis (8, 10, 11). Moreover, the TNF-induced NF- κ B signaling pathway is a precisely regulated and therapeutically relevant pathway and a potential target for drug discovery (12, 13). The binding of TNF to its cognate receptor (TNF-R1) directly activates the canonical NF-KB signaling pathway, leading to the transcription of antiapoptotic genes (12, 14). Cancer cells can evade apoptosis *via* upregulating the expression levels of antiapoptotic proteins such as XIAP, Mcl-1, and Survivin (10). Consequently, there is increasing interest in identifying natural compounds that can inhibit this pathway (13, 15-17).

It is well known that new natural products isolated from medicinal plants are excellent and reliable sources of new anticancer drugs (16, 18–20). Roburic acid (molecular formula: $C_{30}H_{48}O_2$; **Figure 1A**) is a newly identified tetracyclic triterpene acid originally isolated from oak galls, and later also found in *Gentiana macrophylla* Pall (21). Roburic acid has been shown to exert anti-inflammatory effects (21–23); however, whether it exhibits additionally bioactivities, especially anticancer effects, remains unknown. Given the anti-inflammatory properties of roburic acid and the critical role of TNF/TNF-R1-mediated NF- κ B signaling in colorectal cancer development and progression,

we speculated that roburic acid might disrupt TNF/TNF-R1mediated NF- κ B signaling and suppress the growth of human colorectal cancer cells. In the present study, we provide evidence that roburic acid binds to TNF with high affinity, which disrupts its interaction with TNF-R1 and leads to inhibition of the NF- κ B signaling pathway, both *in vitro* and *in vivo*.

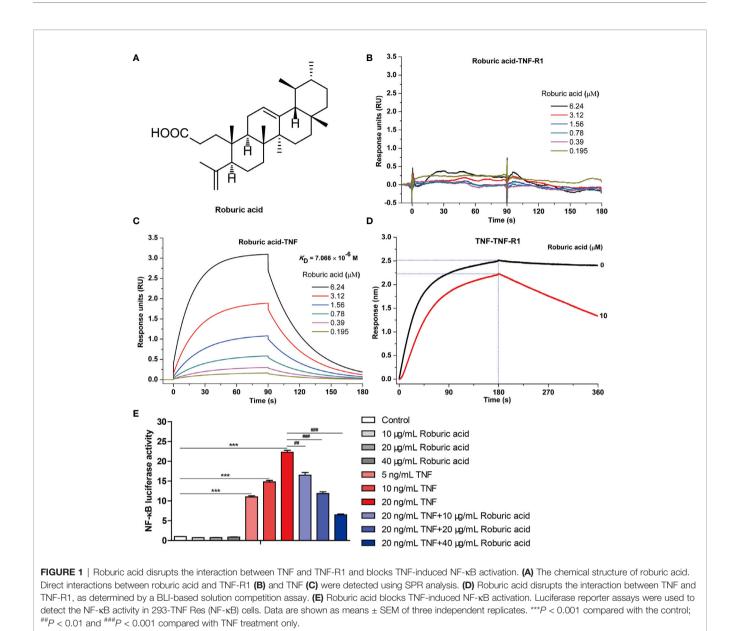
MATERIALS AND METHODS

Chemicals and Reagents

Roburic acid of high purity grade (≥99%) was purchased from Chengdu Biopurify Phytochemicals Ltd (Chengdu, China). Purified cremophor (>98%) and crystal violet were purchased from Calbiochem, Inc. (San Diego, CA, USA) and Aladdin Bio-Chem Technology Co., Ltd (Shanghai, China), respectively. Dimethyl sulfoxide (DMSO) and 3-(4,5-dimethylthiazol-2-yl)-2,5-diphenyltetrazolium bromide (MTT) were obtained from Sigma-Aldrich (Saint Louis, MO, USA). RPMI-1640 medium (Gibco) and fetal bovine serum (FBS) were obtained from ThermoFisher Biochemical Products (Beijing) Co., Ltd and Biological Industries (Kibbutz Beit Haemek, Israel), respectively. Phosphate-buffered saline (PBS), a mixed penicillin-streptomycin solution (P/S), 4% paraformaldehyde, Triton X-100, antifade mounting medium with DAPI, radioactive immunoprecipitation assay (RIPA) buffer, phenylmethylsulfonyl fluoride (PMSF), and the nuclear protein extraction kit were purchased from Solarbio (Beijing, China). The BeyoClick EdU cell proliferation kit with Alexa Fluor 488 was purchased from Beyotime Biotechnology (Shanghai, China). Propidium Iodide (PI) and the Annexin V-FITC/PI detection kit were purchased from Beijing 4A Biotech Co., Ltd (Beijing, China). Anti-TNF-R1 antibody was purchased from HuaAn Biotechnology Co., Ltd (Hangzhou, China). Specific primary antibodies against Bcl-xL, Survivin, Cyclin B1, and Cyclin D1 were purchased from Abcam (Cambridge, MA, USA). Anti-Cyclin E1 and anti-XIAP antibodies were obtained from Santa Cruz Biotechnology (Santa Cruz, CA, USA). Antibodies against PARP, cleaved Caspase3, Caspase7, Caspase9, Bcl-2, Bax, Mcl-1, c-Myc, phospho (p)-ΙΚΚα/β, ΙΚΚα, ΙΚΚβ, p-ΙκΒα, ΙκΒα, p-p65 (Ser536), p65, p-JNK, JNK, p-ERK, ERK, p-p38, p38, p-AKT, AKT, p-STAT3, STAT3, Histone H3, β-tubulin, Ki-67, and rabbit IgG (H+L), F(ab')₂ Fragment (Alexa Fluor 594 conjugate) were purchased from Cell Signaling Technology (Beverly, MA, USA). Recombinant human TNF protein and horseradish peroxidase-conjugated secondary antibodies were obtained from R&D Systems (Minneapolis, MN, USA).

Molecular Interaction Assay

Interactions between human TNF and TNF-R1 proteins and roburic acid were investigated using surface plasmon resonance (SPR) analysis. The human TNF soluble form (NP-000585.2) N-terminal fragment (Val 77–Leu 233) and the TNF-R1 (NP-001056.1) extracellular domain (Met 1–Thr 211) (Sino Biological Inc; Beijing, China) were prepared. SPR studies were performed using a Biacore S200 instrument (GE Healthcare, Sweden) at 25° C. Briefly, 50 μ g/mL TNF-R1 and TNF in 10 mM sodium acetate



buffer (pH 5.0) were respectively immobilized in flow cell-2 and -4 of the Series S CM5 Sensor Chip using an amine coupling kit (GE Healthcare), according to the standard Immobilization Wizard program. Roburic acid was double-diluted in PBS-P buffer (GE Healthcare) supplemented with 5% DMSO to concentrations ranging from 0.195 to 6.24 μ M. The analytes were then injected to flow over the reference and active chip surfaces at a flow rate of 30 μ L/min and the response units were measured. The association and dissociation times were both 90 s. The binding kinetics of TNF-R1 and TNF to roburic acid were analyzed with Biacore S200 Evaluation Software Version 1.1 using a 1:1 binding model.

In addition, solution competition biolayer interferometry (BLI) analysis was performed using an Octet Red 96 instrument (ForteBio, USA) at 25°C, as previously described (24). Briefly, TNF-R1 was biotinylated using amine-PEG3-biotin and then desalted using a Zeba Spin desalting column. The biotinylated TNF-R1 protein was loaded onto the surface of Super Streptavidin (SSA) biosensors (ForteBio). Roburic acid (0 or 20 μ M) was preincubated with the immobilized TNF-R1 for 180 s. Subsequently, a 1 μ M TNF solution supplemented with 0 or 20 μ M roburic acid was allowed to interact with the immobilized TNF-R1 for 180 s, and dissociation was followed for 180 s in 0 or 20 μ M roburic acid. Kinetic parameters and affinities were calculated from a non-linear global fit of the monitored binding curves using Octet Data Analysis software version 7.0 (Fortebio).

Luciferase Reporter Assays

293-TNF Res (NF- κ B) cell line purchased from Novoprotein Technology Co., Ltd (Shanghai, China) was used for luciferase

reporter assays. The cells were cultured in serum free DMEM with or without roburic acid in the presence of TNF for 4 h. Luciferase activities were measured consecutively using the firefly luciferase reporter assay kit (Meilunbio, Dalian, China) with the GloMax[®] 96 Microplate Luminometer (Promega, Madison, WI).

Cell Lines and Cell Culture

All the cell lines (HCT-116, HCT-15, HT29, Colo205, SK-BR-3, BT549, BT-474, U251, 786-O, ACHN, A498, A549, NCI-H460, NCI-H226, NCI-H23, OVCAR-3, SK-OV-3, DU145, PC-3, and CCRF-CEM) used in this study were purchased from the American Type Culture Collection (ATCC; Manassas, VA, USA). All the cells were cultured in RPMI-1640 medium supplemented with 10% FBS and 1% P/S. Cells were cultured in an incubator (BINDER GmbH; Tuttlingen, Germany) with 95% air and 5% CO_2 at 37°C.

Cell Viability Assay

Cell viability was determined using the MTT method as previously described (25). For all the cancer cell lines, 2×10^4 cells/well were seeded into 96-well plates and allowed to adhere for 24 h. The following day, the cells were treated with various concentrations of roburic acid (0–20 μ M). After 48 h, MTT solution (5 mg/mL) was added to the cells. After 4 h, the supernatant was aspirated and 200 μ L of DMSO was added to dissolve the formazan crystals. The optical density at 492 nm was then detected using a FlexStation 3 Multi-Mode Microplate Reader (Molecular Devices; Sunnyvale, CA, USA) and IC₅₀ values were calculated.

Colony Formation Assay

For clonogenicity analysis, 4×10^3 viable HCT-116 and HCT-15 cells were seeded into 60-mm plates and incubated overnight. Then, vehicle or roburic acid was added to each plate at the respective concentrations (4, 8, or 16 μ M) and the culture medium was changed every 2 days. After 8 days of incubation, the cells were fixed in 4% paraformaldehyde and then stained with a 1% crystal violet solution. The colonies were imaged and the number of colonies counted.

Cell Proliferation Assay

HCT-116 and HCT-15 cells (5 \times 10⁴ cells/well) were seeded into 12-well plates and allowed to adhere overnight. The following day, the cells were treated with various concentrations of roburic acid (0, 4, 8, or 16 µM) for 24 h. Then, HCT-116 and HCT-15 proliferation was determined using a BeyoClick EdU cell proliferation kit with Alexa Fluor 488 according to the manufacturer's instructions. Briefly, the cells were treated with 10 µM EdU for 2 h, fixed in 4% paraformaldehyde for 20 min, washed twice with PBS, and permeabilized with 0.5% Triton X-100 for 30 min. Subsequently, the cells were incubated in 200 µL of click reaction buffer at room temperature for 30 min and then washed twice with PBS. Finally, the cells were mounted using antifade mounting medium with DAPI and observed under a fluorescence microscope (Leica). Images were captured at ×200 magnification and merged using ImageJ software (National Institutes of Health, Bethesda, MD, USA).

Cell Cycle Analysis

HCT-116 and HCT-15 cells (2×10^5 cells per plate) were seeded into 60-mm plates and incubated overnight. Subsequently, the cells were treated with various concentrations of roburic acid as described above. After incubation for 24 h, the cells were harvested, washed with PBS, and then fixed in 70% ethanol at -20°C overnight. After fixation, the cells were washed twice with pre-cooled PBS and incubated with binding buffer containing 100 µg/mL PI and 25 µg/mL RNase A in the dark for 30 min at 37°C. Finally, the fluorescence intensities of these samples were detected by BD FACSCalibur flow cytometry (BD Biosciences; San Jose, CA, USA) and FlowJo v.X.7.6.5 software was used to determine the cell cycle phase distributions.

Cell Apoptosis Analysis

Cell apoptosis was analyzed using the Annexin V–FITC/PI detection kit according to the manufacturer's instructions. Briefly, HCT-116 and HCT-15 cells (3×10^5 cells per plate) were treated with different concentrations of roburic acid in serum-free medium for 24 h. The harvested cells were then incubated with 100 µL of binding buffer containing 5 µL of Annexin V–FITC and 10 µL of PI (20 µg/mL) in the dark for 5 min at room temperature. Subsequently, the prepared samples were analyzed by BD FACSCalibur flow cytometry within 1 h and the percentage of apoptotic cells was determined using FlowJo software.

Immunoblotting Analysis

For protein extraction, after the corresponding treatments, HCT-116 and HCT-15 cells, as well as tumor tissues, were washed twice with pre-cooled PBS and lysed on ice using RIPA lysis buffer containing 1 mM PMSF. Cell lysates were quantified using an Enhanced BCA Protein Assay Kit (Beyotime Biotechnology) according to the manufacturer's protocol. Subsequently, equal amounts of proteins were separated by 10% SDS-PAGE and electrophoretically transferred onto polyvinylidene fluoride (PVDF) membranes (Millipore). After blocking with 5% nonfat milk in PBST, the membranes were incubated with diluted specific primary antibodies at 4°C overnight, followed by incubation with the corresponding rabbit or mouse IgG horseradish peroxidase-conjugated secondary antibodies (diluted 1:5,000). Protein bands were detected with an Ultrasensitive Enhanced Chemiluminescent Substrate Kit (4A Biotech) and visualized using a FluorChem E System (ProteinSimple, San Jose, CA, USA). The protein expression level was detected using AlphaView software (Cell Biosciences, Santa Clara, CA, USA).

Nuclear and Cytoplasmic Protein Extraction

HCT-116 and HCT-15 cells (2.5×10^6 cells per plate) were seeded into 100-mm plates and allowed to adhere overnight. The following day, cells were cultured in serum-free medium for 12 h and then pretreated with or without roburic acid (8 μ M) for 4 h, followed by stimulation with TNF (10 ng/mL) for the indicated times. A nuclear protein extraction kit was used to isolate and

extract nuclear and cytoplasmic proteins, according to the manufacturer's protocol. In brief, the collected cells were incubated in cytoplasm lysis buffer containing 1 mM PMSF on ice for 10 min. The supernatants collected after centrifugation at $16,000 \times g$ for 10 min at 4°C were considered cytoplasmic protein extracts. The pellets were then dissolved in nuclear lysis buffer containing 1 mM PMSF on ice for 10 min, and the supernatants obtained by centrifuging were regarded as the nuclear protein fractions. Finally, the cytoplasmic and nuclear protein extracts were subjected to immunoblotting analysis with the corresponding primary antibodies.

Immunofluorescence Staining

HCT-116 and HCT-15 cells (5×10^4 cells/well) were seeded into 12-well plates and allowed to adhere overnight. Cells were treated with or without roburic acid (8μ M) for 4 h and subsequently stimulated with TNF (10 ng/mL) for 30 min in serum-free medium. Then, the cells were washed twice with precooled PBS, fixed in 4% paraformaldehyde for 20 min, washed twice with PBS, blocked with 1% bovine serum albumin (BSA) for 1 h at room temperature, incubated with anti-p65 antibody at 4°C overnight, gently washed twice with PBS, and incubated with Alexa Fluor 594-conjugated secondary antibody for 1 h at temperature in the dark. Subsequently, the slides were washed twice with PBS and mounted using antifade mounting medium with DAPI. Images were taken at ×400 magnification using a fluorescence microscope, and merged using ImageJ software.

In Vivo Xenograft Studies

All animal experiments were carried out in accordance with the National Institutes of Health's Guidelines for the Care and Use of Laboratory Animals and were approved by the Yunnan Agricultural University institutional ethics committee. Care was taken to minimize the discomfort, distress, and pain of the experimental animals. Eighteen 5-week-old male BALB/c nude mice were purchased from Cawens Lab Animal Co. (Changzhou, China) and allowed to acclimate for 1 week. The animals were housed in polypropylene cages with sterile paddy husk and were maintained under standard pathogen-free conditions (ambient temperature $24 \pm 1^{\circ}$ C, humidity 50–60%, 12 h light/dark cycle) with free access to a standard laboratory diet and water. HCT-116 (5×10^6) and HCT-15 (4×10^6) cells were harvested and suspended in 200 µL of a physiological saline solution, and injected subcutaneously into the left and right flanks of each mouse, respectively. One week after xenotransplantation, mice with tumors of approximately 100 mm³ were randomly and averagely divided into three groups. The tumor-bearing mice started daily intraperitoneal injection with either a vehicle (10% DMSO, 70% cremophor/ethanol (3:1), and 20% PBS) as previously described (18), or 5 or 10 mg/kg body weight roburic acid for 18 days. Body weight was recorded and tumor size was determined using electronic calipers every 2 days, and tumor volume was calculated in an unblinded manner according to the formula $(L \times W^2) \times 0.5$, where L is the length and W the width. At the end of the treatments, mice were euthanized by cervical dislocation and the isolated tumors were weighed,

photographed, and used for immunoblotting analysis and immunohistochemical staining.

Immunohistochemical Staining

Immunohistochemistry was performed according to standard methods. Paraffin-embedded xenograft tumor tissues were cut into 3-µm sections, deparaffinized, and rehydrated in different percentages (100, 95, 85, 75, and 65%) of ethanol. For antigen retrieval and to quench endogenous peroxidases, sections were incubated with 10 mM citric buffer (pH 6.0) and BLOXALL Blocking Solution (Vector Laboratories; Burlingame, CA, USA), respectively. The slides were incubated overnight at 4°C with primary antibodies against p-p65, cleaved Caspase3, and Ki-67. Detection was performed using the VECTASTAIN Elite ABC-Peroxidase Kit (Vector Laboratories) and an Enhanced HRP-DAB Chromogenic Kit (TIANGEN Biotech Co., Ltd; Beijing, China) according to the manufacturer's instructions, followed by counterstaining with Mayer's hematoxylin (Sigma-Aldrich). The slides were dehydrated with different concentrations of ethanol (65, 75, 85, 95, and 100%) and then mounted in Permount Mounting Medium (Fisher Scientific). Images were captured at ×400 magnification under a CKX41 microscope (Olympus, Tokyo, Japan).

Statistical Analysis

Data are shown as means \pm the standard error of the mean (SEM). All experiments were performed at least three times and representative images are shown. The Student's *t*-test was performed using SPSS v17.0 (IBM, Armonk, NY, USA). A value of P < 0.05 was considered significant. The statistical parameters of quantitative data are reported in the corresponding figure legends.

RESULTS

Roburic Acid Disrupts the Interaction Between TNF and TNF-R1 and Blocks TNF-Induced NF-κB Activation

Protein-protein interactions between TNF and its receptor TNF-R1 are known to regulate the canonical TNF-induced NF-κB pathway and are therefore considered a pivotal therapeutic target for the treatment of TNF-associated autoimmune diseases, including cancer (10, 26, 27). Given that roburic acid can exhibit anti-inflammatory activity and the underlying molecular mechanism is still unknown (21, 23), we investigated whether roburic acid could directly disrupt the interaction between TNF and TNF-R1.

We first detected the direct interactions between roburic acid and TNF-R1 and TNF using SPR analysis. The results showed that roburic acid could directly interact with TNF, but not with TNF-R1 (**Figures 1B, C**). The apparent association (K_{on}) and dissociation (K_{off}) constants of roburic acid were calculated as $4.21 \times 10^3 \text{ M}^{-1}\text{s}^{-1}$ and $2.97 \times 10^{-2} \text{ s}^{-1}$, respectively, and the TNFbinding affinity (K_D) was calculated as 7.066 µM, suggesting that the TNF-roburic acid complex is relatively stable.

A Novel TNF-Targeting Therapeutics Agent

Importantly, the BLI-based solution competition assay showed that roburic acid could compete with TNF-R1 for TNF binding (**Figure 1D**), indicating that roburic acid disrupts the interaction between the two proteins. Analysis of the intrinsic kinetic parameters indicated that roburic acid inhibited the association between TNF and TNF-R1, with the $K_{\rm on}$ value decreasing from 2.94×10^4 to 1.30×10^4 M⁻¹s⁻¹; roburic acid also promoted the dissociation between TNF and TNF-R1, with the $K_{\rm off}$ value increasing from 2.16×10^{-4} to 2.74×10^{-3} s⁻¹. This demonstrated that roburic acid disrupted the interaction between TNF and TNF-R1, with the binding affinity ($K_{\rm D}$) decreasing from 7.33×10^{-9} to 2.11×10^{-7} M.

To further identify whether roburic acid could inhibit TNFinduced NF- κ B activation, we directly performed NF- κ B luciferase reporter assays *in vitro*. TNF significantly increased the NF- κ B luciferase activity in a concentration-dependent manner, and roburic acid significantly blocked TNF-induced NF- κ B activation in a concentration-dependent manner (**Figure 1E**).

Collectively, these results indicated that roburic acid directly binds to TNF with high affinity, blocks the interaction between TNF and TNF-R1, and inhibits TNF-induced NF- κ B activation. This demonstrates that TNF is a direct target of roburic acid in the inhibition of the TNF-induced NF- κ B activation, which prompted us to investigate whether roburic acid exerts antitumor effects through inhibition of TNF-induced NF- κ B signaling.

The HCT-116 and HCT-15 Cell Lines Showed the Greatest Sensitivity to Roburic Acid Treatment

To evaluate the potential cytotoxicity of roburic acid against human colorectal cancer cells, HCT-116, HCT-15, HT29, and Colo205 cells were treated with various concentrations of roburic acid for 2 days in vitro and cell viability was determined by the standard MTT method. As shown in Figures 2A-D, roburic acid greatly inhibited the viability of HCT-116, HCT-15, HT29, and Colo205 cells, with half-maximal inhibitory concentration (IC_{50}) values of 3.90, 4.77, 5.35, and 14.54 µM, respectively. To further investigate whether roburic acid exhibits cytotoxicity against other types of cancer cells, we determined the IC₅₀ values for three breast cancer cell lines (SK-BR-3, BT549, and BT-474), one central nervous system cancer cell line (U251), three kidney cancer cell lines (786-O, ACHN, and A498), four lung cancer cell lines (A549, NCI-H460, NCI-H226, and NCI-H23), two ovarian cancer cell lines (OVCAR-3 and SK-OV-3), two prostate cancer cell lines (DU145 and PC-3), and one leukemia cancer cell line (CCRF-CEM). As shown in **Supplementary Table S1**, the IC₅₀ values for roburic acid ranged from 5-15 µM in these seven human cancer cell types. Taken together, the above results indicated that the HCT-116 and HCT-15 cell lines were the most sensitive to roburic acid cytotoxicity.

Notably, colorectal cancer has been shown to exhibit extensive inflammatory infiltrates with high levels of cytokine expression in the tumor microenvironment and TNF can activate NF- κ B to promote colorectal cancer cell growth (9). Consistently, the high expression levels of TNF-R1 were detected

in the HCT-116 and HCT-15 cell lines and TNF could effectively promote the growth of these cells in a concentration-dependent manner (**Supplementary Figure S1**). Therefore, we selected HCT-116 and HCT-15 cell lines for further studies. As expected, the flat plate colony formation assays showed that roburic acid could significantly inhibit HCT-116 and HCT-15 colony formation in a concentration-dependent manner (**Figure 2E-G**).

Roburic Acid Suppressed DNA Synthesis in HCT-116 and HCT-15 Cells

To provide direct evidence for the cytotoxic response to roburic acid treatment in human colorectal cancer cell lines, we further investigated whether roburic acid could inhibit DNA synthesis in these cells. EdU incorporation assays showed that roburic acid treatment (4–16 μ M) markedly suppressed DNA synthesis in both colorectal cancer cell lines (**Supplementary Figure S2**).

Roburic Acid Treatment Triggered G0/G1 Cell Cycle Arrest in HCT-116 and HCT-15 Cells

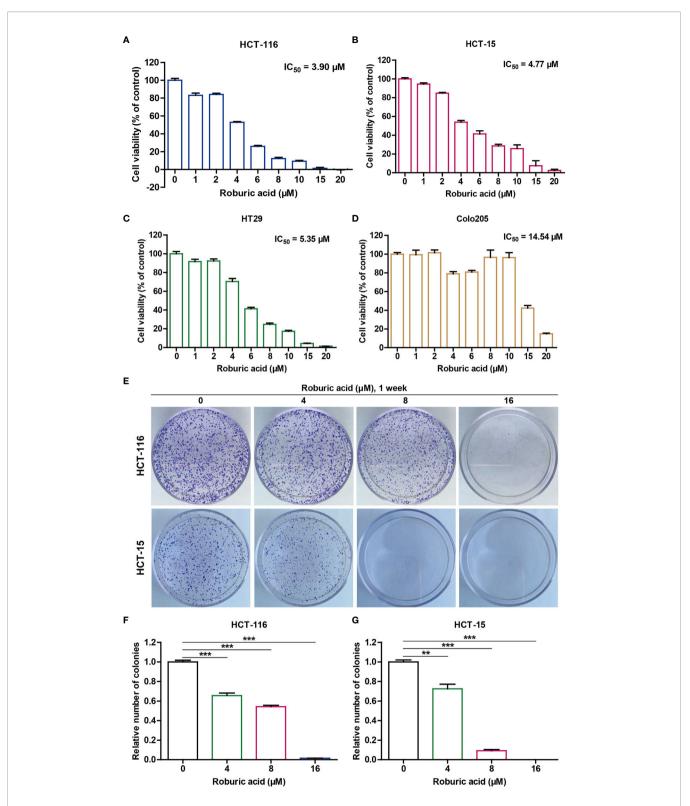
Given that roburic acid could effectively suppress DNA synthesis in colorectal cancer cells, we speculated that it might induce cell cycle arrest. To test this, we treated HCT-116 and HCT-15 cells with different concentrations of roburic acid (4–16 μ M) for 24 h and detected the cell cycle phase distribution using flow cytometry. As expected, roburic acid significantly increased the percentage of G0/G1 phase cells in both cell lines, and this effect was concentration-dependent (**Figure 3**). In addition, the percentages of cells in the S and G2 phases were significantly decreased in roburic acid-treated colorectal cancer cells (data not shown).

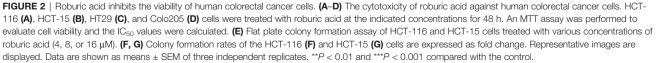
Roburic Acid Triggered Apoptosis in HCT-116 and HCT-15 Cells

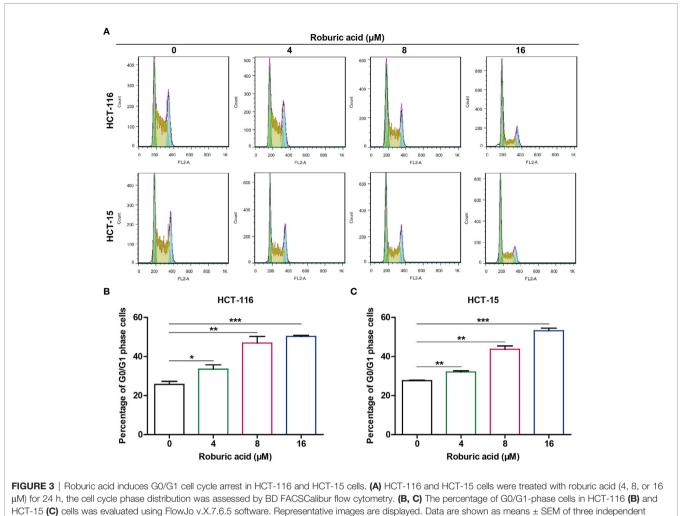
Because we found that roburic acid could significantly inhibit the viability of HCT-116 and HCT-15 cells within 2 days, we speculated that roburic acid triggers cell death in addition to disrupting cell cycle distribution. Interestingly, we observed that HCT-116 and HCT-15 cells treated with roburic acid (8 μ M) for 24 h exhibited a shrunk morphology, detached, and died (**Figure 4A**). We further determined the proapoptotic effect of roburic acid (4–16 μ M) for 24 h, the number of Annexin V–FITC/PI staining and flow cytometric analysis. After treatment with roburic acid (4–16 μ M) for 24 h, the number of Annexin V–FITC-positive (apoptotic) HCT-116 and HCT-15 cells exhibited a significant, concentration-dependent increase (**Figures 4B–D**). These results demonstrated that roburic acid triggers cell death through the induction of cell cycle arrest and apoptosis.

Roburic Acid Modulated the Expression Levels of Multiple Cell Cycle- and Apoptosis-Related Regulators in Colorectal Cancer Cells

Because roburic acid markedly induced cell cycle arrest and apoptosis in colorectal cancer cells, we further investigated the







replicates. *P < 0.05, **P < 0.01 and ***P < 0.001 compared with the control.

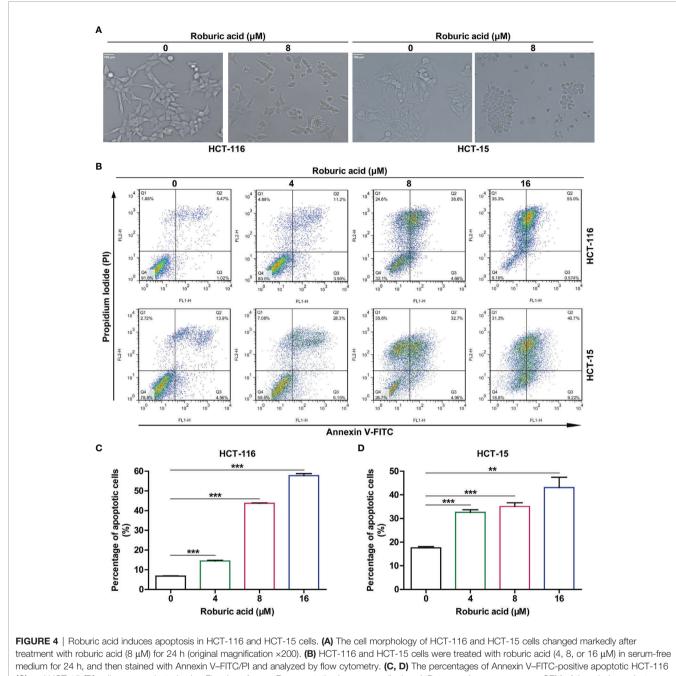
protein levels of multiple cell cycle- and apoptosis-related regulators in HCT-116 and HCT-15 cells treated with roburic acid (4-16 µM) for 24 h. As expected, roburic acid treatment led to a significant decrease in the protein expression levels of cell cyclerelated markers, including Cyclin B1, Cyclin D1, and Cyclin E1, in both HCT-116 and HCT-15 cells (Supplementary Figure S3). In addition, roburic acid treatment greatly enhanced the cleavage of poly (ADP-ribose) polymerase (PARP), Caspase3, Caspase7, and Caspase9 in these colorectal cancer cells in a concentrationdependent manner (Supplementary Figure S3). Importantly, roburic acid treatment also reduced the expression levels of several antiapoptotic proteins in both cell lines, including that of Bcl-2, Bcl-xL, XIAP, Mcl-1, and Survivin, in a concentrationdependent manner (Supplementary Figure S3). c-Myc is an oncogenic transcription factor that is highly expressed through different mechanisms in many cancer types, and is closely associated with promotion of the transition from the G0/G1 phase to the S phase of the cell cycle (28). Interestingly, we found that treatment with roburic acid significantly decreased the protein expression level of c-Myc in human colorectal cancer

cells in a concentration-dependent manner (Supplementary Figure S3).

Roburic Acid Inhibited the TNF-Induced NF-κB Signaling Pathway in Colorectal Cancer Cells

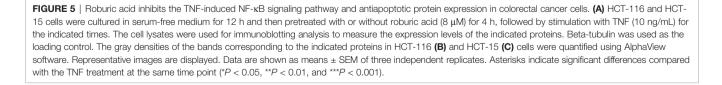
Several studies have indicated that roburic acid inhibits the NF- κ B and MAPK signaling pathways and exerts anti-inflammatory effects (21, 23). Recently, it has become clear that TNF-induced NF- κ B signaling also plays a critical role in colorectal cancer development and progression, and is a potential therapeutic target for the treatment of these conditions (9, 29, 30). Notably, pathways that activate NF- κ B signaling can inhibit apoptosis through upregulation of the expression of antiapoptotic proteins such as XIAP, Mcl-1, and Survivin (16).

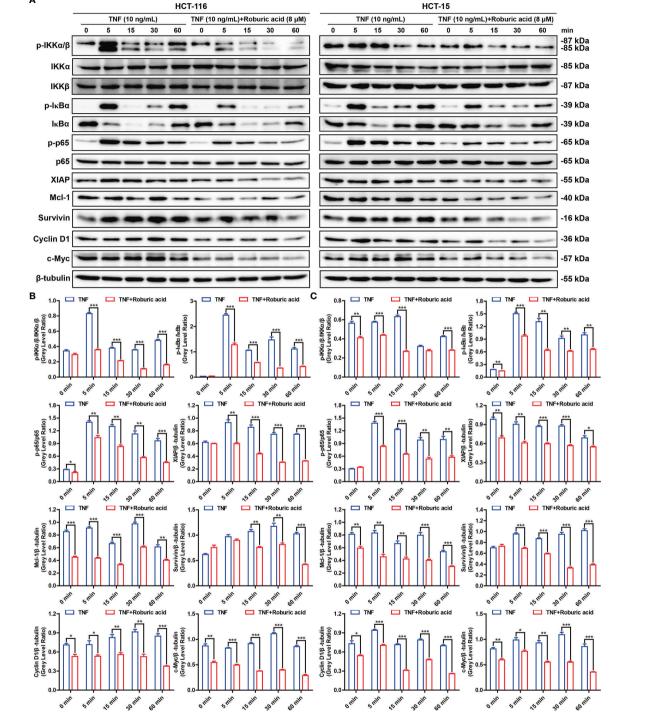
To further explore the molecular mechanisms by which roburic acid suppresses the expression of antiapoptotic proteins, we investigated whether roburic acid could block TNF-induced NF- κ B signaling. As expected, TNF (10 ng/mL) treatment led to a marked activation of the NF- κ B signaling pathway in both



(C) and HCT-15 (D) cells were evaluated using FlowJo software. Representative images are displayed. Data are shown as means ± SEM of three independent replicates. **P < 0.01 and ***P < 0.001 compared with the control.

HCT-116 and HCT-15 cells, as determined by the observed increase in the levels of IKKα/β, IκBα, and p65 phosphorylation, degradation of IκBα, and induction of the protein expression of XIAP, Mcl-1, and Survivin (**Figure 5**). However, these effects were significantly inhibited by roburic acid treatment (8 μ M) (**Figure 5**), which was consistent with the results of the BLI-based solution competition assay and NF-κB luciferase reporter assays (**Figures 1D, E**). Notably, roburic acid treatment had no effect on the protein expression level of p65 in either cell line (**Figure 5**). NF-κB can transactivate the expression of Cyclin D1 and c-Myc, which promotes cell proliferation, and suppress the expression of the proliferation factor JNK (10). As expected, roburic acid treatment significantly suppressed the expression of Cyclin D1 and c-Myc (**Figure 5**), and increased the levels of phosphorylated JNK in both HCT-116 and HCT-15 cells (**Supplementary Figure S4**). Moreover, the TNF-stimulated phosphorylation of ERK, p38, AKT, and STAT3 was decreased in both colorectal cancer cell lines (**Supplementary Figure S4**). Collectively, these results indicated





Α

that roburic acid inhibits TNF-induced NF- κ B signaling in colorectal cancer cells.

Roburic Acid Inhibited TNF-Induced P65 Nuclear Translocation in Colorectal Cancer Cells

Nuclear translocation of p65 is a pivotal event in TNF-induced NF- κ B pathway activation. We further investigated whether roburic acid could block the TNF-stimulated p65 nuclear translocation in HCT-116 and HCT-15 cells. As expected, roburic acid significantly inhibited p65 nuclear translocation at 0 to 30 min in HCT-116 cells and at 30 to 60 min in HCT-15 cells (**Figure 6A**). To further confirm this result, we performed immunofluorescence staining for p65 in HCT-116 and HCT-15 cells. As shown in **Figure 6B**, TNF (10 ng/mL) treatment greatly stimulated p65 nuclear translocation in both cell lines at 30 min; however, this effect was significantly inhibited by roburic acid (8 μ M).

Roburic Acid Reduced Tumor Growth by Blocking NF-kB Signaling in a Xenograft Mouse Model of Colorectal Cancer

Having established the inhibitory effects of roburic acid on human colorectal cancer cells in vitro, we next investigated whether roburic acid could suppress cancer cell growth in vivo using a xenograft mouse model of colorectal cancer. Initially, HCT-116 and HCT-15 cells were injected subcutaneously into nude mice. One week after the xenotransplantation, the tumorbearing mice were randomized into three groups and treated as described in the "Materials and methods" section. We found that roburic acid treatment effectively suppressed the growth of the xenografted colorectal tumors, as indicated by the significantly decreased tumor volume and weight (Figures 7A-F), and was consistent with the results of the in vitro experiments. In addition, treatment with roburic acid at the concentrations tested over 18 days did not affect the body weight of mice (Figure 7G), suggesting that roburic acid treatment had no side effects at the tested concentrations.

To further investigate whether roburic acid suppresses tumor growth by inhibiting the NF-KB signaling pathway in vivo, we performed western blotting analysis and immunohistochemical staining for the xenografted HCT-116 and HCT-15 tumor tissues. Consistent with the molecular findings in vitro, western blotting analysis showed that treatment with roburic acid inhibited the phosphorylation of p65, promoted the cleavage of Caspase3, and suppressed the protein expression of Bcl-xL, XIAP, and Cyclin D1 in the xenografted colorectal tumor tissues (Figure 7H). Furthermore, immunohistochemical staining of the tumor sections indicated that roburic acid treatment downregulated the expression of p-p65, while increasing the level of cleaved Caspase3 (Figure 7I and Supplementary Figure S5). These results were consistent with those of the immunoblotting analysis. Ki-67 is a specific marker for cell proliferation in vivo. As expected, we found that the expression of Ki-67 was decreased in the roburic acid-treated group compared with the control group (Figure 7I and

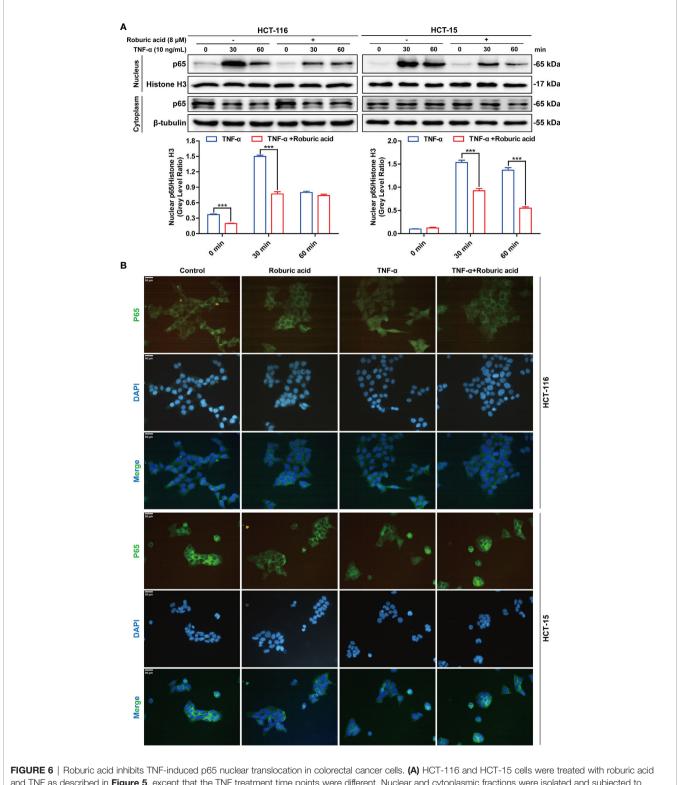
Supplementary Figure S5). Taken together, these results demonstrated that roburic acid can suppress tumor growth by blocking NF- κ B signaling in a xenograft mouse model of colorectal cancer.

DISCUSSION

Cancer remains a major public health problem worldwide, affecting millions of individuals and resulting in extensive morbidity and mortality (31–33). Approximately 18 million new cancer cases and 9 million cancer deaths were reported in 2018 (1). Although a substantial amount of work has been undertaken on cancer research and development of numerous drugs for cancer treatment, further investigation is urgently required to identify more specific therapeutic targets as well as drugs with reduced side effects. Currently, extracting new antitumor compounds from traditional medicinal plants is recognized as one of the main cancer treatment strategies (18). However, to date, no study has elucidated whether roburic acid isolated from oak galls exhibits antitumor activity, nor have its interaction target and the underlying mechanisms been identified.

In the present study, we investigated the cytotoxicity of roburic acid in 24 cancer cell lines comprising eight cancer types and identified the colorectal cancer cell lines HCT-116 and HCT-15 as being the most sensitive to roburic acid treatment, with IC₅₀ values of 3.90 and 4.77 μ M, respectively. These cell lines were then used to further investigate the anticancer effects of roburic acid in vitro and in vivo. Our results demonstrated that roburic acid effectively suppressed colorectal cancer cell proliferation by inducing G0/G1 cell cycle arrest and downregulating the protein expression of Cyclin B1, Cyclin D1, and Cyclin E1. In addition, roburic acid induced the apoptosis of colorectal cancer cells by promoting the cleavage of PARP, Caspase3, Caspase7, and Caspase9, as well as downregulating the levels of the antiapoptotic proteins Bcl-2, Bcl-xL, XIAP, Mcl-1, and Survivin. Importantly, roburic acid inhibited the TNF-induced NF-kB signaling pathway and suppressed the expression of these antiapoptotic proteins in colorectal cancer cells. Molecular interaction studies further demonstrated that roburic acid directly bound to TNF with high affinity ($K_D = 7.066 \ \mu M$) and blocked the interaction between TNF and its receptor, TNF-R1. Consistent with the in vitro results, roburic acid also suppressed tumor growth by blocking NF-KB signaling in a xenograft mouse model of colorectal cancer.

Recent studies have shown that most natural compounds with anti-inflammatory properties exhibit excellent antitumor activity by inhibiting NF- κ B pathway activation (15, 34, 35). The NF- κ B signaling pathway is aberrantly activated in many tumor cells, contributing to cancer cell survival, proliferation, differentiation, apoptosis, inflammation, and cell signaling transduction (11, 36, 37). Interestingly, roburic acid was detected in the resin fraction that is secreted when plants are attacked by insects, and it was shown to exhibit anti-inflammatory properties (21, 23),



and TNF as described in **Figure 5**, except that the TNF treatment time points were different. Nuclear and cytoplasmic fractions were isolated and subjected to western blotting using an anti-p65 antibody. Beta-tubulin and Histone H3 were respectively used as loading control for the nuclear and cytoplasmic fractions. The gray densities of the bands corresponding to the indicated proteins in HCT-116 and HCT-15 cells were quantified using AlphaView software. **(B)** p65 nuclear translocation in HCT-116 and HCT-15 cells was determined by immunofluorescence staining. HCT-116 and HCT-15 cells were treated with TNF for 30 min. p65 was detected using the corresponding primary antibody and nuclei were stained with DAPI. The corresponding images (original magnification ×400) were merged using ImageJ software. Representative images are displayed. Data are shown as means \pm SEM of three independent replicates. Asterisks indicate significant differences compared with the TNF treatment at the same time point (***P < 0.001).

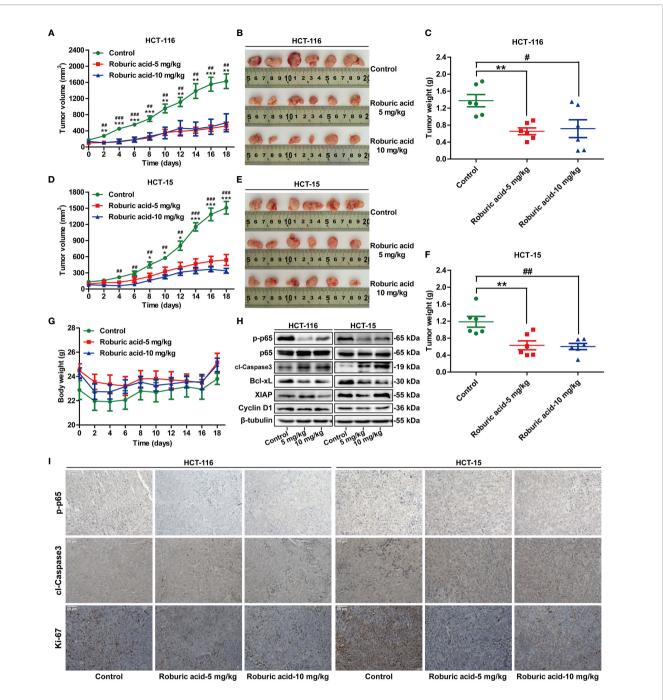


FIGURE 7 | Roburic acid inhibits tumor growth by blocking NF- κ B signaling in a xenograft mouse model of colorectal cancer. Roburic acid treatment inhibits tumor growth and weight of HCT-116 (**A–C**) and HCT-15 (**D–F**) human colorectal cancer xenografts in nude mice, but does not affect the body weight (**G**) of either group. (**H**) Tumor tissues from HCT-116 and HCT-15 xenografts were used for immunoblotting analysis to assess the protein expression of p-p65, p65, cleaved Caspase3 (cl-Caspase3), Bcl-xL, XIAP, and Cyclin D1. Beta-tubulin was used as loading control. (**I**) Paraffin-embedded HCT-116 and HCT-15 tumor tissue sections were immunostained with antibodies against p-p65, cl-Caspase3, and Ki-67 (original magnification ×400). Representative images are displayed. Data are shown as means \pm SEM of six mice per group. **P* < 0.05, ***P* < 0.01, and ****P* < 0.001, low-dose roburic acid group vs the control group; **P* < 0.05, #**P* < 0.01, and ###*P* < 0.001, high-dose roburic acid group vs the control group.

suggesting that it can serve as an insect repellant and might exert protective effects on human health (38). In this study, roburic acid exhibited marked cytotoxic effects in different types of cancer cells (IC_{50} <15 μ M), including colorectal, breast, central

nervous system, kidney, lung, ovarian, prostate, and leukemia cancer cells. Based on these findings, we speculated that roburic acid likely suppresses cancer cell growth by inhibiting the activation of the NF- κ B pathway.

22

It is well established that a dynamic and complex network of interacting proteins regulates cellular behavior (13). Interactions between TNF with TNF-R1 activate the NF-KB signaling pathway, which plays important roles in cancer development and progression (39). Consequently, targeting protein-protein interactions is a promising strategy for the treatment of cancer (40, 41). TNF is an inflammatory cytokine that initiates dynamic intracellular signals through binding to its receptor TNF-R1 (13). Upon TNF binding, TNF-R1 forms a trimer, which then becomes a key regulator of inflammation-dependent NF-KB signaling. The NF- κ B inhibitor protein (I κ B) is degraded soon after phosphorylation by activated IKB kinase (IKK), and the p65 transcription factor translocates into the nucleus to activate TNF-induced NF- κ B signaling (12, 13). In this study, we found that roburic acid treatment significantly inhibited the TNF-induced phosphorylation of IKK α/β , I κ B α , and p65, degradation of IkBa, and nuclear translocation of p65 in human colorectal cancer cells. Regarding the detailed molecular mechanisms, molecular interaction studies demonstrated that roburic acid can directly bind to TNF with high affinity ($K_D = 7.066 \ \mu M$), but not to its receptor, TNF-R1. Interestingly, roburic acid also blocked the interaction between TNF and TNF-R1, with a decrease in binding affinity (K_D) from 7.33 to 211 nM, which explains why roburic acid can inhibit the TNF-induced NF-κB signaling pathway. However, the mechanisms underlying how roburic acid binds to TNF remain unclear and require further investigation.

Apoptosis is the process of programmed cell death, and plays a pivotal role in the development and progression of cancer (16). Excessive NF- κ B signaling in cancer cells can suppress apoptosis via inducing the expression of apoptosis inhibitors such as XIAP, Mcl-1, and Survivin (10, 12). In this study, we demonstrated that roburic acid suppressed the TNF-induced expression of antiapoptotic proteins, including XIAP, Mcl-1, and Survivin. Without exogenous TNF stimulation, roburic acid also inhibited the expression of these antiapoptotic proteins in colorectal cancer cells. NF-KB can promote cell proliferation by transactivating the expression of Cyclin D1 and c-Myc (10). In the current study, we found that roburic acid could significantly downregulate Cyclin D1 and c-Myc protein levels in colorectal cancer cells, with or without TNF stimulation. In vitro studies have established that roburic acid can effectively suppress human colorectal cancer cell growth through inhibition of the NF-KB signaling pathway; however, whether roburic acid also exhibited antitumor activity in vivo through the same mechanism has not been clarified. In the present study, we further demonstrated that roburic acid can also inhibit tumor growth in vivo by blocking NFκB signaling in a xenograft mouse model of colorectal cancer.

Roburic acid is a natural small-molecule compound isolated from medicinal plants, and its biological activities and mechanism of action have not been thoroughly studied. Additionally, roburic acid may have many limitations, such as poor water solubility and bioavailability, and potential side effects. Therefore, these issues need to be urgently solved before roburic acid can be used clinically in the treatment of patients with colorectal cancer. Notably, in addition to contributing to cancer development and progression, TNF/ TNF-R1-mediated NF- κ B signaling has crucial roles in many other autoimmune diseases such as rheumatoid arthritis and Crohn's disease (17, 42, 43). Based on the findings in this study, we speculate that roburic acid could also be used in the treatment of other TNF-related diseases. However, further investigation is urgently needed to test this hypothesis, which is the subject of ongoing work in our laboratory.

CONCLUSIONS

Taken together, our findings showed that roburic acid directly binds to TNF with high affinity, thereby disrupting the interaction between TNF and TNF-R1 and leading to inhibition of the NF- κ B signaling pathway, both *in vitro* and *in vivo*. The results indicated that roburic acid is a novel TNFtargeting therapeutics agent in colorectal cancer as well as other cancer types.

DATA AVAILABILITY STATEMENT

The original contributions presented in the study are included in the article/**Supplementary Material**. Further inquiries can be directed to the corresponding authors.

ETHICS STATEMENT

This study was carried out in accordance with the National Institutes of Health's Guidelines for the Care and Use of Laboratory Animals and was approved by the Yunnan Agricultural University institutional ethics committee.

AUTHOR CONTRIBUTIONS

HX, TL, and ZX conceived and designed the experiments. TL, HX, JL, FC, JX, LH, and LJ performed the experiments. HX and TL analyzed the data. JS and XW contributed reagents/materials/ analysis tools. HX and TL wrote the manuscript. All authors read and approved the final manuscript.

FUNDING

This work was supported by grants from the Scientific Research Fund Project of Yunnan Provincial Education Office (2022J0297), the Yunnan Fundamental Research Project (202101AU070216, 202101AU070086, and 202101AT070749), the Yunnan Provincial Key Programs of Yunnan Eco-friendly Food International Cooperation Research Center Project (2019ZG00904 and 2019ZG00909), and the Science and Technology Plan Project of Yunnan Province (2018IA060).

ACKNOWLEDGMENTS

We thank all members of the laboratory for their kindness and help.

REFERENCES

- Bray F, Ferlay J, Soerjomataram I, Siegel RL, Torre LA, Jemal A. Global Cancer Statistics 2018: GLOBOCAN Estimates of Incidence and Mortality Worldwide for 36 Cancers in 185 Countries. *CA Cancer J Clin* (2018) 68 (6):394–424. doi: 10.3322/caac.21492
- Sun L, Fang Y, Wang X, Han Y, Du F, Li C, et al. miR-302a Inhibits Metastasis and Cetuximab Resistance in Colorectal Cancer by Targeting NFIB and CD44. *Theranostics* (2019) 9(26):8409–25. doi: 10.7150/thno.36605
- Guo M, Li Z, Huang Y, Shi M. Polysaccharides From Nostoc Commune Vaucher Activate Macrophages via NF-kappaB and AKT/JNK1/2 Pathways to Suppress Colorectal Cancer Growth In Vivo. Food Funct (2019) 10 (7):4269–79. doi: 10.1039/c9fo00595a
- DeLaria GA, Hunter JA. Deep Venous Thrombosis. Implications After Open Heart Surgery. Chest (1991) 99(2):284–8. doi: 10.1378/chest.99.2.284
- Yang L, Wang S, Lee JJ, Lee S, Lee E, Shinbrot E, et al. An Enhanced Genetic Model of Colorectal Cancer Progression History. *Genome Biol* (2019) 20 (1):168. doi: 10.1186/s13059-019-1782-4
- Brenner H, Kloor M, Pox CP. Colorectal Cancer. Lancet (2014) 383 (9927):1490–502. doi: 10.1016/S0140-6736(13)61649-9
- Lu YX, Ju HQ, Wang F, Chen LZ, Wu QN, Sheng H, et al. Inhibition of the NF-kappaB Pathway by Nafamostat Mesilate Suppresses Colorectal Cancer Growth and Metastasis. *Cancer Lett* (2016) 380(1):87–97. doi: 10.1016/ j.canlet.2016.06.014
- Karin M, Greten FR. NF-Kappab: Linking Inflammation and Immunity to Cancer Development and Progression. *Nat Rev Immunol* (2005) 5(10):749– 59. doi: 10.1038/nri1703
- De Simone V, Franze E, Ronchetti G, Colantoni A, Fantini MC, Di Fusco D, et al. Th17-Type Cytokines, IL-6 and TNF-Alpha Synergistically Activate STAT3 and NF-kB to Promote Colorectal Cancer Cell Growth. *Oncogene* (2015) 34(27):3493–503. doi: 10.1038/onc.2014.286
- Lin Y, Bai L, Chen W, Xu S. The NF-kappaB Activation Pathways, Emerging Molecular Targets for Cancer Prevention and Therapy. *Expert Opin Ther Targets* (2010) 14(1):45–55. doi: 10.1517/14728220903431069
- Aggarwal BB. Nuclear Factor-Kappab: The Enemy Within. Cancer Cell (2004) 6(3):203–8. doi: 10.1016/j.ccr.2004.09.003
- Van Quickelberghe E, De Sutter D, van Loo G, Eyckerman S, Gevaert K. A Protein-Protein Interaction Map of the TNF-Induced NF-kappaB Signal Transduction Pathway. *Sci Data* (2018) 5:180289. doi: 10.1038/sdata.2018.289
- Pabon NA, Zhang Q, Cruz JA, Schipper DL, Camacho CJ, Lee REC. A Network-Centric Approach to Drugging TNF-Induced NF-KappaB Signaling. *Nat Commun* (2019) 10(1):860. doi: 10.1038/s41467-019-08802-0
- 14. Ju W, Wang X, Shi H, Chen W, Belinsky SA, Lin Y. A Critical Role of Luteolin-Induced Reactive Oxygen Species in Blockage of Tumor Necrosis Factor-Activated Nuclear factor-kappaB Pathway and Sensitization of Apoptosis in Lung Cancer Cells. *Mol Pharmacol* (2007) 71(5):1381–8. doi: 10.1124/mol.106.032185
- Saleem M, Kweon MH, Yun JM, Adhami VM, Khan N, Syed DN, et al. A Novel Dietary Triterpene Lupeol Induces Fas-Mediated Apoptotic Death of Androgen-Sensitive Prostate Cancer Cells and Inhibits Tumor Growth in a Xenograft Model. *Cancer Res* (2005) 65(23):11203–13. doi: 10.1158/0008-5472.CAN-05-1965
- Kong Y, Li F, Nian Y, Zhou Z, Yang R, Qiu MH, et al. KHF16 Is a Leading Structure From Cimicifuga Foetida That Suppresses Breast Cancer Partially by Inhibiting the NF-kappaB Signaling Pathway. *Theranostics* (2016) 6(6):875– 86. doi: 10.7150/thno.14694
- O'Connell J, Porter J, Kroeplien B, Norman T, Rapecki S, Davis R, et al. Small Molecules That Inhibit TNF Signalling by Stabilising an Asymmetric Form of the Trimer. *Nat Commun* (2019) 10(1):5795. doi: 10.1038/s41467-019-13616-1

SUPPLEMENTARY MATERIAL

The Supplementary Material for this article can be found online at: https://www.frontiersin.org/articles/10.3389/fimmu.2022. 853165/full#supplementary-material

- Yang H, Chen D, Cui QC, Yuan X, Dou QP. Celastrol, a Triterpene Extracted From the Chinese "Thunder of God Vine," Is a Potent Proteasome Inhibitor and Suppresses Human Prostate Cancer Growth in Nude Mice. *Cancer Res* (2006) 66(9):4758–65. doi: 10.1158/0008-5472.CAN-05-4529
- Ruan H, Zhan YY, Hou J, Xu B, Chen B, Tian Y, et al. Berberine Binds RXRalpha to Suppress Beta-Catenin Signaling in Colon Cancer Cells. Oncogene (2017) 36(50):6906–18. doi: 10.1038/onc.2017.296
- Wang Y, Huang J, Li B, Xue H, Tricot G, Hu L, et al. A Small-Molecule Inhibitor Targeting TRIP13 Suppresses Multiple Myeloma Progression. *Cancer Res* (2020) 80(3):536–48. doi: 10.1158/0008-5472.CAN-18-3987
- Chen Y, Ji N, Pan S, Zhang Z, Wang R, Qiu Y, et al. Roburic Acid Suppresses NO and IL-6 Production via Targeting NF-kappaB and MAPK Pathway in RAW264.7 Cells. Inflammation (2017) 40(6):1959–66. doi: 10.1007/s10753-017-0636-z
- 22. Cao H, Yu R, Choi Y, Ma ZZ, Zhang H, Xiang W, et al. Discovery of Cyclooxygenase Inhibitors From Medicinal Plants Used to Treat Inflammation. *Pharmacol Res* (2010) 61(6):519-24. doi: 10.1016/ j.phrs.2010.02.007
- 23. Verhoff M, Seitz S, Paul M, Noha SM, Jauch J, Schuster D, et al. Tetra- and Pentacyclic Triterpene Acids From the Ancient Anti-Inflammatory Remedy Frankincense as Inhibitors of Microsomal Prostaglandin E(2) Synthase-1. J Nat Prod (2014) 77(6):1445–51. doi: 10.1021/np500198g
- 24. Xu H, Liu T, Li J, Xu J, Chen F, Hu L, et al. Oxidation Derivative of (-)-Epigallocatechin-3-Gallate (EGCG) Inhibits RANKL-Induced Osteoclastogenesis by Suppressing RANK Signaling Pathways in RAW 264.7 Cells. *BioMed Pharmacother* (2019) 118:109237. doi: 10.1016/ j.biopha.2019.109237
- 25. Liu T, Ding S, Yin D, Cuan X, Xie C, Xu H, et al. Pu-Erh Tea Extract Ameliorates Ovariectomy-Induced Osteoporosis in Rats and Suppresses Osteoclastogenesis In Vitro. Front Pharmacol (2017) 8:324. doi: 10.3389/ fphar.2017.00324
- 26. Chen S, Feng Z, Wang Y, Ma S, Hu Z, Yang P, et al. Discovery of Novel Ligands for TNF-Alpha and TNF Receptor-1 Through Structure-Based Virtual Screening and Biological Assay. J Chem Inf Model (2017) 57 (5):1101–11. doi: 10.1021/acs.jcim.6b00672
- Saddala MS, Huang H. Identification of Novel Inhibitors for TNFalpha, TNFR1 and TNFalpha-TNFR1 Complex Using Pharmacophore-Based Approaches. J Transl Med (2019) 17(1):215. doi: 10.1186/s12967-019-1965-5
- Karkhanis V, Alinari L, Ozer HG, Chung J, Zhang X, Sif S, et al. Protein Arginine Methyltransferase 5 Represses Tumor Suppressor miRNAs That Down-Regulate CYCLIN D1 and C-MYC Expression in Aggressive B-Cell Lymphoma. J Biol Chem (2020) 295(5):1165–80. doi: 10.1074/ jbc.RA119.008742
- Karin M. Nuclear factor-kappaB in Cancer Development and Progression. Nature (2006) 441(7092):431–6. doi: 10.1038/nature04870
- 30. Sheng YH, He Y, Hasnain SZ, Wang R, Tong H, Clarke DT, et al. MUC13 Protects Colorectal Cancer Cells From Death by Activating the NF-kappaB Pathway and Is a Potential Therapeutic Target. Oncogene (2017) 36(5):700– 13. doi: 10.1038/onc.2016.241
- Siegel RL, Miller KD, Jemal A. Cancer Statistics 2017. CA Cancer J Clin (2017) 67(1):7–30. doi: 10.3322/caac.21387
- Li J, Van Valkenburgh J, Hong X, Conti PS, Zhang X, Chen K. Small Molecules as Theranostic Agents in Cancer Immunology. *Theranostics* (2019) 9(25):7849–71. doi: 10.7150/thno.37218
- Siegel RL, Miller KD, Jemal A. Cancer Statistics 2020. CA Cancer J Clin (2020) 70(1):7–30. doi: 10.3322/caac.21590
- Saleem M. Lupeol, a Novel Anti-Inflammatory and Anti-Cancer Dietary Triterpene. Cancer Lett (2009) 285(2):109–15. doi: 10.1016/j.canlet. 2009.04.033

- Callejas BE, Mendoza-Rodriguez MG, Villamar-Cruz O, Reyes-Martinez S, Sanchez-Barrera CA, Rodriguez-Sosa M, et al. Helminth-Derived Molecules Inhibit Colitis-Associated Colon Cancer Development Through NF-kappaB and STAT3 Regulation. *Int J Cancer* (2019) 145(11):3126–39. doi: 10.1002/ ijc.32626
- Sarkar FH, Li Y. NF-Kappab: A Potential Target for Cancer Chemoprevention and Therapy. Front Biosci (2008) 13:2950–9. doi: 10.2741/2900
- Zhuang Z, Li H, Lee H, Aguilar M, Gocho T, Ju H, et al. NEMO Peptide Inhibits the Growth of Pancreatic Ductal Adenocarcinoma by Blocking NF-kappaB Activation. *Cancer Lett* (2017) 411:44–56. doi: 10.1016/j.canlet.2017.09.018
- Liu L, Lauro BM, Ding L, Rovere M, Wolfe MS, Selkoe DJ. Multiple BACE1 Inhibitors Abnormally Increase the BACE1 Protein Level in Neurons by Prolonging Its Half-Life. *Alzheimers Dement* (2019) 15(9):1183-94. doi: 10.1016/j.jalz.2019.06.3918
- Zhang C, Li A, Wang R, Cao Y, Jiang H, Ouyang S, et al. Recombinant Expression, Purification and Bioactivity Characterization of Extracellular Domain of Human Tumor Necrosis Factor Receptor 1. Protein Expr Purif (2019) 155:21–6. doi: 10.1016/j.pep.2018.11.002
- Ivanov AA, Khuri FR, Fu H. Targeting Protein-Protein Interactions as an Anticancer Strategy. *Trends Pharmacol Sci* (2013) 34(7):393-400. doi: 10.1016/j.tips.2013.04.007
- Lim S, Cho HY, Kim DG, Roh Y, Son SY, Mushtaq AU, et al. Targeting the Interaction of AIMP2-DX2 With HSP70 Suppresses Cancer Development. *Nat Chem Biol* (2020) 16(1):31–41. doi: 10.1038/s41589-019-0415-2

- He MM, Smith AS, Oslob JD, Flanagan WM, Braisted AC, Whitty A, et al. Small-Molecule Inhibition of TNF-Alpha. *Science* (2005) 310(5750):1022–5. doi: 10.1126/science.1116304
- Zhao Y, Li Y, Qu R, Chen X, Wang W, Qiu C, et al. Cortistatin Binds to TNF-Alpha Receptors and Protects Against Osteoarthritis. *EBioMedicine* (2019) 41:556–70. doi: 10.1016/j.ebiom.2019.02.035

Conflict of Interest: The authors declare that the research was conducted in the absence of any commercial or financial relationships that could be construed as a potential conflict of interest.

Publisher's Note: All claims expressed in this article are solely those of the authors and do not necessarily represent those of their affiliated organizations, or those of the publisher, the editors and the reviewers. Any product that may be evaluated in this article, or claim that may be made by its manufacturer, is not guaranteed or endorsed by the publisher.

Copyright © 2022 Xu, Liu, Li, Chen, Xu, Hu, Jiang, Xiang, Wang and Sheng. This is an open-access article distributed under the terms of the Creative Commons Attribution License (CC BY). The use, distribution or reproduction in other forums is permitted, provided the original author(s) and the copyright owner(s) are credited and that the original publication in this journal is cited, in accordance with accepted academic practice. No use, distribution or reproduction is permitted which does not comply with these terms.





Localized Intra-Cavitary Therapy to Drive Systemic Anti-Tumor Immunity

Vera S. Donnenberg^{1,2,3*}, Patrick L. Wagner^{4,5}, James D. Luketich^{1,3}, David L. Bartlett^{4,5} and Albert D. Donnenberg^{1,2,6*}

¹ University of Pittsburgh Medical Center (UPMC) Hillman Cancer Centers, Pittsburgh, PA, United States, ² McGowan Institute for Regenerative Medicine, Pittsburgh, PA, United States, ³ Department of Cardiothoracic Surgery, University of Pittsburgh School of Medicine, Pittsburgh, PA, United States, ⁴ Surgical Oncology, Allegheny Health Network Cancer Institute, Pittsburgh, PA, United States, ⁵ College of Medicine, Drexel University, Pittsburgh, PA, United States, ⁶ Department of Medicine, University of Pittsburgh School of Medicine, Pittsburgh, PA, United States

Metastasis to the pleural and peritoneal cavities is a common terminal pathway for a wide variety of cancers. This article explores how these unique environments both promote aggressive tumor behavior and suppresses anti-tumor immunity, and ways in which local delivery of protein therapeutics can leverage the contained nature of these spaces to a therapeutic advantage, achieving high intra-cavital concentrations while minimizing systemic toxicity.

OPEN ACCESS

Edited by:

Xuyao Zhang, Fudan University, China

Reviewed by:

Luciano Mutti, Temple University, United States

*Correspondence:

Albert D. Donnenberg donnenbergad@upmc.edu Vera S. Donnenberg donnenbergvs@upmc.edu

Specialty section:

This article was submitted to Cancer Immunity and Immunotherapy, a section of the journal Frontiers in Immunology

Received: 30 December 2021 Accepted: 20 January 2022 Published: 11 February 2022

Citation:

Donnenberg VS, Wagner PL, Luketich JD, Bartlett DL and Donnenberg AD (2022) Localized Intra-Cavitary Therapy to Drive Systemic Anti-Tumor Immunity. Front. Immunol. 13:846235. doi: 10.3389/fimmu.2022.846235 Keywords: malignant pleural effusion, malignant ascites, local therapy, intratumoral, epithelial to mesenchymal transition (EMT), video assisted thoracoscopic surgery (VATS)

INTRODUCTION

Malignant pleural effusions (MPE) have a US incidence of more than 150,000 cases per year (1, 2) and a life expectancy measured in months (3). Likewise, patients with malignant peritoneal ascites (MPA) and peritoneal carcinomatosis also have abysmal survival (4) and poor quality of life (QOL (5),) with patients experiencing multiple hospitalizations for bowel obstruction and pain (6). Both MPE and MPA are common, painful, difficult to treat, and most importantly are uniformly fatal. Despite significant clinical progress in immuno-oncology, there has been almost no change in survival or quality of life for patients with MPE or MPA, which become the proximate cause of death in many cases of advanced cancer

SUBSECTIONS

An Incomplete Understanding of the Pleural and Peritoneal Cavity Environments

In states of normal health, the pleural and peritoneal cavities contain physiologic fluid with a dynamic array of immune cells and unique secretomes. In non-neoplastic pathologic states, fluid can accumulate in these cavities due either to transudative mechanisms (vascular pressure and decreased resorption), or exudative mechanisms (tissue inflammation and immune cell infiltration). These processes result in dramatic changes to the cavitary secretome and immune environment. Malignant effusions and ascites also exhibit similar shifts in the secretome and cellular infiltrate,

but several additional cytokines and chemokines distinguish them from benign effusions (Figure 1A). The presence of additional malignancy-specific components notwithstanding, the combination of cytokines seen across the spectrum of benign and malignant conditions is predicted to drive both aggressive tumor behavior and polarize pleural immune cells away from tumor-specific immunity and instead, toward a maladaptive repair-and-regenerate mode. Understanding the interplay between the secretome and the resident cell populations will provide much needed foundation for the development of innovative immunotherapeutics targetable to the cavitary spaces and specific to the mechanisms relevant to malignant effusions and ascites.

The Secretomic Signatures of Malignant Peritoneal Ascites and Pleural Effusions Are Indistinguishable

One of the most striking features of Figure 1A, which contrasts the secretomes of ovarian cancer ascites and pleural effusions with that of benign pleural effusions, is the similarity between the cytokine and chemokine profiles in pleural and peritoneal malignancies. In the healthy cavitary spaces, a physiologic secretome and a complement of immune cells are dedicated to maintenance and repair of the mesothelial lining through a process involving the epithelial to mesenchymal transition (EMT, detachment, migration) and the mesenchymal to epithelial transition (MET, reattachment, re-epithelialization) (9). In malignant fluid, the environment is transformed into an inflammatory milieu that promotes wound healing and suppresses adaptive immune effector responses. As mentioned above, this tumor-related cavitary fluid environment has all the inflammatory components of benign effusions (IL-6, sIL-6Ra, CCL2, CXCL10, TGFβ, CCL22, IL-8, IL-5 Figure 1), but includes additional tumor and endothelial growth factors, as well as a blunted effector cytokine response (IFN α 2) that is not seen in physiologic cavitary fluid or benign effusions.

Effects of the Malignant Secretome on Mesothelial Maintenance, Intra-Cavitary Tumor and Anti-Tumor Responses

Because the pleural and peritoneal spaces are lined by mesothelial cells, and because effusions and ascites result from a net inflow from the peripheral circulation, these cavities develop a unique cytokine environment. In the context of malignancy, the milieu of cytokines is predicted to play a maladaptive, tumor-supporting role, with negative effects not only in the cavitary environment, but systemically as well, promoting motility and solid organ metastasis. Figure 1B illustrates mechanisms by which the inflammatory cavitary secretome, initiated by tumor metastasis and supplemented by tumor-secreted cytokines, is predicted to establish an environment that promotes aggressive tumor behavior. These mechanisms include EMT, suppression of adaptive T-cell effector responses, and polarization of macrophages to support rather than oppose tumor growth. Although ovarian cancer is presented here as an example, the malignant cavitary secretome,

and the resulting tumor pathobiology is common to a wide range of cancers (7, 8).

A Rationale for Intra-Cavitary Therapy Using Immune-Oncology Drugs

The physiologically isolated pleural and peritoneal environments provide ideal anatomical spaces for the localized administration of large protein drugs. The pleura as well as the peritoneum are lined with mesothelial cells joined by tight junctions (10) creating a unique and isolated cavitary environment. Unlike chemotherapeutics, high molecular weight immuno-oncology drugs remain concentrated when administered directly to these cavities, reaching a high target occupancy even with protein drugs with a narrow therapeutic index when administered systemically (11–14).

Local administration of therapeutics may be used to directly target the tumor, support local immune cells, and condition cancer associated stromal cells (15). Despite the net inflow of serous fluid, IgG levels are lower in pleural effusions (16) and peritoneal ascites than in the peripheral circulation. Thus, intravenous administration of protein therapeutics may not be the most effective way to achieve the necessary therapeutic levels within the cavitary spaces. Conversely, localized intra-cavitary administration of these therapeutics has been shown to result in low systemic exposure, and negligible on-target off-tumor effects, while reducing adverse events associated with systemic toxicity (13, 14). The same principle applies to intra-cavitary injection of RNA-based therapeutics (17, 18). This mode of administration is greatly facilitated by the use of minimally invasive surgical techniques and placement of indwelling catheters. While these catheters are traditionally used for palliative decompression of the cavitary spaces, they have been repurposed as drug delivery devices, for example the instillation of pleurodesis agents or cytotoxic chemotherapy. Video assisted thoracoscopic surgery [VATS (19)] or laparoscopic peritoneal catheter placement (20) can likewise be used to guide intracavital-intratumoral drug delivery for agents such as oncovaccines and mRNA therapeutics, which are injected directly into tumor foci. Further, indwelling catheters allow for iterative sampling of cavitary fluid to monitor the response to therapy, the impact on the cavitary immune environment, the pharmacokinetics and pharmacodynamics (PK/ PD) of personalized drug dosing, and the real time determination of minimal anticipated biological effect levels [MABEL (21)]. Finally, anti-tumor effector responses initiated in the confines of the cavitary spaces would be expected to propagate systemically through the draining lymphatics, where they could combat solid organ metastases. Although most studies of single-agent intracavital immunotherapies have not measured effects on systemic immunity directly, the intrapleural (14) and intraperitoneal (13) experience with the bispecific anti-CD3/anti-EpCAM antibody catumaxomab is informative. Even though the systemic catumaxomab concentration was <1% of the intracavitary concentration, both studies observed transient increases in serum transaminases, which were attributed to systemic cytokine release. Similarly, intracavitary IL-2 administration resulted in an increase in peripheral CD8 T cells expressing granzyme B (22) and in peripheral NK cell activity (12), and intracavitary administration of an adenovirus/interferon β construct resulted in increased peripheral NK activity and anti-tumor antibodies (23).

In this manner, the cavitary spaces can be conceived of as 'bioreactors' into which novel immunotherapeutic agents could be instilled or injected intratumorally with the aim of selecting and stimulating effector cytotoxic T cells for cavitary and abscopal activity. We argue for local rather than systemic administration of protein-based therapies, since systemic administration may not achieve the necessary intracavitary therapeutic levels (11).

Intra-cavitary therapy can be considered as a special case of intra-tumoral therapy (reviewed in (24). Intra-tumoral immunotherapies have been explored extensively with the intention of altering the immune microenvironment of solid tumors to promote adaptive immunity. The peritoneal and pleural cavities are fluid-phase environments that may be more amenable to targeted manipulation. Although clusters of tumor cells are usually demonstrable in the fluid phase, the bulk of the lesions cake the mesothelium and adhere to internal organs, where they are bathed in the fluid phase.

Effusions and Ascites as a Source for Adoptive Cellular Therapy

Adoptive T-cell therapy using autologous tumor infiltrating lymphocytes (TIL) has been reported to induce salvage responses in a variety of refractory solid tumors (25). Conventionally, TIL therapy requires large-scale expansion of a small number of T-cells grown out from tumor tissue fragments stimulated with high dose IL-2 and anti-CD3 antibody. Since the expanded TIL depend on the continued presence of IL-2 for their survival, TIL infusion must be accompanied by repeated systemic administration of high dose IL-2, stopping only when doselimiting toxicity is reached. TIL infusion is often preceded by treatment with immunosuppressive chemotherapeutic agents such as cyclophosphamide and fludarabine to make space for the therapeutic cells. Therapeutic drainage of MPE frequently vields on the order of 0.25 to 0.5 x 10^6 pleural T cells/mL. In our experience, it is not unusual to drain a liter of fluid, yielding up to 5×10^8 T cells. Macrophages are also prevalent, constituting up to 50% of total nucleated MPE cells. Thus, in a single drainage it is often possible to obtain potentially therapeutic doses of pleural T cells following short-term activation or expansion. The ex vivo activated cells can be positively selected for CD45+ T cells and macrophages and then re-instilled into the pleural or peritoneal cavity. Potential advantages over conventionally expanded TIL include greatly simplified and rapid manufacture, potentially eliminating the requirement for systemic administration of toxic high dose IL-2 to ensure cell survival after reintroduction.

Potential Drawbacks to Intra-Cavitary Therapeutics

The principal problems facing intra-cavitary therapies are determining the most efficacious combination of therapeutics and the logistics associated with intra-cavitary and intratumoral administration. Additionally, the high cost of biologics, and particularly patient-specific cellular therapeutics must also be considered. There are a broad range of potential modalities that can be locally delivered, and within these modalities a variety of agents with similar targets or mechanisms of action, with many more in pre-clinical or early phase clinical trials (24, 26, 27). The varied formulations and compatibilities of potentially useful therapeutics must be considered if they are to be coadministered through indwelling catheters. Some therapeutics will be administered into the cavities, but others will require precise intratumoral delivery, which is limited to accessible tumor. Drug retention at intratumoral injection sites poses an additional potential difficulty and must be addressed by choosing appropriate agents and vehicles. For example, intratumoral injection of liposomal IL-12 mRNA (28) is more likely to remain localized than injection of the cytokine itself. Unexpected toxicities resulting from localized immune hyperresponsiveness, or interference with normal tissue maintenance may also pose problems, especially if they are delayed. Quantification of responses will likely require objective criteria similar to the RECIST score for solid tumors (29).

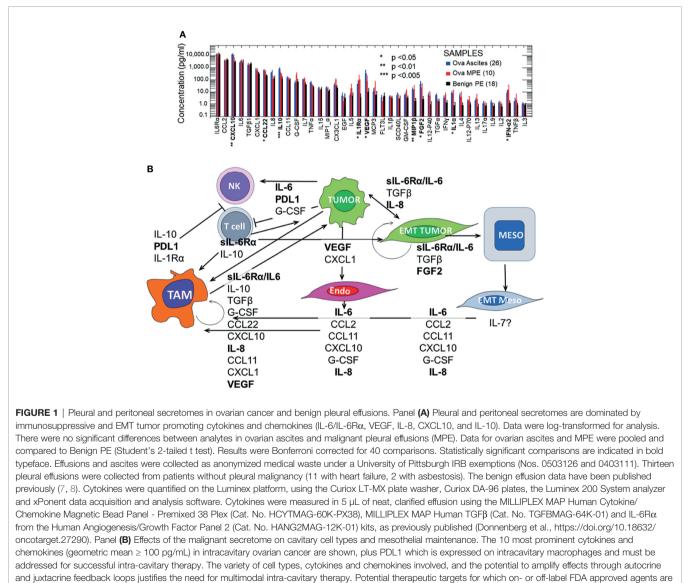
Technical challenges to implementation of intra-cavitary therapy include the need for dedicated personnel and facilities, including those required for image guided drug delivery. For drug delivery protocols requiring general anesthesia, the ability to administer repeated doses will be limited. Toxicities specific to intraperitoneal immunotherapy may be anticipated based on the experience with intra-peritoneal IL-2 (30) and monoclonal antibody (31) therapy (pyrexia, abdominal pain, nausea/ vomiting). These toxicities may be cavity specific as they were far milder with intrapleural administration of the same cytokine (12, 32) or antibody (14).

Finally, maximizing benefit with respect to cost is a challenge that must be met if intracavitary therapy is to gain acceptance. Given the dire prognosis and current palliative approaches to cavitary malignancies, any therapeutic combination that can provide an objective increase in response rates and survival with improved quality of life may justify the current high cost of immunotherapeutics. However, once Phase I/II trials have been completed, it will be important to initiate therapy while patients still have acceptable performance status and limited disease burden (33).

DISCUSSION

Since tumors that metastasize to the pleura and peritoneum exist in an environment tailored to EMT and immune suppression, combination therapy directed toward conditioning the local environment as well as activating anti-tumor immunity is warranted. **Figure 2A** divides these goals into four categories that can be addressed with intra-cavitary and intratumoral therapies: 1) Turning *cold* tumors *hot*; 2) Increasing tumorassociated antigen presentation; 3) Supporting effector T cell responses; and 4) Conditioning the local environment to block EMT. Tumors can be made more immunogenic by inducing damage associated molecular patterns (DAMPS) with therapies such as radiation, or pathogen associated molecular patterns (PAMPS) *via* oncolytic virus therapy (35). Tumors may also constitutively express receptors for PAMPS and DAMPs (toll-like receptors, TLR), but their prognostic significance varies with disease and receptor type (36). Introduction of TLR ligands through natural infection of the pleura (empyema) has been associated with prolonged survival in patients with cancer metastatic to the pleura or lung cancer (37, 38). This response may be due to PAMP-associated repolarization of the local immune environment, with concomitant alternation of the cytokine profile and augmentation of tumor antigen presentation by resident macrophages and dendritic cells. Numerous attempts have been made to exploit TLR receptor agonists as single agent therapeutics with limited success. This does not rule out the possibility that they will be a highly effective adjuvant to other immune oncology interventions.

IL-12 plays a central role in inducing and maintaining Th1 Tcell polarization (39). The low levels of IL-12p70 in pleural and ascites fluid (**Figure 1A**) suggest that IL-12 can be a key therapeutic for conditioning the intra-cavital environment. Multiple clinical trials of IL-12 protein and IL-12 mRNA support its potential use in intra-cavitary therapy, where systemic adverse effects can be limited. IFN γ promotes T-cell and NK effector cells both directly and indirectly. Like IL-12, local administration may be advantageous to achieve functional concentrations while limiting systemic toxicity. Finally, therapeutic T cells may be activated or expanded *ex vivo* for intra-cavitary administration, provided that they are not reintroduced into an immunosuppressive environment.



currently available are shown in bold typeface.

	resentation
 Works across tumor types. Drives co-stimulation (increases GM Stimulates IFNy production by T cell 	used as "adjuvant" in anti-tumor immunity. A-CSF), DC maturation, macrophage polarization. Ils. umor immunity by TLR-activation and viral-
Maintain a TH1 environment	
 environment Decreases T reg activity. Increases DC/Ag presentation. Supports DC trafficking to draining Increases cytotoxic CD4. 	ral IL-12 as the central mediator of TH1 LN and tertiary lymphoid structures. duction: Discovery of antibody-bound tumor
Support effector T cells	
 TH1 cytokine cascade Support effector T cells and NK cell Recruit and support M1 macrophag Repolarize T-regs to produce more 	ges.
Condition intra-cavitary environment	:
 High levels of secreted IL-6/IL-6Rα in invasion and polarize local immune r Block tumor EMT with anti-IL-6Rα c Conditioning local environment awa Prevent IL-6 induced cachexia. 	or anti-IL-6.
B	
Onco-immune targeting	EMT and cavitary environment targeting
To support the nascent anti-tumor response and PD-protect • Anti-PD/PD-L: pembrolizumab, nivolumab, atezolizumab • IFNγ • IL-2 • IL-12: MEDI1191/lipid nanoparticle- formulated hIL-12 mRNA, hrIL-12 protein • Anti-CTLA4: ipilimumab	 To reverse the maladaptive milieu and EMT LPS (TLR4) and other TLR agonists: imiquimod (TLR7), resiquimod (TLR7/8) Anti-IL-6: siltuximab Anti-IL-6Rα: tocilizumab, satralizumab, sarilumab Anti-VEGF: bevacizumab Anti-IL-8: HuMax-IL8 (BMS-986253), rivanicline Anti-TGFβ and integrin inhibitors: anti-TGFb antibodies (NIS793, SAR439459, LY3022859,

FIGURE 2 | Intra-cavitary therapeutics to drive systemic immunity and reverse EMT. Panel (A) Since tumors that metastasize to the pleural and peritoneum exist in an environment tailored to EMT and immune suppression, combination therapy directed toward conditioning the local environment as well as activating anti-tumor immunity is required. Panel (B) A list of potential therapeutics directed toward reversing tumor EMT, repolarizing the cavitary maladaptive milieu, and driving local and systemic anti-tumor immunity. *Summarized in Addeo et al. (21) **Targeting histamine and related cytokines. Discussed in Li et al. (34).

Our secretomic data supports the role of IL-6/sIL-6R α receptor trans-signaling as the key driver of tumor EMT and associated therapy resistance and increased metastatic potential. IL-6 and its secreted receptor sIL-6R α are increasingly recognized as master

cytokines (40, 41), upstream of a wide array of inflammatory processes, including pathologies as diverse as cytokine release syndrome (42), acute allograft rejection (43), rheumatoid arthritis (44), asbestosis (45) and cachexia (46). Complexes of soluble

IL-6/IL-6Ra elicit responses from gp130-expressing cells that lack the complete IL-6 receptor by a process known as trans-signaling (40, 47). Figure 1A and our findings in NSCLC-associated MPE (7) reveal a profound degree of cytokine-chemokine polarization dominated by ng/mL concentrations of IL-6/sIL6Ra. Neutralizing pleural IL-6 or IL-6Ra activity with therapeutic antibodies may not only diminish IL-6-driven aggressive tumor behavior associated with EMT (48) (Figure 1B), but may also reverse downstream negative regulation of tumor-specific immune effector responses, thereby enhancing the efficacy of other immune oncology therapies. Although long-term antagonism of IL-6Ra is immunosuppressive (49), single dose exposure has been shown to break the cytokine storm associated with CAR-T therapy without compromising effector responses (50) or incurring serious adverse events (51). Intra-cavitary administration of anti-IL-6 or anti-IL-6Ra may likewise be expected to exert profound effects on the pleural or peritoneal environments.

Histamine has been shown to play a role in conferring resistance to immunotherapy. H1 antihistamine therapy counteracts histamine-mediated immunosuppression by counteracting M2 macrophage polarization and promoting CD8+ effector T cell responses (34). In the intracavitary space, cytokines such as IL-4 and IL-5 that are elevated in MPE (**Figure 1**) and are central to the allergy cascade (52) and may provide additional targets of therapy.

The pleura and peritoneum are common sites of metastasis for a wide variety of cancers. Their unique physiology makes them ideal tumor sanctuaries that promote aggressive behavior while inhibiting immune effector responses. The contained nature of these spaces also presents an opportunity to therapeutically manipulate the tumor environment in ways that are not possible for other metastatic lesions. There is a wealth of agents available for combination intra-cavitary therapy (**Figure 2B**), many of which have already shown some activity as single agents. We argue that combination therapies designed to condition the maladaptive cavitary environment, reverse EMT and stimulate immune priming locally and systemically will succeed where single agents have ultimately failed. However,

REFERENCES

- Zamboni MM, da Silva CTJr., Baretta R, Cunha ET, Cardoso GP. Important Prognostic Factors for Survival in Patients With Malignant Pleural Effusion. *BMC Pulm Med* (2015) 15:29–. doi: 10.1186/s12890-015-0025-z
- Directors ATSBo. Management of Malignant Pleural Effusions. Am J Respir Crit Care Med (2000) 162(5):1987–2001. doi: 10.1164/ajrccm.162.5.ats8-00
- Clive AO, Kahan BC, Hooper CE, Bhatnagar R, Morley AJ, Zahan-Evans N, et al. Predicting Survival in Malignant Pleural Effusion: Development and Validation of the LENT Prognostic Score. *Thorax* (2014) 69(12):1098–104. doi: 10.1136/thoraxjnl-2014-205285
- Ayantunde AA, Parsons SL. Pattern and Prognostic Factors in Patients With Malignant Ascites: A Retrospective Study. Ann Oncol (2007) 18(5):945–9. doi: 10.1093/annonc/mdl499
- Hodge C, Badgwell BD. Palliation of Malignant Ascites. J Surg Oncol (2019) 120(1):67–73. doi: 10.1002/jso.25453
- Franke AJ, Iqbal A, Starr JS, Nair RM, George TJ. Management of Malignant Bowel Obstruction Associated With GI Cancers. J Oncol Pract (2017) 13 (7):426–34. doi: 10.1200/JOP.2017.022210
- 7. Donnenberg AD, Luketich JD, Donnenberg VS. Secretome of Pleural Effusions Associated With Non-Small Cell Lung Cancer (NSCLC) and

the devil is in the details, and the challenge will be to design and implement the most agile adaptive therapeutic trials (53) designed to determine the safest and most effective therapeutic combinations and dosing schedules.

DATA AVAILABILITY STATEMENT

The raw data supporting the conclusions of this article will be made available by the authors, without undue reservation.

AUTHOR CONTRIBUTIONS

AD and VD wrote the manuscript, created and analyzed the data. PW contributed the section on peritoneal malignancies and edited the manuscript. JL provided samples and contributed to the discussion and ideas. DB contributed to the discussion and ideas. All authors contributed to the article and approved the submitted version.

FUNDING

This work was supported by BC032981, BC044784, W81XWH-12-1-0415 and BC132245_W81XWH-14-0258 from the Department of Defense, National Cancer Institute (NCI) grant R21 CA191647, MetaVivor FP00002718, the Glimmer of Hope Foundation, the Pennsylvania Breast Cancer Coalition, and the David Downing Fund. The Hillman Cancer Center Luminex Facility is supported by Cancer Center Support Grant P30CA047904.

ACKNOWLEDGMENTS

The authors would like to thank Bosko Popov and Denise Prosser for their excellent technical assistance.

Malignant Mesothelioma: Therapeutic Implications. Oncotarget (2019) 10 (60):6456-65. doi: 10.18632/oncotarget.27290

- Donnenberg ADDVS.. The Secretome of Malignant Pleural Effusions: Clues to Targets of Therapy. *Leukemia Res* (2019) 85:S11–2. doi: 10.1016/S0145-2126(19)30222-X
- Koopmans T, Rinkevich Y. Mesothelial to Mesenchyme Transition as a Major Developmental and Pathological Player in Trunk Organs and Their Cavities. *Commun Biol* (2018) 1(1):170. doi: 10.1038/s42003-018-0180-x
- Amasheh S, Markov AG, Volgin GN, Voronkova MA, Yablonsky PK, Fromm M. Barrier Function of Human Pleura Mesothelium is Constituted by Tight Junctions. *FASEB J* (2011) 25(1_supplement):1036.3–.3. doi: 10.1096/fasebj. 25.1_supplement.1036.3
- Donnenberg AD, Luketich JD, Dhupar R, Donnenberg VS. Treatment of Malignant Pleural Effusions: The Case for Localized Immunotherapy. *J ImmunoTher Cancer* (2019) 7(1):110. doi: 10.1186/s40425-019-0590-4
- Goey SH, Eggermont AM, Punt CJ, Slingerland R, Gratama JW, Oosterom R, et al. Intrapleural Administration of Interleukin 2 in Pleural Mesothelioma: A Phase I-II Study. Br J Cancer (1995) 72(5):1283–8. doi: 10.1038/bjc.1995.501
- Ruf P, Kluge M, Jager M, Burges A, Volovat C, Heiss MM, et al. Pharmacokinetics, Immunogenicity and Bioactivity of the Therapeutic Antibody Catumaxomab Intraperitoneally Administered to Cancer Patients.

Br J Clin Pharmacol (2010) 69(6):617–25. doi: 10.1111/j.1365-2125.2010. 03635.x

- 14. Sebastian M, Kiewe P, Schuette W, Brust D, Peschel C, Schneller F, et al. Treatment of Malignant Pleural Effusion With the Trifunctional Antibody Catumaxomab (Removab) (Anti-EpCAM×Anti-CD3): Results of a Phase 1/2 Study. J Immunother (2009) 32(2):195–202. doi: 10.1097/CJI. 0b013e318195b5bb
- Sahai E, Astsaturov I, Cukierman E, DeNardo DG, Egeblad M, Evans RM, et al. A Framework for Advancing Our Understanding of Cancer-Associated Fibroblasts. *Nat Rev Cancer* (2020) 20(3):174–86. doi: 10.1038/s41568-019-0238-1
- Telvi L, Jaubert F, Eyquem A, Andreux JP, Labrousse F, Chretien J. Study of Immunoglobulins in Pleura and Pleural Effusions. *Thorax* (1979) 34(3):389– 92. doi: 10.1136/thx.34.3.389
- Hewitt SL, Bailey D, Zielinski J, Apte A, Musenge F, Karp R, et al. Intratumoral IL12 mRNA Therapy Promotes TH1 Transformation of the Tumor Microenvironment. *Clin Cancer Res* (2020) 26(23):6284–98. doi: 10.1158/1078-0432.CCR-20-0472
- Di Trani CA, Fernandez-Sendin M, Cirella A, Segués A, Olivera I, Bolaños E, et al. Advances in mRNA-Based Drug Discovery in Cancer Immunotherapy. *Expert Opin Drug Discov* (2021) 17(1):1–13. doi: 10.1080/17460441. 2021.1978972
- Pennathur A, Abbas G, Christie N, Landreneau R, Luketich JD. Video Assisted Thoracoscopic Surgery and Lobectomy, Sublobar Resection, Radiofrequency Ablation, and Stereotactic Radiosurgery: Advances and Controversies in the Management of Early Stage non-Small Cell Lung Cancer. Curr Opin Pulmonary Med (2007) 13(4):267–70. doi: 10.1097/ MCP.0b013e3281c61a85
- Chang E, Alexander HR, Libutti SK, Hurst R, Zhai S, Figg WD, et al. Laparoscopic Continuous Hyperthermic Peritoneal Perfusion1. J Am Coll Surgeons (2001) 193(2):225–9. doi: 10.1016/S1072-7515(01)00980-2
- Muller PY, Milton M, Lloyd P, Sims J, Brennan FR. The Minimum Anticipated Biological Effect Level (MABEL) for Selection of First Human Dose in Clinical Trials With Monoclonal Antibodies. *Curr Opin Biotechnol* (2009) 20(6):722–9. doi: 10.1016/j.copbio.2009.10.013
- Hu CY, Zhang YH, Wang T, Chen L, Gong ZH, Wan YS, et al. Interleukin-2 Reverses CD8(+) T Cell Exhaustion in Clinical Malignant Pleural Effusion of Lung Cancer. *Clin Exp Immunol* (2016) 186(1):106–14. doi: 10.1111/cei.12845
- 23. Sterman DH, Recio A, Carroll RG, Gillespie CT, Haas A, Vachani A, et al. A Phase I Clinical Trial of Single-Dose Intrapleural IFN- β Gene Transfer for Malignant Pleural Mesothelioma and Metastatic Pleural Effusions: High Rate of Antitumor Immune Responses. *Clin Cancer Res* (2007) 13(15):4456–66. doi: 10.1158/1078-0432.CCR-07-0403
- Zeltsman M, Mayor M, Jones DR, Adusumilli PS. Surgical Immune Interventions for Solid Malignancies. *Am J Surg* (2016) 212(4):682–90.e5. doi: 10.1016/j.amjsurg.2016.06.008
- Chandran SS, Somerville RPT, Yang JC, Sherry RM, Klebanoff CA, Goff SL, et al. Treatment of Metastatic Uveal Melanoma With Adoptive Transfer of Tumour-Infiltrating Lymphocytes: A Single-Centre, Two-Stage, Single-Arm, Phase 2 Study. *Lancet Oncol* (2017) 18(6):792–802. doi: 10.1016/S1470-2045 (17)30251-6
- Murthy V, Katzman D, Sterman DH. Intrapleural Immunotherapy: An Update on Emerging Treatment Strategies for Pleural Malignancy. *Clin Respir J* (2019) 13(5):272–9. doi: 10.1111/crj.13010
- Addeo A, Friedlaender A, Giovannetti E, Russo A, de Miguel-Perez D, Arrieta O, et al. A New Generation of Vaccines in the Age of Immunotherapy. *Curr Oncol Rep* (2021) 23(12):137. doi: 10.1007/s11912-021-01130-x
- Miao L, Zhang Y, Huang L. mRNA Vaccine for Cancer Immunotherapy. *Mol Cancer* (2021) 20(1):41. doi: 10.1186/s12943-021-01335-5
- Eisenhauer EA, Therasse P, Bogaerts J, Schwartz LH, Sargent D, Ford R, et al. New Response Evaluation Criteria in Solid Tumours: Revised RECIST Guideline (Version 1.1). *Eur J Cancer* (2009) 45(2):228–47. doi: 10.1016/ j.ejca.2008.10.026
- Edwards RP, Gooding W, Lembersky BC, Colonello K, Hammond R, Paradise C, et al. Comparison of Toxicity and Survival Following Intraperitoneal Recombinant Interleukin-2 for Persistent Ovarian Cancer After Platinum: Twenty-Four-Hour Versus 7-Day Infusion. J Clin Oncol (1997) 15(11):3399– 407. doi: 10.1200/JCO.1997.15.11.3399

- 31. Sehouli J, Pietzner K, Wimberger P, Vergote I, Rosenberg P, Schneeweiss A, et al. Catumaxomab With and Without Prednisolone Premedication for the Treatment of Malignant Ascites Due to Epithelial Cancer: Results of the Randomised Phase IIIb CASIMAS Study. *Med Oncol* (2014) 31(8):76. doi: 10.1007/s12032-014-0076-7
- Elkadi D, Wiernik PH, Tong TR. Resolution of Massive Pleural Effusion Due to Lymphoma With Intrapleural Interleukin-2. *Am J Hematol* (2010) 85 (9):711–2. doi: 10.1002/ajh.21604
- Santini D, Zeppola T, Russano M, Citarella F, Anesi C, Buti S, et al. PD-1/PD-L1 Checkpoint Inhibitors During Late Stages of Life: An Ad-Hoc Analysis From a Large Multicenter Cohort. J Transl Med (2021) 19(1):270. doi: 10.1186/s12967-021-02937-9
- 34. Li H, Xiao Y, Li Q, Yao J, Yuan X, Zhang Y, et al. The Allergy Mediator Histamine Confers Resistance to Immunotherapy in Cancer Patients via Activation of the Macrophage Histamine Receptor H1. Cancer Cell (2022) 40(1):36–52.e9. doi: 10.1016/j.ccell.2021.11.002
- Ekeke CN, Russell KL, Joubert K, Bartlett DL, Luketich JD, Soloff AC, et al. Fighting Fire With Fire: Oncolytic Virotherapy for Thoracic Malignancies. *Ann Surg Oncol* (2021) 28(5):2715–27. doi: 10.1245/s10434-020-09477-4
- Urban-Wojciuk Z, Khan MM, Oyler BL, Fåhraeus R, Marek-Trzonkowska N, Nita-Lazar A, et al. The Role of TLRs in Anti-Cancer Immunity and Tumor Rejection. *Front Immunol* (2019) 10(2388). doi: 10.3389/fimmu.2019.02388
- Bone G. Postoperative Empyema and Survival in Lung Cancer. Br Med J (1973) 1(5852):504–5. doi: 10.1136/bmj.1.5852.504-a
- Ruckdeschel JC, Codish SD, Stranahan A, McKneally MF. Postoperative Empyema Improves Survival in Lung Cancer. Documentation and Analysis of a Natural Experiment. N Engl J Med (1972) 287(20):1013–7. doi: 10.1056/ NEJM197211162872004
- Brombacher F, Kastelein RA, Alber G. Novel IL-12 Family Members Shed Light on the Orchestration of Th1 Responses. *Trends Immunol* (2003) 24 (4):207–12. doi: 10.1016/S1471-4906(03)00067-X
- Uciechowski P, Dempke WCM. Interleukin-6: A Masterplayer in the Cytokine Network. Oncology (2020) 98(3):131–7. doi: 10.1159/000505099
- Scheller J, Chalaris A, Schmidt-Arras D, Rose-John S. The Pro- and Anti-Inflammatory Properties of the Cytokine Interleukin-6. *Biochim Biophys Acta* (BBA) Mol Cell Res (2011) 1813(5):878–88. doi: 10.1016/j.bbamcr.2011.01.034
- Maude SL, Barrett D, Teachey DT, Grupp SA. Managing Cytokine Release Syndrome Associated With Novel T Cell-Engaging Therapies. *Cancer J* (2014) 20(2):119–22. doi: 10.1097/PPO.000000000000035
- Iacono A, Dauber J, Keenan R, Spichty K, Cai J, Grgurich W, et al. Interleukin 6 and Interferon-Gamma Gene Expression in Lung Transplant Recipients With Refractory Acute Cellular Rejection: Implications for Monitoring and Inhibition by Treatment With Aerosolized Cyclosporine. *Transplantation* (1997) 64(2):263–9. doi: 10.1097/00007890-199707270-00015
- Davies R, Choy E. Clinical Experience of IL-6 Blockade in Rheumatic Diseases —Implications on IL-6 Biology and Disease Pathogenesis. Semin Immunol (2014) 26(1):97–104. doi: 10.1016/j.smim.2013.12.002
- 45. Doré P, Lelièvre E, Morel F, Brizard A, Fourcin M, Clemént C, et al. IL-6 and Soluble IL-6 Receptors (sIL-6R and Sgp130) in Human Pleural Effusions: Massive IL-6 Production Independently of Underlying Diseases. *Clin Exp Immunol* (1997) 107(1):182–8. doi: 10.1046/j.1365-2249.1997.d01-889.x
- Rupert JE, Narasimhan A, Jengelley DHA, Jiang Y, Liu J, Au E, et al. Tumor-Derived IL-6 and Trans-Signaling Among Tumor, Fat, and Muscle Mediate Pancreatic Cancer Cachexia. J Exp Med (2021) 218(6). doi: 10.1084/ jem.20190450
- Lo C-W, Chen M-W, Hsiao M, Wang S, Chen C-A, Hsiao S-M, et al. IL-6 Trans-Signaling in Formation and Progression of Malignant Ascites in Ovarian Cancer. *Cancer Res* (2011) 71(2):424. doi: 10.1158/0008-5472.CAN-10-1496
- Lu H, Clauser KR, Tam WL, Frose J, Ye X, Eaton EN, et al. A Breast Cancer Stem Cell Niche Supported by Juxtacrine Signalling From Monocytes and Macrophages. *Nat Cell Biol* (2014) 16(11):1105–17. doi: 10.1038/ncb3041
- Pawar A, Desai RJ, Solomon DH, Santiago Ortiz AJ, Gale S, Bao M, et al. Risk of Serious Infections in Tocilizumab Versus Other Biologic Drugs in Patients With Rheumatoid Arthritis: A Multidatabase Cohort Study. Ann Rheumatic Dis (2019) 78(4):456. doi: 10.1136/annrheumdis-2018-214367
- Davila ML, Riviere I, Wang X, Bartido S, Park J, Curran K, et al. Efficacy and Toxicity Management of 19-28z CAR T Cell Therapy in B Cell Acute Lymphoblastic Leukemia. *Sci Trans Med* (2014) 6(224):224ra25.

- Xu X, Han M, Li T, Sun W, Wang D, Fu B, et al. Effective Treatment of Severe COVID-19 Patients With Tocilizumab. *ChinaXiv* (2020) 00026v1. doi: 10.1073/pnas.2005615117
- 52. Krouwels FH, Hol BE, Lutter R, Bruinier B, Bast A, Jansen HM, et al. Histamine Affects Interleukin-4, Interleukin-5, and Interferon-Gamma Production by Human T Cell Clones From the Airways and Blood. Am J Respir Cell Mol Biol (1998) 18(5):721–30. doi: 10.1165/ajrcmb.18.5.2909
- Park JJ, Thorlund K, Mills EJ. Critical Concepts in Adaptive Clinical Trials. Clin Epidemiol (2018) 10:343–51. doi: 10.2147/CLEP.S156708

Conflict of Interest: The authors declare that the research was conducted in the absence of any commercial or financial relationships that could be construed as a potential conflict of interest.

Publisher's Note: All claims expressed in this article are solely those of the authors and do not necessarily represent those of their affiliated organizations, or those of the publisher, the editors and the reviewers. Any product that may be evaluated in this article, or claim that may be made by its manufacturer, is not guaranteed or endorsed by the publisher.

Copyright © 2022 Donnenberg, Wagner, Luketich, Bartlett and Donnenberg. This is an open-access article distributed under the terms of the Creative Commons Attribution License (CC BY). The use, distribution or reproduction in other forums is permitted, provided the original author(s) and the copyright owner(s) are credited and that the original publication in this journal is cited, in accordance with accepted academic practice. No use, distribution or reproduction is permitted which does not comply with these terms.





Advances of DNA Damage Repair-Related Drugs and Combination With Immunotherapy in Tumor Treatment

Yumin Wang^{1,2†}, Meihan Duan^{3†}, Zhouying Peng^{1,2†}, Ruohao Fan¹, Yuxiang He^{2,4}, Hua Zhang¹, Wei Xiong⁵ and Weihong Jiang^{1,2*}

¹ Department of Otolaryngology Head and Neck Surgery, Xiangya Hospital, Central South University, Changsha, China, ² National Clinical Research Center for Geriatric Disorders, Xiangya Hospital, Changsha, China, ³ School of Medicine, Tsinghua University, Beijing, China, ⁴ Department of Oncology, Xiangya Hospital, Central South University, Changsha, China, ⁵ Key Laboratory of Carcinogenesis and Cancer Invasion of the Chinese Ministry of Education, Cancer Research Institute, Central South University, Changsha, China

OPEN ACCESS

Edited by:

Yubin Li, University of Pennsylvania, United States

Reviewed by:

Xi Lou, University of Alabama at Birmingham, United States Ling Li, University of North Dakota, United States Wentao Huang, Massachusetts Institute of Technology, United States

*Correspondence: Weihong Jiang weihongjiang@csu.edu.cn

[†]These authors have contributed equally to this work

Specialty section:

This article was submitted to Cancer Immunity and Immunotherapy, a section of the journal Frontiers in Immunology

Received: 14 January 2022 Accepted: 31 January 2022 Published: 23 February 2022

Citation:

Wang Y, Duan M, Peng Z, Fan R, He Y, Zhang H, Xiong W and Jiang W (2022) Advances of DNA Damage Repair-Related Drugs and Combination With Immunotherapy in Tumor Treatment. Front. Immunol. 13:854730. doi: 10.3389/fimmu.2022.854730 Cancer therapy has been an important and popular area in cancer research. With medical technology developing, the appearance of various targeted drugs and immunotherapy offer more choices to cancer treatment. With the increase in drug use, people have found more and more cases in which tumors are resistant to DNA damage repair (DDR)-based drugs. Recently, the concept of combination therapy has been brought up in cancer research. It takes advantages of combining two or more therapies with different mechanisms, aiming to benefit from the synergistic effects and finally rescue patients irresponsive to single therapies. Combination therapy has the potential to improve current treatment of refractory and drug-resistant tumors. Among the methods used in combination therapy, DDR is one of the most popular methods. Recent studies have shown that combined application of DDR-related drugs and immunotherapies significantly improve the therapeutic outcomes of malignant tumors, especially solid tumors.

Keywords: DNA damage, DNA repair, immunotherapy, combination, tumor treatment

INTRODUCTION

Genome instability is one of the 10 hallmarks of cancer (1). Cells are exposed to various sources of DNA damage in metabolic activities such as reactive oxygen species (ROS). To cope with it, human cells have developed a complex series of DNA repair strategies to protect the integrity and stability of genome (2). However, when the repair fails, the destruction leads to carcinogenesis and genome instability. Studies show that the formation of many malignant tumors is apparently related to the defects in DNA repair (3). On the other hand, the defects may indicate the weakness of cancer cells in DNA repair, which can be targeted in treatment. Therefore, people have developed a great

Abbreviations: MMR, mismatch repair; HR, homologous recombination; DDR, DNA damage and repair; PD-1, programmed cell death protein 1; MGMT, O-6-methylguanine-DNA methyltransferase; NSCLC, non-small cell lung cancer; HNSCC, head and neck squamous cell carcinoma; RCC, renal cell carcinoma; UC, urothelial carcinoma; PARP, poly-ADP-ribose polymerase; SSB, single-strand break; DSB, double-strand break; PARP, poly-ADP-ribose polymerase; TIL, tumor-infiltrating lymphocyte; PD-L1, programmed cell death-ligand 1; cGAS, cyclic GMP-AMP synthase; circRNA, circular RNA; lncRNA, long noncoding RNA.

number of drugs targeting DDR to treat cancer, such as cisplatin and Olaparib. These DDR-related drugs greatly improve the survival time and therapeutic outcomes of cancer patients.

Immunotherapy is a newly developed method emerging these years. At present, there have been different approaches for immunotherapy applied in clinical practice. Targeting the immunological changes in cancer, people designed many strategies acting on various kinds of targets (4). Immunotherapy represented by PD-1/PD-L1 inhibitor and chimeric antigen receptor T cell (CAR-T) has shown satisfactory targeting ability and curative effect in cancer therapy, implying its promising prospect in treatment (5). However, both experiments and clinical trials suggest that immunotherapy has very limited effect in solid tumors. Therefore, improving the outcome of immunotherapy in solid tumors has become a critical issue in recent studies.

With the increase in chemotherapy use, people have found more and more cases in which tumors are resistant to DDRbased drugs. As research moves along, the concept of combination therapy has been brought up in cancer studies (6). It takes advantages of combining two or more therapies with different mechanisms, aiming to benefit from the synergistic effects and finally rescue patients irresponsive to single therapies. Combination therapy has the potential to improve current treatment of refractory and drug-resistant tumors. This review summarizes the progress on the association among DNA repair defects, host immune response, and the tumor sensitivity to immunotherapy.

APPLICATIONS AND MECHANISM OF DDR-RELATED DRUGS

Complicated mechanisms are necessary to keep genetic code intact from endogenous and exogenous impairment. There are several DDR pathways now that are usually divided into DNA single- and DNA double-strand DNA repair. DNA single-strand repair pathway mainly responds to impaired or mismatched basic groups (e.g., base excision repair, nucleotide excision repair, direct repair, and mismatch repair), while DNA double-strand repair pathway is mainly in charge of DNA double-strand breaks (DSBs) (e.g., homologous recombination, non-homologous end joining, and Fanconi anemia pathway) (7). When DNA repair fails, oncogenes and antioncogenes may obtain somatic mutations, resulting into uncontrolled proliferation and carcinogenesis. It has been found that cancer susceptibility can be caused by several diseases, most of which are associated with genetic defects in certain DNA repair pathways (8). Further studies show that DNA repair defects oftentimes play a vital role in tumor formation and progression. Recently, researchers have analyzed the DNA repair defects in 33 types of cancer. The results show that about one-third of cancers harbor somatic mutations such as BRCA1/2-mutated breast cancer or ovarian cancer and MGMT-methylated glioblastoma, which may give us a hint on the treatment. Both in vivo and in vitro experiments suggest that chemotherapytargeting DDR have satisfactory effects on these cancers lacking functional DDR (9) (Table 1). Below, we will introduce several representative DDR-related drugs (Figure 1).

Drug name	Anti-tumor mechanism	Tumor type	Immunotherapy combination	
PARPi (Olaparib, PARP1, PARP2 etc.)		Breast cancer; ovarian cancer	Combine with Pembrolizumab in recurrent ovarian cancer	
Cisplatin	DNA crosslinker	Sarcoma; carcinoma (lung cancer, head and neck cancer; cervical cancer, etc.)	Combine with Nivolumab and Ipilimumab in NSCLC, combine with PD1 inhibitor in head and neck cance	
Doxorubicin	Anthracycline	Blood disorders; sarcoma; carcinoma (breast, bladder, lung ovarian)		
Etoposide	TOP2	Lung cancer, lymphoma; Ewing's sarcoma; GBM	Combine with Tezolizumab and carboplatin in small cell lung cancer	
Gemcitabine	Pyrimidine antimetabolite	NSCLC; pancreatic cancer; breast cancer; bladder cancer; etc.		
Methotrexate	Antimetabolite	Breast cancer; leukemia; lung cancer; osteosarcoma		
Mitomycin-C	DNA crosslinker	Gastric cancer; pancreatic cancer; bladder cancer		
Pemetrexed	DNA replication	Pleural mesothelioma; non-small cell lung cancer (NSCLC).		
Temozolomide	DNA alkylating agent	Brain cancers; astrocytoma; glioblastoma Olaparib in combination with temozolomide demonstrated substantial clinical activity in relapsed small cell lung cancer	Combine with PD-1 inhibitor in glioma	
Camptothecin	TOP1	Gastric cancer; esophageal cancer, cardiac cancer, colon cancer, rectal cancer, primary liver cancer; Acute and chronic myelogenous leukemia, choriocarcinoma, lung cancer, and bladder cancer; Breast cancer		
Carmustine	DNA replication	Glioma, glioblastoma multiforme, medulloblastoma and astrocytoma, multiple myeloma, and lymphoma		
Cyclophosphamide	Alkylating agent	Lymphoma; leukemia; brain cancer		
Epirubicin	Anthracycline	Breast cancer		
rinotecan	TOP1	Colorectal cancer and small cell carcinoma		
Vitoxantrone	DNA replication	Breast cancer, acute lymphoblastic leukemia, and non-Hodgkin's lymphoma		
Oxaliplatin	DNA alkylating agent	Colorectal cancer		
Topotecan	TOP1	Ovarian cancer and lung cancer		

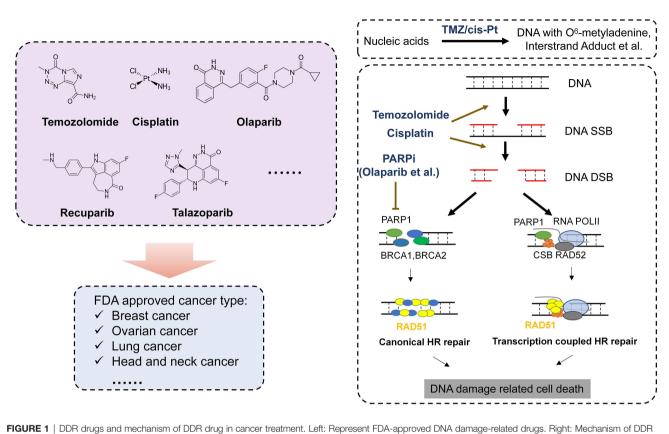


FIGURE 1 | DDR drugs and mechanism of DDR drug in cancer treatment. Left: Represent FDA-approved DNA damage-related drugs. Right: Mechanism of DDR drugs in DNA repair progress.

Temozolomide

Temozolomide (TMZ) is one of the widely used chemotherapy drugs targeting DDR. Studies showed that O6 methylguanine (O6 MeG) is the main cytotoxic DNA damage (10). TMZ can methylate DNA, which most often occurs at the N-7 or O-6 positions of guanine residues. Experiments using the cancer cell lines in which high-level methylation or mutation leads to diminished MGMT functions, and transgenic or gene knockout mice experiments all prove that dysfunctional MGMT is one of the main reasons why cells are sensitive to TMZ. In all of the cases and experiments, MGMT deficiency turns cells to be more sensitive to methylating anti-cancer drugs (11). Similarly, when using small-molecule soluble substrates such as O6-benzylguanine and O6-bromothiopheneguanine to inhibit the repair activity of MGMT, the MGMT-tolerant cells turn to be sensitive to TMZ. Moreover, this phenomenon is independent of cancer types. Besides the lethal effect to tumor cells, TMZ also has severe cytotoxicity, mutagenicity, and genotoxicity. The main mechanism of cytotoxicity is mismatch repair (MMR) (12). DNA O6 MeG causes the mismatch of deoxyribonucleotide and thymine, which can be recognized and repaired by MMR complex proteins like MSH2, MSH6, MLH1, and PMS2, resulting in the excision of thymine. In the process, activated EXO1 may produce long nicks (>1,000 bp), which will be repaired later. But during the repair, O6 MeG will match

thymine again due to the mismatch feature of lesions. Consequently, a vain, repetitive repair cycle is initiated. Apparently, this is an obstacle to the subsequent DNA replication in S phase (13), and finally, it will cause DNA DSB (14) in MGMT- and MMR+ cancer cells. Although the detailed molecular mechanism has not been fully understood yet, many have verified that DSB produced by O6 MeG processing is lethal by triggering apoptosis. Moreover, it is reported that cells activate apoptosis to detect O6 MeG-T mismatch directly through ataxiatelangiectasia mutated and rad3-related (ATR)/ATR-interacting protein (ATRIP) signal pathway in MTR. This finding also reveals that DDR activation, DSB formation, and the initiation of cell death pathway only happen when DNA replicates twice after DNA damage induction. Therefore, most studies support the model in which DSB formed in the second replication cycle triggers cell apoptosis and finally caused cell death (15). It should be noted that restriction enzyme-induced DSB has high selectivity and efficiency in inducing cell apoptosis, which may explain why TMZ can lead to severe cell apoptosis. Importantly, studies using mutated Cricetulus griseus lacking HR pathway show that this cell line is extremely sensitive to O6-methylating agents. The phenomenon strongly supports the model in which HR repairs processed O6 products and generates MeG/MMR intermediate to trigger cell death from another aspect. A study specifically utilizing phosphatase and tensin homolog (PTEN)-

lacked primary astrocyte also demonstrates this. The expression of RAD51B, RD51C, and RAD51D is downregulated to weaken HR in the cell line. Since 36% glioma has PTEN mutation, this finding has significant meaning and potential in therapy (16).

PARP Inhibitors

For now, as the first tumor-targeted drug approved by Food and Drug Administration (FDA), PARPi has attracted much attention from its discovery. Studies have found that various types of human cancer have latent defects in HR pathway, including ovarian cancer, breast cancer, prostate cancer, and pancreas cancer (17). Despite the reasons of their HR dysfunction are not clear, the defect does provide more genome instability for cancer cells, and lead to more mutations that may promote cancer progression. The defective HR pathway offers an excellent condition for PARPis. Epidemiological investigation shows that 50% high-grade serous ovarian cancer (HGSOC) have latent defects in HR repair pathway, which result in one or more germ-line or somatic mutations in BRCA or other DDR-related genes (18). Moreover, 10%-20% breast cancer (mainly triple-negative breast cancer), metastatic prostate cancer, or pancreas cancer have biallelic mutations in HR genes, which leads them also to be sensitive to PARPi. Classically, BRCA1/2 mutated cancer is supposed to respond to PARPis via synthetic lethality; that is, PARPis inhibit BER so that SSB converts into DSB subsequently. If cancer cells have underlying HR defects due to BRCA1/2 deficiency, they will be unable to repair DSB and finally die (19). Besides this mechanism, it is also believed that PARPis combine and arrest PARP1 enzyme on chromatin, forming lesions that can only be repaired by HR. Some PARPis like Talazoparib are more effective PARP predators than others (8, 20, 21). Recently, the third mechanism has already been discovered (9, 22). In this case, DSB is excised in S phase as normal. However, cancer cells have to rely on the other DSB repair pathway due to HR defects. It is microhomology-mediated end-joining (MMEJ, also known as Alt-EJ), which depends on PARP1 and DNA polymerase θ (POLQ). In fact, PARP1 is necessary for DSB to recruit POLQ. Therefore, the inhibitors of PARP1 or POLQ block Alt-EJ pathway and kill HRdefective cancer cells. Recent studies show that PARPi-tolerant cancer cells have relatively higher POLQ expression, and they are sensitive to POLQ inhibitor (17).

Cisplatin

Cisplatin is another type of widely used chemotherapy drugs targeting DDR. Similar to other DDR-based drugs, cisplatin is activated after entering cells. In cytoplasm, the atomic chlorine of cisplatin is replaced by water (23). The aquo complex is a potent electrophile that can react with any nucleophile, including the sulfhydryl of proteins and nitrogen donor atoms of nucleic acid. Cisplatin combines with the N7 reaction center of purine residues, causing DNA damage in cancer cells, inhibiting cell proliferation and finally leading to cell apoptosis. In this process, the 1,2-intrastrand crosslinking between purine bases and cisplatin is the most apparent DNA change (24). It includes 1,2-intrastrand d(GpG) adducts and 1,2-intrastrand d(ApG) adducts, accounting for 90% and 10%, respectively. According to the report, 1,3-intrastrand d(GpXpG) adducts and others (e.g., inter-strand and non-functional adducts) have contributions to the toxicity of cisplatin (25). Despite that it has been observed that cisplatin impairs cancer cells through many aspects, many published results still support that DNA is the key target of cisplatin toxicity.

DDR Combination Treatment

Besides single-drug treatment, the combination therapy of multiple drugs is a remarkable direction in the future. Many types of tumors like GBM is treated by radiotherapy and TMZ for now. Despite of this, the prognosis of patients is still unsatisfactory, indicating that more studies on combination therapy are required to improve the therapeutic outcome of cancer especially advanced cancer. In the GBM mouse model, people found that PARPis had synergistic effects with radiotherapy and TMZ, slowing down tumor growth and improving patients' survival (26). In various types of cancer models, PARPis can play as a good radiosensitizer, which significantly raises the mortality of tumor cells (27). Their effects include inhibiting tumor cell proliferation, reducing the survival rate of clones, slowing tumor growth, and improving the survival rate of mice. This also indicates that the combined application of chemotherapy drugs will play an important role in the prospective cancer therapy.

APPLICATION AND PROGRESS OF THE COMBINATION OF DDR ANTI-TUMOR DRUGS AND IMMUNOTHERAPY

Applications and Research Progress of Cancer Immunotherapy

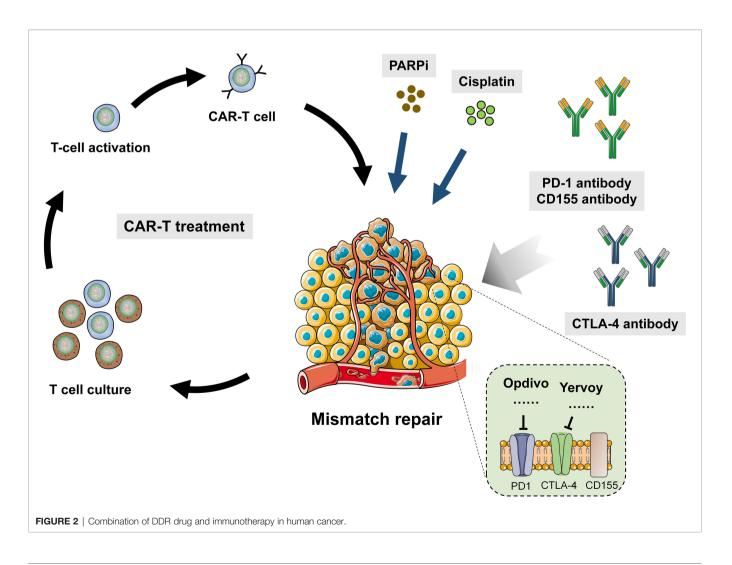
The interaction between tumor and immune system is dynamic during tumor formation and progression. Thus, cancer limitation of the immune system and the immune escape of cancer are also in a dynamic balance. Tumor-infiltrated lymphocytes (TILs) have important functions in the dynamic control of tumor. A great number of studies have found that TILs could predict the response of tumors to immunotherapy (28), especially CD8+ T lymphocytes. As the core of anti-tumor immune response, its ability to infiltrate tumors is related to the survival rate of patients (29). Specifically activated CD8+ lymphocytes induce the basic anti-tumor response to cope with the infiltration of tumor antigen. Therefore, TILs are the key to restrict tumor growth. TAA recognized by T lymphocyte induces the specific immune response. Further studies discover that growing tumors contain TILs. They are invalid to eliminate cancer cells in vivo, but they can proliferate and function when being removed from the immune-suppressive microenvironment. This is because cancer cells have developed the mechanisms to avoid being recognized and eliminated, including downregulating the components that process and present antigens; recruiting inhibitive immunocytes like regulative T cell, MDSC, and TAM; and producing soluble cytokines involved in immune suppression like transforming growth factor beta (TGF- β) and interleukin (IL)-10. Meanwhile, cancer cells also downregulate the expression like PD-L1.

It has achieved great success to use CTLA-4 and PD-1 in cancer immunotherapy. Pierre Goldstein discovered CTLA-4 in 1987. Later on, several groups independently proves that CTLA4 played a role as inhibitive receptor both in vitro and in gene knockout mice. These led James Allison to start a pioneering work in 1996, which demonstrated that CTLA-4 blocker could eliminate tumors in mice and provide theoretical basis for the clinical development of CTLA-4 antibody. In 2011, FDA approved CTLA-4 antibody (ipilimumab) to be applied in melanoma, which marked a new era of cancer immunotherapy. At present, people has raised many models to explain the mechanism of CTLA-4 functions. The most simple one is the competition between CD28 and CTLA-4. It is similar to other endogenous inhibitive signaling model. Although CTLA-4defective mice have overactive CD4+ T cells exhibiting pathogenetic clinical phenotypes, chimera can still prevent diseases and normalize the phenotype of defective cells by the part of cells expressing CTLA-4. Consistent with cellular structure, there is another molecular mechanism to capture CD80 and CD86 physically and then remove them from antigen-presenting cells (APC), which is called transendocytosis (30). In this procedure, T cells recognize certain

peptides and present them to APC. In this way, CD80 and CD86 expression in APC is regulated. Despite that the molecular mechanism by which endocytosis controls gene transcription is unknown (31), there are other receptor–ligand pairs employing this pathway besides CTLA-4. It was found that the Notch–Delta pathway was also one of them. The combination with Delta (ligand) removes Notch (receptor) from neighbor cells (32) (**Figure 2**).

PD-1 and PD-L1 Drug Treatment

The clinical development of PD-1 inhibitor owes to a series of discovery in basic science. It was first cloned by Tasuku Honjo in 1992, and its ligand (PD-L1) was discovered by two groups led by Lieping Chen and Gordon Freeman independently approximately 10 years later (32). Chen further proved that many human cancers upregulate dPD-L1, and the blocking by its antibody resulted in tumor regression. These findings lay the root for the successful clinical results that PD-1 blocking treats advanced solid tumors. PD-1 is a member of B7/CD28 costimulatory receptor family. It combines the ligand including PD-L1 and PD-L2 to regulate the activation of T cells (33). Like CTLA-4 signaling, the binding of PD-1 and its ligands inhibits T



cells to proliferate; reduces the production of interferon gamma (IFN- γ), tumor necrosis factor alpha (TNF- α), and IL-2; and also lowers the survival rate of T cells. If the presentation and recognition of TCR and the combination of PD-1 happens simultaneously in T cells, PD-1 signaling will prevent critical TCR signaling intermediate from phosphorylation. Thus, the early TCR signaling is suspended, and T-cell activation decreases. In normal cells, the main function of PD-1 is making the CD4+ T cells that experience high-level stimulation to be exhausted (34). It also happens in patients with chronic infection of malignant tumors. The characteristic is T-cell dysfunction, resulting in inadequate control for them. As the target of PD-L1 inhibitor, the ligand PD-L1 expression is a natural potential biomarker. However, in the present studies, there are contradictory conclusions. According to the expression of PD-L1 in melanoma, NSCLC, and urogenital cancer and the sensitivity of their response to PD-L1 inhibitor, the recurrent ratio of PD-L1 positive and negative cancer is 34.1% and 19.9%, respectively. Cancer types and certain CPI make some differences, while the lack of standardized test and the heterogeneity of tumor itself may also be one of the reasons that cause these inconsistent results. Collectively, the real value of PD-1 as a biomarker in prediction is still uncertain. Other features of tumor microenvironment like the infiltration of effector immunocytes and the expression of inflammatory genes can also suggest stronger activity. For now, people are studying the functions of some molecules in inflammatory reactions and looking for potential biomarkers in CPI treatment.

CAR technique was first reported by Zelig Eshhar and colleagues in 1993. They used chimeric genes coding singlestrand antibody to transduct T cell. This single-strand antibody connects trans-membrane region and the intracellular domain coding T-cell receptor adaptor. It proved that CAR-T enables T cells to redirect to the cells expressing antibody-related antigen (35). The subsequent studies found that CD19 CAR-mediated human peripheral blood T lymphocytes can eradicate the lymphoma and leukemia in immune-compromised mice. In 2010, a case report revealed that the therapeutic effect of CD19 CAR-T in lymphoma patients was very satisfactory. From then, CAR-T has shown impressive results in recurrent or refractory B-cell malignant tumors such as acute and chronic lymphocytic leukemia. CAR-T cells targeting solid tumors have also been tested but has not shown an ideal result yet. According to the costimulatory molecules (CM), CAR-T cells can be classified into four generations (36). However, due to lacking assistance of CM, infused CAR-T cells are poor at proliferation, resulting in unsatisfying results. The second generation of CAR-T has CM like CD28, CD27, and 41BB (CDB7). They can add OX40 (CD134) or inducible CM to T cells in order to overcome the problems of the first generation. Therefore, the second generation has significantly improved in killing cancer cells compared to the first one. As for the third generation, another CM such as CD28, 4-1BB, or CD3 is added to T cells so that they contain two CMs resulting in the further improvement of T-cell proliferation activity, cytotoxicity, and survival rate. The fourth generation is called TRUCKs. Compared to the structures of previous CAR-T, it has additional proinflammatory cytokines such as IL-12 and CM ligand (4-1 BBL and CD40L), which enable CAR-T cells to be released to kill cancer cells. Moreover, the fourth generation saves the pretreatment like routine or highdose chemotherapy, which raises patients' quality of life (37).

Combination of DDR Anti-Tumor Drugs and Immunotherapy

As the studies go further, people gradually found that the mechanisms of DNA damage and immunology are connected in some aspects. Therefore, they came up with combined therapy to treat the cancer that is insensitive to DNA repair-related drugs or immunotherapy. As immunology, especially tumor immunology, develops in recent years, it has been a hot spot to combine immunotherapy and DNA repair, which is proved in defective cancer. Among the drugs, immune checkpoint inhibitors exhibit high activity. CPI is a type of drug that targets the negative inhibitive receptors on T lymphocytes in the host, such as CTLA-4 and PD-1. These receptors are often abducted by cancer in case of effective anti-tumor response (38). Monoclonal antibodies that can block these checkpoints have been developed and show impactful ability to induce deep and enduring response in some late-stage refractory cancer. Consequently, it is approved in many subtypes of cancer including melanoma, NSCLC, HNSCC, RCC, UC, and Hodgkin's lymphoma. Despite of the excellent performances in these cancers, it seems that only a few patients can benefit from this in clinical trials. It is still vital to develop reliable biomarkers to predict patients' response and help in selection; these findings also lay foundation for studying the other sources of genome instability, which may also be used as biomarkers for selecting patients who should accept immunotherapy.

More and more evidence shows that HR-defective cancer cells have stronger immunogenicity and have potential effects on CPI. In HGSOC, BRCA1/2-mutated cells have higher predictive new antigen load and more TILs infiltration. In addition, the expression of PD-1/PD-L1 is enhanced (39). A similar increased TIL is also observed in DNA repair-defective breast cancer. In PDA, the transcriptome analysis suggests that the DSB repair-defective subtype is associated with anti-tumor immunological genetic markers (40). A recent large-scale study using the next-generation sequencing to analyze various types of cancer shows that at least 25% HR genes have defects. The TMB of HRD group is significantly higher than that of non-HRD one. People also found that BRCA/Fanconi anemia pathway defective breast cancer cells also have increased cytoplasmic DNA associated with cGAS/STING/TBK1/IRF3 pathway (41, 42).

By affecting TILs, especially the functions and composition of CTLs, PARPi may have immune-suppressive functions or improve anti-tumor response. Anti-PD-1/PD-L1 may deteriorate the former and have synergistic effect with the latter. If PARPis enhance immune response, anti CTLA-4 can coordinate with it and strengthen the effect (43). Higuchi et al. revealed that the binding of anti PD-L1 and PARPis did not induce anti-tumor response. However, the latest studies provide a new perspective on the combination of anti PD-L1 and

DDR Drug and Immunotherapy in Cancer

PARPi (Olaparib). This therapy was tested on triple-negative breast cancer (TNBC) both in vivo and in vitro. The histological results showed that protein formylation in human breast cancer is negatively related to the expression of PD-L1 (20, 44). When inoculated to homogenic mice model, PARP upregulated PD-L1 on the surface of EMT6 cancer cells (TNBC cell line) both in vitro and in vivo, which was mediated by inactive GSK3β pathway and induced TIL to decrease. Therefore, PARPi suppresses immunity by the decrease in TILs. Compared to PARPi or anti PD-L1 alone, anti PD-L1 may reverse the inhibitive functions of TIL and enhance anti-tumor response when combined with PARPis. These data collectively support further studies on the combination of PARPis and anti PD-L1/ PD-1. A recent clinical trial in Stage I applied anti-PD-1 durvalumab and olaparib into patients with breast cancer, establishing good tolerance and achieving improvement in therapeutic effects (44). At present, two combinations have been used in the study of breast cancer therapy, Veliparib and anti-CTLA-4, and Olaparib and anti-PD-L1. Noticeably, immunotherapy is applied in both situations. In future studies, we need to choose different kinds of PARPis according to the cancer types and need more studies to confirm the influences of PARPis on anti-tumor response.

In the *in vitro* experiments, IFN γ , TNF α , and PARPis (Veliparib) can coordinate to inhibit the proliferation of BRCA-deficient cancer cell line. In the mice model inoculated in this cancer cell line, the synergistic effects of anti CTLA-4 and PARPis have better anti-tumor results than any single drug, and the mice in this groups have the highest survival rate. This response is mediated by the infiltration of intraperitoneal CD8+T cells that produce IFN γ . As the response to anti CTLA-4 and PARPis, the increase in local IFN γ is competent to prohibit tumor growth, while this drug combination does not have similar roles to BRCA1-sufficient ovarian cancer. For now, there is no conclusion if it functions in the immunotherapy in human. Therefore, more studies are required to confirm the roles of PARPis on anti-tumor response.

Combining PARPi and immunotherapy has been the latest progress. In contrast, the synergistic effects of radiotherapy and immunotherapy have been fully vindicated (45). Many studies based on animal models have shown that radiation has anti-tumor immunological effects, mainly by regulating CD8+ T lymphocytes. Besides, ionizing radiation induces proinflammatory lesions and fibration, which is partially mediated by regulating cytokines. A similar process has been observed in cancer, with the infiltration of leukocytes (7, 46). Ionizing radiation activates CTl by a variety of mechanisms, including inducing TAA production and killing tumor-specific T cells. In addition, exposure in ionizing radiation upregulates major histocompatibility complex 1 (MHC-1) expression in cancer cells so that the TAA presenting of CD8+ lymphocytes is enhanced. Ionizing radiation also regulates damage-associated molecular patterns (DAMPs) release in the tumor bed, which then activate macrophages and DC. Finally, CTL production is raised. Ionizing radiation can also upregulate MHC expression to raise the production of TAA. It can improve immuno-response and coordinate with immunotherapy.

Since TTA might be caused by cancer mutations, the tumors with higher mutations may have better response to the combination of ionizing radiation and immunotherapy. Not only IR but also cytotoxic effector molecules targeting DNA repair such as PARPis can enhance the mutation load in tumors. DNA repair is already defective. Therefore, PARPis and ionizing radiation may improve therapeutic effects as immune checkpoint inhibitors.

Since the coupling of radiotherapy and PARPis has become a used treatment, its influences on anti-tumor immune response are also required to be tested. Studies have shown that PARPis and radiation can upregulate the expression and secretion of chemokines, such as CCL2 and CCL5 (PARPis, CXCL-16, and CXCL-10), and facilitate tumor infiltrating by CTL. The effects of this group is undetermined. PARPis and ionizing radiation can upregulate PD-L1 on the surface of cancer cells to suppress immunity (45). Thereby, we should investigate the changes in immunological molecular spectra in cancer cells after the induction of radiation plus PARPis and TIL (especially CTL), so that we can gain insight into the underlying mechanisms (6, 17). Animal models are needed to be developed in order to study the effects of triple therapy incorporating PARPis, radiation, and immune checkpoint inhibitors or T cell therapy, and confirm if they can improve anti-tumor response. In this situation, it is quite meaningful to compare the effects of heavily charged particles and photon radiation on anti-tumor immune response and to prove that the combination of radiosensitizer and PARPis can reduce radiotoxicity.

By far, dMMR has still been the only proven genome biomarker that responds to CPI. A large portion of cancer has profound and lasting response. The abnormal high TMB may be the basis of the immunogenecity and instructs a new direction for exploring other genomic biomarkers especially other cancer-related DNA repair pathways defects (47). However, how DNA damage and repair affect the immunogenicity of these cancer seems to be versatile and complex. Particularly, how the different features of DNA damage affect the immunogenicity is largely unknown. In a study in which 60 patients with UC accept PD-1 or PD-L1 inhibitor treatment, the targeting exon sequencing shows that the existence of DDR changes is associated with 67.9% recurrence. Different reaction pathways make different influences. The effects are maximum in the cancer with POLE or NER mutation. Prospective study is required to confirm the contribution of defects in certain pathway in the possibility of CPI response.

Now, there are some ongoing clinical trials on DDR-related drugs with immunotherapy (**Table 2**). However, currently, both DDR and immunotherapeutic drugs have their limitations and resistance reported. Resistance to DDR drugs has now been widely reported, while immunotherapy, especially PD-1 inhibitors, has not been very effective in some solid tumors. For example, although some studies have shown that PD-1 and chemotherapeutic agents such as cisplatin can improve the survival time of some patients with nasopharyngeal carcinoma, the expression of PDL1 in most patients with nasopharyngeal carcinoma, PD-1 inhibitor does not show a good effect respond. This also needs to be further explored in future studies.

TABLE 2 | Ongoing clinical trials on DDR-related drugs with immunotherapy.

Research title	Tumor type	Drugs	Locations	
Camrelizumab Combined With Apatinib, Etoposide and Cisplatin Treat Small- cell Lung Cancer.	Lung Neoplasm Small Cell Lung Cancer	Camrelizumab; Apatinib; Etoposide; Cisplatin	The 900th Hospital of Joint Logistic Support Force Fuzhou, Fujian, China	
Anlotinib in Combination With PD1 With Gemcitabine Plus(+)Cisplatin for Unresectable or Metastatic Biliary Tract Cancer	Biliary Tract Cancer	PD1 inhibitor; Cisplatin	Zhejiang Cancer Hospital Hangzhou, Zhejiang, China	
Concurrent Immunotherapy With Postoperative Radiotherapy in Intermediate/ High Risk HNSCC Patients Unfit for Cisplatin: The IMPORT Study (IMPORT)	Head and Neck Squamous Cell Carcinoma	PD1 inhibitor; Cisplatin	Guopei Zhu Shanghai, China	
Neoadjuvant Anti-PD-1 and TP Versus TPF on Pathological Response in OSCC	Oral Squamous Cell Carcinoma	Toripalimab; Albumin paclitaxel; Cisplatin	Ninth People's Hospital, Shanghai Jiao Tong University School of Medicine Shanghai, Shanghai, China	
A Clinical Trial Comparing HLX10 With Placebo Combined With Chemotherapy (Cisplatin + 5-fu) in the First-line Treatment of Locally Advanced/Metastatic Esophageal Squamous Cell Carcinoma (ESCC)	Esophageal Squamous Cell Carcinoma	HLX10; Cisplatin	Ethics Committee of cancer hospital, Chinese academy of medical sciences, Beijing, Beijing, China et al.	
Camrelizumab Combined With Chemotherapy for Recurrent or Advanced Cervical Neuroendocrine Carcinomas	Cervical Neuroendocrine Carcinoma	Camrelizumab; Cisplatin	Lei Li Beijing, Beijing, China	
Efficacy and Safety of BCD-100 (Anti-PD-1) in Combination With Platinum- Based Chemotherapy as First Line Treatment in Patients With Advanced Non- Squamous NSCLC	Non-Squamous Non- Small Cell Neoplasm of Lung	Pemetrexed; Cisplatin (or carboplatin)	Regional Hospital Liberec Liberec, Czechia University Hospital Olomouc, Czechia et al.	
Toripalimab Combined With Gemcitabine and Cisplatin Treating Resectable Locally Advanced HNSCC	Locally Advanced Head and Neck Squamous Cell Carcinoma	PD-1 inhibitor; Gemcitabine; Cisplatin	Fifth Affilliated Hospital of Sun Yat-sen University Zhuhai, Guangdong, China	
Perioperative Pembrolizumab (MK-3475) Plus Neoadjuvant Chemotherapy Versus Perioperative Placebo Plus Neoadjuvant Chemotherapy for Cisplatin- eligible Muscle-invasive Bladder Cancer (MIBC) (MK-3475-866/KEYNOTE- 866)	Urinary Bladder Cancer, Muscle- invasive	Pembrolizumab; Gemcitabine; Cisplatin	Scripps MD Anderson, California, United States et al.	
Clinical Study of Camrelizumab in Combination With Neoadjuvant Chemotherapy for Operable Locally Advanced Head and Neck Squamous Cell Carcinoma	Head and Neck Cancer Squamous Cell Carcinoma	PD-1 inhibitor; Albumin Paclitaxel; Cisplatin	Hunan cancer Hospital Changsha, Hunan, China	
Efficacy and Safety of Pembrolizumab Plus Investigational Agents in Combination With Chemotherapy as First-Line Treatment in Extensive-Stage Small Cell Lung Cancer (ES-SCLC) (MK-3475-B99/KEYNOTE-B99)	Small Cell Lung Cancer	Pembrolizumab; MK- 4830; MK-5890	Banner MD Anderson Cancer Center Gilbert, Arizona, United States et al.	
Placebo-controlled, Study of Concurrent Chemoradiation Therapy With Pembrolizumab Followed by Pembrolizumab and Olaparib in Newly Diagnosed Treatment-Naïve Limited-Stage Small Cell Lung Cancer (LS-SCLC) (MK 7339-013/KEYLYNK-013)	Small Cell Lung Cancer	Pembrolizumab; Olaparib	Ironwood Cancer & Research Centers et al.	
Study of Pembrolizumab With Concurrent Chemoradiation Therapy Followed by Pembrolizumab With or Without Olaparib in Stage III Non-Small Cell Lung Cancer (NSCLC) (MK-7339-012/KEYLYNK-012)	Lung Neoplasms Carcinoma, Non-Small- Cell Lung	Pembrolizumab; Olaparib	University of South Alabama, Mitchell Cancer Institute, Alabama, United States et al.	
Phase II Umbrella Study of Novel Anti-cancer Agents in Patients With NSCLC Who Progressed on an Anti-PD-1/PD-L1 Containing Therapy	Non-Small Cell Lung Cancer	Durvalumab; AZD9150; AZD6738	Research Site Duarte, California, United States et al.	
Phase II Study of Olaparib and Pembrolizumab in Advanced Melanoma With Homologous Recombination (HR) Mutation	Metastatic Melanoma	Olaparib; Pembrolizumab	California Pacific Medical Center Research Institute, San Francisco, California, United States	
Paclitaxel, Pembrolizumab and Olaparib in Previously Treated Advanced Gastric Adenocarcinoma	Advanced Gastric Adenocarcinoma	Paclitaxel; Olaparib; Pembrolizumab	Sidney Kimmel Comprehensive Cancer Center Baltimore, Maryland, United States	

CONCLUSIONS AND FUTURE PERSPECTIVES

In the past decades, we have made great progress on understanding how cancer cells escape from the surveillance of immune system, which offers us new approaches based on how to prevent immune escape and eliminate cancer cells. The immune system has vital functions in the progression and restriction of cancer. The immunological surveillance of cancer includes three stages, namely, elimination, balance, and escape (48, 49). In this process, IFN γ and lymphocytes inhibit primary tumor progression. In the stage of elimination, the immunoresponse can induce effective exogenous tumor-suppressing system, while the bad side is that it also causes an immunological selection of cancer cells that are more capable to survive in the immune-competent host. Next, the chosen tumor cells enter the stage of immune escape. Between these two stages, it is called immune balancing stage, in which tumor does not grow or grow slowly under the pressure of the immune system (50). Both innate and adaptive immunity particulate in countering cancer. Besides, cytokine IFN γ has pleiotropic effects, especially in the activation of NK cells and CTL. IFN γ signaling upregulates the expression of MHC I and MHC II and raises the expression of TAA in lymphocytes. IFN γ also induces specific TAA-activated CD8+ lymphocytes, thereby initiating CTL-mediated anti-tumor response. CTL infiltration enhances the lethal effect of immune system to cancer cells. A body of evidence has shown that CTL infiltration is related to the good prognosis of many tumors (51–53).

So far, people have found that MDSC plays an important role in tumorigenesis and progression as well besides TILs. Studies show MDSC can directly support the growth and metastasis of tumor besides suppressing the immune system. Similar to TILs, MDSC can also be considered as a factor for prognosis of cancer immunotherapy and the target of drugs according to the clinical data of patients. In sum, tumor-related myeloid including MDSC and TAM reprogram to create an immune-suppressing environment in tumorigenesis. Meanwhile, it also promotes tumor stem, angiogenesis, the transformation from epithelium to mesenchyme and metastasis, which directly drive the progression of tumors. As an important kind of RNA, noncoding RNA also may play an important role in tumor treatment. Non-coding RNAs have been found to play important functions in tumor immunity and DNA damage repair in a variety of tumors, such as lncRNA and circRNA, which suggest that they may serve as important targets for combination drug delivery.

DDR drugs cause biological behaviors such as apoptosis of tumor cells through DNA damage, thus leading to the death of tumor cells. In contrast, immunosuppressants, especially immune checkpoint inhibitors represented by PD-1, promote the killing of tumor cells by immune cells *via* attenuating the immune escape of tumor cells. Recent studies also have found that DDR drugs lead to changes in tumor microenvironment, which mechanistically explains why the combination of DDR drugs and immunotherapy may have better effects on the treatment of tumors. The common pathway between DDR and immunotherapy has also been one of the main focuses of research in recent years, and studies have identified molecules represented by cGAS, which play important functions in both DNA damage repair and immunity. The roles of cGAS in

REFERENCES

- Hanahan D, Weinberg RA. Hallmarks of Cancer: The Next Generation. Cell (2011) 144(5):646–74. doi: 10.1016/j.cell.2011.02.013
- Aparicio T, Baer R, Gautier J. DNA Double-Strand Break Repair Pathway Choice and Cancer. DNA Repair (Amst) (2014) 19:169–75. doi: 10.1016/j.dnarep.2014.03.014
- Lord CJ, Ashworth A. BRCAness Revisited. Nat Rev Cancer (2016) 16(2):110– 20. doi: 10.1038/nrc.2015.21
- Yang Y. Cancer Immunotherapy: Harnessing the Immune System to Battle Cancer. J Clin Invest (2015) 125(9):3335–7. doi: 10.1172/JCI83871
- Esfahani K, Roudaia L, Buhlaiga N, Del Rincon SV, Papneja N, Miller WH Jr. A Review of Cancer Immunotherapy: From the Past, to the Present, to the Future. *Curr Oncol* (2020) 27(Suppl 2):S87–97. doi: 10.3747/co.27.5223
- Drean A, Lord CJ, Ashworth A. PARP Inhibitor Combination Therapy. Crit Rev Oncol Hematol (2016) 108:73–85. doi: 10.1016/j.critrevonc.2016.10.010
- Alhmoud JF, Woolley JF, Al Moustafa AE, Malki MI. DNA Damage/Repair Management in Cancers. *Cancers (Basel)* (2020) 12(4):1–22. doi: 10.3390/ cancers12041050

immunity and DNA repair is noteworthy. Previous studies reported the existence of cytoplasmic DNA damage in late S phase. In addition, there has been evidence proving that cells can actively export DNA segment from the nucleus, which possibly contributes to the prevention of incorporating mistakes into DNA. Reversely, when efficient DNA repair is lacking, cytoplasmic DNA will trigger cGAS-mediated innate immunoresponse (54, 55). Studies have shown that the downregulation of cGAS and STING successfully reverses the effects of combining DNA repair-related anti-tumor drugs and PD-L1 in prohibiting tumor growth. Therefore, cGAS can also be a molecule worth further investigation. However, although the combination of immunotherapy and DDR drugs has achieved good results in some tumors, current clinical studies have shown that most solid tumors are not sensitive to immunotherapy or immunotherapy plus chemotherapy, which requires further investigation of the mechanisms and development of new immunotherapy drugs in future studies.

AUTHOR CONTRIBUTIONS

YW, MD and ZP collected the related paper and finished the manuscript and figures. YH, WX, HZ and RF gave constructive guidance and made critical revisions. WJ participated in the design of this review. All authors read and approved the final manuscript.

FUNDING

This research was funded by the National Natural Science Foundation of China (81770985), Xiangya Hospital Funds for Young Scholar (2020Q13), Hunan Postdoctoral Program for Innovative Talent (2021RC2017), and Natural Science Foundation of Hunan Province (2021JJ41027). The funders had no role in study design, data collection and analysis, decision to publish, or preparation of the manuscript.

- Wei L, Nakajima S, Böhm S, Bernstein KA, Shen Z, Tsang M, et al. DNA Damage During the G0/G1 Phase Triggers RNA-Templated, Cockayne Syndrome B-Dependent Homologous Recombination. *PNAS* (2015) 112 (27):E3495–504. doi: 10.1073/pnas.1507105112
- Keung MYT, Wu Y, Vadgama JV. PARP Inhibitors as a Therapeutic Agent for Homologous Recombination Deficiency in Breast Cancers. J Clin Med (2019) 8(4):1–24. doi: 10.3390/jcm8040435
- Newlands ES, Stevens MF, Wedge SR, Wheelhouse RT, Brock C. Temozolomide: A Review of Its Discovery, Chemical Properties, Pre-Clinical Development and Clinical Trials. *Cancer Treat Rev* (1997) 23 (1):35-61. doi: 10.1016/S0305-7372(97)90019-0
- 11. Abe H, Natsumeda M, Kanemaru Y, Watanabe J, Tsukamoto Y, Okada M, et al. MGMT Expression Contributes to Temozolomide Resistance in H3K27M-Mutant Diffuse Midline Gliomas and MGMT Silencing to Temozolomide Sensitivity in IDH-Mutant Gliomas. *Neurol Med Chir* (*Tokyo*) (2018) 58(7):290–5. doi: 10.2176/nmc.ra.2018-0044
- 12. Lu Y, Zhao Z, Wang J, Lv W, Lu L, Fu W, et al. Safety and Efficacy of Combining Capecitabine and Temozolomide (CAPTEM) to Treat Advanced

Neuroendocrine Neoplasms: A Meta-Analysis. Med (Baltimore) (2018) 97 (41):e12784. doi: 10.1097/MD.00000000012784

- Chua J, Nafziger E, Leung D. Evidence-Based Practice: Temozolomide Beyond Glioblastoma. Curr Oncol Rep (2019) 21(4):30. doi: 10.1007/s11912-019-0783-5
- Peng Z, Wang Y, Wang Y, Fan R, Gao K, Zhang H, et al. Preliminary Efficacy Report and Prognosis Analysis of Endoscopic Endonasal Nasopharyngectomy for Recurrent Nasopharyngeal Carcinoma. *Front Surg* (2021) 8:713926. doi: 10.3389/fsurg.2021.713926
- Syro LV, Rotondo F, Camargo M, Ortiz LD, Serna CA, Kovacs K. Temozolomide and Pituitary Tumors: Current Understanding, Unresolved Issues, and Future Directions. *Front Endocrinol (Lausanne)* (2018) 9:318. doi: 10.3389/fendo.2018.00318
- Karachi A, Dastmalchi F, Mitchell DA, Rahman M. Temozolomide for Immunomodulation in the Treatment of Glioblastoma. *Neuro Oncol* (2018) 20(12):1566–72. doi: 10.1093/neuonc/noy072
- Kamel D, Gray C, Walia JS, Kumar V. PARP Inhibitor Drugs in the Treatment of Breast, Ovarian, Prostate and Pancreatic Cancers: An Update of Clinical Trials. *Curr Drug Targets* (2018) 19(1):21–37. doi: 10.2174/1389450118666170711151518
- Jiang X, Li X, Li W, Bai H, Zhang Z. PARP Inhibitors in Ovarian Cancer: Sensitivity Prediction and Resistance Mechanisms. J Cell Mol Med (2019) 23 (4):2303–13. doi: 10.1111/jcmm.14133
- Damaskos C, Garmpi A, Nikolettos K, Vavourakis M, Diamantis E, Patsouras A, et al. Triple-Negative Breast Cancer: The Progress of Targeted Therapies and Future Tendencies. *Anticancer Res* (2019) 39(10):5285–96. doi: 10.21873/anticanres.13722
- Weil MK, Chen AP. PARP Inhibitor Treatment in Ovarian and Breast Cancer. Curr Probl Cancer (2011) 35(1):7–50. doi: 10.1016/j.currproblcancer.2010.12.002
- Teng Y, Yadav T, Duan M, Tan J, Xiang Y, Gao B, et al. ROS-Induced R Loops Trigger a Transcription-Coupled But BRCA1/2-Independent Homologous Recombination Pathway Through CSB. *Nat Commun* (2018) 9(1):4115. doi: 10.1038/s41467-018-06586-3
- 22. Khanna KK, Jackson SP. DNA Double-Strand Breaks: Signaling, Repair and the Cancer Connection. *Nat Genet* (2001) 27(3):247–54. doi: 10.1038/85798
- Pabla N, Dong Z. Cisplatin Nephrotoxicity: Mechanisms and Renoprotective Strategies. *Kidney Int* (2008) 73(9):994–1007. doi: 10.1038/sj.ki.5002786
- Miller RP, Tadagavadi RK, Ramesh G, Reeves WB. Mechanisms of Cisplatin Nephrotoxicity. *Toxins (Basel)* (2010) 2(11):2490–518. doi: 10.3390/ toxins2112490
- Rocha CRR, Silva MM, Quinet A, Cabral-Neto JB, Menck CFM. DNA Repair Pathways and Cisplatin Resistance: An Intimate Relationship. *Clinics (Sao Paulo)* (2018) 73(suppl 1):e478s. doi: 10.6061/clinics/2018/e478s
- Filippini SE, Vega A. Breast Cancer Genes: Beyond BRCA1 and BRCA2. Front Biosci (Landmark Ed) (2013) 18:1358–72. doi: 10.2741/4185
- Watkins J, Weekes D, Shah V, Gazinska P, Joshi S, Sidhu B, et al. Genomic Complexity Profiling Reveals That HORMAD1 Overexpression Contributes to Homologous Recombination Deficiency in Triple-Negative Breast Cancers. *Cancer Discov* (2015) 5(5):488–505. doi: 10.1158/2159-8290.CD-14-1092
- Yi M, Jiao D, Xu H, Liu Q, Zhao W, Han X, et al. Biomarkers for Predicting Efficacy of PD-1/PD-L1 Inhibitors. *Mol Cancer* (2018) 17(1):129. doi: 10.1186/ s12943-018-0864-3
- Hall M, Liu H, Malafa M, Centeno B, Hodul PJ, Pimiento J, et al. Expansion of Tumor-Infiltrating Lymphocytes (TIL) From Human Pancreatic Tumors. *J Immunother Cancer* (2016) 4:61. doi: 10.1186/s40425-016-0164-7
- Rowshanravan B, Halliday N, Sansom DM. CTLA-4: A Moving Target in Immunotherapy. *Blood* (2018) 131(1):58–67. doi: 10.1182/blood-2017-06-741033
- Buchbinder EI, Desai A. CTLA-4 and PD-1 Pathways: Similarities, Differences, and Implications of Their Inhibition. *Am J Clin Oncol* (2016) 39(1):98–106. doi: 10.1097/COC.00000000000239
- 32. Linsley PS, Bradshaw J, Greene J, Peach R, Bennett KL, Mittler RS. Intracellular Trafficking of CTLA-4 and Focal Localization Towards Sites of TCR Engagement. *Immunity* (1996) 4(6):535–43. doi: 10.1016/S1074-7613 (00)80480-X
- Wang Y, Zhang L, Yang Y, Lu S, Chen H. Progress of Gastric Cancer Surgery in the era of Precision Medicine. *Int J Biol Sci* (2021) 17(4):1041-9. doi: 10.7150/ijbs.56735
- 34. Phan GQ, Yang JC, Sherry RM, Hwu P, Topalian SL, Schwartzentruber DJ, et al. Cancer Regression and Autoimmunity Induced by Cytotoxic T Lymphocyte-Associated Antigen 4 Blockade in Patients With Metastatic Melanoma. *Proc Natl Acad Sci USA* (2003) 100(14):8372–7. doi: 10.1073/pnas.1533209100

- 35. Kershaw MH, Westwood JA, Parker LL, Wang G, Eshhar Z, Mavroukakis SA, et al. A Phase I Study on Adoptive Immunotherapy Using Gene-Modified T Cells for Ovarian Cancer. Clin Cancer Res an Off J Am Assoc Cancer Res (2006) 12(20 Pt 1):6106–15. doi: 10.1158/1078-0432.CCR-06-1183
- 36. Carpenito C, Milone MC, Hassan R, Simonet JC, Lakhal M, Suhoski MM, et al. Control of Large, Established Tumor Xenografts With Genetically Retargeted Human T Cells Containing CD28 and CD137 Domains. Proc Natl Acad Sci USA (2009) 106(9):3360–5. doi: 10.1073/pnas.0813101106
- Yu H, Pan J, Guo Z, Yang C, Mao L. CART Cell Therapy for Prostate Cancer: Status and Promise. Onco Targets Ther (2019) 12:391–5. doi: 10.2147/OTT.S185556
- Calabrese LH, Calabrese C, Cappelli LC. Rheumatic Immune-Related Adverse Events From Cancer Immunotherapy. Nat Rev Rheumatol (2018) 14(10):569– 79. doi: 10.1038/s41584-018-0074-9
- Young A, Quandt Z, Bluestone JA. The Balancing Act Between Cancer Immunity and Autoimmunity in Response to Immunotherapy. *Cancer Immunol Res* (2018) 6(12):1445–52. doi: 10.1158/2326-6066.CIR-18-0487
- Mo Y, Wang Y, Zhang S, Xiong F, Yan Q, Jiang X, et al. Circular RNA circRNF13 inhibits proliferation and metastasis of nasopharyngeal carcinoma via SUMO2. *Mol Cancer* (2021) 20(1):112. doi: 10.1186/s12943-021-01409-4
- 41. Park Y, Chui MH, Suryo Rahmanto Y, Yu ZC, Shamanna RA, Bellani MA, et al. Loss of ARID1A in Tumor Cells Renders Selective Vulnerability to Combined Ionizing Radiation and PARP Inhibitor Therapy. *Clin Cancer Res an Off J Am Assoc Cancer Res* (2019) 25(18):5584–94. doi: 10.1158/1078-0432.CCR-18-4222
- Tabano S, Azzollini J, Pesenti C, Lovati S, Costanza J, Fontana L, et al. Analysis of BRCA1 and RAD51C Promoter Methylation in Italian Families at High-Risk of Breast and Ovarian Cancer. *Cancers (Basel)* (2020) 12(4):1–8. doi: 10.3390/cancers12040910
- Cesaire M, Thariat J, Candeias SM, Stefan D, Saintigny Y, Chevalier F. Combining PARP Inhibition, Radiation, and Immunotherapy: A Possible Strategy to Improve the Treatment of Cancer? *Int J Mol Sci* (2018) 19(12):1– 18. doi: 10.3390/ijms19123793
- 44. >Coleman RL, Fleming GF, Brady MF, Swisher EM, Steffensen KD, Friedlander M, et al. Veliparib With First-Line Chemotherapy and as Maintenance Therapy in Ovarian Cancer. N Engl J Med (2019) 381 (25):2403-15. doi: 10.1056/NEJMoa1909707
- 45. Wirsdorfer F, de Leve S, Jendrossek V. Combining Radiotherapy and Immunotherapy in Lung Cancer: Can We Expect Limitations Due to Altered Normal Tissue Toxicity? *Int J Mol Sci* (2018) 20(1):1–21. doi: 10.3390/ ijms20010024
- Memon H, Patel BM. Immune Checkpoint Inhibitors in Non-Small Cell Lung Cancer: A Bird's Eye View. Life Sci (2019) 233:116713. doi: 10.1016/j.lfs.2019.116713
- Oliveira AF, Bretes L, Furtado I. Review of PD-1/PD-L1 Inhibitors in Metastatic dMMR/MSI-H Colorectal Cancer. Front Oncol (2019) 9:396. doi: 10.3389/fonc.2019.00396
- Sugie T. Immunotherapy for Metastatic Breast Cancer. Chin Clin Oncol (2018) 7(3):28. doi: 10.21037/cco.2018.05.05
- Helmy KY, Patel SA, Nahas GR, Rameshwar P. Cancer Immunotherapy: Accomplishments to Date and Future Promise. *Ther Deliv* (2013) 4(10):1307– 20. doi: 10.4155/tde.13.88
- Sampson JH, Maus MV, June CH. Immunotherapy for Brain Tumors. J Clin Oncol (2017) 35(21):2450–6. doi: 10.1200/JCO.2017.72.8089
- Pettenati C, Ingersoll MA. Mechanisms of BCG Immunotherapy and Its Outlook for Bladder Cancer. Nat Rev Urol (2018) 15(10):615–25. doi: 10.1038/ s41585-018-0055-4
- Kakimi K, Karasaki T, Matsushita H, Sugie T. Advances in Personalized Cancer Immunotherapy. *Breast Cancer* (2017) 24(1):16–24. doi: 10.1007/ s12282-016-0688-1
- Emens LA, Ascierto PA, Darcy PK, Demaria S, Eggermont AMM, Redmond WL, et al. Cancer Immunotherapy: Opportunities and Challenges in the Rapidly Evolving Clinical Landscape. *Eur J Cancer* (2017) 81:116–29. doi: 10.1016/j.ejca.2017.01.035
- Sen T, Rodriguez BL, Chen L, Corte CMD, Morikawa N, Fujimoto J, et al. Targeting DNA Damage Response Promotes Antitumor Immunity Through STING-Mediated T-Cell Activation in Small Cell Lung Cancer. *Cancer Discov* (2019) 9(5):646–61. doi: 10.1158/2159-8290.CD-18-1020
- 55. Ahmadzadeh M, Johnson LA, Heemskerk B, Wunderlich JR, Dudley ME, White DE, et al. Tumor Antigen-Specific CD8 T Cells Infiltrating the Tumor

Express High Levels of PD-1 and Are Functionally Impaired. *Blood* (2009) 114 (8):1537-44. doi: 10.1182/blood-2008-12-195792

Conflict of Interest: The authors declare that the research was conducted in the absence of any commercial or financial relationships that could be construed as a potential conflict of interest.

Publisher's Note: All claims expressed in this article are solely those of the authors and do not necessarily represent those of their affiliated organizations, or those of the publisher, the editors and the reviewers. Any product that may be evaluated in this article, or claim that may be made by its manufacturer, is not guaranteed or endorsed by the publisher.

Copyright © 2022 Wang, Duan, Peng, Fan, He, Zhang, Xiong and Jiang. This is an open-access article distributed under the terms of the Creative Commons Attribution License (CC BY). The use, distribution or reproduction in other forums is permitted, provided the original author(s) and the copyright owner(s) are credited and that the original publication in this journal is cited, in accordance with accepted academic practice. No use, distribution or reproduction is permitted which does not comply with these terms.





GPC2 Is a Potential Diagnostic, Immunological, and Prognostic Biomarker in Pan-Cancer

Guoming Chen¹, Dongqiang Luo², Nan Zhong², Danyun Li², Jiyuan Zheng², Hui Liao², Zhuoyao Li², Xiaoxiao Lin², Qiqi Chen², Cheng Zhang¹, Yuanjun Lu¹, Yau-Tuen Chan¹, Qing Ren¹, Ning Wang¹ and Yibin Feng^{1*}

¹ School of Chinese Medicine, Li Ka Shing Faculty of Medicine, The University of Hong Kong, Hong Kong SAR, China, ² Guangzhou University of Chinese Medicine, Guangzhou, China

OPEN ACCESS

Edited by:

Yubin Li, University of Pennsylvania, United States

Reviewed by:

Ling Li, University of North Dakota, United States Wentao Huang, Massachusetts Institute of Technology, United States

*Correspondence:

Yibin Feng yfeng@hku.hk

Specialty section:

This article was submitted to Cancer Immunity and Immunotherapy, a section of the journal Frontiers in Immunology

Received: 18 January 2022 Accepted: 01 February 2022 Published: 08 March 2022

Citation:

Chen G, Luo D, Zhong N, Li D, Zheng J, Liao H, Li Z, Lin X, Chen Q, Zhang C, Lu Y, Chan Y-T, Ren Q, Wang N and Feng Y (2022) GPC2 Is a Potential Diagnostic, Immunological, and Prognostic Biomarker in Pan-Cancer. Front. Immunol. 13:857308. doi: 10.3389/fimmu.2022.857308 **Background:** Glypican 2 (GPC2), a member of glypican (GPC) family genes, produces proteoglycan with a glycosylphosphatidylinositol anchor. It has shown its ascending significance in multiple cancers such as neuroblastoma, malignant brain tumor, and small-cell lung cancer. However, no systematic pan-cancer analysis has been conducted to explore its function in diagnosis, prognosis, and immunological prediction.

Methods: By comprehensive use of datasets from The Cancer Genome Atlas (TCGA), Cancer Cell Line Encyclopedia (CCLE), Genotype-Tissue Expression Project (GTEx), cBioPortal, Human Protein Atlas (HPA), UALCAN, StarBase, and Comparative Toxicogenomics Database (CTD), we adopted bioinformatics methods to excavate the potential carcinogenesis of GPC2, including dissecting the correlation between GPC2 and prognosis, gene mutation, immune cell infiltration, and DNA methylation of different tumors, and constructed the competing endogenous RNA (ceRNA) networks of GPC2 as well as explored the interaction of GPC2 with chemicals and genes.

Results: The results indicated that GPC2 was highly expressed in most cancers, except in pancreatic adenocarcinoma, which presented at a quite low level. Furthermore, GPC2 showed the early diagnostic value in 16 kinds of tumors and was positively or negatively associated with the prognosis of different tumors. It also verified that GPC2 was a gene associated with most immune-infiltrating cells in pan-cancer, especially in thymoma. Moreover, the correlation with GPC2 expression varied depending on the type of immune-related genes. Additionally, GPC2 gene expression has a correlation with DNA methylation in 20 types of cancers.

Conclusion: Through pan-cancer analysis, we discovered and verified that GPC2 might be useful in cancer detection for the first time. The expression level of GPC2 in a variety of tumors is significantly different from that of normal tissues. In addition, the performance of GPC2 in tumorigenesis and tumor immunity also confirms our conjecture. At the same

45

time, it has high specificity and sensitivity in the detection of cancers. Therefore, GPC2 can be used as an auxiliary indicator for early tumor diagnosis and a prognostic marker for many types of tumors.

Keywords: GPC2, pan-cancer, diagnosis, prognosis, immunization

INTRODUCTION

Cancer brings immense suffering to individuals (1). From radiotherapy and chemotherapy to targeted therapy and immunotherapy, persistent efforts enhance our understanding toward the complex pathogenesis of tumor and raise the level of treatment (2). However, immunotherapy calls for more investigation in different cancers to validate itself (3, 4). Pancancer analysis is the analysis of genes in a wide variety of cancers, in which the differences and similarities of the expression of extracted genes are compared (5). Thanks to public databases like The Cancer Genome Atlas (TCGA), valuable factors can be mined for diagnosis, prognosis, and immunotherapy (6).

Glypican 2 (GPC2) is a protein-coding gene expressing cell surface proteoglycan bearing heparan sulfate (7). The glypican (GPC) family genes encode GPC which attaches to the cell membrane by means of a glycosylphosphatidylinositol (GPI) anchor (8). Studies manifest that these glypicans work as protein co-receptor, playing a part in signal transduction of wingless (Wnts), hedgehogs (Hhs), fibroblast growth factors (FGFs), and bone morphogenetic proteins (BMPs) (7). Six species of GPC (GPC1-6) have been identified in mammals, and all of them are shown as cancer therapeutic targets with high expression in cancers (9). Their expression varies in different tissues, and among them GPC2 is mainly active in growing nervous tissues and thyroid cancer tissues (10-14). It participates in the growth and differentiation of neuronal axons (15). Increasing evidence has demonstrated the overexpression of GPC2 in neuroblastoma, a kind of childhood cancer (9, 16, 17). Based on previous research, immunotherapy and targeted therapy have shown good therapeutic prospects in neuroblastoma and malignant brain tumors (16, 18, 19). A research identified immunotherapy targets in 12 pediatric cancers, and GPC2 was analyzed in 8 diseases such as osteosarcoma (OS) and Ewing sarcoma (EWS), which makes it evident that GPC2 has a wide range of functions in childhood cancers (20). Some papers consider that it keeps silent relatively in various adult normal tissues such as brain, heart, lung, and kidney (9, 21). However, small-cell lung cancer and prostate cancer were discovered to have an upregulated expression (17, 22). Moreover, experiences show that a high expression of GPC2 may lead to favorable prognosis in early pancreatic duct adenocarcinoma after pancreaticoduodenectomy (23). Generally, GPC2 has an effect on protein transduction, cell proliferation and differentiation, and oncogenic signatures (7, 23).

In view of the lack of pan-cancer study and inconsistencies in past research, we retrieved diverse data resources containing TCGA, Cancer Cell Line Encyclopedia (CCLE), Genotype-Tissue Expression Project (GTEx), cBioPortal, and Human Protein Atlas (HPA) and extracted corresponding data subsequently. With the analysis and comparison of the expression of GPC2 in types of malignancies, we further conducted immune infiltration levels, co-expression analysis of immune-related genes with GPC2, and DNA methylation across 33 types of cancer. Besides, we also investigated competing endogenous RNA (ceRNA) networks and interacting chemicals and genes of GPC2. There is a discovery that GPC2 can be employed as a diagnostic, prognostic, and immunological predictor of generalized cancers. The study may broaden the train of thought toward application of GPC2 in immunotherapy.

MATERIALS AND METHODS

Data Preprocessing and Differential Expression Analysis

The mRNA expression profiles and correlative clinical data from 33 types of cancer samples and corresponding normal samples were downloaded from TCGA (https://www.cancer.gov/about-nci/organization/ccg/research/structural-genomics/tcga), which involve 11,315 samples in all. The differentially expression genes (DEGs) between tumor tissues and adjacent tissues were identified using the log₂ transformation and t-tests in TCGA cohorts with a p-value <0.05. The intersection genes were screened from the cancer species with significant differential expression.

We downloaded gene expression data from GTEx (https:// commonfund.nih.gov/GTEx) from 31 different tissues. The CCLE database (https://sites.broadinstitute.org/ccle) is a large, public cancer genome database, which includes information of thousands of cell lines and methylation gene expression profiles. We downloaded the data of cancer cell lines from 37 human tissues in CCLE and analyzed their GPC2 expression.

The downloaded data enabled us to evaluate the expression levels of GPC2 in 31 normal tissues as well as 33 tumor tissues and compare the cancer samples with paired standard samples in 33 cancers. Log_2 transformation and t-tests were performed on the expression data and these tumor types. The expression difference between tumor and normal tissue samples was identified by the standard of p-value < 0.05. R software (Version 4.0.2, https://www. Rproject.org) was used for data analysis, and the "ggplot2" R package was applied to draw the box diagrams.

Immunohistochemistry Staining of GPC2

HPA (https://www.proteinatlas.org/) is a human proteome atlas database containing information on the protein distribution of human tissues and cells. To analyze the differential expression of GPC2 at the protein level, we downloaded immunohistochemical images of 15 kinds of tumor tissues with their corresponding normal tissues from HPA. These included liver cancer, testis

cancer, thyroid cancer, lymphoma, ovarian cancer, skin cancer, prostate cancer, breast cancer, stomach cancer, pancreatic cancer, cervical cancer, endometrial cancer, renal cancer, colorectal cancer, and lung cancer.

Analysis of the Diagnosis Value of GPC2

Mined from each sample provided by TCGA, the clinical phenotype, tumor stage, was chosen and its link with GPC2 expression was analyzed, which was carried out benefiting from "ggplot2" R packages. "ggplot2" is a kind of drawing package that can separate drawing and data, data-related drawing, and data irrelevant drawing. To evaluate the diagnostic accuracy of GPC2, the ROC curve analysis based on sensitivity and specificity was conducted using the "pROC" package. The area under the curve (AUC) ranges from 1.0 (perfect diagnostic) to 0.5 (no diagnostic value) (24).

Analysis of the Relationships Between GPC2 and Prognosis

We also had access to the survival data profiting from the samples downloaded from TCGA. Overall survival (OS), disease-specific survival (DSS), and progression-free interval (PFI) were considered as the indicators to explore the relevancy between GPC2 expression and patient prognosis. When it comes to survival analyses, the Kaplan–Meier method and log-rank test were used in each cancer type. R packages "survival" and "survminer" were used to draw the survival curves. Moreover, we employed the R packages "forestplot" to ascertain the relationship between GPC2 expression and survival in pan-cancer.

Relationship Between GPC2 Expression and Immunity

The relative scores for 24 immune cells in 33 cancers were calculated by a metagene tool, CIBERSORT (https://cibersort. stanford.edu/), which can predict the phenotypes of immunocytes. What is more, the correlations between GPC2 and each immune cell infiltration level were assessed based on R software packages "ggplot2" and "ggpubr"("ggplot2" is a flexible package for elegant data visualization in R. The "ggpubr" package provides some easy-to-use functions for creating and customizing "ggplot2"-based publication-ready plots).

Additionally, we analyzed the co-expression of GPC2 and immune-related genes, specifically involving genes encoding the major histocompatibility complex (MHC) and immune activation, immunosuppressive, chemokine, and chemokine receptor proteins. Moreover, the visualization results were presented by "reshape2" and "RColorBrewer" packages. "Reshape2" is applied for the interaction between wide-format data and long-format data while "RColorBrewer" is applied to configure colors.

Correlation of GPC2 Expression With DNA Methylation

UALCAN (http://ualcan.path.uab.edu/) is a interactive web portal that is used to conduct an in-depth analysis of TCGA

gene expression data (25). In this study, UALCAN was used to investigate the promoter methylation level of GPC2 in cancers.

cBioPortal (http://www.cbioportal.org/) is a platform that contains all tumor gene data in TCGA database and can provide researchers with multidimensional visual data. We selected data from 32 cancers, a total of 10,953 samples, and used cBioPortal for further analysis. The type and frequency of GPC2 gene mutation in all tumors were analyzed in "OncoPrint" and "CancerTypesSummary." "OncoPrint" shows the mutation, copy number, and expression of the target gene in all samples in the form of a heat map. In addition, "CancerTypesSummary" shows the mutation rate of the target gene in generalized carcinoma in the form of a bar chart.

Target miRNA Prediction and ceRNA Network Construction

We retrieved target miRNAs of GPC2 from five prediction databases of miRNAs, including DIANA-microT (http://diana. imis.athena-innovation.gr/DianaTools/index.php?r=microT_ CDS/index), RNA22 (http://cbcsrv.watson.ibm.com/rna22.html/), miRDB (http://mirdb.org/miRDB/), miRWalk (http://mirwalk. umm.uni-heidelberg.de/), and miRcode (http://www.mircode. org/index.php). Target miRNAs were defined as miRNAs found in at least three databases. StarBase v2.0 (https://starbase.sysu.edu. cn/index.phpStarBase) constructed the most comprehensive miRNA-lncRNA and miRNA-circRNA interaction networks (26), providing lncRNA and circRNA information about GPC2. The screening criteria were mammal, human, hg19, strict stringency (≥5) of CLIP-Data, and with or without data of Degradome-Data. The Cytoscape was applied to visualize the ceRNA networks according to the relationship among noncoding RNAs (ncRNAs), miRNAs, and mRNAs.

Interaction of GPC2 With Chemicals and Genes

The Comparative Toxicogenomics Database (CTD, http:// ctdbase.org/) is a digital resource contributing to investigation in novel connections of molecular mechanisms by which chemicals influence health outcomes (27). We used this database to query the interacting chemicals of GPC2 and explore the genes with high similarity to GPC2 in terms of common interacting chemicals.

The GeneMANIA database (http://www.genemania.org) is a user-friendly website that can find functionally similar genes according to the given gene list based on a wealth of genomics and proteomics data (23). Through detection of similar gene functions in GeneMANIA, we identified genes whose expression patterns were similar to those of GPC2.

RESULTS

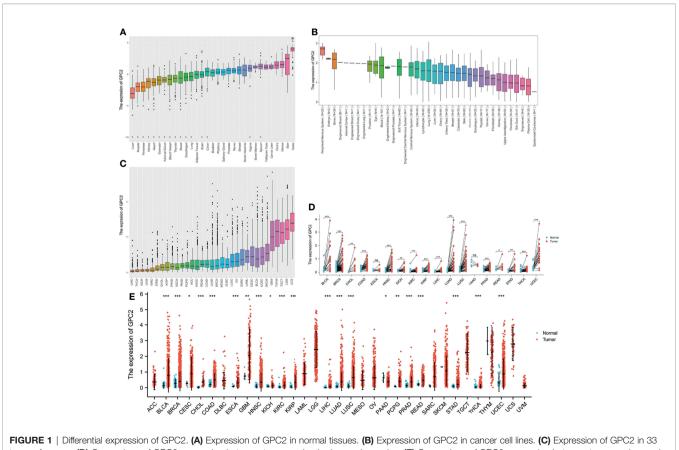
Differential Expression of GPC2 Between Tumor and Normal Tissue Samples

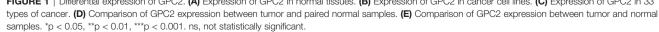
The GTEx datasets were used to analyze the expression levels of the GPC2 gene across different tissues under physiological conditions (**Figure 1A**). It is not difficult to find that GPC2 expression levels were highest in testis (compared with other tissues, the differences were statistically significant), but low in most other normal tissues. **Figure 1B** presents the relative GPC2 expression levels in various cancer cell lines from CCLE. It can be seen from the results that the expression levels of GPC2 are generally increased in cancer cell lines from different tissue sources, which is consistent with the analysis result of TCGA database, and it is significantly expressed in the peripheral nervous system.

Whereafter, we ranked GPC2 expression levels in various cancers from lowest to highest (**Figure 1C**). GPC2 was expressed in all tumors, with the highest level in uterine carcinosarcoma (UCS) and, conversely, lowest in liver hepatocellular carcinoma (LIHC). We also made a comparison between cancer and paired normal samples on GPC2 expression levels in 33 cancers, based on TCGA data (**Figure 1E**). Except for those cancers in which no normal tissue data were available or only had very few normal samples, it was detected that the expression of GPC2 in 21 types of cancer was significantly different from that in normal tissue. Thereinto, GPC2 levels were upregulated in bladder urothelial carcinoma (BLCA), breast invasive carcinoma (BRCA), cervical squamous cell carcinoma (CHOL), colon adenocarcinoma

(COAD), esophageal carcinoma (ESCA), head and neck squamous cell carcinoma (HNSC), kidney chromophobe (KICH), kidney renal clear cell carcinoma (KIRC), kidney renal papillary cell carcinoma (KIRP), LIHC, lung adenocarcinoma (LUAD), lung squamous cell carcinoma (LUSC), pheochromocytoma and paraganglioma (PCPG), prostate adenocarcinoma (PRAD), rectum adenocarcinoma (READ), stomach adenocarcinoma (STAD), thyroid carcinoma (THCA), uterine corpus endometrial carcinoma (UCEC), and glioblastoma multiforme (GBM). In contrast, GPC2 had a low expression in tumor relative to normal tissues in pancreatic adenocarcinoma (PAAD). However, there was no significant difference in GPC2 levels between sarcoma (SARC), skin cutaneous melanoma (SKCM), thymoma (THYM), and nontumor tissues. Besides, a noteworthy increase in GPC2 expression in 16 types of cancer was observed respectively in paired tumor samples compared with corresponding normal samples (Figure 1D). These results suggest that GPC2 expression is upregulated in various types of cancer, indicating that GPC2 may play a potentially pivotal role in cancer diagnosis.

Furthermore, to assess the expression of GPC2 in terms of protein level, we elicited the immunohistochemical images taking advantage of the HPA database. From **Figure 2**, it can be intuitively seen that the protein expression of GPC2 was significantly higher in 15 cancers than in normal tissues.





48

Diagnosis Value of GPC2 Across Cancers

In the examination on the tumor stage relevance, we discovered it was in 16 types of cancer that the GPC2 expression significantly increased in the early tumor stage (Figure 3), including CHOL, LUSC, LUAD, KIRP, HNSC, LIHC, ESCA, KIRC, UCEC, BLCA, COAD, READ, STAD, PRAD, THCA, and BRCA, indicating that GPC2 may have important clinical value in the early diagnosis of these tumors. The ROC curves were utilized to make an evaluation of the performance of the gene signature for diagnostic accuracy. A different AUC cutoff has been considered to indicate high diagnostic accuracy (AUC: 1.0-0.9), relative diagnostic accuracy (AUC: 0.9-0.7), or low diagnostic accuracy (AUC: 0.7-0.5). Figure 4 shows that the AUC of ROC analysis of the model has high diagnostic accuracy in 6 types of cancer, relative diagnostic accuracy in 16 types of cancer, and low diagnostic accuracy in 7 types of cancer. It is worth emphasizing that the AUC achieved 1.0 in CHOL.

Prognostic Significance of GPC2 Across Cancers

Aiming to investigate the association between GPC2 expression level and prognosis, we performed a survival association analysis for each cancer, concentrating on OS, DSS, and PFI. One the one hand, Cox proportional hazards model analysis illustrated that the expression levels of GPC2 were associated with OS in COAD (p < 0.001), PAAD (p < 0.001), acute myeloid leukemia (LAML) (p < 0.001), ACC (p < 0.001), SARC (p < 0.001), KIRC (p < 0.001), KIRC (p < 0.001), Comparison of the statement of the stat

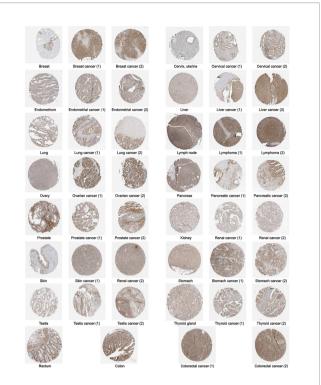
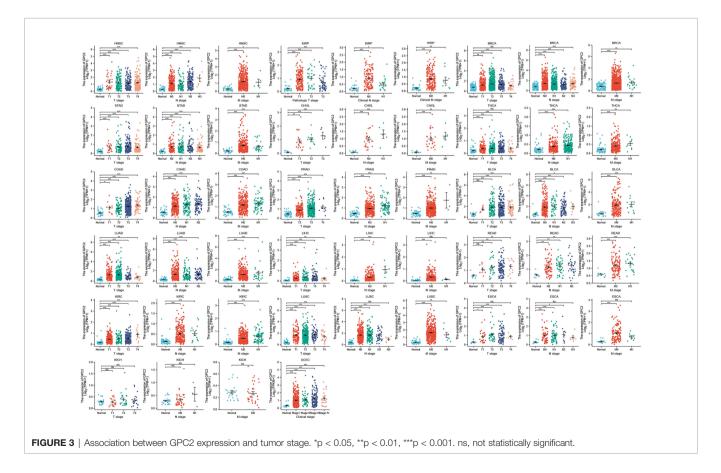
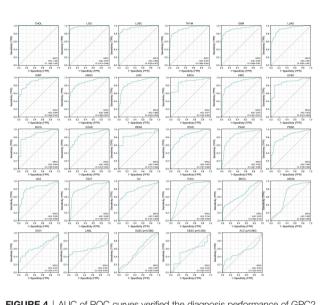


FIGURE 2 | The protein expression of GPC2 in immunohistochemical images of normal (left) and tumor (right) groups.





 $\ensuremath{\mbox{Figure 4}}\xspace$ | AUC of ROC curves verified the diagnosis performance of GPC2 in the TCGA cohort.

0.001), BLCA (p = 0.001), PRAD (p = 0.003), brain lower grade glioma (LGG) (p = 0.003), HNSC (p = 0.005), mesothelioma (MESO) (p = 0.005), THYM (p = 0.009), LIHC (p = 0.013), ESCA (p = 0.016), BRCA (p = 0.035), UCEC (p = 0.035), uveal

melanoma (UVM) (p = 0.049), and THCA (p = 0.049) (**Figure 5**). On the other hand, GPC2 was a low-risk factor in PAAD, LAML, BLCA, LGG, HNSC, THYM, and ESCA, while it was a high-risk factor in other types of cancer, especially PRAD (hazard ratio = 10.20) (**Figure 5**). Kaplan–Meier survival analysis also demonstrated that among patients with PAAD, LAML, BLCA, LGG, HNSC, THYM, and ESCA, high GPC2 expression was associated with better OS, while in patients with COAD, ACC, SARC, KIRC, PRAD, MESO, LIHC, BRCA, UCEC, UVM, and THCA, those with high GPC2 expression had shorter survival times.

Moreover, DSS data analysis presented in **Figure 6** reflected associations between low GPC2 expression and poor prognosis in patients with BLCA (p = 0.001), PAAD (p = 0.002), HNSC (p = 0.007), KIRP (p = 0.013), LGG (p = 0.015), and ESCA (p = 0.047); however, in patients with other 8 types of cancer, GPC2 expression exhibited the opposite relationship with prognosis.

Referring to associations between GPC2 expression and PFI, high expression of GPC2 was associated with poor PFI in ACC (p < 0.001), PRAD (p < 0.001), KIRC (p = 0.001), COAD (p = 0.001), BRCA (p = 0.001), MESO (p = 0.002), STAD (p = 0.003), PCPG (p = 0.003), THCA (p = 0.014), READ (p = 0.039), and CHOL (p = 0.042), while low expression was associated with poor PFI in patients with PAAD (p = 0.003), THYM (p = 0.004), GBM (p = 0.013), BLCA (p = 0.015), HNSC (p = 0.021), KIRP (p = 0.025), and LGG (p = 0.026) (**Figure 7**).

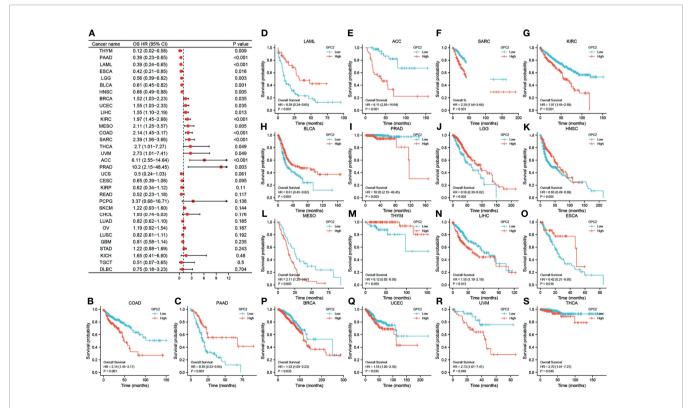


FIGURE 5 | Association between GPC2 expression and overall survival (OS). (A) Forest plot of OS associations in 33 types of tumor. (B–S) Kaplan–Meier analysis of the association between GPC2 expression and OS.

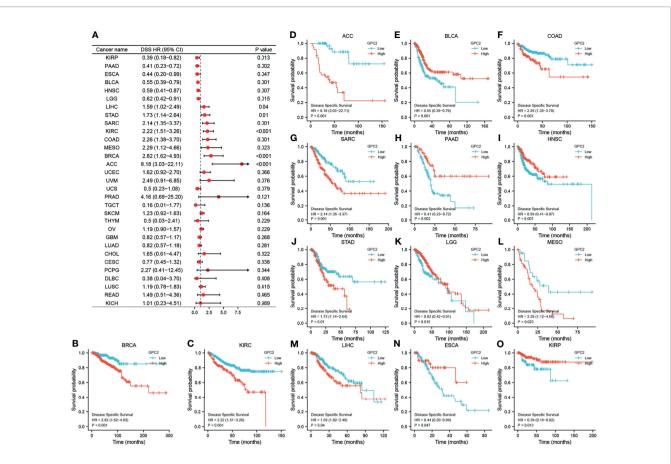


FIGURE 6 | Association between GPC2 expression levels and disease-specific survival (DSS). (A) Forest plot of association of GPC2 expression and DSS in 33 types of tumor. (B–O) Kaplan–Meier analysis of the association between GPC2 expression and DSS.

Relationship Between GPC2 Expression Level and Tumor Immune Cell Infiltration

Our result of CIBERSORT revealed that for most types of cancer, the association between levels of immune cell infiltration and GPC2 expression was significant (**Figure 8**). Especially, GPC2 expression level had a positive relation with infiltrating T cells, T helper cells, Tcm, Th17 cells, and Th2 cells in THYM.

Moreover, a co-expression analysis was carried out in 33 tumors, in order to detect the relationships between GPC2 expression and immune-related genes. From the heat map (**Figure 9**), we can intuitively see that almost all immune-related genes were co-expressed with GPC2, and except LUSC and SARC, majority of immune-related genes were positively correlated with GPC2 in all types of tumor (p < 0.05).

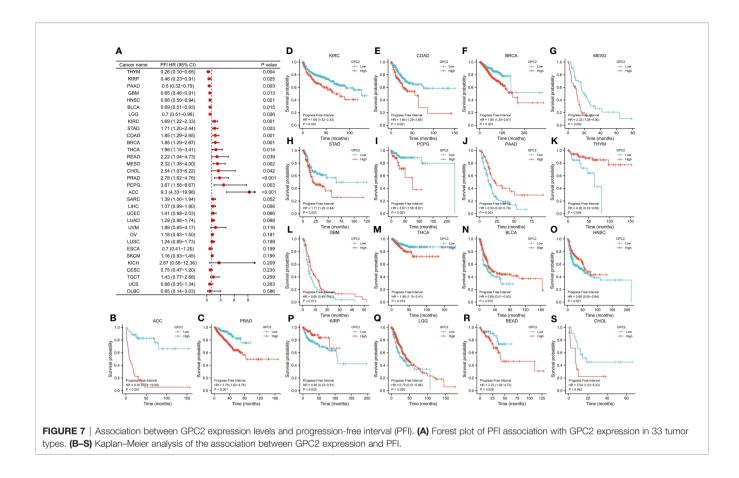
Correlation of GPC2 Expression With DNA Methylation

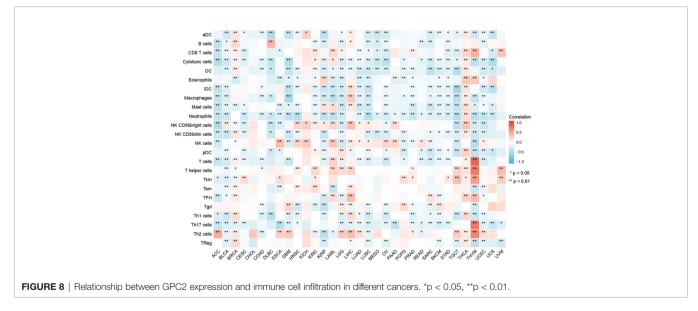
The UALCAN online tool provided a platform for us to investigate promoter methylation levels of GPC2 among groups of patients and normals according to different cancers. The beta value indicates level of DNA methylation ranging from 0 (unmethylated) to 1 (fully methylated). A different beta value cutoff has been considered to indicate hypermethylation (betavalue: 0.7–0.5) or hypomethylation (beta-value: 0.3–0.25). **Figure 10** shows that the promoter methylation levels of GPC2 were significantly higher in 12 tumor groups than those in normal groups.

The mutation of the GPC2 gene in all tumor tissues was analyzed by the cBioPortal platform. 10,953 patients from the TCGA database were analyzed. The amplification of GPC2 accounted for the largest proportion of all mutation types, of which esophageal squamous cell carcinoma, esophagogastric adenocarcinoma, and CHOL had the highest occurrence rates of 8.42%, 6.42%, and 5.56%, respectively (**Figure 11**). Amplification is the most common type.

Prediction of Target miRNAs and Construction of the Co–Expressed Network

It is well known that miRNAs are able to induce gene silencing and downregulate gene expression *via* combining mRNAs. The ceRNA network is the connection built on the interaction among mRNAs, miRNAs, and their corresponding ncRNAs. NcRNAs, including circRNAs and lncRNAs, are regarded as upstream molecules, which can influence the miRNAs' function through binding miRNA response elements and further upregulating



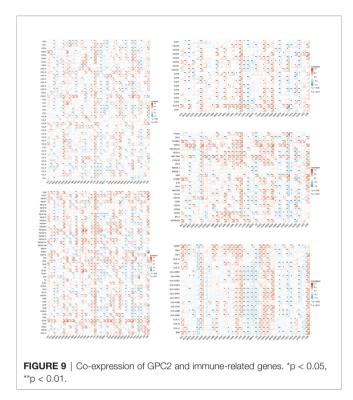


gene expression (28). In the end, we acquired 22 target miRNAs of GPC2 from five databases. However, only 8 target miRNAs can be retrieved in StarBase to predict their circRNAs and lncRNAs. As a result, 121 target lncRNAs and 149 target circRNAs were obtained about the target miRNAs of GPC2. The ceRNA networks shown in **Figure 12** were accorded to the

prediction results, which might provide a basis for us to research the potential drugs regulating GPC2.

Interacting Chemicals and Genes of GPC2

The data from the CTD database listed that GPC2 is associated with 50 chemicals, in which 21 chemicals can upregulate GPC2



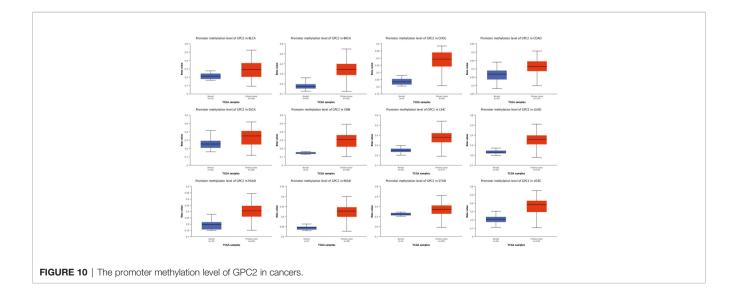
while 21 can downregulate it. Additionally, 8 chemicals were confirmed to have an effect on the expression of GPC2 with unclear specific roles (**Table 1**).

Furthermore, we discovered the top 20 relationships between GPC2 and other genes *via* chemical associations. The results showed that GPC2 is highly correlated with Synaptotagmin-Like 5 (SYTL5), Transmembrane protein 108 (TMEM108), ST8 Alpha-N-Acetyl-Neuraminide Alpha-2,8-Sialyltransferase 2 (ST8SIA2), Hes-Related Family BHLH Transcription Factor With YRPW Motif Like (HEYL), and Transmembrane protein 231 (TMEM231) (**Table 2**).

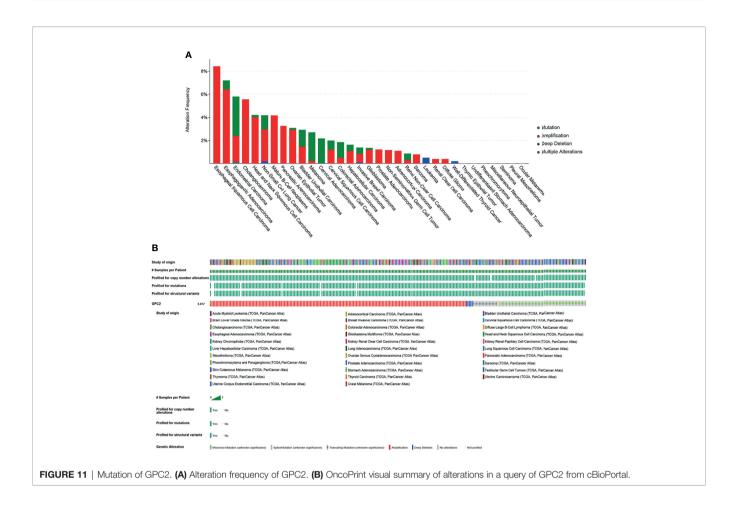
The gene–gene interaction network for GPC2 and similar genes was constructed by GeneMANIA. The results showed that the 20 most frequently altered genes closely correlated with GPC2, in which Midkine (MDK) has the most significant correlation to GPC2. Moreover, the functional analysis suggested that GPC2 and its similar genes were prominently associated with the glycosaminoglycan metabolic process, aminoglycan metabolic process, and aminoglycan biosynthetic process (**Figure 13**).

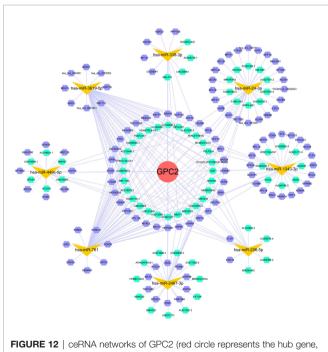
DISCUSSION

Hitherto, cancer-related research has always been a research focus in the current medical domain. 33 cancer-related data from TCGA and CCLE platforms were used to explore biomarkers suitable for broad-spectrum cancer diagnosis through gene expression difference analysis. By pan-cancer analysis, GPC2 emerged from a number of genes due to its significant upregulation in many types cancer, and we illuminate the significant difference in its expression between cancer and normal tissues in many ways and discussed its early detection value, regulatory pathways, associated genes, and compounds. GPC2 is a member of glypicans. Heretofore, GPC3 and GPC1, which show excellent diagnostic effects in specific cancer types, respectively, have monopolized most studies of glypicans. For example, GPC1, the same subfamily gene of GPC2, has been proved to be a diagnostic biomarker and therapeutic target for pancreatic cancer and trigger a wave of interest of glypicans (29). Also reported in the literature, GPC3 has been proved to have high specificity in the diagnosis of hepatocellular carcinoma and can be used as a marker to distinguish hepatocellular carcinoma from other liver tumors (17, 30). In a further study of GPC3, Tetsuya Nakatsura et al. found that it could also be used as an auxiliary indicator for the early diagnosis of melanoma (31). GPC2 was originally identified in rat brain at locus 7q22.1, encoding a 579-amino acid protein, but the mechanism of



53





yellow vs. represent the miRNAs, green hexagons represent the IncRNAs, and purple hexagons represent the circRNAs).

action has not been revealed (7, 32). The UniProt (https://www. uniprot.org/) platform predicts that GPC2 has five hydrogen sulfur bond insertion sites, and it has been reported that the unique structure of GPC2 helps to bind to the Wnt signaling pathway, thus affecting the expression of MYCN Proto-Oncogene (MYCN) and regulating the proliferation of tumor cells (33).

In our comprehensive analysis and screening of a large number of genes, GPC2 has captured our attention because of its preeminent detection performance. Except for cancers with no normal tissue data or only an insufficient number of normal tissue samples, our results detected the significant differences of GPC2 expression between tumors and normal tissues of 20 forms of cancer. Among them, GPC2 expression levels were upregulated in BLCA, BRCA, CESC, CHOL, COAD, ESCA, HNSC, and so on. A mere one form of cancer (PAAD) shows a downregulation between PAAD tumor tissues and nontumor tissues.

Unfortunately, due to the insufficient number of normal samples in the database, the data of GPC2 in the expression difference analysis of THYM, SKCM, and SARC were not statistically significant. In cancers such as LGG, UCS, TGCT, OV, LAML, DLBC, ACC, UVM, and MESO, the analysis was not successful due to the lack of normal group samples. With the accumulation of datasets, this part is worth a further exploration

TABLE 1 | Interacting chemicals of GPC2 from CTD.

Chemical name	ID	Interaction actions	Chemical name	ID	Interaction actions
2,2',3',4,4',5-Hexachlorobiphenyl	C029790	Decreases	Flusilazole	C061365	Decreases
		expression			expression
2,4,4'-Trichlorobiphenyl	C081766	Increases	Folic acid	D005492	Decreases
		expression			expression
2,4,5,2',4',5'-Hexachlorobiphenyl	C014024	Increases	Glycidol	C004312	Decreases
		expression			expression
2,4,5,2',5'-Pentachlorobiphenyl	C009828		Methyleugenol	C005223	Increases
		expression	_		expression
2,5,2',5'-Tetrachlorobiphenyl	C009407		Paraquat	D010269	Decreases
		expression			expression
4-(5-Benzo(1,3)dioxol-5-yl-4-pyridin-2-yl-1H-imidazol-2-yl)	C459179		PCB 180	C410127	
benzamide		expression		0040040	expression
Acetamide	C030686		Pentanal	C046012	Increases
A to	D000000	expression		D010000	expression
Acetaminophen	D000082		Phenylmercuric acetate	D010662	Decreases
	D000100	expression		D011441	expression
Acrylamide	D020106		Propylthiouracil	D011441	Increases
Amindarana	D000600	expression	Cadium dutamata	D010070	expression
Amiodarone	D000638	Affects expression	Sodium glutamate	D012970	Increases
Ammonium chloride	D000642	Affects expression	Sunitinib	D077010	expression Decreases
Annonium chionde	D000043	Allects expression	Sulliulius	D077210	
Atrazine	0001280	Increases	T-2 toxin	D013605	expression Decreases
Alidzine	D001200	expression	1-2 10/11	D013003	expression
Benzo(a)pyrene	D001564		Testosterone	D013739	Increases
Delizo(a)pyrelie	D001304	expression	restosterone	D010/03	expression
Bisphenol A	C006780		Tetrachlorodibenzodioxin	D013749	Decreases
	0000700	expression		0010740	expression
Butyraldehyde	C018475	Increases	Tetracycline	D013752	Affects expression
		expression			
Chlorpromazine	D002746		Thioacetamide	D013853	Affects expression
Cuprizone	D003471	1	Titanium dioxide	C009495	Decreases
		expression			expression
Cyclosporine	D016572	Affects expression	Tobacco smoke pollution	D014028	Decreases
					expression
Dexamethasone	D003907	Decreases	Trichostatin A	C012589	Affects expression
		expression			
Dietary Fats	D004041	Increases	Tris(1,3-dichloro-2-propyl)	C016805	Increases
		expression	phosphate		expression
Diethylhexyl phthalate	D004051	Increases	Tunicamycin	D014415	Decreases
		expression			expression
Dorsomorphin	C516138	Decreases	Urethane	D014520	Decreases
		expression			expression
Estradiol	D004958	Increases	Valproic acid	D014635	Decreases
		expression			expression
Ethinyl estradiol	D004997	Affects expression	Vanadates	D014638	Increases
					expression
Exemestane	C056516	Increases	Vorinostat	D077337	Decreases
		expression			expression

in the future. For instance, recent studies have manifested that GPC2 expression is low in normal pediatric tissues but elevated in optic neuroblastoma tissues, and it has been selected as an excellent chimeric antigen receptor T cell therapy target for optic neuroblastoma, and its therapeutic effect is attracting much attention (16).

In addition, GPC2 expression was significantly increased in 16 cancers in paired sample expression differential analysis. Immunohistochemical analysis confirmed higher levels of GPC2 protein at the protein level in almost all cancers. By and large, these findings confirm that GPC2 expression is upregulated in a

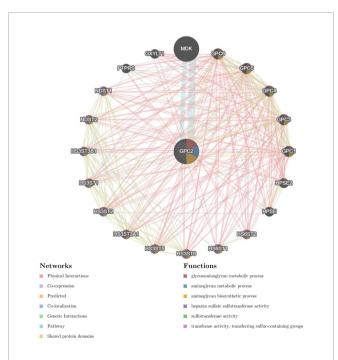
variety of cancers, suggesting that the prospect of GPC2 in cancer diagnosis is worth looking forward to.

For the time being, the early cancer detection is of great clinical significance, to push back the frontier of the early cancer detection; thereby, we explored the differential expression of GPC2 in the samples marked with cancer staging information. Analysis showed an early elevation of GPC2 in 16 of the 17 cancers in which staging and normal control samples were collected. The AUC of the ROC curve also confirmed the superior performance of GPC2 in the diagnosis of multiple cancers. GPC2 showed high diagnostic accuracy in 6 forms of

TABLE 2 | Relationship of GPC2 with genes via chemical interaction, based on the CTD database.

Gene	Similarity index	Common interacting chemicals
SYTL5	0.3929	27
TMEM108	0.3676	23
ST8SIA2	0.3580	28
HEYL	0.3373	24
TMEM231	0.3333	30
CDH18	0.3284	22
DCAF17	0.3281	22
SLC25A27	0.3253	23
DACT1	0.3243	31
DOK6	0.3194	22
KNDC1	0.3188	23
ANK1	0.3163	36
GPR137C	0.3151	27
SLITRK4	0.3143	22
TESMIN	0.3143	21
PXYLP1	0.3125	22
USP31	0.3117	28
MFAP3L	0.3111	29
PPFIA3	0.3108	25
RCOR2	0.3103	33

cancer (AUC: 1.0–0.9), and it is worth noting that 1.0 was reached in CHOL. Sixteen cancer forms showed relative diagnostic accuracy (AUC: 0.9–0.7). To investigate the association between GPC2 expression levels and prognosis, survival association analysis was performed using Kaplan-Meier survival curves for each type of cancer, including OS, DSS, and PFI. Combining these results, we found that high GPC2 expression had a good prognosis in PAAD, BLCA, LGG, HNSC,





ESCA, THYM, LAML, and GBM and a poor prognosis in COAD, ACC, SARC, KIRC, PRAD, MESO, LIHC, BRCA, UCEC, UVM, and THCA.

By understanding the relationship between GPC2 gene expression and the level of tumor immune cell infiltration, we can find that the expression of GPC2 is mostly negatively correlated with the level of immune cell infiltration. GPC2 is believed to be involved in the transduction of the Wnt/ β -catenin signaling pathway, which can regulate the differentiation and development of macrophages, B cells, and other immune cells and regulates the immune response process through multiple ways (34–36), These may also be the mechanism of GPC2 affecting the number of immune cells. This predicts that GPC2 is a good indicator that can reveal the occurrence of cancer *in vivo* from the side and play a very good supporting role in the diagnosis of tumor. Also, there is a significant positive correlation between GPC2 and immune-related genes.

From the results interpreted in the cBioPortal platform, we know that GPC2 is mutated in most forms of tumors. Thereinto, the incidence of esophageal squamous cell carcinoma, esophagogastric adenocarcinoma, and CHOL is the highest, which suggests that we should pay attention to the relationship between GPC2 gene mutation and digestive system tumors.

In our study, an elevated methylation level of the GPC2 promoter and a high expression level of GPC2 appeared simultaneously, which is not uncommon in tumor tissues. Smith et al. discussed several possible mechanisms of promoter DNA hypermethylation leading to paradoxical gene activation in detail, such as binding to transcription inhibitors, combining to remote control elements, or inducing alternative promoter activation (37). This study shows that there is a more complex network mechanism for gene expression regulation (37, 38). In order to demonstrate the upstream and downstream expression mechanisms of GPC2 in vivo more comprehensively, we constructed an intuitive ceRNA expression network containing ncRNAs, circRNAs, and lncRNAs. Based on these prediction results, we identified compounds that may regulate GPC2 expression and constructed the gene interaction network of 20 genes that are most closely related to GPC2 through chemical association.

To put it in a nutshell, we found that GPC2 was widely differentially expressed between tumor tissues and normal tissues through pan-cancer analysis and revealed the correlation between GPC2 expression and clinical prognosis. Our findings suggest that GPC2 has the potential to become an independent prognostic factor for many tumors and that the level of GPC2 expression may vary in different types of tumor. In the most recent study by Clevers et al., GPC2 is designed as a therapeutic target for optic neuroblastoma (39). By silencing GPC2, Wnt/β-catenin signaling is inactivated and MYCN expression is reduced, which is a driver of optic neuroblastoma. The specific role of GPC2 in each tumor needs to be further studied. Furthermore, the analysis results of tumor immune cell infiltration level and immune-related genes also showed that the expression level of GPC2 was mostly positively correlated with immune-related expression level. We also investigated GPC2 from the aspects of methylation level, immunohistochemical analysis, and mutation analysis, which will

be helpful to further elucidate the mechanism of GPC2 in tumor development in the future.

DATA AVAILABILITY STATEMENT

Publicly available datasets were analyzed in this study. These data can be found as follows. The RNA sequencing data, somatic mutation data, and clinicopathological and survival data of 33 cancers were downloaded from TCGA (https://www.cancer.gov/ about-nci/organization/ccg/research/structural-genomics/tcga). Tumor cell line data were downloaded from the CCLE database (https://portals.broadinstitute.org/ccle/). GPC2 expressions in 31 various tissues were downloaded from GTEx (https:// commonfund.nih.gov/GTEx). Immunohistochemistry images of GPC2 protein expression were downloaded from the Human Protein Atlas (HPA) (http://www.proteinatlas.org/). The methylation HM450 data were downloaded from cBioPortal database (http://www.cbioportal.org/).

REFERENCES

- Iskandar AC, Rochmawati E, Wiechula R. Patient's Experiences of Suffering Across the Cancer Trajectory: A Qualitative Systematic Review Protocol. J Adv Nurs (2021) 77(2):1037–42. doi: 10.1111/jan.14628
- Singh AK, McGuirk JP. CAR T Cells: Continuation in a Revolution of Immunotherapy. *Lancet Oncol* (2020) 21(3):e168–78. doi: 10.1016/S1470-2045(19)30823-X
- Kennedy LB, Salama AKS. A Review of Cancer Immunotherapy Toxicity. CA Cancer J Clin (2020) 70(2):86–104. doi: 10.3322/caac.21596
- Yiping Y. Cancer Immunotherapy: Harnessing the Immune System to Battle Cancer. J Clin Invest (2015) 125(9):3335–7. doi: 10.1172/JCI83871
- Srivastava S, Hanash S. Pan-Cancer Early Detection: Hype or Hope? Cancer Cell (2020) 38(1):23–4. doi: 10.1016/j.ccell.2020.05.021
- Blum A, Wang P, Zenklusen JC. SnapShot: TCGA-Analyzed Tumors. *Cell* (2018) 173(2):530. doi: 10.1016/j.cell.2018.03.059
- Filmus J, Capurro M, Rast J. Glypicans. Genome Biol (2008) 9(5):224–4. doi: 10.1186/gb-2008-9-5-224
- Filmus J, Selleck SB. Glypicans: Proteoglycans With a Surprise. J Clin Invest (2001) 108(4):497–501. doi: 10.1172/JCI200113712
- Li N, Gao W, Zhang YF, Ho M. Glypicans as Cancer Therapeutic Targets. *Trends Cancer* (2018) 4:741–54. doi: 10.1016/j.trecan.2018.09.004
- Rauvala H, Paveliev M, Kuja-Panula J, Kulesskaya N. Inhibition and Enhancement of Neural Regeneration by Chondroitin Sulfate Proteoglycans. *Neural Regener Res* (2017) 12(5):687–91. doi: 10.4103/1673-5374.206630
- Lugert S, Kremer T, Jagasia R, Herrmann A, Aigner S, Giachino C, et al. Glypican-2 Levels in Cerebrospinal Fluid Predict the Status of Adult Hippocampal Neurogenesis. *Sci Rep* (2017) 7:46543. doi: 10.1038/srep46543
- Kurosawa N, Chen G-Y, Kadomatsu K, Ikematsu S, Sakuma S, Muramatsu T. Glypican-2 Binds to Midkine: The Role of Glypican-2 in Neuronal Cell Adhesion and Neurite Outgrowth. *Glycoconjugate J* (2001) 18(6):499–507. doi: 10.1023/ a:1016042303253
- Zhang T, Liu Y, Ren X, Wang Z, Wang H. Glypican 2 Regulates Cell Proliferation and Metastasis in Thyroid Cancer Cells. *Mol Cell Toxicol* (2020) 16(2):203–9. doi: 10.1007/s13273-020-00073-x
- Smith FI, Qu Q, Hong SJ, Kim KS, Gilmartin TJ, Head SR. Gene Expression Profiling of Mouse Postnatal Cerebellar Development Using Oligonucleotide Microarrays Designed to Detect Differences in Glycoconjugate Expression. *Gene Expr Patterns* (2005) 5(6):740–9. doi: 10.1016/j.modgep.2005.04.006
- Appelbaum JS, Pinto N, Orentas RJ. Promising Chimeric Antigen Receptors for Non-B-Cell Hematological Malignancies, Pediatric Solid Tumors, and Carcinomas. Amsterdam, Netherlands: Elsevier. (2020). pp. 137–63.

AUTHOR CONTRIBUTIONS

YF contributed to the conception and design of the study. GC, DqL, NZ, DyL, JZ, and HL drafted the manuscript. ZL, XL, QC, CZ, YL, Y-TC, and QR collected and analyzed the data. NW and YF revised the manuscript. All authors contributed to the manuscript revision and read and approved the submitted version.

FUNDING

This study was funded by the Hong Kong Health and Medical Research Fund (Project Code: 18192141), RGC General Research Fund (Project Code: 17121419; 17119621), Hong Kong Chinese Medicine Development Fund (Project Code: 19SB2/002A), Wong's donation (Project Code: 200006276), and a donation from the Gaia Family Trust of New Zealand (Project Code: 200007008).

- Bosse KR, Raman P, Zhu Z, Lane M, Martinez D, Heitzeneder S, et al. Identification of GPC2 as an Oncoprotein and Candidate Immunotherapeutic Target in High-Risk Neuroblastoma. *Cancer Cell* (2017) 32(3):295–309.e12. doi: 10.1016/j.ccell.2017.08.003
- Raman S, Buongervino SN, Lane MV, Zhelev DV, Zhu Z, Cui H. A GPC2 Antibody-Drug Conjugate is Efficacious Against Neuroblastoma and Small-Cell Lung Cancer via Binding a Conformational Epitope. *Cell Rep Med* (2021) 2(7):100344. doi: 10.1016/j.xcrm.2021.100344
- Buongervino S, Lane MV, Garrigan E, Zhelev DV, Dimitrov DS, Bosse KR Antibody-Drug Conjugate Efficacy in Neuroblastoma: Role of Payload, Resistance Mechanisms, Target Density, and Antibody Internalization. *Mol Cancer Ther* (2021) 20:2228–39. doi: 10.1158/1535-7163.MCT-20-1034
- Foster J, Griffin C, Stern A, Brimley C, Buongervino S, Storm P, et al. IMMU-16. Targeting Glypican 2 (Gpc2) On Pediatric Malignant Brain Tumors With Mrna Car T Cells. *Neuro-Oncology* (2021) 23(Supplement1):i30. doi: 10.1093/ neuonc/noab090.123
- Orentas RJ, Yang JJ, Wen X, Wei JS, Mackall CL, Khan J. Identification of Cell Surface Proteins as Potential Immunotherapy Targets in 12 Pediatric Cancers. *Front Oncol* (2012) 2:194. doi: 10.3389/fonc.2012.00194
- Li N, Torres MB, Spetz MR, Wang R, Peng L, Tian M, et al. CAR T Cells Targeting Tumor-Associated Exons of Glypican 2 Regress Neuroblastoma in Mice. Cell Rep Med (2021) 2(6):100297. doi: 10.1016/j.xcrm.2021.100297
- Xu N, Wu YP, Yin HB, Xue XY, Gou X. Molecular Network-Based Identification of Competing Endogenous RNAs and mRNA Signatures That Predict Survival in Prostate Cancer. J Transl Med (2018) 16(1):274. doi: 10.1186/s12967-018-1637-x
- Liu JQ, Liao XW, Wang XK, Yang CK, Zhou X, Liu ZQ, et al. Prognostic Value of Glypican Family Genes in Early-Stage Pancreatic Ductal Adenocarcinoma After Pancreaticoduodenectomy and Possible Mechanisms. BMC Gastroenterol (2020) 20(1):415. doi: 10.1186/s12876-020-01560-0
- Smoot BJ, Wong JF, Dodd MJ. Comparison of Diagnostic Accuracy of Clinical Measures of Breast Cancer-Related Lymphedema: Area Under the Curve. *Arch Phys Med Rehabil* (2011) 92(4):603–10. doi: 10.1016/j.apmr.2010.11.017
- Chandrashekar DS, Bashel B, Balasubramanya SAH, Creighton CJ, Ponce-Rodriguez DS, Chakravarthi BVSK, et al. UALCAN: A Portal for Facilitating Tumor Subgroup Gene Expression and Survival Analyses. *Neoplasia* (2017) 19 (8):649–58. doi: 10.1016/j.neo.2017.05.002
- Li JH, Liu S, Zhou H, Qu LH, Yang JH. Starbase V2.0: Decoding miRNA-ceRNA, miRNA-ncRNA and Protein-RNA Interaction Networks From Large-Scale CLIP-Seq Data. Nucleic Acids Res (2014) 42(Database issue):D92–7. doi: 10.1093/nar/gkaa891
- Davis AP, Grondin CJ, Johnson RJ, Sciaky D, Wiegers J, Wiegers TC, et al. Comparative Toxicogenomics Database (CTD): Update 2021. Nucleic Acids Res (2021) 49(D1):D1138–43. doi: 10.1093/nar/gkaa891

- Salmena L, Poliseno L, Tay Y, Kats L, Pandolfi PP. A ceRNA Hypothesis: The Rosetta Stone of a Hidden RNA Language? *Cell* (2011) 146(3):353–8. doi: 10.1016/j.cell.2011.07.014
- Melo SA, Luecke LB, Kahlert C, Fernandez AF, Gammon ST, Kaye J. Glypican-1 Identifies Cancer Exosomes and Detects Early Pancreatic Cancer. *Nature* (2015) 523(7559):177–82. doi: 10.1038/nature14581
- Zhou F, Shang W, Yu X, Tian J. Glypican-3: A Promising Biomarker for Hepatocellular Carcinoma Diagnosis and Treatment. *Med Res Rev* (2018) 38 (2):741–67. doi: 10.1002/med.21455
- Nakatsura T, Kageshita T, Ito S, Wakamatsu K, Monji M, Ikuta Y, et al. Identification of Glypican-3 as a Novel Tumor Marker for Melanoma. *Clin Cancer Res* (2004) 10(19):6612–21. doi: 10.1158/1078-0432.CCR-04-0348
- Herndon ME, Lander AD. A Diverse Set of Developmentally Regulated Proteoglycans Is Expressed in the Rat Central Nervous System. *Neuron* (1990) 4(6):949–61. doi: 10.1016/0896-6273(90)90148-9
- Li N, Spetz MR, Li D, Ho M. Advances in Immunotherapeutic Targets for Childhood Cancers: A Focus on Glypican-2 and B7-H3. *Pharmacol Ther* (2021) 223:107892. doi: 10.1016/j.pharmthera.2021.107892
- 34. Xu WD, Wang J, Yuan TL, Li YH, Yang H, Liu Y, et al. Interactions Between Canonical Wnt Signaling Pathway and MAPK Pathway Regulate Differentiation, Maturation and Function of Dendritic Cells. Cell Immunol (2016) 310:170–7. doi: 10.1016/j.cellimm.2016.09.006
- Grzywacz B, Kataria N, Kataria N, et al. Natural Killer-Cell Differentiation by Myeloid Progenitors. Blood (2011) 117(13):3548–58. doi: 10.1182/blood-2010-04-281394
- Luis TC, Naber BA, Roozen PP, et al. Canonical Wnt Signaling Regulates Hematopoiesis in a Dosage-Dependent Fashion. *Cell Stem Cell* (2011) 9 (4):345–56. doi: 10.1016/j.stem.2011.07.017

- Smith J, Sen S, Weeks RJ, Eccles MR, Chatterjee A. Promoter DNA Hypermethylation and Paradoxical Gene Activation. *Trends Cancer* (2020) 6(5):392–406. doi: 10.1016/j.trecan.2020.02.007
- Pellacani D, Packer RJ, Frame FM, et al. Interactions Between Canonical Wnt Signaling Pathway and MAPK Pathway Regulate Differentiation, Maturation and Function of Dendritic Cells. *Mol Cancer* (2011) 10:94. doi: 10.1186/1476-4598-10-94
- Clevers H, Nusse R. Wnt/beta-Catenin Signaling and Disease. Cell (2012) 149 (6):1192–205. doi: 10.1016/j.cell.2012.05.012

Conflict of Interest: The authors declare that the research was conducted in the absence of any commercial or financial relationships that could be construed as a potential conflict of interest.

Publisher's Note: All claims expressed in this article are solely those of the authors and do not necessarily represent those of their affiliated organizations, or those of the publisher, the editors and the reviewers. Any product that may be evaluated in this article, or claim that may be made by its manufacturer, is not guaranteed or endorsed by the publisher.

Copyright © 2022 Chen, Luo, Zhong, Li, Zheng, Liao, Li, Lin, Chen, Zhang, Lu, Chan, Ren, Wang and Feng. This is an open-access article distributed under the terms of the Creative Commons Attribution License (CC BY). The use, distribution or reproduction in other forums is permitted, provided the original author(s) and the copyright owner(s) are credited and that the original publication in this journal is cited, in accordance with accepted academic practice. No use, distribution or reproduction is permitted which does not comply with these terms.





The Heterogeneity of Immune Cell Infiltration Landscape and Its Immunotherapeutic Implications in Hepatocellular Carcinoma

OPEN ACCESS

Edited by:

Xuyao Zhang, Fudan University, China

Reviewed by:

Shuai Wang, Harvard Medical School, United States Lijie Zhao, University of Michigan, United States

*Correspondence:

Hua Gao gaohua_2008@163.com Xin Tian tianx@zzu.edu.cn Xiaojian Zhang zhxj0524@hotmail.com Quancheng Kan kanqc@zzu.edu.cn

Specialty section:

This article was submitted to Cancer Immunity and Immunotherapy, a section of the journal Frontiers in Immunology

Received: 24 January 2022 Accepted: 11 February 2022 Published: 10 March 2022

Citation:

Guo Y, Yang J, Ren K, Tian X, Gao H, Tian X, Zhang X and Kan Q (2022) The Heterogeneity of Immune Cell Infiltration Landscape and Its Immunotherapeutic Implications in Hepatocellular Carcinoma. Front. Immunol. 13:861525. doi: 10.3389/fimmu.2022.861525 Yuanyuan Guo^{1,2}, Jing Yang^{1,2}, Kaidi Ren^{1,2}, Xueke Tian^{1,2}, Hua Gao^{3*}, Xin Tian^{1,2*}, Xiaojian Zhang^{1,2*} and Quancheng Kan^{1,2*}

¹ Department of Pharmacy, The First Affiliated Hospital of Zhengzhou University, Zhengzhou, China, ² Henan Key Laboratory of Precision Clinical Pharmacy, Zhengzhou University, Zhengzhou, China, ³ Department of Radiotherapy, The First Affiliated Hospital of Zhengzhou University, Zhengzhou, China

Immunotherapy, closely associated with immune infiltration and tumor mutation burden (TMB), is emerging as a promising strategy for treating tumors, but its low response rate in hepatocellular carcinoma (HCC) remains a major challenge. Herein, we applied two algorithms to uncover the immune infiltration landscape of the immune microenvironment in 491 HCC patients. Three immune infiltration patterns were defined using the CIBERSORT method, and the immune cell infiltration (ICI) scores were established using principal component analysis. In the high ICI score group, the activation of the Wnt/β-catenin pathway was significantly enriched and expressions of immune checkpoint genes increased, which showed a pessimistic outcome. The low ICI score group was characterized by increased TMB and enrichment of metabolism-related pathways. Further analysis found that the ICI score exhibited a significant difference in age ≥65/age <65, grade I/grade II-IV, and response to immunotherapy. Moreover, the CTNNB1 mutation status was found to be closely associated with prognosis and immunotherapeutic efficiency, significantly affecting the ICI score and TMB, which might be regarded as a potential marker for the treatment of HCC. The evaluation of immune infiltration patterns can improve the understanding of the tumor immune microenvironment and provide new directions for the study of individualized immunotherapy strategies for HCC.

Keywords: immune cell infiltration, tumor heterogeneity, immune microenvironment, hepatocellular carcinoma, tumor mutational burden

Abbreviations: HCC, hepatocellular carcinoma; TMB, tumor mutational burden; ICI, immune cell infiltration; TME, tumor microenvironment; t-SNE, t-distributed stochastic neighbor embedding; GSEA, gene set enrichment analysis; PCA, principal component analysis.

INTRODUCTION

Liver cancer ranks as the fourth leading cause of most common malignancies in the world (1, 2), 90% of which is hepatocellular carcinoma (HCC). At present, the main treatment options are liver transplantation, transarterial chemoembolization, radiofrequency ablation, surgery in the early stage, and molecular targeting agents (e.g., sorafenib, regorafenib, and lenvatinib) in the advanced stage (3). Although these treatment strategies lead to a modest survival benefit, the overall survival of HCC is still challenging due to the heterogeneity of HCC.

Immunotherapy can recognize and eliminate tumor cells by activating and enhancing the host immune system. Emerging evidence has highlighted that immunotherapy has been clinically proven to be an effective treatment for a variety of cancers (4). However, a major limitation is that only 10% to 20% of cancer patients can benefit from this treatment, which could be due to the difference in the amount of immune cell infiltration or somatic variants in tumor types (5). Therefore, it is an urgent need to identify the new therapeutic markers to determine the ideal HCC subgroups for immunotherapy.

Immune cells and stromal cells constitute the main part of the tumor microenvironment (TME), which are responsible for tumor spread, recurrence, metastasis, the effect of immunotherapy, and prognosis (6-9). For example, tumorinfiltrating CD4⁺ and CD8⁺ T lymphocytes play an antitumor role, which is associated with favorable prognosis (10-14). Tumor-associated macrophages (TAMs) exert a tumorpromoting effect by secreting immunosuppressive factors, thereby reducing survival outcomes (15, 16). In addition, excessive invasion of stromal components in tumor tissues hinders the transport of immune cells to tumor, suggesting that the intercellular communication in TME, rather than the single-cell population, is more likely to affect the occurrence and development of tumors (17-20). Thus, it is more important to elucidate the composition and characteristics of the complex tumor immune medium than in single-cell populations in TME.

In the study, we performed two calculation algorithms, Cell-type Identification by Estimating Relative Subsets of RNA Transcripts (CIBERSORT) and ESTIMATE, to analyze the gene-expression profiles of HCC samples and comprehensively describe the immune landscape of HCC. Besides, we classified HCC samples into three immune subtypes according to the immune infiltration patterns. The ICI score was established to characterize various immune statuses, which can accurately predict HCC patients' response and prognosis to immunotherapy.

MATERIALS AND METHODS

Data Collection From TCGA and GEO Databases

A total of 376 HCC samples were downloaded from TCGA database (https://portal.gdc.cancer.gov/), and 115 samples were downloaded from GSE76427 (https://www.ncbi.nlm.nih.gov/geo/query/acc.cgi?acc=GSE76427). The detailed description of

the clinical information of HCC samples is provided in **Supplementary Table S1**. Another 80 samples from GSE10141 were used as an external validation set. To be consistent with the data of the microarrays (21), the fragments per kilobase million (FPKM) values in TCGA dataset were normalized as TPMs (transcripts per kilobase million). Then the TCGA-LIHC and GEO data were converted to log2 (TPM +1) to avoid negative values. Meanwhile, the deviation between different datasets caused by batch effects was removed using the "ComBat" algorithm (22).

Immune Profile Analysis

The "CIBERSORT" (Cell-type Identification by Estimating Relative Subsets of RNA Transcripts) algorithm was used to assess the proportion of distinct immune cells in each sample from TCGA-LIHC and GSE76427 datasets. The principle was to infer the proportion of cell types from tumor samples with mixed cell types using support vector regression based on the signature of 22 different immune cells (LM22, including B cells, T cells, natural killer cells, monocytes, macrophages, dendritic cells, and mast cells). Using the gene expression signature of LM22 as a reference, the "CIBERSORT" R package was used to infer the composition of immune cells in HCC samples by the deconvolution algorithm (23).

The "MCP-counter" (24) (Microenvironment Cell Populations-counter) algorithm was used to obtain information about the abundance of distinct specific cell lineage (including nine different cell types such as T cells, cytotoxic T cells, NK cells, and monocytic lineage) infiltration in HCC samples with or without CTNNB1. It was also a deconvolution method that used marker genes to quantify the relative abundance of immune cells by the "MCPcounter" R package.

Tumor Microenvironment Analysis

ImmuneScore, StromalScore, and ESTIMATEScore were quantified for each HCC sample by the ESTIMATE algorithm (25). ImmuneScore captured the infiltration of immune cells, while StromalScore represented the presence of stroma in tumor tissue. Specifically, ESTIMATEScore was calculated as the sum of ImmuneScore and StromalScore.

Consensus Cluster of Tumor-Infiltrating Immune Cell Analysis

According to the immune cell infiltration profiles, the number of unsupervised clusters was assessed *via* the "ConsensuClusterPlus" R package (26). The unsupervised clustering "Pan" method was performed based on Euclidean and Ward's linkage analysis, and the procedure was repeated 1,000 times to ensure the classification stability. The result was visualized using the "heatmap" R package, and the subtype assignments were verified using t-distributed stochastic neighbor embedding (t-SNE).

Differential Gene Screening of Different Immune Infiltration Patterns

The molecular characteristics of different immunophenotypes were further explored by screening differential genes. p < 0.05

and absolute fold change >1.5 were set as the cutoff criteria, which was implemented using the "Limma" R package after running a log2 (TPM + 1) transformation.

Immune Cell Infiltration Score (ICI Score) Algorithm

According to gene expression, the unsupervised clustering method was used to classify HCC patients. Genes positively correlated with clusters were named gene signatures A, and genes negatively correlated were named gene signatures B. The dimension reduction of gene signatures A and B was performed by the "Boruta" algorithm. The signature score was extracted using principal component analysis (PCA). Then, the ICI score for each sample was defined using a method similar to the Gene expression Grade Index (27) as follows:

Immune cell infiltration (ICI) score = $\sum PC1A - \sum PC1B$

In the formula, PC1A and PC1B represented the first component of gene signature A and gene signature B, respectively.

Collection and Assessment of Tumor Mutation Burden

The somatic alteration data of the TCGA-LIHC cohort were downloaded from the TCGA data portal website (https://www. cancer.gov/tcga/). The tumor mutation burden (TMB) for each sample was determined by counting the total number of variants through the full length of exons. The "Maftool" R package (28) was used to identify the oncogenic drivers of HCC, and the somatic alterations of the oncogenic drivers were compared between high and low ICI scores. The top 20 oncogenic drivers with the highest alteration frequency were further analyzed to screen potential targets for immunotherapy.

Gene Set Enrichment Analysis

Gene set enrichment analysis (GSEA) was performed to compare the differences of a predefined set of genes between the high and low ICI score groups. The "c2.cp.kegg.v7.4symbols" downloaded from MSigDB v7.4 (Molecular Signatures Database) was chosen as the reference to calculate the gene set enrichment scores using GSEA software (v4.1.0). NOM *p*-value < 0.05 and FDR *q*-value <0.05 were considered as significant.

Evaluation of the Immunotherapy Efficacy

The response to immunotherapy was predicted by the Immune Cell Abundance Identifier (http://bioinfo.life.hust.edu.cn/ ImmuCellAI) website. The difference of the ICI score between response and non-response groups was analyzed by the Wilcoxon test. Besides, a total of 127 HCC cases with mutation information were downloaded from the cBioPortal database (https://www.cbioportal.org/). Patients who received immunotherapy were analyzed to verify the effect of CTNNB1 mutation on immunotherapy.

Statistical Analyses

All statistical analyses were performed using SPSS version 22.0 or GraphPad Prism version 7.0 or R version 4.0.3 software.

The Kaplan–Meier curve was employed for survival curve analysis with the log-rank test. Two groups were compared by the Wilcoxon test, and three or more groups were compared by the Kruskal–Wallis test. Correlation analysis was performed using the Spearman rank test. A p value less than 0.05 was regarded as statistically significant.

RESULTS

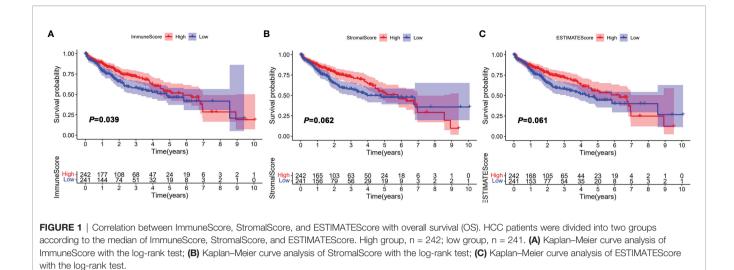
ImmuneScore Revealed More Prognostic Value in HCC Versus StromalScore

The workflow of the study design is illustrated in Figure S1. In this study, a total of 491 HCC samples from the TCGA-LIHC and GSE76427 were included. The average age of these patients was 60.4 years, and 70.7% of the patients were male, which was 2.41 times higher than that of women (Supplementary Table S1). To assess the infiltrating proportion of immune/stromal cells, the ImmuneScore, StromalScore, and ESTIMATEScore for each sample were calculated by the ESTIMATE algorithm, respectively. ImmuneScore ranged from -931.61 to 3,171.87, while the distribution of StromalScore was -1,632.97 to 1,212.68 (Supplementary Table S2). The median of ESTIMATEScore was -186.74 ranging from -2,564.58 to 3,808.98, which was calculated by integrating the two scores. According to the median, HCC patients were divided into high and low groups, and the survival analysis was performed to estimate the prognostic value of the three scores. The log-rank test showed that the difference in immune score was statistically significant, and HCC patients with low scores had poor survival outcomes (Figure 1A, p = 0.039). However, StromalScore and ESTIMATEScore showed no significant correlation with the overall survival (Figures 1B, C, p = 0.062, p = 0.061, respectively). These results suggest that the immune status of TME was more suitable for predicting the prognosis of HCC patients.

The Landscape of Immune Cell Infiltration in the TME of HCC

The abundance of 22 tumor-infiltrating immune cells in the TME of HCC was determined using the CIBERSORT algorithm, as depicted in **Supplementary Table S3**. In the immune microenvironment, M2 macrophages and resting memory $CD4^+$ T cells were the most abundant (**Figure 2A**). The abundance of different tumor-infiltrating immune cells was found to be weakly to moderately correlated. Of the 22 immune cells, $CD8^+$ T cells correlated best not only with immune score but also with $CD4^+$ T cells (**Figure 2B**). In general, the correlation heatmap showed that T cell exhaustion was the main feature of immune cell dysfunction in the tumor microenvironment, which was one of the key links of tumor immunotherapy.

Considering the interindividual difference in the proportion of immune cell infiltration, unsupervised hierarchical clustering was performed on all samples. The optimal number of clusters was three (**Supplementary Table S4**), and t-SNE analysis



confirmed that three subtypes of patients could be completely distinguished (**Figure 2C**). The clinical characteristic and immune cell proportions of each cluster are shown in **Figure 2D**. Cluster A exhibited the best prognosis, and cluster C possessed the worst outcome (**Figure 2E**). Furthermore, there were significant differences in the immune-checkpoint expressions (e.g., CTLA-4, PD-1, and TIM-3, **Figure 2F**) and HCC stage (**Supplementary Figures S2A, B**) among the three immune patterns, which were significantly correlated with tumor progression.

Then, the effect of distinct immune cell infiltration patterns on the clinical prognosis of HCC patients was further investigated. As shown in **Figure 2G**, the subjects in cluster A showed higher resting memory CD4⁺T cells, which were associated with favorable prognosis. Cluster B was defined by a high level of follicular helper T cell (Tfh) and M2 macrophages. Cluster C with a low level of CD8⁺ T cells and a high level of Treg cells had a pessimistic outcome. These results suggested that three clusters had distinct immune cell infiltration features in the composition.

Identification of Gene Subtypes of HCC Based on Immune Profiles

To reveal the underlying biological features of distinct immunophenotypes, 214 genes were obtained by differential expression analysis (**Supplementary Table S5**). Three gene clusters were identified by the unsupervised hierarchical clustering, namely, gene subtypes A–C (**Supplementary Table S4**). The transcriptomic profiles of identified gene subtypes were depicted as a heatmap in **Figure 3A**, and t-SNE analysis confirmed that patients in three subtypes could be completely distinguished (**Figure 3B**). Through Kaplan–Meier plotter analysis, we found that patients in gene subtype A presented a favorable prognosis, while those in gene subtype C had a poor prognosis (**Figure 3C**).

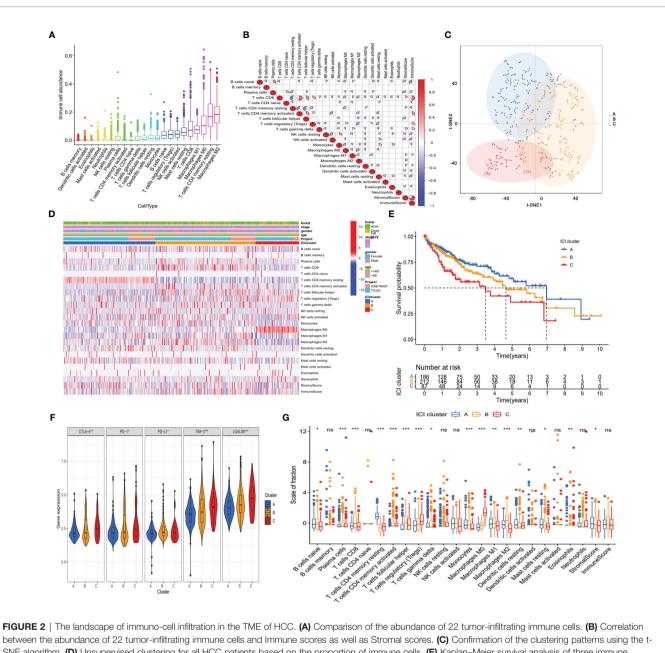
As depicted in **Figure 3D**, the three gene clusters had distinct TME features. Expression levels of immune checkpoints such as PD-1 and CTLA4 were significantly different in the three gene

subtypes (Figure 3E). Taken together, the concordance of immune profile-based genotypes with prognosis indicated that the molecular typing of HCC had important clinical prognostic significance.

Construction and Functional Enrichment Analysis of the ICI Score Based on Immune Infiltration-Related Genes

To further obtain a quantitative indicator of immune cell infiltration in HCC patients, the Boruta algorithm was used to reduce the redundant genes to obtain the optimal feature genes (**Supplementary Table S5**) and PCA was performed to construct the ICI score for each patient. **Figure 4A** shows the ICI score distribution of HCC patients in three gene subtypes. The expression of genes associated with immune checkpoints was significantly increased in the high ICI score group (**Figure 4B**). Meanwhile, the ICI score was significantly positively correlated with ImmuneScore, but not StromalScore and ESTIMATEScore (**Supplementary Figure S3**), which implied that the ICI score established could better reflect the immune status of the TME.

Additionally, the significant biological process of GO enrichment analysis for signature genes A and B is displayed in Figures 4C, D, respectively (Supplementary Tables S8, S9). The gene set enrichment analysis (GSEA) revealed that the differentially expressed genes for the high ICI score group were mainly involved in the Wnt/ β -catenin pathway (Figure 4E and Supplementary Table S10). Metabolism pathways related to fatty acid, tryptophan, and propanoate were significantly enriched in the low ICI score group (Figure 4F and Supplementary Table S11). Kaplan-Meier plotter analysis revealed that the patients in the low ICI score group had poor prognosis than those in the high ICI score group (median OS 3.32 vs. 6.29 years, Figure 4G and Supplementary Table S12). In addition, the ICI score also exhibited good performance in predicting prognosis in external validation cohort (GSE10141, Figure 4H) and internal validation cohorts (TCGA-LIHC, Figure 5A; GSE76427, Figure 5D).



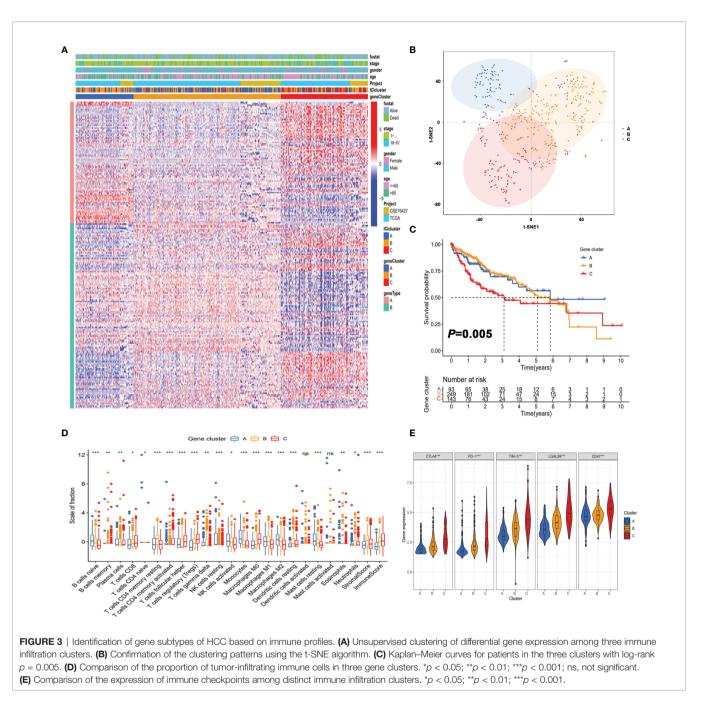
SNE algorithm. (D) Unsupervised clustering for all HCC patients based on the proportion of immune cells. (E) Kaplan–Meier survival analysis of three immune infiltration clusters. (F) Comparison of the expression of immune checkpoints among distinct immune infiltration clusters. *p < 0.05; **p < 0.01; ***p < 0.001. (G) Comparison of fraction of tumor-infiltrating immune cells in immune infiltration clusters. *p < 0.05; **p < 0.01; ***p < 0.001; mmune cells in immune infiltration clusters. *p < 0.05; **p < 0.001; ***p <

The Role of the ICI Score in the Prediction of Immunotherapeutic Benefits

To further determine the role of the ICI score in predicting the benefit of immunotherapy, the ImmuCell analysis website was used to predict the therapeutic effect of immune checkpoint inhibitors based on the transcriptome. Patients with a high ICI score in both TCGA-LIHC and GSE76427 cohorts had better prognosis than those in the low score group (**Figures 5A, D**). As shown in **Figures 5B, E**, the ICI score of the immunotherapy response group was lower than that of the non-response group.

Besides, the objective response rate to immunotherapy was higher in the high ICI score group, which indicated that the ICI score was associated with objective response to immunotherapy (**Figures 5C, F**). Overall, these data manifested that ICI score could better predict the response to immunotherapy.

To further explore the utility of the ICI score in predicting the clinic therapeutic benefits in HCC patients, we analyzed the correlation between ICI score and clinical parameters. As depicted in **Figures 5G, H**, patients aged >65 years and grade I showed a significantly lower ICI score than those aged < 65 years and grades



II–IV. Notably, the proportion of early-stage HCC (grade I) in the low score group was 51%, which was much higher than the 28% in the high score group. Collectively, the results obtained could be important for optimizing current immunotherapies targeting the aging world populations and contribute to the development of precise treatment of early-stage HCC.

The Correlation Between the ICI Score and Tumor Mutation Burden

Considering that genetic instability was a hallmark of tumor and the significant clinical implications of TMB, we explored whether TMB status and ICI score play independent or synergistic roles in predicting prognosis. First, we sought to determine the TMB values (**Supplementary Table S13**) and compare the differences in TMB between patients with high and low scores. Correlation analysis showed that the ICI score was negatively correlated with TMB (**Figure 6A**). Moreover patients with a low ICI score showed a significantly higher TMB than those in the high ICI score group (**Figure 6B**). Then the distribution of the prevalent TOP 20 oncogenic drivers with the highest alteration frequency in the low and high ICI score groups is shown in **Figures 6C, D**. Among the 20 genes, the majority of genes were associated with increased

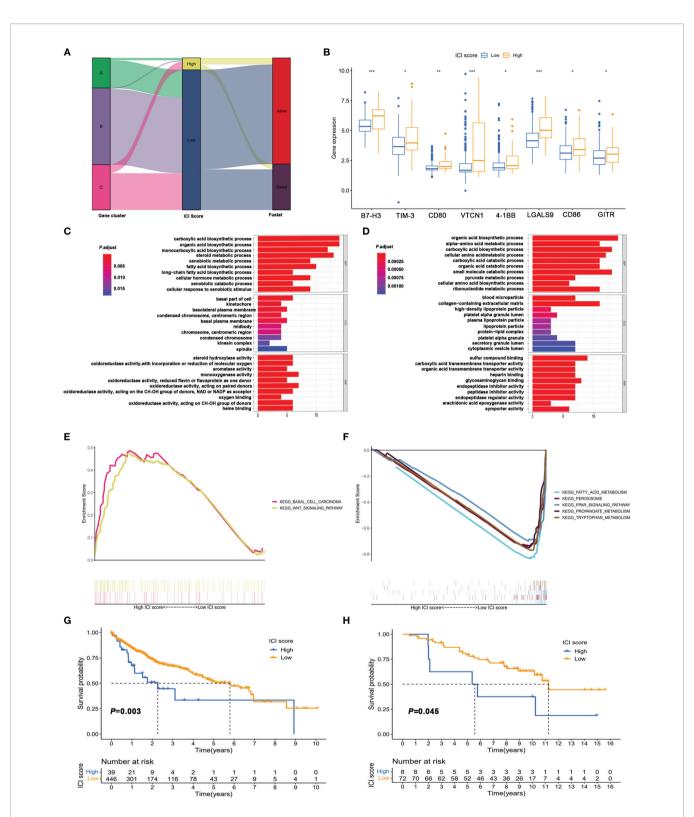


FIGURE 4 | Construction of immune score and functional enrichment analysis based on immune infiltration-related genes. (A) Alluvial plot of distribution of the ICI score and prognosis in different immune infiltration gene clusters. (B) Expression of immune checkpoint in high and low ICI score groups. *p < 0.05; **p < 0.05; **p < 0.01; ***p < 0.001; ns, not significant. (C, D) GO enrichment analysis of signature genes A (C) and B (D). (E, F) Gene set enrichment analysis (GSEA) of high score (E) and low score group (F). (G) Kaplan–Meier survival analysis of high score and low score groups divided based on the optimal cutoff value. (H) Kaplan–Meier survival analysis of high score and low score groups in the validation cohort (GSE10141).

65

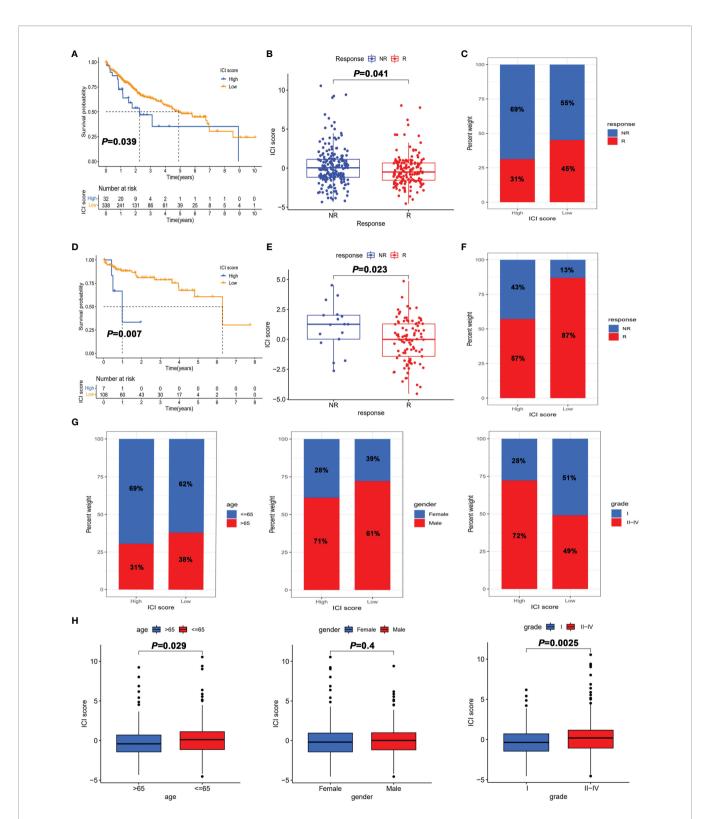
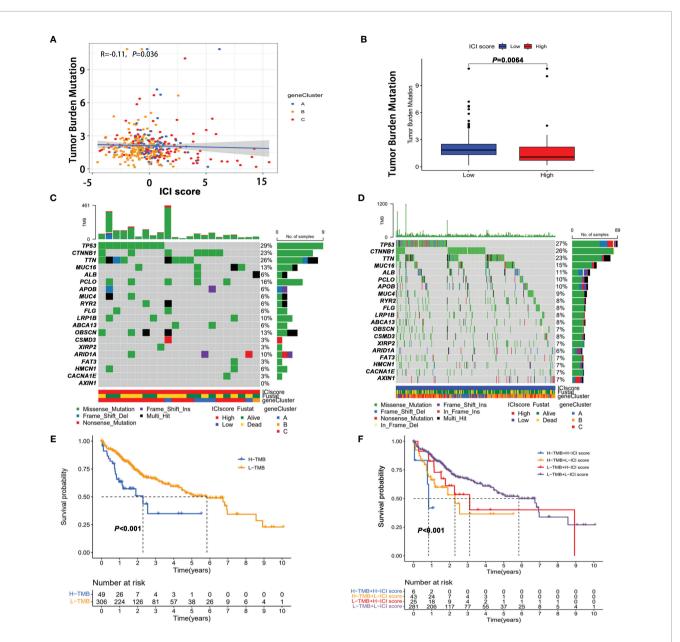


FIGURE 5 | The role of the ICI score in the prediction of immunotherapeutic benefits. (A) Kaplan–Meier curves for patients with high and low ICI score in the TGCA-LIHC cohort. (B) Comparison of the ICI score in response and non-response to immunotherapy in the TGCA-LIHC cohort. (C) Percentage of objective response rate to immunotherapy for high score and low score groups in the TGCA-LIHC cohort. (D) Kaplan–Meier curves for patients with high and low ICI scores in the GSE76427 cohort. (E) Comparison of ICI scores in response and non-response to immunotherapy in the GSE76427 cohort. (F) Percentage of objective response rate to immunotherapy for the high score and low score groups in the GSE76427 cohort. (G) Percentage of clinical parameters for high score and low score groups. (H) Comparison of clinical parameters between high score and low score groups.





TMB value except for ABCA13, APOB, ARID1A, AXIN1, and MUC4 (**Supplementary Figure S4**). After stratifying patients according to TMB status, ICI score subgroups still strongly correlated with patient prognosis regardless of TMB values (**Figures 6E, F**), supporting the superior prognostic power of molecular features of the immune infiltration patterns.

CTNNB1 Mutation Might Be Predictive of Response to Immunotherapy

To further screen potential biomarkers for immunotherapy of HCC, we analyzed the top 20 oncogenic drivers with the

highest alteration frequency. Among them, the significant difference in ICI score only existed between the patients with CTNNB1 mutation and those without CTNNB1 mutation (**Supplementary Figure S5**). Similarly, CTNNB1 status was also significantly related to the prognosis of patients with HCC (**Figure 7A**). Using the Kaplan–Meier curve analysis, we also found that only CTNNB1 expression was associated with poor outcomes (**Supplementary Figure S6**). Furthermore, in the TCGA-LIHC cohort, the mutation frequency of CTNNB1 was lower in the immunotherapy response group (15.9%) than in the non-response group (36.1%) (**Figure 7B**). A similar result was

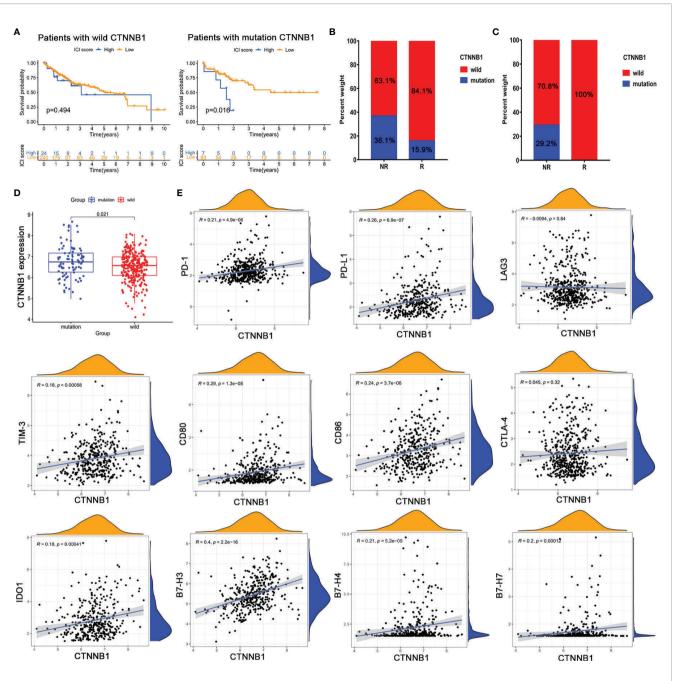


FIGURE 7 | (CTNNB1 mutation might be predictive of response to immunotherapy. Kaplan–Meier survival curve of the (A) CTNNB1 wild-type group and (B) CTNNB1 mutation group in TCGA-LIHC. (C) CTNNB1 mutation status in the response and non-response groups from TCGA-LIHC (left) and cBioPortal database (right). (D) Comparison of the expression of CTNNB1 in wild-type and mutant groups. (E) Correlation between CTNNB1 expression and T-cell checkpoint expressions.

observed in the cBioPortal dataset, and none of the patients who responded to immunotherapy had CTNNB1 mutation (**Figure 7C**). The infiltration levels of T cells, B lineage, monocytic lineage, dendritic cells, neutrophils, and NK cells were significantly reduced in CTNNB1-mutated HCC patients (all *p* values were less than 0.05, **Supplementary Figure S7**). To sum up, CTNNB1 mutation tended toward higher TMB, higher ICI score, and lower immune cell infiltration, which better predicted immunotherapy response and may be a prognostic predictor in HCC patients.

To test whether CTNNB1 mutation affected CTNNB1 function, we compared the expression level of CTNNB1 wild type and mutant type and found that its expression was significantly upregulated in the CTNNB1-mutated group (**Figure 7D**). We then assessed the correlation between CTNNB1 expression and the expression of critical immune

checkpoints that have emerged as biomarkers for the selection of HCC patients for immunotherapy. The results showed that CTNNB1 expression was weakly associated with the expression of classical T cell immune checkpoint pathway-related molecules (e.g., PD-1/PD-L1, LAG3/TIM-3, B7-1/B7-2/CTLA-4) (**Figure 7E**). Besides, there were no significant correlations between CTNNB1 expression and the majority of killer immunoglobulin-like receptors (e.g., KIR2DL1, KIR2DS4, and KIR3DL1) that play an essential role in the regulation of natural killer (NK) activity (**Supplementary Figure S8**). The findings partly explained why patients with CTNNB1 mutation were innate resistant to immune checkpoint inhibitors. Taken together, CTNNB1 mutation might serve as a predictive marker of response to immunotherapy, which contributed to the precise decision-making of immunotherapy in HCC patients.

DISCUSSION

Immunotherapy is emerging as a promising option for advanced HCC patients. A significant limitation of immunotherapy is that only a subset of HCC patients benefit from it. Given the individual heterogeneity of the immune environment, there is an urgent need to quantify the tumor immune infiltration patterns across individuals. In this study, we comprehensively analyzed the immune infiltration landscape of 491 HCC samples and categorized the HCC samples into three distinct immune infiltration subtypes. Furthermore, we established the ICI score to comprehensively quantify the immune environment of HCC, which might be an effective prognostic biomarker and predictor for evaluating immunotherapy response.

Currently, the mechanism of immunotherapy is based on the activation of T cells, especially $CD8^+$ T, because of their role in tumor cell cytolysis. In the study, we found that $CD8^+$ T cells had the best correlation with other 21 immune cells. It indicated that $CD8^+$ T cells were the main cause of immune exhaustion in the immune microenvironment, which was consistent with the core concept of clinical immunotherapy. Besides, $CD8^+$ T cells were also highly related to $CD4^+$ T cells, which might partly explain the insufficient immune response of $CD8^+$ T cells to eliminate tumors and why scientists had shifted their focus to the "supporting role" of $CD4^+$ T cells. Overall, the results further confirmed that T cells were the core cells of immunotherapy, which partially explained why immune checkpoints targeting T cells could generate markedly specific immune responses.

Growing evidence manifests that immune cell dysfunction in the TME promoted immune suppression, thereby promoting tumorigenesis and progression (29–31). For instance, $CD4^+$ T cells, $CD8^+$ T cells, and Treg cells play important roles in tumor recurrence, metastasis, and immunotherapy response (32, 33). Here, we found that cluster A with the best prognosis was characterized by the highest $CD4^+$ T cell infiltration and exhibited an active immune phenotype, which was routinely so-called hot tumor (34–36). The cluster C with the worst prognosis had a low $CD8^+$ /regulatory T cell ratio, which implied an immune-cold phenotype (37, 38). However, the results of the ESTIMATE algorithm showed no significant difference in the ImmuneScore of the three clusters, which seemed to be inconsistent with the CIBERSORT algorithm. It implied that immune components, rather than the quantity, were more likely to affect the prognosis of immune subtypes.

Based on the differential genes among distinct immune infiltration patterns, we established the ICI score to fully quantify immune infiltration patterns by PCA analysis. The high ICI score group exhibited poor prognosis, and the expressions of immune checkpoints such as PD-L1 and TIM-3 were significantly increased. The prognostic value of the ICI score was validated in the external validation cohort (GSE10141). Age is associated with many changes in immune function, primarily a reduction in the number of lymphocytes, especially T cells, and a decrease in the diversity of the T-cell receptor repertoire (39, 40). Stratified analysis showed that patients aged >65 years and grade I showed significantly lower ICI score than those aged <65 years and grades II-IV, suggesting that the ICI score was important for optimizing current immunotherapy targeting an aging world population and developing precise treatments for early HCC. Through GSEA, we found that genes involved in the high ICI score group were enriched in the Wnt/ β -catenin pathway, now commonly defined as immune exclusion HCC class, also known as HCC "cold" tumors (41). Furthermore, the ImmuCell analysis website predicted response to immunotherapy in the TCGA-LIHC and GSE76427 cohorts. The results showed a lower ICI score in the immunotherapy response group. In contrast, the objective response rate of immunotherapy was lower in the high ICI score group. Taken together, these data manifested that the ICI score could better predict the response to immunotherapy and had important clinical significance.

Previous studies have shown that TMB is a predictive biomarker of the efficacy of immunotherapy, and the higher the TMB, the better the efficacy of immunotherapy (42, 43). In the study, our current study showed that high TMB was a poor prognosis factor for patients with HCC, which was consistent with HCC being a genetic disease requiring only four mutations on average. Besides, we also found a significant difference in the mutation frequency of multiple genes between the high and low ICI score groups. The ICI score was significantly negatively correlated with TMB, with a correlation coefficient of -0.17, and TMB was significantly increased in patients with a low ICI score. The stratified analysis showed that the ICI score could synergistically predict HCC patients' prognosis with TMB, which implies that the molecular alterations may interfere with cell-tocell communication between infiltrating immune cells during tumorigenesis.

Considering the limitation of the ICI score that can only be obtained by transcriptome analysis of surgical specimens, we analyzed the somatic mutation genes in the high and low score groups to screen potential biomarkers for HCC immunotherapy and found that the ICI score was significantly increased in patients with CTNNB1 mutation. Previous studies have shown that 30% of HCC patients harbor CTNNB1 mutation, which may represent those with innate resistance to immune checkpoint inhibitors (41-44). Compared with wild-type CTNNB1, HCC patients with CTNNB1 mutation in TCGA-LIHC and cBioPortal databases were resistant to immunotherapies, suggesting that CTNNB1 might represent the biomarkers for predicting resistance to immune checkpoint inhibitors. Moreover, T cells, B lineage, monocytic lineage, dendritic cells, neutrophils, and NK cells exhibited lower infiltration levels in CTNNB1-mutated HCC patients. This was in line with previous studies showing that CTNNB1 mutation was characterized by an immune excluded class, so-called cold tumors (41). The reason is that, on the one hand, CTNNB1 mutation caused its expression to be significantly upregulated, which was closely related to the activation of the Wnt/β-catenin pathway. On the other hand, CTNNB1 expression was weakly correlated with immune checkpoint expression, which can partially explain why patients with CTNNB1 mutation were refractory to antibodies targeting PD-1/PD-L, or LAG3, or KIR (45). However, CTNNB1 expression was moderately correlated with B7-H3 (CD276), a new checkpoint target for cancer immunotherapy with an expression frequency of 91.8% in HCC (46), which suggested that CTNNB1-mutated HCC patients might escape immunotherapy through the non-classical immune checkpoint pathway, providing a novel direction for the treatment of CTNNB1-mutated HCC patients and precise decision-making for HCC management. Certainly, all the results were based on theoretical analysis of transcriptome data. The effective target and molecular mechanism for the treatment of CTNNB1mutated HCC patients still need to be further explored and verified.

CONCLUSION

In summary, we performed a comprehensive analysis of the immune landscape in the TME of HCC. We found that the difference in immune infiltration patterns of the immune microenvironment of HCC was closely related to tumor heterogeneity, treatment response, and prognosis. Therefore, the systematic evaluation of the tumor immune infiltration model in this study could help determine the optimal immunotherapy strategy for patients, which had important clinical significance.

DATA AVAILABILITY STATEMENT

The datasets presented in this study can be found in online repositories. The names of the repository/repositories and accession number(s) can be found in the article/**Supplementary Material**.

AUTHOR CONTRIBUTIONS

XZ and QK designed and directed the completion of the project. XT was involved in writing of the review and editing. YG performed the data analysis and drawing. XT and KR performed the data download and clinical data collection. YG and HG performed the statistical analyses. JY supervised the study. All authors contributed to the article and approved the submitted version.

FUNDING

This work was supported by the National Key Research and Development Program of China (No. 2020YFC2008304) and the Medical Science and Technology Joint Project of Henan Province (No. LHGJ20210282).

ACKNOWLEDGMENTS

We thank all the participants in the TCGA-LIHC, GSE76427, GSE10141, and cBioPortal cohorts. We also thank the other members of the laboratory for their help and assistance.

SUPPLEMENTARY MATERIAL

The Supplementary Material for this article can be found online at: https://www.frontiersin.org/articles/10.3389/fimmu.2022.861525/ full#supplementary-material

Supplementary Table S1 | Detailed description of the clinical characteristics for HCC samples from TCGA-LIHC, GSE76427 and GSE10141.

Supplementary Table S2 | ImmuneScore, StromalScore and ESTIMATEScore quantified for each HCC sample by ESTIMATE algorithm.

Supplementary Table S3 | The abundance of 22 types of tumor-infiltrating immune cells using the CIBERSORT method.

Supplementary Table S4 | Unsupervised clustering for all HCC patients according to the proportion of immune cells.

Supplementary Table S5 | Unsupervised clustering of differentially expressed genes among three immune infiltration clusters.

Supplementary Table S6 | Differentially gene expression profiles of the three immune infiltration clusters.

Supplementary Table S7 | Signature gene expression profiles for different immunity patterns based on Boruta algorithm.

Supplementary Table S8 | The gene ontology analysis of ICI signature genes A ranked according to the adjusted P-value.

Supplementary Table S9 | The gene ontology analysis of ICI signature genes B ranked according to the adjusted P-value.

Supplementary Table S10 | KEGG pathway enrichment analysis of high ICI Score group.

Supplementary Table S11 | KEGG pathway enrichment analysis of low ICI Score group.

Supplementary Table S12 | ICI score of HCC patients from TCGA-LIHC and GSE76427.

Supplementary Table S13 | Mutation status of HCC samples from TCGA-LIHC (0, absence of mutations; 1, presence of mutations).

Supplementary Table S14 | Mutation status of HCC samples from TCGA-LIHC (0, absence of mutations; 1, presence of mutations).

Supplementary Figure S1 | The workflow of the study design.

Supplementary Figure S2 | Comparison of stages of HCC among distinct immune infiltration clusters. (A) HCC stage; (B) The proportion of HCC stage divided into early (I) and late HCC (II-IV).

Supplementary Figure S3 | Correlations between ImmuneScore/StromalScore/ ESTIMATEScore and ICI score.

Supplementary Figure S4 | Correlations between TMB value and expressions of the TOP 20 oncogenic drivers with the highest alteration frequency.

REFERENCES

- 1. Villanueva A. Hepatocellular Carcinoma. N Engl J Med (2019) 380:1450–62. doi: 10.1056/NEJMra1713263
- Bray F, Ferlay J, Soerjomataram I, Siegel RL, Torre LA, Jemal A. Global Cancer Statistics 2018: GLOBOCAN Estimates of Incidence and Mortality Worldwide for 36 Cancers in 185 Countries. *CA Cancer J Clin* (2018) 68:394– 424. doi: 10.3322/caac.21492
- Lin J, Zhao H. Systemic Management for Patients With Hepatobiliary Tumors in a Multi-Dimensional View. *Hepatobiliary Surg Nutr* (2019) 8:626–8. doi: 10.21037/hbsn.2019.07.21
- Davis AA, Patel VG. The Role of PD-L1 Expression as a Predictive Biomarker: An Analysis of All US Food and Drug Administration (FDA) Approvals of Immune Checkpoint Inhibitors. J Immunother Cancer (2019) 7:278. doi: 10.1186/s40425-019-0768-9
- Osipov A, Lim SJ, Popovic A, Azad NS, Laheru DA, Zheng L, et al. Tumor Mutational Burden, Toxicity, and Response of Immune Checkpoint Inhibitors Targeting PD(L)1, CTLA-4, and Combination: A Meta-Regression Analysis. *Clin Cancer Res* (2020) 26:4842–51. doi: 10.1158/1078-0432.CCR-20-0458
- Ge Z, Ding S. The Crosstalk Between Tumor-Associated Macrophages (TAMs) and Tumor Cells and the Corresponding Targeted Therapy. *Front* Oncol (2020) 10:590941. doi: 10.3389/fonc.2020.590941
- Qi X, Qi C, Qin B, Kang X, Hu Y, Han W. Immune-Stromal Score Signature: Novel Prognostic Tool of the Tumor Microenvironment in Lung Adenocarcinoma. *Front Oncol* (2020) 10:541330. doi: 10.3389/fonc. 2020.541330
- Obradovic A, Chowdhury N, Haake SM, Ager C, Wang V, Vlahos L, et al. Single-Cell Protein Activity Analysis Identifies Recurrence-Associated Renal Tumor Macrophages. *Cell* (2021) 184:2988–3005. doi: 10.1016/j.cell. 2021.04.038
- Bagaev A, Kotlov N, Nomie K, Svekolkin V, Gafurov A, Isaeva O, et al. Conserved Pan-Cancer Microenvironment Subtypes Predict Response to Immunotherapy. *Cancer Cell* (2021) 39:845–65. doi: 10.1016/j.ccell. 2021.04.014
- Maibach F, Sadozai H, Seyed Jafari SM, Hunger RE, Schenk M. Tumor-Infiltrating Lymphocytes and Their Prognostic Value in Cutaneous Melanoma. *Front Immunol* (2020) 11:2105. doi: 10.3389/fimmu.2020.02105
- Ostroumov D, Fekete-Drimusz N, Saborowski M, Kuhnel F, Woller N. CD4 and CD8 T Lymphocyte Interplay in Controlling Tumor Growth. *Cell Mol Life Sci* (2018) 75:689–713. doi: 10.1007/s00018-017-2686-7
- Chen H, Molberg K, Strickland AL, Castrillon DH, Carrick K, Jiang Q, et al. PD-L1 Expression and CD8+ Tumor-Infiltrating Lymphocytes in Different Types of Tubo-Ovarian Carcinoma and Their Prognostic Value in High-Grade Serous Carcinoma. *Am J Surg Pathol* (2020) 44:1050–60. doi: 10.1097/ PAS.000000000001503
- Chatzopoulos K, Kotoula V, Manoussou K, Markou K, Vlachtsis K, Angouridakis N, et al. Tumor Infiltrating Lymphocytes and CD8+ T Cell Subsets as Prognostic Markers in Patients With Surgically Treated Laryngeal Squamous Cell Carcinoma. *Head Neck Pathol* (2020) 14:689–700. doi: 10.1007/s12105-019-01101-6

Supplementary Figure S5 | Comparison of ICI score between HCC samples with mutation and without mutation of the TOP 20 oncogenic drivers with the highest alteration frequency.

Supplementary Figure S6 | Effect of expressions of the TOP 20 oncogenic drivers with the highest alteration frequency on prognosis.

Supplementary Figure S7 | Comparison of the infiltration levels of immune cells between HCC samples with and without CTNNB1 mutation.

Supplementary Figure S8 | Correlations between CTNNB1 expression and expression of killer immunoglobulin-like receptors.

- Davis D, Tretiakova MS, Kizzar C, Woltjer R, Krajbich V, Tykodi SS, et al. Abundant CD8+ Tumor Infiltrating Lymphocytes and Beta-2-Microglobulin Are Associated With Better Outcome and Response to Interleukin-2 Therapy in Advanced Stage Clear Cell Renal Cell Carcinoma. *Ann Diagn Pathol* (2020) 47:151537. doi: 10.1016/j.anndiagpath.2020.151537
- Xiang X, Wang J, Lu D, Xu X. Targeting Tumor-Associated Macrophages to Synergize Tumor Immunotherapy. *Signal Transduct Target Ther* (2021) 6:75. doi: 10.1038/s41392-021-00484-9
- Liu H, Liang Z, Zhou C, Zeng Z, Wang F, Hu T, et al. Mutant KRAS Triggers Functional Reprogramming of Tumor-Associated Macrophages in Colorectal Cancer. Signal Transduct Target Ther (2021) 6:144. doi: 10.1038/s41392-021-00534-2
- Zhang M, Yang H, Wan L, Wang Z, Wang H, Ge C, et al. Single-Cell Transcriptomic Architecture and Intercellular Crosstalk of Human Intrahepatic Cholangiocarcinoma. J Hepatol (2020) 73:1118–30. doi: 10.1016/j.jhep.2020.05.039
- Fabris L, Sato K, Alpini G, Strazzabosco M. The Tumor Microenvironment in Cholangiocarcinoma Progression. *Hepatology* (2021) 73:75–85. doi: 10.1002/ hep.31410
- Dai J, Su Y, Zhong S, Cong L, Liu B, Yang J, et al. Exosomes: Key Players in Cancer and Potential Therapeutic Strategy. *Signal Transduct Target Ther* (2020) 5:145. doi: 10.1038/s41392-020-00261-0
- Cao R, Yuan L, Ma B, Wang G, Tian Y. Tumour Microenvironment (TME) Characterization Identified Prognosis and Immunotherapy Response in Muscle-Invasive Bladder Cancer (MIBC). *Cancer Immunol Immunother* (2021) 70:1–18. doi: 10.1007/s00262-020-02649-x
- Wagner GP, Kin K, Lynch VJ. Measurement of mRNA Abundance Using RNA-Seq Data: RPKM Measure Is Inconsistent Among Samples. *Theory Biosci* (2012) 131:281–5. doi: 10.1007/s12064-012-0162-3
- Johnson WE, Li C, Rabinovic A. Adjusting Batch Effects in Microarray Expression Data Using Empirical Bayes Methods. *Biostatistics* (2007) 8:118– 27. doi: 10.1093/biostatistics/kxj037
- Newman AM, Liu CL, Green MR, Gentles AJ, Feng W, Xu Y, et al. Robust Enumeration of Cell Subsets From Tissue Expression Profiles. *Nat Methods* (2015) 12:453–7. doi: 10.1038/nmeth.3337
- 24. Becht E, Giraldo NA, Lacroix L, Buttard B, Elarouci N, Petitprez F, et al. Estimating the Population Abundance of Tissue-Infiltrating Immune and Stromal Cell Populations Using Gene Expression. *Genome Biol* (2016) 17:218. doi: 10.1186/s13059-016-1070-5
- Yoshihara K, Shahmoradgoli M, Martinez E, Vegesna R, Kim H, Torres-Garcia W, et al. Inferring Tumour Purity and Stromal and Immune Cell Admixture From Expression Data. *Nat Commun* (2013) 4:2612. doi: 10.1038/ncomms3612
- Yu G, Wang LG, Han Y, He QY. Clusterprofiler: An R Package for Comparing Biological Themes Among Gene Clusters. OMICS (2012) 16:284–7. doi: 10.1089/omi.2011.0118
- Sotiriou C, Wirapati P, Loi S, Harris A, Fox S, Smeds J, et al. Gene Expression Profiling in Breast Cancer: Understanding the Molecular Basis of Histologic Grade to Improve Prognosis. J Natl Cancer Inst (2006) 98:262–72. doi: 10.1093/jnci/djj052
- Mayakonda A, Lin DC, Assenov Y, Plass C, Koeffler HP. Maftools: Efficient and Comprehensive Analysis of Somatic Variants in Cancer. *Genome Res* (2018) 28:1747–56. doi: 10.1101/gr.239244.118

- Perez-Romero K, Rodriguez RM, Amedei A, Barcelo-Coblijn G, Lopez DH. Immune Landscape in Tumor Microenvironment: Implications for Biomarker Development and Immunotherapy. *Int J Mol Sci* (2020) 21:5521. doi: 10.3390/ ijms21155521
- 30. Job S, Rapoud D, Dos Santos A, Gonzalez P, Desterke C, Pascal G, et al. Identification of Four Immune Subtypes Characterized by Distinct Composition and Functions of Tumor Microenvironment in Intrahepatic Cholangiocarcinoma. *Hepatology* (2020) 72:965–81. doi: 10.1002/hep.31092
- DeCordova S, Shastri A, Tsolaki AG, Yasmin H, Klein L, Singh SK, et al. Molecular Heterogeneity and Immunosuppressive Microenvironment in Glioblastoma. *Front Immunol* (2020) 11:1402. doi: 10.3389/fimmu.2020.01402
- Jiang Y, Zhang Q, Hu Y, Li T, Yu J, Zhao L, et al. ImmunoScore Signature: A Prognostic and Predictive Tool in Gastric Cancer. Ann Surg (2018) 267:504– 13. doi: 10.1097/SLA.00000000002116
- Zeng D, Zhou R, Yu Y, Luo Y, Zhang J, Sun H, et al. Gene Expression Profiles for a Prognostic Immunoscore in Gastric Cancer. *Br J Surg* (2018) 105:1338– 48. doi: 10.1002/bjs.10871
- Ostrand-Rosenberg S, Horn LA, Ciavattone NG. Radiotherapy Both Promotes and Inhibits Myeloid-Derived Suppressor Cell Function: Novel Strategies for Preventing the Tumor-Protective Effects of Radiotherapy. *Front Oncol* (2019) 9:215. doi: 10.3389/fonc.2019.00215
- Galon J, Bruni D. Approaches to Treat Immune Hot, Altered and Cold Tumours With Combination Immunotherapies. *Nat Rev Drug Discov* (2019) 18:197–218. doi: 10.1038/s41573-018-0007-y
- Maleki Vareki S. High and Low Mutational Burden Tumors Versus Immunologically Hot and Cold Tumors and Response to Immune Checkpoint Inhibitors. J Immunother Cancer (2018) 6:157. doi: 10.1186/ s40425-018-0479-7
- Bonaventura P, Shekarian T, Alcazer V, Valladeau-Guilemond J, Valsesia-Wittmann S, Amigorena S, et al. Cold Tumors: A Therapeutic Challenge for Immunotherapy. *Front Immunol* (2019) 10:168. doi: 10.3389/fimmu. 2019.00168
- Ochoa de Olza M, Navarro Rodrigo B, Zimmermann S, Coukos G. Turning Up the Heat on Non-Immunoreactive Tumours: Opportunities for Clinical Development. *Lancet Oncol* (2020) 21:e419–30. doi: 10.1016/S1470-2045(20) 30234-5
- Reitsema RD, Hid Cadena R, Nijhof SH, Abdulahad WH, Huitema MG, Paap D, et al. Effect of Age and Sex on Immune Checkpoint Expression and Kinetics in Human T Cells. *Immun Ageing* (2020) 17:32. doi: 10.1186/s12979-020-00203-y
- Valiathan R, Ashman M, Asthana D. Effects of Ageing on the Immune System: Infants to Elderly. Scand J Immunol (2016) 83:255–66. doi: 10.1111/sji.12413

- Sia D, Jiao Y, Martinez-Quetglas I, Kuchuk O, Villacorta-Martin C, Castro de Moura M, et al. Identification of an Immune-Specific Class of Hepatocellular Carcinoma, Based on Molecular Features. *Gastroenterology* (2017) 153:812– 26. doi: 10.1053/j.gastro.2017.06.007
- Samstein RM, Lee CH, Shoushtari AN, Hellmann MD, Shen R, Janjigian YY, et al. Tumor Mutational Load Predicts Survival After Immunotherapy Across Multiple Cancer Types. *Nat Genet* (2019) 51:202–6. doi: 10.1038/s41588-018-0312-8
- Sha D, Jin Z, Budczies J, Kluck K, Stenzinger A, Sinicrope FA. Tumor Mutational Burden as a Predictive Biomarker in Solid Tumors. *Cancer Discov* (2020) 10:1808–25. doi: 10.1158/2159-8290.CD-20-0522
- Llovet JM, Montal R, Sia D, Finn RS. Molecular Therapies and Precision Medicine for Hepatocellular Carcinoma. Nat Rev Clin Oncol (2018) 15:599– 616. doi: 10.1038/s41571-018-0073-4
- 45. Harding JJ, Nandakumar S, Armenia J, Khalil DN, Albano M, Ly M, et al. Prospective Genotyping of Hepatocellular Carcinoma: Clinical Implications of Next-Generation Sequencing for Matching Patients to Targeted and Immune Therapies. *Clin Cancer Res* (2019) 25:2116–26. doi: 10.1158/1078-0432.CCR-18-2293
- Michelakos T, Kontos F, Barakat O, Maggs L, Schwab JH, Ferrone CR, et al. B7-H3 Targeted Antibody-Based Immunotherapy of Malignant Diseases. *Expert Opin Biol Ther* (2021) 21:587–602. doi: 10.1080/14712598. 2021.1862791

Conflict of Interest: The authors declare that the research was conducted in the absence of any commercial or financial relationships that could be construed as a potential conflict of interest.

Publisher's Note: All claims expressed in this article are solely those of the authors and do not necessarily represent those of their affiliated organizations, or those of the publisher, the editors and the reviewers. Any product that may be evaluated in this article, or claim that may be made by its manufacturer, is not guaranteed or endorsed by the publisher.

Copyright © 2022 Guo, Yang, Ren, Tian, Gao, Tian, Zhang and Kan. This is an openaccess article distributed under the terms of the Creative Commons Attribution License (CC BY). The use, distribution or reproduction in other forums is permitted, provided the original author(s) and the copyright owner(s) are credited and that the original publication in this journal is cited, in accordance with accepted academic practice. No use, distribution or reproduction is permitted which does not comply with these terms.





MAOI Antidepressants: Could They Be a Next-Generation ICB Therapy?

James Brown^{1†}, Bo Li^{1*†} and Lili Yang^{1,2,3,4*}

¹ Department of Microbiology, Immunology & Molecular Genetics, University of California, Los Angeles, Los Angeles, CA, United States, ² Eli and Edythe Broad Center of Regenerative Medicine and Stem Cell Research, University of California, Los Angeles, Los Angeles, CA, United States, ³ Jonsson Comprehensive Cancer Center, The David Geffen School of Medicine, University of California, Los Angeles, Los Angeles, CA, United States, ⁴ Molecular Biology Institute, University of California, Los Angeles, Los Angeles, CA, United States

Keywords: monoamine oxidase inhibitor, immune checkpoint blockade, T cell, tumor-associated macrophage, immunotherapy, nanoformulation

OPEN ACCESS

Edited by:

Xuyao Zhang, Fudan University, China

Reviewed by:

Wei Chen, Stanford University, United States Yanqing Liu, Columbia University, United States

*Correspondence:

Bo Li bo.li@ucla.edu Lili Yang liliyang@ucla.edu

[†]These authors have contributed equally to this work

Specialty section:

This article was submitted to Cancer Immunity and Immunotherapy, a section of the journal Frontiers in Immunology

Received: 12 January 2022 Accepted: 21 February 2022 Published: 14 March 2022

Citation:

Brown J, Li B and Yang L (2022) MAOI Antidepressants: Could They Be a Next-Generation ICB Therapy? Front. Immunol. 13:853624. doi: 10.3389/fimmu.2022.853624

INTRODUCTION

The serotonin signaling pathway has been well understood in the neurons for decades (1, 2). During regular neuronal processes, serotonin released by the presynaptic neuron is used to communicate feelings of happiness and other behavioral changes with the postsynaptic neuron through binding to the 5-hydroxytryptamine receptor (5-HTR) (3, 4). After signaling, the presynaptic neuron reuptakes free serotonin to avoid overstimulation of 5-HTR, which is then broken down by the enzyme monoamine oxidase-A (MAO-A). The investigation of this critical neurotransmitter pathway has resulted in the development of many drugs capable of utilizing the diverse signaling regulators associated with serotonin to mitigate the effects of clinical depression and other neurological disorders. One of the first classes of small-molecule inhibitory drugs approved for the treatment of depression are MAO inhibitors (MAOIs), which prevent MAO-A from cleaving serotonin upon reuptake into the cells (3, 5). However, the MAO-A-serotonin signaling pathway outside of neurons is largely unknown. Recent discoveries have opened the door for understanding the function of MAO-A as an immunomodulatory molecule as well as examining its potential as a candidate for immune checkpoint blockade (ICB) therapy.

ICB therapy is the subject of growing interest as oncology is becoming an increasingly immunological field (6, 7). Anti-PD-1/PD-L1 therapy, which blocks PD-1-PD-L1 binding, circumventing T-cell exhaustion brought about by the immunosuppressive tumor microenvironment (TME), has been approved by the FDA as a treatment for solid tumors (5, 8). Another approved ICB therapy is anti-cytotoxic T lymphocyte-associated antigen 4 (anti-CTLA-4), which blocks the CTLA4 receptor from binding the apoptotic signaling ligand B7-1 (9). However, while these therapies have demonstrated significant or complete remission, factors such as multiple immune checkpoint pathways and their different roles in regulating specific cancer types can limit the efficacy of current ICB therapies (10). Therefore, it is of continuing interest to researchers that novel ICB candidates be developed in order to augment the effects of clinically-proven ICB through combination therapy that can improve immune cell infiltration and block suppressive pathways of tumor infiltrating immune cells (TIIs), increasing the tumor-type range and specificity of the field (10, 11). A number of ICB therapies are currently undergoing clinical trials, such as anti-CD47, which improves classically activated macrophage activity, as well as anti-Tim3 and anti-LAG3, which target common T cell negative immune checkpoints (12, 13). With the discovery of the serotonin pathway as a potential immune regulator, the promise of repurposing drugs that already have FDA approval as treatments for clinical depression offers the potential for a novel therapy that may increase the efficacy of current ICB treatments and broaden the reach of the field. This, in turn, makes the investigation of MAOIs as candidates of combination ICB therapy an incredibly interesting and exciting field of research with regards to cancer treatment.

MAO-A AS AN IMMUNE REGULATOR

MAO-A was recently discovered to be upregulated in TIIs, especially in exhausted intratumoral CD8 T cells. This led to the hypothesis that MAO-A may be a negative regulator of antitumor T cell immunity through some unknown mechanism, so further studies examining the functions of knockout MAO-A T cells in tumor-challenged mice were conducted to determine whether there was any impact on oncolytic activity. Wang et al. reported that MAO-A-KO mice exhibited significantly suppressed tumor growth in two syngeneic mouse tumor models (5). This improved tumor-suppression response was accompanied by an increase in cytokine and cytotoxic molecule release in MAO-A-KO mice, indicating that the knockout of MAO-A results in increased cytotoxic lymphocyte (CTL) activity. To further dissect the mechanisms underlying the antitumor effects of MAO-A-KO T cells, researchers demonstrated that MAO-A-KO CD8 T cells produce higher levels of serotonin, which acts as an autocrine immune regulator to activate the downstream immunostimulatory mitogen-activated protein kinase (MAPK) pathway through 5-HTRs (5). This signaling pathway in turn "cross-talks" with the T cell receptor (TCR) signaling pathway, resulting in the enhanced effector function observed in MAO-A-KO T cells (Figure 1A) (5).

In addition to MAO-A's role as a T cell regulator, another recent study revealed that MAO-A activity in tumor-associated macrophages (TAMs) was positively correlated with immune suppression (14). A knockout study comparing tumor-laden MAO-A-deficient mice and WT mice revealed that MAO-A-KO TAMs expressed lower levels of immunosuppressive markers and higher levels of immunostimulatory molecules (14). This led to the elucidation of a novel immunosuppressive mechanism of action associated with MAO-A in TAMs in addition to its role in T cells (5). The oxidation of monoamines in neurotransmitters such as serotonin by MAO-A results in the intracellular accumulation of reactive oxygen species (ROS) (14, 15). These ROS cause oxidative stress that polarizes the TME through the

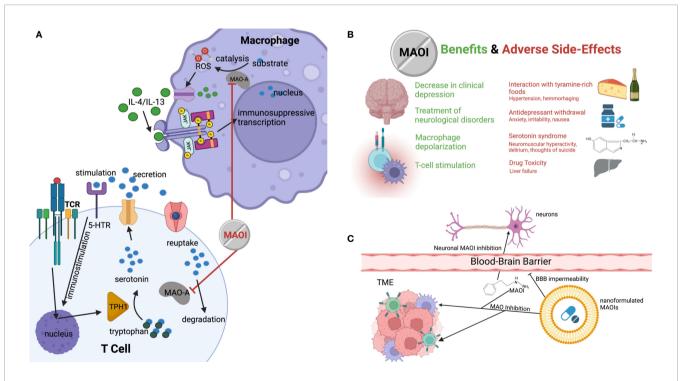


FIGURE 1 | The potential of MAOI as a next-generation ICB therapy. (A) Diagram demonstrating how MAOIs inhibit MAO-A activity in immune cells, increasing free, immunostimulatory serotonin for intratumoral CD8 T cell stimulation and decreasing immunosuppression-inducing ROS produced by MAO-A oxidation of monoamine substrates in TAMs. (B) Current and potential clinical therapeutic benefits of MAOIs and the known associated side effects and symptoms. (C) Demonstration of nanoformulation of MAOIs preventing administered drugs from crossing the blood-brain barrier while maintaining ability to deliver drugs to target cells in tumor, avoiding the systemic application of the drug and mitigating side effects.

stimulation of the immunosuppressive JAK-Stat6 pathway and the production of immunosuppressive cytokines (**Figure 1A**) (16, 17). This demonstrated the multifaceted effects that MAO-A has on immune function in the TME.

POTENTIAL OF MAOIS AS ICB THERAPY

MAO-A regulation of T cell activity was further investigated through the administration of MAOIs as a means of artificially inhibiting MAO-A activity and the breakdown of serotonin. In a mouse B16-OVA melanoma model, Wang et al. demonstrated dramatic tumor-suppressive effects of the MAOI antidepressants phenelzine, clorgyline, and moclobemide, which represented three classes of MAOIs, varying in the reversibility of the drug's effects (reversible vs irreversible) and the selectivity for the serotonin-degrading MAO-A isoform over MAO-B (selective vs nonselective) (5). There was no observed significant difference in efficacy between the nonselective, reversible phenelzine; the selective, reversible moclobemide; and the nonselective, irreversible clorgyline, indicating that MAO-A specificity and drug irreversibility do not provide a therapeutic advantage with respect to antitumor response. Because phenelzine is commercially available in the United States, it was selected as a representative to determine whether MAOIs are a feasible candidate for ICB therapy. Phenelzine exhibited tumorsuppressive effects in mice of multiple mouse syngeneic tumor models (e.g. B16-OVA, MC38) as well as a human xenograft model (e.g. A375) (5). CTL antitumor activity was continuously demonstrated to be improved by the administration of phenelzine. In addition, phenelzine has been shown to exhibit tumor-suppressive effects in a stage II clinical trial by Gross et al. on patients with prostate cancer (18). Therefore, these findings suggest the translational potential of MAOIs as ICB therapy.

The efficacy of phenelzine as an ICB therapy was also demonstrated to inhibit immunosuppression through TAM polarization (14). This provides an interesting mechanism by which MAO-A inhibits the immune system's natural antitumor abilities through the downregulation of ROS production, further demonstrating the immunological reasoning behind the efficacy of MAOIs as ICB candidates (Figure 1A). Strikingly, two reports demonstrated MAOI efficacy as both a monotherapy and combination therapy with anti-PD-1 in the typically responsive colon cancer MC38, as well as in B16 melanoma cells, which have historically been less responsive to immunotherapy (5). Phenelzine showed nearly identical efficacy to anti-PD-1, proving its utility as a monotherapy. What was even more promising, however, was the high significance in therapeutic improvement in the melanoma combination therapy model. This suggests that MAOIs may be able to drastically improve the reach of classical ICB therapies and opens the door for further testing to determine whether MAOIs have an effect in historically unresponsive cancer types such as breast, lung, prostate, and ovarian cancers.

POSSIBLE ISSUES WITH MAOIS FOR ICB THERAPY

While MAOIs were the primary class of antidepressants for the majority of the second half of the 20th century, they have fallen largely out of fashion due to the adverse side effects associated with their administration and the rise of alternative drugs (Figure 1B) (19). MAOIs have been known to cause severe dizziness due to hypertension, especially in elderly patients (20, 21). This presents an issue when considering MAOIs as cancer therapies for older patients, who are an important demographic for cancer treatments due to the high incidence of disease (22). These hypertensive side effects can also be made worse by an increase of dietary tyramine, which is typically metabolized by MAOs and can result in fatal brain hemorrhaging (23). Consequently, patients are often placed on restrictive diets excluding tyramine-rich foods such as cheese (hence the name "cheese effects"), making them a less appealing candidate for both neurological disorders and as ICB therapies when compared to other available options (14, 23). MAOIs have also been linked to significant liver toxicity when applied in high doses, making their long-term application less feasible when dealing with chronic illnesses (3). Additionally, MAOIs have been linked to serotonin syndrome when administered with other serotonergic drugs, which results from the accumulation of serotonin and can cause life threatening behavioral and physical maladies such as delirium, neuromuscular hyperactivity, and even thoughts of suicide (3, 20).

Despite these potential negatives, the utilization of MAOIs still shows significant promise, and the process should be optimized to increase drug efficacy and patient wellbeing. One potential source of side-effect remediation is through the development of nanoformulated MAOIs that can be targeted for delivery to the tumor. This would prevent many of the systemic side-effects of the drug and restrict its effects only to TIIs demonstrated to experience immunosuppression as a result of MAO-A activity (Figure 1C) (24). Liposomal drug delivery has been shown to limit systemic toxicity and improve drug delivery efficacy by inhibiting the diffusion of the nanoformulated particle across the blood-brain barrier (25). Currently, crosslinked multilamellar liposomes are the subject of ongoing trials for cancer drug delivery, and, by nanoformulating such liposomes for MAOI delivery, researchers may be able to increase drug payload size and decrease detrimental side effects, improving efficacy and avoiding life-threatening risks associated with these astounding, multifaceted drugs (26).

DISCUSSION

The discovery of MAO-A as an immune checkpoint offers an exciting new pathway that can be explored for the development of novel therapies repurposing drugs developed for the regulation of neuronal serotonin signaling (5, 14). Research has demonstrated that MAOIs have the ability not only to prevent

the degradation of autocrine, immunostimulatory serotonin by MAO-A in T cells, but also to decrease immunosuppressive TAM polarization by inhibiting the production of ROS that results from MAO-A activity. Further studies are needed to investigate the clinical correlations between MAOI treatment and clinical outcomes in patients with cancer. Moreover, the identification and description of MAO-A as an immune checkpoint in CD8 T cells and TAMs suggests promising possibilities for investigation into its role as a checkpoint in other immune cell types.

While the potential associated with the use of a multifaceted ICB therapy such as MAOIs is impressive, it is important to consider the adverse side-effects that can greatly threaten the comfort and safety of the patient. However, there are several avenues of research that may help mitigate these side effects while successfully downregulating immunosuppressive pathways. As discussed, the use of liposomal drug delivery systems has shown significant promise in increasing the specificity of small-molecule drug delivery, and the development of a liposomal MAOI could provide the necessary specificity to avoid the adverse side effects currently associated with MAOI treatment (14, 18).

Additionally, the serotonergic pathway is complex, and, while the direct administration of serotonin would likely have limited lasting effects, other important protein targets in the serotonin production, reception, transport, and degradation pathway could potentially lead to more effective or less adverse ICB (5, 27). Because this pathway is well understood in the brain, there are already many types of drugs developed for the improvement of serotonin reception, several of which could potentially be repurposed for ICB therapy if demonstrated to have antitumor effects in future studies.

Because of the nature of cancer, novel drugs that can target the multifaceted pathways by which the disease avoids the immune system are always needed (6, 28). MAOIs in effect increase the amount of antitumor T cell stimulation by decreasing the expression of immunosuppressive markers *via* autologous serotonin-MAPK signaling, which is nonredundant

REFERENCES

- Pintar JE, Breakefield XO. Monoamine Oxidase (MAO) Activity as a Determinant in Human Neurophysiology. *Behavior Genetics* (1982) 12:53– 68. doi: 10.1007/BF01065740
- Deneris E, Gaspar P. Serotonin Neuron Development: Shaping Molecular and Structural Identities. Wiley Interdiscip Rev: Dev Biol (2018) 7:1–26. doi: 10.1002/wdev.301
- Bortolato M, Chen K, Shih JC. Monoamine Oxidase Inactivation: From Pathophysiology to Therapeutics. *Adv Drug Deliv Rev* (2008) 60:1527–33. doi: 10.1016/j.addr.2008.06.002
- Jacobs BL, Azmitia EC. Structure and Function of the Brain Serotonin System. *Physiological Rev* (1992) 72:165–230. doi: 10.1152/physrev.1992.72.1.165
- Wang X, Li B, Kim YJ, Wang Y-C, Li Z, Yu J, et al. Targeting Monoamine Oxidase a for T Cell-Based Cancer Immunother (2021). Available at: http:// immunology.sciencemag.org/.
- Vermaelen K, Waeytens A, Kholmanskikh O, van den Bulcke M, van Valckenborgh E. Perspectives on the Integration of Immuno-Oncology Biomarkers and Drugs in a Health Care Setting. *Semin Cancer Biol* (2018) 52:166–77. doi: 10.1016/j.semcancer.2017.11.011

to other immune checkpoint regulatory pathways, suggesting that they may have widespread applications as a combination therapy that increases the efficacy of classical ICBs. MAOIs' inhibition of alternative macrophage polarization also plays a major role in increasing the host antitumor response (14). It remains to be seen whether combination with new ICB therapies which act directly on macrophage activity to promote immune infiltration, such as anti-CD47, increases patient response. In addition to their efficacy as an immune checkpoint blockade, MAOIs' status as antidepressants could also be beneficial, as the dual role of this drug could help alleviate the depression experienced by many cancer patients while also assisting their immune system in combating their malignancy (14). While there is still much work to be done surrounding the full potential of serotonin regulation as an ICB therapy, the demonstration of MAOIs as an effective antitumor drug is a promising and inspiring development in the effort against cancer.

AUTHOR CONTRIBUTIONS

This manuscript was written by JB, BL, and LY. All authors contributed to the article and approved the submitted version.

FUNDING

This work was supported by a Magnolia Council Senior Investigator Grant Award from the Tower Cancer Research Foundation (to LY).

ACKNOWLEDGMENTS

The authors would like to acknowledge the members fo the Yang Lab for contributing insights and discussion surrounding the topic. Figures were created in biorender.com.

- Chen DS, Mellman I. Oncology Meets Immunology: The Cancer-Immunity Cycle. *Immunity* (2013) 39:1–10. doi: 10.1016/j.immuni.2013.07.012
- Page DB, Postow MA, Callahan MK, Allison JP, Wolchok JD. Immune Modulation in Cancer With Antibodies. *Annu Rev Med* (2014) 65:185–202. doi: 10.1146/annurev-med-092012-112807
- Wang H, Kaur G, Sankin AI, Chen F, Guan F, Zang X. Immune Checkpoint Blockade and CAR-T Cell Therapy in Hematologic Malignancies. *J Hematol* Oncol (2019) 12:1–20. doi: 10.1186/s13045-019-0746-1
- Yeon Yeon S, Jung SH, Jo YS, Choi EJ, Kim MS, Chung YJ, et al. Immune Checkpoint Blockade Resistance-Related B2M Hotspot Mutations in Microsatellite-Unstable Colorectal Carcinoma. *Pathol Res Pract* (2019) 215:209–14. doi: 10.1016/j.prp.2018.11.014
- Ngiow SF, Young A, Jacquelot N, Yamazaki T, Enot D, Zitvogel L, et al. A Threshold Level of Intratumor CD8+ T-Cell PD1 Expression Dictates Therapeutic Response to Anti-PD1. *Cancer Res* (2015) 75:3800–11. doi: 10.1158/0008-5472.CAN-15-1082
- Zhang X, Chen W, Fan J, Wang S, Xian Z, Luan J, et al. Disrupting CD47-Sirpα Axis Alone or Combined With Autophagy Depletion for the Therapy of Glioblastoma. *Carcinogenesis* (2018) 39:689–99. doi: 10.1093/ carcin/bgy041

- Patel SA, Minn AJ. Combination Cancer Therapy With Immune Checkpoint Blockade: Mechanisms and Strategies. *Immunity* (2018) 48:417–33. doi: 10.1016/j.immuni.2018.03.007
- Wang YC, Wang X, Yu J, Ma F, Li Z, Zhou Y, et al. Targeting Monoamine Oxidase a-Regulated Tumor-Associated Macrophage Polarization for Cancer Immunotherapy. *Nat Commun* (2021) 12:1–17. doi: 10.1038/s41467-021-23164-2
- Ding F, Liu B, Zou W, Tian D, Li Q, Dai J, et al. LPS Exposure in Early Life Protects Against Mucus Hypersecretion in Ovalbumin-Induced Asthma by Down-Regulation of the IL-13 and JAK-STAT6 Pathways. *Cell Physiol Biochem* (2018) 46:1263–74. doi: 10.1159/000489109
- Nappo G, Handle F, Santer FR, McNeill R v., Seed RI, Collins AT, et al. The Immunosuppressive Cytokine Interleukin-4 Increases the Clonogenic Potential of Prostate Stem-Like Cells by Activation of STAT6 Signalling. Oncogenesis (2017) 6:1–12. doi: 10.1038/oncsis.2017.23
- Charras A, Arvaniti P, le Dantec C, Dalekos GN, Zachou K, Bordron A, et al. JAK Inhibitors and Oxidative Stress Control. *Front Immunol* (2019) 10:2814. doi: 10.3389/fimmu.2019.02814
- Gross ME, Agus DB, Dorff TB, Pinski JK, Quinn DI, Castellanos O, et al. Phase 2 Trial of Monoamine Oxidase Inhibitor Phenelzine in Biochemical Recurrent Prostate Cancer. Prostate Cancer Prostatic Dis (2021) 24:61–8. doi: 10.1038/s41391-020-0211-9
- Tran BX, Ha GH, Vu GT, Nguyen LH, Latkin CA, Nathan K, et al. Indices of Change, Expectations, and Popularity of Biological Treatments for Major Depressive Disorder Between 1988 and 2017: A Scientometric Analysis. *Int J Environ Res Public Health* (2019) 16:1–15. doi: 10.3390/ijerph16132255
- 20. Sabri MA, Saber-Ayad MM. *Mao Inhibitors*. Treasure Island, FL: StatPearls Publishing (2021).
- Volz H-P, Gleiter CH. Monoamine Oxidase Inhibitors a Perspective on Their Use in the Elderly. *Drugs & Aging* (1998) 13:341–55. doi: 10.2165/00002512-199813050-00002
- Ellison EC, Pawlik TM, Way DP, Satiani B, Williams TE. The Impact of the Aging Population and Incidence of Cancer on Future Projections of General Surgical Workforce Needs. Surg (United States) (2018) 163:553–9. doi: 10.1016/ j.surg.2017.09.035
- Carradori S, Secci D, Petzer JP. MAO Inhibitors and Their Wider Applications: A Patent Review. *Expert Opin Ther Patents* (2018) 28:211–26. doi: 10.1080/13543776.2018.1427735

- Mancini S, Nardo L, Gregori M, Ribeiro I, Mantegazza F, Delerue-Matos C, et al. Functionalized Liposomes and Phytosomes Loading Annona Muricata L. Aqueous Extract: Potential Nanoshuttles for Brain-Delivery of Phenolic Compounds. *Phytomedicine* (2018) 42:233–44. doi: 10.1016/j.phymed.2018.03.053
- Rip J, Chen L, Hartman R, van den Heuvel A, Reijerkerk A, van Kregten J, et al. Glutathione Pegylated Liposomes: Pharmacokinetics and Delivery of Cargo Across the Blood-Brain Barrier in Rats. *J Drug Targeting* (2014) 22:460– 7. doi: 10.3109/1061186X.2014.888070
- Joo K, Xiao L, Liu S, Liu Y, Lee CL, Conti PS, et al. Crosslinked Multilamellar Liposomes for Controlled Delivery of Anticancer Drugs. *Biomaterials* (2013) 34:3098–109. doi: 10.1016/j.biomaterials.2013.01.039
- Taciak PP, Lysenko N, Mazurek AP. Drugs Which Influence Serotonin Transporter and Serotonergic Receptors: Pharmacological and Clinical Properties in the Treatment of Depression. *Pharmacol Rep* (2018) 70:37–46. doi: 10.1016/j.pharep.2017.07.011
- Chowdhury PS, Chamoto K, Honjo T. Combination Therapy Strategies for Improving PD-1 Blockade Efficacy: A New Era in Cancer Immunotherapy. *J Internal Med* (2018) 283:110–20. doi: 10.1111/joim.12708

Conflict of Interest: L.Y. in an inventor on patents related to this topic filed by UCLA.

The remaining authors declare that the research was conducted in the absence of any commercial or financial relationships that could be construed as a potential conflict of interest.

Publisher's Note: All claims expressed in this article are solely those of the authors and do not necessarily represent those of their affiliated organizations, or those of the publisher, the editors and the reviewers. Any product that may be evaluated in this article, or claim that may be made by its manufacturer, is not guaranteed or endorsed by the publisher.

Copyright © 2022 Brown, Li and Yang, This is an open-access article distributed under the terms of the Creative Commons Attribution License (CC BY). The use, distribution or reproduction in other forums is permitted, provided the original author(s) and the copyright owner(s) are credited and that the original publication in this journal is cited, in accordance with accepted academic practice. No use, distribution or reproduction is permitted which does not comply with these terms.





Real-World Data of Different Immune Checkpoint Inhibitors for Non-Small Cell Lung Cancer in China

Kang Miao, Xiaotong Zhang, Hanping Wang, Xiaoyan Si, Jun Ni, Wei Zhong, Jing Zhao, Yan Xu, Minjiang Chen, Ruili Pan, Mengzhao Wang^{*†} and Li Zhang^{*†}

OPEN ACCESS

Edited by:

Xuyao Zhang, Fudan University, China

Reviewed by:

Zeguo Sun, Icahn School of Medicine at Mount Sinai, United States Qiaosi Tang, Calico Life Sciences LLC, United States

*Correspondence:

Li Zhang zhanglipumch1026@sina.com Mengzhao Wang mengzhaowang@sina.com [†]These authors share last authorship

Specialty section:

This article was submitted to Cancer Immunity and Immunotherapy, a section of the journal Frontiers in Oncology

Received: 22 January 2022 Accepted: 14 February 2022 Published: 15 March 2022

Citation:

Miao K, Zhang X, Wang H, Si X, Ni J, Zhong W, Zhao J, Xu Y, Chen M, Pan R, Wang M and Zhang L (2022) Real-World Data of Different Immune Checkpoint Inhibitors for Non-Small Cell Lung Cancer in China. Front. Oncol. 12:859938. doi: 10.3389/fonc.2022.859938 Department of Pulmonary and Critical Care Medicine, Peking Union Medical Hospital, Chinese Academy of Medical Science and Peking Union Medical College, Beijing, China

Background: Patients treated with immunotherapy in the real-world may have significantly different responses to those meeting inclusion criteria for random controlled clinical studies. There is a partial overlap in approved indications for the use of the different immune checkpoint inhibitors (ICIs) currently available. A comprehensive assessment of the efficacy, safety and economic effects of various ICIs is a problem that clinicians need to address.

Methods: Analyzed real-world data was collected from non-small cell lung cancer (NSCLC) patients who were treated with ICIs from hospitalized patients in the Lung Cancer Center of Peking Union Medical College Hospital between 2018 and 2021. The objectives were to evaluate the efficacy and safety of different ICIs for the treatment of NSCLC in China and to investigate the factors affecting their curative effects.

Results: Overall, 351 patients were included in the retrospective study. The median PFS for the NSCLC patient cohort treated with medication regimens that included ICIs was 9.5 months, with an ORR of 47.3%. There were no significant discrepancies in efficacy and safety between the different ICIs administered. Factors that had the greatest impact on the efficacy of ICIs were the disease stage, ECOG-PS scores and treatment lines. Gender, age, smoking history, PD-L1 TPS expression, history of targeted therapy and irAEs all had a degree of influence on patient prognosis.

Conclusions: The study reports the experience of real-world usage of ICIs for the treatment of NSCLC patients in China. The results were generally consistent with those of clinical trials, while the efficacy and safety of different ICIs exhibited no statistically significant differences. Therefore, physicians can make a comprehensive choice based on the indications and cost of different ICIs and the preferences of patients.

Keywords: immune checkpoint inhibitors (ICIs), immunotherapy, non-small cell lung cancer (NSCLC), objective response rate (ORR), progression-free survival (PFS), real-world data (RWD)

BACKGROUND

Immune checkpoint inhibitors (ICIs) are a class of antitumor drug that activate lymphocytes, which then attack tumor cells by relieving immune checkpoint-mediated immune-suppression (1, 2). In 2015, two types of ICIs (nivolumab and pembrolizumab) were approved by the U.S. Food and Drug Administration for the treatment of patients with advanced non-small cell lung cancer (NSCLC) (3). Subsequently, immunotherapy was officially introduced into China with the launch of nivolumab and pembrolizumab in June 2018 and July 2018, respectively (4).

Clinical studies under strictly controlled experimental conditions provided an objective assessment of the efficacy and safety of various ICIs, and were the main basis for their approval. However, in the real-world, patients given immunotherapy may have significantly different treatment criteria from those enrolled in clinical trials (5). Based on Keynote 407 and Keynote 189 studies, pembrolizumab was approved for the treatment of NSCLC as combination chemotherapy (6, 7). Further approval of pembrolizumab for monotherapy in PD-L1 positive NSCLC was based on Keynote 042 and Keynote 024 studies (8, 9). Pembrolizumab, which has the most extensive clinical study data available, is usually the first-choice treatment for patients with NSCLC. However, there is partial overlap in the approved indications for different ICIs. Currently, 8 ICIs have been approved for clinical use in China, including 2 imported PD-1 inhibitors (nivolumab and pembrolizumab), 2 imported PD-L1 inhibitors (atezolizumab and durvalumab) and 4 PD-1 inhibitors manufactured in China (camrelizumab, tislelizumab, sintilimab and toripalimab) (10). Therefore, a comprehensive assessment of the efficacy, safety and economic effects of various ICIs has become a problem that clinicians need to address. Studies based on real-world data (RWD) provide a reference for understanding patient outcomes outside of clinical trials and better guide treatment decisions (11). Most of the current clinical studies used patients on conventional chemotherapy as the controls, but unfortunately this resulted in a paucity of data with regard to direct efficacy comparisons between the different ICIs administered. An RWD-based cross-sectional study will help to compare the efficacy and safety of different ICIs.

Thus, a real-world retrospective observational study was conducted to explore the efficacy and safety of different types of ICIs in a cross-sectional manner. In addition, we also investigated the possible risk factors that may affect the efficacy of ICIs to provide guidance for optimization of clinical decision making.

METHODS Study Objectives

This was a retrospective, observational, single-center study that collected and analyzed data from real-world NSCLC patients

treated with ICIs. The objectives were to evaluate the efficacy and safety of different ICIs for the treatment of NSCLC in China and to investigate the impact of factors affecting their curative effects.

Ethics Approval Statement

The study was performed in accordance with the principles of the Declaration of Helsinki and approved by the Ethics Review Committee of Peking Union Medical College Hospital (2020-12-24/HS-2195). Written informed consent was provided by all enrolled patients.

Data Collection

Data from the digital hospital information management system (HIS database) of Peking Union Medical College Hospital were analyzed. Inclusion criteria were patients with NSCLC who had been treated with ICIs and followed up for at least 6 months.

Information about each enrolled patient was carefully documented including: gender; age; pathology type; disease stage; date of diagnosis; targeted drug history; history of smoking; alcohol consumption; Eastern Cooperative Oncology Group performance status (ECOG-PS) scores; PD-L1 TPS (PD-L1 tumor cell proportion score: The percentage of PD-L1 membrane stained tumor cells in the total number of tumor cells); type of ICIs administered; time of initiation of ICI therapy; lines of ICIs; combination chemotherapy; combination antivascular therapy; real-world PFS; optimal efficacy; and immune-related adverse effects (irAEs).

Statistical Analysis

Descriptive analyses of the characteristics of patients, their disease states and treatment were conducted who were then stratified into subgroups of interest. Enumeration data are described according to statistical quantities and percentages. Only one data measurement was included (age in years), presented as the median and interquartile range, because the data were not normally distributed. The implications of different characteristics for PFS were compared using the Kaplan-Meier method and a log-rank test. Median survival estimates and the hazard ratio (HR) from a Cox proportional hazards model, as well as the 95% confidence intervals (CIs) are reported. The PFS was defined as the duration from the onset of treatment with ICIs to disease progression or death, which was assessed based on the date of disease progression as indicated by CT or PET/CT scans confirmed by the supervising physician, or in-hospital death recorded in the HIS database. Logistic regression was used to analyze the effects of different factors on the ORR, and the ORR for each subgroup of interest, the odds ratios (OR) from logistic regression and the corresponding 95% CIs are reported. Indicators from univariate analysis that reached the threshold (P < 0.1) were employed in the multivariate analysis, with a *P*value < 0.05 deemed to be a statistically significant finding. Fisher exact test was used to analyze differences in the incidence rate of irAEs between various ICIs. All statistical analyses were conducted using SPSS (ver. 24.0) and Kaplan-Meier survival curves were constructed using GraphPad Prism (ver. 8.0.1).

Abbreviations: ICIs, immune checkpoint inhibitors; NSCLC, non-small cell lung cancer; ORR, objective response rate; PFS, progression-free survival; RWD, real-world data; ECOG-PS, Eastern Cooperative Oncology Group performance status; irAEs, immune-related adverse effects; HR, hazard ratio; CIs, confidence intervals; OR, odds ratios; NOS, not otherwise specified; CIP, checkpoint inhibitor pneumonitis.

RESULTS

Data from 1,832 patients who received therapy from January 2018 to December 2021 were analyzed. Among them, 461 were NSCLC patients treated with ICIs. To ensure completeness of the survival information, only data from patients followed up for ≥ 6 months were included in the analysis. A total of 110 patients were excluded due to insufficient follow-up, and finally 351 patients were formally included in the study.

The majority (73.8%) were male, with a median age of 65 years. Slightly more patients had non-squamous carcinoma (55.0%) than squamous carcinoma (40.2%), with the remaining 17 patients not otherwise specified (NOS). About 64.7% patients had a history of smoking and 32.8% a history of alcohol consumption. The majority of NSCLC patients were able to take care of themselves at the time of starting immunotherapy (ECOG-PS scores 0 – 1), but the other 11.7% required long-term bed rest (ECOG-PS scores 2 - 4). Circa 78.3% patients treated with ICIs were at stage IV and 19.4% patients with the EGFR/ ALK mutation had previously received targeted therapy. The type of ICIs used for NSCLC was predominantly pembrolizumab (65.2%), with the remaining therapy including nivolumab (5.1%), camrelizumab (6.0%), tislelizumab (6.8%) and sintilimab (7.7%). Basic information had no significant impact on the choice of different types of ICIs except for histology pathology type (P = 0.015) (**Table S1**). ICIs were given as firstline treatment to 53.6% patients, 28.8% for second line treatment and 9.1% for third-line treatment and beyond. ICIs were administered to 30 patients for other reasons including maintenance treatment after radiotherapy and for neoadjuvant treatment before surgery. Immunotherapy was usually administered in combination with chemotherapy (75.2%) for 4-6 courses before being switched to maintenance therapy of ICIs. Only 10.5% patients chose immunotherapy in conjunction with anti-vascular therapy (Table 1). The regimen containing ICIs produced an overall median PFS of 9.5 months, with an ORR of 47.3% (Figure 1A). The 1-year PFS rate was 35.9% and the 2-year PFS rate 8.5%. There was no significant difference between the efficacy of various ICIs, with good overlap of survival curves (P = 0.942) (Figure 1B). The median PFS for pembrolizumab was 9.6 months with an ORR of 45.0%; for nivolumab, the median PFS was 9.2 months with an ORR of 50%; for camrelizumab, the median PFS was 10.4 months with an ORR of 47.6%; for tislelizumab, the median PFS was 10.3 months with an ORR of 54.2%; and for sintilimab, the median PFS was 6.8 months, with an ORR of 51.9% (Table 2). The longest median PFS was produced by camrelizumab (10.4 months) and the highest ORR by tislelizumab (54.2%).

Different application mode of ICIs and patient baseline characteristics may have an impact on prognosis. Lung cancer stage, line of therapy and ECOG-PS scores were the three factors that have the greatest impact on survival (**Table S2**). Thus, the population of stage IV NSCLC patients with ECOG-PS scores of 0 - 1, given ICIs as first-line treatment were selected as the subgroup study population (**Table 3**). The median PFS for this subgroup population was 10.6 months, with an ORR of 51.5% (**Figure 1C**). The most commonly administered ICIs were

TABLE 1 | Basic information.

Basic information	Number	Percentage
Patients	351	100.0%
Sex		
Male	259	73.8%
Female	92	26.2%
Age	65 (60-70)	
< 60	97	27.6%
60-74	221	63.0%
≥ 75	33	9.4%
Histology	100	EE 00/
Non-squamous carcinoma	193 141	55.0% 40.2%
Squamous carcinoma NOS	17	40.2%
	17	4.8%
Lung cancer stage	76	21.7%
IV	275	78.3%
History of targeted therapy	210	10.070
No	283	80.6%
Yes	68	19.4%
Cl type	00	10.470
Pembrolizumab	229	65.2%
Nivolumab	18	5.1%
Camrelizumab	21	6.0%
Tislelizumab	24	6.8%
Sintilimab	27	7.7%
Others	32	9.1%
Line of therapy	02	011/0
First-line	188	53.6%
Second-line	101	28.8%
Third-line and beyond	32	9.1%
Others	30	8.5%
Combined chemotherapy		
No	87	24.8%
Mono chemotherapy	41	11.7%
Doublet chemotherapy	223	63.5%
Combined anti-vascular therapy		
No	314	89.5%
Yes	37	10.5%
Smoking status		
No	124	35.3%
Yes	227	64.7%
Drinking status		
No	236	67.2%
Yes	115	32.8%
ECOG-PS		
0	148	42.2%
1	162	46.2%
2	27	7.7%
3	7	2.0%
4	7	2.0%
Recorded irAEs (need glucocorticoids)	60	
Grade 1	8	13.3%
Grade 2	18	30.0%
Grade 3	14	23.3%
Grade 4	20	33.3%
PD-L1 TPS	91	
0%	21	23.1%
1-49%	37	40.7%
≥ 50%	33	36.3%
Primary efficacy assessment		
PR	166	47.3%
SD	130	37.0%
PD	55	15.7%

NOS, not otherwise specified; ICI, immune checkpoint inhibitor; ECOG-PS, Eastern Cooperative Oncology Group performance status; irAEs, immune-related adverse events; TPS, turnor cell proportion score; PR, partial response; SD, stable disease; PD, progressive disease.

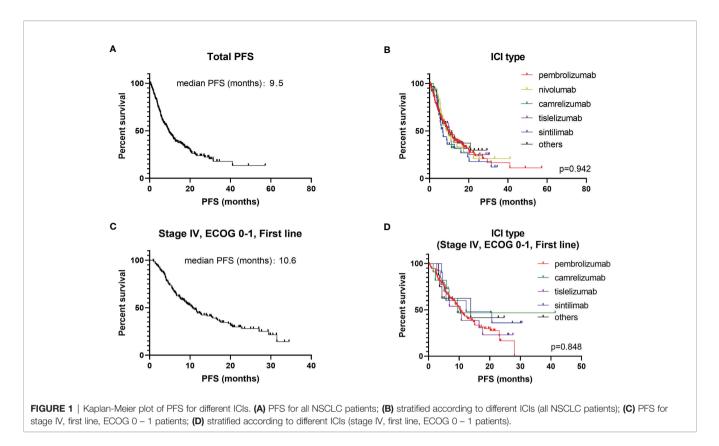


TABLE 2	Differences in	efficacy b	etween ICIs	(all NSCLC)	natients)
	Dilici choco in	childady b	000000000000000000000000000000000000000		pationitoj.

	number	Cox regression			Logistic regression				
		Median PFS	HR	95%CI	P-value	ORR	OR	95%CI	P-value
Total	351								
Pembrolizumab	229	9.6 months	Reference		0.943	45.0%	Reference		0.894
Nivolumab	18	9.2 months	0.945	0.545-1.638	0.840	50.0%	0.817	0.313-2.135	0.681
Camrelizumab	21	10.4 months	1.077	0.610-1.901	0.799	47.6%	0.899	0.367-2.201	0.816
Tislelizumab	24	10.3 months	0.917	0.547-1.537	0.741	54.2%	0.692	0.297-1.609	0.392
Sintilimab	27	6.8 months	1.212	0.773-1.903	0.402	51.9%	0.759	0.342-1.687	0.499
Others	32	9.7 months	0.909	0.563-1.466	0.695	53.1%	0.721	0.344-1.514	0.388

ICIs, immune checkpoint inhibitors; PFS, progression-free survival; HR, hazard ratio; 95% CI, 95% confidence interval; ORR, objective response rate; OR, odds ratio;

pembrolizumab, camrelizumab, tislelizumab and sintilimab. Nivolumab is less commonly used in first-line therapy due to its price and lack of associated single-agent indications. The results of survival analysis showed that there was no significant difference in efficacy between the various ICIs in this subgroup, with a median PFS of 9.4–13.8 months and ORR of 47.9–63.6% (P = 0.846) (**Figure 1D**).

For the safety analysis, immune-related adverse effects (irAEs) that required glucocorticoids intervention or discontinuation of ICIs were counted. A total of 60 patients (17.1%) had concerning irAEs, of which 34 (9.7%) were of grade 3 or higher. The types of adverse events mainly included immune-related pneumonia (39 cases, 11.1%), liver toxicity (8 cases, 2.2%), skin toxicity (13 cases, 3.7%), colitis (10 cases, 2.8%), myocarditis (4 cases, 1.1%), and other types of irAEs (9 cases, 2.6%) (**Table 4**). There was no statistical difference in the

incidence of irAEs or severe irAEs for the different ICIs administered (P = 0.607). Death occurred in 9 patients due to severe irAEs, including 5 cases of pneumonia, 2 cases of myocarditis, 1 case of colitis and 1 case of liver toxicity. Additionally, patients who developed grade 1 to 2 irAEs (median PFS: 17.4 months, ORR: 61.7%) had a significantly better survival prognosis than those without irAEs (median PFS: 8.7 months, ORR: 44.3%) and those patients who developed grades 3 to 4 irAEs (median PFS: 7.5 months, ORR. 44.4%) (P = 0.017) (**Figure 2A**).

The patients were stratified according to their basic condition and treatment regimen. Factors included gender, age, pathology type, disease stage, type of ICIs, treatment line of ICIs, combination chemotherapy, combination anti-vascular therapy, history of smoking, history of alcohol consumption and ECOG-PS scores. After univariate Cox regression analysis,

TABLE 3 | Differences in efficacy between ICIs (Stage IV, first line, ECOG 0-1 patients).

	cox regression				logistic regression				
	number	Median PFS	HR	95%CI	p-value	ORR	OR	95%CI	p-value
Total	136								
Pembrolizumab	94	10.2 months	R	Reference		47.9%	R	eference	0.768
Camrelizumab	11	9.4 months	0.779	0.313-1.940	0.592	63.6%	0.525	0.144-1.913	0.329
Tislelizumab	13	10.4 months	0.825	0.409-1.662	0.590	53.8%	0.787	0.246-2.519	0.687
Sintilimab	10	12.3 months	0.664	0.285-1.550	0.344	60.0%	0.612	0.162-2.311	0.469
Others	8	13.8 months	0.703	0.256-1.993	0.495	62.5%	0.551	0.125-2.439	0.432

ICIs, immune checkpoint inhibitors; PFS, progression-free survival; HR, hazard ratio; 95% CI, 95% confidence interval; ORR, objective response rate; OR, odds ratio.

TABLE 4 | Differences in safety between ICIs.

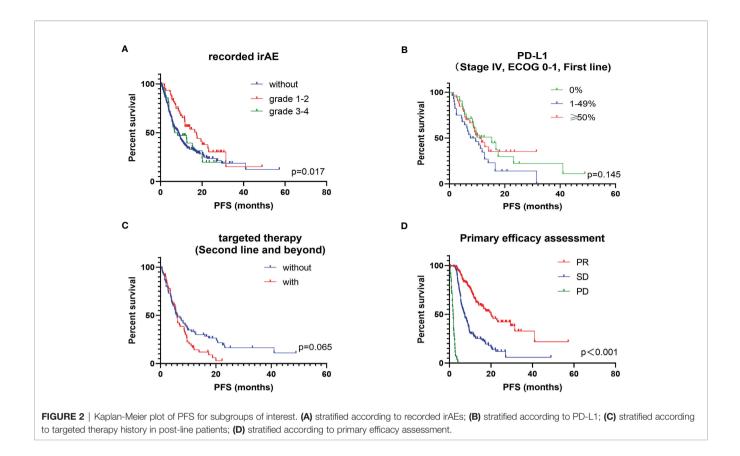
ICI		Pembrolizumab	Camrelizumab	Tislelizumab	Nivolumab	Sintilimab	Others	Total
Patients		229	21	24	18	27	32	351
Pneumonia	All grade	26 (11.4%)	2 (9.6%)	3 (12.5%)	2 (11.2%)	2 (7.4%)	4 (12.6%)	39 (11.1%)
	≥3 grade	10 (4.4%)	1 (4.8%)	2 (8.3%)	1 (5.6%)	1 (3.7%)	2 (6.3%)	22 (4.8%)
Myocarditis	All grade	2 (0.9%)	1 (4.7%)	1 (4.2%)	0 (0.0%)	0 (0.0%)	0 (0.0%)	4 (1.1%)
	≥3 grade	1 (0.4%)	1 (4.7%)	1 (4.2%)	0 (0.0%)	0 (0.0%)	0 (0.0%)	3 (0.8%)
Skin toxicity	All grade	9 (3.9%)	0 (0.0%)	1 (4.2%)	1 (5.6%)	1 (3.1%)	1 (3.7%)	13 (3.7%)
	≥3 grade	4 (1.7%)	0 (0.0%)	1 (4.2%)	0 (0.0%)	1 (3.1%)	1 (3.7%)	7 (2.0%)
Colitis	All grade	7 (3.1%)	0 (0.0%)	1 (4.2%)	0 (0.0%)	2 (7.4%)	0 (0.0%)	10 (2.8%)
	≥3 grade	4 (1.7%)	0 (0.0%)	1 (4.2%)	0 (0.0%)	2 (7.4%)	0 (0.0%)	7 (2.0%)
Liver toxicity	All grade	6 (2.6%)	0 (0.0%)	1 (4.2%)	0 (0.0%)	0 (0.0%)	1 (3.1%)	8 (2.2%)
	≥3 grade	4 (1.7%)	0 (0.0%)	0 (0.0%)	0 (0.0%)	0 (0.0%)	0 (0.0%)	4 (1.1%)
Others	All grade	4 (1.7%)	1 (4.7%)	0 (0.0%)	1 (5.6%)	2 (7.4%)	1 (3.1%)	9 (2.6%)
	≥3 grade	2 (0.9%)	0 (0.0%)	0 (0.0%)	1 (5.6%)	1 (3.1%)	0 (0.0%)	4 (1.1%)
Total	All grade	41 (17.9%)	3 (14.3%)	4 (16.7%)	3 (16.7%)	4 (14.8%)	5 (15.6%)	60 (17.1%)
	≥3 grade	22 (9.6%)	2 (9.6%)	3 (12.5%)	2 (11.2%)	2 (7.4%)	3 (9.4%)	34 (9.7%)

ICI, immune checkpoint inhibitor.

most factors were found to influence PFS to some extent (Figures S1A-K). Females had a significantly worse prognosis than males (P = 0.005) and also the prognosis was worse in patients < 60 years old and in those \geq 75 years old (P = 0.085). Patients with squamous carcinoma had a slightly better survival benefit from treatment with ICIs than those with non-squamous carcinoma (P = 0.059). The survival benefit resulting from ICIs therapy was significantly better in NSCLC patients with stage III disease compared to those with stage IV disease (P < 0.001). The prolongation of PFS produced by giving ICIs as first-line treatment was longer than that for post-line treatment (P < 0.001). In terms of combination therapy, a platinumbased chemotherapy regimen was significantly better than mono chemotherapy or de-chemotherapy regimens (P < 0.001). However, instead of contributing to the prolongation of PFS, a combination with anti-vascular therapy had a negative effect (P = 0.041). De-chemotherapy was chosen by 46.7% of patients who adopted ICIs in combination with antivascular therapy, while only 9.1% patients without combined anti-vascular therapy chose the de-chemotherapy regimen (Figure S1L). Patients with a history of smoking may benefit more from ICI therapy (P < 0.001). In addition, a poor general condition (ECOG-PS scores 2 to 4) was a significant associated risk factor for a poor prognosis (P < 0.001). Eight indicators, with significant differences in the univariate Cox regression, were included in the multivariate Cox regression analysis. It was found

that the 3 indicators with the most significant influence on PFS were the disease stage, lines of ICIs administered and the ECOG-PS score (**Table S2**). A similar conclusion was reached when data were analyzed in terms of the ORR for NSCLC patients with therapeutic regimens containing ICIs. The overall ORR for the NSCLC cohort who received treatment regimens that included ICIs was 47.3%. After multifactorial logistic regression analysis, the 3 most influential risk factors for ORR remained the disease stage, line of ICIs and the ECOG-PS score (**Table S3**).

Other factors that may influence the efficacy of ICIs were also explored, mainly the PD-L1 TPS expression status, history of targeted therapy and the results of first efficacy assessment on overall PFS. PD-L1 TPS expression was recorded in 91 patients. Patients with high PD-L1 TPS expression (\geq 50%) had a longer PFS benefit compared to those with a low PD-L1 TPS expression (1-49%). Surprisingly, patients with negative PD-L1 TPS expression did not show a worse survival benefit, which was slightly better than those with low PD-L1 TPS expression (P =0.145) (Figure 2B). Previous studies concluded that patients with positive driver genes were the population with a poor prognosis for immunotherapy (12, 13). Of the 351 patients we studied, 133 received ICIs as a backline treatment, among which 59 had received targeted therapy. In post-line therapy, patients who had received targeted therapy had an ORR of 31.1% and a median PFS of 5.9 months, while patients without driver mutations had an ORR of 28.8% and a median PFS of 6.0



months. Although the survival benefit did not reach a statistically significant difference between the two groups (P = 0.065), a trend of shorter PFS benefit was observed in patients with a history of targeted therapy on the survival curves (**Figure 2C**). In clinical practice, the therapeutic efficacy evaluated by impactology was generally conducted after every 2 cycles of treatment, while initial efficacy provided a good indication of the long-term survival benefit. The median PFS was 7.4 months for patients with a first evaluation of stable disease (SD) and 20.1 months for patients with a first evaluation of a partial response (PR) (P < 0.001) (**Figure 2D**).

DISCUSSION

To the best of our knowledge, this is the first large study conducted in China to cross-sectionally compare the efficacy and safety of different ICIs with RWD. The overall median PFS was 9.5 months and the ORR was 47.3%. The survival data were significantly better than those reported in earlier real-world studies, which may be attributed to a difference in the ratio of patients enrolled (14, 15). Recently, with the rapid development of immunotherapy, the use of ICIs has gradually expanded to become first-line treatment for patients with NSCLC (16). For real-world application of ICIs, Khozin et al. reported a median PFS time of 3.2 months, while Areses et al. reported a median PFS of 4.8 months (15, 16). However, ICIs were used primarily for post-line therapy in the latter study, whereas the population included in the present study was comprised of a much greater proportion of patients given first-line ICIs treatment. In contrast to real-world studies, randomized controlled trials tend to have strict screening criteria for enrolling subjects. We singled out patients with stage IV disease, ECOG-PS scores of 0 to 1 and who had received first-line ICIs treatment, which are factors considered in the screening criteria for most clinical trials. In this subgroup, the median PFS time was 10.6 months with an ORR of 51.5%, which was generally consistent with data from the clinical studies of first-line application of ICIs combined with chemotherapy (PFS: 8.0–11.3 months, ORR: 48.3–64.8%) (6, 7, 17).

The choice of ICIs has been a troubling issue for physicians, as clinical trials of different ICIs cannot be compared cross-sectionally (18). Therefore, we sought to explore the discrepancies in the efficacy and safety of different ICIs in a real-world study. Pembrolizumab in combination with chemotherapy for NSCLC demonstrated a significant survival benefit over chemotherapy in the Keynote 407 and Keynote 189 studies, with a median PFS of 8.0–9.0 months and ORR of 48.3 – 57.9% (6, 7). In our real-world cohort of patients, pembrolizumab exhibited a median PFS of 9.6 months and an ORR of 45.0%, similar to the results of clinical studies. NSCLC patients treated with camrelizumab had median PFS of 8.5 – 11.3 months and ORRs of 60.0 – 64.8% in the Camel-sq study and Camel study, respectively (17, 19). In terms of absolute values of median PFS and ORR, the efficacy of camrelizumab seems to be better than

pembrolizumab. However, in our cohort of patients, there was no significant difference between the efficacy of camrelizumab (median PFS: 10.4 months; ORR: 47.6%) and pembrolizumab. Tislelizumab produced a median PFS of 7.6 months and 9.7 months in the Ratinale 307 and Ratinale 304 studies, with ORRs of 72.5% and 57.4%, respectively (20). In our cohort of patients, it produced a median PFS of 10.3 months with an ORR of 54.2%, which was not statistical difference from pembrolizumab. In the Orient 11 study, sintilimab combined with chemotherapy resulted in a median PFS of 8.9 months and an ORR of 51.9% for nonsquamous NSCLC patients (21). In our cohort, the ORR for sintilimab was 51.9%, similar to that reported in the Orient 11 study, and not significantly dissimilar to other ICIs. However, it had a median PFS of only 6.8 months, significantly lower than other ICIs in our cohort of patients. Considering the impact of baseline information on survival prognosis, we analyzed the baseline treatment information and found that the majority population treated with sintilimab were post-line. Therefore, we further analyzed a subgroup population (stage IV, first line, ECOG 0-1) and found that the efficacy of sintilimab was not any worse than that of other ICIs.

For the safety analysis, as our study was a retrospective analysis, recording the occurrence of all adverse events was rather difficult. Therefore, we focused on irAEs that required glucocorticoid interventions or suspension of ICIs, which were of most concern to clinicians. The results showed that there was no statistically difference in the incidence of irAEs produced by different PD-1 inhibitors. The most common irAEs that require glucocorticoids treatment was checkpoint inhibitor pneumonitis (CIP). The incidence of CIP in our cohort was 11.1%, and 4.8% for severe CIP (grade 3 or above), similar to previous reports (3.5–19%) (22). In addition, there was a significant correlation between the incidence of CIP and radiotherapy. CIP occurred in 26.3% patients who had chest radiotherapy during immunotherapy, compared with 8.6% patients without radiotherapy (P = 0.001). As there were no significant differences in efficacy and safety between the various types of ICIs, physicians can make a comprehensive choice based on indications and the cost of different ICIs, and the preference of patients. In fact, the occurrence of irAEs does not always imply a poor prognosis. Patients who developed severe irAEs need to discontinue ICIs and be treated with glucocorticoids or even immunosuppressive drugs, which can promote tumor growth (23). Therefore, severe irAEs do lead to a poor prognosis for NSCLC patients. However, mild irAEs not only do not affect tumor treatment, they have a positive impact on prognosis, compared to those who do not develop irAEs. Recently, irAEs have emerged as a potential clinical biomarker for predicting the efficacy of ICIs (24). Our results reconfirmed the idea that patients with grade 1-2 irAEs had a longer median PFS than those without irAEs.

More than 75% of patients included in the present study were over 60 years old. Previous research suggested that the efficacy of ICIs, as well as the patient tolerance of ICIs, was not significantly correlated with age (25). However, our results indicated that the 60-74-year-old population exhibited a longer PFS time, but there was no significant difference in ORR. Younger patients (< 60 years old) tend to be metabolically active with high tumor malignancy (26), while elderly patients (\geq 75 years old) frequently have poor ECOG-PS scores, which is an inherent risk factor for the efficacy of ICIs (27). The influence of gender on the efficacy of ICIs has been reported in a number of studies. Keynote 024 revealed that males were more likely to benefit from ICI therapy (8). In contrast, the real-world study by Khozin et al. found that females achieved longer PFS and OS times after ICI therapy (16). The findings of the present study showed that males benefited more than females from ICI therapy in the overall NSCLC cohort of patients.

Researchers have been trying to establish the best combination immunotherapy regimens. Currently, the most commonly used immunotherapy regimens include ICIs combined with chemotherapy, as well as single ICI (6, 9). In addition, double immunization combination regimens and the combination of ICIs with anti-vascular therapy are also directions worthy of further investigation (28, 29). Currently, CTLA-4 inhibitors have not yet been marketed in China, thus real-world data on double immunization combination regimens are lacking. In contrast, anti-vascular drugs, such as bevacizumab and anlotinib, have occupied a pivotal position for the treatment of NSCLC. The efficacy and safety of immunotherapy in combination with antivascular therapy has been confirmed (30). However, the findings of the present study revealed that anti-vascular therapy combined with immunotherapy failed to improve the efficacy of ICIs. On the one hand, the majority of patients who opted for combined antivascular therapy chose a concurrent de-chemotherapy regimen. On the other hand, a 4-drug combination regimen (platinumbased chemotherapy + ICIs + anti-vascular therapy) has not yet been authorized for relevant clinical applications (29). In the realworld, this regimen has been used primarily in young patients with high expectations of a good prognosis or having liver metastases. Anti-vascular therapy has been used in 16.7% of young patients (< 60 years old) compared to 8.6% of elderly patients (\geq 75 years old) (P = 0.036), and in 17.1% of patients with liver metastases compared to 7.8% patients without liver metastases. These data might partially explain why the median PFS was shorter after combination anti-vascular therapy.

Despite great heterogeneity, PD-L1 expression levels remain the best biomarker to predict the efficacy of PD-1 inhibitors in NSCLC patients (31, 32). Patients with a high PD-L1 TPS expression (> 50%) had a better PFS benefit than those with low expression of PD-L1 TPS (< 50%). However, the survival prognosis of patients with low PD-L1 TPS expression appears to be inferior to that of patients with negative PD-L1 TPS expression. This finding indicates that PD-L1 still has a great defect as a biomarker for predicting the efficacy of immunotherapy, and indirectly supports the idea that PD-L1 expression is highly heterogeneous in tumor tissues. Khozin et al. concluded that the presence of driver gene mutations was a risk factor for poor prognosis after treatment with ICIs (33). To avoid interference by treatment lines, NSCLC patients who used ICIs as first-line treatment were excluded. The majority of first-line treatment options for patients with driver mutations are targeted therapy. We divided the patient population who would receive post-line ICI therapy into 2 subgroups, namely those given chemotherapy as first-line treatment and those who received

targeted therapy as first-line treatment. The results indicated that the presence of driver gene mutations and a history of targeted therapy did affect the efficacy of subsequent treatment with ICIs in the long-term PFS but not the ORR.

Inevitably, there were some limitations to our study. First, the HIS database only recorded the survival endpoints of a small number of patients (patients who died in our hospital) and thus there is a lack of OS data. Second, the gene mutation status, PD-L1 expression information and irAEs were incompletely recorded in the HIS database, which may lead to analysis bias. Third, the number of cases for each type of ICIs except pembrolizumab were small, so that the results may be affected by random effects. Fourth, our study focused on the current status of ICI therapy in China, with all enrolled patients being Asian and therefore the results may not be completely applicable to other races.

CONCLUSIONS

A single-center, real-world study in China was conducted to explore the efficacy and safety of different ICIs for NSCLC therapy, along with the impact of patient baseline characteristics and treatment regimens on prognosis. The overall median PFS for the NSCLC patient cohort treated with regimens including ICIs was 9.5 months, with an ORR of 47.3%. There were no significant discrepancies in efficacy and safety between the different ICIs administered. Factors that had the greatest impact on the efficacy of ICIs were the disease stage, ECOG-PS scores and treatment lines. It is noteworthy that gender, age, smoking history, PD-L1 expression, history of targeted therapy, and irAEs all had a degree of influence on patient prognosis.

DATA AVAILABILITY STATEMENT

The original contributions presented in the study are included in the article/**Supplementary Material**. Further inquiries can be directed to the corresponding authors.

REFERENCES

- Duma N, Santana-Davila R, Molina JR. Non-Small Cell Lung Cancer: Epidemiology, Screening, Diagnosis, and Treatment. *Mayo Clin Proc* (2019) 94:1623–40. doi: 10.1016/j.mayocp.2019.01.013
- Morgensztern D, Herbst RS. Nivolumab and Pembrolizumab for Non-Small Cell Lung Cancer. Clin Cancer Res (2016) 22:3713–7. doi: 10.1158/1078-0432.Ccr-15-2998
- Lurienne L, Cervesi J, Duhalde L, de Gunzburg J, Andremont A, Zalcman G, et al. NSCLC Immunotherapy Efficacy and Antibiotic Use: A Systematic Review and Meta-Analysis. J Thorac Oncol (2020) 15:1147–59. doi: 10.1016/j.jtho.2020.03.002
- Sheng J, Li H, Yu X, Yu S, Chen K, Pan G, et al. Efficacy of PD-1/PD-L1 Inhibitors in Patients With Non-Small Cell Lung Cancer and Brain Metastases: A Real-World Retrospective Study in China. *Thorac Cancer* (2021) 12:3019–31. doi: 10.1111/1759-7714.14171
- Kim HS, Lee S, Kim JH. Real-World Evidence Versus Randomized Controlled Trial: Clinical Research Based on Electronic Medical Records. J Korean Med Sci (2018) 33:e213. doi: 10.3346/jkms.2018.33.e213

ETHICS STATEMENT

The studies involving human participants were reviewed and approved by Ethics Review Committee of Peking Union Medical College Hospital. The patients/participants provided their written informed consent to participate in this study.

AUTHOR CONTRIBUTIONS

KM: Drafting the manuscript and revising it for important intellectual content. XZ, HW, XS, JN, WZ, JZ, YX, MC, and RP: Provision of clinical data, article revision and correction. LZ and MW: Substantial contributions to the conception or design of the work and final approval of the version to be published.

ACKNOWLEDGMENTS

The authors would like to thank all medical staff at the Lung Cancer Center of Peking Union Medical College Hospital.

SUPPLEMENTARY MATERIAL

The Supplementary Material for this article can be found online at: https://www.frontiersin.org/articles/10.3389/fonc.2022. 859938/full#supplementary-material

Supplementary Figure 1 | Kaplan-Meier plot of PFS for subgroups for basic Information. (A) stratified according to sex; (B) stratified according to age; (C) stratified according to histology; (D) stratified according to lung cancer stage; (E) stratified according to the ICI type; (F) stratified according to the line of therapy; (G) stratified according to whether combined with chemotherapy; (H) stratified according to whether combined with anti-vascular therapy; (I) stratified according to smoking status; (J) stratified according to drinking status; (K) stratified according to the ECOG-PS score; (L) Correlation between chemotherapy and anti-vascular therapy. PFS, progression-free survival; ECOG-PS, Eastern Cooperative Oncology Group performance status; ICI, immune checkpoint inhibitor; PR: partial response; SD: stable disease; PD: progressive disease.

- Paz-Ares L, Vicente D, Tafreshi A, Robinson A, Soto Parra H, Mazières J, et al. A Randomized, Placebo-Controlled Trial of Pembrolizumab Plus Chemotherapy in Patients With Metastatic Squamous NSCLC: Protocol-Specified Final Analysis of KEYNOTE-407. *J Thorac Oncol* (2020) 15:1657– 69. doi: 10.1016/j.jtho.2020.06.015
- Gadgeel S, Rodríguez-Abreu D, Speranza G, Esteban E, Felip E, Dómine M, et al. Updated Analysis From KEYNOTE-189: Pembrolizumab or Placebo Plus Pemetrexed and Platinum for Previously Untreated Metastatic Nonsquamous Non-Small-Cell Lung Cancer. J Clin Oncol (2020) 38:1505– 17. doi: 10.1200/jco.19.03136
- Reck M, Rodríguez-Abreu D, Robinson AG, Hui R, Csőszi T, Fülöp A, et al. Updated Analysis of KEYNOTE-024: Pembrolizumab Versus Platinum-Based Chemotherapy for Advanced Non-Small-Cell Lung Cancer With PD-L1 Tumor Proportion Score of 50% or Greater. *J Clin Oncol* (2019) 37:537–46. doi: 10.1200/jco.18.00149
- Mok TSK, Wu YL, Kudaba I, Kowalski DM, Cho BC, Turna HZ, et al. Pembrolizumab Versus Chemotherapy for Previously Untreated, PD-L1-Expressing, Locally Advanced or Metastatic Non-Small-Cell Lung Cancer

(KEYNOTE-042): A Randomised, Open-Label, Controlled, Phase 3 Trial. Lancet (2019) 393:1819-30. doi: 10.1016/s0140-6736(18)32409-7

- Gan J, Huang Y, Fang W, Zhang L. Research Progress in Immune Checkpoint Inhibitors for Lung Cancer in China. *Ther Adv Med Oncol* (2021) 13:17588359211029826. doi: 10.1177/17588359211029826
- Pasello G, Pavan A, Attili I, Bortolami A, Bonanno L, Menis J, et al. Real World Data in the Era of Immune Checkpoint Inhibitors (ICIs): Increasing Evidence and Future Applications in Lung Cancer. *Cancer Treat Rev* (2020) 87:102031. doi: 10.1016/j.ctrv.2020.102031
- Qiao M, Jiang T, Liu X, Mao S, Zhou F, Li X, et al. Immune Checkpoint Inhibitors in EGFR-Mutated NSCLC: Dusk or Dawn? J Thorac Oncol (2021) 16:1267–88. doi: 10.1016/j.jtho.2021.04.003
- Wu L, Ke L, Zhang Z, Yu J, Meng X. Development of EGFR TKIs and Options to Manage Resistance of Third-Generation EGFR TKI Osimertinib: Conventional Ways and Immune Checkpoint Inhibitors. *Front Oncol* (2020) 10:2020.602762. doi: 10.3389/fonc.2020.602762
- Youn B, Trikalinos NA, Mor V, Wilson IB, Dahabreh IJ. Real-World Use and Survival Outcomes of Immune Checkpoint Inhibitors in Older Adults With Non-Small Cell Lung Cancer. *Cancer* (2020) 126:978–85. doi: 10.1002/ cncr.32624
- 15. Areses Manrique MC, Mosquera Martínez J, García González J, Afonso Afonso FJ, Lázaro Quintela M, Fernández Núñez N, et al. Real World Data of Nivolumab for Previously Treated Non-Small Cell Lung Cancer Patients: A Galician Lung Cancer Group Clinical Experience. *Transl Lung Cancer Res* (2018) 7:404–15. doi: 10.21037/tlcr.2018.04.03
- Khozin S, Miksad RA, Adami J, Boyd M, Brown NR, Gossai A, et al. Real-World Progression, Treatment, and Survival Outcomes During Rapid Adoption of Immunotherapy for Advanced Non-Small Cell Lung Cancer. *Cancer* (2019) 125:4019–32. doi: 10.1002/cncr.32383
- Zhou C, Chen G, Huang Y, Zhou J, Lin L, Feng J, et al. Camrelizumab Plus Carboplatin and Pemetrexed Versus Chemotherapy Alone in Chemotherapy-Naive Patients With Advanced Non-Squamous Non-Small-Cell Lung Cancer (CameL): A Randomised, Open-Label, Multicentre, Phase 3 Trial. *Lancet Respir Med* (2021) 9:305–14. doi: 10.1016/s2213-2600(20)30365-9
- Kitagawa S, Hakozaki T, Kitadai R, Hosomi Y. Switching Administration of Anti-PD-1 and Anti-PD-L1 Antibodies as Immune Checkpoint Inhibitor Rechallenge in Individuals With Advanced Non-Small Cell Lung Cancer: Case Series and Literature Review. *Thorac Cancer* (2020) 11:1927–33. doi: 10.1111/ 1759-7714.13483
- Ren S, Chen J, Xu X, Jiang T, Cheng Y, Chen G, et al. Camrelizumab Plus Carboplatin and Paclitaxel as First-Line Treatment for Advanced Squamous Non-Small-Cell Lung Cancer (CameL-Sq): A Phase 3 Trial. J Thorac Oncol (2021) 21:1556–0864. doi: 10.1016/j.jtho.2021.11.018
- Lu S, Wang J, Yu Y, Yu X, Hu Y, Ai X, et al. Tislelizumab Plus Chemotherapy as First-Line Treatment for Locally Advanced or Metastatic Nonsquamous NSCLC (RATIONALE 304): A Randomized Phase 3 Trial. J Thorac Oncol (2021) 16:1512–22. doi: 10.1016/j.jtho.2021.05.005
- 21. Yang Y, Sun J, Wang Z, Fang J, Yu Q, Han B, et al. Updated Overall Survival Data and Predictive Biomarkers of Sintilimab Plus Pemetrexed and Platinum as First-Line Treatment for Locally Advanced or Metastatic Nonsquamous NSCLC in the Phase 3 ORIENT-11 Study. *J Thorac Oncol* (2021) 16:2109–20. doi: 10.1016/j.jtho.2021.07.015
- Gomatou G, Tzilas V, Kotteas E, Syrigos K, Bouros D. Immune Checkpoint Inhibitor-Related Pneumonitis. *Respiration* (2020) 99:932–42. doi: 10.1159/ 000509941
- Obradović MMS, Hamelin B, Manevski N, Couto JP, Sethi A, Coissieux MM, et al. Glucocorticoids Promote Breast Cancer Metastasis. *Nature* (2019) 567:540–4. doi: 10.1038/s41586-019-1019-4

- Das S, Johnson DB. Immune-Related Adverse Events and Anti-Tumor Efficacy of Immune Checkpoint Inhibitors. J Immunother Cancer (2019) 7:306. doi: 10.1186/s40425-019-0805-8
- 25. Grossi F, Crinò L, Logroscino A, Canova S, Delmonte A, Melotti B, et al. Use of Nivolumab in Elderly Patients With Advanced Squamous Non-Small-Cell Lung Cancer: Results From the Italian Cohort of an Expanded Access Programme. *Eur J Cancer* (2018) 100:126–34. doi: 10.1016/j.ejca.2018.05.015
- Tricoli JV, Bleyer A. Adolescent and Young Adult Cancer Biology. Cancer J (2018) 24:267–74. doi: 10.1097/ppo.0000000000343
- Muchnik E, Loh KP, Strawderman M, Magnuson A, Mohile SG, Estrah V, et al. Immune Checkpoint Inhibitors in Real-World Treatment of Older Adults With Non-Small Cell Lung Cancer. J Am Geriatr Soc (2019) 67:905–12. doi: 10.1111/jgs.15750
- Paz-Ares L, Ciuleanu TE, Cobo M, Schenker M, Zurawski B, Menezes J, et al. First-Line Nivolumab Plus Ipilimumab Combined With Two Cycles of Chemotherapy in Patients With Non-Small-Cell Lung Cancer (CheckMate 9LA): An International, Randomised, Open-Label, Phase 3 Trial. *Lancet Oncol* (2021) 22:198–211. doi: 10.1016/s1470-2045(20)30641-0
- Reck M, Shankar G, Lee A, Coleman S, McCleland M, Papadimitrakopoulou VA, et al. Atezolizumab in Combination With Bevacizumab, Paclitaxel and Carboplatin for the First-Line Treatment of Patients With Metastatic Non-Squamous Non-Small Cell Lung Cancer, Including Patients With EGFR Mutations. *Expert Rev Respir Med* (2020) 14:125–36. doi: 10.1080/ 17476348.2020.1701439
- Mo DC, Luo PH, Huang SX, Wang HL, Huang JF. Safety and Efficacy of Pembrolizumab Plus Lenvatinib Versus Pembrolizumab and Lenvatinib Monotherapies in Cancers: A Systematic Review. *Int Immunopharmacol* (2021) 91:107281. doi: 10.1016/j.intimp.2020.107281
- Brody R, Zhang Y, Ballas M, Siddiqui MK, Gupta P, Barker C, et al. PD-L1 Expression in Advanced NSCLC: Insights Into Risk Stratification and Treatment Selection From a Systematic Literature Review. *Lung Cancer* (2017) 112:200–15. doi: 10.1016/j.lungcan.2017.08.005
- Bassanelli M, Sioletic S, Martini M, Giacinti S, Viterbo A, Staddon A, et al. Heterogeneity of PD-L1 Expression and Relationship With Biology of NSCLC. Anticancer Res (2018) 38:3789–96. doi: 10.21873/anticanres.12662
- 33. Khozin S, Carson KR, Zhi J, Tucker M, Lee SE, Light DE, et al. Real-World Outcomes of Patients With Metastatic Non-Small Cell Lung Cancer Treated With Programmed Cell Death Protein 1 Inhibitors in the Year Following U.S. Regulatory Approval. Oncologist (2019) 24:648–56. doi: 10.1634/ theoncologist.2018-0307

Conflict of Interest: The authors declare that the research was conducted in the absence of any commercial or financial relationships that could be construed as a potential conflict of interest.

Publisher's Note: All claims expressed in this article are solely those of the authors and do not necessarily represent those of their affiliated organizations, or those of the publisher, the editors and the reviewers. Any product that may be evaluated in this article, or claim that may be made by its manufacturer, is not guaranteed or endorsed by the publisher.

Copyright © 2022 Miao, Zhang, Wang, Si, Ni, Zhong, Zhao, Xu, Chen, Pan, Wang and Zhang. This is an open-access article distributed under the terms of the Creative Commons Attribution License (CC BY). The use, distribution or reproduction in other forums is permitted, provided the original author(s) and the copyright owner(s) are credited and that the original publication in this journal is cited, in accordance with accepted academic practice. No use, distribution or reproduction is permitted which does not comply with these terms.



The Therapeutic Effect and Clinical Outcome of Immune Checkpoint Inhibitors on Bone Metastasis in Advanced Non-Small-Cell Lung Cancer

OPEN ACCESS

Edited by:

Yubin Li, University of Pennsylvania, United States

Reviewed by:

Ling Yin, University of Texas MD Anderson Cancer Center, United States Xia Wu, Peking Union Medical College Hospital (CAMS), China

*Correspondence:

Akihiko Takeuchi a_take@med.kanazawa-u.ac.jp

Specialty section:

This article was submitted to Cancer Immunity and Immunotherapy, a section of the journal Frontiers in Oncology

Received: 08 February 2022 Accepted: 11 March 2022 Published: 01 April 2022

Citation:

Asano Y, Yamamoto N, Demura S, Hayashi K, Takeuchi A, Kato S, Miwa S, Igarashi K, Higuchi T, Yonezawa H, Araki Y, Morinaga S, Saito S, Sone T, Kasahara K and Tsuchiya H (2022) The Therapeutic Effect and Clinical Outcome of Immune Checkpoint Inhibitors on Bone Metastasis in Advanced Non-Small-Cell Lung Cancer. Front. Oncol. 12:871675. doi: 10.3389/fonc.2022.871675 Yohei Asano¹, Norio Yamamoto¹, Satoru Demura¹, Katsuhiro Hayashi¹, Akihiko Takeuchi^{1*}, Satoshi Kato¹, Shinji Miwa¹, Kentaro Igarashi¹, Takashi Higuchi¹, Hirotaka Yonezawa¹, Yoshihiro Araki¹, Sei Morinaga¹, Shiro Saito¹, Takashi Sone², Kazuo Kasahara² and Hiroyuki Tsuchiya¹

¹ Department of Orthopedic Surgery, Kanazawa University Graduate School of Medical Sciences, Kanazawa, Japan, ² Department of Respiratory Medicine, Kanazawa University Hospital, Kanazawa, Japan

Introduction: In advanced non-small-cell lung cancer (NSCLC), immune checkpoint inhibitors (ICIs) have been reported a better treatment outcome on primary lesions, however, the therapeutic effect on bone metastases has not been clarified. This study investigates the therapeutic effect of ICIs on bone metastases in advanced NSCLC.

Methods: The data of patients with advanced NSCLC, treated with ICIs from 2016 to 2019 at our hospital, were analyzed. The therapeutic effects of ICIs on primary lung and metastatic bone lesions, concomitant use of bone modifying agents (BMA), treatment outcomes, and frequency of immune-related adverse events (irAEs) and skeletal-related events (SREs) were investigated.

Results: A total of 29 patients were included (19 men and 10 women; mean age, 64.2 years). Among the ICIs, pembrolizumab was the most used (55.2%), and concomitant use of BMA was prevalent in 21 patients (zoledronic acid=1, denosumab=20). The therapeutic effect was partial response (PR) in 10.3% (n=3) on primary lung lesions by RECIST 1.1, complete response (CR) in 6.9% (n=2) and PR in 17.2% (n=5) on bone metastatic lesions by MDA criteria. ICIs suppressed the progression of bone metastasis in 21 cases (72.4%). All patients in CR and PR were treated with pembrolizumab and denosumab. SREs and irAEs were developed in 3.4% (n=1) and 20.7% (n=6), respectively. The median survival time after treatment with ICIs was 11.0 months. Concomitant therapy with ICIs and denosumab significantly prolonged the overall survival compared to ICI-only therapy (16.0 months vs. 2.5 months, p<0.01).

87

Conclusions: This study showed that treatment with ICIs may successfully suppress the progression of bone metastasis in advanced NSCLC. Pembrolizumab with denosumab had the highest therapeutic effect on both primary lung lesions and bone metastases. Systemic treatment with this combination and conservative treatment of bone metastasis could be one of the options in the treatment of advanced NSCLC.

Keywords: immune checkpoint inhibitor, non-small cell lung cancer, bone metastasis, bone modifying agent (BMA), denosumab

INTRODUCTION

Lung cancer is a malignant neoplasm that is responsible for distant metastases at a relatively early stage in the disease, to the breast, prostate, and bones (1-3). It has been reported that 48% of patients with advanced (stage III, IV) non-small-cell lung cancer (NSCLC) have bone metastases at initial diagnosis (4). Bone metastases can cause skeletal-related events (SREs) such as severe bone pain, pathological fractures, spinal cord compression, and hypercalcemia (5), and can result in the deterioration of the quality of life (QOL). In advanced cases of lung cancer with bone metastasis, 20-30% of patients already have SREs at the time of diagnosis (4, 6, 7), and they have a worse prognosis than that of other cancers (8). SREs themselves could be independent predictors of worse prognosis in terms of overall survival (OS) (7), therefore, the treatment strategy for bone metastases is essential in NSCLC. A multidisciplinary approach with radiation therapy, surgical treatment, and bone modifying agents (BMAs) is necessary for the management of these cases. Zoledronic acid and denosumab have been reported to significantly reduce the incidence of SREs (9, 10) and prolong OS (11).

In recent years, it has been reported that immune checkpoint inhibitors (ICIs), which target the Programmed death-1 receptor (PD-1)/PD-1 ligand (PD-L1) pathway, have more favorable outcomes than conventional anticancer drugs on metastatic lung cancer (12–14). We have reported two cases of advanced NSCLC with a high risk of lower extremity long bone fracture due to metastases that were drastically improved by systemic treatment with pembrolizumab and denosumab (15). Two other case reports have shown the therapeutic effect of ICIs on bone metastasis in lung cancer (16, 17). Based on these findings, ICIs as well as their combination with BMAs such as denosumab may be one of the treatment options for NSCLC with bone metastases.

There is insufficient data regarding the therapeutic effect of ICIs on bone metastasis in NSCLC. The purpose of this study was to evaluate the therapeutic effect of ICIs on bone metastasis in advanced NSCLC and to seek a novel treatment strategy.

MATERIALS AND METHODS

Study Design

This retrospective study analyzed patients diagnosed with advanced NSCLC and treated with ICIs between February

2016 and November 2019 in the Department of Respiratory Medicine of Kanazawa University Hospital, Japan. Patients diagnosed with bone metastases before the initiation of ICI treatment [PD-1 inhibitors (nivolumab and pembrolizumab) or PD-L1 inhibitor (atezolizumab)] and who received treatment for more than six months were included. Patients who died within six months were also included to assess the clinical outcomes of ICI treatment. On the other hand, patients who received concomitant therapy with a PD-1 inhibitor and Cytotoxic T-lymphocyte-associated protein 4 (CTLA-4) inhibitor were excluded. This study was approved by the ethics committee of the Kanazawa University Hospital (no. 3339-1) and has been carried out in accordance with the Declaration of Helsinki. Informed consent from the patients was obtained.

Data Collection

The medical information used in this study was collected from the database at Kanazawa University Hospital. The collected data included patient demographics such as age and sex, disease details such as histological type, stage, Eastern Cooperative Oncology Group performance status (ECOG PS), metastatic sites, driver gene mutation, PD-L1 tumor proportion score (TPS), and treatment history. The therapeutic effects of ICIs on primary lung lesions and bone metastases were evaluated based on Response Evaluation Criteria in Solid Tumors (RECIST) version 1.1 (18) and MD Anderson Cancer Center (MDA) criteria (19), respectively. Change of the size of primary lung lesions and osteosclerotic change or tracer uptake of bone metastatic lesions were evaluated by computed tomography (CT) or bone scintigraphy. The evaluation at the final examination was investigated as the therapeutic effects of ICIs. In addition, concomitant use of BMAs such as zoledronic acid and denosumab, treatment outcomes, frequency of Immunerelated adverse events (irAEs), and SREs were investigated.

Statistical Analyses

Categorical variables were presented as frequencies and percentages, whereas continuous ones were presented as median (IQR). The Kaplan-Meier curve was used to evaluate the OS of the participants, and the log-rank test was performed for comparison amongst groups. The OS was defined as the period from the initiation of ICI treatment to death. A p-value < 0.05 was used to denote statistical significance. These analyses were performed using EZR (Saitama Medical Center, Jichi Medical University, Saitama, Japan) (20).

RESULTS

Characteristics of Participants

A total of 29 patients (19 men and 10 women) were included in this study. The mean age was 64.2 years (44 - 81 years). The mean follow-up period after treatment with ICIs was 13.1 months (1 -35 months). The most common histological type was adenocarcinoma in 75.9% (n = 22), and the most common disease stage was IVB (93.1%). The most common bone metastatic sites were the ribs (55.2%) and pelvis (55.2%), and most patients had multiple bone metastases (89.7%). In addition, metastases to other organs were observed in 75.9% (n = 22) of patients. The examination of driver gene mutation was performed in 25 patients and only one was positive for anaplastic lymphoma kinase mutation. The TPS, used for ICI treatment indication, was examined in 16 patients and 81.3% exhibited > 1% (n = 13) and 18.7% exhibited < 1% (n = 3). ICIs were the first-line therapy in 27.6% (n = 8), second-line in 44.8% (n =13), and third-line in 27.6% (n = 8) of the patients. Among them, eight patients who were treated with first-line ICIs had high PD-L1 TPS expression (≥ 50%). In the other patients who received ICI treatment as secondline or further treatment, surgery and radiation therapy for primary lung lesions were performed in 23.8% (n = 5) and 9.5% (n = 2), respectively, while anticancer drug treatment was performed in 100% (n = 21). None of the patients was treated with molecular-targeted drugs prior to ICI treatment. BMAs were administrated in 21 patients, 20 of whom received denosumab (69.0%), and one received zoledronic acid (3.4%) (Table 1).

Therapeutic Effects

Treatment with ICIs suppressed the progression of bone metastasis in 21 out of the 29 cases (72.4%). The most commonly used ICI was pembrolizumab (55.2%, n = 16), which had the best therapeutic effect on both primary lung lesions (partial response (PR) in 18.8% (n = 3) according to RECIST 1.1) and bone metastases where osteosclerotic changes were noted, indicating a response to therapy (complete response [CR] in 12.5% [n = 2] and PR in 31.2% [n = 5] according to the MDA criteria) (**Table 2** and **Figure 1**). Nivolumab and atezolizumab on lung lesions and bone metastases resulted in either stable disease (SD) or progressive disease (PD) in all patients (**Table 2**).

All patients whose evaluations showed CR or PR with regard to bone metastases were treated with pembrolizumab as the firstor second-line therapy and received concomitant use of denosumab. Moreover, three patients had PR in terms of primary lung lesions (**Table 3**). In these patients, denosumab was initiated at the same time as ICI treatment compared with those who were evaluated as SD or PD (71.4% vs. 0%, p<0.01). However, there was no significant difference in the duration of concomitant use of ICIs and denosumab (CR or PR; 7.9 months vs. SD or PD; 7.5 months, p=0.92).

Prognosis

During the study period, the median survival time after treatment with ICIs was 11.0 months (4 - 20 months) and 72.4% of the patients died from the disease (n = 21) (**Table 4**). The 1-year and 2-year survival rates were 44.8% and 24.0%, respectively.

TABLE 1 | Characteristics of patients with advanced NSCLC treated with ICIs.

		Number (%)
Sex	Male	19 (65.5
	Female	10 (34.5
ECOG PS	0-2	26 (89.7
	3-4	3 (10.3)
listology	Adenocarcinoma	22 (75.9
	Squamous cell carcinoma	3 (10.3)
	Pulmonary pleomorphic carcinoma	2 (6.9)
	Poor-differentiated carcinoma	2 (6.9)
Priver gene mutation: positive/total)	EGFR	0/25
	ALK	1/24
	ROS1	0/8
	Untested	4
lumber of bone netastasis	Solitary	3 (10.3)
	Multiple	26 (89.7
Site of bone metastasis	Ribs	16 (55.2
	Pelvis	16 (55.2
	Thoracic spine	15 (51.7
	Lumbar spine	11 (37.9
	Long bone of the extremities	5 (17.2)
	Scapula	5 (17.2)
	Other	6 (20.7)
Netastasis to other Irgans	Yes	22 (75.9)
0	No	7 (24.1)
PD-L1 TPS	≥50%	9 (36.0)
-	1-49%	4 (16.0)
	<1%	3 (12.0)
	Untested	13 (52.0)
CI	Nivolumab	11 (37.9
-	Pembrolizumab	16 (55.2)
	Atezolizumab	2 (6.9)
herapy line	1st	8 (27.6)
	2nd	13 (44.8)
	>3rd	8 (27.6)
reatment history prior to	Surgery of primary lung lesions	5 (23.8)
Cl treatment		. ,
	Radiation therapy of primary lung lesions	2 (9.5)
	Anticancer drug	21 (100)
	0	, ,
BMA	Molecular-targeted drug Denosumab	0
AIVIC		20 (69.0)
	Zoledronic acid	1 (3.4)

ECOG PS, Eastern Cooperative Oncology Group Performance Status; EGFR, epidermal growth factor receptor; ALK anaplastic lymphoma kinase; PD-L1 programmed deathligand 1; TPS, tumor proportion score; ICI, immune checkpoint inhibitor; BMA, bone modifying agent.

Concomitant therapy with ICIs and denosumab significantly prolonged the OS compared to ICI-only therapy (16.0 months vs. 2.5 months, p<0.005) (**Figure 2**). In the concomitant therapy and ICI-only therapy groups, ICIs were used as more than third-line therapy in 25% (n = 5) and 25% (n = 2) of patients, respectively, and there was no significant difference (p=0.98). In addition, there were no significant differences in the type of ICI used for treatment (p=0.25) or in the ECOG PS before ICI treatment (p=0.35) between the groups. Moreover, the OS of the group that ICIs responded to bone metastatic lesions was significantly prolonged than that of the non-responsive group (19.3 months vs. 10.3 months, p=0.0072) (**Figure 3**).

TABLE 2 | Therapeutic effect of ICIs on primary lung lesions and bone metastases.

	Nivolumab	Pembrolizumab	Atezolizumab	Total
	N = 11 (37.9%)	N = 16 (55.2%)	N = 2 (6.9%)	N = 29
Therapy line: N (%)				
1st	O (O)	8 (50.0)	O (O)	8 (27.6)
2nd	7 (63.7)	5 (31.2)	1 (50.0)	13 (48.3)
≧3rd	4 (33.3)	3 (18.8)	1 (50.0)	8 (24.1)
RECIST 1.1: N (%)				
CR	O (O)	O (O)	O (O)	0 (0)
PR	O (O)	3 (18.8)	O (O)	3 (10.3)
SD	2 (18.2)	3 (18.8)	O (O)	5 (17.2)
PD	8 (72.7)	9 (56.2)	2 (100)	19 (65.5)
N/A	1 (9.1)	1 (6.2)	O (O)	2 (7.0)
MDA criteria: N (%)				
CR	O (O)	2 (12.5)	O (O)	2 (7.0)
PR	O (O)	5 (31.2)	O (O)	5 (17.2)
SD	5 (45.4)	7 (43.8)	2 (100)	14 (48.3)
PD	5 (45.4)	2 (12.5)	O (O)	7 (24.1)
N/A	1 (9.1)	0 (0)	0 (0)	1 (3.4)

ICI, immune checkpoint inhibitor; RECIST 1.1, Response Evaluation Criteria in Solid Tumors version 1.1; MDA criteria, MD Anderson Cancer Center criteria; CR, complete response; PR, partial response; SD, stable disease; PD, progressive disease; N/A, not available.

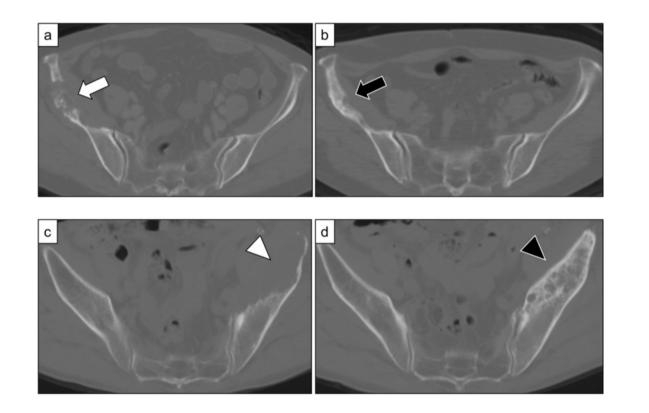


FIGURE 1 | (A) Metastatic bone lesions in the right ilium of a 77-year-old woman (Case 17). (B) Osteosclerotic changes three months after treatment with pembrolizumab and denosumab. The patient was in partial remission (MDA criteria). (C) Metastatic bone lesions in the left ilium of a 64-year-old man (Case 29). (D) Osteosclerotic changes five months after treatment with pembrolizumab and denosumab. The patient was in partial remission (MDA criteria).

Adverse Events

irAEs were observed in 20.7% (n = 6) and were encephalitis (Common Terminology Criteria for Adverse Events (CTCAE) grade 5), pneumonitis (grade 2), cholangitis (grade 2), drug eruption (grade 2) and hypothyroidism (grade 2). One patient

who developed encephalitis and died was treated with nivolumab and developed irAEs after two cycles of treatment; magnetic resonance imaging (MRI) revealed abnormal lesions in the bilateral temporal lobes. Based on these results, nivolumabinduced autoimmune encephalitis was diagnosed clinically.

TABLE 3 Therapeutic effect of ICI and DEMb concomitant therapy compared
to ICI-only or ICI and ZOL therapy.

	ICI only		ICI + DMAb (N = 20)					
	(n = 8) or ICI + ZOL (n = 1)	Nivolumab (N = 10)	Pembrolizumab (N = 9)	Atezolizumab (N = 1)				
RECIST 1.1								
CR	0	0	0	0				
PR	0	0	3	0				
SD	2	1	2	0				
PD	6	8	4	1				
N/A	1	1	0	0				
MDA criteria								
CR	0	0	2	0				
PR	0	0	5	0				
SD	7	4	2	1				
PD	2	5	0	0				
N/A	0	1	0	0				

ICI, immune checkpoint inhibitor; DMAb, Denosumab; ZOL, Zolendronic acid; RECIST 1.1, Response Evaluation Criteria in Solid Turnors version 1.1; MDA criteria, MD Anderson Cancer Center criteria; CR, complete response; PR, partial response; SD, stable disease; PD, progressive disease; N/A, not available.

In contrast, the other five patients with irAEs were stable after ICI discontinuation and steroid treatment. Among those who died, nivolumab was used in two patients, pembrolizumab in three, and atezolizumab in one (**Table 4**). Only one patient developed SRE

(spinal cord compression at the level of the 5th thoracic spine) after the initiation of nivolumab and was treated by radiation therapy.

DISCUSSION

In this study, the bone metastasis control rate of advanced NSCLC treated with ICIs was 72.4%, two of those patients were in CR and five were in PR based on MDA criteria. All patients received pembrolizumab and denosumab, implying that the combined treatment may have high therapeutic effects on bone metastases in advanced NSCLC.

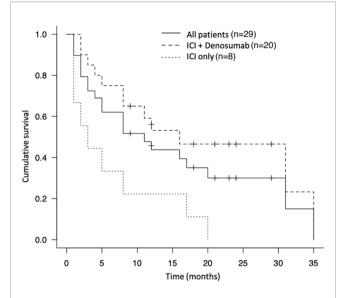
In recent years, immunotherapy, including ICIs, has made remarkable progress and led to a paradigm shift in cancer treatment (21). Some reports have shown that ICIs prolong OS and progression-free survival (PFS) in patients with metastatic NSCLC compared with conventional anticancer medications (12–14), and they are expected to improve the prognosis and QOL of these patients. However, in advanced NSCLC, there are few reports on the therapeutic effects of ICIs on bone metastases. Therefore, this study examined the efficacy of ICIs on bone metastases in advanced NSCLC.

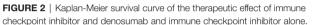
In this study, seven patients (24.1%) had osteosclerotic changes of bone metastases after the initiation of ICIs, showing

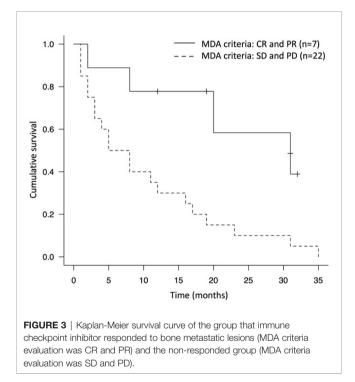
TABLE 4 | Patient characteristics, disease features, treatment details, and outcomes of study population.

Case/Age/Sex	Histology	Number of bone metastasis	PD-L1 TPS (%)	ICI	MDA criteria	RECIST 1.1	BMA	irAEs (Grade)	Outcome
1/67/M	SQCC	solitary	N/T	NIV	SD	PD	DMAb	No	DOD
2/77/F	ADC	multiple	N/T	NIV	PD	N/A	DMAb	No	DOD
3/47/F	ADC	multiple	N/T	NIV	PD	PD	DMAb	No	DOD
4/54/M	ADC	multiple	N/T	NIV	PD	PD	DMAb	No	DOD
5/59/M	PPC	multiple	N/T	NIV	SD	PD	DMAb	Encephalitis (G5)	DOD
6/57/M	P/D	multiple	N/T	NIV	SD	SD	DMAb	No	AWD
7/60/M	PPC	multiple	N/T	NIV	SD	SD	No	No	DOD
8/66/M	ADC	multiple	N/T	NIV	PD	PD	DMAb	No	DOD
9/61/M	ADC	solitary	N/T	NIV	N/A	PD	DMAb	No	DOD
10/67/M	ADC	multiple	N/T	NIV	PD	PD	DMAb	Hypothyroidism (G2)	DOD
11/71/M	SQCC	solitary	N/T	PEM	PD	PD	ZOL	No	DOD
12/60/M	ADC	multiple	25-49	PEM	SD	PD	No	No	DOD
13/62/M	ADC	multiple	<1	NIV	SD	PD	DMAb	No	AWD
14/74/F	ADC	multiple	75	PEM	CR	PR	DMAb	No	AWD
15/68/F	ADC	multiple	>75	PEM	SD	SD	DMAb	No	DOD
16/46/M	ADC	multiple	N/T	PEM	SD	PD	No	No	DOD
17/77/F	ADC	multiple	>75	PEM	PR	PD	DMAb	Pneumonitis (G2)	AWD
18/66/F	ADC	multiple	100	PEM	SD	N/A	No	No	DOD
19/81/M	ADC	multiple	>75	PEM	SD	PD	DMAb	Drug eruption (G2)	DOD
20/64/M	ADC	multiple	80-90	PEM	SD	SD	No	No	DOD
21/46/F	ADC	multiple	11-24	PEM	PR	PD	DMAb	No	DOD
22/75/F	ADC	multiple	>75	PEM	PR	SD	DMAb	Cholangitis (G2)	DOD
23/73/M	SQCC	multiple	25-49	PEM	SD	PD	No	No	DOD
24/69/M	ADC	multiple	24	PEM	PD	PD	No	No	DOD
25/44/F	P/D	multiple	70-80	PEM	PR	PD	DMAb	No	AWD
26/69/F	ADC	multiple	<1	ATE	SD	PD	No	No	DOD
27/66/M	ADC	multiple	N/T	ATE	SD	PD	DMAb	Hypothyroidism (G2)	AWD
28/71/M	ADC	multiple	>75	PEM	CR	PR	DMAb	No	AWD
29/64/M	ADC	multiple	<1	PEM	PR	PR	DMAb	No	AWD

ICI, immune checkpoint inhibitor; ADC, adenocarcinoma; SQCC, squamous cell carcinoma; PPC, pulmonary pleomorphic carcinoma; P/D poor-differentiated carcinoma; N/T, not tested; RECIST 1.1, Response Evaluation Criteria in Solid Tumors version 1.1; MDA criteria, MD Anderson Cancer Center criteria; CR, complete response; PR, partial response; SD, stable disease; PD, progressive disease; N/A, not available; DMAb, Denosumab; ZOL, Zolendronic acid; DOD, dead of disease; AWD, alive with disease.







response to therapy (CR in two patients and PR in five patients). All these patients had been treated with pembrolizumab as firstline therapy in six patients and second-line in one patient. The two patients with CR of bone metastases were in PR in terms of the primary lung lesions (15). Similarly, two case reports showed the remarkable effectiveness of pembrolizumab on both primary lung lesions and bone metastases (16, 17). In both these case reports, pembrolizumab was used as first-line therapy, and the bone metastases disappeared. Moreover, the seven patients who showed improvement in the osteosclerotic changes of bone metastases had been received the combined treatment of ICIs and denosumab. In NSCLC, although denosumab has been reported to prolong OS and prevent SREs (9, 11, 22), there have been no reports on the correlation between osteosclerotic changes in osteolytic lesions of bone metastases, including impending fractures, and ICIs. Therefore, it was considered that denosumab may enhance the therapeutic effects of ICIs. There are only a few reports regarding the therapeutic effect of ICIs on the primary lung lesions treated with the combined therapy of ICIs and denosumab for NSCLC (23), but none have investigated the therapeutic effect on bone metastases. Thus, the correlation between these drugs has not been clarified. In previous case reports where metastatic bone lesions disappeared after treatment with pembrolizumab, BMAs such as denosumab were not used (16, 17). Our results show that among ICIs, pembrolizumab may have the highest therapeutic effects both on primary lung lesions and bone metastases.

The combined effect of ICIs and denosumab have been previously studied in other malignancies. Angela et al. reported that the combined treatment of PD-1 inhibitor and denosumab resulted in osteosclerotic changes on bone metastases in 62% of stage IV melanoma (24). Furthermore, in a clinical study, a longer mean duration of concomitant use of ICIs and denosumab was associated with increased overall response rate (ORR) (CR + PR) in melanoma and NSCLC as well as increased overall survival in NSCLC (23). On the other hand, Qin et al. reported that the use of BMA was not associated with decreased SREs or differences in survival in patients with metastatic NSCLC (25). Thus, the influence of the concomitant use of denosumab in ICI treatment on clinical outcomes has not yet been clarified, and the prognostic significance of ICI treatment in NSCLC with bone metastases remains inconsistent (26).

It has been shown that Receptor activator of nuclear factor kappa-B ligand (RANKL) inhibitors improve the anti-metastatic activity of PD-1/PD-L1 inhibitors, resulting in subcutaneous growth suppression in mouse models of melanoma, prostate cancer, and colon cancer (27). Additionally, the RANKL/RANK axis has been shown to affect the immune response such as regulatory, CD8+ and CD4+ T cells, as well as myeloid suppressor cells (28-32). Ahern et al. reported that optimal antitumor effects were observed when anti-RANKL was initiated concurrently with or after ICI treatment (27). In our study, denosumab was initiated at the same time as ICI treatment in cases where the therapeutic effect on bone metastasis was CR or PR. These reports support the results of our study, except for the duration of concomitant use of denosumab. Regarding that duration, our results showed no significant difference in the response of ICIs to bone metastasis. However, five out the seven patients evaluated as CR or PR based on the MDA criteria were still treated with combined therapy, which may make a significant difference in the future. The exact mechanism underlying the antitumor effect of the concomitant use of ICIs and denosumab requires further analysis.

In this study, TPS was evaluated in six out the seven patients who had CR and PR in terms of bone metastases, and high

expression was observed in five patients, but only one patient exhibited < 1%. TPS is measured before the initiation of pembrolizumab in unresectable advanced or recurrent NSCLC. If it is > 1%, first-line treatment with pembrolizumab alone is possible (14). High expression of PD-L1 in NSCLC is a predictive factor of the therapeutic effectiveness of pembrolizumab on primary lung lesions (33, 34), however, there are no reports regarding the effect on bone metastases. The results of this study implied that the high TPS expression might be a predictive factor of high therapeutic effect on both bone metastases and primary lung lesions.

The irAEs of ICIs are other important issues that need to be considered. Sun et al. reported that the overall incidence of irAEs in NSCLC was 22% for all grades and 4% for high grades in a systematic review and meta-analysis (35). In our study, 20.7% (n = 6) developed irAEs and 3.4% (n = 1) of those who developed encephalitis died (grade 5), consistent with the report. From these patients, two had achieved PR and the others had SD on bone metastasis evaluation. In NSCLC patients who were treated with ICIs, it has been reported that PFS, OS, and ORR of the patients who developed irAEs were more favorable than those who did not (36–39). However, there have been no studies regarding the therapeutic effect association with irAEs and bone metastases. Our results show that the incidence of irAEs might correlate with the therapeutic effect, and further studies are necessary to clarify these correlations.

In our study, three patients had impending fractures of the long bone of the lower extremity, two of them who were in CR based on the MDA criteria (15) and had Mirels scores (40) of 9 and 11 points. Since they were simultaneously diagnosed with primary lung cancer and bone metastasis, systemic treatment with pembrolizumab was prioritized, and conservative treatment was decided upon regarding the bone metastases after multidisciplinary discussions. The bone remodeling of the metastatic lesions was observed during the follow-up period, and they were able to return to their normal daily life without prophylactic surgery for impending fractures. One of the patients with SD in terms of bone metastasis was prioritized systemic treatment with pembrolizumab due to brain metastasis. Since the bone metastasis progression was suppressed by the systemic treatment, prophylactic surgery was not necessary. In addition, three other patients had extremity long bone metastases, the proximal humerus in one patient and the femoral trochanter in two patients. The Mirels scores of these patients were < 8 points for the proximal humerus, but 9 points for the patient with the femoral trochanter metastasis.

Prophylactic surgery for impending fractures of the lower extremities is a reasonable approach (41, 42), however, it is not always beneficial for advanced-stage patients due to poor general health and systemic treatment delays. This study revealed two cases of impending fractures that responded to ICIs and one whose progression was suppressed, and thus avoided prophylactic surgery. These results suggested that the systemic treatment of pembrolizumab and denosumab with conservative treatment with regards to bone metastasis could be one of the options for advanced NSCLC, although further studies are needed. There were some limitations in this study. The number of patients was small. In addition, no control group received medication therapy other than ICIs, and the therapeutic effects of ICIs could not be compared with the effects of these therapies. Moreover, the effects of chemotherapy administered concurrently with ICIs were not considered. Although the concomitant use of denosumab in ICI treatment might enhance the therapeutic effect, the mechanism has not been sufficiently elucidated, and further verification of this finding is required.

In conclusion, ICIs suppressed the progression of bone metastasis in advanced NSCLC in 72.4% of this limited case series, although most cases were combined with BMAs. Pembrolizumab with denosumab had the highest therapeutic effect on not only primary lung lesions but bone metastases as well. These results suggest that the systemic treatment of pembrolizumab with denosumab with conservative treatment of bone metastasis could be one of the options for advanced NSCLC even in cases of impending lower extremity fracture. Future research should focus on validating these results, as well as creating guidelines to manage the bone metastasis from advanced NSCLC with a multidisciplinary approach including ICIs, anticancer drugs, molecular-targeted drugs, BMAs, surgical intervention, and radiotherapy.

DATA AVAILABILITY STATEMENT

The original contributions presented in the study are included in the article/supplementary material. Further inquiries can be directed to the corresponding author.

ETHICS STATEMENT

Written informed consent was obtained from the individual(s) for the publication of any potentially identifiable images or data included in this article.

AUTHOR CONTRIBUTIONS

The manuscript was drafted by YoA, and AT. YoA, SD, KH, AT, SK, ShM, KI, TH, HY, YA, SeM, SS, and TS collected and analyzed the data and YoA wrote the manuscript. NY, AT, KK, and HT revised the manuscript. All authors were involved in the preparation of this study, and read and approved the final manuscript.

ACKNOWLEDGMENTS

We would like to thank Editage (www.editage.com) for English language editing.

REFERENCES

- Roodman GD. Mechanisms of Bone Metastasis. N Engl J Med (2004) 350:1655–64. doi: 10.1056/NEJMra030831
- Kuchuk M, Addison CL, Clemons M, Kuchuk I, Wheatley-Price P. Incidence and Consequences of Bone Metastases in Lung Cancer Patients. *J Bone Oncol* (2013) 2:22–9. doi: 10.1016/j.jbo.2012.12.004
- Coleman RE. Clinical Features of Metastatic Bone Disease and Risk of Skeletal Morbidity. *Clin Cancer Res* (2006) 12:6243s–9s. doi: 10.1158/1078-0432.CCR-06-0931
- Katakami N, Kunikane H, Takeda K, Takayama K, Sawa T, Saito H, et al. Prospective Study on the Incidence of Bone Metastasis (BM) and Skeletal-Related Events (SREs) in Patients (Pts) With Stage IIIB and IV Lung Cancer-CSP-HOR 13. J Thorac Oncol (2014) 9:231–8. doi: 10.1097/JTO.00000000 0000051
- Kan C, Vargas G, Pape FL, PClézardin P. Cancer Cell Colonisation in the Bone Microenvironment. *Int J Mol Sci* (2016) 17:1674. doi: 10.3390/ ijms17101674
- Oster G, Lamerato L, Glass AG, Richert-Boe KE, Lopez A, Chuang K, et al. Natural History of Skeletal-Related Events in Patients With Breast, Lung, or Prostate Cancer and Metastases to Bone: A 15-Year Study in Two Large US Health Systems. *Support Care Cancer* (2013) 21:3279–86. doi: 10.1007/ s00520-013-1887-3
- Tsuya A, Kurata T, Tamura K, Fukuoka M. Skeletal Metastases in Non-Small Cell Lung Cancer: A Retrospective Study. *Lung Cancer* (2007) 57:229–32. doi: 10.1016/j.lungcan.2007.03.013
- Bauml J, Mick R, Zhang Y, Watt CD, Vachani A, Aggarwal C, et al. Determinants of Survival in Advanced Non-Small-Cell Lung Cancer in the Era of Targeted Therapies. *Clin Lung Cancer* (2013) 14:581–91. doi: 10.1016/ j.cllc.2013.05.002
- Henry DH, Costa L, Goldwasser F, Hirsh V, Hungria V, Prausova J, et al. Randomized, Doubled-Blind Study of Denosumab Versus Zoledronic Acid in the Treatment of Bone Metastases in Patients With Advanced Cancer (Excluding Breast and Prostate Cancer) or Multiple Myeloma. *J Clin Oncol* (2011) 29:1125–32. doi: 10.1200/JCO.2010.31.3304
- Rosen LS, Gordon D, Tchekmedyian NS, Yanagihara R, Hirsh V, Krzakowski M, et al. Long-Term Efficacy and Safety of Zoledronic Acid in the Treatment of Skeletal Metastases in Patients With Nonsmall Cell Lung Carcinoma and Other Solid Tumors: A Randomized, Phase III, Double-Blind, Placebo-Controlled Trial. *Cancer* (2004) 100:2613–21. doi: 10.1002/cncr.20308
- Scagliotti GV, Hirsh V, Siena S, Henry DH, Woll PJ, Manegold C, et al. Overall Survival Improvement in Patients With Lung Cancer and Bone Metastases Treated With Denosumab Versus Zoledronic Acid: Subgroup Analysis From a Randomized Phase 3 Study. J Thorac Oncol (2012) 7:1823– 9. doi: 10.1097/JTO.0b013e31826aec2b
- Brahmer J, Reckamp KL, Baas P, Crinò L, Eberhardt WE, Poddubskaya E, et al. Nivolumab Versus Docetaxel in Advanced Squamous-Cell Non-Small-Cell Lung Cancer. N Eng J Med (2015) 373:123–35. doi: 10.1056/ NEJMoa1504627
- Borghaei H, Paz-Ares L, Horn L, Spigel DR, Steins M, Ready NE, et al. Nivolumab Versus Docetaxel in Advanced Nonsquamous Non-Small-Cell Lung Cancer. N Eng J Med (2015) 373:1627–39. doi: 10.1056/NEJMoa1507643
- Reck M, Rodríguez-Abreu D, Robinson AG, Hui R, Csőszi T, Fülöp A, et al. Pembrolizumab Versus Chemotherapy for PD-L1-Positive Non-Small-Cell Lung Cancer. N Eng J Med (2016) 375:1823–33. doi: 10.1056/NEJMoa1606774
- Asano Y, Yamamoto N, Hayashi K, Takeuchi A, Miwa S, Igarashi K, et al. Complete Response of Bone Metastasis in Non-Small Cell Lung Cancer With Pembrolizumab: Two Case Reports. *Anticancer Res* (2021) 41:1693–99. doi: 10.21873/anticanres.14933
- Sidhu G, Tam E. Complete Resolution of Bone Metastases With Pembrolizumab. Jpn J Clin Oncol (2019) 49:691–92. doi: 10.1093/jjco/hyz077
- Tang Y, Li Y, Zhang L, Tong G, Ou Z, Wang Z, et al. Pathologic Complete Response to Preoperative Immunotherapy in a Lung Adenocarcinoma Patient With Bone Metastasis: A Case Report. *Thorac Cancer* (2020) 11:1094–8. doi: 10.1111/1759-7714.13361
- Eisenhauer EA, Therasse P, Bogaerts J, Schwartz LH, Sargent D, Ford R, et al. New Response Evaluation Criteria in Solid Tumours: Revised RECIST

Guideline (Version 1.1). Eur J Cancer (2009) 45:228-47. doi: 10.1016/ j.ejca.2008.10.026

- Hamaoka T, Madewell JE, Podoloff DA, Hortobagyi GN, Ueno NT. Bone Imaging in Metastatic Breast Cancer. J Clin Oncol (2004) 22:2942–53. doi: 10.1200/JCO.2004.08.181
- Kanda Y. Investigation of the Freely Available Easy-to-Use Software 'Ezr' for Medical Statistics. *Bone Marrow Transpl* (2012) 48:452–8. doi: 10.1038/ bmt.2012.244
- Anagnostou VK, Brahmer JR. Cancer Immunotherapy: A Future Paradigm Shift in the Treatment of Non-Small Cell Lung Cancer. *Clin Cancer Res* (2015) 21:976–84. doi: 10.1158/1078-0432.CCR-14-1187
- 22. De Castro J, García R, Garrido P, Isla D, Massuti B, Blanca B, et al. Therapeutic Potential of Denosumab in Patients With Lung Cancer: Beyond Prevention of Skeletal Complications. *Clin Lung Cancer* (2015) 16:431-46. doi: 10.1016/j.cllc.2015.06.004
- Liede A, Hernandez RK, Wade SW, Bo R, Nussbaum NC, Ahern E, et al. An Observational Study of Concomitant Immunotherapies and Denosumab in Patients With Advanced Melanoma or Lung Cancer. *Oncoimmunology* (2018) 7:e1480301. doi: 10.1080/2162402X.2018.1480301
- 24. Angela Y, Haferkamp S, Weishaupt C, Ugurel S, Becker JC, Oberndörfer F, et al. Combination of Denosumab and Immune Checkpoint Inhibition: Experience in 29 Patients With Metastatic Melanoma and Bone Metastases. *Cancer Immunol Immunother* (2019) 68:1187–94. doi: 10.1007/s00262-019-02353-5
- 25. Qin A, Zhao S, Miah A, Wei L, Patel S, Johns A, et al. Bone Metastases, Skeletal-Related Events, and Survival in Patients With Metastatic Non-Small Cell Lung Cancer Treated With Immune Checkpoint Inhibitors. J Natl Compr Canc Netw (2021) 19:915–21. doi: 10.6004/jnccn.2020.7668
- 26. Liu C, Wang M, Xu C, Li B, Chen J, Chen J, et al. Immune Checkpoint Inhibitor Therapy for Bone Metastases: Specific Microenvironment and Current Situation. J Immunol Res (2021) 2021:8970173. doi: 10.1155/2021/ 8970173
- Ahern E, Harjunpää H, O'Donnell JS, Allen S, Dougall WC, Teng MWL, et al. RANKL Blockade Improves Efficacy of PD1-PD-L1 Blockade or Dual PD1-PD-L1 and CTLA4 Blockade in Mouse Models of Cancer. Oncoimmunology (2018) 7:e1431088. doi: 10.1080/2162402X.2018.1431088
- Peggs KS, Quezada SA, Chambers CA, Korman AJ, Allison JP. Blockade of CTLA-4 on Both Effector and Regulatory T Cell Compartments Contributes to the Antitumor Activity of Anti–CTLA-4 Antibodies. J Exp Med (2009) 206:1717–25. doi: 10.1084/jem.20082492
- 29. Vilain RE, Menzies AM, Wilmott JS, Kakavand H, Madore J, Guminski A, et al. Dynamic Changes in PD-L1 Expression and Immune Infiltrates Early During Treatment Predict Response to PD-1 Blockade in Melanoma. *Clin Cancer Res* (2017) 23:5024–33. doi: 10.1158/1078-0432.CCR-16-0698
- 30. Chen P-L, Roh W, Reuben A, Cooper ZA, Spencer CN, Prieto PA, et al. Analysis of Immune Signatures in Longitudinal Tumor Samples Yields Insight Into Biomarkers of Response and Mechanisms of Resistance to Immune Checkpoint Blockade. *Cancer Discov* (2016) 6:827–37. doi: 10.1158/2159-8290.CD-15-1545
- 31. Selby MJ, Engelhardt JJ, Johnston RJ, Lu LS, Han M, Thudium K, et al. Preclinical Development of Ipilimumab and Nivolumab Combination Immunotherapy: Mouse Tumor Models, *In Vitro* Functional Studies, and Cynomolgus Macaque Toxicology. *PloS One* (2016) 11:e0161779. doi: 10.1371/journal.pone.0161779
- Mittal D, Vijayan D, Putz EM, Aguilera AR, Markey KA, Straube J, et al. Interleukin-12 From CD103(C) Batf3-Dependent Dendritic Cells Required for NK-Cell Suppression of Metastasis. *Cancer Immunol Res* (2017) 5:1098– 108. doi: 10.1158/2326-6066.CIR-17-0341
- 33. Incorvaia L, Fanale D, Badalamenti G, Barraco N, Bono M, Corsini LR. Et al. Programmed Death Ligand 1 (PD-L1) as a Predictive Biomarker for Pembrolizumab Therapy in Patients With Advanced Non-Small-Cell Lung Cancer (NSCLC). Adv Ther (2019) 36:2600–17. doi: 10.1007/s12325-019-01057-7
- 34. Aguilar EJ, Ricciuti B, Gainor JF, Kehl KL, Kravets S, Dahlberg S, et al. Outcomes to First-Line Pembrolizumab in Patients With Non-Small-Cell Lung Cancer and Very High PD-L1 Expression. Ann Oncol (2019) 30:1653–9. doi: 10.1093/annonc/mdz288

- 35. Sun X, Roudi R, Dai T, Chen S, Fan B, Li H, et al. Immune-Related Adverse Events Associated With Programmed Cell Death Protein-1 and Programmed Cell Death Ligand 1 Inhibitors for Non-Small Cell Lung Cancer: A PRISMA Systematic Review and Meta-Analysis. BMC Cancer (2019) 19:558. doi: 10.1186/s12885-019-5701-6
- Haratani K, Hayashi H, Chiba Y, Kudo K, Yonesaka K, Kato R, et al. Association of Immune-Related Adverse Events With Nivolumab Efficacy in Non-Small-Cell Lung Cancer. JAMA Oncol (2018) 4:374–8. doi: 10.1001/jamaoncol.2017.2925
- 37. Teraoka S, Fujimoto D, Morimoto T, Kawachi H, Ito M, Sato Y, et al. Early Immune-Related Adverse Events and Association With Outcome in Advanced Non-Small Cell Lung Cancer Patients Treated With Nivolumab: A Prospective Cohort Study. J Thorac Oncol (2017) 12:1798–805. doi: 10.1016/ j.jtho.2017.08.022
- Hosoya K, Fujimoto D, Morimoto T, Kumagai T, Tamiya A, Taniguchi Y, et al. Association Between Early Immune-Related Adverse Events and Clinical Outcomes in Patients With Non-Small Cell Lung Cancer Treated With Immune Checkpoint Inhibitors. *Clin Lung Cancer* (2020) 21:e315–28. doi: 10.1016/j.cllc.2020.01.003
- Sato K, Akamatsu H, Murakami E, Sasaki S, Kanai K, Hayata A, et al. Correlation Between Immune-Related Adverse Events and Efficacy in Non-Small Cell Lung Cancer Treated With Nivolumab. *Lung Cancer* (2018) 115:71–4. doi: 10.1016/j.lungcan.2017.11.019
- Mirels H. Metastatic Disease in Long Bones. A Proposed Scoring System for Diagnosing Impending Pathologic Fractures. *Clin Orthop Relat Res* (1989) 249:256–64. doi: 10.1097/00003086-198912000-00027

- Ward WG, Holsenbeck S, Dorey FJ, Spang J, Howe D. Metastatic Disease of the Femur: Surgical Treatment. *Clin Orthop Relat Res* (2003) 415 Suppl:S230– 44. doi: 10.1097/01.blo.0000093849.72468.82
- Mavrogenis AF, Pala E, Romagnoli C, Romantini M, Calabro T, Ruggieri P. Survival Analysis of Patients With Femoral Metastases. J Surg Oncol (2012) 105:135–41. doi: 10.1002/jso.22061

Conflict of Interest: The authors declare that the research was conducted in the absence of any commercial or financial relationships that could be construed as a potential conflict of interest.

Publisher's Note: All claims expressed in this article are solely those of the authors and do not necessarily represent those of their affiliated organizations, or those of the publisher, the editors and the reviewers. Any product that may be evaluated in this article, or claim that may be made by its manufacturer, is not guaranteed or endorsed by the publisher.

Copyright © 2022 Asano, Yamamoto, Demura, Hayashi, Takeuchi, Kato, Miwa, Igarashi, Higuchi, Yonezawa, Araki, Morinaga, Saito, Sone, Kasahara and Tsuchiya. This is an open-access article distributed under the terms of the Creative Commons Attribution License (CC BY). The use, distribution or reproduction in other forums is permitted, provided the original author(s) and the copyright owner(s) are credited and that the original publication in this journal is cited, in accordance with accepted academic practice. No use, distribution or reproduction is permitted which does not comply with these terms.



Identification and Validation in a Novel Quantification System of Ferroptosis Patterns for the Prediction of Prognosis and Immunotherapy Response in Leftand Right-Sided Colon Cancer

OPEN ACCESS

Edited by:

Yubin Li, University of Pennsylvania, United States

Reviewed by:

Ling Yin, University of Texas MD Anderson Cancer Center, United States Chongming Jiang, Baylor College of Medicine, United States

*Correspondence:

Bin-Bin Cui cbbhrb@163.com Yan-Long Liu liuyanlong@hrbmu.edu.cn

[†]These authors have contributed equally to this work

Specialty section:

This article was submitted to Cancer Immunity and Immunotherapy, a section of the journal Frontiers in Immunology

Received: 16 January 2022 Accepted: 07 March 2022 Published: 04 April 2022

Citation:

Zhang H-C, Deng S-H, Pi Y-N, Guo J-N, Xi H, Shi X, Yang X-F, Zhang B-M, Xue W-N, Cui B-B and Liu Y-L (2022) Identification and Validation in a Novel Quantification System of Ferroptosis Patterns for the Prediction of Prognosis and Immunotherapy Response in Leftand Right-Sided Colon Cancer. Front. Immunol. 13:855849. doi: 10.3389/fimmu.2022.855849 Heng-Chun Zhang^{1†}, Shen-Hui Deng^{2†}, Ya-Nan Pi³, Jun-Nan Guo¹, Hua Xi¹, Xin Shi⁴, Xue-Fei Yang⁵, Bo-Miao Zhang¹, Wei-Nan Xue¹, Bin-Bin Cui^{1*} and Yan-Long Liu^{1*}

¹ Department of Colorectal Surgery, Harbin Medical University Cancer Hospital, Harbin, China, ² Department of Anesthesiology, The Fourth Affiliated Hospital of Harbin Medical University, Harbin, China, ³ Department of Gynecology, Harbin Medical University Cancer Hospital, Harbin, China, ⁴ Department of Rehabilitation Medicine, The Second Affiliated Hospital of Harbin Medical University, Harbin, China, ⁵ The First Department of Oncology, The First Affiliated Hospital of Harbin Medical University, Harbin, China

Background: This study aimed to establish a novel quantification system of ferroptosis patterns and comprehensively analyze the relationship between ferroptosis score (FS) and the immune cell infiltration (ICI) characterization, tumor mutation burden (TMB), prognosis, and therapeutic sensitivity in left-sided and right-sided colon cancers (LCCs and RCCs, respectively).

Methods: We comprehensively evaluated the ferroptosis patterns in 444 LCCs and RCCs based on 59 ferroptosis-related genes (FRGs). The FS was constructed to quantify ferroptosis patterns by using principal component analysis algorithms. Next, the prognostic value and therapeutic sensitivities were evaluated using multiple methods. Finally, we performed weighted gene co-expression network analysis (WGCNA) to identify the key FRGs. The IMvigor210 cohort, TCGA-COAD proteomics cohort, and Immunophenoscores were used to verify the predictive abilities of FS and the key FRGs.

Results: Two ferroptosis clusters were determined. Ferroptosis cluster B demonstrated a high degree of congenital ICI and stromal-related signal enrichment with a poor prognosis. The prognosis, response of targeted inhibitors, and immunotherapy were significantly different between high and low FS groups (HSG and LSG, respectively). HSG was characterized by high TMB and microsatellite instability-high subtype with poor prognosis. Meanwhile, LSG was more likely to benefit from immunotherapy. ALOX5 was identified as a key FRG based on FS. Patients with high protein levels of ALOX5 had poorer prognoses.

Conclusion: This work revealed that the evaluation of ferroptosis subtypes will contribute to gaining insight into the heterogeneity in LCCs and RCCs. The quantification for ferroptosis patterns played a non-negligible role in predicting ICI characterization, prognosis, and individualized immunotherapy strategies.

Keywords: colon cancer, left-sided, right-sided, ferroptosis, immunity, prognosis, immunotherapy response

1 INTRODUCTION

Colon cancer (CC) is a common gastrointestinal malignancy, with an incidence second only to that of gastric and esophageal cancers, and is associated with a high mortality rate (1). Approximately 900,000 people die from CC every year worldwide, accounting for about 10% of the total cancer-related deaths (2). Based on the anatomical structure of the colon, CC can be classified as left-sided CC (LCCs) or right-sided CC (RCCs) (3–5). Previous studies have demonstrated that primary tumor site is an independent prognostic factor in CC, and it is used as a basis for the development of treatment strategies (6–8). Thus, understanding cellular and molecular biological mechanisms between LCCs and RCCs is key in advancing tumor therapy (4).

Multiple studies have identified different CC subtypes based on the tumor cells, immune infiltration, molecular pathways, mutation status, and m6A methylation. Besides, these studies have characterized the differences between these subtypes, including metastasis tendency, recurrence, prognosis, and response to treatment (9-11). Immunotherapy works by recognizing and eliminating tumor cells by activating the body's natural defense system. Although immunotherapy is gradually becoming the most preferred strategy for cancer treatment, low overall response presents a major hindrance (12). Growing evidence shows that the tumor microenvironment (TME) plays an important role in tumor progression, immune escape, and immunotherapy responses. Recent studies have demonstrated that ferroptosis exerts a dual role in tumor promotion and suppression, as well as affecting the efficacy of chemotherapy, radiotherapy, and immunotherapy. Ferroptosis is an iron-dependent new type of cell death characterized by the accumulation of intracellular reactive oxygen species (ROS). The process is dependent on the release of damage-associated molecular patterns in the TME and the immune response triggered by ferroptosis cell damage. Regulation of ferroptosis can suppress cell migration, invasion, and proliferation of CC (13). On the other hand, β -elemene combined with cetuximab can inhibit the migration of KRAS mutant CC; induce the accumulation of intracellular ROS, glutathione depletion, lipid peroxidation, and transferrin increase; and decrease the negative regulatory protein of ferroptosis, all of which could be reversed by inhibitors of ferroptosis (13). Therefore, targeting the pathway modulating tumor cell ferroptosis is an emerging antitumor strategy, and its combination with other therapeutic approaches could yield huge improvement in the clinical management of cancer. At present, it is possible to use a combination of iron levels, gene expression, and mutations to assess the patients who could benefit from the ferroptosis-promoting treatment. In addition, through a comprehensive analysis of the heterogeneity and complexity of the TME, it is possible to identify different tumor subtypes and novel biomarkers, and the ability to improve prediction of treatment sensitivity. This will also help to find and validate new therapeutic targets. Data on the characteristics of ferroptosisrelated subtypes in LCC and RCC remain scanty.

Here, we integrated ferroptosis-related genes (FRGs) and identified ferroptosis-related subtypes in LCCs and RCCs from The Cancer Genome Atlas (TCGA) and Gene Expression Omnibus (GEO) databases. Surprisingly, our data demonstrated that different ferroptosis-related subtypes have unique immune cell infiltration (ICI) characteristics. The data showed that ferroptosis plays a vital role in shaping the TME. Thus, we established a scoring model to quantify the characteristics of ferroptosis and analyzed the relationship between the ferroptosis score (FS) and tumor mutation burden (TMB), prognosis, and treatment sensitivity. Our results provided a novel and accurate method for predicting the prognosis and potential benefits of treatment.

2 MATERIALS AND METHODS

The flowchart of the entire study is shown in Figure 1.

2.1 Colon Cancer Datasets and Preprocessing

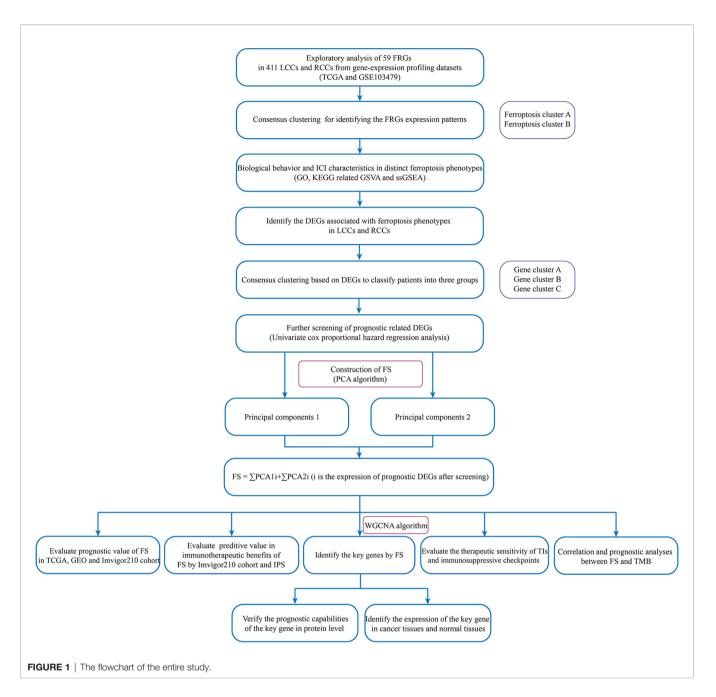
A total of 629 CC samples from two high-throughput platforms were included in this study: 473 samples from TCGA (https:// tcga-data.nci.nih.gov/tcga/) and 156 samples from GEO (GSE103479) (http://www.ncbi.nlm.nih.gov/geo/). Other information included somatic mutation information, copy number variation (CNV), primary tumor site, clinical information, and survival data. The inclusion criteria were as follows: 1) the primary sites of the tumor were all in the left or right colon. The tumor primary sites in the cecum, ascending colon, and hepatic flexure are RCCs. The tumor primary sites in splenic flexure, descending colon, sigmoid colon, and rectosigmoid junction are LCCs (2). All patients must have complete follow-up information and RNA-seq data. Patients with incomplete survival information were excluded from the subsequent analysis. Following the screening, 444 samples were admitted to the study, including 322 TCGA samples and 122 GEO samples. The normalized matrix files were downloaded from GEO and RNA sequencing data (FPKM value) of gene expression from TCGA. Then the FPKM value was converted to transcripts per kilobase million (TPM) values for the combined analysis. The "ComBat" algorithm (14) in the R package "SVA" was used to reduce the batch effect caused by nonbiotechnology deviations.

2.2 Unsupervised Clustering Based on Ferroptosis-Related Genes

To identify different iron ferroptosis-related patterns mediated by FRGs, a total of 59 FRGs was retrieved from previously published literature and available data and extracted the expression of these genes from integrated datasets (15–19). Hierarchical agglomerative clustering was used for sample clustering using the R package "ConsensusClusterPlus" (20). Stability evidence was then employed in unsupervised analysis to determine cluster count and membership. The process was repeated 1,000 times to ensure the stability of clustering.

2.3 Gene Set Variation Analysis

To study the differences in biological processes of the ferroptosis subtypes, the R package "GSVA" (21) was used to perform enrichment analysis. The gene set variation analysis (GSVA)



was conducted, a non-parametric and unsupervised method, to evaluate enrichment variation, if any, of pathways and biological process activities in different expression datasets. Gene Ontology (GO) and Kyoto Encyclopedia of Genes and Genomes (KEGG) gene sets were downloaded from the MSigDB database (http:// software.broadinstitute.org/gsea/msigdb/) and used to perform the GSVA. Heatmaps were used to show the ferroptosis-related pathways with an adjusted p < 0.05.

2.4 Estimating of Immune Cell Infiltration

To evaluate and quantify the ICI in each sample, single-sample gene-set enrichment analysis (ssGSEA) by the R package "GSVA" (21) was used. After immune cell marker gene

expression information was obtained from Charoentong's research, the enrichment score calculated by ssGSEA was used to represent the relative infiltration abundance of each immune cell. Finally, the differences in ICI between ferroptosis subtypes were analyzed.

2.5 Identification of Differentially Expressed Genes Between Ferroptosis Subtypes in Left-Sided Colon Cancer and Right-Sided Colon Cancer

The R package "Limma" (22) was used to identify differentially expressed genes (DEGs) between different ferroptosis subtypes

(adjusted *p*-value <0.01). Considering the molecular biological differences, the DEGs in LCCs and RCCs were also identified ($|\log 2$ foldchange| > 0.5, adjusted *p*-value <0.05). Then the intersection of the two groups of DEGs was taken, and their expression in all samples was extracted for subsequent analysis. The GO and KEGG functional annotations analyses were performed by the R package "clusterProfiler" (23).

2.6 Construction of Ferroptosis Score

To quantify the characteristics of ferroptosis in the LCCs and RCCs, an algorithm was developed, and the outcome was defined as FS. First, univariate Cox proportional hazards regression analysis (COX) on the intersection DEGs by the R package "glmnet" (24) was performed. Thereafter, genes with a significant difference in the prognosis were extracted for further analysis. To classify the patients into several groups for in-depth analysis, unsupervised clustering was performed. Afterward, principal component analysis (PCA) was performed to extract the main components of these genes, and then a ferroptosisrelevant gene signature was constructed. Principal components 1 and 2 were selected as signature scores. A method similar to the gene expression rank index was performed to define the FS of each patient: $FS = \Sigma PCA1i + \Sigma PCA2i$ (i is the expression of prognostic DEGs after screening). To distinguish the high and low FS groups (HSG and LSG, respectively) associated with prognosis, the best cutoff value was estimated by the R package "maxstat" (25).

2.7 Prediction of Multiple Therapeutic Sensitivities

The difference in therapeutic sensitivities between HSG and LSG from targeted inhibitor (TI) therapy and immunotherapy was analyzed. The concentration causing 50% reduction growth (IC50) of TIs was calculated by the R package "pRRophetic" (26), including Notch, Hedgehog (HH), and Wnt inhibitors. Wilcoxon rank-sum test was applied for comparing the difference of IC50 between HSG and LSG.

Meanwhile, immunogenicity is determined by multiple genes, including genes associated with effector cells, MHC molecules, immune regulatory factors, and immunosuppressive cells. Immunogenicity can be estimated and quantified without bias by machine learning. The Immunophenoscores (IPS) of CC were downloaded from The Cancer Immunome Atlas (TCIA) database (https://tcia.at/) (27). Then, the IPS between the HSG and LSG in different immunotherapy methods were compared to predict immunotherapy sensitivity. Meanwhile, a comprehensive search was conducted on the gene expression profile of publicly available datasets treated with immunotherapy, and the metastatic urothelial tumors cohort (28) (IMvigor210: http:// research-pub.gene.com/IMvigor210CoreBiologies) and the advanced melanoma cohort (BMS038: https://github.com/ riazn/bms038_analysis) (29) were included in the study. The IMvigor210 data were preprocessed by the R package "IMvigor210CoreBiologies." The RNA-seq data were filtered and normalized by the R package "edgeR" (30), and the data were transformed by "voom" in the R package "limma" (22). The

prognostic information and immunotherapy outcomes were also collated. The FS of each sample in the IMvigor210 cohort and BMS038 cohort were also quantified.

2.8 Identification of Key Genes Related to Ferroptosis

To identify key prognostic genes related to ferroptosis in the LCC and RCC, weighted gene co-expression network analysis (WGCNA) was performed based on the intersection of DEGs and FS. First, a suitable power exponent was selected to convert the adjacency matrix (AM) to the topological overlap matrix. A correlation analysis between the gene consensus modules with FS was then performed, and the modules negatively correlated with FS were selected for subsequent analyses. The key genes were identified by the intersection of the module genes and the FRGs obtained from the literature. To evaluate the expression of the key FRGs at the protein level, the TCGA-COAD proteomics cohort was downloaded from the Clinical Proteomic Tumor Analysis Consortium (CPTAC) database (https://proteomics. cancer.gov/programs/cptac), which included 29 normal samples and 64 tumor samples. The prognostic value and characteristics of the expression of the key genes were analyzed.

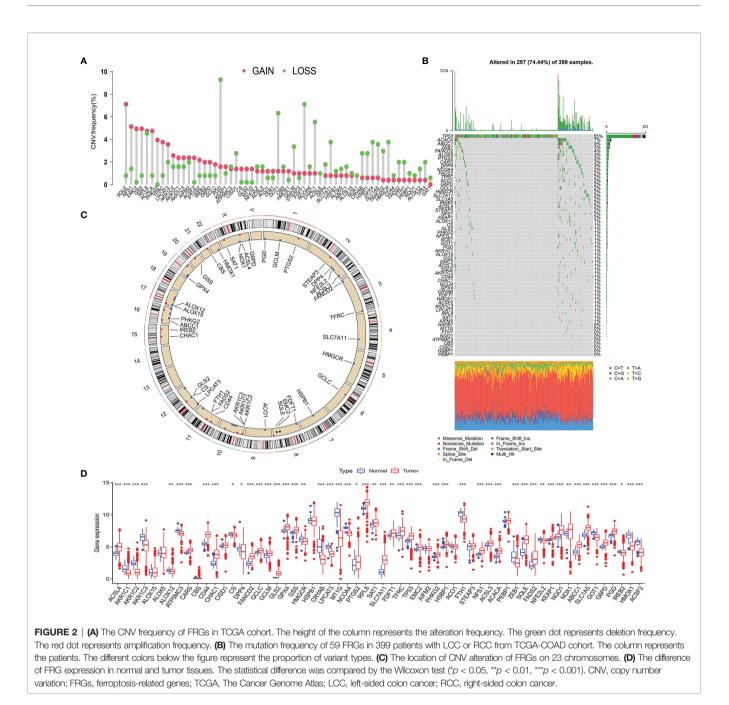
2.9 Statistical Analyses

All statistical analyses were conducted by R statistical language (version 4.0.5). Wilcoxon test and Kruskal–Wallis test were used for the comparison between the two groups and more than two groups, respectively. The Kaplan–Meier plotter was used to draw the prognostic survival curve, and the log-rank test was used to evaluate the significance of the statistical difference. Spearman's test was used for correlation analysis and calculation of correlation coefficient. The R package "maftool" (31) was used to illustrate the gene mutation status in different groups. The R package "rcircos" (32) was used to plot the CNV of FRGs on 23 pairs of chromosomes. In all analyses, p < 0.05 was considered statistically significant.

3 RESULTS

3.1 Genetic Variation of the Ferroptosis-Related Genes in Left-Sided Colon Cancer and Right-Sided Colon Cancer

Based on recent literature reports, a total of 59 FRGs were included in this study. First, we calculated and demonstrated that FRGs have prevalent CNV alteration in LCC and RCC, and most were focused on the deletion in copy number, while nearly half of the FRGs have a wider frequency of CNV amplification (**Figure 2A**). Out of 399 samples, 297 carried FRG mutations, representing a 74.44% mutation frequency. Among these, TP53 had the highest mutation frequency, followed by ACACA, ABCC1, and ZEB1 (**Figure 2B**). The data showed that there was a frequent occurrence of CNV, and deletions or amplifications of different FRGs had unique characteristics. Genes with a higher frequency of copy number amplification included SQLE, NFS1, EMC2, and GSS. The genes with higher



deletion frequency included PGD, GOT1, FDFT1, and CHAC1. We also demonstrated the prevalence of the CNV on these FRGs on the chromosome (**Figure 2C**). To determine whether the above genetic variations affect the mRNA expression in LCC and RCC, we analyzed the mRNA expression levels in normal and cancer tissues and showed that the CNV might be mediating the difference in FRG expression. Compared with normal tissues, the expression of FRGs with higher amplification frequency increased significantly in cancer tissues (e.g., SQLE, NFS1, and ACACA), and vice versa (e.g., GOT1, HMGCR, and FTH1) (**Figure 2D**). In addition, the expression of the FRGs in normal and cancer tissues was highly heterogeneous, indicating that the

differential FRG expression plays an important role in the occurrence and development of LCC and RCC.

3.2 The Initial Clustering: Ferroptosis Subtypes Have Unique Immune Infiltration Characteristics and Biological Behaviors 3.2.1 Two Ferroptosis Phenotypes Were Identified Based on the Expression Pattern of Ferroptosis-Related Genes

To further explore the interactions, connection, and prognostic impact of the FRGs, we employed univariate COX and

correlation analyses on these genes. The results showed that 27 FRGs affected the prognosis (all p < 0.05) of the LCC and RCC. There was a significant positive correlation between the FRGs with the same prognostic impact; for example, the KEPA1 expression has a positive correlation with the expression of GPX4, AIFM2, RPL8, and HSPB1 (**Figure 3A**). Meanwhile, there was a significant negative correlation between the prognostic favorable FRGs and unfavorable FRGs, such as the unfavorable factor GPX4 has a negative correlation with favorable prognostic factors HMGCR, GCLM, and FANCD2. The favorable prognostic factors CRYAB, CBS, and ALOX12 (**Figure 3A**). The data demonstrated that there might be complex crosstalk between the FRGs, which is important for the prognosis of patients and the cell-infiltrating characterization in the TME.

Subsequently, we used the R package "ConsensusClusterPlus" (20) to perform a cluster analysis of the patients based on different FRG expression patterns. The analysis identified 2 ferroptosis-related phenotypes, which were defined as ferroptosis clusters A and B (**Figure 3B**). The prognostic analysis showed that ferroptosis cluster A yielded a better prognosis as compared to ferroptosis cluster B (p = 0.017) (**Figure 3C**). Next, we used a heatmap to illustrate the expression pattern of the FRGs and showed that the FRGs were differentially expressed in the 2 clusters (**Figure 3D**).

3.2.2 The Immune Cell Infiltration Characteristics and Biological Behaviors in Distinct Ferroptosis Phenotypes

The analysis of the ICI showed that there was no significant difference in CD4⁺ and CD8⁺ T cells between the two clusters. Although most immune cells in ferroptosis cluster B were highly infiltrated, they contained many immunosuppressive cells, such as eosinophil, myeloid-derived suppressor cells (MDSCs), macrophages, mast cells, and regulatory T cells (Tregs) (Figure 3E). These results are somewhat interesting. Previous research has indicated that ferroptotic damage can cause immunosuppression associated with inflammation in tumor ICI (33). Ferroptosis could be induced by cytotoxic T celldriven immunity (34), but in specific conditions, ferroptosis can promote tumor progression through other immune cells. Ferroptotic cancer cells can release HMGB1 and promote macrophage inflammatory response (35). Additionally, pancreatic cancer cells release KRAS-G12D via exosomes during ferroptosis, and macrophages then take up these KRAS-G12D and undergo M2 polarization mediated by AGER to promote tumor progression (36). Neutrophils have been shown to maintain inflammation and promote tumor progression. In lung cancer, neutrophils could secrete pro-inflammatory leukotrienes to change vascular permeability and stimulate cell adhesion (37). The presence of tumor-infiltrating mast cells and FOXP3⁺ Tregs was correlated with the downregulation of HLA-I molecules on tumor cells, resulting in the lack of CD8⁺ T-cell infiltration in these tumor regions (38).

To explore the differences in the biological behaviors between the ferroptosis clusters, we conducted GO- and KEGG-related GSVAs. The results showed that tumor stem cells and stromalrelated signals were significantly enriched in ferroptosis cluster B. The signals included the non-canonical Wnt signaling pathway, Hedgehog signaling pathway, TGF β signaling pathway, and extracellular matrix (ECM) receptor interaction (Figures 3F, **G**). The upregulation of the TGF β signaling pathway and ECM receptor interaction reflected the immunosuppressive nature in ferroptosis cluster B. This upregulation pattern was also observed in some stage III colorectal cancer (CRC) regardless of the microsatellite instability (MSI) status (39). Besides, signaling pathways related to genome stability, such as the P53 signaling pathway, base excision repair, and mismatch repair pathway, were significantly enriched in ferroptosis cluster A. The enriched pathways also included ferroptosis-related signaling, such as fatty acid metabolism, peroxisome, glutamate metabolism, and glutathione metabolism. It has been shown that ferroptosis is caused by excessive lipid peroxidation, which can be induced by exogenous or endogenous pathways. The exogenous pathways are initiated by inhibition of cell-membrane transporters, such as cystine/glutamate transporters, while the endogenous pathways are activated by blocking antioxidant enzymes, such as glutathione peroxidase 4 (33). In addition, the p53 signaling pathway is closely associated with ferroptosis and inhibits transcription of SLC7A11, which promotes ferroptosis in cancer cells (40). Some metabolism-related genes, such as SAT1, FDXR, and GLS2, have been reported to be direct targets of p53mediated ferroptosis under different conditions (41, 42).

3.3 The Secondary Clustering: Ferroptosis Phenotype-Related Differentially Expressed Gene Cluster Patients More Stably and Quantify Ferroptosis Patterns to Better Predict Prognosis 3.3.1 The Secondary Clustering Using the

Differentially Expressed Genes More Stably Identified Prognostic-Related Subtypes

To further study the potential biological behavior of each ferroptosis phenotype, we obtained 8,087 DEGs related to ferroptosis phenotypes using the R package "Limma." In view of the obvious differences between LCCs and RCCs, we analyzed the DEGs in the LCCs and RCCs. After intersection analysis, 508 overlapped DEGs were obtained. GO and KEGG enrichment analyses of the DEGs showed significant enrichment of many biological processes related to immunity, which confirmed that ferroptosis plays a crucial role in TME. To further verify this effect, we performed an unsupervised cluster analysis based on the 508 overlapped DEGs and stratified patients into three ferroptosis phenotype-related DEG clusters (gene clusters A-C) (Figure 4A). The stratification aimed at further distinguishing other phenotypic differences caused by the ferroptosis patterns. Under this clustering algorithm, we demonstrated that patients in gene cluster A had the most favorable prognosis (p < 0.001) (Figure 4B). Most patients in gene cluster A belonged to ferroptosis cluster A, while those in gene clusters B and C with relatively poor prognosis belonged to ferroptosis cluster B (Figure 4C). The significant differences in the expression of the FRGs were found within the different gene clusters

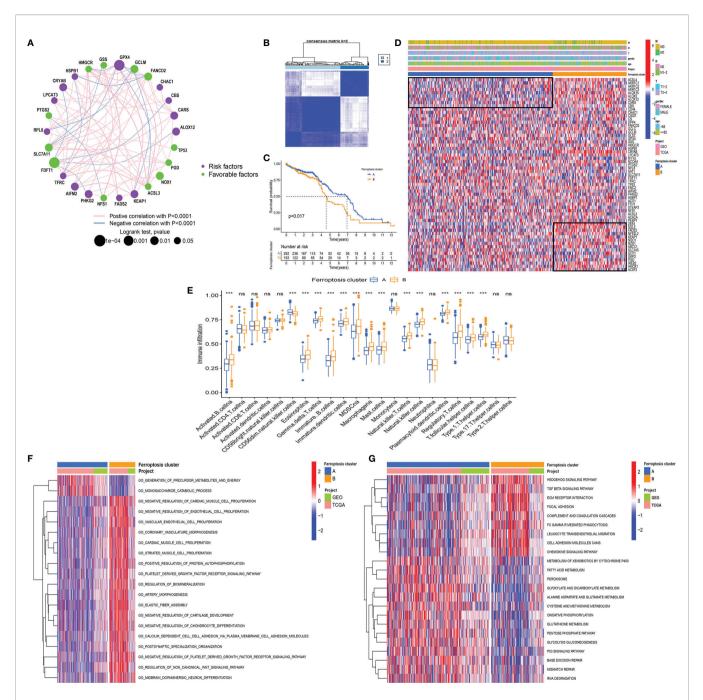


FIGURE 3 | (A) The interaction between FRGs in LCCs and RCCs. The circle size represents the range of significance values of each FRG on the prognosis. The *p*-values were calculated by log-rank test. Green dots represent favorable factors for prognosis, and purple dots represent risk factors for prognosis. The lines linking FRGs represent their correlation. The thickness of the lines represents the strength of correlation between FRGs. Negative and positive correlations were marked with blue and red, respectively. (B) The consensus matrixes for all CC samples displayed the clustering stability with 1,000 iterations. All samples were clustered into an appropriate number of subtypes (k = 2). (C) Kaplan–Meier curves showed the overall survival difference between ferroptosis clusters A and B (p = 0.017). (D) The heatmap demonstrates the expression of FRGs in different ferroptosis clusters. Heatmap colors indicate relative FRG expression levels. (E) The abundance of each ICI in ferroptosis clusters A and B (***p < 0.001, ^{ns}p > 0.05). (F, G) GO-related (F) and KEGG-related (G) GSVA showing the activation status of biological behaviors in ferroptosis clusters A and (B) The heatmap demonstrates these biological pathways. Red and blue represent activated and inhibited pathways, respectively. FRGs, ferroptosis-related genes; LCC, left-sided colon cancer; RCC, right-sided colon cancer; CC, colon cancer; ICI, immune cell infiltration; GO, Gene Ontology; KEGG, Kyoto Encyclopedia of Genes and Genomes; GSVA, gene set variation analysis.

(**Figure 4D**), which were in accordance with the expected results caused by ferroptosis patterns.

3.3.2 The Ferroptosis Score Had Satisfactory and Consistent Predictive Power for Prognosis in Multiple Independent Cohorts

Given the heterogeneity and complexity of individual ferroptosis patterns and the subsequent identification of key FRGs, we used PCA to quantify the ferroptosis patterns in the LCCs and RCCs and defined the results as FS. Next, we evaluated the value of the FS in predicting prognosis. After the best cutoff value was obtained through the R package "maxstat," we distributed all the patients from TCGA and GSE103479 cohorts into HSG and LSG. The patients in the LSG showed a better prognosis compared to those in the HSG (p < 0.001) (Figure 4E). To evaluate the predictive prognostic consistency of the FS, we calculated the FS and performed a prognostic analysis in the Imvigor210 cohort, GSE17536 cohort, and BMS038 cohort. The results showed that the patients in LSG had a significantly better prognosis than those in HSG in the Imvigor210 cohort (p =0.004) (Figure 4F), GSE17536 cohort (p = 0.019) (Figure 4G), and BMS038 cohort (p = 0.050) (Figure 4H). Thus, the consistency of the predictive effectiveness of the FS was demonstrated, indicating that the FS had robust predictive ability in the cross-validation cohort.

A Sankey plot was used to visualize the primary tumor sites, ferroptosis clusters, gene clusters, and FS in each patient (**Figure 4I**). The LCCs and RCCs patients were classified into 2 ferroptosis clusters and then divided into 3 gene clusters. Compared with gene cluster A, which showed better prognoses, the patients in gene cluster C with poor prognoses belonged to the HSG. Similarly, most patients in gene cluster B with poor prognoses belonged to HSG.

Since the overlapped DEGs were significantly enriched in immune-related pathways, we explored the relationship between the FS and ICI and generated a correlation heatmap (**Figure 4J**). The data showed that there was a significant positive correlation between the FS and most infiltrated immune cells.

In addition, we explored the relationship between the FS and the two clustering modes and showed significant differences in the FS among the different clustering modes. The median FS in ferroptosis cluster B was significantly higher as compared to that in ferroptosis cluster A (p < 0.001) (**Figure 4K**). The median FS of gene cluster C was significantly higher than that in gene clusters A and B (p < 0.001) (**Figure 4L**). Besides, the patients in ferroptosis cluster B, gene cluster C, and HSG had a relatively worse prognosis, thus demonstrating the consistency of the predictive effectiveness. Therefore, the quantified ferroptosis patterns could be used as an indicator to predict prognosis and ICI.

3.4 The Ferroptosis Score Had Significant Associations With Tumor Mutation Burden and Genomic Instability

Our analysis showed that genome stability-related pathways were significantly enriched in the GSVA of ferroptosis clusters. We then performed a series of analyses on somatic mutations in the HSG and LSG. First, we analyzed the difference between the TMB in the HSG and LSG and demonstrated that the TMB in the HSG was significantly higher compared to that in the LSG (p < 0.001) (**Figure 5A**). Previous studies have shown that high TMB predicts poor prognosis in a variety of cancers. In our study, the HSG had a worse prognosis, and the results were consistent. Furthermore, there was a positive correlation between the FS and TMB (Spearman's coefficient: r=0.4, p < 0.001) (**Figure 5B**). The distribution of gene clusters varied with the increase of the FS. Gene cluster A with a better prognosis was mainly distributed at the bottom left of the coordinate axis (**Figure 5B**).

CC was classified into microsatellite stable (MSS), MSI-low (MSI-L), and MSI-high (MSI-H) by TCGA project. In the 2017 National Comprehensive Cancer Network guidelines, the immune checkpoint inhibitor anti-PD-1 was recommended as an end-line treatment of CC with deficient mismatch repair (dMMR)/MSI-H subtype [27]. Our analysis showed significant FS differences between the molecular subtypes. The median FS in the MSI-H subtype was significantly higher than that in the other two subtypes (all p < 0.001) (Figure 5C). A larger portion of patients in the HSG belonged to the MSI-H subtype and had a worse prognosis, while almost all patients in the LSG belonged to the MSS and MSI-L subtypes and had better prognoses (Figure 5D). The above results indicated that the ferroptosis patterns not only affect ICI but also have a potential relationship with somatic mutation, which leads to a poorer prognosis of patients under their synergistic influence.

3.5 The Synergistic Effect of Ferroptosis Score and Tumor Mutation Burden Further Refined Prognostic Prediction

We performed a prognostic analysis of TMB and found that there was a significant difference in the prognosis of patients in the high and low TMB groups (**Figure 5E**). Taking the synergistic effect of the TMB and FS on the prognosis, we performed a stratified prognostic analysis. We found that patients with a combination of low FS and low TMB showed a great survival advantage (**Figure 5F**). These data indicated that the FS could be a potential prognostic indicator, and the combination with TMB could further refine prognostic prediction for patients.

We then analyzed the differences in the distribution of somatic mutation in the HSG and LSG human populations. The top 20 driver genes with the highest mutation frequency were used for presentation. The data showed that the mutation frequency of the genes in the HSG was generally higher compared to that in the LSG (**Figures 5G, H**).

3.6 The Ferroptosis Score Had Great Potential for Predicting Immunotherapy Efficacy

To evaluate the value of FS in predicting the clinical therapeutic efficacy of CC, we analyzed the difference in sensitivity of TIs between the groups. In sunitinib (VEGFR2 inhibitor)

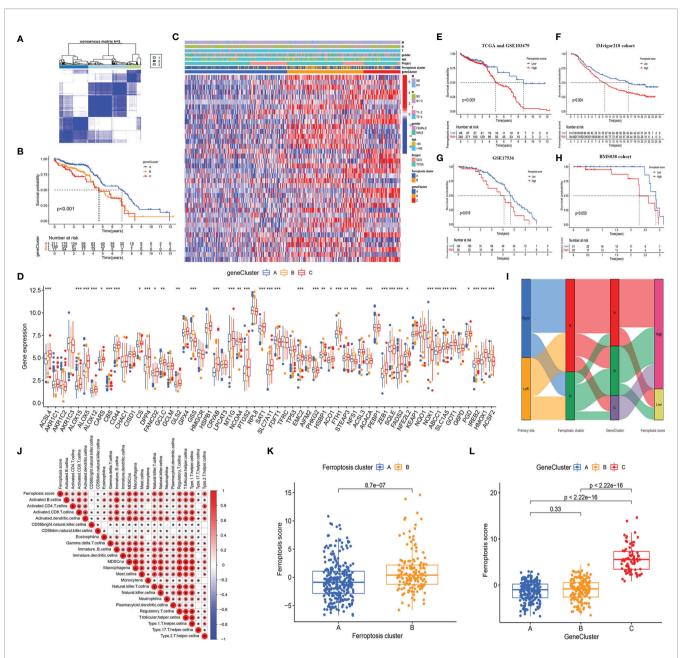


FIGURE 4 | (A) The consensus matrixes for TCGA-COAD cohorts based on the DEGs among the 2 ferroptosis clusters. TCGA samples were clustered into an appropriate number of subtypes (k = 3). (B) Kaplan–Meier curves showed an overall survival difference between gene clusters (p < 0.001). (C) The heatmap shows the expression of the ferroptosis-related DEGs in different ferroptosis clusters and gene clusters. (D) The difference of FRG expression in normal and tumor tissues. The statistical difference was compared by the Kruskal–Wallis test (p < 0.05, *p < 0.01, **p < 0.001). (E–H) Kaplan–Meier curves show overall survival difference between HSG and LSG in TCGA and GSE103479 cohort (p < 0.001) (E), IMvigor210 cohort (p = 0.004) (F), GSE17536 cohort (p = 0.019) (G), and BMS038 cohort (p = 0.050) (H). (I) The Sankey diagram demonstrates the distribution of patients with primary tumor sites, ferroptosis clusters, and FS. (J) Correlations between FS and the abundance of each ICI in TCGA cohort using Spearman's analysis. Positive correlation with red and negative correlation is marked in blue. (K) Differences in FS between 2 ferroptosis clusters. The Wilcoxon test was used to compare the statistical difference between 2 ferroptosis clusters (p < 0.001). (L) Differences in FS among 3 gene clusters. The Kruskal–Wallis test was used to compare the statistical difference between 3 gene clusters. DEGs, differentially expressed genes; TCGA, The Cancer Genome Atlas; FRG, ferroptosis-related gene; HSG, high ferroptosis score group; LSG, low ferroptosis score group; FS, ferroptosis score; ICI, immune cell infiltration.

(Figure 6A), the median IC50 of LSG was significantly lower than that of HSG (p = 0.0025). In elesclomol (inducer of oxidative stress) (Figure 6B), embelin (NF- κ B inhibitor) (Figure 6C), JNK Inhibitor VIII (Figure 6D), cyclopamine

(HH signaling inhibitor) (**Figure 6E**), CGP.60474 (cyclindependent kinase inhibitor) (**Figure 6F**), and GDC0941 (PI3K inhibitor) (**Figure 6G**), the median IC50 of HSG was significantly lower than that of LSG (all p < 0.05).

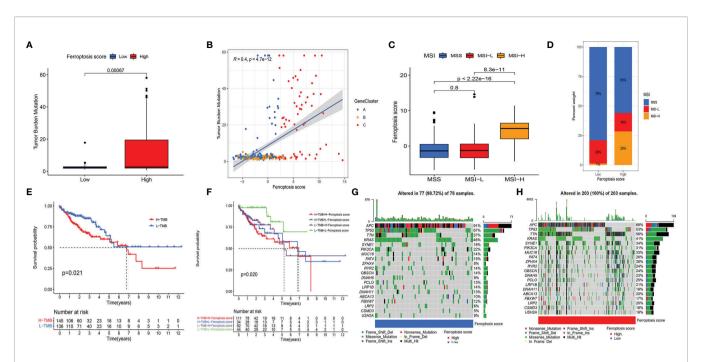


FIGURE 5 | (A) Differences in TMB between HSG and LSG. The Wilcoxon test was used to compare the statistical difference between HSG and LSG (p < 0.001). (B) The scatterplots show that there was a significant positive correlation between FS and TMB. The correlation coefficient between FS and TMB was 0.4 (p < 0.001). (C) The median FS in the MSI-H subtype was significantly higher than that in MSS and MSI-L subtypes (all p < 0.001) (D) The proportion of CC molecular subtypes in HSG and LSG. MSS subtype, blue; MSI-L subtype, red; MSI-H, yellow. (E) Kaplan–Meier curves show an overall survival difference between TMB subgroups (p = 0.021). (F) Kaplan–Meier curves show overall survival differences stratified by TMB and FS (p = 0.02). (G, H) The waterfall diagram demonstrates the top 20 driver genes with the highest mutation frequency in HSG (G) and LSG (H). TMB, tumor mutation burden; HSG, high ferroptosis score group; LSG, low ferroptosis score group; FS, ferroptosis score; MSI-H, microsatellite instability-high; MSS, microsatellite stable; MSI-L, microsatellite instability-low; CC, colon cancer.

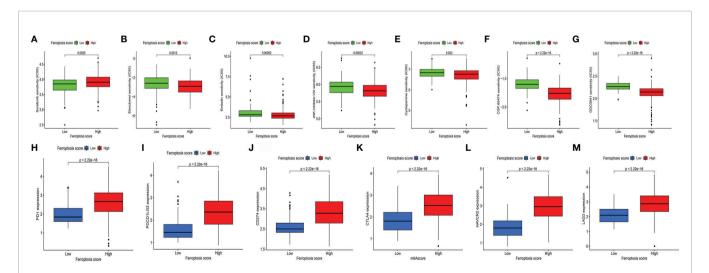


FIGURE 6 | (A–G) The difference of multiple TI sensitivity in HSG and LSG. In sunitinib (A), the median IC50 of LSG was significantly lower than that of HSG (p < 0.01). In elescionol (B), embelin (C), JNK Inhibitor VIII (D), cyclopamine (E), CGP.60474 (F), and GDC0941(G), HSG had a significantly lower median IC50 than LSG (all p < 0.05). (H–M) The difference of immune-suppressive checkpoint gene expressions between HSG and LSG. The expressions of PD1 (H), PDCD1LG2 (I), CD274 (J), CTLA4 (K), HAVCR2 (L), and LAG3 (M) were higher in HSG than in LSG (all p < 0.001). The statistical difference was compared by the Wilcoxon test. TI, targeted inhibitor; HSG, high ferroptosis score group; LSG, low ferroptosis score group.

For immune-suppressive checkpoint genes, the expressions of PDCD1, PDCD1LG2, CD274, HAVCR2, CTLA4, and LAG3 were higher in HSG than those in LSG (all p < 0.001) (Figures 6H-M). In addition, two methods were performed to verify the predictive ability of FS in immunotherapeutic benefits. Several researchers have identified the ability of IPS calculated by immunogenicity on predicting the immunotherapy response in melanoma patients. So we analyzed the difference of IPS between HSG and LSG. The IPS, IPS-PD1/PD-L1/PD-L2, IPS-CTLA4, and IPS-PD1/PD-L1/PD-L2 + CTLA4 were used to evaluate the potential application of FS. The IPS (Figure 7A), IPS-CTLA4 (Figure 7C), and IPS-PD1/PD-L1/PD-L2 + CTLA4 (Figure 7D) were significantly different in HSG and LSG (all p < 0.05). There was no statistically significant difference in IPS-PD1/PD-L1/PD-L2 between HSG and LSG (p = 0.21) (Figure 7B). The proportion of complete response/partial response (CR/PR) patients in LSG was significantly higher than that in HSG (p < 0.05) (Figure 7E), and the FS in the CR/PR group was significantly lower than that in the stable disease (SD)/ progressive disease (PD) group (p = 0.022) (Figure 7F). Also, in the BMS038 cohort, the proportion of CR/PR patients in LSG was significantly higher than that in HSG (p < 0.05) (Figure 7G).

Overall, the FS had greater predictive potential in prognosis and immunotherapy efficacy.

3.7 ALOX5 Was Identified as the Prognostic Key Gene Based on Ferroptosis Score

To further analyze the key genes, a gene co-expression network was built by using WGCNA to identify modules with the highest correlation with FS. We selected the number 10 as the appropriate soft threshold (**Figure 8A**) and built a scale-free co-expression network. Ultimately, 5 gene modules were obtained (**Figure 8B**). It was apparent that only the gray module had a negative correlation with FS (correlation coefficient = -0.22, p < 0.001), while the other modules had a positive correlation with FS (**Figure 8C, D**). To narrow the scope of key genes, we selected the unique gray module for further screening.

To identify the key FRGs associated with prognosis, we selected the genes of the gray module, crossed them with the 59 FRGs collected in the literature, and finally obtained ALOX5. At the protein level, we found that the expression of ALOX5 was significantly more expressed in cancer tissues than in normal tissues (p < 0.001) (**Figure 8E**). Meanwhile, patients with higher

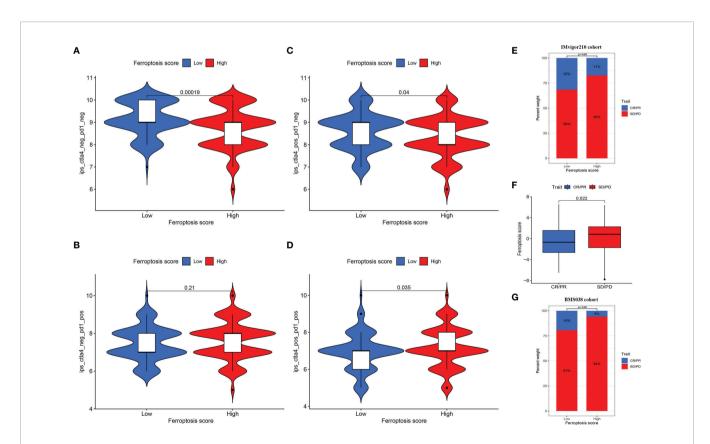


FIGURE 7 | (A–D) The differences of IPS between HSG and LSG. The IPS (A), IPS-CTLA4 (B), and IPS-PD1/PD-L1/PD-L2 + CTLA4 (D) were significantly different between HSG and LSG (all p < 0.05). (E) Proportion of patients with different treatment outcomes in HSG and LSG. The proportion of CR/PR patients in LSG was significantly higher than that in HSG in IMvigor210 cohort (p < 0.05). (F) The difference of FS between treatment outcome groups (p = 0.022). The statistical difference above was compared by the Wilcoxon test. (G) The proportion of CR/PR patients in LSG was significantly higher than that in HSG in BMS038 cohort (p < 0.05). IPS, Immunophenoscores; HSG, high ferroptosis score group; LSG, low ferroptosis score group; CR/PR, complete response/partial response.

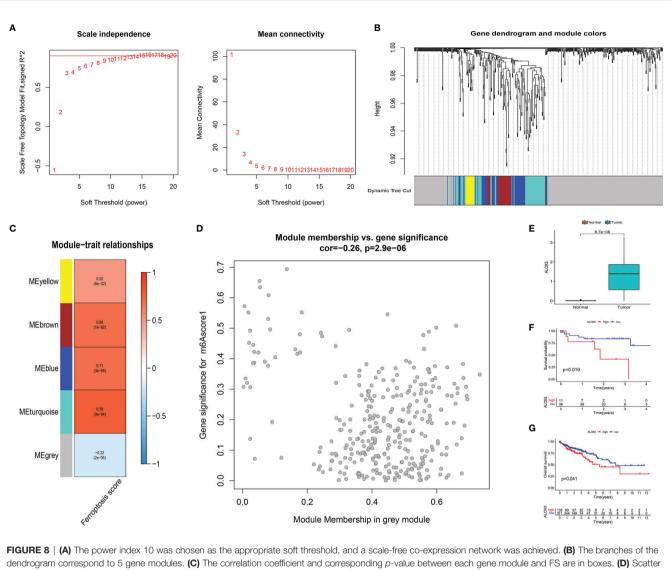


FIGURE 8 (A) The power index 10 was chosen as the appropriate soft threshold, and a scale-free co-expression network was achieved. (b) The branches of the dendrogram correspond to 5 gene modules. (C) The correlation coefficient and corresponding *p*-value between each gene module and FS are in boxes. (D) Scatter plot of module eigengenes in the gray module. (E) There were significant differences in ALOX5 expression between cancer tissues and normal tissues at protein level (p < 0.001). The statistical difference was compared by the Wilcoxon test. (F, G) Kaplan–Meier curves showed overall survival difference between high and low ALOX5 expression groups at protein level (p = 0.019) (F) and RNA level (p = 0.041) (G). FS, ferroptosis score.

expression of ALOX5 in protein level and RNA level were all related to poor prognosis (all p < 0.05) (**Figures 8F, G**).

Furthermore, the first neighbor of ALOX5 was found in the DisNor database (43) (**Supplementary Figure 1**). The upstream upregulators of ALOX5 included ERK1/2, MAPKAPK2, MAPK1, MAPK3, SP1, and CAMK2A; and upstream downregulators involved zileuton, MBD2, PRKACA, MECP2, and MBD1. Leukotriene A4 was the downstream regulator of ALOX5.

4 DISCUSSION

Herein, we first revealed two different ferroptosis clusters using 27 FRGs. The two clusters had significantly different characteristics in the ICI and FRG expression patterns. The analysis of the ICI in the

TME showed that ferroptosis cluster A had an immune-desert phenotype, while ferroptosis cluster B had a congenital immune infiltration. The analysis showed that eosinophils, MDSCs, macrophages, mast cells, and Tregs were the main infiltrating immune cells in cluster B. Previous studies have shown that eosinophils have high catalytic content of Fe(II), and increasing the concentration of Fe(II) could yield ROS through Fenton reaction and eventually induce ferroptosis (44). MDSCs have strong immunosuppressive activity, inhibiting the function of T cells and NK cells and promoting immune escape (45). Macrophages can regulate iron metabolism and iron homeostasis (46). The M1 and M2 macrophages formed by macrophage polarization showed iron isolation and iron release phenotypes, respectively (47). Macrophages and iron metabolism play a major role in tumor development. On the other hand, Tregs (Foxp3⁺ CD25⁺ CD4⁺ T cells) have been shown to be recruited by tumor cells in TME to fight antitumor immunity (48). Hong et al. established a ferroptosis-related 12-gene signature in clear cell renal cell carcinoma and demonstrated that macrophages, mast cells, and Tregs were significantly enriched in the FRG model through immunoannotation analysis (49). These results suggested that there was potential regulation between tumor immunity and ferroptosis. In addition, stromal-related signals were significantly enriched in ferroptosis cluster B, especially TGF β signaling pathway and ECM receptor activation, confirming the stromal activation in cluster B. Stromal activation can inhibit antitumor functions of immune cells. Immunosuppressive characteristics might explain the poor prognosis of ferroptosis cluster B. In this study, we obtained ferroptosis-related DEGs and crossed them with the DEGs in the LCCs and RCCs. Enrichment analyses of these overlapped DEGs revealed significant enrichment of many immune-related biological processes, robustly demonstrating that ferroptosis plays a key role in the tumor immune microenvironment (TIME).

Subsequently, we identified 3 ferroptosis-related DEG clusters, which were also significantly associated with stromal and immune activation. We once again demonstrated the importance of changes in the ferroptosis in shaping different TIME landscapes. In addition, we constructed a scoring system to quantify the ferroptosis pattern of each CCs patient, defined as FS, to guide individualized prognostic analysis and precise treatment of CC. Studies have shown that an FRG-based prognostic nomogram could improve the estimation of the survival rate of patients with clear cell renal cell carcinoma (50). Similarly, a novel ferroptosis risk signature could be useful in predicting prognosis and reflecting immune infiltration in adrenocortical carcinoma (51). These analyses also suggested that the FS might be a potential and reliable prognostic biomarker in CC.

Mutations in the DNA damage response genes are the main cause of TMB elevation, which can be used to predict the immune checkpoint inhibitor response (52). Many mutations in the somatic exon region lead to an increase in the production of neoantigens, which are recognized by T cells and thus enhance the antitumor immune response. Therefore, patients with high TMB might develop a stronger immune response and be more sensitive to the immune checkpoint inhibitors treatment. MSI status is used as a symbol of dMMR. dMMR tumors often generate more effective antitumor immune responses and have a higher likelihood of immunotherapeutic responses (53). Le et al. demonstrated that mismatch repair status played a role in predicting the clinical benefit of pembrolizumab immune checkpoint blockade (54). Our data confirmed that the FS could also be predictive indicators for immune checkpoint inhibitor response and prognosis independent of the TMB and is potentially effective in evaluating the MSI status of patients.

Nowadays, there is diversification in cancer treatment strategies. Clinical trial results showed that anti-PD-1 antibodies ultimately achieve a lasting CR in patients with CRC (55). Ferroptosis mediates the tumor-suppressive activity of IFN- γ secreted by CD8⁺ T cells against immune checkpoint blockade. The significant clinical benefits of immunotherapy such as immune checkpoint blockade might be derived, at least in part, from ferroptosis-induced tumor cells. In our analysis, gene expression at immunosuppressive checkpoints was significantly different between the HSG and LSG. Besides, FS can be used to predict the efficacy of TIs and response to immunotherapy. Currently, many clinical trials aim to investigate the use of immunotherapy in combination with a variety of other therapies in the treatment of CC (56–58). Ferroptosis regulators might enable the CC patients to achieve a better therapeutic response by leveraging the iron-philic activity of the immune system in conjunction with immunotherapy and targeted therapy (59, 60).

Given the vital roles played by ferroptosis in TIME and prognosis, we screened out key adverse prognostic regulators. Interestingly, our analysis showed that ALOX5 was a key FRG related to poor prognosis. The main mechanism of ferroptosis is metabolic necrosis caused by the peroxidation of polyunsaturated fatty acids, resulting in the accumulation of toxic products and rapture of the cell membrane (61). ALOX5 is a non-heme iron-containing dioxygenase that encodes lipoxygenase and metabolizes arachidonic acid into 5hydroperoxyeicosatetraenoic acid (62). ALOX5 was shown to regulate ferroptosis in cancer cells through lipid peroxidation (19, 63). In gastric cancer and hepatocellular carcinoma, ALOX5 expression was significantly higher than that in normal tissues in the promotion of tumor progression (64, 65). On the other hand, ALOX5 inhibition augments the efficacy of other chemotherapeutic agents in the treatment of gastric cancer. Zhou et al. demonstrated that abnormal activation of ALOX5 is associated with HER2 overexpression, mediates the growth and migration of breast cancer, and has prognostic value (66). Previous studies have demonstrated that ALOX5 is associated with macrophage infiltration. ALOX5 induces leukotriene synthesis to create a pro-inflammatory environment. Besides, increased 5-LOX metabolites from hypoxic ovarian cancer cells promote macrophage migration and invasion (67). In this study, we demonstrated the overexpression and adverse prognostic value of ALOX5 in CC. FDAapproved ALOX5 inhibitors already exist. For example, zileuton, a selective ALOX5 inhibitor, is used to prevent and treat chronic asthma (68). In addition, clinical trials have been conducted to evaluate the efficacy of zileuton monotherapy or combination therapy in lung cancer (Clinical trial numbers: NCT00056004 and NCT00070486). We constructed upstream and downstream regulatory networks of ALOX5, whose interaction network could provide the basis for follow-up studies. These results implied that ALOX5 is a potential target for CC tumor therapy and an effective prognostic biomarker.

However, several limitations remain, as follows: we need more independent immunotherapy cohorts to verify the predictive robustness and consistency of FS for prognosis and immunotherapy efficacy. For the key gene, additional experiments are required to investigate the unique role of ALOX5 in LCCs and RCCs.

In summary, this study comprehensively explored the association between ferroptosis and ICI in LCC and RCC. The identification of ferroptosis subtypes will help gain insight into the heterogeneity in LCC and RCC. By establishing a system to quantify ferroptosis patterns, the FS could serve as an effective biomarker to predict prognosis and immunotherapy response. The key gene ALOX5 identified by the FS also showed good predictive abilities. Our study provided a novel tool for the identification of ferroptosis

immunophenotypes, predicting prognosis, and provision of individualized immunotherapy in LCCs and RCCs.

DATA AVAILABILITY STATEMENT

Publicly available datasets were analyzed in this study. These datasets can be found here: TCGA database (http://cancergenome.nih.gov/), the NCBI Gene Expression Omnibus database (GSE103479) (GSE17536) (https://www.ncbi.nlm.nih.gov/), TCIA database (https://tcia.at/) (27), IMvigor210 cohort (http://research-pub.gene.com/IMvigor210CoreBiologies) (28), BMS038 cohort (https://github.com/riazn/bms038_analysis) (29), DISNOR (https:// disnor.uniroma2.it/) (43), The CPTAC database (https:// proteomics.cancer.gov/programs/cptac).

AUTHOR CONTRIBUTIONS

B-BC and Y-LL designed the study. H-CZ, S-HD, and Y-NP drafted the manuscript and collected, analyzed, and interpreted the data. J-NG, HX, and XS drew the figures. B-BC, Y-LL, B-MZ,

REFERENCES

- Ladabaum U, Dominitz JA, Kahi C, Schoen RE. Strategies for Colorectal Cancer Screening. *Gastroenterology* (2020) 158(2):418–32. doi: 10.1053/ j.gastro.2019.06.043
- Dekker E, Tanis PJ, Vleugels JLA, Kasi PM, Wallace MB. Colorectal Cancer. Lancet (London England) (2019) 394(10207):1467–80. doi: 10.1016/S0140-6736(19)32319-0
- Gervaz P, Bucher P, Morel P. Two Colons-Two Cancers: Paradigm Shift and Clinical Implications. J Surg Oncol (2004) 88(4):261–6. doi: 10.1002/jso.20156
- Bufill JA. Colorectal Cancer: Evidence for Distinct Genetic Categories Based on Proximal or Distal Tumor Location. *Ann Intern Med* (1990) 113(10):779– 88. doi: 10.7326/0003-4819-113-10-779
- Iacopetta B. Are There Two Sides to Colorectal Cancer? Int J Cancer (2002) 101(5):403–8. doi: 10.1002/ijc.10635
- Grass F, Lovely JK, Crippa J, Ansell J, Hubner M, Mathis KL, et al. Comparison of Recovery and Outcome After Left and Right Colectomy. *Colorectal Dis* (2019) 21(4):481–6. doi: 10.1111/codi.14543
- Wu C. Systemic Therapy for Colon Cancer. Surg Oncol Clin N Am (2018) 27 (2):235–42. doi: 10.1016/j.soc.2017.11.001
- Blakely AM, Lafaro KJ, Eng OS, Ituarte PHG, Fakih M, Lee B, et al. The Association of Tumor Laterality and Survival After Cytoreduction for Colorectal Carcinomatosis. J Surg Res (2020) 248:20–7. doi: 10.1016/ j.jss.2019.10.001
- Guinney J, Dienstmann R, Wang X, de Reynies A, Schlicker A, Soneson C, et al. The Consensus Molecular Subtypes of Colorectal Cancer. *Nat Med* (2015) 21(11):1350–6. doi: 10.1038/nm.3967
- Blair HA. Immunoscore((R)): A Diagnostic Assay for Clinical Management of Colon Cancer. *Mol Diagn Ther* (2020) 24(3):365–70. doi: 10.1007/s40291-020-00459-6
- Pages F, Mlecnik B, Marliot F, Bindea G, Ou FS, Bifulco C, et al. International Validation of the Consensus Immunoscore for the Classification of Colon Cancer: A Prognostic and Accuracy Study. *Lancet* (2018) 391(10135):2128– 39. doi: 10.1016/S0140-6736(18)30789-X
- Varade J, Magadan S, Gonzalez-Fernandez A. Human Immunology and Immunotherapy: Main Achievements and Challenges. *Cell Mol Immunol* (2020) 18(4):805–28. doi: 10.1038/s41423-020-00530-6
- Chen P, Li X, Zhang R, Liu S, Xiang Y, Zhang M, et al. Combinative Treatment of β-Elemene and Cetuximab is Sensitive to KRAS Mutant Colorectal Cancer Cells by Inducing Ferroptosis and Inhibiting Epithelial-Mesenchymal

and W-NX helped with the final revision of the article. All authors have read and approved the final manuscript.

FUNDING

This work was supported by the Nn10 Program of Harbin Medical University Cancer Hospital (Nn102017-02), the Postdoctoral Scientific Research Developmental Fund of Heilongjiang (LBH-Q18085), the Youth Science Foundation of Heilongjiang (JJ2018QN0724), and the Natural Science Foundation of Heilongjiang Province (QC2018111).

SUPPLEMENTARY MATERIAL

The Supplementary Material for this article can be found online at: https://www.frontiersin.org/articles/10.3389/fimmu.2022. 855849/full#supplementary-material

Supplementary Figure 1 | The causal interaction of the key gene ALOX5 in DisNor. The database consisted the direct targets and their intracellular localization of ALOX5.

Transformation. Theranostics (2020) 10(11):5107-19. doi: 10.7150/ thno.44705

- Johnson WE, Li C, Rabinovic A. Adjusting Batch Effects in Microarray Expression Data Using Empirical Bayes Methods. *Biostatistics* (2007) 8 (1):118–27. doi: 10.1093/biostatistics/kxj037
- Stockwell BR, Friedmann Angeli JP, Bayir H, Bush AI, Conrad M, Dixon SJ, et al. Ferroptosis: A Regulated Cell Death Nexus Linking Metabolism, Redox Biology, and Disease. *Cell* (2017) 171(2):273–85. doi: 10.1016/j.cell.2017.09.021
- Hassannia B, Vandenabeele P, Vanden Berghe T. Targeting Ferroptosis to Iron Out Cancer. Cancer Cell (2019) 35(6):830–49. doi: 10.1016/ j.ccell.2019.04.002
- Bersuker K, Hendricks JM, Li Z, Magtanong L, Ford B, Tang PH, et al. The CoQ Oxidoreductase FSP1 Acts Parallel to GPX4 to Inhibit Ferroptosis. *Nature* (2019) 575(7784):688–92. doi: 10.1038/s41586-019-1705-2
- Doll S, Freitas FP, Shah R, Aldrovandi M, da Silva MC, Ingold I, et al. FSP1 is a Glutathione-Independent Ferroptosis Suppressor. *Nature* (2019) 575 (7784):693–8. doi: 10.1038/s41586-019-1707-0
- Zhu L, Yang F, Wang L, Dong L, Huang Z, Wang G, et al. Identification the Ferroptosis-Related Gene Signature in Patients With Esophageal Adenocarcinoma. *Cancer Cell Int* (2021) 21(1):124. doi: 10.1186/s12935-021-01821-2
- Wilkerson MD, Hayes DN. ConsensusClusterPlus: A Class Discovery Tool With Confidence Assessments and Item Tracking. *Bioinformatics* (2010) 26 (12):1572–3. doi: 10.1093/bioinformatics/btq170
- Hanzelmann S, Castelo R, Guinney J. GSVA: Gene Set Variation Analysis for Microarray and RNA-Seq Data. BMC Bioinf (2013) 14:7. doi: 10.1186/1471-2105-14-7
- Ritchie ME, Phipson B, Wu D, Hu Y, Law CW, Shi W, et al. Limma Powers Differential Expression Analyses for RNA-Sequencing and Microarray Studies. *Nucleic Acids Res* (2015) 43(7):e47. doi: 10.1093/nar/gkv007
- Yu G, Wang LG, Han Y, He QY. Clusterprofiler: An R Package for Comparing Biological Themes Among Gene Clusters. OMICS (2012) 16(5):284–7. doi: 10.1089/omi.2011.0118
- 24. Friedman J, Hastie T, Tibshirani R. Regularization Paths for Generalized Linear Models *via* Coordinate Descent. *J Stat Softw* (2010) 33(1):1–22. doi: 10.18637/jss.v033.i01
- Laska E, Meisner M, Wanderling J. A Maximally Selected Test of Symmetry About Zero. Stat Med (2012) 31(26):3178–91. doi: 10.1002/sim.5384
- Geeleher P, Cox N, Huang RS. Prrophetic: An R Package for Prediction of Clinical Chemotherapeutic Response From Tumor Gene Expression Levels. *PloS One* (2014) 9(9):e107468. doi: 10.1371/journal.pone.0107468

- Charoentong P, Finotello F, Angelova M, Mayer C, Efremova M, Rieder D, et al. Pan-Cancer Immunogenomic Analyses Reveal Genotype-Immunophenotype Relationships and Predictors of Response to Checkpoint Blockade. *Cell Rep* (2017) 18(1):248–62. doi: 10.1016/j.celrep.2016.12.019
- Mariathasan S, Turley SJ, Nickles D, Castiglioni A, Yuen K, Wang Y, et al. TGFbeta Attenuates Tumour Response to PD-L1 Blockade by Contributing to Exclusion of T Cells. *Nature* (2018) 554(7693):544–8. doi: 10.1038/ nature25501
- Riaz N, Havel JJ, Makarov V, Desrichard A, Urba WJ, Sims JS, et al. Tumor and Microenvironment Evolution During Immunotherapy With Nivolumab. *Cell* (2017) 171(4):934–949 e916. doi: 10.1016/j.cell.2017.09.028
- Robinson MD, McCarthy DJ, Smyth GK. Edger: A Bioconductor Package for Differential Expression Analysis of Digital Gene Expression Data. *Bioinformatics* (2010) 26(1):139–40. doi: 10.1093/bioinformatics/btp616
- Mayakonda A, Lin DC, Assenov Y, Plass C, Koeffler HP. Maftools: Efficient and Comprehensive Analysis of Somatic Variants in Cancer. *Genome Res* (2018) 28(11):1747–56. doi: 10.1101/gr.239244.118
- Zhang H, Meltzer P, Davis S. RCircos: An R Package for Circos 2D Track Plots. BMC Bioinf (2013) 14:244. doi: 10.1186/1471-2105-14-244
- Chen X, Kang R, Kroemer G, Tang D. Broadening Horizons: The Role of Ferroptosis in Cancer. Nat Rev Clin Oncol (2021) 18(5):280–96. doi: 10.1038/ s41571-020-00462-0
- Wang W, Green M, Choi JE, Gijon M, Kennedy PD, Johnson JK, et al. CD8(+) T Cells Regulate Tumour Ferroptosis During Cancer Immunotherapy. *Nature* (2019) 569(7755):270–4. doi: 10.1038/s41586-019-1170-y
- Wen Q, Liu J, Kang R, Zhou B, Tang D. The Release and Activity of HMGB1 in Ferroptosis. *Biochem Biophys Res Commun* (2019) 510(2):278–83. doi: 10.1016/j.bbrc.2019.01.090
- 36. Dai E, Han L, Liu J, Xie Y, Kroemer G, Klionsky DJ, et al. Autophagy-Dependent Ferroptosis Drives Tumor-Associated Macrophage Polarization via Release and Uptake of Oncogenic KRAS Protein. Autophagy (2020) 16 (11):2069–83. doi: 10.1080/15548627.2020.1714209
- Spicer JD, McDonald B, Cools-Lartigue JJ, Chow SC, Giannias B, Kubes P, et al. Neutrophils Promote Liver Metastasis via Mac-1-Mediated Interactions With Circulating Tumor Cells. Cancer Res (2012) 72(16):3919–27. doi: 10.1158/0008-5472.CAN-11-2393
- Somasundaram R, Connelly T, Choi R, Choi H, Samarkina A, Li L, et al. Tumor-Infiltrating Mast Cells are Associated With Resistance to Anti-PD-1 Therapy. *Nat Commun* (2021) 12(1):346. doi: 10.1038/s41467-020-20600-7
- Fakih M, Ouyang C, Wang C, Tu TY, Gozo MC, Cho M, et al. Immune Overdrive Signature in Colorectal Tumor Subset Predicts Poor Clinical Outcome. J Clin Invest (2019) 129(10):4464–76. doi: 10.1172/JCI127046
- Jiang L, Kon N, Li T, Wang SJ, Su T, Hibshoosh H, et al. Ferroptosis as a P53-Mediated Activity During Tumour Suppression. *Nature* (2015) 520(7545):57– 62. doi: 10.1038/nature14344
- Ou Y, Wang SJ, Li D, Chu B, Gu W. Activation of SAT1 Engages Polyamine Metabolism With P53-Mediated Ferroptotic Responses. *Proc Natl Acad Sci* USA (2016) 113(44):E6806–12. doi: 10.1073/pnas.1607152113
- Zhang Y, Qian Y, Zhang J, Yan W, Jung YS, Chen M, et al. Ferredoxin Reductase Is Critical for P53-Dependent Tumor Suppression *via* Iron Regulatory Protein 2. *Genes Dev* (2017) 31(12):1243–56. doi: 10.1101/gad.299388.117
- Lo Surdo P, Calderone A, Iannuccelli M, Licata L, Peluso D, Castagnoli L, et al. DISNOR: A Disease Network Open Resource. *Nucleic Acids Res* (2018) 46 (D1):D527–34. doi: 10.1093/nar/gkx876
- 44. He YJ, Liu XY, Xing L, Wan X, Chang X, Jiang HL. Fenton Reaction-Independent Ferroptosis Therapy via Glutathione and Iron Redox Couple Sequentially Triggered Lipid Peroxide Generator. Biomaterials (2020) 241:119911. doi: 10.1016/j.biomaterials.2020.119911
- Bunt SK, Sinha P, Clements VK, Leips J, Ostrand-Rosenberg S. Inflammation Induces Myeloid-Derived Suppressor Cells That Facilitate Tumor Progression. *J Immunol* (2006) 176(1):284–90. doi: 10.4049/jimmunol.176.1.284
- Recalcati S, Locati M, Marini A, Santambrogio P, Zaninotto F, De Pizzol M, et al. Differential Regulation of Iron Homeostasis During Human Macrophage Polarized Activation. *Eur J Immunol* (2010) 40(3):824–35. doi: 10.1002/ eji.200939889
- Cairo G, Recalcati S, Mantovani A, Locati M. Iron Trafficking and Metabolism in Macrophages: Contribution to the Polarized Phenotype. *Trends Immunol* (2011) 32(6):241–7. doi: 10.1016/j.it.2011.03.007

- 48. Shang B, Liu Y, Jiang SJ, Liu Y. Prognostic Value of Tumor-Infiltrating FoxP3 + Regulatory T Cells in Cancers: A Systematic Review and Meta-Analysis. *Sci Rep* (2015) 5:15179. doi: 10.1038/srep15179
- Hong Y, Lin M, Ou D, Huang Z, Shen P. A Novel Ferroptosis-Related 12-Gene Signature Predicts Clinical Prognosis and Reveals Immune Relevancy in Clear Cell Renal Cell Carcinoma. *BMC Cancer* (2021) 21(1):831. doi: 10.1186/ s12885-021-08559-0
- Zhao GJ, Wu Z, Ge L, Yang F, Hong K, Zhang S, et al. Ferroptosis-Related Gene-Based Prognostic Model and Immune Infiltration in Clear Cell Renal Cell Carcinoma. *Front Genet* (2021) 12:650416. doi: 10.3389/fgene. 2021.650416
- 51. Chen X, Yan L, Jiang F, Lu Y, Zeng N, Yang S, et al. Identification of a Ferroptosis-Related Signature Associated With Prognosis and Immune Infiltration in Adrenocortical Carcinoma. *Int J Endocrinol* (2021) 2021:4654302. doi: 10.1155/2021/4654302
- 52. Klempner SJ, Fabrizio D, Bane S, Reinhart M, Peoples T, Ali SM, et al. Tumor Mutational Burden as a Predictive Biomarker for Response to Immune Checkpoint Inhibitors: A Review of Current Evidence. *Oncologist* (2020) 25 (1):e147–59. doi: 10.1634/theoncologist.2019-0244
- Dudley JC, Lin MT, Le DT, Eshleman JR. Microsatellite Instability as a Biomarker for PD-1 Blockade. *Clin Cancer Res* (2016) 22(4):813–20. doi: 10.1158/1078-0432.Ccr-15-1678
- Le DT, Uram JN, Wang H, Bartlett BR, Kemberling H, Eyring AD, et al. PD-1 Blockade in Tumors With Mismatch-Repair Deficiency. N Engl J Med (2015) 372(26):2509–20. doi: 10.1056/NEJMoa1500596
- Brahmer JR, Drake CG, Wollner I, Powderly JD, Picus J, Sharfman WH, et al. Phase I Study of Single-Agent Anti-Programmed Death-1 (MDX-1106) in Refractory Solid Tumors: Safety, Clinical Activity, Pharmacodynamics, and Immunologic Correlates. J Clin Oncol (2010) 28(19):3167–75. doi: 10.1200/ jco.2009.26.7609
- Chen EX, Jonker DJ, Loree JM, Kennecke HF, Berry SR, Couture F, et al. Effect of Combined Immune Checkpoint Inhibition vs Best Supportive Care Alone in Patients With Advanced Colorectal Cancer: The Canadian Cancer Trials Group CO.26 Study. JAMA Oncol (2020) 6(6):831–8. doi: 10.1001/ jamaoncol.2020.0910
- 57. Kim DW, Tan E, Zhou JM, Schell MJ, Martinez M, Yu J, et al. A Phase 1/2 Trial of Ibrutinib in Combination With Pembrolizumab in Patients With Mismatch Repair Proficient Metastatic Colorectal Cancer. *Br J Cancer* (2021) 124(11):1803–8. doi: 10.1038/s41416-021-01368-z
- Yarchoan M, Huang CY, Zhu Q, Ferguson AK, Durham JN, Anders RA, et al. A Phase 2 Study of GVAX Colon Vaccine With Cyclophosphamide and Pembrolizumab in Patients With Mismatch Repair Proficient Advanced Colorectal Cancer. *Cancer Med* (2020) 9(4):1485–94. doi: 10.1002/cam4.2763
- Xia Y, Liu S, Li C, Ai Z, Shen W, Ren W, et al. Discovery of a Novel Ferroptosis Inducer-Talaroconvolutin A-Killing Colorectal Cancer Cells *In Vitro* and *In Vivo*. *Cell Death Dis* (2020) 11(11):988. doi: 10.1038/s41419-020-03194-2
- 60. Chen P, Li X, Zhang R, Liu S, Xiang Y, Zhang M, et al. Combinative Treatment of Beta-Elemene and Cetuximab Is Sensitive to KRAS Mutant Colorectal Cancer Cells by Inducing Ferroptosis and Inhibiting Epithelial-Mesenchymal Transformation. *Theranostics* (2020) 10(11):5107–19. doi: 10.7150/thno.44705
- Dixon SJ, Lemberg KM, Lamprecht MR, Skouta R, Zaitsev EM, Gleason CE, et al. Ferroptosis: An Iron-Dependent Form of Nonapoptotic Cell Death. *Cell* (2012) 149(5):1060–72. doi: 10.1016/j.cell.2012.03.042
- 62. Li QQ, Li Q, Jia JN, Liu ZQ, Zhou HH, Mao XY. 12/15 Lipoxygenase: A Crucial Enzyme in Diverse Types of Cell Death. *Neurochem Int* (2018) 118:34–41. doi: 10.1016/j.neuint.2018.04.002
- Li C, Zhang Y, Liu J, Kang R, Klionsky DJ, Tang D. Mitochondrial DNA Stress Triggers Autophagy-Dependent Ferroptotic Death. *Autophagy* (2021) 17 (4):948–60. doi: 10.1080/15548627.2020.1739447
- Tang J, Zhang C, Lin J, Duan P, Long J, Zhu H. ALOX5-5-HETE Promotes Gastric Cancer Growth and Alleviates Chemotherapy Toxicity via MEK/ERK Activation. Cancer Med (2021) 10(15):5246–55. doi: 10.1002/cam4.4066
- Liu Y, Zhang X, Zhang J, Tan J, Li J, Song Z. Development and Validation of a Combined Ferroptosis and Immune Prognostic Classifier for Hepatocellular Carcinoma. Front Cell Dev Biol (2020) 8:596679. doi: 10.3389/ fcell.2020.596679
- 66. Zhou X, Jiang Y, Li Q, Huang Z, Yang H, Wei C. Aberrant ALOX5 Activation Correlates With HER2 Status and Mediates Breast Cancer Biological Activities

Through Multiple Mechanisms. *BioMed Res Int* (2020) 2020:1703531. doi: 10.1155/2020/1703531

- Wen Z, Liu H, Li M, Li B, Gao W, Shao Q, et al. Increased Metabolites of 5-Lipoxygenase From Hypoxic Ovarian Cancer Cells Promote Tumor-Associated Macrophage Infiltration. *Oncogene* (2015) 34(10):1241–52. doi: 10.1038/onc.2014.85
- Morina N, Boçari G, Iljazi A, Hyseini K, Halac G. Maximum Time of the Effect of Antileukotriene - Zileuton in Treatment of Patients With Bronchial Asthma. Acta Inform Med (2016) 24(1):16–9. doi: 10.5455/aim.2016.24.16-19

Conflict of Interest: The authors declare that the research was conducted in the absence of any commercial or financial relationships that could be construed as a potential conflict of interest.

Publisher's Note: All claims expressed in this article are solely those of the authors and do not necessarily represent those of their affiliated organizations, or those of the publisher, the editors and the reviewers. Any product that may be evaluated in this article, or claim that may be made by its manufacturer, is not guaranteed or endorsed by the publisher.

Copyright © 2022 Zhang, Deng, Pi, Guo, Xi, Shi, Yang, Zhang, Xue, Cui and Liu. This is an open-access article distributed under the terms of the Creative Commons Attribution License (CC BY). The use, distribution or reproduction in other forums is permitted, provided the original author(s) and the copyright owner(s) are credited and that the original publication in this journal is cited, in accordance with accepted academic practice. No use, distribution or reproduction is permitted which does not comply with these terms.



Case Report: Immune Checkpoint Inhibitors as a Single Agent in the Treatment of Metastatic Cervical Cancer

Manasa Anipindi^{1*}, Ryan J. Smith² and Madiha Gilani³

¹ Internal Medicine residency, Einstein Medical Center Montgomery, East Norriton, PA, United States, ² Department of Radiology, Einstein Medical Center Montgomery, East Norriton, PA, United States, ³ Department of Oncology, Einstein Medical Center Montgomery, East Norriton, PA, United States

OPEN ACCESS

Edited by:

Xian Zeng, Fudan University, China

Reviewed by:

Eric Leung, University of Toronto, Canada Nicholas Pavlidis, University of Ioannina, Greece

> *Correspondence: Manasa Anipindi AnipindM@einstein.edu

Specialty section:

This article was submitted to Cancer Immunity and Immunotherapy, a section of the journal Frontiers in Oncology

Received: 17 January 2022 Accepted: 07 March 2022 Published: 06 April 2022

Citation:

Anipindi M, Smith RJ and Gilani M (2022) Case Report: Immune Checkpoint Inhibitors as a Single Agent in the Treatment of Metastatic Cervical Cancer. Front. Oncol. 12:856944. doi: 10.3389/fonc.2022.856944 The incidence of cervical cancer has decreased in recent years due to widespread vaccination and routine screenings. It can be treated successfully, and the prognosis is also excellent if detected early. However, the 5-year survival rate for patients with stage IV cervical cancer is only 17% even with aggressive systemic chemotherapy. With the Food and Drug Administration (FDA)'s approval of immunotherapy, the prognosis has improved. We present a patient with stage IV cervical cancer who could not tolerate platinum-based chemotherapy and bevacizumab, so she was started on an immune checkpoint inhibitor, as her tumor was 100% programmed cell death ligand-1 (PD-L1) positive. She survived more than 2 years since the diagnosis of stage IV cervical cancer without any significant side effects. Based on our patient's response, the use of immune checkpoint inhibitors as a single agent needs further research and probably can be considered in patients with stage 4 cervical cancer who cannot tolerate standard chemotherapy.

Keywords: metastatic cervical cancer, immune checkpoint inhibitors, pembrolizumab, PD-L1, singleagent immunotherapy

INTRODUCTION

Cervical cancer remains a common cancer worldwide despite widespread preventive strategies (1). The American Cancer Society 2021 estimates there are about 14,480 new cervical cancer cases, out of which about 4,290 women will die, averaging about 11 deaths every day (2, 3). Prognosis remains poor even with the addition of bevacizumab to cytotoxic chemotherapy in patients with metastatic

Abbreviations: PD-1, programmed cell death protein-1; PD-L1, programmed cell death ligand-1; OB/GYN, obstetriciangynecologist; ASCUS, atypical cells of undetermined significance; HPV, human papillomavirus; TSH, thyroid-stimulating hormone; PET, positron emission tomography; FDG, fluorodeoxyglucose; ICIs, immune checkpoint inhibitors; CD, cluster differentiation; B cell, mature in bone marrow, so B cell; NK cell, natural killer cell; T cell, final stage of development in thymus, so T cell; IgG, immunoglobulin G; FDA, Food and Drug Administration.

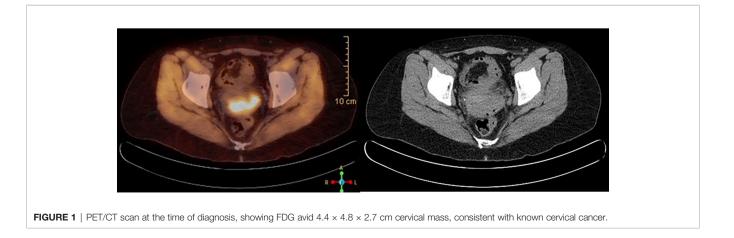
cervical cancer. Bevacizumab improves overall median survival by 3.7 months and was associated with severe side effects (4). The response to chemotherapy is usually limited, as most patients with advanced cervical cancers have a very brief response, and patients cannot receive multiple agents due to adverse side effects. Also, there is no evidence suggesting an increase in disease-free progression rate or overall survival in patients treated with second-line chemotherapy (5). The discovery of immune checkpoint inhibitors (ICIs) has changed the field of oncology over the past few years. The addition of programmed cell death protein-1 (PD-1) inhibitors to the treatment has further improved survival in metastatic cervical cancer patients (6, 7). Our patient has progressed to stage IV within a few months of her initial stage IB2 cervical cancer diagnosis. She received 6 cycles of weekly cisplatin with pelvic external beam radiation therapy and brachytherapy for her initial diagnosis of stage IB2 cervical cancer. Then she proceeded with chemotherapy for stage IV cervical cancer after lung metastasis, but she could not tolerate cisplatin-based chemotherapy or bevacizumab due to poor bone marrow reserve and renal issues. She was started on pembrolizumab, as her tumor was 100% programmed cell death ligand-1 (PD-L1) positive. She has been disease-free for more than 2 years and is continuing to maintain that response without any significant side effects.

CASE DISCUSSION

A 39-year-old female with a past medical history of anxiety, recurrent bacterial vaginosis, atypical squamous cells of undetermined significance (ASCUS) at age 28 status post loop electrosurgical excision procedure (s/p LEEP) with biopsy negative for cervical intraepithelial lesion or malignancy, and tobacco abuse went to her obstetrician–gynecologist (OB/GYN) for the complaints of vaginal odor and postcoital bleeding. She also reported unintentional weight loss of 18 pounds in the past 6 months. She had recurrent urinary tract infections and bacterial vaginosis diagnoses earlier that year that were successfully

treated each time. Since the diagnosis of ASCUS, she had one human papillomavirus (HPV)/pap co-test negative at age 34. Her physical examination at the office showed a friable cervix with bleeding and discharge. She was treated for bacterial vaginosis infection first and was reexamined a week later after the infection has cleared. Reexamination under anesthesia revealed a cervical mass, so cystoscopy and proctoscopy with cervical biopsy were done. The results demonstrated a moderate to poorly differentiated invasive squamous cell carcinoma. She was diagnosed with stage I B2 cervical cancer in late 2018 after the biopsy and was started on chemoradiation. She received cisplatin weekly for six doses with a cumulative dose of 55.8 Gray of pelvic external beam radiation therapy, and suspicious lymph nodes were boosted. This was followed by five fractions of 3.000 centigray cervix 3-D image brachytherapy. Pretreatment MRI of the pelvis with and without contrast demonstrated a $4.4 \times 4.8 \times 2.7$ cm of cervical mass with disruption of outer contour in the left aspect of the cervix. PET/CT demonstrated FDG activity in cervical $4.4 \times 4.8 \times 2.7$ cm mass (Figure 1). Repeat MRI 2 months later showed interval and decrease in the size of cervical mass with small sub-centimeter bilateral internal iliac lymph nodes. She required frequent blood transfusions for anemia in this process.

About 5 months after diagnosis of initial stage I B2 cervical cancer, she was seen in the emergency department with fevers and cough. CT chest with contrast done showed multiple pulmonary parenchymal nodules of varying sizes throughout the lungs consistent with diffuse pulmonary metastasis, and mediastinal and hilar adenopathy (Figure 2). She was started on treatment with three chemotherapy agents, i.e., cisplatin, paclitaxel, and bevacizumab, at 50% dose considering her delayed bone marrow recovery from pelvic radiation therapy. As she required frequent blood transfusions for anemia and had severe hypomagnesemia requiring frequent replacements, cisplatin was substituted for carboplatin during the 2nd cycle of chemotherapy. She could not tolerate the third cycle of chemotherapy due to severely compromised bone marrow and borderline kidney function. So systemic chemotherapy had to be discontinued considering her poor bone marrow reserve and associated nephrotoxicity. Her lung nodules biopsy came back 100% PD-L1 positive, so she was



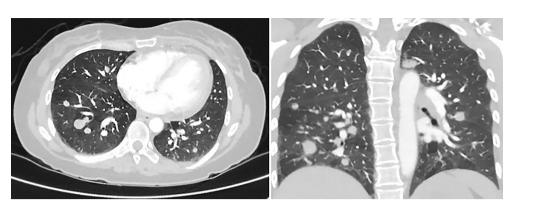
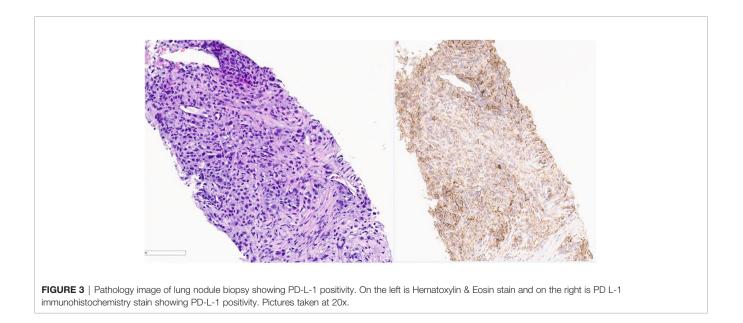


FIGURE 2 | CT chest with contrast, 5 months later, revealing multiple pulmonary parenchymal nodules of varying sizes throughout the lungs, consistent with diffuse pulmonary metastasis. It also showed mediastinal and hilar adenopathy.

started on pembrolizumab only without additional chemotherapy, and imaging done a month later showed an interval decrease in the size of lung nodules (**Figure 3**).

A total of 4 months after starting on pembrolizumab, she had complaints of severe fatigue more than usual without complaints of palpitations, heat intolerance, and sweats. Blood work showed low thyroid-stimulating hormone (TSH) at 0.02. Prior to the initiation of pembrolizumab, TSH was within normal limits. Pembrolizumab can cause thyroid dysfunction and adrenal insufficiency, so cortisol was also checked; 8 a.m. cortisol came back normal at 6.4, so hypophysitis was ruled out. She was diagnosed with pembrolizumab-induced hyperthyroidism. Endocrinology was consulted, and she was started on propylthiouracil with a very good response. Her TSH started increasing, so propylthiouracil was discontinued. A decision was made to continue with pembrolizumab, as she had a very good response to treatment. Unfortunately, about 10 days after stopping propylthiouracil even before the next blood work, the patient was admitted to the intensive care unit with altered mental status and sinus bradycardia. She was intubated due to acute respiratory failure with hypercapnia secondary to myxedema coma and required pressor support with norepinephrine. She was treated with intravenous hydrocortisone and levothyroxine. Twenty-four hours later she was extubated, and 2 days later, she was discharged home with levothyroxine 100 μ g daily. About 15 days later, there was a significant improvement in TSH to 25.74 from TSH of 200 at the time of presentation to the emergency department, so she was restarted on Keytruda. Follow-up imaging 2 months later to monitor response to Keytruda showed continued improvement in lung metastasis.

Throughout the course of treatment, CT chest/abdomen/ pelvis with contrast was repeated every 3 to 6 months, and PET skull base to mid-thigh with CT initial was repeated every 4 to 6 months to monitor the response to treatment. She showed

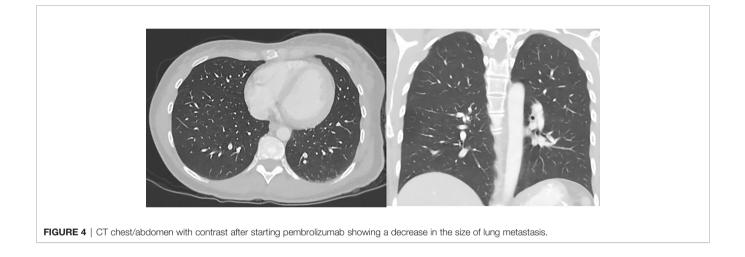


consistent improvement in lung metastases (Figure 4). Pembrolizumab was continued every 3 weeks since diagnosis with some diarrhea as a side effect was well controlled with Imodium. Hypothyroidism was also well controlled with the help of levothyroxine. As of today, she continues to receive pembrolizumab every 3 weeks for the past 18 months. She finished 44 treatments with pembrolizumab till now. The last PET/CT in late 2021 showed no metabolically active cancer (Figure 5). She is doing clinically very well and is continuing to work full-time. She is currently completely asymptomatic without any pulmonary or systemic symptoms.

DISCUSSION

Cervical cancer is still the most common cancer detected in women worldwide. About 30 to 40 years ago, it was the most

diagnosed gynecological cancer (8). The incidence has decreased in recent decades in developed countries due to screening and widespread HPV vaccinations (9, 10). However, it is still a common gynecological cancer in developing countries due to lack of resources and poor sanitation. Cervical cancer is caused by high-risk subtypes of HPVs. The common risk factors for this cancer are early sexual debut, multiple sexual partners, history of sexually transmitted infections, and tobacco abuse. It usually presents with symptoms of postcoital bleeding (11). Like every other cancer, it is divided into four stages depending on invasion to adjacent and distant organs. Treatment of cervical cancer is based on the stage at the time of diagnosis and the patient's wish to preserve fertility. The relapse rate for cervical cancer is between 11% and 22% in the International Federation of Gynecology and Obstetrics (FIGO) stages 1B-IIA and 28%-64% in FIGO stages IIB-IVA. The persistence and local recurrence of cervical cancer often exceed the distant metastasis



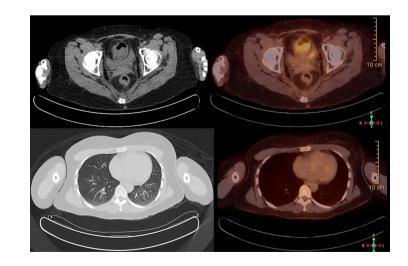


FIGURE 5 | PET/CT scan showing no abnormal FDG avidity is seen in cervix, uterus, or lungs. No pulmonary nodules or metabolically active lymph nodes are identified in the mediastinum, axilla, abdomen, and pelvis. No axillary or supraclavicular lymphadenopathy.

rate with increased pelvic tumor burden (12). Stage IV cervical cancer is a cancer that spreads to distant organs or it involves adjacent organs including the mucosa of the bladder or rectum (13). The overall survival rate of stage IV cervical cancer is only 17% compared to 85% in localized cervical cancer even with aggressive chemotherapy (14).

Treatment for metastatic cervical cancer is cisplatin-based chemotherapy, but according to research, no statistical benefit in overall survival was noted with platinum-based therapy (15). Its use is also limited due to significant toxicity and subsequent resistance to therapy (16). Bevacizumab is a monoclonal antibody with antiangiogenic properties and is also approved for metastatic cervical cancer. Adding bevacizumab to platinumbased chemotherapy in metastatic cervical cancer patients improved survival by 3.4 months, but it is associated with an increased risk for thromboembolism, fistulas, and a rare risk of bowel perforation (4). ICIs with chemotherapy or as a single agent raised a new hope in metastatic cancer treatments, as they are associated with improved overall survival rate and diseasefree progression rates. Since the approval of ICIs by the Food and Drug Administration (FDA), their use has been incorporated in the treatment of about 19 different cancer types. There has been an increase in survival rates with the addition of ICIs in the treatment plan of patients with metastatic cancers including lung, cervix, colon, breast, esophagus, malignant melanomas, classical Hodgkin's lymphoma, and other cancers (17).

PD-1, also called CD 279, was identified for the first time in 1992. CD 279 is expressed in activated cells including CD4 T, CD8 T, B cell, NK T cell, and CD4 CD8 negative T cells. It is a T-cell coinhibitory receptor, and its expression is increased in apoptotic cells, tumor cells, and virus infections (18, 19). The binding of PD-L1, the ligand for the PD-1 receptor, activates the PD-1/PD-L1 pathway leading to inhibition of T-cell activity (19, 20). The main role is to protect against excessive inflammatory responses and autoimmunity by increasing apoptosis in activated T cells (21). This mechanism also helps cancer cells escape our immune system leading to decreased antitumor response and progression of malignancies (22, 23). PD-1 and PD-L-I expression is upregulated in HPV-associated cervical tumor cells (24). Synthetic anti-PD-1 antibodies including pembrolizumab, nivolumab, and cemiplimab block this PD-1/PD-L-1 pathway leading to an improved immune response against tumor cells (25).

Pembrolizumab is a humanized IgG4 antibody against the PD-1 receptor accepted by the FDA. It was approved in 2014 for melanoma and non-small cell lung cancer by the FDA for the first time (26).

The treatment of stage IV cervical cancer is usually nonsurgical with chemoradiotherapy, as combined radical surgery with chemoradiotherapy is associated with significant adverse events. Cisplatin-based chemotherapy with angiogenesis inhibitor bevacizumab has been the treatment for stage IV cervical cancer for many years. KEYNOTE-158 trial showed impressive results with pembrolizumab in previously treated advanced PD-L1-positive cervical cancer patients (27). Based on the results of the KEYNOTE-158 trial, in the year 2018, FDA granted accelerated approval of pembrolizumab use as a single agent for patients with metastatic cervical cancer with disease progression on or after receiving chemotherapy (28). It was the first immunotherapy agent approved for advanced gynecological cancer. EMPOWER-Cervical 1 trial compared anti-PD-1 cemiplimab with investigator choice (IC) single-agent chemotherapy in patients who progressed despite first-line platinum-based treatment. This landmark trial showed promising improvement in the overall survival of patients treated with immunotherapy compared to single-agent chemotherapy in patients regardless of their PD-1 status (29).

On October 13, 2021, pembrolizumab is accepted by the FDA as a first-line agent for use in combination with chemotherapy with or without bevacizumab in PD-L1-positive metastatic tumors based on the KEYNOTE-826 trial (6). Pembrolizumab now has regular approval by the FDA as a single agent for metastatic cervical cancer PD-L1 tumor-positive patients with disease progression on or after chemotherapy based on confirmatory data from the KEYNOTE-826 trial (4, 6, 30). The dose of pembrolizumab for cervical cancer is 200 mg 30-min infusion every 3 weeks or 400 mg 30-min infusion every 6 weeks until disease progression, until unacceptable toxicity, or up to 24 months (17). PD-L1-positive cervical cancer is a tumor with PD-L1 expression more than or equal to 1% in tumor cells. It is mostly used in combination with cisplatin-based chemotherapy, but as a single agent, the response rate remains low (31). Response to ICIs is determined by PD-L1 biomarker expression levels on tumor cells using in vitro immunohistochemistry assays. The assay shows the percentage of PD-L1-positive tumor cells compared to the viable cells in the sample (32). ICIs improve progressionfree survival and overall survival in PD-L1-positive patients. Research shows that ICIs can also benefit PD-L1 negative patients with response rates between 11% and 20%. While the biomarker assay also identifies other PD-L1-positive cells including lymphocytes and macrophages, it has been shown that increased lymphocyte infiltration is associated with improved survival in many cancers. Increased CD-8+ T cells were noted in pretreatment melanoma cells in responders to pembrolizumab (33).

Cervical cancer was once the most common gynecological cancer even in developed countries. The incidence has decreased in the past few decades due to effective screening methods and HPV vaccinations. It remains an important cause of death in developing countries (34). It has a 75% to 85% overall 5-year survival rate if detected early (35). However, the overall 5-year survival rate is very low in patients with recurrent, persistent, or metastatic cancer (36). Our patient had metastatic cervical cancer to the lungs, and she could not tolerate cisplatin-based chemotherapy and bevacizumab, so she was treated with pembrolizumab as a single agent. She was 100% PD-L1positive and responded very well to the immunotherapy for more than 2 years. Her last PET scan showed no FDG activity in lung nodules and cervix. We clearly understand the limitations of this case report. We treated only one young patient, and she could tolerate the immunotherapy without any toxicity. We also know she could not tolerate the standard chemotherapy, so we tried alternate immunotherapy, as we did not have any other

option. To summarize, treating any metastatic cancer can be very challenging not only to the physicians but also to the patients. The treatment is physically and emotionally draining for the patients. Most patients are afraid not only about the side effects but also about their quality of life after starting the treatment for metastatic cancers. Immunotherapy increased expectations among oncologists about better treatment options for their patients. ICI as a monotherapy worked well in our patients, showing that it can possibly be used as a single agent in patients who cannot tolerate a combination of platinum-based chemotherapy and bevacizumab. The good outcome in our patients probably warrants further research on the use of immunotherapy as a single agent in patients with metastatic cervical cancer.

REFERENCES

- Sung H, Ferlay J, Siegel RL, Laversanne M, Soerjomataram I, Jemal A, et al. Global Cancer Statistics 2020: GLOBOCAN Estimates of Incidence and Mortality Worldwide for 36 Cancers in 185 Countries. *CA: Cancer J Clin* (2021) 71(3):209–49. doi: 10.3322/caac.21660
- 2. Key Statistics for Cervical Cancer (Date of Access- 10/10/2021). Available at: https://www.cancer.org/cancer/cervical-cancer/about/key-statistics.html.
- Siegel RL, Miller KD, Fuchs HE, Jemal A. Cancer Statistics, 2021. CA: Cancer J Clin (2021) 71(1):7–33. doi: 10.3322/caac.21654
- Tewari KS, Sill MW, Long HJIII, Penson RT, Huang H, Ramondetta LM, et al. Improved Survival With Bevacizumab in Advanced Cervical Cancer. New Engl J Med (2014) 370(8):734–43. doi: 10.1056/NEJMoa1309748
- McLachlan J, Boussios S, Okines A, Glaessgen D, Bodlar S, Kalaitzaki R, et al. The Impact of Systemic Therapy Beyond First-Line Treatment for Advanced Cervical Cancer. *Clin Oncol* (2017) 29(3):153–60. doi: 10.1016/ j.clon.2016.10.002
- Shapira-Frommer R, Alexandre J, Monk B, Fehm TN, Colombo N, Caceres MV, et al. KEYNOTE-826: A Phase 3, Randomized, Double-Blind, Placebo-Controlled Study of Pembrolizumab Plus Chemotherapy for First-Line Treatment of Persistent, Recurrent, or Metastatic Cervical Cancer. J Clin Oncol (2019) 37(15_suppl). doi: 10.1200/JCO.2019.37.15_ suppl.TPS5595
- Feng CH, Mell LK, Sharabi AB, McHale M, Mayadev JS. Immunotherapy With Radiotherapy and Chemoradiotherapy for Cervical Cancer. *InSeminars Radiat Oncol* (2020) 30 No. 4:273–80. WB Saunders. doi: 10.1016/ j.semradonc.2020.05.003
- Schiffman M, Castle PE, Jeronimo J, Rodriguez AC, Wacholder S. Human Papillomavirus and Cervical Cancer. *Lancet* (2007) 370(9590):890–907. doi: 10.1016/S0140-6736(07)61416-0
- American College of Obstetricians and Gynecologists. Practice Bulletin No. 157: Cervical Cancer Screening and Prevention. *Obstet Gynecol* (2016) 127(1): e1–20. doi: 10.1097/AOG.00000000001263
- Arbyn M, Xu L, Simoens C, Martin-Hirsch PP. Prophylactic Vaccination Against Human Papillomaviruses to Prevent Cervical Cancer and its Precursors. *Cochrane Database Systematic Rev* (2018) 5. doi: 10.1002/ 14651858.CD009069.pub3
- Tarney CM, Han J. Postcoital Bleeding: A Review on Etiology, Diagnosis, and Management. Obstetrics Gynecol Int (2014). doi: 10.1155/2014/192087
- 12. Boussios S, Seraj E, Zarkavelis G, Petrakis D, Kollas A, Kafantari A, et al. Management of Patients With Recurrent/Advanced Cervical Cancer Beyond First Line Platinum Regimens: Where do We Stand? A Literature Review. Crit Rev Oncol/Hematol (2016) 108:164–74. doi: 10.1016/j.critrevonc.2016.11.006
- Bhatla N, Berek JS, Cuello Fredes M, Denny LA, Grenman S, Karunaratne K, et al. Revised FIGO Staging for Carcinoma of the Cervix Uteri. *Int J Gynecol Obstetrics* (2019) 145(1):129–35. doi: 10.1002/ijgo.12749
- Survival Rates of Cervical Cancer (Date of Access 10/17/2021). Available at: https://www.cancer.org/cancer/cervical-cancer/detection-diagnosis-staging/ survival.html.

DATA AVAILABILITY STATEMENT

The original contributions presented in the study are included in the article/supplementary material. Further inquiries can be directed to the corresponding author.

AUTHOR CONTRIBUTIONS

MA wrote the case report under the guidance of MG. MG is the medical oncologist who is treating this patient. RS is the radiologist who added appropriate images pertinent to the text. All authors were involved in making appropriate changes as needed and approved the final case report.

- Monk BJ, Sill MW, McMeekin DS, Cohn DE, Ramondetta LM, Boardman CH, et al. Phase III Trial of Four Cisplatin-Containing Doublet Combinations in Stage IVB, Recurrent, or Persistent Cervical Carcinoma: A Gynecologic Oncology Group Study. J Clin Oncol (2009) 27(28):4649. doi: 10.1200/ JCO.2009.21.8909
- Zhu H, Luo H, Zhang W, Shen Z, Hu X, Zhu X. Molecular Mechanisms of Cisplatin Resistance in Cervical Cancer. *Drug Design Dev Ther* (2016) 10:1885. doi: 10.2147/DDDT.S106412
- 17. *Keytruda Prescribing Information (Date of Access 10/17/2021).* Available at: https://www.accessdata.fda.gov/drugsatfda_docs/label/2021/125514s121 s122lbl.pdf.
- Okazaki T, Chikuma S, Iwai Y, Fagarasan S, Honjo T. A Rheostat for Immune Responses: The Unique Properties of PD-1 and Their Advantages for Clinical Application. *Nat Immunol* (2013) 14(12):1212–8. doi: 10.1038/ ni.2762
- Jiang Y, Chen M, Nie H, Yuan Y. PD-1 and PD-L1 in Cancer Immunotherapy: Clinical Implications and Future Considerations. *Hum Vaccines Immunotherapeutics* (2019) 15(5):1111–22. doi: 10.1080/21645515.2019. 1571892
- Salmaninejad A, Valilou SF, Shabgah AG, Aslani S, Alimardani M, Pasdar A, et al. PD-1/PD-L1 Pathway: Basic Biology and Role in Cancer Immunotherapy. J Cell Physiol (2019) 234(10):16824–37. doi: 10.1002/ jcp.28358
- Francisco LM, Sage PT, Sharpe AH. The PD-1 Pathway in Tolerance and Autoimmunity. *Immunol Rev* (2010) 236(1):219–42. doi: 10.1111/j.1600-065X.2010.00923.x
- Syn NL, Teng MW, Mok TS, Soo RA. *De-Novo* and Acquired Resistance to Immune Checkpoint Targeting. *Lancet Oncol* (2017) 18(12):e731–41. doi: 10.1016/S1470-2045(17)30607-1
- Iwai Y, Ishida M, Tanaka Y, Okazaki T, Honjo T, Minato N. Involvement of PD-L1 on Tumor Cells in the Escape From Host Immune System and Tumor Immunotherapy by PD-L1 Blockade. *Proc Natl Acad Sci* (2002) 99(19):12293– 7. doi: 10.1073/pnas.192461099
- Mezache L, Paniccia B, Nyinawabera A, Nuovo GJ. Enhanced Expression of PD L1 in Cervical Intraepithelial Neoplasia and Cervical Cancers. *Modern Pathol* (2015) 28(12):1594–602. doi: 10.1038/modpathol. 2015.108
- De Sousa Linhares A, Battin C, Jutz S, Leitner J, Hafner C, Tobias J, et al. Therapeutic PD-L1 Antibodies are More Effective Than PD-1 Antibodies in Blocking PD-1/PD-L1 Signaling. *Sci Rep* (2019) 9(1):1–9. doi: 10.1038/ s41598-019-47910-1
- Twomey JD, Zhang B. Cancer Immunotherapy Update: FDA-Approved Checkpoint Inhibitors and Companion Diagnostics. AAPS J (2021) 23(2):1. doi: 10.1208/s12248-021-00574-0
- Ros W, Delord JP, Perets R, Italiano A, Shapira-Frommer R, Manzuk L, et al. Efficacy and Safety of Pembrolizumab in Previously Treated Advanced Cervical Cancer: Results From the Phase 2 KEYNOTE-158 Study. *Early Phase Clin Stud Novel Immunotherapeutics Oncol* (2019) 37:117. doi: 10.1200/JCO.18.01265

- Cohen PA, Jhingran A, Oaknin A, Denny L. Cervical Cancer. Lancet (2019) 393(10167):169–82. doi: 10.1016/S0140-6736(18)32470-X
- Tewari KS, Monk BJ, Vergote I, Miller A, deMeto AC, Kim HS, et al. VP4-2021: EMPOWER-Cervical 1/GOG-3016/ENGOT-Cx9: Interim Analysis of Phase III Trial of Cemiplimab vs. Investigator's Choice (IC) Chemotherapy (Chemo) in Recurrent/Metastatic (R/M) Cervical Carcinoma. *Ann Oncol* (2021) 32(7):940–1. doi: 10.1016/j.annonc.2021.04.009
- 30. FDA Approves Pembrolizumab Combination for First Line Treatment of Cervical Cancer. (Date of Access-10/15/2021). Available at: https://www.fda. gov/drugs/resources-information-approved-drugs/fda-approvespembrolizumab-combination-first-line-treatment-cervical-cancer.
- Borcoman E, Le Tourneau C. Keynote-158 Study, FDA Granted Accelerated Approval of Pembrolizumab for the Treatment of Patients With Advanced PD-L1-Positive Cervical Cancer. Ann Trans Med (2020) 8(23):20–2656. doi: 10.21037/atm-20-2656
- Ilie M, Khambata-Ford S, Copie-Bergman C, Huang L, Juco J, Hofman V, et al. Use of the 22C3 Anti–PD-L1 Antibody to Determine PD-L1 Expression in Multiple Automated Immunohistochemistry Platforms. *PloS One* (2017) 12 (8):e0183023. doi: 10.1371/journal.pone.0183023
- Revythis A, Shah S, Kutka M, Moschetta M, Ozturk MA, Pappas-Gogos G, et al. Unraveling the Wide Spectrum of Melanoma Biomarkers. *Diagnostics* (2021) 11(8):1341. doi: 10.3390/diagnostics11081341
- 34. Sung H, Ferlay J, Siegel RL, Laversanne M, Soerjomataram I, Jemal A, et al. Global Cancer Statistics 2020: GLOBOCAN Estimates of Incidence and Mortality Worldwide for 36 Cancers in 185 Countries. CA: Cancer J Clin (2021) 71(3):209–49. doi: 10.3322/caac.21660

- Landoni F, Maneo A, Colombo A, Placa F, Milani R, Perego P, et al. Randomised Study of Radical Surgery Versus Radiotherapy for Stage Ib-Iia Cervical Cancer. *Lancet* (1997) 350(9077):535–40. doi: 10.1016/S0140-6736 (97)02250-2
- 36. Gardner AB, Charo LM, Mann AK, Kapp DS, Eskander RN, Chan JK. Ovarian, Uterine, and Cervical Cancer Patients With Distant Metastases at Diagnosis: Most Common Locations and Outcomes. *Clin Exp Metastasis* (2020) 37(1):107–13. doi: 10.1007/s10585-019-10007-0

Conflict of Interest: The authors declare that the research was conducted in the absence of any commercial or financial relationships that could be construed as a potential conflict of interest.

Publisher's Note: All claims expressed in this article are solely those of the authors and do not necessarily represent those of their affiliated organizations, or those of the publisher, the editors and the reviewers. Any product that may be evaluated in this article, or claim that may be made by its manufacturer, is not guaranteed or endorsed by the publisher.

Copyright © 2022 Anipindi, Smith and Gilani. This is an open-access article distributed under the terms of the Creative Commons Attribution License (CC BY). The use, distribution or reproduction in other forums is permitted, provided the original author(s) and the copyright owner(s) are credited and that the original publication in this journal is cited, in accordance with accepted academic practice. No use, distribution or reproduction is permitted which does not comply with these terms.



Identification of a Tumor Immunological Phenotype-Related Gene Signature for Predicting Prognosis, Immunotherapy Efficacy, and Drug Candidates in Hepatocellular Carcinoma

OPEN ACCESS

Edited by:

Xian Zeng, Fudan University, China

Reviewed by:

Lei Yang, Harbin Medical University, China Jianzhong Su, Wenzhou Medical University, China

*Correspondence:

Yongqiang Zhang zyq1014zyq1014@163.com Dong Wang dwang@cdutcm.edu.cn

[†]These authors have contributed equally to this work

Specialty section:

This article was submitted to Cancer Immunity and Immunotherapy, a section of the journal Frontiers in Immunology

Received: 26 January 2022 Accepted: 22 March 2022 Published: 12 April 2022

Citation:

Tang Y, Guo C, Yang Z, Wang Y, Zhang Y and Wang D (2022) Identification of a Tumor Immunological Phenotype-Related Gene Signature for Predicting Prognosis, Immunotherapy Efficacy, and Drug Candidates in Hepatocellular Carcinoma. Front. Immunol. 13:862527. doi: 10.3389/fimmu.2022.862527 Yuqin Tang^{1†}, Chengbin Guo^{2†}, Zhao Yang³, Yumei Wang¹, Yongqiang Zhang^{4*} and Dong Wang^{1*}

¹ State Key Laboratory of Southwestern Chinese Medicine Resources, School of Basic Medical Sciences, Chengdu University of Traditional Chinese Medicine, Chengdu, China, ² Faculty of Medicine, Macau University of Science and Technology, Macau, China, ³ West China School of Medicine, West China Hospital, Sichuan University, Chengdu, China, ⁴ Guangzhou Women and Children's Medical Center, Guangzhou Medical University, Guangzhou, China

Hepatocellular carcinoma (HCC) is the predominant subtype of primary liver cancer and represents a highly heterogeneous disease, making it hard to predict the prognosis and therapy efficacy. Here, we established a novel tumor immunological phenotype-related gene index (TIPRGPI) consisting of 11 genes by Univariate Cox regression and the least absolute shrinkage and selection operator (LASSO) algorithm to predict HCC prognosis and immunotherapy response. TIPRGPI was validated in multiple datasets and exhibited outstanding performance in predicting the overall survival of HCC. Multivariate analysis verified it as an independent predictor and a TIPRGPI-integrated nomogram was constructed to provide a quantitative tool for clinical practice. Distinct mutation profiles, hallmark pathways, and infiltration of immune cells in tumor microenvironment were shown between the TIPRGPI high and low-risk groups. Notably, significant differences in tumor immunogenicity and tumor immune dysfunction and exclusion (TIDE) were observed between the two risk groups, suggesting a better response to immune checkpoint blockade (ICB) therapy of the low-risk group. Besides, six potential drugs binding to the core target of the TIPRGPI signature were predicted via molecular docking. Taken together, our study shows that the proposed TIPRGPI was a reliable signature to predict the risk classification, immunotherapy response, and drugs candidate with potential application in the clinical decision and treatment of HCC. The novel "TIP genes"-guided strategy for predicting the survival and immunotherapy efficacy, we reported here, might be also applied to more cancers other than HCC.

Keywords: hepatocellular carcinoma, tumor immunological phenotype, immunotherapy efficacy, immune infiltration, prognosis, molecular docking

INTRODUCTION

Liver cancer is one of the deadliest malignancies in the world and hepatocellular carcinoma (HCC) is the dominant type, accounting for ~75% of all cases (1). In the past decade, despite the great progress of surveillance, diagnosis and management in HCC, the mortality rate of HCC remains unacceptably high (2, 3). Due to the poor prognosis, the incidence and mortality rates of HCC are roughly equivalent (4). In 2018, the incidence rate per 100,000 in Eastern Asia was 17.7, whereas the corresponding mortality rate was 16.0 (5). The high prevalence and poor survival of HCC largely result from the heterogeneity of pathogenic factors, treatment responses, and molecular profiles. For instance, multiple factors, including chronic infections of Hepatitis B virus (HBV) or Hepatitis C virus (HCV), alcohol consumption, metabolic syndrome are strong causes for the incidence of HCC (2, 6, 7). While the HBV vaccine has been introduced by a number of countries to eliminate HBV-related HCC, there is still no vaccine available for HCV-related HCC and nonviral HCC (4). The presently used clinical characteristics including the tumor-node-metastasis (TNM) staging system, vascular invasion, and tumor burden status are limited in predicting the prognosis and treatment sensitivities for HCC (8, 9). Thus, novel prognostic classifiers or therapeutic biomarkers are urgently needed to improve the clinical benefits of HCC patients.

Tumor immune microenvironment (TIME) is proven to play a vital role in tumorigenesis and development (10). Immunotherapy with immune checkpoint inhibitors (ICIs), reversing the inactivation of immune cells to eliminate tumor cells, has emerged as a promising therapy for a variety of cancers in recent years (11). Multiple ICIs were approved for cancer therapy such as nivolumab, pembrolizumab, and cemiplimab targeting programmed death-1 (PD-1) and ipilimumab targeting cytotoxic T-lymphocyte-associated protein 4 (CTLA-4) (12). More agents targeting novel immune checkpoints such as T cell immunoglobulin and mucin-domain containing-3 (TIM-3), lymphocyte activation gene-3 (LAG-3), and T cell immunoglobulin and ITIM domain (TIGIT) are under investigation to expand the scope of immunotherapy (13-15). Adequate evidences suggested that chronic inflammation was a major risk factor for the development of HCC and immunotherapy might be the ideal approach to improve the prognosis of HCC (16, 17). The composition of tumor microenvironment (TME) of HCC is complex, in which a number of immune and stromal cells interact to form an immunosuppressive microenvironment and eventually lead to a worse prognosis of HCC (11). Hopefully, checkpoint-based therapy was effective and beneficial against advanced HCC clinically (18, 19). However, owing to the low sensitivity and unexpected resistance to ICIs, more useful and reliable biomarkers should be identified to improve the accuracy of predicting the prognosis and immunotherapy efficiency in HCC (20). How to choose available and suitable targets for personalized therapy is still a tricky question to be answered for HCC patients.

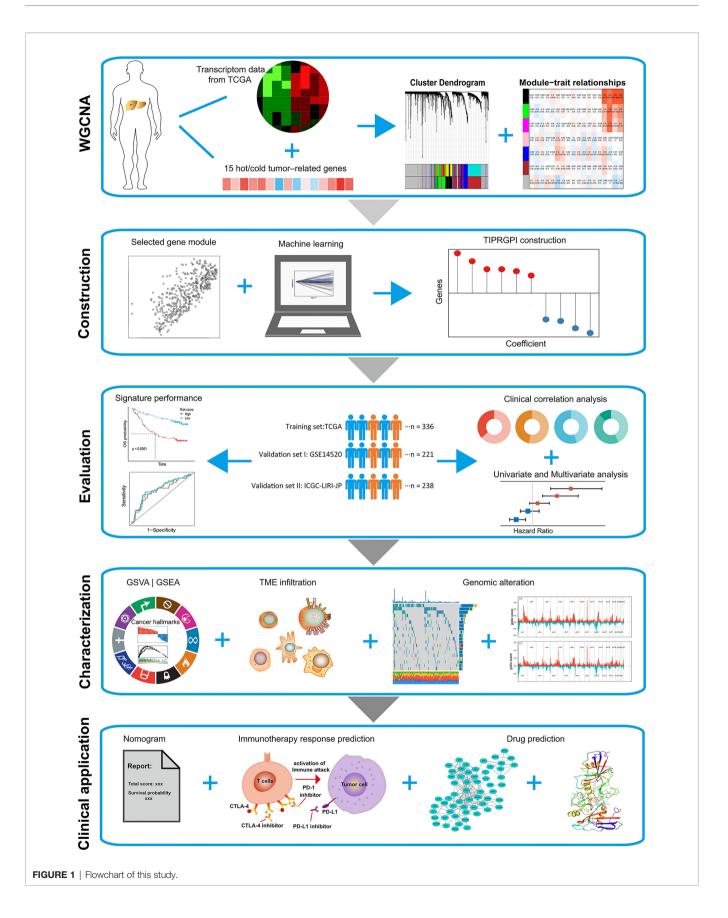
TME is a highly heterogeneous ecosystem involving different types of stromal cells, vascular cells, and immune cells perturbed by therapy, which are recognized as the potential determinants of treatment response in cancer (21, 22). Tumor immunological phenotype (TIP) is an emerging concept to evaluate the immunological heterogeneity depending on the relative infiltration of immune cells (23), and tumors are generally classified into two TIPs: "hot" (inflamed) and "cold" (noninflamed) (23). Particular genes and pathways genetically regulate the immunological phenotypes have been identified to aid immunotherapy (24-27). Wang et al. recently reported 12 hot tumor-related genes and three cold tumor-related genes to constitute the TIP gene signature using a text-mining approach (26), which is significantly associated with the survival outcomes of cancer patients and shows superior performance in predicting immunotherapeutic responses than widely used immune signatures such as tumor mutation burden (TMB), and tumor immune dysfunction and exclusion (TIDE). Thus, these "TIP genes" hold great promise in clinical application especially for postoperative risk stratification and the discovery of immuno therapeutic predictors.

Accumulating immune-based signatures have been established to predict HCC patients' outcomes. However, the predictive accuracies of most signatures are still insufficient for clinical practice and a more reliable and accurate signature predicting the survival as well as the immunotherapy response of HCC patients is urgently needed (28, 29). In this study, a "TIP genes"-guided strategy was employed with several statistical algorithms to construct TIP-related gene prognostic index (TIPRGPI), a novel HCC signature, followed by comprehensive validation to predict the prognosis and immunotherapy efficiency for HCC patients. Besides, it is estimated that the low-risk group might respond better to immunotherapies than those in the highrisk group. Furthermore, we identified six potential drugs binding well to the core target of TIPRGPI with molecular docking. The workflow for this study is shown in **Figure 1**.

MATERIALS AND METHODS

Data Source

We carefully reviewed the mRNA expression datasets deposited in the Cancer Genome Atlas (TCGA), International Cancer Genome Consortium (ICGC), and Gene Expression Omnibus (GEO), database and enrolled the patients with complete annotation of overall survival (OS).Those patients with an overall survival time of <30 days were excluded due to other possible causes of mortality (29). Subsequently, the RNA-seq gene expression data of 336 HCC patients was derived from the TCGA database (https://portal.gdc.cancer.gov/) (TCGA-LIHC). The corresponding clinical information and survival outcomes including overall survival, progression-free survival (PFS), disease-specific survival (DSS) and disease-free survival (DFS) were also collected. Another RNA-seq expression profiling dataset (ICGC-LIRI-JP) containing 238 patients with survival information was obtained from the ICGC database



(https://dcc.icgc.org). In addition, we acquired a transcriptomic microarray dataset (GSE14520) including a total of 221 HCC patients (30, 31) from the GEO database (https://www.ncbi.nlm. nih.gov/geo/). The summary of the demographic information was listed in **Supplementary Table 1**. For the TCGA-LIHC dataset, the Fragments per Kilobase Million (FPKM) value was used to generate the Transcripts per Kilobase Million (TPM) and further subjected to log2 transformation for normalization. For the ICGC-LIRI-JP and GSE14520 datasets, data were preprocessed as previously reported (32, 33). The ESTIMATE algorithm was utilized to calculate the immune score, stromal score, estimate score, and tumor purity for all the patients in the TCGA-LIHC dataset (34, 35).

Somatic mutation information of TCGA-LIHC was gathered from the TCGA data portal (http://tcga-data.nci.nih.gov/tcga/) as the mutation annotation format (MAF) format by the R package "maftools" (36). The CNV profile contained in the "Masked Copy Number Segment" data type was downloaded from TCGA.

Correlations of TIP Score With Prognosis and TME of HCC

TIP score was calculated as previously reported (26) with some modifications. Briefly, the gene expression matrix of three predefined cold tumor-related genes (CXCL1, CXCL2, and CCL20) and 12 predefined hot tumor-related genes (CXCR3, CXCR4, CXCL9, CXCL10, CXCL11, CCL5, CD3, CD4, CD8a, CD8b, CD274, and PDCD1) was extracted, followed by the generation of expression z scores. TIP score was computed by a summary score of RNA-seq z scores for the tumor immunological phenotype genes. To evaluate the prognostic value of the TIP score, all patients with available survival information for OS, DFS, PFS, and DSS were divided into the high- and low-score group by the optimal cutoff of TIP scores, respectively (34), followed by the Kaplan-Meier analysis with a log-rank test. To examine the relationship between TIP score and TME, we carried out the Spearman correlation analysis between TIP score and the ESTIMATE derived scores including immune score, stromal score, estimate score, and tumor purity. And we also checked the correlations of the TIP score and the fractions of the activated CD4 and the activated CD8, as well as two immune checkpoint molecules (PD1 and CTLA-4).

Weighted Gene Co-Expression Network Analysis (WGCNA) and TIPRGPI Establishment

WGCNA was performed on the expression data of TCGA-LIHC using the "WGCNA" R package (37). Generally, all genes were sorted by the median absolute deviation (MAD), and the top 5,000 genes were used for sample clustering, followed by the removal of outlier samples. Then, the optimal soft threshold power was specified to generate a scale-free network. Next, the topological overlap matrix (TOM)-based dissimilarity (dissTOM) was computed and further used to perform the gene dendrogram and module recognition with the minClusterSize of 30. Similar dynamic modules were merged by the cutline of 0.2. Pearson correlation coefficients (PCC) and

corresponding P values between module eigengenes and clinicopathological parameters were subsequently calculated and visualized by a heatmap. The most significant module that correlated with the TIP score was identified and used for further analysis.

Gene Ontology (GO) enrichment and Kyoto Encyclopedia of Genes and Genomes (KEGG) pathway analysis were completed for the most significant module by the "clusterProfiler" R package (38) with the cutoff of p.adjust <0.05.

To establish a scoring system regarding TIP score, we first adopted the Univariate Cox (UniCox) hazard regression to screen the candidate genes from the most significant module. Next, the popular least absolute shrinkage and selection operator (LASSO) algorithm was applied for the best subset of prognostic genes using the "glmnet" R package (39). For the purpose of minimization of the overfitting risk, we conducted LASSO 200 times and chose the robust genes that appeared in the model more than 160 times. A linear equation called "TIPRGPI" was then established to predict the overall survival of HCC patients: Risk score = Σ (coef (β)*EXP_{β}), where β represents each selected gene.

Survival Analysis

The TIPRGPI score was calculated for each patient of the TCGA-LIHC training set, the ICGC-LIRI-JP validation set, and the GSE14520 validation set. For each dataset, patients were separated into the high- and low-risk groups by the median value of the training set, which is crucial for clinical practice. Kaplan-Meier survival curves were depicted to compare the difference of distinct risk groups with a log-rank test, and time-dependent receiver operating characteristic (tROC) curves were drawn to assess the predictive power. Moreover, stratified analysis was performed to further validate the additional prognostic value of the TIPRGPI model, and univariate and multivariate analyses were used to determine the independent prognostic indicators for HCC. Additionally, we also compared the 3- and 5-year ROC values of the TIPRGPI and popular biomarkers for immunotherapy and other published gene signatures of HCC, including a TP53related transcriptomic signature by Long et al. ("Long signature") (40), a metabolic gene signature by Huo et al. ("Huo signature") (27), a ferroptosis-related gene signature ("Liang signature") (41), an immune-related prognostic signature ("Wang signature") (42), and a hypoxia-related risk signature by Zeng et al. ("Zeng signature") (43).

Construction of a Predictive Nomogram

A TIPRGPI-integrated nomogram was constructed to quantitatively evaluate the prognostic risk based on the result of univariate analysis. Calibration curves for the 3- and 5-year were drawn to examine the predictive capability of the nomogram. The 1-, 3-, and 5-year DCA plots were utilized to measure the net benefits of the nomogram and TNM stage, as well as tumor burden. Moreover, Kaplan-Meier analysis was further used for OS, DFS, PFS, and DSS on the TCGA-LIHC set to validate the prognostic value of the nomogram.

Genomic Variation Analysis

To explore the somatic mutations regarding TIPRGPI, the "maftools" R package was used to depict the waterfall plots manifesting the mutation landscape for the high- and low-risk groups of HCC patients. TMB values reflecting total mutation numbers for each HCC patient were calculated with non-synonymous mutations using 38MB as the estimate of the exome size (44, 45). Somatic copy number alterations between the two different risk groups were investigated *via* the GISTIC2.0 algorithm. The correlations of expression values and CNV types for two oncogenic hub genes (NDC80 and RFC4) (32, 33) in HCC were accomplished by the Kruskal-Wallis test.

Gene Set Variation Analysis (GSVA) and Gene Set Enrichment Analysis (GSEA)

To determine the underlying hallmark pathways related to TIPRGPI, the R package "GSVA" was utilized to obtain the GSVA enrichment scores (46) of the 50 hallmark pathways (h.all.v7.1.symbols) deposited in the molecular signature database (47, 48) for each patient in the high- and low-risk groups of the TCGA-LIHC dataset, followed by the contrast of GSVA scores using a linear model as previously reported (49). Significant gene sets were defined by an adj.*P*.Val of < 0.01. GSEA for the same 50 hallmark gene sets was operated in the two risk groups with the recommended criteria of FDR<0.25 and NES>1. Venn diagram analysis was performed to identify the overlapping hallmark pathways by GSVA and GSEA, and Kaplan-Meier analysis was further used to verify the prognostic value of oncogenic hallmark pathways.

Exploration of Immune Infiltration

To investigate the relative infiltration of TME cells in the highand low-risk groups of HCC, the ssGSEA algorithm was utilized for immune deconvolution analyses with the gene sets of 28 reported immune cell types (50) and two stromal components (fibroblasts and endothelial cells) (51) of TME. Differential infiltration analysis was conducted and visualized by a violin plot and the relationship of the TIPRGPI score and each type of the 30 TME cells was determined by the Spearman correlation analysis. Kaplan-Meier survival analysis was also performed to assess the prognostic values of these TME cells.

Estimation of Immunotherapeutic Response Prediction

According to previous publications, the correlations between TIPRGPI and potential immunotherapeutic markers including 50 ICB-related genes (52–54), IFN-gamma pathway markers (55), and m6A regulators (56, 57) were explored by Wilcoxon test. The Tumor Immune Dysfunction and Exclusion (TIDE) algorithm (58) (http://tide.dfci.harvard.edu/), was utilized to infer the clinical response to immunotherapy with the gene expression profile of TCGA-LIHC. Additionally, Immunophenoscore (IPS), which was designed to determine immunogenicity using the machine learning approach, was further obtained from The Cancer Immunome Atlas (TCIA) (https://tcia.at/home) (50). Higher IPS indicates a better response to immunotherapy.

Identification of the Core Target of TIPRGPI

To identify the core target of the TIPRGPI signature, all genes were uploaded to the online database of the Search Tool for the Retrieval of Interacting Genes (STRING) (version 11.0; http:// string-db.org/) for the construction of the protein-protein interaction (PPI) network with default settings (Interaction score \geq 0.4). Cytoscape (version 3.2.1; http://www.cytoscape. org) was used for visualization. Next, we calculated the topological parameters with the Network Analyzer plugin and obtained the degrees of all nodes in the network. The core target was recognized as the node with the highest degree.

Molecular Docking

For the screening of the putative small molecules stably binding to the core target, molecular docking was performed with Glide of Schrodinger. Firstly, we collected the 3D protein structures of totally 9800 small molecules as well as the core target from zinc15 database and PDB database (www.rcsb.org), respectively. Next, the protein preparation wizard tool was utilized to process the crystal structure. Subsequently, the ligand-binding pocket was predicted with the deepsite module (59) of Play Molecule (www.playmolecule.org), which was a knowledge-based approach using convolutional neural networks. Finally, the binding mode and interaction force of the core target and small molecules were evaluated to identify potential compounds.

Statistical Analysis

The correlations of TIP score and immune signatures were conducted using Spearman correlation by the "ggplot2" package. Kaplan-Meier analysis was performed using the "survival" package with a log-rank test. The correlations of the TIPRGPI group and other clinicopathological features were determined by the Pearson Chi-square test. Univariate and multivariate analyses were applied by the "survival" package to identify independent prognostic indicators. The optimal cutoff for survival analysis was generated by the R package "survminer". All statistical analyses were completed by the R software (version 3.6.1). Unless specified otherwise, P < 0.05 was considered statistically significant.

RESULTS

TIP Score Was Associated With the Prognosis and the Immune State of HCC

To determine whether TIP score was effective in HCC, we carried out a series of survival analyses, applying Kaplan-Meier (K-M) survival curves and log-rank tests to investigate the discrepancy between low- and high- TIP score groups. As expected, patients with HCC in the high TIP score group had a better prognosis (**Figure 2A**). Next, we confirmed the correlations between TIP score and the immune score, stromal score, estimate score, and tumor purity respectively. As shown in **Figure 2B**, TIP score was positively associated with immune score, stromal score, and estimate score, but negatively associated with tumor purity. Moreover, given that effective T cells such as activated CD4 and CD8 T cells play a pivotal role in the tumor microenvironment (60), we also calculated their correlations with TIP score, and we found they were both correlated with TIP score positively (**Figure 2C**). Besides, considering that PD-1 or CTLA-4 is the key immune checkpoint, we also verified they were positively correlated with TIP score (**Figure 2C**).

Construction of TIPRGPI

In order to identify the gene module associated with TIP score, WGCNA was applied to the TCGA-LIHC RNA-seq dataset. The MAD top 5000 genes were extracted to construct a co-expression network. Four outlier samples were removed prior to network construction (**Supplementary Figure 1A**). The optimal soft-thresholding power of 10 (scale-free $R^2 = 0.86$) was picked to ensure the scale-free topology (**Supplementary Figure 1B**). The

established co-expression network showed that these 5000 genes were clustered into seven modules (Figure 3A) and the network heatmap plot of the clustering dendrogram among modules was shown (Supplementary Figure 1C). Then, we calculated the correlations of module eigengenes (ME) with multiple indicated variables by computing the Pearson correlation coefficient (PCC), and among which, we focused on the black module showing highly positive correlation with TIP score (PCC = 0.78, P = 3E-70) (Figure 3B). Also, we plotted a scatterplot of gene significance vs. module membership of the black module containing 432 genes (Figure 3C). GO enrichment analysis revealed that the most significant terms enriched by the black module were the biological process (BP) of T cell activation, cellular component (CC) of side of membrane, and molecular function (MF) of peptide antigen binding (Figure 3D). KEGG analysis suggested that they mostly participated in the pathway

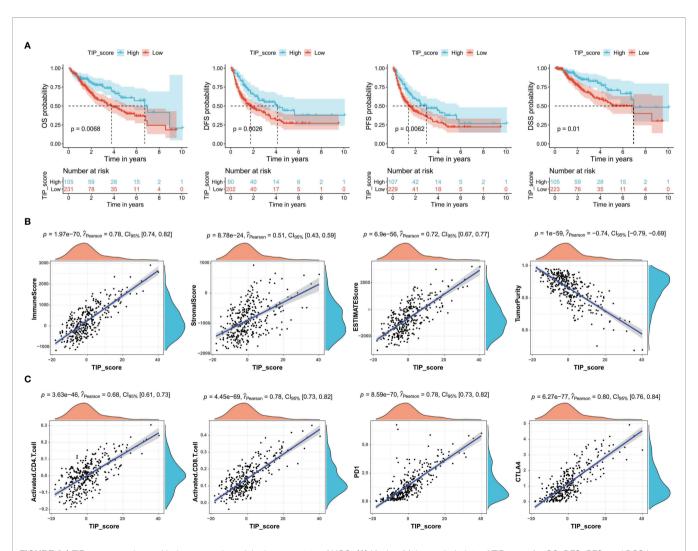


FIGURE 2 | TIP score correlates with the prognosis and the immune state of HCC. (A) Kaplan–Meier survival plots of TIP score for OS, DFS, PFS, and DSS in TCGA-HCC cohort. (B) Correlations between TIP score and immune score, stromal score, estimate score, and tumor purity in HCC. (C) Correlations between TIP score and biomarkers of cancer immunotherapy including activated CD4/CD8 and PD-1/CTLA-4. TIP, tumor immunological phenotype. OS, overall survival; DFS, disease-free survival; PFS, progression-free survival; DSS, disease-specific survival.

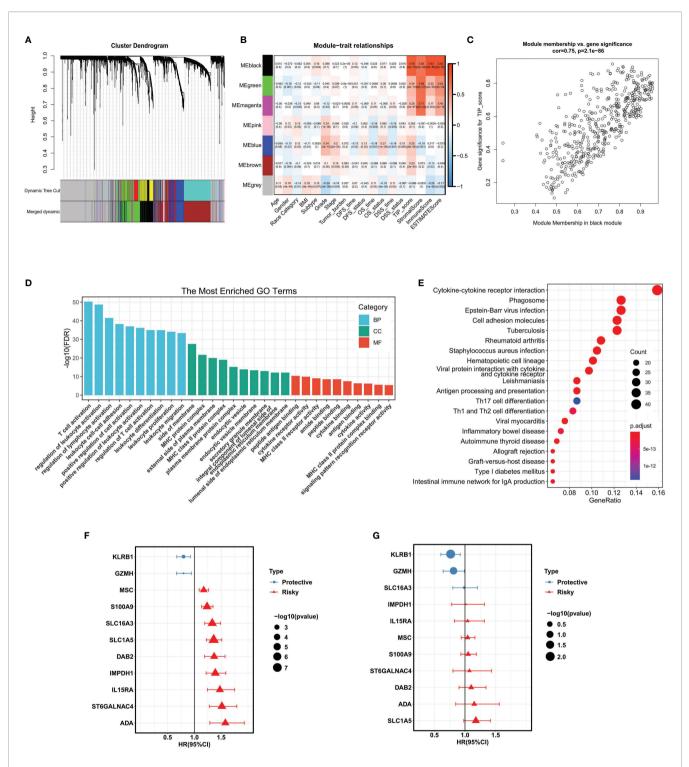


FIGURE 3 | WGCNA analysis and the construction of TIPRGPI for HCC. (A) Cluster dendrogram of MAD top 5000 genes. (B) Table cells showing Pearson's correlation coefficients and corresponding *P*-value between module eigengenes (ME) and the variables. (C) Scatter plot showing the relationship between gene significance (GS) for TIP score and module membership (MM) in the black module. (D, E) GO enrichment analysis (D) and KEGG (E) enrichment analysis for the black module genes. (F, G) Hazard ratio with 95%CI of each gene in the TIPRGPI signature computed by UniCox and MultiCox, respectively. GO, gene oncology; KEGG, Kyoto Encyclopedia of Genes and Genomes; WGCNA, weighted gene co-expression network analysis; MAD, median absolute deviation; TIPRGPI, TIP-related gene prognostic index.

of cytokine-cytokine receptor interaction (**Figure 3E**). Subsequently, we inputted the genes of the black module into UniCox regression analysis and found 128 significant genes with *P* value lower than 0.05 (**Supplementary Table 2**). Next, we conducted LASSO Cox regression with the 128 genes and obtained 11 robust genes (KLRB1, GZMH, SLC16A3, IMPDH1, IL15RA, MSC, S100A9, ST6GALNAC4, DAB2, ADA, SLC1A5) that were significantly correlated with the OS of HCC patients from TCGA-HCC dataset. MultiCox was applied to analyze the 11 genes, which were subsequently incorporated into a TIPRGPI model for predicting the prognosis of HCC. **Figures 3F, G** showed the UniCox and MultiCox results of the selected 11 genes with the corresponding hazard ratio (HR) and statistical significance.

Evaluation and Validation of the TIPRGPI Signature

After the construction of TIPRGPI, we proceeded with evaluation and validation analysis. First, we computed the risk score for individual patients using the expression and the risk coefficients of the 11 TIPRGPI genes in HCC datasets, and based on the median value derived from the training set, HCC patients from TCGA-LIHC (training dataset), GSE14520 (validation dataset 1) and ICGC-LIRI-JP (validation dataset 2) were separated into low- and high-risk groups, respectively (Figure 4A). As shown in Figure 4B, the low-risk group had a lower death rate than the high-risk group. Afterward, by Kaplan-Meier analysis, significant differences in the OS possibility were observed between the low- and high-risk groups in the training and validation datasets (Figure 4C). Further, the time-dependent receiver operating characteristic curve analysis was applied to evaluate the accuracy of the TIPRGPI signature. For the TCGA-HCC training dataset, the area under the ROC curve (AUC) was 0.836, 0.775, and 0.741 in 1-year, 3-year, and 5-year survival, respectively. Moreover, ROC curve analysis of GSE14520 and ICGC validation dataset exhibited that TIPRGPI had excellent predictive performance (GSE14520: AUC = 0.664 for 1-year, 0.708 for 3-years and 0.666 for 5-year survival; ICGC: AUC = 0.769 for 1-year, 0.637 for 3-years and 0.656 for 4-year survival) (Figure 4D). Compared with several other published signatures and popular biomarkers, TIPRGPI had the highest AUC for either 3-year or 5-year survival (Figure 4E). Besides, stratified analysis revealed an additional predictive value of TIPRGPI in subgroups divided by age, gender, BMI, race, stage, grade, and tumor burden (Supplementary Figure 2). Correlation analysis between TIPRGPI and multiple clinical traits revealed that the tumor grade and stage of HCC were significantly correlated with risk score (Figure 4F). These results indicated that TIPRGPI was a highly reliable signature.

Establishment of the Prognostic Nomogram

To figure out whether the TIPRGPI predicting model was an independent prognostic indicator in HCC, univariate and multivariate analyses were performed. The HR of the TIPRGPI risk level was 3.049 (95%CI: 2.083-4.465) and 3.056 (95%CI:

1.976-4.725) in the univariate and multivariate analysis, respectively, and an elevated HR was observed compared with the pathologic stage (**Figure 5A**). Importantly, multivariate analysis demonstrated TIPRGPI was an independent prognostic factor in HCC.

To provide a quantitative instrument for the clinician, a nomogram was built by tumor burden, stage, and TIPRGPI (**Figure 5B**). The calibration plot showing the observed versus predicted rates of the 3- and 5-year OS indicates the ideal consistency of the nomogram (**Figure 5C**). As **Figures 5D–F** showed, the TIPRGPI-integrated nomogram achieved a better net benefit than clinical traits in predicting 1-year, 3-year, and 5-year OS in HCC patients from the TCGA-LIIHC dataset. In addition, we confirmed the prognostic value of the nomogram, which was found to be significantly associated with OS, DFS, PFS, and DSS, respectively (**Figure 5G**).

The Underlying Molecular Mechanisms of TIPRGPI

To investigate the potential mechanisms of the risk level defined by TIPRGPI in HCC, we downloaded the available somatic mutation profiles and analyzed the mutation landscape of the high- and low-risk patients from the TCGA-LIHC dataset (Figures 6A, B). We exhibited the top 20 mutated genes in two groups respectively. The gene with the most mutation frequency is TP53 (43%) in the high-risk group and that in the low-risk group is CTNNB1 (29%). The summary of the mutation information with statistical calculation was shown in Supplementary Figure 3. Further, the significant differentially mutated genes between the TIPRGPI high- and low-risk groups were detected by Fisher's exact test. As shown in Figure 6C, TP53 was found with a much higher mutation rate in the highrisk group compared with the low-risk group (P < 0.001), and a lollipop plot was depicted to indicate the different mutation spots of TP53 for the two risk groups (Figure 6D). Meanwhile, the coincident and exclusive associations across the top 25 mutated genes from the high- and low-risk groups were also analyzed, in which blue represents the co-occurrence while red represents mutual exclusion (Figure 6E). Additionally, the CNV alteration landscapes of the high- and low-risk groups were generated after removing the germline features (Figure 6F). Interestingly, the hub genes of HCC (32, 33) were widely amplified in the high-risk group in comparison with the low-risk group (Figure 6G). NDC80 and RFC4 were two examples demonstrating the positive correlations of gene expression and copy number in the TIPRGPI high-risk group (Figure 6H).

To explore the associated cancer hallmark pathways regarding TIPRGPI, we performed GSVA in high- and low-risk groups. According to the predefined cutoff, 16 hallmark pathways significantly increased in the high-risk group compared with the low-risk group (**Figure 7A**). GSEA confirmed that 12 of them were upregulated in the high-risk group, most of which were related to well-known oncogenic pathways (61) (**Figure 7B** and **Supplementary Table 3**). Kaplan-Meier survival analysis was applied to evaluate the prognostic values of the upregulated hallmark pathways and different OS probabilities were observed

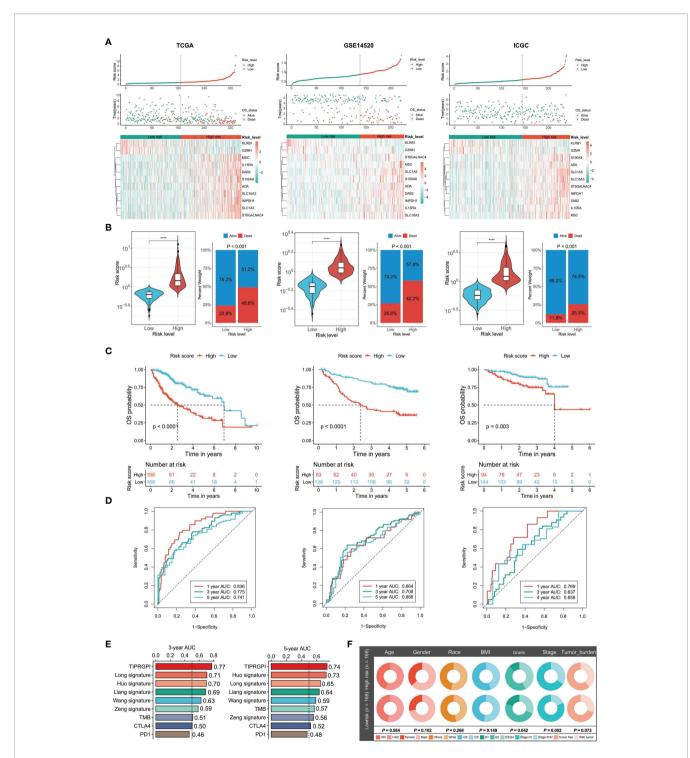


FIGURE 4 | Validation of the TIPRGPI predicting model and performance analysis in HCC. (A) Risk score distribution, survival status, and the expression of 11 TIPRGPI genes for patients in low- and high-risk groups from TCGA training dataset and two validation datasets (GSE14520 and ICGC-LIRI-JP). (B) Risk score and mortality rate of patients in low- and high-risk groups from three datasets. (C) Kaplan-Meier survival curves showing the comparison of overall survival (OS) between the low- and high-risk groups from three datasets. (D) Time-dependent receiver operating characteristic (tROC) curves of three datasets. (E) The area under the ROC curve (AUC) in 3-year and 5-year survival for TIPRGPI and other published signatures and common immunotherapeutic biomarkers. (F) Correlation analysis between the TIPRGPI low-/high-risk groups and clinical traits ****P < 0.0001.

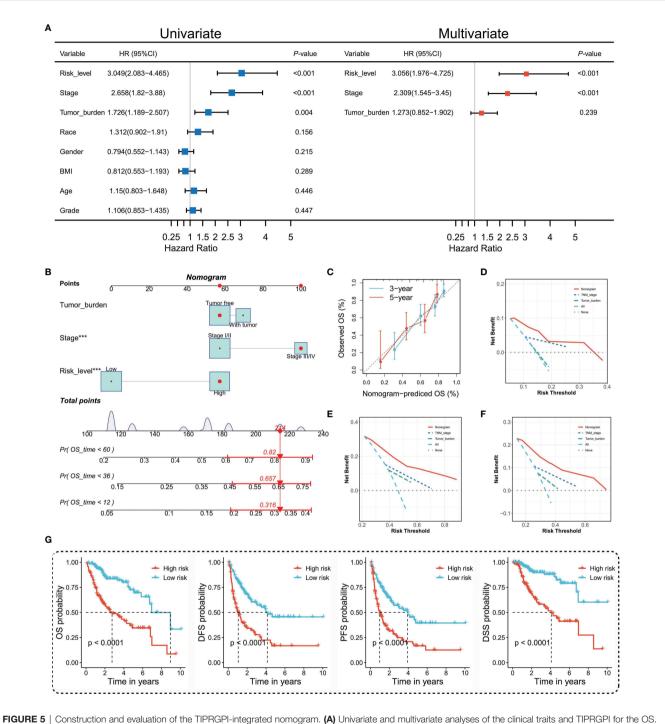
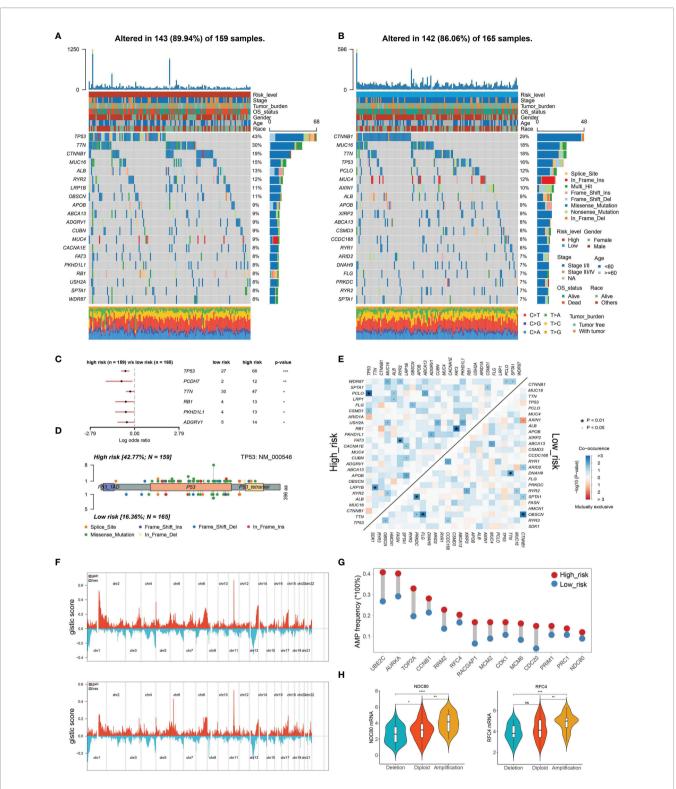


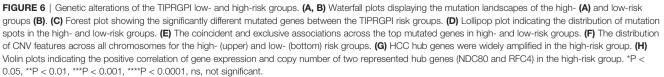
FIGURE 5 | Construction and evaluation of the TIPRGPI-integrated nomogram. (A) Univariate and multivariate analyses of the clinical traits and TIPRGPI for the OS. (B) Nomogram for predicting the probability of 1-, 3-, and 5-year overall survival in HCC. (C) The calibration plots of the nomogram predicting the probability of the 3- and 5-year OS. (D–F) Decision curves showing the comparison of net benefits of the nomogram, TNM stage, tumor burden for 1-year (D), 3-year (E), and 5-year (F) OS. (G) Kaplan-Meier survival analysis of the integrated nomogram for OS, DFS, PFS, and DSS of HCC. ***P < 0.001.

between the high- and low-score groups for these oncogenic hallmark pathways, such as PI3K_AKT_MTOR_SIGNALING, G2M_CHECKPOINT, WNT_BETA_CATENIN_SIGNALING, and MYC_TARGETS_V1 (**Figure 7C**). Taken together, TIPRGPI was tightly associated with oncogenic pathways.

TIPRGPI Was Associated With HCC Immune Status

Given that TIPRGPI was constructed on the basis of TIP score, which was significantly related to other immune signatures, we explored the potential relationship between TIPRGPI and the





infiltration of TME cells. The boxplots showed the differential distribution of infiltrating TME cells inferred by ssGSEA algorithm between low- and high-risk groups and revealed that the infiltration of most TME cell types including activated B cell, activated CD4 T cell, gamma delta T cell, memory B cell, activated CD8 T cell, immature B cell, effector memory CD8 T cell, type 1 T helper cell, natural killer T cell, eosinophil, activated dendritic cell, immature dendritic cell, plasmacytoid dendritic cell, endothelial cell and fibroblast cell (P < 0.05) were significantly associated with risk group (Figure 8A). In addition, correlation analysis was used to pick out the TME cell types significantly correlated with the risk score and the result showed that four types were positively correlated with risk score while seven types were negatively correlated with it (Figure 8B). We also analyzed the relationships between OS and the infiltration of TME cells, whose expression levels were classed into low- and high-infiltration groups from the TCGA-HCC dataset, and the results showed 13 TME cell types were

involved in the significant differences between the high- and lowinfiltration groups (**Supplementary Figure 4**). Finally, overlapping Venn plot revealed 10 intersected TME cell types including four adaptive immune cell types (red), five innate immune cell types (green), and one stromal cell type (blue) among differential analysis, correlation analysis, and survival analysis (**Figure 8C**). These findings strongly suggested that the infiltration of TME cells plays a vital role in the postoperative risk stratification of HCC.

TIPRGPI May be a Potential Indicator to Predict Immunotherapeutic Sensitivity in HCC Patients

ICB-related gene expression levels have been reported to be correlated with therapeutic responses of immune checkpoint inhibitors (62) and ICB targeting promising checkpoints has emerged as a promising strategy in treating cancers (63). To evaluate the potential of TIPRGPI for predicting the response of

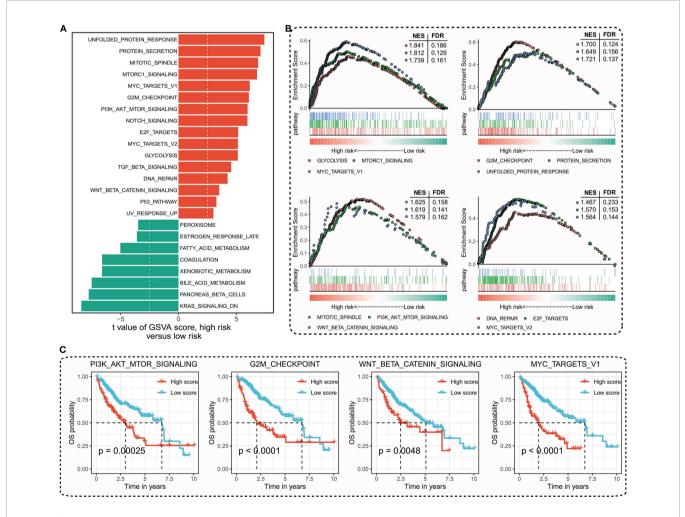
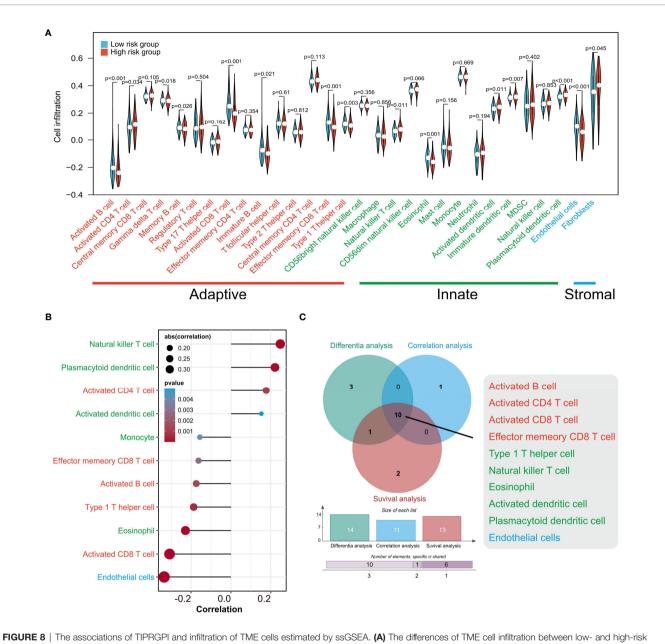
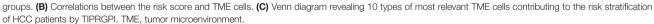


FIGURE 7 | Determination of the distinct hallmark pathways of the TIPRGPI low- and high-risk groups. (A) Differences in cancer hallmark pathway activities between the high- and low-risk groups scored by GSVA. (B) The GSEA results for the 12 overlapping upregulated hallmark pathways in terms of the TIPRGPI risk groups. (C) Kaplan-Meier survival plots showing the significant correlations between the OS and GSVA scores of typical oncogenic hallmark pathways. GSVA, gene set variation analysis. GSEA, gene set enrichment analysis.





HCC patients to immunotherapy, we first determined the expression of 50 immunomodulators in low- and high-risk groups. As shown in **Figure 9A**, the expressions of more than half of the presented immunomodulators were significantly associated with the risk score. Considering the significant correlation between the risk score and CD8 T cell and the important role of m6A methylation in impairing the antitumor ability of CD8 T cell, we next analyzed the expression of the CD8 T cell-related IFN-gamma pathway markers and m6A regulators in low- and high-risk groups and found most of them were significantly associated with the risk score (**Figures 9B, C**). These findings demonstrated the TIPRGPI had great potential in evaluating the response of immunotherapy for HCC. Subsequently, we explored the correlation between the TIPRGPI risk group and immunophenoscore (IPS), which is a recognized model based on machine learning to predict patients' responses to immune checkpoints blockade by estimating the immunogenicity. We found that the low-risk group has a higher IPS score, indicating patients in the low-risk group might respond better to immunotherapy (**Figure 9D**). We also used the TIDE algorithm to predict the immunotherapeutic efficacy for immune checkpoint blockade in TCGA-LIHC, GSE14520,

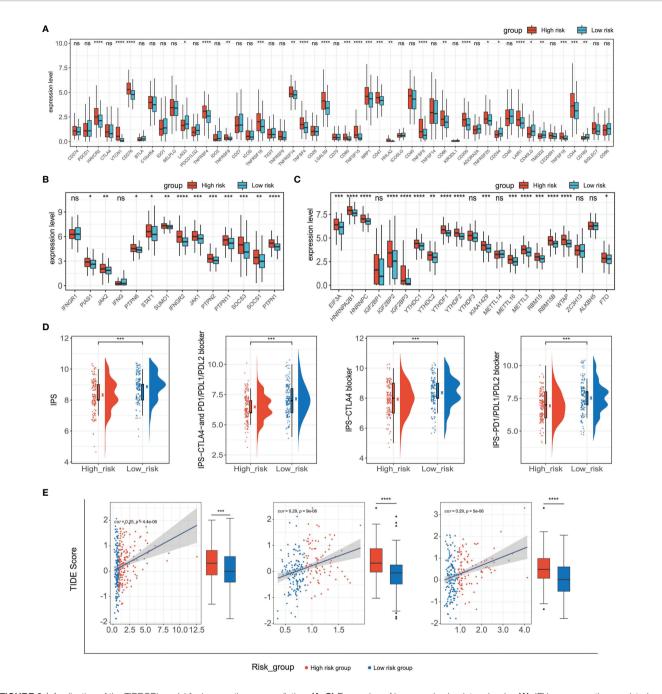


FIGURE 9 | Application of the TIPRGPI model for immunotherapy prediction. (A–C) Expression of immune checkpoint molecules (A), IFN-gamma pathway-related markers (B), and m6A regulators (C) in low- and high-risk groups. (D) The relationship between TIPRGPI and IPS. (E) Distribution of TIDE scores in the TCGA-LIHC, GSE14520, and ICGC-LIRI-JP datasets. *P < 0.05, **P < 0.01, ***P < 0.001, ****P < 0.0001, ns, not significant.

and ICGC datasets and the high-risk group had a higher TIDE score, indicating that high-risk patients might have a worse response to immunotherapy (**Figure 9E**).

Core Target Identification and Candidate Molecules Prediction

To identify the core target concerning TIPRGPI, a PPI network was built using the STRING database (confidence score > 0.4)

and visualized by the Cytoscape software (**Supplementary Figure 5**). The highly interactive network contains 58 nodes and 182 edges with the clustering coefficient of 0.595. As shown in **Supplementary Figure 5**, CD44 lies at the hub of the network and has the highest degree among all the nodes. Thus, CD44 was considered as the core target.

Molecular docking is a structure-based computational algorithm for compound screening. In this study, the structures for a total of

9800 purchasable small molecules from the libraries of zinc15 database were obtained and subjected to molecular docking. **Supplementary Table 4** showed the top six molecules (Pentostatin, Allantoin, Mizoribine, Xylose, Deoxynojirimycin, and 6-Hydroxyetodolac) that had the highest affinity with the predicted binding pocket of CD44. The 3D diagrams for the six docking models presenting the detailed binding energy were displayed in **Figure 10**. For instance, Mizoribine (ZINC000003812887) forms hydrogen bonds with amino acid residues ILE-96, CYS-77, ARG-78, TYR-42, and ILE-91. Besides, the probable formation of salt bridge interaction between ARG-78 and the side-chain hydroxyl group of the ligand also helped the compound connect to the active site of CD44.

DISCUSSIONS

It is well established that the tumor immune microenvironment is closely related to tumorigenesis and cancer progression (64-66). Here, using the "TIP genes"-guided strategy with multiple statistical approaches, we developed a novel immune-relevant and independent predictive model - TIPRGPI - for prognosis and immunotherapy in HCC. Based on the training (TCGA-LIHC) and two external validation (ICGC-LIRI-JP and GSE14520) datasets, the TIPRGPI signature was applied to divide HCC patients into low-risk and high-risk groups. As expected, high-risk patients had a worse prognosis and response to immunotherapy. Univariate and multivariate analysis verified it was an independent predictor for the prognosis of HCC. Moreover, a TIPRGPIintegrated nomogram model was established, which showed a better net benefit than the clinical traits in predicting 1-year, 3year, and 5-year OS for HCC patients, thus demonstrating enhanced accuracy and potential implication in clinical practice. Besides, potential drugs targeting the signature could be predicted via molecular docking. Therefore, the TIPRGPI signature was a reliable model to predict prognosis and immunotherapeutic response in HCC and might provide valuable insight for seeking the treatment for HCC.

A growing body of gene signatures has been established to shed light on the prognosis classification of HCC. For example, Long et al. established a four-gene prognostic model that showed a good performance for HCC prognosis prediction (40). Gao et al. reported a six-gene signature for predicting OS of HCC (67). However, few studies focused on gene signatures on the basis of key genes in the tumor immune microenvironment. Tumor immunological phenotype has been emerging to be significantly related to prognosis and therapeutic responses in various types of cancer by mounting evidence (26, 68-71). TIP score, representing the expression level of fifteen TIP genes that were obtained from a previously study (26), was significantly associated with the prognosis and other immune signatures in HCC. Thus, we, for the first time, conducted WGCNA to uncover the specific gene expression pattern related to TIP score in HCC, identifying the black module that contained 432 genes, which generated an 11-gene signature called "TIPRGPI" for prognosis prediction of HCC. Another advantage of this study is the larger sample size and higher AUCs than that of most previous studies trying to building an effective risk classifier for HCC. Besides, unlike previous studies only describing a prognostic gene signature, we engaged an integrative analysis to get a deeper and comprehensive understanding of the risk model, and putative drugs were even predicted based on the model, which was rarely reported by other similar studies.

All genes involved are either related to the immune system or tumorigenesis. For example, adenosine deaminase (ADA) is produced in all cells but highest in lymphocytes and loss of ADA causes the immune system to collapse (72). IL-15RA is expressed in multiple types of immune cells including dendritic cells (DC), macrophages, and natural killer cells (NK), and it plays a prominent role in TME (73). Disabled-2 (DAB2) is considered to be an immune-regulatory factor (74), and has recently been found to be involved in the regulation of tumor-related signaling pathways (75, 76). To sum up, TIPRGPI is likely to be a prognostic indicator strongly related to the immune status in HCC.

Systematically exploring the hallmark gene sets between the lowand high-risk groups provided us more insights into the transcriptomic regulatory mechanisms of TIPRGPI in HCC. Those hallmark pathways with an increased level in the high-risk group were found to be relevant to well-recognized oncogenic signaling pathways, including PI3K pathway, Wnt pathway, Myc pathway, and Cell cycle pathway (61). The similarities and disparities of mutation status or CNV profiles gave a hint of oncogenes that linked to the TIPRGPI model. These preliminary data strongly implied the inherent associations between immune-derived signature and oncogenic pathways and could provide more clues or new strategies for candidate drug discovery in future studies.

In consideration of the importance of immune infiltration in the tumor ecosystem, ssGSEA algorithm was used to estimate the activities of TME cells in low- and high-risk groups. 11 types of immune cells were significantly associated with the risk score. In line with the survival analysis, a higher abundance of activated B cell, effector memory CD8+ T cell, and activated CD8+ T cell in the low-risk group might contribute to a better prognosis. These results suggest that the poor survival outcomes of high-risk group patients are probably due to the low infiltration of these protective immune cells, which is also the main cause for the low objective response rates to immunotherapy, agreeing with previous observations (43, 77).

In the past decade, anti-cancer immunotherapies targeting PD-1/ PD-L1 and CTLA-4, have achieved positive response in HCC patients (78, 79). However, as mentioned above, only a small proportion of HCC patients can respond to immunotherapies, and the main reason might be the limitations in their tumor immunity status (80). To determine whether TIPRGPI was capable of predicting the efficiency of anti-cancer immunotherapies in HCC patients, we measured the expression levels of 50 common immune checkpoints in low- and high-risk groups and found more than half of them were significantly associated with the risk level. It is widely known that cancer immunotherapy restores or enhances the antitumor function of CD8+T cells in the tumor microenvironment (81). Thus, we estimated the expression levels of the key molecules in two CD8+ T cells anti-tumor related pathways (IFN-gamma (82) and

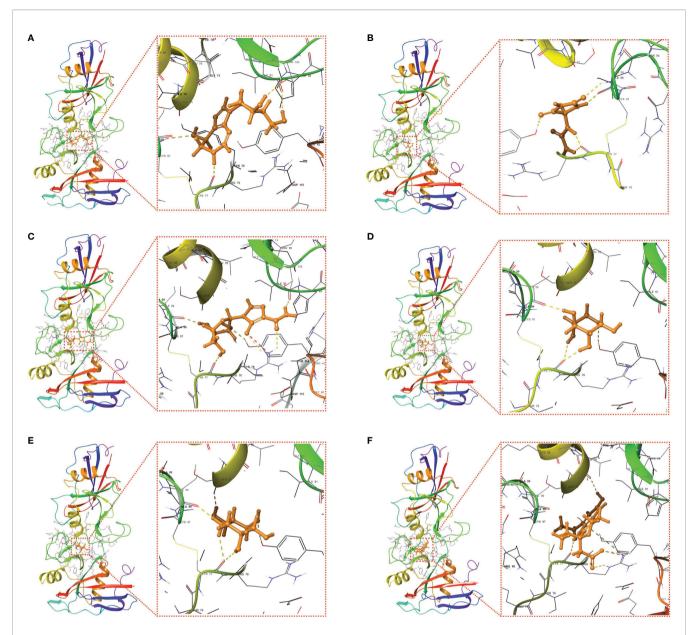


FIGURE 10 | Putative docking models of the six candidate drugs and the core target using molecular docking analysis. 3D structures and binding modes showing the formed hydrogen bonds between the predicted pocket of CD44 and Pentostatin (A), Allantoin (B), Mizoribine (C), Xylose (D), Deoxynojirimycin (E), and 6-Hydroxyetodolac (F).

m6A pathway (83)) in low- and high-risk groups, and the results indicated that the majority of these molecules were expressed differently between two groups of HCC patients. IPS, developed from a panel of immune-related genes belonging to the four classeseffector cells, immunosuppressive cells, MHC molecules, and selected immunomodulators, was a superior predictor of response to immune checkpoint inhibitors (50). Our study showed that the low-risk group had higher IPS, IPS-PD-11/PD-L1/PD-L2, and IPS-CTLA4 scores, suggesting that HCC patients in the low-risk group might have a better response to anti-CTLA-4 and anti-PD-1 antibodies. Also, TIDE analysis showed that the low-risk group had a lower TIDE score than the high-risk group in three different datasets. Taken together, these results suggested that patients in the low-risk group might have a better response to immunotherapies and TIPGPI could be a potential biomarker for predicting the efficiency of immunotherapies in HCC.

As another application of the prognostic classifier, we demonstrated the feasibility of searching candidate drugs by combining the core target and structure-based approaches. A PPI network was constructed for these signature genes, among which CD44 was found to be the hub node. Interestingly, CD44 was a well-defined cancer stem cell (CSC) marker that was involved in tumor initiation, epithelial-mesenchymal transition (EMT), and therapy resistance in multiple types of cancer.

Therefore, substantial efforts have been exerted to develop effective anti-cancer drugs or antibodies by targeting CD44 (84–87). Preclinical and clinical trials of CD44 monoclonal antibodies have also been performed to evaluate the pharmacokinetics, efficacy, and drug-related toxicity in cancer (88). In the present study, we identified six drugs with high affinity to CD44 from a total of 9800 small molecules. Among them, Pentostatin has been reported in clinical trials for chronic lymphocytic leukemia (CLL) (89). Noticeably, Deoxynojirimycin could exert anti-HCV activity through inhibiting alphaglucosidase (90). Although more in-depth investigations should be conducted for the specific mechanisms of the small compounds, our results indicated their potential in cancer immunotherapy especially for the immunological high-risk group of HCC patients.

CONCLUSION

In summary, we constructed an immune-related TIPRGPI model to predict the prognosis and immunotherapy efficacy of HCC patients using a novel "TIP genes"- guided strategy, and it was well-validated from multiple aspects. Combining these results and the linkage between TIPRGPI and oncogenic hallmark pathways, our study provides new perspectives for the identification of prognostic classifiers and even the discovery of immunotherapeutic drugs. Notably, in the era, where immunotherapy offers new hope for effective cancer treatment, TIPRGPI provides certain guiding significance for clinical judgment and personalized treatment.

DATA AVAILABILITY STATEMENT

The data achieved and analyzed in the current study are available in the TCGA repository (https://portal.gdc.cancer.gov/), ICGC

REFERENCES

- Petrick JL, Florio AA, Znaor A, Ruggieri D, Laversanne M, Alvarez CS, et al. International Trends in Hepatocellular Carcinoma Incidence, 1978-2012. *Int J Cancer* (2020) 147(2):317–30. doi: 10.1002/ijc.32723
- Yang JD, Hainaut P, Gores GJ, Amadou A, Plymoth A. Roberts LR. A Global View of Hepatocellular Carcinoma: Trends, Risk, Prevention and Management. *Nat Rev Gastroenterol Hepatol* (2019) 16(10):589–604. doi: 10.1038/s41575-019-0186-y
- Valery PC, Laversanne M, Clark PJ, Petrick JL, McGlynn KA, Bray F. Projections of Primary Liver Cancer to 2030 in 30 Countries Worldwide. *Hepatology* (2018) 67(2):600–11. doi: 10.1002/hep.29498
- Bray F, Ferlay J, Soerjomataram I, Siegel RL, Torre LA, Jemal A. Global Cancer Statistics 2018: Globocan Estimates of Incidence and Mortality Worldwide for 36 Cancers in 185 Countries. *CA Cancer J Clin* (2018) 68 (6):394–424. doi: 10.3322/caac.21492
- Singal AG, Lampertico P, Nahon P. Epidemiology and Surveillance for Hepatocellular Carcinoma: New Trends. J Hepatol (2020) 72(2):250–61. doi: 10.1016/j.jhep.2019.08.025
- de Martel C, Maucort-Boulch D, Plummer M, Franceschi S. World-Wide Relative Contribution of Hepatitis B and C Viruses in Hepatocellular Carcinoma. *Hepatology* (2015) 62(4):1190–200. doi: 10.1002/hep.27969

database (https://icgc.org/), and GEO database (https://www. ncbi.nlm.nih.gov/geo/) under the accession number GSE14520.

AUTHOR CONTRIBUTIONS

YT, YZ, and DW conceived the study. YT, YZ, and CG contributed to data collection, analysis, and interpretation. ZY helped with data visualization. YZ and CG completed the drafting of the manuscript. YT, YW, and DW revised the manuscript. DW supervised the research. All authors contributed to the article and approved the submitted version.

FUNDING

This work was supported by the National Natural Science Foundation of China (Grant No. 82172723, 81673460), Science and Technology Department of Sichuan Province (Grant No. 2021ZYD0079), and the Sichuan Youth Science and Technology Innovation Research Team of Experimental Formulology (2020JDTD0022).

ACKNOWLEDGMENTS

We acknowledge the Gene Expression Omnibus (GEO) database, Cancer Genome Atlas (TCGA), and International Cancer Genome Consortium (ICGC) for data sharing.

SUPPLEMENTARY MATERIAL

The Supplementary Material for this article can be found online at: https://www.frontiersin.org/articles/10.3389/fimmu.2022. 862527/full#supplementary-material

- Sung H, Ferlay J, Siegel RL, Laversanne M, Soerjomataram I, Jemal A, et al. Global Cancer Statistics 2020: Globocan Estimates of Incidence and Mortality Worldwide for 36 Cancers in 185 Countries. *CA Cancer J Clin* (2021) 71 (3):209–49. doi: 10.3322/caac.21660
- Bruix J, Reig M, Sherman M. Evidence-Based Diagnosis, Staging, and Treatment of Patients With Hepatocellular Carcinoma. *Gastroenterology* (2016) 150(4):835–53. doi: 10.1053/j.gastro.2015.12.041
- Xu Q, Xu H, Chen S, Huang W. Immunological Value of Prognostic Signature Based on Cancer Stem Cell Characteristics in Hepatocellular Carcinoma. *Front Cell Dev Biol* (2021) 9:710207. doi: 10.3389/fcell. 2021.710207
- Schreiber RD, Old LJ, Smyth MJ. Cancer Immunoediting: Integrating Immunity's Roles in Cancer Suppression and Promotion. *Science* (2011) 331(6024):1565–70. doi: 10.1126/science.1203486
- Sangro B, Sarobe P, Hervas-Stubbs S, Melero I. Advances in Immunotherapy for Hepatocellular Carcinoma. Nat Rev Gastroenterol Hepatol (2021) 18 (8):525–43. doi: 10.1038/s41575-021-00438-0
- Vaddepally RK, Kharel P, Pandey R, Garje R, Chandra AB. Review of Indications of Fda-Approved Immune Checkpoint Inhibitors Per Nccn Guidelines With the Level of Evidence. *Cancers (Basel)* (2020) 12(3):738. doi: 10.3390/cancers12030738

- Anderson AC, Joller N, Kuchroo VK. Lag-3, Tim-3, and Tigit: Co-Inhibitory Receptors With Specialized Functions in Immune Regulation. *Immunity* (2016) 44(5):989–1004. doi: 10.1016/j.immuni.2016.05.001
- Zhang Q, Bi J, Zheng X, Chen Y, Wang H, Wu W, et al. Blockade of the Checkpoint Receptor Tigit Prevents Nk Cell Exhaustion and Elicits Potent Anti-Tumor Immunity. *Nat Immunol* (2018) 19(7):723–32. doi: 10.1038/s41590-018-0132-0
- Visan I. New Ligand for Lag-3. Nat Immunol (2019) 20(2):111. doi: 10.1038/ s41590-018-0307-8
- Yang YM, Kim SY, Seki E. Inflammation and Liver Cancer: Molecular Mechanisms and Therapeutic Targets. Semin Liver Dis (2019) 39(1):26–42. doi: 10.1055/s-0038-1676806
- Ringelhan M, Pfister D, O'Connor T, Pikarsky E, Heikenwalder M. The Immunology of Hepatocellular Carcinoma. *Nat Immunol* (2018) 19(3):222– 32. doi: 10.1038/s41590-018-0044-z
- Sangro B, Gomez-Martin C, de la Mata M, Inarrairaegui M, Garralda E, Barrera P, et al. A Clinical Trial of Ctla-4 Blockade With Tremelimumab in Patients With Hepatocellular Carcinoma and Chronic Hepatitis C. J Hepatol (2013) 59(1):81–8. doi: 10.1016/j.jhep.2013.02.022
- El-Khoueiry AB, Sangro B, Yau T, Crocenzi TS, Kudo M, Hsu C, et al. Nivolumab in Patients With Advanced Hepatocellular Carcinoma (Checkmate 040): An Open-Label, Non-Comparative, Phase 1/2 Dose Escalation and Expansion Trial. *Lancet* (2017) 389(10088):2492–502. doi: 10.1016/S0140-6736(17)31046-2
- Miamen AG, Dong H, Roberts LR. Immunotherapeutic Approaches to Hepatocellular Carcinoma Treatment. *Liver Cancer* (2012) 1(3-4):226–37. doi: 10.1159/000343837
- Sammut SJ, Crispin-Ortuzar M, Chin SF, Provenzano E, Bardwell HA, Ma W, et al. Multi-Omic Machine Learning Predictor of Breast Cancer Therapy Response. *Nature* (2021) 601(7894):623–9. doi: 10.1038/s41586-021-04278-5
- Marusyk A, Janiszewska M, Polyak K. Intratumor Heterogeneity: The Rosetta Stone of Therapy Resistance. *Cancer Cell* (2020) 37(4):471–84. doi: 10.1016/ j.ccell.2020.03.007
- Nagarsheth N, Wicha MS, Zou W. Chemokines in the Cancer Microenvironment and Their Relevance in Cancer Immunotherapy. Nat Rev Immunol (2017) 17(9):559–72. doi: 10.1038/nri.2017.49
- 24. Cai Y, Ji W, Sun C, Xu R, Chen X, Deng Y, et al. Interferon-Induced Transmembrane Protein 3 Shapes an Inflamed Tumor Microenvironment and Identifies Immuno-Hot Tumors. *Front Immunol* (2021) 12:704965. doi: 10.3389/fimmu.2021.704965
- Ollauri-Ibanez C, Ayuso-Inigo B, Pericacho M. Hot and Cold Tumors: Is Endoglin (Cd105) a Potential Target for Vessel Normalization? *Cancers* (*Basel*) (2021) 13(7):1552. doi: 10.3390/cancers13071552
- Wang H, Li S, Wang Q, Jin Z, Shao W, Gao Y, et al. Tumor Immunological Phenotype Signature-Based High-Throughput Screening for the Discovery of Combination Immunotherapy Compounds. *Sci Adv* (2021) 7(4):eabd7851. doi: 10.1126/sciadv.abd7851
- Huo J, Wu L, Zang Y. Development and Validation of a Ctnnb1-Associated Metabolic Prognostic Model for Hepatocellular Carcinoma. J Cell Mol Med (2021) 25(2):1151–65. doi: 10.1111/jcmm.16181
- Chew V, Chen J, Lee D, Loh E, Lee J, Lim KH, et al. Chemokine-Driven Lymphocyte Infiltration: An Early Intratumoural Event Determining Long-Term Survival in Resectable Hepatocellular Carcinoma. *Gut* (2012) 61 (3):427–38. doi: 10.1136/gutjnl-2011-300509
- Cai WY, Dong ZN, Fu XT, Lin LY, Wang L, Ye GD, et al. Identification of a Tumor Microenvironment-Relevant Gene Set-Based Prognostic Signature and Related Therapy Targets in Gastric Cancer. *Theranostics* (2020) 10 (19):8633–47. doi: 10.7150/thno.47938
- Roessler S, Jia HL, Budhu A, Forgues M, Ye QH, Lee JS, et al. A Unique Metastasis Gene Signature Enables Prediction of Tumor Relapse in Early-Stage Hepatocellular Carcinoma Patients. *Cancer Res* (2010) 70(24):10202–12. doi: 10.1158/0008-5472.CAN-10-2607
- Roessler S, Long EL, Budhu A, Chen Y, Zhao X, Ji J, et al. Integrative Genomic Identification of Genes on 8p Associated With Hepatocellular Carcinoma Progression and Patient Survival. *Gastroenterology* (2012) 142(4):957–66 e12. doi: 10.1053/j.gastro.2011.12.039
- 32. Zhang Y, Tang Y, Guo C, Li G. Integrative Analysis Identifies Key Mrna Biomarkers for Diagnosis, Prognosis, and Therapeutic Targets of Hcv-

Associated Hepatocellular Carcinoma. Aging (Albany NY) (2021) 13:12865-95. doi: 10.18632/aging.202957

- 33. Tang Y, Zhang Y, Hu X. Identification of Potential Hub Genes Related to Diagnosis and Prognosis of Hepatitis B Virus-Related Hepatocellular Carcinoma via Integrated Bioinformatics Analysis. BioMed Res Int (2020) 2020:4251761. doi: 10.1155/2020/4251761
- 34. Guo C, Tang Y, Zhang Y, Li G. Mining Tcga Data for Key Biomarkers Related to Immune Microenvironment in Endometrial Cancer by Immune Score and Weighted Correlation Network Analysis. *Front Mol Biosci* (2021) 8:645388. doi: 10.3389/fmolb.2021.645388
- 35. Yoshihara K, Shahmoradgoli M, Martinez E, Vegesna R, Kim H, Torres-Garcia W, et al. Inferring Tumour Purity and Stromal and Immune Cell Admixture From Expression Data. *Nat Commun* (2013) 4:2612. doi: 10.1038/ ncomms3612
- Mayakonda A, Lin DC, Assenov Y, Plass C, Koeffler HP. Maftools: Efficient and Comprehensive Analysis of Somatic Variants in Cancer. *Genome Res* (2018) 28(11):1747–56. doi: 10.1101/gr.239244.118
- Langfelder P, Horvath S. Wgcna: An R Package for Weighted Correlation Network Analysis. BMC Bioinf (2008) 9:559. doi: 10.1186/1471-2105-9-559
- Yu G, Wang LG, Han Y, He QY. Clusterprofiler: An R Package for Comparing Biological Themes Among Gene Clusters. OMICS (2012) 16(5):284–7. doi: 10.1089/omi.2011.0118
- Friedman J, Hastie T, Tibshirani R. Regularization Paths for Generalized Linear Models via Coordinate Descent. J Stat Softw (2010) 33(1):1–22. doi: 10.18637/jss.v033.i01
- 40. Long J, Wang A, Bai Y, Lin J, Yang X, Wang D, et al. Development and Validation of a Tp53-Associated Immune Prognostic Model for Hepatocellular Carcinoma. *EBioMedicine* (2019) 42:363–74. doi: 10.1016/ j.ebiom.2019.03.022
- Liang JY, Wang DS, Lin HC, Chen XX, Yang H, Zheng Y, et al. A Novel Ferroptosis-Related Gene Signature for Overall Survival Prediction in Patients With Hepatocellular Carcinoma. *Int J Biol Sci* (2020) 16(13):2430–41. doi: 10.7150/ijbs.45050
- Wang Z, Zhu J, Liu Y, Liu C, Wang W, Chen F, et al. Development and Validation of a Novel Immune-Related Prognostic Model in Hepatocellular Carcinoma. J Transl Med (2020) 18(1):67. doi: 10.1186/s12967-020-02255-6
- Zeng F, Zhang Y, Han X, Zeng M, Gao Y, Weng J. Employing Hypoxia Characterization to Predict Tumour Immune Microenvironment, Treatment Sensitivity and Prognosis in Hepatocellular Carcinoma. *Comput Struct Biotechnol J* (2021) 19:2775–89. doi: 10.1016/j.csbj.2021.03.033
- 44. Chalmers ZR, Connelly CF, Fabrizio D, Gay L, Ali SM, Ennis R, et al. Analysis of 100,000 Human Cancer Genomes Reveals the Landscape of Tumor Mutational Burden. *Genome Med* (2017) 9(1):34. doi: 10.1186/s13073-017-0424-2
- 45. Sun J, Shi R, Zhang X, Fang D, Rauch J, Lu S, et al. Characterization of Immune Landscape in Papillary Thyroid Cancer Reveals Distinct Tumor Immunogenicity and Implications for Immunotherapy. *Oncoimmunology* (2021) 10(1):e1964189. doi: 10.1080/2162402X.2021.1964189
- Hanzelmann S, Castelo R, Guinney J. Gsva: Gene Set Variation Analysis for Microarray and Rna-Seq Data. BMC Bioinf (2013) 14:7. doi: 10.1186/1471-2105-14-7
- 47. Subramanian A, Tamayo P, Mootha VK, Mukherjee S, Ebert BL, Gillette MA, et al. Gene Set Enrichment Analysis: A Knowledge-Based Approach for Interpreting Genome-Wide Expression Profiles. *Proc Natl Acad Sci U States America* (2005) 102(43):15545–50. doi: 10.1073/pnas.0506580102
- Liberzon A, Birger C, Thorvaldsdottir H, Ghandi M, Mesirov JP, Tamayo P. The Molecular Signatures Database (Msigdb) Hallmark Gene Set Collection. *Cell Syst* (2015) 1(6):417–25. doi: 10.1016/j.cels.2015.12.004
- Lambrechts D, Wauters E, Boeckx B, Aibar S, Nittner D, Burton O, et al. Phenotype Molding of Stromal Cells in the Lung Tumor Microenvironment. *Nat Med* (2018) 24(8):1277–89. doi: 10.1038/s41591-018-0096-5
- Charoentong P, Finotello F, Angelova M, Mayer C, Efremova M, Rieder D, et al. Pan-Cancer Immunogenomic Analyses Reveal Genotype-Immunophenotype Relationships and Predictors of Response to Checkpoint Blockade. *Cell Rep* (2017) 18(1):248–62. doi: 10.1016/j.celrep.2016.12.019
- 51. Becht E, Giraldo NA, Lacroix L, Buttard B, Elarouci N, Petitprez F, et al. Estimating the Population Abundance of Tissue-Infiltrating Immune and

Stromal Cell Populations Using Gene Expression. *Genome Biol* (2016) 17 (1):218. doi: 10.1186/s13059-016-1070-5

- Wu XN, Su D, Mei YD, Xu MQ, Zhang H, Wang ZY, et al. Identified Lung Adenocarcinoma Metabolic Phenotypes and Their Association With Tumor Immune Microenvironment. *Cancer Immunol Immunother* (2021) 70 (10):2835–50. doi: 10.1007/s00262-021-02896-6
- 53. Wu J, Li L, Zhang H, Zhao Y, Zhang H, Wu S, et al. A Risk Model Developed Based on Tumor Microenvironment Predicts Overall Survival and Associates With Tumor Immunity of Patients With Lung Adenocarcinoma. *Oncogene* (2021) 40(26):4413–23. doi: 10.1038/s41388-021-01853-y
- 54. Liu Z, Lu T, Wang L, Liu L, Li L, Han X. Comprehensive Molecular Analyses of a Novel Mutational Signature Classification System With Regard to Prognosis, Genomic Alterations, and Immune Landscape in Glioma. *Front Mol Biosci* (2021) 8:682084. doi: 10.3389/fmolb.2021.682084
- 55. Xu F, Chen JX, Yang XB, Hong XB, Li ZX, Lin L, et al. Analysis of Lung Adenocarcinoma Subtypes Based on Immune Signatures Identifies Clinical Implications for Cancer Therapy. *Mol Ther Oncolytics* (2020) 17:241–9. doi: 10.1016/j.omto.2020.03.021
- 56. Xu Q, Xu H, Deng R, Li N, Mu R, Qi Z, et al. Landscape of Prognostic M6a Rna Methylation Regulators in Hepatocellular Carcinoma to Aid Immunotherapy. *Front Cell Dev Biol* (2021) 9:669145. doi: 10.3389/fcell.2021.669145
- Li Y, Xiao J, Bai J, Tian Y, Qu Y, Chen X, et al. Molecular Characterization and Clinical Relevance of M(6)a Regulators Across 33 Cancer Types. *Mol Cancer* (2019) 18(1):137. doi: 10.1186/s12943-019-1066-3
- Jiang P, Gu S, Pan D, Fu J, Sahu A, Hu X, et al. Signatures of T Cell Dysfunction and Exclusion Predict Cancer Immunotherapy Response. *Nat Med* (2018) 24(10):1550–8. doi: 10.1038/s41591-018-0136-1
- Jimenez J, Doerr S, Martinez-Rosell G, Rose AS, De Fabritiis G. Deepsite: Protein-Binding Site Predictor Using 3d-Convolutional Neural Networks. *Bioinformatics* (2017) 33(19):3036–42. doi: 10.1093/bioinformatics/btx350
- van der Leun AM, Thommen DS, Schumacher TN. Cd8(+) T Cell States in Human Cancer: Insights From Single-Cell Analysis. *Nat Rev Cancer* (2020) 20 (4):218–32. doi: 10.1038/s41568-019-0235-4
- Sanchez-Vega F, Mina M, Armenia J, Chatila WK, Luna A, La KC, et al. Oncogenic Signaling Pathways in the Cancer Genome Atlas. *Cell* (2018) 173 (2):321–37 e10. doi: 10.1016/j.cell.2018.03.035
- Goodman A, Patel SP, Kurzrock R. Pd-1-Pd-L1 Immune-Checkpoint Blockade in B-Cell Lymphomas. Nat Rev Clin Oncol (2017) 14(4):203–20. doi: 10.1038/nrclinonc.2016.168
- Postow MA, Callahan MK, Wolchok JD. Immune Checkpoint Blockade in Cancer Therapy. J Clin Oncol: Off J Am Soc Clin Oncol (2015) 33(17):1974–82. doi: 10.1200/JCO.2014.59.4358
- Gajewski TF, Schreiber H, Fu YX. Innate and Adaptive Immune Cells in the Tumor Microenvironment. Nat Immunol (2013) 14(10):1014–22. doi: 10.1038/ni.2703
- Hinshaw DC, Shevde LA. The Tumor Microenvironment Innately Modulates Cancer Progression. *Cancer Res* (2019) 79(18):4557–66. doi: 10.1158/0008-5472.CAN-18-3962
- Melaiu O, Lucarini V, Cifaldi L, Fruci D. Influence of the Tumor Microenvironment on Nk Cell Function in Solid Tumors. Front Immunol (2019) 10:3038. doi: 10.3389/fimmu.2019.03038
- Liu G-M, Zeng H-D, Zhang C-Y, Xu J-W. Identification of a Six-Gene Signature Predicting Overall Survival for Hepatocellular Carcinoma. *Cancer Cell Int* (2019) 19(1):138. doi: 10.1186/s12935-019-0858-2
- Wang S, Zhang Q, Yu C, Cao Y, Zuo Y, Yang L. Immune Cell Infiltration-Based Signature for Prognosis and Immunogenomic Analysis in Breast Cancer. Brief Bioinform (2020) 22(2):2020–31. doi: 10.1093/bib/bbaa026
- Sui S, An X, Xu C, Li Z, Hua Y, Huang G, et al. An Immune Cell Infiltration-Based Immune Score Model Predicts Prognosis and Chemotherapy Effects in Breast Cancer. *Theranostics* (2020) 10(26):11938–49. doi: 10.7150/thno.49451
- Fu H, Zhu Y, Wang Y, Liu Z, Zhang J, Xie H, et al. Identification and Validation of Stromal Immunotype Predict Survival and Benefit From Adjuvant Chemotherapy in Patients With Muscle-Invasive Bladder Cancer. *Clin Cancer Res* (2018) 24(13):3069–78. doi: 10.1158/1078-0432.CCR-17-2687
- 71. Zhou R, Zhang J, Zeng D, Sun H, Rong X, Shi M, et al. Immune Cell Infiltration as a Biomarker for the Diagnosis and Prognosis of Stage I-Iii Colon Cancer. *Cancer Immunol Immunother* (2019) 68(3):433–42. doi: 10.1007/s00262-018-2289-7

- 72. Carbonaro Sarracino D, Tarantal AF, Lee CC, Martinez M, Jin X, Wang X, et al. Effects of Vector Backbone and Pseudotype on Lentiviral Vector-Mediated Gene Transfer: Studies in Infant Ada-Deficient Mice and Rhesus Monkeys. *Mol Ther* (2014) 22(10):1803–16. doi: 10.1038/mt.2014.88
- Di Pilato M, Kfuri-Rubens R, Pruessmann JN, Ozga AJ, Messemaker M, Cadilha BL, et al. Cxcr6 Positions Cytotoxic T Cells to Receive Critical Survival Signals in the Tumor Microenvironment. *Cell* (2021) 184 (17):4512–30 e22. doi: 10.1016/j.cell.2021.07.015
- 74. Figliuolo da Paz V, Ghishan FK, Kiela PR. Emerging Roles of Disabled Homolog 2 (Dab2) in Immune Regulation. *Front Immunol* (2020) 11:580302. doi: 10.3389/fimmu.2020.580302
- Adamson SE, Griffiths R, Moravec R, Senthivinayagam S, Montgomery G, Chen W, et al. Disabled Homolog 2 Controls Macrophage Phenotypic Polarization and Adipose Tissue Inflammation. J Clin Invest (2016) 126 (4):1311–22. doi: 10.1172/JCI79590
- 76. Hocevar BA, Prunier C, Howe PH. Disabled-2 (Dab2) Mediates Transforming Growth Factor Beta (Tgfbeta)-Stimulated Fibronectin Synthesis Through Tgfbeta-Activated Kinase 1 and Activation of the Jnk Pathway. J Biol Chem (2005) 280(27):25920–7. doi: 10.1074/jbc.M501150200
- Havel JJ, Chowell D, Chan TA. The Evolving Landscape of Biomarkers for Checkpoint Inhibitor Immunotherapy. *Nat Rev Cancer* (2019) 19(3):133–50. doi: 10.1038/s41568-019-0116-x
- Flynn MJ, Sayed AA, Sharma R, Siddique A, Pinato DJ. Challenges and Opportunities in the Clinical Development of Immune Checkpoint Inhibitors for Hepatocellular Carcinoma. *Hepatology* (2019) 69(5):2258–70. doi: 10.1002/hep.30337
- Duffy AG, Ulahannan SV, Makorova-Rusher O, Rahma O, Wedemeyer H, Pratt D, et al. Tremelimumab in Combination With Ablation in Patients With Advanced Hepatocellular Carcinoma. J Hepatol (2017) 66(3):545–51. doi: 10.1016/j.jhep.2016.10.029
- Ramos-Casals M, Brahmer JR, Callahan MK, Flores-Chavez A, Keegan N, Khamashta MA, et al. Immune-Related Adverse Events of Checkpoint Inhibitors. Nat Rev Dis Primers (2020) 6(1):38. doi: 10.1038/s41572-020-0160-6
- Lang X, Green MD, Wang W, Yu J, Choi JE, Jiang L, et al. Radiotherapy and Immunotherapy Promote Tumoral Lipid Oxidation and Ferroptosis via Synergistic Repression of Slc7a11. Cancer Discov (2019) 9(12):1673–85. doi: 10.1158/2159-8290.CD-19-0338
- St Paul M, Ohashi PS. The Roles of Cd8(+) T Cell Subsets in Antitumor Immunity. Trends Cell Biol (2020) 30(9):695–704. doi: 10.1016/ j.tcb.2020.06.003
- Wang L, Hui H, Agrawal K, Kang Y, Li N, Tang R, et al. M(6) a Rna Methyltransferases Mettl3/14 Regulate Immune Responses to Anti-Pd-1 Therapy. *EMBO J* (2020) 39(20):e104514. doi: 10.15252/embj.2020104514
- Phua SZF, Yang G, Lim WQ, Verma A, Chen H, Thanabalu T, et al. Catalase-Integrated Hyaluronic Acid as Nanocarriers for Enhanced Photodynamic Therapy in Solid Tumor. ACS Nano (2019) 13(4):4742–51. doi: 10.1021/ acsnano.9b01087
- Chan LS, Man OY, Kwok HH, Chen L, Chan KC, Lung HL, et al. The Wnt Modulator Icg001 Mediates the Inhibition of Nasopharyngeal Carcinoma Cell Migration in Vitro via the Mir150/Cd44 Axis. Int J Oncol (2019) 54(3):1010– 20. doi: 10.3892/ijo.2018.4664
- Lv Y, Xu C, Zhao X, Lin C, Yang X, Xin X, et al. Nanoplatform Assembled From a Cd44-Targeted Prodrug and Smart Liposomes for Dual Targeting of Tumor Microenvironment and Cancer Cells. ACS Nano (2018) 12(2):1519– 36. doi: 10.1021/acsnano.7b08051
- Wang S, Tian Y, Tian W, Sun J, Zhao S, Liu Y, et al. Selectively Sensitizing Malignant Cells to Photothermal Therapy Using a Cd44-Targeting Heat Shock Protein 72 Depletion Nanosystem. ACS Nano (2016) 10(9):8578–90. doi: 10.1021/acsnano.6b03874
- Xu H, Niu M, Yuan X, Wu K, Liu A. Cd44 as a Tumor Biomarker and Therapeutic Target. *Exp Hematol Oncol* (2020) 9(1):36. doi: 10.1186/s40164-020-00192-0
- Zent CS, Taylor RP, Lindorfer MA, Beum PV, LaPlant B, Wu W, et al. Chemoimmunotherapy for Relapsed/Refractory and Progressive 17p13-Deleted Chronic Lymphocytic Leukemia (Cll) Combining Pentostatin, Alemtuzumab, and Low-Dose Rituximab Is Effective and Tolerable and Limits Loss of Cd20 Expression by Circulating Cll Cells. Am J Hematol (2014) 89(7):757-65. doi: 10.1002/ajh.23737

 Wohlfarth C, Efferth T. Natural Products as Promising Drug Candidates for the Treatment of Hepatitis B and C. Acta Pharmacol Sin (2009) 30(1):25–30. doi: 10.1038/aps.2008.5

Conflict of Interest: The authors declare that the research was conducted in the absence of any commercial or financial relationships that could be construed as a potential conflict of interest.

Publisher's Note: All claims expressed in this article are solely those of the authors and do not necessarily represent those of their affiliated organizations, or those of the publisher, the editors and the reviewers. Any product that may be evaluated in this article, or claim that may be made by its manufacturer, is not guaranteed or endorsed by the publisher.

Copyright © 2022 Tang, Guo, Yang, Wang, Zhang and Wang. This is an open-access article distributed under the terms of the Creative Commons Attribution License (CC BY). The use, distribution or reproduction in other forums is permitted, provided the original author(s) and the copyright owner(s) are credited and that the original publication in this journal is cited, in accordance with accepted academic practice. No use, distribution or reproduction is permitted which does not comply with these terms.



Case Report: Fulminant Celiac Disease With Combination Immune Checkpoint Therapy

Ayo S. Falade^{1*}, Kerry L. Reynolds², Leyre Zubiri², Vikram Deshpande³, Florian J. Fintelmann⁴, Michael Dougan² and Meghan J. Mooradian^{2*}

¹ Department of Medicine, Salem Hospital, Salem, MA, United States, ² Department of Medicine, Massachusetts General Hospital, Boston, MA, United States, ³ Department of Pathology, Massachusetts General Hospital, Boston, MA, United States, ⁴ Department of Radiology, Massachusetts General Hospital, Boston, MA, United States

OPEN ACCESS

Edited by:

Yubin Li, University of Pennsylvania, United States

Reviewed by:

Qiao Lu, NYU Grossman School of Medicine, United States Ling Yin, University of Texas MD Anderson Cancer Center, United States Weiwei Li, University of Cincinnati, United States

> *Correspondence: Ayo S. Falade afalade@partners.org Meghan J. Mooradian mmooradian@mgh.harvard.edu

Specialty section:

This article was submitted to Cancer Immunity and Immunotherapy, a section of the journal Frontiers in Immunology

Received: 08 February 2022 Accepted: 07 March 2022 Published: 14 April 2022

Citation:

Falade AS, Reynolds KL, Zubiri L, Deshpande V, Fintelmann FJ, Dougan M and Mooradian MJ (2022) Case Report: Fulminant Celiac Disease With Combination Immune Checkpoint Therapy. Front. Immunol. 13:871452. doi: 10.3389/fimmu.2022.871452 Since the first approval of immune checkpoint inhibitors (ICIs) in 2011, these agents have rapidly become an integral treatment option across tumor types. However, with the increased adoption of ICIs, the incidence of immune-related adverse events (irAEs) continues to rise, and rare toxicity continues to be reported. Here, we present a case of a 70-year-old male patient with widespread metastatic melanoma who developed rapid onset anasarca and transaminitis after initiation of dual anti-PD-1/CTLA-4 inhibition with nivolumab and ipilimumab. An extensive workup was performed with serologies returning positive for anti-tissue transglutaminase immunoglobulin (tTG-IgA) and endoscopy revealing duodenal mucosal atrophy with duodenal biopsies confirming celiac disease. All symptoms resolved after initiation of a gluten-free diet without the addition of immunosuppression. This case highlights the importance of considering celiac disease in patients with suspected protein-losing enteropathy on ICI, the fulminant nature this uncommon irAE can present with, and underscores the broad differential clinicians must maintain when managing presumed irAEs.

Keywords: immunotherapy, celiac disease, immune-related adverse effects, immune checkpoint inhibitors, immune-related celiac disease

INTRODUCTION

Over the last decade, immune checkpoint inhibitors (ICIs) have revolutionized oncology care with these agents now approved in over a dozen tumor types with indications in the neoadjuvant, adjuvant, and metastatic setting. With their increasing use comes a critical need for clinicians to recognize the variable presentations of immune-related adverse events (irAEs). Luminal gastrointestinal (GI) irAEs are a well-known sequela of ICI (1) with common presentations ranging from mild dyspepsia to severe gastroenterocolitis; however, in rare cases, GI toxicity can also manifest as extraluminal symptoms (2).

ICI-associated celiac disease (ICI-CeD), though rare, is an established irAE (3-5). Similar to traditional celiac disease (CeD), a well-known T-cell-mediated reaction to dietary gluten, it frequently presents with diarrhea and vague abdominal discomfort. When a diagnosis is

suspected in a patient with positive tissue transglutaminase (tTG)-IgA antibody, an upper endoscopy with a small bowel biopsy is recommended to confirm the diagnosis. Classic endoscopic and histologic features include mucosal inflammation, crypt hyperplasia, and villous atrophy of the small bowel (6). Recent data demonstrate that the clinical presentation, endoscopic findings, and response to gluten withdrawal in ICI-CeD mirror those seen in CeD (3). Whether ICI-CeD represents exacerbation of an underlying subclinical disease versus a *de-novo* condition is unclear. According to Badran et al., the approximate incidence of ICI-CeD based on a melanoma cohort is 0.3% of cases of diarrhea on ICI, which highlights the low incidence of CeD among patients treated with ICI therapy (3).

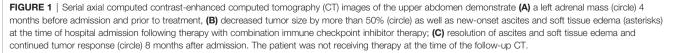
Here, we report an unusual and fulminant presentation of ICI-CeD in a patient with metastatic melanoma receiving combination nivolumab and ipilimumab.

CASE REPORT

A 70-year-old Caucasian male patient with widespread metastatic melanoma (Figure 1A) was initiated on first-line nivolumab (1 mg/kg) and ipilimumab (3 mg/kg) administered every 3 weeks. Restaging scans after two cycles of combination therapy demonstrated a partial response, and the patient reported an improvement in energy and appetite. However, shortly after cycle 2, he developed diarrhea, which slowly escalated from a baseline of two solid bowel movements per day to 4-6 per day by the end of cycle 4. These bowel movements were initially watery but became more formed over time, and he lacked additional GI complaints such as dyspepsia, nausea, vomiting, abdominal cramping, or hematochezia. Infectious stool studies, including Clostridioides difficile testing, were negative. Endoscopy was deferred given improvement in diarrhea. During this time, he developed 1+ edema of the bilateral lower extremities (right > left). A right lower extremity deep venous thrombosis was diagnosed, and he was

started on low molecular weight heparin (LMWH). Despite LMWH, his edema worsened, and serial lab tests demonstrated a slowly downtrending albumin. Upon presentation to the clinic for consideration of cycle 5 of immunotherapy with single-agent nivolumab (his regimen consists of 4 cycles of ipilimumab and nivolumab followed by nivolumab monotherapy), he reported dyspnea on exertion and his exam revealed periorbital edema, ascites, and 3+ pitting edema of bilateral lower extremities. Laboratory evaluation demonstrated significant hypoalbuminemia (1.7 g/dl), hypophosphatemia (1.4 mg/dl), and a rising transaminitis (ALT 65 U/L and AST 62 U/L). Alkaline phosphatase (ALP) was 503 U/L, with the remaining liver function tests within normal limits. He was first admitted to an outside hospital where the cause of his symptoms could not be identified and subsequently transferred to a tertiary care facility for an expedited workup of a suspected immune-mediated toxicity. On arrival, he was hypotensive, and a broad differential was considered for his anasarca and hemodynamic compromise including sepsis, tumor progression, Budd-Chiari syndrome, nephritis with an evolving nephrotic syndrome, myocarditis, heart failure, endocrinopathies (including myxedema and adrenal insufficiency), and protein-losing enteropathy with potential concurrent hepatitis. An extensive workup was performed including viral hepatitis and CMV serologies and Helicobacter pylori stool antigen which were all negative. Urinalysis did not show proteinuria and the protein/ urine creatinine ratio was normal. CT imaging of the chest, abdomen, and pelvis demonstrated continued tumor control although new bilateral ground-glass opacities (GGOs) and pleural effusions were noted, as well as diffuse soft tissue edema and ascites in the abdomen and pelvis (Figure 1B). These findings raised the concern for potential pulmonary and/or cardiac immune-mediated toxicities, as the occurrence of multiple irAEs is a common pattern in hospitalized patients, especially after treatment with combination therapy. A TTE demonstrated a normal ejection fraction. EKG and troponin levels were normal, with an NT-proBNP of 9,768. While hospitalized, his ALP continued to rise with a peak of 566 U/L





with ALT/AST peaking at 91 and 71 U/L, respectively. Stool alpha 1-antitrypsin and tTG Ab IgA were sent. Gastroenterology was consulted due to concern for a protein-losing enteropathy, and an upper and a lower endoscopy were performed with extensive biopsies taken. Endoscopy visualized mild gastric erythema and diffuse mucosal atrophy throughout the duodenum with the visualized colon appearing normal. Duodenal biopsies demonstrated marked villous blunting, intraepithelial lymphocytosis, and expansion of lamina propria (**Figure 2**). Shortly after endoscopy was performed, stool anti-alpha 1-antitrypsin returned negative and tTG-IgA returned positive (>100 U/ml) confirming a diagnosis of celiac disease. In the hospital, the patient received intravenous albumin (12.5 g on October 6, 2020) and furosemide (10 mg IV on October 6, 2020, and 20 mg orally on October 8, 2020) which improved his

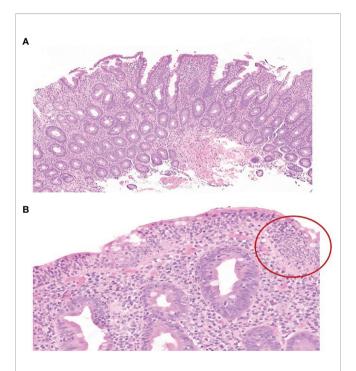


FIGURE 2 | **(A)** H&E-stained slide (×10) of duodenal biopsy demonstrating marked villous blunting, crypt hyperplasia, and expansion of lamina propria by lymphocytes and plasma cells. **(B)** H&E-stained slide (×10) of duodenal biopsy highlights the marked intraepithelial lymphocytosis (circled) without evidence of epithelial injury or neutrophils.

hypotension, bilateral lower extremity edema, and dyspnea. He was ultimately initiated on a gluten-free diet once tTG-IgA resulted. The use of systemic immunosuppression was deferred. His edema resolved after several weeks of dietary adherence. Four months later (**Table 1**), labs demonstrated normalization of albumin values and a decline in tTG-IgA levels (4.40 U/ml). While recovering, immunotherapy was held. Subsequent CT scan (**Figure 1C**) demonstrated persistent disease control and resolution of volume overload.

DISCUSSION

Clinicians are now well trained to identify the most common irAEs. However, less frequent toxicities with atypical presentations remain challenging to diagnose. The initial differential diagnoses entertained in this case due to the severity of symptoms included the more common and/or wellknown irAEs such as enterocolitis, pneumonitis, hepatitis, myocarditis, hypothyroidism, and adrenal insufficiency. However, after an extensive workup, this patient was found to have a fulminant presentation of ICI-CeD where the initial GI complaints were mild (grade 1 diarrhea) and largely resolved despite ongoing duodenal inflammation resulting in a significant protein-losing enteropathy and hepatitis.

Data on ICI-CeD are limited and largely comprised of case reports (4, 5, 7). The largest case series highlighted eight cases of ICI-CeD, confirmed by tTG-IgA. In this report, the authors compared ICI-CeD to CeD as well as to ICI-duodenitis. The clinical presentation and histological findings in CeD, ICI-CeD, and ICIduodenitis were similar; however, patients with CeD and ICI-CeD had positive serologies, and specifically in cases of ICI-CeD, tTG-IgA titers ranged from 104 to >300 IU/ml. Notably, in our case, rather than the common presentation of mild upper GI complaints, ICI-CeD manifested as a severe clinical syndrome of malabsorption with significant hypoalbuminemia resulting in hypotension and diffuse anasarca. As seen in our case, effective management of ICI-CeD centers on strict adherence to a gluten-free diet rather than initiation of systemic immunosuppression. This dietary change does not onlylead to the resolution of symptoms but also spares patients from systemic immunosuppression, which may reduce ICI efficacy (8). In addition to emphasizing the optimal treatment of ICI-CeD and the importance of including this toxicity in the differential diagnosis of potential GI toxicity, this case highlights the

TABLE 1 | Lab values of interest on admission, discharge, and 3 months post-discharge.

	During admission (September 29, 2020)	On discharge (October 8, 2020)	3 months later (January 14, 2021)
Albumin (g/dl)	1.6	1.9	4.0
ALK phos (U/L)	460	371	68
ALT (U/L)	54	61	16
AST (U/L)	44	40	21
tTG-IgA (U/ml)	On October 1, 2020	On November 12, 2020	On March 5, 2021
	>100	16.88	4.40
Magnesium (mg/dl)	1.6	1.7	1.8
Calcium (mg/dl)	7.2	7.4	9.3
LDH (U/L)	237	217	162

extraluminal manifestations of ICI-CeD. Rather than a concomitant ICI hepatotoxicity, our patient's transaminitis and elevated alkaline phosphatase were secondary to ICI-CeD. Though the exact mechanism of cryptogenic liver injury in celiac disease is unknown, levels often normalize after dietary gluten exclusion as was the case in our patient.

Like other irAEs, such as inflammatory arthritis or other rheumatologic disorders, it is difficult to discern if the development of ICI-CeD represents an unmasking of a longstanding subclinical disease or de-novo development of immunemediated gluten sensitivity triggered by ICI use. In the absence of pretreatment tTG-IgA titers in this case, we are unable to discern the exact mechanism of this patient's toxicity. Though ICI-CeD is rare, there may be utility to obtain tTG-IgA titers prior to ICI initiation to identify patients at risk for the evolution of subclinical disease to symptomatic gluten sensitivity. At this time, there are no reliable clinical factors (e.g., age, sex, tumor type, or type of ICI) that are associated with the development of ICI-CeD. Additionally, like other well-known immune-mediated toxicities, we currently lack predictive biomarkers (clinical and/or translational) to identify patients and/or tumor types at risk to develop ICI-CeD. Further research in this space is critical.

In conclusion, ICI-CeD is a rare irAE that often resembles ICImediated colitis; however, it can also present with extraluminal manifestations. As highlighted in our case, ICI-CeD can be a fulminant process. Clinicians needs to maintain a high level of suspicion for ICI-CeD in patients with new-onset GI complaints including LFT abnl as early and accurate diagnosis is important to avoid complications. Furthemore, with an accurate diagnosis of

REFERENCES

- Naidoo J, Page D, Li B, Connell L, Schindler K, Lacouture M, et al. Toxicities of the Anti-PD-1 and Anti-PD-L1 Immune Checkpoint Antibodies. *Ann Of Oncol* (2015) 26(12):2375–91. doi: 10.1093/annonc/mdv383
- Dougan M, Wang Y, Rubio-Tapia A, Lim J. AGA Clinical Practice Update on Diagnosis and Management of Immune Checkpoint Inhibitor Colitis and Hepatitis: Expert Review. *Gastroenterology* (2021) 160(4):1384–93. doi: 10.1053/ j.gastro.2020.08.063
- Badran Y, Shih A, Leet D, Mooradian M, Coromilas A, Chen J, et al. Immune Checkpoint Inhibitor-Associated Celiac Disease. J For Immunother Of Cancer (2020) 8(1):e000958. doi: 10.1136/jitc-2020-000958
- Sethi A, Helfand A, Balikani L, Bunker M, Finley G. Association of Celiac Disease With Pembrolizumab. *Cureus* (2021) 13(6):e15565. doi: 10.7759/cureus.15565
- Arnouk J, Mathew D, Nulton E, Rachakonda V. A Celiac Disease Phenotype After Checkpoint Inhibitor Exposure: An Example of Immune Dysregulation After Immunotherapy. ACG Case Rep J (2019) 6(8):e00158. doi: 10.14309/ crj.000000000000158
- Rubio-Tapia A, Hill I, Kelly C, Calderwood A, Murray J. ACG Clinical Guidelines: Diagnosis and Management of Celiac Disease. Am J Gastroenterol (2013) 108(5):656–76. doi: 10.1038/ajg.2013.79
- Alsaadi D, Shah NJ, Charabaty A, Atkins MB. A Case of Checkpoint Inhibitor-Induced Celiac Disease. J For Immunother Cancer (2019) 7(1):203. doi: 10.1186/ s40425-019-0694-x
- Bai X, Hu J, Betof Warner A, Quach H, Cann C, Zhang M, et al. Early Use of High-Dose Glucocorticoid for the Management of irAE Is Associated With Poorer Survival in Patients With Advanced Melanoma Treated With Anti–PD-1 Monotherapy. *Clin Cancer Res* (2021) 27(21):5993–6000. doi: 10.1158/1078-0432.ccr-21-1283

ICI-CeD, clinicians can employ the optimal treatment of gluten restriction rather than high-dose immunosuppresssion.

DATA AVAILABILITY STATEMENT

The original contributions presented in the study are included in the article/supplementary material. Further inquiries can be directed to the corresponding authors.

ETHICS STATEMENT

Ethical review and approval was not required for the study on human participants in accordance with the local legislation and institutional requirements. The patients/participants provided their written informed consent to participate in this study. Written informed consent was obtained from the individual(s) for the publication of any potentially identifiable images or data included in this article.

AUTHOR CONTRIBUTIONS

AF and MM drafted and edited the case report. KR, LZ, and MD edited the case report. VD edited the case report and provided the pathology slides. FF edited the case report and provided and edited the images for publication. All authors contributed to the article and approved the submitted version.

Conflict of Interest: MM served as a consultant or received honorarium from AstraZeneca, Bristol Myers Squibb, Immunia, Istari Oncology, and Nektar Therapeutics. MD received research funding from Novartis and Eli Lilly; received consulting fees from Tillotts Pharma, ORIC Pharmaceuticals, Partner Therapeutics, SQZ Biotech, AzurRx, Mallinckrodt Pharmaceuticals, and Moderna; received honoraria from WebMD, Experts at Your Fingertips, and Sandoz Academy; and is a member of the Scientific Advisory Board for Neoleukin Therapeutics. KR received research funding from Project DataSphere. LZ served as a consultant for Merck.

The remaining authors declare that the research was conducted in the absence of any commercial or financial relationships that could be construed as a potential conflict of interest.

Publisher's Note: All claims expressed in this article are solely those of the authors and do not necessarily represent those of their affiliated organizations, or those of the publisher, the editors and the reviewers. Any product that may be evaluated in this article, or claim that may be made by its manufacturer, is not guaranteed or endorsed by the publisher.

Copyright © 2022 Falade, Reynolds, Zubiri, Deshpande, Fintelmann, Dougan and Mooradian. This is an open-access article distributed under the terms of the Creative Commons Attribution License (CC BY). The use, distribution or reproduction in other forums is permitted, provided the original author(s) and the copyright owner(s) are credited and that the original publication in this journal is cited, in accordance with accepted academic practice. No use, distribution or reproduction is permitted which does not comply with these terms.



miR-582 Suppresses the Proliferation of B-Cell Precursor Acute Lymphoblastic Leukemia (BCP-ALL) Cells and Protects Them From Natural Killer Cell-Mediated Cytotoxicity

OPEN ACCESS

Edited by:

Yubin Li, University of Pennsylvania, United States

Reviewed by:

Yisi Lu, Boston Children's Hospital and Harvard Medical School, United States Dongxu Jiang, Cleveland Clinic, United States

*Correspondence:

Siyong Huang huangsiyong1980@126.com Minhua Zheng zhengmh@fmmu.edu.cn Hua Han huahan@fmmu.edu.cn [†]These authors have contributed equally to this work

Specialty section:

This article was submitted to Cancer Immunity and Immunotherapy, a section of the journal Frontiers in Immunology

Received: 12 January 2022 Accepted: 16 March 2022 Published: 20 April 2022

Citation:

Li X, Zhang Y, He F, Gao D, Che B, Cao X, Huang S, Zheng M and Han H (2022) miR-582 Suppresses the Proliferation of B-Cell Precursor Acute Lymphoblastic Leukemia (BCP-ALL) Cells and Protects Them From Natural Killer Cell-Mediated Cytotoxicity. Front. Immunol. 13:853094. doi: 10.3389/fimmu.2022.853094 Xinxin Li^{1,2†}, Yufei Zhang^{3†}, Fei He^{4†}, Dan Gao³, Bo Che³, Xiuli Cao⁵, Siyong Huang^{6*}, Minhua Zheng^{5*} and Hua Han^{3*}

¹ Xi'an Key Laboratory of Stem Cell and Regenerative Medicine, Institute of Medical Research, Northwestern Polytechnical University, Xi'an, China, ² Research and Development Institute of Northwestern Polytechnical University in Shenzhen, Shenzhen, China, ³ State Key Laboratory of Cancer Biology, Department of Biochemistry and Molecular Biology, Fourth Military Medical University, Xi'an, China, ⁴ Department of Hepatobiliary Surgery, Xijing Hospital, Fourth Military Medical University, Xi'an, China, ⁵ Department of Medical Genetics and Developmental Biology, Fourth Military Medical University, Xi'an, China, ⁶ Department of Hematology, Xi'an International Medical Center Hospital, Xi'an, China

B-cell precursor acute lymphoblastic leukemia (BCP-ALL) is a malignancy characterized by the aberrant accumulation of immature B-cell precursors in bone marrow and other lymphoid organs. Although several intrinsic regulatory signals participating in BCP-ALL have been clarified, detailed intrinsic and extrinsic mechanisms that regulate BCP-ALL progression have not been fully understood. In the current study, we report that miR-582 is downregulated in BCP-ALL cells compared with normal B cells. Forced overexpression of miR-582 attenuated BCP-ALL cell proliferation and survival. We found that miR-582 overexpression disturbed the mitochondrial metabolism of BCP-ALL cells, leading to less ATP but more ROS production. Mechanistically, we identified PPTC7 as a direct target of miR-582. MiR-582 overexpression inhibited the activity of CoQ10, which is downstream of PPTC7 and played an important positive regulatory role in mitochondrial electron transportation. Finally, we found that overexpression of miR-582 upregulated the expression of immune checkpoint molecule CD276 and reduced NK cell-mediated cytotoxicity against BCP-ALL cells. CD276 blockade significantly increased NK cellmediated cytotoxicity against miR-582-overexpressing BCP-ALL cells. Together, our research demonstrates that miR-582 acts as a negative regulator of BCP-ALL cells by reducing proliferation and survival, but protects BCP-ALL cells from NK cell-mediated cytotoxicity, suggesting that miR-582 may be a new therapeutic biomarker for BCP-ALL with CD276 blocker.

Keywords: BCP-ALL, miR-582, PPTC7, mitochondria, metabolism, NK cells, immune checkpoint, CD276

INTRODUCTION

B-cell precursor acute lymphoblastic leukemia (BCP-ALL) is a type of hematopoietic malignancy found both in children and adults, and is characterized by the aberrant expansion of immature clonal B-cell precursors in bone marrow (BM), peripheral blood and lymphoid organs (1, 2). Although the prognosis of BCP-ALL has improved, the therapeutic effect of BCP-ALL patients with relapsed and drug-resistant remain unsatisfactory, and specifically, the 5-year survival rate for these types of patients is 35-40% (3). Previous studies have reported that during the development of B cells in BM, the disruption of the balance between pre-B cell proliferation and apoptosis is one of the important factors leading to the pathogenesis of BCP-ALL (4). Therefore, elucidating the regulatory mechanisms of BCP-ALL cells' proliferation and survival is an important research focus for developing novel therapeutic approaches for BCP-ALL.

The progression of BCP-ALL is influenced by cell-intrinsic programs and the tumor microenvironment (TME) (5). In the TME of progressive BCP-ALL, anti-tumor immune cells, such as natural killer (NK) cells and CD8⁺ T cells, are prone to exhaust, lose or attenuate their cytotoxic activity against tumor cells, thus promoting tumor cell survival and proliferation (6, 7). Cellintrinsic programs such as energy metabolism also play critical roles in regulating the survival and proliferation of BCP-ALL cells (8). For instance, electron transport chain (ETC) in mitochondria plays an essential role in energy metabolism, which is critically involved in the expansion of BCP-ALL cells (9). Specifically, the main function of ETC is transports electrons to generate ATP, which ultimately provides energy for cell survival and proliferation (10). Coenzyme Q10 (CoQ10), which is a crucial electron transporter of ETC, is involved in regulating the survival of B cells and T cells (11). Previous studies have shown that, compared with the control group, increasing the concentration of CoQ10 can promote the electron transport and improve the ATP synthesis, and reduce the generation of reactive oxygen species (ROS) (12). Protein phosphatase targeting CoQ7 (PPTC7), an important member of the protein phosphatase 2C (PP2C) family, has been reported to regulate the phosphorylation and dephosphorylation of protein complexassociated molecules which involved in electron transport (13) and CoQ10 production (14). Previous studied have shown that PPTC7 is a regulator of CoQ10 biosynthesis, and PPTC7/CoQ10 signaling facilitates ATP synthesis while preventing the accumulation of ROS, further promoting cell survival (14). However, whether PPTC7/CoQ10 signaling regulates BCP-ALL cell proliferation and survival, and the underlying regulatory mechanisms, remain unknown. Therefore, more studies are required to elucidate the exact regulatory mechanisms of PPTC7/CoQ10 signaling in BCP-ALL cell proliferation and survival.

miRNAs are endogenous ~22 nt non-coding RNAs that downregulate protein expression by inhibiting target mRNA translation or promoting mRNA degradation (15). Previous reports indicated that miR-582 serves as an anti-oncogenic biomarker in many cancers, such as in intermediate risk AML (16), colorectal carcinoma (17). Recently, our lab found that miR-582 was highly expressed in murine pre-B cells, and knockout of miR-582 promotes the proliferation of murine pre-B cells (18). Relevant clinical studies also found that, compared with normal B cells, the expression of miR-582 is significantly lower in B cells of multiple sclerosis and B cells of dysregulated chronic lymphocytic leukemia (19, 20). MiR-582 expression in B cells from MLL rearranged pediatric acute lymphoblastic leukemia patients was significantly lower than that in other ALL patients (21). The above-mentioned research results indicated that dysregulated miR-582 expression may be involved in BCP-ALL progression. However, the specific regulation and mechanism of miR-582 in BCP-ALL needs further verification.

In the TME, miRNAs can not only regulate intracellular signaling pathways involved in cell survival and proliferation, but also alter the expression of immune checkpoint (IC) proteins on cell surface, such as PD-1/PD-L1 (22), CTLA-4 (23), CD276 (24), to subvert host immune surveillance. Recently, increasing evidence has indicated that IC molecules regulate the cytotoxic activity of T cells and NK cells. NK cells are important innate immune cells and have the ability to directly kill tumor cells without prior sensitization (25). Previous researches have shown that, in the TME, low expression of miR-29c and miR-142-5p upregulates the expression of some IC molecules such as CD276 and PD-L1, which further suppress the cytotoxic activity of NK cells and CD8⁺ T cells (26, 27). In diffuse large B cell lymphoma (DLBCL), overexpression of miR-5590-3p upregulates PD-L1 expression, and the high expression of PD-L1 on DLBCL cells promotes immune escape by inhibiting the cytotoxic activity of CD8⁺ T cells (28). However, whether miR-582 can regulate the expression of IC molecules on BCP-ALL cells and affect the cytotoxic activity of NK cells remains unknown. In this study, we show that overexpression of miR-582 inhibits the proliferation and survival of BCP-ALL cells. Moreover, we demonstrate that miR-582 directly regulates PPTC7/CoQ10 signaling to regulate BCP-ALL. We also showed that miR-582 overexpression promotes the expression of CD276 and protect BCP-ALL cells from NK cell-mediated cytotoxicity, which was reversed by anti-CD276 antibody.

MATERIALS AND METHODS

Human Samples

BM samples were collected from BCP-ALL patients (n = 5) and non-BCP-ALL controls (n = 4, patients with unexplained anemia but excluded hematopoietic malignancies) hospitalized in the Department of Hematology, Xi'an International Medical Center Hospital, with signed informed consent and approved by the Ethics Committee of Fourth Military Medical University for use of human samples (**Supplementary Table S2**). B cells were enriched from BM by using MACSxpress B cell isolation kit (Miltenyi Biotec, USA) and erythrocyte depletion kit (Miltenyi Biotec, USA). The purity of the enriched B cells was > 90% as determined by using flow cytometry after CD19 staining. In some cases, B cells were further purified to > 99% purity by using FACS Aria II cell sorter (BD Biosciences, USA) after gating on $CD19^+$ cells.

Mice

NCG (NOD/ShiLtJGpt-*Prkdc*^{em26Cd52}*Il2rg*^{em26Cd22}/Gpt) mice (8 weeks old, female) were purchased from Gem Pharmatech (Nanjing, China). Mice were maintained in a specific pathogen-free (SPF) facility. All animal experiments were performed in accordance with the protocols approved by the Animal Experiment Administration Committee of the Fourth Military Medical University.

Cell Culture, Infection, and Treatment

BCP-ALL cell lines (NALM-6, KOPN-8, and SUP-B15) and NK cells were obtained from the Beijing Beina Chuanglian Biotechnology Institute (Beijing, China). Specifically, NALM-6 and SUP-B15 cells were maintained in Roswell Park Memorial Institute 1640 (RPMI-1640) medium (Invitrogen, USA) supplemented with 10% FBS, 2 mM L-glutamine, 100 U/mL penicillin and 100 μ g/mL streptomycin. KOPN-8 cells were maintained in Iscove's Modified Dulbecco Medium (IMDM) (Invitrogen, USA) supplemented with 10% FBS, 2 mM L-glutamine, 100 U/mL penicillin and 100 μ g/mL streptomycin and incubated at 37°C in 5% CO₂ and 95% air. NK cells were maintained in complete medium with 1000 U/ml recombinant human IL-2. Cells were routinely tested for the absence of mycoplasma using MycoAlertTM PLUS Mycoplasma Detection Kit (Lonza, USA).

In order to test the infection efficiency of lentivirus on BCP-ALL cells, we infect cells with EGFP-labeled lentivirus (MOI of 60), after 24 hours (h), we tested the infection efficiency by flow cytometry, and found that the infection efficiency of BCP-cells > 99% (Supplementary Figure S1A). Then, to overexpress human single-stranded mature miR-582 in BCP-ALL cells, a synthetic precursor miR-582 [pre-miR-582] gene fragment was inserted into the lentiviral vector GV309. After the lentivirus package and infection of BCP-ALL cells, pre-miR-582 was expressed and further cleaved by Dicer to form single-stranded, mature miR-582. Specifically, for infection, cells $(1 \times 10^6/\text{well})$ were seeded in 96-well plates. Lentivirus particles were added at a multiplicity of infection (MOI of 60), and cultured for 12 h, then the medium was changed and cultured for 72h according to experimental designs. In some experiments, PPTC7 overexpressing lentivirus (MOI of 60), PPTC7 overexpressing lentivirus (MOI of 60) with premiR-582 overexpressing lentivirus (MOI of 60) was used to infect BCP-ALL cells. In some experiments, the anti-CD276 antibody (100ng/well, MGA271) was added to the cultures.

Cell Proliferation and Apoptosis

Cell proliferation and apoptosis assays were performed as described previously (18). Specifically, after infection with lentivirus for 48 h, NALM-6, KOPN-8 and SUP-B15 cells (1 × 10^6 /well) were resuspended in PBS in tubes and incubated with 5,6-carboxyfluorescein diacetate succinimidyl ester (CFSE) (Biolegand, USA) at the concentration of 3 μ M for 20 min in cell incubator, followed by adding 10% FBS-containing medium

to quench CFSE. After washing twice by using10% FBS medium, cells were resuspended in culture medium and cultured in 96-well U bottom plates for another 24 h, and the proliferation was analyzed by flow cytometry.

To evaluate apoptosis, cells $(1 \times 10^6 \text{ cells/well})$ were resuspended in 100 µl binding buffer, prior to the addition of 5 µL Annexin V (Biolegand, USA) and incubated for 15 min. Then, cells were washed twice with the binding buffer, and 200 µL of binding buffer and 5 µL 7-AAD were added. The percentage of live cells, early and lately apoptotic cells were analyzed by flow cytometry.

ATP Measurement

ATP level was determined by using an ATP assay kit (Beyotime Biotechnology, China) according to the manufacturer's instructions. Briefly, cells were broken by the lysis buffer, and the supernatant was gathered and mixed with the ATP detecting solution. The ATP level was detected by firefly luciferase activities with a luciferase assay system (Promega, USA).

Extracellular Flux Analysis

Extracellular flux analyses were carried out with a Seahorse XF-24 analyzer. BCP-ALL cells (5×10^{5} /well) are adhere-cultured with PLL-coated plate for 12 h. Then, cells were washed three times in the Seahorse assay medium. Mitochondrial metabolism (OCRs) was analyzed with Seahorse Mito Test kits (Agilent, Waldbronn, Germany) according to the manufacturer's instructions.

ROS Generation Assay

For cellular total ROS detect, 2^{-} ,7'-dichlorofluorescin diacetate (DCFH-DA, Beyotime, China) was diluted by serum-free medium to a concentration of 10 μ M. Then, cells were resuspended in DCFH-DA medium and incubated at 37°C for 30 min. For mitochondrial ROS detect, cells were re-suspended in medium containing 10 μ M DCFH-DA and 25 nM MitoTacker (Invitrogen, USA), and incubated at 37°C for 30 min. Cells were washed twice with serum-free medium and analyzed by flow cytometry.

Glucose Uptake Assay

For glucose uptake assay, cells were pelleted at 500 g for 5 min at 4°C and then washed twice with glucose-free medium. The 2-deoxy-2-[(7-nitro-2,1,3-benzoxadiazol-4-yl)amino]-D-glucose (2-NBDG, Cayman Technologies, USA) was diluted to the concentration of 150 μ g/mL in glucose-free medium. Then, the 2-NBDG dilution (100 μ L) was added to the glucose-free medium and incubated at 37°C for 30 min. Finally, the cells were washed twice with PBS to remove the residual 2-NBDG and analyzed by flow cytometry.

RNA-Seq Analysis

NALM-6 cells were infected with pre-miR-582 lentivirus or premiR-Ctrl lentivirus for 72 h, and total cellular RNA was isolated using the TRIzol reagent. RNA was reverse-transcribed into cDNA for constructing the library. Then, RNA sequencing was conducted with the cDNA library. RNA sequencing using Illumina Novaseq6000 by Gene Denovo Biotechnology Co. (Guangzhou, China). The raw reads were filtered, and clean reads were mapped to Ensembl_release103 whole genome using HISAT2.2.4. The mapped reads of each sample were assembled by using StringTie v1.3.1 in a reference-based approach. For each transcription region, a FPKM (fragment per kilobase of transcript per million mapped reads) value was calculated to quantify its expression abundance and variations, using the StringTie software. Original RNA-seq data have been deposited in the NCBI (https://www.ncbi.nlm.nih.gov/sra/PRJNA811525). The online tools (http://www.omicshare.com/tools) were used for the subsequent bioinformatic analysis.

Human BCP-ALL Xenograft Mouse Model

NCG mice were inoculated with 1×10^6 NALM-6 cells which infected with lentivirus expressing pre-miR-Ctrl or pre-miR-582 together with luciferase through tail veins (day 0). On day 14 and 21, tumor burden was determined by IVIS[®] Spectrum *In Vivo* Imaging System in each mouse. BM and spleen cells were collected on day 21, and the proportion and number of human CD19⁺ NALM-6 cells were detected by flow cytometry. Finally, the survival days of tumor-bearing mice were recorded and a survival curve was drawn.

Cytotoxicity Assay

Cytotoxicity assays were performed as described previously (25). NALM-6, KOPN-8 and SUP-B15 cells were co-cultured with the effector NK cells in a 96-well V-bottom plate at 37°C for 4 h. At the end of the co-culture, cells were collected and incubated with anti-human CD56, anti-human CD107a antibodies against surface markers to label NK cells and the degranulation marker of NK cells. Cells were then washed and resuspended in Cytofix/Cytoperm solution (BD Biosciences) at 4°C for 30 min. Fixed and permeabilized cells were stained with anti-human Granzyme B (GZMB) antibody for analysis by flow cytometry. Data were analyzed using FlowJo V10 software (Tree Star, Ashland, OR).

Statistical Analysis

GraphPad Prism 7.0 software (GraphPad Software, USA) and SAS8e software were used for statistical analyses. Student's t-test or paired t-test was used to compare two independent or paired groups. Kaplan-Meier method was used to estimate survival functions and log-rank test was used to compare any two survival curves. All results are expressed as mean \pm SD. *P* < 0.05 was considered statistically significant.

RESULTS

miR-582 Is Downregulated in BCP-ALL Cells

Aberrant expression of miR-582 has been implicated in several solid tumors including non-small cell lung cancer (29, 30), prostate cancer (31), and hepatocellular carcinoma (32). Our lab recently found that miR-582 represses pre-B proliferation in early B cell development in mice (18). To evaluate whether miR-582 regulates BCP-ALL progression, we examined the expressions of

miR-582-5p and miR-582-3p in B cells from BCP-ALL patients or controls, and BCP-ALL cell lines NALM-6, KOPN-8, and SUP-B15. The results showed that, compared with the controls, miR-582-5p and miR-582-3p were downregulated in B cells from BCP-ALL patients and the BCP-ALL cell lines (**Figures 1A, B**), suggesting that miR-582 is potentially involved in BCP-ALL.

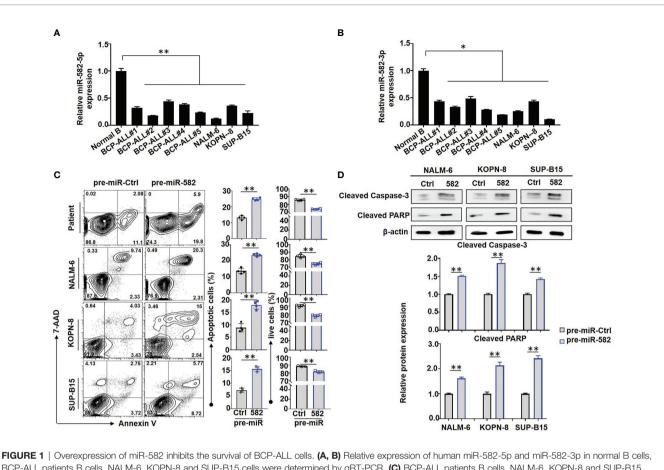
miR-582 Inhibits the Proliferation and Promotes the Apoptosis of BCP-ALL Cells

We next accessed the function of miR-582 in BCP-ALL cells. BCP-ALL cells were infected with pre-miR-582 or pre-miR-Ctrl (control) lentivirus, firstly, we evaluate the overexpression efficiency by using qRT-PCR method, the results showed that, compared with control group, the expression of miR-582-5p is significantly increased in pre-miR-582 group (Supplementary Figure S1B). Then we stained with Annexin V and 7-AAD prior to flow cytometry. The result showed that, compared with premiR-Ctrl infected cells, the proportion of apoptosis (Annexin $V^{+}/7$ -AAD^{+/-}) cells was significantly increased and the proportion of live (Annexin V⁻/7-AAD⁻) cells was significantly decreased in pre-miR-582 infected cells (Figure 1C). Western blotting confirmed that overexpression of miR-582 significantly increased the expression of Cleaved caspase-3 and Cleaved PARP proteins, two makers of apoptosis (33, 34) (Figure 1D). We also examined the role of miR-582 in regulating BCP-ALL proliferation. BCP-ALL cells were infected with pre-miR-582 or control lentivirus for 48 h, and labeled with CFSE for another 24 h prior to flow cytometry analysis. The result showed that, compared with the control infected cells, the proportion of CFSE^{low/-} BCP-ALL cells in pre-miR-582 infected cells was significantly decreased (Figure 2A). By using the MTT assay, we found that, compared with control group, the cell viability and proliferation ability in pre-miR-582 infected BCP-ALL cells were significantly reduced, which confirming the above data (Figure 2B). These results suggested that miR-582 inhibits the proliferation and promotes the apoptosis of BCP-ALL cells.

Next, firefly luciferase-expressing NALM-6 cells were infected with pre-miR-582 or control lentivirus for 24 h, and cells were injected intravenously (i.v) into NCG mice to establish an orthotopic xenograft NALM-6 model. Tumor growth was monitored by bioluminescence imaging, starting at day 14 after the infusion of tumor cells (**Figure 2C**). The results showed that, compared with the control group, tumor progression in the premiR-582 infected group was significantly inhibited on day 14 and 21 (**Figure 2D**). Consistently, the proportion and number of tumor cells in BM and spleen were significantly decreased in premiR-582 infected group as compared with the control (**Figures 2E, F**). The survival of tumor-bearing mice was significantly longer in the pre-miR-582 infected group than the control group (**Figure 2G**).

miR-582 Inhibits Mitochondrial Energy Metabolism of BCP-ALL Cells

Previous studies have demonstrated that mitochondrial energy metabolism plays an important role in regulating BCP-ALL cell survival and proliferation (8). We next tested whether



BCP-ALL patients B cells, NALM-6, KOPN-8 and SUP-B15 cells were determined by qRT-PCR. (C) BCP-ALL patients B cells, NALM-6, KOPN-8 and SUP-B15 cells were infected with pre-miR-582 lentivirus or their control lentivirus, and cultured for 72 h. Apoptosis was evaluated by using flow cytometry after staining of Annexin V and 7-AAD. The percentages of infected live (Annexin V⁻⁷7-AAD) BCP-ALL cells, infected early and late apoptotic (Annexin V⁺/7-AAD^{-/+}) BCP-ALL cells were quantitatively compared (n = 3-4). (D) BCP-ALL cells were infected with pre-miR-582 lentivirus or their control lentivirus for 72 h, and Cleaved Caspase-3, Cleaved PARP proteins were determined by Western blotting, with β -actin as an internal control (n = 3). Bars represent means \pm SD, **P* < 0.05, ***P* < 0.01.

mitochondrial energy metabolism is involved in regulating BCP-ALL cell proliferation and survival by miR-582. We found that overexpression of miR-582 significantly reduced the content of ATP in BCP-ALL cells (Figure 3A). We then used the extracellular flux analyses with a Seahorse device to detect the O₂ consumption rate (OCR) of BCP-ALL cells. The result showed that overexpression of miR-582 reduced the OCR (the basal respiration, ATP production and maximal respiration) of BCP-ALL cells (Figure 3B). However, the spare respiratory capacity did not decrease significantly in pre-miR-582-infected BCP-ALL cells, except in NALM-6 cells (Figure 3B and Supplementary Figure S3). These results suggested that miR-582 inhibits mitochondrial energy metabolism of BCP-ALL cells, but there is no difference in the ability of BCP-ALL cells to respond to the demand for spare respiratory capacity, except in NALM-6 cells.

Next, we investigated the effect of miR-582 on ROS production in BCP-ALL cells, the results showed that miR-582 overexpression significantly increased total and mitochondrial ROS production in BCP-ALL cells as compared with the control (**Figures 3C, D; Supplementary Figure S2**). Moreover, compared with the control, overexpression of miR-582 significantly inhibit the glucose uptake in BCP-ALL cells (**Figure 3E**). These results indicated that miR-582 overexpression inhibits mitochondrial energy metabolism and promotes ROS production in BCP-ALL cells.

miR-582 Downregulates PPTC7 in BCP-ALL Cells

To address the molecular mechanism of miR-582 regulating energy metabolism in BCP-ALL cells, we compared the transcriptomes of NALM-6 cells infected with pre-miR-582 or control lentivirus. The result showed that miR-582 overexpression upregulated the mRNA expression of 106 genes and downregulated 140 genes (Figure 4A). Among the 140 downregulated genes, 94 genes are metabolism-related genes (Figure 4B). Further analyses of RNA-seq data and potential miR-582 targets using the TargetScan 6.2 database identified 7 metabolism-related and downregulated genes as predicted target genes of human miR-582-5p (Figure 4C), including PPTC7, a gene reported to play an important role in mitochondrial energy metabolism (Figures 4D, E). QRT-PCR confirmed that infection of the pre-miR-582 lentivirus significantly downregulated the

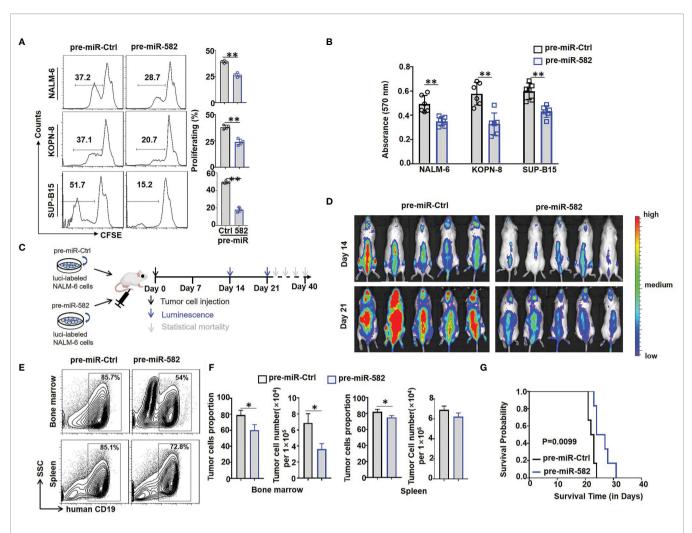


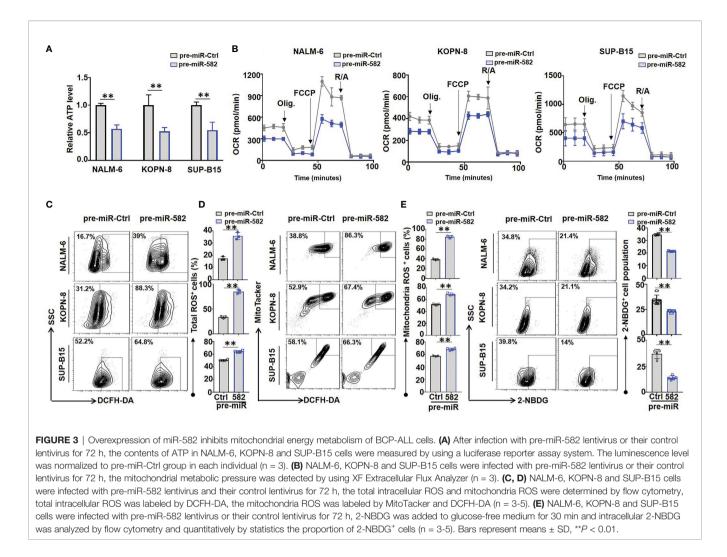
FIGURE 2 | Overexpression of miR-582 inhibits the proliferation of BCP-ALL cells. (A) NALM-6, KOPN-8 and SUP-B15 cells were infected with pre-miR-582 lentivirus or their control lentivirus. Cell proliferation of infected cells was determined using the CFSE labeling assay (n = 3-6). (B) NALM-6, KOPN-8 and SUP-B15 cells were infected with pre-miR-582 lentivirus or their control lentivirus or their control lentivirus or their control lentivirus, and cultured for 72 h. Cell viability was detected by MTT method (n = 6). (C, D) Experimental timeline for *in vivo* study. luciferase (luci)-labeled NALM-6 were infected with pre-miR-582 lentivirus or their control lentivirus, then, an orthotopic xenograft BCP-ALL mouse model was established by i.v injecting 1 × 10⁶ luci-labeling pre-miR-582 NALM-6 cells or pre-miR-Ctrl NALM-6 cells into NCG mice on day 0. Tumor burden was determined on day 14 and 21. (E, F) On Day 21, single cell suspensions of BM and spleen from BCP-ALL mouse model were analyzed by flow cytometry (E), and the percentage of human CD19⁺ B cells were quantitatively compared (F) (n = 3). (G) Survival of NCG mice which injected with miR-582-overexpressing NALM-6 cells and control NALM-6 cells. Bars represent means \pm SD, **P* < 0.05, ***P* < 0.01.

mRNA expression of PPTC7 in all three BCP-ALL cell lines (Figure 4F).

The 3'UTR of PPTC7 contains a miR-582-5p recognition site. We cloned the PPTC7 3'UTR fragment harboring the miR-582-5p binding site, and constructed reporter genes with the wild type of fragment or the fragment with the mutated binding site (**Figures 4G, H**). Transfection of miR-582-5p mimics into HEK-293T cells significantly suppressed the wild-type (WT) reporter activity but failed to suppress the reporter with the mutated (MUT) PPTC7 3'UTR (**Figure 4I**). Moreover, we found that overexpression of miR-582 significantly inhibited the protein expression of PPTC7 in NALM-6, KOPN-8 and SUP-B15 cells (**Figures 4J, K**). Taken together, these results verified that miR-582 directly targets the 3'UTR of PPTC7 to inhibit PPTC7 expression in BCP-ALL cells.

miR-582 Attenuates Mitochondrial Energy Metabolism by Inhibiting PPTC7/CoQ10 Signaling in BCP-ALL Cells

To further evaluate the role of PPTC7 in miR-582-mediated mitochondrial energy metabolism, we examined the effects of miR-582 overexpression on CoQ10 production, which is reported to be a downstream molecule of PPTC7 in Hela cells (14). BCP-ALL cells were infected with pre-miR-582 or control lentivirus for 72 h, and CoQ10 content was examined. The results showed that miR-582 overexpression inhibited the CoQ10 production in the three BCP-ALL cell lines (**Figure 5A**). We then infected BCP-ALL cells with PPTC7 overexpression lentivirus, and found that PPTC7 overexpression strongly promotes the mitochondrial energy metabolism, including promote the production of CoQ10 and



ATP, inhibit the production of ROS (**Figures 5B–E**), which demonstrated that PPTC7 positively regulate mitochondrial energy metabolism through COQ10 in BCP-ALL cells. However, compared with the PPTC7 overexpression group, simultaneous overexpression of PPTC7 and miR-582 partially suppressed the increase in COQ10 and ATP production, and promoted the generation of ROS (**Figures 5B–E**). These results suggested that miR-582 attenuates mitochondrial energy metabolism of BCP-ALL cells *via* inhibiting PPTC7/CoQ10 signaling.

miR-582 Overexpression Protects BCP-ALL Cells From NK Cell-Mediated Cytotoxicity

The IC molecules, such as PD-1, CTLA-4 and CD276, inhibit the cytotoxic activity and promote the exhaustion of NK cells and T cells (26, 27). RNA-seq results of NALM-6 cells showed that, compared with the control, miR-582 overexpression significantly upregulated the mRNA expression of CD276, which is an important IC molecule inhibiting NK-mediated cytotoxicity (26) (**Figure 6A**). Then, three BCP-ALL cell lines were infected with pre-miR-582 and control lentivirus for 72 h, and the expression of CD276 was

examined. The results showed that, compared with the control, miR-582 overexpression significantly increased the mRNA and protein expression of CD276 (Figures 6B, C and Supplementary Figure S4A). We further determined whether miR-582 overexpression could protect BCP-ALL cells from NK cellmediated cytotoxicity by upregulating CD276. The cytotoxicity assay showed that, compared with the control group, the expression of CD107a and GZMB was significantly reduced in NK cells co-cultured with miR-582-overexpressing BCP-ALL (NALM-6, KOPN-8, as well as SUP-B15) cells (Figures 6D, E; Supplementary Figures S4B, C). Treat with anti-CD276 antibody significantly increased the NK cell-mediated cytotoxicity on BCP-ALL cells with miR-582 overexpression (Figures 6D, E). These results suggested that miR-582 upregulates CD276 to protect BCP-ALL cells from NK cell-mediated cytotoxicity.

DISCUSSION

In this study, we report that miR-582 regulates BCP-ALL progression by negatively regulating the survival and proliferation of BCP-ALL

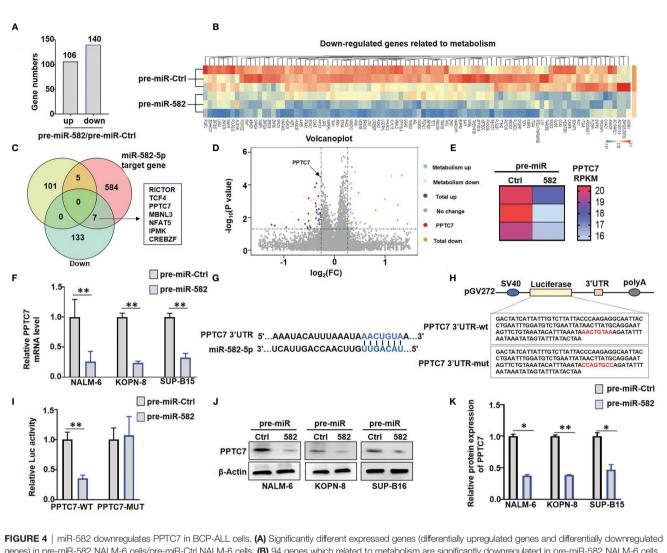
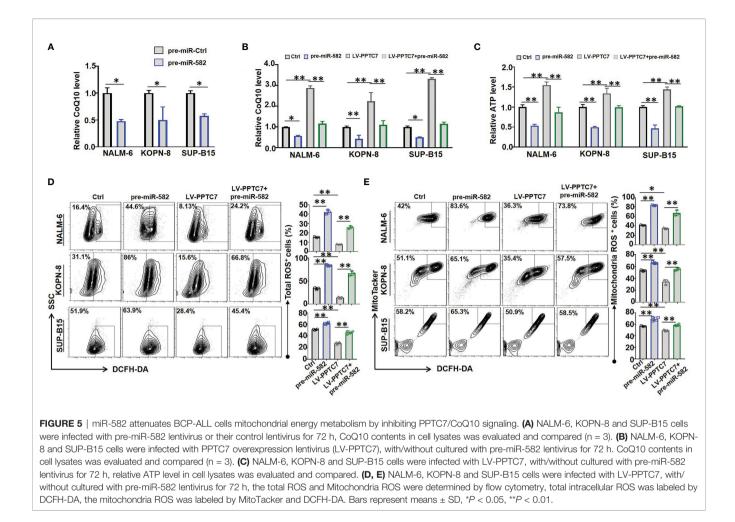


FIGURE 4 | miR-582 downregulates PPTC7 in BCP-ALL cells. (A) Significantly different expressed genes (differentially upregulated genes and differentially downregulated genes) in pre-miR-582 NALM-6 cells/pre-miR-Ctrl NALM-6 cells. (B) 94 genes which related to metabolism are significantly downregulated in pre-miR-582 NALM-6 cells. (C) 7 significantly downregulated metabolism-related genes were predicted target genes of human miR-582-5p by combined with RNA-seq data and TargetScan 6.2 database. (D, E) The mRNA expression of PPTC7 in pre-miR-Ctrl NALM-6 cells and pre-miR-582 NALM-6 cells were showed by volcano plot and heatmap. (F) NALM-6, KOPN-8 and SUP-B15 cells were infected with pre-miR-582 lentivirus or their control lentivirus for 72 h, and PPTC7 mRNA were determined by qRT-PCR, with β-actin as an internal control (n = 3). (G) Alignment of the seed sequence of human miR-582-5p with human PPTC7 3'UTR. Complementary bases are marked with blue color. (H) The sequences of PPTC7 3'UTR-wut used for schematic of the reporter constructs. (I) HEK293T cells were transfected with miR-582-5p and different 3'UTR reporters of human PPTC7 for 72 h. Luciferase activity in cell lysates were determined by the dual luciferase reporter assay (n = 3). (J, K) NALM-6, KOPN-8 and SUP-B15 cells were infected with pre-miR-582 lentivirus or their controls for 72 h, and PPTC7 protein were determined by Western blotting, with β-actin as an internal control (n = 3). Bars represent means \pm SD, *P < 0.05,**P < 0.01.

cells. We have identified that the PPTC7, which regulates CoQ10 production and mitochondrial energy metabolism, is the downstream target of miR-582 involved in regulating the survival and proliferation of BCP-ALL cells. We also found that miR-582 overexpression promotes the expression of CD276 and protects BCP-ALL cells from NK cell-mediated cytotoxicity, which can be overcome by CD276 blockade with a specific antibody (**Figure 6F**). Our observations in clinical samples suggest that miR-582 is downregulated in BCP-ALL, therefore these findings provide a new molecular mechanism of BCP-ALL progression, and suggest that low miR-582 may provide progression advantages in human BCP-ALL, which may insensitive to anti-CD276 therapy.

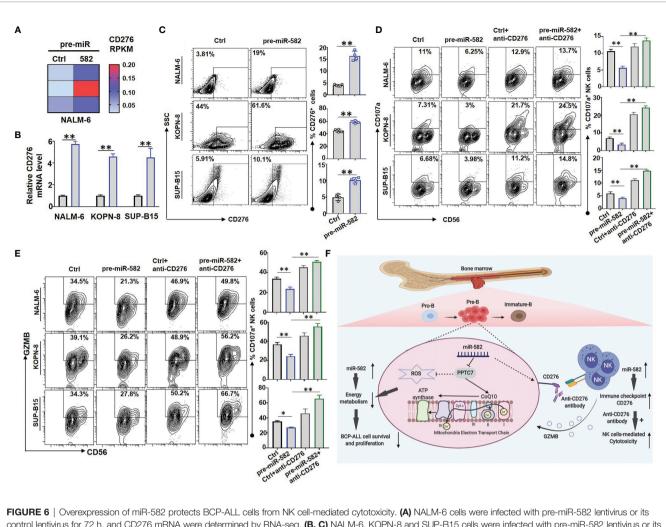
Previous studies have established a link between miR-582 and tumor procession (30, 35). For instance, in hematopoietic malignancies and solid tumors, such as acute myeloid leukemia (36), chronic lymphocytic leukemia (37), multiple myeloma (38), bladder cancer (39), and human colorectal carcinoma (17), miR-582 serves as an anti-oncogenic biomarker and can inhibit proliferation and induce apoptosis of these malignant cells by targeting different genes, such as cyclin B2, HNRNPA1, HMGB2 and Rab27a (17, 35–38). These studies have shown that miR-582 plays a negative regulatory role in tumor progression. Recently, miR-582 has also been found to participate in regulating several energy metabolism-related genes, such as ERO1A (40) and AKT/



mTOR signaling (41), in different biological processes. Our lab has found that miR-582 is highly expressed in murine pre-B cells, and knockout of miR-582 promotes pre-B cell proliferation, while overexpression of miR-582 inhibits pre-B cell proliferation (18). Consistently, in this study, we revealed an anti-oncogenic role of miR-582 in BCP-ALL. These findings indicated that miR-582 may serve as an important molecule in BCP-ALL progression, and miR-582 overexpression in BCP-ALL cells could be a potential strategy for inhibit BCP-ALL progression.

Tumor cells are characterized by extensive proliferation, in which mitochondrial energy metabolism plays an important role (42). Previous researches have shown that improving mitochondrial energy metabolism promotes the survival and proliferation of BCP-ALL cells (8). A recent study further found that mitochondrial energy metabolism was significantly decreased in PPTC7 downregulated cells, resulting in decreased ATP synthesis and increased ROS production (13), indicating that PPTC7 plays a key role in the mitochondrial energy metabolism pathway of cells. In our study, we have provided evidence that miR-582 downregulates mitochondria energy metabolism at least partially *via* directly targeting PPTC7, which contributes to attenuated the survival and proliferation of BCP-ALL cells. Moreover, a previous research has shown that CoQ10, which is an crucial downstream molecule of PPTC7, facilitates ATP synthesis while prevents the accumulation of ROS, further promoting cell survival (14). In our study, we have provided functional evidence that miR-582 negatively regulates CoQ10 synthesis through inhibiting PPTC7, resulting in less ATP synthesis and more ROS production. Therefore, we suggest that miR-582 downregulates PPTC7 and reduces CoQ10 production by directly targeting PPTC7, and thereby functions as a novel negative regulator of the electron transport chain in mitochondrial energy metabolism of BCP-ALL cells.

During the progression of various tumors, tumor cells in the TME often tend to promote the exhaustion of anti-tumor immune cells, such as NK cells, by upregulating the expression of IC molecules, to reduce cytotoxicity and enhance immune escape (43). Previous researches have shown that CD276, an important IC molecule, is often highly expressed in neuroblastoma (44) and non-small cell lung cancer cells (45), inhibits the cytotoxicity of NK cells. CD276-CAR NK cells or blocking CD276 with anti-CD276 antibody often rescues the anti-tumor ability of NK cells (44–46). A previous study showed that miR-29c negatively regulates CD276 expression in tumor cells (43). However, in our



control lentivirus for 72 h, and CD276 mRNA were determined by RNA-seq. (**B**, **C**) NALM-6, KOPN-8 and SUP-B15 cells were infected with pre-miR-582 lentivirus or its control lentivirus for 72 h, and CD276 mRNA were determined by qRT-PCR (**B**); the proportion of CD276⁺ cells were determined by flow cytometry (**C**). (**D**, **E**) NALM-6, KOPN-8 and SUP-B15 cells were infected with pre-miR-582 lentivirus and their control lentivirus, cultured with or without anti-CD276 antibody, and co-cultured with NK cells for 4 h, the proportion of CD107a⁺ NK and GZMB⁺ NK cells were determined by flow cytometry. (**F**) The signaling pathway of miR-582 regulate the progression of BCP-ALL and protect BCP-ALL cells from natural killer cell-mediated cytotoxicity, figure created with BioRender.com. Bars represent means ± SD, **P* < 0.01.

research, we found that miR-582 positively regulates the CD276 expression in BCP-ALL cells, resulting in reduced NK cellmediated cytotoxicity to BCP-ALL cells. The specific mechanism of miR-582 in regulating the expression of CD276 is still unknown. miR-582-mediated metabolic remodeling could be involved in, but more studies are required to access this question. Our study further suggests that CD276 blockade can relieve the inhibition of NK cellmediated cytotoxicity likely in BCP-ALL cells with high miR-582 expression, and therefore miR-582 may serve as a biomarker for anti-CD276 therapy of BCP-ALL.

In conclusion, our research reported here has uncovered a role of miR-582 as a negative regulator of human BCP-ALL cells proliferation and survival. Our findings provide novel insights into how miR-582 inhibits the proliferation and survival of BCP-ALL cells by targeting PPTC7 to reduce CoQ10 level and further inhibit mitochondrial energy metabolism in BCP-ALL cells. miR-582 also promotes the expression of CD276 and protect BCP-ALL

cells from NK cell-mediated cytotoxicity, which might of significance in treatment of BCP-ALL with anti-CD276 antibodies.

DATA AVAILABILITY STATEMENT

The datasets presented in this study can be found in online repositories. The names of the repository/repositories and accession number(s) can be found below: NCBI - PRJNA811525.

ETHICS STATEMENT

The studies involving human participants were reviewed and approved by the Ethics Committee of Fourth Military Medical University for use of human samples. Written informed consent to participate in this study was provided by the participants' legal guardian/next of kin.

AUTHOR CONTRIBUTIONS

Conception and design: MZ and HH. Performing methodology: XL, YZ, FH, and BC. Analysis of data: DG and XC. Critical materials: XL and SH. Writing manuscript: XL and HH. Study supervision: HH. All authors contributed to the article and approved the submitted version.

FUNDING

This work was supported by Natural Science Basic Research Program of Shaanxi (Program No. 2020JQ-147), Guangdong

REFERENCES

- Geron I, Savino AM, Tal N, Brown J, Turati V, James C, et al. An Instructive Role for IL7RA in the Development of Human B-Cell Precursor Leukemia. *Nat Commun* (2022) 13(1):659. doi: 10.1038/s41467-022-28218-7
- Wang W, Wu F, Ma P, Gan S, Li X, Chen L, et al. LncRNA CRNDE Promotes the Progression of B-Cell Precursor Acute Lymphoblastic Leukemia by Targeting the miR-345-5p/CREB Axi. *Mol Cells* (2020) 43(8):718–27. doi: 10.14348/molcells.2020.0065
- Neri LM, Cani A, Martelli A, Simioni C, Junghanss C, Tabellini G, et al. Targeting the PI3K/Akt/mTOR Signaling Pathway in B-Precursor Acute Lymphoblastic Leukemia and Its Therapeutic Potential. *Leukemia* (2014) 28 (4):739–48. doi: 10.1038/leu.2013.226
- Buske C, Becker D, Feuring-Buske M, Hannig H, Wulf G, Schäfer C, et al. TGF-β Inhibits Growth and Induces Apoptosis in Leukemic B Cell Precursors. *Leukemia* (1997) 11(3):386–92. doi: 10.1038/sj.leu.2400586
- Heisterkamp N, ji Joo E, Yang L, Groffen J, Fei F. Cell-Intrinsic and Extrinsic Effects of Galectin-1 and Galectin-3 in B-Cell Precursor Acute Lymphoblastic Leukemia. *bioRxiv* (2021). doi: 10.1101/2021.09.22.461145
- Pastorczak A, Domka K, Fidyt K, Poprzeczko M, Firczuk M. Mechanisms of Immune Evasion in Acute Lymphoblastic Leukemia. *Cancers* (2021) 13 (7):1536. doi: 10.3390/cancers13071536
- Rouce RH, Shaim H, Sekine T, Weber G, Ballard B, Ku S, et al. The TGF-β/ SMAD Pathway Is an Important Mechanism for NK Cell Immune Evasion in Childhood B-Acute Lymphoblastic Leukemia. *Leukemia* (2016) 30(4):800–11. doi: 10.1038/leu.2015.327
- Sbirkov Y, Ivanova T, Burnusuzov H, Gercheva K, Petrie K, Schenk T, et al. The Protozoan Inhibitor Atovaquone Affects Mitochondrial Respiration and Shows *In Vitro* Efficacy Against Glucocorticoid-Resistant Cells in Childhood B-Cell Acute Lymphoblastic Leukaemia. *Front Oncol* (2021) 11:632181:632181. doi: 10.3389/fonc.2021.632181
- Anselmi L, Bertuccio SN, Lonetti A, Prete A, Masetti R, Pession A. Insights on the Interplay Between Cells Metabolism and Signaling: A Therapeutic Perspective in Pediatric Acute Leukemias. *Int J Mol Sci* (2020) 21(17):6251. doi: 10.3390/ijms21176251
- Birk A, Chao W, Bracken C, Warren J, Szeto H. Targeting Mitochondrial Cardiolipin and the Cytochrome C/Cardiolipin Complex to Promote Electron Transport and Optimize Mitochondrial ATP Synthesis. *Br J Pharmacol* (2014) 171(8):2017–28. doi: 10.1111/bph.12468
- Gollapudi S, Gupta S. Reversal of Oxidative Stress-Induced Apoptosis in T and B Lymphocytes by Coenzyme Q10 (Coq10). *Am J Clin Exp Immunol* (2016) 5(2):41–7.
- Xie T, Wang C, Jin Y, Meng Q, Liu Q, Wu J, et al. CoenzymeQ10-Induced Activation of AMPK-YAP-OPA1 Pathway Alleviates Atherosclerosis by Improving Mitochondrial Function, Inhibiting Oxidative Stress and Promoting Energy Metabolism. *Front Pharmacol* (2020) 11:1034. doi: 10.3389/fphar.2020.01034
- Niemi NM, Wilson GM, Overmyer KA, Vögtle FN, Myketin L, Lohman DC, et al. Pptc7 Is an Essential Phosphatase for Promoting Mammalian Mitochondrial Metabolism and Biogenesis. *Nat Commun* (2019) 10(1):3197. doi: 10.1038/s41467-019-11047-6

Basic and Applied Basic Research Foundation (2020A15 15110094) and the Fundamental Research Funds for the Central Universities of China (3102019YX01004), and National Natural Science Foundation (31730041, 91339115, 31671523) of China.

SUPPLEMENTARY MATERIAL

The Supplementary Material for this article can be found online at: https://www.frontiersin.org/articles/10.3389/fimmu.2022. 853094/full#supplementary-material

- González-Mariscal I, Martin-Montalvo A, Vazquez-Fonseca L, Pomares-Viciana T, Sánchez-Cuesta A, Fernández-Ayala DJ, et al. The Mitochondrial Phosphatase PPTC7 Orchestrates Mitochondrial Metabolism Regulating Coenzyme Q10 Biosynthesis. *Biochim Biophys Acta Bioenerg* (2018) 1859 (11):1235–48. doi: 10.1016/j.bbabio.2018.09.369
- Shyu AB, Wilkinson MF, Van Hoof A. Messenger RNA Regulation: To Translate or to Degrade. *EMBO J* (2008) 27(3):471–81. doi: 10.1038/ sj.emboj.7601977
- Wang X, Feng Y, Zhang P, Chen H, Bai J, Wang F, et al. miR-582-5p Serves as an Antioncogenic Biomarker in Intermediate Risk AML With Normal Cytogenetics and Could Inhibit Proliferation and Induce Apoptosis of Leukemia Cells. Cell Biol Int (2020) 44(10):2021–30. doi: 10.1002/cbin.11408
- Zhang X, Zhang Y, Yang J, Li S, Chen J. Upregulation of miR-582-5p Inhibits Cell Proliferation, Cell Cycle Progression and Invasion by Targeting Rab27a in Human Colorectal Carcinoma. *Cancer Gene Ther* (2015) 22(10):475–80. doi: 10.1038/cgt.2015.44
- Li X, Zhang Y, Zheng M, Cao X, Guo M, Gao X, et al. miR-582 Negatively Regulates Pre-B Cell Proliferation and Survival Through Targeting Hif1α and Rictor. Cell Death Dis (2022) 13(2):107. doi: 10.1038/s41419-022-04560-y
- Ma X, Zhou J, Zhong Y, Jiang L, Mu P, Li Y, et al. Expression, Regulation and Function of microRNAs in Multiple Sclerosis. *Int J Med Sci* (2014) 11(8):810– 8. doi: 10.7150/ijms.8647
- Li J, Qin Y, Zhang H. Identification of Key miRNA–Gene Pairs in Chronic Lymphocytic Leukemia Through Integrated Analysis of mRNA and miRNA Microarray. Oncol Lett (2018) 15(1):361–67. doi: 10.3892/ol.2017.7287
- de Oliveira JC, Brassesco MS, Scrideli CA, Tone LG, Narendran A. MicroRNA Expression and Activity in Pediatric Acute Lymphoblastic Leukemia (ALL). *Pediatr Blood Cancer* (2012) 59(4):599–604. doi: 10.1002/pbc.24167
- Yong H, Fu J, Gao G, Shi H, Zheng D, Zhou X. MiR-34a Suppresses the Proliferation and Invasion of Gastric Cancer by Modulating PDL1 in the Immune Microenvironment. *Mol Cell Probes* (2020) 53:101601. doi: 10.1016/ j.mcp.2020.101601
- Sonkoly E, Janson P, Majuri ML, Savinko T, Fyhrquist N, Eidsmo L, et al. MiR-155 Is Overexpressed in Patients With Atopic Dermatitis and Modulates T-Cell Proliferative Responses by Targeting Cytotoxic T Lymphocyte– Associated Antigen 4. J Allergy Clin Immunol (2010) 126(3):581–9. doi: 10.1016/j.jaci.2010.05.045
- Kanchan RK, Perumal N, Atri P, Chirravuri Venkata R, Thapa I, Klinkebiel DL, et al. MiR-1253 Exerts Tumor-Suppressive Effects in Medulloblastoma *via* Inhibition of CDK6 and CD276 (B7-H3). *Brain Pathol* (2020) 30(4):732–45. doi: 10.1111/bpa.12829
- 25. Li X, Dong W, Nalin AP, Wang Y, Pan P, Xu B, et al. The Natural Product Chitosan Enhances the Anti-Tumor Activity of Natural Killer Cells by Activating Dendritic Cells. Oncoimmunology (2018) 7(6):e1431085. doi: 10.1080/2162402X.2018.1431085
- Deng M, Wu D, Zhang Y, Jin Z, Miao J. MiR-29c Downregulates Tumor-Expressed B7-H3 to Mediate the Antitumor NK-Cell Functions in Ovarian Cancer. *Gynecol Oncol* (2021) 162(1):190–9. doi: 10.1016/j.ygyno. 2021.04.013
- 27. Jia L, Xi Q, Wang H, Zhang Z, Liu H, Cheng Y, et al. miR-142-5p Regulates Tumor Cell PD-L1 Expression and Enhances Anti-Tumor Immunity.

Biochem Biophys Res Commun (2017) 488(2):425-31. doi: 10.1016/ j.bbrc.2017.05.074

- Zhao L, Liu Y, Zhang J, Liu Y, Qi Q. LncRNA SNHG14/miR-5590-3p/ZEB1 Positive Feedback Loop Promoted Diffuse Large B Cell Lymphoma Progression and Immune Evasion Through Regulating PD-1/PD-L1 Checkpoint. *Cell Death Dis* (2019) 10(10):731. doi: 10.1038/s41419-019-1886-5
- Zhu B, Finch-Edmondson M, Lee Y, Wan Y, Sudol M, DasGupta R. miR-582-5p Is a Tumor Suppressor microRNA Targeting the Hippo-YAP/TAZ Signaling Pathway in Non-Small Cell Lung Cancer. *Cancers* (2021) 13 (4):756. doi: 10.3390/cancers13040756
- Wang L, Zhang M. miR-582-5p Is a Potential Prognostic Marker in Human Non-Small Cell Lung Cancer and Functions as a Tumor Suppressor by Targeting MAP3K2. *Eur Rev Med Pharmacol Sci* (2018) 22(22):7760–7. doi: 10.26355/eurrev_201811_16397
- Huang S, Zou C, Tang Y, Wa Q, Peng X, Chen X, et al. miR-582-3p and miR-582-5p Suppress Prostate Cancer Metastasis to Bone by Repressing TGF-β Signaling. *Mol Ther Nucleic Acids* (2019) 16:91–104. doi: 10.1016/ j.omtn.2019.01.004
- 32. Zhang Y, Huang W, Ran Y, Xiong Y, Zhong Z, Fan X, et al. miR-582-5p Inhibits Proliferation of Hepatocellular Carcinoma by Targeting CDK1 and AKT3. *Tumour Biol* (2015) 36(11):8309–16. doi: 10.1007/s13277-015-3582-0
- 33. Godbersen JC, Humphries LA, Danilova OV, Kebbekus PE, Brown JR, Eastman A, et al. The Nedd8-Activating Enzyme Inhibitor MLN4924 Thwarts Microenvironment-Driven NF-κb Activation and Induces Apoptosis in Chronic Lymphocytic Leukemia B Cells. *Clin Cancer Res* (2014) 20(6):1576–89. doi: 10.1158/1078-0432.CCR-13-0987
- 34. Oh YS, Lee YJ, Kang Y, Han J, Lim OK, Jun H. Exendin-4 Inhibits Glucolipotoxic ER Stress in Pancreatic β Cells via Regulation of SREBP1c and C/Ebpβ Transcription Factors. J Endocrinol (2013) 216(3):343–52. doi: 10.1530/JOE-12-0311
- 35. Xie M, Yu T, Jing X, Ma L, Fan Y, Yang F, et al. Exosomal Circshkbp1 Promotes Gastric Cancer Progression *via* Regulating the miR-582-3p/HUR/ VEGF Axis and Suppressing HSP90 Degradation. *Mol Cancer* (2020) 19 (1):112. doi: 10.1186/s12943-020-01208-3
- 36. Li H, Tian X, Wang P, Huang M, Xu R, Nie T. MicroRNA-582-3p Negatively Regulates Cell Proliferation and Cell Cycle Progression in Acute Myeloid Leukemia by Targeting Cyclin B2. Cell Mol Biol Lett (2019) 24(1):66. doi: 10.1186/s11658-019-0184-7
- Wang Z, Li Y, Kuang X, Guo F, Lang T, Mao M, et al. Anti-Proliferation and Pro-Apoptosis Effects of miR-582-5p in Chronic Lymphocytic Leukemia *via* Targeting HNRNPA1 and Suppression of NF-κb. *Mol Cell Toxicol* (2021) 17:357–65. doi: 10.1007/s13273-021-00143-8
- Wang F, Luo Y, Zhang L, Younis M, Yuan L. The LncRNA RP11-301g19. 1/ miR-582-5p/HMGB2 Axis Modulates the Proliferation and Apoptosis of Multiple Myeloma Cancer Cells via the PI3K/AKT Signalling Pathway. *Cancer Gene Ther* (2021) 29(3-4):293–303. doi: 10.1038/s41417-021-00309-5

- Tian Y, Guan Y, Su Y, Luo W, Yang G, Zhang Y. MiR-582-5p Inhibits Bladder Cancer-Genesis by Suppressing TTK Expression. *Cancer Manag Res* (2020) 12:11933–44. doi: 10.2147/CMAR.S274835
- Huang D, Li C. Circ–ACACA Promotes Proliferation, Invasion, Migration and Glycolysis of Cervical Cancer Cells by Targeting the Mir–582–5p/ERO1A Signaling Axis. Oncol Lett (2021) 22(5):795. doi: 10.3892/ol.2021.13056
- Dai T, Liang J, Liu W, Zou Y, Niu F, Li M, et al. The MIRNA Mir-582-3p Suppresses Ovarian Cancer Progression by Targeting AKT/MTOR Signaling via lncRNA Tug1. Bioengineered (2021) 12(2):10771–81. doi: 10.1080/ 21655979.2021.2003662
- 42. Stein M, Dütting S, Mougiakakos D, Bösl M, Fritsch K, Reimer D, et al. A Defined Metabolic State in Pre B Cells Governs B-Cell Development and Is Counterbalanced by Swiprosin-2/Efhd1. *Cell Death Differ* (2017) 24(7):1239– 52. doi: 10.1038/cdd.2017.52
- Lee CC, Ho KH, Huang TW, Shih CM, Hsu SY, Liu AJ, et al. A Regulatory Loop Among CD276, miR-29c-3p, and Myc Exists in Cancer Cells Against Natural Killer Cell Cytotoxicity. *Life Sci* (2021) 277:119438. doi: 10.1016/ j.lfs.2021.119438
- Grote S, Chan KCH, Baden C, Bösmüller H, Sulyok M, Frauenfeld L, et al. CD276 as a Novel CAR NK-92 Therapeutic Target for Neuroblastoma. *Adv Cell Gene* (2021) 4(1):e105. doi: 10.1002/acg2.105
- 45. Yang S, Cao B, Zhou G, Zhu L, Wang L, Zhang L, et al. Targeting B7-H3 Immune Checkpoint With Chimeric Antigen Receptor-Engineered Natural Killer Cells Exhibits Potent Cytotoxicity Against Non-Small Cell Lung Cancer. *Front Pharmacol* (2020) 11:1089. doi: 10.3389/fphar.2020.01089
- Picarda E, Ohaegbulam KC, Zang X. Molecular Pathways: Targeting B7-H3 (CD276) for Human Cancer Immunotherapy. *Clin Cancer Res* (2016) 22 (14):3425–31. doi: 10.1158/1078-0432.CCR-15-2428

Conflict of Interest: The authors declare that the research was conducted in the absence of any commercial or financial relationships that could be construed as a potential conflict of interest.

Publisher's Note: All claims expressed in this article are solely those of the authors and do not necessarily represent those of their affiliated organizations, or those of the publisher, the editors and the reviewers. Any product that may be evaluated in this article, or claim that may be made by its manufacturer, is not guaranteed or endorsed by the publisher.

Copyright © 2022 Li, Zhang, He, Gao, Che, Cao, Huang, Zheng and Han. This is an open-access article distributed under the terms of the Creative Commons Attribution License (CC BY). The use, distribution or reproduction in other forums is permitted, provided the original author(s) and the copyright owner(s) are credited and that the original publication in this journal is cited, in accordance with accepted academic practice. No use, distribution or reproduction is permitted which does not comply with these terms.



IL-27 Improves Prophylactic Protection Provided by a Dead Tumor Cell Vaccine in a Mouse Melanoma Model

Kyle Seaver¹, Olena Kourko¹, Katrina Gee¹, Peter A. Greer² and Sameh Basta^{1*}

¹ Department of Biomedical and Molecular Sciences, Queen's University, Kingston, ON, Canada, ² Department of Pathology and Molecular Medicine, Queen's University, Kingston, ON, Canada

OPEN ACCESS

Edited by:

Yubin Li, University of Pennsylvania, United States

Reviewed by:

Xi Lou, University of Alabama at Birmingham, United States Qiaosi Tang, University of Pennsylvania, United States Chongming Jiang, Baylor College of Medicine, United States

*Correspondence:

Sameh Basta bastas@queensu.ca

Specialty section:

This article was submitted to Cancer Immunity and Immunotherapy, a section of the journal Frontiers in Immunology

Received: 27 February 2022 Accepted: 28 March 2022 Published: 21 April 2022

Citation:

Seaver K, Kourko O, Gee K, Greer PA and Basta S (2022) IL-27 Improves Prophylactic Protection Provided by a Dead Tumor Cell Vaccine in a Mouse Melanoma Model. Front. Immunol. 13:884827. doi: 10.3389/fimmu.2022.884827 The protocol used to induce cell death for generating vaccines from whole tumor cells is a critical consideration that impacts vaccine efficacy. Here we compared how different protocols used to induce cell death impacted protection provided by a prophylactic whole tumor cell vaccine in a mouse melanoma model. We found that melanoma cells exposed to γ -irradiation or lysis combined with UV-irradiation (LyUV) provided better protection against tumor challenge than lysis only or cells exposed to UV-irradiation. Furthermore, we found that the immunoregulatory cytokine, IL-27 enhanced protection against tumor growth in a dose-dependent manner when combined with either LyUV or γ -irradiated whole tumor cell vaccine preparations. Taken together, this data supports the use of LyUV as a potential protocol for developing whole tumor cell prophylactic cancer vaccines. We also showed that IL-27 can be used at low doses as a potent adjuvant in combination with LyUV or γ -irradiation treated cancer cells to improve the protection provided by a prophylactic cancer vaccine in a mouse melanoma model.

Keywords: IL-27, adjuvant, cancer vaccine, cell death, prophylactic, melanoma

INTRODUCTION

A key objective of cancer immunotherapy is to enhance immune recognition of tumors for elimination. Cancer vaccines can be delivered therapeutically to treat established tumors (1) or applied prophylactically to prevent tumor development or recurrence (2, 3). The immune system recognizes tumors using tumor associated antigens (TAAs), which provide targets for antigen specific CD8⁺ T lymphocyte (CTL) activation (4–8). Therefore, a successful cancer vaccine has the potential to promote robust CTL activation against TAAs (9). In addition to activating CTLs, cancer vaccines have also investigated the role of CD4⁺ T helper cells. Studies have elucidated a prominent role of CD4⁺ T cells in cancer vaccine clinical trials against multiple cancer types, including melanoma (10, 11).

In addition to providing TAAs, therapeutic cancer vaccines need to overcome an immunosuppressive tumor microenvironment (TME). Therefore, early intervention with prophylactic vaccination may be highly effective in preventing a tumor while also reducing the

potential for recurrence following surgical removal of the tumor (12). Whole tumor cell vaccines consisting of dead tumor cells (DTCVs) can be used in prophylactic settings. Different protocols are used to produce DTCVs, including exposure to irradiation, y-irradiation and ultraviolet (UV)-irradiation, oxidizing treatment, and lysis using heat-shock/snap-freezing and thawing (F/T) (13-15). Cancer cells exposed to these treatments can undergo immunogenic cell death (ICD) (16), releasing danger-associated molecular patterns (DAMPs), such as adenosine triphosphate (ATP), high mobility group box protein 1 (HMGB1), and heat shock proteins (HSPs) (17). DAMPs can activate professional antigen presenting cells (pAPCs), including dendritic cells (DCs). This activation is characterized by an increase in co-stimulatory molecule expression and release of cytokines that can enhance T cell activation (18, 19). CTL activation can be achieved when pAPCs present TAAs on major histocompatibility complex (MHC) class I to CTLs via antigen cross-presentation (20-23). DTCVs reduce the need to select a predictive TAA as it provides access to all potential tumor antigens, including uncharacterized and unique antigens not yet identified. Additionally, cancer cell variants can escape immune detection by downregulating antigens. Using DTCVs in a prophylactic setting may reduce escape variants from arising because they provide access to multiple antigens at once (24). However, tumor cells alone are poorly immunogenic, and studies have investigated how adjuvants can improve cancer vaccine efficacy (16).

The use of cytokines as adjuvants to enhance cancer vaccine efficacy has been well documented and can influence both innate and adaptive immune responses (25–28). Interleukin (IL)-12, for example, has been used as a cancer vaccine adjuvant; however, toxicity is a concern, and dosage requires careful consideration (29, 30). IL-27, a cytokine belonging to the IL-12 family of cytokines, has been identified as a potential cancer vaccine adjuvant (31). IL-27 can signal in T cells, macrophages, and monocytes while also directly impacting cancer cell death and proliferation (32, 33). Although IL-27 has been associated with both pro- and anti-tumor effects (34), elevated levels of IL-27 have demonstrated success in reducing cancer progression (31, 35). However, the use of IL-27 as an adjuvant to improve prophylactic cancer vaccines needs further investigation. Furthermore, understanding the impacts of different doses of IL-27 in combination with DTCVs has yet to be investigated.

In the present study, we examined how different protocols were used to generate a DTCV in combination with recombinant mouse (rm)IL-27 as an adjuvant, impact tumor growth focusing on the potential MHC-I/CD8⁺ T cell interactions. Using the B16-OVA murine melanoma model, we determined that the addition of rmIL-27 at a lower dose, rather than a higher dose, improved protection by a DTCV against tumor challenge. We also showed that despite the added protection against initial tumor challenge with the addition of rmIL-27 to a DTCV, rmIL-27 did not protect against tumor rechallenge. These results have implications on the potential use of IL-27 as an adjuvant in combination with vaccines generated from whole tumor cells.

METHODS

Mice and Cell Lines

Male and female C57BL/6 (H-2^b) mice (6-8 weeks old) were purchased from JAX[®] Laboratories (Bar Harbour, USA) and kept under specific pathogen-free conditions. All animal experiments were conducted in accordance with the Canadian Council of Animal Use and approved by Queen's University Animal Care Services.

The murine melanoma cell line B16F10 (H-2k^b) was maintained in DMEM (Gibco, Fisher Scientific, Canada) supplemented with 5% FBS (Gibco, Fisher Scientific, Canada) (36). B16F10 cells transfected with chicken ovalbumin (OVA), a gift from Dr. Yewdell (NIAID, NIH, USA), were maintained under 500 μ g/mL of G418 sulfate (Bioshop, Canada) selection in complete DMEM medium. The DC2.4 cell line (kindly provided by Dr. Rock, University of Massachusetts Medical School, USA), isolated from C57BL/6 mice bone marrow and transduced with retroviral vectors expressing murine granulocyte-macrophage colony-stimulating factor (GM-CSF) and myc and raf oncogenes (37), was maintained in RPMI media (Gibco, Fisher Scientific, Canada) supplemented with 5% FBS. All cells were maintained at 37°C and 5% CO₂.

Induction of Cell Death

B16-OVA cells were exposed to one of the following protocols of inducing cell death. *Cell lysis*: five consecutive rounds of F/T where cells were frozen using liquid nitrogen and thawed in a water bath at 37°C. *Ultraviolet-irradiation (UV-irradiation)*: Cells were exposed to UV-irradiation at a total exposure of 1500 mJ//cm² using a CL-1000 ultraviolet crosslinker (Ultra-Violet Products Ltd., United Kingdom). *LyUV*: Cells were exposed to a single F/T cycle followed by UV-irradiation, as previously described (38, 39). γ -irradiation: Cells were exposed to 60 Gys of irradiation using a cesium irradiator as the source (Cs¹³⁷ GammaCell 20 Irradiator, Queen's University).

Microscopy

Light microscopy was used to visualize the morphology of cancer cells following the protocols used to induce cell death. Cells were seeded into 6-well plates at a density of $1x10^6$ cell/well and observed using a light microscope (Lecia DM IRE2, Germany) at 20X magnification. Images were acquired using Lecia DFC340 cooled monochrome digital camera.

Detection of Cell Viability

To measure the induction of cell death, annexin-V (AV) and propidium iodide (PI) staining was conducted as outlined by the manufacturer. Briefly, B16-OVA cells were washed twice in AV binding buffer (10 mM Hepes, pH 7.4, 0.14mM NaCl and 2.5 mM CaCl₂) followed by staining with APC-conjugated AV (Biolegend, USA) for 15 min protected from light at room temperature. PI (Biolegend, USA) was then added 5 min before acquisition at a concentration of 1.5 μ g/mL. Data was acquired using a CytoFLEX flow cytometer (Beckman Coulter, USA) and analyzed using FlowJo software (BD, USA).

Evaluation of MHC-I Expression on Irradiated Tumor Cell by Flow Cytometry

Following exposure to either γ -irradiation or UV-irradiation or treatment with 50 ng/mL of interferon- γ (IFN- γ) (Shenandoah Biotechnology, USA), B16-OVA cells were incubated for 18 hrs. in a 6-well plate at a density of 1.0×10^6 cells/well. After incubation, the cells were harvested and washed with 1X PBS, then transferred to a 96-well round-bottom plate (Corning, USA). Cells were then washed twice in flow staining buffer (1X PBS, 0.1% sodium azide, 1% BSA) and then stained with PE-anti-MHC-I (Biolegend, clone: 28-8-6) for 30 min at 4°C. Data was acquired using a CytoFLEX flow cytometer and analyzed using FlowJo software (BD, USA).

Co-Incubation of DC2.4 Cells With Dead B16-OVA Supernatants

B16-OVA cells were exposed to the indicated protocol of inducing cell death as described earlier. After exposure, cancer cells were left to incubate for 24 hrs. in complete RPMI media at a concentration of 1.0x10⁶ cells/mL in a 6-well plate (Corning, USA) constituting the tumor conditioned media (TCM). Following the incubation period, supernatants were collected and centrifuged at 1000g for 5 min to remove debris and immediately added at a 1:1 ratio by volume (TCM: complete media) to 1.0x10⁶ DC2.4 cells in a total volume of 1.5 mL. The DC2.4 cells were subsequently left to incubate for 24 hrs, after which cells were collected and prepared for flow cytometry, as previously described. Cells were then stained with the following antibodies: FITC-anti-MHC-II IA/IE (Biolegend, clone: M5/ 114.15.2), PE-anti-CD80 (Biolegend, clone: 16-10A1), APCanti-CD86 (Biolegend, clone: GL-1), and PerCP-anti-CD40 (Biolegend, clone: 3/23) for 30 min at 4°C. Data was acquired using a CytoFLEX flow cytometer and analyzed using FlowJo software (BD, USA).

Phagocytosis Assay

The phagocytosis assay was performed as previously reported (40). Briefly, cancer cells were stained with carboxyfluorescein succinimidyl ester (CFSE) (0.2 μ M/mL) for 15 min at 37°C then washed extensively and exposed to the indicated protocols to induce cell death. Cancer cells were then co-cultured with DC2.4 cells at a ratio of 3:1 in a 96-well round-bottom plate for 3 hrs. at 37°C in a total volume of 200 μ L/well. After the co-incubation, DCs were stained with PE-Cy7-anti-CD11c (Biolegend, clone: N418) for 30 min at 4°C. Data was acquired using a CytoFLEX flow cytometer and analyzed using FlowJo software to identify the cells that were CFSE⁺/CD11c⁺ double-positive cells.

Preparation of a Prophylactic Cancer Vaccine Containing IL-27

B16-OVA cells were harvested and exposed to the indicated protocol to induce cell death. Cells were then resuspended at $5.0x10^6$ cells in 0.2 mL 1X PBS and delivered to each mouse *via* intraperitoneal (i.p) injection. Mice were injected with the corresponding vaccine 14 and 7 days before the tumor challenge. For vaccines that included rmIL-27 (Biolegend,

USA), mice received 0.2 mL of either 10 ng/mouse or 100 ng/ mouse of rmIL-27 suspended in 1X PBS alone or with dead tumor cells. For tumor engraftment, 1.0×10^6 live B16-OVA cells were injected subcutaneously (s.c) into the right hind flank. Tumor growth was monitored by calipers every second day by measuring volume using the modified ellipsoidal formula: V=1/2 (length x widgth²) (41).

For tumor rechallenge experiments, mice that remained tumor free following the prophylactic vaccination and tumor engraftment were rechallenged on day 60 with 1.0×10^6 live B16-OVA cells s.c into the opposite hind flank of the original engraftment.

Statistical Analysis

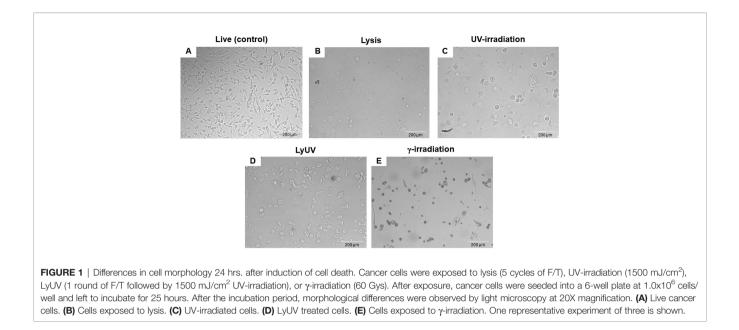
Statistical significance was determined using GraphPad Prism. Comparison between two groups was done using Student's t-test. One-way ANOVA was used when comparing differences between more than two groups. For Kaplan-Meier survival curves the Log-rank (Mantel-Cox) test was used. All values are reported as mean \pm SD. A p-value ≤ 0.05 was considered significant.

RESULTS

Cell Morphology Is Influenced by the Protocol Used to Induce Cell Death

The protocol used to induce cell death can result in differences in the level of protection observed by a prophylactic vaccine. Using B16-OVA melanoma cells, we visualized the impact of four different protocols used to induce cell death. Cancer cells were exposed to five consecutive rounds of freeze/thaw (lysis) which resulted in higher mean fluorescence intensity (MFI) of PI-positive cells although no differences in the percent of PI-positive cells was detected when compared to one round of lysis (Supplementary Figure 1). B16 cells were exposed to UV-irradiation at a total exposure of 1500 mJ/ cm², either delivered alone (UV-irradiation) or in combination with a single round of F/T (LyUV) as has been previously described (40, 42). For γ -irradiation, a range of doses (20 – 100 Gy) were tested but yielded no differences in the induction of cell death 24 hrs. after exposure (Supplementary Figure 2), or proliferation (data not shown). Based on these results and previous literature, we used 60 Gys of γ -irradiation exposure based on previous literature using B16 cells (43).

Following induction of cell death, B16-OVA cells were incubated for 24 hrs, and morphological differences and adherence were determined *via* light microscopy (**Figure 1**). Exposure to lysis resulted in few detectable intact cells with a large quantity of debris. Exposure to UV-irradiation did not yield adherent cells, most cells remained intact with a circular and swelled appearance compared to the elongated appearance of live (control) B16-OVA cells. Interestingly, LyUV yielded a combination of debris (similar to lysis) and intact cells (similar to UV). Compared to UV-irradiation, cells exposed to γ irradiation did not demonstrate the same swelled appearance and yielded a mixture of adherent and non-adherent cells. Taken together, each protocol used to induce cell death yields morphological differences.



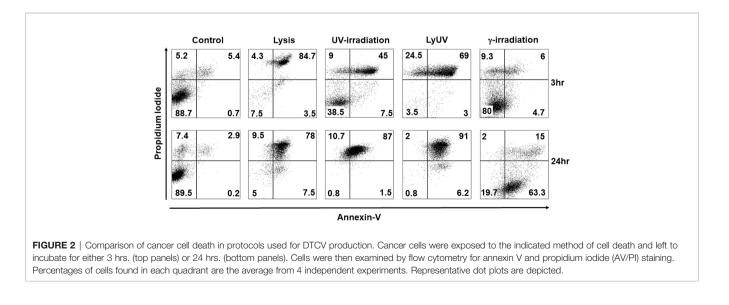
Generating Apoptotic and Necrotic Cancer Cells for Use in a DTCV

With observable differences in cell morphology, we next assessed cell viability using AV and PI staining at 3 hrs. and 24 hrs. after cell death was induced. After 3 hrs. of incubation following induction of cell death, lysis and LyUV resulted in a majority of the cells being late apoptotic (AV^+/PI^+) with 84.7% and 69%, respectively, with LyUV yielding a greater number of necrotic cells (AV^-/PI^+ , 24.5%) (**Figure 2**). Cell viability following exposure to lysis and LyUV remained similar between the 3 hr and 24 hr time points. There were differences observed in cell viability when B16-OVA cells were exposed to UV- or γ -irradiation. Following 3 hrs. post-exposure to UV- or γ -irradiation, cancer cells that remained alive (AV^-/PI^-) were 38.5% and 80%, respectively (**Figure 2**). After 24 hrs. post-

exposure, UV-irradiation resulted in most of the cells being late apoptotic (87%) whereas γ -irradiation resulted in the majority of cells being early apoptotic (AV⁺/PI⁻) (63.3%) (**Figure 2**). Overall, these results indicated that lysis and LyUV are comparable in the type of cell death induced, while UV- and γ -irradiation result in different proportions of apoptotic and necrotic cells while requiring 24 hrs. to yield the greatest reduction in cell viability.

Irradiation Can Promote B16-OVA Cell Immunogenicity by Increasing MHC-I Expression

In addition to inducing cell death, exposure to irradiation can enhance MHC-I expression (44–47). Increasing MHC-I expression has the potential to enhance CTL recognition of



poorly immunogenic tumor cells. The expression of MHC-I on B16-OVA was measured by flow cytometry, and IFN- γ (50 ng/mL) stimulation was used as a positive control. We observed a significant increase in MHC-I on B16-OVA cells exposed to either UV- or γ -irradiation (**Figure 3A**). Compared to γ -irradiation, UV-irradiation resulted in a greater increase of MHC-I expression, although neither form of irradiation could increase the expression of MHC-I to the same extent as IFN- γ (**Figure 3B**). These results indicate that both forms of irradiation increase the expression of MHC-I on B16-OVA cancer cells, although UV-irradiation does this to a greater extent.

Supernatants From B16-OVA Cells Impact Dendritic Cell Activation Which Is Dependent on the Protocol Used to Induce Cell Death

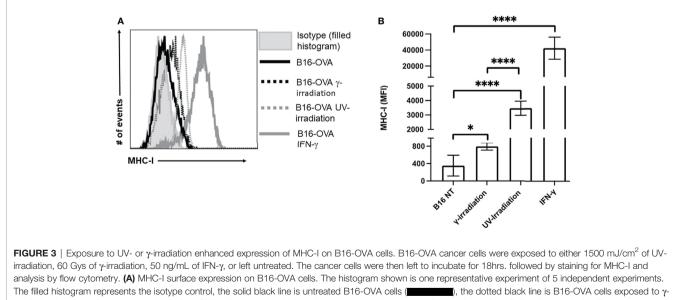
In addition to inducing cell death, lysis and irradiation can result in the release of DAMPs, which can influence DC activation, assessed by an increased expression of co-stimulatory molecules (CD80, CD86, CD40) and MHC-II (48). To evaluate DC activation, we used the well-characterized dendritic cell line, DC2.4, originally derived from the bone marrow of C57BL/6 mice (37). Regardless of the protocol used to induce cell death, B16-OVA supernatants did not affect the expression of MHC-II on DC2.4 cells (Figure 4A). DC2.4 cultured in lysis, LyUV or UV-irradiation supernatants had a significant increase in CD80, whereas a significant reduction in CD80 was seen in DC2.4 cell culture in γ -irradiation supernatants (Figure 4B). DC2.4 cells incubated with LyUV or UV-irradiation supernatants both displayed an increase in CD86 and CD40 expression (Figures 4C, D). Taken together, these results indicate that the protocol used to induce cell death can influence the impact of the TCM on DC2.4 activation.

The Mode of Cancer Cell Death Influences the Rate of Their Phagocytosis by Dendritic Cells

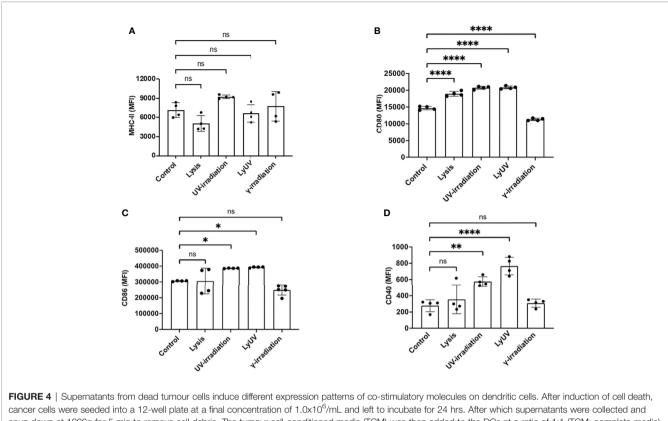
Phagocytosis of dead cancer cells by antigen presenting cells leads to TAA presentation resulting in T cell priming. Therefore, we next determined how DCs phagocytosed tumor cells following exposure to each of the methods of cell death being evaluated. Cancer cells were stained with CFSE and exposed to the protocols of cell death induction. After exposure cancer cells were left to rest for 3- or 24hrs, after which the cancer cells were co-incubated with DCs (3:1) for 3 hrs. to evaluate phagocytosis. Following co-incubation, cancer cell phagocytosis by DCs was determined based on the percent of double-positive DC cells (CFSE $^+$ /CD11c $^+$). After incubation times of 3 and 24 hrs, we observed the greatest amount of phagocytosis with lysed cells (Figure 5). 25% of cancer cells exposed to LyUV were phagocytosed after 3 hrs, which increased to 40% if the cells were left to incubate for 24 hrs. before incubation with DCs. In comparison, UV- and γ -irradiation resulted in lower percentages of phagocytosis after 3 hrs., 15% and 7% respectively. However, if the cancer cells were left for 24 hrs. before co-incubation with DCs, the rate of phagocytosis increased significantly compared to live cells with UV-irradiation increasing to 21% and γ -irradiation increasing to 17%. Overall, these results indicate that when cancer cells are exposed to either lysis or LyUV, phagocytosis by DCs can occur more rapidly than when cancer cells are exposed to UV- or γ-irradiation.

Prophylactic Vaccination With LyUV-Treated or γ-Irradiated B16-OVA Cells Promotes Better Tumor Free Survival When Compared to Unvaccinated Control Mice

We next proceeded to determine how each protocol used to induce cell death impacted the efficacy of a DTCV delivered in a



irradiation (\blacksquare \blacksquare), dotted grey line is B16-OVA cell exposed to UV-irradiation (\blacksquare \blacksquare), and the solid grey line is B16-OVA cell treated with IFN- γ (**B**) Bar graph showing the mean fluorescence intensity (MFI) ± SD of 5 independent experiments. *p < 0.05,**** $p \leq 0.0001$.



cancer cells were seeded into a 12-well plate at a final concentration of $1.0 \times 10^{\circ}$ /mL and left to incubate for 24 hrs. After which supernatants were collected and spun down at 1000g for 5 min to remove cell debris. The tumour cell-conditioned media (TCM) was then added to the DCs at a ratio of 1:1 (TCM: complete media). The DCs were incubated for 24 hrs. in the presence or absence of TCM before being analyzed by flow cytometry for surface marker expression. Bar graphs show expression levels of **(A)** MHC-II, **(B)** CD80, **(C)** CD86, and **(D)** CD40. The control represents DCs incubated in complete media alone. Each bar graph shows the mean fluorescence intensity (MFI) \pm SD of 4 independent experiments. *p < 0.05,**p < 0.01, **** $p \leq 0.0001$. ns denotes not significant.

prophylactic model. A prime-boost model of vaccination showed that two DTCV injections provided greater tumor protection than a single injection (**Supplementary Figure 3**). Vaccines were administered immediately following induction of cell death on days -14 and -7, followed by live tumor challenge on day 0 (**Figure 6A**).

Compared to PBS control mice, prophylactic vaccines consisting of lysed or UV-irradiated B16-OVA cancer cells did not provide significant protection against tumor challenge (**Figure 6B**). However, increased survival was observed when mice were vaccinated with B16-OVA cells exposed to LyUV or γ irradiation, with 12% and 25% of the mice remaining tumor free for 60 days post tumor engraftment, respectively (**Figure 6B**). These results indicate that in addition to γ -irradiation, LyUV has the potential to be used as a protocol for generating DTCV and should be explored further in cancer vaccine development.

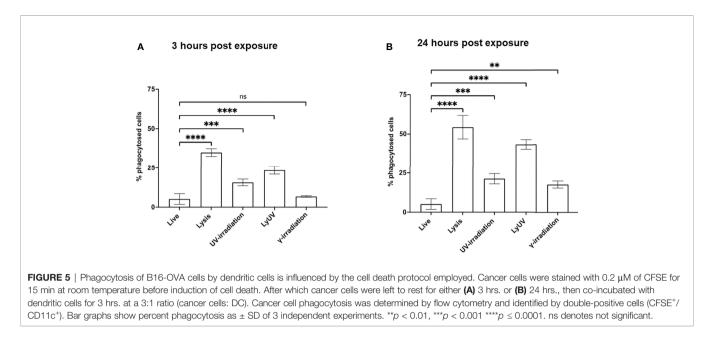
IL-27 Improves the Efficacy of the Prophylactic Cancer Vaccine With a Lower Dose Providing Enhanced Protection

In our model, we observed partial protection against tumor growth using B16-OVA cells that were exposed to LyUV or γ -irradiation. Therefore, we wanted to determine if rmIL-27 could influence the efficacy of the LyUV or γ -irradiated DTCV. Using the same vaccination schedule as previously described (**Figure 6A**), rmIL-

27 was added at 10 or 100 ng/mouse in combination with the DTCV (LyUV or γ -irradiation) at days -14 and -7. While rmIL-27 alone at 10 ng/mouse showed a slight increase in protection relative to PBS, 100 ng/mouse rmIL-27 did not (data not shown). The combination of rmIL-27 at 10 ng/mouse provided significant improvement in protection in both LyUV and γ -irradiation DTCV models compared to unvaccinated controls (PBS), with \geq 50% of the mice remaining tumor free at 60 days post engraftment (Figure 7). Interestingly, the combination of rmIL-27 at 100 ng/mouse to mice vaccinated with either LyUV or y-irradiation based DTCV did not improve protection when compared to the DTCV alone. We also observed a similar trend with DTCVs produced using the B16 melanoma cells that do not express OVA following LyUV exposure, where the lower dose of rmIL-27 provided better protection than the higher dose (Supplementary Figure 4). Although the use of rmIL-27 as an adjuvant in our model provided significant protection against tumor growth, the differential effects observed with the addition of rmIL-27 indicate that the dose required careful consideration.

IL-27 Can Improve Protection Against Initial Tumor Engraftment but Not Tumor Rechallenge

With the increased protection observed using rmIL-27 as a vaccine adjuvant, we next evaluated whether the addition of rmIL-27



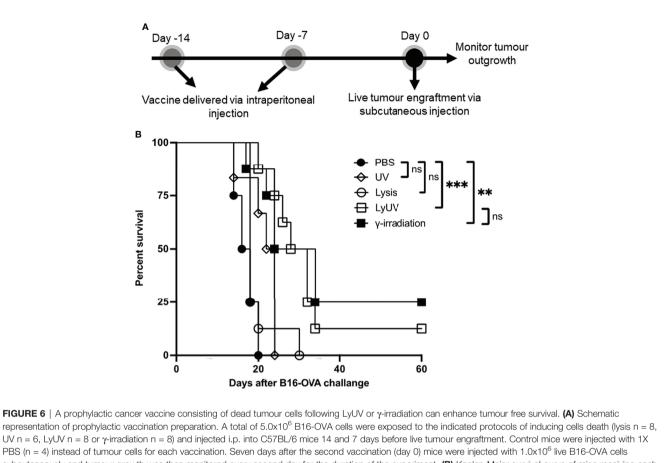
could provide long-term protection in a tumor rechallenge model. To assess this, mice that remained tumor free after the first challenge were later rechallenged at day 60 (**Figure 8A**). Upon rechallenge, all mice that were clear of tumors initially after 60 days exhibited rapid tumor growth which resulted in no significant improvement in tumor free survival when compared to the agematched controls challenged at day 60 (**Figures 8B, C**). This indicates that in our model rmIL-27, as an adjuvant in the prophylactic vaccine preparations provides initial protection against tumor development; however, is not effective in providing protection against further tumor challenges.

DISCUSSION

A challenge that immunotherapies face is to overcome an immunosuppressive TME to enhance an anti-tumor immune response (49, 50). Prophylactic therapies, such as cancer vaccines, promote an anti-tumor immune response in the absence of an immunosuppressive TME (3, 51, 52). Although there are different types of cancer vaccines being studied, those vaccines designed to target multiple TAAs increase the potential for tumor recognition and reduce the potential for escape variants (53-58). Using whole tumor cells provides access to all potential TAAs, and targets that may be unidentified for use by immune cells. In addition, whole tumor cell vaccines that incorporate dead or dying tumor cells resulting from ICD provide a more robust immune response (59, 60), and constitute what we refer to as a DTCV. The robust immune response associated with induction of ICD is attributed to the increase in DAMPs including high HMGB1 (61, 62), HSPs (63, 64), and pentraxin-3 (PTX3) (65), and ATP (66). In addition to the presence of DAMPs, exposure to irradiation can increase the expression of calreticulin (CRT) and phosphatidylserine (PS) on the surface of the cancer cells (67–70) which also contributes to immune recognition of dying cells.

Previous studies have reported that the protocol used for generating a DTCV impacts their efficacy. For example, cancer vaccines consisting of apoptotic cells demonstrated better protection than necrotic cells in colon, melanoma, and renal cancer models (15). However, opposing results have been reported in melanoma where comparable protection was observed when DCs were pre-loaded with necrotic or apoptotic cancer cells (71). Exposing cancer cells to irradiation, UVirradiation and γ -irradiation can result in apoptosis (72, 73), while necrosis can be achieved through repeated F/T cycles, with the number of cycles contributing to the necrotic state of the cells (74). UV and γ -irradiation have previously been compared in colon cancer (75), and in human melanoma (76). Vandenberk et al. showed that irradiating lysed tumor cells in a model of highgrade glioma is more effective than either irradiation or lysis alone (13). In the present study, we focused on comparing four different protocols used to generate a DTCV, consisting of cancer cells that were either exposed to lysis, UV-irradiation, LyUV, or γ-irradiation. LyUV utilized a single round of F/T as multiple rounds induced more necrosis and debris, while a single cycle had the potential to promote antigen cross-presentation, while also keeping membranes intact (22, 74). By using a single round of F/T, subsequent exposure to UV-irradiation, which is the case in our LyUV treatment, has the potential to act on tumor cells that may have partially intact membranes.

We found that LyUV, although by visual observation appears to be a combination of lysis and UV-irradiation. Further analysis by flow cytometry 24 hrs. post induction of cell death results in minimal differences between lysis, UV-irradiation and LyUV. However, at the 3 hr time point after induction of cell death, there are greater differences seen in the flow cytometry analysis, with LyUV resembling UV-irradiation, although UV-irradiation

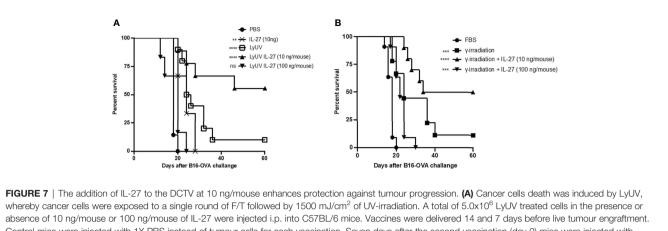


subcutaneously and tumour growth was then monitored every second day for the duration of the experiment. (B) Kaplan-Meier survival curve of mice receiving each of the vaccinations. $*^{*}\rho < 0.005$, $*^{**}\rho < 0.001$. ns denotes not significant.

alone yielded live cells. Lysis and LyUV resulted in more rapid induction of cell death when compared to UV- or γ -irradiation alone. The induction of cell death can increase the potential of TAA acquisition by APCs. With antigen quality being an important factor to consider when designing antigen specific immune responses (77); this may provide insight into the improved protection of LyUV (single round of F/T) compared to lysis (5 rounds of F/T), as repeated F/T cycles may decrease TAA quality (78).

Cancer cells develop immune escape mechanisms (79), and each of these mechanisms highlight challenges and potential targets for cancer immunotherapies. An example of this is through the downregulation of MHC-I on cancer cells, making these cells less immunogenic (80) and unable to be detected by CD8⁺ T cells (24). We show that exposure to both UV- and γ irradiation can increase MHC-I expression, and in the B16-OVA model, UV-irradiation was able to increase MHC-I expression to a greater extent than γ -irradiation at the doses compared. We were not able to test MHC-I expression levels following exposure to lysis or LyUV because the large increase in cellular debris present after 24 hrs. of incubation rendered these protocols of inducing cell death unsuitable for analysis by flow cytometry. However, with LyUV having the potential to yield intact cells these cells may have increased MHC-I expression that could promote $CD8^+$ T cell recognition of the tumor cells. Although the focus of inducing cell death was to evaluate changes in MHC-I expression, which would have the potential to improve $CD8^+$ T cell recognition of cancer cells, future studies could also investigate how DTCVs could impact $CD4^+$ T cell development, as $CD4^+$ T cells can help promote and sustain anti-tumor $CD8^+$ T cell responses (81).

Appropriate DC stimulation can promote effective T cell activation, while the absence of appropriate co-stimulation can lead to T cell anergy (82). In our study, supernatants from dead cancer cells influenced DC2.4 activation. We observed an increase in the co-stimulatory molecules CD80, CD86 and CD40 following UV and LyUV protocols. Indicating, that the supernatants from these cells can promote co-stimulatory molecule expression on DCs, which are required for T cell activation. Interestingly we observed an increase in CD80 expression following lysis, while following exposure to γ -irradiation we observed a decrease in expression. This may be attributed to the timing at which CD80 expression was observed, as CD80 is increased later when compared to CD86 (83). To this point, supernatants from cancer cells exposed to γ -irradiation did not result in DC upregulation of any markers tested. This may be



Control mice were injected with 1X PBS instead of tumour cells for each vaccination. Seven days after the second vaccination (day 0) mice were injected with 1.0×10^6 live B16-OVA cells subcutaneously and tumour growth was then monitored. **(B)** Following the same vaccination schedule as in A, however, cancer cells death was induced by γ -irradiation at a dose of 60 Gys. Kapan-Meier survival graph of n= 7 mice. **p < 0.01, ***p < 0.001, ****p < 0.0001. ns denotes not significant. The statistical difference is compared to PBS for each vaccination group.

a result of γ -irradiation yielding many cells in early apoptosis following the 24 hr incubation, leading to fewer DAMPs being present at the time of collection. Previous research has indicated that apoptotic or necrotic tumor cells can activate DCs, while other studies indicated opposing results (84).

We demonstrated that LyUV can induce rapid cancer cell death and effective activation of DCs. The timing of DC activation and maturation can dictate antigen cross-presentation (20, 85). We found that DC phagocytosis of cancer cells was greater 3 hrs. after LyUV compared to UV-irradiation or γ -irradiation but not that of lysis. If cancer cells were left for 24 hrs. before co-incubation with DCs, LyUV still

resulted in greater phagocytosis than UV- or γ -irradiation, but the difference between lysis and LyUV was not significant. This indicates that LyUV can provide the benefits of lysis (increased antigen acquisition) and the benefits of UV-irradiation (DC activation). Furthermore, induction of cell lysis by F/T cycles has been shown to be poor at activating the immune response (86). However, cell lysis results in the formation of cellular fragments that are easier for acquisition by DCs. This may help indicate why a more significant amount of phagocytosis was observed with lysis when compared to LyUV. Moreover, DCs in an immature state are well recognized for their capacity for endocytosis of extracellular components, however upon

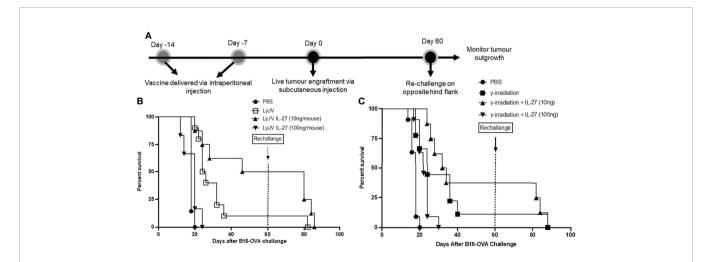


FIGURE 8 | The use of IL-27 as a vaccine adjuvant does not provide long-term protection against tumour rechallenge. (**A**) Schematic representation of prophylactic vaccination preparation with tumour rechallenge. A total of 5.0x10⁶ B16-OVA cells were exposed to the indicated protocol of inducing cells death (LyUV or γirradiation) in the presence or absence of 10 ng/mouse or 100 ng/mouse of rmIL-27 and subsequently injected i.p. into C57BL/6 mice 14 and 7 days before live B16-OVA cancer cell engraftment. Control mice were injected with 1X PBS instead of cancer cells for each vaccination. Seven days after the second vaccination (day 0) mice were injected with 1.0x10⁶ live B16-OVA cells over the opposite hind flank. (**B, C**) LyUV and γ-irradiation Kapan-Meier survival curve. No significant differences were observed.

maturation they have reduced antigen acquisition and improved antigen processing and presentation (87). This may explain why cell lysis would allow a higher degree of phagocytosis while not improving DC activation as compared to LyUV.

We next wanted to determine how other protocols for generating DTCVs influenced protection against tumor challenge. A prime-boost model was used because it provides better protection than a single vaccination in our model. We found that LyUV, but not lysis or UV-irradiation, significantly improved protection compared to PBS. B16-OVA cells exposed to UV-irradiation and y-irradiation had comparable effects on DC activation and resulting phagocytosis, however γ -irradiation provided better protection against tumor challenge than UVirradiation. This may be attributed to the high dose of UV irradiation used in this study impacting the resulting cell death observed following injection. In contrast γ -irradiation results in a more gradual induction of cell death going through early apoptotic and late apoptotic stages. However, at the high dose of UV-irradiation used here the cells progress from live to dead rapidly after vaccination, potentially explaining the reduced efficacy in protection observed. Although others have reported that cancer cell death induced by lysis or UV-irradiation alone or antigen preloaded DCs can enhance protection (71, 88). The increase in the protection provided by LyUV was comparable to γ -irradiation. These results indicate that LyUV can be used as an additional protocol of inducing cell death that can be completed faster and safely.

Studies have explored using irradiated tumor cells that are transduced with genes encoding an adjuvant, such as a cytokine, in cancer vaccines to help orchestrate a desired immune response (89, 90). With LyUV, it is not possible to transfect these cells and ensure continual expression of the desired cytokine after exposure. Therefore, with incomplete protection and an inability to transfect LyUV exposed B16-OVA cells, we next wanted to determine how the addition of a recombinant cytokine could improve the efficacy of our DTCVs.

IL-12 has been explored as a cancer vaccine adjuvant by promoting anti-tumor effects (30, 91), however, the use of IL-12 has been limited due to toxicity concerns (92, 93). Studies have used inducible IL-12 expression in chimeric antigen receptor (CAR) T cell therapy to reduce toxicity associated with IL-12 (94). Furthermore, IL-27 is a member of the IL-12 family of cytokines and is well tolerated and does not exhibit toxicity concerns (31). In the current study, we asked whether rmIL-27 would be capable of enhancing the efficacy of the DTCV. IL-27 can promote Th1 differentiation (95, 96), while also providing enhanced CTL activation in vivo (97, 98). In addition, IL-27 can improve DC-mediated antigen presentation and result in Treg depletion (35, 99). However, IL-27 has been identified as a pleiotropic cytokine (32) with the capacity to also activate Tregs (100) and induce immunosuppression through DCs (101, 102), which may depend on their maturation state (103). In this study, we tested two different doses of rmIL-27 to determine the effects of IL-27 in our DTCVs. We observed that rmIL-27 was able to enhance protection by both LyUV and γ -irradiated DTCVs; however, the dose of rmIL-27

drastically impacted the efficacy of the vaccine in the B16-OVA model used. Interestingly, the addition of rmIL-27 at a lower dose (10 ng/mouse) to vaccinations consisting of LyUV or γ -irradiated B16-OVA cells provided significant increases in survival of mice challenged with live tumors. However, at a higher concentration of rmIL-27 (100ng/mouse), there was a decrease in protection compared to LyUV or γ -irradiated cells alone. This indicates the potential of rmIL-27 at higher doses having an immunosuppressive effect. Previous studies using IL-27 transfected B16 cells have non-specified concentrations (104, 105), while delivery using viral vectors yields varying concentrations (35, 106). The levels of IL-27 may be an important factor to consider where higher amounts may reduce the potential for an anti-tumor immune response to ensue in a prophylactic model.

With a significant improvement in survival observed with the addition of rmIL-27 at a lower dose, we asked if the surviving mice could be protected against tumor rechallenge. Regardless of the protocol used to induce cell death, or the addition of rmIL-27 to the DTCVs, mice that originally demonstrated protection did not survive longer than 30 days following tumor rechallenge. This may indicate that in our model, rmIL-27 can promote antitumor effector T cell responses without the induction of memory. Other researchers have indicated that IL-27 is required for the induction of T cell activation and memory in response to immunization (107, 108). The development of effector versus memory responses can be dictated by distinct cytokines and transcription factors (109). Based on our results, it appears that the effects of IL-27 as an adjuvant in a DTCV to develop antitumor responses are not long-lasting and could be due to the lack of establishing robust memory responses. The lack of a robust memory response could also be attributed to weak induction of CD4⁺ T cell help, which is required for memory CD8⁺ T cell generation (81). However, the presence of IL-27 during the initial vaccination may help promote innate immune cell activation to establish strong anti-tumor responses. NK cells can also respond to IL-27 and promote effector cell function in viral and tumor models (110, 111). Therefore, future research should investigate how a prophylactic vaccine consisting of tumor cells exposed to a method of ICD and IL-27 affects T cell (effector and memory) and NK cell responses.

Although LyUV and γ -irradiation could protect against tumor challenges, it is essential to recognize the limitations of these methods. The main restriction is the need to obtain high cell number; unlike DNA and peptide cancer vaccines, where the target can be synthetically made, DTCVs require isolating tumor cells in large quantities. The DTCVs evaluated here would be easier to prepare and deliver following tumor resection from the patient, to prevent tumor recurrence, similarly to that of BCG vaccination protocol to avoid the recurrence of bladder cancer (112). These challenges would not be present if a DTCV was used therapeutically, where the tumor cells would be detectable and accessible. IL-27 is known to directly impact both CD4⁺ and CD8⁺ T cells and both cell types have a role in promoting cancer vaccine efficacy. Therefore, future studies should investigate the mechanisms involved in establishing the increase in DTCV efficacy with the addition of IL-27.

In conclusion, we demonstrate in a prophylactic setting that different protocols to induce cell death can impact the efficacy of DTCVs and that the LyUV is a robust protocol of inducing cell death that can give significant protection against tumor growth *in vivo*. Moreover, we highlight the potential of using rmIL-27 as an adjuvant to improve cancer vaccines, while emphasizing the importance of dose consideration. Therefore, IL-27 shows promise in enhancing anti-tumor responses but requires further investigation into the mechanisms that are responsible for its pleiotropic effects.

DATA AVAILABILITY STATEMENT

The original contributions presented in the study are included in the article/**Supplementary Material**. Further inquiries can be directed to the corresponding author.

ETHICS STATEMENT

The animal study was reviewed and approved by Queen's University Animal Care Services.

AUTHOR CONTRIBUTIONS

KS, KG, and SB conceptualized the project. KS and OK performed experiments. KS analyzed and wrote the manuscript. PG provided experimental insight. All authors reviewed and edited the manuscript.

REFERENCES

- Mougel A, Terme M, Tanchot C. Therapeutic Cancer Vaccine and Combinations With Antiangiogenic Therapies and Immune Checkpoint Blockade. *Front Immunol* (2019) 10:467. doi: 10.3389/fimmu.2019.00467
- Crews DW, Dombroski JA, King MR. Prophylactic Cancer Vaccines Engineered to Elicit Specific Adaptive Immune Response. *Front Oncol* (2021) 11:626463. doi: 10.3389/fonc.2021.626463
- Finn OJ. The Dawn of Vaccines for Cancer Prevention. Nat Rev Immunol (2018) 18(3):183–94. doi: 10.1038/nri.2017.140
- Yee C, Thompson JA, Byrd D, Riddell SR, Roche P, Celis E, et al. Adoptive T Cell Therapy Using Antigen-Specific Cd8+ T Cell Clones for the Treatment of Patients With Metastatic Melanoma: *In Vivo* Persistence, Migration, and Antitumor Effect of Transferred T Cells. *Proc Natl Acad Sci U.S.A.* (2002) 99 (25):16168–73. doi: 10.1073/pnas.242600099
- 5. Dudley ME, Wunderlich JR, Robbins PF, Yang JC, Hwu P, Schwartzentruber DJ, et al. Cancer Regression and Autoimmunity in Patients After Clonal Repopulation With Antitumor Lymphocytes. *Science* (2002) 298(5594):850–4. doi: 10.1126/science.1076514
- Boon T, Coulie PG, Van den Eynde B. Tumor Antigens Recognized by T Cells. *Immunol Today* (1997) 18(6):267–8. doi: 10.1016/s0167-5699(97) 80020-5
- Greenberg PD. Adoptive T Cell Therapy of Tumors: Mechanisms Operative in the Recognition and Elimination of Tumor Cells. *Adv Immunol* (1991) 49:281–355. doi: 10.1016/s0065-2776(08)60778-6
- Zamora AE, Crawford JC, Thomas PG. Hitting the Target: How T Cells Detect and Eliminate Tumors. *J Immunol* (2018) 200(2):392–9. doi: 10.4049/ jimmunol.1701413

SUPPLEMENTARY MATERIAL

The Supplementary Material for this article can be found online at: https://www.frontiersin.org/articles/10.3389/fimmu.2022. 884827/full#supplementary-material

Supplementary Figure 1 | Evaluation of propidium iodide staining following exposure to different numbers of F/T cycles. Cancer cells were exposed to the indicated number of rounds of F/T cycles (0, 1, or 5) and subsequently stained with propidium iodide (1.5 µg/mL) and analyzed *via* flow cytometry. **(A)** Fold change in MFI compared to untreated cells with data expressed as \pm SD of three independent experiments. **(B)** Representative dot plot of total PI positive cells as a percent following the indicated number of rounds of F/T cycles. The percent PI positive cells are shown in the dot plots. n = 3, **p < 0.01. ns denotes not significant.

Supplementary Figure 2 | Comparison of different doses of γ -irradiation on B16-OVA cell death 24 hrs. after treatment. Cancer cells were exposed to the indicated dose of γ -irradiation and left to incubate for 24 hrs. Cells were then harvested, and the type of cell death was determined through AV/PI staining and flow cytometry.

Supplementary Figure 3 | Prophylactic cancer vaccine consisting of γ -irradiated B16-OVA cells delivered in a prime-boost vaccination model provides better protection than a single vaccination with DTCV. γ -irradiated B16-OVA cancer cells were injected intraperitoneally (i.p.) at 5.0x10⁶ cells/mouse: either once, one week before engraftment; or twice, one and two weeks before engraftment. Seven days after the final vaccination, mice were engrafted with 1.0x10⁶ live B16-OVA cells subcutaneously and tumour growth was monitored. Kapan-Meier survival analysis, n = at least 5. *p < 0.05, ns denotes not significant.

Supplementary Figure 4 | The addition of IL-27 at a lower dose to the prophylactic cancer vaccine consisting of LyUV-treated B16 cells improved protection. B16 cells (not expressing OVA) were exposed to LyUV treatment and were injected intraperitoneally (i.p.) at 5.0×10^6 cells/mouse in the absence or presence of rmIL-27 at 10ng/mouse or 100 ng/mouse. The vaccine was delivered 14 and 7 days before tumour engraftment with 1.0×10^6 B16 cells injected subcutaneously on day 0. Tumour outgrowth was then monitored. Kapan-Meier survival analysis, n = 3. *p < 0.05.

- van der Bruggen P, Traversari C, Chomez P, Lurquin C, De Plaen E, Van den Eynde B, et al. A Gene Encoding an Antigen Recognized by Cytolytic T Lymphocytes on a Human Melanoma. *Science* (1991) 254(5038):1643–7. doi: 10.1126/science.1840703
- Slingluff CL Jr, Petroni GR, Olson W, Czarkowski A, Grosh WW, Smolkin M, et al. Helper T-Cell Responses and Clinical Activity of a Melanoma Vaccine With Multiple Peptides From Mage and Melanocytic Differentiation Antigens. J Clin Oncol (2008) 26(30):4973-80. doi: 10.1200/JCO.2008.17.3161
- Knutson KL, Block MS, Norton N, Erskine CL, Hobday TJ, Dietz AB, et al. Rapid Generation of Sustainable Her2-Specific T-Cell Immunity in Patients With Her2 Breast Cancer Using a Degenerate Hla Class Ii Epitope Vaccine. *Clin Cancer Res* (2020) 26(5):1045–53. doi: 10.1158/1078-0432.CCR-19-2123
- Sabel MS, Sondak VK. Tumor Vaccines: A Role in Preventing Recurrence in Melanoma? *Am J Clin Dermatol* (2002) 3(9):609–16. doi: 10.2165/00128071-200203090-00003
- Vandenberk L, Garg AD, Verschuere T, Koks C, Belmans J, Beullens M, et al. Irradiation of Necrotic Cancer Cells, Employed for Pulsing Dendritic Cells (Dcs), Potentiates Dc Vaccine-Induced Antitumor Immunity Against High-Grade Glioma. Oncoimmunology (2016) 5(2):e1083669. doi: 10.1080/ 2162402X.2015.1083669
- Vandenberk L, Belmans J, Van Woensel M, Riva M, Van Gool SW. Exploiting the Immunogenic Potential of Cancer Cells for Improved Dendritic Cell Vaccines. *Front Immunol* (2015) 6:663. doi: 10.3389/ fimmu.2015.00663
- Scheffer SR, Nave H, Korangy F, Schlote K, Pabst R, Jaffee EM, et al. Apoptotic, But Not Necrotic, Tumor Cell Vaccines Induce a Potent Immune Response in Vivo. Int J Cancer (2003) 103(2):205–11. doi: 10.1002/ijc.10777

- Galluzzi L, Buque A, Kepp O, Zitvogel L, Kroemer G. Immunogenic Cell Death in Cancer and Infectious Disease. *Nat Rev Immunol* (2017) 17(2):97– 111. doi: 10.1038/nri.2016.107
- Hernandez C, Huebener P, Schwabe RF. Damage-Associated Molecular Patterns in Cancer: A Double-Edged Sword. Oncogene (2016) 35(46):5931– 41. doi: 10.1038/onc.2016.104
- Seya T, Shime H, Ebihara T, Oshiumi H, Matsumoto M. Pattern Recognition Receptors of Innate Immunity and Their Application to Tumor Immunotherapy. *Cancer Sci* (2010) 101(2):313–20. doi: 10.1111/j.1349-7006.2009.01442.x
- Nace G, Evankovich J, Eid R, Tsung A. Dendritic Cells and Damage-Associated Molecular Patterns: Endogenous Danger Signals Linking Innate and Adaptive Immunity. J Innate Immun (2012) 4(1):6–15. doi: 10.1159/000334245
- van Mierlo GJ, Boonman ZF, Dumortier HM, den Boer AT, Fransen MF, Nouta J, et al. Activation of Dendritic Cells That Cross-Present Tumor-Derived Antigen Licenses Cd8+ Ctl to Cause Tumor Eradication. *J Immunol* (2004) 173(11):6753–9. doi: 10.4049/jimmunol.173.11.6753
- Huang AY, Golumbek P, Ahmadzadeh M, Jaffee E, Pardoll D, Levitsky H. Role of Bone Marrow-Derived Cells in Presenting Mhc Class I-Restricted Tumor Antigens. *Science* (1994) 264(5161):961–5. doi: 10.1126/ science.7513904
- Kim J, Gambhir V, Alatery A, Basta S. Delivery of Exogenous Antigens to Induce Cytotoxic Cd8+ T Lymphocyte Responses. J BioMed Biotechnol (2010) 2010:218752. doi: 10.1155/2010/218752
- 23. Chen W, Masterman KA, Basta S, Haeryfar SM, Dimopoulos N, Knowles B, et al. Cross-Priming of Cd8+ T Cells by Viral and Tumor Antigens Is a Robust Phenomenon. *Eur J Immunol* (2004) 34(1):194–9. doi: 10.1002/eji.200324257
- Dhatchinamoorthy K, Colbert JD, Rock KL. Cancer Immune Evasion Through Loss of Mhc Class I Antigen Presentation. *Front Immunol* (2021) 12:636568. doi: 10.3389/fimmu.2021.636568
- Tovey MG, Lallemand C. Adjuvant Activity of Cytokines. *Methods Mol Biol* (2010) 626:287–309. doi: 10.1007/978-1-60761-585-9_19
- Rizza P, Ferrantini M, Capone I, Belardelli F. Cytokines as Natural Adjuvants for Vaccines: Where Are We Now? *Trends Immunol* (2002) 23 (8):381–3. doi: 10.1016/s1471-4906(02)02276-7
- Nohria A, Rubin RH. Cytokines as Potential Vaccine Adjuvants. *Biotherapy* (1994) 7(3-4):261–9. doi: 10.1007/BF01878491
- Capitini CM, Fry TJ, Mackall CL. Cytokines as Adjuvants for Vaccine and Cellular Therapies for Cancer. Am J Immunol (2009) 5(3):65–83. doi: 10.3844/ajisp.2009.65.83
- Rakhmilevich AL, Janssen K, Turner J, Culp J, Yang NS. Cytokine Gene Therapy of Cancer Using Gene Gun Technology: Superior Antitumor Activity of Interleukin-12. *Hum Gene Ther* (1997) 8(11):1303–11. doi: 10.1089/hum.1997.8.11-1303
- Brunda MJ, Luistro L, Warrier RR, Wright RB, Hubbard BR, Murphy M, et al. Antitumor and Antimetastatic Activity of Interleukin 12 Against Murine Tumors. J Exp Med (1993) 178(4):1223–30. doi: 10.1084/ jem.178.4.1223
- Hisada M, Kamiya S, Fujita K, Belladonna ML, Aoki T, Koyanagi Y, et al. Potent Antitumor Activity of Interleukin-27. *Cancer Res* (2004) 64(3):1152– 6. doi: 10.1158/0008-5472.can-03-2084
- Beizavi Z, Zohouri M, Asadipour M, Ghaderi A. Il-27, a Pleiotropic Cytokine for Fine-Tuning the Immune Response in Cancer. *Int Rev Immunol* (2021) 40(5):319–29. doi: 10.1080/08830185.2020.1840565
- 33. Kourko O, Smyth R, Cino D, Seaver K, Petes C, Eo SY, et al. Poly(I:C)-Mediated Death of Human Prostate Cancer Cell Lines Is Induced by Interleukin-27 Treatment. J Interferon Cytokine Res (2019) 39(8):483–94. doi: 10.1089/jir.2018.0166
- Kourko O, Seaver K, Odoardi N, Basta S, Gee K. Il-27, Il-30, and Il-35: A Cytokine Triumvirate in Cancer. *Front Oncol* (2019) 9:969. doi: 10.3389/ fonc.2019.00969
- 35. Zhu J, Liu JQ, Shi M, Cheng X, Ding M, Zhang JC, et al. Il-27 Gene Therapy Induces Depletion of Tregs and Enhances the Efficacy of Cancer Immunotherapy. JCI Insight (2018) 3(7):e98745. doi: 10.1172/ jci.insight.98745

- 36. Fidler IJ. Biological Behavior of Malignant Melanoma Cells Correlated to Their Survival *in Vivo. Cancer Res* (1975) 35(1):218–24.
- Shen Z, Reznikoff G, Dranoff G, Rock KL. Cloned Dendritic Cells Can Present Exogenous Antigens on Both Mhc Class I and Class Ii Molecules. *J Immunol* (1997) 158(6):2723–30.
- Basta S, Stoessel R, Basler M, van den Broek M, Groettrup M. Cross-Presentation of the Long-Lived Lymphocytic Choriomeningitis Virus Nucleoprotein Does Not Require Neosynthesis and Is Enhanced Via Heat Shock Proteins. J Immunol (2005) 175(2):796–805. doi: 10.4049/ jimmunol.175.2.796
- Siddiqui S, Basta S. Cd8+ T Cell Immunodominance in Lymphocytic Choriomeningitis Virus Infection Is Modified in the Presence of Toll-Like Receptor Agonists. J Virol (2011) 85(24):13224–33. doi: 10.1128/JVI.05996-11
- 40. Alothaimeen T, Seaver K, Mulder R, Gee K, Basta S. Granulocyte/ Macrophage Colony-Stimulating Factor-Derived Macrophages Exhibit Distinctive Early Immune Response to Lymphocytic Choriomeningitis Virus Infection. Viral Immunol (2020) 33(6):477–88. doi: 10.1089/ vim.2019.0178
- Tomayko MM, Reynolds CP. Determination of Subcutaneous Tumor Size in Athymic (Nude) Mice. *Cancer Chemother Pharmacol* (1989) 24(3):148–54. doi: 10.1007/BF00300234
- Alatery A, Basta S. An Efficient Culture Method for Generating Large Quantities of Mature Mouse Splenic Macrophages. J Immunol Methods (2008) 338(1-2):47–57. doi: 10.1016/j.jim.2008.07.009
- Lemay CG, Rintoul JL, Kus A, Paterson JM, Garcia V, Falls TJ, et al. Harnessing Oncolytic Virus-Mediated Antitumor Immunity in an Infected Cell Vaccine. *Mol Ther* (2012) 20(9):1791–9. doi: 10.1038/mt.2012.128
- 44. Golden EB, Frances D, Pellicciotta I, Demaria S, Helen Barcellos-Hoff M, Formenti SC. Radiation Fosters Dose-Dependent and Chemotherapy-Induced Immunogenic Cell Death. Oncoimmunology (2014) 3:e28518. doi: 10.4161/onci.28518
- 45. Sharabi AB, Nirschl CJ, Kochel CM, Nirschl TR, Francica BJ, Velarde E, et al. Stereotactic Radiation Therapy Augments Antigen-Specific Pd-1-Mediated Antitumor Immune Responses Via Cross-Presentation of Tumor Antigen. Cancer Immunol Res (2015) 3(4):345–55. doi: 10.1158/2326-6066.CIR-14-0196
- Mosch B, Mueller K, Steinbach J, Pietzsch J. Influence of Irradiation on Metabolism and Metastatic Potential of B16-F10 Melanoma Cells. Int J Radiat Biol (2009) 85(11):1002–12. doi: 10.3109/09553000903258871
- Reits EA, Hodge JW, Herberts CA, Groothuis TA, Chakraborty M, Wansley EK, et al. Radiation Modulates the Peptide Repertoire, Enhances Mhc Class I Expression, and Induces Successful Antitumor Immunotherapy. *J Exp Med* (2006) 203(5):1259–71. doi: 10.1084/jem.20052494
- Subauste CS, de Waal Malefyt R, Fuh F. Role of Cd80 (B7.1) and Cd86 (B7.2) in the Immune Response to an Intracellular Pathogen. *J Immunol* (1998) 160 (4):1831–40.
- Garner H, de Visser KE. Immune Crosstalk in Cancer Progression and Metastatic Spread: A Complex Conversation. *Nat Rev Immunol* (2020) 20 (8):483–97. doi: 10.1038/s41577-019-0271-z
- Rabinovich GA, Gabrilovich D, Sotomayor EM. Immunosuppressive Strategies That Are Mediated by Tumor Cells. Annu Rev Immunol (2007) 25:267–96. doi: 10.1146/annurev.immunol.25.022106.141609
- Sobol RE. The Rationale for Prophylactic Cancer Vaccines and Need for a Paradigm Shift. *Cancer Gene Ther* (2006) 13(8):725–31. doi: 10.1038/ sj.cgt.7700950
- Finn OJ. Vaccines for Cancer Prevention: A Practical and Feasible Approach to the Cancer Epidemic. *Cancer Immunol Res* (2014) 2(8):708–13. doi: 10.1158/2326-6066.CIR-14-0110
- Slingluff CLJr., Petroni GR, Chianese-Bullock KA, Smolkin ME, Hibbitts S, Murphy C, et al. Immunologic and Clinical Outcomes of a Randomized Phase Ii Trial of Two Multipeptide Vaccines for Melanoma in the Adjuvant Setting. *Clin Cancer Res* (2007) 13(21):6386–95. doi: 10.1158/1078-0432.CCR-07-0486
- Tagliamonte M, Petrizzo A, Tornesello ML, Buonaguro FM, Buonaguro L. Antigen-Specific Vaccines for Cancer Treatment. *Hum Vaccin Immunother* (2014) 10(11):3332–46. doi: 10.4161/21645515.2014.973317

- 55. Slingluff CLJr., Petroni GR, Yamshchikov GV, Hibbitts S, Grosh WW, Chianese-Bullock KA, et al. Immunologic and Clinical Outcomes of Vaccination With a Multiepitope Melanoma Peptide Vaccine Plus Low-Dose Interleukin-2 Administered Either Concurrently or on a Delayed Schedule. J Clin Oncol (2004) 22(22):4474–85. doi: 10.1200/JCO.2004.10.212
- 56. Fang J, Hu B, Li S, Zhang C, Liu Y, Wang P. A Multi-Antigen Vaccine in Combination With an Immunotoxin Targeting Tumor-Associated Fibroblast for Treating Murine Melanoma. *Mol Ther Oncolytics* (2016) 3:16007. doi: 10.1038/mto.2016.7
- Neller MA, Lopez JA, Schmidt CW. Antigens for Cancer Immunotherapy. Semin Immunol (2008) 20(5):286–95. doi: 10.1016/j.smim.2008.09.006
- Suzuki H, Fukuhara M, Yamaura T, Mutoh S, Okabe N, Yaginuma H, et al. Multiple Therapeutic Peptide Vaccines Consisting of Combined Novel Cancer Testis Antigens and Anti-Angiogenic Peptides for Patients With Non-Small Cell Lung Cancer. J Transl Med (2013) 11:97. doi: 10.1186/1479-5876-11-97
- Demaria S, Formenti SC. Radiation as an Immunological Adjuvant: Current Evidence on Dose and Fractionation. *Front Oncol* (2012) 2:153. doi: 10.3389/ fonc.2012.00153
- 60. Fucikova J, Kepp O, Kasikova L, Petroni G, Yamazaki T, Liu P, et al. Detection of Immunogenic Cell Death and Its Relevance for Cancer Therapy. Cell Death Dis (2020) 11(11):1013. doi: 10.1038/s41419-020-03221-2
- Scaffidi P, Misteli T, Bianchi ME. Release of Chromatin Protein Hmgb1 by Necrotic Cells Triggers Inflammation. *Nature* (2002) 418(6894):191–5. doi: 10.1038/nature00858
- Rovere-Querini P, Capobianco A, Scaffidi P, Valentinis B, Catalanotti F, Giazzon M, et al. Hmgb1 Is an Endogenous Immune Adjuvant Released by Necrotic Cells. *EMBO Rep* (2004) 5(8):825–30. doi: 10.1038/ sj.embor.7400205
- Creagh EM, Sheehan D, Cotter TG. Heat Shock Proteins–Modulators of Apoptosis in Tumour Cells. *Leukemia* (2000) 14(7):1161–73. doi: 10.1038/ sj.leu.2401841
- 64. Basu S, Binder RJ, Suto R, Anderson KM, Srivastava PK. Necrotic But Not Apoptotic Cell Death Releases Heat Shock Proteins, Which Deliver a Partial Maturation Signal to Dendritic Cells and Activate the Nf-Kappa B Pathway. *Int Immunol* (2000) 12(11):1539–46. doi: 10.1093/intimm/12.11.1539
- 65. Rovere P, Peri G, Fazzini F, Bottazzi B, Doni A, Bondanza A, et al. The Long Pentraxin Ptx3 Binds to Apoptotic Cells and Regulates Their Clearance by Antigen-Presenting Dendritic Cells. *Blood* (2000) 96(13):4300–6. doi: 10.1182/blood.V96.13.4300
- 66. Martins I, Wang Y, Michaud M, Ma Y, Sukkurwala AQ, Shen S, et al. Molecular Mechanisms of Atp Secretion During Immunogenic Cell Death. *Cell Death Differ* (2014) 21(1):79–91. doi: 10.1038/cdd.2013.75
- Hoffmann PR, deCathelineau AM, Ogden CA, Leverrier Y, Bratton DL, Daleke DL, et al. Phosphatidylserine (Ps) Induces Ps Receptor-Mediated Macropinocytosis and Promotes Clearance of Apoptotic Cells. J Cell Biol (2001) 155(4):649–59. doi: 10.1083/jcb.200108080
- 68. Fadok VA, de Cathelineau A, Daleke DL, Henson PM, Bratton DL. Loss of Phospholipid Asymmetry and Surface Exposure of Phosphatidylserine Is Required for Phagocytosis of Apoptotic Cells by Macrophages and Fibroblasts. J Biol Chem (2001) 276(2):1071–7. doi: 10.1074/jbc.M003649200
- Fadok VA, Voelker DR, Campbell PA, Cohen JJ, Bratton DL, Henson PM. Exposure of Phosphatidylserine on the Surface of Apoptotic Lymphocytes Triggers Specific Recognition and Removal by Macrophages. J Immunol (1992) 148(7):2207–16.
- Obeid M, Tesniere A, Ghiringhelli F, Fimia GM, Apetoh L, Perfettini JL, et al. Calreticulin Exposure Dictates the Immunogenicity of Cancer Cell Death. *Nat Med* (2007) 13(1):54–61. doi: 10.1038/nm1523
- Kotera Y, Shimizu K, Mule JJ. Comparative Analysis of Necrotic and Apoptotic Tumor Cells as a Source of Antigen(S) in Dendritic Cell-Based Immunization. *Cancer Res* (2001) 61(22):8105–9.
- Rieber MS, Rieber M. Uv Radiation Induces DNA Fragmentation and Cell Death in B16 Melanoma Sensitized by Bromodeoxyuridine: Impaired C-Jun Induction and Defective Tyrosine Phosphorylation Signalling. *Biochem Biophys Res Commun* (1994) 203(3):1629–37. doi: 10.1006/bbrc.1994.2373

- Zhao H, Spitz MR, Tomlinson GE, Zhang H, Minna JD, Wu X. Gamma-Radiation-Induced G2 Delay, Apoptosis, and P53 Response as Potential Susceptibility Markers for Lung Cancer. *Cancer Res* (2001) 61(21):7819–24.
- 74. Sauter B, Albert ML, Francisco L, Larsson M, Somersan S, Bhardwaj N. Consequences of Cell Death: Exposure to Necrotic Tumor Cells, But Not Primary Tissue Cells or Apoptotic Cells, Induces the Maturation of Immunostimulatory Dendritic Cells. J Exp Med (2000) 191(3):423–34. doi: 10.1084/jem.191.3.423
- 75. Obeid M, Panaretakis T, Joza N, Tufi R, Tesniere A, van Endert P, et al. Calreticulin Exposure Is Required for the Immunogenicity of Gamma-Irradiation and Uvc Light-Induced Apoptosis. *Cell Death Differ* (2007) 14 (10):1848–50. doi: 10.1038/sj.cdd.4402201
- Deacon DH, Hogan KT, Swanson EM, Chianese-Bullock KA, Denlinger CE, Czarkowski AR, et al. The Use of Gamma-Irradiation and Ultraviolet-Irradiation in the Preparation of Human Melanoma Cells for Use in Autologous Whole-Cell Vaccines. *BMC Cancer* (2008) 8:360. doi: 10.1186/ 1471-2407-8-360
- 77. Salewski I, Gladbach YS, Kuntoff S, Irmscher N, Hahn O, Junghanss C, et al. In Vivo Vaccination With Cell Line-Derived Whole Tumor Lysates: Neoantigen Quality, Not Quantity Matters. J Transl Med (2020) 18(1):402. doi: 10.1186/s12967-020-02570-y
- Gao YC, Yuan ZB, Yang YD, Lu HK. Effect of Freeze-Thaw Cycles on Serum Measurements of Afp, Cea, Ca125 and Ca19-9. Scand J Clin Lab Invest (2007) 67(7):741–7. doi: 10.1080/00365510701297480
- Tang S, Ning Q, Yang L, Mo Z, Tang S. Mechanisms of Immune Escape in the Cancer Immune Cycle. *Int Immunopharmacol* (2020) 86:106700. doi: 10.1016/j.intimp.2020.106700
- Restifo NP, Marincola FM, Kawakami Y, Taubenberger J, Yannelli JR, Rosenberg SA. Loss of Functional Beta 2-Microglobulin in Metastatic Melanomas From Five Patients Receiving Immunotherapy. J Natl Cancer Inst (1996) 88(2):100–8. doi: 10.1093/jnci/88.2.100
- Ahrends T, Busselaar J, Severson TM, Babala N, de Vries E, Bovens A, et al. Cd4(+) T Cell Help Creates Memory Cd8(+) T Cells With Innate and Help-Independent Recall Capacities. *Nat Commun* (2019) 10(1):5531. doi: 10.1038/s41467-019-13438-1
- Quill H, Schwartz RH. Stimulation of Normal Inducer T Cell Clones With Antigen Presented by Purified Ia Molecules in Planar Lipid Membranes: Specific Induction of a Long-Lived State of Proliferative Nonresponsiveness. *J Immunol* (1987) 138(11):3704–12.
- Greene JL, Leytze GM, Emswiler J, Peach R, Bajorath J, Cosand W, et al. Covalent Dimerization of Cd28/Ctla-4 and Oligomerization of Cd80/Cd86 Regulate T Cell Costimulatory Interactions. J Biol Chem (1996) 271 (43):26762–71. doi: 10.1074/jbc.271.43.26762
- Brouckaert G, Kalai M, Krysko DV, Saelens X, Vercammen D, Ndlovu MN, et al. Phagocytosis of Necrotic Cells by Macrophages Is Phosphatidylserine Dependent and Does Not Induce Inflammatory Cytokine Production. *Mol Biol Cell* (2004) 15(3):1089–100. doi: 10.1091/mbc.e03-09-0668
- West MA, Wallin RP, Matthews SP, Svensson HG, Zaru R, Ljunggren HG, et al. Enhanced Dendritic Cell Antigen Capture Via Toll-Like Receptor-Induced Actin Remodeling. Science (2004) 305(5687):1153–7. doi: 10.1126/ science.1099153
- Hatfield P, Merrick AE, West E, O'Donnell D, Selby P, Vile R, et al. Optimization of Dendritic Cell Loading With Tumor Cell Lysates for Cancer Immunotherapy. J Immunother (2008) 31(7):620–32. doi: 10.1097/ CJI.0b013e31818213df
- Dudek AM, Martin S, Garg AD, Agostinis P. Immature, Semi-Mature, and Fully Mature Dendritic Cells: Toward a Dc-Cancer Cells Interface That Augments Anticancer Immunity. *Front Immunol* (2013) 4:438. doi: 10.3389/ fimmu.2013.00438
- Rainone V, Martelli C, Ottobrini L, Biasin M, Texido G, Degrassi A, et al. Immunological Characterization of Whole Tumour Lysate-Loaded Dendritic Cells for Cancer Immunotherapy. *PloS One* (2016) 11(1): e0146622. doi: 10.1371/journal.pone.0146622
- Berraondo P, Sanmamed MF, Ochoa MC, Etxeberria I, Aznar MA, Perez-Gracia JL, et al. Cytokines in Clinical Cancer Immunotherapy. *Br J Cancer* (2019) 120(1):6–15. doi: 10.1038/s41416-018-0328-y

- Briukhovetska D, Dorr J, Endres S, Libby P, Dinarello CA, Kobold S. Interleukins in Cancer: From Biology to Therapy. Nat Rev Cancer (2021) 21(8):481–99. doi: 10.1038/s41568-021-00363-z
- Zeh HJ3rd, Hurd S, Storkus WJ, Lotze MT. Interleukin-12 Promotes the Proliferation and Cytolytic Maturation of Immune Effectors: Implications for the Immunotherapy of Cancer. J Immunother Emphasis Tumor Immunol (1993) 14(2):155–61. doi: 10.1097/00002371-199308000-00012
- Lasek W, Zagozdzon R, Jakobisiak M. Interleukin 12: Still a Promising Candidate for Tumor Immunotherapy? *Cancer Immunol Immunother* (2014) 63(5):419–35. doi: 10.1007/s00262-014-1523-1
- Car BD, Eng VM, Lipman JM, Anderson TD. The Toxicology of Interleukin-12: A Review. *Toxicol Pathol* (1999) 27(1):58–63. doi: 10.1177/ 019262339902700112
- 94. Chmielewski M, Kopecky C, Hombach AA, Abken H. Il-12 Release by Engineered T Cells Expressing Chimeric Antigen Receptors Can Effectively Muster an Antigen-Independent Macrophage Response on Tumor Cells That Have Shut Down Tumor Antigen Expression. *Cancer Res* (2011) 71 (17):5697–706. doi: 10.1158/0008-5472.CAN-11-0103
- 95. Hibbert L, Pflanz S, De Waal Malefyt R, Kastelein RA. Il-27 and Ifn-Alpha Signal Via Stat1 and Stat3 and Induce T-Bet and Il-12rbeta2 in Naive T Cells. J Interferon Cytokine Res (2003) 23(9):513-22. doi: 10.1089/ 10799900360708632
- 96. Pflanz S, Timans JC, Cheung J, Rosales R, Kanzler H, Gilbert J, et al. Il-27, a Heterodimeric Cytokine Composed of Ebi3 and P28 Protein, Induces Proliferation of Naive Cd4+ T Cells. *Immunity* (2002) 16(6):779–90. doi: 10.1016/s1074-7613(02)00324-2
- Liu Z, Liu JQ, Talebian F, Wu LC, Li S, Bai XF. Il-27 Enhances the Survival of Tumor Antigen-Specific Cd8+ T Cells and Programs Them Into Il-10-Producing, Memory Precursor-Like Effector Cells. *Eur J Immunol* (2013) 43 (2):468–79. doi: 10.1002/eji.201242930
- Salcedo R, Stauffer JK, Lincoln E, Back TC, Hixon JA, Hahn C, et al. Il-27 Mediates Complete Regression of Orthotopic Primary and Metastatic Murine Neuroblastoma Tumors: Role for Cd8+ T Cells. J Immunol (2004) 173(12):7170–82. doi: 10.4049/jimmunol.173.12.7170
- Jung JY, Roberts LL, Robinson CM. The Presence of Interleukin-27 During Monocyte-Derived Dendritic Cell Differentiation Promotes Improved Antigen Processing and Stimulation of T Cells. *Immunology* (2015) 144 (4):649–60. doi: 10.1111/imm.12417
- 100. Park YJ, Ryu H, Choi G, Kim BS, Hwang ES, Kim HS, et al. Il-27 Confers a Protumorigenic Activity of Regulatory T Cells Via Cd39. Proc Natl Acad Sci USA (2019) 116(8):3106–11. doi: 10.1073/pnas.1810254116
- 101. Mascanfroni ID, Yeste A, Vieira SM, Burns EJ, Patel B, Sloma I, et al. Il-27 Acts on Dcs to Suppress the T Cell Response and Autoimmunity by Inducing Expression of the Immunoregulatory Molecule Cd39. *Nat Immunol* (2013) 14(10):1054–63. doi: 10.1038/ni.2695
- 102. Karakhanova S, Bedke T, Enk AH, Mahnke K. Il-27 Renders Dc Immunosuppressive by Induction of B7-H1. J Leukoc Biol (2011) 89 (6):837–45. doi: 10.1189/jlb.1209788
- Zhou F, Zhang GX, Rostami A. Distinct Role of Il-27 in Immature and Lps-Induced Mature Dendritic Cell-Mediated Development of Cd4(+) Cd127(+)

3g11(+) Regulatory T Cell Subset. Front Immunol (2018) 9:2562. doi: 10.3389/fimmu.2018.02562

- 104. Chiba Y, Mizoguchi I, Furusawa J, Hasegawa H, Ohashi M, Xu M, et al. Interleukin-27 Exerts Its Antitumor Effects by Promoting Differentiation of Hematopoietic Stem Cells to M1 Macrophages. *Cancer Res* (2018) 78 (1):182–94. doi: 10.1158/0008-5472.CAN-17-0960
- 105. Shimizu M, Shimamura M, Owaki T, Asakawa M, Fujita K, Kudo M, et al. Antiangiogenic and Antitumor Activities of Il-27. J Immunol (2006) 176 (12):7317–24. doi: 10.4049/jimmunol.176.12.7317
- 106. Hu A, Ding M, Zhu J, Liu JQ, Pan X, Ghoshal K, et al. Intra-Tumoral Delivery of 1l-27 Using Adeno-Associated Virus Stimulates Anti-Tumor Immunity and Enhances the Efficacy of Immunotherapy. *Front Cell Dev Biol* (2020) 8:210. doi: 10.3389/fcell.2020.00210
- 107. Pennock ND, Gapin L, Kedl RM. Il-27 Is Required for Shaping the Magnitude, Affinity Distribution, and Memory of T Cells Responding to Subunit Immunization. *Proc Natl Acad Sci USA* (2014) 111(46):16472–7. doi: 10.1073/pnas.1407393111
- 108. Kilgore AM, Pennock ND, Kedl RM. Cdc1 Il-27p28 Production Predicts Vaccine-Elicited Cd8(+) T Cell Memory and Protective Immunity. *J Immunol* (2020) 204(3):510–7. doi: 10.4049/jimmunol.1901357
- Danilo M, Chennupati V, Silva JG, Siegert S, Held W. Suppression of Tcf1 by Inflammatory Cytokines Facilitates Effector Cd8 T Cell Differentiation. *Cell Rep* (2018) 22(8):2107–17. doi: 10.1016/j.celrep.2018.01.072
- Kumar P, Rajasekaran K, Nanbakhsh A, Gorski J, Thakar MS, Malarkannan S. Il-27 Promotes Nk Cell Effector Functions *Via* Maf-Nrf2 Pathway During Influenza Infection. *Sci Rep* (2019) 9(1):4984. doi: 10.1038/s41598-019-41478-6
- 111. Wei J, Xia S, Sun H, Zhang S, Wang J, Zhao H, et al. Critical Role of Dendritic Cell-Derived Il-27 in Antitumor Immunity Through Regulating the Recruitment and Activation of Nk and Nkt Cells. J Immunol (2013) 191 (1):500–8. doi: 10.4049/jimmunol.1300328
- 112. Guallar-Garrido S, Julian E. Bacillus Calmette-Guerin (Bcg) Therapy for Bladder Cancer: An Update. *Immunotargets Ther* (2020) 9:1–11. doi: 10.2147/ITT.S202006

Conflict of Interest: The authors declare that the research was conducted in the absence of any commercial or financial relationships that could be construed as a potential conflict of interest.

Publisher's Note: All claims expressed in this article are solely those of the authors and do not necessarily represent those of their affiliated organizations, or those of the publisher, the editors and the reviewers. Any product that may be evaluated in this article, or claim that may be made by its manufacturer, is not guaranteed or endorsed by the publisher.

Copyright © 2022 Seaver, Kourko, Gee, Greer and Basta. This is an open-access article distributed under the terms of the Creative Commons Attribution License (CC BY). The use, distribution or reproduction in other forums is permitted, provided the original author(s) and the copyright owner(s) are credited and that the original publication in this journal is cited, in accordance with accepted academic practice. No use, distribution or reproduction is permitted which does not comply with these terms.



DNA Hypermethylation-Regulated CX3CL1 Reducing T Cell Infiltration Indicates Poor Prognosis in Wilms Tumour

Tao Mi^{1,2,3}, Liming Jin^{1,2,3}, Zhaoxia Zhang^{1,2,3}, Jinkui Wang^{1,2,3}, Mujie Li^{1,2,3}, Chenghao Zhanghuang^{1,2,3}, Xiaojun Tan^{1,2,3}, Zhang Wang^{1,2,3}, Xiaomao Tian^{1,2,3}, Bin Xiang^{1,2,3} and Dawei He^{1,2,3*}

¹ Department of Urology, Children's Hospital of Chongqing Medical University, Chongqing, China, ² Chongqing Key Laboratory of Children Urogenital Development and Tissue Engineering, Chongqing, China, ³ China International Science and Technology Cooperation Base of Child Development and Critical; National Clinical Research Center for Child Health and Disorders, Chongqing; Ministry of Education Key Laboratory of Child Development and Disorders; Chongqing Key Laboratory of Pediatrics, Chongqing, China

OPEN ACCESS

Edited by: Xuyao Zhang, Fudan University, China

Reviewed by:

Zeguo Sun, Icahn School of Medicine at Mount Sinai, United States Qiaosi Tang, Calico Life Sciences LLC, United States

***Correspondence:** Dawei He hedawei@hospital.cqmu.edu.cn

Specialty section:

This article was submitted to Cancer Immunity and Immunotherapy, a section of the journal Frontiers in Oncology

Received: 24 February 2022 Accepted: 21 March 2022 Published: 22 April 2022

Citation:

Mi T, Jin L, Zhang Z, Wang J, Li M, Zhanghuang C, Tan X, Wang Z, Tian X, Xiang B and He D (2022) DNA Hypermethylation-Regulated CX3CL1 Reducing T Cell Infiltration Indicates Poor Prognosis in Wilms Tumour. Front. Oncol. 12:882714. doi: 10.3389/fonc.2022.882714 **Objective:** To investigate the role of chemokines in Wilms tumours, especially their chemotaxis to immune cells and the role of DNA methylation in regulating the expression level of chemokines.

Methods: RNAseqV2 gene expression and clinical data were downloaded from the TARGET database. DNA methylation data were downloaded from the GEO and cBioPortal database. The difference analysis and Kaplan-Meier(KM) analysis of chemokines were performed by edgeR package. Then predictive model based on chemokines was constructed by lasso regression and multivariate COX regression. ROC curve, DCA curve, Calibration curve, and Nomogram were used to evaluate the prognostic model. MCPcounter and Cibersort algorithm was used to calculate the infiltration of immune cells in Wilms tumour and para-tumour samples. Then the difference analysis of the immune cells was performed. The relationship between chemokines and immune cells were calculated by Pearson correlation. In addition, DNA methylation differences between Wilms tumour and para-tumour samples was performed. The correlation between DNA methylation and mRNA expression was calculated by Pearson correlation. Western blot (WB)and immunofluorescence were used to confirm the differential expression of CX3CL1 and T cells, and the correlation between them.

Results: A total of 16 chemokines were differentially expressed in tumour and paratumour samples. A total of seven chemokines were associated with survival. CCL2 and CX3CL1 were positively correlated with prognosis, while high expression of CCL3, CCL8, CCL15, CCL18 and CXCL9 predicted poor prognosis. By lasso regression and multivariate COX regression, CCL3, CCL15, CXCL9 and CX3CL1 were finally included to construct a prediction model. The model shows good prediction ability. MCPcounter and Cibersort algorithm both showed that T cells were higher in para-tumour tissues than cancer tissues. Correlation analysis showed that CX3CL1 had a strong correlation with T cells. These were verified by Weston blot and immunofluorescence. DNA methylation analysis showed that various chemokines were different in para-tumours and tumours. CX3CL1 was hypermethylated in tumours, and the degree of methylation was negatively correlated with mRNA expression.

Conclusion: 1. There is low T cell infiltration in nephroblastoma. 2. Chemokines such as CX3CL1 indicate a favourable prognosis and positively correlate with the number of T cells. 3. chemokines such as CX3CL1 are negatively regulated by DNA hypermethylation.

Keywords: Wilms tumour, chemokine, immune infiltration, T cells, DNA methylation

INTRODUCTION

Wilms tumour is a common abdominal malignant tumour in children, accounting for 90% of renal tumours in children aged 0-14 years (1). Surgery combined with radiotherapy and chemotherapy has made significant progress in treating nephroblastoma, with a 5-year overall survival rate of 90% (1, 2). However, there are still some recurrent subgroups (3). Some cases remain challenging to heal, and new treatment options need to be explored (2). At present, the treatment of cancer has entered a new era. The discovery of PD1 and PDL1 brought immunotherapy into a new field. Nivolumab and Pembrolizumab are the main PD-1 inhibitors that have been approved in clinical practice (4). They are humanized IgG4 antibodies targeting PD-1 with high affinity, Approved for non-small cell lung cancer metastatic melanoma (4). However, none of these new methods has been applied in Wilms tumours. The progress of nephroblastoma treatment seems to enter a plateau. Fresh calls have been made to explore targeted therapies and immunotherapy (2).

Immune checkpoint inhibitors have been successful in various adult tumours but are rarely reported in children with solid tumours. The causes of poor immunotherapy in children with tumours are related to ' cold tumours', which are known as tumours that lack infiltration of effector CD8+ T cells or include massive accumulation of Tregs that suppress their activities (5, 6).

Despite this immune deficiency, this does not imply that immunotherapy is useless for 'cold tumours'. There are two complementary solutions in response to this part of the patients with ineffective immunotherapy. One focuses on accurate identification of immune therapy sensitive patients. Another is committed to converting immune-insensitive patients into immune-sensitive patients or combining them with traditional treatment methods (5). For the second strategy, some successes have been achieved. For example, U3 - 1402 can enhance the infiltration of immune cells to enhance the therapeutic effect of PD1 monoclonal antibodies (7). More extensive research has focused on interfering with chemokines to induce immune cell infiltration (5, 8, 9). GPR182 ablation increases the concentration of various chemokines in tumours, making tumours with poor immunogenicity sensitive to immune checkpoint blockade and excessive cell therapy (10). Those inspired our interest to explore the role of chemokines in nephroblastoma.

Chemokines are a class of secretory inflammatory cytokines with the directional movement of chemokine cells. The primary

function is to manage the migration of white blood cells to their respective positions during inflammation and homeostasis (11). According to the amino acid particular structure and conserved sequence of cysteine amino acid residues, they are divided into four categories: XC, CC, CXC and CX3C. These chemokines mainly produce a series of biological effects by binding to the homologous receptors of the G protein-coupled receptor (GPR) family located on the cell membrane surface. They are widely involved in the physiological functions of cell growth, development, cellular immunity and humoral immunity and play an essential role in various pathological processes, such as the aggregation of lymphocytes to inflammatory sites, HIV infection, and tumour growth and metastasis (11).

Chemokines play an essential role in tumour metastasis, homing and regulating the tumour microenvironment (9, 12). In different types of cancer, the role of chemokines in tumours is controversial because chemokines have the effects of both promoting and inhibiting cancer (9, 13–15). This dual role of chemokines may be associated with the chemotaxis to immune cells (8). For example, in Mouse skin melanoma cancer, CX3CL1 kills tumour cells by chemotaxis of NK cells and T cells (16). However, the role of chemokines in nephroblastoma and their chemotaxis to immune cell is not clear. Here, we analyzed the chemokines and immune cell infiltration in nephroblastoma and the potential relationship between them. In addition, we analyzed the regulation of DNA methylation on chemokine expression.

MATERIALS AND METHODS

Data Download and Processing

The nephroblastoma (TARGET-WT) mRNA expression and clinical data were downloaded by the TCGAbiolink package of R software (R4.0.1) from the TARGET database. Screening criteria are as follows: 1. From primary tumours and paratumour samples. 2. There are both mRNA expression data and clinical data. A total of 130 samples were obtained, including 124 tumour samples and 6 para-tumour samples. The clinical data collected included gender, age at diagnosis, stage, survival status and survival days. We downloaded the corresponding DNA methylation-related data from the cBioPortal database. DNA methylation data and mRNA expression data. In addition, another DNA methylation data were downloaded from the

GEO database (GSE163372), including a total of 7 pairs of primary tumours and para-tumour.

Analysis of Differentially Expressed Chemokines

We used raw counts for the difference analysis. The genes with an average expression level of less than 3 were removed. And finally, we obtained 32 chemokines that were expressed in Wilms tumour. These chemokines are used for differential analysis. | Log2FC | > 1 and p < 0.05 were considered significant. Peatmap and ggplot2 packages were used to draw a pheatmap.

KM Analysis

Survival and Survminer R packages were used for KM analysis, and the samples were divided into high and low groups according to the median expression value. p < 0.05 was considered statistically significant.

Construction and Validation of Prediction Model

To find the chemokines most related to prognosis and solve the collinearity problem, all chemokines were included in the lasso regression, and the parameters were set as family = 'cox', nlambda = 100. The variables screened by lasso were used for multiple stepwise regression. The R packages used here were Glmnet and Survminer. To verify the model's prediction ability, the ROC curve, Calibration curves, and DCA curve were used. In addition, to verify whether the prediction model is independent of clinical information, we further conducted multiple stepwise regression based on the risk scores, gender, age at diagnosis and stage, then we draw a nomograms through the rms package.

Immune Infiltration

There are mainly two algorithms to evaluate immune infiltration based on gene expression data. One is the ssGSEA-like algorithm based on marker genes, represented by MCPcounter (17). The other algorithm is based on deconvolution, and the classic one is Cibersort (18). They were both used to infer the infiltration of immune cells in Wilms tumour samples. Visualization mainly uses the ggplot2 package.

Correlation Analysis Between Chemokines and Immune Cells

The correlation between immune cells and chemokines were analyzed by Pearson correlation. The Ggcorrplot package was used to calculate correlation, and p < 0.05 was conspicuous.

DNA Methylation Difference Analysis and DNA Methylation Regulation mRNA Identification

To further understand the reasons for the change of chemokines, the differences analysis of DNA Methylation was performed by limma package between the para-tumour and tumour tissues. In addition, we analyzed the correlation between the degree of methylation and the expression of this mRNA by Pearson. p < 0.05 and $|\mathbf{r}|$ >0.3 were considered significant.

Patient Samples

A total of 24 Wilms tumour tissues and 24 para-tumour tissues from patients undergoing urological surgery in the children's Hospital of Chongqing Medical University were collected. This study has got the approval of the Ethics Committee of Children's Hospital of Chongqing Medical University, and all patients and their parents signed informed consent before joining this study. Immediately, specimens were placed in liquid nitrogen and stored at -80°C for further examination.

Western Blot

Protein samples were lysed in RIPA buffer (Beyotime) supplemented with 1% proteinase inhibitors (Beyotime). The protein concentration was determined using a bicinchoninic acid (BCA) assay kit (Beyotime). Equal amounts of proteins (10 µg) were separated on an 8% SDS-PAGE (sodium dodecyl sulfate-polyacrylamide gel electrophoresis) gel and transferred onto polyvinylidene fluoride (PVDF; Millipore) membranes. The membranes were then blocked in rapid blocking solution and incubated with the primary antibodies overnight at 4°C. The following antibodies were used: CD4 (1:1,000), CD8 (1:1,000), CD3(1:1,000), CX3CL1(1:1000, GAPDH (1:1,000). Finally, the membranes were incubated with HRP-conjugated secondary antibody (1:1,000) for 2 h at room temperature. The immunoblots were visualized using the Immobilon Western Chemiluminescent HRP Substrate, and the bands were quantified, relative to GAPDH, by densitometric analysis (GeneGnome, Syngene UK).

Immunofluorescence

We co-stained CX3CL1 with T cell markers CD3, CD4 and CD8. The details are as follows. tumour and para-tumour samples were fixed with 4% paraformaldehyde (PFA), dehydrated overnight at 4°C. Paraffin embedding, sectioning, routine deparaffinization, 0.5% BSA blocking and incubated with primary antibody overnight. The primary antibodies were rabbit anti-CD4 (1: 200), rabbit anti-CD3 (1: 200), and mouse anti-CX3CL1 (1: 200). CY3 – coupled and FITC - coupled fluorescent secondary antibodies (1:200) were incubated at 25°C for 30 min, and the nucleus was stained with DAPI for 15 min. At least three optical fields were selected for each section for morphological evaluation.

Statistical Method

Difference analysis was undergoing by edgeR package and limma package. The KM method was performed to evaluate the expression of patients' chemokines and immune cells and OS. A log-rank test was used to compare the survival differences between the groups. Lasso and multi-factor Cox regression were used to constructing the model, and the ROC curve and correction curve was used for evaluation. The difference of immune cells between tumour tissues and para-tumour was compared by Kruskal.test. Pearson correlation analysis was used. The above statistics were performed using R software (version 4.0.1). Bilateral P < 0.05 was considered statistically significant.

RESULTS

Chemokines Are Abnormally Expressed in Wilms Tumour

Of all 32 chemokines, 16 were differentially expressed between Wilms tumour and para-tumour sample (**Figure 1A**) Three chemokines were down-regulated in Wilms tumour samples, and 13 chemokines were up-regulated. Comprehensively evaluating the expression abundance and stability of chemokines, it was found that the three down-regulated chemokines CX3CL1, CXCL14 and CXCL2 had extremely significant differences and high expression abundance.

Chemokines Are Associated With Prognosis

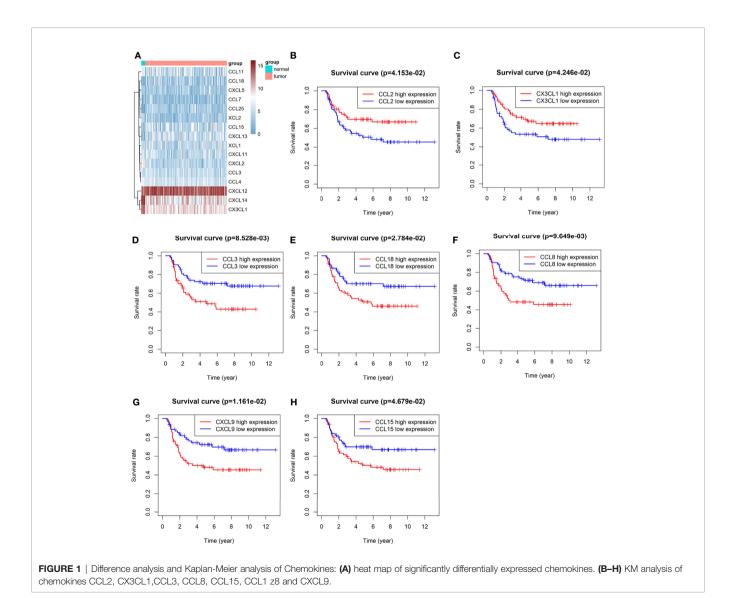
A total of 7 chemokines were associated with survival, of which CCL2 and CX3CL1 were positively correlated with prognosis, while high expression of CCL3, CCL8, CCL15, CCL18 and CXCL9 predicted poor prognosis (**Figures 1B-H**).

Establishment of an Chemokines-Based Prognosis Model

Four genes were included in the final model, namely CCL3, CCL15, CXCL9 and CX3CL1 (**Figures 2A–C**). CX3CL1 was associated with a good prognosis, while CCL3, CCL15 and CXCL9 predicted poor prognosis. This is consistent with the previous KM analysis results.

Verification of the Predictive Power of the Model

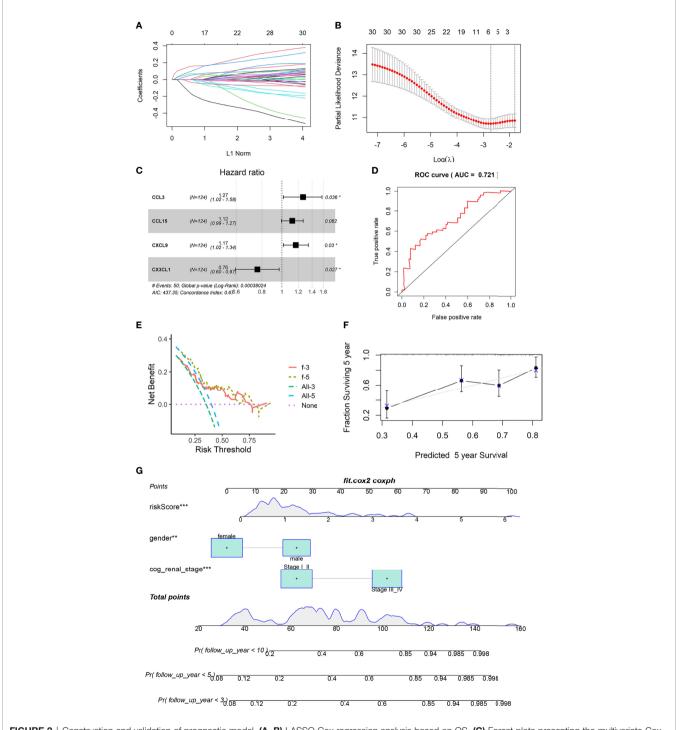
The area under the ROC curve was 0.721 (**Figure 2D**). The Calibration curves and DCA curves showed that the prognostic model composed of four chemokines had a good predictive ability (**Figures 2E, F**). Nomograms shows that age and clinical stage are associated with prognosis, and the role of risk scores in judging prognosis is independent of clinical information (**Figure 2G**).

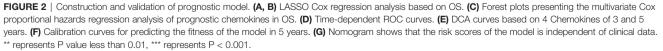


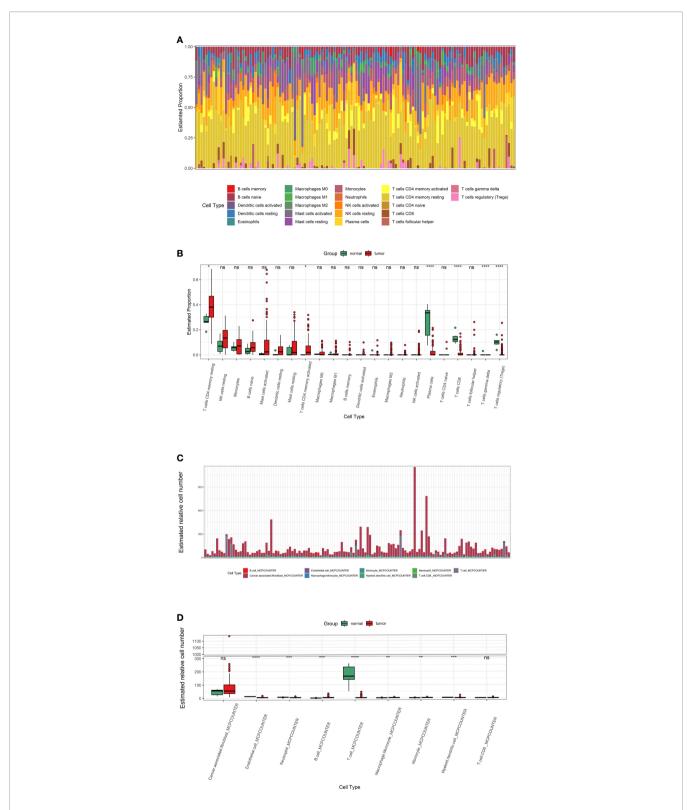
Low Infiltration of T Cells in Tumors

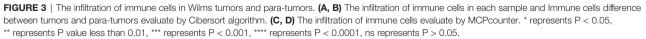
Cibersort and MCPcounter algorithm calculated the infiltration of 22 and 9 immune cells in Wilms tumour (**Figures 3A, C**). Cibersort algorithm showed that T cells, including CD8+ T cells,

CD4+ T cells and regulatory T cells, were lower in tumour tissues than para-tumor tissues. (**Figure 3B**). MCPcounter showed significant different expression of total T cells while CD8+ T cells did not differ between tumour and para-tumour (**Figure 3D**).









The Number of T Cells Correlates With CX3CL1 Expression

Most chemokines are positively correlated with immune cells (**Figures 4A, B**). MCPcounter algorithms consistently showed that CX3CL1 was positively correlated with T cells, with a correlation coefficient of 0.6 (**Figure 4A**). Cibersort algorithms showed that CX3CL1 was positively correlated with CD8+ T cells, with a correlation coefficient of 0.6 (**Figure 4B**).

The Expression of Chemokines Is Regulated by DNA Methylation

We found that the DNA methylation state of Wilms tumour tissue was significantly different from that of the para-tumour tissues. Further analysis of the methylation status of chemokines showed that 35 methylation sites were differentially methylated in 19 chemokines (**Figure 5A**). The mRNA expression levels of 12 chemokines correlated with the degree of DNA methylation. It is worth noting that all chemokine methylation levels were negatively associated with mRNA expression (**Figure 5B**). The degree of DNA methylation of CCL28, CX3CL1 and CCL5 was strongly correlated with mRNA expression, with a correlation coefficient of -0.71, -0.52, and-0.52, respectively.

The Differential Expression and Correlation of CX3CL1 and T Cells Were Verified by WB and Immunofluorescence

The result of Weston blot showed that CX3CL1 was more abundant in para-tumor samples (Figure 6). CD3+ T cells, CD4+ T cells, and CD8+ T cells were lower in tumor samples than para-tumor samples (Figure 6). Immunofluorescence also showed that CX3CL1 was highly expressed in para-tumour, mainly around renal tubules (Figures 7A-C). This is consistent with previous reports (19, 20). The degree of T cell infiltration was lower in tumor. Most tumor samples were difficult to find T cells, but there were still a small number of tumor samples with high T cells infiltration. These T cells were mainly distributed in the tumor stroma, especially around the blood vessels. In the area with abundant blood vessels, the number of T cells was even higher than the average amount of T cells in kidney (Figures 7A-C). The expression of CD4+ and CD8+ subsets was similar to that of total T cells. Additionally, to verify the relationship between T cell infiltration and CX3CL1 expression, we divided tumor tissues into high T cell infiltration and low T cell infiltration. In tumor tissues, the higher the expression of CX3CL1, the higher the number of T cells, whether it is CD8+ T cells or CD4+ T cells (Figure 7D).

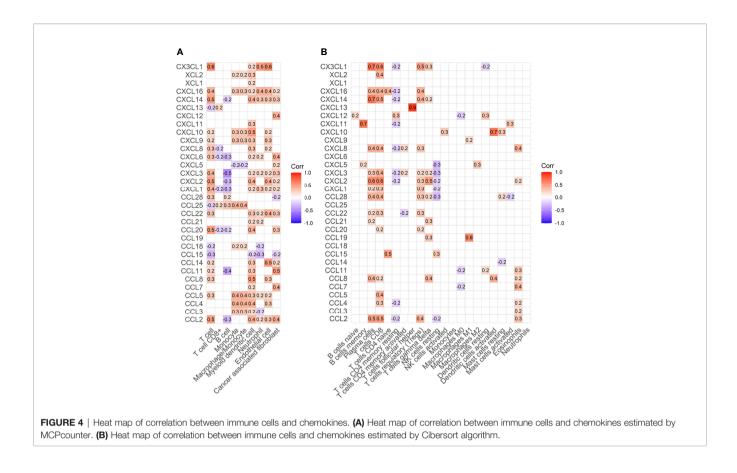
DISCUSSION

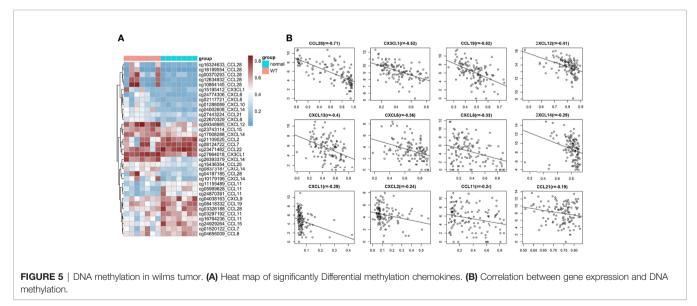
As a common solid tumour in children, nephroblastoma has made significant progress in treatment. At present, the treatment of nephroblastoma is mainly surgery, radiotherapy and chemotherapy (2). However, radiotherapy and chemotherapy may have serious side effects on children, the long-term impact on patients is unclear (2). Some patients are poorly treated, and new treatments need to be explored. Immunotherapy has shown significant advantages in clinical practice. Drugs based on PD1 and PDL1 block have been successful in many tumours, such as lung cancer and melanoma (21, 22). But there are few reports of childhood tumours. Previous studies have shown that a significant increase in plasma EV PD-L1 in WT patients contributes to the immunosuppression of peripheral CD8+ T cells (23). This suggests that nephroblastoma also has immunosuppression similar to that in adult tumors. However, children with Wilms tumors are faced with another major problem, low T cell infiltration. Therefore, the effect of immune checkpoint inhibitors alone may not be ideal. Although we found that a small number of patients also have rich immune cell infiltration. accurate selection of such patients for individual immune checkpoint inhibition therapy may have some effect. But for most nephroblastoma patients, increasing immune cells infiltration in tumor is the key to immunosuppressive therapy. After all, if there is no T cells, how can the function of T cells be enhanced by immune checkpoint inhibitors? in fact, Studies have shown that the therapeutic effect of immunosuppressants is related to tumour immune checkpoints and the infiltration degree of immune cells (24).

To solve the problem of low infiltration of immune cells in tumour. We focused our attention on chemokines. Chemokines are named for their chemotaxis to immune cells. Numerous studies have shown that chemokines regulate immune cell trafficking in tumours and are associated with tumour development, progression and angiogenesis (16, 25). Chemokines can recruit tumourassociated macrophages and regulatory T cells to promote tumour progression, which is related to poor prognosis (26-28). At the same time, chemokines can also recruit CD8+ T cells to inhibit tumour progression (29, 30). For example, chemokines can increase the aggregation of CD8+ T cells in melanoma, thereby promoting immune monitoring and controlling cancer growth (30). CX3CL1 exerts antitumor activity through NK cells and T cells (16). CCL7 is a key chemokine that recruits dendritic cells (DCs) (25). This role of chemokines undoubtedly laid the foundation for immunotherapy.

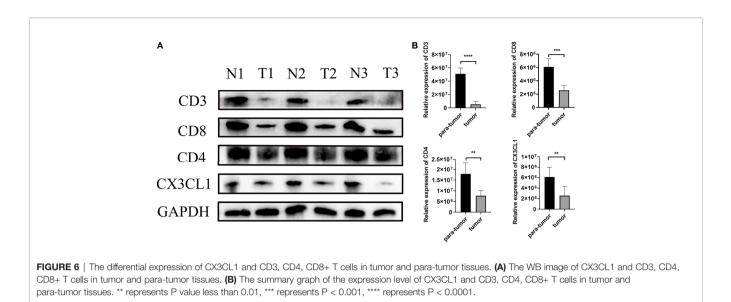
In this study, we performed a comprehensive analysis of chemokines in nephroblastoma. We found that nearly half of the chemokines were abnormally expressed in nephroblastoma. The expression of CX3CL1, CXCL14 and CXCL2 in nephroblastoma was significantly decreased. Further, we explored the chemokines related to prognosis. CCL2 and CX3CL1 were positively correlated with prognosis, while the high expression of CCL3, CCL8, CCL15, CCL18 and CXCL9 predicted a poor prognosis.

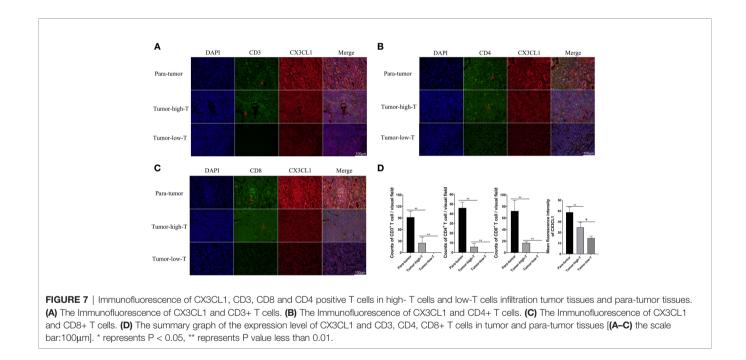
To explore the immune infiltration of nephroblastoma, we evaluated the immune cells both by MCPcounter and Cibersort algorithm. We found that the expression of total T cells in tumours was significantly reduced. Further analysis of the T-cell subpopulation found that the CD8+ T cell infiltration calculated by Cibersort was significantly reduced in tumours, while MCPcounter showed no difference. To identify whether T cells differ in the Wilms tumour and para-tumour,





We experimentally verified by WB and immunofluorescence. The expression of CD3 in the tumour was significantly lower than that in para-tumour, indicating that total T cells were poorly infiltrated in tumours. Furthermore, we performed WB and immunofluorescence to investigate the expression and distribution of CD3+, CD4+ and CD8+ T cells in the tumour and para-tumour tissues. It was found that CD8+ T cells were scattered around renal, but almost no distribution in most tumour tissues. This is a little different from the previous calculation of MCPcounter which showed that CD8+ T cells was no differentially expression in the tumour and paratumour tissues, while identical to the Cibersort algorithm.





These results suggest that, In Wilms tumour, Cibersort can be used to assess immune cells Infiltration more accurately than MCPcounter. There are still a small number of patients with abundant immune cell infiltration, and these immune cells are mainly distributed in tumor stroma, especially in areas rich in blood vessels.

To explore the chemotaxis of chemokines to immune cells, we conducted a correlation analysis between chemokines and immune cells. Whether MCPcounter or Cibersort algorithm, It was found that CX3CL1 was strongly correlated with total T cells. Cibersort algorithm shows that CX3CL1 was positively correlated with CD8+ T cells with a correlation coefficient of 0.6. In addition, we found that T cells were positively correlated not only with CX3CL1 but also with CCL2, CXCL12 and other chemokines, indicating that a variety of chemokines can show chemotaxis to T cells. Co-staining confirmed that CX3CL1 strongly expressed tumor tissues had more T cell infiltration.

The expression of chemokines is affected by many pathways; NF-kappa B, NOTCH, MYC or WNT are related to the expression of chemokines (27, 31). It has been reported that TNF α , IL-1 β , and LPS can stimulate the expression of CX3CL1 (32). The hypoxia microenvironment of tumours affects the expression of chemokines (33). In addition, DNA methylation plays an essential

role in the expression of chemokines (34). It has been reported that DNA methylation is the main negative regulatory mechanism of CCL5, and low-dose DNA methyltransferase inhibitor 5 azacytidine can affect the expression of chemokines and immune infiltration (35). Here, we found that CX3CL1 was down-regulated in Wilms' tumour. To explore the reasons for the abnormal expression of chemokines, we analyzed the methylation of gene expression sites of chemokines. It was found that the methylation of chemokine DNA was significantly different in tumours and para-tumour tissue, and the CX3CL1 gene was seriously hypermethylated at cg27664018 in Wilms tumour tissues. Further correlation analysis between methylation level and mRNA expression was performed. The degree of methylation of all chemokines was negatively correlated with mRNA, which was consistent with the negative regulation of gene expression by DNA methylation (36). In particular, the correlation between the methylation BETA value of CX3CL1 and the expression of CX3CL1 reached -0.52. This evidence provides a basis for applying DNA methylation inhibitors in tumour immunotherapy.

In summary, this study found a deficiency of T cells and other immune cells in Wilms tumours. This phenomenon may be caused by the lack of chemokines such as CX3CL1. Furthermore, we found that chemokine deficiency was associated with DNA hypermethylation. Regulating immune cell infiltration by regulating chemokine expression with DNA methylation inhibitors may provide a new approach for treating nephroblastoma in the future.

DATA AVAILABILITY STATEMENT

The datasets presented in this study can be found in online repositories. The names of the repository/repositories and accession number(s) can be found in the article/**Supplementary Material**.

REFERENCES

- Pastore G, Znaor A, Spreafico F, Graf N, Pritchard-Jones K, Steliarova-Foucher E. Malignant Renal Tumours Incidence and Survival in European Children (1978-1997): Report From the Automated Childhood Cancer Information System Project. *Eur J Cancer* (2006) 42(13):2103–14. doi: 10.1016/j.ejca.2006.05.010
- Szychot E, Apps J, Pritchard-Jones K. Wilms' Tumor: Biology, Diagnosis and Treatment. *Trans Pediatr* (2014) 3(1):12–24. doi: 10.3978/j.issn.2224-4336.2014.01.09
- Vujanić GM, Gessler M, Ooms A, Collini P, Coulomb-l'Hermine A, D'Hooghe E, et al. The Umbrella Siop-Rtsg 2016 Wilms Tumour Pathology and Molecular Biology Protocol. *Nat Rev Urol* (2018) 15(11):693–701. doi: 10.1038/s41585-018-0100-3
- Fessas P, Lee H, Ikemizu S, Janowitz T. A Molecular and Preclinical Comparison of the Pd-1-Targeted T-Cell Checkpoint Inhibitors Nivolumab and Pembrolizumab. *Semin Oncol* (2017) 44(2):136–40. doi: 10.1053/ j.seminoncol.2017.06.002
- Karin N. Chemokines in the Landscape of Cancer Immunotherapy: How They and Their Receptors Can Be Used to Turn Cold Tumors Into Hot Ones? *Cancers* (2021) 13(24). doi: 10.3390/cancers13246317
- 6. Pender A, Titmuss E, Pleasance ED, Fan KY, Pearson H, Brown SD, et al. Genome and Transcriptome Biomarkers of Response to Immune Checkpoint

ETHICS STATEMENT

The studies involving human participants were reviewed and approved by The Institutional Review Board, Children's Hospital of Chongqing Medical University. Written informed consent to participate in this study was provided by the participants' legal guardian/next of kin. Written informed consent was obtained from the individual(s), and minor(s)' legal guardian/next of kin, for the publication of any potentially identifiable images or data included in this article.

AUTHOR CONTRIBUTIONS

Conceptualization: (TM, LJ, DH); Data curation: (TM, LJ, ZZ, DH); Formal analysis: (LJ, JW, ML, CZ); Funding acquisition: (DH); Methodology: (XJT, ZW, XMT, BX); Writing—original draft: (TM, ZZ, DH); Resources: (DH); Supervision: (DH). All authors contributed to the article and approved the submitted version.

FUNDING

The present study was supported by the Special Project of Science and Technology Innovation for Social Undertakings and Livelihood Guarantee of Chongqing (Grant Nos. cstc2019jscx-tjsbX0003 and cstc2017shmsA130103).

SUPPLEMENTARY MATERIAL

The Supplementary Material for this article can be found online at: https://www.frontiersin.org/articles/10.3389/fonc.2022.882714/ full#supplementary-material

Inhibitors in Advanced Solid Tumors. Clin Cancer Res: Off J Am Assoc Cancer Res (2021) 27(1):202–12. doi: 10.1158/1078-0432.Ccr-20-1163

- Haratani K, Yonesaka K, Takamura S, Maenishi O, Kato R, Takegawa N, et al. U3-1402 Sensitizes Her3-Expressing Tumors to Pd-1 Blockade by Immune Activation. J Clin Invest (2020) 130(1):374–88. doi: 10.1172/jci126598
- Nagarsheth N, Wicha MS, Zou W. Chemokines in the Cancer Microenvironment and Their Relevance in Cancer Immunotherapy. Nat Rev Immunol (2017) 17(9):559–72. doi: 10.1038/nri.2017.49
- Mollica Poeta V, Massara M, Capucetti A, Bonecchi R. Chemokines and Chemokine Receptors: New Targets for Cancer Immunotherapy. Front Immunol (2019) 10:379. doi: 10.3389/fimmu.2019.00379
- Torphy RJ, Sun Y, Lin R, Caffrey-Carr A, Fujiwara Y, Ho F, et al. Gpr182 Limits Antitumor Immunity Via Chemokine Scavenging in Mouse Melanoma Models. Nat Commun (2022) 13(1):97. doi: 10.1038/s41467-021-27658-x
- 11. Baggiolini M. Chemokines in Pathology and Medicine. J Internal Med (2001) 250(2):91–104. doi: 10.1046/j.1365-2796.2001.00867.x
- Bikfalvi A, Billottet C. The Cc and Cxc Chemokines: Major Regulators of Tumor Progression and the Tumor Microenvironment. Am J Physiol Cell Physiol (2020) 318(3):C542–c54. doi: 10.1152/ajpcell.00378.2019
- Liu P, Liang Y, Jiang L, Wang H, Wang S, Dong J. Cx3cl1/Fractalkine Enhances Prostate Cancer Spinal Metastasis by Activating the Src/Fak Pathway. *Int J Oncol* (2018) 53(4):1544–56. doi: 10.3892/ijo.2018.4487

- Kehlen A, Greither T, Wach S, Nolte E, Kappler M, Bache M, et al. High Coexpression of Ccl2 and Cx3cl1 Is Gender-Specifically Associated With Good Prognosis in Soft Tissue Sarcoma Patients. *Int J Cancer* (2014) 135 (9):2096–106. doi: 10.1002/ijc.28867
- Matsuo K, Yoshie O, Nakayama T. Multifaceted Roles of Chemokines and Chemokine Receptors in Tumor Immunity. *Cancers* (2021) 13(23). doi: 10.3390/cancers13236132
- Xin H, Kikuchi T, Andarini S, Ohkouchi S, Suzuki T, Nukiwa T, et al. Antitumor Immune Response by Cx3cl1 Fractalkine Gene Transfer Depends on Both Nk and T Cells. *Eur J Immunol* (2005) 35(5):1371–80. doi: 10.1002/ eji.200526042
- Becht E, Giraldo NA, Lacroix L, Buttard B, Elarouci N, Petitprez F, et al. Estimating The Population Abundance of Tissue-Infiltrating Immune and Stromal Cell Populations Using Gene Expression. *Genome Biol* (2016) 17 (1):218. doi: 10.1186/s13059-016-1070-5
- Chen B, Khodadoust MS, Liu CL, Newman AM, Alizadeh AA. Profiling Tumor Infiltrating Immune Cells With Cibersort. *Methods Mol Biol (Clifton* NJ) (2018) 1711:243–59. doi: 10.1007/978-1-4939-7493-1_12
- Durkan AM, Alexander RT, Liu GY, Rui M, Femia G, Robinson LA. Expression and Targeting of Cx3cl1 (Fractalkine) in Renal Tubular Epithelial Cells. J Am Soc Nephrol: JASN (2007) 18(1):74–83. doi: 10.1681/ asn.2006080862
- Kassianos AJ, Wang X, Sampangi S, Afrin S, Wilkinson R, Healy H. Fractalkine-Cx3cr1-Dependent Recruitment and Retention of Human Cd1c+ Myeloid Dendritic Cells by in Vitro-Activated Proximal Tubular Epithelial Cells. *Kidney Int* (2015) 87 (6):1153–63. doi: 10.1038/ki.2014.407
- Garon EB, Rizvi NA, Hui R, Leighl N, Balmanoukian AS, Eder JP, et al. Pembrolizumab for the Treatment of Non-Small-Cell Lung Cancer. N Engl J Med (2015) 372(21):2018–28. doi: 10.1056/NEJMoa1501824
- Brahmer JR, Tykodi SS, Chow LQ, Hwu WJ, Topalian SL, Hwu P, et al. Safety and Activity of Anti-Pd-L1 Antibody in Patients With Advanced Cancer. *N Engl J Med* (2012) 366(26):2455–65. doi: 10.1056/NEJMoa1200694
- Zhang X, Liu Z, Hou Y, Jiao H, Ren J, Wang G. Ev Pd-L1 Contributes to Immunosuppressive Cd8(+) T Cells in Peripheral Blood of Pediatric Wilms Tumor. *Technol Cancer Res Treat* (2021) 20:15330338211041264. doi: 10.1177/ 15330338211041264
- Lei Q, Wang D, Sun K, Wang L, Zhang Y. Resistance Mechanisms of Anti-Pd1/Pd11 Therapy in Solid Tumors. *Front Cell Dev Biol* (2020) 8:672. doi: 10.3389/fcell.2020.00672
- 25. Zhang M, Yang W, Wang P, Deng Y, Dong YT, Liu FF, et al. Ccl7 Recruits Cdc1 to Promote Antitumor Immunity and Facilitate Checkpoint Immunotherapy to Non-Small Cell Lung Cancer. *Nat Commun* (2020) 11 (1):6119. doi: 10.1038/s41467-020-19973-6
- 26. Zhou SL, Zhou ZJ, Hu ZQ, Huang XW, Wang Z, Chen EB, et al. Tumor-Associated Neutrophils Recruit Macrophages and T-Regulatory Cells to Promote Progression of Hepatocellular Carcinoma and Resistance to Sorafenib. *Gastroenterology* (2016) 150(7):1646–58.e17. doi: 10.1053/ j.gastro.2016.02.040
- Ji L, Qian W, Gui L, Ji Z, Yin P, Lin GN, et al. Blockade of β-Catenin-Induced Ccl28 Suppresses Gastric Cancer Progression Via Inhibition of Treg Cell Infiltration. Cancer Res (2020) 80(10):2004–16. doi: 10.1158/0008-5472.Can-19-3074

- 28. Zeng Y, Li B, Liang Y, Reeves PM, Qu X, Ran C, et al. Dual Blockade of Cxcl12-Cxcr4 and Pd-1-Pd-L1 Pathways Prolongs Survival of Ovarian Tumor-Bearing Mice by Prevention of Immunosuppression in the Tumor Microenvironment. FASEB J (2019) 33(5):6596–608. doi: 10.1096/ fj.201802067RR
- Dangaj D, Bruand M, Grimm AJ, Ronet C, Barras D, Duttagupta PA, et al. Cooperation Between Constitutive and Inducible Chemokines Enables T Cell Engraftment and Immune Attack in Solid Tumors. *Cancer Cell* (2019) 35 (6):885–900.e10. doi: 10.1016/j.ccell.2019.05.004
- Harlin H, Meng Y, Peterson AC, Zha Y, Tretiakova M, Slingluff C, et al. Chemokine Expression in Melanoma Metastases Associated With Cd8+ T-Cell Recruitment. *Cancer Res* (2009) 69(7):3077–85. doi: 10.1158/0008-5472.Can-08-2281
- 31. Yang RC, Chang CC, Sheen JM, Wu HT, Pang JH, Huang ST. Davallia Bilabiata Inhibits Tnf-α-Induced Adhesion Molecules and Chemokines by Suppressing Ikk/Nf-Kappa B Pathway in Vascular Endothelial Cells. Am J Chin Med (2014) 42(6):1411–29. doi: 10.1142/s0192415x1450089x
- Jang J, Yoon Y. Oh DJ. A Calpain Inhibitor Protects Against Fractalkine Production in Lipopolysaccharide-Treated Endothelial Cells. *Kidney Res Clin Pract* (2017) 36(3):224–31. doi: 10.23876/j.krcp.2017.36.3.224
- 33. Korbecki J, Kojder K, Barczak K, Simińska D, Gutowska I, Chlubek D, et al. Hypoxia Alters the Expression of Cc Chemokines and Cc Chemokine Receptors in a Tumor-A Literature Review. Int J Mol Sci (2020) 21(16). doi: 10.3390/ijms21165647
- Peng D, Kryczek I, Nagarsheth N, Zhao L, Wei S, Wang W, et al. Epigenetic Silencing of Th1-Type Chemokines Shapes Tumour Immunity and Immunotherapy. *Nature* (2015) 527(7577):249–53. doi: 10.1038/nature15520
- 35. Li H, Chiappinelli KB, Guzzetta AA, Easwaran H, Yen R-WC, Vatapalli R, et al. Immune Regulation by Low Doses of the DNA Methyltransferase Inhibitor 5-Azacitidine in Common Human Epithelial Cancers. Oncotarget (2014) 5(3):587–98. doi: 10.18632/oncotarget.1782
- Klutstein M, Nejman D, Greenfield R, Cedar H. DNA Methylation in Cancer and Aging. Cancer Res (2016) 76(12):3446–50. doi: 10.1158/0008-5472.Can-15-3278

Conflict of Interest: The authors declare that the research was conducted in the absence of any commercial or financial relationships that could be construed as a potential conflict of interest.

Publisher's Note: All claims expressed in this article are solely those of the authors and do not necessarily represent those of their affiliated organizations, or those of the publisher, the editors and the reviewers. Any product that may be evaluated in this article, or claim that may be made by its manufacturer, is not guaranteed or endorsed by the publisher.

Copyright © 2022 Mi, Jin, Zhang, Wang, Li, Zhanghuang, Tan, Wang, Tian, Xiang and He. This is an open-access article distributed under the terms of the Creative Commons Attribution License (CC BY). The use, distribution or reproduction in other forums is permitted, provided the original author(s) and the copyright owner(s) are credited and that the original publication in this journal is cited, in accordance with accepted academic practice. No use, distribution or reproduction is permitted which does not comply with these terms.



Molecular Characteristics of T Cell-Mediated Tumor Killing in Hepatocellular Carcinoma

Wei-feng Hong¹, Mou-yuan Liu², Li Liang^{3,4}, Yang Zhang¹, Zong-juan Li¹, Keqi Han⁵, Shi-suo Du^{1*}, Yan-jie Chen^{6*} and Li-heng Ma^{2*}

¹ Department of Radiation Oncology, Zhongshan Hospital, Fudan University, Shanghai, China, ² Department of Medical Imaging, The First Affiliated Hospital of Guangdong Pharmaceutical University, Guangzhou, China, ³ Department of Medical Oncology, Zhongshan Hospital, Fudan University, Shanghai, China, ⁴ Cancer Center, Zhongshan Hospital, Fudan University, Shanghai, China, ⁵ Department of Oncology, Luodian Hospital Affiliated to Shanghai University, Shanghai, China, ⁶ Department of Gastroenterology, Zhongshan Hospital, Fudan University, Shanghai, China

OPEN ACCESS

Edited by:

Yubin Li, University of Pennsylvania, United States

Reviewed by:

Shixiang Wang, Sun Yat-sen University Cancer Center (SYSUCC), China Minghui Li, Soochow University, China

*Correspondence:

Li-heng Ma maliheng@gdpu.edu.cn Yan-jie Chen chen.yanjie@zs-hospital.sh.cn Shi-suo Du du.shisuo@zs-hospital.sh.cn

Specialty section:

This article was submitted to Cancer Immunity and Immunotherapy, a section of the journal Frontiers in Immunology

Received: 02 February 2022 Accepted: 31 March 2022 Published: 29 April 2022

Citation:

Hong W-f, Liu M-y, Liang L, Zhang Y, Li Z-j, Han K, Du S-s, Chen Y-j and Ma L-h (2022) Molecular Characteristics of T Cell-Mediated Tumor Killing in Hepatocellular Carcinoma. Front. Immunol. 13:868480. doi: 10.3389/fimmu.2022.868480 **Background:** Although checkpoint blockade is a promising approach for the treatment of hepatocellular carcinoma (HCC), subsets of patients expected to show a response have not been established. As T cell-mediated tumor killing (TTK) is the fundamental principle of immune checkpoint inhibitor therapy, we established subtypes based on genes related to the sensitivity to TKK and evaluated their prognostic value for HCC immunotherapies.

Methods: Genes regulating the sensitivity of tumor cells to T cell-mediated killing (referred to as GSTTKs) showing differential expression in HCC and correlations with prognosis were identified by high-throughput screening assays. Unsupervised clustering was applied to classify patients with HCC into subtypes based on the GSTTKs. The tumor microenvironment, metabolic properties, and genetic variation were compared among the subgroups. A scoring algorithm based on the prognostic GSTTKs, referred to as the TCscore, was developed, and its clinical and predictive value for the response to immunotherapy were evaluated.

Results: In total, 18 out of 641 GSTTKs simultaneously showed differential expression in HCC and were correlated with prognosis. Based on the 18 GSTTKs, patients were clustered into two subgroups, which reflected distinct TTK patterns in HCC. Tumor-infiltrating immune cells, immune-related gene expression, glycolipid metabolism, somatic mutations, and signaling pathways differed between the two subgroups. The TCscore effectively distinguished between populations with different responses to chemotherapeutics or immunotherapy and overall survival.

Conclusions: TTK patterns played a nonnegligible role in formation of TME diversity and metabolic complexity. Evaluating the TTK patterns of individual tumor will contribute to enhancing our cognition of TME characterization, reflects differences in the functionality of T cells in HCC and guiding more effective therapy strategies.

Keywords: hepatocellular carcinoma, T cell-mediated tumor killing, tumor microenvironment, glycolipid metabolism, somatic mutation analysis

BACKGROUND

Hepatocellular carcinoma (HCC) is the most common primary malignant cancer in the liver. It ranks sixth in morbidity and fourth in mortality among cancers worldwide. The mortality rate of HCC in the United States increased by 43% % between 2000 and 2016, and the average 5-year survival is only 12% in China and 18% worldwide (1, 2). The World Health Organization predicts that in 2030, HCC will account for approximately one million deaths (3).

The single or combined administration of checkpoint inhibitors has shown good efficacy in HCC. In the CheckMate-040 trial, patients with advanced HCC received nivolumab as a single second-line agent and showed a median overall survival (OS) time ranging from 15.6 to 28.6 months, irrespective of the use of sorafenib (4). A clinical trial in China (NCT02989922) involving 220 patients with progressive HCC from 13 centers showed a similar treatment efficacy for camrelizumab and other PD-1 monoclonal antibodies, with an objective response rate of 14.7%, 6-month survival rate of 74.4%, and median OS time of 13.8 months (5).

Although immune checkpoint blockade has become an effective immunotherapeutic approach for HCC, it is very difficult to identify subsets of patients expected to benefit from this strategy before the start of therapy. Immune cells (especially various T cell subtypes), stromal cells, and molecules expressed in the tumor microenvironment (TME) are key determinants of the response to checkpoint blockade. Thorsson et al. classified 33 tumors into six immune subtypes based on data from The Cancer Genome Atlas (TCGA), among which HCC cases were classified as inflammatory or lymphocyte-depleted subtypes (6). In a proteomic study of paired tumor and adjacent normal tissues, 159 cases of hepatitis B virus-related HCC were divided into subtypes with metabolic, proliferative, and tumor immune microenvironment (TIME) disorders, and PYCR2 and ADH1A were found to be differentially expressed and involved in metabolic reprogramming in the subtypes (7). However, the clinical utility of these models for predicting the response to immunotherapy in HCC is limited, and they have not been verified in clinical cohorts.

Using a genome-scale gRNA library knockout screen, Pan et al. revealed that inactivation of *Prbm1*, *Arid2*, and *Brd7*, encoding components of the polybromo and BRG1-associated factors chromatin remodeling complex sensitized melanoma cells to T cell-mediated killing (8). Ru et al. integrated high-throughput screening data including CRISPR/Cas9, shRNA, and

RNAi data, and determined that *PTPN2* and *CD47* are genes associated with the sensitivity of tumor cells to T cell-mediated killing (referred to as GSTTKs) (9).

In this study, we utilized a set of identified GSTTKs to distinguish between HCC patient populations with different immunophenotypes and immune cell infiltration characteristics. Additionally, we investigated the metabolic and genomic features of patients and developed a new independent prognostic marker based on T cell-mediated tumor killing (TTK) with the potential to guide individualized treatment of HCC.

METHODS

Raw Data Retrieval and Preprocessing

A total of 660 HCC samples datasets were procured from three publicly available datasets. Raw RNA sequencing data were standardized by variance-stabilizing transformation (VST) using the DESeq2 package in R, include 349 samples from the Cancer Genome Atlas (https://portal.gdc.cancer.gov/) TCGA-LIHC cohort (10) and 196 samples from the International Cancer Genome Consortium (https://dcc.icgc.org/) ICGC-LIRI-JP cohort (11). The microarray datasets, 115 samples of GSE76427, was downloaded from the Gene Expression Omnibus database (GEO, https://www.ncbi.nlm.nih.gov/geo/) (12). Genes associated with a favorable response to TTK in cancer immunotherapy were obtained from the TISIDB database (http://cis.hku.hk/TISIDB/) and used to established a gene set, referred to as GSTTKs (9).

Integrated Multi-Omics Analysis

GSTTKs differentially expressed between paracancerous and cancerous tissues were identified using the R package DESeq2 (13), with a false discovery rate < 0.05 and |Log fold change| > 1as thresholds for significance. GSTTKs significantly associated with OS in HCC were identified by univariate Cox regression using the Survival package in R. A Venn diagram was generated using the VennDiagram package to identify the intersection of differentially expressed GSTTKs and prognostic GSTTKs. Somatic mutations in these genes in patients were described using the maftools R package (14). The copy number variation (CNV) status of each gene was retrieved from TCGA and delineated using GISTIC 2.0 to obtain chromosome information along with the gain or loss status, which was visualized in a circos plot (15). A principal component analysis (PCA) was performed using the PCAtools package in R to determine whether specific GSTTKs in the TCGA-LIHC dataset can distinguish between liver tumor samples and nontumor samples.

Recognition of Different TTK Patterns by Unsupervised Clustering

The ConsensusClusterPlus package was employed for unsupervised clustering using the following parameter settings: partitioning around medoid (PAM) based on the center point, merge based on Ward's distances using the minimum variance

Abbreviations: CNV, copy number variation; ES, enrichment score; GEO, Gene Expression Omnibus; GSEA, gene set enrichment analysis; GSTTKs, genes sensitive to T cell-mediated tumor killing; GSVA, gene set variation analysis; HCC, hepatocellular carcinoma; HR, hazard ratio; IC50, half-maximal inhibitory concentration; ICGC, International Cancer Genome Consortium; KEGG: Kyoto Encyclopedia of Genes and Gnomes, LIHC, liver hepatocellular carcinoma; MSigDB, Molecular Signatures Database; ORA, over-representation analysis; OS, overall survival; PCA, principal component analysis; RTK, receptor tyrosine kinase; SD, stable disease; ssGEEA, single sample gene set enrichment analysis; TCGA, The Cancer Genome Atlas; Th, T helper; TIME, tumor immune microenvironment; TME, tumor microenvironment; tSNE, t-distributed stochastic neighbor embedding; TTK, T cell-mediated tumor killing.

method (16). In addition, 1000 times repetitions were conducted for guaranteeing the stability of classification. The proportion of ambiguous clustering (PAC) was used to automatically select the optimal number of subtypes. PCA and tSNE analysis were performed to compare the transcriptional profiles between the different immune subtypes. For the clustering results for the TCGA-LIHC and ICGC-LIRI-JP cohorts, Kaplan–Meier survival curves were plotted and log-rank tests were performed using the survininer and survival packages in R.

Evaluation of Tumor-Infiltrating Immune Cells

Based on TCGA-LIHC dataset, a single sample gene set enrichment analysis (ssGSEA) was performed to quantitatively detect the relative levels of infiltration of 28 immune cells in the TME (17). The genetic signatures for these 28 immune cells were derived from Charoentong et al. (18). In the ssGSEA, differentially expressed marker genes were employed to evaluate the abundance of immune cells in individual samples. The relative abundance of each type of immune cell was represented as an enrichment score. To further explore the relationship between HCC subtypes and immune cell infiltration in HCC, the Wilcoxon rank sum test was used to analyze the differences in immune cell abundance between HCC subtypes. TIDE (Tumor Immune Dysfunction and Exclusion) algorithm developed by Liu can simulate the two main mechanisms of tumor immune escape: the induction of T cell dysfunction at high cytotoxic T lymphocyte (Cytotoxic T Lymphocytes, CTL) and the prevention of T cell infiltration at low CTL, and predict the response potential of tumor immunotherapy. This algorithm was used to evaluate the LIHC cohort, which is verified with the results of ssGSEA analysis to explore the difference of TME among different TTK patterns of HCC (19). The stromal and immune score was determined using the ESTIMATE package in R to assess the level of immune infiltration. These analyses were performed using the gene set variation analysis (GSVA) (20), ComplexHeatmap and estimate packages in R.

Annotation and Functional Enrichment Analyses

To evaluate the correlation between molecular subtypes and immune markers, the characteristic signatures related to differentially infiltrating immune cells in the HCC subtypes were collected from previous studies. Data for 148 immunomodulators and inhibitory immune checkpoints, including 41 chemokines, 21 major histocompatibility complex molecules, 18 receptor molecules, 44 immunostimulant molecules, and 24 inhibitory immune checkpoint molecules, were collected from previous studies (18, 21, 22). The Wilcoxon rank sum test was used to analyze the differential expression of these genes between the HCC subtypes. To determine the correlation between molecular subtypes and specific biological processes, annotated gene sets derived from the Kyoto Encyclopedia of Genes and Genomes (KEGG), Molecular Signatures Database (MSigDB), and a study by Mariathasan et al. were used for enrichment analysis and for comparing biological processes among subtypes (20, 23). For typing based on glycolipid metabolism, a glycolysis-cholesterol synthesis axis-related gene set was obtained from Schaeffer et al. (24) and modeling was completed using the R package ConsensusClusterPlus package. GSEA, GSVA, and overrepresentation analysis (ORA) were performed using the ClusterProfiler (25) and GSVA (20) packages in R.

Study of Etiology Based on Whole-Genome Data

Somatic mutation information in the mutect2 format for patients with HCC in TCGA-LIHC was converted to the mutation annotation format. The maftools package was used to generate waterfall diagrams to visually represent genes with high mutation frequencies. To investigate differences in the distribution of mutations among the HCC subtypes, differentially mutated genes were identified using p < 0.05 as the threshold for significance. Non-negative matrix factorization was carried out to reduce the dimensionality of the mutation matrix for the LIHC dataset, and the optimal number of mutation signatures in different HCC subtypes was identified (26). Thirty tumor mutational signatures that have been reported in COSMIC (https://cancer.sanger.ac.uk/cosmic) were downloaded for comparison with signatures identified by NMF, and mutational signature features of HCC were determined (27). A bar graph of 96 trinucleotide changes was generated for each sample to show the base change profile of each mutation feature. The whole process was performed using the NMF, BSgenome, and MutationalPatterns packages in R.

Calculation of the TCscore and Assessments of Clinical Significance

The index to represent the TTK level was establish based on the expression data for 18 GSTTKs including risk factors of CA9, SLC1A7, E2F1, RECQL4, AURKA, CENPF, RFPL4B, H2AFZ, KIF11, CDC7, TGIF2LX, MCM10, GRM4 and protective factors of SLC4A10, CAPN11, MYO1B, NR4A3, FGF12. The enrichment score (ES) of gene set that positively or negatively regulated TTK was calculated using single sample gene set enrichment analysis (ssGSEA) in the GSVA package (20), and the normalized differences between the ES of the risk factors minus protective factors was defined as the TTK potential index (TCscore) to computationally dissect the TTK trends of each sample:

TCscore = *ESforriskfactors* - *ESforprotectivefactors*

The relationships between the TCscore and clinical characteristics, sensitivity to chemotherapeutics were evaluated. AJCC guidelines recommend the use of antineoplastic drugs such as doxorubicin, mitomycin, vincristine, cisplatin and sorafenib in the treatment of HCC. We predicted the chemotherapy response of each sample to these five drugs based on the GDSC database (the Genomics of Drug Sensitivity in Cancer, https://www.cancerrxgene.org/). The prediction process is realized by pRRophetic (28) packages in R.

Statistical Analysis

All statistical analyses were conducted using R versions 3.6.3 and 4.0.2. For comparisons of continuous variables between two groups, normally distributed variables were evaluated using independent Student's t-tests, and non-normally distributed data were analyzed using Mann-Whitney U tests (the Wilcoxon rank sum test). The chi-square test or Fisher's exact test was used for comparisons of categorical variables between two groups. The relationships between gene expression levels were evaluated on the basis of Spearman correlation coefficients. Univariate and multivariate Cox analyses were used to identify independent prognostic factors. Receiver operating characteristic curves were plotted using the SurvivalROC package, and the area under the curve was used to evaluate the accuracy of the TCscore in predicting prognosis. The Rtsne package was used for a tdistributed stochastic neighbor embedding (tSNE) analysis. Two-sided p < 0.05 was the threshold for significance.

RESULTS

Identification and Characterization of GSTTKs Involved in HCC Progression

Comprehensive analysis of GSTTKs using multi-group data of TCGA-LIHC cohort. The result of difference analysis of transcriptome data shows that 92 of 641 GSTTKs were upregulated or downregulated in HCC, as shown in a volcano map in Figure 1A and a heatmap in Figure S1A. Univariate Cox regression analysis revealed that 125 out of 641 GSTTKs were related to prognosis in HCC. Taking the intersection of the two sets of genes, 37 GSTTKs simultaneously exhibited differential expression and prognostic value in HCC (Figure 1B). The univariate Cox analysis of 37 GSTTKs showed that 11 GSTTKs were protective factors with HR < 1 and 16 GSTTKs were risk factors with HR > 1 for HCC prognosis (Figure 1C). According to the genomic data of TCGA-LIHC, the top 10 oncogenic pathways and effects of HCC are shown in Figure S1B. The mutational landscape for the 37 GSTTKs is displayed in a waterfall plot in Figure 1D. Eighteen out of the 37 GSTTKs had a mutation frequency of >1% and were closely associated with progression or recurrence in HCC. Results of univariate cox regression analysis and differential analysis for 18 GSTTKs were shown in Table S1. As shown in Figure S1C, the co-occurrence of CA9 mutations and MCM10 mutations was significantly overrepresented in HCC. In addition, we detected widespread CNV in these 18 GSTTKs (Figure 1E). Copy number gains were most frequent, and RECQL4, CAPN11, and FGF12 showed extensive CNV amplification, whereas H2AFZ showed a copy number loss. The chromosomal locations of the 18 GSTTKs with CNV are shown in Figure 1F. HCC and non-tumor samples could be completely separated by the PCA (Figure 1G) based on these 18 GSTTKs with differential mRNA levels (Figure 1H), indicating high heterogeneity in the mutation status and expression of GSTTKs between normal and HCC tissues. Thus, GSTTK expression changes may play a crucial role in HCC occurrence and progression.

TTK Patterns in HCC

Based on RNA-seq data and clinical data for TCGA-LIHC, we identified four different patterns which show that comprehensive landscape of 18 GSTTKs interactions and their prognostic significance for HCC patients was depicted with the 18 GSTTKs network correlations (Figure 2A). The R package of ConsensusClusterPlus was used to classify patients with qualitatively different TTK patterns based on the expression of 18 GSTTKs, and two distinct modification patterns were eventually identified using unsupervised clustering, including 146 cases in Cluster1 and 203 cases in Cluster2 (Figure 2B). PCA algorithm and tSNE algorithm are used to evaluate the differences between the two TTK patterns, and it is found that there are significant differences in transcriptional profile among different TTK patterns (Figures 2C, D). To verify the stability and applicability of two TTK patterns in HCC, we repeated the unsupervised clustering analysis using LIRI-JP cohort from ICGC (Figure S2A) and GSE76427 cohort from GEO (Figure **S2D**); both populations could be well classified into two groups. The PCA (Figures S2B, E) and tSNE analysis (Figures S2C, F) results corroborated the two distinct patterns of TTK in HCC. Based on TCGA-LIHC expression profiling data, 16 out of 18 GSTTKs in the two clusters were significantly differentially expressed (Figure S2G). The clinical prognostic value of TTK patterns in patients with HCC was assessed through a survival analysis. Patients in the two clusters showed a significant difference in survival in both TCGA dataset (p = 0.0016, **Figure 2E**) and the ICGC dataset (p = 0.0025, **Figure 2F**).

Mechanisms Underlying the Immunotherapy Response in Patients With Different TTK Subtypes

By comparing the infiltrating immune cell composition in the TME of HCC between the two TTK subtypes (**Figure 3A**), we obtained the following key findings. 1) Samples in Cluster 1 mostly showed low immune cell infiltration, whereas samples in Cluster 2 mostly exhibited high immune cell infiltration. 2) The high immune infiltration zone in the heatmap contains immune cells that are established to mediate antitumor immune response (e.g., activated CD8+ T cells, type 1 T helper (Th1) cells, and dendritic cells) and multiple immunosuppressive cells (e.g., bone marrow-derived suppressor cells, regulatory T cells(Treg), immature dendritic cells, and neutrophils), suggesting that there may be a feedback mechanism, that is, TME may promote the recruitment or differentiation of immunosuppressive cells.

In order to determine the specific immune components that cause the difference of TME between Cluster 1 and Cluster 2, the differences of 28 immune cells among different subtypes were calculated. Combined with the results of the survival analysis (**Figure 2E**), samples in Cluster 2 corresponding to favorable survival outcome showed abundant infiltration by effector memory CD8⁺ T cells, Th1 cells, CD56 natural killer cells, eosinophils, natural killer T cells, neutrophils, and plasmacytoid dendritic cells, whereas those in Cluster 1 corresponding to an unfavorable clinical prognosis showed the infiltration of activated CD4⁺ T cells, effector memory CD4⁺ T

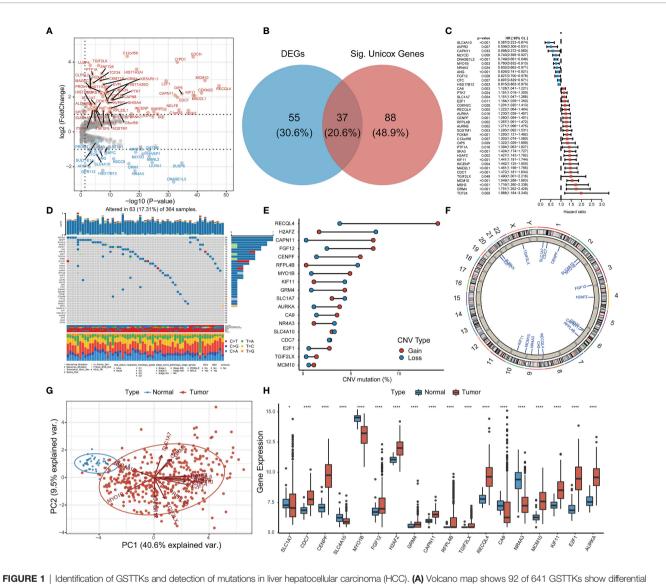


FIGURE 1 | Identification of GSTTKs and detection of mutations in liver hepatocellular carcinoma (HCC). (A) Volcano map shows 92 of 641 GSTTKs show differential mRNA expression in HCC based on transcriptome profiling data for patients with HCC from TCGA-LIHC cohort. Red indicates up-regulation and blue indicates down-regulation. (B) Venn diagram shows 37 GSTTKs exhibiting both differential expression and prognostic value in HCC. (C) Univariate Cox regression analysis of 37 GSTTKs associated with clinical prognosis in HCC. (D) Waterfall plot displays the mutational landscape of the 37 GSTTKs along with clinicopathological characteristics. (E) Copy number variation (CNV) in 18 GSTTKs in HCC. Deletions, blue dots; Amplifications, red dots. (F) CNV locations of 18 GSTTKs are labeled on the chromosome. (G) Principal component analysis separates tumor (green) and normal samples (red). (H) The 18 GSTTKs are differentially expressed between HCC and normal tissues. Tumor, red; Normal, blue. The upper and lower ends of boxes represent the interquartile range. Lines in the boxes represent median values, and black dots show outliers. Asterisks indicate significance, *p < 0.05; **p < 0.001; ***p < 0.0001; ***p < 0.0001;

cells, Th2 cells, and natural killer T cells (**Figure 3B**). A TIDE analysis based on RNA-sequencing data revealed that samples in Cluster 2 had higher scores for T cell dysfunction, microsatellite instability, and tumor-associated fibroblasts than those in Cluster 1, whereas samples in Cluster 1 scored higher for T cell exclusion, myeloid-derived suppressor cells, and tumor-associated M2 macrophages than those in Cluster 2; these findings were generally consistent with the ssGSEA results (**Figure 3C**).

Furthermore, we compared the two clusters with respect to biomarkers of infiltrating immune cells (Figure S3A) and

molecular markers of the response to immunotherapy, including 41 chemokines, 21 major histocompatibility complex molecules, 18 receptor molecules, 44 immunostimulant molecules, and 24 inhibitory immune checkpoint molecules (**Figure S3B**). In addition, we also evaluated the correlations between the 18 GSTTKs and immune-infiltrating cells (**Figure S4A**) and identified significant correlations between *NR4A3* and *RECQL4* expression and most immune cells. Analysis of the differences in immune-infiltrating cells between the groups with high and low *NR4A3* and *RECQL4* expression were further

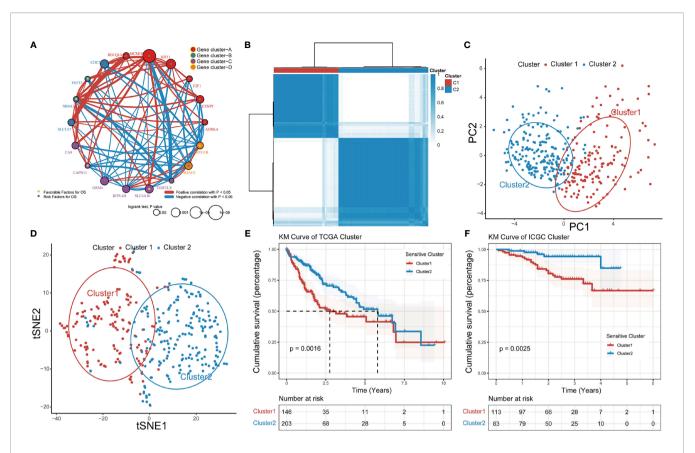
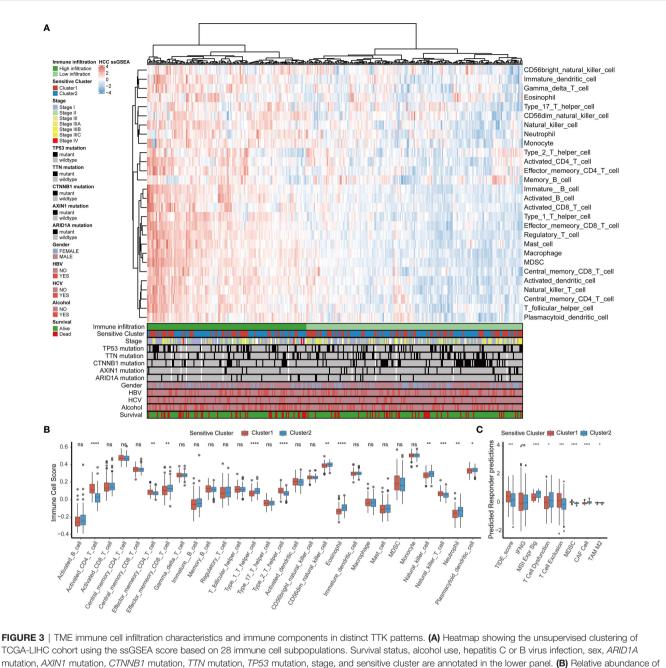


FIGURE 2 | Patterns of TTK and their prognostic value in HCC. (A) Interactions among 18 GSTTKs in HCC. The circle size represents the effect of each regulator on prognosis, and comparisons were made using the log-rank test (p < 0.05, p < 0.001, p < 1E-05 and p < 1E-08). Green dots in the circle represent risk factors for prognosis; gray dots represent favorable factors for prognosis. The lines linking the regulators show interactions, and the line thickness indicates the strength of the correlation. Positive correlations are marked in red and negative correlations are shown in blue. The regulator clusters A–D are marked in red, blue, purple, and orange, respectively. (B) Two patterns of TTK were identified by unsupervised clustering. Cluster1, red; Cluster2, blue. (C, D) PCA and tSNE verified the two patterns in HCC. Two subgroups without intersection were identified, indicating that Cluster1 and Cluster2 samples could be clearly distinguished based on GSTTK expression profiles. (E, F) Survival analysis indicated that patients assigned to the two clusters had significantly different survival outcomes in TCGA-LIHC and ICGC-LIRI-JP cohorts.

analyzed (**Figures S4B, C**), and these results indicated that these genes may contribute to the difference between the TTK patterns.

TTK Patterns and the Metabolic Microenvironment in HCC

Based on an enrichment analysis of TCGA-LIHC dataset by GSVA (**Figure 4A**), the two TTK clusters differed significantly with respect to metabolic pathways, suggesting that metabolic alterations as well as the TIME contributed to the distinct TTK patterns. Subsequent ORA (**Figure S5A**) and GSEA (**Figure S5B**) confirmed the difference in metabolic status between the two clusters. Next, we extracted glycolytic and cholesterogenic genes (**Figure S6A**) and used them to classify HCC into four metabolic subtypes: quiescent, glycolytic, cholesterogenic, and mixed (**Figure 4B**). PCA revealed a substantial separation among these four metabolic patterns (**Figure S6B**). The expression levels of genes involved in glycolipid metabolism are presented in **Figure S6C**. We detected significant differences in OS among the four metabolic clusters, with the quiescent and cholesterogenic subtypes being superior to the glycolytic and mixed subtypes (Figure 4C, p = 0.0032). This is consistent with the Warburg effect, in which aerobic glycolysis contributes to the aggressive cellular proliferation in malignant tumors. To investigate whether expression patterns across the glycolytic-cholesterogenic axis could underlie the differences between previously established immune subtypes (29), we determined the various HCC subtypes for each sample and investigated their degree of overlap with the metabolic phenotypes (Table S2). Quiescent and cholesterogenic subtypes could be classified into Cluster 2, whereas the glycolytic and mixed subtypes were mostly assigned to Cluster 1 or Lymphocyte Depleted Subtype (Figure 4D), suggesting that there is a relationship between TTK subtypes and the metabolic microenvironment in HCC. Analysis of the expression levels of the 18 GSTTKs (Figure S7A) and tumorinfiltrating cells (Figure S7B) according to the metabolic clusters uncovered the relationship between the immune and metabolic microenvironment in HCC.

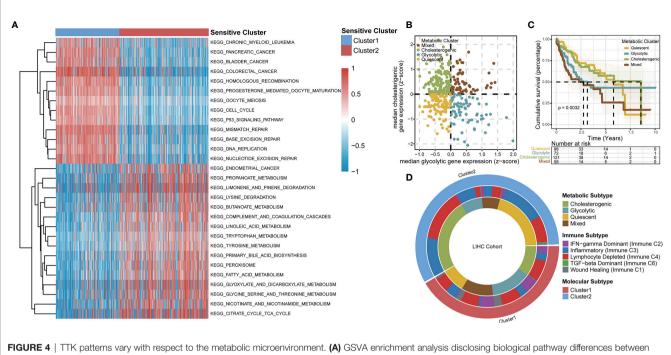


TCGA-LIHC cohort using the ssGSEA score based on 28 immune cell subpopulations. Survival status, alcohol use, hepatitis C or B virus infection, sex, *ARID1A* mutation, *AXIN1* mutation, *CTNNB1* mutation, *TTN* mutation, *TP53* mutation, stage, and sensitive cluster are annotated in the lower panel. **(B)** Relative abundance of each infiltrating cell type that differed between the two clusters. **(C)** Box plots showing the TIDE score for the two clusters in HCC. The upper and lower ends of the boxes indicate the interquartile range. Lines in the boxes indicate median values, and black dots show outliers. *p < 0.05; **p < 0.01; ***p < 0.001; ****p < 0.001; ns, no statistical significance.

Genomic Features and Signaling Pathways Associated With the Two TTK Subtypes of HCC

We analyzed the distribution of somatic mutations in the two clusters using genomic data from TCGA-LIHC datasets (**Figures 5A, B**). Mutations in *CTNNB1*, a common therapy resistance gene in HCC, were predominant in Cluster 1, whereas mutations in *TP53*, a cardinal driver gene of HCC, were predominant in Cluster 2. Comparison of the mutant genes in

the two clusters (**Figure 5C**) and revealed that both *TP53* and *RB1* showed the largest difference in mutation frequency between the two clusters. As somatic mutations are the result of multiple mutation processes, including DNA repair defects, and exposure to exogenous or endogenous mutagens, different mutation processes contribute to different combinations of mutation types or characteristics. To comprehensively characterize the landscape of genomic features, we identified five mutational signatures for the two HCC subtypes (**Figure S8**). C > A_DNA_Repair and



(B) Socket and the patterns way with respect to the metabolic microenvironment. (A) GSVA enrichment analysis disclosing biological pathway dimensions way enriched by enrichment analysis disclosing biological pathway dimensions way enriched by enrichment analysis disclosing biological pathway dimensions way enriched by enrichment analysis disclosing biological pathway dimensions way enriched by enrichment analysis disclosing biological pathway dimensions way enriched by enrichment analysis disclosing biological pathway dimensions way enriched by enrichment analysis disclosing biological pathway dimensions way enriched by enrichment analysis disclosing biological pathway dimensions way enriched by enrichment analysis disclosing biological pathway enrichment analysis disclosing biological pathway enriched by enrichment analysis of the enriched biological pathway enriched by enrichment analysis of the enriched by enriched by enriched by enrited expression levels of enriched by enriched by enriched by en

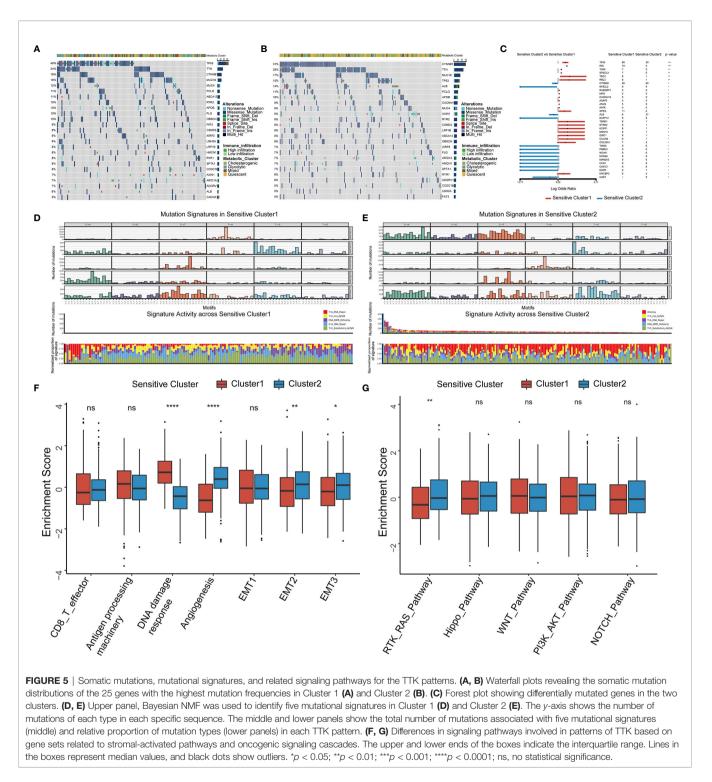
DNA_MMR_Deficiency predominated in Cluster 1 (Figure 5D), whereas Smoking and DNA_MMR_Deficiency were the main patterns in Cluster 2 (Figure 5E).

We selected several markers of the stromal TME for a ssGSEA and found that the score for DNA damage response was significantly higher for Cluster 1 than for Cluster 2, whereas the scores for angiogenesis and epithelial interstitial transformation were significantly higher for Cluster 2 than for Cluster 1 (Figure 5F). To confirm these results, we calculated the stromal score as well as the ESTIMATE score for cases in TCGA-LIHC using the ESTIMATE algorithm and found significant differences between the two TTK types (Figures S9A, B). Moreover, there were significant differences in the stromal and ESTIMATE scores among the four metabolic subtypes (Figures **S9C**, **D**). Based on the differences in expression patterns and mutation frequencies between the two clusters, we selected genes involved in oncogenic pathways from the MsigDB and KEGG databases for a ssGSEA and found that only the receptor tyrosine kinase (RTK)-RAS pathway differed significantly between the groups (Figure 5G). Thus, RTK-RAS is the main pathway mediating the TTK patterns.

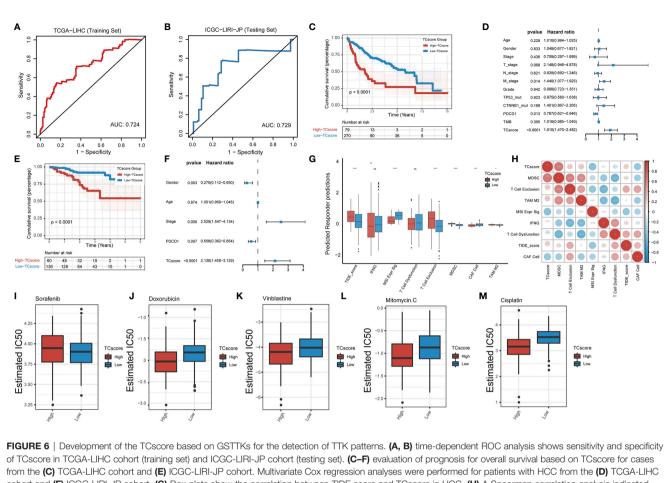
Establishment of the TCscore to Predict the TTK Type in Patients With HCC

We developed a scoring system, referred to as the TCscore, to quantify TTK patterns based on the expression levels of the above 18 GSTTKs from TCGA-LIHC. A Spearman correlation analysis of the TCscore, stromal pathway score, and oncogenic pathway score revealed relationships between the TCscore and intertumoral or tumor microenvironment signaling pathways (Figure S9E). Most variables were negatively correlated with TCscore, but angiogenesis was most strongly related. TCscore were calculated for patients in the ICGC-LIRI-JP cohort using the formula applied to the TCGA-LIHC cohort to validate the prognostic ability of the GSTTKs signature. The sensitivity and specificity of the TCscore was assessed through time-dependent ROC analysis. The AUC values were 0.724 in TCGA-LIHC cohort (training set) and 0.729 in ICGC-LIRI-JP cohort (testing set), respectively (Figures 6A, B). A best threshold value of 0.738 was further selected for classification and Kaplan-Meier and cox regression analysis was performed after classification. Kaplan-Meier curves for OS were plotted according to the optimal cutoff value for TCscore for cases from TCGA-LIHC (p < 0.0001, Figure 6C) and ICGC-LIRI-JP (p < 0.0001, Figure 6E). Patients with high TCscore showed a relative shorter survival time than that of patients with low TCscore. The univariate (Figure S10) and multivariate \mbox{cox} regression analyses suggested that the TCscore is an independent prognostic factor for patients with HCC in TCGA-LIHC (p < 0.0001, hazard ratio (HR) = 1.910, 95% confidence interval (CI): 1.470-2.482, Figure 6D) and ICGC-LIRI-JP (p < 0.0001, HR = 2.136, 95% CI: 1.458-3.129, Figure 6F).

We combined the TCscore with other factors, including the mutation status of known oncogenes (e.g., *TP53*, *ARID1A*, *AXIN1*, *CTNNB1*, and *TTN*) and clinical characteristics (e.g.,



history of alcoholism, hepatitis B or C virus infection, expression of PDCD1, and tumor mutation burden), and plotted the Kaplan–Meier survival curves based on these parameters for cases from the TCGA database (**Figure S11**). When we also investigated the relationships between the TCscore and clinicopathological characteristics, we found significant correlations of the TCscore with survival, sex, T stage, grade, clinical stage, and TP53 and CTNNB1 mutation statuses (**Figure S12**). To assess the predictive value of the TCscore in immunotherapy, we used the TIDE algorithm to evaluate the associations with the treatment response and found that the differences in the TIDE score in view of the TCscore were similar to the TTK patterns (**Figure 6G**). A Spearman correlation analysis showed that the TCscore was negatively correlated



from the (C) TCGA-LIHC cohort and (E) ICGC-LIRI-JP cohort. Multivariate Cox regression analyses were performed for patients with HCC from the (D) TCGA-LIHC cohort and (F) ICGC-LIRI-JP cohort. (G) Box plots show the correlation between TIDE score and TCscore in HCC. (H) A Spearman correlation analysis indicated that the TCscore is positively related to the TIDE score. (I–M) Response to four common chemotherapeutics for high and low TCscore in HCC. *p < 0.05; ***p < 0.001; ****p < 0.0001; ns, no statistical significance.

with CAF cell (r = -0.4) and positively correlated with MDSC (r = 0.68, **Figure 6H**).

Using drug information from the GDSC database to calculate the half-maximal inhibitory concentration (IC50) values of common chemotherapeutics for HCC, we found that the IC50 value of sorafenib in the high TCscore group than in the low TCscore group (**Figure 6I**), whereas the IC50 values of four other drugs (doxorubicin, vinblastine, mitomycin, and cisplatin) showed the opposite pattern (**Figures 6J-M**), providing a basis for the selection of chemotherapy drugs when immunotherapy is combined with chemotherapy in clinical practice.

DISCUSSION

Immunotherapy agents, such as anti-PD1, anti-PD-L1, and anti-CTLA4 antibodies, are increasingly being used in cancer treatment; however, only a subset of patients with HCC benefits from these therapies. Therefore, it is crucially important to characterize the organ-specific TME in HCC and to identify the patient population expected to respond to treatment.

We adopted GSTTKs identified by high-throughput experimental methods to subtype HCC and used unsupervised clustering analysis to further identify TTK patterns. Next, we performed an integrated analysis to evaluate differences in the TIME (e.g., the abundance of tumor-infiltrating cells, molecular markers of immune cells, and immunomodulatory gene expression) and metabolic features (e.g., glycolipid metabolism) between the TTK subtypes. In addition, we evaluated genetic variation, including somatic mutations, mutational signatures, and related signaling pathways, to explore the etiological drivers of the TTK patterns. Finally, we developed a scoring system, the TCscore, based on the TTK types and investigated its clinical and predictive value for the response to immunotherapy.

There is a close connection between immune infiltration and the response to immunotherapy; immune cell dysfunction facilitates the immunosuppressive status in tumors. In this study, we stratified patients with HCC into two stratified according to clinical data from TCGA and validated our findings in an Asian population using data from LIRI-JP in the ICGC. We found that Cluster 2 was dominated by immune cells mediating anti-tumor therapy and that patients in this cluster showed better survival than those in Cluster 1, which was enriched in some of the same immune cells. Chen et al. have reported that tumors with the immune-excluded phenotype also could show abundant infiltration of immune cells trapped in the stroma and excluded from the parenchyma. Conversely, tumors with the immune-inflamed phenotype had greater levels of immune cell infiltration and activation and a better response to immunotherapy (30). Thorsson et al. performed an immunogenomic analysis of cases of 33 cancer types in TCGA and found that HCC can be classified into two types: C3 (inflammatory) and C4 (lymphocyte-depleted) (6). The former type is characterized by the activation of Th1 and Th17 cells and low-to-moderate proliferation of tumor cells, whereas the latter type is characterized by the suppression of Th1 cells and a high response by M2 tumor-associated macrophages. In fact, some pro-inflammatory factors and effector cytokines are released by tumors with the immune-inflamed phenotype, and in some cases, PD-L1 is also expressed, indicating that patients with the immune-inflamed phenotype may show a clear response to immunotherapy (31–33).

We found that NR4A3 and RECQL4, which are involved in the regulation of immunity and metabolism, showed significant associations with most immune-infiltrating cells (34-37). NR4A3, a member of the steroid-thyroid hormone-retinoid receptor superfamily, acts as a transcriptional activator by binding to promoter regions to regulate gene expression (38). NR4A3 binds to NBRE to induce the expression of VCAM1 and ICAM1 and the adhesion of monocytes, resulting in a tumor necrosis factor-stimulating inflammatory response (39). Li et al. have suggested that NR4A3 regulates Treg differentiation and maintains the Treg/Th17 balance to improve the symptoms of immune thrombocytopenic purpura (40). Liu et al. have found that NR4A3 augments glucose uptake in insulin target cells by promoting the translocation of the glucose transporter SLC2A4 to the cell surface for glucose transport (41). Wang et al. have demonstrated that the suppression of NR4A3 promotes cell proliferation and disease progression in HCC (42). RECQL4 is a DNA helicase that modulates chromosome segregation. Wang et al. have revealed that cancer-related RECQL4 mutations stimulate abnormally high levels of mitochondrial DNA synthesis, resulting in disorders in mitochondrial metabolism. Kumari et al. have reported that RECQL4 localizes to the mitochondria and dysfunctions in mitochondrial RECQL4 promote aerobic glycolysis and invasive phenotypes in cells (43). The results of our bioinformatics analyses may guide further experimental studies of the functions and mechanisms of action of these genes (43).

Genes involved in glycolysis-cholesterol synthesis axis have been associated with immune infiltration and prognosis in ovarian, cervical, endometrial, breast, and pancreatic cancers, indicating that there is an interaction between the TME and tumor metabolism (24, 44, 45). Glucose deprivation attenuates the anti-tumor immune response triggered by Cytotoxic T Lymphocytes (CTLs) in glycolytic-dependent tumor cells, whereas checkpoint antagonists, such as anti-PD1 or anti PDL1 antibodies, provide glucose to CTLs by inhibiting glycolysis (46, 47). We hypothesized that this metabolic competition also contributes to TKK and identified four metabolic subtypes in HCC with differences in prognosis, tumor immune-infiltrating cells, GSTTKs expression, and the stromal score.

A recent study revealed that tumor mutations are correlated with the responsiveness or tolerance to immunotherapy (48). Comprehensive genomic analyses have indicated that mutation profiles, including the frequencies of TP53 and CTNNB1 mutations, which act as major oncogenic drivers, rather than drug targets in HCC, vary among subtypes (49). In this study, Cluster 1 was characterized by CTNNB1 mutations and the lymphocyte-depleted phenotype in the TME, suggesting that patients with CTNNB1 mutations may not be sensitive to immunotherapy. These results were in agreement with those reported by Pinyol et al. (50). Cluster 2 was characterized by a high frequency of TP53 mutations and the inflammatory phenotype in the TME, suggesting that patients with TP53 mutations may show favorable responses to immunotherapy. These results were consistent with the previous finding that TP53 mutations represent the tumor mutational burden in HCC and predict a longer survival time in patients receiving immunotherapy (51). Furthermore, this study revealed other significant indicators of the response to combination therapies. For instance, as EGFR and TSC2 mutations were detected in Clusters 1 and 2, immunotherapy combined with EGFR tyrosine kinase inhibitors (erlotinib or gefitinib) or mTOR inhibitors (sirolimus or everolimus) may be effective for individuals with characteristics of both subtypes.

We identified five mutational signatures in Clusters 1 and 2. Samples in Cluster 1 mainly exhibited two signatures: $C > A_DNA_Repair$ and $DNA_MMR_Deficiency$, whereas samples in Cluster 2 displayed various signatures, such as Smoking and $DNA_MMR_Deficiency$. Baecker et al. have reported that tobacco smoking is a risk factor for HCC (52). The difference in DNA damage repair between Clusters 1 and 2 may explain why patients in Cluster 1 showed a worse response to immunotherapy. The mutation pattern in Cluster 1 may contribute to lymphocyte depletion in the TME and the response to immunotherapy. Additional studies are needed to verify these hypotheses.

The mitogen-activated protein kinase pathway and RTKs make up the RKT-RAS-ERK axis, which is crucial for the malignant behavior of common tumors (53). Akalu et al. have reported that TAM receptors, a subfamily of RTKs comprising three members (Tyro3, Axl, and Mer), are an emerging innate immune checkpoint for immune escape and that the inhibition of TAM signaling may promote T cell checkpoint blockade (54). Our results indicated that the RTK-RAS pathway may be the key signaling pathway mediating different TTK modes in HCC. This finding improves our understanding of the biological function and mechanisms of action of T cells in HCC.

We integrated transcriptome data and data for the 18 GSTTKs to establish a new independent quantitative

marker, the TCscore, which could be used for individual evaluations of clinicopathological characteristics, sensitivity to chemotherapeutics, and survival outcomes.

This study had some shortcomings. The TTK patterns and TCscore were based on bioinformatics analyses and require validation in a clinical trial with a large sample size. Key GSTTKs and related pathways in TTK patterns, such as *NR4A3*, *RECQL4*, and RTK-RAS signaling, need to be experimentally validated in the future.

CONCLUSIONS

In summary, we identified two TTK patterns in HCC based on GSTTKs, providing insight into T cell activity in HCC. Additionally, we evaluated the mechanism underlying the TTK patterns, including characteristics of the TME, metabolic processes, and multi-omics properties. Finally, the newly developed TCscore, a composite reflection of the TTK patterns of individual tumors, is expected to improve our understanding of the TME and genomic features and to be useful for guiding immunotherapy and combination therapy strategies.

DATA AVAILABILITY STATEMENT

All data used in this work can be acquired from the GDC portal (https://portal.gdc.cancer.gov/), the International Cancer Genome Consortium (ICGC, https://dcc.icgc.org/) and the Gene-Expression Omnibus under the accession number GSE76427.

ETHICS STATEMENT

The patient data used in this study were acquired from the publicly available datasets with complete informed consent of patients.

AUTHOR CONTRIBUTIONS

W-fH and L-hM contributed to conception, design, acquisition, analysis, and interpretation of data. W-fH, Y-jC, and M-yL contributed to the interpretation of result and manuscript preparation. LL, YZ, and Z-jL contributed to the acquisition and interpretation of data. W-fH, KqH, and S-sD revised the manuscript critically. All the authors participated in the discussion and editing of the manuscript. All authors contributed to the article and approved the submitted version.

FUNDING

This study was funded by the National Natural Science Foundation of China (No. 81900482), Chinese Society of Clinical Oncology-

Youth Innovation Research Fund (Y-young2019-057), and Natural Science Foundation of Shanghai (21ZR1412500).

SUPPLEMENTARY MATERIAL

The Supplementary Material for this article can be found online at: https://www.frontiersin.org/articles/10.3389/fimmu.2022.868480/full#supplementary-material

Supplementary Figure 1 | Identification of GSTTKs and survey of mutations in these genes in HCC. (A) Heatmap displaying 92 GSTTKs differentially expressed in HCC. (B) Cellular signaling pathways enriched in mutated genes in HCC. (C) Co-occurrence of mutations in pairs of GSTTKs.

Supplementary Figure 2 | Patterns of TTK in HCC. (A–C) Qualitative classification by unsupervised clustering based on 18 GSTTKs in cases from the LIRI-JP dataset in the ICGC followed by PCA and tSNE analyses. (D–F) Qualitative classification by unsupervised clustering based on 18 GSTTKs in cases from the GSE76427 dataset followed by PCA and tSNE analyses. (G). Expression of the 18 GSTTKs in the two TTK patterns in TCGA-LIHC cohort.

Supplementary Figure 3 | Immunomodulator biomarkers and involvement in patterns of TTK in HCC. (**A**, **B**) Heatmaps suggested that signatures of (**A**) nine tumor-associated immune cells and (**B**) immunomodulators as well as immune checkpoints were differently expressed between the two patterns. *p < 0.05; **p < 0.01; ***p < 0.001.

Supplementary Figure 4 | Eighteen GSTTKs are related to tumor immune cell infiltration. (A–C) Correlations among 18 GSTTKs and tumor-infiltrating immune cells were studied (A). The expression levels of (B) *NR4A3* and (C) *RECQL4* were positively associated with various immune cells. *p < 0.05; **p < 0.01; ***p < 0.001; ***p < 0.001.

Supplementary Figure 5 | Enrichment analysis indicates a difference in metabolic status between the TTK patterns. A, B. (A) ORA and (B) GSEA revealed differences in metabolic processes between the TTK patterns.

Supplementary Figure 6 | Re-clustering of patients according to the glycolipid metabolism patterns in HCC. (A) The TCGA-LIHC cohort was re-clustered according to both glycolytic and cholesterogenic genes. (B) PCA suggested satisfactory separation among four metabolic patterns. (C) A heatmap shows glycolytic and cholesterogenic genes expressed in the four subgroups.

Supplementary Figure 7 | Tumor immune microenvironment differed among the four metabolic subgroups. (A) Eighteen GSTTKs were generally differentially expressed among the four metabolic subtypes. (B) Most tumor immune cells showed differential infiltration among the four metabolic subtypes. *p < 0.05; **p < 0.01; ***p < 0.001; ***p < 0.001;

Supplementary Figure 8 | Comprehensive genomic analyses revealed distinct mutational signatures between the TTK patterns. (A, C) Bayesian non-negative matrix factorization was used to determine the optimal number of mutational signatures. (B, D) Based on 30 mutation features summarized in the COSMIC database, five signatures for the two clusters were annotated.

Supplementary Figure 9 | Investigation of the stromal TME in HCC. (A–D) The stromal tumor microenvironments (A, B) for the two clusters and (C, D) four metabolic subtypes were assessed based on the stromal score and ESTIMATE score. e A Spearman correlation analysis was performed to evaluate relationships among the TCscore, stromal pathway score, and oncogenic pathway score.

Supplementary Figure 10 | The TCscore predicts prognoses in HCC. **(A, B)** Univariate cox regression analysis suggests that the TCscore is associated with a poor prognosis in patients in the TCGA **(A)** and ICGC **(B)** datasets. Supplementary Figure 11 | Survival analysis using the TCscore combined with other factors. (A–J). Kaplan–Meier survival analyses were performed based on the TCscore plus the following factors: mutation statuses of (A) *TP53*, (B) *ARID1A*, (C) *AXIN1*, (D) *CTNNB1*, and (E) *TTN*, (F) history of alcoholism, (G) hepatitis B virus infection, (H) hepatitis C virus infection, (I) PDCD1 expression, and (J) tumor mutation burden.

REFERENCES

- Craig AJ, von Felden J, Garcia-Lezana T, Sarcognato S, Villanueva A. Tumour Evolution in Hepatocellular Carcinoma. *Nat Rev Gastroenterol Hepatol* (2020) 17:139–52. doi: 10.1038/s41575-019-0229-4
- Zheng R, Qu C, Zhang S, Zeng H, Sun K, Gu X, et al. Liver Cancer Incidence and Mortality in China: Temporal Trends and Projections to 2030. *Chin J Cancer Res* (2018) 30:571–9. doi: 10.21147/j.issn.1000-9604.2018.06.01
- Villanueva A. Hepatocellular Carcinoma. N Engl J Med (2019) 380:1450–62. doi: 10.1056/NEJMra1713263
- El-Khoueiry AB, Sangro B, Yau T, Crocenzi TS, Kudo M, Hsu C, et al. Nivolumab in Patients With Advanced Hepatocellular Carcinoma (CheckMate 040): An Open-Label, Non-Comparative, Phase 1/2 Dose Escalation and Expansion Trial. *Lancet* (2017) 389:2492–502. doi: 10.1016/ S0140-6736(17)31046-2
- Qin S, Ren Z, Meng Z, Chen Z, Chai X, Xiong J, et al. Camrelizumab in Patients With Previously Treated Advanced Hepatocellular Carcinoma: A Multicentre, Open-Label, Parallel-Group, Randomised, Phase 2 Trial. *Lancet* Oncol (2020) 21:571–80. doi: 10.1016/S1470-2045(20)30011-5
- Thorsson V, Gibbs DL, Brown SD, Wolf D, Bortone DS, Ou Yang TH, et al. The Immune Landscape of Cancer. *Immunity* (2018) 48:812–30.e14. doi: 10.1016/j.immuni.2018.03.023
- Gao Q, Zhu H, Dong L, Shi W, Chen R, Song Z, et al. Integrated Proteogenomic Characterization of HBV-Related Hepatocellular Carcinoma. *Cell* (2019) 179:1240. doi: 10.1016/j.cell.2019.10.038
- Pan D, Kobayashi A, Jiang P, Ferrari de Andrade L, Tay RE, Luoma AM, et al. A Major Chromatin Regulator Determines Resistance of Tumor Cells to T Cell-Mediated Killing. *Science* (2018) 359:770–5. doi: 10.1126/ science.aao1710
- Ru B, Wong CN, Tong Y, Zhong JY, Zhong SSW, Wu WC, et al. TISIDB: An Integrated Repository Portal for Tumor-Immune System Interactions. *Bioinformatics* (2019) 35:4200–2. doi: 10.1093/bioinformatics/btz210
- Hutter C, Zenklusen JC. The Cancer Genome Atlas: Creating Lasting Value Beyond Its Data. *Cell* (2018) 173:283-5. doi: 10.1016/j.cell. 2018.03.042
- Zhang J, Bajari R, Andric D, Gerthoffert F, Lepsa A, Nahal-Bose H, et al. The International Cancer Genome Consortium Data Portal. *Nat Biotechnol* (2019) 37:367–9. doi: 10.1038/s41587-019-0055-9
- Grinchuk OV, Yenamandra SP, Iyer R, Singh M, Lee HK, Lim KH, et al. Tumor-Adjacent Tissue Co-Expression Profile Analysis Reveals Pro-Oncogenic Ribosomal Gene Signature for Prognosis of Resectable Hepatocellular Carcinoma. *Mol Oncol* (2018) 12:89–113. doi: 10.1002/1878-0261.12153
- Love MI, Huber W, Anders S. Moderated Estimation of Fold Change and Dispersion for RNA-Seq Data With Deseq2. *Genome Biol* (2014) 15:550. doi: 10.1186/s13059-014-0550-8
- Mayakonda A, Lin DC, Assenov Y, Plass C, Koeffler HP. Maftools: Efficient and Comprehensive Analysis of Somatic Variants in Cancer. *Genome Res* (2018) 28:1747–56. doi: 10.1101/gr.239244.118
- Mermel CH, Schumacher SE, Hill B, Meyerson ML, Beroukhim R, Getz G. GISTIC2.0 Facilitates Sensitive and Confident Localization of the Targets of Focal Somatic Copy-Number Alteration in Human Cancers. *Genome Biol* (2011) 12:R41. doi: 10.1186/gb-2011-12-4-r41
- Wilkerson MD, Hayes DN. ConsensusClusterPlus: A Class Discovery Tool With Confidence Assessments and Item Tracking. *Bioinformatics* (2010) 26:1572–3. doi: 10.1093/bioinformatics/btq170
- Hackl H, Charoentong P, Finotello F, Trajanoski Z. Computational Genomics Tools for Dissecting Tumour-Immune Cell Interactions. *Nat Rev Genet* (2016) 17:441–58. doi: 10.1038/nrg.2016.67

Supplementary Figure 12 | The TCscore was related to clinicopathological characteristics of patients with HCC. (A–G) Relationships between the TCscore and clinicopathological characteristics, such as (A) survival status, (B) gender, (C) TP53 mutations, (D) CTNNB mutations, (E) T stage, (F) grade, and (G) TNM stage, were investigated.

- Charoentong P, Finotello F, Angelova M, Mayer C, Efremova M, Rieder D, et al. Pan-Cancer Immunogenomic Analyses Reveal Genotype-Immunophenotype Relationships and Predictors of Response to Checkpoint Blockade. *Cell Rep* (2017) 18:248–62. doi: 10.1016/j.celrep.2016.12.019
- Jiang P, Gu S, Pan D, Fu J, Sahu A, Hu X, et al. Signatures of T Cell Dysfunction and Exclusion Predict Cancer Immunotherapy Response. *Nat Med* (2018) 24:1550–8. doi: 10.1038/s41591-018-0136-1
- Hanzelmann S, Castelo R, Guinney J. GSVA: Gene Set Variation Analysis for Microarray and RNA-Seq Data. BMC Bioinf (2013) 14:7. doi: 10.1186/1471-2105-14-7
- Auslander N, Zhang G, Lee JS, Frederick DT, Miao B, Moll T, et al. Robust Prediction of Response to Immune Checkpoint Blockade Therapy in Metastatic Melanoma. Nat Med (2018) 24:1545–9. doi: 10.1038/s41591-018-0157-9
- 22. Chen PL, Roh W, Reuben A, Cooper ZA, Spencer CN, Prieto PA, et al. Analysis of Immune Signatures in Longitudinal Tumor Samples Yields Insight Into Biomarkers of Response and Mechanisms of Resistance to Immune Checkpoint Blockade. *Cancer Discov* (2016) 6:827–37. doi: 10.1158/2159-8290.CD-15-1545
- Mariathasan S, Turley SJ, Nickles D, Castiglioni A, Yuen K, Wang Y, et al. TGFbeta Attenuates Tumour Response to PD-L1 Blockade by Contributing to Exclusion of T Cells. *Nature* (2018) 554:544-8. doi: 10.1038/nature25501
- Karasinska JM, Topham JT, Kalloger SE, Jang GH, Denroche RE, Culibrk L, et al. Altered Gene Expression Along the Glycolysis-Cholesterol Synthesis Axis Is Associated With Outcome in Pancreatic Cancer. *Clin Cancer Res* (2020) 26:135–46. doi: 10.1158/1078-0432.CCR-19-1543
- Yu G, Wang LG, Han Y, He QY. Clusterprofiler: An R Package for Comparing Biological Themes Among Gene Clusters. OMICS (2012) 16:284–7. doi: 10.1089/omi.2011.0118
- Kim J, Akbani R, Creighton CJ, Lerner SP, Weinstein JN, Getz G, et al. Invasive Bladder Cancer: Genomic Insights and Therapeutic Promise. *Clin Cancer Res* (2015) 21:4514–24. doi: 10.1158/1078-0432.CCR-14-1215
- Alexandrov LB, Nik-Zainal S, Wedge DC, Aparicio SA, Behjati S, Biankin AV, et al. Signatures of Mutational Processes in Human Cancer. *Nature* (2013) 500:415–21. doi: 10.1038/nature12477
- Hong W, Liang L, Gu Y, Qi Z, Qiu H, Yang X, et al. Immune-Related lncRNA to Construct Novel Signature and Predict the Immune Landscape of Human Hepatocellular Carcinoma. *Mol Ther Nucleic Acids* (2020) 22:937–47. doi: 10.1016/j.omtn.2020.10.002
- Thorsson V, Gibbs DL, Brown SD, Wolf D, Bortone DS, Ou Yang TH, et al. The Immune Landscape of Cancer. *Immunity* (2019) 51:411–2. doi: 10.1016/ j.immuni.2019.08.004
- Chen DS, Mellman I. Elements of Cancer Immunity and the Cancer-Immune Set Point. Nature (2017) 541:321–30. doi: 10.1038/nature21349
- Harlin H, Meng Y, Peterson AC, Zha Y, Tretiakova M, Slingluff C, et al. Chemokine Expression in Melanoma Metastases Associated With CD8+ T-Cell Recruitment. *Cancer Res* (2009) 69:3077–85. doi: 10.1158/0008-5472.CAN-08-2281
- Fehrenbacher L, Spira A, Ballinger M, Kowanetz M, Vansteenkiste J, Mazieres J, et al. Atezolizumab Versus Docetaxel for Patients With Previously Treated non-Small-Cell Lung Cancer (POPLAR): A Multicentre, Open-Label, Phase 2 Randomised Controlled Trial. *Lancet* (2016) 387:1837–46. doi: 10.1016/ S0140-6736(16)00587-0
- 33. Rosenberg JE, Hoffman-Censits J, Powles T, van der Heijden MS, Balar AV, Necchi A, et al. Atezolizumab in Patients With Locally Advanced and Metastatic Urothelial Carcinoma Who Have Progressed Following Treatment With Platinum-Based Chemotherapy: A Single-Arm, Multicentre, Phase 2 Trial. *Lancet* (2016) 387:1909–20. doi: 10.1016/S0140-6736(16)00561-4

- 34. Chi Z, Nie L, Peng Z, Yang Q, Yang K, Tao J, et al. RecQL4 Cytoplasmic Localization: Implications in Mitochondrial DNA Oxidative Damage Repair. Int J Biochem Cell Biol (2012) 44:1942–51. doi: 10.1016/ j.biocel.2012.07.016
- Ordelheide AM, Gerst F, Rothfuss O, Heni M, Haas C, Thielker I, et al. Nor-1, a Novel Incretin-Responsive Regulator of Insulin Genes and Insulin Secretion. *Mol Metab* (2013) 2:243-55. doi: 10.1016/ j.molmet.2013.06.003
- 36. Gupta S, De S, Srivastava V, Hussain M, Kumari J, Muniyappa K, et al. RECQL4 and P53 Potentiate the Activity of Polymerase Gamma and Maintain the Integrity of the Human Mitochondrial Genome. *Carcinogenesis* (2014) 35:34–45. doi: 10.1093/carcin/bgt315
- 37. Jennings E, Elliot TAE, Thawait N, Kanabar S, Yam-Puc JC, Ono M, et al. Nr4a1 and Nr4a3 Reporter Mice Are Differentially Sensitive to T Cell Receptor Signal Strength and Duration. *Cell Rep* (2020) 33:108328. doi: 10.1016/j.celrep.2020.108328
- Park K, Mikulski Z, Seo GY, Andreyev AY, Marcovecchio P, Blatchley A, et al. The Transcription Factor NR4A3 Controls CD103+ Dendritic Cell Migration. *J Clin Invest* (2016) 126:4603–15. doi: 10.1172/JCI87081
- Zhao Y, Howatt DA, Gizard F, Nomiyama T, Findeisen HM, Heywood EB, et al. Deficiency of the NR4A Orphan Nuclear Receptor NOR1 Decreases Monocyte Adhesion and Atherosclerosis. *Circ Res* (2010) 107:501–11. doi: 10.1161/CIRCRESAHA.110.222083
- Li JQ, Tian JM, Fan XR, Wang ZY, Ling J, Wu XF, et al. miR-106b-5p Induces Immune Imbalance of Treg/Th17 in Immune Thrombocytopenic Purpura Through NR4A3/Foxp3 Pathway. *Cell Cycle* (2020) 19:1265–74. doi: 10.1080/ 15384101.2020.1746485
- 41. Liu Q, Zhu X, Xu L, Fu Y, Garvey WT. 6-Mercaptopurine Augments Glucose Transport Activity in Skeletal Muscle Cells in Part via a Mechanism Dependent Upon Orphan Nuclear Receptor NR4A3. Am J Physiol Endocrinol Metab (2013) 305:E1081–92. doi: 10.1152/ajpendo. 00169.2013
- Wang H, Guo Q, Nampoukime KB, Yang P, Ma K. Long non-Coding RNA LINC00467 Drives Hepatocellular Carcinoma Progression via Inhibiting NR4A3. J Cell Mol Med (2020) 24:3822–36. doi: 10.1111/jcmm.14942
- Kumari J, Hussain M, De S, Chandra S, Modi P, Tikoo S, et al. Mitochondrial Functions of RECQL4 are Required for the Prevention of Aerobic Glycolysis-Dependent Cell Invasion. J Cell Sci (2016) 129:1312–8. doi: 10.1242/jcs.181297
- 44. Wang G, Liu X, Wang D, Sun M, Yang Q. Identification and Development of Subtypes With Poor Prognosis in Pan-Gynecological Cancer Based on Gene Expression in the Glycolysis-Cholesterol Synthesis Axis. *Front Oncol* (2021) 11:636565. doi: 10.3389/fonc.2021.636565
- 45. Zhong PC, Shu R, Wu HW, Liu ZW, Shen XL, Hu YJ. Altered Gene Expression in Glycolysis-Cholesterol Synthesis Axis Correlates With Outcome of Triple-Negative Breast Cancer. Exp Biol Med (Maywood) (2021) 246:560–71. doi: 10.1177/1535370220975206

- Chang CH, Qiu J, O'Sullivan D, Buck MD, Noguchi T, Curtis JD, et al. Metabolic Competition in the Tumor Microenvironment Is a Driver of Cancer Progression. *Cell* (2015) 162:1229–41. doi: 10.1016/j.cell.2015.08.016
- Ho PC, Bihuniak JD, Macintyre AN, Staron M, Liu X, Amezquita R, et al. Phosphoenolpyruvate Is a Metabolic Checkpoint of Anti-Tumor T Cell Responses. *Cell* (2015) 162:1217–28. doi: 10.1016/j.cell.2015.08.012
- George S, Miao D, Demetri GD, Adeegbe D, Rodig SJ, Shukla S, et al. Loss of PTEN Is Associated With Resistance to Anti-PD-1 Checkpoint Blockade Therapy in Metastatic Uterine Leiomyosarcoma. *Immunity* (2017) 46:197– 204. doi: 10.1016/j.immuni.2017.02.001
- Kahn M. Can We Safely Target the WNT Pathway? Nat Rev Drug Discov (2014) 13:513–32. doi: 10.1038/nrd4233
- Pinyol R, Sia D, Llovet JM. Immune Exclusion-Wnt/CTNNB1 Class Predicts Resistance to Immunotherapies in HCC. *Clin Cancer Res* (2019) 25:2021–3. doi: 10.1158/1078-0432.CCR-18-3778
- Assoun S, Theou-Anton N, Nguenang M, Cazes A, Danel C, Abbar B, et al. Association of TP53 Mutations With Response and Longer Survival Under Immune Checkpoint Inhibitors in Advanced Non-Small-Cell Lung Cancer. *Lung Cancer* (2019) 132:65–71. doi: 10.1016/j.lungcan.2019.04.005
- Baecker A, Liu X, La Vecchia C, Zhang ZF. Worldwide Incidence of Hepatocellular Carcinoma Cases Attributable to Major Risk Factors. *Eur J Cancer Prev* (2018) 27:205–12. doi: 10.1097/CEJ.00000000000428
- 53. Imperial R, Toor OM, Hussain A, Subramanian J, Masood A. Comprehensive Pancancer Genomic Analysis Reveals (RTK)-RAS-RAF-MEK as a Key Dysregulated Pathway in Cancer: Its Clinical Implications. Semin Cancer Biol (2019) 54:14–28. doi: 10.1016/j.semcancer.2017.11.016
- Akalu YT, Rothlin CV, Ghosh S. TAM Receptor Tyrosine Kinases as Emerging Targets of Innate Immune Checkpoint Blockade for Cancer Therapy. *Immunol Rev* (2017) 276:165–77. doi: 10.1111/imr.12522

Conflict of Interest: The authors declare that the research was conducted in the absence of any commercial or financial relationships that could be construed as a potential conflict of interest.

Publisher's Note: All claims expressed in this article are solely those of the authors and do not necessarily represent those of their affiliated organizations, or those of the publisher, the editors and the reviewers. Any product that may be evaluated in this article, or claim that may be made by its manufacturer, is not guaranteed or endorsed by the publisher.

Copyright © 2022 Hong, Liu, Liang, Zhang, Li, Han, Du, Chen and Ma. This is an open-access article distributed under the terms of the Creative Commons Attribution License (CC BY). The use, distribution or reproduction in other forums is permitted, provided the original author(s) and the copyright owner(s) are credited and that the original publication in this journal is cited, in accordance with accepted academic practice. No use, distribution or reproduction is permitted which does not comply with these terms.



Noncanonical PD-1/PD-L1 Axis in Relation to the Efficacy of Anti-PD Therapy

Yiru Long^{1,2†}, Xiaolu Yu^{1,2†}, Runqiu Chen^{1,3}, Yongliang Tong^{1,2} and Likun Gong^{1,2,4*}

¹ State Key Laboratory of Drug Research, Shanghai Institute of Materia Medica, Chinese Academy of Sciences, Shanghai, China, ² University of Chinese Academy of Sciences, Beijing, China, ³ Department of Pharmaceutics, Wuya College of Innovation, Shenyang Pharmaceutical University, Shenyang, China, ⁴ Zhongshan Institute for Drug Discovery, Shanghai Institute of Materia Medica, Chinese Academy of Sciences, Zhongshan, China

With programmed death 1/ligand 1 (PD-1/PD-L1) as the cornerstone, anti-PD antibodies have pioneered revolutionary immunotherapies for malignancies. But most patients struggled to respond to anti-PD owing to primary or acquired resistance or even hyperprogression, pointing to more efforts needed to explore this axis. PD-1 constrains T-cell immunoreactivity via engaging with PD-L1 of tumor/myeloid cells is the canonical PD-1/PD-L1 axis function mode. Studies are increasingly aware of the impact of noncanonical PD-1/PD-L1 expression in various cancers. PD-L1 induced on activated T-cells ligates to PD-1 to mediate self-tolerance or acts on intratumoral myeloid cells and other T-cells, affecting their survival, differentiation and immunophenotyping, leading to tumor immunosuppression. Myeloid PD-1 interferes with their proliferation, differentiation, cytokine secretion and phagocytosis, mediating remarkable pro-tumor effects. Tumor cell intrinsic PD-1 signaling has diverse functions in different tumors, resulting in proproliferation or proliferation inhibition. These nonclassical PD-1/PD-L1 functions may be novel anti-PD mechanisms or causes of treatment resistance. This review highlights the nonnegligible role of T-cell-intrinsic PD-L1 and tumor/myeloid PD-1 in the cell interplay network and the complex impact on the efficacy of anti-PD antibodies. Reconsidering and rational utilization of the comprehensive PD-1/PD-L1 axis could cumulate breakthroughs in precision treatment and combination for anti-PD therapies.

Keywords: noncanonical PD-1/PD-L1 axis, T-cells, tumor cells, myeloid cells, anti-PD therapy

INTRODUCTION

Programmed death-1 (PD-1) was discovered in 1992 as an apoptosis-associated gene (1). Subsequent studies identified PD-1 as a negative regulatory immune molecule to maintain self-tolerance, containing cytoplasmic immunoreceptor tyrosine-based inhibitory motif (ITIM) and switch motif (ITSM), and predominantly expressed in T/B-lymphocytes (2–5). Programmed death ligand 1 (PD-L1) was discovered in 1999 as a novel member of the B7 family (6). In 2000, PD-L1 was found to be a ligand for PD-1, which inhibits T-cell proliferation (7). Later studies revealed that PD-L1, abundantly expressed on tumor and myeloid cells, induces T-cell apoptosis and immunosuppression to achieve tumor escape, and is a potential tumor therapeutic target (8–10).

OPEN ACCESS

Edited by:

Xuyao Zhang, Fudan University, China

Reviewed by: Yi Lu, Tongji University, China

***Correspondence:** Likun Gong Ikgong@simm.ac.cn

[†]These authors have contributed equally to this work

Specialty section:

This article was submitted to Cancer Immunity and Immunotherapy, a section of the journal Frontiers in Immunology

Received: 01 April 2022 Accepted: 21 April 2022 Published: 18 May 2022

Citation:

Long Y, Yu X, Chen R, Tong Y and Gong L (2022) Noncanonical PD-1/ PD-L1 Axis in Relation to the Efficacy of Anti-PD Therapy. Front. Immunol. 13:910704. doi: 10.3389/fimmu.2022.910704 Since 2012, numerous clinical reports (11–19) have shown the unprecedented efficacy of anti-PD antibodies for the treatment of metastatic bladder cancer, renal-cell cancer, colorectal cancer (CRC), non–small-cell lung cancer (NCSLC), and melanoma, etc. Frustratingly, durable responses to PD-1/PD-L1 antibodies are only achieved in about 10-40% of patients, with the majority not benefiting (20). In parallel to the necessity to address resistance and hyperprogression, immune-related adverse events cannot be neglected (21, 22), emphasizing in-depth investigation of the physiological-pathological functions and regulatory mechanisms of the PD-1/PD-L1 axis is paramount.

This review focuses on significant advances in the nonclassical PD-1/PD-L1 axis, summarizes and discusses the roles of T-cell-intrinsic PD-L1 and myeloid/tumor cell-intrinsic PD-1 in cancer progression and the complex implications for anti-PD efficacy, hoping to inspire more rational anti-PD drug design and combination strategies.

CLASSICAL EXPRESSION AND LOCATION OF PD-1/PD-L1

Generally, the PD-1/PD-L1 axis is involved in tumor immune escape *via* antigen-presenting cell (APC) or tumor cell surface PD-L1 mediating suppression of PD-1⁺ CD8⁺ T-cells and blocking PD-1/PD-L1 ligation can reinvigorate anti-tumor adaptive immunity (20, 23). The classical PD-1/PD-L1 axis is the main attraction for drug development.

PD-1 on T-Cells

Earlier studies concluded that PD-1 was mainly expressed on thymic and splenic T-cells (3, 24, 25) and that PD-1 ligation on CD8⁺ T-cells inhibits naive-to-effector differentiation, cytotoxicity, proliferation, and survival during chronic infections and tumor progression (26-32). PD-1/PD-L1 blockade rescues CD8⁺ T-cells from exhaustion or dysfunction (26, 29, 32). Increased PD-1⁺ CD8⁺ T-cells are positively correlated with anti-PD responses (33, 34). Notably, PD-1 expression does not necessarily determine T-cell exhaustion (35). Partial PD-1 intermediate T-cells maintain proliferation and interferon- γ (IFN- γ)/tumor necrosis factor- α (TNF- α) secretion and show well potential for anti-PD reinvigoration (36, 37). PD-1 signaling also affects other T-cell subsets. PD-L1 engagement on CD4⁺ T-cells affects cytokine secretion and induces differentiation into regulatory T-cells (Tregs) (38-40). Follicular helper T-cells, natural killer T-cells (NKT) and $\gamma\delta$ Tcells also reduce antitumor activity or exert regulatory functions due to PD-1 function (41-45). Recent advances demonstrated that PD-1 ligation also regulates the metabolic reprogramming and migration of T-cells (45-47).

PD-L1 on Tumor Cells and Myeloid Cells

PD-L1, abundantly expressed on tumor or myeloid cells, engages on antitumor T-cells to accelerate their apoptosis and malfunction (8, 10). Anti-PD-L1 antibodies are effective in reversing the tumor immunosuppression microenvironment (9, 10). The contribution of host and tumor PD-L1 to the efficacy of anti-PD blockade remains controversial. Recently, researchers suggested that PD-L1 of host myeloid cells mainly determines the efficacy of PD-L1 antibodies (48-51). Tumor cell-derived PD-L1 exosomes were also shown to inhibit the anticancer activity of T-lymphocytes (52). Additionally, complicated membranal protein interactions and intracellular signaling of PD-L1 were revealed, suggesting there are multiple unresolved gaps in PD-L1 function. The cis-CD80/PD-L1 interactions on APCs impede PD-L1/PD-1 and CD80/cytotoxic T-lymphocyte-associated antigen-4 (CTLA-4) inhibitory signaling but do not affect CD28 co-stimulatory signaling (53, 54). Ongoing studies have indicated that PD-L1 as a receptor could transmit signals and impact the anti-apoptosis, chemotaxis, neoantigen presentation, and glycolysis of tumor cells or APCs (55-59). Moreover, cytoplasmic or nuclear translocation of PD-L1 could modulate genomic stability, DNA damage response, pyroptosis, and gene transcription of tumor cells (60-63).

PD-L1 EXPRESSED ON T CELLS

Although the T-cells-intrinsic-PD-L1 has been insufficiently studied, in fact, as early as when PD-L1 was identified, Lieping Chen's team already found that although PD-L1 was not expressed in freshly isolated human and mouse T-cells, but could be upregulated in activated T-cells (6, 64), especially in CD4⁺ T-cells and CD45RO⁺ memory T-cells (65). They also found that autoantibodies against PD-L1 in rheumatoid arthritis patients acted on primary CD4⁺ T-cells to promote apoptosis of activated CD4⁺ T-cells in an interleukin-10 (IL-10)-dependent manner. Subsequently, via PD-L1-deficient mice, researchers found that PD-L1 depleting led to increased CD4⁺ T-cell cytokine production, increased CD8⁺ T-cell expansion and cytotoxicity, and increased intrahepatic accumulation and survival of CD8⁺ T-cells, as well as impaired autoimmune tolerance (25, 66, 67). Su-Kil Seo et al. reported that T-cell-associated PD-L1 interacted with PD-1 on Tcells via the alloreactive T-T interaction, resulting in reduced T-cell proliferation and IFN-y and IL-2 production (68). And Nuriban Valero-Pacheco et al. observed that PD-L1⁺ CD8⁺ T-cells were related to a lower T-cell proportion in patients infected with the H1N1 virus (69). These early findings revealed that PD-L1 was expressed on activated T cells and may also act as a receptor to receive signals that affect T-cell activation and selftolerance maintenance.

Nonetheless, several researches conducted during the same period discussed that T-cell-intrinsic-PD-L1 functions appeared to contradict the preceding conclusions. Oezcan Talay et al. demonstrated that activation and proliferation of PD-L1^{-/-} CD8⁺ T-cells in the initial phase against influenza virus was impaired and that PD-L1 expressed on naive T-cells was required for T-cell-mediated dendritic cell (DC) maturation (70). Seung-Joo Lee and colleagues also found a significant increase in PD-L1 on CD4⁺ T-cells during *Salmonella* infection and that PD-L1-deficiency did not affect specific antibody production and CD4⁺ T-cell expansion but

affected CD4⁺ T-cell maturation and function (71). For anti-tumor immunity, Vesna Pulko et al. found that PD-L1 upregulation on primed T-cells helped effector T-cells survive the contraction phase, but anti-PD-L1 hindered T-cell survival (72). Their results also showed that PD-L1-deficient CD8⁺ T-cells were more sensitive to cytotoxicity, whereas adoptive PD-L1-deficient T-cell therapy was ineffective in restraining the growth of B16-OVA tumors. According to Asim Saha et al., upregulated PD-L1 expression in donor T-cells promoted graft-versus-host responses (73). PD-L1deficient T-cells had fewer gut homing receptors, produced fewer inflammatory cytokines, enhanced apoptosis and multiple bioenergetic pathways.

Additional studies have reported puzzling roles for anti-PD-L1 antibodies in antitumor, anti-infection and anti-autoimmune diseases (74-77). For example, two publications found that Listeria infection enhanced T-cell PD-L1 expression, whereas PD-L1 antibody blockade selectively obstructed the antiintracellular bacterial responses of CD8⁺ T-cells (75, 76). Notably, partial anti-PD-L1 antibodies caused apoptosis of PD-L1⁺ T-cells, even PD-1-knockout T-cells, by activating p38 MAPK, and that such antibodies failed to suppress B16-OVA and RENCA tumor growth in vivo (77). And these PD-L1⁺ Tcells inhibited the apoptosis of activated CD8⁺ T-cells via altering phosphorylation of p38 MAPK through intracellular interactions with DNA-PK. These results have sparked a debate about whether T-cell-intrinsic PD-L1 regulates the immune system positively or negatively. Researchers are reminded to focus on the complexity of T-cell-intrinsic PD-L1 function, where the different phases of immune responses, immune cell crosstalks, unexpected protein interactions, and specific anti-PD-L1 functions all require careful exploration.

In recent years, important progresses have been made regarding the expression pattern and immunomodulatory function of T-cell-intrinsic PD-L1 (Figure 1). Donnele Daley and colleagues found that PD-L1 expression switched positive in approximately 50% of $\gamma\delta$ T-cells in human and murine pancreatic ductal adenocarcinoma (PDA), and that blocking PD-L1 in $\gamma\delta$ Tcells enhanced activation and infiltration of CD4⁺ and CD8⁺ Tcells (78). Subsequently, Brian Diskin et al. used extensive experiments to elucidate the regulatory role and mechanisms of T-cell-intrinsic PD-L1 in PDA tumors (79). They detected that PD-L1 was expressed on >50% of intratumoral T-cells in the orthotopic PDA model and increased with progressive oncogenesis. And 63% of T-cells in B16 tumors and 17% of Tcells in MCA38 tumors also expressed PD-L1. Intriguingly, the highest PD-L1 expression in human PDA was found in T-cells, rather than in tumor cells or macrophages as commonly thought. Based on the fact that conditional ablation of PD-L1 in T-cells promoted adaptive anti-tumor responses and activated macrophages, they elucidated that PD-L1⁺ T-cells reinforce an immune tolerant environment to accelerate carcinogenesis through three ways: (1) PD-L1 engagement on T-cells inhibits Th1 differentiation but promotes Th17 differentiation via a STAT3-dependent manner, while inducing an anergic phenotype in CD8⁺ T-cells (2) PD-L1⁺ T-cells deliver inhibitory signals to PD-1⁺ T-cells; (3) PD-L1⁺ T-cells engage PD-1⁺

macrophages to promote M2-preference differentiation. Giorgia Fanelli et al. proved that PD-L1 ligation accompanied by CD3/ TCR stimulation tended to transform memory T-cells but not naive T-cells into highly suppressive Tregs by triggering the PD-L1 intracellular pathway as reducing ERK phosphorylation and decreasing AKT/mTOR/S6 signaling (80). And Fabienne Mazerolles et al. suggested that T-cell proliferation was correlated with the PD-L1 expression of activated naive CD4⁺ effector T-cells regulated by DCs and Tregs (81). Thus, T-cells-intrinsic PD-L1 has bidirectional signaling that affects CD4⁺ T-cell and macrophage differentiation and attenuates cytotoxic T-cell effects to drive immune tolerance.

In addition, numerous evidences have shown peripheral or tumor-infiltrating PD-L1⁺ T-cell levels have the potential to be served as clinical indicators. Two papers reported that melanoma patients had greater PD-L1⁺ circulating T-cell levels than healthy volunteers, and PD-L1⁺ CD8⁺ T-cells were raised in disease relapsed or disease-related dead patients (82, 83). Furthermore, PD-L1⁺ circulating CD4⁺/CD8⁺ T-cells may be a predictive biomarker for anti-CTLA-4 therapy resistance. Bruktawit A. Goshu et al. demonstrated that anti-PD-L1 (Avelumab) targeting PD-L1⁺ HIVGag-specific-CD8⁺ T-cells combined with rhIL-15 enhanced CD8⁺ T-cell activity during HIV infection (84). Xia Li et al. identified dynamic fluctuations in PD-L1 on CD4⁺/CD8⁺ T-cells around the partial mission phase of type 1 diabetes and suggested PD-L1 may be a potential target for prolonging this phase (85). Several analyses (86-91) of patient samples involving ovarian cancer, NSCLC, and chronic lymphocytic leukemia (CLL) suggested an association between low circulating or infiltrating PD-L1⁺ CD8⁺ T-cells and prolonged survival, but high PD-L1⁺ CD8⁺ T-cell levels predicted a better anti-PD-1/PD-L1 therapy response. Among them, Libin Zhang et al. used a cohort of 378 NSCLC cases to speculate that CD8⁺ PD-L1⁺ TILs might indicate a hot but immunosuppressive tumor microenvironment with a high mutation burden (90). Nikolaos Ioannou et al. found that avadomide, via triggering IFN signaling in T-cells to increase PD-L1 expression on T cells, reprogramed patients' T-cells, which complements PD-L1/PD-1 blockade (91).

TUMOR CELL-INTRINSIC PD-1

Given the predominant biofunction of PD-1 on T-lymphocytes, T-cell-extrinsic PD-1 has been largely neglected. Yet persistent studies focusing on the non-classical PD-1 are shedding further light on previously incomprehensible biological and clinical phenomena. Currently, PD-1 has been identified to be expressed on various clinical tumor cells or tumor cell lines of CRC, melanoma, hepatocellular carcinoma (HCC), NSCLC and PDA (92–102). However, the ramifications of tumor cellintrinsic PD-1 on oncogenesis have sparked much controversy.

For most oncological diseases, tumor cell-intrinsic PD-1 augmented cancer advancement independently of adaptive immunity (**Figure 2A**). Sonja Kleffel and colleagues earlier identified that preferential expression of PD-1 by ABCB5⁺-

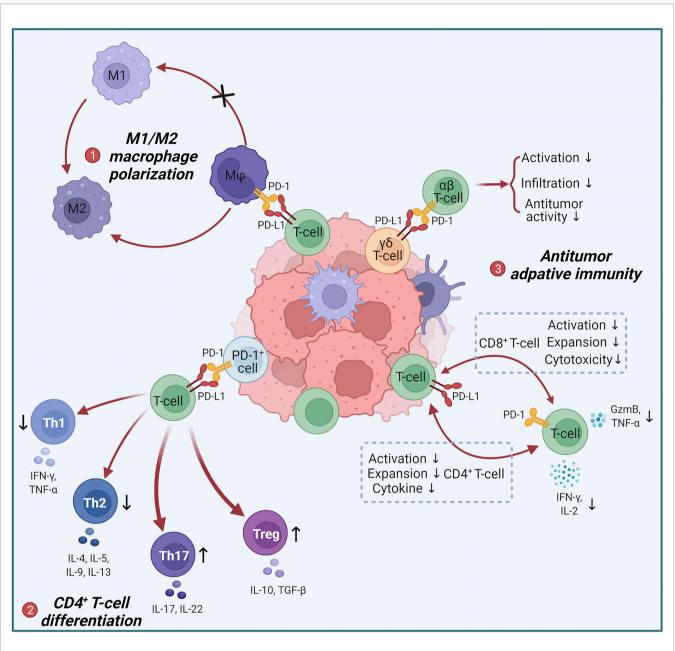


FIGURE 1 | Negative regulation of anti-tumor immune responses by T-cell intrinsic PD-L1. (1) Tumor-infiltrating PD-L1⁺ T-cells act on intratumoral PD-1⁺ macrophages to induce M2 polarization. M2 can promote tumor progression. (2) PD-1⁺ cells act on PD-L1⁺ T-cells to limit the differentiation of Th1 and Th2 and promote the differentiation of Th17 and Tregs, leading to an increase in pro-tumor immunosuppressive factors such as IL-10, IL-17 and TGF- β . (3) PD-L1⁺ T-cells and PD-1⁺ T-cells achieve bidirectional signaling through PD-1/PD-L1 interactions, resulting in bidirectional immunosuppression: inhibition of CD4⁺ T-cells activation, expansion and cytotoxicity. PD-L1⁺ $\gamma\delta$ T-cells suppress the activation, intratumoural infiltration and antitumor activity of $\alpha\beta$ T-cells *via* the PD-L1/PD-1 axis.

melanoma cells mediated increased tumorigenic capacity (94). Then they noticed that 3.5% to 16.5% of clinical melanoma cells expressed PD-1, and PD-1 positive frequencies ranged from 11.3% to 29.5% in eight human melanoma cell lines and from 6.6% to 9.4% in two murine melanoma cell lines (95). Through PD-1 knockdown/overexpressing B16 phenotype in NSG, they determined tumor PD-1 on B16 promoted tumorigenesis independently of immunity. By mutating the tyrosine sites of ITIM and ITSM, it was determined that melanoma-PD-1-driven tumorigenesis required the interactions between melanoma-PD-1 and host/melanoma-PD-L1 to initiate the PD-1 intracellular signaling *via* the mTOR pathway. Hui Li et al. later reported that five HCC cell lines and clinical HCC tissues contained subpopulations upregulating PD-1 (96). PD-1 interacted with and promoted phosphorylation of the mTOR effectors eIF4E and S6 to enhance tumor growth. Ning Pu et al. believed that PD-1 of

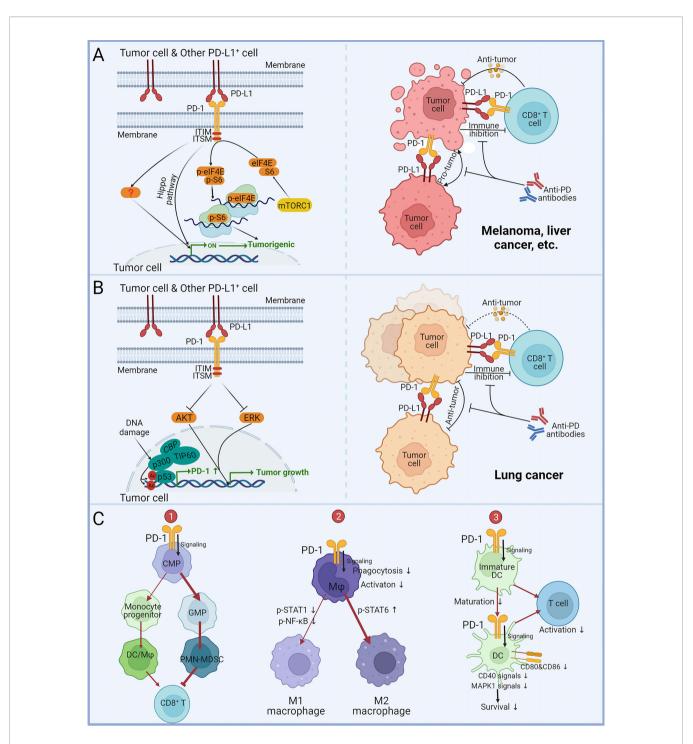


FIGURE 2 | Impact of tumor and myeloid cell-intrinsic PD-1 on tumor progression. (**A**) The effect of tumor cell-intrinsic PD-1 on melanoma, liver cancer, and other malignancies. PD-L1 expressed by tumor cells or other cells acts on PD-1⁺ tumor cells to mediate PD-1 signaling in tumor cells *via* ITIM and ITSM. The Hippo pathway and phosphorylation of mTOR downstream effector molecules eIF4E and S6 can enhance tumor-promoting gene transcription and protein expression. Anti-PD antibodies can block the PD-1/PD L1-mediated tumor promotion independent of adaptive immunity. (**B**) The role of tumor cell-intrinsic PD-1 in lung cancer. PD-L1 expressed by tumor cells or other cells acts on PD-1⁺ tumor cells to suppress tumor growth by dampening AKT and ERK signaling. Acetylation of p53 promotes gene transcription of PD-1. Anti-PD antibodies block PD-1/PD-L1-mediated tumor suppression, leading to hyperprogression in immunocompromised patients. (**C**) Effects of myeloid PD-1 on cell development, differentiation and function. (1) PD-1 expression promotes common myeloid progenitors (CMP) differentiation into granulocyte/macrophage progenitors (GMP), leading to increased MDSCs in granulocyte lineages and suppressing the activity of anti-tumor CD8⁺ T-cells. (2) PD-1 suppresses M1 polarization by reducing STAT1 and NF-κB phosphorylation and promoted M2 polarization by increasing STAT6 phosphorylation. (3) PD-1 suppresses DC maturation, survival and co-stimulatory molecules expression, consequently downregulating antigen-specific T-cell activity.

PDA cells promoted tumor growth and apoptotic resistance *via* PD-L1 ligation and Hippo signaling (99).

These teams also showed that blocking PD-1 inhibited the growth of xenografts in immunodeficient mice, and innovative combination strategies have been proposed and practiced (95, 96, 99). Li Hui et al. tried mTOR inhibitors in combination with anti-PD-1 to accomplish more durable and synergistic tumor regression (96). Ning Pu et al. found that Hippo pathway inhibitors together with anti-PD-1 treatment showed remarkable tumor eradication (99). Besides, the two teams highlighted that tumor cell PD-1 levels were positively correlated with poorer prognosis, further underlining the clinical value of tumor PD-1.

Nevertheless, tumor cell-intrinsic PD-1 has been found to depress malignancies in several lung cancer studies (Figure 2B). Shisuo Du et al. described a NSCLC patient with hyperprogression after palliative radiotherapy and pembrolizumab treatment, and tumor biopsy found PD-1 positive NSCLC cells (97). Increased viability of PD-1⁺-NSCLC cells M109 following PD-1 blockade was measured in vitro. Anti-PD-1 could significantly promote M109 growth in NSG. Yunlong Zhao et al. reported that PD-1 and PD-L1 were co-expressed in NSCLC subpopulations (98). They found that co-expressed PD-1 bound to PD-L1 in cis and inhibited PD-L1 to bind T-cell-PD-1 in trans to repress canonical PD-1/PD-L1 signaling. Selective blockade of tumor-intrinsic PD-1 could release tumor PD-1 to inhibit T-cell function. Xiaodong Wang et al. identified four lung cancer cell lines and 2/7 NSCLC patients expressing PD-1 protein (100). They demonstrated that in an immune-free condition, knockdown/overexpression of PD-1 in tumor cells altered AKT and ERK1/2 phosphorylation dependent on PD-L1, while Nivolumab and Pembrolizumab administration activated AKT and ERK1/2 signaling to promote the growth of PD-1⁺ lung cancer cells and even colon cancer cells. This suggests that the anti-tumor function of PD-1 may not be confined to NSCLC. Zhijie Cao et al. unexpectedly identified that the acetylated p53 preferentially recruited the transcriptional coactivator p300/CBP/TIP60 to the promoter region of PD-1 and elevated the accessibility of PD-1 transcription by upregulating the local histores H3K18/27 and H4K16 acetylation (101). PD-1 in cancer cells inhibited NSCLC (H1299) tumor growth, whereas interference with PD-1 transcriptional activation significantly attenuated the p53-dependent tumor suppression, confirming the materiality of the p53-PD-1 axis. These findings imply that anti-PD-1 for PD-1⁺ NSCLC patients may result in tumor hyperprogression. However, a recent study has suggested that PD-1 expression in lung cancer cell lines (A549, H1975, H1299 and HCC827) can enhance their proliferation and clone formation (102). Therefore, the multifaceted effects of PD-1 on NSCLC still need further research and debate.

MYELOID CELL-INTRINSIC PD-1

Soon after PD-1 was identified, Tasuku Honjo's team noted that PD-1 was also expressed on myeloid cells (103). Studies have

confirmed that PD-1 is expressed on monocytes (104-106), macrophages (79, 107-113), DCs (114-119) and myeloidderived suppressor cells (MDSCs) (120). Myeloid-PD-1 was markedly upregulated during infections, tumor progression, organ injury and compound induction. Researchers have found that toll-like receptor (TLR) agonists, NOD-like receptor agonists, cytokines, and growth factors all augmented myeloid-PD-1 expression dependent on NF-KB and STAT3, etc. Alexander P. R. Bally and colleagues revealed an NF-KB binding site located in conserved region C upstream of PDCD1 was required for NF-KB-dependent macrophages PD-1 induction (109). Sorim Nam et al. also noticed that PD-1 of MDSCs was regulated by the NK- κ B signaling (120). Purushottam Lamichhane et al. found that IL-10 mediated increase in PD-1 of DCs was STAT3 dependent (119). Besides, histone modifications in the PD-1 promoter region are also involved in myeloid-PD-1 induction (109, 112). However, controversy remains in these studies. For example, Sheng Yao et al. reported that PD-1 of spleen DCs was inhibited by TLR9 agonists but not affected by IL-6 and TNF- α (114), but Elias A Said et al. found that TLR9 agonists, IL-6 and TNF- α all promoted PD-1 upregulation in monocytes (104). The differential responses of inducers may be due to cell types and microenvironment, emphasizing that much work remains to be done to investigate the regulatory mechanisms of myeloid-PD-1.

PD-1 engagement affects the differentiation, maturation, survival, metabolism, and effects of myeloid cells (Figure 2C). Myeloid-PD-1 altered the balance of differentiation into monocyte and granulocyte cells (106). PD-1 suppressed M1 polarization by reducing STAT1 and NF-KB phosphorylation and promoted M2 polarization by increasing STAT6 phosphorylation (108, 110, 121). Classical phosphorylation of ITIM and ITSM of PD-1 and recruitment of SHP-2 remained upstream of these signals (110). But PD-1 on DCs suppressed antigen presentation via MHC I expression inhibition dependent on the NF-kB pathway but independent of SHP-2 (117). In addition to host/tumor cells PD-L1 acting on PD-1⁺ macrophages, T-cell PD-L1 ligation induced M2 differentiation (79). Notably, studies have observed that anti-PD-1 promoted M1 polarization, which may directly function on PD-1⁺ macrophages besides the indirect effect of PD-1⁺ T-cells (122-124). PD-1 ligation on myeloid cells hampered glycolysis and cholesterol metabolism (105, 106). In addition, PD-1deficient DCs exhibited prolonged longevity dependent on increased MAPK1 and CD40 signaling, as well as maturationpromoting and increased cytokines and co-stimulatory molecules expression, consequently promoting antigen-specific T-cells activity (114-116, 118). Similar phenomena have been observed in monocytes/macrophages (104, 107).

Myeloid-PD-1 expression has been shown in ovarian cancer (115), melanoma (125), gastric cancer (121), NSCLC (98), pleural mesothelioma (112), etc, and generally increased with tumor progression. Tumor-infiltrating PD-1⁺ myeloid cells exhibited immunosuppressive phenotypes with upregulated of PD-L1 and IL-10 and could directly inhibit anti-tumor T-cells infiltration or effects *via* the PD-1/PD-L1 axis (115, 119).

New mechanisms of myeloid-PD-1 involvement in tumor immunity have been unearthed in recent years. Sydney R. Gordon et al. found that tumor-associated macrophages (TAMs) PD-1 expression impeded phagocytic potency against tumor cells, and blockade of PD-1 increased phagocytosis and reduced oncogenesis dependent on macrophages (111). Yunlong Zhao et al. reported that co-expressed PD-1 bound to PD-L1 in cis on APCs to hinder PD-L1 acts on T-cell-intrinsic PD-1 in trans (98). The work of Laura Strauss et al. focused on how myeloid-PD-1 affected myeloid cell differentiation, metabolism and effects, particularly during cancer-driven emergency myelopoiesis (79). They discovered a significant reduction in granulocyte/macrophage progenitors (GMP) in PD-1-deficient mice, and myeloid cells of tumor-bearing mice were skewed toward the LY6C⁺ monocytic lineage, which was determined by myeloid-PD-1 deletion. PD-1 deficiency or blockade suppressed monocytic immunosuppressive functions. Myeloid-PD-1knockout was superior to systemic PD-1-knockdout and T-cell PD-1 conditional knockout for tumor inhibition, even in MC38 tumors where T-cells PD-1 knockout functioned slightly but myeloid-PD-1 deletion completely inhibited MC38 growth. Notably, anti-PD-1 antibodies were still effective in mice lacking T-cells.

Thus, the role of myeloid-PD-1 in anti-PD-1 therapy is gaining attention, and several combination strategies have been proposed. Purushottam Lamichhane et al. found that DCs responded to PD-1 blockade by increasing IL-10 production (119). The combination of PD-1 and IL-10 blockade significantly reduced tumor burden. Hirotake Tsukamoto et al. found that blocking PD-1/PD-L1 prompted PD-1⁺ TAMs to produce IL-6. Depletion of macrophages in melanoma-bearing mice reduced the levels of IL-6 during PD-1/PD-L1 blockade, suggesting that IL-6-neutralizing antibodies are potential candidates for combination with anti-PD-1 antibodies (125). In addition, inhibition of EZH2 methyltransferase was found to promote PD-1 expression on macrophages, and the combination of EZH2 inhibitors and anti-PD-1 antibodies could achieve better anti-tumor efficacy (112).

OTHER NONCANONICAL PD-1/PD-L1 EXPRESSION

In addition to the above discussion, unacquainted PD-1/PD-L1 expression in other cell types also requires attention. Taking NK cells as an example, although less studied, available reports have supported that NK cells can express PD-1/PD-L1. PD-L1 engagement can inhibit PD-1⁺ NK cell-mediated antitumor responses (126, 127). Increased NK cell PD-1 expression is associated with tumor progression and poor prognosis in patients (128, 129). Anti-PD-1 treatment can promote NK cell activation, intratumoral recruitment, and anti-tumor cytotoxicity (130–132). Studies on PD-L1 in NK cells are much rarer. Existing results suggest that the TME can upregulate PD-L1 in NK cells (129, 133). PD-L1 inhibitors can not only block the inhibitory signal of PD-1, surprisingly, also directly activate PD-L1⁺ NK cells (133).

Furthermore, the expression of PD-1/PD-L1 in other nonimmune cells may also affect the efficacy or safety of anti-PD therapy. For example, PD-1 was found to be expressed by primary sensory neurons in the dorsal root ganglion and to affect their signaling, and administration of anti-PD-1 antibodies to mice or non-human primates led to altered opioid-induced antinociception (134).

DISCUSSION OF NONCANONICAL PD-1/PD-L1 AXIS ASSOCIATED THERAPY STRATEGIES

Shifting the focus of anti-PD therapies from the classical PD-1/PD-L1 axis to noncanonical axis may provide opportunities to broaden the benefits of PD-1/PD-L1 blockade through rational drug design and combination based on the regulatory role of noncanonical PD-1/PD-L1 axis in tumorigenesis.

The involvement of T-cell intrinsic PD-L1 in immunosuppression is increasingly recognized as an additional mechanism for anti-PD-L1 efficacy. Considering several studies emphasized that many anti-PD-L1 antibodies could trigger apoptosis of PD-L1⁺ T-cells (72, 77), excluding such antibodies via T-cell apoptosis assays and using of Fc with weak effects are spurred. Besides, potential cis-interactions of PD-1/PD-L1 and CD80/PD-L1 on Tcells need to be investigated. They have been shown to contend with PD-1/PD-L1 and CD80/CTLA-4 trans-interactions (54, 98), so that anti-PD-1/PD-L1 antibodies alone lead to the release of inhibitory signals after breaking cis-interactions. Coadministration of anti-PD-1, anti-PD-L1 and anti-CTLA-4 antibodies or treatment of anti-PD-1/PD-L1/CTLA-4 trispecific antibodies may be candidate approaches to completely unleash innate and adaptive immunity to eradicate tumors, which also fits well with cancers with PD-1⁺ tumor or myeloid cells.

Intracellular signals of tumor-intrinsic PD-1 as accomplices of malignancies are candidate strategies for combination with anti-PD-1 antibodies, such as Hippo and mTOR pathways. Notably, PD-1 of tumor cells has been found to depress NSCLC tumor growth, and anti-PD-1 treatment may even lead to tumor hyperprogression. In general, anti-PD therapies result in significant activation of T-cells in patients to eliminate tumors. However, in immunocompromised patients with low initial activated T-cells, anti-PD antibodies administration could not normalize the intratumoral T-cells function, but may raise the pro-tumor signaling, thus leading to tumor hyperprogression (21). Therefore, for NSCLC or cancers with hyperprogression caused by immunotherapies, caution is needed for anti-PD-1/ PD-L1 treatment. Combination with AKT and ERK1/2 inhibitors is an approach to contain the tumor-promoting signaling activated by anti-PD-1 antibodies (100), and combination with innate immune agonists can boost the antitumor responses of patients. Combining them may be a beneficial strategy for patients with hyperprogression.

For myeloid cells, increased secretion of IL-6/IL-10 induced by anti-PD-1 antibodies is also a potential target for combination to further repress the alternative inhibitory molecules (119, 125). In addition, the noncanonical expression of other checkpoint molecules such as lymphocyte activation gene-3 (LAG-3) (135, 136) and T cell immunoglobulin domain and mucin domain-3 (TIM-3) (137) on myeloid cells also needs attention and investigation, and combination with these checkpoint inhibitors holds promise for overcoming antitumor resistance.

CONCLUSION AND PERSPECTIVES

In summary, the noncanonical PD-1/PD-L1, represented by Tcell-intrinsic PD-L1, tumor cell-intrinsic PD-1, and myeloid PD-1, exhibits unique protein interactions, signaling and cell crosstalk to regulate cell growth, differentiation, metabolism and effects dependently on immunity or not. But noncanonical signaling contributes to both anti-PD efficacy and resistance, and further studies are needed to resolve, balance, or even exploit these controversies for clinical applications of the noncanonical PD-1/ PD-L1 axis. Integrating the classical and non-classical PD-1/PD-L1 axes and revisiting the role of the holistic PD-1/PD-L1 axis on tumor progression in specific cancer types and stages, improved

REFERENCES

- Ishida Y, Agata Y, Shibahara K, Honjo T. Induced Expression of Pd-1, a Novel Member of the Immunoglobulin Gene Superfamily, Upon Programmed Cell Death. *EMBO J* (1992) 11(11):3887–95. doi: 10.1002/ j.1460-2075.1992.tb05481.x
- Shinohara T, Taniwaki M, Ishida Y, Kawaichi M, Honjo T. Structure and Chromosomal Localization of the Human Pd-1 Gene (Pdcd1). *Genomics* (1994) 23(3):704–6. doi: 10.1006/geno.1994.1562
- Agata Y, Kawasaki A, Nishimura H, Ishida Y, Tsubata T, Yagita H, et al. Expression of the Pd-1 Antigen on the Surface of Stimulated Mouse T and B Lymphocytes. Int Immunol (1996) 8(5):765–72. doi: 10.1093/intimm/ 8.5.765
- Finger LR, Pu J, Wasserman R, Vibhakar R, Louie E, Hardy RR, et al. The Human Pd-1 Gene: Complete Cdna, Genomic Organization, and Developmentally Regulated Expression in B Cell Progenitors. *Gene* (1997) 197(1-2):177–87. doi: 10.1016/s0378-1119(97)00260-6
- Nishimura H, Nose M, Hiai H, Minato N, Honjo T. Development of Lupus-Like Autoimmune Diseases by Disruption of the Pd-1 Gene Encoding an Itim Motif-Carrying Immunoreceptor. *Immunity* (1999) 11(2):141–51. doi: 10.1016/s1074-7613(00)80089-8
- Dong H, Zhu G, Tamada K, Chen L. B7-H1, A Third Member of the B7 Family, Co-Stimulates T-Cell Proliferation and Interleukin-10 Secretion. *Nat Med* (1999) 5(12):1365–9. doi: 10.1038/70932
- Freeman GJ, Long AJ, Iwai Y, Bourque K, Chernova T, Nishimura H, et al. Engagement of the Pd-1 Immunoinhibitory Receptor by a Novel B7 Family Member Leads to Negative Regulation of Lymphocyte Activation. *J Exp Med* (2000) 192(7):1027–34. doi: 10.1084/jem.192.7.1027
- Dong H, Strome SE, Salomao DR, Tamura H, Hirano F, Flies DB, et al. Tumor-Associated B7-H1 Promotes T-Cell Apoptosis: A Potential Mechanism of Immune Evasion. *Nat Med* (2002) 8(8):793-800. doi: 10.1038/nm730
- Iwai Y, Ishida M, Tanaka Y, Okazaki T, Honjo T, Minato N. Involvement of Pd-L1 on Tumor Cells in the Escape From Host Immune System and Tumor Immunotherapy by Pd-L1 Blockade. *Proc Natl Acad Sci USA* (2002) 99(19):12293–7. doi: 10.1073/pnas.192461099
- Curiel TJ, Wei S, Dong H, Alvarez X, Cheng P, Mottram P, et al. Blockade of B7-H1 Improves Myeloid Dendritic Cell-Mediated Antitumor Immunity. *Nat Med* (2003) 9(5):562–7. doi: 10.1038/nm863

therapeutic efficacy and safety of anti-PD therapies will be achieved through rational drug design and combination.

AUTHOR CONTRIBUTIONS

YL and LG conceived the topic. YL and XY drafted the manuscript and prepared the figures. Others reviewed the manuscript. All authors read and approved the final manuscript. All authors contributed to the article and approved the submitted version.

FUNDING

This work was supported by Foundation of Shanghai Science and Technology Committee (No. 22S11902100), Zhongshan Municipal Bureau of Science and Technology (No. 2020SYF08) and the Strategic Priority Research Program of the Chinese Academy of Sciences (No. XDA 12050305).

ACKNOWLEDGMENTS

All the figures were created with BioRender.com.

- Brahmer JR, Tykodi SS, Chow LQM, Hwu W-J, Topalian SL, Hwu P, et al. Safety and Activity of Anti-Pd-L1 Antibody in Patients With Advanced Cancer. N Engl J Med (2012) 366(26):2455-65. doi: 10.1056/ NEJMoa1200694
- Topalian SL, Hodi FS, Brahmer JR, Gettinger SN, Smith DC, McDermott DF, et al. Safety, Activity, and Immune Correlates of Anti–Pd-1 Antibody in Cancer. N Engl J Med (2012) 366(26):2443–54. doi: 10.1056/ NEJMoa1200690
- Powles T, Eder JP, Fine GD, Braiteh FS, Loriot Y, Cruz C, et al. Mpdl3280a (Anti-Pd-L1) Treatment Leads to Clinical Activity in Metastatic Bladder Cancer. Nature (2014) 515(7528):558–62. doi: 10.1038/nature13904
- Borghaei H, Paz-Ares L, Horn L, Spigel DR, Steins M, Ready NE, et al. Nivolumab Versus Docetaxel in Advanced Nonsquamous Non-Small-Cell Lung Cancer. N Engl J Med (2015) 373(17):1627–39. doi: 10.1056/ NEJMoa1507643
- Motzer RJ, Escudier B, McDermott DF, George S, Hammers HJ, Srinivas S, et al. Nivolumab Versus Everolimus in Advanced Renal-Cell Carcinoma. *N Engl J Med* (2015) 373(19):1803–13. doi: 10.1056/NEJMoa1510665
- Robert C, Schachter J, Long GV, Arance A, Grob JJ, Mortier L, et al. Pembrolizumab Versus Ipilimumab in Advanced Melanoma. N Engl J Med (2015) 372(26):2521–32. doi: 10.1056/NEJMoa1503093
- Ferris RL, Blumenschein G Jr, Fayette J, Guigay J, Colevas AD, Licitra L, et al. Nivolumab for Recurrent Squamous-Cell Carcinoma of the Head and Neck. N Engl J Med (2016) 375(19):1856–67. doi: 10.1056/NEJMoa1602252
- Herbst RS, Baas P, Kim DW, Felip E, Pérez-Gracia JL, Han JY, et al. Pembrolizumab Versus Docetaxel for Previously Treated, Pd-L1-Positive, Advanced Non-Small-Cell Lung Cancer (Keynote-010): A Randomised Controlled Trial. *Lancet (Lond Engl)* (2016) 387(10027):1540–50. doi: 10.1016/s0140-6736(15)01281-7
- Kaufman HL, Russell J, Hamid O, Bhatia S, Terheyden P, D'Angelo SP, et al. Avelumab in Patients With Chemotherapy-Refractory Metastatic Merkel Cell Carcinoma: A Multicentre, Single-Group, Open-Label, Phase 2 Trial. *Lancet Oncol* (2016) 17(10):1374–85. doi: 10.1016/s1470-2045(16)30364-3
- Zou W, Wolchok JD, Chen L. Pd-L1 (B7-H1) and Pd-1 Pathway Blockade for Cancer Therapy: Mechanisms, Response Biomarkers, and Combinations. *Sci Transl Med* (2016) 8(328):328rv4. doi: 10.1126/scitranslmed.aad7118
- Adashek JJ, Subbiah IM, Matos I, Garralda E, Menta AK, Ganeshan DM, et al. Hyperprogression and Immunotherapy: Fact, Fiction, or Alternative Fact? *Trends Cancer* (2020) 6(3):181–91. doi: 10.1016/j.trecan.2020.01.005

- Naidoo J, Page DB, Li BT, Connell LC, Schindler K, Lacouture ME, et al. Toxicities of the Anti-Pd-1 and Anti-Pd-L1 Immune Checkpoint Antibodies. Ann Oncol (2015) 26(12):2375–91. doi: 10.1093/annonc/ mdv383
- Sanmamed MF, Chen L. A Paradigm Shift in Cancer Immunotherapy: From Enhancement to Normalization. *Cell* (2018) 175(2):313–26. doi: 10.1016/ j.cell.2018.09.035
- Yamazaki T, Akiba H, Iwai H, Matsuda H, Aoki M, Tanno Y, et al. Expression of Programmed Death 1 Ligands by Murine T Cells and Apc. *J Immunol* (2002) 169 (10):5538–45. doi: 10.4049/jimmunol.169.10.5538
- Liang SC, Latchman YE, Buhlmann JE, Tomczak MF, Horwitz BH, Freeman GJ, et al. Regulation of Pd-1, Pd-L1, and Pd-L2 Expression During Normal and Autoimmune Responses. *Eur J Immunol* (2003) 33(10):2706–16. doi: 10.1002/eji.200324228
- Barber DL, Wherry EJ, Masopust D, Zhu B, Allison JP, Sharpe AH, et al. Restoring Function in Exhausted Cd8 T Cells During Chronic Viral Infection. *Nature* (2006) 439(7077):682–7. doi: 10.1038/nature04444
- Freeman GJ, Wherry EJ, Ahmed R, Sharpe AH. Reinvigorating Exhausted Hiv-Specific T Cells Via Pd-1-Pd-1 Ligand Blockade. J Exp Med (2006) 203 (10):2223–7. doi: 10.1084/jem.20061800
- Petrovas C, Casazza JP, Brenchley JM, Price DA, Gostick E, Adams WC, et al. Pd-1 Is a Regulator of Virus-Specific Cd8+ T Cell Survival in HIV Infection. J Exp Med (2006) 203(10):2281–92. doi: 10.1084/jem.20061496
- Trautmann L, Janbazian L, Chomont N, Said EA, Gimmig S, Bessette B, et al. Upregulation of Pd-1 Expression on Hiv-Specific Cd8+ T Cells Leads to Reversible Immune Dysfunction. *Nat Med* (2006) 12(10):1198–202. doi: 10.1038/nm1482
- Goldberg MV, Maris CH, Hipkiss EL, Flies AS, Zhen L, Tuder RM, et al. Role of Pd-1 and Its Ligand, B7-H1, in Early Fate Decisions of Cd8 T Cells. *Blood* (2007) 110(1):186–92. doi: 10.1182/blood-2006-12-062422
- 31. Ahmadzadeh M, Johnson LA, Heemskerk B, Wunderlich JR, Dudley ME, White DE, et al. Tumor Antigen-Specific Cd8 T Cells Infiltrating the Tumor Express High Levels of Pd-1 and Are Functionally Impaired. *Blood* (2009) 114(8):1537–44. doi: 10.1182/blood-2008-12-195792
- Ahn E, Araki K, Hashimoto M, Li W, Riley JL, Cheung J, et al. Role of Pd-1 During Effector Cd8 T Cell Differentiation. *Proc Natl Acad Sci* (2018) 115 (18):4749–54. doi: 10.1073/pnas.1718217115
- Simon S, Labarriere N. Pd-1 Expression on Tumor-Specific T Cells: Friend or Foe for Immunotherapy? Oncoimmunology (2017) 7(1):e1364828. doi: 10.1080/2162402X.2017.1364828
- 34. Kamphorst AO, Pillai RN, Yang S, Nasti TH, Akondy RS, Wieland A, et al. Proliferation of Pd-1+ Cd8 T Cells in Peripheral Blood After Pd-1-Targeted Therapy in Lung Cancer Patients. *Proc Natl Acad Sci USA* (2017) 114 (19):4993–8. doi: 10.1073/pnas.1705327114
- Shen Y, Teng Y, Lv Y, Zhao Y, Qiu Y, Chen W, et al. Pd-1 Does Not Mark Tumor-Infiltrating Cd8+ T Cell Dysfunction in Human Gastric Cancer. *J Immunother Cancer* (2020) 8(2):e000422. doi: 10.1136/jitc-2019-000422
- Blackburn SD, Shin H, Freeman GJ, Wherry EJ. Selective Expansion of a Subset of Exhausted Cd8 T Cells by αpd-L1 Blockade. Proc Natl Acad Sci USA (2008) 105(39):15016–21. doi: 10.1073/pnas.0801497105
- Paley MA, Kroy DC, Odorizzi PM, Johnnidis JB, Dolfi DV, Barnett BE, et al. Progenitor and Terminal Subsets of Cd8+ T Cells Cooperate to Contain Chronic Viral Infection. *Science* (2012) 338(6111):1220–5. doi: 10.1126/ science.1229620
- Francisco LM, Salinas VH, Brown KE, Vanguri VK, Freeman GJ, Kuchroo VK, et al. Pd-L1 Regulates the Development, Maintenance, and Function of Induced Regulatory T Cells. J Exp Med (2009) 206(13):3015–29. doi: 10.1084/jem.20090847
- 39. Park HJ, Park JS, Jeong YH, Son J, Ban YH, Lee BH, et al. Pd-1 Upregulated on Regulatory T Cells During Chronic Virus Infection Enhances the Suppression of Cd8+ T Cell Immune Response Via the Interaction With Pd-L1 Expressed on Cd8+ T Cells. J Immunol (2015) 195(12):5841–2. doi: 10.4049/jimmunol.1502256
- Laba S, Mallett G, Amarnath S. The Depths of Pd-1 Function Within the Tumor Microenvironment Beyond Cd8(+) T Cells. Semin Cancer Biol (2021) \$1044-579X(21):00153–X. doi: 10.1016/j.semcancer.2021.05.022
- Hoeres T, Holzmann E, Smetak M, Birkmann J, Wilhelm M. Pd-1 Signaling Modulates Interferon-Gamma Production by Gamma Delta (Gammadelta)

T-Cells in Response to Leukemia. Oncoimmunology (2019) 8(3):1550618. doi: 10.1080/2162402X.2018.1550618

- 42. Chang WS, Kim JY, Kim YJ, Kim YS, Lee JM, Azuma M, et al. Cutting Edge: Programmed Death-1/Programmed Death Ligand 1 Interaction Regulates the Induction and Maintenance of Invariant Nkt Cell Anergy. *J Immunol* (2008) 181(10):6707–10. doi: 10.4049/jimmunol.181.10.6707
- 43. Iwasaki M, Tanaka Y, Kobayashi H, Murata-Hirai K, Miyabe H, Sugie T, et al. Expression and Function of Pd-1 in Human Gammadelta T Cells That Recognize Phosphoantigens. *Eur J Immunol* (2011) 41(2):345–55. doi: 10.1002/eji.201040959
- 44. Chen Y, Yu M, Zheng Y, Fu G, Xin G, Zhu W, et al. Cxcr5(+)Pd-1(+) Follicular Helper Cd8 T Cells Control B Cell Tolerance. *Nat Commun* (2019) 10(1):4415. doi: 10.1038/s41467-019-12446-5
- 45. Shi J, Hou S, Fang Q, Liu X, Liu X, Qi H. Pd-1 Controls Follicular T Helper Cell Positioning and Function. *Immunity* (2018) 49(2):264–74.e4. doi: 10.1016/j.immuni.2018.06.012
- 46. Patsoukis N, Bardhan K, Chatterjee P, Sari D, Liu B, Bell LN, et al. Pd-1 Alters T-Cell Metabolic Reprogramming by Inhibiting Glycolysis and Promoting Lipolysis and Fatty Acid Oxidation. *Nat Commun* (2015) 6:6692. doi: 10.1038/ncomms7692
- Honda T, Egen JG, Lammermann T, Kastenmuller W, Torabi-Parizi P, Germain RN. Tuning of Antigen Sensitivity by T Cell Receptor-Dependent Negative Feedback Controls T Cell Effector Function in Inflamed Tissues. *Immunity* (2014) 40(2):235–47. doi: 10.1016/j.immuni.2013.11.017
- Lau J, Cheung J, Navarro A, Lianoglou S, Haley B, Totpal K, et al. Tumour and Host Cell Pd-L1 Is Required to Mediate Suppression of Anti-Tumour Immunity in Mice. *Nat Commun* (2017) 8:14572. doi: 10.1038/ ncomms14572
- Lin H, Wei S, Hurt EM, Green MD, Zhao L, Vatan L, et al. Host Expression of Pd-L1 Determines Efficacy of Pd-L1 Pathway Blockade-Mediated Tumor Regression. J Clin Invest (2018) 128(2):805–15. doi: 10.1172/JCI96113
- Tang H, Liang Y, Anders RA, Taube JM, Qiu X, Mulgaonkar A, et al. Pd-L1 on Host Cells Is Essential for Pd-L1 Blockade–Mediated Tumor Regression. *J Clin Invest* (2018) 128(2):580–8. doi: 10.1172/jci96061
- Oh SA, Wu D-C, Cheung J, Navarro A, Xiong H, Cubas R, et al. Pd-L1 Expression by Dendritic Cells Is a Key Regulator of T-Cell Immunity in Cancer. Nat Cancer (2020) 1(7):681–91. doi: 10.1038/s43018-020-0075-x
- Poggio M, Hu T, Pai CC, Chu B, Belair CD, Chang A, et al. Suppression of Exosomal Pd-L1 Induces Systemic Anti-Tumor Immunity and Memory. *Cell* (2019) 177(2):414–27.e13. doi: 10.1016/j.cell.2019.02.016
- Sugiura D, Maruhashi T, Okazaki IM, Shimizu K, Maeda TK, Takemoto T, et al. Restriction of Pd-1 Function by Cis-Pd-L1/Cd80 Interactions Is Required for Optimal T Cell Responses. *Science* (2019) 364(6440):558–66. doi: 10.1126/science.aav7062
- Zhao Y, Lee CK, Lin C-H, Gassen RB, Xu X, Huang Z, et al. Pd-L1:Cd80 Cis-Heterodimer Triggers the Co-Stimulatory Receptor Cd28 While Repressing the Inhibitory Pd-1 and Ctla-4 Pathways. *Immunity* (2019) 51(6):1059– 73.e9. doi: 10.1016/j.immuni.2019.11.003
- Azuma T, Yao S, Zhu G, Flies AS, Flies SJ, Chen L. B7-H1 Is a Ubiquitous Antiapoptotic Receptor on Cancer Cells. *Blood* (2008) 111(7):3635–43. doi: 10.1182/blood-2007-11-123141
- Gato-Canas M, Zuazo M, Arasanz H, Ibanez-Vea M, Lorenzo L, Fernandez-Hinojal G, et al. Pdl1 Signals Through Conserved Sequence Motifs to Overcome Interferon-Mediated Cytotoxicity. *Cell Rep* (2017) 20(8):1818– 29. doi: 10.1016/j.celrep.2017.07.075
- Chang CH, Qiu J, O'Sullivan D, Buck MD, Noguchi T, Curtis JD, et al. Metabolic Competition in the Tumor Microenvironment Is a Driver of Cancer Progression. *Cell* (2015) 162(6):1229–41. doi: 10.1016/j.cell.2015. 08.016
- Okada M, Shimizu K, Iyoda T, Ueda S, Shinga J, Mochizuki Y, et al. Pd-L1 Expression Affects Neoantigen Presentation. *iScience* (2020) 23(6):101238. doi: 10.1016/j.isci.2020.101238
- Lucas ED, Schafer JB, Matsuda J, Kraus M, Burchill MA, Tamburini BAJ. Pd-L1 Reverse Signaling in Dermal Dendritic Cells Promotes Dendritic Cell Migration Required for Skin Immunity. *Cell Rep* (2020) 33(2):108258. doi: 10.1016/j.celrep.2020.108258
- 60. Tu X, Qin B, Zhang Y, Zhang C, Kahila M, Nowsheen S, et al. Pd-L1 (B7-H1) Competes With the Rna Exosome to Regulate the DNA Damage Response

and Can Be Targeted to Sensitize to Radiation or Chemotherapy. *Mol Cell* (2019) 74(6):1215–26.e4. doi: 10.1016/j.molcel.2019.04.005

- Hou J, Zhao R, Xia W, Chang CW, You Y, Hsu JM, et al. Pd-L1-Mediated Gasdermin C Expression Switches Apoptosis to Pyroptosis in Cancer Cells and Facilitates Tumour Necrosis. *Nat Cell Biol* (2020) 22(10):1264–75. doi: 10.1038/s41556-020-0575-z
- 62. Zhang W, Jin J, Wang Y, Fang L, Min L, Wang X, et al. Pd-L1 Regulates Genomic Stability *Via* Interaction With Cohesin-Sa1 in the Nucleus. *Signal Transduct Target Ther* (2021) 6(1):81. doi: 10.1038/s41392-021-00463-0
- Gao Y, Nihira NT, Bu X, Chu C, Zhang J, Kolodziejczyk A, et al. Acetylation-Dependent Regulation of Pd-L1 Nuclear Translocation Dictates the Efficacy of Anti-Pd-1 Immunotherapy. *Nat Cell Biol* (2020) 22(9):1064–75. doi: 10.1038/s41556-020-0562-4
- Tamura H, Dong H, Zhu G, Sica GL, Flies DB, Tamada K, et al. B7-H1 Costimulation Preferentially Enhances Cd28-Independent T-Helper Cell Function. *Blood* (2001) 97(6):1809–16. doi: 10.1182/blood.v97.6.1809
- 65. Dong H, Strome SE, Matteson EL, Moder KG, Flies DB, Zhu G, et al. Costimulating Aberrant T Cell Responses by B7-H1 Autoantibodies in Rheumatoid Arthritis. J Clin Invest (2003) 111(3):363–70. doi: 10.1172/ JCI16015
- 66. Latchman YE, Liang SC, Wu Y, Chernova T, Sobel RA, Klemm M, et al. Pd-L1-Deficient Mice Show That Pd-L1 on T Cells, Antigen-Presenting Cells, and Host Tissues Negatively Regulates T Cells. *Proc Natl Acad Sci USA* (2004) 101(29):10691–6. doi: 10.1073/pnas.0307252101
- Dong H, Zhu G, Tamada K, Flies DB, van Deursen JM, Chen L. B7-H1 Determines Accumulation and Deletion of Intrahepatic Cd8(+) T Lymphocytes. *Immunity* (2004) 20(3):327–36. doi: 10.1016/s1074-7613(04) 00050-0
- Seo SK, Seo HM, Jeong HY, Choi IW, Park YM, Yagita H, et al. Co-Inhibitory Role of T-Cell-Associated B7-H1 and B7-Dc in the T-Cell Immune Response. *Immunol Lett* (2006) 102(2):222–8. doi: 10.1016/ j.imlet.2005.09.007
- 69. Valero-Pacheco N, Arriaga-Pizano L, Ferat-Osorio E, Mora-Velandia LM, Pastelin-Palacios R, Villasis-Keever MA, et al. Pd-L1 Expression Induced by the 2009 Pandemic Influenza a(H1n1) Virus Impairs the Human T Cell Response. *Clin Dev Immunol* (2013) 2013:989673. doi: 10.1155/2013/989673
- Talay O, Shen CH, Chen L, Chen J. B7-H1 (Pd-L1) on T Cells Is Required for T-Cell-Mediated Conditioning of Dendritic Cell Maturation. *Proc Natl Acad Sci U S A* (2009) 106(8):2741–6. doi: 10.1073/pnas.0813367106
- Lee SJ, O'Donnell H, McSorley SJ. B7-H1 (Programmed Cell Death Ligand 1) Is Required for the Development of Multifunctional Th1 Cells and Immunity to Primary, But Not Secondary, Salmonella Infection. J Immunol (2010) 185 (4):2442–9. doi: 10.4049/jimmunol.1000743
- Pulko V, Harris KJ, Liu X, Gibbons RM, Harrington SM, Krco CJ, et al. B7-H1 Expressed by Activated Cd8 T Cells Is Essential for Their Survival. J Immunol (2011) 187(11):5606–14. doi: 10.4049/jimmunol.1003976
- Saha A, O'Connor RS, Thangavelu G, Lovitch SB, Dandamudi DB, Wilson CB, et al. Programmed Death Ligand-1 Expression on Donor T Cells Drives Graft-Versus-Host Disease Lethality. J Clin Invest (2016) 126(7):2642–60. doi: 10.1172/JCI85796
- 74. Kanai T, Totsuka T, Uraushihara K, Makita S, Nakamura T, Koganei K, et al. Blockade of B7-H1 Suppresses the Development of Chronic Intestinal Inflammation. J Immunol (2003) 171(8):4156–63. doi: 10.4049/ jimmunol.171.8.4156
- Rowe JH, Johanns TM, Ertelt JM, Way SS. Pdl-1 Blockade Impedes T Cell Expansion and Protective Immunity Primed by Attenuated Listeria Monocytogenes. J Immunol (2008) 180(11):7553–7. doi: 10.4049/ jimmunol.180.11.7553
- Seo SK, Jeong HY, Park SG, Lee SW, Choi IW, Chen L, et al. Blockade of Endogenous B7-H1 Suppresses Antibacterial Protection After Primary Listeria Monocytogenes Infection. *Immunology* (2008) 123(1):90–9. doi: 10.1111/j.1365-2567.2007.02708.x
- 77. Liu X, Wu X, Cao S, Harrington SM, Yin P, Mansfield AS, et al. B7-H1 Antibodies Lose Antitumor Activity Due to Activation of P38 Mapk That Leads to Apoptosis of Tumor-Reactive Cd8(+) T Cells. *Sci Rep* (2016) 6:36722. doi: 10.1038/srep36722
- 78. Daley D, Zambirinis CP, Seifert L, Akkad N, Mohan N, Werba G, et al. Gammadelta T Cells Support Pancreatic Oncogenesis by Restraining

Alphabeta T Cell Activation. *Cell* (2016) 166(6):1485–99.e15. doi: 10.1016/j.cell.2016.07.046

- 79. Diskin B, Adam S, Cassini MF, Sanchez G, Liria M, Aykut B, et al. Pd-L1 Engagement on T Cells Promotes Self-Tolerance and Suppression of Neighboring Macrophages and Effector T Cells in Cancer. *Nat Immunol* (2020) 21(4):442–54. doi: 10.1038/s41590-020-0620-x
- Fanelli G, Romano M, Nova-Lamperti E, Werner Sunderland M, Nerviani A, Scotta C, et al. Pd-L1 Signaling on Human Memory Cd4+ T Cells Induces a Regulatory Phenotype. *PloS Biol* (2021) 19(4):e3001199. doi: 10.1371/ journal.pbio.3001199
- Mazerolles F, Rieux-Laucat F. Pd-L1 Is Expressed on Human Activated Naive Effector Cd4+ T Cells. Regulation by Dendritic Cells and Regulatory Cd4+ T Cells. *PloS One* (2021) 16(11):e0260206. doi: 10.1371/ journal.pone.0260206
- Jacquelot N, Roberti MP, Enot DP, Rusakiewicz S, Ternes N, Jegou S, et al. Predictors of Responses to Immune Checkpoint Blockade in Advanced Melanoma. Nat Commun (2017) 8(1):592. doi: 10.1038/s41467-017-00608-2
- Brochez L, Meireson A, Chevolet I, Sundahl N, Ost P, Kruse V. Challenging Pd-L1 Expressing Cytotoxic T Cells as a Predictor for Response to Immunotherapy in Melanoma. *Nat Commun* (2018) 9(1):2921. doi: 10.1038/s41467-018-05047-1
- Goshu BA, Chen H, Moussa M, Cheng J, Catalfamo M. Combination Rhil-15 and Anti-Pd-L1 (Avelumab) Enhances Human Hivgag-Specific Cd8 T-Cell Function. J Infect Dis (2020) 222(9):1540–9. doi: 10.1093/infdis/jiaa269
- Li X, Zhong T, Tang R, Wu C, Xie Y, Liu F, et al. Pd-1 and Pd-L1 Expression in Peripheral Cd4/Cd8+ T Cells Is Restored in the Partial Remission Phase in Type 1 Diabetes. J Clin Endocrinol Metab (2020) 105(6):1947–56. doi: 10.1210/clinem/dgaa130
- Liu Y, Zugazagoitia J, Ahmed FS, Henick BS, Gettinger SN, Herbst RS, et al. Immune Cell Pd-L1 Colocalizes With Macrophages and Is Associated With Outcome in Pd-1 Pathway Blockade Therapy. *Clin Cancer Res* (2020) 26 (4):970–7. doi: 10.1158/1078-0432.CCR-19-1040
- 87. Bekos C, Pils D, Dekan S, Hofstetter G, Horak P, Reinthaller A, et al. Tumor Specimens (Ovarian Tumor Tissues and Intraperitoneal Metastases) of 111 Patients Were Used to Investigate Pd-1 and Pd-L1 Expression on Tils in Peritoneal Metastases Compared to Ovarian Tumor Tissues and Its Associations With Clinical Outcome. *Sci Rep* (2021) 11(1):6400. doi: 10.1038/s41598-021-85966-0
- Dart SJ, Cook AM, Millward MJ, McDonnell AM, Chin WL, Hakeem MU, et al. Changes in Expression of Pd-L1 on Peripheral T Cells in Patients With Melanoma and Lung Cancer Treated With Pd-1 Inhibitors. *Sci Rep* (2021) 11(1):15312. doi: 10.1038/s41598-021-93479-z
- Li L, Lu G, Liu Y, Gong L, Zheng X, Zheng H, et al. Low Infiltration of Cd8+ Pd-L1+ T Cells and M2 Macrophages Predicts Improved Clinical Outcomes After Immune Checkpoint Inhibitor Therapy in Non-Small Cell Lung Carcinoma. Front Oncol (2021) 11:658690. doi: 10.3389/fonc.2021.658690
- Zhang L, Chen Y, Wang H, Xu Z, Wang Y, Li S, et al. Massive Pd-L1 and Cd8 Double Positive Tils Characterize an Immunosuppressive Microenvironment With High Mutational Burden in Lung Cancer. J Immunother Cancer (2021) 9 (6):e002356. doi: 10.1136/jitc-2021-002356
- Ioannou N, Hagner PR, Stokes M, Gandhi AK, Apollonio B, Fanous M, et al. Triggering Interferon Signaling in T Cells With Avadomide Sensitizes Cll to Anti-Pd-L1/Pd-1 Immunotherapy. *Blood* (2021) 137(2):216–31. doi: 10.1182/blood.2020006073
- Gasser M, Grimm M, Nichiporuk E, Bueter M, Lutz J, Lebedeva T, et al. Pd-1/Pd-L1 Expression in Colorectal Cancer and Its Implications for Apoptosis and Tumor Immune Evasion. *Cancer Res* (2006) 66(8_Supplement):1118-. doi: 10.1200/jco.2006.24.18_suppl.10046
- Gasser M, Grimm M, Nichiporuk E, Bueter M, Lutz J, Lebedeva T, et al. Pd-1/Pdl-1 Expression in Colorectal Cancer and Its Implications for Tumor Immune Evasion. J Clin Oncol (2006) 24(18_suppl):10046–. doi: 10.1200/ jco.2006.24.18_suppl.10046
- Schatton T, Schutte U, Frank NY, Zhan Q, Hoerning A, Robles SC, et al. Modulation of T-Cell Activation by Malignant Melanoma Initiating Cells. *Cancer Res* (2010) 70(2):697–708. doi: 10.1158/0008-5472.CAN-09-1592
- Kleffel S, Posch C, Barthel SR, Mueller H, Schlapbach C, Guenova E, et al. Melanoma Cell-Intrinsic Pd-1 Receptor Functions Promote Tumor Growth. *Cell* (2015) 162(6):1242–56. doi: 10.1016/j.cell.2015.08.052

- 96. Li H, Li X, Liu S, Guo L, Zhang B, Zhang J, et al. Programmed Cell Death-1 (Pd-1) Checkpoint Blockade in Combination With a Mammalian Target of Rapamycin Inhibitor Restrains Hepatocellular Carcinoma Growth Induced by Hepatoma Cell-Intrinsic Pd-1. *Hepatology* (2017) 66(6):1920–33. doi: 10.1002/hep.29360
- Du S, McCall N, Park K, Guan Q, Fontina P, Ertel A, et al. Blockade of Tumor-Expressed Pd-1 Promotes Lung Cancer Growth. *Oncoimmunology* (2018) 7(4):e1408747. doi: 10.1080/2162402X.2017.1408747
- Zhao Y, Harrison DL, Song Y, Ji J, Huang J, Hui E. Antigen-Presenting Cell-Intrinsic Pd-1 Neutralizes Pd-L1 in Cis to Attenuate Pd-1 Signaling in T Cells. Cell Rep (2018) 24(2):379–90.e6. doi: 10.1016/j.celrep.2018.06.054
- Pu N, Gao S, Yin H, Li JA, Wu W, Fang Y, et al. Cell-Intrinsic Pd-1 Promotes Proliferation in Pancreatic Cancer by Targeting Cyr61/Ctgf Via the Hippo Pathway. Cancer Lett (2019) 460:42–53. doi: 10.1016/j.canlet.2019.06.013
- 100. Wang X, Yang X, Zhang C, Wang Y, Cheng T, Duan L, et al. Tumor Cell-Intrinsic Pd-1 Receptor Is a Tumor Suppressor and Mediates Resistance to Pd-1 Blockade Therapy. *Proc Natl Acad Sci USA* (2020) 117(12):6640–50. doi: 10.1073/pnas.1921445117
- 101. Cao Z, Kon N, Liu Y, Xu W, Wen J, Yao H, et al. An Unexpected Role for P53 in Regulating Cancer Cell-Intrinsic Pd-1 by Acetylation. *Sci Adv* (2021) 7 (14):eabf4148. doi: 10.1126/sciadv.abf4148
- 102. Gan F, Zhang C, Xia L, Deng S. Tumor-Endogenous Pd-1 Promotes Cell Proliferation and Predicts Poor Survival in Non-Small Cell Lung Cancer. *Transl Cancer Res* (2022) 11(1):3–13. doi: 10.21037/tcr-21-1644
- 103. Nishimura H, Minato N, Nakano T, Honjo T. Immunological Studies on Pd-1 Deficient Mice: Implication of Pd-1 as a Negative Regulator for B Cell Responses. *Int Immunol* (1998) 10(10):1563–72. doi: 10.1093/intimm/10.10.1563
- 104. Said EA, Dupuy FP, Trautmann L, Zhang Y, Shi Y, El-Far M, et al. Programmed Death-1-Induced Interleukin-10 Production by Monocytes Impairs Cd4+ T Cell Activation During Hiv Infection. *Nat Med* (2010) 16 (4):452–9. doi: 10.1038/nm.2106
- 105. Qorraj M, Bruns H, Bottcher M, Weigand L, Saul D, Mackensen A, et al. The Pd-1/Pd-L1 Axis Contributes to Immune Metabolic Dysfunctions of Monocytes in Chronic Lymphocytic Leukemia. *Leukemia* (2017) 31 (2):470–8. doi: 10.1038/leu.2016.214
- 106. Strauss L, Mahmoud MAA, Weaver JD, Tijaro-Ovalle NM, Christofides A, Wang Q, et al. Targeted Deletion of Pd-1 in Myeloid Cells Induces Antitumor Immunity. *Sci Immunol* (2020) 5(43):eaay1863. doi: 10.1126/ sciimmunol.aay1863
- 107. Huang X, Venet F, Wang YL, Lepape A, Yuan Z, Chen Y, et al. Pd-1 Expression by Macrophages Plays a Pathologic Role in Altering Microbial Clearance and the Innate Inflammatory Response to Sepsis. *Proc Natl Acad Sci U.S.A.* (2009) 106(15):6303–8. doi: 10.1073/pnas.0809422106
- 108. Yao A, Liu F, Chen K, Tang L, Liu L, Zhang K, et al. Programmed Death 1 Deficiency Induces the Polarization of Macrophages/Microglia to the M1 Phenotype After Spinal Cord Injury in Mice. *Neurotherapeutics* (2014) 11 (3):636–50. doi: 10.1007/s13311-013-0254-x
- 109. Bally AP, Lu P, Tang Y, Austin JW, Scharer CD, Ahmed R, et al. Nf-Kappab Regulates Pd-1 Expression in Macrophages. J Immunol (2015) 194(9):4545– 54. doi: 10.4049/jimmunol.1402550
- 110. Chen W, Wang J, Jia L, Liu J, Tian Y. Attenuation of the Programmed Cell Death-1 Pathway Increases the M1 Polarization of Macrophages Induced by Zymosan. Cell Death Dis (2016) 7:e2115. doi: 10.1038/cddis.2016.33
- 111. Gordon SR, Maute RL, Dulken BW, Hutter G, George BM, McCracken MN, et al. Pd-1 Expression by Tumour-Associated Macrophages Inhibits Phagocytosis and Tumour Immunity. *Nature* (2017) 545(7655):495–9. doi: 10.1038/nature22396
- 112. Hamaidia M, Gazon H, Hoyos C, Hoffmann GB, Louis R, Duysinx B, et al. Inhibition of Ezh2 Methyltransferase Decreases Immunoediting of Mesothelioma Cells by Autologous Macrophages Through a Pd-1-Dependent Mechanism. JCI Insight (2019) 4(18):e128474. doi: 10.1172/ jci.insight.128474
- 113. Triantafyllou E, Gudd CL, Mawhin MA, Husbyn HC, Trovato FM, Siggins MK, et al. Pd-1 Blockade Improves Kupffer Cell Bacterial Clearance in Acute Liver Injury. J Clin Invest (2021) 131(4):e140196. doi: 10.1172/JCI140196
- 114. Yao S, Wang S, Zhu Y, Luo L, Zhu G, Flies S, et al. Pd-1 on Dendritic Cells Impedes Innate Immunity Against Bacterial Infection. *Blood* (2009) 113 (23):5811–8. doi: 10.1182/blood-2009-02-203141

- 115. Krempski J, Karyampudi L, Behrens MD, Erskine CL, Hartmann L, Dong H, et al. Tumor-Infiltrating Programmed Death Receptor-1+ Dendritic Cells Mediate Immune Suppression in Ovarian Cancer. J Immunol (2011) 186 (12):6905–13. doi: 10.4049/jimmunol.1100274
- 116. Park SJ, Namkoong H, Doh J, Choi JC, Yang BG, Park Y, et al. Negative Role of Inducible Pd-1 on Survival of Activated Dendritic Cells. *J Leukoc Biol* (2014) 95(4):621–9. doi: 10.1189/jlb.0813443
- 117. Karyampudi L, Lamichhane P, Krempski J, Kalli KR, Behrens MD, Vargas DM, et al. Pd-1 Blunts the Function of Ovarian Tumor-Infiltrating Dendritic Cells by Inactivating Nf-Kappab. *Cancer Res* (2016) 76(2):239–50. doi: 10.1158/0008-5472.CAN-15-0748
- Lim TS, Chew V, Sieow JL, Goh S, Yeong JP, Soon AL, et al. Pd-1 Expression on Dendritic Cells Suppresses Cd8(+) T Cell Function and Antitumor Immunity. Oncoimmunology (2016) 5(3):e1085146. doi: 10.1080/ 2162402X.2015.1085146
- 119. Lamichhane P, Karyampudi L, Shreeder B, Krempski J, Bahr D, Daum J, et al. Il10 Release Upon Pd-1 Blockade Sustains Immunosuppression in Ovarian Cancer. *Cancer Res* (2017) 77(23):6667–78. doi: 10.1158/0008-5472.CAN-17-0740
- 120. Nam S, Lee A, Lim J, Lim JS. Analysis of the Expression and Regulation of Pd-1 Protein on the Surface of Myeloid-Derived Suppressor Cells (Mdscs). *Biomol Ther (Seoul)* (2019) 27(1):63–70. doi: 10.4062/biomolther.2018.201
- 121. Wang F, Li B, Wei Y, Zhao Y, Wang L, Zhang P, et al. Tumor-Derived Exosomes Induce Pd1(+) Macrophage Population in Human Gastric Cancer That Promotes Disease Progression. *Oncogenesis* (2018) 7(5):41. doi: 10.1038/s41389-018-0049-3
- 122. Dhupkar P, Gordon N, Stewart J, Kleinerman ES. Anti-Pd-1 Therapy Redirects Macrophages From an M2 to an M1 Phenotype Inducing Regression of Os Lung Metastases. *Cancer Med* (2018) 7(6):2654–64. doi: 10.1002/cam4.1518
- 123. Ho TTB, Nasti A, Seki A, Komura T, Inui H, Kozaka T, et al. Combination of Gemcitabine and Anti-Pd-1 Antibody Enhances the Anticancer Effect of M1 Macrophages and the Th1 Response in a Murine Model of Pancreatic Cancer Liver Metastasis. J Immunother Cancer (2020) 8(2):e001367. doi: 10.1136/ jitc-2020-001367
- 124. Rao G, Latha K, Ott M, Sabbagh A, Marisetty A, Ling X, et al. Anti-Pd-1 Induces M1 Polarization in the Glioma Microenvironment and Exerts Therapeutic Efficacy in the Absence of Cd8 Cytotoxic T Cells. *Clin Cancer Res* (2020) 26(17):4699–712. doi: 10.1158/1078-0432.CCR-19-4110
- 125. Tsukamoto H, Fujieda K, Miyashita A, Fukushima S, Ikeda T, Kubo Y, et al. Combined Blockade of Il6 and Pd-1/Pd-L1 Signaling Abrogates Mutual Regulation of Their Immunosuppressive Effects in the Tumor Microenvironment. *Cancer Res* (2018) 78(17):5011–22. doi: 10.1158/0008-5472.CAN-18-0118
- 126. Vari F, Arpon D, Keane C, Hertzberg MS, Talaulikar D, Jain S, et al. Immune Evasion Via Pd-1/Pd-L1 on Nk Cells and Monocyte/Macrophages Is More Prominent in Hodgkin Lymphoma Than Dlbcl. *Blood* (2018) 131(16):1809– 19. doi: 10.1182/blood-2017-07-796342
- 127. Concha-Benavente F, Kansy B, Moskovitz J, Moy J, Chandran U, Ferris RL. Pd-L1 Mediates Dysfunction in Activated Pd-1(+) Nk Cells in Head and Neck Cancer Patients. *Cancer Immunol Res* (2018) 6(12):1548–60. doi: 10.1158/2326-6066.CIR-18-0062
- 128. Liu Y, Cheng Y, Xu Y, Wang Z, Du X, Li C, et al. Increased Expression of Programmed Cell Death Protein 1 on Nk Cells Inhibits Nk-Cell-Mediated Anti-Tumor Function and Indicates Poor Prognosis in Digestive Cancers. Oncogene (2017) 36(44):6143–53. doi: 10.1038/onc.2017.209
- 129. Iraolagoitia XL, Spallanzani RG, Torres NI, Araya RE, Ziblat A, Domaica CI, et al. Nk Cells Restrain Spontaneous Antitumor Cd8+ T Cell Priming Through Pd-1/Pd-L1 Interactions With Dendritic Cells. J Immunol (2016) 197(3):953–61. doi: 10.4049/jimmunol.1502291
- 130. Trefny MP, Kaiser M, Stanczak MA, Herzig P, Savic S, Wiese M, et al. Pd-1
 (+) Natural Killer Cells in Human Non-Small Cell Lung Cancer Can Be Activated by Pd-1/Pd-L1 Blockade. *Cancer Immunol Immunother* (2020) 69 (8):1505–17. doi: 10.1007/s00262-020-02558-z
- 131. Hsu J, Hodgins JJ, Marathe M, Nicolai CJ, Bourgeois-Daigneault MC, Trevino TN, et al. Contribution of Nk Cells to Immunotherapy Mediated by Pd-1/Pd-L1 Blockade. J Clin Invest (2018) 128(10):4654–68. doi: 10.1172/ JCI99317
- 132. Benson DMJr., Bakan CE, Mishra A, Hofmeister CC, Efebera Y, Becknell B, et al. The Pd-1/Pd-L1 Axis Modulates the Natural Killer Cell Versus Multiple

Myeloma Effect: A Therapeutic Target for Ct-011, a Novel Monoclonal Anti-Pd-1 Antibody. *Blood* (2010) 116(13):2286–94. doi: 10.1182/blood-2010-02-271874

- 133. Dong W, Wu X, Ma S, Wang Y, Nalin AP, Zhu Z, et al. The Mechanism of Anti-Pd-L1 Antibody Efficacy Against Pd-L1-Negative Tumors Identifies Nk Cells Expressing Pd-L1 as a Cytolytic Effector. *Cancer Discov* (2019) 9 (10):1422–37. doi: 10.1158/2159-8290.CD-18-1259
- 134. Wang Z, Jiang C, He Q, Matsuda M, Han Q, Wang K, et al. Anti–Pd-1 Treatment Impairs Opioid Antinociception in Rodents and Nonhuman Primates. Sci Transl Med (2020) 12(531):. doi: 10.1126/scitranslmed.aaw6471
- Workman CJ, Wang Y, El Kasmi KC, Pardoll DM, Murray PJ, Drake CG, et al. Lag-3 Regulates Plasmacytoid Dendritic Cell Homeostasis. J Immunol (2009) 182(4):1885–91. doi: 10.4049/jimmunol.0800185
- 136. Chiba S, Baghdadi M, Akiba H, Yoshiyama H, Kinoshita I, Dosaka-Akita H, et al. Tumor-Infiltrating Dcs Suppress Nucleic Acid-Mediated Innate Immune Responses Through Interactions Between the Receptor Tim-3 and the Alarmin Hmgb1. *Nat Immunol* (2012) 13(9):832–42. doi: 10.1038/ ni.2376
- 137. de Mingo Pulido A, Gardner A, Hiebler S, Soliman H, Rugo HS, Krummel MF, et al. Tim-3 Regulates Cd103(+) Dendritic Cell Function and Response

to Chemotherapy in Breast Cancer. Cancer Cell (2018) 33(1):60–74.e6. doi: 10.1016/j.ccell.2017.11.019

Conflict of Interest: The authors declare that the research was conducted in the absence of any commercial or financial relationships that could be construed as a potential conflict of interest.

Publisher's Note: All claims expressed in this article are solely those of the authors and do not necessarily represent those of their affiliated organizations, or those of the publisher, the editors and the reviewers. Any product that may be evaluated in this article, or claim that may be made by its manufacturer, is not guaranteed or endorsed by the publisher.

Copyright © 2022 Long, Yu, Chen, Tong and Gong. This is an open-access article distributed under the terms of the Creative Commons Attribution License (CC BY). The use, distribution or reproduction in other forums is permitted, provided the original author(s) and the copyright owner(s) are credited and that the original publication in this journal is cited, in accordance with accepted academic practice. No use, distribution or reproduction is permitted which does not comply with these terms.



Changes in Neutrophil to Lymphocyte Ratio, Lymphocyte to Monocyte Ratio, and Platelet to Lymphocyte Ratio During Palliative Radiotherapy May Predict Efficacy of Immune Checkpoint Inhibitor as Re-Challenge Treatment in Advanced Gastric Cancer: A Case Report

OPEN ACCESS

Edited by:

Xuyao Zhang, Fudan University, China

Reviewed by:

Xiaobin Shang, Tianjin Medical University Cancer Institute and Hospital, China Masaichi Ohira, Osaka City University, Japan Zhiru Wang, Zhengzhou University, China

> ***Correspondence:** Junhui Wang wangjunhui7526@163.com

Specialty section:

This article was submitted to Cancer Immunity and Immunotherapy, a section of the journal Frontiers in Oncology

Received: 10 February 2022 Accepted: 15 April 2022 Published: 19 May 2022

Citation:

Chen J, Wu X, Zhu S and Wang J (2022) Changes in Neutrophil to Lymphocyte Ratio, Lymphocyte to Monocyte Ratio, and Platelet to Lymphocyte Ratio During Palliative Radiotherapy May Predict Efficacy of Immune Checkpoint Inhibitor as Re-Challenge Treatment in Advanced Gastric Cancer: A Case Report. Front. Oncol. 12:873213. doi: 10.3389/fonc.2022.873213 Jianxin Chen, Xilin Wu, Shijian Zhu and Junhui Wang*

The Quzhou Affiliated Hospital of Wenzhou Medical University, Quzhou People's Hospital, Quzhou, China

Introduction: Immunotherapy with programmed death-1 (PD-1) inhibitors has emerged as frontline option in patients with advanced or metastatic gastric cancer. However, two-thirds of patients who received PD-1 inhibitors treatment still had disease progression in 1 year. Subsequent treatment strategies as salvage options always lead to limited efficacy.

Case Description: Herein, we presented a case of recurrent metastatic gastric adenocarcinoma that had progressed on first-line treatment with nivolumab, in which systematic inflammation parameters with neutrophil to lymphocyte ratio (NLR), lymphocyte to monocyte ratio (LMR), and platelet to lymphocyte ratio (PLR) were significantly changed by palliative radiotherapy on metastatic lymph nodes. The patient achieved persistent response to the re-challenge of immune checkpoint inhibitor, which resulted in survival time reaching 52 months, and is still in extension.

Conclusions: We supposed that the palliative radiotherapy may lead to the correction of NLR, LMR, and PLR and finally contribute to the efficacy of the re-challenge treatment by PD-1 inhibitor.

Keywords: gastric cancer, re-challenge, neutrophil to lymphocyte ratio, programmed death-1 inhibitor, lymphocyte to monocyte ratio

INTRODUCTION

Gastric cancer constitutes a global health problem, with more than one million new cases and 768,000 deaths in 2020, making it the fifth most frequently diagnosed cancer and the third leading cause of cancer-related deaths all over the world (1, 2). Patients with gastric cancer always had a poor prognosis, since gastric cancer is generally diagnosed at an advanced or metastatic stage, with

206

limited opportunity to receive radical operation. The median survival time for patients diagnosed with advanced or metastatic disease is <12 months (3, 4). It should be an urgent need to prolong the survival time in such patients.

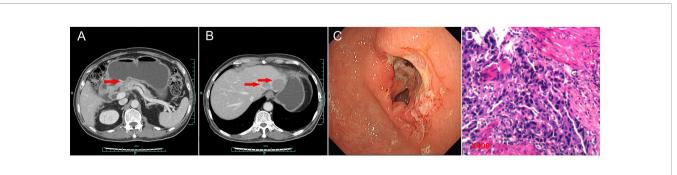
Nivolumab, a fully human IgG4 monoclonal antibody inhibitor of programmed death-1, has emerged as the first one to show superior survival time, with a median overall survival time exceeding 1 year in the first-line setting for patients with non-HER2-positive gastric, gastroesophageal junction, or esophageal adenocarcinoma (5). However, 64% of patients who received nivolumab plus chemotherapy as first-line regimen still had disease progression in 1 year (5). Subsequent monotherapy with pembrolizumab, another immune checkpoint inhibitor, has failed to improve survival time compared with paclitaxel for advanced gastric or gastroesophageal junction cancer with PD-L1 CPS of 1 or higher (6). The current efficacy of further line treatment strategies could not satisfy clinical demand.

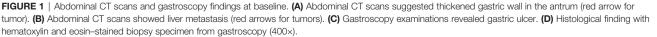
In most recent years, it is reported that the re-challenge of PD-1/PD-L1 inhibitors as further line treatment might still be effective in selective patients (7). However, few studies were conducted to investigate the specific profiting population, with the mechanism of re-challenge remaining to be explored. A recent retrospective pooled analysis demonstrated that high pretreatment neutrophil to lymphocyte ratio (NLR) was significantly associated with poorer progression-free survival time (PFS, HR = 1.44, 95% CI 1.26-1.65; p < 0.001) and overall survival time (OS, HR = 2.86, 95% CI 2.11-3.87; p < 0.001) compared with those with low pretreatment NLR in patients with non-small cell lung cancer (8). In addition, similar outcomes were also observed in metastatic melanoma and renal cell carcinoma (9, 10). Even so, a majority of publications focused on the relationship between pretreated level of systematic inflammation markers including NLR, lymphocyte to monocyte ratio (LMR), and platelet to lymphocyte ratio (PLR), and clinical outcomes. Few studies have been conducted to investigate the strategies to correct the level of NLR, LMR, and PLR, aiming to improve the clinical outcomes. Herein, we presented a case of recurrent metastatic gastric adenocarcinoma that had progressed on first-line treatment with nivolumab, in which systematic inflammation parameters with NLR, LMR, and PLR were changed by palliative radiotherapy on metastatic lymph nodes. The patient achieved persistent response to the re-challenge

of immune checkpoint inhibitor, which resulted in survival time reaching 52 months, and is still in extension. We supposed that the palliative radiation may lead to the correction of NLR, LMR, and PLR and finally contributed to the persistent efficacy of the re-challenge treatment by PD-1 inhibitor.

CASE DESCRIPTION

A 74-year-old Chinese man was admitted to our hospital on September 11, 2017 with repeated abdominal distension for 3 months. The patient denied smoking, alcohol, or any other medical or family history. Abdominal CT showed thickened gastric wall in the antrum and surrounded by enlarged lymph nodes (Figure 1A), along with multiple lesions in liver, suggesting metastasis (Figure 1B). Subsequently, the patient received gastroscopy examination, the results of which revealed a large ulcer (3.5 cm \times 3.5 cm), with dirty surface and scattered bleeding spots (Figure 1C). Based on the biopsy findings by gastroscopy, the patient was diagnosed as having gastric adenocarcinoma, with metastasis on interstitial lymph nodes of the liver and stomach, and liver (Figure 1D). Immunohistochemistry outcomes were presented as CDX2 (positive), CK18 (positive), CK19 (positive), CEA (negative), CK20 (negative), and Her-2 (negative). Additionally, results of next-generation sequencing (NGS) using tissues revealed microsatellite stability (MSS), programmed cell death ligand-1 (PD-L1) negative, and low tumor mutation burden (TMB). His palliative therapy was started with regimen XELOX (oxaliplatin of 130 mg/m² on day 1 and oral capecitabine of 1,000 mg/m² twice a day, from day 1 to 14, every 21 days) combined with immune checkpoint inhibitor nivolumab on September 15, 2017. After three cycles' exposure of the treatment strategy, the efficacy was evaluated as partial response (PR), with complete response (CR) for lesions on liver according to the criteria of Response Evaluation Criteria in Solid Tumors (RECIST) version 1.1. He finally completed six cycles of first-line treatment, with manageable toxicities, and subsequently received maintenance therapy with mono-nivolumab. However, after 2 months of maintenance, significantly elevated glutamic-pyruvic transaminase (ALT = 637 U/ml) was detected, which was





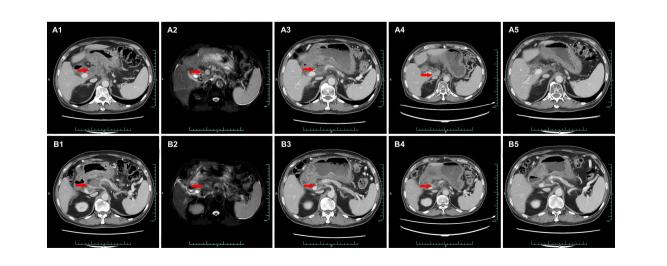
considered as immunotherapy-related hepatitis. Based on that, maintenance therapy was terminated, but follow-up continued. On July 11, 2020, his regular abdomen CT showed reenlargement and fused interstitial lymph nodes of the liver and stomach (Figure 2A1), suggesting progressive disease (PD). Metastatic lymph nodes invaded the portal and splenic veins (Figure 2B1). The symptom of abdominal distension appeared again, leading to performance status (PS) being degraded to 3. The patient refused any cytotoxic medication treatment but agreed to receive palliative medical care. After discussion by the multidisciplinary team including medical oncologist, surgical oncologist, radiation oncologist, and medical imaging doctors, intensity modulated radiotherapy (IMRT) on enlarged and fused interstitial lymph nodes of the liver and stomach was finally adopted as symptomatic care. Radiation schedule was set as 95% planning-gross target volume (P-GTV), with a total of 50 Gy for 25 times. The palliative radiation was started on August 11, 2020 and ended on September 19, 2020. Abdominal distension was relieved. Efficacy assessment for radiation was conducted by abdomen CT scan in October 2020 (Figures 2A2,B2), which suggested a stable disease (SD, by 16% regression for target lymph nodes). During the radiotherapy, we surprisingly detected a dynamic change in elevated level of LMR, accompanied with lowered level of NLR and PLR (Figure 3A), which suggested a potential response to systematic therapy with immune checkpoint inhibitor (11-14). In addition, we also observed a significant variation in the means of LMR, NLR, and mPLR (PLR/50) before radiotherapy (2 months before radiotherapy) and after radiotherapy (2 months from the beginning of radiotherapy), the results of which are presented in Figure 3B. Based on this, re-challenge treatment of PD-1 inhibitor was considered as consolidation therapy. However, due to the elevated ALT observed during the treatment of nivolumab, monotherapy of sintilimab, another PD-1 inhibitor, was prescribed as maintenance treatment from November 20, 2020. After 2 months treatment of sintilimab, repeat abdomen CT scan

revealed a partial response (PR, by 64% regression for target lymph nodes; Figures 2A3, B3). The latest CT scan was performed on August 4, 2021, the results of which still suggested a continuous PR, with complete regression on portal vein and splenic vein (by 67% regression for target lymph nodes; Figures 2A5, B5). There was no treatment-related adverse event observed during the administration of sintilimab. The patient still received the regimen regularly, with overall survival time of 52 months. The variation in tumor size for target lymph nodes is presented in Table 1. It should be noticed that the main gastric tumor was presented as thickened gastric wall with ulceration. There was no clear boundary for the thickened gastric wall with ulceration, which caused difficulty in measurement. That was the reason why the enlarged and fused interstitial lymph nodes of the liver and stomach, rather than the main gastric tumor, were selected as target lesion. In addition, the timeline with relevant data during the treatment is presented in Table 2.

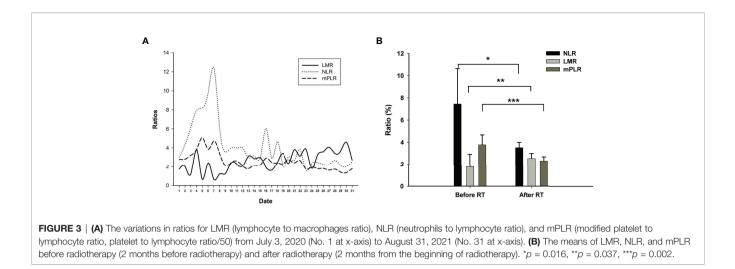
DISCUSSION

We herein presented a case of recurrent metastatic gastric adenocarcinoma, in which systematic inflammation parameters with NLR, LMR, and PLR have been changed by palliative radiotherapy and has achieved persistent response to the rechallenge of immune checkpoint inhibitor, with survival time reaching 52 months, and is still in extension.

In recent years, systematic inflammation markers including NLR, LMR, and PLR have been reported as indicators of systematic response for cancer treatment strategies. High NLR and PLR and low LMR are supposed as markers of unspecific immune system activation, correlating significant poor clinical outcomes in various cancers including advanced gastric cancer patients (15), small cell lung cancer (16), colorectal cancers (17, 18), pancreatic cancer (19), and non-small cell lung cancers (8). However, in previous literatures, only internal factors including







NLR, LMR, and PLR, which were evaluated before systematic treatment, had been adequately investigated. For patients with possible negative prognostic parameters (higher NLR, higher PLR, and lower LMR, without a standard range), few studies have been conducted to explore strategies to correct the unspecific immune system activation, such as lowering the level of NLR and PLR and improving the level of LMR. In recent decades, published literatures suggested a significant association between tumor response and treatment-related neutropenia and thrombocytopenia (20-22). In a pooled analysis, researchers performed a post-hoc analysis pooling data prospectively collected in six randomized phase III trials in nonsmall cell lung cancer. In multivariable overall survival (OS) analysis, chemotherapy-induced neutropenia (CIN) was significantly predictive of prognosis (hazard ratio of death, 0.71; 95%CI: 0.53-0.95) (22), which might be caused by the decline in NLR, as lymphocytes were little influenced by cytotoxic agents (23-25). In addition, NLR was also reported as a meaningful predictor of outcome in patients with extensive small-cell lung cancer who received radiation treatment (26). It was reported that radiotherapy also reduced the level of NLR, which may contribute to a longer survival time, even in patients with advanced or metastatic disease (27). Although the above clinical evidence reported a meaningful predictive value of NLR/ LMR/PLR in practice, few basic experiments were conducted to investigate the intrinsic mechanism for the phenomenon. According to the varied data of NLR in the present case, we

detected that the decrease in neutrophil might be the dominant reason for the decrease in NLR. We supposed that the count of neutrophil, rather than lymphocyte, may be easier influenced by anti-tumor treatment including chemotherapy or radiotherapy. We speculated that the ratio of circulating neutrophils to lymphocytes was supposed to correlate with the interaction between inflammation and immunity, especially the potential mechanism in tumor microenvironment. The potential mechanism of the interesting clinical phenomenon has been discussed with our basic experimental researchers. We hope that there would be something to be discovered by the cooperation of basic and clinical findings in the future. Even so, parameters correction (NLR/PLR/LMR) by systematic or local treatment is supposed to be beneficial for the improvement of clinical outcomes, which is also suggested in our study. In the present case, we scheduled palliative radiation on the metastatic fused interstitial lymph nodes of the liver and stomach nodes. As a result, we amazingly found the correction of immune systematic parameters including the reduction in NLR and PLR and the improvement of LMR (Figure 3A). Based on this, re-challenge of immunotherapy was administrated, which may have finally led to the persistent response in the present case.

Most recently, there were several retrospective studies that reported the efficacy and safety of the re-challenge of PD-1/PD-L1 inhibitors (7, 28), the results of which indicate that the effectiveness of treatment with a PD-1 inhibitor is maintained during retreatment and that this may be a valid therapeutic

TABLE 1	Variations of enlarged lymph	nodes size after recurrence	according to RECIST version 1.1.

Date	Exposure	Duration	Enlarged lymph nodes of A area (LD×SD, mm)	Enlarged lymph nodes of B area (LD×SD, mm)
2020.07	Radiation		54×39	43×33
2020.10	Radiation		39×29	42×25
2021.01	Sintilimab	2 month	36×17	26×21
2021.04	Sintilimab	5 months	27×17	17×16
2021.08	Sintilimab	9 months	18×15	14×13

LD, longest diameter; SD, shortest diameter. A area, enlarged lymph nodes of A1–A5 in Figure 2. B area, enlarged lymph nodes of B1–B5 in Figure 2.

TABLE 2 | Timeline with relevant data during the treatment.

Timeline	Intervention	Best response	Adverse events
September 2017 to February 2018	Nivolumab, Xelox	PR	Neutropenia grade 2
March 2018 to May 2018	Nivolumab	PR	Elevated ALT grade 3
June 2018 to July 2020	Follow-up	NA	NA
August 2020 to September 2020	Radiotherapy	SD	NO
November 2020 to present	Sintilimab	PR	NO

Xelox, Oxaliplatin, Capecitabine; PR, partial response; NA, not applicable; SD, stable disease; NO, not observed; ALT, glutamic-pyruvic transaminase.

option for routine clinical practice in selected patients. Although the mechanism of PD-1 inhibitors re-challenge still remains uncovered, authors described that the patients who received a second course of PD-1 inhibitor after an intervening course of standard chemotherapy presented a better survival time compared to a drug holiday following nivolumab discontinuation (median OS of 18.1 versus 14.8 months) (7). However, it was not mentioned whether or not the variation in immune systematic parameters (NLR/PLR/LMR) contributes to the difference between the groups (7). Even so, with the superior efficacy presented in the present case, we still supposed that intervening treatment with radiotherapy may lead to the correction of immune systematic parameters, which might finally contribute to the response of cancer and the extension of survival time.

The leading limitation of the present case report comes from the nature of a case report. Although we supposed that the improvement of systematic inflammation parameters with NLR, PLR, and LMR may contribute to the re-challenge of immune checkpoint inhibitor in advanced gastric cancer, the conclusion still needs further identification in prospective clinical practice and basic experiments.

Briefly, we presented a case of recurrent metastatic gastric adenocarcinoma, whose systematic inflammation parameters with NLR, LMR, and PLR were changed by palliative radiation and has achieved persistent response to the re-challenge of immune checkpoint inhibitor, with survival time reaching 52 months, and is still in extension.

REFERENCES

- Siegel RL, Miller KD, Jemal A. Cancer Statistics, 2020. CA Cancer J Clin (2020) 70:7–30. doi: 10.3322/caac.21590
- World Health Organization. International Agency for Research on Cancer. In: GLOBOCAN 2020: Stomach Cancer Fact Sheet (2020). Available at: https:// gco.iarc.fr/today/data/factsheets/cancers/7-Stomach-fact-sheet.pdf.
- Bang YJ, Van Cutsem E, Feyereislova A, Chung HC, Shen L, Sawaki A, et al. Trastuzumab in Combination With Chemotherapy Versus Chemotherapy Alone for Treatment of HER2-Positive Advanced Gastric or Gastro-Oesophageal Junction Cancer (ToGA): A Phase 3, Open-Label, Randomised Controlled Trial. *Lancet* (2010) 376:687–97. doi: 10.1016/ S0140-6736(10)61121-X
- Song J, Lee HJ, Cho GS, Han SU, Kim MC, Ryu SW, et al. Recurrence Following Laparoscopy-Assisted Gastrectomy for Gastric Cancer: A Multicenter Retrospective Analysis of 1,417 Patients. *Ann Surg Oncol* (2010) 17:1777–86. doi: 10.1245/s10434-010-0932-4
- 5. Janjigian YY, Shitara K, Moehler M, Garrido M, Salman P, Shen L, et al. First-Line Nivolumab Plus Chemotherapy Versus Chemotherapy Alone for Advanced Gastric, Gastro-Oesophageal Junction, and Oesophageal

DATA AVAILABILITY STATEMENT

The raw data supporting the conclusions of this article will be made available by the authors, without undue reservation.

ETHICS STATEMENT

The studies involving human participants were reviewed and approved by the Ethical Committee of People's Hospital of Quzhou. The patients/participants provided their written informed consent to participate in this study.

AUTHOR CONTRIBUTIONS

JC contributed to conception and design of the study. XW organized the database. SZ performed the statistical analysis. JC wrote the first draft of the manuscript. SZ and JW wrote sections of the manuscript. All authors contributed to the article and approved the submitted version.

ACKNOWLEDGMENTS

The authors thank the patient for his participation and agreement to the publication of the report.

Adenocarcinoma (CheckMate 649): A Randomised, Open-Label, Phase 3 Trial. Lancet (2021) 398:27-40. doi: 10.1016/S0140-6736(21)00797-2

- Shitara K, Ozguroglu M, Bang YJ, Di Bartolomeo M, Mandala M, Ryu MH, et al. Pembrolizumab Versus Paclitaxel for Previously Treated, Advanced Gastric or Gastro-Oesophageal Junction Cancer (KEYNOTE-061): A Randomised, Open-Label, Controlled, Phase 3 Trial. *Lancet* (2018) 392:123–33. doi: 10.1016/S0140-6736(18)31257-1
- Giaj Levra M, Cotte FE, Corre R, Calvet C, Gaudin AF, Penrod JR, et al. Immunotherapy Rechallenge After Nivolumab Treatment in Advanced non-Small Cell Lung Cancer in the Real-World Setting: A National Data Base Analysis. *Lung Cancer* (2020) 140:99–106. doi: 10.1016/j.lungcan.2019.12.017
- Li Y, Zhang Z, Hu Y, Yan X, Song Q, Wang G, et al. Pretreatment Neutrophil-To-Lymphocyte Ratio (NLR) May Predict the Outcomes of Advanced Non-Small-Cell Lung Cancer (NSCLC) Patients Treated With Immune Checkpoint Inhibitors (ICIs). *Front Oncol* (2020) 10:654. doi: 10.3389/ fonc.2020.00654
- Ferrucci PF, Gandini S, Battaglia A, Alfieri S, Di Giacomo AM, Giannarelli D, et al. Baseline Neutrophil-to-Lymphocyte Ratio is Associated With Outcome of Ipilimumab-Treated Metastatic Melanoma Patients. *Br J Cancer* (2015) 112:1904–10. doi: 10.1038/bjc.2015.180

- Kuzman JA, Stenehjem DD, Merriman J, Agarwal AM, Patel SB, Hahn AW, et al. Neutrophil-Lymphocyte Ratio as a Predictive Biomarker for Response to High Dose Interleukin-2 in Patients With Renal Cell Carcinoma. *BMC Urol* (2017) 17:1. doi: 10.1186/s12894-016-0192-0
- Yang T, Hao L, Yang X, Luo C, Wang G, Lin Cai C, et al. Prognostic Value of Derived Neutrophil-to-Lymphocyte Ratio (dNLR) in Patients With Non-Small Cell Lung Cancer Receiving Immune Checkpoint Inhibitors: A Meta-Analysis. *BMJ Open* (2021) 11:e049123. doi: 10.1136/bmjopen-2021-049123
- Vinal D, Gutierrez-Sainz L, Martinez D, Garcia-Cuesta JA, Pedregosa J, Villamayor J, et al. Prognostic Value of Neutrophil-to-Lymphocyte Ratio in Advanced Cancer Patients Receiving Immunotherapy. *Clin Trans Oncol Off Publ Fed Spanish Oncol Soc Natl Cancer Inst Mexico* (2021) 23:1185–92. doi: 10.1007/s12094-020-02509-1
- Shang J, Han X, Zha H, Tao H, Li X, Yuan F, et al. Systemic Immune-Inflammation Index and Changes of Neutrophil-Lymphocyte Ratio as Prognostic Biomarkers for Patients With Pancreatic Cancer Treated With Immune Checkpoint Blockade. *Front Oncol* (2021) 11:585271. doi: 10.3389/ fonc.2021.585271
- Fujimoto A, Toyokawa G, Koutake Y, Kimura S, Kawamata Y, Fukuishi K, et al. Association Between Pretreatment Neutrophil-to-Lymphocyte Ratio and Immune-Related Adverse Events Due to Immune Checkpoint Inhibitors in Patients With Non-Small Cell Lung Cancer. *Thorac Cancer* (2021) 12:2198– 204. doi: 10.1111/1759-7714.14063
- Konopka K, Micek A, Ochenduszko S, Streb J, Potocki P, Kwinta L, et al. Combined Neutrophil-To-Lymphocyte and Platelet-Volume-To-Platelet Ratio (NLR and PVPR Score) Represents a Novel Prognostic Factor in Advanced Gastric Cancer Patients. J Clin Med (2021) 10. doi: 10.3390/ jcm10173902
- Chen C, Yang H, Cai D, Xiang L, Fang W, Wang R. Preoperative Peripheral Blood Neutrophil-to-Lymphocyte Ratios (NLR) and Platelet-to-Lymphocyte Ratio (PLR) Related Nomograms Predict the Survival of Patients With Limited-Stage Small-Cell Lung Cancer. *Transl Lung Cancer Res* (2021) 10:866–77. doi: 10.21037/tlcr-20-997
- Ergen SA, Barlas C, Yildirim C, Oksuz DC. Prognostic Role of Peripheral Neutrophil-Lymphocyte Ratio (NLR) and Platelet-Lymphocyte Ratio (PLR) in Patients With Rectal Cancer Undergoing Neoadjuvant Chemoradiotherapy. J Gastrointest Cancer (2021) 53:151-60. doi: 10.1007/ s12029-020-00578-7
- Naszai M, Kurjan A, Maughan TS. The Prognostic Utility of Pre-Treatment Neutrophil-to-Lymphocyte-Ratio (NLR) in Colorectal Cancer: A Systematic Review and Meta-Analysis. *Cancer Med* (2021) 10:5983–97. doi: 10.1002/ cam4.4143
- Zhou L, Wang J, Zhang XX, Lyu SC, Pan LC, Du GS, et al. Prognostic Value of Preoperative NLR and Vascular Reconstructive Technology in Patients With Pancreatic Cancer of Portal System Invasion: A Real World Study. *Front* Oncol (2021) 11:682928. doi: 10.3389/fonc.2021.682928
- Chabot GG, Abigerges D, Catimel G, Culine S, de Forni M, Extra JM, et al. Population Pharmacokinetics and Pharmacodynamics of Irinotecan (CPT-11) and Active Metabolite SN-38 During Phase I Trials. *Ann Oncol* (1995) 6:141– 51. doi: 10.1093/oxfordjournals.annonc.a059109

- Osumi H, Shinozaki E, Ooki A, Wakatsuki T, Kamiimabeppu D, Sato T, et al. Early Hypertension and Neutropenia are Predictors of Treatment Efficacy in Metastatic Colorectal Cancer Patients Administered FOLFIRI and Vascular Endothelial Growth Factor Inhibitors as Second-Line Chemotherapy. *Cancer Med* (2021) 10:615–25. doi: 10.1002/cam4.3638
- 22. Gargiulo P, Arenare L, Gridelli C, Morabito A, Ciardiello F, Gebbia V, et al. Chemotherapy-Induced Neutropenia and Treatment Efficacy in Advanced Non-Small-Cell Lung Cancer: A Pooled Analysis of 6 Randomized Trials. *BMC Cancer* (2021) 21:549. doi: 10.1186/s12885-021-08323-4
- Cho MY, Joh YG, Kim NR, Jung SI, Bae JW, Kim YC, et al. T-Lymphocyte Subsets in Patients With AJCC Stage III Gastric Cancer During Postoperative Adjuvant Chemotherapy. American Joint Committee on Cancer. Scand J Surg (2002) 91:172–7. doi: 10.1177/145749690209100207
- 24. Wang Y, Qu H, Xu B, Wu J, Lu K, Liu C, et al. Expression of FOXA1 Is Associated With the Tumor-Infiltrating M2 Macrophage, Cytotoxic T Lymphocyte, and Effect of Chemotherapy in Bladder Cancer. Urol Int (2021), 1–6. doi: 10.1159/000519129
- 25. Ishibashi Y, Tsujimoto H, Hiraki S, Kouzu K, Tsuchiya S, Itazaki Y, et al. Predictive Value of Immuno-Inflammatory and Nutritional Measures Modulated by Neoadjuvant Chemotherapy on the Response of Neoadjuvant Chemotherapy and Long-Term Outcomes in Patients With Esophageal Cancer. Oncol Lett (2020) 19:487–97.
- Suzuki R, Lin SH, Wei X, Allen PK, Welsh JW, Byers LA, et al. Prognostic Significance of Pretreatment Total Lymphocyte Count and Neutrophil-to-Lymphocyte Ratio in Extensive-Stage Small-Cell Lung Cancer. *Radiother* Oncol (2018) 126:499–505. doi: 10.1016/j.radonc.2017.12.030
- Ho YC, Lai YC, Lin HY, Ko MH, Wang SH, Yang SJ, et al. Low Cardiac Dose and Neutrophil-to-Lymphocyte Ratio Predict Overall Survival in Inoperable Esophageal Squamous Cell Cancer Patients After Chemoradiotherapy. *Sci Rep* (2021) 11:6644. doi: 10.1038/s41598-021-86019-2
- Dolladille C, Ederhy S, Sassier M, Cautela J, Thuny F, Cohen AA, et al. Immune Checkpoint Inhibitor Rechallenge After Immune-Related Adverse Events in Patients With Cancer. JAMA Oncol (2020) 6:865–71. doi: 10.1001/ jamaoncol.2020.0726

Conflict of Interest: The authors declare that the research was conducted in the absence of any commercial or financial relationships that could be construed as a potential conflict of interest.

Publisher's Note: All claims expressed in this article are solely those of the authors and do not necessarily represent those of their affiliated organizations, or those of the publisher, the editors and the reviewers. Any product that may be evaluated in this article, or claim that may be made by its manufacturer, is not guaranteed or endorsed by the publisher.

Copyright © 2022 Chen, Wu, Zhu and Wang. This is an open-access article distributed under the terms of the Creative Commons Attribution License (CC BY). The use, distribution or reproduction in other forums is permitted, provided the original author(s) and the copyright owner(s) are credited and that the original publication in this journal is cited, in accordance with accepted academic practice. No use, distribution or reproduction is permitted which does not comply with these terms.



Oncolytic Adenoviral Vector-Mediated Expression of an Anti-PD-L1-scFv Improves Anti-Tumoral Efficacy in a Melanoma Mouse Model

OPEN ACCESS

Edited by:

Yubin Li, University of Pennsylvania, United States

Reviewed by:

Chongming Jiang, Baylor College of Medicine, United States Liang He, University of California, San Francisco, United States

*Correspondence:

Lucio Pastore lucio.pastore@unina.it

[†]These authors have contributed equally to this work

Specialty section:

This article was submitted to Cancer Immunity and Immunotherapy, a section of the journal Frontiers in Oncology

Received: 22 March 2022 Accepted: 14 April 2022 Published: 20 May 2022

Citation:

Vitale M, Scialò F, Passariello M, Leggiero E, D'Agostino A, Tripodi L, Gentile L, Bianco A, Castaldo G, Cerullo V, De Lorenzo C and Pastore L (2022) Oncolytic Adenoviral Vector-Mediated Expression of an Anti-PD-L1-scFv Improves Anti-Tumoral Efficacy in a Melanoma Mouse Model. Front. Oncol. 12:902190. doi: 10.3389/fonc.2022.902190 Maria Vitale^{1,2†}, Filippo Scialò^{2,3†}, Margherita Passariello^{1,2}, Eleonora Leggiero², Anna D'Agostino², Lorella Tripodi², Laura Gentile², Andrea Bianco³, Giuseppe Castaldo^{1,2}, Vincenzo Cerullo^{1,4}, Claudia De Lorenzo^{1,2} and Lucio Pastore^{1,2*}

¹ Dipartimento di Medicina Molecolare e Biotecnologie Mediche, Università di Napoli Federico II, Naples, Italy,
 ² CEINGE-Biotecnologie Avanzate, Naples, Italy, ³ Dipartimento di Scienze Mediche Traslazionali, Università della Campania
 "L. Vanvitelli", Naples, Italy, ⁴ Laboratory of Immunovirotherapy, Drug Research Program, Faculty of Pharmacy, University of Helsinki, Helsinki, Finland

Oncolytic virotherapy is an emerging therapeutic approach based on replicationcompetent viruses able to selectively infect and destroy cancer cells, inducing the release of tumor-associated antigens and thereby recruiting immune cells with a subsequent increase in antitumoral immune response. To increase the anticancer activity, we engineered a specific oncolytic adenovirus expressing a single-chain variable fragment of an antibody against PD-L1 to combine blockage of PD-1/PD-L1 interaction with the antitumoral activity of Onc.Ad5. To assess its efficacy, we infected B16.0VA cells, a murine model of melanoma, with Ad5∆24 -anti-PD-L1-scFv and then co-cultured them with C57BL/6J naïve splenocytes. We observed that the combinatorial treatments were significantly more effective in inducing cancer cell death. Furthermore, we assessed the efficacy of intratumoral administrations of Ad5∆24-anti-PD-L1-scFv in C57BL/6J mice engrafted with B16.0VA and compared this treatment to that of the parental Ad5 Δ 24 or placebo. Treatment with the scFv-expressing Onc.Ad induced a marked reduction of tumor growth concerning the parental Onc.Ad. Additionally, the evaluation of the lymphocytic population infiltrating the treated tumor reveals a favorable immune profile with an enhancement of the CD8⁺ population. These data suggest that Onc.Ad-mediated expression of immune checkpoint inhibitors increases oncolytic virotherapy efficacy and could be an effective and promising tool for cancer treatments, opening a new way into cancer therapy.

Keywords: oncolytic virotherapy, oncolytic adenoviruses, programmed death ligand 1 (PD-L1), Programmed cell death 1 (PD-1), single-chain variable antibody fragment (scFv), B16.0VA cells, C57BL/6J mice

Anti-PD-L1 Ocolityc Adenovirus for Melanoma Therapy

INTRODUCTION

Despite scientific efforts and the development of new therapies, cancer remains one of the leading causes of death in the 21st century (1). Recently, some promising findings involving the use of the immune system (IS) as a weapon against tumors have been reported (2). Indeed, the IS can be activated, making it able to identify and eradicate tumor cells (3). However, some hurdles make the work difficult for the IS; the most relevant of these is the tumor microenvironment (TME). The TME is a very complex structure with multiple components (4), which altogether create an immune-suppressive environment and induce the immuneescape of cancer cells (Figure 1A) (5). Programmed cell death ligand 1 (PD-L1)/programmed cell death (PD-1) interaction and its downstream pathway plays a crucial role in cancer cell immune-escape (6). At TME, the interaction between PD-L1 on the surface of tumor cells and PD-1 on the surface of T cells induces suppression of T-cell function, causing T-cell tolerance, inhibition of their proliferation, and lowering their cytokine production. This combination produces, as a result, the immune escape of tumor cells (7, 8). To prevent PD-1/PD-L1 interaction several approaches have been developed; the most popular one consists of the use of antibodies (Abs) against one of the two partners, thus interfering with their binding (9, 10). Clinical efficacy and safety of monoclonal Abs (mAbs) have been demonstrated in several studies (11-14), and recently, different types of antibody-like proteins have been developed: they are capable of antigen-binding but have modifications that change some of their properties. The single-chain Fragment variable (scFv) is an antibody fragment made up of the variable regions of heavy (VH) and light chains (VL) joined by a flexible linker peptide, and it is the smallest immunoglobulin fragment endowed with antigen-binding activities. The scFv smaller size, compared to that of the whole mAbs, could offer several advantages in therapeutic applications, such as: i) major penetration capability into the tissue and, in particular, into the tumor; ii) Efficient localization at the tumor sites and no up-take by the kidney; iii) faster blood clearance than the whole-sized antibody; and iv) adaptable size for development of specific viral and non-viral targeting vectors for therapeutic gene delivery. Additionally, to overcome this hostile and immunosuppressive TME, strategies that involve the use of oncolytic viruses (OVs) have been adopted (15). OVs can exert anticancer activity in different ways: i) virusmediated direct lysis of cancer cells mediates the release of tumor neoantigens (TNAs) and tumor-associated antigens (TAAs) that induce a tumor-specific T-cell response; ii) infected cells can promote a potent inflammatory response by stimulating cytokine production, leading to a lower immunosuppressive TME; and iii) induction of immunogenic cell death (ICD) due to the release of danger-associated molecular patterns (DAMPs) and pathogen-associated molecular patterns (PAMPs) as viral DNA or capsid proteins (16, 17). Adenoviruses (Ads) are among the most extensively studied OVs because their genome can be easily modified (18) without interfering with their capacity to infect host cells (19). After two decades of clinical studies, Ads appear safe and can be used as effective therapies against cancer (20). They can be engineered to express one or multiple transgenes (20) and can accommodate a thousand base pairs of extra genomic DNA. In this study, we decided to evaluate the efficacy of an engineered Ad5 Δ 24 expressing an anti-PD-L1-scFv (Ad5 Δ 24-anti-PD-L1-scFv). This approach can exert antitumoral activity in two ways: i) reduction of immune escape following the mobilization of the immune system, principally CD8⁺ T cells; and ii) Ad-mediated cell lysis with consequent TANs and TAAs release (**Figure 1A**). In other words, the immune system can be awakened against tumor cells killing them with mechanisms that are properly used for canonical defense (21).

MATERIALS AND METHODS

Cloning Techniques

The expression cassette for the anti-PD-L1scFv has been excised by pcDNA3.1-anti-PD-L1 (Proteogenix) with BsiWI and MfeI (New England Biolabs) digestion and inserted into pTHSN, generating pTHSN-anti-PD-L1. The resulting shuttle vector with the gene of interest (pTHSN-scFv-anti-PD-L1 plasmid) was recombined with pAd5 Δ 24 (IVT lab, Faculty of Pharmacy, Helsinki) in the *Escherichia coli* BJ5183 strain (Agilent) *via* electroporation. The electroporation was performed using cuvettes according to the standard protocol from Bi-orad and bacterial cells were plated on LB-agar with kanamycin resistance.

ELISA

To confirm the binding specificity of the purified immunomodulatory scFv, ELISA assays were performed on both human and mouse chimeric proteins (coated at 5 µg/ml on microplates), and untreated or activated hPBMCs. The ELISA assays on coated chimeric protein were performed by coating NuncTM flat-bottom 96-well plates (ThermoFisher Scientific) with 5 µg/ml of recombinant proteins in a solution of 0.05 M NaHCO3 for 72 h at 37°C. After blocking off the coated 96-well plates with 5% nonfat dry milk in PBS for 1 h at 37°C, the purified scFv was added at increasing concentrations (10-200 nM) to the plates in 2.5% nonfat dry milk in PBS and incubated for 2 h at room temperature by gently shaking. Cell ELISA assays were performed by plating the cells in roundbottom 96-well plates ($2 \times 10E5$ lymphocytes for each well) and incubating them with increasing concentrations of the scFv in 2.5% nonfat dry milk for 2 h at room temperature with gentle agitation. After the incubation with the primary antibodies, extensive washes were carried out with PBS, then the plates were incubated with an appropriate HRP-conjugated antibody for 1 h at room temperature, washed again, and incubated with 3,3',5,5'-tetramethylbenzidine (Sigma-Aldrich) reagent for 10 min before quenching with an equal volume of 1 N HCl. Absorbance at 450 nm was measured by the Envision plate reader (Perkin Elmer, 2102).

Competitive ELISA Assays

To investigate the ability of the selected anti-PD-L1-scFv to compete in the PD-L1/PD-1 or PD-L1/B7.1 binding, competitive ELISA assays were performed by testing the binding of each biotinylated chimeric protein (PD-1/Fc or B7.1/Fc) to PD-L1 in

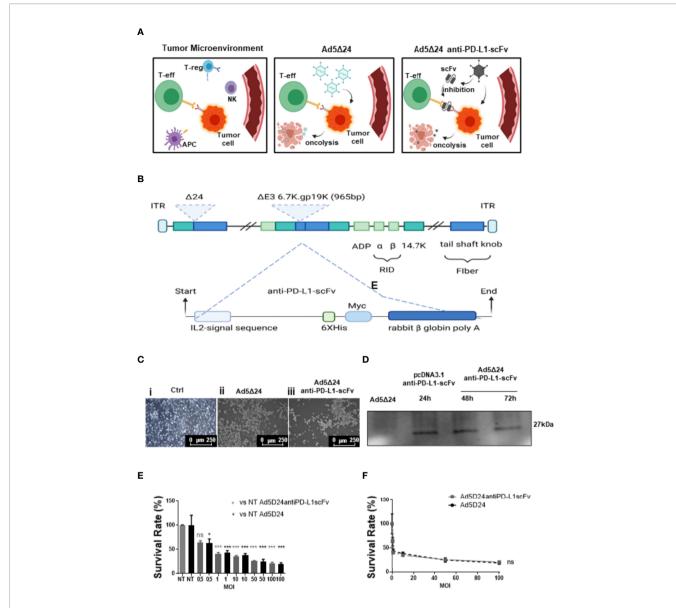


FIGURE 1 | Design and characterization of a novel Ad5delta24-anti-PD-L1-scFv. (A) The interaction between PD-L1 on the surface of tumor cells and PD-1 on the surface of T cells induces as a result the immune escape (left panel). The injection of Ad5Δ24 into TME, results in a potent lytic effect on tumor cells, leading to a tumorspecific T cells response (central panel). The injection of Ad5₄24-anti-PD-L1-scFv into TME, induces not only a potent lytic effect on tumor cells, due to Ov. Ads, but also, inhibit the interaction between PD-L1 and PD-1 through the expression of an scFv, resulting in a failure of immune escape (right panel). Regulatory T cells (Tregs), natural killer (NK) cells, tumor cells, and effector T (Teff) cells in the tumor microenvironment (TME). (B) A schematic representation of oncolytic adenovirus serotype 5 (Ad5) DNA viral backbone containing a deletion of 24 bp (Δ24 or D24) in the Rentinoblastoma (Rb) binding constant region 2 of E1 gene. Dashed line indicate the insertion site of a nucleic acid sequence encoding a single chain fragment variable (scFv) anti-PD-L1, in the place of the deleted gp 19k/6 in the adenoviral E3 region. (C) A549 cells were infected with 50MOI of Ad5Δ24 (ii) or Ad5Δ24-anti-PD-L1-scFv (iii). Images show that compared to control cells (i) at 48hrs post-infection a potent lytic effect was noted confirming that the remodeling of Ad5delta24 DNA does not interfere with its oncolytic action. (D) To test the scFv production A549 cells were infected with 500 MOI of Ad5d24-anti-PD-L1-scFv, and the media was collected at 48 and 72 h to test the presence of scFv by using an anti-Hys-tag as primary antibody. Collected media from A549 cells infected with Ad5Δ24 were used as a negative control, while media from A549 cells transfected with pcDNA 3.1+ scFv anti-PD-L1 at 24 h was used as positive control. A band of 27 kD was detected in the media of infected or transfected cells while was absent in the negative control. (E) A549 were infected with increasing MOI of Ad5Δ24 (in black) or Ad5delta24-anti-PD-L1-scFv (in gray) and cell count was performed at 48hrs post-infection. The graphs show the survival rate expressed in the percentage of the cell still alive and compared to the uninfected control. The data were analyzed with GraphPad Prism version 5.02 through One-way analysis of variance. The significance was evaluated with Turkey's Multiple Comparison Test comparing each condition to the uninfected control. In the graph, SEM is reported for each column. (F) Comparison of survival rate in A549 infected with different MOI of Ad5deta24-anti-PD-L1-scFv at 48 h post-infection. The graphics were obtained through GraphPad Prism 5.02 version. *< 0.05, *** < 0.001 and ns, not significant.

the absence or presence of unlabeled competitive scFv. For this aim, a 96-well plate was coated with 200 ng/ml of PD-L1 recombinant protein in 0.005 M NaHCO3 solution for 72 h at 4°C. Then, the PD-L1 coated plate was pre-incubated with competitor scFv (at a 10:1 M/M excess ratio), and then further treated with biotinylated PD-1 or B7.1 chimeric proteins, which were added to the plate at the same concentrations of competitive antibodies (2 µg/ml). For detecting bound biotinylated proteins, HRP-conjugated Streptavidin (Biorad) was added to the plate, whereas an anti-human antibody was used in parallel assays for the detection of bound anti-PD-L1 antibodies. The error bars were based on the results obtained in triplicate by at least two independent experiments.

Adenovirus Production and Purification

The replication-competent pAd5₂₄ adenovirus was provided by the IVT lab (IVT lab, Faculty of Pharmacy, Helsinki). The plasmid containing the anti-PD-L1-scFv gene was provided by Proteogenix. A549 cells were transfected with Lipofectamine 2000 (Invitrogen) according to the instructions of the manufacturer. After 14 days, cells were harvested, centrifuged at 1,000 rpm for 10 min, and stored at -80°C. Then, we performed three freeze-thaw cycles to lyse cells and obtain virions. The supernatant was collected, treated with DNase, and then subjected to two rounds of ultracentrifugation in a CsCl (Roche) gradient (2.5 ml of CsCl 1.45 gr/ml and 3 ml of CsCl 1.25 gr/ml) for 2 h and, subsequently, for 20 h at 27,000 rpm at 4°C. The viral band was collected and transferred to a dialysis cassette (Thermo Scientific) with 1 L of dialyzing solution (TM: 10 mM Tris-HCl, pH 8.0; 2 mM MgCl2). After 2 h, the TM solution was substituted with 1 L of freezing solution (10 mM Tris-HCl, pH 8.0; 2 mM MgCl2; 4% sucrose) and dialyzed overnight. Finally, the virus was collected, aliquoted, and stored at -80°C. The concentration was measured as the number of viral particles, determining absorbance at 260 nm. Furthermore, virus infectious units (ifu) have been calculated using the Adeno-XTM Rapid Titer Kit (Clontech Laboratories Inc.) based on immunodetection of the adenoviral hexon protein in transduced cells, according to the instructions of the manufacturer. The titer of Ad5A24-anti-PD-L1-scFv after amplification and purification was 2.4×10^{12} vp/ml. The titer of Ad5 Δ 24, was 2.2 × 10¹³ vp/ml.

PCR Analysis

Viral DNA was extracted with a standard phenol/chloroform (Sigma) extraction protocol. DNA is quantified with Nanodrop (Euroclone) and analyzed by PCR. We used HotMasterMix from Quantabio, following the instructions of the manufacturer. Primers were synthesized by the DNA LAB facility at the CEINGE-Biotecnologie Avanzate:

Forward oligonucleotide -5'AAAACACCACCCTCCTTAC CT3'-

Reverse oligonucleotide -3'GCTCCGTTCAAATCCTCTTC G5' -.

Their complementary regions are at both ends of the transgene.

Cell Culture and Transfection

The A549 and SK-MEL-28 cells (provided by CEINGE-Biotecnologie Avanzate cell culture facility) were cultured respectively with alpha-MEM and D-MEM (Sigma Aldrich), supplemented with 10% fetal bovine serum (FBS, Gibco), 50 U penicillin/50 μ g streptomycin (Microgem) and 4 mM Lglutamine (Gibco) in a humified incubator at 37°C with 5% CO2. A549 were seeded in a 60-mm dish and transfected the following day with Lipofectamine 2000 transfection reagent (Life Technologies, USA), according to the instructions of the manufacturer. B16.OVA cells (donated by the IVT lab of Vincenzo Cerullo, Helsinki, Finland) were cultured with RPMI (Gibco) supplemented with 10% FBS, 50 U penicillin/50 μ g streptomycin, and 4 mM L-glutamine in a humified incubator at 37°C with 5% CO2.

Co-Culture Experiments

B16-OVA cell lines were seeded in 96-well plates and were infected with a range of 1 to 100 MOI of modified or unmodified Ads as a control. The splenocytes were extracted from the C57BL/6J naïve spleen, smashed with a cell strainer 70 μ m Nylon (Falcon), and cultured in R10 medium (RPMI supplemented with 10% FBS, 50 U penicillin/50 μ g streptomycin, and 4 mM L-glutamine, 1% sodium pyruvate 100 m, and 0.1% 2beta-mercaptoethanol 50 mM Gibco). The splenocytes were primed for 24 h with 100 MOI of Ad5 Δ 24 or Ad5 Δ 24-anti-PD-L1-scFv in a humified incubator at 37°C with 5% CO2. After 24 h, primed splenocytes were added to the B16-OVA cells. After 24 h B16-OVA cells that were still alive were counted with the trypan blue (0.4%, Sigma) method.

Western Blot Analysis

Three 100 mm dishes of A549 were infected with 500 MOI of our modified Ads; infections were collected at three different times (24, 48, and 72 h), centrifuged at 1,000 rpm for 5 min, and subjected to 4 freeze-thaw cycles. Later, 40 µl of supernatant of each sample was added with 5 μ l of loading + reducing buffer (Life Technologies) and denatured at 75°C for 5 min. These samples were loaded onto a 12% SDS-polyacrylamide gel and separated for ~3 h at 80 V. Proteins were electrophoretically transferred onto a nitrocellulose membrane (Life Technologies) and then blocked with 5% BSA in PBS/Tween (0.1%) for 1 h at 37°C to prevent non-specific antibody binding. Subsequent immunostaining was obtained using an anti-His HPRconjugated antibody that recognizes His-tag in the an-ti-PD-L1-scFv. It was diluted 1:2,500 in 1% BSA with PBS/Tween (0.1%). The Pierce[®] ECL Western Blotting Substrate from Thermo Scientific was used according to the instructions of the manufacturer to reveal the signal. We cannot normalize the sample using a housekeeping protein but for volume used (22).

Animal Studies

Animal studies were conducted by the National Institutes of Health guidelines in accordance with ethical and safety rules and guidelines for the use of animal studies in biomedical research provided by relevant Italian laws and European Union's directives (no.86/609/EC). The Ministry of Health has approved this work. All efforts were made to minimize the suffering of the animal. Food and water were provided *ad libitum*. For all the experiments, we used an 8-week-old female C57BL/6J (Jackson Laboratory) engrafted subcutaneously into the right and left flank with 3×105 B16.OVA cells. The viral dose was $2 \times 1,010$ vp/kg and was injected directly into the tumor.

Flow Cytometry

Surface staining was conducted using the following antibodies: CD3 PerCP-Cy5.5 (eBio-science, San Diego, California); CD8 FITC (eBioscience); CD4 PeCy7 (eBioscience); CD45R/B220 APC (Biolegend, San Diego, California); anti-mouse CD45 APC-Cy7 (Sony Biotechnology, San Jose, California). Cells were initially stained with surface markers (CD3, CD8, CD4, CD45R/B220, and CD45) and then stained for FOXP3 (Fox-P3/ Transcription Factor Staining Buffer Set, eBioscience) using a protocol for nuclear detection, according to the instructions of the manufacturer.

Statistical Analysis

Statistical analysis was performed using GraphPad Prism 5.02 for Windows (GraphPad Software, La Jolla, California, USA) as reported in each figure legend. As reported in the figure legend, the statistical significance was evaluated with a one-way analysis of variance (ANOVA) analysis with a p-value <0.05. Tukey's Multiple Comparison test was used to compare the difference between un-treated values and other values. All data are reported as \pm SEM.

RESULTS

Ad5∆24-Anti-PD-L1-scFv Infection Induces Tumor Cell Lysis and Interferes in PD-L1/PD-1 Binding

We isolated a novel human anti-PDL1-scFv by phage display technology that allows for selecting binders from large antibody phage libraries containing up to 10¹⁰ different variants. The isolation of anti-PD-L1 scFvs consisted of alternate panning rounds of the phage antibody library on live activated hPBMCs expressing the target protein and on immobilized recombinant purified targets to increase the specificity. This approach guaranteed the efficient selection of a large number of clones with high specificity for PD-L1 antigen in its native conformation, like that presented on the cell membrane. Subtractive selection rounds to subtract the phages that recognize the Fc domain present in the PD-L1/Fc chimeric proteins used in the following two parallel rounds, as previously reported for other selections (23-25) The screening of scFvs cross-reactive for human and mouse PD-L1 proteins was performed by parallel ELISA assays on both human and mouse recombinant proteins. We identified a clone capable of recognizing both mouse and human targets and we expressed it in bacteria for its biological characterization. After purification from the periplasmic extract by IMAC (Supplementary

Figures 1A, B), we tested it by ELISA assays for its binding to recombinant PD-L1 at increasing concentrations (Supplementary Figure 1C). The scFv showed high affinity for its target with an obvious Kd value of 4nM. Then we tested for its ability to inhibit the interaction between PD-L1/PD-1 and PD-L1/B7.1, the principal receptors involved in the interaction with PD-L1. To this aim, we performed a competitive ELISA by measuring the binding to immobilized PD-L1 of biotinylated PD-1 or B7.1 in the absence or presence of saturating concentrations of unlabeled anti-PD-L1-scFv. As shown in Supplementary Figure 1D, the samples treated with anti-PD-L1-scFv show a reduction in the absorbance compared to the untreated controls in both cases. These data suggest that the selected anti-PD-L1-scFv can interfere with the interaction of the ligand with its receptors, demonstrating a significant ability to bind to PD-L1 and, consequently, inhibit the interaction with PD-1 and B7. Afterward, we engineered Ad5₄₂₄ introducing an expression cassette containing a cDNA encoding the anti-PD-L1-scFv (Ad5Δ24-anti-PD-L1-scFv, Figure 1B) for subsequent in vitro and in vivo evaluation. Expression and secretion of the anti-PD-L1-scFv were confirmed by infecting adenocarcinoma human alveolar basal epithelial cells (A549) with a dose of 50 vp/cell of either modified or un-modified Ad, used as a control, and assessing scFv secretion by Western blotting analysis with an anti-Hys-tag mAb on media conditioned with infected cells for 48 and 72 h. Cells infected with Ad5∆24-anti-PD-L1-scFv showed a cvtopathic effect 24 h post-infection and at 48 h, cells began to die (Figure 1C). The expression and secretion of the anti-PD-L1scFv were evaluated until 72 h post-infection. As shown in Figure 1D, expression and secretion of scFv in the media are maintained for up to 72 h, suggesting that Ad5Δ24-anti-PD-L1scFv does not only replicate, inducing cytopathic and lytic effects, but also expresses and secretes scFv encoded by the expression cassette, which is stable in the serum at 37°C. Furthermore, we evaluated the effect of Ad5∆24-anti-PD-L1-scFv compared to Ad5 Δ 24 on A549, a PD-L1⁻ cell line. Therefore, we infected A549 with different multiplicity of infection (MOI) of either Ad5Δ24-anti-PD-L1-scFv or Ad5Δ24, used as a control, starting from an MOI of 0.5 up to 100. Both Ads induce the same effect on this cell line, with a mortality rate of almost 37.5% at 0.5 MOI that increases at high MOI (almost 80% of mortality at 100 MOI) (Figure 1E). Additionally, the comparison of the survival rate between the two Ads, related to the increased MOI of the Ads, reveals that both viruses had the same effect on the A549, with differences not significant as shown in Figure 1F.

Ad5∆24-Anti-PD-L1-scFv Infects and Kills Human Melanoma Cell SK-MEL 28

After assessing the ability of Ad5 Δ 24-anti-PD-L1-scFv to express and secrete the anti-PD-L1-scFv, we evaluated its efficacy *in vitro*. For this aim, we evaluated the effects of Ad5 Δ 24-anti-PD-L1-scFv on SK MEL 28, a human malignant melanoma cell line. SK-MEL 28 expresses a high level of PD-L1, making this a suitable model to test the engineered Ad (26). Therefore, we infected SK-MEL 28 with a different multiplicity of infection (MOI) of either Ad5 Δ 24-anti-PD-L1-scFv or Ad5 Δ 24, used as a control, starting from an MOI of 10 up to 100. At the highest MOI of Ad5 Δ 24-anti-PD-L1-scFv, only 40% of cells survived, whereas 60% cell survival was observed with Ad5 Δ 24 (**Figure 2A**). Ad5 Δ 24-anti-PD-L1-scFv retains the typical cytopathic effect of Ad5 Δ 24 (**Figure 2B**). Furthermore, at 48 h post-infection, when the replicative cycle of Ad is almost complete, cell counts demonstrated that cell death increased with the higher MOI of the virus, indicating a dose-response correlation as reported in **Figure 2C**. This suggests that expression of the anti-PD-L1-scFv in the absence of the

immune system had the same effect as Ad5 Δ 24, and indeed, the difference between both Ads was not significant (**Figure 2C**).

Co-Culture of B16.OVA With Naïve C57BL/ 6J Splenocytes Increases the Anti-Tumor Effects of Ad5∆24-Anti-PD-L1-scFv

After assessing the ability of $Ad5\Delta 24$ -anti-PD-L1-scFv to infect and replicate in SK-MEL 28, we determined its ability to infect B16.OVA, a murine melanoma cell line. As reported in the literature, B16.OVA cells express PD-L1 on their surface at

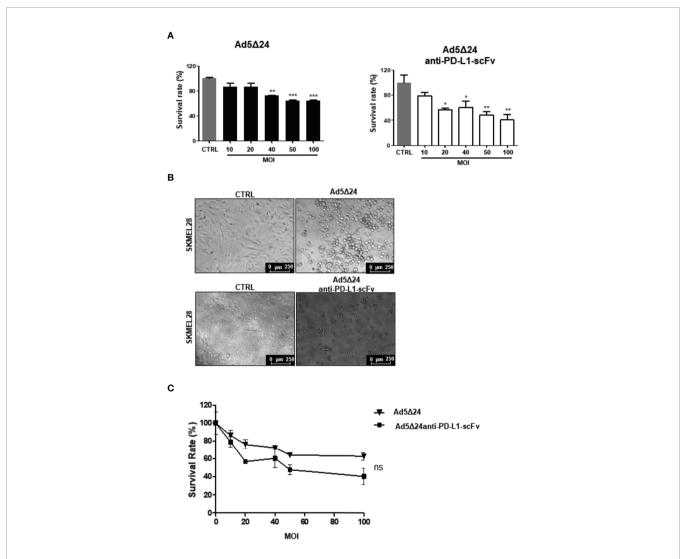


FIGURE 2 | Effects of infection with Ad5Δ24-anti-PD-L1-scFv on human melanoma cell lines SK-MEL28. (**A**) Human melanoma cells line SK-MEL28 were infected with increasing MOI of Ad5Δ24 (in black) or Ad5delta24-anti-PD-L1-scFv (in white) and cell count was performed at 48 h post-infection. The graphs show the survival rate expressed in the percentage of the cell still alive and compared to the uninfected control. The data were analyzed with GraphPad Prism version 5.02 through One-way analysis of variance with a P-value of <0.0001 for Ad5Δ24 and 0.0026 for Ad5delta24-anti-PD-L1-scFv. The significance was evaluated with Turkey's Multiple Comparison Test comparing each condition to the un-infected control. In the graph, SEM is reported for each column. (**B**) Representative images of SK-MEL28 infected with Ad5Δ24 or Ad5delta24-anti-PD-L1-scFv at 48 h post-infection. The images clearly show the cytopathic effect associated with both Ads while absent in the un-infected control. (**C**) Comparison of survival rate in SK-MEL28 infected with different MOI of Ad5Δ24 or Ad5delta24-anti-PD-L1-scFv at 48 h post-infection. The graphics were obtained through GraphPad Prism 5.02 version. The data were analyzed with GraphPad Prism 5.02 version *via* T-test with a P-value of 0.1797 indicating that the differences were not significant (ns). *≤ 0.05, ** ≤ 0.01 and ***≤ 0.001.

constant levels in vitro (27), making these cells a suitable model for testing Ad5Δ24-anti-PD-L1-scFv. Furthermore, to mimic the interaction of IS with tumor cells in vitro, we used naïve C57BL/ 6J splenocytes, which contains a heterogeneous immune cell population composed mainly of B and T lymphocytes. We assume that splenocytes could represent a simplified in vitro IS, that could enhance the oncolytic effect of the Ads in killing cancerous cells. Therefore, to corroborate our hypothesis, we evaluated tumor cell survival after treatment with Ad5Δ24-anti-PD-L1-scFv or Ad5Δ24 alone or along with splenocytes primed by incubation for 24 h with 100 vp/cell of Ad5∆24-anti-PD-L1scFv or Ad5 Δ 24, respectively (Figure 3A). We then infected B16.OVA cells with either Onc.Ads (using MOI from 1 to 100), alone or along with primed splenocytes. Forty-eight hours postinfection, cell counts demonstrated that combinatorial treatments were more effective than Ads alone (Figure 3B). Moreover, a combination of Ad5∆24-anti-PD-L1-scFv and primed splenocytes had a significant efficacy even at the lowest MOI (1 MOI) with only 55% cell survival compared with the 87% observed in B16.OVA cells were treated with Ad5Δ24-anti-PD-L1-scFv alone (Figure 3B). Additionally, we plotted these data in different graphics to compare the effects of both Ads at different MOI with or without splenocytes. Thanks to these comparisons, we are able to observe a trend in the reduction of cell survival when scFv is expressed (Figure 3C). In detail, in Figure 3CI, we compared the Ad5 Δ 24 infection with and without splenocytes. Even though the differences between treatments were not significant, we report a trend in which the presence of the splenocytes improves the virus efficacy; this is probably due to the ability of the lymphocytic population to recognize tumor cells after infection. In Figure 3CII, we compared Ad5∆24-anti-PD-L1-scFv infection with and without splenocytes. In this graphic, the differences between treatments were insignificant, but the presence of the splenocytes induced a reduction in survival rate of 66% compared to the treatment with the virus only, in which the reduction of the survival rate was 54%. In **Figure 3CIII**, we compared the Ad5 Δ 24 and Ad5 Δ 24anti-PD-L1-scFv with splenocytes. Even in this graphic, differences were insignificant. However, we observed a reduction in survival rate of 66% for the Ad5∆24-anti-PD-L1scFv and splenocytes compared to 54% for the Ad5∆24 and splenocytes. In Figure 3CIV, we compared infections with either Ads, that in the absence of the immune system had the same effects on the cells. Indeed, Ad5 Δ 24 induced a cell death of 45% while Ad5∆24-anti-PD-L1-scFv induced a cell death of 55%. In summary, these data suggest that the combinatorial treatment (splenocytes and Onc.Ads) seems to show a trend in which the addition of splenocytes induces a reduction in cancer cell survival compared to any single treatment (splenocytes or Onc.Ads alone). In addition, the best results were obtained with the combination of Ad5∆24-anti-PD-L1-scFv with splenocytes shown in Figure 3CII. However, expression of the anti-PD-L1scFv results in a strengthening of Onc.Ads therapy because it likely blocks PD-1/PD-L1 interactions, stimulating the IS, and in particular, the T cell population, to recognize and kill cancer cells (Figure 1A).

Intratumoral Administration of Ad5∆24-Anti-PD-L1-scFv Improves OV Efficacy in Reducing Tumor Growth in a Melanoma Mouse Model

After assessing the ability of the Ad5A24-anti-PD-L1-scFv in vitro in SK MEL 28 and B16.OVA, we decided to evaluate its efficacy *in vivo*. For this aim, we implanted 3×10^5 B16.OVA cells into the right and left flanks of 6/7-week-old C57BL/6J female mice. After 10 days, when the tumor size was about 5 mm, we intratumorally administered 2×10^{10} vp/kg of either Ad5 Δ 24anti-PD-L1-scFv or Ad5 Δ 24; a control group was treated with PBS. Ads and PBS administrations were repeated three times (11, 14, and 17 days) and tumor growth was evaluated until the day of sacrifice, corresponding to 25 days after B16.OVA cell implantation (Figure 4A). Analysis of tumor growth showed that the administration of Ad5Δ24 produced mild growth inhibition, whereas treatment with Ad5∆24-anti-PD-L1-scFv significantly reduced tumor size at day 19 compared to the other treatments (Figure 4B). These data demonstrate that both Onc.Ads are effective in tumor growth inhibition, underlining a stronger effect of Ad5Δ24-anti-PD-L1-scFv. As previously discussed, we expected that scFv expression could contribute to tumor growth inhibition by blocking PD-L1 interaction with PD-1 on effector T cells and, therefore, increasing lymphocyte recruitment. For this aim, we analyzed by flow cytometry the intratumoral CD3⁺CD8⁺ lymphocyte population, namely the tumor-infiltrating lymphocytes (TILs). Among the $CD3^+$ positive population, $CD8^+$ is increased in tumors treated with Ad5∆24-anti-PD-L1-scFv compared to the other groups, indicating that the Onc. Ad-induced expression of the anti-PD-L1-scFv potentiates T-cell infiltration in treated tumors (Figure 4C). Additionally, the tumor treated with Ad5 Δ 24 showed a mild increase in CD8⁺, a feature of the Onc. Ads treatment (Figures 4CI). Furthermore, immunological analyses performed on TIL (Table 1) revealed that administration of Ad5A24-anti-PD-L1-scFv induced an expansion of the CD3⁺CD8⁺ cell population; indeed, the percentage is 68% while a milder effect was observed in Ad5 Δ 24 treated tumors with a percentage of 48% (Figure 4C **II-III**). Finally, the B220⁺ cells were significantly decreased in the group treated with Ad5A24-anti-PD-L1-scFv compared to the mock and the group treated with Ad5 Δ 24 in which the B population was 36 and 37% (Figure 4CIV).

DISCUSSION

Melanoma is the most dangerous and aggressive form of skin cancer. Despite the easier detection and the effectiveness of surgery in the early stages, patients with advanced melanoma have a median survival of 7 months and a 5-year survival rate of less than 10% (13, 26), making melanoma among the more difficult cancers to eradicate. The first therapeutic approaches in melanoma treatment involved the administration of IL-2 and interferon alone or in combination with chemotherapy.

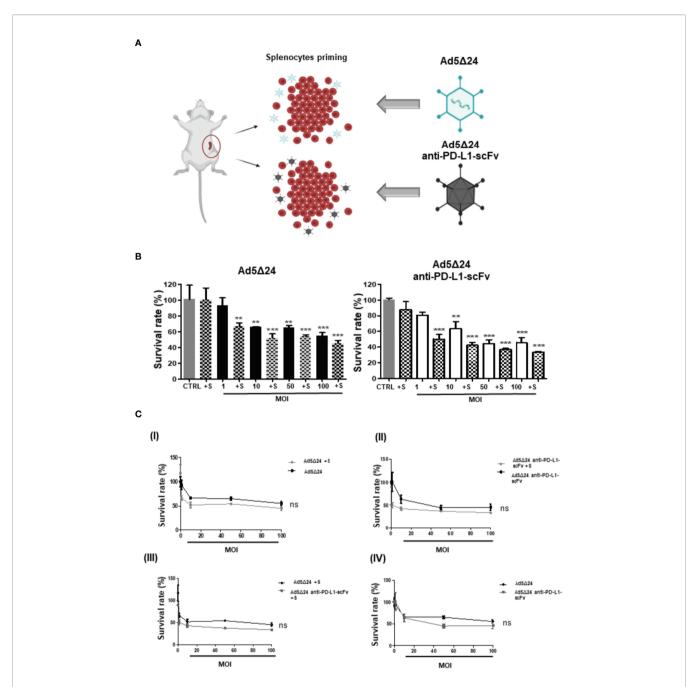


FIGURE 3 | *In vitro* evaluation of Ad5 Δ 24-anti-PD-L1-scFv infection. **(A)** Schematic representation of splenocytes derived from C57BL/6J (6–8 weeks old) naïve, primed with 50 MOI of Ad5 Δ 24-anti-PD-L1-scFv or Ad5 Δ 24 for 16–18 h before the incubation with infected B16 OVA cells. The number of splenocytes was five times more than B16 OVA cells and remains in contact with the cells for 24 (h) **(B)** Mouse melanoma cell line B16. OVA cells were infected with increasing MOI of Ad5 Δ 24 (in black) or Ad5delta24-anti-PD-L1-scFv (in white). At 24 h post-infection the same number of splenocytes were added to the cells and indicated in the graph with "+s". Cell viability was assessed at 48 h post-infection. The graphs show the survival rate expressed in the percentage of cells still alive with or without splenocytes and compared to the uninfected control. The data were analyzed with GraphPad Prism version 5.02 through One-way analysis of variance with a p-value of <0.0001 for both Ads. The significance was evaluated with Turkey's Multiple Comparison Test comparing each condition to the un-infected control. In the graph, SEM is reported for each column. **(C)** I) Comparison of survival rate in B16.0VA infected with different MOI of Ad5 Δ 24 anti-PD-L1-scFv with splenocytes at 48 h post-infection. II) Comparison of survival rate in B16.0VA infected with different MOI of Ad5 Δ 24 anti-PD-L1-scFv with splenocytes at 48 h post-infection. IIV) Comparison of survival rate in B16.0VA infected with different MOI of Ad5 Δ 24 anti-PD-L1-scFv with splenocytes at 48 h post-infection. IV) Comparison of survival rate in B16.0VA infected with different MOI of Ad5 Δ 24 anti-PD-L1-scFv with splenocytes at 48 h post-infection. IV) Comparison of survival rate in B16.0VA infected with different MOI of Ad5 Δ 24 anti-PD-L1-scFv with splenocytes at 48 h post-infection. IV) Comparison of survival rate in B16.0VA infected with different MOI of Ad5 Δ 24 anti-PD-L1-scFv with splenocytes at 48 h post-infection. IV) Comparison of survival rate

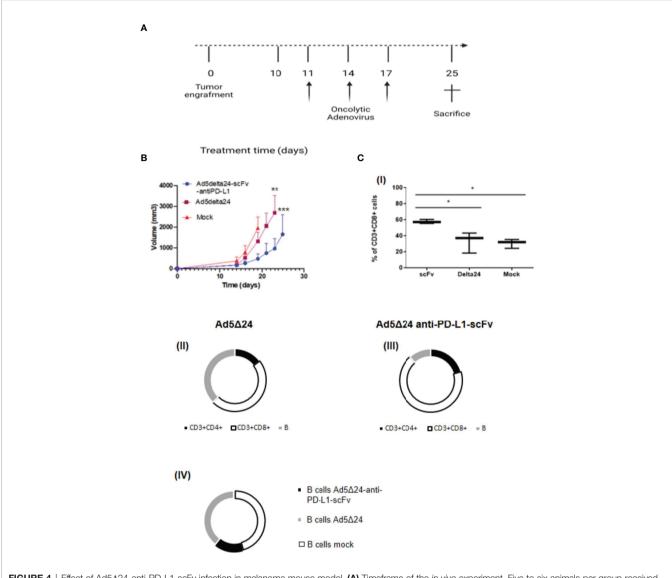


FIGURE 4 | Effect of Ad5 Δ 24-anti-PD-L1-scFv infection in melanoma mouse model. (**A**) Timeframe of the *in vivo* experiment. Five to six animals per group received subcutaneous B16.OVA melanoma cells (day 0) that were left to grow for 10 days. Then, 2 × 10E10 vp/kg mice of Ad5 Δ 24 or Ad5 Δ 24-anti-PD-L1-scFv or PBS were injected intratumorally. The intratumoral injection is repeated at days 11, 14, and 17 while at day 25 mice were sacrificed and tumors were collected. (**B**) Analysis of tumor size described in panel (**A**). Tumors volumes were analyzed for each experimental group every 2–3 days until the day of sacrifice. The data are plotted as the mean ± SEM. The statistical analysis was performed with GraphPad Prism 5.02 version *via* Spearman test, with a p-value of 0.0028 for Ad5delta24 and 0.0004 for Ad5delta24-scFv-anti-PD-L1. (**C**) Percentage of CD3⁺ CD8⁺ tumor-infiltrating lymphocytes by flow cytometric analysis are plotted by Tukey box and whiskers for each group of animals (I). Statistical analysis was done by two-way ANOVA with a p-value of 0.0134. Flow cytometric analysis of CD3⁺CD4⁺, CD3⁺CD8⁺, and B220⁺ cells in tumor samples from each group of mice (II–III–IV). *< 0.05, ** < 0.01 and *** < 0.001.

TABLE 1 | Cytofluorimetric evaluation of TILs.

	B220+	CD3 ⁺ CD4 ⁺	CD3 ⁺ CD8 ⁺
Mock	36%	27%	37%
Ad5∆24	37%	15%	48%
Ad5∆24scFv-anti-PD-L1	11%	21%	68%

We evaluated the mean percentages of TILs population from different tumors treated with PBS (Mock), Ad5 Δ 24, or Ad5 Δ 24 anti-PD-L1-scFv. In the groups of animals that received the Ad5 Δ 24 anti-PD-L1-scFv was observed an enhancement of the CD3+CD8+ T-cell population. In fact, as can be seen from the table the percentage of CD3+CD8+ T-cell population in the tumors treated with Ad5 Δ 24 anti-PD-L1-scFv is 68% compared with 48 and 37% of Ad5 Δ 24 and Mock, respectively.

Although these treatments have had some success, the most relevant progress has been made with therapies based on the use of ICIs (12). The first ICI therapy for melanoma approved by the FDA was ipilimumab (12, 13). Ipilimumab is a mAb that targets CTLA-4, resulting in a blockade of inhibitory signals allowing T cells to respond against TAAs. An additional extremely relevant target for immunotherapy is the PD-1/PD-L1 binding that also causes a block of T-cell response. Antibodies against PD-1 and PD-L1 block interactions between these proteins (28). Unfortunately, despite several immune-based cancer treatments being currently available, not all patients benefit from them or respond to treatments only for an initial period (13). Additionally, mAb production is expensive and requires maintenance of transfected cells (29), and the Fc domain of mAb induces immunogenicity that can lead to complement fixation or phagocytosis of bound cells interfering with therapeutic effects. Furthermore, systemic administration of mAbs is hampered by several limitations that include: i) unpredictable patient response, ii) low tumor penetration, and iii) slow clearance from the blood with retention in several organs, including the liver (30). Finally, several tumor types have poor lymphocyte infiltration and are defined as "cold" tumors; in these tumors, immunotherapy has a poor effect due to the lack of a suitable number of cells to be primed by TAAs (15, 27). To overcome some of these obstacles, we have decided to develop an anti-PD-L1 antibody in scFv format and express it in an OV. After intratumoral administration, Ad5 Δ 24 induces an antiviral as well as antitumoral immune response. The antiviral response is directly involved in the initial priming of the antitumoral response, promoting the recruitment of immune cells. It has been observed that OVs can turn a "cold" TME into a "hot" one; therefore, even tumors defined as "desert" for the absence of a lymphocytic population could benefit from a viroimmunotherapeutic treatment (31). Additionally, OVs induce cancer cell lysis, generating the immunogenic cell death signal (ICD) that has a main role in the activation of tumor-specific responses mediated by CD4⁺ helper cells, CD4⁺ and CD8⁺ cells (2). Hence, the association of OVs with classical immunotherapy has been proven extremely powerful (27) in animal models and clinical trials are underway to evaluate this combination in patients. The use of scFvs can also promote a more potent and specific immune response against cancer. Indeed, the smaller size of the scFv overcomes some of the limitations (large size) and possible unwanted side-effects of the whole antibodies, such as non-specific activation of circulating lymphocytes due to prolonged half-life, and promotes more efficient tumor tissue penetration (32). In this work, we have expressed the scFv-anti-PD-L1 in Ad5∆24. We have chosen the Onc.Ad5₄₂₄ because of its well-known ability to induce an antitumoral immune response in the immunogenic tumor model of melanoma. Expression of the anti-PD-L1-scFv in Ad5 Δ 24 is a way to combine the advantages of "passive" immunotherapy with "active" virotherapy, capable of inducing recruitment of immune cells. Recently, it has been demonstrated that OV-based virotherapy is less effective in advanced melanoma management compared to OV virotherapy combined with ICIs, suggesting that the addition of ICIs increases efficacy (33). Furthermore, additional studies have examined the treatment with different OVs in combination or expressing a variety of scFv targeting ICIs (18, 34, 35). For example, Wu et al. engineered a vesicular stomatitis virus (VSV) to express an scFv-anti-PD-L1, demonstrating that this system shows a potent therapeutic effect in a lung carcinoma mouse model (35), while Tanoue et al., in 2017, demonstrated that the PD-L1 mini body expressed by a system of Onc.Ads and helper-dependent Ads

(HD-Ad) blocks, with high efficacy, the PD-1/PD-L1 pathway enhanced the antitumoral effect in a prostate cancer engraft mouse model. In this study we explored the combination of the antitumor effect of the Ad5∆24 Onc.Ad together with the expression of an anti-PD-L1-scFv identified by phage display, in a C57BL/6J melanoma mouse model. The selected anti-PD-L1-scFv binds to PD-L1 thus interfering in PD-1 and B7.1 interactions, representing the principal PD-L1 receptors on immune cells, and does not interfere with the ability of Ad5 Δ 24 to induce cell death in an *in vitro* model of melanoma, actually enhancing it. Treatment of the B16.OVA murine melanoma cells with different MOI of Ad5∆24 anti-PD-L1-scFv in the presence of splenocytes, resembling an *in-vitro* simplified tumoral immune system environment, induced a more robust effect compared to the treatments with the virus or splenocytes alone. A major effect on cell death was seen (Figures 3B, C), demonstrating that PD-L1-scFv expression enhanced the splenocyte action. Most importantly, in vivo intratumoral administration of Ad5∆24-anti-PD-L1-scFv in murine melanoma model resulted in the prolonged survival of mice compared to the unmodified Ad5 Δ 24 (Figure 4B). Specifically, we observed that untreated mice showed a rapid increase in tumor size, progressive deterioration of physical conditions and, consequently, had to be sacrificed on day 19. In contrast, mice treated with $Ad5\Delta 24$ resulted in a mild reduction of tumor progression, highlighting that the sole oncolytic process is not sufficient to completely block tumor growth. In this study, the addition of a control group treated with an anti-PD-L1 mAb was not considered appropriate, since scFvs have different features, as we previously described; in addition, for the purpose of this study, we did not purify the anti-PDL-1 scFv. Finally, we observed that although mice treated with Ad5∆24-anti-PD-L1-scFv did not show a complete remission, the association of the oncolytic process with PD-L1 inhibition significantly slowed down tumor progression resulting in an important reduction of tumor size and an amelioration of survival condition. In support of the hypothesis that reduction in tumor growth was due to increased antitumoral immune response, we observed an increment in the CD8⁺ Tcell population in the tumors of mice treated with Ad5 Δ 24 anti-PD-L1-scFv, suggesting that the combination of OV action and PD-L1 inhibition is beneficial for the recruitment and activation of cytotoxic T cells. Furthermore, this data confirmed the main role of the CD8⁺ T-cell population in the detection and destruction of tumor cells (36-38). Additionally, based on the literature and our observation of the T and B population analysis, we assumed that the anti-PD-L1-scFv could also act on Breg, reducing the PD-1 positive Breg population at the tumor site and therefore restoring an antitumoral response mediated by the CD8⁺ T-cell population that increased in mice treated with $Ad5\Delta 24$ -anti-PD-L1-scFv (39). Finally, we plan to compare in future studies the efficacy and toxicity of Ad5Δ24-anti-PD-L1-scFv with the commercially available mAbs and, additionally, to evaluate its efficacy in different tumor models characterized by lower Tcell infiltrations.

CONCLUSIONS

This study demonstrates that combining Onc.Ads with anti-PD-L1-scFv can lead to a more effective antitumoral therapeutic approach by combining active and passive immunotherapy. Although more efforts need to be made to improve the versatility and safety of Onc.Ads, this intriguing approach could have the potential to usher in a new era in cancer treatment.

DATA AVAILABILITY STATEMENT

The raw data supporting the conclusions of this article will be made available by the authors, without undue reservation.

ETHICS STATEMENT

The animal study was reviewed and approved by the Ministry of Health, Italy.

AUTHOR CONTRIBUTIONS

Study concept and design: MV, FS, EL, LT, and LP. Data collection and analysis: AD'A, MV, LG, MP, and LT. Interpretation: MV, FS, MP, EL, VC, CL, and LP. Manuscript preparation: MV, FS, and LP. Critical revision: AB, GC, VC, CL, and LP. All authors listed have made a substantial, direct, and intellectual contribution to the work and approved it for publication.

REFERENCES

- Qiao Y, Wan J, Zhou L, Ma W, Yang Y, Luo W, et al. Stimuli-Responsive Nanotherapeutics for Precision Drug Delivery and Cancer Therapy. *Wiley Interdiscip Rev Nanomed Nanobiotechnol* (2019) 11(1):1–20. doi: 10.1002/ wnan.1527
- Gujar S, Pol JG, Kim Y, Lee PW, Kroemer G. Antitumor Benefits of Antiviral Immunity: An Underappreciated Aspect of Oncolytic Virotherapies. *Cell Press Trends Immunol* (2018) 39(3):209–21. doi: 10.1016/j.it.2017.11.006
- Hegde PS, Chen DS. Top 10 Challenges in Cancer Immunotherapy. *Immunity* (2020) 52(1):17–35. doi: 10.1016/j.immuni.2019.12.011
- Najafi M, Goradel NH, Farhood B, Salehi E, Solhjoo S, Toolee H, et al. Tumor Microenvironment: Interactions and Therapy. J Cell Physiol (2019) 234 (5):5700–21. doi: 10.1002/jcp.27425
- Hinshaw DC, Shevde LA. The Tumor Microenvironment Innately Modulates Cancer Progression. *Cancer Res* (2019) 79(18):4557–67. doi: 10.1158/0008-5472.CAN-18-3962
- Lau J, Cheung J, Navarro A, Lianoglou S, Haley B, Totpal K, et al. Tumour and Host Cell PD-L1 Is Required to Mediate Suppression of Anti-Tumour Immunity in Mice. Nat Commun (2017) 8:1–11. doi: 10.1038/ncomms14572
- Kawakami Y, Ohta S, Sayem MA, Tsukamoto N, Yaguchi T. Immune-Resistant Mechanisms in Cancer Immunotherapy. Int J Clin Oncol (2020) 25(5):810–7. doi: 10.1007/s10147-019-01611-x
- Balar AV, Weber JS. PD-1 and PD-L1 Antibodies in Cancer: Current Status and Future Directions. *Cancer Immunol Immunother* (2017) 66(5):551–64. doi: 10.1007/s00262-017-1954-6

FUNDING

This research was funded by the SATIN CUP B6C1700007-SURF 17061BP00000002 and the University of Naples Federico II, Dipartimento di Medicina Molecolare e Biotecnologie Mediche.

ACKNOWLEDGMENTS

The author wishes to acknowledge Dr. Silvia Esposito for her expert assistance in animal studies. This work was realized using the CEINGE-Biotecnologie Avanzate Institute shared facilities and laboratory. Figures were created using BioRender. MV is supported by a PhD program of di Medicina Molecolare e Biotecnologie Mediche of University of Naples Federico II.

SUPPLEMENTARY MATERIAL

The Supplementary Material for this article can be found online at: https://www.frontiersin.org/articles/10.3389/fonc.2022. 902190/full#supplementary-material

Supplementary Figure 1 | Figure Legend: Purification and characterization of anti-PD-L1 scFv. (A) SDS-PAGE of periplasmic extract of bacteria cells transformed with the cDNA encoding the anti-PD-L1 scFv before (lane 3) and after purification (lanes 4-6) by affinity chromatography. An unrelated scFv (lane 2) was used as a control. (B) Western blotting analysis of the eluted fraction (as in lane 5 of panel A).
(C) ELISA assays of the purified scFv on recombinant PD-L1/Fc at increasing concentrations (nM). (D) A competitive ELISA assay performed by PD-L1 coating on the plate, followed by saturation with the unlabeled scFv and incubation with biotinylated PD-1 or B7, demonstrate the ability of anti-PD-L1-scFv to interfere in the interaction between PD-1 and B7. Error bars were calculated on the basis of the results obtained in triplicates by at least two independent experiments.

- Zimmer L, Apuri S, Eroglu Z, Kottschade LA, Forschner A, Gutzmer R, et al. Ipilimumab Alone or in Combination With Nivolumab After Progression on Anti-PD-1 Therapy in Advanced Melanoma. *Eur J Cancer* (2017) 75:47–55. doi: 10.1016/j.ejca.2017.01.009
- Robert C, Thomas L, Bondarenko I, O'Day S, Weber J, Garbe C, et al. Ipilimumab Plus Dacarbazine for Previously Untreated Metastatic Melanoma. N Engl J Med (2011) 364(26):2517–26. doi: 10.1056/NEJMoa1104621
- Johnson RMG, Dong H. Functional Expression of Programmed Death-Ligand 1 (B7-H1) by Immune Cells and Tumor Cells. *Front Immunol* (2017) 8:1–9. doi: 10.3389/fimmu.2017.00961
- Zito CR, Kluger HM. Immunotherapy for Metastatic Melanoma. J Cell Biochem (2012) 113(3):725–34. doi: 10.1002/jcb.23402
- Redman JM, Gibney GT, Atkins MB. Advances in Immunotherapy for Melanoma. BMC Med (2016) 14(1):1–11. doi: 10.1186/s12916-016-0571-0
- Bianco A, Malapelle U, Rocco D, Perrotta F, Mazzarella G. Targeting Immune Checkpoints in non Small Cell Lung Cancer. *Curr Opin Pharmacol* (2018) 40:46–50. doi: 10.1016/j.coph.2018.02.006
- Ylösmäki E, Cerullo V. Design and Application of Oncolytic Viruses for Cancer Immunotherapy. *Curr Opin Biotechnol* (2020) 65:25–36. doi: 10.1016/ j.copbio.2019.11.016
- Lemos de Matos A, Franco LS, McFadden G. Oncolytic Viruses and the Immune System: The Dynamic Duo. *Mol Ther - Methods Clin Dev* (2020) 17:349–58. doi: 10.1016/j.omtm.2020.01.001
- Feola S, Russo S, Ylösmäki E, Cerullo V. Oncolytic ImmunoViroTherapy: A Long History of Crosstalk Between Viruses and Immune System for Cancer Treatment. *Pharmacol Ther* (2021) 236:108103. doi: 10.1016/j.pharmthera.2021.108103

- Tanoue K, Shaw AR, Watanabe N, Porter C, Rana B, Gottschalk S, et al. Armed Oncolytic Adenovirus-Expressing PD-L1 Mini-Body Enhances Antitumor Effects of Chimeric Antigen Receptor T Cells in Solid Tumors. *Cancer Res* (2017) 77(8):2040–51. doi: 10.1158/0008-5472.CAN-16-1577
- Cervera-Carrascon V, Havunen R, Hemminki A. Oncolytic Adenoviruses: A Game Changer Approach in the Battle Between Cancer and the Immune System. *Expert Opin Biol Ther* (2019) 19(5):443–55. doi: 10.1080/ 14712598.2019.1595582
- Tripodi L, Vitale M, Cerullo V, Pastore L. Oncolytic Adenoviruses for Cancer Therapy. Int J Mol Sci (2021) 22(5):1–15. doi: 10.3390/ijms22052517
- Cervera-Carrascon V, Siurala M, Santos JM, Havunen R, Tähtinen S, Karell P, et al. TNFa and IL-2 Armed Adenoviruses Enable Complete Responses by Anti-PD-1 Checkpoint Blockade. *Oncoimmunology* (2018) 7(5):1–11. doi: 10.1080/2162402X.2017.1412902
- Rafiq S, Yeku OO, Jackson HJ, Purdon TJ, van Leeuwen DG, Drakes DJ, et al. Targeted Delivery of a PD-1-Blocking scFV by CAR-T Cells Enhances Anti-Tumor Efficacy *In Vivo. Nat Biotechnol* (2018) 36(9):847–58. doi: 10.1038/ nbt.4195
- Passariello M, D'Alise AM, Esposito A, Vetrei C, Froechlich G, Scarselli E, et al. Novel Human Anti-PD-L1 Mabs Inhibit Immune-Independent Tumor Cell Growth and PD-L1 Associated Intracellular Signalling. *Sci Rep* (2019) 9 (1):1–13. doi: 10.1038/s41598-019-49485-3
- Sasso E, D'Avino C, Passariello M, D'Alise AM, Siciliano D, Esposito ML, et al. Massive Parallel Screening of Phage Libraries for the Generation of Repertoires of Human Immunomodulatory Monoclonal Antibodies. *MAbs* (2018) 10(7):1060–72. doi: 10.1080/19420862.2018.1496772
- Passariello M, Vetrei C, Sasso E, Froechlich G, Gentile C, D'alise AM, et al. Isolation of Two Novel Human Anti-Ctla-4 Mabs With Intriguing Biological Properties on Tumor and Nk Cells. *Cancers (Basel)* (2020) 12(8):1–24. doi: 10.3390/cancers12082204
- Kuryk L, Møller ASW, Jaderberg M. Combination of Immunogenic Oncolytic Adenovirus ONCOS-102 With Anti-PD-1 Pembrolizumab Exhibits Synergistic Antitumor Effect in Humanized A2058 Melanoma huNOG Mouse Model. Oncoimmunology (2019) 8(2):1–11. doi: 10.1080/ 2162402X.2018.1532763
- Feola S, Capasso C, Fusciello M, Martins B, Tähtinen S, Medeot M, et al. Oncolytic Vaccines Increase the Response to PD-L1 Blockade in Immunogenic and Poorly Immunogenic Tumors. *Oncoimmunology* (2018) 7(8):1–10. doi: 10.1080/2162402X.2018.1457596
- Bianco A, Perrotta F, Barra G, Malapelle U, Rocco D, De Palma R. Prognostic Factors and Biomarkers of Responses to Immune Checkpoint Inhibitors in Lung Cancer. Int J Mol Sci (2019) 20(19):4931. doi: 10.3390/ijms20194931
- Ahmad ZA, Yeap SK, Ali AM, Ho WY, Alitheen NBM, Hamid M. ScFv Antibody: Principles and Clinical Application. *Clin Dev Immunol* (2012) 2012. doi: 10.1155/2012/980250
- Shin J, Phelan PJ, Gjoerup O, Bachovchin W, Bullock PA. Characterization of a Single Chain Variable Fragment of Nivolumab That Targets PD-1 and Blocks PD-L1 Binding. *Protein Expr Purif* (2021) 177:105766. doi: 10.1016/ j.pep.2020.105766

- Bommareddy PK, Shettigar M, Kaufman HL. Integrating Oncolytic Viruses in Combination Cancer Immunotherapy. Nat Rev Immunol (2018) 18(8):498– 513. doi: 10.1038/s41577-018-0014-6
- 32. Nannini F, Parekh F, Wawrzyniecka P, Mekkaoui L, Righi M, Dastjerdi FV, et al. A Primer Set for the Rapid Isolation of scFv Fragments Against Cell Surface Antigens From Immunised Rats. *Sci Rep* (2020) 10(1):1–15. doi: 10.1038/s41598-020-76069-3
- 33. Zou P, Tang R, Luo M. Oncolytic Virotherapy, Alone or in Combination With Immune Checkpoint Inhibitors, for Advanced Melanoma: A Systematic Review and Meta-Analysis. *Int Immunopharmacol* (2020) 78(87):106050. doi: 10.1016/j.intimp.2019.106050
- Engeland CE, Grossardt C, Veinalde R, Bossow S, Lutz D, Kaufmann JK, et al. CTLA-4 and PD-L1 Checkpoint Blockade Enhances Oncolytic Measles Virus Therapy. *Mol Ther* (2014) 22(11):1949–59. doi: 10.1038/mt.2014.160
- Wu C, Wu M, Liang M, Xiong S, Dong C. A Novel Oncolytic Virus Engineered With PD-L1 scFv Effectively Inhibits Tumor Growth in a Mouse Model. *Cell Mol Immunol* (2019) 16(9):780–2. doi: 10.1038/s41423-019-0264-7
- Chiaro J, Kasanen HHE, Whalley T, Capasso C, Grönholm M, Feola S, et al. Viral Molecular Mimicry Influences the Antitumor Immune Response in Murine and Human Melanoma. *Cancer Immunol Res* (2021) 9(8):981–93. doi: 10.1158/2326-6066.CIR-20-0814
- Bentzen AK, Such L, Jensen KK, Marquard AM, Jessen LE, Miller NJ, et al. T Cell Receptor Fingerprinting Enables in-Depth Characterization of the Interactions Governing Recognition of Peptide–MHC Complexes. *Nat Biotechnol* (2018) 36(12):1191–6. doi: 10.1038/nbt.4303
- Tumeh PC, Harview CL, Yearley JH, Shintaku IP, Taylor EJM, Robert L, et al. PD-1 Blockade Induces Responses by Inhibiting Adaptive Immune Resistance. *Nature* (2014) 515(7528):568–71. doi: 10.1038/nature13954
- Xiao X, Lao XM, Chen MM, Liu RX, Wei Y, Ouyang FZ, et al. PD-1hi Identifi Es a Novel Regulatory B-Cell Population in Human Hepatoma That Promotes Disease Progression. *Cancer Discovery* (2016) 6(5):546–59. doi: 10.1158/2159-8290.CD-15-1408

Conflict of Interest: The authors declare that the research was conducted in the absence of any commercial or financial relationships that could be construed as a potential conflict of interest.

Publisher's Note: All claims expressed in this article are solely those of the authors and do not necessarily represent those of their affiliated organizations, or those of the publisher, the editors and the reviewers. Any product that may be evaluated in this article, or claim that may be made by its manufacturer, is not guaranteed or endorsed by the publisher.

Copyright © 2022 Vitale, Scialò, Passariello, Leggiero, D'Agostino, Tripodi, Gentile, Bianco, Castaldo, Cerullo, De Lorenzo and Pastore. This is an open-access article distributed under the terms of the Creative Commons Attribution License (CC BY). The use, distribution or reproduction in other forums is permitted, provided the original author(s) and the copyright owner(s) are credited and that the original publication in this journal is cited, in accordance with accepted academic practice. No use, distribution or reproduction is permitted which does not comply with these terms.



Potentialities and Challenges of mRNA Vaccine in Cancer Immunotherapy

Li-Juan Duan^{1†}, Qian Wang^{2†}, Cuilian Zhang^{2*}, Dong-Xiao Yang^{1*} and Xu-Yao Zhang^{1*}

¹ Medical School, Huanghe Science and Technology College, Zhengzhou, China, ² Reproductive Medicine Center, Henan Provincial People's Hospital, People's Hospital of Zhengzhou University, Zhengzhou, China

Immunotherapy has become the breakthrough strategies for treatment of cancer in recent years. The application of messenger RNA in cancer immunotherapy is gaining tremendous popularity as mRNA can function as an effective vector for the delivery of therapeutic antibodies on immune targets. The high efficacy, decreased toxicity, rapid manufacturing and safe administration of mRNA vaccines have great advantages over conventional vaccines. The unprecedent success of mRNA vaccines against infection has proved its effectiveness. However, the instability and inefficient delivery of mRNA has cast a shadow on the wide application of this approach. In the past decades, modifications on mRNA structure and delivery methods have been made to solve these questions. This review summarizes recent advancements of mRNA vaccines in cancer immunotherapy and the existing challenges for its clinical application, providing insights on the future optimization of mRNA vaccines for the successful treatment of cancer.

Keywords: mRNA, cancer vaccine, immunotherapy, efficient delivery, optimization, strategies

INTRODUCTION

Cancer is one of the most lethal diseases in the world. In the recent decades, achievements in the understanding of the immune system have shed light on the treatment of cancer by immunotherapies (1). Various immune cells are able to identify antigens on the surface of cancer cells and interact with the antigenetic peptides to destroy cancer cells. Therefore, immunotherapies including immune cell-based cancer vaccines were considered as promising approaches to cure cancer. Cancer vaccines have drawn great attention since the clinical application of several novel cancer vaccines such as immune cell-based vaccines, viral vector-based vaccines and RNA or DNAbased vaccines (2, 3). Among these, mRNA-based cancer vaccines demonstrate exceptional advantages in comparison with the other types of vaccines (4). First, unlike virus-based vaccines which can be infectious in some circumstances, mRNA-based vaccines are safer and free of contamination. Second, once delivered into the cells, the genetic information of antigen carried by mRNA can be translated into protein very rapidly. Third, mRNA-based cancer vaccines can stimulate immune response and overcome vaccine resistance that is often observed in conventional chemotherapies. In addition, mRNA-based cancer vaccines encode the cancer antigens in fulllength and thus can overcome the restrictions of human leukocyte antigen to activate a broader immune response. Last but not least, mRNA-based cancer vaccines are free of mutations since mRNA can't insert into the chromosome. Given the advantages of mRNA vaccines over

OPEN ACCESS

Edited by:

Xian Zeng, Fudan University, China

Reviewed by:

Yan Cao, Sun Yat-sen University Cancer Center (SYSUCC), China

*Correspondence:

Cuilian Zhang luckyzcl@qq.com Dong-Xiao Yang dongxiaoyang2@gmail.com Xu-Yao Zhang hhstuyxz@outlook.com

[†]These authors have contributed equally to this work

Specialty section:

This article was submitted to Cancer Immunity and Immunotherapy, a section of the journal Frontiers in Immunology

Received: 19 April 2022 Accepted: 02 May 2022 Published: 26 May 2022

Citation:

Duan L-J, Wang Q, Zhang C, Yang D-X and Zhang X-Y (2022) Potentialities and Challenges of mRNA Vaccine in Cancer Immunotherapy. Front. Immunol. 13:923647. doi: 10.3389/fimmu.2022.923647 conventional cancer vaccines, this novel immunotherapy has become the hotspot of research for the development of new generation cancer therapies. However, the expected substantial application of mRNA-based cancer vaccines was not seen due to several problems regarding the instability of mRNA, immunogenicity and the inefficiency of *in vivo* delivery.

Research on mRNA-based vaccines have focused on overcoming the instability and the delivery of mRNA. One strategy is to use synthetic mRNA or modified mRNA analogs, which can enhance the stability and protein expression of mRNA. For example, circular RNA is used to avoid the detection of pathogen-associated pattern receptors; selfamplifying RNA greatly increased the expression level of proteins (5). Another strategy is to modify the *in vivo* delivery methods of RNA vaccines to achieve higher efficiency. For instance, in addition to electroporation, novel vectors such as polyplexes, lipid nanoparticles, peptides and cationic nanoemulsions have been used for the delivery of RNA vaccines (6). The success of RNA-based vaccines for the COVID19 pandemic has witnessed the significant progress made on the clinical application of mRNA vaccines and the increasing necessity of developing novel RNA vaccines for treatment of diseases (7).

In this review, we will focus on the most recent progress that have been made on the stability and *in vivo* delivery of mRNAbased vaccines for the treatment of cancer and discuss the existing challenges on the current clinical application of mRNA-based immunotherapies, hoping to accelerate the clinical application of mRNA-based cancer immunotherapy.

EVOLUTION OF MRNA-BASED VACCINES IN CANCER IMMUNOTHERAPY

The first introduction of mRNA to activate immune response in vivo could be dated to the year 1993, when Martinon and coworkers constructed a liposome-mRNA expressing influenza hemagglutinin that activated CD8⁺ T cell responses for the detection and lysing of virus-infected cells (8). In 1995, mRNA construct expressing cancer embryonic antigen was reported to induce the generation of antibodies in mice, demonstrating the potential of mRNA vaccines in cancer therapies (9, 10). Over the past decades, mRNA vaccines quickly became the spotlight of cancer immunotherapy due to their abilities to provide safe vaccination, to improve antigen expression and to avoid gene integration. The earliest mRNA vaccines in cancer immunotherapy normally use RNA virus genomes, which have shown good efficacy against viral cancer in mouse models (11). Later, a liposome-mRNA vaccine was developed and its ability to induce cognate cytotoxic T cells has resulted in the destroy of melanoma cancer cells (12). These mRNAbased vaccines have demonstrated great advantage over conventional vaccines and thus have been established as novel strategies for cancer therapies. Since then, more and more kinds of mRNA-based vaccines are developed for treatment of cancer.

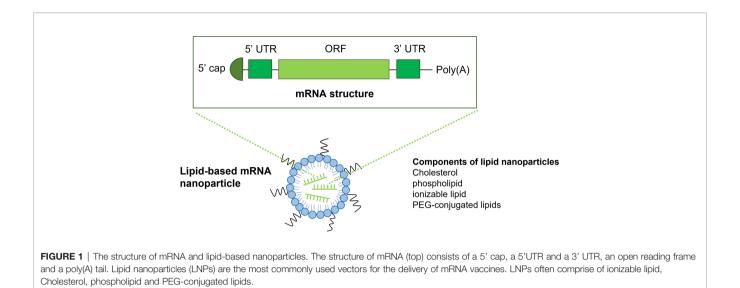
To date, replicating modified mRNA, unmodified mRNA, and virus-derived mRNA are the three main types of mRNA vaccines in cancer immunotherapy (1). The basic structure of non-replicating mRNA consists of an open reading frame flanked by a 5'-prime region and a 3'-prime untranslated region (UTR), a 5' cap structure and a 3' poly (A) tails (13). The ORF of mRNA encodes the sequences of the target antigen. The target antigen will be translated into proteins once mRNA is transited to the cytosol of the cell. The expressed antigen will further be post-translationally modified and fold into a fullfunctional protein whereas the remaining mRNA will be quickly degraded to reduce potential toxicity. However, the rapid degradation of naked mRNA also dramatically affects its stability. In addition, the intrinsic immunogenicity of mRNA further promotes the rapid degradation of mRNA, resulting in decreased expression levels of antigen. Moreover, the inefficient in vivo delivery of mRNA-based vaccines will reduce the protein expression of mRNA. These disadvantages have greatly limited the clinical application of mRNA vaccines in cancer immunotherapy. We will discuss the limitations and highlight the current state-of-the-art strategies to overcome these limitations in the next section.

STRATEGIES TO IMPROVE THE STABILITY OF MRNA-BASED CANCER VACCINES

Previous studies have found that the inadequate methylation of mRNA, impurity and immunogenicity could lead to low efficiency of mRNA translation (14, 15). A better understanding of the structure of mRNA has provided new strategies to improve the stability and the translation efficiency of mRNA.

mRNA consists of an ORF, a 5'-prime UTR, a 3'-prime UTR, a 5' cap structure and a 3' poly (A) tails (Figure 1). Firstly, modification of the 5' cap of mRNA has been utilized to improve stability. There are mainly two types of mRNA capping methods: the in vitro post-translational capping enzymatic method that utilizes the Vaccinia virus Capping Enzyme (VCE) and the chemical capping methods (16). These capping methods largely improve mRNA translation but are limited by reverse incorporation. This limitation could be overcome by the development of anti-reverse cap analogs (ARCA), which is methylated at the C3 position. ARCA significantly increases the expression of mRNA. However, the disadvantages of ARCA including de-capping of mRNA, exogeneous motif, and relatively low capping efficiency (60-80%) in contrast to the enzymatic capping method (100%) (17, 18). To increase the capping efficiency and prevent de-capping of ARCA, a novel cotranscriptional cap analog termed CleanCap has been developed, which can generate an unmodified cap structure with high efficiency (>90%) (19).

Secondly, post-translational modifications of mRNA can inhibit the immune recognition of mRNA. Studies have revealed that minimization of mRNA reorganization by the



innate immune system could prevent sensing and destruction of mRNA translation, resulting in increased expression (15, 20). For example, removal of the uncapped phosphate of mRNA by phosphatases can effectively avoid immunogenicity. In addition, modifications of mRNA through substitution of natural uridine and cytidine with pseudouridine (Ψ) or 1methylpseudouridine (m1 Ψ) can also effectively avoid immunogenicity and improve stability (21, 22). Pseudouridine is an isomer of uridine in which the nitrogen-carbon glycosidic bond of uridine is replaced by a carbon-carbon bond. N1-Methylpseudouridine is the methylated derivative of pseudouridine and is usually used for mRNA vaccines. Substitution of uridine with pseudouridine (Ψ) or 1methylpseudouridine (m1 Ψ) in mRNA synthesis can reduce cytotoxicity of mRNA vaccines because $\Psi/m1\Psi$ mRNAs trigger low-to-no immune responses to the cells and enhance the expression of tumor antigen (23, 24).

Thirdly, increased purity of RNA and removal of impurities can prevent the degradation of mRNA. During the process of transcription, double stranded RNA impurities are easily formed, which leads to the immunogenicity of mRNA cancer vaccines. Thess and co-workers have shown that the RNA impurities could be removed by optimization of the sequence and purification of RNA by high-pressure liquid chromatography (HPLC), which could result in reduced immunogenicity and improved stability of mRNA vaccines (25). However, HPLC is limited by low yield and high cost. A better way to achieve high purity of mRNA is to use synthetic mRNA (26).

Fourthly, optimization of the ORF of mRNA can improve mRNA translation. Increased GC content in the ORF can be applied to improve stability (27). Methods to increase GC content including codon optimization of ORF and depletion of uridine (28). For example, rare codons in ORF are often substituted by codons with higher tRNA abundance to achieve higher translation rate (29). However, high translation rate sometimes can be harmful, which is the major limitation of codon optimization (30). The reason underlying this observation is that the correctly folding of some proteins may require a low translation rate rather than a high translation rate. Despite the defects of codon optimization, this strategy is one of the most important methods for improving mRNA translation.

Finally, optimization of the untranslated 5' UTR and 3' UTR of mRNA can also significantly improve stability and protein expression (31). For example, start codon AUG or CUG at 5' UTR can inhibit the translation of mRNA (22). Therefore, avoiding these can improve translation rate of mRNA. Increasing the 3'UTR sequence in tandem may also improve mRNA translation (32). In conclusion, modifications of mRNA structure have proven to be of great importance to improve the stability and protein expression of mRNA vaccines. Future studies will focus on overcoming the limitations of current strategies and developing novel mRNA vaccines with higher stability and translation rate.

OPTIMIZATION OF THE VECTORS FOR EFFICIENT DELIVERY OF MRNA CANCER VACCINES

Despite the many advantages of mRNA cancer vaccine described above, the difficulties of *in vivo* delivery of mRNA vaccine have greatly inhibited its clinical application. Therefore, it is of urgency to increase the delivery efficiency of mRNA vaccines. There are mainly three types of vectors used for *in vivo* delivery: viral, non-viral and cell-based vectors. Dendritic cells (DCs) are usually used as cell-based vectors for adoptive transfer of mRNA cancer vaccines. Designated 'nature's adjuvants', dendritic cells (DCs) are a group of bone marrow-derived antigen-presenting cells that play essential roles in activating and mediating immune response (33, 34). DCs can transit antigen to T cells and facilitate the transduction of immunomodulatory signals *via* cytokines and cell interactions. The generation of mRNA-based cancer vaccines using DCs as vectors involves the use of mRNA extracted from autologous cancers (35). In this process, dendritic cells were isolated from patients, cultured ex vivo, induced to maturation via adjuvant, loaded with mRNA encoding target antigens and injected back to patients to activate efficient anti-cancer immunity (36). DC-based mRNA cancer vaccines have been examined by clinical trials (Table 1). The initial results from phase I/II have shown that these mRNA vaccines display dramatically increased survival rate and reduced toxicity (37). However, the differentiation, maturation and antigen loading of DCs impact T cell co-stimulation and lead to weak immune response (38, 39). In addition, low production and high variability of mRNA-based DC vaccines have limited the application of this novel immunotherapy. Future studies may focus on the direct injection of mRNA as an alternative approach to overcome the limitations of mRNA-based DC vectors.

Viral vectors have been extensively studied for the development of mRNA cancer vaccines, with promising preliminary results being reported (33, 40, 41). For instance, mRNA vaccines for Covid19 pandemic have used viral vectors. In fact, an adenovirus type-5 (Ad5) vector-based RNA vaccines had been on clinical trials in China as early as March 2020 (42). The most used viral vector is self-amplifying mRNA (replicons or saRNA), which encodes target antigen and self-replicates in the cytoplasm of the host cell for expression of target antigen. The viral structural protein is deleted from the sequences of the self-amplifying mRNA thus it is unable to generate infectious virus in the host cells. In the past decades, we have witnessed the utilization of self-amplifying mRNA derived from the genomes of RNA viruses including picornaviruses, alphaviruses and flaviviruses (43, 44). In comparison with non-viral vectors, viral-based mRNA vaccines demonstrate advantages such as modular design, rapid manufacturing and low dose

requirement because of its self-replicative properties (45). Viral-based mRNA vaccines against colorectal tumor, urothelial carcinoma, gastroesophageal tumor and rabies have been applied in clinical trials (46). However, the infectious property of virus vectors and the difficulties for large-scale manufacturing of virus vectors have limited the applicability of this approach.

The most famous non-viral vector used for mRNA vaccine is the lipid nanoparticle-based mRNA delivery system, which has been used for the mRNA vaccine of Covid19 and has been very successful (47, 48). LNPs usually consists of an ionizable lipid-like molecule, polyethylene glycol (PEG)-conjugated lipid, cholesterol and a helper phospholipid. Lipid-based nanoparticles (LNPs) could significantly improve delivery efficiency of mRNA cancer vaccines and reduce the system toxicity. Since the ionized lipid is positively charged at low pH, it could enhance the encapsulation of the negatively charged mRNA by electrostatic interaction and promote membrane fusion and destabilization upon delivery. In addition, the neutrality of lipid at the physiological environment improves the stability of mRNA. The first-generation lipids used for LNPs including Dlin-DMA, DLin-KC2-DMA and cKK-E12, etc (49, 50). The second-generation lipids are the derivatives of DLin-KC2-DMA and cKK-E12 (51). In addition to lipid, the other components of LNPs such as cholesterol and phospholipid could facilitate membrane fusion and improve mRNA stability, whereas the diffusive PEG could inhibit particle aggregation, leading to increased stability of mRNA vaccines. Over the past decades, improvements have been made to LPNs. Current LPNs have demonstrated enhanced delivery specificity and improved capacity to be rapidly metabolized and cleared, leading to reduced toxicity of the system and increased stability of mRNA vaccines. Studies have shown that LNPs act as an effective vector for delivery of mRNA vaccines to liver cancers (52, 53). In addition, LPNs have also been

TABLE 1 | Representative clinical trials of LNP-based and DC-based mRNA cancer vaccines.

Name	RNA encoding antigen	Tumour	Formulation type	Administration route	NCT number	Phase
FixVac	MAGE-A3, NY-ESO-1, tyrosinase, TPTE	Melanoma	LNP	intravenous	NCT02410733	Ι
mRNA-2416	OX40L	Solid Tumor Malignancies or Lymphoma	LNP	Intratumoural	NCT03323398	1/11
mRNA-2752	OX40L, IL-23, IL-36Y	Solid Tumor Malignancies or Lymphoma	LNP	Intratumoural	NCT03739931	1
mRNA-4157	Personalized neoantigens	Melanoma	LNP	intramuscular	NCT03897881	Ш
mRNA-4650	Personalized neoantigens	Gastrointestinal cancer	LNP	intramuscular	NCT03480152	1/11
mRNA-5671/ V941	KRAS antigens	Colorectal cancer, non-small-cell lung cancer, pancreatic adenocarcinoma	LNP	intramuscular	NCT03948763	Ι
W_ova1	Ovarian cancer antigens	Ovarian cancer	LNP	intravenous	NCT04163094	1
HARE-40	HPV oncoproteins E6 and E7	HPV oncoproteins E6 and E7	LNP	intradermal	NCT03418480	1/11
RO7198457	Personalized neoantigens	Melanoma	LNP	intravenous	NCT03815058	Ш
TNBC-MERIT	Personalized neoantigens	Triple-negative breast cancer	LNP	intravenous	NCT02316457	1
MEDI1191	IL-12	Solid tumours	LNP	Intratumoural	NCT03946800	1
SAR441000	IL-12sc, IL-15sushi, IFNα and GM-CSF	Solid tumours	LNP	Intratumoural	NCT03871348	Ι
TriMixDC- MEL	MAGE-A3, MAGE-C2, tyrosinase, gp100	Melanoma	DC-based	intravenous and intradermal	NCT01066390	Ι
TriMixDC- MEL	MAGE-A3, MAGE-C2, tyrosinase, gp100	Melanoma	DC-based	intravenous and intradermal	NCT01676779	Ш
TriMixDC- MEL	CTLA-4 inhibitor ipilimumab	Melanoma	DC-based	intravenous and intradermal	NCT01302496	II
Not available	TAA-transfected DC	melanoma	DC-based	intradermal	NCT01278940	1/11

reported to target tumours in other organs such as lung, spleen and bone marrow. For example, the Selective Organ Targeting approach developed by Cheng and co-workers using cationic or anionic lipid can target liver, lung and spleen (54, 55). Overall, LNPs have made great contributions to the clinical application of mRNA vaccines.

In addition to LNP vectors, peptide vectors and polymer vectors also play important roles in facilitating the delivery of mRNA cancer vaccines. Polyethylenimine (PEI) is one of the most commonly used polymer-based vectors for mRNA vaccine delivery (56, 57). The efficacy of PEI-based hemagglutinin antigen from influenza virus has been evaluated in mice models (58). In comparison with LNP-based delivery system, polymer vectors display lower purity and reduced clearance rate but higher toxicity. Peptide-based delivery system have been widely studied (59–61). For example, cationic cell-penetrating peptides (CPPs) can condense mRNA complexes and induce strong immune response upon injection (62). However, the precise mechanism of this delivery system remains to be understood.

CONCLUSION AND FUTURE PERSPECTIVES

The successful application of mRNA vaccines for Covid19 has demonstrated the great potential of mRNA vaccines as novel therapies for the treatment of lethal diseases. It's reported that mRNA-based vaccines can induce immune response in cancer cells, leading to the destruction of cancer cells and the control of tumour growth. Conventional therapies of cancer treatment such as chemotherapy and radiotherapy often suffer from multi-drug

REFERENCES

- Huff AL, Jaffee EM, Zaidi N. Messenger RNA Vaccines for Cancer Immunotherapy: Progress Promotes Promise. J Clin Invest (2022) 132(6): e156211. doi: 10.1172/JCI156211
- Van Lint S, Wilgenhof S, Heirman C, Corthals J, Breckpot K, Bonehill A, et al. Optimized Dendritic Cell-Based Immunotherapy for Melanoma: The TriMix-Formula. *Cancer Immunol Immunother* (2014) 63(9):959–67. doi: 10.1007/ s00262-014-1558-3
- Zeng C, Zhang C, Walker PG, Dong Y. Zeng C, Zhang C, Walker PG, Dong Y. "Formulation and Delivery Technologies for mRNA Vaccines,". In: *Current Topics in Microbiology and Immunology*. Berlin: Springer Press (2020) 1–40. doi: 10.1007/82_2020_217
- Pastor F, Berraondo P, Etxeberria I, Frederick J, Sahin U, Gilboa E, et al. An RNA Toolbox for Cancer Immunotherapy. *Nat Rev Drug Discov* (2018) 17 (10):751–67. doi: 10.1038/nrd.2018.132
- Flemming A. Vaccines: Self-Amplifying RNA in Lipid Nanoparticles: A Next-Generation Vaccine? Nat Rev Drug Discov (2012) 11(10):748–9. doi: 10.1038/ nrd3854
- Faghfuri E, Pourfarzi F, Faghfouri AH, Abdoli Shadbad M, Hajiasgharzadeh K, Baradaran B. Recent Developments of RNA-Based Vaccines in Cancer Immunotherapy. *Expert Opin Biol Ther* (2021) 21(2):201–18. doi: 10.1080/ 14712598.2020.1815704
- Baden LR, El Sahly HM, Essink B, Kotloff K, Frey S, Novak R, et al. Efficacy and Safety of the mRNA-1273 SARS-CoV-2 Vaccine. N Engl J Med (2021) 384 (5):403–16. doi: 10.1056/NEJMoa2035389
- Martinon F, Krishnan S, Lenzen G, Magne R, Gomard E, Guillet JG, et al. Induction of Virus-Specific Cytotoxic T Lymphocytes *In Vivo* by Liposome-

resistance and strong toxicity, whereas mRNA-based cancer vaccines have shown enhanced efficacy and reduced toxicity. Therefore, mRNA-based vaccines have gained more and more popularity for the development of novel immunotherapies. However, the instability and *in vivo* delivery of mRNA cancer vaccine have impaired its clinical application. Although progress has been made over the past decades to overcome these limitations, challenges still exist on the development of mRNA cancer vaccines. To promote the wide application of mRNA cancer vaccines, more strategies should be taken to improve the stability and translation rate of mRNA vaccines.

In conclusion, mRNA vaccines have the potential to significantly affect the battle against cancer. Future studies should cast more investigations on the combination of mRNA cancer vaccines and conventional cancer therapies.

AUTHOR CONTRIBUTIONS

X-YZ, D-XY and CZ conceived the topic, revised and proofread the manuscript. L-JD and QW drafted the paper and prepared the figure and table. All authors approved the submitted version.

FUNDING

This study was supported by the Major Projects in Provincial and National Union Construction of Henan Medical Science Research Plan (SBGJ202001002).

Entrapped mRNA. Eur J Immunol (1993) 23(7):1719–22. doi: 10.1002/ eji.1830230749

- Conry RM, LoBuglio AF, Loechel F, Moore SE, Sumerel LA, Barlow DL, et al. A Carcinoembryonic Antigen Polynucleotide Vaccine has *In Vivo* Antitumor Activity. *Gene Ther* (1995) 2(1):59–65.
- Conry RM, LoBuglio AF, Loechel F, Moore SE, Sumerel LA, Barlow DL, et al. A Carcinoembryonic Antigen Polynucleotide Vaccine for Human Clinical Use. *Cancer Gene Ther* (1995) 2(1):33–8.
- Ying H, Zaks TZ, Wang RF, Irvine KR, Kammula US, Marincola FM, et al. Cancer Therapy Using a Self-Replicating RNA Vaccine. *Nat Med* (1999) 5 (7):823–7. doi: 10.1038/10548
- Zhou WZ, Hoon DS, Huang SK, Fujii S, Hashimoto K, Morishita R, et al. RNA Melanoma Vaccine: Induction of Antitumor Immunity by Human Glycoprotein 100 mRNA Immunization. *Hum Gene Ther* (1999) 10 (16):2719–24. doi: 10.1089/10430349950016762
- Emens LA, Adams S, Cimino-Mathews A, Disis ML, Gatti-Mays ME, Ho AY, et al. Society for Immunotherapy of Cancer (SITC) Clinical Practice Guideline on Immunotherapy for the Treatment of Breast Cancer. *J Immunother Cancer* (2021) 9(8):e002597. doi: 10.1136/jitc-2021-002597
- Foster JB, Choudhari N, Perazzelli J, Storm J, Hofmann TJ, Jain P, et al. Purification of mRNA Encoding Chimeric Antigen Receptor Is Critical for Generation of a Robust T-Cell Response. *Hum Gene Ther* (2019) 30(2):168– 78. doi: 10.1089/hum.2018.145
- Kranz LM, Diken M, Haas H, Kreiter S, Loquai C, Reuter KC, et al. Systemic RNA Delivery to Dendritic Cells Exploits Antiviral Defence for Cancer Immunotherapy. *Nature* (2016) 534(7607):396–401. doi: 10.1038/nature18300
- Muttach F, Muthmann N, Rentmeister A. Synthetic mRNA Capping. Beilstein J Org Chem (2017) 13:2819–32. doi: 10.3762/bjoc.13.274

- Rydzik AM, Kulis M, Lukaszewicz M, Kowalska J, Zuberek J, Darzynkiewicz ZM, et al. Synthesis and Properties of mRNA Cap Analogs Containing Imidodiphosphate Moiety–Fairly Mimicking Natural Cap Structure, Yet Resistant to Enzymatic Hydrolysis. *Bioorg Med Chem* (2012) 20(5):1699– 710. doi: 10.1016/j.bmc.2012.01.013
- Shuman S. Catalytic Activity of Vaccinia mRNA Capping Enzyme Subunits Coexpressed in Escherichia Coli. J Biol Chem (1990) 265(20):11960–6. doi: 10.1016/S0021-9258(19)38494-7
- Vaidyanathan S, Azizian KT, Haque A, Henderson JM, Hendel A, Shore S, et al. Uridine Depletion and Chemical Modification Increase Cas9 mRNA Activity and Reduce Immunogenicity Without HPLC Purification. *Mol Ther Nucleic Acids* (2018) 12:530–42. doi: 10.1016/j.omtn.2018.06.010
- Kariko K, Buckstein M, Ni H, Weissman D. Suppression of RNA Recognition by Toll-Like Receptors: The Impact of Nucleoside Modification and the Evolutionary Origin of RNA. *Immunity* (2005) 23(2):165–75. doi: 10.1016/ j.immuni.2005.06.008
- Durbin AF, Wang C, Marcotrigiano J, Gehrke L. RNAs Containing Modified Nucleotides Fail To Trigger RIG-I Conformational Changes for Innate Immune Signaling. *mBio* (2016) 7(5):e00833–16. doi: 10.1128/mBio.00833-16
- Andries O, Mc Cafferty S, De Smedt SC, Weiss R, Sanders NN, Kitada T. N(1)-Methylpseudouridine-Incorporated mRNA Outperforms Pseudouridine-Incorporated mRNA by Providing Enhanced Protein Expression and Reduced Immunogenicity in Mammalian Cell Lines and Mice. J Control Release (2015) 217:337–44. doi: 10.1016/j.jconrel.2015.08.051
- Svitkin YV, Cheng YM, Chakraborty T, Presnyak V, John M, Sonenberg N. N1-Methyl-Pseudouridine in mRNA Enhances Translation Through Eif2alpha-Dependent and Independent Mechanisms by Increasing Ribosome Density. *Nucleic Acids Res* (2017) 45(10):6023–36. doi: 10.1093/nar/gkx135
- Parr CJC, Wada S, Kotake K, Kameda S, Matsuura S, Sakashita S, et al. N 1-Methylpseudouridine Substitution Enhances the Performance of Synthetic mRNA Switches in Cells. *Nucleic Acids Res* (2020) 48(6):e35. doi: 10.1093/nar/gkaa070
- Thess A, Grund S, Mui BL, Hope MJ, Baumhof P, Fotin-Mleczek M, et al. Sequence-Engineered mRNA Without Chemical Nucleoside Modifications Enables an Effective Protein Therapy in Large Animals. *Mol Ther* (2015) 23 (9):1456–64. doi: 10.1038/mt.2015.103
- Nelson J, Sorensen EW, Mintri S, Rabideau AE, Zheng W, Besin G, et al. Impact of mRNA Chemistry and Manufacturing Process on Innate Immune Activation. *Sci Adv* (2020) 6(26):eaaz6893. doi: 10.1126/sciadv.aaz6893
- Cannarozzi G, Schraudolph NN, Faty M, von Rohr P, Friberg MT, Roth AC, et al. A Role for Codon Order in Translation Dynamics. *Cell* (2010) 141 (2):355–67. doi: 10.1016/j.cell.2010.02.036
- Mauger DM, Cabral BJ, Presnyak V, Su SV, Reid DW, Goodman B, et al. mRNA Structure Regulates Protein Expression Through Changes in Functional Half-Life. *Proc Natl Acad Sci U S A* (2019) 116(48):24075–83. doi: 10.1073/pnas.1908052116
- Linares-Fernandez S, Lacroix C, Exposito JY, Verrier B. Tailoring mRNA Vaccine to Balance Innate/Adaptive Immune Response. *Trends Mol Med* (2020) 26(3):311–23. doi: 10.1016/j.molmed.2019.10.002
- Schlake T, Thess A, Fotin-Mleczek M, Kallen KJ. Developing mRNA-Vaccine Technologies. RNA Biol (2012) 9(11):1319–30. doi: 10.4161/rna.22269
- Holtkamp S, Kreiter S, Selmi A, Simon P, Koslowski M, Huber C, et al. Modification of Antigen-Encoding RNA Increases Stability, Translational Efficacy, and T-Cell Stimulatory Capacity of Dendritic Cells. *Blood* (2006) 108(13):4009–17. doi: 10.1182/blood-2006-04-015024
- 32. Orlandini von Niessen AG, Poleganov MA, Rechner C, Plaschke A, Kranz LM, Fesser S, et al. Improving mRNA-Based Therapeutic Gene Delivery by Expression-Augmenting 3' UTRs Identified by Cellular Library Screening. *Mol Ther* (2019) 27(4):824–36. doi: 10.1016/j.ymthe.2018.12.011
- Palucka K, Banchereau J. Cancer Immunotherapy via Dendritic Cells. Nat Rev Cancer (2012) 12(4):265–77. doi: 10.1038/nrc3258
- Wculek SK, Cueto FJ, Mujal AM, Melero I, Krummel MF, Sancho D. Dendritic Cells in Cancer Immunology and Immunotherapy. *Nat Rev Immunol* (2020) 20(1):7–24. doi: 10.1038/s41577-019-0210-z
- Perez CR, De Palma M. Engineering Dendritic Cell Vaccines to Improve Cancer Immunotherapy. Nat Commun (2019) 10(1):5408. doi: 10.1038/ s41467-019-13368-y
- Sabado RL, Balan S, Bhardwaj N. Dendritic Cell-Based Immunotherapy. Cell Res (2017) 27(1):74–95. doi: 10.1038/cr.2016.157

- Beck JD, Reidenbach D, Salomon N, Sahin U, Tureci O, Vormehr M, et al. mRNA Therapeutics in Cancer Immunotherapy. *Mol Cancer* (2021) 20(1):69. doi: 10.1186/s12943-021-01348-0
- Kongsted P, Borch TH, Ellebaek E, Iversen TZ, Andersen R, Met O, et al. Dendritic Cell Vaccination in Combination With Docetaxel for Patients With Metastatic Castration-Resistant Prostate Cancer: A Randomized Phase II Study. *Cytotherapy* (2017) 19(4):500–13. doi: 10.1016/j.jcyt.2017.01.007
- Gu YZ, Zhao X, Song XR. Ex Vivo Pulsed Dendritic Cell Vaccination Against Cancer. Acta Pharmacol Sin (2020) 41(7):959–69. doi: 10.1038/s41401-020-0415-5
- Fiedler K, Lazzaro S, Lutz J, Rauch S, Heidenreich R. mRNA Cancer Vaccines. Recent Results Cancer Res (2016) 209:61–85. doi: 10.1007/978-3-319-42934-2_5
- Diken M, Kranz LM, Kreiter S, Sahin U. mRNA: A Versatile Molecule for Cancer Vaccines. *Curr Issues Mol Biol* (2017) 22:113–28. doi: 10.21775/ cimb.022.113
- 42. Cohen J. Vaccine Designers Take First Shots at COVID-19. *Science* (2020) 368 (6486):14–6. doi: 10.1126/science.368.6486.14
- Tews BA, Meyers G. Self-Replicating RNA. Methods Mol Biol (2017) 1499:15– 35. doi: 10.1007/978-1-4939-6481-9_2
- Bloom K, van den Berg F, Arbuthnot P. Self-Amplifying RNA Vaccines for Infectious Diseases. *Gene Ther* (2021) 28(3-4):117–29. doi: 10.1038/s41434-020-00204-y
- Li Y, Teague B, Zhang Y, Su Z, Porter E, Dobosh B, et al. *In Vitro* Evolution of Enhanced RNA Replicons for Immunotherapy. *Sci Rep* (2019) 9(1):6932. doi: 10.1038/s41598-019-43422-0
- Gebre MS, Brito LA, Tostanoski LH, Edwards DK, Carfi A, Barouch DH. Novel Approaches for Vaccine Development. *Cell* (2021) 184(6):1589–603. doi: 10.1016/j.cell.2021.02.030
- 47. Thomas SJ, Perez JL, Lockhart SP, Hariharan S, Kitchin N, Bailey R, et al. Efficacy and Safety of the BNT162b2 mRNA COVID-19 Vaccine in Participants With a History of Cancer: Subgroup Analysis of a Global Phase 3 Randomized Clinical Trial. *Vaccine* (2022) 40(10):1483–92. doi: 10.1016/j.vaccine.2021.12.046
- Buschmann MD, Carrasco MJ, Alishetty S, Paige M, Alameh MG, Weissman D. Nanomaterial Delivery Systems for mRNA Vaccines. Vaccines (Basel) (2021) 9(1):65. doi: 10.3390/vaccines9010065
- Jayaraman M, Ansell SM, Mui BL, Tam YK, Chen J, Du X, et al. Maximizing the Potency of siRNA Lipid Nanoparticles for Hepatic Gene Silencing In Vivo. *Angew Chem Int Ed Engl* (2012) 51(34):8529–33. doi: 10.1002/anie.201203263
- Love KT, Mahon KP, Levins CG, Whitehead KA, Querbes W, Dorkin JR, et al. Lipid-Like Materials for Low-Dose, *In Vivo* Gene Silencing. *Proc Natl Acad Sci* U S A (2010) 107(5):1864–9. doi: 10.1073/pnas.0910603106
- Maier MA, Jayaraman M, Matsuda S, Liu J, Barros S, Querbes W, et al. Biodegradable Lipids Enabling Rapidly Eliminated Lipid Nanoparticles for Systemic Delivery of RNAi Therapeutics. *Mol Ther* (2013) 21(8):1570–8. doi: 10.1038/mt.2013.124
- 52. Lai I, Swaminathan S, Baylot V, Mosley A, Dhanasekaran R, Gabay M, et al. Lipid Nanoparticles That Deliver IL-12 Messenger RNA Suppress Tumorigenesis in MYC Oncogene-Driven Hepatocellular Carcinoma. J Immunother Cancer (2018) 6(1):125. doi: 10.1186/s40425-018-0431-x
- Stadler CR, Bahr-Mahmud H, Celik L, Hebich B, Roth AS, Roth RP, et al. Elimination of Large Tumors in Mice by mRNA-Encoded Bispecific Antibodies. *Nat Med* (2017) 23(7):815–7. doi: 10.1038/nm.4356
- 54. Parhiz H, Shuvaev VV, Pardi N, Khoshnejad M, Kiseleva RY, Brenner JS, et al. PECAM-1 Directed Re-Targeting of Exogenous mRNA Providing Two Orders of Magnitude Enhancement of Vascular Delivery and Expression in Lungs Independent of Apolipoprotein E-Mediated Uptake. *J Control Release* (2018) 291:106–15. doi: 10.1016/j.jconrel.2018.10.015
- 55. Basha G, Novobrantseva TI, Rosin N, Tam YY, Hafez IM, Wong MK, et al. Influence of Cationic Lipid Composition on Gene Silencing Properties of Lipid Nanoparticle Formulations of siRNA in Antigen-Presenting Cells. *Mol Ther* (2011) 19(12):2186–200. doi: 10.1038/mt.2011.190
- Khan OF, Kowalski PS, Doloff JC, Tsosie JK, Bakthavatchalu V, Winn CB, et al. Endothelial siRNA Delivery in Nonhuman Primates Using Ionizable Low-Molecular Weight Polymeric Nanoparticles. *Sci Adv* (2018) 4(6): eaar8409. doi: 10.1126/sciadv.aar8409
- Romano E, Pascolo S, Ott P. Implications of mRNA-Based SARS-CoV-2 Vaccination for Cancer Patients. J Immunother Cancer (2021) 9(6):e002932. doi: 10.1136/jitc-2021-002932

- Vogel AB, Lambert L, Kinnear E, Busse D, Erbar S, Reuter KC, et al. Self-Amplifying RNA Vaccines Give Equivalent Protection Against Influenza to mRNA Vaccines But at Much Lower Doses. *Mol Ther* (2018) 26(2):446–55. doi: 10.1016/j.ymthe.2017.11.017
- Sebastian M, Schroder A, Scheel B, Hong HS, Muth A, von Boehmer L, et al. A Phase I/IIa Study of the mRNA-Based Cancer Immunotherapy CV9201 in Patients With Stage IIIB/IV non-Small Cell Lung Cancer. *Cancer Immunol Immunother* (2019) 68(5):799–812. doi: 10.1007/s00262-019-02315-x
- Kubler H, Scheel B, Gnad-Vogt U, Miller K, Schultze-Seemann W, Vom Dorp F, et al. Self-Adjuvanted mRNA Vaccination in Advanced Prostate Cancer Patients: A First-in-Man Phase I/IIa Study. J Immunother Cancer (2015) 3:26. doi: 10.1186/s40425-015-0068-y
- 61. De Keersmaecker B, Claerhout S, Carrasco J, Bar I, Corthals J, Wilgenhof S, et al. TriMix and Tumor Antigen mRNA Electroporated Dendritic Cell Vaccination Plus Ipilimumab: Link Between T-Cell Activation and Clinical Responses in Advanced Melanoma. J Immunother Cancer (2020) 8(1): e000329. doi: 10.1136/jitc-2019-000329
- 62. Udhayakumar VK, De Beuckelaer A, McCaffrey J, McCrudden CM, Kirschman JL, Vanover D, et al. Arginine-Rich Peptide-Based mRNA Nanocomplexes Efficiently Instigate Cytotoxic T Cell Immunity Dependent

on the Amphipathic Organization of the Peptide. *Adv Healthc Mater* (2017) 6 (13):1601412. doi: 10.1002/adhm.201601412

Conflict of Interest: The authors declare that the research was conducted in the absence of any commercial or financial relationships that could be construed as a potential conflict of interest.

Publisher's Note: All claims expressed in this article are solely those of the authors and do not necessarily represent those of their affiliated organizations, or those of the publisher, the editors and the reviewers. Any product that may be evaluated in this article, or claim that may be made by its manufacturer, is not guaranteed or endorsed by the publisher.

Copyright © 2022 Duan, Wang, Zhang, Yang and Zhang. This is an open-access article distributed under the terms of the Creative Commons Attribution License (CC BY). The use, distribution or reproduction in other forums is permitted, provided the original author(s) and the copyright owner(s) are credited and that the original publication in this journal is cited, in accordance with accepted academic practice. No use, distribution or reproduction is permitted which does not comply with these terms.



SQLE, A Key Enzyme in Cholesterol Metabolism, Correlates With Tumor Immune Infiltration and Immunotherapy Outcome of Pancreatic Adenocarcinoma

OPEN ACCESS

Edited by:

Xian Zeng, Fudan University, China

Reviewed by:

Ying Ma, Tianjin Medical University Cancer Institute and Hospital, China Qing Li, The Chinese University of Hong Kong, Hong Kong SAR, China Yandong Gong, Fifth Medical Center of the PLA General Hospital, China

> ***Correspondence:** Xiaoiian Wu

wuxjian@mail.sysu.edu.cn

Specialty section:

This article was submitted to Cancer Immunity and Immunotherapy, a section of the journal Frontiers in Immunology

Received: 28 January 2022 Accepted: 26 April 2022 Published: 26 May 2022

Citation:

You W, Ke J, Chen Y, Cai Z, Huang Z-p, Hu P and Wu X (2022) SQLE, a Key Enzyme in Cholesterol Metabolism, Correlates With Tumor Immune Infiltration and Immunotherapy Outcome of Pancreatic Adenocarcinoma. Front. Immunol. 13:864244. doi: 10.3389/fimmu.2022.864244 Weiqiang You, Jia Ke, Yufeng Chen, Zerong Cai, Ze-ping Huang, Peishan Hu and Xiaojian Wu *

Department of Colorectal Surgery, Guangdong Provincial Key Laboratory of Colorectal and Pelvic Floor Diseases, Guangdong Institute of Gastroenterology, The Sixth Affiliated Hospital, Sun Yat-sen University, Guangzhou, China

Background: Pancreatic adenocarcinoma (PAAD) is a treatment-refractory cancer with poor prognosis. Accumulating evidence suggests that squalene epoxidase (SQLE) plays a pivotal role in the development and progression of several cancer types in humans. However, the function and underlying mechanism of SQLE in PAAD remain unclear.

Methods: SQLE expression data were downloaded from The Cancer Genome Atlas and the Genotype-Tissue Expression database. SQLE alterations were demonstrated based on the cBioPortal database. The upstream miRNAs regulating SQLE expression were predicted using starBase. The function of miRNA was validated by Western blotting and cell proliferation assay. The relationship between SQLE expression and biomarkers of the tumor immune microenvironment (TME) was analyzed using the TIMER and TISIDB databases. The correlation between SQLE and immunotherapy outcomes was assessed using Tumor Immune Dysfunction and Exclusion. The log-rank test was performed to compare prognosis between the high and low SQLE groups.

Results: We demonstrated a potential oncogenic role of SQLE. SQLE expression was upregulated in PAAD, and it predicted poor disease-free survival (DFS) and overall survival (OS) in patients with PAAD. "Amplification" was the dominant type of SQLE alteration. In addition, this alteration was closely associated with the OS, disease-specific survival, DFS, and progression-free survival of patients with PAAD. Subsequently, hsa-miR-363-3p was recognized as a critical microRNA regulating SQLE expression and thereby influencing PAAD patient outcome. *In vitro* experiments suggested that miR-363-3p could knock down the expression of SQLE and inhibit the proliferation of PANC-1. SQLE was significantly associated with tumor immune cell infiltration, immune checkpoints (including PD-1 and CTLA-4), and biomarkers of the TME. KEGG and GO analyses indicated that cholesterol metabolism-associated RNA functions are implicated in the

mechanisms of SQLE. SQLE was inversely associated with cytotoxic lymphocytes and predicted immunotherapy outcomes.

Conclusions: Collectively, our results indicate that cholesterol metabolism-related overexpression of SQLE is strongly correlated with tumor immune infiltration and immunotherapy outcomes in patients with PAAD.

Keywords: pancreatic adenocarcinoma, SQLE, prognosis, miRNA, tumor immune infiltration, immunotherapy

INTRODUCTION

Pancreatic adenocarcinoma (PAAD) is currently one of the most aggressive and malignant tumors with a 5-year survival rate of only 10% (1, 2). It is the seventh leading cause of cancer-related death worldwide (3). Given the long asymptomatic disease progression and poor early detection, 80% of patients with PAAD have an advanced or metastatic stage at diagnosis, rendering a grim prognosis (4-6). In recent years, despite improvements in perioperative chemotherapy, radiotherapy techniques, immune checkpoint inhibitors, and comprehensive treatments, the number of deaths due to PAAD has been steadily increasing (7, 8). Immunotherapy has shown favorable prospects for the treatment of solid tumors, especially when combined with other targeted drugs (9). Although tumor mutational burden (TMB), microsatellite status, and programmed cell death-ligand 1 (PD-L1) expression have been used to predict the effect of immunotherapy (10, 11), the efficiency was limited in PAAD. Therefore, there is an urgent need to identify more effective therapeutic targets and develop new promising strategies for PAAD.

Cholesterol is the major sterol in mammalian cell membranes, maintaining cell integrity and fluidity and forming intracellular homeostasis (12). The biosynthetic pathway from acetyl-CoA to cholesterol involves nearly 30 enzymatic reactions, including the initial mevalonate (MVA) pathway, subsequent squalene biosynthesis, and ultimate sterol conversion (13–15). Squalene epoxidase (SQLE) is the second rate-limiting enzyme in cholesterol biosynthesis that catalyzes the conversion of squalene to 2,3-epoxysqualene (16, 17). SQLE promotes the initiation and progression of non-alcoholic steatohepatitis by regulating cholesterol metabolism (18). Notably, an increasing number of studies have shown that SQLE expression is closely correlated with the progression, invasion, and metastasis of multiple tumors, such as breast cancer (19), hepatocellular carcinoma (20), esophageal cancer (21), prostate cancer (22), colorectal cancer (23), and lung cancer (24). In addition, the inhibitor terbinafine, which targets SQLE, showed efficient tumor suppression and represents a new strategy for solid tumor treatment (25). Recent research has emphasized that the glycolysis-cholesterol synthesis axis affects the outcome and prognosis of PAAD (26). However, a comprehensive analysis, including the expression, prognosis, and mechanism of SQLE in PAAD, has not yet been conducted. Additionally, the relationship between SQLE and the tumor immune microenvironment in PAAD remains unclear.

In this study, we first analyzed the expression level of SQLE and its prognostic value in various types of human cancers, illustrating its potential oncogenic role. Subsequently, microRNAs (miRNAs) were determined to be vital regulators of SQLE and to influence the outcome of patients with PAAD. Our results confirmed that SQLE is significantly associated with tumor immune cell infiltration, immune checkpoints, and biomarkers of the tumor immune microenvironment. RNA functions associated with cholesterol metabolism were found to be implicated in the mechanisms of SQLE. Finally, a high SQLE level was indicative of a poor immunotherapy effect in melanoma and PAAD. Together, cholesterol metabolism-related overexpression of SQLE is strongly correlated with poor prognosis, tumor immune infiltration, and immunotherapy outcomes in PAAD.

MATERIALS AND METHODS

Cell Culture

The human PDAC cell line PANC-1 was obtained from the American Type Culture Collection (ATCC) and cultured in DMEM medium (Gibco, Carlsbad, CA) supplemented with 10% FBS (Gibco, Carlsbad, CA) and 1% penicillin/ streptomycin (Gibco, Carlsbad, CA) in 5% CO_2 at 37°C.

Western Blotting

Total proteins were extracted in RIPA buffer, and the protein concentration was measured by BCA Protein Assay Kit (Thermo Fisher Scientific, Waltham, MA). Protein was resolved in 10% Tris-SDS-PAGE gels and transferred to PVDF membranes (Millipore, Darmstadt, Germany). The membranes were incubated with antihuman SQLE antibody (Proteintech, Chicago, IL) at a dilution of

Abbreviations: PAAD, pancreatic adenocarcinoma; SQLE, squalene epoxidase; OS, overall survival; DFS, disease-free survival; DSS, disease-specific survival; PFS, progression-free survival; TIME, tumor immune microenvironment; BLCA, bladder urothelial carcinoma; BRCA, breast invasive carcinoma; CESC, cervical squamous cell carcinoma and endocervical adenocarcinoma; COAD, colon adenocarcinoma; ESCA, esophageal carcinoma; HNSC, head and neck squamous cell carcinoma; LIHC, liver hepatocellular carcinoma; LUSC, lung squamous cell carcinoma, READ, rectal adenocarcinoma; STAD, stomach adenocarcinoma; UCEC, uterine corpus endometrial carcinoma; KIRP, kidney renal papillary cell carcinoma; PRAD, prostate adenocarcinoma; THCA, thyroid carcinoma; ACC, adrenocortical carcinoma; DLBC, lymphoid neoplasm diffuse large B-cell lymphoma; OV, ovarian serous cystadenocarcinoma; THYM, thymoma; UCS, uterine carcinosarcoma; LGG, lower grade glioma, SKCM, skin cutaneous melanoma; TGCT, testicular germ cell tumors; PDCD1, programmed cell death protein 1; LAG3, lymphocyte activation gene 3; CTLA-4, cytotoxic Tlymphocyte-associated protein 4; TMB, tumor mutation burden; CTL, cytotoxic T lymphocyte.

1:1000 and then probed with HRP-conjugated secondary antibody (Proteintech, Chicago, IL).

Cell Transfection

The miR-363-3p mimics (Genepharma, Shanghai, China) or negative control (NC) was transfected into PANC-1 cells using Lipofectamine 3000 Transfection Reagent (Invitrogen, Karlsruhe, Germany) according to the manufacturer's instructions.

Cell Viability

Cells were plated in 96-well plates at a density of 2000 cells per well. Cell viability was assessed using CCK-8 (Gaithersburg, MD). OD450 values were determined on Day 0, 1, 2, 3, and 4.

Correlation Between SQLE Expression and Immune Cell Infiltration

TIMER (27) and TIMER2.0 (28) were used as servers for the comprehensive analysis of SQLE expression in 33 types of human cancer, infiltration of tumor immune cells, and the expression of immune checkpoints in PAAD. EPIC (29) and McP-Counter (30) were used to validate the immune cell infiltration from SQLE expression profiles. One-way ANOVA was used to test the significant differences. Statistical significance was set at p < 0.05.

GEPIA Database Analysis

GEPIA (31) is a web tool for gene expression analyses based on The Cancer Genome Atlas (TCGA) and Genotype-Tissue Expression databases. We used GEPIA to analyze SQLE expression in 10 types of human cancers, namely, ACC, DLBC, LAML, LGG, OV, PAAD, SKCM, TGCT, THYM, and UCS. Statistical significance was set at p < 0.05. We also conducted survival analyses for SQLE, including overall survival (OS) and disease-free survival (DFS). The correlation of SQLE with ACAT2, HMGCR, HMGCS1, ID11, and LDLR in PAAD and pan-cancer was analyzed, and the top 100 SQLE-correlated genes were identified using GEPIA.

StarBase Database Analysis

The Starbase database (32) was first used to predict the miRNAs upstream of SQLE. PITA, RNA22, miRmap, microT, miRanda, PicTar, and TargetScan were used to identify miRNAs binding to SQLE, and miRNAs that were present in more than two programs were included in further analyses. We also used starBase to perform miRNA expression and correlation analyses for miRNA and SQLE in PAAD.

Kaplan-Meier Plotter Analysis

Kaplan-Meier plotter (33), a database evaluating the genes or miRNAs that are associated with survival in human cancer types, including PAAD, was used to perform survival analysis for miRNAs in PAAD. A log-rank p < 0.05 was defined as statistically significant.

Genetic Alteration Analysis

cBioPortal web (34, 35) was used to analyze the alteration frequency, mutation type, and copy number alteration of SQLE

in human cancers. The mutated site information of SQLE is displayed in a schematic diagram of the protein structure. The prognostic value of SQLE alterations, including OS, diseasespecific survival (DSS), DFS, and progression-free survival (PFS), was determined using survival analysis. In addition, immunohistochemical images of SQLE in tumor and normal tissues were obtained. Log-rank p-values were also generated.

TISIDB Database Analysis

TISIDB is a web portal for tumor and immune system interaction (36). The relationship between SQLE expression and tumor immune biomarkers in PAAD, including lymphocytes, MHC molecules, immune inhibitors, and immunostimulators, was analyzed using TISIDB. The p-value and Spearman's correlation coefficients (rho) were calculated automatically.

Gene Enrichment Analysis

STRING website (37) was used to determine the SQLE-binding proteins network. Kyoto Encyclopedia of Genes and Genomes (KEGG) pathway analysis was performed by "hiplot" (unpublished, https://hiplot.com.cn), which is a free and comprehensive cloud platform for scientific computation and visualization. Gene ontology (GO) analyses, including biological process (BP), cellular component (CC), and molecular function (MF), were obtained from the DAVID database (https://david.nci fcrf.gov). A two-tailed p < 0.05 was considered statistically significant.

Statistical Analysis

Data are shown as the mean \pm standard deviation of at least three independent experiments. Kaplan-Meier survival analysis was used to compare survival times with the log-rank test. Spearman's correlation coefficient was used to determine the relationship between the two variables. Statistical significance was set at p < 0.05.

RESULTS

SQLE Expression in the Pan-Cancer Analysis

We first explored SQLE expression levels in 33 types of human cancers based on TCGA dataset. As shown in **Figure 1A**, SQLE expression was significantly higher in tumors than in normal tissues in BLCA, BRCA, CESC, COAD, ESCA, HNSC, LIHC, LUSC, READ, STAD, and UCEC. SQLE expression was distinctly downregulated in KIRC, KIRP, PRAD, and THCA cells. Owing to an insufficient number of normal tissues as controls for several cancer types in the TCGA dataset, we verified the difference in SQLE expression between normal and tumor tissues in 10 types of human cancers by including normal tissue from the GTEx consortium of the GEPIA database. SQLE expression level was prominently increased in ACC, DLBC, OV, PAAD, THYM, and UCS and was dramatically downregulated in LAML. However, no significant differences were observed in LGG, SKCM, and TGCT (**Figures 1B-K**). Notably, SQLE

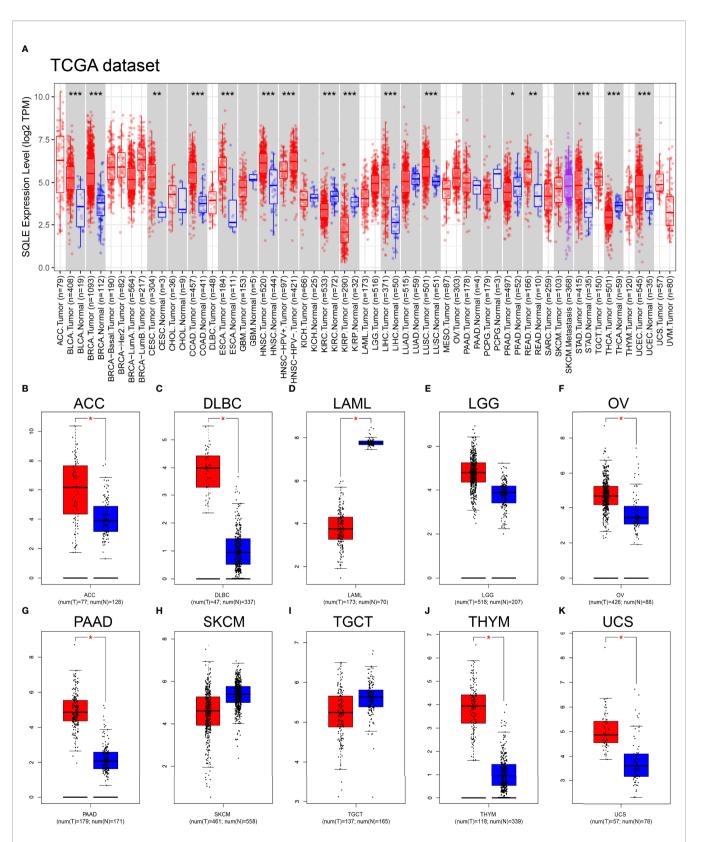


FIGURE 1 | SQLE expression level in human cancers. (A) SQLE expression in 33 types of human cancer based on TCGA dataset. (B–K) SQLE expression in ACC (B), DLBC (C), LAML (D), LGG (E), OV (F), PAAD (G), SKCM (H), TGCT (I), THYM (J), and UCS (K) compared with corresponding TCGA and GTEx normal tissues. *p < 0.05; **p < 0.01; **p < 0.01; **p < 0.01;

expression in PAAD was markedly upregulated when an adequate number of normal tissues were used as controls. In summary, aberrant SQLE expression was observed in 22 types of human cancers, implying that SQLE has a tumorigenic function.

SQLE Is Associated With the Prognosis of Multiple Human Cancer

To further reveal the significance of SQLE in tumors, we performed survival analyses, including OS and DFS, in 33 types of human cancers. As shown in **Figure 2**, high SQLE expression predicted unfavorable OS in the following 11 cancer types: ACC (p = 0.02), BRCA (p = 0.041), CESC (p = 0.018), HNSC (p < 0.001), KIRP (p = 0.021), LUAD (p < 0.001), MESO (p = 0.016), PAAD (p = 0.0031), SARC (p < 0.001), THCA (p < 0.001), and UVM (p = 0.0026). Moreover, overexpression of SQLE was linked to poor DFS in ACC, BLCA, HNSC, LUSC, PAAD, SARC, and UVM (**Supplementary Figure S1**, p < 0.05). In other types of human cancers, there was no significant difference observed in SQLE expression between the high and low groups. Taken together, our results reveal that SQLE overexpression correlates with poor prognosis in patients with PAAD.

Analysis of SQLE Alterations in PAAD

To investigate the frequency and category of SQLE mutations in human cancers, we conducted a gene alteration analysis. The highest alteration frequency of SQLE (> 25%) was observed in patients with ovarian epithelial tumors, with "amplification" as the dominant type (Figure 3A). Significantly, more than 10% of SQLE alterations (including "amplification" and "mutation") were detected in PAAD patients (Figure 3A). Furthermore, we explored the location and number of SQLE alterations and found that the P85Lfs*25/E86* domain was detected in 4 cases, which was the most mutated location (Figure 3B). Additionally, the relationship between SQLE alterations and PAAD prognosis was demonstrated. Our results indicate that PAAD patients with SQLE alterations had worse OS (p = 2.603e-4), DSS (p = 0.0347), DFS (p = 1.021e-3), and PFS (p = 1.425e-3) than patients without SLQE alterations (Figures 3C-F). Together, SQLE alterations were frequently probed in PAAD and found associated with an unfavorable prognosis in patients with PAAD.

Analysis of Upstream miRNAs Regulating SQLE in PAAD

MicroRNAs (miRNAs) can bind to and regulate the expression of target genes. To identify the miRNAs that regulate SQLE expression, we analyzed the upstream miRNAs that could potentially target SQLE. We found 21 miRNAs that could be responsible for regulating SQLE expression in the pan-cancer analysis (**Table 1**). Next, we focused on these miRNAs in PAAD. As shown in **Figures 4A–C**, the expression of hsa-miR-194-5p, hsa-miR-363-3p, and hsa-miR-429 was different in the tumor and normal tissues, and therefore these miRNAs were confirmed as vital regulatory molecules (p < 0.05). High expression of these three miRNAs predicted favorable OS in PAAD (**Figures 4D–F**, p < 0.05). This phenomenon was not observed for the other 18 miRNAs in PAAD. It is well known that miRNAs negatively regulate their target genes (38). As presented in **Table 1**, SQLE expression showed a negative correlation with hsa-miR-363-3p but a positive correlation with hsa-miR-194-5p and hsa-miR-429 in PAAD. Thus, we hypothesized that hsa-miR-363-3p is an upstream miRNA of SQLE.

To explore the function of hsa-miR-363-3p in PAAD, we performed *in vitro* experiments using miR-363-3p mimic. Western blot results confirmed that both 50 nM and 100 nM mimics could effectively knock down the expression of SQLE in PANC-1 (**Figure 4G**). Subsequently, CCK8 results showed that the mimic could inhibit the proliferation ability of PANC-1 (**Figure 4H**). These results indicated that miR-363-3p could regulate the expression of SQLE and then inhibit cell proliferation in PAAD.

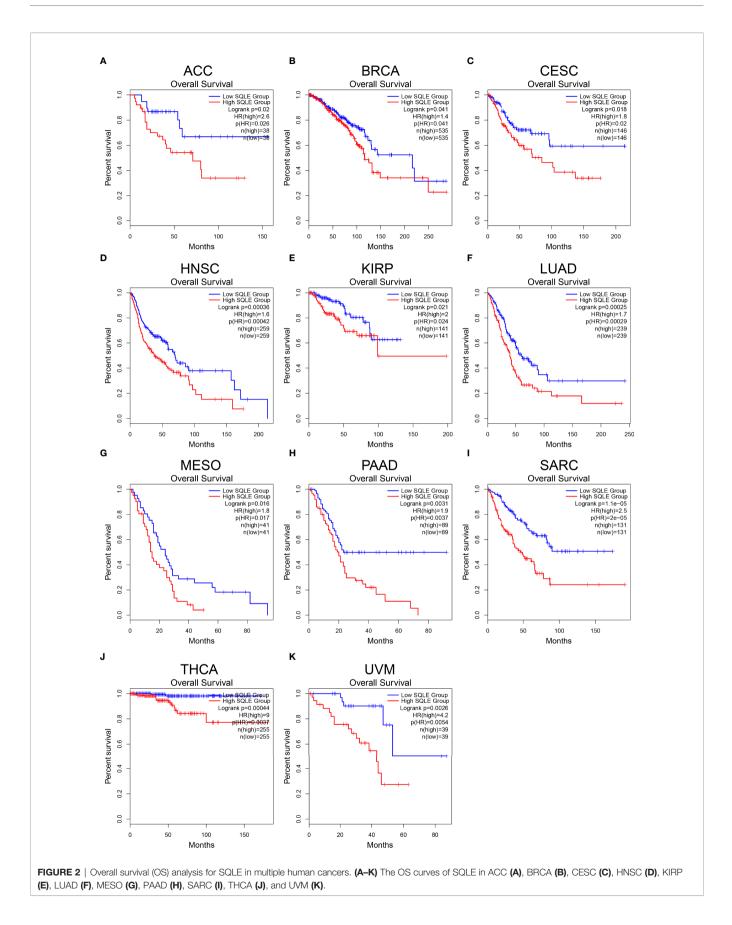
SQLE Expression Was Closely Related to Immune Cell Infiltration in PAAD

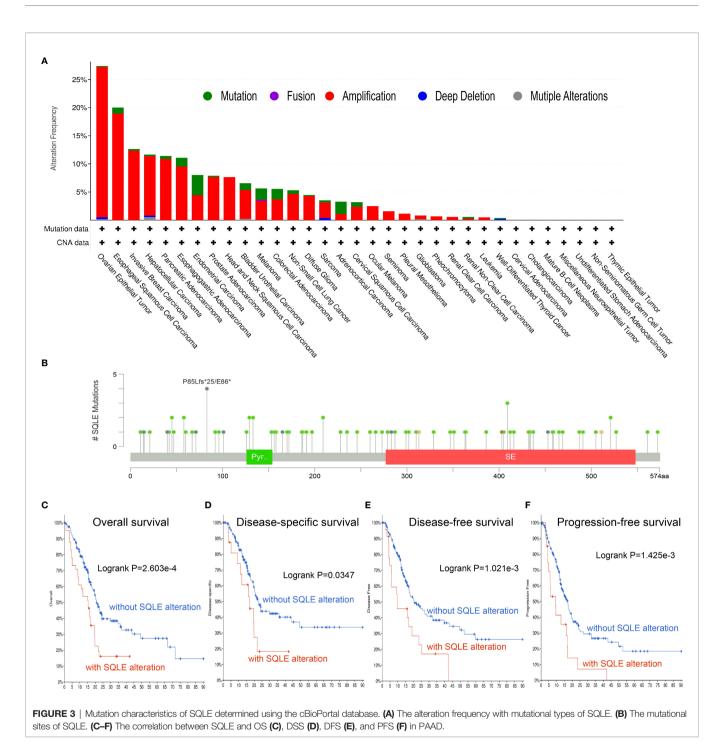
SQLE is a key enzyme in cholesterol metabolism and is involved in important lymphocyte functions (39, 40). Therefore, we explored the relationship between SQLE expression and immune cell infiltration in PAAD patients. The copy number of SQLE could affect the infiltration of B cells, CD8+ T cells, and CD4+ T cells (**Figure 5A**). In addition, SQLE expression was negatively correlated with CD4+ T cells (**Figure 5B**). In contrast, SQLE expression positively correlated with the infiltration of CD8+ T cells (**Figure 5C**) and neutrophils (**Figure 5D**). Our results also demonstrated that SQLE expression did not affect the infiltration of the other three types of immune cells: B cells, dendritic cells (DCs), and macrophages (**Figures 5E–G**).

Furthermore, these results were validated in 178 patients with PAAD from the TCGA cohort. Patients were divided into two groups according to the median expression level of SQLE. McP-Counter and EPIC methods were performed to validate the immune cell infiltration in 2 groups. The McP-Counter results showed that there were significant differences in T cell, CD8+ T cell, B cell, NK cell, DC, and endothelial cell (**Figure 5H**), which was consistent with EPIC results (**Figure 5I**). In conclusion, SQLE expression has a complex regulatory effect on immune cell infiltration in PAAD.

Correlation of SQLE With Biomarkers of Tumor Immune Microenvironment

To further investigate the relationship between SQLE and tumor immune biomarkers, we used the GEPIA and TISIDB databases. Our results showed that SQLE expression was significantly negatively correlated with PDCD1 (**Figure 6A**), LAG3 (**Figure 6C**), cytotoxic T-lymphocyte associated protein 4 (CTLA4, **Figure 6E**), and CD160 (**Figure 6G**)-all checkpoint inhibitors in the GEPIA database analysis. Our TISIDB database analysis confirmed these findings. SQLE expression was related to PDCD1 (**Figure 6B**, rho = -0.347, p < 0.01), LAG3 (**Figure 6D**, rho = -0.334, p < 0.01), CTLA4 (**Figure 6F**, rho = -0.241, p < 0.01), and CD160 (**Figure 6H**, rho = -0.447, p < 0.01). We performed further analyses to reveal the correlation among SQLE expression, copy number, methylation, and tumor immune features in PAAD,





including lymphocytes (**Supplementary Figure S2-A**), immunoinhibitors (**Supplementary Figure S2-B**), MHC molecules (**Supplementary Figure S2-C**), and immunostimulators (**Supplementary Figure S2-D**). Remarkably, the relationship between SQLE expression and tumor immune features was always contrary to the results of SQLE methylation (**Supplementary Figure S2**). Our results indicate that SQLE might function as a regulator of the immune microenvironment in PAAD.

Enrichment Analysis of SQLE

SQLE is a pivotal gene regulating cholesterol biosynthesis. Therefore, we performed an enrichment analysis of SQLE-related partners. A list of 50 SQLE-binding proteins was obtained from the STRING database. We constructed a network of 20 proteins that were most strongly associated (**Figure 7A**), and most of these proteins were involved in cholesterol metabolism. The top 100 genes related to SQLE expression pan-cancer were selected from the GEPIA2

TABLE 1 | The expression correlation between predicted miRNAs and SQLE in PAAD analyzed by starBase database.

Gene	miRNA	R-value	P-value
SQLE	hsa-miR-584-5p	0.187	1.24E-02*
SQLE	hsa-miR-194-5p	0.216	3.77E-03*
SQLE	hsa-miR-579-3p	-0.011	8.84E-01
SQLE	hsa-miR-664b-3p	-0.040	5.95E-01
SQLE	hsa-miR-205-5p	0.049	5.17E-01
SQLE	hsa-miR-367-3p	-0.040	5.98E-01
SQLE	hsa-miR-363-3p	-0.189	1.17E-02*
SQLE	hsa-miR-25-3p	0.068	3.67E-01
SQLE	hsa-miR-92a-3p	0.123	1.02E-01
SQLE	hsa-miR-32-5p	-0.012	8.76E-01
SQLE	hsa-miR-92b-3p	0.048	5.24E-01
SQLE	hsa-miR-429	0.190	1.10E-02*
SQLE	hsa-miR-371a-5p	-0.093	2.19E-01
SQLE	hsa-miR-200c-3p	0.072	3.37E-01
SQLE	hsa-miR-200b-3p	0.230	1.97E-03*
SQLE	hsa-miR-495-3p	0.012	8.76E-01
SQLE	hsa-miR-133b	-0.143	5.69E-02
SQLE	hsa-miR-381-3p	-0.011	8.80E-01
SQLE	hsa-miR-495-3p	0.012	8.76E-01
SQLE	hsa-miR-133a-3p	-0.179	1.67E-02*
SQLE	hsa-miR-1298-5p	0.167	2.54E-02*

*p value < 0.05.

database analysis. As presented in Figures 7B-F, SQLE expression level was positively correlated with ACAT2 (R = 0.53), HMGCR (R = 0.5), HMGCS1 (R = 0.56), IDI1 (R = 0.51), and LDLR (R = 0.49) genes (all p < 0.001). We obtained similar results for PAAD (Figures 7G-K, all p < 0.001). A combined analysis of the two datasets suggested three common molecules, namely, DHCR7, NSDHL, and MSMO1 (Figure 7L). Subsequently, we conducted KEGG and GO enrichment analyses. The results of the former showed that "metabolic pathways" and "steroid biosynthesis" were involved in the function of SQLE in carcinogenesis (Figure 7M). The results of the latter implied that these genes were related to oxidationreduction, cholesterol biosynthesis, iron ion binding, and oxidoreductase activity, among other reactions (Figure 7N). The annotations of the X-axis in Figure 7N are presented in Supplementary Table S1.

SQLE Is Associated With Immunotherapy Outcome of Cancer

TMB is a favorable predictor of immunotherapy. Our results suggest that SQLE alteration correlated with high TMB pancancer and in PAAD (**Figure 8A**, p < 0.001). We also analyzed the results of two clinical trials of anti-PD1 treatment in melanoma and found that SQLE expression was inversely associated with cytotoxic lymphocyte levels (CTLs), OS, and PFS in melanoma patients (**Figure 8B**, p < 0.05). Subsequently, we analyzed SQLE expression and its association with biomarkers of MHC (B2M, HLA-B, HLA-C, TAP1, and TAP2), dendritic cells (BATF3), macrophages (CD68 and IL1A), type-I anti-tumor responses (CD8A and GZMB), and cell proliferation (MKI67) in 178 PAAD tissues (**Figure 8C**). SQLE was positively associated with MHC molecules (B2M, r =0.221; HLA-B, r = 0.146; HLA-C, r = 0.143; TAP1, r = 0.187; and TAP2, r = 0.240), macrophages (CD68, r = 0.196 and IL1A, r = 0.275), and cell proliferation (MKI67, r = 0.380) but negatively associated with dendritic cells (BATF3, r = -0.181) and type-I anti-tumor responses (CD8A, r = -0.173 and GZMB, r = -0.171). Furthermore, our results showed that high SQLE expression indicated low CTL infiltration and poor OS in PAAD patients (**Figure 8D**, p < 0.05). These results suggest that high SQLE expression predicted depletion of cytotoxic lymphocytes and loss of anti-tumor ability, leading to unfavorable responses to immunotherapy.

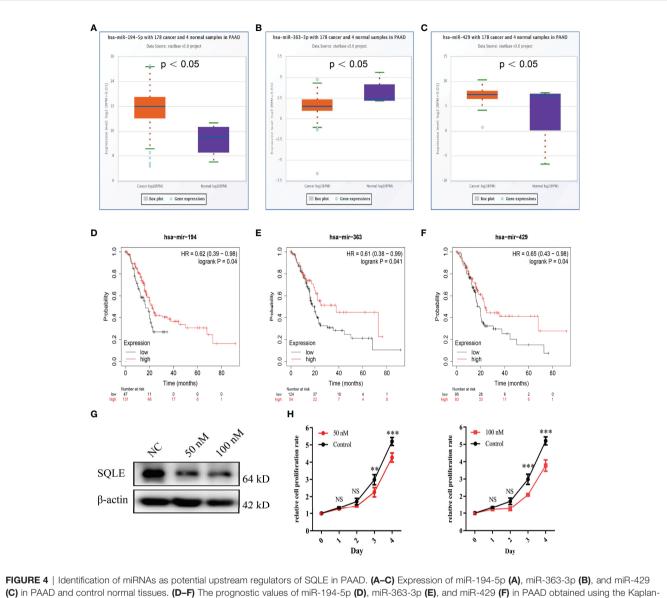
DISCUSSION

Presently, the prognosis of PAAD remains poor despite radical resection, mainly because of the lack of effective adjuvant therapy; therefore, the development of effective target biomarkers or promising drugs is urgently needed. Previous studies have demonstrated that SQLE promotes oncogenesis and metastasis in multiple human cancers by regulating cholesterol metabolism. However, a comprehensive understanding of SQLE in PAAD remained to be achieved.

In this study, we first performed pan-cancer analysis of SQLE expression and demonstrated that SQLE is highly expressed in PAAD. Survival and gene alteration analyses suggested that high expression and alteration of SQLE predicted the grim prognosis of PAAD, including OS, DFS, DSS, and PFS. miRNAs can modulate target gene expression through complex regulatory networks (41, 42). Therefore, it is essential to identify upstream miRNAs that participate in regulating SQLE expression. Twentyone miRNAs were identified as pivotal regulators of SQLE. Among them, miR-194-5p was considered to potentiate the survival of tumor-repopulating cells, leading to radiotherapy failure in PAAD (43). Interestingly, microRNA-205, as a tumor suppressor, could re-sensitize gemcitabine-resistant pancreatic cancer cells and reduce the proliferation of cancer stem cells and tumor growth in mouse models (44). In addition, miR-92a-3p promotes EMT progression and metastasis by inhibiting PTEN and activating Akt/Snail signaling in hepatocellular carcinoma (45). miR-429 can be inhibited by an X-inactive specific transcript and upregulate the expression of ZEB1 to promote migration and invasion in PAAD (46).

After a comprehensive analysis of these 21 miRNAs in PAAD, including expression and survival analyses, miR-363-3p was recognized as the most potential upstream regulator of SQLE. Reportedly, miR-363-3p may play a crucial role in the progression of ovarian cancer (47). However, the role and function of miR-363-3p in PAAD have not been previously reported. We therefore speculate that miR-363-3p is involved in the pathological processes of PAAD by regulating SQLE function.

Immune cell infiltration into the tumor microenvironment is closely related to the therapeutic efficiency and prognosis of multiple human cancers, including gastric cancer (48) and colorectal cancer (49–51). Different immune cell-infiltrating subsets in the PAAD microenvironment were considered as



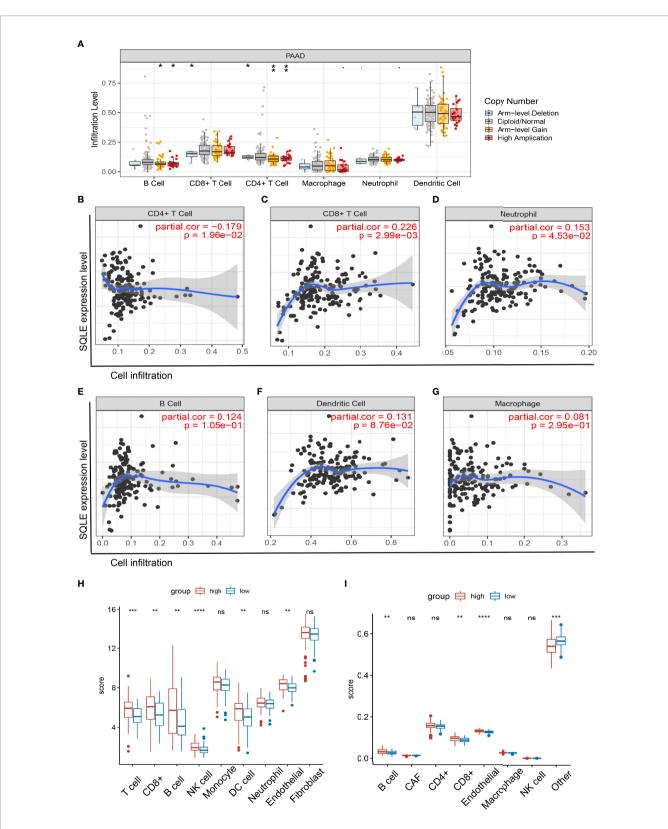
(C) in PAAD and control normal tissues. (D–F) The prognostic values of miR-194-5p (D), miR-363-3p (E), and miR-429 (F) in PAAD obtained using the Kaplan-Meier plotter. (G) The SQLE knockdown efficiency of 50 nM and 100 nM of miR-363-3p mimics on Day 2. (H) The effects of 50 nM and 100 nM of miR-363-3p mimics on *in vitro* proliferation in PANC-1. Two-way ANOVA test (n=3). **p value < 0.01; ***p value < 0.001; NS, no significance.

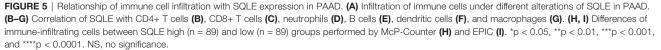
independent prognostic characteristic factors (52). Furthermore, single-cell transcriptomics of PAAD indicated substantial immunological heterogeneities and T cell infiltration differences in the microenvironment. (53, 54). Our results emphasized that SQLE expression is negatively correlated with the infiltration of CD4+ T cells and NK cells, whereas it is positively correlated with the infiltration of CD8+ T cells and neutrophils in PAAD. Our findings suggest that SQLE may regulate the immune microenvironment in PAAD.

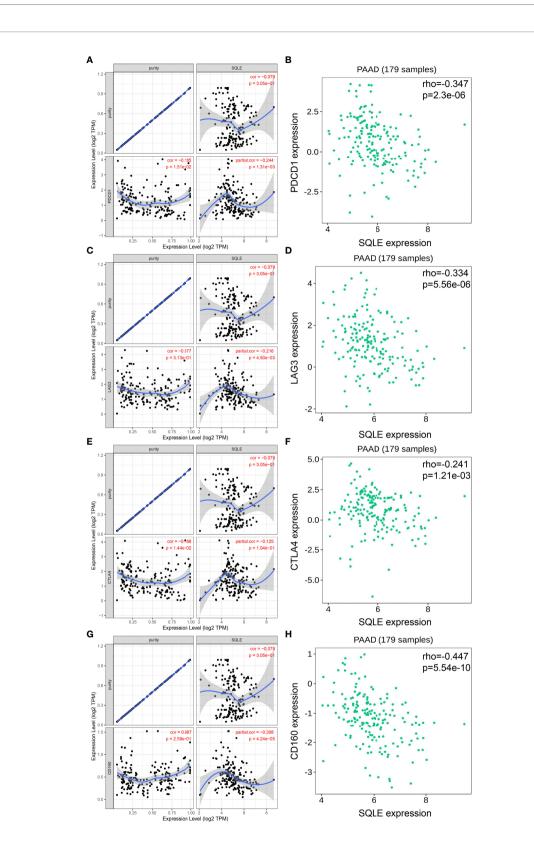
Immune checkpoint inhibitors comprise the most promising strategy for treating solid tumors (55), especially targeting PD-1 and CTLA4. However, the PD-1/PD-L1 blockade has proven to have limited effectiveness in PAAD (56). Therefore, we evaluated

the relationship between SQLE expression and tumor immune biomarkers to identify new therapeutic strategies. Our results showed that SQLE expression was negatively correlated with PDCD1, LAG3, CTLA4, and CD160 expression, suggesting that the combined application of the SQLE inhibitor terbinafine and immune checkpoint blockade may improve the efficacy of PAAD. Moreover, the relation between SQLE expression and tumor immune feature was always consistent with the copy number of SQLE, whereas contrary to the results of SQLE methylation. We hypothesized that the methylation may inhibit the expression of SQLE, and thus caused these results.

We hypothesized that SQLE regulates the immune microenvironment through metabolic pathways. Enrichment









241

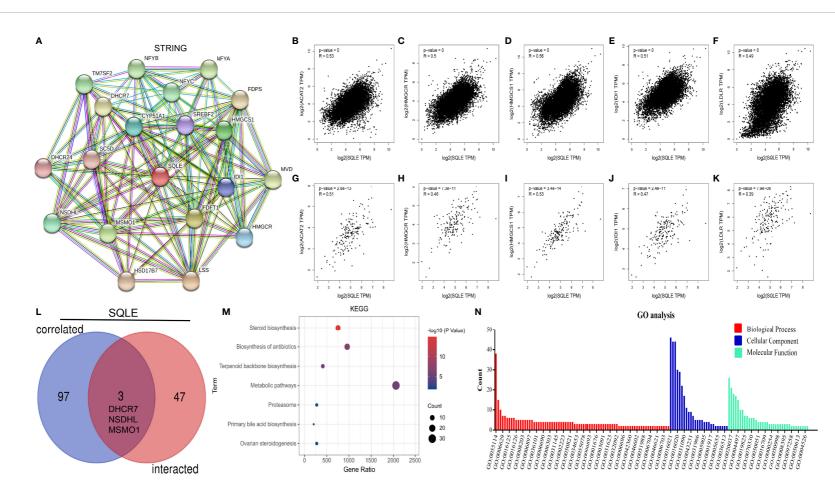
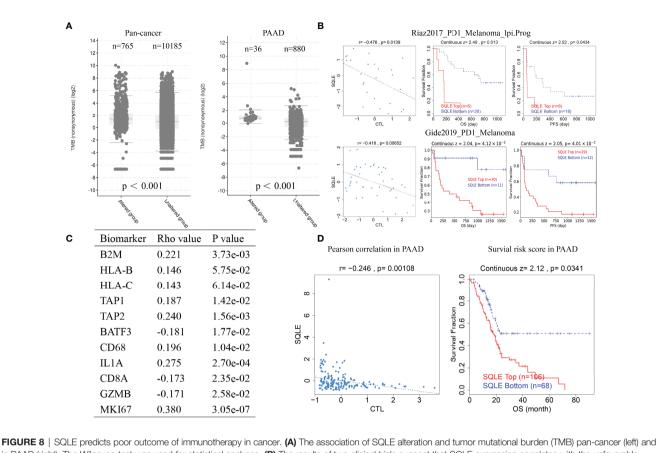


FIGURE 7 | SQLE-related gene enrichment analysis. (A) The top 20 SQLE-binding proteins using the STRING tool. (B–F) The expression correlation between SQLE and the targeting genes ACAT2 (B), HMGCR (C), HMGCS1 (D), IDI1 (E), and LDLR (F) in human cancers. (G–K) The expression correlation between SQLE and the targeting genes ACAT2 (G), HMGCR (H), HMGCS1 (I), IDI1 (J), and LDLR (K) in PAAD. (L) Interaction analysis of the SQLE-binding and related genes. (M) KEGG pathway analysis of the SQLE-binding and interacting genes. (N) GO analysis for the molecular function of the SQLE-binding and interacting genes.



in PAAD (right). The Wilcoxon test was used for statistical analyses. (B) The results of two clinical trials suggest that SQLE expression correlates with the unfavorable outcome of immunotherapy in melanoma. (C) Correlation between SQLE expression and biomarkers of MHC (B2M, HLA-B, HLA-C, TAP1, and TAP2), dendritic cells (BATF3), macrophages (CD68 and IL1A), type-I anti-tumor responses (CD8A and GZMB), and cell proliferation (MKI67) in 178 tumor tissues of PAAD. (D) SQLE correlates with the outcome of immunotherapy in PAAD.

analysis showed that SQLE-related partners are involved in cholesterol and lipid metabolism. KEGG and GO analyses suggested that "metabolic pathways" and "steroid biosynthesis" are associated with the function of SQLE in carcinogenesis. Yang et al. reported that cholesterol metabolism affects CD8+ T lymphocyte function (39). Cholesterol homeostasis is regulated by SCAP-SREBP2 and is essential for macrophage function (57). Moreover, statin use, by inhibiting cholesterol biosynthesis, could reduce mortality risk and improve survival of patients with PAAD (58). Finally, SQLE alteration was associated with high TMB, and its expression is negatively correlated with the infiltration of CTLs in melanoma and PAAD, leading to poor outcome of immunotherapy. Although the correlation between TMB and outcome of immunotherapy for PAAD has not been adequately elucidated, the lack of CTLs appears to underlie the ineffectiveness of immunotherapy in PAAD (59-61). Preclinical mouse models have suggested that increasing the infiltration of CTLs could improve the efficiency of checkpoint blockade in PAAD (62). In summary, our results indicate that SQLE influences the immune microenvironment and immunotherapy outcomes in patients with PAAD. Immunotherapy based on metabolic intervention may be a novel

approach in treating PAAD, and interdisciplinary combination therapy may help overcome the bottleneck of cancer treatment.

Taken together, we demonstrate that SQLE expression is upregulated in multiple types of human cancer (including PAAD) and negatively correlated with the prognosis of PAAD. We also report an upstream miRNA, miR-363-3p, as a key regulator of SQLE expression in PAAD. SQLE could regulate the infiltration of tumor immune cells and the expression of immune checkpoints. SQLE plays a crucial role in cholesterol metabolism, and high SQLE expression is associated with poor immunotherapy outcomes. SQLE blockade may improve the efficiency of PAAD immunotherapy. Nevertheless, these results should be validated through additional wet experiments and clinical trials in the future.

DATA AVAILABILITY STATEMENT

The datasets presented in this study can be found in online repositories. The names of the repository/repositories and accession number(s) can be found in the article/**Supplementary Material**.

AUTHOR CONTRIBUTIONS

XW designed this study. WY, YC, ZC, Z-pH, and PH performed bioinformatic analyses. WY performed the wet experiments and wrote the manuscript. JK revised the manuscript. All authors have read the final version of this manuscript.

FUNDING

This study was supported by the National Key R&D Program of China (No. 2017YFC1308800), National Key Clinical Discipline, National Natural Science Foundation of China (No. 81972212, No. 82003197), Guangdong Natural Science Foundation (No. 2019A1515010063), Science and Technology Planning Project of Guangdong Province, China (No. 2021A0505030028), Science and Technology Planning Project of Guangzhou City (No. 202102020186), the program of Guangdong Provincial Clinical Research Center for Digestive Diseases (2020B1111170004), Postdoctoral Fund project of The Sixth Affiliated Hospital, Sun Yat-sen University (No. R20210217202102987), and Youth Fund

REFERENCES

- 1. Mizrahi JD, Surana R, Valle JW, Shroff RT. Pancreatic Cancer. Lancet (2020) 395(10242):2008–20. doi: 10.1016/s0140-6736(20)30974-0
- Siegel RL, Miller KD, Jemal A. Cancer Statistics 2020. CA Cancer J Clin (2020) 70(1):7–30. doi: 10.3322/caac.21590
- Bray F, Ferlay J, Soerjomataram I, Siegel RL, Torre LA, Jemal A. Global Cancer Statistics 2018: GLOBOCAN Estimates of Incidence and Mortality Worldwide for 36 Cancers in 185 Countries. *CA Cancer J Clin* (2018) 68 (6):394–424. doi: 10.3322/caac.21492
- Winter JM, Cameron JL, Campbell KA, Arnold MA, Chang DC, Coleman J, et al. 1423 Pancreaticoduodenectomies for Pancreatic Cancer: A Single-Institution Experience. J Gastrointest Surg (2006) 10(9):1199–210. doi: 10.1016/j.gassur.2006.08.018
- Zhou B, Xu JW, Cheng YG, Gao JY, Hu SY, Wang L, et al. Early Detection of Pancreatic Cancer: Where Are We Now and Where Are We Going? *Int J Cancer* (2017) 141(2):231–41. doi: 10.1002/ijc.30670
- Hessmann E, Buchholz SM, Demir IE, Singh SK, Gress TM, Ellenrieder V, et al. Microenvironmental Determinants of Pancreatic Cancer. *Physiol Rev* (2020) 100(4):1707–51. doi: 10.1152/physrev.00042.2019
- Grossberg AJ, Chu LC, Deig CR, Fishman EK, Hwang WL, Maitra A, et al. Multidisciplinary Standards of Care and Recent Progress in Pancreatic Ductal Adenocarcinoma. *CA Cancer J Clin* (2020) 70(5):375–403. doi: 10.3322/caac. 21626
- Zhang X, Huang X, Xu J, Li E, Lao M, Tang T, et al. NEK2 Inhibition Triggers Anti-Pancreatic Cancer Immunity by Targeting PD-L1. *Nat Commun* (2021) 12(1):4536. doi: 10.1038/s41467-021-24769-3
- Rizzo A, Dadduzio V, Ricci AD, Massari F, Di Federico A, Gadaleta-Caldarola G, et al. Lenvatinib Plus Pembrolizumab: The Next Frontier for the Treatment of Hepatocellular Carcinoma? *Expert Opin Investig Drugs* (2021) 31(4):371–8. doi: 10.1080/13543784.2021.1948532
- Rizzo A, Brandi G. Biochemical Predictors of Response to Immune Checkpoint Inhibitors in Unresectable Hepatocellular Carcinoma. *Cancer Treat Res Commun* (2021) 27:100328. doi: 10.1016/j.ctarc.2021.100328
- Rizzo A, Ricci AD, Brandi G. Recent Advances of Immunotherapy for Biliary Tract Cancer. *Expert Rev Gastroenterol Hepatol* (2021) 15(5):527–36. doi: 10.1080/17474124.2021.1853527
- Espinosa G, Lopez-Montero I, Monroy F, Langevin D. Shear Rheology of Lipid Monolayers and Insights on Membrane Fluidity. *Proc Natl Acad Sci* USA (2011) 108(15):6008–13. doi: 10.1073/pnas.1018572108

for Basic and Applied Basic Research of Guangdong Province (No. 2021A1515111128).

ACKNOWLEDGMENTS

The authors would like to express our sincere gratitude to the reviewers and appreciation for the language editing services provided by ELSEVIER.

SUPPLEMENTARY MATERIAL

The Supplementary Material for this article can be found online at: https://www.frontiersin.org/articles/10.3389/fimmu.2022. 864244/full#supplementary-material

Supplementary Figure 1 | Disease-free survival (DFS) analysis for SQLE in multiple human cancers. (A–G) DFS curves of SQLE in ACC (A), BLCA (B), HNSC (C), LUSC (D), PAAD (E), SARC (F), and UVM (G).

Supplementary Figure 2 | SQLE expression, copy number, and methylation are associated with tumor immune features. (A–D) Correlation of SQLE with lymphocyte (A), immuno-inhibitor (B), MHC molecule (C), and immunostimulator (D).

- Mullen PJ, Yu R, Longo J, Archer MC, Penn LZ. The Interplay Between Cell Signalling and the Mevalonate Pathway in Cancer. *Nat Rev Cancer* (2016) 16 (11):718–31. doi: 10.1038/nrc.2016.76
- Gobel A, Rauner M, Hofbauer LC, Rachner TD. Cholesterol and Beyond -The Role of the Mevalonate Pathway in Cancer Biology. *Biochim Biophys Acta Rev Cancer* (2020) 1873(2):188351. doi: 10.1016/j.bbcan.2020. 188351
- Xu H, Zhou S, Tang Q, Xia H, Bi F. Cholesterol Metabolism: New Functions and Therapeutic Approaches in Cancer. *Biochim Biophys Acta* (*BBA*) - *Rev Cancer* (2020) 1874(1):188394. doi: 10.1016/j.bbcan.2020. 188394
- Gill S, Stevenson J, Kristiana I, Brown AJ. Cholesterol-Dependent Degradation of Squalene Monooxygenase, a Control Point in Cholesterol Synthesis Beyond HMG-CoA Reductase. *Cell Metab* (2011) 13(3):260–73. doi: 10.1016/j.cmet.2011.01.015
- Cerqueira NM, Oliveira EF, Gesto DS, Santos-Martins D, Moreira C, Moorthy HN, et al. Cholesterol Biosynthesis: A Mechanistic Overview. *Biochemistry* (2016) 55(39):5483–506. doi: 10.1021/acs.biochem.6b00342
- Liu D, Wong CC, Zhou Y, Li C, Chen H, Ji F, et al. Squalene Epoxidase Induces Nonalcoholic Steatohepatitis *Via* Binding to Carbonic Anhydrase III and is a Therapeutic Target. *Gastroenterology* (2021) 160(7):2467–2482.e2463. doi: 10.1053/j.gastro.2021.02.051
- Qin Y, Hou Y, Liu S, Zhu P, Wan X, Zhao M, et al. A Novel Long Non-Coding RNA Lnc030 Maintains Breast Cancer Stem Cell Stemness by Stabilizing SQLE mRNA and Increasing Cholesterol Synthesis. *Adv Sci (Weinh)* (2021) 8 (2):2002232. doi: 10.1002/advs.202002232
- Liu D, Wong CC, Fu L, Chen H, Zhao L, Li C, et al. Squalene Epoxidase Drives NAFLD-Induced Hepatocellular Carcinoma and Is a Pharmaceutical Target. *Sci Transl Med* (2018) 10(437). doi: 10.1126/scitranslmed.aap9840
- Qin Y, Zhang Y, Tang Q, Jin L, Chen Y. SQLE Induces Epithelial-to-Mesenchymal Transition by Regulating of miR-133b in Esophageal Squamous Cell Carcinoma. Acta Biochim Biophys Sin (Shanghai) (2017) 49 (2):138–48. doi: 10.1093/abbs/gmw127
- Stopsack KH, Gerke TA, Sinnott JA, Penney KL, Tyekucheva S, Sesso HD, et al. Cholesterol Metabolism and Prostate Cancer Lethality. *Cancer Res* (2016) 76(16):4785–90. doi: 10.1158/0008-5472.Can-16-0903
- He L, Li H, Pan C, Hua Y, Peng J, Zhou Z, et al. Squalene Epoxidase Promotes Colorectal Cancer Cell Proliferation Through Accumulating Calcitriol and Activating CYP24A1-Mediated MAPK Signaling. *Cancer Commun (Lond)* (2021) 41(8):726–46. doi: 10.1002/cac2.12187

- Zhang HY, Li HM, Yu Z, Yu XY, Guo K. Expression and Significance of Squalene Epoxidase in Squamous Lung Cancerous Tissues and Pericarcinoma Tissues. *Thorac Cancer* (2014) 5(4):275–80. doi: 10.1111/1759-7714.12087
- Feltrin S, Ravera F, Traversone N, Ferrando L, Bedognetti D, Ballestrero A, et al. Sterol Synthesis Pathway Inhibition as a Target for Cancer Treatment. *Cancer Lett* (2020) 493:19–30. doi: 10.1016/j.canlet.2020.07.010
- 26. Karasinska JM, Topham JT, Kalloger SE, Jang GH, Denroche RE, Culibrk L, et al. Altered Gene Expression Along the Glycolysis–Cholesterol Synthesis Axis Is Associated With Outcome in Pancreatic Cancer. *Clin Cancer Res* (2020) 26(1):135–46. doi: 10.1158/1078-0432.Ccr-19-1543
- Li T, Fan J, Wang B, Traugh N, Chen Q, Liu JS, et al. TIMER: A Web Server for Comprehensive Analysis of Tumor-Infiltrating Immune Cells. *Cancer Res* (2017) 77(21):e108–10. doi: 10.1158/0008-5472.CAN-17-0307
- Li T, Fu J, Zeng Z, Cohen D, Li J, Chen Q, et al. TIMER2.0 for Analysis of Tumor-Infiltrating Immune Cells. *Nucleic Acids Res* (2020) 48(W1):W509– 14. doi: 10.1093/nar/gkaa407
- 29. Racle J, de Jonge K, Baumgaertner P, Speiser DE, Gfeller D. Simultaneous Enumeration of Cancer and Immune Cell Types From Bulk Tumor Gene Expression Data. *Elife* (2017) 6:e26476. doi: 10.7554/eLife.26476
- Becht E, Giraldo NA, Lacroix L, Buttard B, Elarouci N, Petitprez F, et al. Estimating the Population Abundance of Tissue-Infiltrating Immune and Stromal Cell Populations Using Gene Expression. *Genome Biol* (2016) 17 (1):218. doi: 10.1186/s13059-016-1070-5
- Tang Z, Li C, Kang B, Gao G, Li C, Zhang Z. GEPIA: A Web Server for Cancer and Normal Gene Expression Profiling and Interactive Analyses. *Nucleic Acids Res* (2017) 45(W1):W98–102. doi: 10.1093/nar/gkx247
- Li JH, Liu S, Zhou H, Qu LH, Yang JH. Starbase V2.0: Decoding miRNA-ceRNA, miRNA-ncRNA and Protein-RNA Interaction Networks From Large-Scale CLIP-Seq Data. Nucleic Acids Res (2014) 42:D92–7. doi: 10.1093/nar/gkt1248
- Nagy A, Munkacsy G, Gyorffy B. Pancancer Survival Analysis of Cancer Hallmark Genes. Sci Rep (2021) 11(1):6047. doi: 10.1038/s41598-021-84787-5
- Cerami E, Gao J, Dogrusoz U, Gross BE, Sumer SO, Aksoy BA, et al. The Cbio Cancer Genomics Portal: An Open Platform for Exploring Multidimensional Cancer Genomics Data. *Cancer Discov* (2012) 2(5):401–4. doi: 10.1158/2159-8290.CD-12-0095
- 35. Gao J, Aksoy BA, Dogrusoz U, Dresdner G, Gross B, Sumer SO, et al. Integrative Analysis of Complex Cancer Genomics and Clinical Profiles Using the Cbioportal. *Sci Signal* (2013) 6(269):11. doi: 10.1126/scisignal. 2004088
- Ru B, Wong CN, Tong Y, Zhong JY, Zhong SSW, Wu WC, et al. TISIDB: An Integrated Repository Portal for Tumor-Immune System Interactions. *Bioinformatics* (2019) 35(20):4200–2. doi: 10.1093/bioinformatics/btz210
- Szklarczyk D, Gable AL, Nastou KC, Lyon D, Kirsch R, Pyysalo S, et al. The STRING Database in 2021: Customizable Protein-Protein Networks, and Functional Characterization of User-Uploaded Gene/Measurement Sets. *Nucleic Acids Res* (2021) 49(D1):D605–12. doi: 10.1093/nar/gkaa1074
- Peng F, Fan H, Li S, Peng C, Pan X. MicroRNAs in Epithelial-Mesenchymal Transition Process of Cancer: Potential Targets for Chemotherapy. *Int J Mol Sci* (2021) 22(14):7526. doi: 10.3390/ijms22147526
- 39. Yang W, Bai Y, Xiong Y, Zhang J, Chen S, Zheng X, et al. Potentiating the Antitumour Response of CD8(+) T Cells by Modulating Cholesterol Metabolism. *Nature* (2016) 531(7596):651–5. doi: 10.1038/nature17412
- Baek AE, Yu YA, He S, Wardell SE, Chang CY, Kwon S, et al. The Cholesterol Metabolite 27 Hydroxycholesterol Facilitates Breast Cancer Metastasis Through its Actions on Immune Cells. *Nat Commun* (2017) 8(1):864. doi: 10.1038/s41467-017-00910-z
- Gao S, Ding B, Lou W. microRNA-Dependent Modulation of Genes Contributes to ESR1's Effect on ERalpha Positive Breast Cancer. Front Oncol (2020) 10:753. doi: 10.3389/fonc.2020.00753
- Lou W, Ding B, Wang J, Xu Y. The Involvement of the Hsa_Circ_0088494miR-876-3p-CTNNB1/CCND1 Axis in Carcinogenesis and Progression of Papillary Thyroid Carcinoma. *Front Cell Dev Biol* (2020) 8:605940. doi: 10.3389/fcell.2020.605940
- Jiang MJ, Chen YY, Dai JJ, Gu DN, Mei Z, Liu FR, et al. Dying Tumor Cell-Derived Exosomal miR-194-5p Potentiates Survival and Repopulation of Tumor Repopulating Cells Upon Radiotherapy in Pancreatic Cancer. *Mol Cancer* (2020) 19(1):68. doi: 10.1186/s12943-020-01178-6

- 44. Chaudhary AK, Mondal G, Kumar V, Kattel K, Mahato RI. Chemosensitization and Inhibition of Pancreatic Cancer Stem Cell Proliferation by Overexpression of microRNA-205. *Cancer Lett* (2017) 402:1–8. doi: 10.1016/j.canlet.2017.05.007
- 45. Yang B, Feng X, Liu H, Tong R, Wu J, Li C, et al. High-Metastatic Cancer Cells Derived Exosomal Mir92a-3p Promotes Epithelial-Mesenchymal Transition and Metastasis of Low-Metastatic Cancer Cells by Regulating PTEN/Akt Pathway in Hepatocellular Carcinoma. *Oncogene* (2020) 39(42):6529–43. doi: 10.1038/s41388-020-01450-5
- 46. Shen J, Hong L, Yu D, Cao T, Zhou Z, He S. LncRNA XIST Promotes Pancreatic Cancer Migration, Invasion and EMT by Sponging miR-429 to Modulate ZEB1 Expression. *Int J Biochem Cell Biol* (2019) 113:17–26. doi: 10.1016/j.biocel.2019.05.021
- Lou W, Ding B, Zhong G, Du C, Fan W, Fu P. Dysregulation of Pseudogene/ lncRNA-hsa-miR-363-3p-SPOCK2 Pathway Fuels Stage Progression of Ovarian Cancer. Aging (Albany NY) (2019) 11(23):11416–39. doi: 10.18632/aging.102538
- Zhang H, Liu H, Shen ZB, Lin C, Wang XF, Qin J, et al. Tumor-Infiltrating Neutrophils is Prognostic and Predictive for Postoperative Adjuvant Chemotherapy Benefit in Patients With Gastric Cancer. Ann Surg (2018) 267(2):311–8. doi: 10.1097/Sla.00000000002058
- Waniczek D, Lorenc Z, Snietura M, Wesecki M, Kopec A, Muc-Wierzgon M. Tumor-Associated Macrophages and Regulatory T Cells Infiltration and the Clinical Outcome in Colorectal Cancer. Arch Immunol Ther Exp (Warsz) (2017) 65(5):445–54. doi: 10.1007/s00005-017-0463-9
- Pagès F, Mlecnik B, Marliot F, Bindea G, Ou F-S, Bifulco C, et al. International Validation of the Consensus Immunoscore for the Classification of Colon Cancer: A Prognostic and Accuracy Study. *Lancet* (2018) 391(10135):2128– 39. doi: 10.1016/s0140-6736(18)30789-x
- Zhang L, Yu X, Zheng L, Zhang Y, Li Y, Fang Q, et al. Lineage Tracking Reveals Dynamic Relationships of T Cells in Colorectal Cancer. *Nature* (2018) 564(7735):268–72. doi: 10.1038/s41586-018-0694-x
- Ino Y, Yamazaki-Itoh R, Shimada K, Iwasaki M, Kosuge T, Kanai Y, et al. Immune Cell Infiltration as an Indicator of the Immune Microenvironment of Pancreatic Cancer. Br J Cancer (2013) 108(4):914–23. doi: 10.1038/bjc.2013.32
- 53. Bernard V, Semaan A, Huang J, San Lucas FA, Mulu FC, Stephens BM, et al. Single-Cell Transcriptomics of Pancreatic Cancer Precursors Demonstrates Epithelial and Microenvironmental Heterogeneity as an Early Event in Neoplastic Progression. *Clin Cancer Res* (2019) 25(7):2194–205. doi: 10.1158/1078-0432.CCR-18-1955
- 54. Lin W, Noel P, Borazanci EH, Lee J, Amini A, Han IW, et al. Single-Cell Transcriptome Analysis of Tumor and Stromal Compartments of Pancreatic Ductal Adenocarcinoma Primary Tumors and Metastatic Lesions. *Genome Med* (2020) 12(1):80. doi: 10.1186/s13073-020-00776-9
- Rotte A. Combination of CTLA-4 and PD-1 Blockers for Treatment of Cancer. J Exp Clin Cancer Res (2019) 38(1):255. doi: 10.1186/s13046-019-1259-z
- Paz-Ares L, Dvorkin M, Chen Y, Reinmuth N, Hotta K, Trukhin D, et al. Durvalumab Plus Platinum–Etoposide Versus Platinum–Etoposide in First-Line Treatment of Extensive-Stage Small-Cell Lung Cancer (CASPIAN): A Randomised, Controlled, Open-Label, Phase 3 Trial. *Lancet* (2019) 394 (10212):1929–39. doi: 10.1016/s0140-6736(19)32222-6
- Guo C, Chi Z, Jiang D, Xu T, Yu W, Wang Z, et al. Cholesterol Homeostatic Regulator SCAP-SREBP2 Integrates NLRP3 Inflammasome Activation and Cholesterol Biosynthetic Signaling in Macrophages. *Immunity* (2018) 49 (5):842–856.e847. doi: 10.1016/j.immuni.2018.08.021
- Huang BZ, Chang JI, Li E, Xiang AH, Wu BU. Influence of Statins and Cholesterol on Mortality Among Patients With Pancreatic Cancer. J Natl Cancer Inst (2017) 109(5). doi: 10.1093/jnci/djw275
- Morrison AH, Byrne KT, Vonderheide RH. Immunotherapy and Prevention of Pancreatic Cancer. *Trends Cancer* (2018) 4(6):418–28. doi: 10.1016/ j.trecan.2018.04.001
- Balachandran VP, Beatty GL, Dougan SK. Broadening the Impact of Immunotherapy to Pancreatic Cancer: Challenges and Opportunities. *Gastroenterology* (2019) 156(7):2056–72. doi: 10.1053/j.gastro.2018.12.038
- Bear AS, Vonderheide RH, O'Hara MH. Challenges and Opportunities for Pancreatic Cancer Immunotherapy. *Cancer Cell* (2020) 38(6):788–802. doi: 10.1016/j.ccell.2020.08.004
- 62. Winograd R, Byrne KT, Evans RA, Odorizzi PM, Meyer AR, Bajor DL, et al. Induction of T-Cell Immunity Overcomes Complete Resistance to PD-1 and

CTLA-4 Blockade and Improves Survival in Pancreatic Carcinoma. *Cancer Immunol Res* (2015) 3(4):399–411. doi: 10.1158/2326-6066.CIR-14-0215

Conflict of Interest: The authors declare that the research was conducted in the absence of any commercial or financial relationships that could be construed as a potential conflict of interest.

Publisher's Note: All claims expressed in this article are solely those of the authors and do not necessarily represent those of their affiliated organizations, or those of the publisher, the editors and the reviewers. Any product that may be evaluated in this article, or claim that may be made by its manufacturer, is not guaranteed or endorsed by the publisher.

Copyright © 2022 You, Ke, Chen, Cai, Huang, Hu and Wu. This is an open-access article distributed under the terms of the Creative Commons Attribution License (CC BY). The use, distribution or reproduction in other forums is permitted, provided the original author(s) and the copyright owner(s) are credited and that the original publication in this journal is cited, in accordance with accepted academic practice. No use, distribution or reproduction is permitted which does not comply with these terms.



Combination of Radiofrequency Ablation With Resiquimod to Treat Hepatocellular Carcinoma *Via* Inflammation of Tumor Immune Microenvironment and Suppression of Angiogenesis

Zhou Tian¹, Baojian Hong², Jianzhong Chen^{3,4*} and Zhe Tang^{1,5*}

¹ Department of Surgery, The Fourth Affiliated Hospital, International Institutes of Medicine, Zhejiang University School of Medicine, Yiwu, China, ² Laboratory Medicine Center, Department of Clinical Laboratory, Zhejiang Provincial People's Hospital (Affiliated People's Hospital, Hangzhou Medical College), Hangzhou, China, ³ Institute of Immunology School of Medicine, Zhejiang University, Hangzhou, China, ⁴ Key Laboratory of Immunity and Inflammatory Diseases of Zhejiang Province, Hangzhou, China, ⁵ Department of Surgery, The Second Affiliated Hospital, Zhejiang University School of Medicine, Hangzhou, China

OPEN ACCESS

Edited by:

Xian Zeng, Fudan University, China

Reviewed by:

Marieke F. Fransen, Academic Medical Center, Netherlands Jian Kong, Capital Medical University, China

*Correspondence:

Jianzhong Chen chenjianzhong@zju.edu.cn Zhe Tang 8xi@zju.edu.cn

Specialty section:

This article was submitted to Cancer Immunity and Immunotherapy, a section of the journal Frontiers in Oncology

Received: 08 March 2022 Accepted: 22 April 2022 Published: 02 June 2022

Citation:

Tian Z, Hong J, Chen J and Tang Z (2022) Combination of Radiofrequency Ablation With Resiquimod to Treat Hepatocellular Carcinoma Via Inflammation of Tumor Immune Microenvironment and Suppression of Angiogenesis. Front. Oncol. 12:891724. doi: 10.3389/fonc.2022.891724 **Background:** Radiofrequency ablation (RFA) destroys tumors through hyperthermic injury, which induces the release of immunogenic intracellular substrates and damages associated molecular patterns (DAMPs) to evoke a systemic immune response, but its therapeutic effect is limited. This study aimed to combine RFA with an immunomodulator, resiguimod (R848), to enhance the RFA-induced antitumor immunity.

Methods: We performed RFA on subcutaneous tumors in immunocompetent mice and intraperitoneally injected R848 to observe the efficacy of the combination therapy. Our research investigated changes in the composition of tumor-infiltrating immune cells in primary and distant tumors by flow cytometry. Natural killer (NK) cell depletion experiment was applied to confirm the role of NK cell in the combination therapy. The expression levels of cytokines and chemokines were detected by real-time quantitative PCR. Immunohistochemical test was conducted to reveal tumor angiogenesis, tumor proliferation, and apoptosis after the different treatments.

Results and Conclusion: Compared with RFA or R848 monotherapy, the combination therapy significantly slowed the tumor growth, prolonged the survival time, and shrank the tumor-draining lymph nodes of tumor-bearing mice. The flow cytometry results showed that tumor-infiltrating immune cells, total T cells, the ratio of CD8⁺ T and NK cells to CD45⁺ cells, and functional NK cells were obviously increased after the combined treatment. Distal tumor growth was also suppressed, and the profile of tumor-infiltrating immune cells was remodeled, too. In addition, the additive effect of the combination therapy disappeared after NK cell depletion. Furthermore, immunohistochemical results verified that R848 inhibited tumor angiogenesis in murine liver cancer, and the combination therapy promoted tumor cell apoptosis. In conclusion, our data suggest that RFA

combined with R848 stimulated a stronger antitumor immune response and effectively inhibited liver cancer progression in a NK cell-dependent manner. Meanwhile, we confirmed that R848 inhibited tumor angiogenesis and promoted apoptosis in murine liver cancer. Overall, this is a promising therapeutic strategy to improve the efficacy of RFA in the treatment of liver cancer and provides a novel option for combined thermal ablation and immunotherapy.

Keywords: radiofrequency ablation, resiquimod, liver cancer, immune response, combination therapy

INTRODUCTION

Hepatocellular carcinoma (HCC) is one of the most common malignant tumors worldwide and the fourth leading cause of cancer-related deaths (1-3). East Asia and Africa are currently the regions with the highest incidence and mortality of HCC. The incidence and mortality of HCC in Europe and the United States have also been increasing in recent years (4, 5). At present, liver transplantation, surgical resection, and local ablation are the three major treatments for HCC (4, 6). However, the occult onset of HCC and the scarcity of donor livers severely limit the clinical application of surgical resection and liver transplantation (7-9). Local ablation therapy is especially suitable for these patients who are not suitable for surgery, and it is estimated that more than half of HCC patients have received local ablation therapy during their lifetime (10).

Radiofrequency ablation (RFA) is the most commonly used local ablation technique for HCC (11), and several studies have shown that RFA can achieve a similar therapeutic effect as surgical resection in the treatment of small HCC (single nodules ≤ 2 to 3 cm) (12–15). Interestingly, RFA induces tumor tissue coagulation necrosis and apoptosis, which lead to the release of immunogenic intracellular substrates to stimulate local anti-tumor immunity (16-20). Nevertheless, for a large tumor or a tumor located close to large blood vessels, RFA cannot completely destroy the tumor (incomplete ablation), and the residual tumor results in the recurrence and distant metastasis of HCC in the future (10, 21, 22). Therefore, it is clear that the anti-tumor immunity elicited by RFA monotherapy is too weak to effectively inhibit tumor recurrence and distant metastasis. In recent years, the combination of local ablation and immunotherapy for liver cancer is considered as a promising approach to boost RFA-induced immune response. Clinical trials of thermal ablation combined with immunotherapy, such as anti-PD1/anti-PDL1/anti-CTLA4 antibody, in the treatment of liver cancer have been widely carried out. Patients who received combination therapy had different degrees of improvement in overall survival or progression-free survival (23).

Resiquimod (R848) is a novel immunomodulatory agent which binds to Toll-like receptor7/8 and stimulates the release of various immunoregulatory cytokines, such as IFN- α , IL-6, and TNF- α , through MyD88-dependent or MyD88-independent pathways, thereby activating a cascade of signaling pathways to induce innate and adaptive immune response (24–26). Although R848 was originally used to study the role of antiviral and antibacterial immunity and the research on tumor has only started in recent years, several studies have shown that R848 significantly increases the number and function of CD8⁺ T cell and inflames the tumor immune microenvironment (TIME) (27–29). In addition, R848 has been used as an adjuvant in combination with anti-PD1/PDL1 antibody to treat colon cancer (30) and squamous cell carcinoma (31, 32) and achieved great therapeutic effects.

Here we demonstrated that the combined treatment of RFA and R848 not only ignited the TIME compared with RFA monotherapy but also increased the number and function of NK cell and CD8⁺ T cell and boosted the expression levels of multiple proinflammatory cytokines and NK cell-related chemokines in tumors. Meanwhile, we found that the combination therapy significantly inhibited HCC angiogenesis and proliferation but promoted tumor apoptosis (**Schematic Illustration**).

MATERIALS AND METHODS

Cell Lines and Mice

Murine liver cancer cell line hepa1-6 was purchased from the cell bank of Chinese Academy of Sciences (Shanghai, China). The cells were cultured in Dulbecco's modified Eagle's medium (DMEM) containing 10% fetal bovine serum and 1% penicillin–streptomycin at 37°C and 5% CO₂. The cells were digested for subsequent use when they reached 70% density.

Six- to 8-week-old male C57BL/6 mice were obtained from Shanghai SLAC Laboratory Animal Co. Ltd. Hepa1-6 cells (4 × 10^6) were resuspended in 100 ul phosphate-buffered saline (PBS) and were subcutaneously injected into the right flank of C57BL/6 mice. In the abscopal effect assay, hepa1-6 tumor cells (3 × 10^6) were simultaneously inoculated into the bilateral flanks of the mice. Tumor progression was measured with a vernier caliper. Tumor volume was calculated with the following formula: (length × width²)/2. At about 1 week later, the tumor-bearing mice were randomly divided into four groups to receive different treatments. All animal experiments followed relevant experimental animal ethic requirements and were approved by the Laboratory Animal Welfare Ethics Review Committee of Zhejiang University.

Radiofrequency Ablation Therapy

For the radiofrequency ablation (RFA) and RFA+R848 groups, the mice were anesthetized with ketamine + xylazine solution (i.p., 90 + 8 mg/kg). After the mice were fully anesthetized, the abdominal hair was shaved, and they were fixed on the electrode

plate in prone position; then, 1 ml PBS was sprayed on the contact area between the electrode plate and the mouse's skin to increase the conductivity. A 480-kHz RFA generator (S-1500, MedSphere, Shanghai) was then connected, and a 17-gauge monopolar electrode was inserted along the long axis of the tumor so that the electrode tip reached the center of the tumor, and the ablation was performed with parameters of 5 W and 15 s. For the control and R848 groups, the mice received the same treatments but with the RFA generator turned off. After the RFA procedure, all mice were resuscitated on a 37°C blanket. A picture of the tumor RFA model is shown in **Supplementary Figure S6**.

Resiguimod Therapy

The powder of resiqumod (R848) was obtained from MedChemExpress (Monmouth Junction, NJ, USA). The powder was prepared into a solution according to the manufacturer's instructions and filtered with a 0.2-um syringe filter before administration. For the mice in the R848 and RFA +R848 groups, R848 solution (1 mg/kg,100 ul) was intraperitoneally injected on the same day as with the RFA treatment and then once every 2 days until the mice were sacrificed or dead. For the control and RFA groups, the mice were injected in the same way with a control solution without R848.

Flow Cytometry

Flow cytometry was performed to analyze the tumor-infiltrating immune cells. In brief, tumors were peeled off the skin after the mice were sacrificed. The edge of the tumor was cut into 1-mm³ size, and then the fragments were placed for an hour in 5 ml DMEM containing 0.1 mg/ml DNase-I and 1 mg/ml collagenase IV at 37°C to get a single-cell suspension. Next, the cell suspensions were filtered through a 70-µm strainer to filter out incompletely digested residues. For cell membrane staining, Zombie Aqua Fixable Viability Kit was first applied, according to the manufacturer's instructions, to distinguish live cells from dead cells, and then a suspension of various antibodies was used for cell membrane staining. For intracellular cytokine staining, the cells need to be stimulated with Cell Activation Cocktail (with Brefeldin A) first, followed by live-dead staining, cell membrane staining, fixation and permeabilization, and incubation of anti-IFN- γ and anti-Granzyme B monoclonal antibodies with cell suspensions. After dyeing, the excess dye was washed off with PBS, and the suspension was filtered again with a 40-µm nylon mesh to get the final single-cell suspension. All samples were acquired on BD LSR Fortessa (BD Biosciences), and data was analyzed with FlowJo 10.5.3 software (FlowJo LLC, Ashland, USA). The gating strategy is provided in Supplementary Figure S2.

The antibodies and reagents used in the flow cytometry analysis were obtained from Bio-Legend (San Diego, CA, USA), namely: Zombie Aqua Fixable Viability Kit, BV605-conjugated anti-CD45, APC-conjugated anti-CD3, Perp-Cy5.5-conjugated anti-NK1.1, PE-conjugated anti-CD4, FITC-conjugated anti-CD8, APC-conjugated anti-TCR β , PE-conjugated anti-CD11b, BV711-conjugated anti-Ly6C, BV650-conjugated anti-Ly6G, APC-conjugated anti-F4/80,

APC-Cy7-conjugated anti-I-A/I-E (MHCII), APC-Cy7-conjugated anti-CD45R (B220), PE-Cy7-conjugated anti-CD11c, FITC-conjugated anti-CD86, PE-Cy7-conjugated anti-IFN- γ and FITC-conjugated Granzyme B, Cell Activation Cocktail (with Brefeldin A), fixation buffer, and permeabilization wash buffer.

NK Cell Deletion

The tumor-bearing mice were divided into three groups, and then they received RFA, RFA+R848, or RFA+R848+anti-NK1.1 antibody (Bio-Legend, San Diego, CA, USA). R848 was administered as previously described. Anti-NK1.1 (300 μ g/ mouse) or sham antibodies were injected intraperitoneally into the mice starting on the day before the RFA and then once every 3 days—for a total of 3 injections. Detection of NK cell in mouse blood was performed using flow cytometry to verify the efficiency of NK1.1 antibody.

Real-Time Quantitative PCR

Approximately 0.1 g of tumor tissue was homogenized, and then total RNA was extracted using RNeasy Mini Kit (Qiagen, Germany), according to the manufacturer's instructions. The synthesis of cDNA from RNA was achieved with Prime-ScriptTM RT reagent kit (TaKaRa). qPCR was performed on LightCycler 480 II system (480II-384, Roche, Germany) in a 10-µl reaction mixture containing SYBR Green I (Yeasen, Shanghai). The parameters are set to 40 cycles of 95°C for 15 s, 60°C for 15 s, and 72°C for 30 s. The expressions of the desired genes were normalized to GAPDH, and data were further analyzed by the $2^{-\Delta\Delta CT}$ formula. The final results are presented as fold change to the control group, and the primer sequences are provided in **Supplementary Table S1**.

Immunochemistry Staining

Tumor tissues were fixed in 10% neutral buffered formalin and then embedded in paraffin. For immunochemistry (IHC), the paraffins are cut into 4-µm slices. In the deparaffinization of sections to water, xylene and various concentrations of ethanol (100, 95, 85, and 75%) were used. Endogenous peroxidase was inactivated, antigen was retrieved, followed by goat serum blocking and incubation with primary anti-CD31 (AF3628, Bio-Techne) antibody, anti-VEGFA (19003-1-AP, Proteintech) antibody, anti-cleaved-caspase3 (9661L, Cell Signaling) antibody, and anti-ki67 (12202S, Cell Signaling) antibody. Next, the samples were incubated with a horseradish peroxidase-conjugated secondary antibody, and a color developer (diaminobenzidine) was used to develop color at an appropriate concentration. Finally, five fields of each section were randomly selected at ×400 magnification for counting of positive cells, and for ki67 staining, the integrated optical density value was calculated by ImageJ software (https://imagej.nih.gov/ nih-image/) under the same threshold conditions.

Statistical Analysis

All data analyses were performed by GraphPad Prism 8.0.2 (GraphPad Software, Inc.), and *p*-value <0.05 was regarded as statistically significant. The detailed statistical methods are presented in the figure legend.

RESULTS

Combination of RFA With R848 Constrains the Growth of HCC and Extends the Survival of Tumor-Bearing Mice

To evaluate whether RFA, R848, and the combo treatment elicit an effective anti-tumor immunity, hepa1-6 liver cancer cells were subcutaneously implanted into the right flank of C57BL/6 mice. At 1 week later, the mice were randomly assigned to four groups when the diameter of the tumor has reached 6–8 mm. The mice in the four groups received no treatment (control), RFA treatment, R848 treatment, and combined treatment (RFA+ R848), respectively. Tumor volume was recorded every day, and tumor growth curves were plotted (**Figure 1A**).

As shown in **Figures 1B–D**, in contrast to the control or monotherapy group, the tumors of mice treated with RFA+R848 grew significantly slower and were smaller at the end of the experiment, whereas only a negligible tumor growth inhibitory effect was detected in the RFA and R848 groups. Combo treatments especially distinctly constrained the growth of tumor in the first 3 days after RFA. The tumor growth kinetics of mice that received different treatments is shown in Figure 1C. Both the RFA and combo treatments evidently reduced the tumor weight compared with the control group, but the tumor in the RFA+R848 group was significantly lighter than that in the RFA group (Figure 1E). Besides this, we observed that the tumor-draining lymph node in the RFA+R848 group was a little bit smaller than that in the control group, but there was no significant difference between the RFA and control groups (Supplementary Figure S1A). In addition, spleen size was not different among the groups (Supplementary Figure S1B). On the other hand, we also showed that combo treatments obviously extended the survival of tumorbearing mice compared with those from the monotherapy or control group (Figure 1F). The median survival for mice treated with RFA+R848 was 15 days, an increase of 36.4 and 57.9% compared with the RFA (11 days) and R848 (9.5 days) group, respectively. We additionally found that RFA alone can also slightly improve the survival time of tumor-bearing mice.

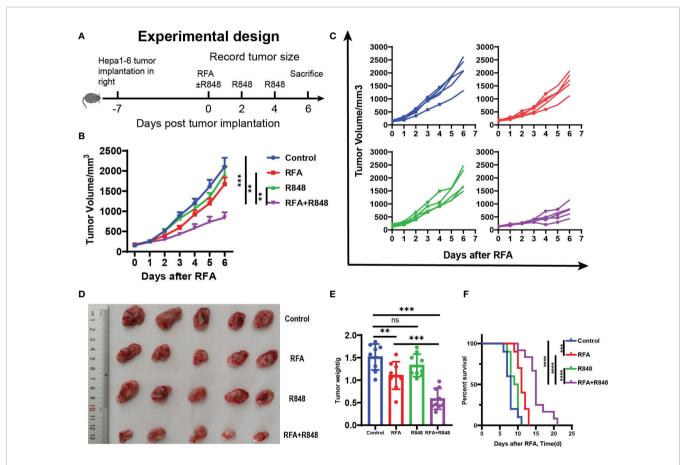


FIGURE 1 | Potent antitumor efficiency following radiofrequency ablation combined with resiquimod. (A) Diagram of the experimental design for assessment combo treatments in mice liver cancer model (hepa1-6). (B) Tumor growth curves of mice that received different treatments. (C) Tumor growth in each mouse after different treatments. (D) Representative image of hepa1-6 tumor excised at day 6. (E) Quantitative analysis of tumor weight at sacrifice in different groups; summary analysis of the result of the two experiments. The experiments represented in (B–E) were repeated 3 times, with 4–6 mice per group. All data are shown as mean \pm SEM, and two-tailed Student's *t*-test was performed to compare the statistical differences between the two groups. (F) Kaplan–Meier overall survival analysis (*n* = 10 for each group), and this experiment was repeated 2 times. Statistical significance was evaluated by log-rank (Mantel–Cox) tests. ***p* < 0.01; ****p* < 0.001; ns, not significant.

Combination of RFA With R848 Modulates the Profiles of Tumor-Infiltrating Immune Cells

We then revealed the effect of the combo treatments on tumorinfiltrating immune cells by flow cytometry (the gating strategy is shown in **Supplementary Figure S2**). Mice that received different treatments were executed on the 6th day, the tumors were peeled off the skin, and the edge of the tumor was cut into pieces to get single-cell suspensions. As shown in **Figure 2A**, there was a distinct increase in intra-tumoral CD45⁺ immune cells after the combined treatments compared with the control or RFA monotherapy, but no significant difference was found between the RFA+R848 group and the R848 group.

Natural killer (NK) cells and $CD8^+$ T cells play an important role in liver cancer progression (33–36). We found that the combination therapy clearly elevated the ratio of NK, $CD3^+T$,

and CD8⁺ T cells to CD45⁺ immune cells compared with those in the control or RFA monotherapy (Figures 2B, C; Supplementary Figure S3A). Furthermore, the proportion of NK cells in the combined treatment group is significantly higher than in the R848 group, whereas the ratio of CD8⁺ T cells is not. In addition, the proportion of IFN γ^+ cells in NK cells in the combined treatment group is higher than that in the RFA or control group (Figure 2D). Only a slight increase was observed after the combo treatments in terms of the frequency of IFN γ^+ CD8⁺ T cells compared with no treatments, and there was no statistical difference between the combined group and the RFA group (Supplementary Figure S3D). Besides this, the ratio of Granzyme B⁺ cells in NK cells and CD8⁺ T cells was not different among the four groups (Supplementary Figures 3E, F). This implies that the combinational effect is mainly attributed to NK cells.

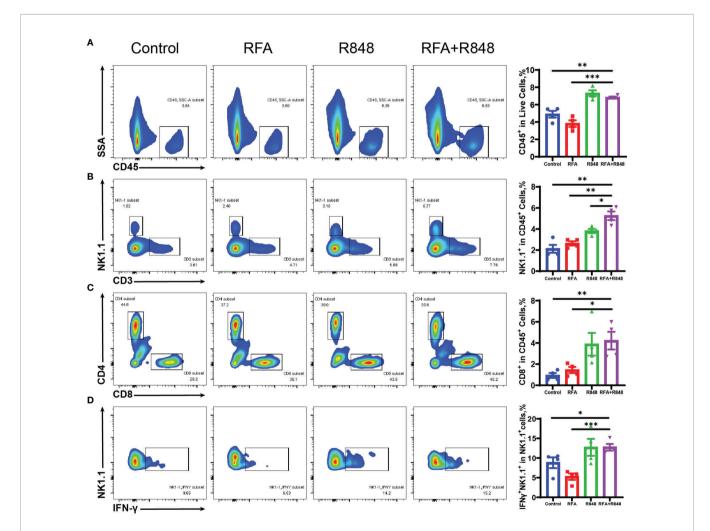


FIGURE 2 | The composition of tumor-infiltrating immune cells is changed after combination therapy. (A) Ratio of tumor-infiltrating immune (CD45⁺) cells to live cells in different groups; quantitative analysis results are shown on the right. (B) Representative flow cytometry plots of the percent of tumor-infiltrating NK (CD3⁻NK1.1⁺) cells in CD45⁺ cells and the corresponding quantitative results. (C) Intra-tumoral CD8⁺ T cells were gated from CD3⁺ cells, and then the ratio of CD8⁺ to CD45⁺ was calculated; %CD8⁺ T in CD45⁺ cells = %(CD8⁺CD3⁺CD45⁺). (D) The proportion of IFN₇-secreting NK (IFN₇⁺NK1.1⁺) cells to total NK cells in the tumors of mice that received different treatments. The experimental results from one of the two independent experiments are shown; *n* = 4 per group. Statistical comparison was performed by two-tailed Student's t-test. All error bars represent mean ± SEM. **p* < 0.05; ***p* < 0.001. IFN₇, interferon γ , NK, natural killer.

The flow cytometric assay also detected that the proportion of CD4⁺ T cells, B cells (CD3⁻CD45R⁺), macrophages (Ly6c⁻CD11B⁺F4/80⁺), monocytes (CD11B⁺MHCII⁻Ly6c⁺Ly6g⁻), and neutrophils (CD11B⁺MHCII⁻Ly6c⁺Ly6g⁺) to CD45⁺ immune cells was not different among the four groups. Moreover, there was also no difference between the ratio of M1 (MHCII⁺ macrophage)/M and M2 (MHCII⁻ macrophage)/M (**Supplementary Figures S3B**, **C**, **S4A–E**). However, interestingly, similar to the role of R848 in pancreatic cancer (27), the percentage of dendritic cells (DCs, CD11B⁺MHCII⁺CD11C⁺F4/80⁻) as a percent of CD45⁺ cells in both the R848 group and the RFA+R848 group was significantly reduced, while there was no difference in the proportion of CD86⁺ DCs to the total DCs between groups (**Supplementary Figures S4F, G**).

Abscopal Effect Is Induced by RFA+R848 Treatments

To investigate the systemic antitumor immune response of combo treatments, we simultaneously implanted hepa1-6 liver cancer cells into the bilateral flanks of C57BL/6 mice. After a week, the mice were divided into four groups when the tumors have reached approximately 100 mm3. The tumor on the right flank was regarded as the primary tumor for RFA therapy, while the contralateral tumor was considered the distant tumor for monitoring and flow cytometry analysis. R848 was injected intraperitoneally once every 2 days-for a total of 4 injections. The mice were sacrificed on the 7th day after RFA (Figure 3A). The volume and weight of distant tumors manifested that only a negligible tumor growth inhibition was induced by RFA or R848 monotherapy. Nevertheless, the RFA+R848 treatment significantly reduced the tumor burden of the tumors that were left untreated (Figure 3B). Corresponding to these results, the flow cytometry analysis revealed that the combo treatments showed a stronger ability to increase the frequencies of both CD45⁺ and NK cells in the distant tumors compared with the control or RFA treatment. Furthermore, the proportion of NK cells to CD45⁺ cells in the combination therapy group was highest among the four groups (Figures 3C, D). This phenomenon further proves the role of NK cells in combination therapy. However, unlike a tumor in situ, no difference was detected in the ratio of CD3⁺ and CD8⁺ T cells to CD45⁺ cells in distant tumors among the four groups. The proportion of CD4⁺ T cells was not changed either (Supplementary Figure S5). What is more, similar to the primary tumor, except for DCs, the tumor-infiltrating myeloid immune cells in mice with different treatments almost did not differ in the distant tumor. The data is not presented.

NK Cells Are Essential for the Antitumor Immunity Elicited by the Combined Treatments

On the basis of the research that we have made, those mice that received the combination therapy not only had the highest proportion of NK cells among the four groups but also had enhanced NK cell function (**Figures 2B, D**). Hence, to directly confirm the role of NK cells in combination therapy, we performed a NK depletion test. Anti-NK1.1 antibody was

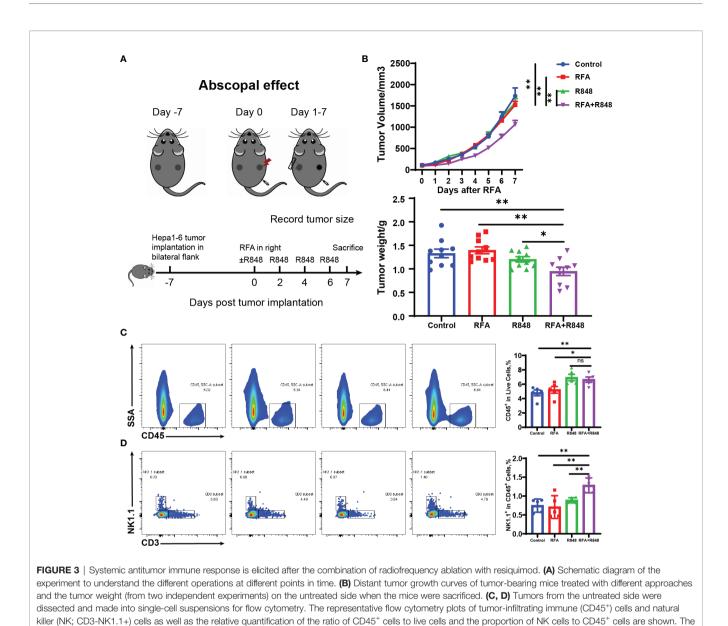
injected intraperitoneally at 1 day before the RFA and then once every 3 days until the mice were sacrificed. The rest of the operation was similar to **Figure 1A**. The depletion efficiency is shown in **Figure 4A**. The tumor growth curves indicate that the RFA+R848 treatment evidently reduced the tumor burden compared with RFA monotherapy, whereas the inhibition of tumor growth disappeared in the absence of NK cells (**Figure 4B**). Correspondingly, the tumors in the RFA+R848 group were the lightest and smallest among the three groups, but the tumor size was not reduced after using anti-NK1.1 antibody (**Figures 4C, D**).

RFA+R848 Treatment Promotes the Expression of Lymphocyte-Related Cytokines and NK Cell-Related Chemokines in Tumor Tissue

Various cytokines and chemokines play a crucial role in the tumor microenvironment (24, 37-39), and chemokine networks are essential for NK cells exerting antitumor effects in solid tumor (40). We discovered that the expression of IL-2, IL-6, and IL-12 in these tumors, associated with the activation of T cells and NK cells, was evidently increased after the combo treatments (**Figures 5A–C**). At the same time, the expression of IFN- $\alpha/\beta R$ and cytokines related to the function of T cells and NK cells, such as TNF- α and IFN- γ , was also significantly increased after the combination therapy (Figures 5D-F). This inflammatory phenomenon is a reflection of the widespread and powerful immune activation within the tumor microenvironment and is consistent with the changes that we observed earlier in tumorinfiltrating lymphocytes. Although NK cells express many chemokine receptors, CCR2, CCR5, CCR7, CXCR3, CX3CR1, and their ligands are thought to play a major role in attracting NK cells to infiltrate tumors (40). As depicted in Figures 5G-O, the expression levels of the ligands corresponding to the aforementioned chemokine receptors in the RFA+R848 group were markedly higher than those in the RFA group. In summary, these multivariate data suggest that the combination therapy evidently reshaped the HCC immune microenvironment, leading to the inhibition of tumor growth.

Combo Treatments Suppress Angiogenesis and Promote the Apoptosis of Liver Cancer

Previous studies have shown that R848 alone can inhibit angiogenesis and promote apoptosis in breast cancer (41). To assess whether R848 plays a similar role in liver cancer, we selected two tumor vascular markers—CD31 and VEGFA—for immunohistochemical staining of tumor tissues. Apparently, the micro-vessel density and VEGFA⁺ cells were decreased in the R848 group and the RFA+R848 group (**Figures 6A, B, E, F**), while RFA+R848 did not further reduce the tumor micro-vessels compared with R848 monotherapy. This indicates that the reduction of tumor micro-vessels is mainly caused by R848. In addition, cleaved caspase3 and ki-67 were stained to indicate tumor apoptosis and proliferation. The number of cleaved caspase3⁺ cells in the RFA+R848 group was significantly



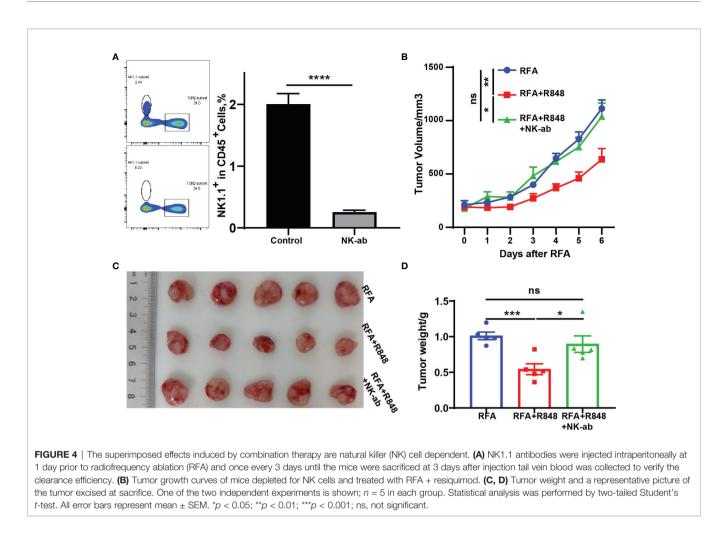
results represent one of two independent experiments; n = 5 in each group. Statistical analysis was performed by two-tailed Student's *t*-test. All error bars represent mean \pm SEM. *p < 0.05; **p < 0.01; ns, not significant.

higher than in the other three groups, and the quantity of cleaved caspase3⁺ cells in the R848 group was also slightly higher than that in the RFA group and the control group (**Figures 6C, G**). Meanwhile, both the RFA and R848 treatments have a certain degree of inhibitory effect on tumor proliferation, but no obvious additive effect was observed in the combined treatment (**Figures 6D, H**). Overall, these findings are consistent with the changes in tumor size and TIME that we described earlier.

DISCUSSION

HCC is one of the most common malignant tumors worldwide and remains a global health challenge (9). Local ablation is one of

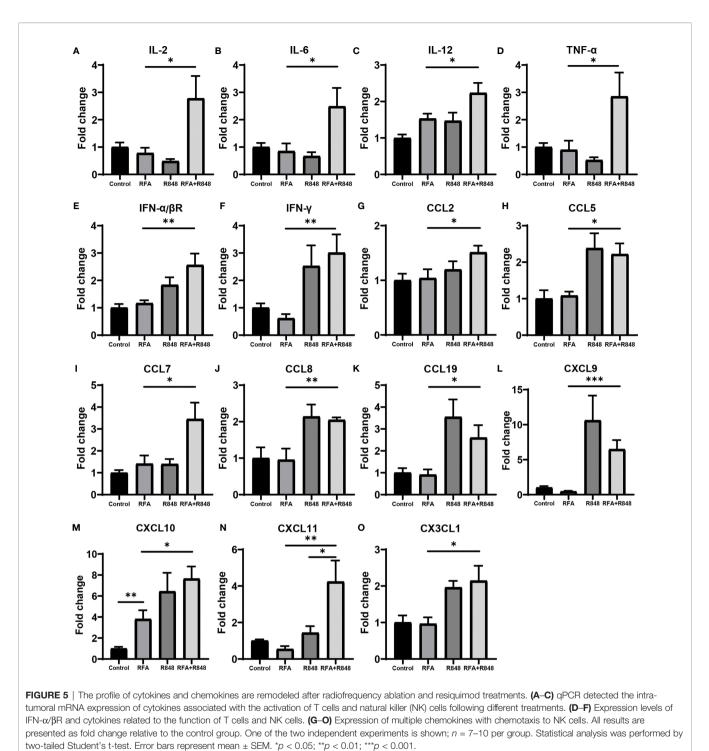
the top three treatment options for HCC, and it is estimated that more than half of HCC patients have received this treatment throughout their lifespan (10). As one of the most commonly used treatment modalities in local ablation, RFA destroys tumor tissues by generating heat through a radiofrequency electrode (16, 42). The heat causes mechanical damage to tumor cells, which, in turn, leads to the release of abundant immunogenic intracellular substrates and damage-associated molecular patterns, such as heat shock proteins, high mobility group protein B1, RNA as well as DNA (16, 43). These elicit a certain degree of anti-tumor immune response as an *in situ* vaccine, but the response is too weak to effectively inhibit tumor progression (10, 42–45). Combined immunotherapy, on the basis of local ablation therapy, is an ideal method to enhance the efficacy of



thermal ablation therapy (10, 23, 46). As a novel immunomodulatory agent, R848 has attracted widespread attention in recent years, which plays an important role in promoting the activation of NK cell and CD8⁺ T cell as well as the release of proinflammatory cytokines, such as IFN- α , IL-2, IL-6, and TNF- α (27, 47–49). The purpose of this study was to examine whether RFA in combination with R848 could meaningfully inhibit HCC progression and inflame the TIME.

Some preclinical studies have confirmed that R848 alone can slightly inhibit the progression of pancreatic cancer (27), breast cancer (41), and colorectal cancer (47). Here we demonstrated that RFA combined with R848 further inhibited HCC growth and prolonged the survival time of tumor-bearing mice compared with R848 or RFA monotherapy. This study also revealed the changes in the composition of tumor-infiltrating immune cells by flow cytometry. We found that the total tumorinfiltrating immune cells, the ratio of CD8⁺ T cells and NK cells to the total immune cells, and the percentage of functional NK cells were effectively increased after the combination therapy compared with RFA treatment alone. However, unlike previous studies about TLR7/8 agonist (50–54), our findings suggest that the systemic administration of R848 (1 mg/kg) did not evidently alter the composition of macrophages nor did it effectively promote type I macrophage polarization in murine liver cancer, and the percentage of DC cells in liver cancer and pancreatic cancer (27) was slightly decreased after R848 administration, which is inconsistent with the stronger antitumor immunity induced by R848—so further research is necessary.

Another critical finding of our research is that the combined treatment of RFA and R848 induced a potent abscopal effect. The total tumor-infiltrating immune cells and NK cells in distant tumor tissues were significantly increased. NK cells are abundant in the liver, and studies have shown that the proportion of NK cells in the liver is approximately five times that in the blood and spleen, but it is significantly decreased in the occurrence and development of HCC (34, 55). Moreover, the number of NK cells is positively correlated with the prognosis of HCC patients (56). Previous research had also shown that both RFA (17, 57) and TLR7/8 agonist (58-61) alone can stimulate the activation of NK cells. Our study shows that the proportion of tumor-infiltrating NK cells in both primary and distant tumors of the combined treatment group was higher than that in the RFA or R848 treatment group, suggesting that the combination therapy further promotes the infiltration of NK cells into the HCC and formed a superimposed effect. Furthermore, the NK deletion test



clearly proved that the inhibition of liver cancer by the combination therapy is NK cell dependent.

Chemokine networks are critical for driving the intra-tumoral infiltration of NK cells (40). Previous studies have confirmed as well that CXCL10, CX3CL1 (62), and CXCL11 (63) play an important role in the infiltration of NK cells into the melanoma. Correspondingly, we observed that the expression levels of NK cell-

related chemokines were the highest in the combined treatment group, especially CCL7, CXCL10, CXCL11, and CX3CL1, which was consistent with the phenomenon that the proportion of NK cells was the highest in the combined treatment group, reflecting that they are responsible for the infiltration of NK cell into the tumor. Moreover, the expression of CXCL11 in the combination therapy group was significantly higher than those in the R848

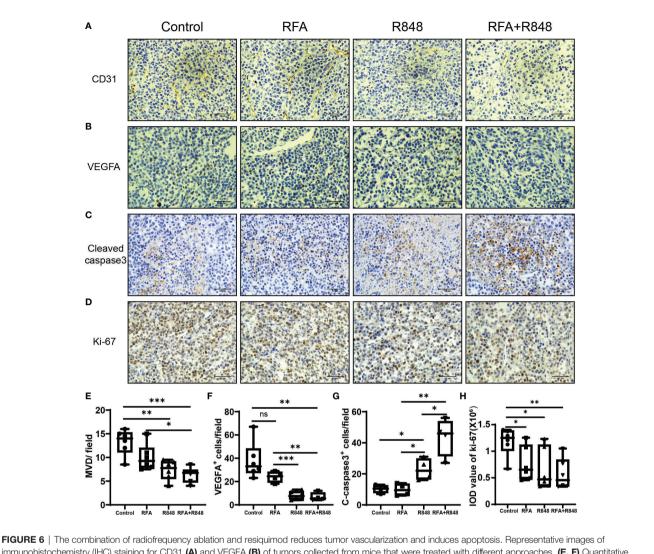


FIGURE 6 | The combination of radiofrequency ablation and resignimod reduces tumor vascularzation and induces apoptosis. Hepresentative images of immunohistochemistry (IHC) staining for CD31 (**A**) and VEGFA (**B**) of tumors collected from mice that were treated with different approaches. (**E**, **F**) Quantitative analysis of tumor micro-vessel density and the number of VEGFA+ cells per field; n = 4-6. (**C**, **G**) Detection of the expression of apoptosis marker cleaved caspase 3 in tumors by IHC and its corresponding quantitative analysis; n = 4. (**D**, **H**) IHC analysis of the tumor sections stained with Ki67 following different treatments; n = 6. Scale bars, 50 µm. The *P*-values were calculated by two-tailed Student's *t*-test. Error bars represent mean \pm SEM. *p < 0.05; **p < 0.01; **p < 0.001; ns, not significant.

group, which might be the reason for the additive effect of the combined treatments. However, we have not been able to clarify which chemokine drives the NK cell to infiltrate liver cancer; this needs to be further explored in the future. The expression level of CXCL10 in the RFA group was higher than that in the control group as well. It is a manifestation of the immunogenic cell death of tumor after RFA. On the other hand, recent studies have demonstrated that R848 binding to TLR7/8 stimulates the production of IFN- α , IL-6, IL-12, TNF- α , and other proinflammatory cytokines through MyD88-dependent or MyD88-independent pathway (24, 25, 47), and RFA treatment can also promote the expression of multiple cytokines, such as IL-1 β , IL-6, IL-8, and TNF- α (16, 43, 64, 65). Our data shows that the expression levels of IL-2, IL-6, IL-12, TNF- α , and IFN- $\alpha/\beta R$ in the combination group were significantly higher than those in the RFA or R848 group. This is evidence that RFA and R848 work together

to activate anti-tumor immunity. In addition, several studies reported that R848 can inhibit angiogenesis and promote apoptosis in breast cancer (24, 41). Our IHC results certified that the RFA+R848 treatment effectively reduced the vascular density and VEGF expression of liver cancer, but the mechanism of this has not been elucidated; it is an aspect for further research. Besides this, cleaved-caspase3 and ki-67 staining indicated that the combination therapy promoted tumor apoptosis but failed to further inhibit tumor proliferation compared with RFA monotherapy.

In conclusion, this study demonstrated that the combination of RFA with R848 ignited a robust anti-tumor response and significantly constrained HCC progression in a NK celldependent manner. Meanwhile, we confirmed that R848 inhibited angiogenesis and promoted apoptosis in murine liver cancer (**Schematic Illustration**). Overall, our research explored the potential of RFA combined with R848 in the treatment of liver cancer and provided a novel insight into the combination of thermal ablation with immunotherapy.

DATA AVAILABILITY STATEMENT

The datasets presented in this study can be found in online repositories. The names of the repository/repositories and accession number(s) can be found in the article/**Supplementary Material**.

ETHICS STATEMENT

The animal study was reviewed and approved by the Laboratory Animal Welfare Ethics Review Committee of Zhejiang University.

AUTHOR CONTRIBUTIONS

ZTi conceived the idea, performed the experiments, and wrote the manuscript. BH provided program guidance. JC and ZTa designed the experiments, directed this study, and revised the manuscript. All authors contributed to the article and approved the submitted version.

FUNDING

This work was supported by the Key Research and Development Project of Zhejiang Province (2021C03048), the Key Project of the Natural Science Foundation of Zhejiang Province (LZ20H160002), and the Medical and Health Science and Technology Project of Zhejiang Province (2019KY290 and 2021KY024).

SUPPLEMENTARY MATERIAL

The Supplementary Material for this article can be found online at: https://www.frontiersin.org/articles/10.3389/fonc.2022.891724/full#supplementary-material

Supplementary Figure 1 | Radiofrequency ablation, in combination with resiquimod, shrinks the tumor-draining lymph node, but monotherapy does not. Representative pictures to show the tumor-draining lymph node (A) and spleen (B)

REFERENCES

- 1. Siegel RL, Miller KD, Fuchs HE, Jemal A. Cancer Statistics, 2021. CA Cancer J Clin (2021) 71(1):7–33. doi: 10.3322/caac.21654
- Kulik L, El-Serag HB. Epidemiology and Management of Hepatocellular Carcinoma. *Gastroenterology* (2019) 156(2):477-91.e1. doi: 10.1053/ j.gastro.2018.08.065
- Sung H, Ferlay J, Siegel RL, Laversanne M, Soerjomataram I, Jemal A, et al. Global Cancer Statistics 2020: Globocan Estimates of Incidence and Mortality Worldwide for 36 Cancers in 185 Countries. *CA Cancer J Clin* (2021) 71 (3):209–49. doi: 10.3322/caac.21660

size in the mice with different treatments. The quantitative analysis of the TLN and the spleen weight were taken from two independent experiments; n=4-5, *P < 0.05. Error bars represent mean ± SEM. Statistical analysis was performed by two-tailed Student's *t*-test.

Supplementary Figure 2 | Gating strategy to facilitate the understanding of how different types of cells are defined.

Supplementary Figure 3 | The profile of tumor-infiltrating lymphoid immune cells is slightly altered after the combination therapy. (A–C) The proportion of tumor-infiltrating CD3+, CD4+, CD45R+ cells to total CD45+ immune cells. (D–F) Cumulated ratio of CD8+ T cells and NK cells expressing IFN- γ or GZMB; n = 4. Statistical significance was calculated by two-tailed Student's *t*-test; *P < 0.05. Error bars indicate mean ± SEM. GZMB, Granzyme B.

Supplementary Figure 4 | Changes in tumor-infiltrating myeloid immune cells after the combination therapy. (A–E) The frequencies of macrophages (Ly6c-CD11B+F4/80+), monocytes (CD11B+MHCII-Ly6c+Ly6g-), and neutrophils (CD11B+MHCII-Ly6c+Ly6g+) in the total CD45+ immune cells and the ratio of M1 (MHCII+ macrophage) and M2 (MHCII- macrophage) to the total macrophages. (F, G) The proportion of dendritic cells (DCs, CD11B+MHCII+CD11C+F4/80-) to CD45+ immune cells and the frequencies of CD86+ DCs in total DCs; n = 4. Statistical significance was calculated by two-tailed Student's *t*-test; *P < 0.05, **P < 0.01. All error bars represent mean ± SEM.

Supplementary Figure 5 | Distant intra-tumoral T lymphocyte composition is not altered by the combination therapy. Hepa1-6 tumor cells were simultaneously inoculated on the bilateral flanks of immunocompetent C57BL/6 mice; the tumor on the right side is seen as a primary tumor for radiofrequency ablation therapy, and the contralateral tumor was considered as a distant tumor for flow cytometry analysis. resiquimod was injected intraperitoneally once every 2 days for a total of 4 injections. **(A–C)** Percentage of CD3+, CD4+, and CD8+ T cells as a percent of CD45+ immune cells in distant tumor; n = 4. Statistically significant differences were calculated by two-tailed Student's *t*-test. All error bars indicate mean ± SEM. ns, no significance.

Supplementary Figure 6 | Representative picture of the tumor radiofrequency ablation model.

Supplementary Table 1 | List of qPCR primer sequences.

Schematic Illustration | Both RFA and R848 can stimulate the production of pro-inflammatory cytokines and chemokines in tumor tissue, thereby stimulating the formation of anti-tumor immunity. The combination of the two treatments further promoted the expression of NK cell-related chemokines and cytotoxic lymphocyte-related cytokines, such as CXCL10, CXCL11, IL2, IFN- γ , TNF- α , *etc.*, which drove lots of NK cells to infiltrate the tumor and enhanced the NK cell function. In addition, R848 inhibited tumor angiogenesis and promoted the apoptosis of liver cancer. As a result, the combination of RFA with R848 improved the anti-tumor immune response induced by RFA and significantly inhibited the progression of liver cancer. RFA, radiofrequency ablation; R848, resiquimod; DAMPs, damage-associated molecular patterns; IICSs, immunogenic intracellular substrates; APC, antigenpresenting cell; NK cell, natural killer cell.

- Llovet JM, Kelley RK, Villanueva A, Singal AG, Pikarsky E, Roayaie S, et al. Hepatocellular Carcinoma. *Nat Rev Dis Primers* (2021) 7(1):6. doi: 10.1038/ s41572-020-00240-3
- McGlynn KA, Petrick JL, London WT. Global Epidemiology of Hepatocellular Carcinoma: An Emphasis on Demographic and Regional Variability. *Clin Liver Dis* (2015) 19(2):223–38. doi: 10.1016/j.cld.2015. 01.001
- European Association for the Study of the Liver. Electronic Address Eee, European Association for the Study of the L. Easl Clinical Practice Guidelines: Management of Hepatocellular Carcinoma. *J Hepatol* (2018) 69(1):182–236. doi: 10.1016/j.jhep.2018.03.019

- Kim HD, Shim JH, Kim GA, Shin YM, Yu E, Lee SG, et al. Optimal Methods for Measuring Eligibility for Liver Transplant in Hepatocellular Carcinoma Patients Undergoing Transarterial Chemoembolization. J Hepatol (2015) 62 (5):1076–84. doi: 10.1016/j.jhep.2014.12.013
- Roayaie S, Jibara G, Tabrizian P, Park JW, Yang J, Yan L, et al. The Role of Hepatic Resection in the Treatment of Hepatocellular Cancer. *Hepatology* (2015) 62(2):440–51. doi: 10.1002/hep.27745
- Forner A, Reig M, Bruix J. Hepatocellular Carcinoma. Lancet (2018) 391 (10127):1301–14. doi: 10.1016/S0140-6736(18)30010-2
- Llovet JM, De Baere T, Kulik L, Haber PK, Greten TF, Meyer T, et al. Locoregional Therapies in the Era of Molecular and Immune Treatments for Hepatocellular Carcinoma. *Nat Rev Gastroenterol Hepatol* (2021) 18(5):293– 313. doi: 10.1038/s41575-020-00395-0
- Nault JC, Sutter O, Nahon P, Ganne-Carrie N, Seror O. Percutaneous Treatment of Hepatocellular Carcinoma: State of the Art and Innovations. *J Hepatol* (2018) 68(4):783–97. doi: 10.1016/j.jhep.2017.10.004
- Xia Y, Li J, Liu G, Wang K, Qian G, Lu Z, et al. Long-Term Effects of Repeat Hepatectomy Vs Percutaneous Radiofrequency Ablation Among Patients With Recurrent Hepatocellular Carcinoma: A Randomized Clinical Trial. JAMA Oncol (2020) 6(2):255–63. doi: 10.1001/jamaoncol.2019.4477
- Xu XL, Liu XD, Liang M, Luo BM. Radiofrequency Ablation Versus Hepatic Resection for Small Hepatocellular Carcinoma: Systematic Review of Randomized Controlled Trials With Meta-Analysis and Trial Sequential Analysis. *Radiology* (2018) 287(2):461–72. doi: 10.1148/radiol.2017162756
- Kudo M, Hasegawa K, Kawaguchi Y, Takayama T, Izumi N, Yamanaka N, et al. A Multicenter Randomized Controlled Trial to Evaluate the Efficacy of Surgery Versus Radiofrequency Ablation for Small Hepatocellular Carcinoma (Surf Trial): Analysis of Overall Survival. J Clin Oncol (2021) 39 (15_suppl):4093–3. doi: 10.1200/JCO.2021.39.15_suppl.4093
- Lee MW, Kang D, Lim HK, Cho J, Sinn DH, Kang TW, et al. Updated 10-Year Outcomes of Percutaneous Radiofrequency Ablation as First-Line Therapy for Single Hepatocellular Carcinoma < 3 Cm: Emphasis on Association of Local Tumor Progression and Overall Survival. *Eur Radiol* (2020) 30(4):2391–400. doi: 10.1007/s00330-019-06575-0
- Chu KF, Dupuy DE. Thermal Ablation of Tumours: Biological Mechanisms and Advances in Therapy. *Nat Rev Cancer* (2014) 14(3):199–208. doi: 10.1038/nrc3672
- Zerbini A, Pilli M, Laccabue D, Pelosi G, Molinari A, Negri E, et al. Radiofrequency Thermal Ablation for Hepatocellular Carcinoma Stimulates Autologous Nk-Cell Response. *Gastroenterology* (2010) 138(5):1931–42. doi: 10.1053/j.gastro.2009.12.051
- den Brok MH, Sutmuller RP, van der Voort R, Bennink EJ, Figdor CG, Ruers TJ, et al. *In Situ* Tumor Ablation Creates an Antigen Source for the Generation of Antitumor Immunity. *Cancer Res* (2004) 64(11):4024–9. doi: 10.1158/0008-5472.CAN-03-3949
- Takaki H, Imai N, Thomas CT, Yamakado K, Yarmohammadi H, Ziv E, et al. Changes in Peripheral Blood T-Cell Balance After Percutaneous Tumor Ablation. *Minim Invasive Ther Allied Technol* (2017) 26(6):331–7. doi: 10.1080/13645706.2017.1310737
- van den Bijgaart RJ, Eikelenboom DC, Hoogenboom M, Futterer JJ, den Brok MH, Adema GJ. Thermal and Mechanical High-Intensity Focused Ultrasound: Perspectives on Tumor Ablation, Immune Effects and Combination Strategies. *Cancer Immunol Immunother* (2017) 66(2):247–58. doi: 10.1007/s00262-016-1891-9
- Lee DH, Lee JM, Lee JY, Kim SH, Yoon JH, Kim YJ, et al. Radiofrequency Ablation of Hepatocellular Carcinoma as First-Line Treatment: Long-Term Results and Prognostic Factors in 162 Patients With Cirrhosis. *Radiology* (2014) 270(3):900–9. doi: 10.1148/radiol.13130940
- 22. Livraghi T, Meloni F, Di Stasi M, Rolle E, Solbiati L, Tinelli C, et al. Sustained Complete Response and Complications Rates After Radiofrequency Ablation of Very Early Hepatocellular Carcinoma in Cirrhosis: Is Resection Still the Treatment of Choice? *Hepatology* (2008) 47(1):82–9. doi: 10.1002/hep.21933
- Bo XW, Sun LP, Yu SY, Xu HX. Thermal Ablation and Immunotherapy for Hepatocellular Carcinoma: Recent Advances and Future Directions. World J Gastrointest Oncol (2021) 13(10):1397–411. doi: 10.4251/wjgo.v13.i10.1397
- Chi H, Li C, Zhao FS, Zhang L, Ng TB, Jin G, et al. Anti-Tumor Activity of Toll-Like Receptor 7 Agonists. *Front Pharmacol* (2017) 8:304. doi: 10.3389/ fphar.2017.00304

- Huang X, Zhang X, Lu M. Recent Trends in the Development of Toll-Like Receptor 7/8-Targeting Therapeutics. *Expert Opin Drug Discov* (2021) 16 (8):869–80. doi: 10.1080/17460441.2021.1898369
- Aranda F, Vacchelli E, Obrist F, Eggermont A, Galon J, Sautes-Fridman C, et al. Trial Watch: Toll-Like Receptor Agonists in Oncological Indications. Oncoimmunology (2014) 3:e29179. doi: 10.4161/onci.29179
- Michaelis KA, Norgard MA, Zhu X, Levasseur PR, Sivagnanam S, Liudahl SM, et al. The Tlr7/8 Agonist R848 Remodels Tumor and Host Responses to Promote Survival in Pancreatic Cancer. *Nat Commun* (2019) 10(1):4682. doi: 10.1038/s41467-019-12657-w
- Cheadle EJ, Lipowska-Bhalla G, Dovedi SJ, Fagnano E, Klein C, Honeychurch J, et al. A Tlr7 Agonist Enhances the Antitumor Efficacy of Obinutuzumab in Murine Lymphoma Models *Via* Nk Cells and Cd4 T Cells. *Leukemia* (2017) 31(7):1611–21. doi: 10.1038/leu.2016.352
- Braunstein MJ, Kucharczyk J, Adams S. Targeting Toll-Like Receptors for Cancer Therapy. *Target Oncol* (2018) 13(5):583–98. doi: 10.1007/s11523-018-0589-7
- Schmid D, Park CG, Hartl CA, Subedi N, Cartwright AN, Puerto RB, et al. T Cell-Targeting Nanoparticles Focus Delivery of Immunotherapy to Improve Antitumor Immunity. *Nat Commun* (2017) 8(1):1747. doi: 10.1038/s41467-017-01830-8
- 31. Nishii N, Tachinami H, Kondo Y, Xia Y, Kashima Y, Ohno T, et al. Systemic Administration of a Tlr7 Agonist Attenuates Regulatory T Cells by Dendritic Cell Modification and Overcomes Resistance to Pd-L1 Blockade Therapy. Oncotarget (2018) 9(17):13301–12. doi: 10.18632/oncotarget.24327
- 32. Tachinami H, Nishii N, Xia YL, Kashima Y, Ohno T, Nagai S, et al. Differences of Tumor-Recruiting Myeloid Cells in Murine Squamous Cell Carcinoma Influence the Efficacy of Immunotherapy Combined With a Tlr7 Agonist and Pd-L1 Blockade. Oral Oncol (2019) 91:21–8. doi: 10.1016/j.oraloncology. 2019.02.014
- Male V, Stegmann KA, Easom NJ, Maini MK. Natural Killer Cells in Liver Disease. Semin Liver Dis (2017) 37(3):198–209. doi: 10.1055/s-0037-1603946
- Sun C, Sun H, Zhang C, Tian Z. Nk Cell Receptor Imbalance and Nk Cell Dysfunction in Hbv Infection and Hepatocellular Carcinoma. *Cell Mol Immunol* (2015) 12(3):292–302. doi: 10.1038/cmi.2014.91
- Kim HD, Song GW, Park S, Jung MK, Kim MH, Kang HJ, et al. Association Between Expression Level of Pd1 by Tumor-Infiltrating Cd8(+) T Cells and Features of Hepatocellular Carcinoma. *Gastroenterology* (2018) 155(6):1936– 50.e17. doi: 10.1053/j.gastro.2018.08.030
- Gabrielson A, Wu Y, Wang H, Jiang J, Kallakury B, Gatalica Z, et al. Intratumoral Cd3 and Cd8 T-Cell Densities Associated With Relapse-Free Survival in Hcc. *Cancer Immunol Res* (2016) 4(5):419–30. doi: 10.1158/2326-6066.CIR-15-0110
- Landskron G, de la Fuente M, Thuwajit P, Thuwajit C, Hermoso MA. Chronic Inflammation and Cytokines in the Tumor Microenvironment. *J Immunol Res* (2014) 2014:149185. doi: 10.1155/2014/149185
- Ortiz Zacarias NV, Bemelmans MP, Handel TM, de Visser KE, Heitman LH. Anticancer Opportunities at Every Stage of Chemokine Function. *Trends Pharmacol Sci* (2021) 42(11):912–28. doi: 10.1016/j.tips.2021.08.001
- Martinez-Sabadell A, Arenas EJ, Arribas J. Ifngamma Signaling in Natural and Therapy-Induced Antitumor Responses. *Clin Cancer Res* (2022) 28(7):1243–9. doi: 10.1158/1078-0432.CCR-21-3226
- Yao X, Matosevic S. Chemokine Networks Modulating Natural Killer Cell Trafficking to Solid Tumors. *Cytokine Growth Factor Rev* (2021) 59:36–45. doi: 10.1016/j.cytogfr.2020.12.003
- Yin T, He S, Wang Y. Toll-Like Receptor 7/8 Agonist, R848, Exhibits Antitumoral Effects in a Breast Cancer Model. *Mol Med Rep* (2015) 12 (3):3515–20. doi: 10.3892/mmr.2015.3885
- Mizukoshi E, Yamashita T, Arai K, Sunagozaka H, Ueda T, Arihara F, et al. Enhancement of Tumor-Associated Antigen-Specific T Cell Responses by Radiofrequency Ablation of Hepatocellular Carcinoma. *Hepatology* (2013) 57 (4):1448–57. doi: 10.1002/hep.26153
- Slovak R, Ludwig JM, Gettinger SN, Herbst RS, Kim HS. Immuno-Thermal Ablations - Boosting the Anticancer Immune Response. J Immunother Cancer (2017) 5(1):78. doi: 10.1186/s40425-017-0284-8
- 44. Fietta AM, Morosini M, Passadore I, Cascina A, Draghi P, Dore R, et al. Systemic Inflammatory Response and Downmodulation of Peripheral Cd25 +Foxp3+ T-Regulatory Cells in Patients Undergoing Radiofrequency Thermal

Ablation for Lung Cancer. *Hum Immunol* (2009) 70(7):477–86. doi: 10.1016/ j.humimm.2009.03.012

- 45. Widenmeyer M, Shebzukhov Y, Haen SP, Schmidt D, Clasen S, Boss A, et al. Analysis of Tumor Antigen-Specific T Cells and Antibodies in Cancer Patients Treated With Radiofrequency Ablation. *Int J Cancer* (2011) 128(11):2653–62. doi: 10.1002/ijc.25601
- 46. Wang K, Wang C, Jiang H, Zhang Y, Lin W, Mo J, et al. Combination of Ablation and Immunotherapy for Hepatocellular Carcinoma: Where We Are and Where to Go. Front Immunol (2021) 12:792781. doi: 10.3389/ fimmu.2021.792781
- Bahmani B, Gong H, Luk BT, Haushalter KJ, DeTeresa E, Previti M, et al. Intratumoral Immunotherapy Using Platelet-Cloaked Nanoparticles Enhances Antitumor Immunity in Solid Tumors. *Nat Commun* (2021) 12 (1):1999. doi: 10.1038/s41467-021-22311-z
- Dovedi SJ, Melis MHM, Wilkinson RW, Adlard AL, Stratford IJ, Honeychurch J, et al. Systemic Delivery of a Tlr7 Agonist in Combination With Radiation Primes Durable Antitumor Immune Responses in Mouse Models of Lymphoma. *Blood* (2013) 121(2):251–9. doi: 10.1182/blood-2012-05-432393
- Aranda F, Vacchelli E, Obrist F, Eggermont A, Galon J, Sautes-Fridman C, et al. Trial Watch: Toll-Like Receptor Agonists in Oncological Indications. Oncoimmunology (2014) 3:e29179. doi: 10.4161/onci.29179
- Lee M, Park CS, Lee YR, Im SA, Song S, Lee CK. Resiquimod, a Tlr7/8 Agonist, Promotes Differentiation of Myeloid-Derived Suppressor Cells Into Macrophages and Dendritic Cells. Arch Pharm Res (2014) 37(9):1234–40. doi: 10.1007/s12272-014-0379-4
- Liu ZP, Xie Y, Xiong Y, Liu SL, Qiu C, Zhu ZH, et al. Tlr 7/8 Agonist Reverses Oxaliplatin Resistance in Colorectal Cancer Via Directing the Myeloid-Derived Suppressor Cells to Tumoricidal M1-Macrophages. Cancer Lett (2020) 469:173–85. doi: 10.1016/j.canlet.2019.10.020
- 52. Li H, Somiya M, Kuroda S. Enhancing Antibody-Dependent Cellular Phagocytosis by Re-Education of Tumor-Associated Macrophages with Resiquimod-Encapsulated Liposomes. *Biomaterials* (2021) 268:120601. doi: 10.1016/j.biomaterials.2020.120601
- 53. Anfray C, Mainini F, Digifico E, Maeda A, Sironi M, Erreni M, et al. Intratumoral Combination Therapy with Poly(I:C) and Resiquimod Synergistically Triggers Tumor-Associated Macrophages for Effective Systemic Antitumoral Immunity. J Immunother Cancer (2021) 9(9): e002408. doi: 10.1136/jitc-2021-002408
- Figueiredo P, Lepland A, Scodeller P, Fontana F, Torrieri G, Tiboni M, et al. Peptide-Guided Resiquimod-Loaded Lignin Nanoparticles Convert Tumor-Associated Macrophages From M2 to M1 Phenotype for Enhanced Chemotherapy. *Acta Biomater* (2021) 133:231–43. doi: 10.1016/j.actbio.2020.09.038
- Sun H, Sun C, Tian Z, Xiao W. Nk Cells in Immunotolerant Organs. Cell Mol Immunol (2013) 10(3):202–12. doi: 10.1038/cmi.2013.9
- Chew V, Chen J, Lee D, Loh E, Lee J, Lim KH, et al. Chemokine-Driven Lymphocyte Infiltration: An Early Intratumoural Event Determining Long-Term Survival in Resectable Hepatocellular Carcinoma. *Gut* (2012) 61 (3):427–38. doi: 10.1136/gutjnl-2011-300509
- 57. Zerbini A, Pilli M, Pelosi G, Biasini E, Negri E, Molinari A, et al. The Enhancement of Nk-Cell Function After Radiofrequency Thermal Ablation

for Hcc Is Predictive of Clinical Outcome. *Digest Liver Dis* (2009) 41(5):A3–A. doi: 10.1016/j.dld.2009.02.015

- Dorfel D, Beck B, Geiger C, Lichtenegger F, Lindner L, Merk M, et al. The Tlr7/8 Ligand R848 Is Superior in Generation of Monocyte Derived Dendritic Cells From Aml Patients for the Induction of Potent T and Nk Cell Immune Responses. *Blood* (2010) 116(21):905–6. doi: 10.1182/blood.V116. 21.2195.2195
- Khanna V, Kim H, Zhang WQ, Larson P, Ferguson D, Panyam J. Agonists for Improving Nk Cell Mediated Antibody-Dependent Cellular Cytotoxicity (Adcc). Sci Rep (2019) 11(1):3346. doi: 10.1038/s41598-021-83005-6
- Hart OM, Athie-Morales V, O'Connor GM, Gardiner CM. Tlr7/8-Mediated Activation of Human Nk Cells Results in Accessory Cell-Dependent Ifn-Gamma Production. J Immunol (2005) 175(3):1636–42. doi: 10.4049/ jimmunol.175.3.1636
- Zhou ZX, Yu X, Zhang J, Tian ZG, Zhang C. Tlr7/8 Agonists Promote Nk-Dc Cross-Talk to Enhance Nk Cell Anti-Tumor Effects in Hepatocellular Carcinoma. *Cancer Lett* (2015) 369(2):298–306. doi: 10.1016/ j.canlet.2015.09.017
- Kim J, Kim JS, Lee HK, Kim HS, Park EJ, Choi JE, et al. Cxcr3-Deficient Natural Killer Cells Fail to Migrate to B16f10 Melanoma Cells. Int Immunopharmacol (2018) 63:66–73. doi: 10.1016/j.intimp.2018.07.026
- 63. Vancsik T, Mathe D, Horvath I, Varallyaly AA, Benedek A, Bergmann R, et al. Modulated Electro-Hyperthermia Facilitates Nk-Cell Infiltration and Growth Arrest of Human A2058 Melanoma in a Xenograft Model. *Front Oncol* (2021) 11:590764. doi: 10.3389/fonc.2021.590764
- Enochson L, Sonnergren HH, Mandalia VI, Lindahl A. Bipolar Radiofrequency Plasma Ablation Induces Proliferation and Alters Cytokine Expression in Human Articular Cartilage Chondrocytes. *Arthroscopy* (2012) 28(9):1275–82. doi: 10.1016/j.arthro.2012.01.005
- 65. Iida N, Nakamoto Y, Baba T, Nakagawa H, Mizukoshi E, Naito M, et al. Antitumor Effect After Radiofrequency Ablation of Murine Hepatoma Is Augmented by an Active Variant of Cc Chemokine Ligand 3/Macrophage Inflammatory Protein-1 Alpha. *Cancer Res* (2010) 70(16):6556–65. doi: 10.1158/0008-5472.Can-10-0096

Conflict of Interest: The authors declare that the research was conducted in the absence of any commercial or financial relationships that could be construed as a potential conflict of interest.

Publisher's Note: All claims expressed in this article are solely those of the authors and do not necessarily represent those of their affiliated organizations, or those of the publisher, the editors and the reviewers. Any product that may be evaluated in this article, or claim that may be made by its manufacturer, is not guaranteed or endorsed by the publisher.

Copyright © 2022 Tian, Hong, Chen and Tang. This is an open-access article distributed under the terms of the Creative Commons Attribution License (CC BY). The use, distribution or reproduction in other forums is permitted, provided the original author(s) and the copyright owner(s) are credited and that the original publication in this journal is cited, in accordance with accepted academic practice. No use, distribution or reproduction is permitted which does not comply with these terms.



Prognostic Significance and Immunological Role of FBXO5 in Human Cancers: A Systematic Pan-Cancer Analysis

Peng Liu^{1,2,3†}, Xiaojuan Wang^{4†}, Lili Pan^{1,2,3}, Bing Han^{4*} and Zhiying He^{1,2,3*}

Shanghai, China, ² Shanghai Engineering Research Center of Stem Cells Translational Medicine, Shanghai, China, ³ Shanghai Institute of Stem Cell Research and Clinical Translation, Shanghai, China, ⁴ Department of Pharmacy, Minhang

¹ Institute for Regenerative Medicine, Shanghai East Hospital, School of Life Sciences and Technology, Tongji University,

OPEN ACCESS

Edited by:

Hospital, Fudan University, Shanghai, China

Yubin Li, University of Pennsylvania, United States

Reviewed by:

Hua Zhu, Renmin Hospital of Wuhan University, China Qiaosi Tang, Calico Life Sciences LLC, United States Dongxiao Yang, University of St Andrews, United Kingdom

*Correspondence:

Zhiying He zyhe@tongji.edu.cn Bing Han hbshcn@163.com

[†]These authors have contributed equally to this work

Specialty section:

This article was submitted to Cancer Immunity and Immunotherapy, a section of the journal Frontiers in Immunology

Received: 22 March 2022 Accepted: 11 May 2022 Published: 03 June 2022

Citation:

Liu P, Wang X, Pan L, Han B and He Z (2022) Prognostic Significance and Immunological Role of FBXO5 in Human Cancers: A Systematic Pan-Cancer Analysis. Front. Immunol. 13:901784. doi: 10.3389/fimmu.2022.901784 F-box protein 5 (FBXO5), an essential subunit of the ubiquitin protein ligase complex, is increasingly recognized to exhibit important biological effects in regulating tumor occurrence and progression. The present research was intended to systematically investigate the latent roles of FBXO5 in prognosis and immunological function across cancers. Pan-cancer analyses of FBXO5 were performed based upon publicly available online databases, mainly including the Cancer Genome Atlas (TCGA), Genotype-Tissue Expression (GTEx), UCSC Xena, cBioPortal, and ImmuCellAI, revealing the possible relationships between FBXO5 and prognosis, DNA methylation, tumor microenvironment (TME), infiltration of immune cells, immune-related genes, immune checkpoints, tumor mutation burden (TMB), and microsatellite instability (MSI). The results suggested that FBXO5 was expressed at a high level in numerous tumor cell lines with significant upregulation in most cancers as opposed to normal tissues. Of note, elevated expression of FBXO5 was significantly related to an unfavorable prognosis in many cancer types. Furthermore, DNA methylation and TME were confirmed to display evident correlation with the expression of FBXO5 in several malignancies. Moreover, FBXO5 expression was remarkably positively correlated with the levels of infiltrating Treg cells and Tcm cells in most tumors, but negatively correlated with tumor-infiltrating CD8+ T cells, NK/NKT cells, and Th2 cells. Meanwhile, FBXO5 was demonstrated to be co-expressed with the genes encoding immune activating and suppressive factors, chemokines, chemokine receptors, and major histocompatibility complex (MHC). Immune checkpoints, TMB, and MSI were also overtly associated with FBXO5 dysregulation among diverse kinds of cancers. Additionally, the enrichment analyses showed close relationships between FBXO5 expression and the processes related to cell cycle and immune inflammatory response. These findings provided a detailed comprehension of the oncogenic function of FBXO5. Because of its crucial roles in cancer immunity and tumorigenesis, FBXO5 may serve as a novel prognostic indicator and immunotherapeutic target for various malignancies.

Keywords: FBXO5, bioinformatics, pan-cancer, prognosis, immunity, tumor microenvironment

INTRODUCTION

Malignant tumor poses a threat to global public health as a leading cause of human death and the main hazard factor reducing people's quality of life, and so far, there is still a lack of absolutely effective treatment for cancer (1). Although early screening and surgery make heavy contributions to decreasing the incidence and mortality of malignancies, the prognosis and survival rate of most cancers remain unsatisfactory due to their characteristics of metastasis, recurrence, and heterogeneity (2). Tumor microenvironment (TME), containing various immune cells, stromal cells, and extracellular matrix, exhibits pivotal effects on tumor invasion and metastasis, cancer immunity, and clinical outcomes (3, 4). In recent years, immunotherapy has gradually become a prominent strategy for tumor treatment, especially immune checkpoint blockade therapy. Immune checkpoint inhibitors, such as CTLA-4-, PD-1-, and PD-L1blocking antibodies, have been approved for the standard therapy in different malignancies (5). Nevertheless, the objective response rate remains minimal in many cancer patients receiving the same therapy (5, 6). Therefore, it is full of prospects to discover novel immunotherapeutic targets by analyzing gene expression in pan-cancer and exploring its correlations with clinical prognosis and tumor immunity.

F-box protein 5 (FBXO5), also referred to as early mitotic inhibitor-1 (EMI1), encodes a member of the F-box protein family and functions as an essential cell cycle regulating gene, which modulates the progression to S-phase and mitosis via the mechanism of blocking the anaphase-promoting complex (APC) (7, 8). According to previous reports, overexpression of FBXO5 produces chromosome instability and mitotic disorder, possibly resulting in the tumorigenesis in ovarian clear cell carcinoma (9), esophageal squamous cell carcinoma (10), breast carcinoma (11), and hepatocellular carcinoma (12). Existing evidence has suggested that FBXO5 affects tumor prognosis and clinical phenotypes. FBXO5 accumulation is tightly related to mitotic abnormalities including centrosome overduplication and aberrant spindle formation, which cause the emergence of tetraploidy in ovarian clear cell carcinoma (9). Moreover, elevated expression of FBXO5 is significantly correlated with an unfavorable prognosis among patients suffering from esophageal squamous cell carcinoma (10) and hepatocellular carcinoma (12). In addition, FBXO5 exhibits a pro-proliferative effect in breast cancer tissues through PI3K/Akt signaling pathway, while PI3K inhibitor can reduce FBXO5 expression and arrest cell growth (11). Based upon these findings, FBXO5 may perform an integral function in cell cycle abnormalities and the disruption of genomic stability, both of which can enhance tumor growth (13). At present, specific studies on FBXO5 in tumors appear to be restricted to certain human cancers, but lack of systematic pan-cancer investigation (9–12). In consequence, it is urgent to elucidate the significance and role of FBXO5 expression and alteration across different cancers.

In this research, we attempted to conduct a thorough datamining analysis using multiple public databases to assess the expression and alteration of FBXO5 and visualize the prognostic profiles of FBXO5 in pan-cancer, as well as analyze its correlations with tumor-infiltrating immune cells along with associated immune indicators. Figure 1 illustrated the design flow and implementing approaches of this study. This work integrally revealed that FBXO5 influenced the prognosis of cancer patients. Upregulation of FBXO5 expression was detrimental to survival in most cancers, with inconsistent findings in only a few types of tumors. Furthermore, the potential biological effects were likely to be linked with DNA methylation, tumor microenvironment, and immune microenvironment. In summary, our findings proposed a comprehensive view of the oncogenic role of FBXO5 in multiple kinds of cancers and suggested that FBXO5 might function as a viable indicator for predicting clinical prognosis and immune therapy response in cancer patients.

MATERIAL AND METHODS

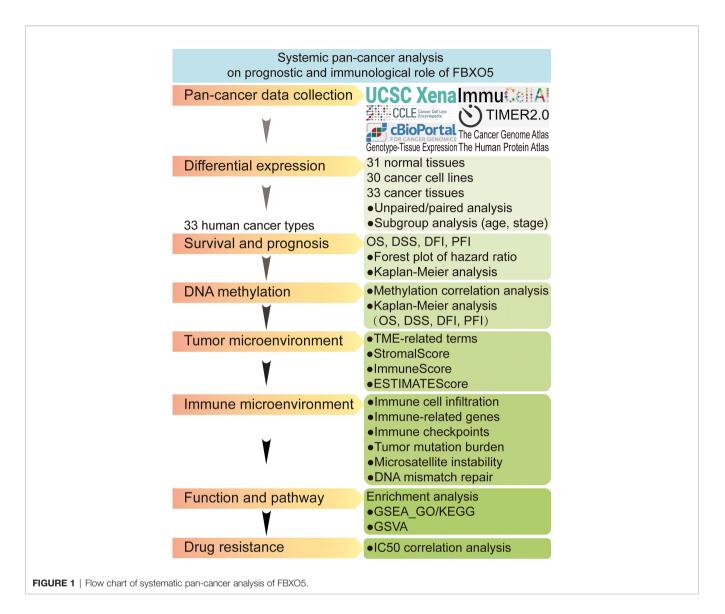
Collection of Pan-Cancer Data and Analysis of Gene Differential Expression

FBXO5 gene expression pattern and clinical data in pan-cancer and corresponding normal tissues obtained from the Cancer Genome Atlas (TCGA, https://portal.gdc.cancer.gov) and Genotype-Tissue Expression (GTEx, https://www.gtexportal.org) were analyzed using UCSC Xena (https://xena.ucsc.edu), an online tool for exploring gene expression and processing clinical and phenotypic information. The Cancer Cell Line Encyclopedia (CCLE, https://portals.broadinstitute.org/ccle) database was employed for the purpose of acquiring tumor cell line-related data. Differential expression of FBXO5 in 33 distinct kinds of cancers in contrast with normal samples was explored by means of merging normal tissue data accessed from both the GTEx and TCGA databases. R language software and publicly available Rpackage "ggplot2" were applied to evaluate the differential expression levels by drawing box plots. All expression data preprocessing and normalization were conducted by log₂ (transcripts per million (TPM)+0.001) or log₂(TPM+1) transformation. Full names and corresponding abbreviations of the 33 types of tumors were listed in the section of Abbreviations.

Survival and Prognostic Analysis of FBXO5

The survival information and clinical phenotype data concerning each sample were acquired from TCGA database. A total of four survival prognosis indexes, namely overall survival (OS), disease-

Abbreviations: ACC, adrenocortical carcinoma; BLCA, bladder urothelial carcinoma; BRCA, breast invasive carcinoma; CESC, cervical squamous cell carcinoma and endocervical adenocarcinoma; CHOL, cholangiocarcinoma; COAD, colon adenocarcinoma; DLBC, lymphoid neoplasm diffuse large B-cell lymphoma; ESCA, esophageal carcinoma; GBM, glioblastoma; LGG, brain lower grade glioma; HNSC, head and neck squamous cell carcinoma; KICH, kidney chromophobe; KIRC, kidney renal clear cell carcinoma; KIRP, kidney renal papillary cell carcinoma; LAML, acute myeloid leukemia; LIHC, liver hepatocellular carcinoma; LUAD, lung adenocarcinoma; LUSC, lung squamous cell carcinoma; MESO, mesothelioma; OV, ovarian serous cystadenocarcinoma; PAAD, pancreatic adenocarcinoma; PCPG, pheochromocytoma and paraganglioma; PRAD, prostate adenocarcinoma; READ, rectum adenocarcinoma; SARC, sarcoma; SKCM, skin cutaneous melanoma; STAD, stomach adenocarcinoma; TGCT, testicular germ cell tumors; THCA, thyroid carcinoma; THYM, thymoma; UCEC, uterine corpus endometrial carcinoma; UCS, uterine carcinosarcoma; UVM, uveal melanoma.



specific survival (DSS), progression-free interval (PFI), and disease-free interval (DFI), were used to investigate the correlation of FBXO5 expression with the prognosis of cancer patients. The R-packages "*survival*" and "*forestplot*" were employed to conduct a univariate Cox analysis. The median levels of FBXO5 expression were recognized as the expression threshold for classifying the low- and high-expression subgroups. Subsequently, the curves of Kaplan-Meier survival were established utilizing the R-packages "*survminer*" and "*survival*". The log-rank test was employed to determine statistically significant differences.

Immunohistochemistry Analysis of FBXO5

The expression pattern of FBXO5 at the protein levels was examined by means of the Human Protein Atlas (HPA, http:// www.proteinatlas.org) database containing the protein data of tumor and normal clinical samples. Immunohistochemistry (IHC) photomicrographs of FBXO5 in different types of tumor

tissues and corresponding normal control were collected from the HPA. Specifically, the immunohistochemical results based on the antibody against FBXO5 (Cat No. HPA029048; Atlas Antibodies, Sigma-Aldrich) in various normal tissues were downloaded from the tissue section of HPA database, while these data in different tumor tissues were obtained from the pathology section. All sample data are independent of each other. FBXO5 protein staining intensity in cancer tissues was quantified as fold of their respective normal control using Image-Pro Plus 6.0 (Media Cybernetics, USA). According to the statistical differences of these data generated from unpaired two-tailed Student's *t*-test, representative FBXO5 protein staining pictures were displayed.

DNA Methylation Analysis of FBXO5

To assess the association between the expression of FBXO5 and DNA methylation in each cancer type involved in this study, we analyzed HM450 methylation data acquired from the cBioPortal

database (http://www.cbioportal.org). The correlation between the levels of FBXO5 expression and gene promoter methylation levels was examined and visualized through the R-package "ggpubr" for each malignancy studied. Further, the correlation analysis between FBXO5 methylation and tumor prognostic value was also evaluated according to the determination of OS, DSS, DFI, and PFI through applying the survival R-packages to construct the Kaplan-Meier curves.

Relevance amongst FBXO5 Expression and Tumor Microenvironment

Numerous research reports have demonstrated that tumor microenvironment (TME) performs an integral function in multidrug resistance and tumorigenesis and metastasis (3, 4). To establish the connection between TME and FBXO5 expression, a previously reported method developed by Zeng et al. was applied to estimate the related effects of FBXO5 within TME of 33 cancers (14). Visualization of the associations between FBXO5 expression and TME indicators such as stromal- and immune-relevant signatures was performed in a heatmap using R-based packages.

In addition, ImmuneScore, StromalScore, and ESTIMATEScore for the 33 types of cancers studied were calculated by the algorithm of ESTIMATE (Estimation of Stromal and Immune Cells in Malignant Tumor Tissues Using Expression Data). Increased scores computed in ImmuneScore or StromalScore were deemed to be favorably correlated with the elevated ratio of immunity or stroma, which signified a greater proportion of the corresponding components in TME. Besides, ESTIMATEScore was described as the sum of ImmuneScore and StromalScore, which denoted the combined percentage of both constituents in TME. In this assessment, ImmuneScore and StromalScore of various tumors were subjected to estimation utilizing the R-package "*estimate*" and Pearson's correlation test.

Immune Infiltration Analysis of FBXO5

A total of three methods were employed for the purpose of investigating the abundance of infiltrating immune cells in diverse cancers, such as neutrophils, dendritic cells (DCs), CD4⁺ and CD8⁺ T cells, natural killer (NK) cells, mast cells, macrophages, monocytes, and B cells. The first method investigated the associations between the levels of FBXO5 expression and the extent of 24 infiltrating immune cells in 32 distinct cancers except for LAML without immune infiltration data by using the R-packages "ggplot2", "ggpubr", and "ggExtra" and the tool CIBERSORT to estimate immune infiltration data from the ImmuCellAI database (http://bioinfo.life.hust.edu.cn/ ImmuCellAI#!/). Besides, the TIMER2.0 database (Tumor Immune Estimation Resource, http://timer.comp-genomics.org/) was employed as the auxiliary technique in order to assess the correlations between FBXO5 expression and the levels of tumorinfiltrating immune cells. The third method involved the use of Rpackages "limma", "reshape2", and "RColorBreyer" for the aim of identifying the relevance between FBXO5 expression and immuneassociated genes, such as immune-activating genes, immunosuppressive genes, chemokine genes, chemokine-receptor genes as well as major histocompatibility complex (MHC) genes.

Correlations Between FBXO5 Expression and Immune Checkpoints, Tumor Mutation Burden, Microsatellite Instability, and DNA Mismatch Repair

The investigation of relationships between FBXO5 and the recognized immune checkpoint genes such as CTLA4, CD274, TIGIT, PDCD1, and LAG3 was conducted in accordance with the database of TCGA. Tumor mutation burden (TMB) is a quantitative biological marker of immune response that reflects the proportion of somatic mutations present in tumor cells (15). The somatic mutation data of the 33 tumors involved in this study were acquired from the UCSC Xena repository (https:// tcga.xenahubs.net) for the calculation of TMB scores using a Perl script with the correction by dividing based upon the total exon length. Microsatellite instability (MSI) as a result of DNA mismatch repair deficiency is related with patient outcomes (16, 17), and the MSI data were acquired according to a previously published report (18). Both TMB and MSI are associated with the effectiveness of immunotherapy across diverse cancers. The correlation between FBXO5 expression and TMB or MSI was explored by means of Pearson correlation coefficient, with these findings displayed in the form of radar plots. Mismatch repair (MMR) is an intracellular DNA repair mechanism. Downregulation or functional defects of MMR genes such as MSH2, MSH6, PMS2, MLH1, and EPCAM can lead to irreparable DNA replication errors, resulting in high-frequency somatic mutations and thereby increasing susceptibility to cancer (19). The correlation between FBXO5 and MMR gene expression was determined based upon gene expression profile data from the TCGA cohort and visualized as a heatmap using the R-packages "reshape2" and "RColorBrewer".

FBXO5-Associated Enrichment Analysis in Pan-Cancer

An investigation into the biological effects of FBXO5 in the human cancers studied was conducted by means of Gene Set Enrichment Analysis (GSEA) and Gene Set Variation Analysis (GSVA). The R-packages "*ClusterProfiler*", "*limma*", and "*enrichplot*" were employed for the enrichment analyses of Gene Ontology (GO) and Kyoto Encyclopedia of Genes and Genomes (KEGG). GO and KEGG gene sets were obtained from the GSEA website (https://www.gsea-msigdb.org/gsea/index.jsp). GSVA gene set was downloaded from the module "hallmark gene sets" in the Molecular Signatures Database (MSigDB, https://www.gsea-msigdb.org/gsea/msigdb/index.jsp). Moreover, GSVA scores were measured as the correlations between 50 well-defined biological processes or states and FBXO5 expression levels for all tumors.

Drug Resistance Analysis of FBXO5

For exploring the correlation of FBXO5 expression with drug resistance or sensitivity of tumor cells, the information of various compounds and the corresponding IC50 values and FBXO5 expression data in cancer cell lines were obtained from the GDSC2 dataset (Genomics of Drug Sensitivity in Cancer,

https://www.cancerrxgene.org). IC50 here refers to the half maximal inhibitory concentration, which represents the concentration of an inhibitor that is required for 50% inhibition of tumor cell survival. IC50 reflects the tolerance of cells to drugs, i.e., the lower the IC50 value, the more sensitive the cells are to drugs. The correlation between IC50 value of each compound and the levels of FBXO5 expression in cancer cells was analyzed using Spearman correlation coefficient and shown in **Table S1**.

Statistical Analysis

Statistical data analyses were carried out with the help of R software (https://www.r-project.org/). Comparison of differences between two groups was conducted using Student's *t*-test or Wilcoxon rank sum test. One-way analysis of variance (ANOVA) was used to compare more than two experimental groups. All survival analyses were performed by applying the Kaplan-Meier product-limit method with a log-rank test and Cox proportional hazards regression model. The correlation between two variables was assessed utilizing Pearson product-moment correlation coefficient. For all statistical differences, *p*-values of less than 0.05, 0.01, 0.001, and 0.0001 were judged to be statistically significant and presented as "*", "**", "***", and "****", respectively. Besides, "ns" indicated no significance.

RESULTS

Differential Expression of FBXO5 Between Tumor and Normal Samples

The physiologic gene expression profiles of FBXO5 among various normal tissues were first analyzed and ranked from low to high, using the GTEx and TCGA data sets (**Figure 2A**). FBXO5 exhibited the highest expression level in bone marrow, but, in general, a majority of other normal samples were found to exhibit low levels of FBXO5 expression. Next, comparative gene expression profiles of FBXO5 among different tumor cell lines that had been obtained from the CCLE database were described in **Figure 2B**, which showed that FBXO5 expression levels were generally higher in up to 30 types of cancer cell lines. Besides, FBXO5 expression levels in various tumors were assayed by the TCGA database, and the findings illustrated that from the 33 cancer tissues analyzed, FBXO5 was expressed with the lowest expression in KICH and with the greatest expression in TGCT (**Figure 2C**).

Moreover, differential expression levels of FBXO5 across tumor and normal samples were computed with the aid of the TCGA database (**Figure 3A**). Apart from those tumors with no available normal tissue data including MESO and UVM, statistical significance of FBXO5 expression differences between normal and tumor samples was detected in 27 types of cancers. Among these, highly expressed FBXO5 was further observed in 24 types of cancers, namely ACC, BLCA, BRCA, CESC, CHOL, COAD, DLBC, ESCA, GBM, HNSC, KIRC, LGG, LIHC, LUAD, LUSC, OV, PAAD, READ, SKCM, STAD, TGCT, THYM, UCEC, and UCS (*p*-value < 0.001 in the above tumors except *p*-value < 0.01 in KIRC). Notably, the fold change of upregulation of FBXO5 expression levels among tumor tissues was the highest in GBM compared with the corresponding normal tissues. On the contrary, FBXO5 expression levels showed significantly downregulated in KICH, LAML, and THCA in comparison to their respective normal control (*p*-value < 0.001). Besides, the expression levels of FBXO5 presented no significant differences in KIRP, PCPG, PRAD, and SARC tissues relative to the corresponding normal tissues.

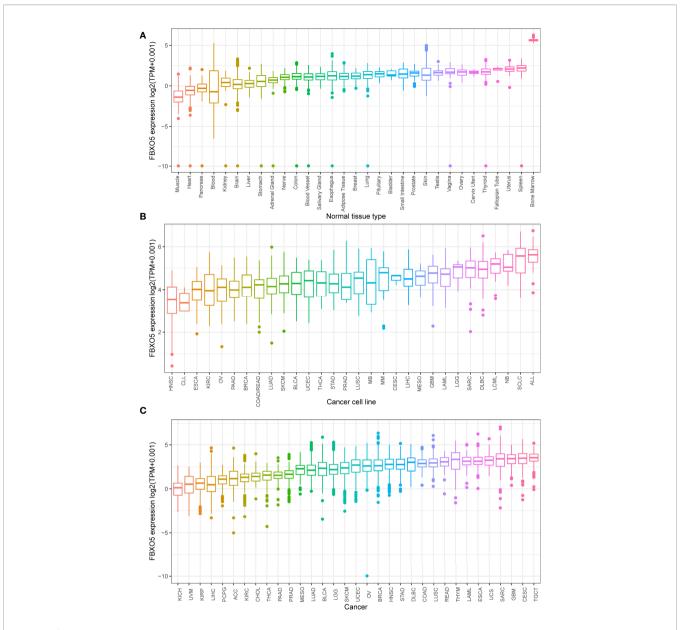
Additionally, the paired differential expression analysis of FBXO5 among tumor and normal tissues was performed followed by a paired Student's *t*-test. Increased expression of FBXO5 in BLCA, BRCA, CHOL, COAD, ESCA, HNSC, LIHC, LUAD, LUSC, and STAD while decreased expression in KICH and THCA was respectively confirmed in comparison of matched normal samples (**Figure 3B**).

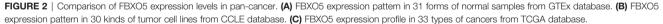
Next, the differential analysis of FBXO5 expression in each tumor type were examined in accordance with the age of patients, which suggested that patients aged > 60 years old had lower expression levels of FBXO5 compared with those aged \leq 60 years old in several tumor types including BRCA, ESCA, HNSC, LIHC, and THYM, while patients aged > 60 years old with OV had higher FBXO5 expression than those aged \leq 60 years old (**Figure 3C**). Moreover, the comparison of FBXO5 expression was higher in more advanced stages of the four malignancies, namely ACC, KICH, LIHC, and UCEC. However, the expression of FBXO5 in higher stages appeared lower in SKCM and THCA (**Figure 3D**).

Subsequently, we further explored the protein expression levels of FBXO5 across tumor and normal clinical samples based upon the HPA database, as depicted in **Supplementary Figures 1A–J**. Quantitative analysis of IHC showed that FBXO5 protein staining intensity in BRCA, CESC, COAD, LIHC, OV, PAAD, STAD, TGCT, and UCEC tissues was respectively detected to be more obvious than weak FBXO5 staining of normal breast, cervix, liver, ovaries, pancreas, and stomach tissues, and also stronger compared with moderate FBXO5 staining of normal colon, testes, and endometrium tissues (**Supplementary Figure 1K**). In contrast, FBXO5 IHC staining in THCA was lighter than that in normal thyroid gland samples (**Supplementary Figure 1K**). Therefore, these IHC staining data were consistent with the sequencing results of FBXO5 at the transcriptome level.

Pan-Cancer Prognostic Value of FBXO5

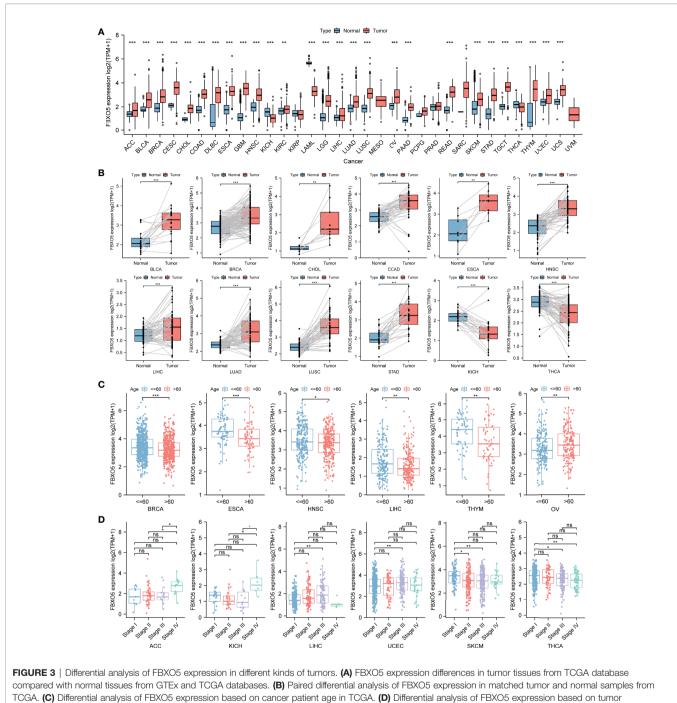
For the purpose of clarifying the correlation between FBXO5 expression and tumor prognosis, hazard ratio statistics for OS, DSS, DFI, and PFI were processed *via* forest plots for each cancer included in this study. According to the univariate Cox regression analysis, FBXO5 was a remarkable risk factor for OS in LGG, ACC, MESO, LIHC, KICH, KIRP, LUAD, and BRCA (*p*-value < 0.001 except LUAD and BRCA in which *p*-value < 0.01), while a protective factor in THYM (*p*-value = 0.008) and READ (*p*-value = 0.009) (**Figure 4A**). Next, Cox regression analysis of DSS identified that FBXO5 was a prominent risk factor in LGG, ACC, MESO, LIHC, KICH, KIRP, and





LUAD (*p*-value < 0.001 other than LUAD in which *p*-value = 0.002). On the other side, FBXO5 served as a protective factor in THYM (*p*-value = 0.036), as displayed in **Figure 4B**. Subsequently, DFI Cox regression analysis regarded FBXO5 as a risk factor in HNSC (*p*-value < 0.001) and LIHC (*p*-value = 0.005) but a protective factor in STAD (*p*-value = 0.044), as depicted in **Figure 4C**. Furthermore, Cox regression analysis of PFI revealed that FBXO5 acted as an unfavorable factor for patients with ACC, LIHC, KIRP, KICH, PRAD, and LGG (*p*-value < 0.001 for ACC and LIHC, *p*-value = 0.001 for KIRP, and *p*-value < 0.01 for KICH, PRAD, and LGG), whereas a protective factor in STAD (*p*-value < 0.05), as shown in **Figure 4D**.

Correspondingly, Kaplan-Meier survival analyses of OS, DSS, DFI, and PFI were further investigated in the 33 forms of cancers studied. Kaplan-Meier survival curves for OS showed that elevated FBXO5 expression levels were evidently correlated with an unfavorable prognosis of cancer patients suffering from ACC, KICH, KIRP, LGG, LIHC, LUAD, and MESO (*p*-value < 0.01 other than KICH in which *p*-value < 0.05), whereas significantly correlated with longer survival time in patients with READ (*p*-value = 0.043) (**Figure 4E**). Meanwhile, Kaplan-Meier DSS survival analysis demonstrated a remarkable relationship of high levels of FBXO5 expression and poor survival outcomes in patients having ACC, ESCA, KICH, KIRP, LGG, LIHC, LUAD,



pathological stages in TCGA. * p-value < 0.05, ** p-value < 0.01, and *** p-value < 0.001. "ns" indicated no significance.

MESO, and SARC (*p*-value < 0.01 other than ESCA and SARC in which *p*-value < 0.05) (**Figure 4F**). Then, Kaplan-Meier survival analysis of DFI revealed a significant connection between high FBXO5 expression and poor prognosis in KIRP (*p*-value = 0.00034) and LIHC (*p*-value = 0.025). Nevertheless, increased expression of FBXO5 exhibited a protective effect on THCA patient outcomes (*p*-value = 0.049) (**Figure 4G**). Moreover, Kaplan-Meier PFI analysis showed that patients with ACC,

KICH, KIRP, LIHC, and MESO had relatively longer survival time probably because of low expression levels of FBXO5 (*p*-value < 0.01 other than KICH and MESO in which *p*-value < 0.05). However, contrasting results were observed in PFI survival of patients with GBM (*p*-value = 0.029) (**Figure 4H**). Taken together, these results implied that high FBXO5 expression generally contributed to unfavorable patient prognosis and survival in a variety of tumor types.

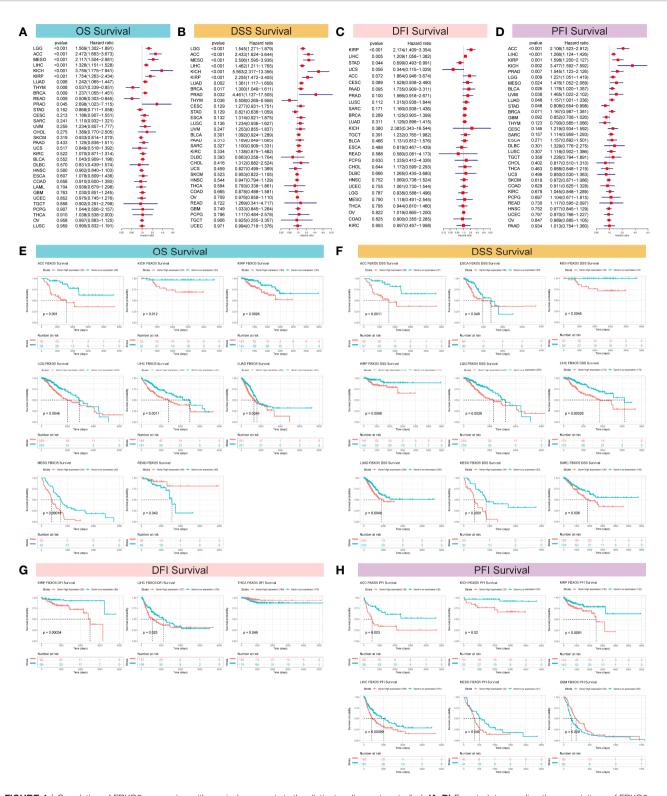
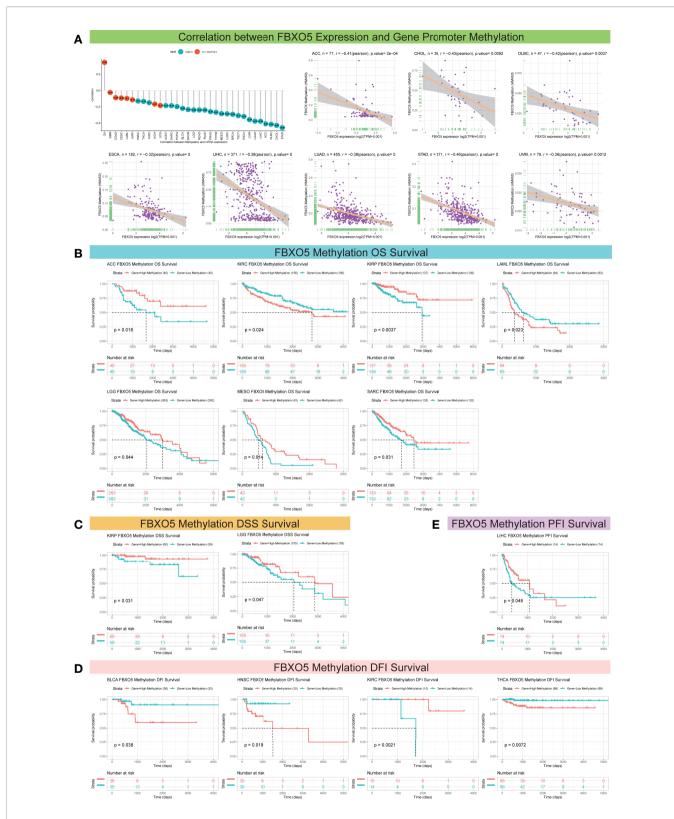
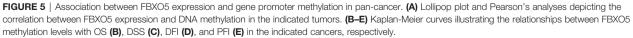


FIGURE 4 | Correlation of FBXO5 expression with survival prognosis in the distinct malignancies studied. (A–D) Forest plots revealing the associations of FBXO5 with OS (A), DSS (B), DFI (C), and PFI (D) in the indicated tumors, respectively. (E–H) Kaplan-Meier curves showing the relationships of FBXO5 expression with OS (E), DFI (G), and PFI (H) in the indicated cancers, respectively.





Correlativity of FBXO5 Expression and DNA Methylation Modification

Next, FBXO5 promoter methylation levels accompanied by changes in FBXO5 expression were estimated using the cBioPortal database and the results reflected significant correlations between FBXO5 expression and methylation in a total of 25 tumors as indicated by the lollipop chart in **Figure 5A**. Among these 25 cancer types, FBXO5 expression all showed Pearson's negative correlations with gene promoter methylation levels, and the former eight malignancies with the greatest inverse association were respectively presented in **Figure 5A**, including STAD, CHOL, DLBC, ACC, LIHC, LUAD, UVM, and ESCA (*p*-value < 0.001 except CHOL, DLBC, and UVM in which *p*-value < 0.01). Pearson's correlation analyses of the other different cancers were displayed in **Supplementary Figure 2**.

On the other hand, for the aim of exploring the correlation between FBXO5 promoter methylation and survival prognosis (OS, DSS, DFI, and PFI), Kaplan-Meier analyses were performed for the 33 forms of cancers studied. Enhanced FBXO5 methylation was demonstrated to be a protective indicator for superior OS in patients diagnosed with ACC, KIRP, LGG, MESO, and SARC (p-value < 0.05 except KIRP in which pvalue < 0.01), whereas a deleterious indicator that was prone to result in low survival probability of KIRC (p-value = 0.024) and LAML (*p*-value = 0.023) (Figure 5B). DSS analysis demonstrated that FBXO5 methylation functioned as a protective marker in patients experiencing KIRP (p-value = 0.031) and LGG (p-value = 0.047) (Figure 5C). Besides, FBXO5 methylation levels exhibited a significant positive correlation with DFI survival in patients experiencing KIRC (p-value = 0.0021) although FBXO5 methylation acted as a harmful factor in patients with BLCA (pvalue = 0.038), HNSC (p-value = 0.019), and THCA (p-value = 0.0072) (Figure 5D). Moreover, as far as PFI be concerned, a lower FBXO5 methylation level was overtly relevant with a poorer prognosis in LIHC patients (*p*-value = 0.048) (Figure 5E).

Association Between FBXO5 Expression and Tumor Microenvironment

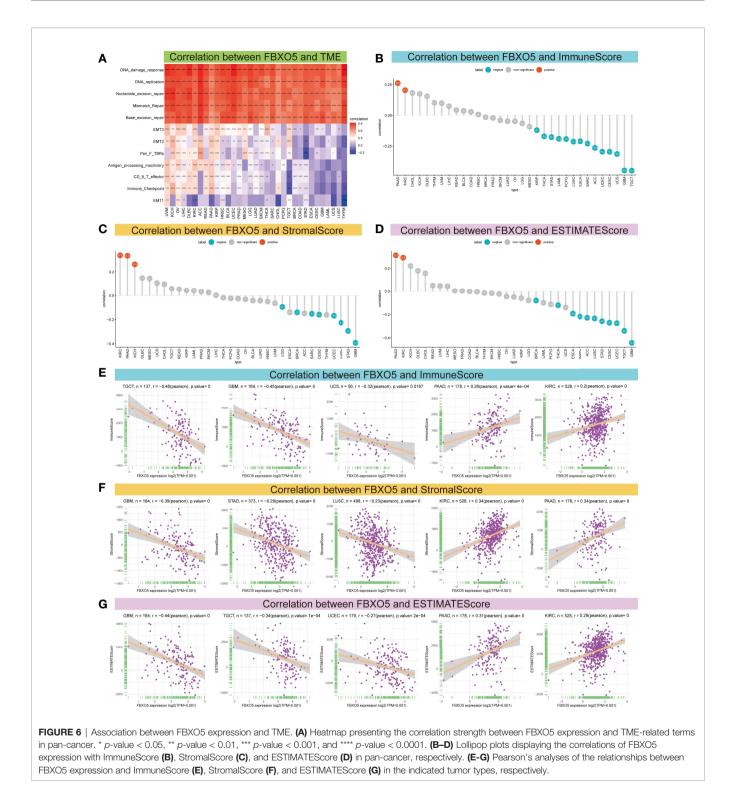
Emerging researches have established that TME exerts a pivotal function during the onset and progression of tumors (3, 4). Therefore, it is essential to examine the correlation between TME and FBXO5 expression levels. Figure 6A described a heatmap of the correlation strength between FBXO5 expression and TME terms, showing that DNA damage response, DNA replication, nucleotide excision repair, mismatch repair as well as base excision repair were highly positively connected to the expression of FBXO5 in the indicated cancers. Subsequently, the ESTIMATE algorithm was implemented to compute the ImmuneScore, StromalScore, and ESTIMATEScore in the 33 distinct malignancies and analyze the Pearson's correlations between the expression of FBXO5 and the above three scores in pan-cancer. The lollipop plots presented an in-depth understanding of FBXO5 expression and TME scores in different cancers (Figures 6B-D). In PAAD and KIRC, the findings indicated that FBXO5 expression exhibited significant positive correlations with the ImmuneScore (Figure 6B),

StromalScore (Figure 6C), and ESTIMATEScore (Figure 6D), respectively. Conversely, notable inverse correlations were discovered between FBXO5 expression and all three scores of SARC, CESC, UCEC, LUSC, STAD, and GBM (Figures 6B-D). Furthermore, regarding the value of Pearson's r, the top three cancers with predominant negative correlations and the top two cancers with remarkable positive correlations of FBXO5 expression and TME-relevant scores included TGCT, GBM, UCS, PAAD, and KIRC (Figure 6E, sorted by ImmuneScore); GBM, STAD, LUSC, KIRC, and PAAD (Figure 6F, sorted by StromalScore); GBM, TGCT, UCEC, PAAD, and KIRC (Figure 6G, sorted by ESTIMATEScore), respectively. In addition, the Pearson's correlations of FBXO5 expression levels with ImmuneScore, StromalScore, and ESTIMATEScore of the other malignancies investigated were separately displayed in Supplementary Figures 3, 4 and 5.

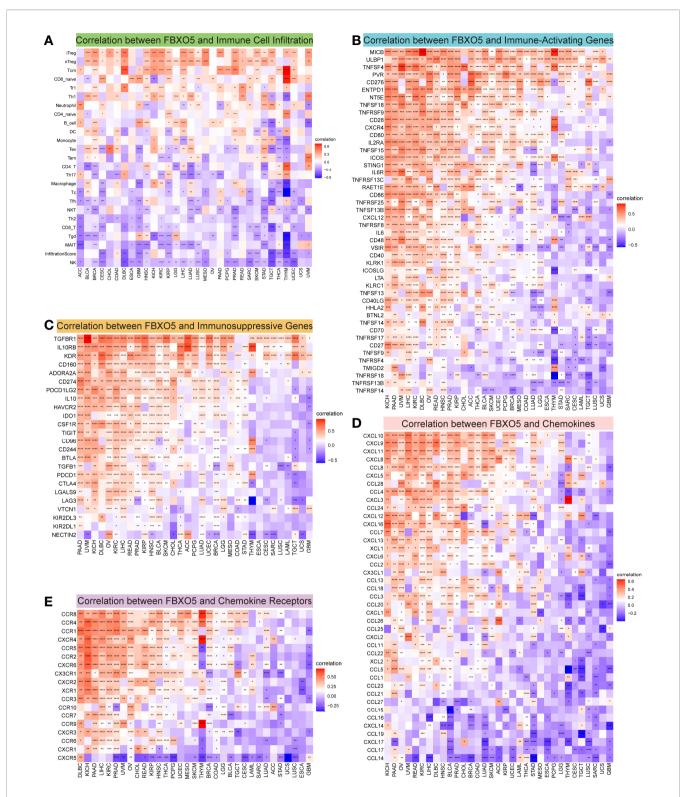
Correlation of FBXO5 Expression With Pan-Cancer Immune Cell Infiltration

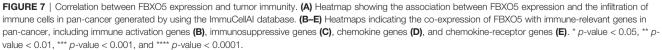
Growing researches have suggested that tumor-infiltrating immunocytes could have a critical impact on the survival status of patients (20). From this point of view, the correlations between the expression levels of FBXO5 and the infiltration abundance of 24 distinct immune cell subtypes were analyzed at a pan-cancer level using the ImmueCellAI database. It was revealed that immune cell infiltration degree was strongly related to FBXO5 expression in most cancers (Figure 7A). For instance, the expression of FBXO5 exhibited a remarkable positive correlation with regulatory T (Treg) cells and central memory T (Tcm) cells. In comparison, the FBXO5 expression exhibited a substantial negative correlation with natural killer (NK) cells, CD8⁺ T cells, and T-helper 2 (Th2) cells. Interestingly, various relationships between FBXO5 expression and distinct T cell subsets were further discovered, as illustrated in Supplementary Figure 6A. For example, the expression of FBXO5 presented an inverse association with the infiltrating levels of CD4⁺ Tcm cells, CD4⁺ effector memory T (Tem) cells, and natural killer T (NKT) cells in most tumors based upon the XCELL algorithm. Besides, a close positive correlation between FBXO5 expression and infiltrating macrophages was observed in PRAD (*p*-value < 0.0001), whereas a notable negative correlation was identified in GBM, THCA, and THYM (p-value < 0.0001 for the three cancers) (Figure 7A). By use of the TIMER2.0 database, similar results about FBXO5 expression-related macrophage infiltration were also found in PRAD based upon the TIMER algorithm, and GBM, THCA, and THYM based upon the XCELL algorithm (Supplementary Figure 6A).

Afterwards, the correlations of expression levels between FBXO5 and immune-related genes that encode immuneactivating, immunosuppressive, chemokine, chemokinereceptor proteins as well as MHC were investigated across cancers (**Figures 7B-E** and **Supplementary Figure 6B**). The heatmaps demonstrated that FBXO5 exhibited a significant coexpression relationship with most immune activation and immunosuppressive genes in various cancers, particularly in KICH, PAAD, UVM, LIHC, KIRC, DLBC, OV, READ, HNSC,



PRAD, and KIRP (**Figures 7B, C**). Furthermore, both chemokine and chemokine-receptor genes were strongly coexpressed with FBXO5 in pan-cancer (**Figures 7D, E**). For example, in KICH and PAAD, there was a positive connection of the expression levels of FBXO5 with most chemokine and chemokine-receptor genes. Concurrently, **Supplementary Figure 6B** elucidated that FBXO5 expression was positively associated with almost all MHC genes in KIRC, UVM, PAAD, KICH, and OV, while inversely correlated in THYM, TGCT, and GBM. To conclude, these data inferred that FBXO5 might





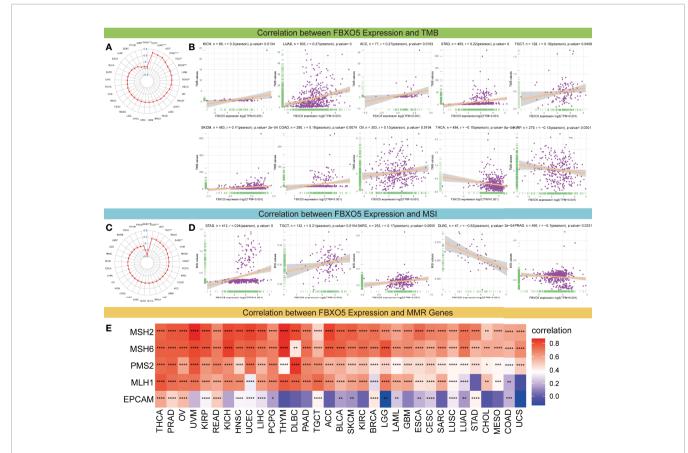
contribute to regulating immune cell infiltration and the biological functions of various immune-related genes in the tumor immune microenvironment of most tumor types.

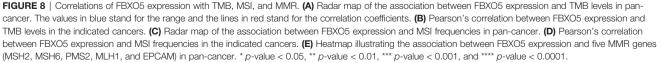
Associations of FBXO5 Expression With Immune Checkpoints, Tumor Mutation Burden, Microsatellite Instability, and DNA Mismatch Repair

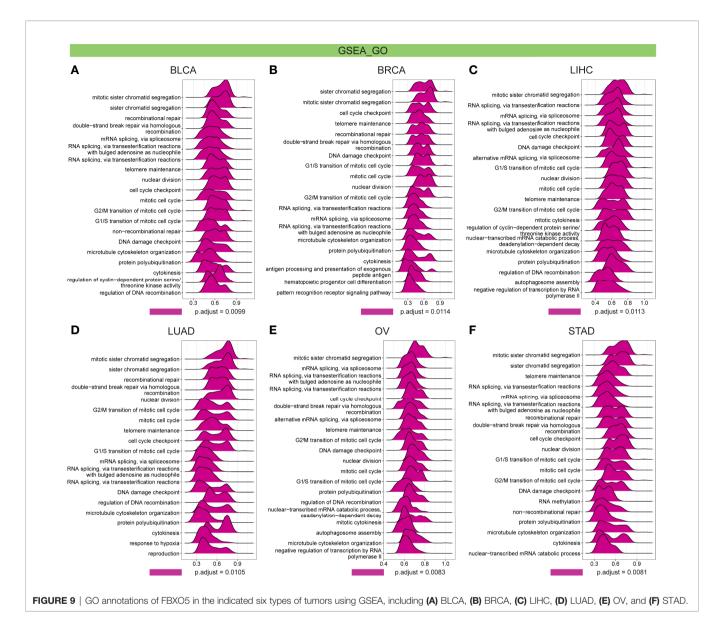
Immune checkpoints that are responsible for regulating the degree of immune activation and play a crucial role in autoimmunity and immune surveillance of tumor cells, have already been identified as the inhibitory targets of cancer immunotherapy (5, 6). Subsequently, the correlations were studied between FBXO5 and five major immune checkpoint genes, namely CTLA4, CD274, TIGIT, PDCD1, and LAG3. In most cancers, FBXO5 expression was highly related with the levels of immune checkpoint gene expression (**Supplementary Figure 7**).

Additionally, considering the essential roles of TMB and MSI in the prediction of the response to immune therapy across cancers, the link between FBXO5 expression and the values of TMB or MSI was also explored. Overall, these two metrics varied remarkably among different cancer types (**Figures 8A, C**). FBXO5 expression showed to be positively relevant to TMB in KICH, LUAD, ACC, STAD, TGCT, SKCM, COAD, and OV (**Figure 8B**). In contrast, FBXO5 expression inversely correlated to TMB in THCA and KIRP (**Figure 8B**). Furthermore, FBXO5 expression had a positive correlation with MSI in STAD, TGCT, and SARC (**Figure 8D**). Nonetheless, FBXO5 expression inversely correlated to MSI in PRAD and DLBC (**Figure 8D**). On balance, the aforementioned results strongly indicated that FBXO5 was well associated with tumor immunity. Thus, FBXO5 might be taken as a viable biomarker for indicating the immunotherapy response in these tumor types.

Furthermore, deficient mismatch repair (dMMR) is an unneglected mechanism of tumorigenesis and development, which suggests that the potential relationship between FBXO5 and MMR needs to be studied in pan-cancer. The results displayed that FBXO5 expression was significantly positively associated with almost each of the five MMR genes (MSH2, MSH6, PMS2, MLH1, and EPCAM) in most tumors (**Figure 8E**). Specially, FBXO5 expression was negatively correlated with







EPCAM in LGG (**Figure 8E**). These data indicated that FBXO5 might regulate the tumor progression by mediating the repairment of DNA mismatch across cancers.

Enrichment Analysis of FBXO5 in Pan-Cancer

Further, GSEA and GSVA were carried out to explore the underlying biological relevance of FBXO5 in tumor tissues. GO analysis indicated that FBXO5 was significantly linked to the functions of cell division and cell cycle regulation, including sister chromatid segregation, telomere maintenance, nuclear division, cell cycle checkpoint, RNA splicing, and DNA damage checkpoint in malignancies of various types, such as BLCA, BRCA, LIHC, LUAD, OV, and STAD (**Figures 9A-F**). KEGG-enriched terms revealed that the major associations of FBXO5 with the above six cancers existed in the processes of nucleocytoplasmic transport, cell cycle, cellular senescence, ubiquitin-mediated proteolysis, and microRNAs in cancer (Figures 10A-F). Of note, FBXO5 was found to be critically involved in immune-associated tumorigenic virus infectious diseases, including hepatitis B, hepatitis C, human T-cell leukemia virus 1 infection, and Epstein-Barr virus infection (Figures 10A-F).

Meanwhile, the GSVA data reinforced that FBXO5 expression was positively correlated with mitotic spindle, G2/ M checkpoint, mTORC1 signaling, PI3K/Akt signaling, and protein secretion in the above six malignancies, as well as inflammatory response of cell immune factors in BLCA, BRCA, and LIHC such as interferon-alpha, interferon-gamma, IL6, and TGF-beta, but in general it was inversely associated with K-ras signaling DN, myogenesis, bile acid metabolism, xenobiotic metabolism, and p53 pathway (**Supplementary**

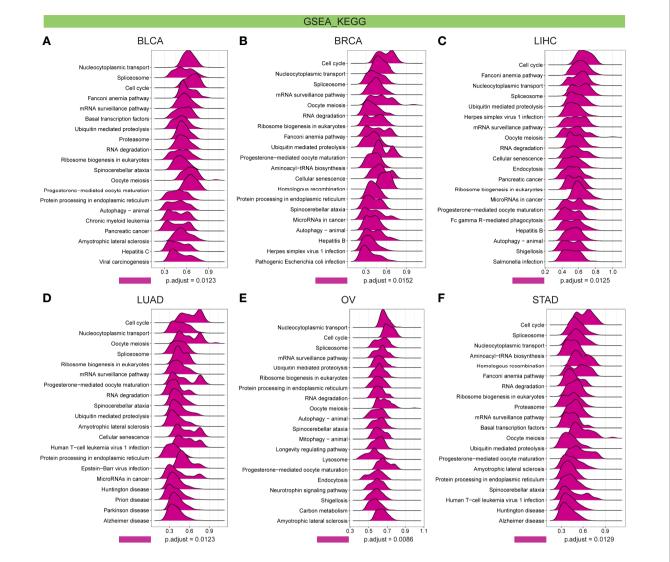


FIGURE 10 | KEGG annotations of FBXO5 in the indicated six types of tumors using GSEA, including (A) BLCA, (B) BRCA, (C) LIHC, (D) LUAD, (E) OV, and (F) STAD.

Figures 8A–F). These results together implied that FBXO5 played a key role in regulating the tumor occurrence and progression and immune microenvironment.

Correlation of FBXO5 Expression With Drug Resistance

At present, in clinical practice, multidrug resistance (MDR) of cancer cells is an unneglected link leading to recurrent tumor and affecting prognosis and survival. Hence, for evaluating the potential of FBXO5 in guiding clinical treatment, the correlation between FBXO5 and drug resistance of tumor cells was computed based upon IC50 values of drugs along with FBXO5 expression levels. The results suggested that FBXO5 exhibited a significant positive association with IC50 values of seven compounds but a notable negative correlation with IC50 values of 153 compounds (**Table S1**). Besides, there were no significant relevance between FBXO5 and IC50 in a total of 32 compounds (**Table S1**). Therefore, increased expression of FBXO5 can make tumor cells more sensitive to most kinds of compounds, which implies that the therapies of most compounds become effective in cancer patients with high FBXO5 expression. From the perspective of translational medicine, detection of FBXO5 expression may be used to guide the efficacy prediction of drug clinical treatment in tumors, and also contribute to the accurate selection of antitumor drugs.

DISCUSSION

APC is well known to be a critical ubiquitin ligase that governs the cell cycle progression through mitosis to G1-phase (21). FBXO5-encoded protein is a significant regulator of APC activity and it functions in cell cycle modulation through effectively stabilizing the ubiquitination substrates of APC after preventing ubiquitin chain elongation (22). Recently, several bioinformatics researches proved that FBXO5 could specifically regulate multiple tumor behaviors and exhibited a crucial role in the tumorigenesis and prognosis of several cancers, including squamous cell lung carcinoma (23), breast cancer (24), hepatocellular carcinoma (25), and HPV-positive cervical cancer (26). Above all, these studies speculated that FBXO5 could be regarded as a potential oncogenic factor or therapeutic target among the above tumor types.

On the premise of existing evidence, the current work performed a thorough investigation for pan-cancer analysis of FBXO5 across malignancies. This study constructed a detailed exploration of FBXO5 expression differences, underlying functions, and prognostic significance in 33 human cancers. Rising FBXO5 expression was confirmed to be remarkably correlated with unfavorable clinical outcomes in a variety of cancers. Further demonstration revealed that abnormal FBXO5 expression in most cancers was significantly correlated with TME, immune infiltration, DNA methylation, immune checkpoints, TMB, MSI, and MMR. Collectively, FBXO5 might confer an instrumental function in indicating tumorigenesis, prognosis, as well as tumor immunity, which is briefly summarized in **Table S2**.

Our data first showed a significant increase of FBXO5 expression in 24 cancers, while decrease in KICH, LAML, and THCA in contrast to the corresponding normal tissues. These findings were in agreement with earlier research reports on ovarian clear cell carcinoma (9), esophageal squamous cell carcinoma (10), squamous cell lung carcinoma (23), breast cancer (11, 24), hepatocellular carcinoma (12, 25), and cervical cancer (26). Meanwhile, FBXO5 expression was analyzed to be correlated with the tumor stage. In patients having UCEC, LIHC, KICH, and ACC, FBXO5 expression was higher at stage III or IV than stage I or II. Hence, the current data provided a hint that FBXO5 could serve as an oncogene in most tumors.

The present research also discovered that FBXO5 expression was related to tumor prognosis, which suggested that the overexpression of FBXO5 was a hazard factor of cancers and could cause a poorer prognosis in terms of OS, DSS, PFI, and DFI. Similarly, existing researches also demonstrated that FBXO5 upregulation was critically correlated to the poor prognosis of esophageal squamous cell carcinoma (10), hepatocellular carcinoma (12), squamous cell lung carcinoma (23), and breast cancer (11, 24). Notably, highly expressed FBXO5 in STAD (stomach adenocarcinoma) was a protective factor for DFI and PFI survival, and this was different from most cancers in which increased FBXO5 acted as an unfavorable prognostic factor, implying that FBXO5 may have specific functions in STAD. A previous study on the role of CRIP1 can well explain the protective role of FBXO5 in gastric cancer (27). Simply put, CRIP1 is overexpressed in gastric cancer and CRIP1 deficiency inhibits the process of homologous recombination and increases susceptibility to chemotherapy in gastric cancer cells. FBXO5 can block CRIP1-promoted homologous recombination repair by preventing nuclear enrichment of RAD51, thereby restoring chemotherapy sensitivity of gastric cancer cells with high CRIP1 expression. Due to the negative

correlation between CRIP1 expression and survival time in gastric cancer patients, FBXO5 may exhibit a potential protective role in the prognosis of gastric cancer through inhibiting the identified function of CRIP1 in this report.

DNA methylation is a type of DNA chemical modification that functions as a crucial regulator of gene transcription. Abnormalities of DNA methylation levels perform an indispensable function in the onset and progression of many tumors (28). Pan-cancer survival analysis showed that FBXO5 promoter methylation levels were obviously correlated with better OS in patients diagnosed as ACC, KIRP, LGG, MESO, and SARC, which was opposite in KIRC and LAML patients. These results uncovered that FBXO5 could be developed as a promising predictive biomarker for clinical prognosis of various malignancies.

TME comprising various infiltrating immune and stromal cells confers instrumental functions in the pathogenesis and development of cancer (3, 4) and meanwhile it can also prominently affect therapeutic response and clinical outcomes (29). The findings of the present research elucidated that FBXO5 expression in 33 malignancies positively correlated to TME involving DNA damage and repair. Of note, DNA damage response (DDR) genes are frequently mutated in almost all cancer types (30). Consequently, deficiency of DDR/DNA repair can lead to accumulative somatic mutations and increased susceptibility to cancer (31). This study suggested that FBXO5 might affect DNA damage and repair and induce carcinogenesis. Typically, the function of ESTIMATEScore is its ability to determine the purity of tumor. The higher the ESTIMATEscore, the lower the tumor purity, and a low purity denotes an advanced cancer stage with a poor prognosis (32, 33). In terms of the ESTIMATEscore, a positive correlation with FBXO5 expression was found only in PAAD and KIRC. On the contrary, a negative relationship with FBXO5 expression existed in diverse cancers.

In addition, tumor-infiltrating immunocytes can promote or antagonize the tumorigenesis and progression in a two-way manner (34). In order to truly comprehend the implications of the tumor immune microenvironment, the correlation between FBXO5 expression and the abundance of infiltrating immune cells in the 33 malignancies described was evaluated in the present study, which highlighted that FBXO5 expression showed a positive correlation with tumor-infiltrating Treg and Tcm cells, and contrastingly a negative correlation with the infiltration degree of NK/NKT cells, CD8⁺ T cells, and Th2 cells. Furthermore, there was a positive relationship between FBXO5 expression and infiltrating macrophages in BLCA, KICH, KIRC, LUAD, and PRAD. Thus, FBXO5 was likely to interact with immunocytes across many malignancies, exhibiting a wide range of applicability. Subsequently, the co-expression correlations of FBXO5 and the genes encoding immune activating and suppressive factors, chemokines, chemokine receptors, as well as MHC were examined, and the findings together illustrated that FBXO5 expression was widely correlated with different immune factors and immunocytes infiltrating into tumors.

MSI and TMB are two valuable indexes both having essential connections with the sensitivity of immune checkpoint inhibitors (35-37). Gastroesophageal cancer patients manifested as highfrequency MSI (MSI-H) present an increased response rate and favorable outcomes to immunotherapy (16). Of note, MSI-H in colorectal cancer is proved to be an independent predictor for clinical features and prognosis (17). Moreover, recent clinical studies also revealed that survival prognosis was effectively improved across cancers with high somatic TMB levels following immune checkpoint inhibitor therapy (38, 39). The present data uncovered that FBXO5 expression had a general relationship with multiple immune checkpoint genes and MMR genes in most cancers. Further, FBXO5 expression was also significantly correlated with MSI or TMB in multiple cancer types. Summarily, the results mentioned above suggested that aberrant FBXO5 expression affected the values of TMB and MSI, thus impacting the treatment effects on patients receiving immunotherapy. Hence, FBXO5 could become a potential immunotherapeutic target for tumors.

Regarding possible regulatory mechanisms, both GO and KEGG enrichment analyses indicated that FBXO5 was closely related to the functions of cell division and cell cycle regulation. Notably, FBXO5 was reported to promote the proliferation of breast cancer cells through PI3K/Akt signaling pathway, leading to a grim prognosis, whereas PI3K inhibitor LY294002 repressed FBXO5 expression and cell proliferative capacity (11). Interestingly, in mammalian cells, FBXO5 initiated the progress of cell cycle via the mechanism of converting from an APC/C^{CDH1} substrate to an APC/C^{CDH1} inhibitor (40). In line with previous studies (9-13, 23-26), GSEA and GSVA analyses obtained herein demonstrated that FBXO5 might influence the pathogenesis or immunity of cancer by participating in the processes of DNA damage checkpoint, cellular senescence, inflammatory response, PI3K/Akt/mTOR signaling pathway, and p53 signaling pathway. In brief, these results offered a theoretical basis for interpreting the oncogenic role and immunological function of FBXO5 in pan-cancer.

However, the current study has several limitations. First, systematic bias exists due to multiple information sources retrieved from different databases for analysis. Second, there are only a few molecular studies on FBXO5 in cancers, including ovarian clear cell carcinoma (9), esophageal squamous cell carcinoma (10), breast carcinoma (11), and hepatocellular carcinoma (12), and thus the findings on FBXO5 in this research need to be further validated in other tumor types. Third, only bioinformatic analyses were conducted to access the correlations between FBXO5 expression and prognostic and immunological features based upon public databases. Therefore, the experimental verification should be performed in the future to overcome this issue.

CONCLUSION

In conclusion, the present research demonstrated that FBXO5 was a potential oncogene that could serve as an independent prognostic biomarker in various cancer types. FBXO5 expression

was also correlated with DNA methylation modification, TME, infiltration of immune cells, immune-related genes, immune checkpoints, MSI, TMB, and MMR. These discoveries expanded the knowledge about the roles of FBXO5 in tumorigenesis and progression, proposing new insights for personalized cancer immunotherapy. Prospective studies focusing on tumor immunity and FBXO5 expression may be beneficial in providing a definite answer, thereby facilitating the development of an immunotherapy approach targeting FBXO5 for tumor in the future.

DATA AVAILABILITY STATEMENT

The datasets presented in this study can be found in online repositories. The names of the repository/repositories and accession number(s) can be found in the article/**Supplementary Material**.

ETHICS STATEMENT

Ethical review and approval was not required for the study on human participants in accordance with the local legislation and institutional requirements. Written informed consent for participation was not required for this study in accordance with the national legislation and the institutional requirements.

AUTHOR CONTRIBUTIONS

PL collected and interpreted the data, organized the illustrations, and wrote the first version of the manuscript. XW collected and processed the data, and contributed to revising the manuscript. LP undertook statistical examination. BH reviewed the manuscript and made valuable academic suggestions. ZH provided the overall guidance for the study. All authors read and approved the final manuscript.

FUNDING

This work was supported by the Major Program of National Key Research and Development Project (2020YFA0112600, 2019YFA0801502), National Natural Science Foundation of China (82103095, 82104242, 82173019), Jiangxi Provincial Natural Science Foundation (20212ACB206033), the Project of Shanghai Science and Technology Commission (19140902900), Program of Shanghai Academic/Technology Research Leader (20XD1434000), and Peak Disciplines (Type IV) of Institutions of Higher Learning in Shanghai.

SUPPLEMENTARY MATERIAL

The Supplementary Material for this article can be found online at: https://www.frontiersin.org/articles/10.3389/fimmu.2022. 901784/full#supplementary-material

REFERENCES

- Sung H, Ferlay J, Siegel RL, Laversanne M, Soerjomataram I, Jemal A, et al. Global Cancer Statistics 2020: GLOBOCAN Estimates of Incidence and Mortality Worldwide for 36 Cancers in 185 Countries. CA Cancer J Clin (2021) 71(3):209–49. doi: 10.3322/caac.21660
- Srivastava S, Koay EJ, Borowsky AD, De Marzo AM, Ghosh S, Wagner PD, et al. Cancer Overdiagnosis: A Biological Challenge and Clinical Dilemma. Nat Rev Cancer (2019) 19(6):349–58. doi: 10.1038/s41568-019-0142-8
- 3. Binnewies M, Roberts EW, Kersten K, Chan V, Fearon DF, Merad M, et al. Understanding the Tumor Immune Microenvironment (TIME) for Effective Therapy. *Nat Med* (2018) 24(5):541–50. doi: 10.1038/s41591-018-0014-x
- Hinshaw DC, Shevde LA. The Tumor Microenvironment Innately Modulates Cancer Progression. *Cancer Res* (2019) 79(18):4557–66. doi: 10.1158/0008-5472.CAN-18-3962
- Ribas A, Wolchok JD. Cancer Immunotherapy Using Checkpoint Blockade. Science (2018) 359(6382):1350–5. doi: 10.1126/science.aar4060
- He X, Xu C. Immune Checkpoint Signaling and Cancer Immunotherapy. *Cell Res* (2020) 30(8):660–9. doi: 10.1038/s41422-020-0343-4
- Miller JJ, Summers MK, Hansen DV, Nachury MV, Lehman NL, Loktev A, et al. Emil Stably Binds and Inhibits the Anaphase-Promoting Complex/ Cyclosome as a Pseudosubstrate Inhibitor. *Genes Dev* (2006) 20(17):2410–20. doi: 10.1101/gad.1454006
- Reimann JD, Freed E, Hsu JY, Kramer ER, Peters JM, Jackson PK. Emil is a Mitotic Regulator That Interacts With Cdc20 and Inhibits the Anaphase Promoting Complex. *Cell* (2001) 105(5):645–55. doi: 10.1016/s0092-8674 (01)00361-0
- Gutgemann I, Lehman NL, Jackson PK, Longacre TA. Emil Protein Accumulation Implicates Misregulation of the Anaphase Promoting Complex/Cyclosome Pathway in Ovarian Clear Cell Carcinoma. *Mod Pathol* (2008) 21(4):445–54. doi: 10.1038/modpathol.3801022
- Guan C, Zhang J, Zhang J, Shi H, Ni R. Enhanced Expression of Early Mitotic Inhibitor-1 Predicts a Poor Prognosis in Esophageal Squamous Cell Carcinoma Patients. Oncol Lett (2016) 12(1):114–20. doi: 10.3892/ ol.2016.4611
- 11. Liu X, Wang H, Ma J, Xu J, Sheng C, Yang S, et al. The Expression and Prognosis of Emi1 and Skp2 in Breast Carcinoma: Associated With PI3K/Akt Pathway and Cell Proliferation. *Med Oncol* (2013) 30(4):735. doi: 10.1007/ s12032-013-0735-0
- Zhao Y, Tang Q, Ni R, Huang X, Wang Y, Lu C, et al. Early Mitotic Inhibitor-1, an Anaphase-Promoting Complex/Cyclosome Inhibitor, can Control Tumor Cell Proliferation in Hepatocellular Carcinoma: Correlation With Skp2 Stability and Degradation of P27(Kip1). *Hum Pathol* (2013) 44(3):365– 73. doi: 10.1016/j.humpath.2012.03.030
- Vaidyanathan S, Cato K, Tang L, Pavey S, Haass NK, Gabrielli BG, et al. In Vivo Overexpression of Emi1 Promotes Chromosome Instability and Tumorigenesis. Oncogene (2016) 35(41):5446–55. doi: 10.1038/onc.2016.94
- Zeng D, Li M, Zhou R, Zhang J, Sun H, Shi M, et al. Tumor Microenvironment Characterization in Gastric Cancer Identifies Prognostic and Immunotherapeutically Relevant Gene Signatures. *Cancer Immunol Res* (2019) 7(5):737–50. doi: 10.1158/2326-6066.CIR-18-0436
- Choucair K, Morand S, Stanbery L, Edelman G, Dworkin L, Nemunaitis J. TMB: A Promising Immune-Response Biomarker, and Potential Spearhead in Advancing Targeted Therapy Trials. *Cancer Gene Ther* (2020) 27(12):841–53. doi: 10.1038/s41417-020-0174-y
- Gryfe R, Kim H, Hsieh ET, Aronson MD, Holowaty EJ, Bull SB, et al. Tumor Microsatellite Instability and Clinical Outcome in Young Patients With Colorectal Cancer. N Engl J Med (2000) 342(2):69–77. doi: 10.1056/ NEJM200001133420201
- van Velzen MJM, Derks S, van Grieken NCT, Haj Mohammad N, van Laarhoven HWM. MSI as a Predictive Factor for Treatment Outcome of Gastroesophageal Adenocarcinoma. *Cancer Treat Rev* (2020) 86:102024. doi: 10.1016/j.ctrv.2020.102024
- Bonneville R, Krook MA, Kautto EA, Miya J, Wing MR, Chen HZ, et al. Landscape of Microsatellite Instability Across 39 Cancer Types. JCO Precis Oncol (2017) 2017:1–15. doi: 10.1200/PO.17.00073

- Li R, Han D, Shi J, Han Y, Tan P, Zhang R, et al. Choosing Tumor Mutational Burden Wisely for Immunotherapy: A Hard Road to Explore. *Biochim Biophys Acta Rev Cancer* (2020) 1874(2):188420. doi: 10.1016/ j.bbcan.2020.188420
- Zhang Y, Zhang Z. The History and Advances in Cancer Immunotherapy: Understanding the Characteristics of Tumor-Infiltrating Immune Cells and Their Therapeutic Implications. *Cell Mol Immunol* (2020) 17(8):807–21. doi: 10.1038/s41423-020-0488-6
- Peters JM. The Anaphase Promoting Complex/Cyclosome: A Machine Designed to Destroy. Nat Rev Mol Cell Biol (2006) 7(9):644–56. doi: 10.1038/nrm1988
- Wang W, Kirschner MW. Emil Preferentially Inhibits Ubiquitin Chain Elongation by the Anaphase-Promoting Complex. *Nat Cell Biol* (2013) 15 (7):797–806. doi: 10.1038/ncb2755
- Wang K, Qu X, Liu S, Yang X, Bie F, Wang Y, et al. Identification of Aberrantly Expressed F-Box Proteins in Squamous-Cell Lung Carcinoma. J Cancer Res Clin Oncol (2018) 144(8):1509–21. doi: 10.1007/s00432-018-2653-1
- Tang J, Kong D, Cui Q, Wang K, Zhang D, Gong Y, et al. Prognostic Genes of Breast Cancer Identified by Gene Co-Expression Network Analysis. Front Oncol (2018) 8:374. doi: 10.3389/fonc.2018.00374
- Xu C, Luo L, Yu Y, Zhang Z, Zhang Y, Li H, et al. Screening Therapeutic Targets of Ribavirin in Hepatocellular Carcinoma. Oncol Lett (2018) 15 (6):9625–32. doi: 10.3892/ol.2018.8552
- 26. Yuan Y, Shi X, Li B, Peng M, Zhu T, Lv G, et al. Integrated Analysis of Key microRNAs /TFs /mRNAs/ in HPV-Positive Cervical Cancer Based on microRNA Sequencing and Bioinformatics Analysis. *Pathol Res Pract* (2020) 216(6):152952. doi: 10.1016/j.prp.2020.152952
- 27. Sun H, Zhou R, Zheng Y, Wen Z, Zhang D, Zeng D, et al. CRIP1 Cooperates With BRCA2 to Drive the Nuclear Enrichment of RAD51 and to Facilitate Homologous Repair Upon DNA Damage Induced by Chemotherapy. Oncogene (2021) 40(34):5342-55. doi: 10.1038/s41388-021-01932-0
- Klutstein M, Nejman D, Greenfield R, Cedar H. DNA Methylation in Cancer and Aging. *Cancer Res* (2016) 76(12):3446–50. doi: 10.1158/0008-5472.CAN-15-3278
- Wu T, Dai Y. Tumor Microenvironment and Therapeutic Response. Cancer Lett (2017) 387:61–8. doi: 10.1016/j.canlet.2016.01.043
- Jeggo PA, Pearl LH, Carr AM. DNA Repair, Genome Stability and Cancer: A Historical Perspective. Nat Rev Cancer (2016) 16(1):35–42. doi: 10.1038/nrc.2015.4
- Brown JS, O'Carrigan B, Jackson SP, Yap TA. Targeting DNA Repair in Cancer: Beyond PARP Inhibitors. *Cancer Discovery* (2017) 7(1):20–37. doi: 10.1158/2159-8290.CD-16-0860
- Aran D, Sirota M, Butte AJ. Systematic Pan-Cancer Analysis of Tumour Purity. Nat Commun (2015) 6:8971. doi: 10.1038/ncomms9971
- 33. Yoshihara K, Shahmoradgoli M, Martinez E, Vegesna R, Kim H, Torres-Garcia W, et al. Inferring Tumour Purity and Stromal and Immune Cell Admixture From Expression Data. *Nat Commun* (2013) 4:2612. doi: 10.1038/ncomms3612
- Lei X, Lei Y, Li JK, Du WX, Li RG, Yang J, et al. Immune Cells Within the Tumor Microenvironment: Biological Functions and Roles in Cancer Immunotherapy. *Cancer Lett* (2020) 470:126–33. doi: 10.1016/j.canlet.2019.11.009
- Chang L, Chang M, Chang HM, Chang F. Microsatellite Instability: A Predictive Biomarker for Cancer Immunotherapy. *Appl Immunohistochem Mol Morphol* (2018) 26(2):e15–21. doi: 10.1097/PAI.00000000000575
- Dudley JC, Lin MT, Le DT, Eshleman JR. Microsatellite Instability as a Biomarker for PD-1 Blockade. *Clin Cancer Res* (2016) 22(4):813–20. doi: 10.1158/1078-0432.CCR-15-1678
- Fumet JD, Truntzer C, Yarchoan M, Ghiringhelli F. Tumour Mutational Burden as a Biomarker for Immunotherapy: Current Data and Emerging Concepts. Eur J Cancer (2020) 131:40–50. doi: 10.1016/j.ejca.2020.02.038
- Liu L, Bai X, Wang J, Tang XR, Wu DH, Du SS, et al. Combination of TMB and CNA Stratifies Prognostic and Predictive Responses to Immunotherapy Across Metastatic Cancer. *Clin Cancer Res* (2019) 25(24):7413–23. doi: 10.1158/1078-0432.CCR-19-0558
- Samstein RM, Lee CH, Shoushtari AN, Hellmann MD, Shen R, Janjigian YY, et al. Tumor Mutational Load Predicts Survival After Immunotherapy Across Multiple Cancer Types. *Nat Genet* (2019) 51(2):202–6. doi: 10.1038/s41588-018-0312-8

 Cappell SD, Mark KG, Garbett D, Pack LR, Rape M, Meyer T. EMI1 Switches From Being a Substrate to an Inhibitor of APC/C(CDH1) to Start the Cell Cycle. *Nature* (2018) 558(7709):313–7. doi: 10.1038/s41586-018-0199-7

Conflict of Interest: The authors declare that the research was conducted in the absence of any commercial or financial relationships that could be construed as a potential conflict of interest.

Publisher's Note: All claims expressed in this article are solely those of the authors and do not necessarily represent those of their affiliated organizations, or those of the publisher, the editors and the reviewers. Any product that may be evaluated in this article, or claim that may be made by its manufacturer, is not guaranteed or endorsed by the publisher.

Copyright © 2022 Liu, Wang, Pan, Han and He. This is an open-access article distributed under the terms of the Creative Commons Attribution License (CC BY). The use, distribution or reproduction in other forums is permitted, provided the original author(s) and the copyright owner(s) are credited and that the original publication in this journal is cited, in accordance with accepted academic practice. No use, distribution or reproduction is permitted which does not comply with these terms.



Identification of Ligand-Receptor Pairs Associated With Tumour Characteristics in Clear Cell Renal Cell Carcinoma

Fahui Liu¹, Ping Wang², Wenjuan Sun³, Yan Jiang^{4*†} and Qiming Gong^{5*†}

¹ Department of Medical Biochemistry and Cell Biology, Institute of Biomedicine, University of Gothenburg, Gothenburg, Sweden, ² Department of Dermatology, Fujian Provincial Geriatric Hospital, Fuzhou, China, ³ Department of Internal Medicine, Chonnam National University Medical School, Gwangju, South Korea, ⁴ Guixi Key Laboratory for High Incidence Diseases, Youjiang Medical University for Nationalities, Baise, China, ⁵ Department of Nephrology, Affiliated Hospital of Youjiang Medical University for Nationalities, Baise, China

OPEN ACCESS

Edited by:

Xian Zeng, Fudan University, China

Reviewed by:

Xiaojian Wu, The Sixth Affiliated Hospital of Sun Yat-sen University, China Wei Song, Wuhan University, China

*Correspondence:

Qiming Gong 15610398015@163.com Yan Jiang jiangyan9hr@yeah.net [†]These authors have contributed

equally to this work

Specialty section:

This article was submitted to Cancer Immunity and Immunotherapy, a section of the journal Frontiers in Immunology

Received: 28 February 2022 Accepted: 10 May 2022 Published: 06 June 2022

Citation:

Liu F, Wang P, Sun W, Jiang Y and Gong Q (2022) Identification of Ligand-Receptor Pairs Associated With Tumour Characteristics in Clear Cell Renal Cell Carcinoma. Front. Immunol. 13:874056. doi: 10.3389/fimmu.2022.874056 The tumour microenvironment (TME) of clear cell renal cell carcinoma (ccRCC) comprises multiple cell types, which promote tumour progression and modulate drug resistance and immune cell infiltrations via ligand-receptor (LR) interactions. However, the interactions, expression patterns, and clinical relevance of LR in the TME in ccRCC are insufficiently characterised. This study characterises the complex composition of the TME in ccRCC by analysing the single-cell sequencing (scRNA-seq) data of patients with ccRCC from the Gene expression omnibus database. On analysing the scRNA-seq data combined with the cancer genome atlas kidney renal clear cell carcinoma (TCGA-KIRC) dataset, 46 LRpairs were identified that were significantly correlated and had prognostic values. Furthermore, a new molecular subtyping model was proposed based on these 46 LRpairs. Molecular subtyping was performed in two ccRCC cohorts, revealing significant differences in prognosis between the subtypes of the two ccRCC cohorts. Different molecular subtypes exhibited different clinicopathological features, mutational, pathway, and immune signatures. Finally, the LR.score model that was constructed using ten essential LR-pairs that were identified based on LASSO Cox regression analysis revealed that the model could accurately predict the prognosis of patients with ccRCC. In addition, the differential expression of ten LR-pairs in tumour and normal cell lines was identified. Further functional experiments showed that CX3CL1 can exert anti-tumorigenic role in ccRCC cell line. Altogether, the effects of immunotherapy were connected to LR.scores, indicating that potential medications targeting these LR-pairs could contribute to the clinical benefit of immunotherapy. Therefore, this study identifies LR-pairs that could be effective biomarkers and predictors for molecular subtyping and immunotherapy effects in ccRCC. Targeting LR-pairs provides a new direction for immunotherapy regimens and prognostic evaluations in ccRCC.

Keywords: ccRCC, ligand-receptor, single-cell, TCGA, tumor microenvironment

INTRODUCTION

Clear cell renal cell carcinoma (ccRCC) is the most common (70%-80%) histological subtype of kidney cancer with the worst prognosis (1). ccRCC exhibits a broad range of metastatic phenotypes, and patients with ccRCC displaying metastases have a 5-year survival rate between 10% and 20% (2). Various clinical trials using immune-based combinations for the treatment of metastatic ccRCC have shown long-term benefits (3). However, a comprehensive analysis of the effect of clinicopathological features on survival in patients treated with first-line immune checkpoint inhibitors and tyrosine kinase inhibitors for ccRCC can aid in clinical decision-making (4) as their efficacy remains limited (5-7). Few patients treated with immune-based combinations displayed unresponsive reactions and intrinsic or acquired resistance (8). A recent study showed that tumour and tumour-infiltrating cells are involved in drug resistance or unresponsiveness to cancer treatment strategies (9). However, the mechanisms underlying these phenomena remain unclear. Therefore, studying the intra-tumoral heterogeneity of cancer is vital to cancer research. ccRCC is highly heterogeneous, and varying patients show significant differences in the composition of the tumour and other cells within the tumour microenvironment (TME), affecting tumour progression and treatment resistance (10). Furthermore, intra-tumoral heterogeneity hinders accurate prognosis prediction and appropriate treatment development. Although the application of genetic signatures from the bulk RNA-seq data shows promise in identifying patient subgroups who respond to treatment, it provides a limited mechanistic understanding of the cell types responsible for regulating clinical benefit (11).

Conversely, single-cell RNA sequencing (scRNA-seq) enables a more comprehensive characterisation of cellular composition and transcriptional state, thereby providing insights into the transcriptional state of different cells and cell-cell interactions in the TME (12) and the impact of these events on disease progression and treatment (10). The TME consists of multiple cell types, including malignant, stromal, and immune cells (13). The heterogeneity of each cell type further increases the complexity and heterogeneity of the tumours, which eventually creates tumour cell or immune cell subpopulations (14). The different cell types in the TME communicate via ligand-receptor (LR) interactions, and this communication is associated with tumorigenesis, tumour progression, therapeutic resistance, immune cells infiltration and inflammation (15, 16). Therefore, it is crucial to understand the cell-cell interactions occurring within the TME and their effect on clinical outcomes to accurately determine risk stratification.

In this study, by combining the analysis of the single-cell dataset of ccRCC and high-throughput large scale sequencing data from TCGA-KIRC, the complex cell types in the TME of ccRCC are described. Additionally, a cellular regulatory network is constructed based on cell-cell communication analysis, and the potential clinical implications of cell-cell interactions in ccRCC are described. On further analysing LR-pairs in different cell types, two LR-pairs associated with molecular subtyping models were established. The molecular subtyping models were significantly associated with survival in both cohorts. Patients grouped using molecular subtyping showed different clinical-pathological characteristics, mutation characteristics, route characteristics, immunological characteristics, and immunotherapy response degrees.

METHODS AND MATERIALS

Datasets

scRNA-seq data (GSE159115) of ccRCC was obtained from the Gene Expression Omnibus (GEO) database, which comprises 14 samples from nine patients with kidney cancer, including seven 'ccRCC' tumour samples, one 'Chromophobe RCC' tumour sample, and six adjacent normal samples. The seven 'ccRCC' tumour samples were included in subsequent analyses. The cell count of the GSE159115 primary tumour sample was obtained from gse159115.raw_cellCount.txt. 526 samples of ccRCC RNA-Seq data downloaded from the TCGA-KIRC portal were used as the training cohort. Additionally, the Research Concept and Research Activities- European Project (RECA-EU) dataset, comprising 91 ccRCC samples downloaded from the International Cancer Genome Consortium (ICGC) database, was used as an independent validation cohort.

scRNA-seq Data Analysis

R (version 3.6.0) and the Seurat R package (version 3.6.3) were used for the analyses. Using the Seurat R package, Seurat objects were created for each sample with the cell-by-gene count matrix using CreateSeuratObject (arguments: min. cells = 5). Cells with high mitochondrial content (25% for tumour libraries) and low gene number detection (<300) were considered low-quality cells and discarded. Potential doublets identified via scrublet were also removed from further analyses. Subsequently, 20851 high-quality cells were obtained after quality checks. The relationship between the percentage of mitochondrial genes and mRNA reads was detected and visualised as the relationship between the number of mRNAs and reads of mRNA. Furthermore, all highly variable genes in single cells were identified after controlling for the average expression and dispersion relationship. Subsequently, principal component analysis with variable genes was used as the input to identify significant principal components (PCs) based on the jackStraw function. When different samples were pooled, highly variable genes were identified, and batch correction using canonical correlation analysis via Seurat was applied based on the highly variable genes to remove the batch effect before clustering. Cells were projected into a 2-D map with tdistributed stochastic neighbour embedding for visualisation. With a resolution of 0.2, cells were clustered using the

Abbreviations: ccRCC, clear cell renal cell carcinoma; DEGs, differentially expressed genes; EGFR, epidermal growth factor receptor; GEO, Gene Expression Omnibus; HLA, human leukocyte antigen; GESA, gene set enrichment analysis; KEGG, Kyoto Encyclopedia of Genes and Genomes; KIRC, Kidney Renal Clear Cell Carcinoma; LR, ligand-receptor; MIF, macrophage migration inhibitory factor; PCs, principal components; RECA-EU, Research Concept and Research Activities- European Project; scRNA-seq, single-cell RNA sequencing; TCGA, The Cancer Genome Atlas; TGFβ, Transforming growth factor-beta; TME, tumour microenvironment; vSMC: vascular smooth muscle cells; WNT, wingless.

'FindClusters' function into 14 different cell types (clusters 0-13). The 'FindAllMarkers' function was used to identify differentially expressed genes (DEGs) in each cluster. Moreover, a few classical markers of cell subset definition were obtained from previous studies (17) and manually annotated according to marker expression.

Cell-Cell Communication Analysis

Cell communication analysis was performed using CellPhoneDB (18). A permutation test calculated the significant mean and significance of cell communication based on cell interactions and the normalised cell matrix. LP-pairs were obtained for each cell pair with nominal p < 0.05. Moreover, LR interactions are based on the annotations from the database included in the current study. At least one gene in the LR-pairs is the receptor. Additionally, receptor-receptor and other receptor-not-defined interactions were excluded.

Correlation of LR-Pairs

The co-expression of a ligand and its corresponding receptor is essential for cell-cell communication. Therefore, Pearson's correlation coefficients for the significant LR-pairs were calculated in the cell communication analysis using the TCGA-KIRC dataset. LR-pairs with Pearson's correlation coefficient greater than 0.4 (p < 0.01) were used for consensus clustering analysis to identify molecular subtypes.

Molecular Subtyping Based on LR-Pairs

Using the significantly relevant LP-pairs, the molecular subtypes of the samples were identified using consensus clustering in both the TCGA-KIRC and RECA-EU cohorts. 'euclidean' was chosen as the distance metric for the PAM algorithm, and 500 bootstrap replicates were performed, each of which included 80% of the training set. The number of clusters (k) was set from 2 to 10, and the best classification was determined by computing the consensus matrix and cumulative distribution function.

Gene Set Enrichment Analysis and Functional Annotation

To study the biological pathways in different molecular subtypes, GSEA was used. The 'hallmark' gene set collection from the molecular signature database was used for pathway enrichment analysis. The clusterProfiler (19) package was used for functional annotation.

Cell Culture and Transfection

Human ccRCC cell line 786-O (KCB200815YJ, Kunming, China) and renal epithelial cell HK-2 (KCB200941YJ, Kunming, China) were obtained from the Chinese Academy of Sciences. All cell lines were cultured in a DMEM medium containing 10% FBS. 786-O cells were infected with CX3CL1 lentivirus (Ubi-MCS-CBh-gcGFP-IRES-Puro-CX3CL1) (Shanghai Gene Chem Co., Ltd.) to against the CX3CL1 gene.

RNA Analysis

Total RNA was extracted from 786-O and HK-2 cells using the TRIzol Reagent (Cowin Biosciences, Beijing, China) and

converted into cDNA using Reverse Transcription Kit (Thermo Fisher Scientific, Waltham, USA). RT-qPCR was performed based on SYBR Green (Cowin Biosciences, Beijing, China) and an ABI 7500 instrument (Thermo Fisher Scientific, Inc.). The sequences of the primer pairs are listed in **Table S1**. RT-qPCR experiment was performed in triplicate.

Cells Clone, Transwell Migration, Invasion, Western Blot and Immunofluorescence Assay

786-O cells were plated onto the upper 8µm transwell chamber (corning, USA) per-coated with Matrigel (Corning, USA). Cells were fixed with paraformaldehyde and stained with 0.1% crystal violet solution to perform Transwell Assay. For Colony Assay, 786-O cells were re-seeded onto 24-well plates at a density of 100 cells per well and stained with 0.1% crystal violet solutions after 4% paraformaldehyde solution was fixed. For Western Blot and Immunofluorescence, cells were incubated with anti-CX3CL1 (Cat# DF12376, Affinity Biosciences), anti- β -Tubulin (Cat#T0023, Affinity Biosciences) and anti-GAPDH (Cat# T0004, Affinity Biosciences) as described by previous study (20).

Analysis of Immune Infiltration in ccRCC

The 22 immune-cell proportions for each sample and immune cell subsets were inferred using the CIBERSORT algorithm (21) with the LM22 gene set. Meanwhile, the scores for stromal cells and immune cell infiltration levels in ccRCC tumour tissues were calculated using the ESTIMATE algorithm.

Risk Model

The risk score for each patient was calculated using the following formula: LR.Score = Σ beta_i × Exp_i, where i indicates the expression level of LR-pairs and beta indicates the coefficient of the LR-pairs of multivariate Cox regression. Based on the threshold of 0, patients were divided into high and low-score groups, and the survival curve was plotted using Kaplan-Meier analysis.

Statistical Analysis

GraphPad Prism 8.0 software was used for data analysis. All data were computed as the means \pm standard (SD) deviation under three independent experiments. The significance of two group differences was analyzed with Student's t-test. P<0.05 was statistically significant.

RESULT

Single-Cell Transcriptome Landscape of ccRCC

Before quality control, correlations between unique molecular identifier (UMI) numbers, mitochondrial genes and mRNA numbers were analysed (**Figure S1A, B**), which revealed that UMI number was not significantly correlated with mitochondrial gene percentage (**Figure S1A**) but was positively correlated with

mRNA number (Figure S1B). Additionally, the number of mRNAs, the readings of mRNA and the distribution of mitochondrial and nuclear chromosome genes were also analysed (Figure S1C). Most gene numbers showed a distribution around 0-8000 while the mitochondrial percentage was below 25%. Further, cells with more than 25% mitochondrial genes and fewer than 300 genes were deleted. Potential doublets were also predicted via 'scrublets,' which were removed in subsequent analyses. The gene expression profile of 20851 cells was obtained, and the number of cells in each sample was counted (Table 1). The number of filtered mRNAs, the readings of mRNA and the distribution of mitochondrial and nuclear chromosome genes are shown in Figure S1D. Highly variable genes (the first 3000) were shortlisted after quality control for further downstream analysis (Figure S1E). Cell features were extracted using principal component analysis, identifying 14 clusters (Figure 1A, B, cell_cluster.txt), with cluster 0 being derived from patient SCS_2023 and cluster 10 from patient SCS_2026 (Figure 1C). The identification of DEGs in each cluster was conducted using Wilcoxon rank and testing, and the top 3 DEGs in each cluster were labelled using a heat map (Figure 1D). Finally, 14 clusters were annotated to eight cell types based on classical markers (Table 2). Further, the Kyoto Encyclopedia of Genes and Genomes pathway enrichment analysis of marker genes for different cellular subsets was performed (Figure 1F), revealing that different cellular subsets share common pathways, such as Antigen processing and presentation, Fluid shear stress and atherosclerosis pathways.

Complex Intercellular Communication Networks in ccRCC

The single-cell analysis identified eight cell types in the TME. To further investigate the potential interactions between different cell types in the TME of ccRCC, cell-to-cell interactions were analysed using cellphoneDB, wherein ccRCC was revealed to have many interactions with other cell subsets, showing the highest interaction strength with endothelial and macrophage cells. Additionally, endothelial cells had a strong interaction with vascular smooth muscle cells(vSMC) (**Figure 2A**). The interaction network between the eight cell subsets aids in visualising the many interactions within and between the cell subsets (**Figure 2B**), with thicker lines and larger nodes indicating more significant LR between the cell subsets. Moreover, the cell subsets of ccRCC, macrophages and vSMC

 TABLE 1
 Statistical analysis of cell numbers for seven clear cell renal cell carcinoma (ccRCC) samples.

Sample	raw_cellCount	clean_cellCount	percent
SCS_2005	1704	1673	0.981807512
SCS_2006	1660	1374	0.827710843
SS_2007	3674	3345	0.910451824
SS_2017	2872	2817	0.980849582
SS_2022	1953	1942	0.99436764
SS_2023	6453	6140	0.951495428
SS_2026	3635	3560	0.979367263

showed the most cell-to-cell interactions within and between the cell subsets (**Figure 2C**). Genes in the Hedgehog, Notch, TGFβ, WNT signalling and EGFR signalling that are related to tumour proliferation, metastasis and progression were selected to further determine the presence of a significant interaction between the cell subsets. The result shows many interactions between the receptor HLA–DPA1 and its corresponding ligand TNFSF9 in the cell subset of macrophage and ccRCC while EGFR and MIF have strong interactions between different cell subsets (endothelia, ccRCC, vSMC) (**Figure 2D**).

Construction of Molecular Subtypes Based on LR-Pairs

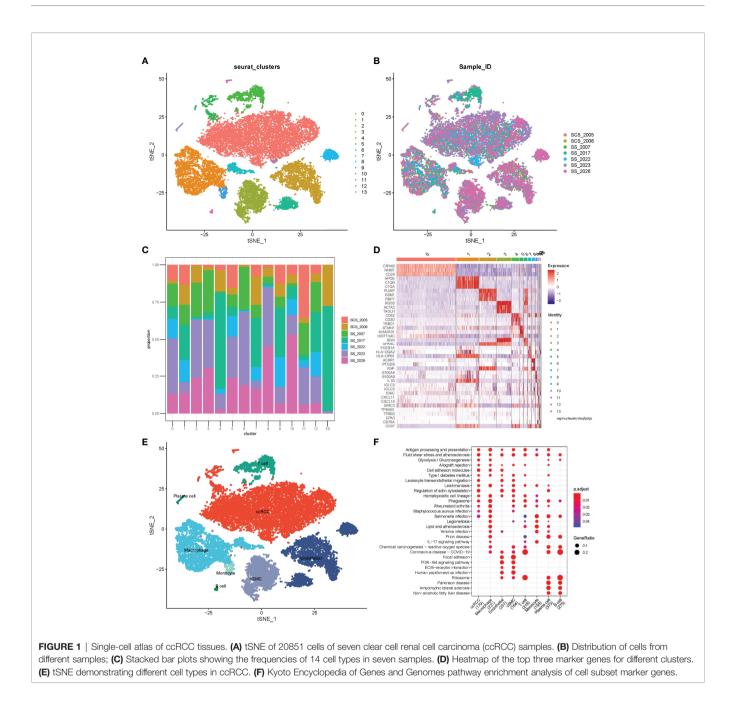
LR interactions between different cell types in the TME play a vital role in the occurrence and development of tumours. Thus, LR-pairs that interact significantly in different cell types were extracted based on Pearson's correlation coefficient between ligand and receptor expressions. A total of 126 LR-pairs that were significantly correlated in TCGA-KIRC were identified (tcga.LR.cor.res.txt). Furthermore, the expression level of LR-pairs was determined by the sum of the expression values of the receptor and ligand genes in TCGA-KIRC. A total of 46 LR-pairs that were significantly associated with patient prognosis in TCGA-KIRC (p < 0.01) (tcga.LR.HR.res.txt) were used in molecular subtyping analysis. A total of 526 ccRCC samples in the TCGA-KIRC cohort were clustered using ConsensusClusterPlus. The optimal number of clusters is determined by the cumulative distribution function and delta area curve (Figures 3A, B), and k = 3 was selected to obtain three molecular subtypes (Figure 3C; tcga.subtype.txt) which showed significant differences in prognosis (p < 0.0001) (Figure 3D). On comparing the three subtypes, the C3 subtype had a better prognosis, while the C1 subtype had a worse prognosis. Similarly, patients with ccRCC in the RECA-EU cohort were typed (icgc.subtype.txt). The results showed that there were significant differences in prognosis among the three molecular subtypes (p = 0.0093) (Figure 3E), which was consistent with the training set.

Comparison of Different Molecular Subgroups With Clinical Features

The distribution of clinical features in the three molecular subtypes was compared using the TCGA-KIRC cohort. The results showed that patients with poor prognosis in the C1 subtype had higher TNM stages, with significant differences between the C1 and C3 subtypes in terms of T and M stage distribution (p < 0.05) (Figures 4A–C). In the C1 and C2 subtypes, patients with Stage III and Stage IV ccRCC were higher in number than those in the C3 subtype (p < 0.05) (Figure 4D). A significant difference was also observed in Grade between different subtypes (p < 0.05) (Figure 4E). Additionally, significant differences in age and gender were observed among different subtypes (Figures 4F, G) (p < 0.05).

Mutational Characteristics of Different Molecular Subtypes

The differences in genomic alterations of these three molecular subtypes in the TCGA cohort were further explored. The C1



and C2 subtypes showed higher levels of an euploidy (p = 5.2e-15), homologous recombination defects (p = 0.019), fraction altered genome (p = 1.4e-20), segment numbers (p = 0.00015) and tumour mutation burdens (p = 0.0093) (**Figure 5A**). Additionally, information on the immune molecular subtypes of TCGA-KIRC was obtained from a previous study (22). The relationship between the six immune subtypes and three molecular subtypes defined in this study was compared. Between the C3 subtypes, the C3 immune subtype accounted for a more significant proportion. Among the C1 subtypes, the C1, C2, C4 and C6 immune subtypes accounted for a more significant proportion (**Figure 5B**). Furthermore, four additional subtypes (KIRC-C1, C2, C3, C4), which were obtained from a previous study (23), were compared with the three molecular subtypes defined in this study. The results showed that KIRC-C4 accounted for more significant proportion in the C1 molecular subtype, while KIRC-C1 accounted for the most proportion in the C3 molecular subtype (**Figure 5C**). Finally, the analysis of the correlation between gene mutations, copy number variants and molecular subtypes revealed a significant correlation between subtypes and gene mutations. The mutation frequencies of VHL, PBRM1 and BAP1 genes vary significantly among subtypes, with more mutation frequencies observed in the C1 subtype (**Figure 5D**).

TABLE 2 | Annotation of cell types for 14 cell clusters.

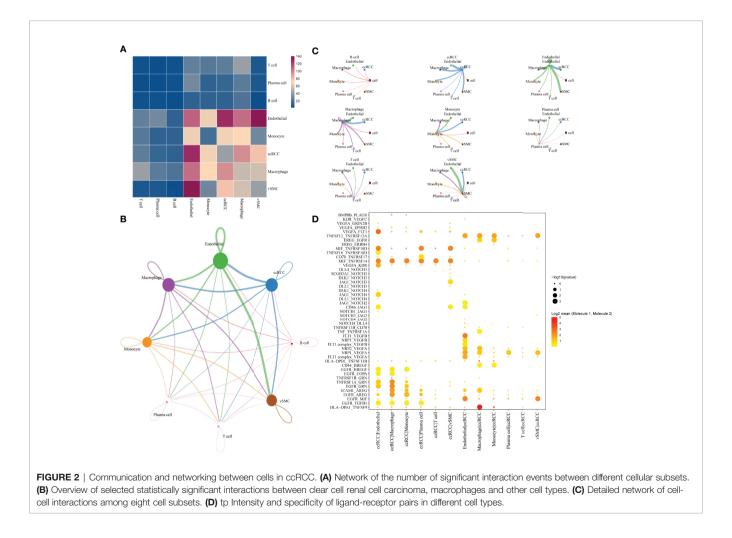
Cell Type	Cluster	Number of Cells
clear cell renal cell carcinoma (ccRCC)	0	8819
Macrophage	1	3382
Endothelial	2	2584
vascular smooth muscle cells (vSMC)	3	2169
T cell	4	1176
ccRCC	5	573
Endothelial	6	534
Macrophage	7	502
Endothelial	8	498
Monocyte	9	248
Plasma cell	10	122
ccRCC	11	87
ccRCC	12	85
B cell	13	72

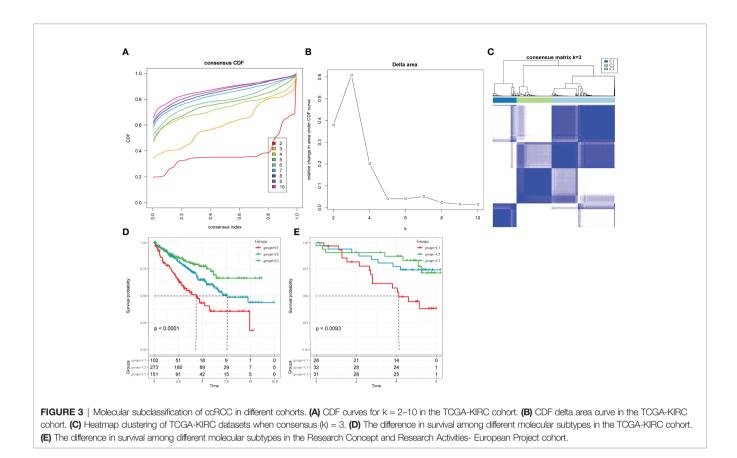
Pathway Analysis of Different Molecular Subtypes

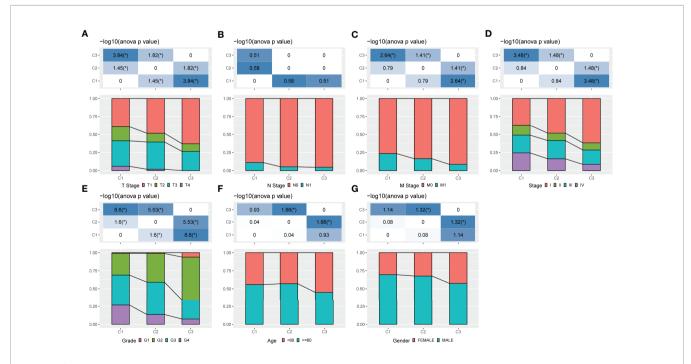
Pathways that are differentiated in different molecular subtypes were analysed using GSEA. The results showed the significant enrichment of 26 pathways in the C1 subtype compared with the C3 subtype in the TCGA cohort and 40 pathways in the RECA-EU cohort (Figures 6A, B). Overall, the inhibition pathways contain few immune marker pathways, such as INTERFERON_GAMM A_RESPONSE, COMPLEMENT, INTERFERON_ALP HA_RESPONSE and INFLAMMATORY_RESPONSE. (Figure 6A). Additionally, abnormal pathways between the C1 and C3 subtypes in different ccRCC cohorts are shown in Figure 6B. The pathways for TCGA-KIRC cohorts between C1 and C2 subtypes, C1 and C3 subtypes and C2 and C3 subtypes are shown in Figure 6C. Overall, immunomodulatory pathways in patients with the C1 subtype are inhibited.

Immune Characteristics of Different Molecular Subtypes

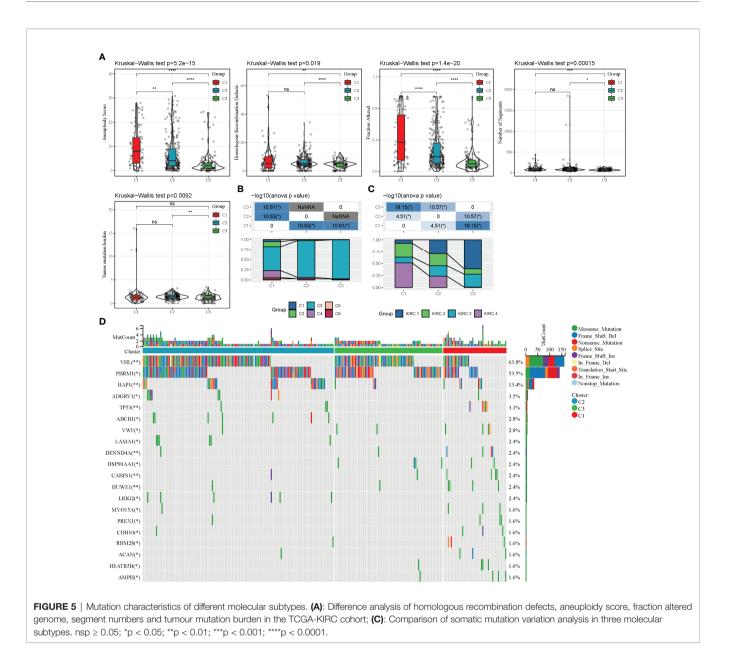
To further elucidate the differences in the immune microenvironment of patients in different molecular subtypes, the degree of infiltration of 22 immune cells in the two ccRCC cohorts was assessed using the CIBERSORT algorithm. In both cohorts, resting mast cells, M1 macrophages and activated/ memory CD4⁺ T cells showed significant differences in different molecular subtypes (**Figures 7A, C**). ESTIMATE algorithm was also used to assess immune cell infiltration in each sample. The 'ImmuneScore' of the C3 subtype in the TCGA and RECA-EU cohorts was higher than the C1 subtype,











indicating that the C3 subtype has a high immune cell infiltration degree (**Figure 7B, D**).

Model Construction Based on the LR-Pairs Score

The above analyses show that the LR-pair molecular subtypes have different mutation landscapes, pathway characteristics and immune infiltration degrees. A total of 46 LR-pairs were significantly associated with patient prognosis, with 37 of them significantly different in both the TCGA-KIRC and RECA-EU datasets (all.LR.genes.diff.kruskal.res.txt) (FDR < 0.001). The 37 LR-pairs with significant differences were further compressed using LASSO cox regression in the TCGA-KIRC cohort to reduce the number of genes in the risk model. The trajectory of each independent variable is shown in **Figure S2A**, wherein

with the gradual increase of lambda, the number of independent coefficients tending to 0 also gradually increases. Model performance was evaluated using 10-fold cross-validation.

On analysing the confidence interval under each lambda (**Figure S2B**), the model was found to be optimal when lambda = 0.0137, and 12 LR-pairs at lambda = 0.0137 were selected for further analysis. Furthermore, the model was optimized using stepwise multivariate regression analysis. Finally, 10 LR-pairs, including 'APLNR_APLN', 'CSF1R_CSF1', 'CX3CR1_CX3CL1', 'EPHA4_EFNB3', 'FGFR3_EPHA4', 'HGF_CD44', 'KDR_VEGFC' 'NGF_NGFR,' 'TEK_ANGPT1' and 'TEK_ANGPT4' were identified as crucial LR-pairs. The multivariate Cox regression coefficient results for these 10 LR-pairs are shown in **Figure S2C**. Furthermore, the LR-pairs to

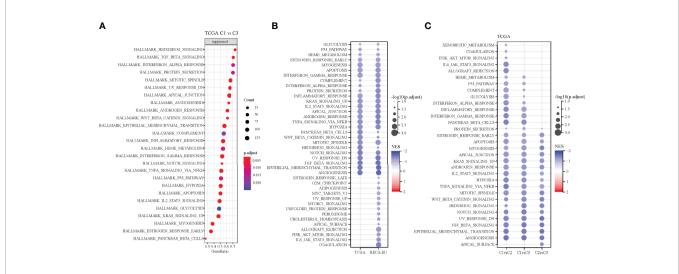
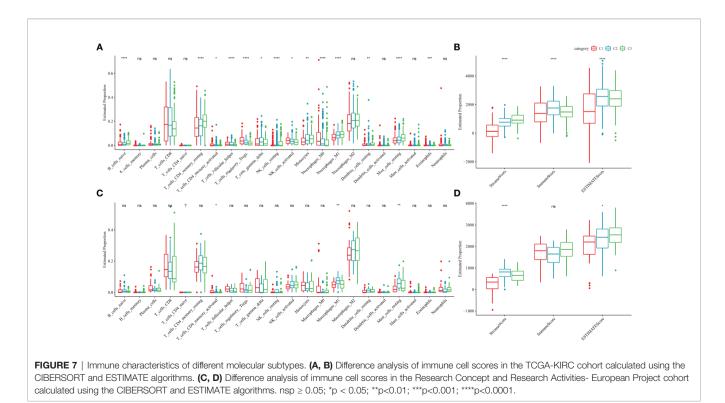


FIGURE 6 | Pathway analysis of different molecular subtypes. (A) Analysis of signalling pathways for differentially expressed genes in the C1 vs. C3 subtypes of the TCGA-KIRC cohort. (B) Pathway analysis of the differentially expressed genes in the C1 vs. C3 subtypes in two clear cell renal cell carcinoma cohorts. (C) Gene set enrichment analysis of the comparison between different molecular subtypes.

facilitate the quantitative analysis of LR-pair scores in patients with ccRCC. The results showed that the LR.score in the C1 subtypes was significantly higher than that in the C2 and C3 subtypes (**Figure 8A**). To further assess the clinical relevance of LR-pair scores, patients were defined as high LR.score group if the LR.score > 0 and low LR.score group otherwise. Patients with low LR.score in the TCGA-KIRC cohort had a better prognosis than patients with high LR.score (p < 0.0001) (**Figure 8B**).

The area under the curve (AUC) of the time-dependent receiver operating characteristic (ROC) curves of the LR.score was 0.79, 0.78 and 0.78 at 1, 3 and 5 years, respectively (**Figure 8C**). Univariate and multivariate cox regression analyses were also used in analysing the TCGA-KIRC cohort, which showed that LR.score is a reliable and independent prognostic biomarker for assessing the prognosis of patients with ccRCC (**Figures 8G, H**). Furthermore, the reliability of the



LR.score was validated using 91 samples from the RECA-EU cohort. A study about LR.score in different molecular subtypes reported similar conclusions using the RECA-EU cohort (**Figure 8D**). Patients with low LR.score in the RECA-EU dataset showed a significant survival benefit (p = 0.001) (**Figure 8E**). The AUC of the time-dependent ROC curves of the LR.score was 0.61, 0.68 and 0.79 at 1, 3 and 5 years, respectively (**Figure 8F**).

Differences in LR.score in Different Clinical Subgroups

To examine the relationship between LR.score and clinical features of ccRCC, the differences in LR.score between subgroups of different clinical features in the TCGA-KIRC dataset were compared. Patients showed significant differences

in TNM stages, pathological stages and histological grades when compared with LR.score. LR.score varied significantly between different clinical feature subgroups, with high malignancy degree correlating to high LR.score (**Figure 9A**). Additionally, the relationship between the LR.score and clinical-pathological features in RECA-EU was analysed. The results showed that the differences in the different subgroups of LR.score were not apparent, possibly due to the insufficient sample size in the RECA-EU cohort (**Figure 9B**).

Correlation Between LR.score and Immune-Related Features

The distribution of 22 immune cells in the TCGA-KIRC cohort and the differences between the LR.score groups were analysed. Significant differences in immune cell infiltration levels were

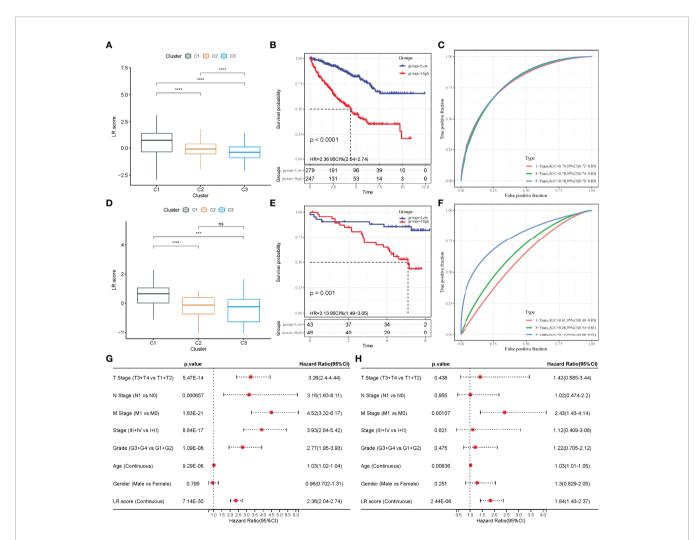


FIGURE 8 | Construction of LR.score model. (A) The difference in LR.score between the different molecular subtype groups in the TCGA-KIRC cohort. (B) Survival benefit of LR.score in the high and low LR.score groups in the TCGA-KIRC cohort. (C) The predictive value of LR.score in patients among the TCGA-KIRC cohort. (D) The difference of LR.score between the different molecular subtype groups in the Research Concept and Research Activities- European Project (RECA-EU) cohort. (E) Survival benefit of LR.score in the high and low LR.score groups in the RECA-EU cohort. (F) The predictive value of LR.score in patients among the RECA-EU cohort. (G) Univariate cox regression analysis of LR.score, age, gender, TNM stage and grade for overall survival (OS) in the TCGA-KIRC cohort. (H) Multivariate cox regression analysis of LR.score, age, gender, TNM stage and grade for OS in the TCGA-KIRC cohort; ns, p≥ 0.05; ***p<0.001; ****p<0.0001.

observed between patients (Figure 10A). Additionally, immune cell infiltration levels showed significant differences between different LR.score groups. Further, CD8⁺ T cells exhibited a high level of infiltration, with the high LR.score group showing significantly higher infiltration levels than the low LR.score group (Figure 10B). Additionally, immune infiltration levels were also compared for different LR.score groups using the ESTIMATE algorithm, wherein the Immune score and ESTIMATE score in the high LR.score group were significantly higher than those in the low LR.score group (Figure 10C). Further, the correlation between LR.score and 22 immune cell scores in the TCGA-KIRC cohort was analysed using Pearson's correlation coefficient. The result shows that LR.score was significantly positively correlated with activated/memory CD4⁺ T cells, follicular helper T cells and regulatory T cells but negatively correlated with resting mast cells (Figure 10D).

The Relationship Between LR.score and Immunotherapy

To identify the relationship between LR.score and immunotherapy, the value of LR.score to predict a patient's response to immune checkpoint blockade(ICB) treatment was examined. In the anti-PD-L1 cohort (IMvigor210 cohort), 348 patients exhibited varying degrees of response to anti-PD-L1 receptor blockers, including complete response (CR), partial response (PR), stable disease (SD) and progressive disease (PD). Patients with SD/PD had a higher LR.score than patients with CR/PR (Figure 11A). Percentage statistics between the high and low LR.score groups showed significantly better treatment outcomes in patients with low LR.score (Figure 11B). Survival analyses further showed that LR.score was associated with overall survival in patients receiving immunotherapy (p < 0.0001) (Figure 11C). In early-stage patients receiving immunotherapy, LR.score was associated with overall survival (p = 0.000051) (Figure 11D) while in advanced patients it was also associated with overall survival (p = 0.097) (Figure 11E).

Additionally, in another cohort of anti-PD1 (GSE78220), patients with SD/PD patients showed higher LR.score than those with CR/PR (**Figure 11F**). Moreover, percentage statistics between the high and low LR.score groups also showed that patients with low LR.score had significantly better treatment outcomes (**Figure 11G**), clinical benefit and prolonged overall survival (p = 0.036) (**Figure 11H**).

CX3CL1 Knockdown Accelerates Migration and Invasion of ccRCC Cell In Vitro

To further confirm the results of databases, 10 LR-pairs, including 'APLNR_APLN,' 'CSF1R_CSF1', 'CX3CR1_CX3CL1', 'EPHA4_EFNB3', 'FGFR3_EPHA4', 'HGF_CD44', 'KDR_VEGFC,' 'NGF_NGFR,' 'TEK_ANGPT1' and 'TEK_ANGPT4' were subjected to RT-qPCR assay in ccRCC cell line. As shown in **Figure 12A**, the mRNA levels of APLNR, APLN, CSF1R, CSF1, CX3CR1, CX3CL1, CD44, KDR, VEGFC, NGF, NGFR, ANGPT1 in the 786-O cell were up-regulated compared with normal renal epithelial cell HK-2, whereas the mRNA levels of EPHA4, EFNB3, FGFR3, HGF, ANGPT4, TEK

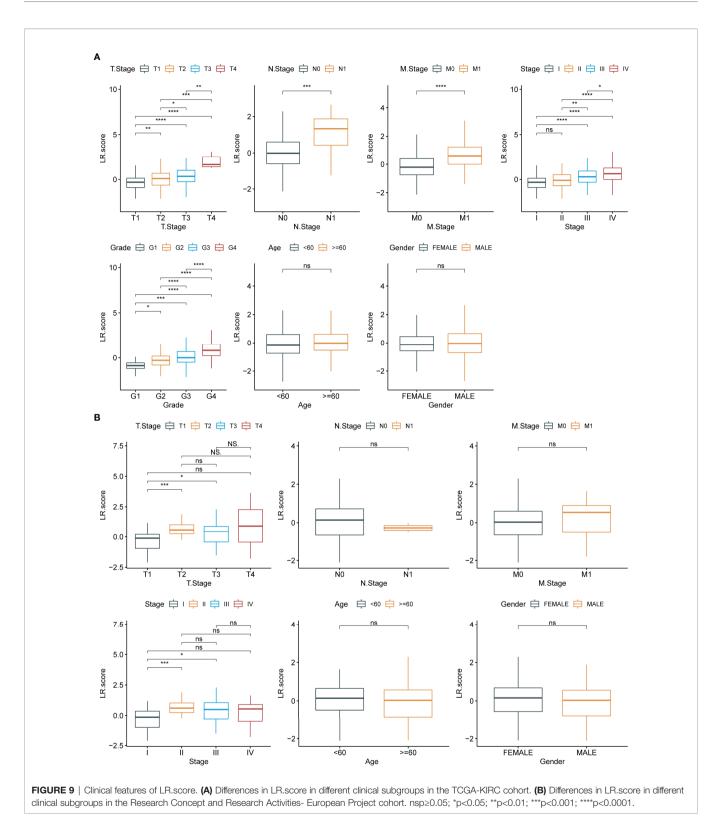
in the 786-O cell were down-regulated compared with HK-2 cell. Recently some research found one such chemokine that plays a critical role in the anti-cancer procession is CX3C chemokine ligand 1 (CX3CL1) and its receptor CX3C chemokine receptor 1 (CX3CR1). In **Figure 12B**, we found that the protein expression of CX3CL1 was increased in the 786-O cell compared with the HK-2 cell. To demonstrate the specific role of CX3CL1, we knocked down the CX3CL1 gene in the 786-O cell (**Figures 12C**, **D**). We found that the numbers of clone formation (**Figure 12D**), as well as the migration (**Figure 12E**) and invasion capacities (**Figure 12F**), were notably increased in 786-O cells with CX3CL1 knockdown.

DISCUSSION

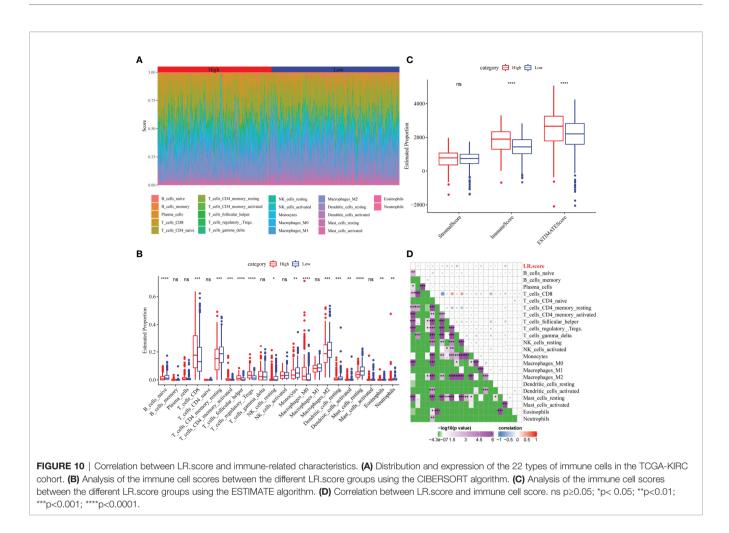
scRNA-seq approaches are rapidly being employed to describe the quantity and functional status of tumour-associated cell types in the TME, revealing previously unknown data about cellular heterogeneity (24). However, in addition to characterising the cellular makeup of tumours, it is crucial to understand how different cell types in the TME interact to initiate tumour progression (25). Although there exist studies examining cell-tocell communication using bulk-seq and scRNA-seq data, investigations relating these features to biological outcomes and studies elucidating the significance of these interactions with specific clinical outcomes remain scarce. This study integrated bulk-Seq and scRNA-Seq data of ccRCC for analyses. After examining cell-to-cell communication, few critical LR-pairs were obtained, revealing cell complexity in the TME. Additionally, two molecular subtyping models were constructed based on these LRpairs, and the prognostic evaluation and immunotherapy utility of different molecular subtyping was found. These findings aid in better understanding the role of cell-cell communication in the TME of ccRCC and developing novel therapy options for ccRCC.

Accumulating evidence shows that immune cell dysfunction within KIRC-TME induces immunosuppression and plays a critical role in tumour growth and treatment (25). In this study, eight different cell types were identified in the ccRCC's TME, indicating its compositional complexity. Malignant solid tumour tissues contain not only tumour cells but also normal epithelial, stromal, immune and vascular cells, with stromal and immune cells as the most prominent components (26). Stromal cells play an essential role in tumorigenesis and drug resistance (27), while infiltrating immune cells are specific to certain environments (28). For example, T cell that infiltrates tumours has been demonstrated to have an anti-cancer effect in ovarian cancer, whereas it is associated with tumour growth, invasion and metastasis in colorectal cancer (28). These cells can impact the results of genomic analysis of tumour samples (such as expression profiles or copy numbers), thus, understanding the TME and the interactions between tumours and other cells could provide important insights into tumour biology and help build reliable prognostic, predictive models.

Therefore, to further study the interaction between different cell types in the TME of ccRCC, a comprehensive and systematic



analysis of cell communication in the TME of ccRCC was conducted. Previous studies have shown that the interaction of ligands and receptors differs significantly in different types of tumours. These differences can lead to the activation or inhibition of different pathways, resulting in tumour development and drug resistance. Therefore, based on the significantly different LR-pairs obtained in this study, a new molecular subtyping model was constructed. According to the



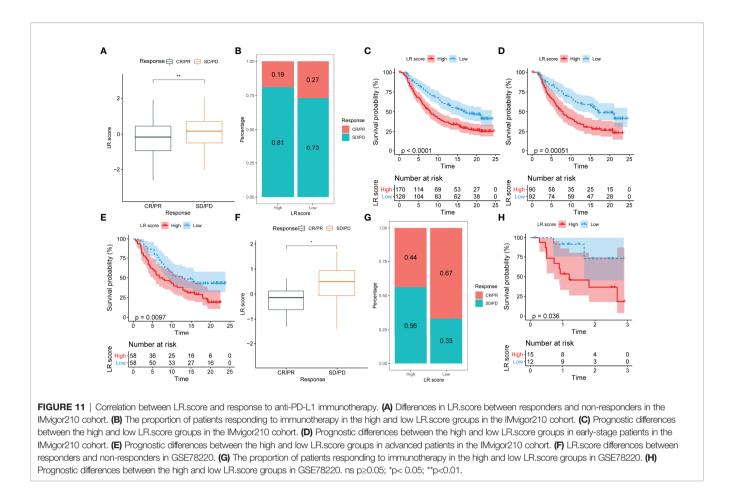
LR-pairs model, patients in different KIRC cohorts can be effectively divided into three subtypes, and the prognosis of patients with different molecular subtypes is significantly different. Additionally, varying clinical-pathological features, mutation features, pathways and immune features showed significant differences in different molecular subtypes.

Furthermore, to further confirm the effectiveness of our typing analysis, data on the immune subtypes of TCGA-KIRC were obtained from a previous pan-cancer study, wherein ccRCC samples were divided into six molecular subtypes based on 160 different immune gene signatures (22). This study compared the relationship between these six immune subtypes and the three LR-pairs subtypes defined in the current study. The results showed that the C3 immune subtypes obtained from the previous study accounted for more of the C3 molecular subtype defined in this study. In previous studies, the C3 immune subtype was described as an 'inflammatory' subtype. Furthermore, the C3 immune subtype was distinguished from other subtypes by increased Th17 and Th1 gene expression, low to medium cancer cell proliferation and lower levels of aneuploidy and total somatic copy number changes. Additionally, it showed the best prognosis among these six immune molecular subtypes, which is consistent with the best

outcome of the C3 molecular subtype defined in the current study. Moreover, the immune subtypes C1, C2, C4 and C6 with worse prognosis accounted for more than the C1 molecular subtypes defined in this study, which coincides with the poor prognosis of C1.

Additional molecular subtypes were provided in previous studies, and four molecular subtypes (KIRC-C1, C2, C3, C4) were identified *via* consensus clustering (23). The KIRC-C3 subtype was associated with the worst prognosis while the KIRC-C1 subtype had the best prognosis. The relationship between these four molecular subtypes and our three molecular subtypes was compared, wherein the KIRC-C4 subtype accounted for more than the C1 subtype, while the KIRC-C1 subtype. Consistent with previous studies, the reliability of the present study is reinforced, providing a base for further understanding of the interactions between cells in the TME and developing new molecular typing methods for patients with ccRCC.

Currently, individualised models based on the specific biomarkers of tumour subtypes have been established in breast and colorectal cancers to improve patients' prognoses (29, 30). However, clinically efficient individualised models for patients



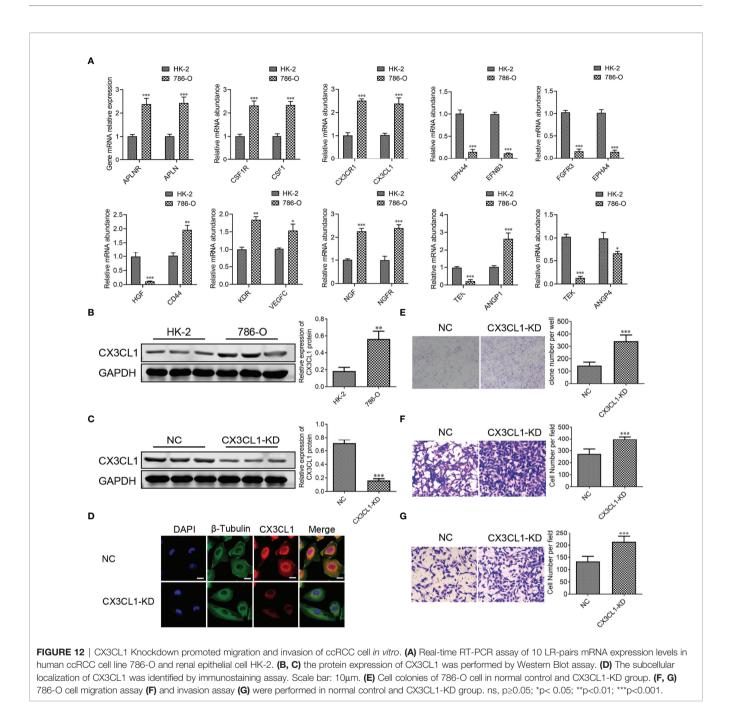
with ccRCC are scarce. Considering the individual heterogeneity of the TME, it is urgent to quantify the scoring pattern of individual tumours and establish an effective treatment and prognosis evaluation model for patients with ccRCC. Although previous studies have explored the value of different signatures in the prognostic evaluation of ccRCC, their validity remains limited (31, 32). Meanwhile, the analysis of cell-cell communication reveals that the expression of ligands and receptors and the type of interaction vary in different tumour types. Therefore, focusing on the communication of different cell types in the TME and their interactions could aid in diagnoses and treatment options. In the current study, based on the previous analysis of LR-pairs with significant differences in both the TCGA-KIRC and RECA-EU datasets, 10 LR-pairs were identified as potential 'subtype biomarkers'. The LR-pairs scores model was established to quantify different risk scores among individuals.

CX3CL1 is a chemokine with a unique motif -Cys-X-X-Cys- at the N-terminal end structure and the only member of the δ -chemokine families. CX3CR1 is a specific receptor for the chemokine CX3CL1. CX3CL1-CX3CR1 plays a critical role in the anticancer immune response (33). Previous studies found that an increase in CX3CL1-CX3CR1 in tumor is associated with the forming of anti-cancer NK cells and CD8⁺T cells in tumor, which improves the prognosis for patients with gastric

adenocarcinoma and glioma (34, 35). In this study, we investigated the anti-cancer effects of CX3CL1 in ccRCC. We found that CX3CL1 knockdown markedly promoted the migration and invasion of ccRCC cell *in vitro*. Targeted CX3CL1 therapy might provide new treatment directions for ccRCC patients.

Furthermore, molecular subtype analyses showed that the LR.score of the C3 subtype was low in both cohorts. Conversely, C1 showed higher scores in both cohorts, which is consistent with previous analyses and thereby confirms the effectiveness of LR-pairs. Meanwhile, in different cohorts, the prognostic model established using LR.score showed high validity and accuracy for the prognostic evaluation of patients. Furthermore, analysis of the differences in the LR.score between different clinicopathological features in two cohorts showed a significant association between the LR.score and patient's malignancy grade. Therefore, LR.score can be used as a reliable biomarker for evaluating the prognosis of patients with ccRCC.

Infiltrating immune cells play various roles in different tumours, hence, the differences in immune score were assessed between patients in the different LR.score groups using ESTIMATE. The result showed that patients in the high-risk group showed higher immune score. A high immune score generally predicts a better prognosis, but patients in the high LR.score group showed a worse prognosis. However, the current findings are consistent with



previous studies, revealing a significant positive correlation between immune score and malignancy degree in patients with ccRCC in the TCGA-KIRC cohort. High immune score and ESTIMATE scores have been associated with worse prognosis (36, 37). Additionally, the high infiltration levels of exhausted CD8⁺ T cells and immunosuppressive M2-like macrophages have been reported in advanced renal disease (8), suggesting that immune scores could indicate progressive T cell dysfunction in patients with ccRCC. This suggestion could also be used to explain a worse prognosis in patients with ccRCC that show a high immune score. Further, to explore the relationship between LR.score and immune cell infiltration levels, the immune cell infiltration levels of patients with ccRCC were quantified using CIBERSORT. Subsequently, the differences in the infiltration of 22 immune cells were compared, revealing that the $CD8^+$ T cell infiltration level was significantly higher in the high LR.score group than in the low LR.score group. Previous studies have confirmed that the infiltration levels of $CD8^+$ T cells are usually associated with a better prognosis in most solid tumours (38). Interestingly, the infiltration of $CD8^+$ T cells was associated with a worse prognosis in ccRCC (39), which is

consistent with the current findings. Therefore, the specificity of the TME of ccRCC can be accurately described using the LR.score model.

ccRCC is an immune-sensitive malignancy, and cytokinebased (IL-2 and IFN-a2b) regimens have been accepted for clinical use. Recent regimens that use immune checkpoints as a therapeutic modality have changed the treatment paradigm of ccRCC (40). However, a significant proportion of patients with kidney cancer do not respond to these therapies and those who initially respond show eventual tumour progression (41). Therefore, this study examined the relationship between immunotherapy and LR.score to assess the benefit of LR.score in different immunotherapy cohorts. The results showed that patients who responded to immunotherapy had significantly lower LR.score than those who responded less. Furthermore, the patients with higher LR.scores showed less favourable responses to immunotherapy. This suggests that single-agent immunotherapy could benefit patients with a lower LR.score. Additionally, the significant differences in survival between the high and low LR.score groups in both immunotherapy cohorts illustrate its association with immunotherapy.

Advances in high-throughput sequencing can lead to personalised therapeutics, wherein each patient's cancer can be treated based on their genomic profile. Although highthroughput sequencing provides a large amount of genomic information, it requires professional bioinformatics analysis and interpretation. Moreover, linking key phenotypes or molecular reactions together remains challenging for most of the data. This study provides concise analysis and novel insights and directions for the personalized treatment of patients with ccRCC. Although high-throughput sequencing could provide a more refined research direction for disease treatment, the current cost of treatment remains high. Reducing treatment costs while maintaining treatment efficacy remains a challenge. Currently, there exists a large amount of research data that require accurate and effective analyses for better clinical application. Although the current study provides a clear view of cell types in the TME of ccRCC and increases our understanding of the importance of LR and cell-to-cell interactions in the microenvironment, there exist a few limitations. While multiple cohorts of patients with ccRCC were used as validation, clinical trial-based validation in larger ccRCC cohorts could better validate the current findings. Additionally, the current high-throughput sequencing data are based on transcriptome data. However, transcription levels are not necessarily associated with protein expression (42)since essential cellular functions are performed and regulated by the proteome, which is also worth considering. The interactions between adjacent cells are the basis of many biological processes, including signalling between cell ligand receptors. Current single-cell genome techniques analyse each cell individually after tissue dissociation, thus losing data on the location between cells. The LR interactions identified by the study may not occur when different cell types do not undergo spatial co-localization in the tumour, thus, spatial transcriptome analysis will help us further understand our

findings. Various bioinformatics methods were used to simulate the cellular composition of TME in patients, and some conclusions are consistent with previous studies. However, in silico cell composition inevitably has limitations; for example, the cellular composition of TME cannot be fully displayed. Therefore, using multiple algorithms to simulate the composition of the patient's TME simultaneously and conducting a more comprehensive analysis could better address the limitations of bioinformatic analyses.

In conclusion, the current study elucidates themicroenvironmental landscape of ccRCC, providing a comprehensive view of the cellular composition of TME in patients with ccRCC. The interaction and communication of LR-pairs between different cell types are evaluated while studying their cellular complexity in the TME. Two valuable LR-pairs models for the molecular subtyping of patients with ccRCC were identified based on LR-pairs in various cell types. Notably, this study provides new insights into cancer immunotherapy, where the expression patterns of LR-pairs effectively evaluate the prognosis of patients with ccRCC and are associated with the efficacy of immunotherapy. Therefore, the development of potential drugs targeting these LR-pairs could contribute to the clinical benefits of immunotherapy. This study provides a new direction in understanding TME and its clinical applications. It also provides novel ideas for identifying different tumour molecular subtypes and developing accurate and personalised tumour immunotherapy.

DATA AVAILABILITY STATEMENT

The datasets presented in this study can be found in online repositories. The names of the repository/repositories and accession number(s) can be found in the article/**Supplementary Material**.

AUTHOR CONTRIBUTIONS

QG, FL and PW designed the study. QG, FL, PW, YJ and WS conducted the study and analysed the data. FL drafted the manuscript. QG and YG revised the manuscript. All authors have read and approved the submitted version.

FUNDING

This research was supported by the Guangxi Natural Science Foundation Project (No. 2020JJB140078).

SUPPLEMENTARY MATERIAL

The Supplementary Material for this article can be found online at: https://www.frontiersin.org/articles/10.3389/fimmu.2022.874056/full#supplementary-material

REFERENCES

- Hoefflin R, Harlander S, Schäfer S, Metzger P, Kuo F, Schönenberger D, et al. Hif-1α and Hif-2α Differently Regulate Tumour Development and Inflammation of Clear Cell Renal Cell Carcinoma in Mice. *Nat Commun* (2020) 11(1):4111. doi: 10.1038/s41467-020-17873-3
- Turajlic S, Xu H, Litchfield K, Rowan A, Chambers T, Lopez JI, et al. Tracking Cancer Evolution Reveals Constrained Routes to Metastases: Tracerx Renal. *Cell* (2018) 173(3):581–94.e12. doi: 10.1016/j.cell.2018.03.057
- Massari F, Rizzo A, Mollica V, Rosellini M, Marchetti A, Ardizzoni A, et al. Immune-Based Combinations for the Treatment of Metastatic Renal Cell Carcinoma: A Meta-Analysis of Randomised Clinical Trials. *Eur J Cancer* (2021) 154:120–7. doi: 10.1016/j.ejca.2021.06.015
- Rizzo A, Mollica V, Santoni M, Ricci AD, Rosellini M, Marchetti A, et al. Impact of Clinicopathological Features on Survival in Patients Treated With First-Line Immune Checkpoint Inhibitors Plus Tyrosine Kinase Inhibitors for Renal Cell Carcinoma: A Meta-Analysis of Randomized Clinical Trials. *Eur Urol Focus* (2021) S2405-4569(21):00058-4. doi: 10.1016/j.euf.2021.03.001
- Porta C, Cosmai L, Leibovich BC, Powles T, Gallieni M, Bex A. The Adjuvant Treatment of Kidney Cancer: A Multidisciplinary Outlook. *Nat Rev Nephrol* (2019) 15(7):423–33. doi: 10.1038/s41581-019-0131-x
- Grimm M-O, Bex A, De Santis M, Ljungberg B, Catto JWF, Rouprêt M, et al. Safe Use of Immune Checkpoint Inhibitors in the Multidisciplinary Management of Urological Cancer: The European Association of Urology Position in 2019. *Eur* Urol (2019) 76(3):368–80. doi: 10.1016/j.eururo.2019.05.041
- Kotecha RR, Motzer RJ, Voss MH. Towards Individualized Therapy for Metastatic Renal Cell Carcinoma. Nat Rev Clin Oncol (2019) 16(10):621–33. doi: 10.1038/s41571-019-0209-1
- Koh MY, Sayegh N, Agarwal N. Seeing the Forest for the Trees—Single-Cell Atlases Link Cd8+ T Cells and Macrophages to Disease Progression and Treatment Response in Kidney Cancer. *Cancer Cell* (2021) 39(5):594–6. doi: 10.1016/j.ccell.2021.03.008
- Wu T, Dai Y. Tumor Microenvironment and Therapeutic Response. Cancer Lett (2017) 387:61–8. doi: 10.1016/j.canlet.2016.01.043
- Marusyk A, Janiszewska M, Polyak K. Intratumor Heterogeneity: The Rosetta Stone of Therapy Resistance. *Cancer Cell* (2020) 37(4):471–84. doi: 10.1016/ j.ccell.2020.03.007
- Motzer RJ, Banchereau R, Hamidi H, Powles T, McDermott D, Atkins MB, et al. Molecular Subsets in Renal Cancer Determine Outcome to Checkpoint and Angiogenesis Blockade. *Cancer Cell* (2020) 38(6):803–17.e4. doi: 10.1016/ j.ccell.2020.10.011
- Wagner A, Regev A, Yosef N. Revealing the Vectors of Cellular Identity With Single-Cell Genomics. Nat Biotechnol (2016) 34(11):1145–60. doi: 10.1038/ nbt.3711
- Yao M, Ventura PB, Jiang Y, Rodriguez FJ, Wang L, Perry JSA, et al. Astrocytic Trans-Differentiation Completes a Multicellular Paracrine Feedback Loop Required for Medulloblastoma Tumor Growth. *Cell* (2020) 180(3):502–20.e19. doi: 10.1016/j.cell.2019.12.024
- Naffar-Abu Amara S, Kuiken HJ, Selfors LM, Butler T, Leung ML, Leung CT, et al. Transient Commensal Clonal Interactions Can Drive Tumor Metastasis. *Nat Commun* (2020) 11(1):5799. doi: 10.1038/s41467-020-19584-1
- Hanahan D, Weinberg RA. Hallmarks of Cancer: The Next Generation. Cell (2011) 144(5):646–74. doi: 10.1016/j.cell.2011.02.013
- Ramilowski JA, Goldberg T, Harshbarger J, Kloppmann E, Lizio M, Satagopam VP, et al. A Draft Network of Ligand-Receptor-Mediated Multicellular Signalling in Human. *Nat Commun* (2015) 6(1):7866. doi: 10.1038/ncomms8866
- Zhang Y, Narayanan SP, Mannan R, Raskind G, Wang X, Vats P, et al. Single-Cell Analyses of Renal Cell Cancers Reveal Insights Into Tumor Microenvironment, Cell of Origin, and Therapy Response. *Proc Natl Acad Sci* (2021) 118(24):e2103240118. doi: 10.1073/pnas.2103240118
- Efremova M, Vento-Tormo M, Teichmann SA, Vento-Tormo R. Cellphonedb: Inferring Cell-Cell Communication From Combined Expression of Multi-Subunit Ligand-Receptor Complexes. *Nat Protoc* (2020) 15(4):1484–506. doi: 10.1038/s41596-020-0292-x
- Wu T, Hu E, Xu S, Chen M, Guo P, Dai Z, et al. Clusterprofiler 4.0: A Universal Enrichment Tool for Interpreting Omics Data. *Innovation* (2021) 2 (3):100141. doi: 10.1016/j.xinn.2021.100141

- Gong Q, Jiang Y, Pan X, You Y. Fractalkine Aggravates Lps-Induced Macrophage Activation and Acute Kidney Injury Via Wnt/B-Catenin Signalling Pathway. J Cell Mol Med (2021) 25(14):6963–75. doi: 10.1111/ jcmm.16707
- Newman AM, Steen CB, Liu CL, Gentles AJ, Chaudhuri AA, Scherer F, et al. Determining Cell Type Abundance and Expression From Bulk Tissues With Digital Cytometry. *Nat Biotechnol* (2019) 37(7):773–82. doi: 10.1038/s41587-019-0114-2
- Thorsson V, Gibbs DL, Brown SD, Wolf D, Bortone DS, Ou Yang T-H, et al. The Immune Landscape of Cancer. *Immunity* (2018) 48(4):812–30.e14. doi: 10.1016/j.immuni.2018.03.023
- Creighton CJ, Morgan M, Gunaratne PH, Wheeler DA, Gibbs RA, Gordon Robertson A, et al. Comprehensive Molecular Characterization of Clear Cell Renal Cell Carcinoma. *Nature* (2013) 499(7456):43–9. doi: 10.1038/ nature12222
- Tanay A, Regev A. Scaling Single-Cell Genomics From Phenomenology to Mechanism. *Nature* (2017) 541(7637):331–8. doi: 10.1038/nature21350
- Greten FR, Grivennikov SI. Inflammation and Cancer: Triggers, Mechanisms, and Consequences. *Immunity* (2019) 51(1):27–41. doi: 10.1016/j.immuni.2019.06.025
- Ma L, Hernandez MO, Zhao Y, Mehta M, Tran B, Kelly M, et al. Tumor Cell Biodiversity Drives Microenvironmental Reprogramming in Liver Cancer. *Cancer Cell* (2019) 36(4):418–30.e6. doi: 10.1016/j.ccell.2019.08.007
- Wang Z, Su G, Dai Z, Meng M, Zhang H, Fan F, et al. Circadian Clock Genes Promote Glioma Progression by Affecting Tumour Immune Infiltration and Tumour Cell Proliferation. *Cell Prolif* (2021) 54(3):e129887. doi: 10.1111/ cpr.12988
- 28. Tian J, Cai Y, Li Y, Lu Z, Huang J, Deng Y, et al. Cancerimmunityqtl: A Database to Systematically Evaluate the Impact of Genetic Variants on Immune Infiltration in Human Cancer. *Nucleic Acids Res* (2020) 49(D1): D1065–D73. doi: 10.1093/nar/gkaa805
- Callari M, Cappelletti V, D'Aiuto F, Musella V, Lembo A, Petel F, et al. Subtype-Specific Metagene-Based Prediction of Outcome After Neoadjuvant and Adjuvant Treatment in Breast Cancer. *Clin Cancer Res* (2016) 22(2):337– 45. doi: 10.1158/1078-0432.Ccr-15-0757
- Bramsen JB, Rasmussen MH, Ongen H, Mattesen TB, Ørntoft M-BW, Árnadóttir SS, et al. Molecular-Subtype-Specific Biomarkers Improve Prediction of Prognosis in Colorectal Cancer. *Cell Rep* (2017) 19(6):1268– 80. doi: 10.1016/j.celrep.2017.04.045
- Xing Q, Zeng T, Liu S, Cheng H, Ma L, Wang Y. A Novel 10 Glycolysis-Related Genes Signature Could Predict Overall Survival for Clear Cell Renal Cell Carcinoma. *BMC Cancer* (2021) 21(1):381. doi: 10.1186/s12885-021-08111-0
- 32. Wu X, Zhao Z, Khan A, Cai C, Lv D, Gu D, et al. Identification of a Novel Signature and Construction of a Nomogram Predicting Overall Survival in Clear Cell Renal Cell Carcinoma. *Front Genet* (2020) 11:1017. doi: 10.3389/ fgene.2020.01017
- Yu Y-RA, Fong AM, Combadiere C, Gao J-L, Murphy PM, Patel DD. Defective Antitumor Responses in Cx3cr1-Deficient Mice. Int J Cancer (2007) 121(2):316–22. doi: 10.1002/ijc.22660
- 34. Hyakudomi M, Matsubara T, Hyakudomi R, Yamamoto T, Kinugasa S, Yamanoi A, et al. Increased Expression of Fractalkine Is Correlated With a Better Prognosis and an Increased Number of Both Cd8+ T Cells and Natural Killer Cells in Gastric Adenocarcinoma. Ann Surg Oncol (2008) 15(6):1775–82. doi: 10.1245/s10434-008-9876-3
- 35. Ren F, Zhao Q, Huang L, Zheng Y, Li L, He Q, et al. The R132h Mutation in Idh1 Promotes the Recruitment Ofnk Cells Through Cx3cl1/Cx3cr1 Chemotaxis and Iscorrelated With a Better Prognosis in Gliomas. *Immunol Cell Biol* (2019) 97(5):457–69. doi: 10.1111/imcb.12225
- Kong G, Wang Y, Huang Y, Shi Z. Identification and Verification of Tumor Immune Microenvironment-Related Prognostic Genes in Kidney Renal Clear Cell Carcinoma. *BioMed Res Int* (2022) 2022:5563668. doi: 10.1155/2022/ 5563668
- 37. Jiang M, Lin J, Xing H, An J, Yang J, Wang B, et al. Microenvironment-Related Gene Tnfsf13b Predicts Poor Prognosis in Kidney Renal Clear Cell Carcinoma. *PeerJ* (2020) 8:e9453. doi: 10.7717/peerj.9453
- Vuong L, Kotecha RR, Voss MH, Hakimi AA. Tumor Microenvironment Dynamics in Clear-Cell Renal Cell Carcinoma. *Cancer Discov* (2019) 9 (10):1349–57. doi: 10.1158/2159-8290.Cd-19-0499

- Fridman WH, Zitvogel L, Sautès-Fridman C, Kroemer G. The Immune Contexture in Cancer Prognosis and Treatment. Nat Rev Clin Oncol (2017) 14(12):717–34. doi: 10.1038/nrclinonc.2017.101
- Motzer RJ, Penkov K, Haanen J, Rini B, Albiges L, Campbell MT, et al. Avelumab Plus Axitinib Versus Sunitinib for Advanced Renal-Cell Carcinoma. N Engl J Med (2019) 380(12):1103–15. doi: 10.1056/ NEJMoa1816047
- 41. Giraldo NA, Becht E, Pagès F, Skliris G, Verkarre V, Vano Y, et al. Orchestration and Prognostic Significance of Immune Checkpoints in the Microenvironment of Primary and Metastatic Renal Cell Cancer. *Clin Cancer Res* (2015) 21(13):3031–40. doi: 10.1158/1078-0432.ccr-14-2926
- 42. Wragg D, Liu Q, Lin Z, Riggio V, Pugh CA, Beveridge AJ, et al. Using Regulatory Variants to Detect Gene–Gene Interactions Identifies Networks of Genes Linked to Cell Immortalisation. *Nat Commun* (2020) 11(1):343. doi: 10.1038/s41467-019-13762-6

Conflict of Interest: The authors declare that the research was conducted in the absence of any commercial or financial relationships that could be construed as a potential conflict of interest.

Publisher's Note: All claims expressed in this article are solely those of the authors and do not necessarily represent those of their affiliated organizations, or those of the publisher, the editors and the reviewers. Any product that may be evaluated in this article, or claim that may be made by its manufacturer, is not guaranteed or endorsed by the publisher.

Copyright © 2022 Liu, Wang, Sun, Jiang and Gong. This is an open-access article distributed under the terms of the Creative Commons Attribution License (CC BY). The use, distribution or reproduction in other forums is permitted, provided the original author(s) and the copyright owner(s) are credited and that the original publication in this journal is cited, in accordance with accepted academic practice. No use, distribution or reproduction is permitted which does not comply with these terms.



Immunotherapy for Pediatric Acute Lymphoblastic Leukemia: Recent Advances and Future Perspectives

Meng Lv^{1†}, Yan Liu^{2†}, Wei Liu³, Yabing Xing^{1*} and Shengnan Zhang^{1*}

¹ Department of Pharmacy, Children's Hospital Affiliated to Zhengzhou University, Zhengzhou, China, ² Department of Pharmacy, The First Affiliated Hospital of Zhengzhou University, Zhengzhou, China, ³ Department of Hematology Oncology, Children's Hospital Affiliated to Zhengzhou University, Zhengzhou, China

OPEN ACCESS

Edited by: Xuyao Zhang, Fudan University, China

Reviewed by:

Yan Cao, Sun Yat-sen University Cancer Center (SYSUCC), China Bowen Xing, Children's Hospital of Philadelphia, United States Longchao Liu, University of Texas Southwester Medical Center, United States

*Correspondence:

Yabing Xing xyb06@live.com Shengnan Zhang zsnphar@126.com

[†]These authors have contributed equally to this work

Specialty section:

This article was submitted to Cancer Immunity and Immunotherapy, a section of the journal Frontiers in Immunology

Received: 16 April 2022 **Accepted:** 19 May 2022 **Published:** 13 June 2022

Citation:

Lv M, Liu Y, Liu W, Xing Y and Zhang S (2022) Immunotherapy for Pediatric Acute Lymphoblastic Leukemia: Recent Advances and Future Perspectives. Front. Immunol. 13:921894. doi: 10.3389/fimmu.2022.921894 Pediatric acute lymphoblastic leukemia (ALL) is the most common subtype of childhood leukemia, which is characterized by the abnormal proliferation and accumulation of immature lymphoid cell in the bone marrow. Although the long-term survival rate for pediatric ALL has made significant progress over years with the development of contemporary therapeutic regimens, patients are still suffered from relapse, leading to an unsatisfactory outcome. Since the immune system played an important role in the progression and relapse of ALL, immunotherapy including bispecific T-cell engagers and chimeric antigen receptor T cells has been demonstrated to be capable of enhancing the immune response in pediatric patients with refractory or relapsed B-cell ALL, and improving the cure rate of the disease and patients' quality of life, thus receiving the authorization for market. Nevertheless, the resistance and toxicities associated with the current immunotherapy remains a huge challenge. Novel therapeutic options to overcome the above disadvantages should be further explored. In this review, we will thoroughly discuss the emerging immunotherapeutics for the treatment of pediatric ALL, as well as side-effects and new development.

Keywords: pediatric ALL, T-cell engagers, CAR T cell therapy, macrophage-based immunotherapy, NK cell-based immunotherapy

INTRODUCTION

Acute lymphoblastic leukemia (ALL), characterized by the abnormal clonal proliferation of the early lymphoid stem cells or progenitor cells and the depletion of the normal hematopoietic cells in the marrow, is the most prevalent subtype of leukemia with a rapidly growing incidence worldwide (1–5). Although ALL occurs in both adults and children, children represent up to 80% of cases (6). Currently, improved long-term survival rates have increased to more than 90% in pediatric ALL thanks to the contemporary therapeutic regimens (7, 8). However, approximately 20% of the patients remain refractory to primary therapy or suffer from relapse after initial complete remission (CR), leading to a poor prognosis (9, 10). Therefore, the exploration of novel therapeutic approaches for pediatric refractory/relapse (R/R) ALL are urgently needed and will eventually benefit this population.

Until now, accumulating evidence has suggested that tumor microenvironment (TME) contributes to the cancer development and progression (11-13). As key members in TME, immune cells consisting of T cells, macrophages, and natural killer cells (NKs) have reduced activity and poise in an immunosuppressive state. Activating the immune system to recognize and eradicate cancer cells rather than remove or directly attack the cancer cells, termed immunotherapy, has been proposed as an alternative to conventional cancer treatment and widely explored over the last decade (14, 15). In particular, immunotherapy promoted rapid development for the treatment of the hematologic malignancies (16-18). The approval for market of blinatumomab, a bispecific CD3/CD19 T-cell engager, and tisagenlecleucel, a CAR T cell therapy, has demonstrated dramatic progress in the treatment of pediatric R/ R B-cell precursor ALL (R/R BCP ALL). Combination or replacement of conventional chemotherapy with immunotherapy to further improve the cure rates and life quality of pediatric patients with ALL has become the priority issue for the moment (19-21). Generally, pediatric cancers are not smaller versions of adult cancers (6, 22). The progress and development in pediatric cancers lags behind adult patients (23). Herein, we aim to provide a comprehensive overview of the emerging immunotherapeutic approaches in pediatric ALL, thus guiding the development of novel therapeutic options. The preclinical research and ongoing clinical trials in this field will be extensively summarized in this review (Table 1). Due to T-cell ALL accounts for merely 15% of the pediatric ALL patients and has a different immunophenotype from B-cell ALL, immunotherapy for pediatric T-cell ALL is outside the scope of this article.

T CELL-BASED IMMUNOTHERAPY

T cells have become an ideal weapon and attracted great research enthusiasm in cancer immunotherapy due to its capacity for antigen-directed cytotoxicity (45–47). Over the last decade, various T cell-based immunotherapeutic approaches, including blocking programmed cell death-1 (PD-1)/programmed cell death-ligand 1 (PD-L1) axis, bispecific/trispecific T-cell engagers, and chimeric antigen receptor (CAR) T cells have revolutionized the field of cancer therapeutics. The following context will highlight the T cell-based immunotherapeutic strategies available to attenuate pediatric B-cell ALL (**Figure 1**).

Bispecific CD3/CD19 T Cell Engagers

Bispecific antibodies are designated to recognize and bind two distinct epitopes or antigens simultaneously, which have demonstrated great therapeutic potential toward cancer immunotherapy and are in rapid clinical development (48, 49). Blinatumomab, which is comprised of two different single-chain variable fragment regions (scFv) linked *via* a glycine-serine linker (50), triggers a cytotoxic immune response and shows significant cytotoxic activity at ultra-low concentrations, through binding specifically to antigen CD19 that is overexpressed on the surface of B-cell ALL lymphocytes and antigen CD3 on the surface of T cells (51-53). As the benchmarking case, blinatumomab conveyed good efficiency and safety in a phase I/II study (NCT01471782), which demonstrated that blinatumomab was maximumly tolerated at 15 μ g/m²/day in 49 children with R/R BCP-ALL, 39% of whom achieved CR with single-agent blinatumomab treatment (24, 25). In the subsequent multi-center, expanded access study (RIALTO trial, NCT02187354), 63% of children had CR and the MRD negativity was obtained in 83% of responders after the first two cycles of blinatumomab treatment, further confirming the efficiency of blinatumomab (26, 27). Accordingly, blinatumomab was approved to treat R/R B-cell ALL in children by the US Food and Drug Administration (FDA) in 2018. Recently, two randomized trials (NCT02393859 and NCT02101853) exemplify the advantages of blinatumomab as post reinduction consolidation treatment vs chemotherapy before allogeneic hematopoietic stem cell transplant (alloHSCT), resulting in superior in eradicating MRD (28, 29). Therefore, blinatumomab gained accelerated approval by FDA to treat BCP ALL with MRD greater than or equal to 0.1% after the first or second CR. Moreover, a phase II study (NCT02807883) has proved the feasibility of blinatumomab maintenance following alloHSCT for patients with B-cell ALL at high-risk for relapse, with the 1-year overall survival (OS), progression-free survival (PFS), and nonrelapse mortality (NRM) rates of 85%, 71%, and 0%, respectively (30). In addition, to incorporate blinatumomab as part of upfront treatment for pediatric B-cell ALL, several trials are currently ongoing (NCT03643276 and NCT03914625) (31). Of note, the main toxicities including cytokine release syndrome (CRS) and neurotoxicity are tolerable under blinatumomab therapy (54, 55).

Although blinatumomab has obtained an authorization for treating pediatric R/R BCP ALL and eliminating the MRD, several disadvantages, such as the short half-life caused by the low molecular weight, leading to the need to continuous intravenous infusion, limited wide clinical application (56). Besides, blinatumomab resistance caused by the loss of CD19 expression and lineage switch in BCP ALL remains a significant problem (57, 58). For example, in a phase I/II study, four patients harboring CD19 negative B-cell ALL relapsed after prior blinatumomabinduced hematologic remission and one patient with CD19negative had disease progression (57). In the future, screening tumor markers to predict CD19-negative relapse should be paid more attention. What's more, overexpression of checkpoint molecules including T-cell immunoglobulin and mucin domain 3 (TIM-3) on T cells and PD-L1 on tumor cells represented an additional potential escape mechanism from immunosurveillance (30, 59, 60). Adding immune checkpoint inhibitors to blinatumomab treatment thus overcoming resistance may be feasible (60) and are under clinical investigation (NCT03160079, NCT03512405 and NCT04546399).

Bispecific CD3/CD20 T-Cell Engagers

In addition to CD19, other antigens on the surface of leukemic blasts are currently under active research and development. CD20 is a signature B cell differentiation antigen and its overexpression is identified as an inferior prognosis marker associated with a worse event-free survival (EFS) in childhood BCP ALL according to the

TABLE 1 | Emerging immunotherapeutic approaches for pediatric B-cell ALL.

Interventions	Target	Patients number	Patients group	Indications	Study phase	Clinical Trial number	Ref.
T cell engagers							
Blinatumomab	CD3/CD19	93	Up to 17 years	R/R BCP ALL	Phase I/II	NCT01471782	(24, 25)
Blinatumomab	CD3/CD19	110	28 days to 18 years	R/R BCP ALL	Expanded access study	NCT02187354	(26, 27)
Blinatumomab	CD3/CD19	111	Up to 17 years	High-risk first relapse BCP ALL	Phase III	NCT02393859	(28)
Blinatumomab	CD3/CD19	670	1 to 30 years	Relapsed B-cell ALL	Phase III	NCT02101853	(29)
Blinatumomab	CD3/CD19	23	1 to 70 years	Maintenance for patients with B-cell ALL after alloHSCT	Phase II	NCT02807883	(30)
Blinatumomab	CD3/CD19	5000	Up to 18 years	ALL	Phase III	NCT03643276	(31)
CMG1A46	CD3/CD19/ CD20	165	18 years and older	B-cell NHL and/or ALL	Phase I/II	NCT05348889	/
CAR T-cell therapy (correspondence)	onding costim	ulatory dom	ain)				
Tisagenlecleucel (4-1BB)	CD19	30	5 to 20 years	R/R CD19 positive B-cell ALL	Phase I/IIa	NCT01626495	(32)
Tisagenlecleucel (4-1BB)	CD19	75	Up to 25 years	R/R B-cell ALL	Phase II	NCT02435849	(33)
Brexucabtagene autoleucel (CD28)	CD19	125	18 years and older	R/R BCP ALL	Phase I/II	NCT02614066	(34– 36)
Brexucabtagene autoleucel (CD28)	CD19	116	Up to 21 years	R/R BCP ALL and R/R B-cell NHL	Phase I/II	NCT02625480	/
CD19CAR T cells (4-1BB)	CD19	167	1 to 26 years old	R/R CD19 positive leukemia	Phase I/II	NCT02028455	/
CD19CAR T cells (4-1BB)	CD19	35	Up to 21 years	R/R CD19 positive ALL	Phase I/II	NCT03573700	/
CD19CAR T cells (CD28 with or without 4-1BB)	CD19	64	Up to 75 years	Advanced B-cell NHL, ALL, and CLL	Phase I	NCT01853631	/
CD19CAR T cells (4-1BB)	CD19	27	Up to 29 years		Phase II	NCT04276870	/
CD19CAR T cells (4-1BB)	CD19	121	Up to 25 years	R/R B-cell ALL and B-cell NHL	Phase I/II	NCT03743246	/
CD19CAR T cells (CD28 or 4- 1BB)	CD19	50	3 years and older	B-cell malignancy	Phase I/II	NCT02782351	/
CD19CAR T cells (CD28)	CD19	23	Up to 26 Years	Relapsed B-cell ALL	Phase I	NCT01860937	/
CD19CAR T cells (not reported)	CD19	54	3 to 70 years		Phase I/II	NCT03016377	/
CD19CAR T cells (CD28)	CD19	53		B-cell leukemia or lymphoma	Phase I	NCT01593696	(37, 38)
CD22CAR T cells(4-1BB)	CD22	208	3 to 39 years	R/R CD22 positive B-cell malignancies	Phase I	NCT02315612	(39)
CD22-CAR T cells (4-1BB)	CD22	5	18 years and older	R/R B-cell ALL	Phase I	NCT02588456	(40)
CD22-CAR T cells (4-1BB)	CD22	15	1 to 24 years	R/R B-cell ALL	Phase I	NCT02650414	/
CD22CAR T cells (4-1BB)	CD22	34	1 to 55 years	R/R B-cell ALL	Observational study	ChiCTR-OIC- 17013523	(41)
AUTO3 (OX40 and 4-1BB)	CD19/CD22	23	1 to 24 years	R/R B-cell ALL	Phase I/II	NCT03289455	(42)
CD19 and CD22 bispecific CAR T cells (4-1BB)	CD19/CD22	87	3 to 39 years	Recurrent or refractory CD19/CD22 positive B-cell malignancies	Phase I	NCT03448393	/
CTA101 (4-1BB)	CD19	72	3 to 70 years	R/R CD19 positive B-cell ALL and NHL	Early Phase I	NCT04227015	(40)
CD19CAR T cells and CD22CAR T cells (4-1BB)	CD19 and CD22	20	1 to 16 years	R/R B-cell ALL	Phase I	ChiCTR-OIB- 17013670	(43)
CD19 CAR T cells (4-1BB)	CD19	32	Up to 24 Years	high risk, relapsed CD19 positive ALL and Burkitt Lymphoma	Phase I	NCT02443831	(44)
CD19 CAR T cells (4-1BB)	CD19	20	1 to 70 years	20	Phase I	ChiCTR190002445	Ø
Combination therapy		10	A · ···			NOTOOTOTOT	(10)
Pembrolizumab Blinatumomab with	PD-1 PD-1, CD3/	12 24	Adults 18 years and	MRD positive ALL R/R B-cell ALL	Phase II Phase I/II	NCT02767934 NCT03160079	(107) /

(Continued)

Interventions	Target	Patients number	Patients group	Indications	Study phase	Clinical Trial number	Ref.
Blinatumomab with pembrolizumab	PD-1, CD3/ CD19	36	18 years and older	recurrent or refractory ALL	Phase I/II	NCT03512405	/
Blinatumomab with nivolumab	PD-1, CD3/ CD19	550	1 to 30 years	first relapsed B-cell ALL	Phase II	NCT04546399	/
Blinatumomab with chemotherapy	CD3/CD19	6720	1 to 31 years	Newly diagnosed B-cell lymphoblastic leukemia	Phase III	NCT03914625	/
Other emerging therapeutic	approaches						
TTTI-621	CD47	260	18 years and older	Hematologic malignancies and solid tumors	Phase I	NCT02663518	/
CAR NK cells	CD19	14	Up to 18 years	B-cell ALL	Phase I	NCT00995137	/
CAR NK cells	CD19	20	Up to 80 years	B-cell ALL	Phase I	NCT01974479	/
TAA-T	Tumor neoantigens	90	6 months to 80 Years	R/R hematopoietic malignancies, AML and MDS	Phase I	NCT02203903	/
BAFF-R-CAR T Cells	BAFF-R	37	18 years and older	R/R B-cell ALL	Phase I	NCT04690595	/

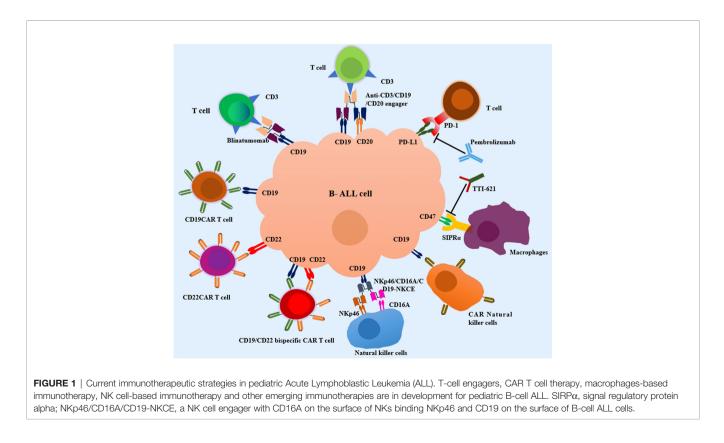
PD-1, programmed cell death-1; MRD, minimal residual disease; R/R, refractory/relapse; BCP ALL, B-cell precursor ALL; NHL, Non-Hodgkin Lymphoma; BAFFR, B-cell activating factor receptor; "/" represents that the detail information about the clinical information could be found in ClinicalTrials.gov or http://www.chictr.org.cn/.

Pediatric Oncology Group treatment protocols (61). Also, CD20 expression was significantly up-regulated in pediatric B-cell leukemias during induction treatment (62), rendering it an appealing target for immunotherapy. Currently, several promising bispecific antibodies of anti-CD3/CD20, such as glofitamab, mosunetuzumab, REGN1979, and epcoritamab, may be of interest for future studies in B-cell Non-Hodgkin Lymphoma

(NHL) (63, 64). However, further investigation is warranted to evaluate this strategy in pediatrics with B-cell ALL.

Trispecific CD3/CD19/CD20 T-Cell Engagers

A-2019, a novel trispecific CD3/CD19/CD20 T-cell engagers possessing the anti-CD19 and anti-CD20 scFvs, was designed



by Wang lab (65). It mediated autologous B cell depletion ex vivo by inducing the activation and proliferation of T cells, and the production and release of cytokines (65). Furthermore, A-2019 bound to CD19 with a lower affinity compared with blinatumomab (1.06 \times 10⁻⁸ mol/L vs. 1.49 \times 10⁻⁹ mol/L, respectively), which potentially reduce the off-target effect on mural cells, thus lowering the risk of neurotoxicity (66). Plus, a general decrease in overall cytokine including IL-6 and IFN- γ induced by A-2019 was observed in preclinical study, reducing the risk of CRS. In short, trispecific T-cell engagers targeting CD3/CD19/CD20 represents a novel strategy for not only preventing and treating CD19 negative relapse, but also has the potential for the treatment of CD20 positive and/or CD19 positive B-cell ALL. In a more recent preclinical study, CMG1A46, another CD3/CD19/CD20 T-cell engager generated from Chimagen's TRIAD platform, displayed superior potency and safety in comparation with CD3/CD20 bispecific T-cell engagers (67). The phase I/II clinical trial is undergoing to evaluate the safety and efficacy of CMG1A46 in adult patients with advanced CD19 and/or CD20 positive B-cell NHL or ALL (NCT05348889).

CAR T Cell Therapy

CAR T cells that commonly consists of an antigen-binding domain and costimulatory signaling domain such as CD28 and/or 4-1BB (68, 69), is a revolutionary and promising immunotherapy approach in cancer treatment (70). Antigen markers on B-cell ALL cells surface such as CD19 and CD22 can be specifically recognized by CAR that is independent from the major histocompatibility complex receptor, thus activating T cells to kill tumor cells.

CD19 Targeting CAR T Cell Therapy

Tisagenlecleucel, also named CTL019, is autologous T cells engineered ex vivo with a CAR containing a 4-1BB domain (71). In 2012, two children diagnosed with R/R B-cell ALL were infused with tisagenlecleucel and both achieved CR, although one patient had a CD19 negative relapse (72, 73). These encouraging data brought a hope of this therapy for the treatment of R/R B-cell ALL. Subsequently, a trial was expanded to 30 patients with the age of 5 to 22 years with R/R B-cell ALL in a phase I/IIa study (NCT01626495), which demonstrated a 90% rate of CR at the first month, an EFS rate of 67% and overall survival (OS) rate of 78% at 6 months after the single infusion of tisagenlecleucel (32). An international phase II study using tisagenlecleucel in pediatric and young adult patients with R/R B-cell ALL showed a CR rate of 81% at 3 months, EFS rate of 73%, and OS rate of 90% at 6 months (NCT02435849) (33). Given the unprecedented successes in clinical trials, tisagenlecleucel was commercially approved by the FDA and was indicated for R/R B-cell ALL patients up to 25 years old in 2017.

Brexucabtagene autoleucel, also named KTE-X19, is another CD19CAR T cell therapy with a CD28 costimulatory subunit generated from peripheral blood monocular cells by removing CD19 positive malignant cells to avoid T cell exhaustion, and has received FDA approval for mantle cell lymphoma (74). Based on the data from the pivotal phase I/II clinical trial (ZUMA-3, NCT02614066), brexucabtagene autoleucel was successfully manufactured and administered as a single infusion in 55 adult patients with R/R BCP ALL (34–36). Ultimately, 31 (56%) patients achieved CR and 8 (15%) patients achieved CR with incomplete haematological recovery, 38 (97%) of whom had MRD negativity. Due to the striking efficacy of brexucabtagene autoleucel in R/R BCP ALL adult patients, study to evaluate brexucabtagene autoleucel in pediatric and young adult patients with BCP ALL is ongoing (ZUMA-4, NCT02625480) and the results will be anticipated. Furthermore, several other CD19CAR T cell therapies are undergoing clinical research (**Table 1**) (75–77).

Although CD19CAR T cell therapy has shown great success for pediatric B-cell ALL, some patients displayed no response and a great part of patients suffered from relapse with poor outcomes (NCT01593696) (37, 38). Unfortunately, even a secondary infusion of CD19CAR T cells can't prevent CD 19positive relapse, which may be partly due to immune-mediated clearance of CAR T cells (78, 79). Antigen loss caused by mutations or alternate splice variants of CD19 have been elucidated as the major resistance mechanism to CD19CAR T cell immunotherapy, which is widely acknowledged as an urgent problem to be solved (80, 81). Therefore, new therapeutic approaches are required for R/R B-cell ALL patients who have failed previous CD19CAR T cell therapy.

CD22 Targeting CAR T Cell Therapy

CD22 represents an alternative target with a high expression level on most B-cell ALL cells, while has restricted expression on normal B cells, especially in the absence of CD19 expression (82-84). Recently, a phase I dose escalation study of CD22CAR T cells with a 4-1BB costimulatory domain in pediatric and young adults with recurrent or refractory CD22 positive B cell malignancies was conducted sponsored by National Cancer Institute (NCT02315612). The results showed that 70.2% of the patients achieved CR and 87.5% of whom were MRD negative (39, 85). However, an CD22CAR possessing the similar structure with the above mentioned CD22CAR but the heavy and light chains were connected by a standard 20aminoacid linker instead of a short 5-amino acid sequence, proved surprisingly poor response in pediatric and adult patients with B-cell ALL (NCT02588456) (40). By performing detailed interrogation responsible for the entirely different findings from the two independent clinical trials, mechanisms that short scFv linker and tonic signaling enhanced the antileukemic function of 4-1BB-based CAR T cells induced the phenomena (40). Based on this work, the pilot study (NCT02650414) was amended to determine the feasibility and safety of a single dose administered CD22CAR T cells expressing 4-1BB costimulatory domains in pediatric R/R B-cell ALL patients (40). Moreover, Pan and his colleges constructed an CD22CAR with a 4-1BB costimulatory domain and initiated a clinical trial, which demonstrated a CR rate of 80% on day 30 after infusion in 34 R/R B-cell ALL pediatric and adult patients who have mostly failed from first CD19CAR T cell therapy (ChiCTR-OIC-17013523) (41). However, most patients relapsed

with a diminished CD22 site density on B-cell ALL cells (85), which raised the question that single target therapy permit the occurrence of resistant variants. Combinatory or tandem CARs, which contain two or more antigen-recognition moieties, may prevent from relapse due to escape variants but need further validation (86, 87).

Dual CD19 and CD22 Targeting CAR T Cell Therapy

The downregulation or loss of pre-designed antigen on ALL cells leads to the failure of CD19CAR T or CD22CAR T cell monotherapy. Therefore, a dual CD19 and CD22 antigen targeting CAR T cell therapy such as CD19/CD22 bispecific CAR T cell therapy and sequential CD19CAR T and CD19CAR T cell therapy, appears to be a strategy to prevent the escape mechanism given that B cells are unlikely to downregulate both CD19 and CD22 simultaneously in a single cell.

AUTO3 is a representative CD19/CD22 bispecific CAR T cell therapy, which is designed and developed through transduction of autologous T cells expressing two CARs targeting CD19 and CD22 by Autolus Therapeutics. A multi-center, phase I/II study has been completed to explore the safety and efficacy in pediatric and young adult patients with B-cell ALL (AMELIA trial, NCT03289455) (42). In the phase I dose-escalation study, dose-limiting toxicities, severe CRS, and neurotoxicity were not reported, which demonstrated a favorable safety profile for clinical application. 13 of 15 patients achieved CR or CR with incomplete bone marrow recovery after AUTO3 infusion for one month. The OS and EFS rates were 60% and 32%, respectively. Consequently, FDA has granted orphan drug designation of AUTO3 for ALL treatment. Nevertheless, unavailability of long-term persistence of AUTO3 in patients resulted in disease relapse. Hence, prolongation of CAR T cell persistence are needed to fully fulfill the therapeutic potential of dual targeting CAR T cell in B-cell ALL. Another phase I trial (NCT03448393) sponsored by National Cancer Institute to evaluate the safety and efficiency of dual CD19/CD22 targeting CAR T cell therapy is undergoing.

CTA101, also called CRISPR-edited allogeneic off-the-shelf CD19/CD22 bispecific CAR T cells, was composed of scFV targeting CD19 and CD22, 4-1BB costimulatory domain, and CRISPR/Cas9-disrupted *TRAC* region to avoid host immune-mediated rejection (88). The phase I clinical trial (NCT04227015) to evaluate the safety and efficiency of a single dose of CTA101 in R/R B-cell ALL patients aged from 3 to 70 years is ongoing.

In addition to CD19/CD22 bispecific CAR T cells, sequential infusion of CD19CAR T and CD22CAR T cells are investigated in a phase I trial in pediatric patients with R/R B-cell ALL (ChiCTR-OIB-17013670). 17 of the 20 patients remained CR at the study end point and only 2 patients relapsed caused by loss of CD19, indicating that the risk of relapse associated with antigen escape was greatly reduced (43).

Strategies to Reduce Toxicities of CAR T Cell Therapy

Despite the huge clinical success, CAR T cell therapy-related severe toxicities such as CRS, cannot be neglected and are remained to be resolved (33, 89, 90). For example, around 50%

of children and young adult patients treated with tisagenlecleucel for R/R B-cell ALL had \geq Grade 3 CRS (33, 91), 24% of adult patients infused with brexucabtagene autoleucel had \geq Grade 3 CRS (36), while lower incidence of \geq Grade 3 CRS, 8.6% and 2.9% respectively, was observed after CD22-CART cell treatment (39, 41). Moreover, no \geq Grade 3 CRS was observed in pediatric patients with R/R B-cell ALL receiving AUTO3, which is in concordance with the modest elevation of cytokines production (42). Finally, extensive studies to ameliorate CAR T cell related toxicities are ongoing, such as altering CAR structure, modifying CAR transduced T cells, and inserting CAR "off-switches" (70, 92, 93). Optimizing CAR binding affinity by developing a new CD19 scFV with a lower affinity than FMC63 could be a useful approach to enhance CAR T cell expansion and persistence, and alleviate toxicity in the pediatric R/R B-cell ALL as illustrated in the CARPALL clinical trial (NCT02443831) (44).

Strategies to Increase the Efficacy of CAR T Cell Therapy

Besides reducing toxicities of CAR T cell therapy, attempts have been made to increase the efficacy of CAR T cell therapy. As mentioned above, targeting two or more antigens by dual CD19 and CD22 targeting CAR T cells or sequential infusion of CD19CAR T and CD22CAR T cells broadened the spectrum of targets, decreased the risk of antigen negative relapse and enhanced the potential therapeutic efficiency. Moreover, tisagenlecleucel and other CAR T cell therapies for pediatric Bcell ALL were commonly composed of the costimulatory domains with CD28 and/or 4-1BB (Table 1), which were the second and third generation CARs (94). CAR T cells were further optimized to secrete cytokines or express cytokine receptors to generate the fourth and fifth generation CARs. In a relapsed patient with B-cell ALL after treatment with CD19CAR and CD22CAR T cell therapy, autologous murine CD19CAR T cells expressing membrane-bound IL-15 achieved CR for five months (95). CD19CAR T cells encoded with interleukin 2 receptor β chain and a STAT3-binding tyrosine-X-X-glutamine motif in the cytoplasmic domain showed grater antitumor effects and superior duration than CAR T cells without this structure (96). Besides, upregulation of TIM-3 increased the risk of relapse in pediatric B-cell ALL (97). Hence, TIM-3-CD28 fusion proteins were combined with the first and second CD19CAR T cells to enhance the proliferation capacity of T cells and improve the functionality of conventional CAR T cells by turning inhibition into activation of T cells (98, 99). Relapse due to the short persistence of CAR T cells and resistance to same murine CAR T cell therapy were attributed to immunogenicity caused by murine scFv (37, 38). 68% of the pediatric and adult patients after failure of murine CD19CAR T cell therapy achieved CR treated with 4-1BB based humanized CD19 CAR-T cells (ChiCT R1900 024456) (100). In brief, various strategies have been developed to increase the efficacy of CAR T cell therapy and warranted to be applied in the treatment of pediatric B-cell ALL.

Combination Therapy

Numerous studies have demonstrated that immune responses by maintaining negative regulatory pathways *via* PD-1/PD-L1 axis

played a significant role in the immune escape, thus leading to growth and spread of malignant tumors (101, 102). In this regard, blocking PD-1/PD-L1 pathway has aroused great success as an effective therapeutic approach in a variety of cancers. Significantly, there is a high expression level of PD-1 on the surface of T cells in B-cell ALL pediatric patients, which is associated with an inferior prognosis (103). Inspired by the encouraging therapeutic outcomes of blocking the PD-1/PD-L1 pathway in the treatment of solid tumors, researchers nowadays have tried to integrate PD-1/PD-L1 inhibitors into the treatment course of hematological malignancy (104, 105). Pembrolizumab is a humanized anti-PD-1 monoclonal antibody with a wide range of indications (106). However, the phase II study of singleagent pembrolizumab in treating minimal residual disease (MRD) in adults with ALL was terminated due to lack of efficacy despite good tolerability (NCT02767934) (107). Immunosuppression due to chemotherapy prior treatment and relatively low mutational rate may lead to the treatment failure of targeting PD-1/PD-L1 pathway (107). That said, monotherapy by blocking PD-1/PD-L1 signaling pathway seems not a viable therapeutic method for the treatment of ALL. Nevertheless, combinatory treatment of immune checkpoint inhibitors including pembrolizumab and nivolumab with blinatumomab for B-cell ALL in adults and pediatrics are undergoing clinical trials (NCT03160079 and NCT03512405 and NCT04546399), which may prove the potential advantage of anti PD-1 antibody as an adjunct or rescue strategy. Besides immune checkpoint inhibitors, blinatumomab in combination of with chemotherapy in patients with newly diagnosed B-lymphoblastic leukemia aged 365 days to 31 years are being investigated (NCT03914625).

Other Emerging T-Cell Based Immunotherapies

Donor-derived tumor associated antigen-specific T cells termed TAA-T (108), reported by Kinoshita and colleges, is capable of targeting three overexpressed and immunogenic tumor associated antigens WT1, PRAME and survivn in most hematologic malignancies (109-111). A phase I clinical is currently ongoing at Children's National and Johns Hopkins Hospitals and Johns Hopkins University to evaluate the safety of TAA-T for the treatment of very high-risk hematopoietic malignancies (NCT02203903). Preliminary results showed that none of the included acute myeloid leukemia (AML) and ALL patients developed CRS or neurotoxicity, and only one patient developed grade 3 graft-versus-host disease (GVHD), which demonstrated the good safety of TAA-T (108). Moreover, persist remissions were observed in high-risk and relapsed patients (108). Later phase of the study is required to determine long-term clinical disease outcomes.

Adoptive cell therapy using T-cell receptor (TCR)-engineered T cells represents another novel and potential strategy for cancer treatment (112–114). ET190L1-AbTCR is one of TCR-T cell therapies generated by replacing the α and β chains of the TCR in the antigen recognition domain with an anti-CD19 antibody-derived Fab fragment (115). Compared with the clinically commonly used CD19CAR T cells with a CD28 or 4-1BB

costimulatory subunit, ET190L1-AbTCR activated cytotoxic Tcell responses, but showed less cytokine release in xenograft mouse models of primary B-cell ALL.

B-cell activating factor receptor (BAFF-R) is a B-lineage marker expressed almost exclusively on B cells (116, 117), making it an ideal target for immunotherapy. BAFF-R-CAR T cells with a 4-1BB costimulatory signaling domain demonstrated therapeutic effects against CD19 negative B-cell ALL *in vitro* and *in vivo* (117), and are currently undergoing clinical trials for the treatment of adult ALL (NCT04690595). Moreover, dual CD19/BAFF-R CAR T cells were developed and exhibited anti-ALL activity *in vivo*, supporting clinical translation of BAFF-R/CD19 dual CAR T cells to treat ALL (118).

MACROPHAGE-BASED IMMUNOTHERAPY

Targeting CD47/SIRPα Pathway

Macrophages are important components of mononuclear phagocytic system, and generates a "don't eat me" signal to suppresses phagocytosis by expressing a signal regulatory protein alpha (SIRPa) that interacts with CD47 (CD47/SIRPa axis), thus contributing to the development and progression of most cancers (119–121). Therefore, the CD47/SIRP α axis has been identified as an essential and promising immune checkpoint in the homeostatic clearance by macrophages. Generally, CD47 is overexpressed on the surface of B-cell ALL cells and recognized as an inferior prognosis marker associated with worse outcomes in pediatric ALL patients, such as treatment failure and even death (122, 123). Additionally, the anti-CD47 antibody and anti-SIRPa antibody both increased phagocytosis of ALL cells in vitro, suggesting that blockade of the CD47/SIRPa signaling enhanced phagocytosis (123). In vivo, anti-CD47 antibody inhibited tumor engraftment and induced remission in ALL engrafted mice (123). These data provided pre-clinical evidence for disrupting CD47/SIRPa signaling as a potential therapy for ALL.

TTI-621 is a novel soluble fusion protein composed of human SIRP α and IgG1, and exerts its effect by blocking CD47/SIRP α pathway (124) (**Figure 1**). Recently, a phase Ia/Ib dose escalation and expansion trial of TTI-621 in R/R hematologic malignancies and selected solid tumors is ongoing (NCT02663518). TTI-621 was well-tolerated in the dose escalation phase. The expansion phase conducted in R/R NHL patients has been completed and demonstrated a sound efficacy. The evaluation of clinical efficacy and safety of TTI-621 in ALL patients is still ongoing.

Additionally, several strategies have been proposed and are being intensively explored, for example, anti-CD47 antibody (124–128), anti-SIRP α antibody (129), bi-specific antibodies to CD47 or SIRP α or other molecules (129), SIRP α -related fusion proteins (130), and others (131), to improve therapeutic efficacy during targeting CD47/ SIRP α pathway while overcome on-target/off-tumor effects (132, 133). A large number of clinical trials related to cutting off the CD47/SIRP α pathway are currently undergoing at various stages, which are centered on solid tumors and hematological malignancies such as NHL and AML (132). The research on blocking the CD47/ SIRP α pathway in pediatric ALL is lagging behind and is undergoing preclinical study. Notably, targeting CD47 induced hematotoxicity including anemia and thrombocytopenia due to the off-target effect on the blocking of CD47 expressed on surface of platelets and erythrocytes (134). Designing and developing SIRP α fusion proteins could diminish the hematotoxicity, thereby safeguarding the clinical safety. For example, TTI-621 exhibited minimal impact on human erythrocytes, resulting in a lower incidence of anemia than that reported in a phase I study of combinatory treatment of humanized anti-CD47 antibody and rituximab (13% vs 41%) (124, 135). Moreover, thrombocytopenia associated with TTI-621 was transient and reversible, and no bleeding events were observed in the clinical trials (136).

NK CELL-BASED IMMUNOTHERAPY

NKs derived from lymphocyte cell lineage were discovered to be critical to the innate immunity (137). NKs are composed of two subtypes, i.e., CD3⁻/CD56^{dim}/CD16⁺ NKs and CD3⁻/CD56^{bright}/ CD16⁻ NKs (138). CD3⁻/CD56^{dim}/CD16⁺ NKs display strong cytotoxic activity on targeted cells by perforin and granzyme B in peripheral blood, and CD3⁻/CD56^{bright}/CD16⁻ NKs produce and release cytokines such as IFN- γ and TNF- α in response cytokines stimulation in lymphoid tissues (139, 140). Mounting studies have demonstrated the innate lymphoid cells as the first line of defense by exerting cytotoxicity against diverse tumor cell types (141, 142), especially in the field of hematologic malignancies (143). The presence of NK cells in bone marrow conferred a better response to chemotherapy and prognosis, and has a high chance of efficacy in pediatric patients with ALL (144, 145). Hence, different artificial engagers have been equipped to selectively redirect NK cells towards tumor cells. In vitro, NKp46/CD16A/CD19-NKCE, a NK cell engager with CD16A on the surface of NKs binding NKp46 and CD19 highly expressed on the surface of B-cell ALL cells, enhanced the activation of NKs and promoted NK cell-mediated lytic effects against pediatric BCP ALL (Figure 1) (146).

Moreover, immunotherapy based on NKs displayed several advantages (147, 148). As the important immune system components, NKs exerted the cytotoxicity upon recognizing specific patterns without prior antigen sensitization. CAR modified NK cells (CAR NKs) are qualified for simultaneously improving efficacy and controlling adverse effects including CRS, neurotoxicity, and GVHD, which offer an alternative option to CAR-T cells (149, 150). To date, two phase I studies to determine the maximum tolerated dose of genetically modified haploidentical NKs infusions targeting CD19 to treat B-cell ALL have been completed in St. Jude Children's Research Hospital (NCT00995137 and NCT01974479). However, the results have not been disclosed.

CONCLUSION AND FUTURE PERSPECTIVES

Immunotherapy represents a novel and promising therapeutic weapon against pediatric B-cell ALL. As alluded to above, T cell

engagers and CAR T cell therapies were successful in treating pediatric R/R B-cell ALL. Currently, blinatumomab has been approved for treating R/R BCP ALL in pediatrics and is further investigated in removing MRD as post-reinduction consolidation treatment, which is believed to be more efficacious and less toxic than chemotherapy. In addition, the approval of tisagenlecleucel, a typical representative of CAR T cell therapies, provided us an alteration when none was available for children and young adults with R/R B-cell ALL, although a large proportion of patients suffered relapse with poor outcomes. However, monotherapy by immune checkpoint inhibitors targeting PD-1/PD-L1 pathway achieved poor clinical efficiency. Immune check inhibitors including anti-PD-1 and anti-CD47 antibodies as an adjunct strategy in pediatric B-cell ALL required to be verified in the further study and may be worth awaiting. Moreover, strategies targeting CD47/SIRPa pathway and CAR-NKs demonstrated potential for treating pediatric ALL and were evaluated in clinical trials.

Since native macrophages are critical effectors and regulators of the innate immune system, CAR macrophages can directly target the desired cancer cells and has been developed to phagocytose human solid tumor cells (151, 152). Nevertheless, treatment of pediatric ALL by using this promising immunotherapy is absent (153). Neoantigen, a new mutationderived protein in tumor cells, is a non-normal cellular product and has proven to be a breakthrough for therapeutic immune targets (154–157). Immunotherapy by harnessing neoepitope-CD8+ T cells to recognize and respond to the neoantigens in pediatric patients with ALL provided us an alternative treatment option (158).

Despite all these advances, the resistance and toxicity should be taken into consideration and further studies should focus on the development of new agents guided to ameliorate some of the toxicities and prevent the recurrence. Variable mechanisms including the downregulation/loss of antigens and antigen escape through lineage switch influence responses to immunotherapy result in resistance or relapse. The relationship between genetic and cytogenetic alterations and immunotherapy responses are warranted to be further explored in the future. Moreover, novel potential targets such as cell surface antigens, kinases and signaling pathways should be consistently identified and explored. On the other hand, blocking a single cell surface antigen or pathway of B-cell ALL may lead to drug resistance. It is anticipated that immunotherapy targeting multiple antigens such as trispecific CD3/CD19/CD20 T-cell engagers and dual CD19 and CD22 targeting CAR T cell therapy will not only overcome the challenge of antigen modulation but also dramatically enhance therapeutic efficacy.

To sum up, the successful outcome of immunotherapy from clinical trials as described in our context has proved the effectiveness of immunotherapy in the treatment of pediatric B-cell ALL and lead to dramatic improvements in outcome for R/R subtype. We believe that the integration and expansion of these therapeutics into frontline therapy and the discovery of novel anti-multiple antigens modifications will further augment efficacy and reduce toxicity, thus improving long-term outcomes in pediatric B-cell ALL patients.

AUTHOR CONTRIBUTIONS

ML and YL designed the study, drafted the initial manuscript, critically reviewed and revised the manuscript, and contributed equally to this work. WL provided us professional knowledge in the field of pediatric ALL. YX and SZ reviewed and revised the manuscript. All authors contributed to the article and approved the submitted version.

REFERENCES

- Liu YF, Wang BY, Zhang WN, Huang JY, Li BS, Zhang M, et al. Genomic Profiling of Adult and Pediatric B-Cell Acute Lymphoblastic Leukemia. *EBioMedicine* (2016) 8:173–83. doi: 10.1016/j.ebiom.2016.04.038
- Siegel RL, Miller KD, Fuchs HE, Jemal A. Cancer Statistics, 2021. CA Cancer J Clin (2021) 71:7–33. doi: 10.3322/caac.21654
- Malard F, Mohty M. Acute Lymphoblastic Leukaemia. Lancet (2020) 395:1146–62. doi: 10.1016/s0140-6736(19)33018-1
- Sung H, Ferlay J, Siegel RL. Global Cancer Statistics 2020: GLOBOCAN Estimates of Incidence and Mortality Worldwide for 36 Cancers in 185 Countries. CA Cancer J Clin (2021) 71:209–49. doi: 10.3322/caac.21660
- Boyiadzis MM, Aksentijevich I, Arber DA, Barrett J, Brentjens RJ, Brufsky J, et al. The Society for Immunotherapy of Cancer (SITC) Clinical Practice Guideline on Immunotherapy for the Treatment of Acute Leukemia. *J Immunother Cancer* (2020) 8:e000810. doi: 10.1136/jitc-2020-000810
- Brown P, Inaba H, Annesley C, Beck J, Colace S, Dallas M, et al. Pediatric Acute Lymphoblastic Leukemia, Version 2.2020, NCCN Clinical Practice Guidelines in Oncology. J Natl Compr Cancer Netw (2020) 18:81–112. doi: 10.6004/jnccn.2020.0001
- Pui CH, Yang JJ, Hunger SP, Pieters R, Schrappe M, Biondi A, et al. Childhood Acute Lymphoblastic Leukemia: Progress Through Collaboration. J Clin Oncol (2015) 33:2938–48. doi: 10.1200/jco. 2014.59.1636
- Hunger SP, Lu X, Devidas M, Camitta BM, Gaynon PS, Winick NJ, et al. Improved Survival for Children and Adolescents With Acute Lymphoblastic Leukemia Between 1990 and 2005: A Report From the Children's Oncology Group. J Clin Oncol (2012) 30:1663–9. doi: 10.1200/jco.2011.37.8018
- Hunger SP, Mullighan CG. Acute Lymphoblastic Leukemia in Children. N Engl J Med (2015) 373:1541–52. doi: 10.1056/NEJMra1400972
- Hunger SP, Raetz EA. How I Treat Relapsed Acute Lymphoblastic Leukemia in the Pediatric Population. *Blood* (2020) 136:1803–12. doi: 10.1182/ blood.2019004043
- Hinshaw DC, Shevde LA. The Tumor Microenvironment Innately Modulates Cancer Progression. *Cancer Res* (2019) 79:4557-66. doi: 10.1158/0008-5472.can-18-3962
- Anderson NM, Simon MC. The Tumor Microenvironment. Curr Biol (2020) 30:R921-r925. doi: 10.1016/j.cub.2020.06.081
- Jin MZ, Jin WL. The Updated Landscape of Tumor Microenvironment and Drug Repurposing. *Signal Transduct Target Ther* (2020) 5:166. doi: 10.1038/ s41392-020-00280-x
- Farkona S, Diamandis EP, Blasutig IM. Cancer Immunotherapy: The Beginning of the End of Cancer? BMC Med (2016) 14:73. doi: 10.1186/ s12916-016-0623-5
- Im A, Pavletic SZ. Immunotherapy in Hematologic Malignancies: Past, Present, and Future. J Hematol Oncol (2017) 10:94. doi: 10.1186/s13045-017-0453-8
- Noh JY, Seo H, Lee J, Jung H. Immunotherapy in Hematologic Malignancies: Emerging Therapies and Novel Approaches. *Int J Mol Sci* (2020) 21:8000. doi: 10.3390/ijms21218000
- Craddock C, Friedberg JW. Immunotherapy for Hematologic Malignancies. J Clin Oncol (2021) 39:343–5. doi: 10.1200/jco.20.03106
- Wang H, Kaur G, Sankin AI, Chen F, Guan F, Zang X. Immune Checkpoint Blockade and CAR-T Cell Therapy in Hematologic Malignancies. *J Hematol* Oncol (2019) 12:59. doi: 10.1186/s13045-019-0746-1
- 19. Jeha S, Pei D, Choi J, Cheng C, Sandlund JT, Coustan-Smith E, et al. Improved CNS Control of Childhood Acute Lymphoblastic Leukemia

ACKNOWLEDGMENTS

We would like to thank Dr. Wenhui Liu for the professional guidance during writing the manuscript. The authors would also like to thank Dr. Zutao Yu, a researcher from Cancer Research UK Cambridge Institute (University of Cambridge), for the manuscript proof-reading.

Without Cranial Irradiation: St Jude Total Therapy Study 16. J Clin Oncol (2019) 37:3377–91. doi: 10.1200/JCO.19.01692

- Teachey DT, Pui CH. Comparative Features and Outcomes Between Paediatric T-Cell and B-Cell Acute Lymphoblastic Leukaemia. *Lancet* Oncol (2019) 20:e142–54. doi: 10.1016/s1470-2045(19)30031-2
- Inaba H, Pui CH. Immunotherapy in Pediatric Acute Lymphoblastic Leukemia. Cancer Metastasis Rev (2019) 38:595–610. doi: 10.1007/s10555-019-09834-0
- 22. Ma X, Liu Y, Liu Y, Alexandrov LB, Edmonson MN, Gawad C, et al. Pan-Cancer Genome and Transcriptome Analyses of 1,699 Paediatric Leukaemias and Solid Tumours. *Nature* (2018) 555:371-6. doi: 10.1038/ nature25795
- Laetsch TW, DuBois SG, Bender JG, Macy ME. Opportunities and Challenges in Drug Development for Pediatric Cancers. *Cancer Discov* (2021) 11:545–59. doi: 10.1158/2159-8290.cd-20-0779
- von Stackelberg A, Locatelli F, Zugmaier G, Handgretinger R, Trippett TM, Rizzari C, et al. Phase I/Phase II Study of Blinatumomab in Pediatric Patients With Relapsed/Refractory Acute Lymphoblastic Leukemia. *J Clin Oncol* (2016) 34:4381–9. doi: 10.1200/JCO.2016.67.3301
- 25. Gore L, Locatelli F, Zugmaier G, Handgretinger R, O'Brien MM, Bader P, et al. Survival After Blinatumomab Treatment in Pediatric Patients With Relapsed/Refractory B-Cell Precursor Acute Lymphoblastic Leukemia. *Blood Cancer J* (2018) 8:80. doi: 10.1038/s41408-018-0117-0
- 26. Locatelli F, Zugmaier G, Mergen N, Bader P, Jeha S, Schlegel PG, et al. Blinatumomab in Pediatric Patients With Relapsed/Refractory Acute Lymphoblastic Leukemia: Results of the RIALTO Trial, an Expanded Access Study. *Blood Cancer J* (2020) 10:77. doi: 10.1038/s41408-020-00342-x
- Locatelli F, Zugmaier G, Mergen N, Bader P, Jeha S, Schlegel PG, et al. Blinatumomab In Pediatric Relapsed/Refractory B-Cell Acute Lymphoblastic Leukemia: RIALTO Expanded Access Study Final Analysis. Blood Adv (2022) 6:1004–14. doi: 10.1182/bloodadvances.2021005579
- Locatelli F, Zugmaier G, Rizzari C, Morris JD, Gruhn B, Klingebiel T, et al. Effect of Blinatumomab vs Chemotherapy on Event-Free Survival Among Children With High-Risk First-Relapse B-Cell Acute Lymphoblastic Leukemia: A Randomized Clinical Trial. *JAMA* (2021) 325:843–54. doi: 10.1001/jama.2021.0987
- Brown PA, Ji L, Xu X, Devidas M, Hogan LE, Borowitz MJ, et al. Effect of Postreinduction Therapy Consolidation With Blinatumomab vs Chemotherapy on Disease-Free Survival in Children, Adolescents, and Young Adults With First Relapse of B-Cell Acute Lymphoblastic Leukemia: A Randomized Clinical Trial. *JAMA* (2021) 325:833–42. doi: 10.1001/jama.2021.0669
- Gaballa MR, Banerjee P, Milton DR, Jiang X. Blinatumomab Maintenance After Allogeneic Hematopoietic Cell Transplantation for B-Lineage Acute Lymphoblastic Leukemia. *Blood* (2022) 139:1908–19. doi: 10.1182/ blood.2021013290
- Tüfekçi Ö, Evim MS, Güneş AM, Celkan T, Karapinar DY, Kaya Z, et al. Assessment of Minimal Residual Disease in Childhood Acute Lymphoblastic Leukemia: A Multicenter Study From Turkey. J Pediatr Hematol Oncol (2022) 44:e396–402. doi: 10.1097/mph.00000000002419
- 32. Maude SL, Frey N, Shaw PA, Aplenc R, Barrett DM, Bunin NJ, et al. Chimeric Antigen Receptor T Cells for Sustained Remissions in Leukemia. *N Engl J Med* (2014) 371:1507–17. doi: 10.1056/NEJMoa1407222
- Maude SL, Laetsch TW, Buechner J, Rives S, Boyer M, Bittencourt H, et al. Tisagenlecleucel in Children and Young Adults With B-Cell Lymphoblastic Leukemia. N Engl J Med (2018) 378:439–48. doi: 10.1056/NEJMoa1709866
- Shah BD, Ghobadi A, Oluwole OO, Logan AC, Boissel N, Cassaday RD, et al. KTE-X19 for Relapsed or Refractory Adult B-Cell Acute Lymphoblastic

Leukaemia: Phase 2 Results of the Single-Arm, Open-Label, Multicentre ZUMA-3 Study. *Lancet* (2021) 398:491–502. doi: 10.1016/s0140-6736(21) 01222-8

- Shah BD, Bishop MR, Oluwole OO. KTE-X19 Anti-CD19 CAR T-Cell Therapy in Adult Relapsed/Refractory Acute Lymphoblastic Leukemia: ZUMA-3 Phase 1 Results. *Blood* (2021) 138:11–22. doi: 10.1182/ blood.2020009098
- Killock D. KTE-X19 Efficacious in Adults With B-ALL. Nat Rev Clin Oncol (2021) 18:470. doi: 10.1038/s41571-021-00537-6
- Shah NN, Lee DW. Long-Term Follow-Up of CD19-CAR T-Cell Therapy in Children and Young Adults With B-ALL. J Clin Oncol (2021) 39:1650–9. doi: 10.1200/jco.20.02262
- Lee DW, Kochenderfer JN, Stetler-Stevenson M, Cui YK, Delbrook C, Feldman SA, et al. T Cells Expressing CD19 Chimeric Antigen Receptors for Acute Lymphoblastic Leukaemia in Children and Young Adults: A Phase 1 Dose-Escalation Trial. *Lancet* (2015) 385:517–28. doi: 10.1016/s0140-6736(14)61403-3
- Shah NN, Highfill SL, Shalabi H, Yates B, Jin J, Wolters PL, et al. CD4/CD8 T-Cell Selection Affects Chimeric Antigen Receptor (CAR) T-Cell Potency and Toxicity: Updated Results From a Phase I Anti-CD22 CAR T-Cell Trial. *J Clin Oncol* (2020) 38:1938–50. doi: 10.1200/jco.19.03279
- Singh N, Frey NV, Engels B, Barrett DM, Shestova O, Ravikumar P, et al. Antigen-Independent Activation Enhances the Efficacy of 4-1BB-Costimulated CD22 CAR T Cells. *Nat Med* (2021) 27:842–50. doi: 10.1038/s41591-021-01326-5
- Pan J, Niu Q, Deng B, Liu S, Wu T, Gao Z, et al. CD22 CAR T-Cell Therapy in Refractory or Relapsed B Acute Lymphoblastic Leukemia. *Leukemia* (2019) 33:2854–66. doi: 10.1038/s41375-019-0488-7
- 42. Cordoba S, Onuoha S, Thomas S, Pignataro DS, Hough R, Ghorashian S, et al. CAR T Cells With Dual Targeting of CD19 and CD22 in Pediatric and Young Adult Patients With Relapsed or Refractory B Cell Acute Lymphoblastic Leukemia: A Phase 1 Trial. *Nat Med* (2021) 27:1797–805. doi: 10.1038/s41591-021-01497-1
- Pan J, Zuo S, Deng B, Xu X, Li C, Zheng Q, et al. Sequential CD19-22 CAR T Therapy Induces Sustained Remission in Children With R/R B-ALL. Blood (2020) 135:387–91. doi: 10.1182/blood.2019003293
- 44. Ghorashian S, Kramer AM, Onuoha S, Wright G, Bartram J, Richardson R, et al. Enhanced CAR T Cell Expansion and Prolonged Persistence in Pediatric Patients With ALL Treated With a Low-Affinity CD19 CAR. *Nat Med* (2019) 25:1408–14. doi: 10.1038/s41591-019-0549-5
- Raskov H, Orhan A, Christensen JP, Gögenur I. Cytotoxic CD8(+) T Cells in Cancer and Cancer Immunotherapy. Br J Cancer (2021) 124:359–67. doi: 10.1038/s41416-020-01048-4
- O'Donnell JS, Teng MWL, Smyth MJ. Cancer Immunoediting and Resistance to T Cell-Based Immunotherapy. Nat Rev Clin Oncol (2019) 16:151–67. doi: 10.1038/s41571-018-0142-8
- Waldman AD, Fritz JM, Lenardo MJ. A Guide to Cancer Immunotherapy: From T Cell Basic Science to Clinical Practice. *Nat Rev Immunol* (2020) 20:651–68. doi: 10.1038/s41577-020-0306-5
- Labrijn AF, Janmaat ML. Bispecific Antibodies: A Mechanistic Review of the Pipeline. Nat Rev Drug Discov (2019) 18:585–608. doi: 10.1038/s41573-019-0028-1
- Rader C. Bispecific Antibodies in Cancer Immunotherapy. Curr Opin Biotechnol (2020) 65:9–16. doi: 10.1016/j.copbio.2019.11.020
- May MB, Glode A. Blinatumomab: A Novel, Bispecific, T-Cell Engaging Antibody. Am J Health Syst Pharm (2016) 73:e6–e13. doi: 10.2146/ajhp150134
- 51. Loüffler A, Kufer P, Lutterbüse R, Zettl F, Daniel PT, Schwenkenbecher JM, et al. A Recombinant Bispecific Single-Chain Antibody, CD19×CD3, Induces Rapid and High Lymphoma-Directed Cytotoxicity by Unstimulated T Lymphocytes. *Blood* (2000) 95:2098–103. doi: 10.1182/ blood.V95.6.2098
- Orentas RJ, Yang JJ, Wen X, Wei JS, Mackall CL, Khan J. Identification of Cell Surface Proteins as Potential Immunotherapy Targets in 12 Pediatric Cancers. Front Oncol (2012) 2:194. doi: 10.3389/fonc.2012.00194
- Wang K, Wei G, Liu D. CD19: A Biomarker for B Cell Development, Lymphoma Diagnosis and Therapy. *Exp Hematol Oncol* (2012) 1:36. doi: 10.1186/2162-3619-1-36
- 54. Beneduce G, De Matteo A. Blinatumomab in Children and Adolescents With Relapsed/Refractory B Cell Precursor Acute Lymphoblastic Leukemia: A Real-Life Multicenter Retrospective Study in Seven AIEOP (Associazione

Italiana Di Ematologia E Oncologia Pediatrica) Centers. Cancers (Basel) (2022) 14:426. doi: 10.3390/cancers14020426

- Queudeville M, Ebinger M. Blinatumomab in Pediatric Acute Lymphoblastic Leukemia-From Salvage to First Line Therapy (A Systematic Review). J Clin Med (2021) 10:2544. doi: 10.3390/jcm10122544
- 56. Zhu M, Wu B, Brandl C, Johnson J, Wolf A, Chow A, et al. Blinatumomab, a Bispecific T-Cell Engager (BiTE((R))) for CD-19 Targeted Cancer Immunotherapy: Clinical Pharmacology and Its Implications. *Clin Pharmacokinet* (2016) 55:1271–88. doi: 10.1007/s40262-016-0405-4
- 57. Mejstrikova E, Hrusak O, Borowitz MJ, Whitlock JA, Brethon B, Trippett TM, et al. CD19-Negative Relapse of Pediatric B-Cell Precursor Acute Lymphoblastic Leukemia Following Blinatumomab Treatment. *Blood Cancer J* (2017) 7:659. doi: 10.1038/s41408-017-0023-x
- Mikhailova E, Gluhanyuk E, Illarionova O, Zerkalenkova E, Kashpor S, Miakova N, et al. Immunophenotypic Changes of Leukemic Blasts in Children With Relapsed/Refractory B-Cell Precursor Acute Lymphoblastic Leukemia, Who Have Been Treated With Blinatumomab. *Haematologica* (2021) 106:2009–12. doi: 10.3324/haematol.2019.241596
- Köhnke T, Krupka C, Tischer J, Knösel T, Subklewe M. Increase of PD-L1 Expressing B-Precursor ALL Cells in a Patient Resistant to the CD19/CD3-Bispecific T Cell Engager Antibody Blinatumomab. *J Hematol Oncol* (2015) 8:111. doi: 10.1186/s13045-015-0213-6
- 60. Feucht J, Kayser S, Gorodezki D, Hamieh M, Döring M, Blaeschke F, et al. T-Cell Responses Against CD19+ Pediatric Acute Lymphoblastic Leukemia Mediated by Bispecific T-Cell Engager (BiTE) are Regulated Contrarily by PD-L1 and CD80/CD86 on Leukemic Blasts. *Oncotarget* (2016) 7:76902–19. doi: 10.18632/oncotarget.12357
- Borowitz MJ, Shuster J, Carroll AJ, Nash M, Look AT, Camitta B, et al. Prognostic Significance of Fluorescence Intensity of Surface Marker Expression in Childhood B-Precursor Acute Lymphoblastic Leukemia. A Pediatr Oncol Group Study. *Blood* (1997) 89:3960–6. doi: 10.1182/ blood.V89.11.3960
- 62. Dworzak MN, Schumich A, Printz D, Pötschger U, Husak Z, Attarbaschi A, et al. CD20 Up-Regulation in Pediatric B-Cell Precursor Acute Lymphoblastic Leukemia During Induction Treatment: Setting the Stage for Anti-CD20 Directed Immunotherapy. *Blood* (2008) 112:3982–8. doi: 10.1182/blood-2008-06-164129
- Lussana F, Gritti G, Rambaldi A. Immunotherapy of Acute Lymphoblastic Leukemia and Lymphoma With T Cell-Redirected Bispecific Antibodies. *J Clin Oncol* (2021) 39:444–55. doi: 10.1200/jco.20.01564
- 64. Hutchings M, Morschhauser F, Iacoboni G. Glofitamab, a Novel, Bivalent CD20-Targeting T-Cell-Engaging Bispecific Antibody, Induces Durable Complete Remissions in Relapsed or Refractory B-Cell Lymphoma: A Phase I Trial. J Clin Oncol (2021) 39:1959–70. doi: 10.1200/jco.20.03175
- 65. Wang S, Peng L, Xu W, Zhou Y, Zhu Z, Kong Y, et al. Preclinical Characterization and Comparison Between CD3/CD19 Bispecific and Novel CD3/CD19/CD20 Trispecific Antibodies Against B-Cell Acute Lymphoblastic Leukemia: Targeted Immunotherapy for Acute Lymphoblastic Leukemia. *Front Med* (2021) 16:139–49. doi: 10.1007/ s11684-021-0835-8
- 66. Parker KR, Migliorini D, Perkey E, Yost KE, Bhaduri A, Bagga P, et al. Single-Cell Analyses Identify Brain Mural Cells Expressing CD19 as Potential Off-Tumor Targets for CAR-T Immunotherapies. *Cell* (2020) 183:126–42.e117. doi: 10.1016/j.cell.2020.08.022
- Zhang J, Zhou Z. Preclinical Study of a Novel Tri-Specific Anti-CD3/CD19/ CD20 T Cell-Engaging Antibody As a Potentially Better Treatment for NHL. *Blood* (2020) 136:22–2. doi: 10.1182/blood-2020-140154
- Jayaraman J, Mellody MP, Hou AJ, Desai RP, Fung AW, Pham AHT, et al. CAR-T Design: Elements and Their Synergistic Function. *EBioMedicine* (2020) 58:102931. doi: 10.1016/j.ebiom.2020.102931
- Mao R, Hussein MS, He Y. Chimeric Antigen Receptor Engineered T Cells and Their Application in the Immunotherapy of Solid Tumours. *Expert Rev* Mol Med (2022) 24:e7. doi: 10.1017/erm.2021.32
- Sterner RC, Sterner RM. CAR-T Cell Therapy: Current Limitations and Potential Strategies. *Blood Cancer J* (2021) 11:69. doi: 10.1038/s41408-021-00459-7
- Milone MC, Fish JD, Carpenito C, Carroll RG, Binder GK, Teachey D, et al. Chimeric Receptors Containing CD137 Signal Transduction Domains

Mediate Enhanced Survival of T Cells and Increased Antileukemic Efficacy In Vivo. Mol Ther (2009) 17:1453–64. doi: 10.1038/mt.2009.83

- Grupp SA, Kalos M, Barrett D, Aplenc R, Porter DL, Rheingold SR, et al. Chimeric Antigen Receptor-Modified T Cells for Acute Lymphoid Leukemia. N Engl J Med (2013) 368:1509–18. doi: 10.1056/NEJMoa1215134
- Rosenbaum L. Tragedy, Perseverance, and Chance The Story of CAR-T Therapy. N Engl J Med (2017) 377:1313–5. doi: 10.1056/NEJMp1711886
- Wang M, Munoz J, Goy A, Locke FL, Jacobson CA, Hill BT, et al. KTE-X19 CAR T-Cell Therapy in Relapsed or Refractory Mantle-Cell Lymphoma. N Engl J Med (2020) 382:1331–42. doi: 10.1056/NEJMoa1914347
- Gardner RA, Finney O, Annesley C. Intent-To-Treat Leukemia Remission by CD19 CAR T Cells of Defined Formulation and Dose in Children and Young Adults. *Blood* (2017) 129:3322–31. doi: 10.1182/blood-2017-02-769208
- Curran KJ, Margossian SP, Kernan NA, Silverman LB, Williams DA, Shukla N, et al. Toxicity and Response After CD19-Specific CAR T-Cell Therapy in Pediatric/Young Adult Relapsed/Refractory B-ALL. *Blood* (2019) 134:2361– 8. doi: 10.1182/blood.2019001641
- Finney OC, Brakke HM, Rawlings-Rhea S, Hicks R, Doolittle D, Lopez M, et al. CD19 CAR T Cell Product and Disease Attributes Predict Leukemia Remission Durability. J Clin Invest (2019) 129:2123–32. doi: 10.1172/jci125423
- Turtle CJ, Hanafi LA, Berger C, Gooley TA, Cherian S, Hudecek M, et al. CD19 CAR-T Cells of Defined CD4+:CD8+ Composition in Adult B Cell ALL Patients. J Clin Invest (2016) 126:2123–38. doi: 10.1172/jci85309
- 79. Cao J, Wang G, Cheng H, Wei C, Qi K, Sang W, et al. Potent Anti-Leukemia Activities of Humanized CD19-Targeted Chimeric Antigen Receptor T (CAR-T) Cells in Patients With Relapsed/Refractory Acute Lymphoblastic Leukemia. Am J Hematol (2018) 93:851–8. doi: 10.1002/ajh.25108
- Sotillo E, Barrett DM, Black KL, Bagashev A, Oldridge D, Wu G, et al. Convergence of Acquired Mutations and Alternative Splicing of CD19 Enables Resistance to CART-19 Immunotherapy. *Cancer Discov* (2015) 5:1282–95. doi: 10.1158/2159-8290.CD-15-1020
- Fischer J, Paret C, El Malki K, Alt F, Wingerter A, Neu MA, et al. CD19 Isoforms Enabling Resistance to CART-19 Immunotherapy Are Expressed in B-ALL Patients at Initial Diagnosis. *J Immunother* (2017) 40:187–95. doi: 10.1097/cji.000000000000169
- Raponi S, De Propris MS, Intoppa S, Milani ML, Vitale A, Elia L, et al. Flow Cytometric Study of Potential Target Antigens (CD19, CD20, CD22, CD33) for Antibody-Based Immunotherapy in Acute Lymphoblastic Leukemia: Analysis of 552 Cases. *Leuk Lymphoma* (2011) 52:1098–107. doi: 10.3109/ 10428194.2011.559668
- Haso W, Lee DW, Shah NN, Stetler-Stevenson M, Yuan CM, Pastan IH, et al. Anti-CD22-Chimeric Antigen Receptors Targeting B-Cell Precursor Acute Lymphoblastic Leukemia. *Blood* (2013) 121:1165–74. doi: 10.1182/ blood-2012-06-438002
- Shah NN, Stevenson MS, Yuan CM, Richards K, Delbrook C, Kreitman RJ, et al. Characterization of CD22 Expression in Acute Lymphoblastic Leukemia. *Pediatr Blood Cancer* (2015) 62:964–9. doi: 10.1002/pbc.25410
- Fry TJ, Shah NN, Orentas RJ, Stetler-Stevenson M, Yuan CM, Ramakrishna S, et al. CD22-Targeted CAR T Cells Induce Remission in B-ALL That is Naive or Resistant to CD19-Targeted CAR Immunotherapy. *Nat Med* (2018) 24:20–8. doi: 10.1038/nm.4441
- Qin H, Ramakrishna S, Nguyen S, Fountaine TJ, Ponduri A, Stetler-Stevenson M, et al. Preclinical Development of Bivalent Chimeric Antigen Receptors Targeting Both CD19 and CD22. *Mol Ther Oncol* (2018) 11:127– 37. doi: 10.1016/j.omto.2018.10.006
- Dai H, Wu Z, Jia H, Tong C, Guo Y, Ti D, et al. Bispecific CAR-T Cells Targeting Both CD19 and CD22 for Therapy of Adults With Relapsed or Refractory B Cell Acute Lymphoblastic Leukemia. *J Hematol Oncol* (2020) 13:30. doi: 10.1186/s13045-020-00856-8
- Hu Y, Zhou Y, Zhang M, Ge W, Li Y, Yang L, et al. CRISPR/Cas9-Engineered Universal CD19/CD22 Dual-Targeted CAR-T Cell Therapy for Relapsed/Refractory B-Cell Acute Lymphoblastic Leukemia. *Clin Cancer Res* (2021) 27:2764–72. doi: 10.1158/1078-0432.CCR-20-3863
- Santomasso BD, Park JH, Salloum D, Riviere I, Flynn J, Mead E, et al. Clinical and Biological Correlates of Neurotoxicity Associated With CAR T-Cell Therapy in Patients With B-Cell Acute Lymphoblastic Leukemia. *Cancer Discov* (2018) 8:958–71. doi: 10.1158/2159-8290.cd-17-1319

- Gofshteyn JS, Shaw PA, Teachey DT, Grupp SA, Maude S, Banwell B, et al. Neurotoxicity After CTL019 in a Pediatric and Young Adult Cohort. Ann Neurol (2018) 84:537–46. doi: 10.1002/ana.25315
- Fitzgerald JC, Weiss SL, Maude SL, Barrett DM, Lacey SF, Melenhorst JJ, et al. Cytokine Release Syndrome After Chimeric Antigen Receptor T Cell Therapy for Acute Lymphoblastic Leukemia. *Crit Care Med* (2017) 45:e124– 31. doi: 10.1097/ccm.00000000002053
- Ying Z, Huang XF, Xiang X, Liu Y, Kang X, Song Y, et al. A Safe and Potent Anti-CD19 CAR T Cell Therapy. *Nat Med* (2019) 25:947–53. doi: 10.1038/ s41591-019-0421-7
- Sheth VS, Gauthier J. Taming the Beast: CRS and ICANS After CAR T-Cell Therapy for ALL. *Bone Marrow Transplant* (2021) 56:552–66. doi: 10.1038/ s41409-020-01134-4
- Voynova E, Kovalovsky D. From Hematopoietic Stem Cell Transplantation to Chimeric Antigen Receptor Therapy: Advances, Limitations and Future Perspectives. *Cells* (2021) 10:2845. doi: 10.3390/cells10112845
- 95. Sun Y, Su Y, Wang Y, Liu N, Li Y, Chen J, et al. CD19 CAR-T Cells With Membrane-Bound IL-15 for B-Cell Acute Lymphoblastic Leukemia After Failure of CD19 and CD22 CAR-T Cells: Case Report. *Front Immunol* (2021) 12:728962. doi: 10.3389/fimmu.2021.728962
- Kagoya Y, Tanaka S, Guo T. A Novel Chimeric Antigen Receptor Containing a JAK-STAT Signaling Domain Mediates Superior Antitumor Effects. *Nat Med* (2018) 24:352–9. doi: 10.1038/nm.4478
- Blaeschke F, Willier S, Stenger D, Lepenies M, Horstmann MA, Escherich G, et al. Leukemia-Induced Dysfunctional TIM-3(+)CD4(+) Bone Marrow T Cells Increase Risk of Relapse in Pediatric B-Precursor ALL Patients. *Leukemia* (2020) 34:2607–20. doi: 10.1038/s41375-020-0793-1
- Zhao S, Wang C, Lu P, Lou Y, Liu H, Wang T, et al. Switch Receptor T3/28 Improves Long-Term Persistence and Antitumor Efficacy of CAR-T Cells. *J Immunother Cancer* (2021) 9:e003176. doi: 10.1136/jitc-2021-003176
- Blaeschke F, Ortner E, Stenger D, Mahdawi J, Apfelbeck A, Habjan N, et al. Design and Evaluation of TIM-3-CD28 Checkpoint Fusion Proteins to Improve Anti-CD19 CAR T-Cell Function. *Front Immunol* (2022) 13:845499. doi: 10.3389/fimmu.2022.845499
- 100. An L, Lin Y, Deng B, Yin Z, Zhao D, Ling Z, et al. Humanized CD19 CAR-T Cells in Relapsed/Refractory B-ALL Patients Who Relapsed After or Failed Murine CD19 CAR-T Therapy. *BMC Cancer* (2022) 22:393. doi: 10.1186/ s12885-022-09489-1
- 101. Chen DS, Mellman I. Elements of Cancer Immunity and the Cancer-Immune Set Point. Nature (2017) 541:321–30. doi: 10.1038/nature21349
- 102. Lei X, Lei Y, Li JK, Du WX, Li RG, Yang J, et al. Immune Cells Within the Tumor Microenvironment: Biological Functions and Roles in Cancer Immunotherapy. *Cancer Lett* (2020) 470:126–33. doi: 10.1016/j.canlet.2019.11.009
- 103. Kang SH, Hwang HJ, Yoo JW, Kim H, Choi ES, Hwang SH, et al. Expression of Immune Checkpoint Receptors on T-Cells and Their Ligands on Leukemia Blasts in Childhood Acute Leukemia. *Anticancer Res* (2019) 39:5531–9. doi: 10.21873/anticanres.13746
- 104. Younes A, Santoro A, Shipp M, Zinzani PL, Timmerman JM, Ansell S, et al. Nivolumab for Classical Hodgkin's Lymphoma After Failure of Both Autologous Stem-Cell Transplantation and Brentuximab Vedotin: A Multicentre, Multicohort, Single-Arm Phase 2 Trial. *Lancet Oncol* (2016) 17:1283–94. doi: 10.1016/s1470-2045(16)30167-x
- 105. Armand P, Rodig S, Melnichenko V, Thieblemont C, Bouabdallah K, Tumyan G, et al. Pembrolizumab in Relapsed or Refractory Primary Mediastinal Large B-Cell Lymphoma. J Clin Oncol (2019) 37:3291–9. doi: 10.1200/jco.19.01389
- 106. Kwok G, Yau TC, Chiu JW, Tse E, Kwong YL. Pembrolizumab (Keytruda). *Hum Vaccin Immunother* (2016) 12:2777–89. doi: 10.1080/21645515.2016.1199310
- 107. Cassaday RD, Garcia KA, Fromm JR, Percival MM, Turtle CJ, Nghiem PT, et al. Phase 2 Study of Pembrolizumab for Measurable Residual Disease in Adults With Acute Lymphoblastic Leukemia. *Blood Adv* (2020) 4:3239–45. doi: 10.1182/bloodadvances.2020002403
- 108. Kinoshita H, Cooke KR, Grant M. Outcome of Donor-Derived TAA T Cell Therapy in Patients With High-Risk or Relapsed Acute Leukemia Post Allogeneic BMT. *Blood Adv* (2022) 6:2520–34. doi: 10.1182/ bloodadvances.2021006831
- 109. Candoni A, Tiribelli M, Toffoletti E, Cilloni D, Chiarvesio A, Michelutti A, et al. Quantitative Assessment of WT1 Gene Expression After Allogeneic

Stem Cell Transplantation is a Useful Tool for Monitoring Minimal Residual Disease in Acute Myeloid Leukemia. *Eur J Haematol* (2009) 82:61–8. doi: 10.1111/j.1600-0609.2008.01158.x

- 110. Rezvani K, Yong AS, Tawab A, Jafarpour B, Eniafe R, Mielke S, et al. Ex Vivo Characterization of Polyclonal Memory CD8+ T-Cell Responses to PRAME-Specific Peptides in Patients With Acute Lymphoblastic Leukemia and Acute and Chronic Myeloid Leukemia. *Blood* (2009) 113:2245–55. doi: 10.1182/ blood-2008-03-144071
- 111. Park E, Gang EJ, Hsieh YT, Schaefer P, Chae S, Klemm L, et al. Targeting Survivin Overcomes Drug Resistance in Acute Lymphoblastic Leukemia. *Blood* (2011) 118:2191–9. doi: 10.1182/blood-2011-04-351239
- Ecsedi M, McAfee MS, Chapuis AG. The Anticancer Potential of T Cell Receptor-Engineered T Cells. *Trends Cancer* (2021) 7:48–56. doi: 10.1016/ j.trecan.2020.09.002
- 113. Liu H, Pan C, Song W, Liu D, Li Z, Zheng L. Novel Strategies for Immuno-Oncology Breakthroughs With Cell Therapy. *Biomark Res* (2021) 9:62. doi: 10.1186/s40364-021-00316-6
- 114. Ping Y, Liu C, Zhang Y. T-Cell Receptor-Engineered T Cells for Cancer Treatment: Current Status and Future Directions. *Protein Cell* (2018) 9:254– 66. doi: 10.1007/s13238-016-0367-1
- 115. Xu Y, Yang Z, Horan LH, Zhang P, Liu L, Zimdahl B, et al. A Novel Antibody-TCR (AbTCR) Platform Combines Fab-Based Antigen Recognition With Gamma/Delta-TCR Signaling to Facilitate T-Cell Cytotoxicity With Low Cytokine Release. *Cell Discov* (2018) 4:62. doi: 10.1038/s41421-018-0066-6
- 116. Rodig SJ, Shahsafaei A, Li B, Mackay CR, Dorfman DM. BAFF-R, the Major B Cell-Activating Factor Receptor, is Expressed on Most Mature B Cells and B-Cell Lymphoproliferative Disorders. *Hum Pathol* (2005) 36:1113–9. doi: 10.1016/j.humpath.2005.08.005
- 117. Qin H, Dong Z. CAR T Cells Targeting BAFF-R can Overcome CD19 Antigen Loss in B Cell Malignancies. *Sci Transl Med* (2019) 11:eaaw9414. doi: 10.1126/scitranslmed.aaw9414
- 118. Wang X, Dong Z, Awuah D, Chang WC, Cheng WA, Vyas V, et al. CD19/ BAFF-R Dual-Targeted CAR T Cells for the Treatment of Mixed Antigen-Negative Variants of Acute Lymphoblastic Leukemia. *Leukemia* (2022) 36:1015–24. doi: 10.1038/s41375-021-01477-x
- 119. Boissonnas A, Combadiere C. Modulating the Tumor-Associated Macrophage Landscape. Nat Immunol (2022) 23:481–2. doi: 10.1038/ s41590-022-01159-5
- 120. Tian L, Lei A, Tan T, Zhu M, Zhang L, Mou H, et al. Macrophage-Based Combination Therapies as a New Strategy for Cancer Immunotherapy. *Kidney Dis (Basel)* (2022) 8:26–43. doi: 10.1159/000518664
- 121. Russ A, Hua AB, Montfort WR, Rahman B, Riaz IB, Khalid MU, et al. Blocking "Don't Eat Me" Signal of CD47-Sirpα in Hematological Malignancies, an in-Depth Review. *Blood Rev* (2018) 32:480-9. doi: 10.1016/j.blre.2018.04.005
- 122. Yang K, Xu J, Liu Q, Li J, Xi Y. Expression and Significance of CD47, PD1 and PDL1 in T-Cell Acute Lymphoblastic Lymphoma/Leukemia. *Pathol Res Pract* (2019) 215:265–71. doi: 10.1016/j.prp.2018.10.021
- 123. Chao MP, Alizadeh AA, Tang C, Jan M, Weissman-Tsukamoto R, Zhao F, et al. Therapeutic Antibody Targeting of CD47 Eliminates Human Acute Lymphoblastic Leukemia. *Cancer Res* (2011) 71:1374–84. doi: 10.1158/0008-5472.CAN-10-2238
- 124. Petrova PS, Viller NN, Wong M, Pang X, Lin GH, Dodge K, et al. TTI-621 (Sirpαfc): A CD47-Blocking Innate Immune Checkpoint Inhibitor With Broad Antitumor Activity and Minimal Erythrocyte Binding. *Clin Cancer Res* (2017) 23:1068–79. doi: 10.1158/1078-0432.ccr-16-1700
- 125. Uno S, Kinoshita Y, Azuma Y, Tsunenari T, Yoshimura Y, Iida S, et al. Antitumor Activity of a Monoclonal Antibody Against CD47 in Xenograft Models of Human Leukemia. Oncol Rep (2007) 17:1189–94. doi: 10.3892/or.17.5.1189
- 126. Puro RJ, Bouchlaka MN, Hiebsch RR, Capoccia BJ, Donio MJ, Manning PT, et al. Development of AO-176, a Next-Generation Humanized Anti-CD47 Antibody With Novel Anticancer Properties and Negligible Red Blood Cell Binding. *Mol Cancer Ther* (2020) 19:835–46. doi: 10.1158/1535-7163.mct-19-1079
- 127. Peluso MO, Adam A, Armet CM, Zhang L, O'Connor RW, Lee BH, et al. The Fully Human Anti-CD47 Antibody SRF231 Exerts Dual-Mechanism

Antitumor Activity via Engagement of the Activating Receptor CD32a. J Immunother Cancer (2020) 8:e000413. doi: 10.1136/jitc-2019-000413

- 128. Ma L, Zhu M, Gai J, Li G, Chang Q, Qiao P, et al. Preclinical Development of a Novel CD47 Nanobody With Less Toxicity and Enhanced Anti-Cancer Therapeutic Potential. J Nanobiotechnol (2020) 18:12. doi: 10.1186/s12951-020-0571-2
- 129. Ring NG, Herndler-Brandstetter D, Weiskopf K, Shan L, Volkmer JP, George BM, et al. Anti-Sirpα Antibody Immunotherapy Enhances Neutrophil and Macrophage Antitumor Activity. *Proc Natl Acad Sci U S A* (2017) 114: E10578–e10585. doi: 10.1073/pnas.1710877114
- 130. Tahk S, Vick B, Hiller B, Schmitt S, Marcinek A, Perini ED, et al. Sirp α - α cd123 Fusion Antibodies Targeting CD123 in Conjunction With CD47 Blockade Enhance the Clearance of AML-Initiating Cells. *J Hematol Oncol* (2021) 14:155. doi: 10.1186/s13045-021-01163-6
- 131. Logtenberg MEW, Jansen JHM, Raaben M, Toebes M, Franke K, Brandsma AM, et al. Glutaminyl Cyclase is an Enzymatic Modifier of the CD47- Sirpα Axis and a Target for Cancer Immunotherapy. *Nat Med* (2019) 25:612–9. doi: 10.1038/s41591-019-0356-z
- Jiang Z, Sun H, Yu J, Tian W, Song Y. Targeting CD47 for Cancer Immunotherapy. J Hematol Oncol (2021) 14:180. doi: 10.1186/s13045-021-01197-w
- 133. Narla RK, Modi H, Bauer D, Abbasian M, Leisten J, Piccotti JR, et al. Modulation of CD47-Sirpα Innate Immune Checkpoint Axis With Fc-Function Detuned Anti-CD47 Therapeutic Antibody. *Cancer Immunol Immunother* (2021) 71:473–89. doi: 10.1007/s00262-021-03010-6
- 134. Chen YC, Shi W, Shi JJ, Lu JJ. Progress of CD47 Immune Checkpoint Blockade Agents in Anticancer Therapy: A Hematotoxic Perspective. J Cancer Res Clin Oncol (2022) 148:1–14. doi: 10.1007/s00432-021-03815-z
- 135. Advani R, Flinn I, Popplewell L, Forero A, Bartlett NL, Ghosh N, et al. CD47 Blockade by Hu5F9-G4 and Rituximab in Non-Hodgkin's Lymphoma. *N Engl J Med* (2018) 379:1711–21. doi: 10.1056/NEJMoa1807315
- 136. Ansell SM, Maris MB, Lesokhin AM, Chen RW, Flinn IW. Phase I Study of the CD47 Blocker TTI-621 in Patients With Relapsed or Refractory Hematologic Malignancies. *Clin Cancer Res* (2021) 27:2190–9. doi: 10.1158/1078-0432.ccr-20-3706
- 137. Vivier E, Artis D, Colonna M, Diefenbach A, Di Santo JP, Eberl G, et al. Innate Lymphoid Cells: 10 Years on. *Cell* (2018) 174:1054–66. doi: 10.1016/ j.cell.2018.07.017
- Abel AM, Yang C, Thakar MS, Malarkannan S. Natural Killer Cells: Development, Maturation, and Clinical Utilization. *Front Immunol* (2018) 9:1869. doi: 10.3389/fimmu.2018.01869
- Poli A, Michel T, Thérésine M, Andrès E, Hentges F, Zimmer J. CD56bright Natural Killer (NK) Cells: An Important NK Cell Subset. *Immunology* (2009) 126:458–65. doi: 10.1111/j.1365-2567.2008.03027.x
- 140. Moretta L, Montaldo E, Vacca P, Del Zotto G, Moretta F, Merli P, et al. Human Natural Killer Cells: Origin, Receptors, Function, and Clinical Applications. Int Arch Allergy Immunol (2014) 164:253–64. doi: 10.1159/ 000365632
- 141. Chiossone L, Dumas PY. Natural Killer Cells and Other Innate Lymphoid Cells in Cancer. Nat Rev Immunol (2018) 18:671–88. doi: 10.1038/s41577-018-0061-z
- 142. Ljunggren HG, Malmberg KJ. Prospects for the Use of NK Cells in Immunotherapy of Human Cancer. Nat Rev Immunol (2007) 7:329–39. doi: 10.1038/nri2073
- Sivori S, Meazza R. NK Cell-Based Immunotherapy for Hematological Malignancies. J Clin Med (2019) 8:1702. doi: 10.3390/jcm8101702
- 144. Mizia-Malarz A, Sobol-Milejska G. NK Cells as Possible Prognostic Factor in Childhood Acute Lymphoblastic Leukemia. *Dis Markers* (2019) 2019:1–4. doi: 10.1155/2019/3596983
- 145. Sullivan EM, Jeha S, Kang G, Cheng C, Rooney B, Holladay M, et al. NK Cell Genotype and Phenotype at Diagnosis of Acute Lymphoblastic Leukemia Correlate With Postinduction Residual Disease. *Clin Cancer Res* (2014) 20:5986–94. doi: 10.1158/1078-0432.ccr-14-0479
- 146. Colomar-Carando N, Gauthier L, Merli P, Loiacono F, Canevali P, Falco M, et al. Exploiting Natural Killer Cell Engagers to Control Pediatric B-Cell Precursor Acute Lymphoblastic Leukemia. *Cancer Immunol Res* (2022) 10:291–302. doi: 10.1158/2326-6066.CIR-21-0843

- 147. Vaněk O, Kalousková B, Abreu C, Nejadebrahim S, Skořepa O. Natural Killer Cell-Based Strategies for Immunotherapy of Cancer. Adv Protein Chem Struct Biol (2022) 129:91–133. doi: 10.1016/bs.apcsb.2022.02.001
- 148. Zhang L, Meng Y, Feng X, Han Z. CAR-NK Cells for Cancer Immunotherapy: From Bench to Bedside. *Biomark Res* (2022) 10:12. doi: 10.1186/s40364-022-00364-6
- 149. Herrera L, Santos S, Vesga MA, Anguita J. Adult Peripheral Blood and Umbilical Cord Blood NK Cells are Good Sources for Effective CAR Therapy Against CD19 Positive Leukemic Cells. Sci Rep (2019) 9:18729. doi: 10.1038/ s41598-019-55239-y
- 150. Müller S, Bexte T, Gebel V, Kalensee F, Stolzenberg E, Hartmann J, et al. High Cytotoxic Efficiency of Lentivirally and Alpharetrovirally Engineered CD19-Specific Chimeric Antigen Receptor Natural Killer Cells Against Acute Lymphoblastic Leukemia. *Front Immunol* (2020) 10:3123. doi: 10.3389/fimmu.2019.03123
- DeNardo DG, Ruffell B. Macrophages as Regulators of Tumour Immunity and Immunotherapy. Nat Rev Immunol (2019) 19:369–82. doi: 10.1038/ s41577-019-0127-6
- Franken L, Schiwon M, Kurts C. Macrophages: Sentinels and Regulators of the Immune System. *Cell Microbiol* (2016) 18:475–87. doi: 10.1111/ cmi.12580
- Klichinsky M, Ruella M. Human Chimeric Antigen Receptor Macrophages for Cancer Immunotherapy. *Nat Biotechnol* (2020) 38:947–53. doi: 10.1038/ s41587-020-0462-y
- Kast F, Klein C. Advances in Identification and Selection of Personalized Neoantigen/T-Cell Pairs for Autologous Adoptive T Cell Therapies. Oncoimmunology (2021) 10:1869389. doi: 10.1080/2162402x.2020.1869389
- 155. Lu F, Ma XJ, Jin WL, Luo Y, Li X. Neoantigen Specific T Cells Derived From T Cell-Derived Induced Pluripotent Stem Cells for the Treatment of

Hepatocellular Carcinoma: Potential and Challenges. *Front Immunol* (2021) 12:690565. doi: 10.3389/fimmu.2021.690565

- 156. Verdon DJ, Jenkins MR. Identification and Targeting of Mutant Peptide Neoantigens in Cancer Immunotherapy. *Cancers (Basel)* (2021) 13:4245. doi: 10.3390/cancers13164245
- 157. Borden ES, Buetow KH, Wilson MA, Hastings KT. Cancer Neoantigens: Challenges and Future Directions for Prediction, Prioritization, and Validation. *Front Oncol* (2022) 12:836821. doi: 10.3389/fonc.2022.836821
- 158. Zamora AE, Crawford JC. Pediatric Patients With Acute Lymphoblastic Leukemia Generate Abundant and Functional Neoantigen-Specific CD8(+) T Cell Responses. *Sci Transl Med* (2019) 11:eaat8549. doi: 10.1126/ scitranslmed.aat8549

Conflict of Interest: The authors declare that the research was conducted in the absence of any commercial or financial relationships that could be construed as a potential conflict of interest.

Publisher's Note: All claims expressed in this article are solely those of the authors and do not necessarily represent those of their affiliated organizations, or those of the publisher, the editors and the reviewers. Any product that may be evaluated in this article, or claim that may be made by its manufacturer, is not guaranteed or endorsed by the publisher.

Copyright © 2022 Lv, Liu, Liu, Xing and Zhang. This is an open-access article distributed under the terms of the Creative Commons Attribution License (CC BY). The use, distribution or reproduction in other forums is permitted, provided the original author(s) and the copyright owner(s) are credited and that the original publication in this journal is cited, in accordance with accepted academic practice. No use, distribution or reproduction is permitted which does not comply with these terms.

309



A Whole Exon Screening-Based Score Model Predicts Prognosis and Immune Checkpoint Inhibitor Therapy Effects in Low-Grade Glioma

Cheng Luo ^{1,2,3†}, Songmao Wang ^{1,3,4†}, Wenjie Shan ^{1,3,5}, Weijie Liao ^{1,3}, Shikuan Zhang ^{1,3,4}, Yanzhi Wang ^{1,3,4}, Qilei Xin ^{1,3,6}, Tingpeng Yang ^{1,3,6}, Shaoliang Hu⁷, Weidong Xie ^{1,3,5}, Naihan Xu ^{1,3,5*} and Yaou Zhang ^{1,3,5*}

OPEN ACCESS

Edited by:

Xuyao Zhang, Fudan University, China

Reviewed by:

Filippo Rossignoli, Brigham and Women's Hospital and Harvard Medical School, United States Shuai Ping, Huazhong University of Science and Technology, China

*Correspondence:

Naihan Xu xu.naihan@sz.tsinghua.edu.cn Yaou Zhang zhangyo@sz.tsinghua.edu.cn [†]These authors have contributed equally to this work

Specialty section:

This article was submitted to Cancer Immunity and Immunotherapy, a section of the journal Frontiers in Immunology

Received: 31 March 2022 Accepted: 16 May 2022 Published: 13 June 2022

Citation:

Luo C, Wang S, Shan W, Liao W, Zhang S, Wang Y, Xin Q, Yang T, Hu S, Xie W, Xu N and Zhang Y (2022) A Whole Exon Screening-Based Score Model Predicts Prognosis and Immune Checkpoint Inhibitor Therapy Effects in Low-Grade Glioma. Front. Immunol. 13:909189. doi: 10.3389/fimmu.2022.909189 ¹ China State Key Laboratory of Chemical Oncogenomics, Tsinghua Shenzhen International Graduate School, Shenzhen, China, ² Department of Biomedical Engineering, Tsinghua University, Beijing, China, ³ Key Lab in Healthy Science and Technology of Shenzhen, Tsinghua Shenzhen International Graduate School, Shenzhen, China, ⁴ School of Life Sciences, Tsinghua University, Beijing, China, ⁵ Open Faculty for Innovation, Education, Science, Technology and Art, Tsinghua Shenzhen International Graduate School, Shenzhen, China, ⁶ Department of Chemical Engineering, Tsinghua University, Beijing, China, ⁷ Research and Development Department, Shenzhen Combined Biotech Co., Ltd, Shenzhen, China

Objective: This study aims to identify prognostic factors for low-grade glioma (LGG) *via* different machine learning methods in the whole genome and to predict patient prognoses based on these factors. We verified the results through *in vitro* experiments to further screen new potential therapeutic targets.

Method: A total of 940 glioma patients from The Cancer Genome Atlas (TCGA) and The Chinese Glioma Genome Atlas (CGGA) were included in this study. Two different feature extraction algorithms – LASSO and Random Forest (RF) – were used to jointly screen genes significantly related to the prognosis of patients. The risk signature was constructed based on these screening genes, and the K-M curve and ROC curve evaluated it. Furthermore, we discussed the differences between the high- and low-risk groups distinguished by the signature in detail, including differential gene expression (DEG), single-nucleotide polymorphism (SNP), copy number variation (CNV), immune infiltration, and immune checkpoint. Finally, we identified the function of a novel molecule, METTL7B, which was highly correlated with PD-L1 expression on tumor cell, as verified by *in vitro* experiments.

Results: We constructed an accurate prediction model based on seven genes (AUC at 1, 3, 5 years= 0.91, 0.85, 0.74). Further analysis showed that extracellular matrix remodeling and cytokine and chemokine release were activated in the high-risk group. The proportion of multiple immune cell infiltration was upregulated, especially macrophages, accompanied by the high expression of most immune checkpoints. According to the *in vitro* experiment, we preliminarily speculate that METTL7B affects the stability of PD-L1 mRNA by participating in the modification of m6A.

Conclusion: The seven gene signatures we constructed can predict the prognosis of patients and identify the potential benefits of immune checkpoint inhibitors (ICI) therapy for LGG. More importantly, METTL7B, one of the risk genes, is a crucial molecule that regulates PD-L1 and could be used as a new potential therapeutic target.

Keywords: METTL7B, PD-L1, prognosis prediction, glioma, m6A (N6-methyladenose), RNA stability

INTRODUCTION

Central nervous system (CNS) malignant tumors have one of the worst prognoses among all cancers, and glioma is the most common primary tumor of the CNS, accounting for approximately 80% of malignant brain tumors (1, 2). At present, the clinical classification of gliomas still follows the histological diagnostic criteria proposed by the WHO in 2007 (3). This classification method has significant limitations (4). One reason is that subjective preference easily differentiates judgments based on tumor histology between observers (5). As a result, the survival time of a group of patients with glioma may vary from weeks to years. It is difficult to explain this difference based only on histological grade. Although diffuse low- and intermediate-grade gliomas collectively constitute low-grade gliomas (LGGs, WHO grades II and III), which are rarer than grade IV gliomas (GBM, glioblastoma) due to their highly invasive nature, complete neurosurgical resection is impossible, leading to recurrence and malignant progression, eventually progressing to glioblastoma (3, 6-8). Therefore, it is necessary to propose new detailed diagnostic criteria that integrate the molecular changes in glioma.

For the treatment of glioma, traditional surgical resection is difficult and the residual tumor cells will further deteriorate. Radiotherapy has also been associated with epilepsy and mild dementia (9). Given these limitations, immune checkpoint inhibitor (ICI) drugs have proven to be promising treatments (10). In a phase III clinical trial of glioblastoma, the overall response rate of patients to nivolumab (PD-1 monoclonal antibody) was only 8%, but the overall survival time doubled (11). Considering the good therapeutic effect and high medical cost of glioma, there is an urgent need for a valuable biomarker to predict the benefits of immunotherapy in patients with glioma.

In this study, we focused on all genes in the LGG transcriptome data. We tried to develop a prognostic marker of LGG that can predict the routine prognosis of patients and the potential benefits of immunotherapy. We found that the immune response, extracellular matrix remodeling, and cytokine release were accelerated in the high-risk groups. In addition, high-risk patients are accompanied by the upregulation of most immune checkpoints represented by PD-1/L1 and the increase in tumor mutation burden (TMB) and CNV, suggesting that patients may respond better to the ICI of PD-L1 (12–15). We proved this through the TIDE score (16). In short, the model can predict the prognosis of patients and determine the possible benefits of ICI treatment. Finally, we also found a new molecule, METTL7B, in glioma, which reduces the expression of PD-L1 in cells by inhibiting the stability of PD-L1 mRNA and lead to the apoptosis of co-cultured T cells.

METHODS

Publicly Available mRNA Data and Immune Gene Sets

Data from two publicly available datasets were incorporated into our study. TCGA RNA-seq data (FPKM) of samples from patients with LGG (Illumina HiSeq 2000) were acquired from the Genomic Data Commons (GDC) (http://portal.gdc.cancer.gov). According to the whole survival time, age, radiotherapy status, and glioma grades, 420 patients were collected and randomly (in a 7:3 ratio) categorized as training set and internal validation set. 529 glioma data was downloaded with complete clinical data and molecular subtyping data (IDH1 mutation, 1p19q codeletion, and MGMT methylation) from Chinese Glioma Genome Atlas (CGGA) (http:// www.cgga.org.cn) to serve as external validation sets.

Construction and Verification of Multivariate Cox Signature

According to the mRNA expression of risk genes, a stepwise Cox proportional hazards regression model was used. RF realized by the R package "randomforestsrc", the number of feature trees was 100, and the number of random splits was 1. LASSO realized by R package "glmnet", and 100 times cross-validation was carried out. Signature genes were obtained by taking the intersection of these two gene lists. Risk score formula was calculated by taking into account the expression of signature genes and correlation estimated Cox regression coefficients: Risk score = (exp Gene1 * coef Gene1) + (exp Gene2 * coef Gene2) +... +(exp Gene7 * coef Gene7). Patients with LGG were classified into a high-risk or low-risk group by ranking the given risk score. The thresholds of high- and low-risk groups were selected through the "survminer" package. The R package "timeROC" was used to test the timedependent receiver operating characteristic curve (ROC) (17). The difference of overall survival (OS) between two groups in the three cohorts was assessed using Kaplan-Meier method and the two-tailed log-rank test. A Cox proportional hazards regression model was used to identify independent prognostic factors.

Construction and Validation of Multigene Containing Nomogram

Nomogram was used to predict the survival probability by specific clinical parameters (18). We constructed the nomogram containing the multigene signature and other independent prognostic factors. The nomogram was calibrated at 1-year, 3-years, and 5-years using the R package "rms". Decision curve analysis (DCA) analysis was used to assess the clinical application benefits of the multigene panel in the TCGA set (19).

Biological Process and Pathway Enrichment Analysis

Using the R package "DESeq2" (20), DEGs between high- and low-risk groups were identified. Then, using Gene Ontology (GO) and Kyoto Encyclopedia of Genes and Genomes (KEGG) enrichment analysis, different pathways and items were identified between the two risk groups. In addition, we used GSEA (21) to dynamically score different enrichment items in the high- and low-risk groups.

Weighted Gene Co-Expression Network Analysis

The R package "WGCNA" (22) was used to perform weighted gene co-expression network analysis (WGCNA) using the TCGA LGG expression matrix (FPKM). To build a scale-free network and calculate the network topology matrix, the gene expression matrix is weighted by a soft threshold. We use a dimension reduction algorithm to visualize the network module composed of co-expressed genes in glioma samples after clustering with the dynamic cut tree algorithm and merging similar modules.

Evaluation of Immune Microenvironment With CIBERSORT and ssGSEA

The LM22 signature matrix, which is included in CIBERSORT, was used to estimate the distribution of 22 immune cell types (23). We ran 1000 iterations in R studio using the script provided in this paper to assess the difference in 22 immune cell infiltrations between the high and low risk groups and displayed the results in heatmap. ssGSEA was realized through the R package "GSVA" according to the analysis process and method provided by the official instruction (24).

Analysis of Gene Mutation and Copy Number Variation

The copy number variation data in the TCGA database was downloaded through the 'TCGAbiolinks' R package (25), and the risk score and CNV were integrated. snp6 grch38 annotation file was downloaded in TCGA and analyzed with GISTIC2.0 (26). Gene mutation data was also obtained from the TCGA database. The occurrence of mutation events was calculated and matched with the risk score. Finally, the 'maftools' R package was used for visualization (27).

Cell Culture and Construction of Stable Cell Lines

U251 cells, A172 cells, and Jurkat cells were purchased from the National Collection of Authenticated Cell Cultures. U251 and A172 were grown in DMEM medium with 10% fetal bovine serum (Gibco, California, USA). Jurkat cells were cultured in RPMI 1640 Medium with 10% fetal bovine serum. All medium was supplemented with 10 U/ml of penicillin-streptomycin, and all cells were cultured in a 5% CO2 humidified incubator at 37°C. The control shRNA and Lentivirus-based LINC00472-targeting shRNA vectors were purchased from GENECHEM (Shanghai, China). U251 cells were transiently transfected with these vectors and screened by puromycin at a 2 mg/ml concentration to generate stable monoclonal cell lines.

PCR and Real-Time Quantitative PCR Analysis

According to the manufacture's protocol, the total RNA was isolated using AG RNAex Pro Reagent AG21101. Real-time quantitative PCR was performed using the TransScript All-in-One First-Strand cDNA Synthesis SuperMix for qPCR (One-Step gDNA Removal) (TRANS, AT341-01) and the PerfectStart SYBR Green qPCR SuperMix (TRANS, AT601-01). The primers used are listed in **Supplemental Table S1**, and all the levels of mRNAs were measured and normalized to β -actin.

Western Blotting

Western blotting was performed as previously described (28). The antibodies used for western blotting include METTL7B (Abclonal, A7200), CD274 (Abcam, 243877), and β -actin (CST, 8480S).

Coculture Study and Assessment of Apoptosis

To examine the effect of tumor cells on lymphocyte apoptosis, a total of 5×10^6 U251 cells were cocultured with 5×10^5 Jurkat leukemia T cells in 6-cm plates for 24 h. Jurkat cells were collected and washed three times with PBS diluted in annexin binding buffer. For each sample, 5 ml (2.5 mg/ml) annexin V–FITC and 5 ml (50 mg/ml) propidium iodide were added to the cell suspension and incubated for 15 min at room temperature (25°C) in the dark. The extent of apoptosis in Jurkat cells was determined by flow cytometry using FITC–annexin V.

Total m6A Modification Level and RNA Stability of Cells

The total amount of m6A in total RNA was measured using the m6A RNA Methylation Assay Kit (Fluorometric) (Abcam, ab233491), following the manufacturer manual. For each sample, 200 ng of total RNA from U251 cells were used. For RNA stability detection, cells were cultured overnight and then treated with actinomycin D 10 mg/mL at 0, 2, 4 and 6 h before trypsinization collection. The total RNA was extracted by TRIzol. Quantitative RT-PCR was conducted to determine the relative level of indicated mRNA.

Statistical Analysis

The R software (version 4.1.2) was used for the statistical analysis. Statistical analysis of cell and molecular biology experiments was performed using GraphPad Prism 8.0 version. "ggplot2", "ggpubr", "vioplot" were applied to visualize the results of data analysis. Wilcoxon Signed Rank test and Student's t test were used for statistical analysis between two groups, while the Kruskal-Wallis test was applied for statistical tests of more than two groups. When p less than 0.05, we considered the difference to be statistically significant.

RESULTS

Identification of Prognosis-Related Genes in Low-Grade Glioma

In this study, 529 LGG samples were acquired from the TCGA database, and a total of 530 patients were obtained from the

CGGA database. The glioma data from TCGA were randomly divided into a training set and a validation set at a ratio of 7:3. The process is shown in **Figure 1**; 32622 genes were selected because the gene expression level in half of the samples was more than zero. The expression of these genes in LGG samples was used for univariate Cox regression analysis. A total of 3432 genes were significantly (p < 0.001) associated with the overall survival of patients in the TCGA training set.

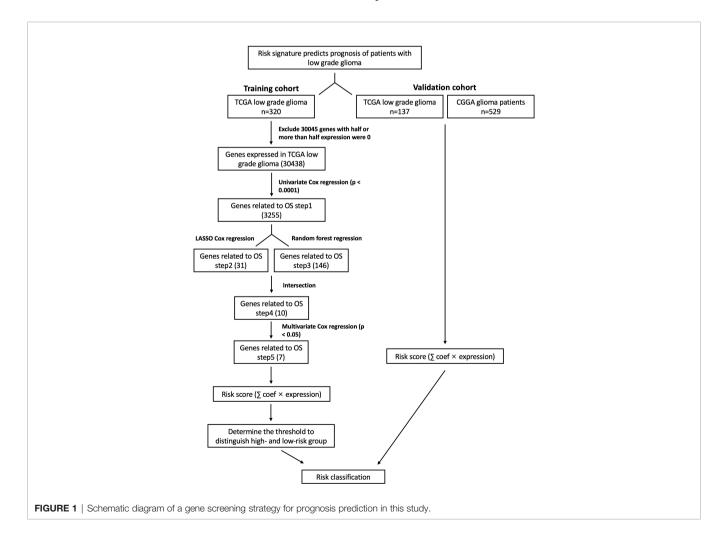
We included these significant genes in LASSO and RF regression (**Figures 2A, B**), two algorithms screened 31 and 146 genes related to the clinical outcome of glioma patients, respectively. Then, we obtain the intersection of these two algorithms. **Figure 2C** shows that 10 genes existed simultaneously in the two regression analysis results. Multivariate Cox regression analysis was performed on these ten genes, and seven genes with P values < 0.05 were selected (**Table 1**).

The 7-Gene Signature Can Accurately Predict the Prognosis of Patients With Low-Grade Glioma

According to the above feature selection algorithm, CTC-548K16.2, EFHB, METTL7B, MLLT3, SEL1L3, SOX13, and FAM66C were used to build a multigene signature for predicting the survival of LGG patients. The risk score of each patient was estimated based on the expression of these genes and their corresponding coefficients, which were obtained by multivariate Cox regression analysis. Patients were categorized into a significant risk group based on the optimized risk value based on the results of ROC analysis.

First, we investigated the performance of the multigene signature in predicting the OS of LGG patients. The K–M curve suggested that the clinical outcome was significantly worse in the high-risk group than in the low-risk group (p < 0.0001) (**Figure 2D**). Furthermore, the time-dependent ROC curve shown in **Figure 2E** shows that the multigene signature has excellent performance in predicting survival events (the areas under the curves (AUC) at one year, three years, and five years were 0.91, 0.85, and 0.74, respectively). **Figure 2F** illustrates the risk score distribution of patients, the survival time, and the heatmap of the seven gene expression profiles in each patient. In short, the risk score proved to be highly significant for patients with glioma in the training set.

We identified clinically independent prognostic factors. As shown in **Figure 2G**, young age (HR = 0.45, 95% CI: $0.28 \sim 0.71$, p < 0.001) and low-risk score (HR = 0.28, 95% CI: $0.17 \sim 0.44$,



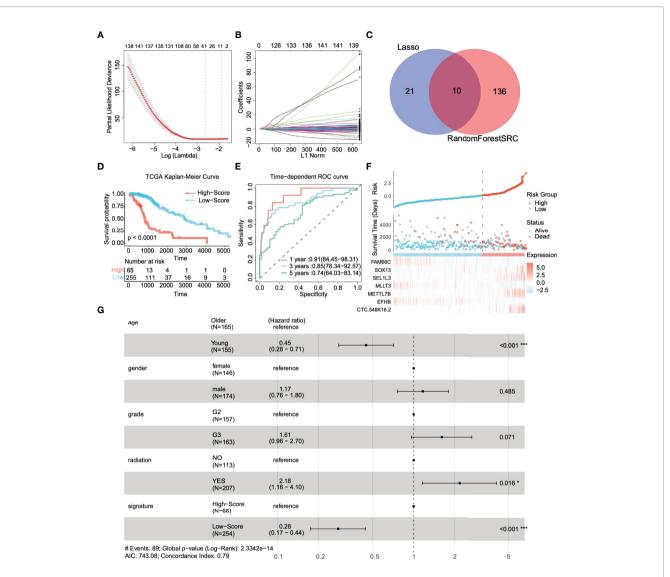


FIGURE 2 | Identification of prognostic genes and survival prediction of patients with low-grade gliomas in the TCGA training cohort. (A) 100-fold cross-validation for tuning parameter selection in the LASSO model. (B) The distribution of regression coefficients of significantly related genes in the model. (C) Gene selection through two algorithms based on the Venn plot. (D) Kaplan–Meier curves of overall survival (OS) in low-grade glioma are based on the risk score. (E) Time-dependent ROC curve of the risk gene signature at 1, 3, and 5 years in the TCGA training cohort. (F) Distribution of risk score, survival time, and gene expression panel. (G) Subgroup analysis shows the effect of different clinical features in TCGA for OS patients with low-grade glioma. Hazard ratios with 95% confidence intervals are shown in each different group. *p < 0.05, ***p < 0.001.

TABLE 1 Multivariate Cox analysis was used to further screen prognostic
factors and corresponding coefficients of the linear model.

Characteristics	Hazard Ratio	CI95	p.value	Coef.	
ARL3	0.67	0.4-1.14	0.143		
CTC-548.K16.2	31.58	1.39-715.54	0.030	3.818	
EFHB	0.60	0.37-0.98	0.040	-0.539	
HILS1	1.12	0.56-2.23	0.741		
METTL7B	1.23	1.02-1.47	0.027	0.194	
MLLT3	0.49	0.29-0.82	0.007	-0.813	
RP11.893F2.14	2.33	0.84-6.47	0.106		
SEL1L3	1.41	1.16-1.72	0.001	0.466	
SOX13	1.57	1.26-1.98	0.000	0.498	
FAM66C	1.32	1.06-1.63	0.032	-0.216	

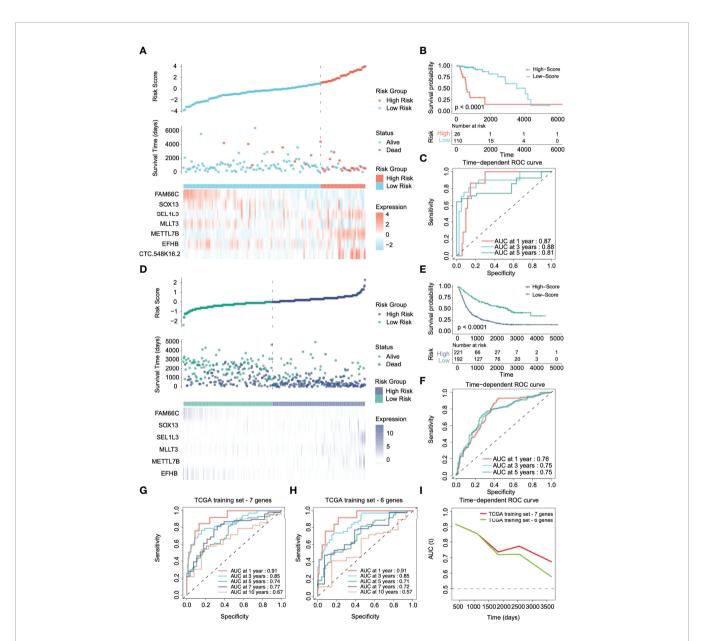
p < 0.001) were protective factors, and glioma grade (HR = 1.61, 95% CI: 0.96~2.70, p = 0.071) and radiotherapy (HR = 2.18, 95% CI: 1.16~4.10, p = 0.016) seemed to be risk.

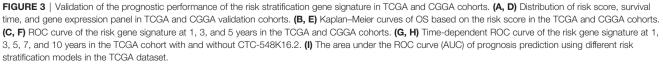
The 7-Gene Signature Still Has Good Performance in the Internal and External Validation Sets

To validate the performance forecast of the multigene signature, we used glioma patient data from TCGA and CGGA as the internal verification and external verification cohort, respectively. With the same coefficients, patients were divided into a high-risk group (N=26 in TCGA, N=221 in CGGA) and a

low-risk group (N=110 in TCGA, N=192 in CGGA) based on the expression of 7 signature genes (**Figures 3A, D**). In the internal verification cohort of TCGA, K–M survival analyses showed that patients in the low-risk group had significantly better OS than those in the high-risk group (**Figure 3B**, p < 0.0001). The time-dependent ROC curve revealed that for predicting prognosis at 1, 3, and 5 years, the AUCs were 0.87, 0.88, and 0.81, respectively (**Figure 3C**). Because the CGGA dataset still contains grade IV gliomas, it suggests that the signature also has potential application value in high-grade gliomas.

However, in the CGGA external verification cohort, CTC-548K16.2 was removed due to probe loss. We used the same coefficient to integrate other genes for analysis. The 6-gene signature in the CGGA external verification set also had a superior ability to distinguish the clinical outcomes of the high-risk group and the low-risk group (**Figure 3E**, p < 0.0001). The 1-, 3-, and 5-year AUCs of the time-dependent ROC curves were 0.76, 0.75, and 0.75, respectively (**Figure 3F**). The results showed that although one variable was removed, the multigene prediction model still had good differentiation for the prognosis of glioma patients.





CTC-548K16.2 is a noncoding RNA that has low expression in the TCGA cohort. Next, we evaluated the significance of CTC-548K16.2 in the prediction signature. In the TCGA dataset, the AUC of the seven-gene model considering CTC-548K16.2 was 0.91 (1 year), 0.85 (3 years), 0.74 (5 years), 0.77 (7 years), and 0.67 (10 years) (**Figure 3G**). With the increase in survival time, the AUC showed a downward tendency. However, the 1-, 3-, 5-, 7-, and 10-year AUCs were 0.91, 0.85, 0.71, 0.72, and 0.57, respectively, when the 6-gene signature was used for prediction (**Figure 3H**). **Figure 3I** shows that the AUC decreased sharply at approximately 1800 days. These results suggest that CTC-548K16.2 may be related to the late prognosis of glioma patients.

The Signature Has Suitable Identification for Different Clinical Subgroups and Molecular Subgroups

We aimed to determine whether the signature has universal applicability, whether it has a more accurate prediction for different types of patients, such as age or gender, and whether is unsuitable for a specific type of patient. We divided the patients into different subgroups according to clinical information. For all subgroups in the internal training set, the OS time of high-risk patients was shorter than that of low-risk patients (**Figure S1**). Signatures can achieve satisfactory identification in most subgroups in the validation set, except for G2 gliomas (**Figure S2**). One reason may be that the prognosis of G2 is usually good, so the number of samples identified as high-risk is minimal (only 3 patients in the high-risk group).

In terms of molecular subgroups, the IDH1 wild-type group (76%) had a higher proportion of high-risk patients than the IDH1 mutant group (34%) (**Figure S3A**). In addition, the percentage of high-risk patients in the 1p19q codeletion group (33%) was lower than that in the nondeletion group (58%) (**Figure S3B**). There was no significant difference in MGMT promoter methylation (**Figure S3C**). Regarding different molecular characteristics, the OS time of the high-risk group was significantly shorter (**Figures S3D-I**).

The Nomogram Integrated Signature Shows That the Clinical Benefit to Patients Has Been Improved

A prognostic nomogram is a quantitative method for clinicians to predict the survival of LGG patients (29). We integrated clinically independent prognostic factors that were identified before. Nomogram was constructed based on these factors to predict the 1-year, 3-year, and 5-year survival probability of glioma patients (**Figure 4A**). The calibration plot closely resembled the ideal diagonal curve at 1-year, 3-year, and 5-year (**Figures 4B–D**), and the C-index of the nomogram was 0.807, suggesting that the performance of the nomogram was reliable.

Figure 4E shows that the AUC of the 1-year ROC curve was significantly higher than that of age (AUC = 0.791) and radiation (AUC = 0.505). In addition, we included independent prognostic factors to compare the decision curve analysis (DCA) of the

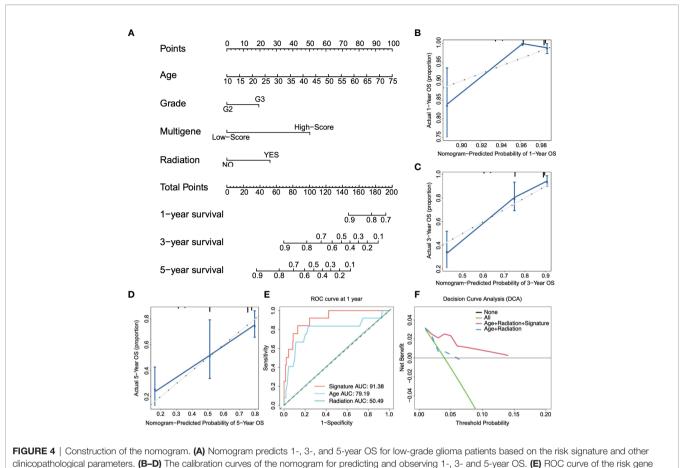
predictive models with or without risk scores. We found that the clinical benefit of patients with risk score integration was much greater than that of patients with only age, grade, and other factor integration (**Figure 4F**). In other words, compared to the conventional clinical classification system, the nomogram with the risk score had a better performance in predicting survival outcomes. Therefore, these results illustrated that the nomogram could be used to predict the prognosis of glioma patients in clinical practice.

Immune Response and Extracellular Matrix Remodeling Were Significantly Activated in High-Risk Patients

To further determine the functional position of risk stratification genes in glioma progression. We selected 20000 genes according to the median absolute deviation and transformed glioma expression profiles (TCGA) into gene co-expression networks using the WGCNA package, as described previously (22). The soft threshold (beta = 4) was selected to build a scale-free network and check the mean connectivity of the network (**Figure S4A**). **Figure S4B** is used to verify the network node connection statistics and scale-free distribution. The fractionalstep algorithm constructs the modules and calculates the correlation (**Figure S4C**). Then, the clusters with a degree of difference less than 0.2 were merged, and 19 different co-expression modules were finally obtained (**Figure 5A**).

Through the enrichment analysis of the WGCNA co-expression modules, we found that the risk stratification genes were located in four different co-expression modules. MLLT3 and FAM66C are light green in the network, and SEL1L3 and SOX13 are turquoise. The genes in these two modules are mainly related to the nervous system and synapses (**Figures S5A, B**). EFHB, which is depicted in brown, is primarily involved in DNA metabolism and chromatin remodeling in gliomas (**Figure S5C**). Finally, METTL7B, depicted in royal blue, is engaged mainly in vasculogenesis and extracellular structure organization (**Figure 5B**), suggesting that METTL7B has the closest relationship with glioma invasion, migration, and vasculogenesis among the risk stratification genes.

Then, based on the DESeq2 algorithm (20), we analyzed the differentially expressed genes between the high- and low-risk groups from the TCGA cohort, including 3883 upregulated and 1101 downregulated genes. The log2 enrichment ratio and -log10 adjusted p were visualized in a volcano plot (Figure 5C). GO analysis indicated that these genes could be categorized into inflammatory signaling pathways and immune responses, including T-cell activation and leukocyte and lymphocyte activation (Figure 5D). GO items with statistical significance were mainly concentrated in three clusters: immune response, extracellular matrix remodeling, and interferon-gamma mediated immune response (Figure 5E). KEGG analysis showed that the DEGs were mainly associated with essential biological processes, including ECM-receptor interactions, phagosomes, focal adhesion, the JAK-STAT signaling pathway, and the cAMP signaling pathway (Figure 5F). Fold changes in the mRNA expression levels of DEGs between the high- and lowrisk groups were calculated and preranked in GSEA, and it



signature and other parameters at one year. (F) The decision curve analysis (DCA) shows the clinical benefits of patients after risk stratification.

revealed that the low-risk group was significantly associated with immune system development (NES = -1.75, p.adj = 0.03, **Figure 5G**) and extracellular matrix structural constituents (NES=-2.46, p.adj < 0.0001, **Figure 5H**).

High-Risk Patients Have Prominent Immune Cell Infiltration and Increased Expression of Immune Checkpoints

Functional enrichment analysis (GO, KEGG and GSEA) found immune response activation in high-risk patients, and we further analyzed this difference. We conducted different machine learning approaches to integrate multidimensional immunerelated variables for every patient. CIBERSORT used a linear model to predict the content of immune cells in the tumor microenvironment and evaluated the accuracy of the results by 1000 permutation tests. In Figure 6A, patients in the high-risk group had a significantly higher proportion of CD8+ T cell, M1, and M2 types of macrophages and a substantially lower proportion of activated mast cells. The increased ratio of macrophage infiltration is associated with a worse prognosis in LGG, which seems to be unrelated to patients with glioblastoma (Figure 6B). We also conducted ssGSEA to evaluate the association with immune-infiltrating cells and the gene signature in individual glioma samples; however, the two

algorithms are different. We obtained similar conclusions, and ssGSEA indicates that we should pay more attention to the general upregulation of the proportion of immune cell infiltration (**Figure 6C**).

The huge difference in the immune landscape suggests that highrisk patients may have different benefits from immunotherapy. Therefore, we expanded our analysis to 28 immune checkpoint molecules, including the B7-CD28 family (30, 31), TNF superfamily (32), and others (33–35). Surprisingly, most immune checkpoints were upregulated (**Figure 6D**), including the B7-CD28 family (p < 0.0001: CD274, CD276, ICOS, PDCD1 and PDCD1LG2), TNF superfamily (p < 0.0001: CD40, CD40LG and TNFRSF14) and others (p < 0.0001: HAVCR2) (**Figure 6E**). Based on the outstanding performance in the therapeutic effect of PD-1/L1 inhibitors, PD-L1 and PD-1 in glioma deserve more attention (36).

The Amplification of TMB and CNV in the High-Risk Group Confirmed the High Response of ICI Therapy

We found that the majority of immune checkpoints in patients in high-risk group were upregulated, especially PD-1/L1. The high expression of these molecules has been proven to be related to patients' better response to ICI therapy. In addition to the detection of PD-1/L1 molecules, the increase in TMB has also

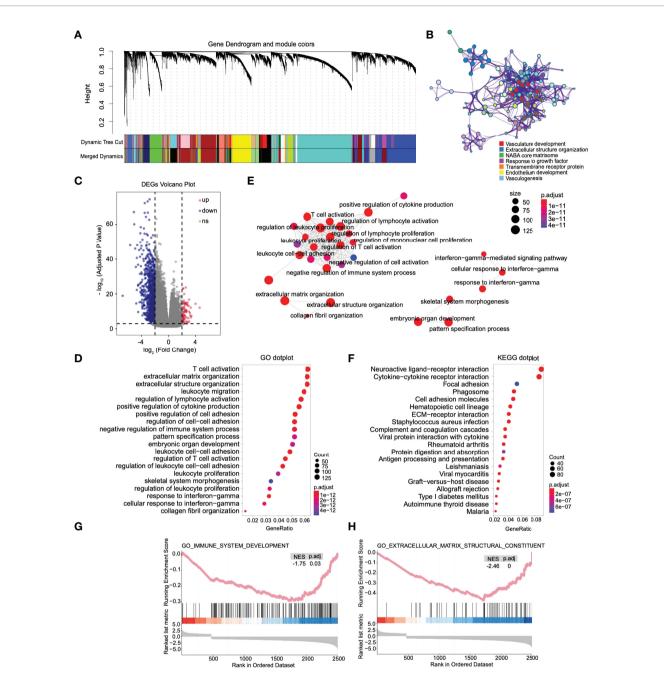
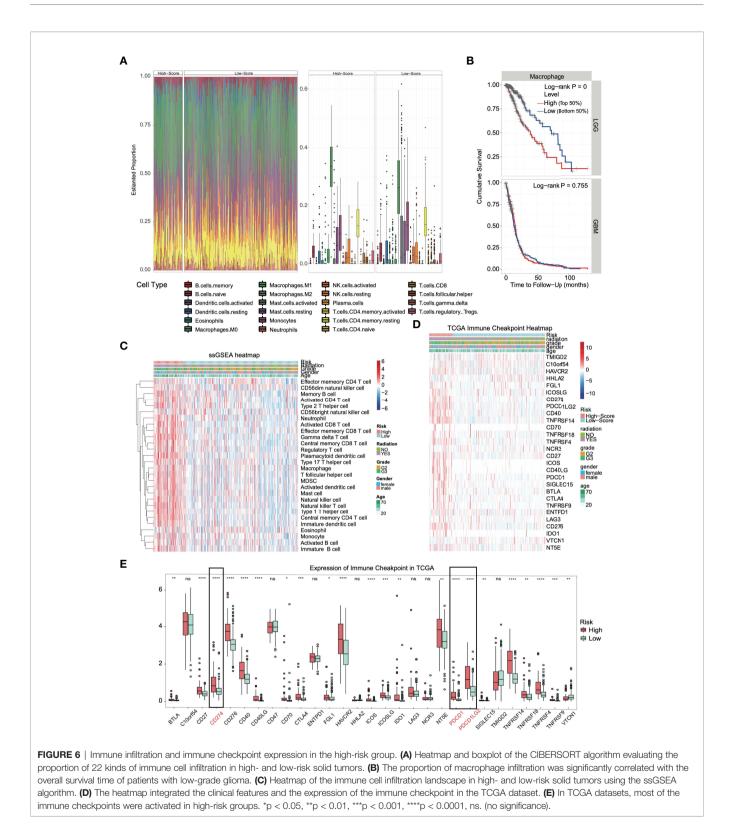


FIGURE 5 | The immune response, extracellular matrix remodeling, and other pathways were significantly activated in high-risk patients. (A) Combining the modules with slight dissimilarity, 19 weighted gene coexpression subnetworks were obtained by a dynamic tree cut algorithm. (B) GO enrichment analysis was performed on all genes in the coexpression module where mettl7b is located. (C) Volcano plot of differentially expressed genes between high- and low-risk patients. (D) Dot plot of Gene Ontology (GO) enriched terms colored by p values. (E) Significant GO items were clustered according to biological function. (F) Dot plot of Kyoto Encyclopedia of Genes and Genomes (KEGG) enriched terms colored by p values. Gene set enrichment analysis between high- and low-risk patients. There was a significant enrichment of immune (G) and extracellular matrix remodeling (H) in the high-risk group. NES, normalized enrichment score.

been proven to be related to the effectiveness of immunotherapy and TMB detection has been used as a clinical reference guide (12, 13). Therefore, we analyzed gene mutation and CNV, hoping to support our view further.

The analysis of SNP in the high- and low-risk groups (Figures 7A, B, respectively) revealed that IDH1 and TP53

were in the top two with the highest frequency of gene mutation. Among them, there were 39% IDH1 mutations in the high-risk group and 91% in the low-risk group, which is consistent with previous reports that IDH1 wild-type gliomas tend to have a significantly worse prognosis (37). We analyzed the TMB (the frequency of mutation events per million bases).



The results showed that the average TMB of high-risk patients was 0.64/MB (**Figure 7C**), and that of low-risk patients was 0.38/MB (**Figure 7D**), which was nearly twice the difference. CNV analysis also showed significant copy number amplification in

the high-risk group, which mainly involved three regions (1q32.1, 7p11.2, and 12q14.1, **Figures 7E, F**). All these conclusions confirm that the high-risk group may have higher benefits from immunotherapy. The TIDE score was used to test

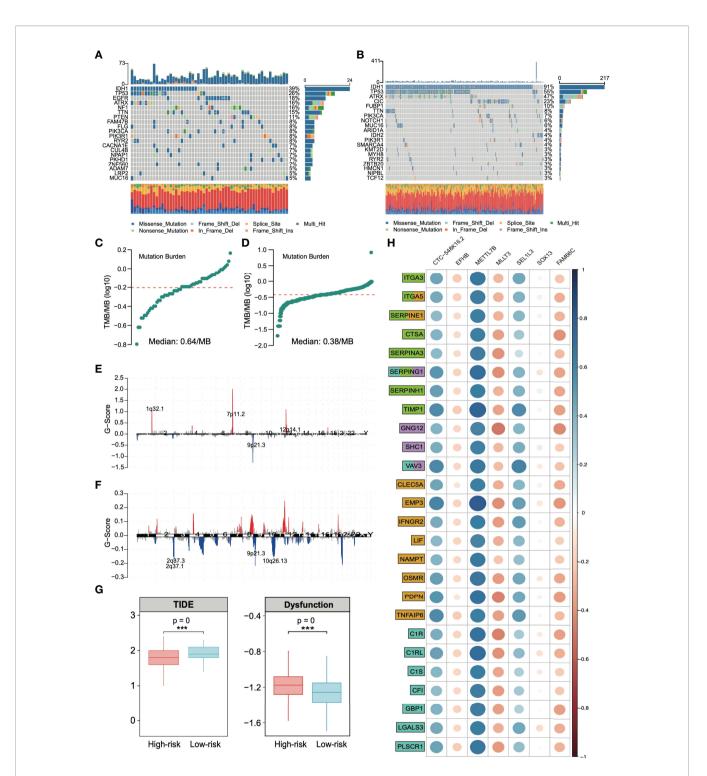


FIGURE 7 | Analysis of single-nucleotide polymorphisms (SNPs) and copy number variations (CNVs) in patients in the high- and low-risk groups. Single-nucleotide polymorphisms in patients in the (A) high- and (B) low-risk groups. Tumor mutation load in patients in the (C) high- and (D) low-risk groups. Copy number variation in patients in the (E) high- and (F) low-risk groups. (G) Based on the calculation of TIDE, the prediction score of each sample (left) the difference of T-cell dysfunction and (right) the difference of TIDE score between high-risk and low-risk groups. ***p < 0.001. (H) Spearman correlation between risk stratification genes and extracellular matrix remodeling markers (green), chemokines (lilac), inflammatory factors (yellow), and immune activation markers (cyan). Gene function annotation is from the MSigDB database.

our conclusion. A higher TIDE score means that patients are unlikely to benefit from immunotherapy (16). We found that the TIDE score in the high-risk group was low, suggesting more significant benefits of immunotherapy. We also observed a higher proportion of T-cell inactivation, indicating the existence of immune escape (**Figure 7G**).

By integrating all the current conclusions, we returned to the risk grading gene itself and selected genes related to extracellular matrix (KEGG_ECM_RECEPTOR_INTERACTION, NABA_ECM_ REGULATORS, and REACTOME_ECM_PROTEDGLYCANS, total of 366 genes), chemokines (KEGG_CHEMOKINE_ SIGNALING_PATHWAY and WP_CHEMOKINE_ SIGNALING_PATHWAY, total of 354 genes), inflammatory factors (HALLMARK_INFLAMMATORT_RESPONSE, total of 200 genes) and immune activation (GO_BP_ACTIVATION_ OF_IMMUNE_RESPONSE, total of 563 genes) from the MsigDB database (https://www.gsea-msigdb.org/gsea/msigdb/) to analyze the relationship of signature genes and these signaling pathways.

We found that the extracellular matrix and immune activation-related genes, chemokines, and inflammatory factors were significantly activated in high-risk solid tumors (**Figure S6**). These results confirm that the signature genes regulate a molecular signaling network in glioma, which is strongly associated with tumor extracellular matrix remodeling and immune response. **Figure 7H** shows that METTL7B has the closest relationship with these immune response-related genes among the risk stratification genes. Additionally, METTL7B has the highest correlation coefficient.

Knockdown of METTL7B in Glioma Promotes the Expression of PD-L1

At present, there is no report on the definite function of METTL7B in glioma, especially its relationship with the immune response. Considering the expression difference between the two risk groups in **Figure 6E**, we analyzed PD-L1, which is mainly expressed on the side of tumor cells and has been widely developed as a target of tumor immunotherapy. The relationship between this molecule and METTL7B was studied *in vitro*.

We selected the human glioma cell line U251 and glioblastoma cell line A172 to realize the knockdown of METTL7B through small interfering RNA (siRNA), as shown in Figure 8A. qRT-PCR showed that the two siMETTL7B targets could achieve a specific inhibition efficiency. We detected the expression of PD-L1 in two cell lines transfected with siMETTL7B and the results showed that the transient inhibition of METTL7B increased the mRNA level of PD-L1 (Figure 8B). We also verified this conclusion by Western blotting (Figure 8C). To further confirm this change, we transfected shRNA with lentivirus and transfected exogenous plasmids to knock out and overexpress METTL7B (Figures 8D, E). Consistent with the above conclusions, knockout of METTL7B further increased the expression of PD-L1, and overexpression reduced the level of PD-L1 (Figures 8F, G). Interferon-gamma is usually produced by activated T cells and

NK cells and is responsible for inhibiting the growth of tumor cells (38). We used interferon-gamma to simulate the immune process of the body. We found that interferon-gamma can make this change more significant, and the Western blot results obtained a consistent conclusion (**Figures 8H, I**).

METTL7B Inhibits the Stability of PD-L1 mRNA, and This May Involve m6A Modification

At present, there are few reports on METTL7B, and there is no thorough report on its role in glioma. We analyzed other family members and found that the three members METTL3, METTL14, and METTL16 of the family have been reported to play the role of m6A writers and play vital roles in the occurrence and development of various tumors (39, 40). Considering an in vitro experiment by Franjic et al., it was verified that METTL7B functions as a methyltransferase via S-adenosylmethionine (SAM) as a methyl donor (41). We tried to study the relationship between METTL7B and intracellular m6A modification. The results showed that siMETTL7B reduced the overall m6A change in cells (Figure 9A), which seemed more evident in the shMETTL7B cell line (Figure 9B). Moreover, an increase in m6A modification was observed in overexpressing cells (Figure 9C). We predicted the posttranscriptional modification of RNA by the SRAMP method (42) and found 15 possible m6A modification sites on PD-L1 mRNA (Figure 9D). One of the most direct consequences of modifying intracellular RNA m6A is the change in the stability of the modified RNA. We verified that METTL7B inhibited the stability of PD-L1 mRNA. As shown in Figure 9E, knockdown of METTL7B in two different glioma cell lines increased the level of PD-L1 mRNA but decreased it in overexpressed cells. All these results suggest that the changes in total m6A modification in cells caused by METTL7B changes may affect the stability of PD-L1 mRNA molecules.

The PD-L1 molecule expressed on the surface of tumor cells binds to the PD-1 receptor on the surface of T lymphocytes, inhibits the function of T lymphocytes, and induces lymphocyte apoptosis. We cocultured Jurkat lymphocytes and U251 glioma cells to simulate the immune process of the body. The results showed that shMETTL7B cells increased the apoptosis of Jurkat lymphocytes coincubated (**Figure 9F**).

All the results show that METTL7B may regulate the expression of PD-L1 molecules through m6A, and m6A modification is likely to be an essential method for METTL7B to play a role in glioma cells, which has not been fully demonstrated at present. In glioma, we analyzed the correlation between METTL7B and the widely reported m6A writer, m6A eraser, and m6A reader. As we speculated, METTL7B has a significant correlation with many molecules, such as ZBP1, IGFBP2, and IGFBP3 (**Figure 9G**).

DISCUSSION

At present, many studies on the prognostic prediction of glioma patients have been reported. Most studies are based on predefined

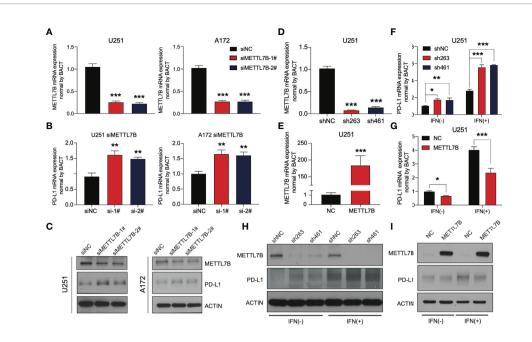


FIGURE 8 | METTL7B affects the expression of PD-L1 in glioma. qRT–PCR showed that the METTL7B siRNAs in (A) U251 and (B) A172 cells could significantly downregulate METTL7B at the transcriptional level. (C) The expression of METTL7B and PD-L1 in U251 siMETTL7B and A172 siMETTL7B cells was detected by Western blot. (D) The expression of METTL7B mRNA in the U251 shMETTL7B cell line was detected by qRT–PCR. (E) The expression of METTL7B mRNA in U251 METTL7B cells was detected by qRT–PCR. (E) The expression of METTL7B mRNA in U251 METTL7B cells was detected by qRT–PCR. The expression of PD-L1 in (F) U251 shMETTL7B and (G) overexpression cell lines in the presence and absence of interferon-gamma (80 ng/mL) was detected by Western blot. *p < 0.05, **p < 0.01, ***p < 0.001.

gene sets to screen prognostic factors. A very detailed analysis based on 24 autophagy characteristic genes constructed an accurate model to predict the prognosis of glioma patients (AUC of 3 years is 0.795) (43). Another study also accurately predicted the prognosis of glioma patients by integrating the expression of 19 lncRNAs related to hypoxia (AUC of 0.862 in one year) (44). We obtained much inspiration from these analyses. The risk prediction model based on a specific gene set can distinguish the prognosis of patients to a certain extent. However, the occurrence and development of the tumor is a highly complex biological process involving a variety of regulatory pathways. We believe that it is not comprehensive to predict only from several aspects of tumor cell development. Given this, we selected the most significant gene as the predictor through various machine learning screening methods starting from the whole genome. We analyzed the tumor as a whole, which achieved an excellent prediction effect (AUC of 0.91 in one year), showing the feasibility of the screening strategy and providing a reference for the development of subsequent cancer prognosis models.

Among these risk genes, the specific biological functions of SEL1L3 and CTC548K16.2 are rarely reported. FAM66C is a long noncoding RNA that has been found to regulate glycolysis and inhibit the proliferation and migration of tumor cells (45, 46). Consistent with these conclusions, we found that the expression of FAM66C in high-risk patients was significantly lower than that in low-risk patients, suggesting that FAM66C is more likely to play the role of a tumor suppressor gene in tumor cells and prevent tumor progression. As a widely reported transcription factor, SOX13

affects cell migration, invasion, and angiogenesis in various cancers and plays a role in an oncogene (47-49). This is closely related to the activation of extracellular matrix remodeling in highrisk people found in our study. For the EFHB gene, Takaoka et al. found through complete exon sequence analysis that EFHB singlenucleotide variation may induce the accumulation of DNA doublestrand breaks in human AML cells (50). Similarly, we found that the coexpression subnetwork of EFHB in glioma regulates DNA metabolism and chromatin remodeling of tumor cells. In addition, MLLT3, as a developmental active epigenetic modifier during the generation of cortical projection neurons, participates in the development of the cerebral cortex by regulating the methylation of histone H3K79 (51). The WGCNA part of this study identified this gene as a factor participant in the development of the nervous system, neuronal differentiation, and ion transport. These results suggest the potential function of MLLT3 in glioma. Most studies on the biological function of risk grading genes are consistent with our results in glioma. These results also suggest that the above genes may have similar roles in glioma.

For predicting whether patients can benefit from PD-1/PD-L1 inhibitor therapy, at present, the detection of PD-L1 has been proven to be an effective method, and the conclusion that patients with high expression of PD-L1 have better overall survival and remission rates after receiving immunotherapy has been widely recognized. In addition to detecting the expression level of PD-L1 at the genomic level, it has also been confirmed that the higher the TMB is, the higher the efficacy of immunotherapy, and the detection of TMB has been written into

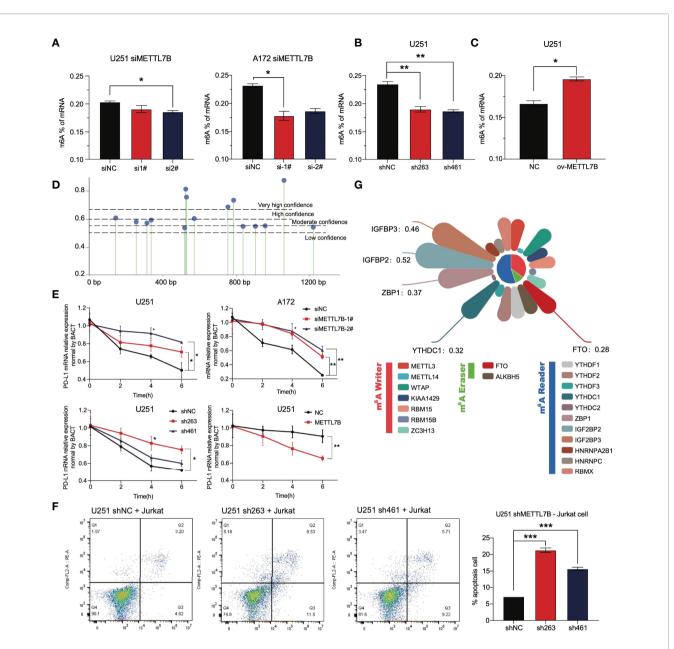


FIGURE 9 | The change in METTL7B in glioma through m6A modification affects the stability of PD-L1 mRNA. (A) In U251 and A172 cells transfected with siMETTL7B, the total level of m6A modification decreased significantly. (B) In the U251 shMETTL7B cell line, the whole level of m6A modification decreased significantly. (C) In U251 cells overexpressing METTL7B, the total level of m6A increased significantly. (D) The potential m6A modification sites on PD-L1 mRNA molecules were predicted based on SRAMP. (E) Actinomycin D (10 µg/mL) inhibited the transcription of nascent RNA in different treatment groups. Cells were collected at 0 h, two h, four h, and six h. The PD-L1 mRNA content in cells was detected by qRT–PCR. (F) The U251 shMETTL7B cell line was incubated with suspended Jurkat lymphocytes for 24 hours (10:1), and the supernatant was collected to detect lymphocyte apoptosis. (G) Correlation coefficient between METTL7B and RNA m6A modification-related molecules in low-grade gliomas. *p < 0.05, **p < 0.01, ***p < 0.001.

the guidance guidelines of multiple clinical immunotherapy trials (52, 53). In addition to these two, a recent study also reported that CNV of plasma cell-free DNA in blood could predict the clinical results of PD-1 inhibitors combined with lenvatinib and other ICI-based hepatobiliary cancer treatments (15). In this study, we found that in the high-risk patients identified by the signature, the expression of PD-L1 increased significantly, accompanied by an increase in TMB and CNV, indicating the

high potential benefits of PD-L1 ICI therapy in high-risk patients in all aspects. Therefore, this signature can accurately predict the prognosis of glioma patients and help identify the benefits of ICI therapy. We verified our conclusion through the TIDE score.

We identified a new functional molecule, METTL7B, for the first time in an *in vitro* experiment in a risk grading gene. We found that knockdown of METTL7B leads to increase in PD-L1, and high expression of PD-L1 is often accompanied by immune escape and malignant progression of the tumor. Recently, Song et al. reported that METTL7B in lung adenocarcinoma reversed resistance to epidermal growth factor receptor (EGFR)-tyrosine kinase inhibitors by changing m6A modification (54). As a new molecule in glioma, we demonstrated that METTL7B participates in the cellular immune response by affecting the mRNA stability of PD-L1 and showed the critical role of m6A in this process. These results suggest that we should pay attention to the role of METTL7B in the occurrence and development of glioma, especially in T cells apoptosis and immune response. In addition, we should also consider the unique correlation between METTL7B and the widely identified m6A participants in gliomas. Considering all the factors, we still need to carry out a large number of *in vitro* experiments to clarify the function of this molecule in gliomas.

DATA AVAILABILITY STATEMENT

The datasets presented in this study can be found in online repositories. The names of the repository/repositories and accession number(s) can be found in the article/**Supplementary Material**.

AUTHOR CONTRIBUTIONS

CL, SW, WX, SH, NX and YZ contributed to conception and design of the study. CL and SW organized the database. WS, SH provides methodological support. CL and SW performed the statistical analysis. QX and TY visualized the project. CL wrote the first draft of the manuscript. WS, WL, SZ, and YW wrote sections of the manuscript. All authors contributed to manuscript revision, read, and approved the submitted version.

FUNDING

This work was supported by the basic research fund of Shenzhen (JCYJ20170405103953336).

REFERENCES

- Ostrom QT, Gittleman H, Truitt G, Boscia A, Kruchko C, Barnholtz-Sloan JS. Cbtrus Statistical Report: Primary Brain and Other Central Nervous System Tumors Diagnosed in the United States in 2011-2015. *Neuro Oncol* (2018) 20 (suppl_4):iv1-iv86. doi: 10.1093/neuonc/noy131
- Ceccarelli M, Barthel FP, Malta TM, Sabedot TS, Salama SR, Murray BA, et al. Molecular Profiling Reveals Biologically Discrete Subsets and Pathways of Progression in Diffuse Glioma. *Cell* (2016) 164(3):550–63. doi: 10.1016/ j.cell.2015.12.028
- Louis DN, Ohgaki H, Wiestler OD, Cavenee WK, Burger PC, Jouvet A, et al. The 2007 Who Classification of Tumours of the Central Nervous System. *Acta Neuropathol* (2007) 114(2):97–109. doi: 10.1007/s00401-007-0243-4
- Perry A, Wesseling P. Histologic Classification of Gliomas. Handb Clin Neurol (2016) 134:71–95. doi: 10.1016/b978-0-12-802997-8.00005-0
- Coons SW, Johnson PC, Scheithauer BW, Yates AJ, Pearl DK. Improving Diagnostic Accuracy and Interobserver Concordance in the Classification and Grading of Primary Gliomas. *Cancer* (1997) 79(7):1381–93. doi: 10.1002/ (sici)1097-0142(19970401)79:7<1381::aid-cncr16>3.0.co;2-w
- Mair MJ, Geurts M, van den Bent MJ, Berghoff AS. A Basic Review on Systemic Treatment Options in Who Grade Ii-Iii Gliomas. *Cancer Treat Rev* (2021) 92:102124. doi: 10.1016/j.ctrv.2020.102124

SUPPLEMENTARY MATERIAL

The Supplementary Material for this article can be found online at: https://www.frontiersin.org/articles/10.3389/fimmu.2022. 909189/full#supplementary-material

Supplementary Figure S1 | Survival analysis of cases in TCGA training cohort stratified by gender, WHO grades and Radiotherapy. Kaplan-Meier curves of OS in (A) male, (B) female, (C) G2, (D) G3, (E) with or (F) without radiotherapy patients based on risk score in low grade glioma population.

Supplementary Figure S2 | Survival analysis of cases in TCGA validation cohort stratified by gender, WHO grades and Radiotherapy. Kaplan-Meier curves of OS in (A) male, (B) female, (C) G2, (D) G3, (E) with or (F) without radiotherapy patients based on risk score in low grade glioma population.

Supplementary Figure S3 | Validation the prognostic performance of patients carrying wild-type IDH1 genes, 1p19q codeletion or MGMT methylation. (A) IDH1 wild-type (WT) and mutation (Mutant) proportions in High Risk or Low Risk. (B) Chromosome 1p19q codeletion or not (Non) proportions in different risk groups. (C) MGMT methylation or not proportions in different risk groups. Kaplan-Meier curves of OS in IDH1 WT (D), IDH1 mutant (E), 1p19q codeletion (F), 1p19q non-codeletion (G), MGMT methylation (H) and MGMT unmethylation (I) based on risk score.

Supplementary Figure S4 | Construction of weighted risk stratification gene coexpression network and functional enrichment analysis. (A) The scale-free fit index for soft thresholding powers. (B) Selecting the soft threshold of 4, checking the node connection number, and verifying the network connectivity of a scale-free network. (C) The correlation between network modules.

Supplementary Figure S5 | Functional enrichment analysis of co-expression networks which containing risk stratification genes. The co-expression module of weighted gene and the Gene Ontology Analysis of all the module gene within (A) MLLT3, FAM66C, (B) SEL1L3, SOX13, (C)EFHB colored by specific cluster ID.

Supplementary Figure S6 | Correlation between marker genes and risk grading genes. Marker genes related to (A) extracellular matrix remodeling, (B) immune response, (C) cytokine, and (D) chemokine release were selected from MsigDB database, and the correlation between the above marker genes and risk grading genes was analyzed in TCGA-LGG data set.

- Smith JS, Chang EF, Lamborn KR, Chang SM, Prados MD, Cha S, et al. Role of Extent of Resection in the Long-Term Outcome of Low-Grade Hemispheric Gliomas. J Clin Oncol (2008) 26(8):1338–45. doi: 10.1200/ jco.2007.13.9337
- McGirt MJ, Chaichana KL, Attenello FJ, Weingart JD, Than K, Burger PC, et al. Extent of Surgical Resection Is Independently Associated With Survival in Patients With Hemispheric Infiltrating Low-Grade Gliomas. *Neurosurgery* (2008) 63(4):700–7; author reply 7-8. doi: 10.1227/01.Neu.0000325729. 41085.73
- Surma-aho O, Niemelä M, Vilkki J, Kouri M, Brander A, Salonen O, et al. Adverse Long-Term Effects of Brain Radiotherapy in Adult Low-Grade Glioma Patients. *Neurology* (2001) 56(10):1285–90. doi: 10.1212/ wnl.56.10.1285
- Daubon T, Hemadou A, Romero Garmendia I, Saleh M. Glioblastoma Immune Landscape and the Potential of New Immunotherapies. Front Immunol (2020) 11:585616. doi: 10.3389/fimmu.2020.585616
- Reardon D, Omuro A, Brandes A, Rieger J, Wick A, Sepulveda J, et al. Os10.3 Randomized Phase 3 Study Evaluating the Efficacy and Safety of Nivolumab Vs Bevacizumab in Patients With Recurrent Glioblastoma: Checkmate 143. *Neuro Oncol* (2017) 19(suppl_3)::iii21-iii. doi: 10.1093/neuonc/nox036.071
- 12. Samstein RM, Lee CH, Shoushtari AN, Hellmann MD, Shen R, Janjigian YY, et al. Tumor Mutational Load Predicts Survival After Immunotherapy Across

Multiple Cancer Types. Nat Genet (2019) 51(2):202-6. doi: 10.1038/s41588-018-0312-8

- Valero C, Lee M, Hoen D, Wang J, Nadeem Z, Patel N, et al. The Association Between Tumor Mutational Burden and Prognosis Is Dependent on Treatment Context. *Nat Genet* (2021) 53(1):11–5. doi: 10.1038/s41588-020-00752-4
- 14. Zhong W, Zhong H, Zhang F, Huang C, Lin Y, Huang J. Characterization of Hypoxia-Related Molecular Subtypes in Clear Cell Renal Cell Carcinoma to Aid Immunotherapy and Targeted Therapy Via Multi-Omics Analysis. Front Mol Biosci (2021) 8:684050. doi: 10.3389/fmolb.2021.684050
- Yang X, Hu Y, Yang K, Wang D, Lin J, Long J, et al. Cell-Free DNA Copy Number Variations Predict Efficacy of Immune Checkpoint Inhibitor-Based Therapy in Hepatobiliary Cancers. *J Immunother Cancer* (2021) 9(5):e001942. doi: 10.1136/jitc-2020-001942
- 16. Jiang P, Gu S, Pan D, Fu J, Sahu A, Hu X, et al. Signatures of T Cell Dysfunction and Exclusion Predict Cancer Immunotherapy Response. *Nat Med* (2018) 24(10):1550–8. doi: 10.1038/s41591-018-0136-1
- Li L, Greene T, Hu B. A Simple Method to Estimate the Time-Dependent Receiver Operating Characteristic Curve and the Area Under the Curve With Right Censored Data. *Stat Methods Med Res* (2018) 27(8):2264–78. doi: 10.1177/0962280216680239
- Balachandran VP, Gonen M, Smith JJ, DeMatteo RP. Nomograms in Oncology: More Than Meets the Eye. *Lancet Oncol* (2015) 16(4):e173–80. doi: 10.1016/s1470-2045(14)71116-7
- Vickers AJ, Elkin EB. Decision Curve Analysis: A Novel Method for Evaluating Prediction Models. *Med Decis Making* (2006) 26(6):565–74. doi: 10.1177/0272989x06295361
- Love MI, Huber W, Anders S. Moderated Estimation of Fold Change and Dispersion for Rna-Seq Data With Deseq2. *Genome Biol* (2014) 15(12):550. doi: 10.1186/s13059-014-0550-8
- Subramanian A, Tamayo P, Mootha VK, Mukherjee S, Ebert BL, Gillette MA, et al. Gene Set Enrichment Analysis: A Knowledge-Based Approach for Interpreting Genome-Wide Expression Profiles. *Proc Natl Acad Sci USA* (2005) 102(43):15545–50. doi: 10.1073/pnas.0506580102
- Langfelder P, Horvath S. Wgcna: An R Package for Weighted Correlation Network Analysis. BMC Bioinform (2008) 9:559. doi: 10.1186/1471-2105-9-559
- Newman AM, Liu CL, Green MR, Gentles AJ, Feng W, Xu Y, et al. Robust Enumeration of Cell Subsets From Tissue Expression Profiles. *Nat Methods* (2015) 12(5):453–7. doi: 10.1038/nmeth.3337
- Charoentong P, Finotello F, Angelova M, Mayer C, Efremova M, Rieder D, et al. Pan-Cancer Immunogenomic Analyses Reveal Genotype-Immunophenotype Relationships and Predictors of Response to Checkpoint Blockade. *Cell Rep* (2017) 18(1):248–62. doi: 10.1016/j.celrep.2016.12.019
- Colaprico A, Silva TC, Olsen C, Garofano L, Cava C, Garolini D, et al. Tcgabiolinks: An R/Bioconductor Package for Integrative Analysis of Tcga Data. *Nucleic Acids Res* (2016) 44(8):e71. doi: 10.1093/nar/gkv1507
- Mermel CH, Schumacher SE, Hill B, Meyerson ML, Beroukhim R, Getz G. Gistic2.0 Facilitates Sensitive and Confident Localization of the Targets of Focal Somatic Copy-Number Alteration in Human Cancers. *Genome Biol* (2011) 12(4):R41. doi: 10.1186/gb-2011-12-4-r41
- Mayakonda A, Lin DC, Assenov Y, Plass C, Koeffler HP. Maftools: Efficient and Comprehensive Analysis of Somatic Variants in Cancer. *Genome Res* (2018) 28(11):1747–56. doi: 10.1101/gr.239244.118
- Liao M, Liao W, Xu N, Li B, Liu F, Zhang S, et al. Lncrna Epb41l4a-As1 Regulates Glycolysis and Glutaminolysis by Mediating Nucleolar Translocation of Hdac2. *EBioMedicine* (2019) 41:200–13. doi: 10.1016/j.ebiom.2019.01.035
- Iasonos A, Schrag D, Raj GV, Panageas KS. How to Build and Interpret a Nomogram for Cancer Prognosis. J Clin Oncol (2008) 26(8):1364–70. doi: 10.1200/jco.2007.12.9791
- Janakiram M, Chinai JM, Zhao A, Sparano JA, Zang X. Hhla2 and Tmigd2: New Immunotherapeutic Targets of the B7 and Cd28 Families. Oncoimmunology (2015) 4(8):e1026534. doi: 10.1080/2162402x.2015.1026534
- Zhang C, Zhang Z, Li F, Shen Z, Qiao Y, Li L, et al. Large-Scale Analysis Reveals the Specific Clinical and Immune Features of B7-H3 in Glioma. Oncoimmunology (2018) 7(11):e1461304. doi: 10.1080/2162402x. 2018.1461304
- Ward-Kavanagh LK, Lin WW, Šedý JR, Ware CF. The Tnf Receptor Superfamily in Co-Stimulating and Co-Inhibitory Responses. *Immunity* (2016) 44(5):1005–19. doi: 10.1016/j.immuni.2016.04.019

- 33. Chrétien S, Zerdes I, Bergh J, Matikas A, Foukakis T. Beyond Pd-1/Pd-L1 Inhibition: What the Future Holds for Breast Cancer Immunotherapy. *Cancers (Basel)* (2019) 11(5):628. doi: 10.3390/cancers11050628
- 34. Wang J, Sanmamed MF, Datar I, Su TT, Ji L, Sun J, et al. Fibrinogen-Like Protein 1 Is a Major Immune Inhibitory Ligand of Lag-3. *Cell* (2019) 176(1-2):334–47. doi: 10.1016/j.cell.2018.11.010
- 35. Wang J, Sun J, Liu LN, Flies DB, Nie X, Toki M, et al. Siglec-15 as an Immune Suppressor and Potential Target for Normalization Cancer Immunotherapy. *Nat Med* (2019) 25(4):656–66. doi: 10.1038/s41591-019-0374-x
- Caccese M, Indraccolo S, Zagonel V, Lombardi G. Pd-1/Pd-L1 Immune-Checkpoint Inhibitors in Glioblastoma: A Concise Review. *Crit Rev Oncol Hematol* (2019) 135:128–34. doi: 10.1016/j.critrevonc.2018.12.002
- Wick W, Hartmann C, Engel C, Stoffels M, Felsberg J, Stockhammer F, et al. Noa-04 Randomized Phase Iii Trial of Sequential Radiochemotherapy of Anaplastic Glioma With Procarbazine, Lomustine, and Vincristine or Temozolomide. J Clin Oncol (2009) 27(35):5874–80. doi: 10.1200/ jco.2009.23.6497
- Lv H, Lv G, Chen C, Zong Q, Jiang G, Ye D, et al. Nad(+) Metabolism Maintains Inducible Pd-L1 Expression to Drive Tumor Immune Evasion. *Cell Metab* (2021) 33(1):110–27.e5. doi: 10.1016/j.cmet.2020.10.021
- Zeng C, Huang W, Li Y, Weng H. Roles of Mettl3 in Cancer: Mechanisms and Therapeutic Targeting. J Hematol Oncol (2020) 13(1):117. doi: 10.1186/ s13045-020-00951-w
- Ruszkowska A. Mettl16, Methyltransferase-Like Protein 16: Current Insights Into Structure and Function. *Int J Mol Sci* (2021) 22(4):2176. doi: 10.3390/ ijms22042176
- Franjic D, Skarica M, Ma S, Arellano JI, Tebbenkamp ATN, Choi J, et al. Transcriptomic Taxonomy and Neurogenic Trajectories of Adult Human, Macaque, and Pig Hippocampal and Entorhinal Cells. *Neuron* (2022) 110 (3):452–69.e14. doi: 10.1016/j.neuron.2021.10.036
- Zhou Y, Zeng P, Li YH, Zhang Z, Cui Q. Sramp: Prediction of Mammalian N6-Methyladenosine (M6a) Sites Based on Sequence-Derived Features. *Nucleic Acids Res* (2016) 44(10):e91. doi: 10.1093/nar/gkw104
- Chen J, Li Y, Han X, Pan Y, Qian X. An Autophagic Gene-Based Signature to Predict the Survival of Patients With Low-Grade Gliomas. *Cancer Med* (2021) 10(5):1848–59. doi: 10.1002/cam4.3748
- 44. Xu S, Tang L, Liu Z, Luo C, Cheng Q. Hypoxia-Related Lncrna Correlates With Prognosis and Immune Microenvironment in Lower-Grade Glioma. *Front Immunol* (2021) 12:731048. doi: 10.3389/fimmu.2021. 731048
- 45. Xiao K, Peng G. Long Non-Coding Rna Fam66c Regulates Glioma Growth Via the Mirna/Lats1 Signaling Pathway. *Biol Chem* (2021) 10.1515/hsz-2021-0333. doi: 10.1515/hsz-2021-0333
- 46. Lei GL, Li Z, Li YY, Hong ZX, Wang S, Bai ZF, et al. Long Noncoding Rna Fam66c Promotes Tumor Progression and Glycolysis in Intrahepatic Cholangiocarcinoma by Regulating Hsa-Mir-23b-3p/Kcnd2 Axis. *Environ Toxicol* (2021) 36(11):2322–32. doi: 10.1002/tox.23346
- Bie LY, Li D, Wei Y, Li N, Chen XB, Luo SX. Sox13 Dependent Pax8 Expression Promotes the Proliferation of Gastric Carcinoma Cells. *Artif Cells Nanomed Biotechnol* (2019) 47(1):3180–7. doi: 10.1080/21691401.2019. 1646751
- Du F, Li X, Feng W, Qiao C, Chen J, Jiang M, et al. Sox13 Promotes Colorectal Cancer Metastasis by Transactivating Snai2 and C-Met. Oncogene (2020) 39 (17):3522–40. doi: 10.1038/s41388-020-1233-4
- 49. Feng M, Fang F, Fang T, Jiao H, You S, Wang X, et al. Sox13 Promotes Hepatocellular Carcinoma Metastasis by Transcriptionally Activating Twist1. *Lab Invest* (2020) 100(11):1400–10. doi: 10.1038/s41374-020-0445-0
- Takaoka K, Kawazu M, Koya J, Yoshimi A, Masamoto Y, Maki H, et al. A Germline Hltf Mutation in Familial Mds Induces DNA Damage Accumulation Through Impaired Pcna Polyubiquitination. *Leukemia* (2019) 33(7):1773–82. doi: 10.1038/s41375-019-0385-0
- Büttner N, Johnsen SA, Kügler S, Vogel T. Af9/Mllt3 Interferes With Tbr1 Expression Through Epigenetic Modification of Histone H3k79 During Development of the Cerebral Cortex. *Proc Natl Acad Sci U S A* (2010) 107 (15):7042–7. doi: 10.1073/pnas.0912041107
- Jardim DL, Goodman A, de Melo Gagliato D, Kurzrock R. The Challenges of Tumor Mutational Burden as an Immunotherapy Biomarker. *Cancer Cell* (2021) 39(2):154–73. doi: 10.1016/j.ccell.2020.10.001

- Addeo A, Friedlaender A, Banna GL, Weiss GJ. Tmb or Not Tmb as a Biomarker: That Is the Question. *Crit Rev Oncol Hematol* (2021) 163:103374. doi: 10.1016/j.critrevonc.2021.103374
- 54. Song H, Liu D, Wang L, Liu K, Chen C, Wang L, et al. Methyltransferase Like 7b Is a Potential Therapeutic Target for Reversing Egfr-Tkis Resistance in Lung Adenocarcinoma. *Mol Cancer* (2022) 21(1):43. doi: 10.1186/s12943-022-01519-7

Conflict of Interest: Author SH was employed by the company Shenzhen Combined Biotech Co., Ltd.

The remaining authors declare that the research was conducted in the absence of any commercial or financial relationships that could be construed as a potential conflict of interest.

The authors declare that this study received funding from the basic research fund of Shenzhen (JCYJ20170405103953336). The funder was not involved in the study

design, collection, analysis, interpretation of data, the writing of this article or the decision to submit it for publication.

Publisher's Note: All claims expressed in this article are solely those of the authors and do not necessarily represent those of their affiliated organizations, or those of the publisher, the editors and the reviewers. Any product that may be evaluated in this article, or claim that may be made by its manufacturer, is not guaranteed or endorsed by the publisher.

Copyright © 2022 Luo, Wang, Shan, Liao, Zhang, Wang, Xin, Yang, Hu, Xie, Xu and Zhang. This is an open-access article distributed under the terms of the Creative Commons Attribution License (CC BY). The use, distribution or reproduction in other forums is permitted, provided the original author(s) and the copyright owner(s) are credited and that the original publication in this journal is cited, in accordance with accepted academic practice. No use, distribution or reproduction is permitted which does not comply with these terms.



Advances in Immune Microenvironment and Immunotherapy of Isocitrate Dehydrogenase Mutated Glioma

Dongming Yan^{1†}, Weicheng Li^{1†}, Qibing Liu^{2,3*} and Kun Yang^{1*}

¹ Department of Neurosurgery, The First Affiliated Hospital of Hainan Medical University, Haikou, China, ² Department of Pharmacology, School of Basic Medicine and Life Sciences, Hainan Medical University, Haikou, China, ³ Department of Pharmacy, The First Affiliated Hospital of Hainan Medical University, Haikou, China

OPEN ACCESS

Edited by:

Xuyao Zhang, Fudan University, China

Reviewed by:

Qiaosi Tang, Calico Life Sciences LLC, United States Yanxin Lu, Zunyi Medical University, China

*Correspondence:

Qibing Liu qibing.liu@hainmc.edu.cn Kun Yang chbyk1379@163.com [†]These authors have contributed equally to this work

Specialty section:

This article was submitted to Cancer Immunity and Immunotherapy, a section of the journal Frontiers in Immunology

Received: 07 April 2022 Accepted: 16 May 2022 Published: 13 June 2022

Citation:

Yan D, Li W, Liu Q and Yang K (2022) Advances in Immune Microenvironment and Immunotherapy of Isocitrate Dehydrogenase Mutated Glioma. Front. Immunol. 13:914618. doi: 10.3389/fimmu.2022.914618 The tumor immune microenvironment and immunotherapy have become current important tumor research concerns. The unique immune microenvironment plays a crucial role in the malignant progression of isocitrate dehydrogenase (IDH) mutant gliomas. IDH mutations in glioma can inhibit tumor-associated immune system evasion of NK cell immune surveillance. Meanwhile, mutant IDH can inhibit classical and alternative complement pathways and directly inhibit T-cell responses by metabolizing isocitrate to D-2-Hydroxyglutaric acid (2-HG). IDH has shown clinically relevant efficacy as a potential target for immunotherapy. This article intends to summarize the research progress in the immunosuppressive microenvironment and immunotherapy of IDH-mutant glioma in recent years in an attempt to provide new ideas for the study of occurrence, progression, and treatment of IDH-mutant glioma.

Keywords: glioma, isocitrate, dehydrogenase, tumor microenvironment, immunotherapy

INTRODUCTION

According to the 2016 WHO revised categorization of central nervous system malignancies and recognized histological characteristics associated with the natural course of the disease, diffuse oligodendrocytes and astrogliomas in adults are rated from grade II to grade IV (1). The presence or absence of isocitrate dehydrogenase (IDH) mutation and chromosomal co-deletion of 1p/19q are used to further classify these malignancies (1, 2). Adult gliomas are classified into three groups: IDH-mutated tumors, 1p/19q co-deletion tumors, and primary oligodendrogliomas. IDH-mutated tumors are associated with a favorable prognosis; non-1p/19q co-deletion tumors and primarily astrocytic gliomas are associated with a moderate prognosis; and IDH wild-type tumors and primarily WHO grade III or IV glioblastomas are associated with a poor prognosis (3). Although most glioblastomas belong to the IDH wild type, IDH mutant glioblastomas have now been identified as a separate disease entity linked to IDH mutant WHO II and III gliomas.

IDH-mutant astrocytomas and oligodendrogliomas (IDH-As and IDH-Os) share the same developmental hierarchy and lineage of glial differentiation, and the volume differences between them can be largely explained by discrete TME and landmark genetic events, as tumor grade increased, malignant cell proliferation was enhanced, undifferentiated glioma cells increased, and

macrophage expression programs overtook microglia in the TME (4). IDH-A is characterized by a loss of function in ATRX that is essentially universal (inactivated in 86 percent of IDH-A). However, in IDH-O, ATRX mutations are uncommon. Comparing IDH-A and IDH-O cells of the same type, there are considerable changes in transcription factor expression and targeting (5). More than 70% of the WHO grade II and III astrocytomas, oligodendrogliomas, and glioblastomas originating from these low-grade lesions have mutations affecting amino acid 132 of IDH1, and alterations affecting IDH2-like amino acids R172 are common in tumors without IDH1 mutations (6). IDH mutations linked to cancer are most commonly found in the arginine residue, which is required for isocitrate recognition (R132 for IDH1, R140, or R172 for IDH2). Isocitrate is effectively converted to D-2-hydroxyglutarate (2-HG) by mutant IDH, resulting in exceptionally high concentrations in TME (7, 8). Tumor-derived 2-HG may operate as an intercellular mediator in TME, affecting nontumor cells.

Immune surveillance relies heavily on the immune system. The immune system can continuously monitor abnormal cells in the body, identify, and destroy them. Immune cells in brain tumors typically include NK cells, T lymphocytes, dendritic cells (DCs), and microglia (9). Tumor-infiltrating immune cells are part of the complex tumor microenvironment (TME) and may play a significant role in either preventing or promoting tumor growth. Tumorigenesis is characterized by immune evasion, which is a significant obstacle to effective treatment for cancer (10). Although significant progress has been made in tumor immunotherapy approaches and clinical efficacy over the previous years, the association between IDH mutations and a better prognosis in glioma remains largely unknown. IDH may be an ideal target for targeted therapy and is expected to become the preferred target of immunotherapy, thus providing a new perspective for the clinical treatment of glioma. Much of the discussion below is primarily related to the immune microenvironment and immunotherapy in IDH-mutant gliomas.

THE IMMUNE MICROENVIRONMENT OF ISOCITRATE DEHYDROGENASE MUTANT GLIOMAS

IDH Mutations Suppress the Tumor-Associated Immune System

In the process of tumorigenesis and malignant progression, tumor-infiltrating immune inflammatory cells play an important role. Once recruited into the tumor microenvironment, these cells can promote the malignant progression of the cancer cell phenotype. In addition, they also establish a complex network of cell-to-cell interactions, which help to improve and maintain the immunosuppressive microenvironment, promote immune escape, and ultimately promote the development of tumors. Immune infiltration is lower in Mutant IDH1/2 gliomas than in wild-type IDH1/2 gliomas (11–13). IDH-As are more heavily infiltrated by monocytic-lineage cells derived from circulation, they upregulate myeloid-cell chemotaxis genes (CSF1, FLT3LG) and upstream transcription factors (NFKB1), compared to IDH-Os (5). Moreover, immune cell (including M0, M1, and M2 macrophages) infiltration in WHO II IDH-As was generally higher than in WHO II IDH-Os, whereas T cells (CD3+, CD4+, and CD8+), cytotoxic cells, and T helper cells infiltrated in IDH-Os were significantly higher than those in IDH-As (14, 15). Reduced tumor purity (i.e., increased invasion of glioma by non-tumor cells such as immune and stromal cells) was linked to higher malignancy and shorter survival (16). A significant increase in T cells (CD3+), cytotoxic cells, and T helper cells infiltration were observed in recurrent IDH-mutant gliomas compared with primary IDH-mutant tumors, while the opposite was observed for regulatory T cells, this change was associated with prior or not radiotherapy (14). CCL-2 is thought to attract white blood cells (monocytes, memory T cells, and DCs) to inflammatory areas caused by tissue damage or infection, CXCL-2 has chemotactic effects on neutrophils, monocytes, and macrophages (17, 18). C5a is a mediator of chemotaxis and cellular release reactions, playing an essential role in innate immunity and adaptive immunity as well (19, 20). Cytokine arrays revealed that the three genes mentioned above were down-regulated at the mRNA and protein levels in IDH1mutated tumors, suggesting that immune infiltration and chemotaxis are regulated by IDH1 mutations and that a reduced aggressive part of the tumor-associated immune system could provide IDH-mutant glioma patients with a longer survival duration (12).

IDH Mutations Evade NK Cell Immune Surveillance

The accumulation of natural killer cells and regulatory T cells leads to leukopenia and immune impairment (21). Natural killer (NK) cells serve as the main effector cells of cancer in innate immunity and are the first line of defense against diseases including malignancies. To evade NK cell-mediated immunity, malignant tumors employ a variety of tissue and mutationspecific strategies. NK cell activity is regulated by the combination of signals that activate and inhibit NK cell surface receptors (22). The activation of NK cells leads to the release of cytotoxic granules containing perforin, various granzymes, and cytokine production, most prominently IFN- γ (23, 24) Killer cell Lectin-like receptor K1 (also known as NKG2D, KLR) is an activated NK cell and CD8+ T cell receptor that mediates cytotoxicity by attaching stress-induced ligands to target cells. MHC class I associated chains A and B (MICA, MICB) and the UL16-binding protein family (ULBP1-6) are among the NKG2D ligands (NKG2DLs) (25). The expression of NKG2DLs in tumor cells is induced by oncogenic stress caused by genetic instability or metabolic derangement, and the expression of these ligands may be essential for antitumor immunity during the elimination phase of innate immune tumor surveillance (26, 27). Following activation of NKG2DLs, NKG2D-activated receptors enhance cytokine production and perforin-mediated cytotoxicity (28), when the expression of NKG2DL in tumors is proportionate to NK-mediated cytotoxicity (29).

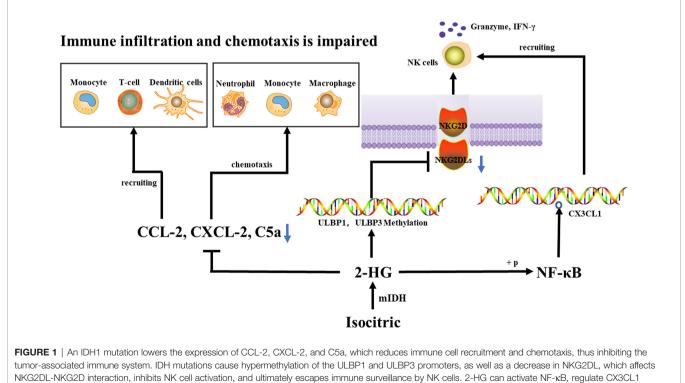
ULBP1 and ULBP3 are MHC class I proteins bound through the glycosylphosphatidylinositol anchor membrane (30). Both ligands are members of the UL16 bound NKG2DLs with 6 members (ULBP₁₋₆) (31). NKG2D receptors on NK cells identify membrane-bound ULBP1 and ULBP3, and these ligands activate NK cells and cause target cell lysis through NKG2D binding (26). IDH wild-type tumors had significantly high levels of NKG2DLs, ULBP1, and ULBP3, while IDH mutant tumors did not, the promoter methylation levels of ULBP1 and ULBP3 were higher in IDH-mutant tumors than in IDH wildtype tumors, ULBP1 and ULBP3 were transcriptionally silenced when their promoters were hypermethylated, thus decreasing the NKG2DL expression, which in turn affected NK cell activation and enhanced resistance to NK-mediated cytotoxicity (32), thereby evading immune surveillance by NK cells. Interestingly, in IDH1-mutant gliomas, 2-HG can activate NFκB, regulate CX3CL1 expression, and then CX3CL1 recruits NK cells to the tumor location (5, 33). Moreover, decreased MHC-I expression in IDH-mutant gliomas is associated with higher DNA methylation levels of MHC-I HLA genes (34). Reduced expression of HLA class I molecules leads to upregulation of activated NK receptor recognized ligands, facilitating NK cells mediated lysis (35) (Figure 1).

2-Hydroxyglutarate Inhibits Classical and Alternative Complement Pathways

Complement is an important aspect of immune surveillance mechanisms in host tumor cells but may play an opposite role in

carcinogenesis, as activating complement causes inflammation, which promotes tumor development. Complement on tumor cells could indeed be directly activated by tumor cells themselves (36, 37), or by tumor-reactive antibodies that attach to neoantigens on the surface of tumor cells, allowing membrane attack complex (MAC) mediated lysis and boosting tumor phagocytosis (38).

C3b (iC3b) was deposited on target cells after complement activation, facilitating phagocytosis (39). C3(C3b) was deposited on the surface of IDH wild-type and mutated glioma cells. Compared with IDH wild-type gliomas, IDH mutants tend to have lower complement depositing on the surface of tiny blood vessels and capillaries. IDH mutant glioblastoma had lower levels of C3 (C3b) deposition in the necrotic area as compared with IDH wild-type glioblastoma. 2-HG significantly reduced C3 deposition on cells through a dose-dependent approach, inhibited C3b (iC3b) complement-mediated phagocytosis and opsonization, and inhibited the assembling of C5 but not C3 convertases in the classical complement activation pathway. Complement-mediated cellular damage is inhibited at numerous phases of the complement activation process (40), rather than inhibiting complement activity through simple calcium linkages (41). The alternate complement route is a separate main complement activation mechanism that amplifies complement activation triggered by other pathways. C3b is required with both C3 but also C5 convertases in the alternate pathway. The assembling of C3/C5 conversion enzymes in the complement activation alternative route was inhibited by



expression, and then CX3CL1 recruit NK cells to the tumor location.

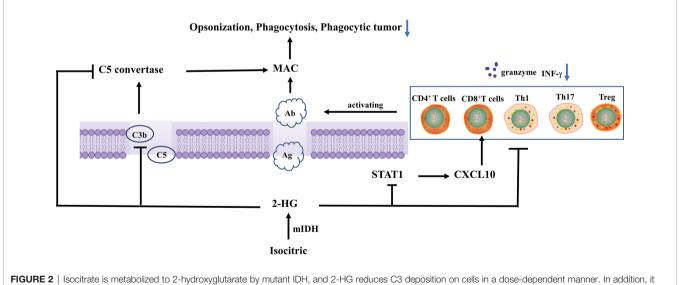
2-HG, while the activity of prebuilt C3/C5 conversion enzymes in the complement activation alternative route was not significantly affected. During pre-assembly and assembly, there was a biochemical and functionality transition that occurs. Complement activation was inhibited by 2-HG, which reduces MAC-mediated brain cancer cell damage (40).

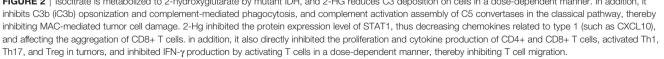
2-Hydroxyglutaric Acid Directly Inhibits T Cell Responses

Tumor-reactive T cells, which are triggered by tumor antigenpresenting cells like DCs, multiply and release cytotoxin-like granzymes and create inflammatory cytokines like IFN-γ, playing a crucial role in tumor immune surveillance (42, 43). T cells also stimulate humoral responses, inducing the production of tumorspecific antibodies to activate complement on tumor cells, resulting in the assembly of MAC pores, lysis, identification, and phagocytosis by giant cells. T-cell factors are a core component of acquired immunity, and DCs plays a key role in T-cell activation. In primary IDH1-R132H grade II/III gliomas, less infiltration of CD8⁺ T cells in the TME is associated with long-term survival (11, 44). Extensive infiltration of Treg cells into tumor tissue is often associated with poor prognosis in cancer patients, and Treg cell depletion enhances antitumor immune responses, but may also trigger autoimmunity (45). Studies demonstrated that 2-HG in IDH mutant grade III and IV gliomas neither decreased the differentiation of DCs nor the functionality of differentiated DCs nor interfered with the processing or presentation of DC antigens. 2-HG did not inhibit T cell function indirectly through DC differentiation, rather it directly suppressed CD4⁺ and CD8⁺ T cells, activated Th1 and Th17, and regulated T cell (Treg) proliferation and

cytokine generation in malignancies. IFN- γ production by activated T cells was inhibited in a dose-dependent manner, which inhibited the migration of T cells (40). In addition, 2-HG reduces antigen-presenting characteristics in macrophages, suppresses macrophage phenotype, and affects T-cell proliferation and effector cytokine production (46). 2-HG generated from tumors with IDH mutations can be taken up by T cells, the accumulation of intracellular 2-HG leads to increased apoptosis, decreased proliferation, and decreased Treg (47). Furthermore, high levels of 2-HG were found in T cells of IDH mutated AML patients, D-2HG caused HIF-1a protein instability, which led to a metabolic shift toward oxidative phosphorylation, an increase in regulatory T cell (Treg) frequency, and a decrease in Th17 polarization (48). It was also reported that NFAT transcription and polyamine synthesis were disturbed after 2-HG uptake, thus decreasing the ATP/ADP ratio and thereby inhibiting T cell activity and proliferation (49).

Cytotoxic CD8⁺ T cells can recognize tumor-associated antigens in the presence of major histocompatibility complex (MHC) class I expressing tumors (50–52). Tumor-specific type 1 CD8⁺ T cells (mainly secreting IFN- γ) can effectively enter brain tumor sites through the type 1 chemokine CXCL10 and effectively kill tumor cells (53–56). Gary et al. (32) detected a lower level of type 1-related effector molecules, chemokines, and CD8⁺ T cells in IDH mutant gliomas after analyzing the clinical specimens and TCGA RNA-seq data. Their orthotopic syngeneic glioma model demonstrated that IDH1 R132H mutation suppressed the STAT1 protein expression *via* 2-HG, thus decreasing the type 1-associated chemokines such as CXCL10 and affecting CD8⁺ T cell aggregation (13) (**Figure 2**).





Tumor-Derived Tiny Extracellular Vesicles and Immune Microenvironment

Tumor-derived tiny extracellular vesicles (TEX) contain a series of proteins, nucleic acids, and lipids that are similar in origin to tumors (57). TEX could transmit information from the tumor to cells near or far away from the tumor (including the bone marrow and lymphatic system), enabling cell-to-cell communication (58). To drive tumor growth, TEX can mediate juxtacrine, paracrine, and endocrine-like signals (59–62). TEX is an appealing candidate for regulating systemic tumor immune responses due to its physiologic origins and biodistribution features. The immunosuppressive effects of TEX are mediated by their immunosuppressive freight, and the intercellular distribution of these cargo components triggers protumorigenic reprogramming of immune cells, which eventually promotes tumor growth (63–65).

Recent studies have shown that IDH mutant glioma cells produced more TEX than IDH wild-type glioma cells and were able to cross the blood-brain barrier to target anatomical sites (bone marrow, spleen) with abundant immune cells for phenotypic/functional regulation of circulating immune cells. Meanwhile, the expression of immune cell-related genes (ULBP1, ULBP3, RBP1, and CCL2) was decreased in IDH mutant glioma TEX, which were important regulators of immunosuppression and shape the immune cell composition of the systemic and local immune landscape (66).

IMMUNOTHERAPY OF ISOCITRATE DEHYDROGENASE MUTANT GLIOMA

Neurosurgical resection and adjuvant chemoradiation can prolong the survival of glioma patients, but recurrence occurs in most diffuse glioma cases, which largely limits the expected lifespan of the patients. Most currently available novel biological therapies have failed to significantly reduce the mortality and recurrence rate, which urges researchers to develop new therapeutic methods for glioma patients. Immunotherapies that target particular immunoregulatory molecules, known as ICIs and vaccine-mediated immunity, have demonstrated clinically meaningful effectiveness in a variety of tumor types, and have emerged as a distinct therapeutic strategy in cancer biology.

Immune checkpoints are a variety of immunosuppressive pathways in the immune system which are important for keeping self-tolerance and controlling the timing and amplitude of physiological immune responses in peripheral tissues to reduce collateral tissue injury (67). Tumor cells stimulate myeloid-derived suppressor cells to upregulate PD-L1 on the cell surface involvement in T cell immune checkpoints (68–71). Under normal circumstances, PD-L1 can bind to PD-1 on T cells and inhibit the activation of T cells, thereby avoiding the occurrence of autoimmune diseases. In tumors, after the combination of PD-L1 on the tumor cell membrane and PD-1, killer CD8+ T cells no longer recognize and kill tumor cells, which provides tumor cells with an opportunity to survive and develop. In gliomas, IDH mutant has been linked to reduced immunological checkpoint(PD-1, CTLA-4, LAG3, and IDO1) expression and immunosuppressive cell infiltration (72, 73). Compared with IDH-Os, IDH-As appear to be more responsive to checkpoint immunotherapy, one reason for the relatively poor anti-checkpoint immunotherapy of IDH-Os is its reduced expression of PD-L1 and other checkpoint molecules, another reason is higher levels of T cell rejection, promoting T cell dysfunction and immunotherapy resistance (15, 74, 75). Berghoff et al. observed that the IDH mutation status was the main factor affecting PD-L1 expression in diffuse gliomas, 2hydroxyglutarate enhanced DNA methylation and suppresses PD-L1 expression (76-78). Because IDH mutant patients have lower PD-L1 expression, inhibitors of the PD1/PD-L1 immunological checkpoint are not recommended and other options should be explored (79). Some scholars have also proposed that targeted immunotherapy of IDH-mutant gliomas with decitabine can recover NKG2DLs expression and NK cell activation in experimental gliomas (32). In lung cancer and colorectal cancer, decitabine triggers tumor PD-L1 expression by inducing DNA hypomethylation, triggering an anticancer immune response, and remodeling the tumor microenvironment to improve the effect of PD-L1 immunotherapy (80, 81). We speculate that decitabine can also trigger PD-L1 expression in IDH-mutant glioma cells.

IDH is a promising target for immunization from an immunological standpoint since it is a tumor-specific latent neoantigen with significant homogeneity and penetration in all cancerous cells (82, 83). In glioma patients, R132H-mutated IDH1 is spontaneously processed, and an immunodominant epitope in the p123-142 region of MHC class II molecules is presented to CD4+ T cells, inducing spontaneous mutationspecific TH1 polarization and generation of mutation-specific antibodies. Schumacher et al. (43) discovered that IDH1R132H contained immunogenic epitopes suitable for mutation-specific vaccination, and inoculation of peptide vaccine IDH1 (R132H) P123-142 in homologous MHC humanized mice induced specific therapeutic T-helper cell responses and mutationspecific antibodies (84).

This notion is further supported by the study of Serena et al. (44), who constructed a mouse intracranial glioma model with IDH1R132H mutation and treated mIDH1-GL261 with mIDH1 peptide glioma mice. They found that the immune system could effectively target the R132H mutation and modify TME, increase the number of peripheral CD8+ T cells, IFN- γ production, and anti-IDH1 mutant antibodies, up-regulated intratumoral IFN- γ , granzyme- β , and perforin-1, and downregulated TGF- β 2 and IL-10, thereby significantly prolonging survival of the mice. NOA-16 is the first IDH1R132H peptide vaccine in a multicenter stage I clinical study in humans. According to the latest report from this trial, more than 90% of patients developed vaccine-induced IDH1R132H-specific T cell reactions and peripheral T cell responses (85).

R132H-IDH1 inhibitor (AGI-5198) blocked, in a dosedependent manner, the ability of the mutant enzyme (mIDH1)

to produce R-2-hydroxyglutarate (R-2HG), delayed growth and promoted differentiation of glioma cells (86). IDH-C35, a unique IDH1 inhibitor, can reverse the immunosuppressive effect of mutant IDH1. In immortalized NHAs and a homogeneous mouse glioma model, Gary et al. demonstrated that restoration of STAT1 with IDH-C35 reversed the reduction in CXCL10 and T cell accumulation, when combined with the vaccine, it could enhance anti-tumor immune function and the performance of peptide vaccines and improve asymptomatic survival of IDHmutant glioma patients (13, 78). In addition, IDH-C35 can also reduce the level of PD-L1 DNA methylation, increase the expression of PD-L1 on mIDH1 glioma cells in vivo, reshape the tumor microenvironment, and improve the effect of PD-L1 immunotherapy (87). Therefore, IDH inhibitors should be used in conjunction with immunotherapy. Moreover, granulocyte colony-stimulating factor (G-CSF) released by mutIDH1 glioma stem-like cells promoted myeloid cell reprogramming, which improved the efficiency of immune-stimulatory gene therapy (88) (Figure 3).

CONCLUSION

IDH1 is a reliable diagnostic and prognostic marker for identifying low-grade gliomas and distinguishing between secondary and primary GBM (89). IDH-mutant gliomas evade immune cell surveillance by reducing the immune-related cellular content and function of effector immune cells, downregulating NKG2D ligand expression, and overproducing 2-HG to inhibit complement pathways and T cell responses to interfere with immune surveillance and affect TME. The immune evasion ability of tumors provides an opportunity to harness immunotherapies against cancer cells.

Immunotherapies, particularly immune checkpoint inhibitors, have seen dramatic responses in various tumor types. Nevertheless, existing immunotherapies do not work on all malignancies, and even when they do, the results aren't necessarily long-lasting. IDH-mutant gliomas have a unique immune microenvironment, 2-hydroxyglutarate is an oncogenic metabolite produced by mutant IDH with neurotoxic effects. Controlling 2-HG production and its effects may hold great promise for glioma therapy. Currently, the therapeutic efficacy of mutation-specific IDH inhibitors may partly depend on restoring the immune response in solid tumors by removing 2-HG. The combination of checkpoint blockade, decitabine, and IDH1R132H-specific vaccine may be more effective. Growing evidence certainly suggests that IDH mutations may play a broad role in glioma-associated immunosuppression. However, our understanding of the molecular mechanisms responsible for this unique immune microenvironment remains limited. For example, Why IDH-Os and IDH-As have different immune cell infiltration and PD-L1 expression? Does the localization of IDH1 in different places (cytoplasmic and peroxisome) affect immune cell infiltration and WHO grade? The research on IDH-mutant

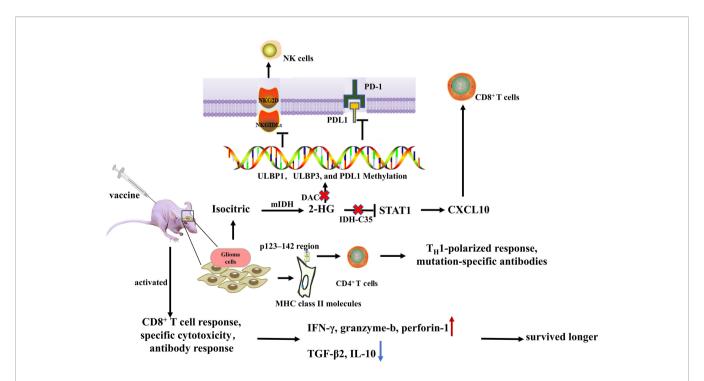


FIGURE 3 | Administration of peptide vaccine IDH1 (R132H) induced specific therapeutic T-helper cell responses and mutation-specific antibodies. After mIDH1 peptide injection, the immune system can effectively target R132H mutation and modify the tumor microenvironment by increasing the number of peripheral CD8+T cells, IFN-γ production and anti-IDH1 mutati antibodies, up-regulating intratumoral IFN- γ, granzyme-b, and perforin-1, and downregulating TGF-β2 and IL-10, thereby significantly prolonging survival of the mice. IDH-C35 reduces ULBP1, ULBP3, and PD-L1 DNA methylation levels and restores STAT1 to reverse CXCL10 and T cell accumulation.

332

gliomas and the immunosuppressive mechanisms in the glioma microenvironment will help develop immunotherapy drugs and design new immunotherapies to target potential glioma therapeutic targets and kill tumor cells more efficiently.

AUTHOR CONTRIBUTIONS

DY, KY, and QL designed the paper and recommended a structure for the review. DY and WL wrote the initial draft and prepared figures. DY, KY, and QL completed the final preparation and editing of the manuscript. DY created the

REFERENCES

- Louis DN, Perry A, Reifenberger G, von Deimling A, Figarella-Branger D, Cavenee WK, et al. The 2016 World Health Organization Classification of Tumors of the Central Nervous System: A Summary. *Acta Neuropathol* (2016) 131(6):803–20. doi: 10.1007/s00401-016-1545-1
- Reifenberger G, Wirsching HG, Knobbe-Thomsen CB, Weller M. Advances in the Molecular Genetics of Gliomas - Implications for Classification and Therapy. Nat Rev Clin Oncol (2017) 14(7):434–52. doi: 10.1038/ nrclinonc.2016.204
- Weller M, Wick W, Aldape K, Brada M, Berger M, Pfister SM, et al. Glioma. Nat Rev Dis Primers (2015) 1:15017. doi: 10.1038/nrdp.2015.17
- Venteicher AS, Tirosh I, Hebert C, Yizhak K, Neftel C, Filbin MG, et al. Decoupling Genetics, Lineages, and Microenvironment in Idh-Mutant Gliomas by Single-Cell Rna-Seq. *Science* (2017) 355(6332):eaai8478. doi: 10.1126/science.aai8478
- Babikir H, Wang L, Shamardani K, Catalan F, Sudhir S, MK A, et al. Atrx Regulates Glial Identity and the Tumor Microenvironment in Idh-Mutant Glioma. *Genome Biol* (2021) 22(1):311. doi: 10.1186/s13059-021-02535-4
- Yan H, Parsons DW, Jin G, McLendon R, Rasheed BA, Yuan W, et al. Idh1 and Idh2 Mutations in Gliomas. N Engl J Med (2009) 360(8):765–73. doi: 10.1056/NEJMoa0808710
- Dang L, White DW, Gross S, Bennett BD, Bittinger MA, Driggers EM, et al. Cancer-Associated Idh1 Mutations Produce 2-Hydroxyglutarate. *Nature* (2009) 462(7274):739–44. doi: 10.1038/nature08617
- Dang L, Yen K, Attar EC. Idh Mutations in Cancer and Progress Toward Development of Targeted Therapeutics. Ann Oncol (2016) 27(4):599–608. doi: 10.1093/annonc/mdw013
- D'Alessio A, Proietti G, Sica G, Scicchitano BM. Pathological and Molecular Features of Glioblastoma and Its Peritumoral Tissue. *Cancers (Basel)* (2019) 11(4):469. doi: 10.3390/cancers11040469
- Hanahan D, Weinberg RA. Hallmarks of Cancer: The Next Generation. Cell (2011) 144(5):646–74. doi: 10.1016/j.cell.2011.02.013
- Bunse L, Pusch S, Bunse T, Sahm F, Sanghvi K, Friedrich M, et al. Suppression of Antitumor T Cell Immunity by the Oncometabolite (R)-2-Hydroxyglutarate. Nat Med (2018) 24(8):1192–203. doi: 10.1038/s41591-018-0095-6
- Amankulor NM, Kim Y, Arora S, Kargl J, Szulzewsky F, Hanke M, et al. Mutant Idh1 Regulates the Tumor-Associated Immune System in Gliomas. *Genes Dev* (2017) 31(8):774–86. doi: 10.1101/gad.294991.116
- Kohanbash G, DA C, Shrivastav S, BJ A, Jahan N, Mazor T, et al. Isocitrate Dehydrogenase Mutations Suppress Stat1 and Cd8+ T Cell Accumulation in Gliomas. J Clin Invest (2017) 127(4):1425–37. doi: 10.1172/JCI90644
- Makarevic A, Rapp C, Dettling S, Reuss D, Jungk C, Abdollahi A, et al. Increased Radiation-Associated T-Cell Infiltration in Recurrent Idh-Mutant Glioma. Int J Mol Sci (2020) 21(20):7801. doi: 10.3390/ijms21207801
- Zhao B, Xia Y, Yang F, Wang Y, Wang Y, Wang Y, et al. Molecular Landscape of Idh-Mutant Astrocytoma and Oligodendroglioma Grade 2 Indicate Tumor Purity as an Underlying Genomic Factor. *Mol Med* (2022) 28(1):34. doi: 10.1186/s10020-022-00454-z

figures. All authors contributed to the article and approved the submitted version.

FUNDING

This work was supported by Hainan Medical University Postgraduate Innovative Research Project Category B (HYYS2021B16)and the National Natural Science Foundation of China (GKJ200032). The funders had no role in the study design, data collection, analysis, decision to publish, or preparation of the manuscript.

- Zhang C, Cheng W, Ren X, Wang Z, Liu X, Li G, et al. Tumor Purity as an Underlying Key Factor in Glioma. *Clin Cancer Res* (2017) 23(20):6279–91. doi: 10.1158/1078-0432.CCR-16-2598
- Rollins BJ. Chemokines. Blood (1997) 90(3):909-28. doi: 10.1182/ blood.V90.3.909
- Yoshie O, Imai T, Nomiyama H. Chemokines in Immunity. Adv Immunol (2001) 78:57–110. doi: 10.1016/S0065-2776(01)78002-9
- Guo RF, Ward PA. Role of C5a in Inflammatory Responses. Annu Rev Immunol (2005) 23:821–52. doi: 10.1146/annurev.immunol.23.021704.115835
- Darling VR, Hauke RJ, Tarantolo S, Agrawal DK. Immunological Effects and Therapeutic Role of C5a in Cancer. *Expert Rev Clin Immunol* (2015) 11 (2):255–63. doi: 10.1586/1744666X.2015.983081
- Sokratous G, Polyzoidis S, Ashkan K. Immune Infiltration of Tumor Microenvironment Following Immunotherapy for Glioblastoma Multiforme. *Hum Vaccin Immunother* (2017) 13(11):2575–82. doi: 10.1080/ 21645515.2017.1303582
- Moretta A, Bottino C, Vitale M, Pende D. Activating Receptors and Coreceptors Involved in Human Natural Killer Cell-Mediated Cytolysis. *Annu Rev Immunol* (2001) 19:197–223. doi: 10.1146/annurev.immunol.19.1.197
- Voskoboinik I, Smyth MJ, Trapani JA. Perforin-Mediated Target-Cell Death and Immune Homeostasis. *Nat Rev Immunol* (2006) 6(12):940–52. doi: 10.1038/nri1983
- Krzewski K, Coligan JE. Human Nk Cell Lytic Granules and Regulation of Their Exocytosis. *Front Immunol* (2012) 3:335. doi: 10.3389/fimmu. 2012.00335
- Eagle RA, Trowsdale J. Promiscuity and the Single Receptor: Nkg2d. Nat Rev Immunol (2007) 7(9):737–44. doi: 10.1038/nri2144
- V Groh TS. Immunobiology of Human Nkg2d and Its Ligands. Curr Top Microbiol Immunol (2006) 298:121–38. doi: 10.1007/3-540-27743-9_6
- Nausch N, Cerwenka A. Nkg2d Ligands in Tumor Immunity. Oncogene (2008) 27(45):5944–58. doi: 10.1038/onc.2008.272
- Bauer S, Groh V, Wu J, Steinle A, Phillips JH, Lanier LL, et al. Activation of Nk Cells and T Cells by Nkg2d, a Receptor for Stress-Inducible Mica. *Science* (1999) 285(5428):727–9. doi: 10.1126/science.285.5428.727
- Pende D, Rivera P, Marcenaro S, Chang C-C. Major Histocompatibility Complex Class I-Related Chain a and Ul16-Binding Protein Expression on Tumor Cell Lines of Different Histotypes: Analysis of Tumor Susceptibility to Nkg2d-Dependent Natural Killer Cell Cytotoxicity. *Cancer Res* (2002) 62 (21):6178–86.
- Paulick MG, Bertozzi CR. The Glycosylphosphatidylinositol Anchor: A Complex Membrane-Anchoring Structure for Proteins. *Biochemistry* (2008) 47(27):6991–7000. doi: 10.1021/bi8006324
- Cosman D, Ilberg JM, Claire L. Sutherland, Wilson Chin, Richard Armitage. Ulbps, Novel Mhc Class I–Related Molecules, Bind to Cmv Glycoprotein Ul16 and Stimulate Nk Cytotoxicity Through the Nkg2d Receptor. *Immunity* (2001) 14(2):123–33. doi: 10.1016/s1074-7613(01)00095-4
- 32. Zhang X, Rao A, Sette P, Deibert C, Pomerantz A, Kim WJ, et al. Idh Mutant Gliomas Escape Natural Killer Cell Immune Surveillance by Downregulation of Nkg2d Ligand Expression. *Neuro Oncol* (2016) 18(10):1402–12. doi: 10.1093/neuonc/now061

- 33. Ren F, Zhao Q, Huang L, Zheng Y, Li L, He Q, et al. The R132h Mutation in Idh1 Promotes the Recruitment of Nk Cells Through Cx3cl1/Cx3cr1 Chemotaxis and Is Correlated With a Better Prognosis in Gliomas. *Immunol Cell Biol* (2019) 97(5):457–69. doi: 10.1111/imcb.12225
- 34. Luoto S, Hermelo I, Vuorinen EM, Hannus P, Kesseli J, Nykter M, et al. Computational Characterization of Suppressive Immune Microenvironments in Glioblastoma. *Cancer Res* (2018) 78(19):5574–85. doi: 10.1158/0008-5472.CAN-17-3714
- Castriconi R, Daga A, Dondero A, Zona G, Poliani PL, Melotti A, et al. Nk Cells Recognize and Kill Human Glioblastoma Cells With Stem Cell-Like Properties. J Immunol (2009) 182(6):3530–9. doi: 10.4049/jimmunol.0802845
- Praz F, Lesavre P. Alternative Pathway of Complement Activation by Human Lymphoblastoid B and T Cell Lines. J Immunol (1983) 131(3):1396–9.
- 37. Kurita M, Matsumoto M, Tsuji S, Kawakami M, Suzuki Y, Hayashi H. Antibody-Independent Classical Complement Pathway Activation and Homologous C3 Deposition in Xeroderma Pigmentosum Cell Lines. Clin Exp Immunol (1999) 116(3):547–53. doi: 10.1046/j.1365-2249.1999.00923.x
- Rogers LM, Veeramani S, Weiner GJ. Complement in Monoclonal Antibody Therapy of Cancer. *Immunol Res* (2014) 59(1-3):203–10. doi: 10.1007/s12026-014-8542-z
- Ehlenberger AG, Nussenzweig V. The Role of Membrane Receptors for C3b and C3d in Phagocytosis. J Exp Med (1977) 145(2):357–71. doi: 10.1084/ jem.145.2.357
- Zhang L, Sorensen MD, Kristensen BW, Reifenberger G, McIntyre TM, Lin F. D-2-Hydroxyglutarate Is an Intercellular Mediator in Idh-Mutant Gliomas Inhibiting Complement and T Cells. *Clin Cancer Res* (2018) 24(21):5381–91. doi: 10.1158/1078-0432.CCR-17-3855
- Unruh D, Schwarze SR, Khoury L, Thomas C, Wu M, Chen L, et al. Mutant Idh1 and Thrombosis in Gliomas. *Acta Neuropathol* (2016) 132(6):917–30. doi: 10.1007/s00401-016-1620-7
- 42. Swann JB, Smyth MJ. Immune Surveillance of Tumors. J Clin Invest (2007) 117(5):1137–46. doi: 10.1172/JCI31405
- Ho PC, Kaech SM. Reenergizing T Cell Anti-Tumor Immunity by Harnessing Immunometabolic Checkpoints and Machineries. *Curr Opin Immunol* (2017) 46:38–44. doi: 10.1016/j.coi.2017.04.003
- 44. Yang I, Tihan T, Han SJ, Wrensch MR, Wiencke J, Sughrue ME, et al. Cd8+ T-Cell Infiltrate in Newly Diagnosed Glioblastoma Is Associated With Long-Term Survival. J Clin Neurosci (2010) 17(11):1381–5. doi: 10.1016/j.jocn.2010.03.031
- Tanaka A, Sakaguchi S. Targeting Treg Cells in Cancer Immunotherapy. Eur J Immunol (2019) 49(8):1140–6. doi: 10.1002/eji.201847659
- 46. van Dierendonck X, de Goede KE, Van den Bossche J. Idh-Mutant Brain Tumors Hit the Achilles' Heel of Macrophages With R-2-Hydroxyglutarate. *Trends Cancer* (2021) 7(8):666–7. doi: 10.1016/j.trecan.2021.06.003
- Richardson LG, Nieman LT, Stemmer-Rachamimov AO, Zheng XS, Stafford K, Nagashima H, et al. Idh-Mutant Gliomas Harbor Fewer Regulatory T Cells in Humans and Mice. *Oncoimmunology* (2020) 9(1):1806662. doi: 10.1080/ 2162402X.2020.1806662
- Bottcher M, Renner K, Berger R, Mentz K, Thomas S, Cardenas-Conejo ZE, et al. D-2-Hydroxyglutarate Interferes With Hif-1alpha Stability Skewing T-Cell Metabolism Towards Oxidative Phosphorylation and Impairing Th17 Polarization. Oncoimmunology (2018) 7(7):e1445454. doi: 10.1080/ 2162402X.2018.1445454
- Friedrich M, Bunse L, Wick W, Platten M. Perspectives of Immunotherapy in Isocitrate Dehydrogenase-Mutant Gliomas. *Curr Opin Oncol* (2018) 30 (6):368–74. doi: 10.1097/CCO.000000000000478
- Liau LM, Black KL, Martin NA, Sykes SN, Bronstein JM, Jouben-Steele L, et al. Treatment of a Glioblastoma Patient by Vaccination With Autologous Dendritic Cells Pulsed With Allogeneic Major Histocompatibility Complex Class I–Matched Tumor Peptides. *Neurosurg Focus* (2000) 9(6):e8. doi: 10.3171/foc.2000.9.6.9
- Prins RM, Liau LM. Immunology and Immunotherapy in Neurosurgical Disease. Neurosurgery (2003) 53(1):144–52. doi: 10.1227/01.neu.0000068865.34216.3a
- Yang I, Kremen TJ, Giovannone AJ, Paik E, Odesa SK, Prins RM, et al. Modulation of Major Histocompatibility Complex Class I Molecules and Major Histocompatibility Complex–Bound Immunogenic Peptides Induced by Interferon- and Interferon- Treatment of Human Glioblastoma Multiforme. J Neurosurg (2004) 100(2):310–9. doi: 10.3171/jns.2004.100.2.0310

- Nishimura F, Dusak JE, Eguchi J, Zhu X, Gambotto A, Storkus WJ, et al. Adoptive Transfer of Type 1 Ctl Mediates Effective Anti-Central Nervous System Tumor Response: Critical Roles of Ifn-Inducible Protein-10. *Cancer Res* (2006) 66(8):4478–87. doi: 10.1158/0008-5472.CAN-05-3825
- 54. Fujita M, Zhu X, Sasaki K, Ueda R, Low KL, Pollack IF, et al. Inhibition of Stat3 Promotes the Efficacy of Adoptive Transfer Therapy Using Type-1 Ctls by Modulation of the Immunological Microenvironment in a Murine Intracranial Glioma. J Immunol (2008) 180(4):2089–98. doi: 10.4049/ jimmunol.180.4.2089
- 55. Fujita M, Zhu X, Ueda R, Sasaki K, Kohanbash G, Kastenhuber ER, et al. Effective Immunotherapy Against Murine Gliomas Using Type 1 Polarizing Dendritic Cells–Significant Roles of Cxcl10. *Cancer Res* (2009) 69(4):1587–95. doi: 10.1158/0008-5472.CAN-08-2915
- Fujita M, Kohanbash G, Fellows-Mayle W, Hamilton RL, Komohara Y, Decker SA, et al. Cox-2 Blockade Suppresses Gliomagenesis by Inhibiting Myeloid-Derived Suppressor Cells. *Cancer Res* (2011) 71(7):2664–74. doi: 10.1158/0008-5472.CAN-10-3055
- 57. Kucharzewska P, Christianson HC, Welch JE, Svensson KJ, Fredlund E, Ringner M, et al. Exosomes Reflect the Hypoxic Status of Glioma Cells and Mediate Hypoxia-Dependent Activation of Vascular Cells During Tumor Development. *Proc Natl Acad Sci USA* (2013) 110(18):7312–7. doi: 10.1073/ pnas.1220998110
- Banks WA, Sharma P, Bullock KM, Hansen KM, Ludwig N, Whiteside TL. Transport of Extracellular Vesicles Across the Blood-Brain Barrier: Brain Pharmacokinetics and Effects of Inflammation. *Int J Mol Sci* (2020) 21 (12):4407. doi: 10.3390/ijms21124407
- Webber J, Steadman R, Mason MD, Tabi Z, Clayton A. Cancer Exosomes Trigger Fibroblast to Myofibroblast Differentiation. *Cancer Res* (2010) 70 (23):9621–30. doi: 10.1158/0008-5472.CAN-10-1722
- Lopatina T, Gai C, Deregibus MC, Kholia S, Camussi G. Cross Talk Between Cancer and Mesenchymal Stem Cells Through Extracellular Vesicles Carrying Nucleic Acids. Front Oncol (2016) 6:125. doi: 10.3389/fonc.2016.00125
- Ludwig N, Yerneni SS, Razzo BM, Whiteside TL. Exosomes From Hnscc Promote Angiogenesis Through Reprogramming of Endothelial Cells. *Mol Cancer Res* (2018) 16(11):1798–808. doi: 10.1158/1541-7786.MCR-18-0358
- Razzo BM, Ludwig N, Hong CS, Sharma P, Fabian KP, Fecek RJ, et al. Tumor-Derived Exosomes Promote Carcinogenesis of Murine Oral Squamous Cell Carcinoma. *Carcinogenesis* (2020) 41(5):625–33. doi: 10.1093/carcin/bgz124
- Chen G, Huang AC, Zhang W, Zhang G, Wu M, Xu W, et al. Exosomal Pd-L1 Contributes to Immunosuppression and Is Associated With Anti-Pd-1 Response. *Nature* (2018) 560(7718):382–6. doi: 10.1038/s41586-018-0392-8
- Azambuja JH, Ludwig N, Yerneni S, Rao A, Braganhol E, Whiteside TL. Molecular Profiles and Immunomodulatory Activities of Glioblastoma-Derived Exosomes. *Neurooncol Adv* (2020) 2(1):vdaa056. doi: 10.1093/ noajnl/vdaa056
- Azambuja JH, Ludwig N, Yerneni SS, Braganhol E, Whiteside TL. Arginase-1
 + Exosomes From Reprogrammed Macrophages Promote Glioblastoma Progression. Int J Mol Sci (2020) 21(11):3990. doi: 10.3390/ijms21113990
- Ludwig N, Rao A, Sandlesh P, Yerneni SS, Swain AD, Bullock KM, et al. Characterization of Systemic Immunosuppression by Idh Mutant Glioma Small Extracellular Vesicles. *Neuro Oncol* (2022) 24(2):197–209. doi: 10.1093/ neuonc/noab153
- Pardoll DM. The Blockade of Immune Checkpoints in Cancer Immunotherapy. Nat Rev Cancer (2012) 12(4):252–64. doi: 10.1038/nrc3239
- Ribas A. Adaptive Immune Resistance: How Cancer Protects From Immune Attack. Cancer Discovery (2015) 5(9):915–9. doi: 10.1158/2159-8290.CD-15-0563
- Alsaab HO, Sau S, Alzhrani R, Tatiparti K, Bhise K, Kashaw SK, et al. Pd-1 and Pd-L1 Checkpoint Signaling Inhibition for Cancer Immunotherapy: Mechanism, Combinations, and Clinical Outcome. *Front Pharmacol* (2017) 8:561. doi: 10.3389/fphar.2017.00561
- 70. Freeman GJ, Long AJ, Iwai Y, Bourque K. Engagement of the Pd-1 Immunoinhibitory Receptor by a Novel B7 Family Member Leads to Negative Regulation of Lymphocyte Activation. J Exp Med (2000) 192 (7):1027–34. doi: 10.1084/jem.192.7.1027
- Keir ME, Liang SC, Guleria I, Latchman YE, Qipo A, Albacker LA, et al. Tissue Expression of Pd-L1 Mediates Peripheral T Cell Tolerance. *J Exp Med* (2006) 203(4):883–95. doi: 10.1084/jem.20051776

- Goldman MJ, Craft B, Hastie M, Repecka K, McDade F, Kamath A, et al. Visualizing and Interpreting Cancer Genomics Data Via the Xena Platform. Nat Biotechnol (2020) 38(6):675–8. doi: 10.1038/s41587-020-0546-8
- Gonzalez N, Asad AS, Gomez Escalante J, Pena Agudelo JA, Nicola Candia AJ, Garcia Fallit M, et al. Potential of Idh Mutations as Immunotherapeutic Targets in Gliomas: A Review and Meta-Analysis. *Expert Opin Ther Targets* (2021) 25(12):1045–60. doi: 10.1080/14728222.2021.2017422
- Joyce JA, Fearon DT. T Cell Exclusion, Immune Privilege, and the Tumor Microenvironment. Science (2015) 348(6230):74–80. doi: 10.1126/science.aaa6204
- Voabil P, de Bruijn M, Roelofsen LM, Hendriks SH, Brokamp S, van den Braber M, et al. An Ex Vivo Tumor Fragment Platform to Dissect Response to Pd-1 Blockade in Cancer. *Nat Med* (2021) 27(7):1250–61. doi: 10.1038/ s41591-021-01398-3
- Berghoff AS, Kiesel B, Widhalm G, Wilhelm D, Rajky O, Kurscheid S, et al. Correlation of Immune Phenotype With Idh Mutation in Diffuse Glioma. *Neuro Oncol* (2017) 19(11):1460–8. doi: 10.1093/neuonc/nox054
- 77. Mu L, Long Y, Yang C, Jin L, Tao H, Ge H, et al. The Idh1 Mutation-Induced Oncometabolite, 2-Hydroxyglutarate, May Affect DNA Methylation and Expression of Pd-L1 in Gliomas. *Front Mol Neurosci* (2018) 11:82. doi: 10.3389/fnmol.2018.00082
- Pirozzi CJ, Yan H. The Implications of Idh Mutations for Cancer Development and Therapy. Nat Rev Clin Oncol (2021) 18(10):645–61. doi: 10.1038/s41571-021-00521-0
- Kayabolen A, Yilmaz E, Bagci-Onder T. Idh Mutations in Glioma: Double-Edged Sword in Clinical Applications? *Biomedicines* (2021) 9(7):799. doi: 10.3390/biomedicines9070799
- Huang KC, Chiang SF, Chen WT, Chen TW, Hu CH, Yang PC, et al. Decitabine Augments Chemotherapy-Induced Pd-L1 Upregulation for Pd-L1 Blockade in Colorectal Cancer. *Cancers (Basel)* (2020) 12(2):462. doi: 10.3390/cancers12020462
- Lai Q, Wang H, Li A, Xu Y, Tang L, Chen Q, et al. Decitibine Improve the Efficiency of Anti-Pd-1 Therapy Via Activating the Response to Ifn/Pd-L1 Signal of Lung Cancer Cells. Oncogene (2018) 37(17):2302–12. doi: 10.1038/s41388-018-0125-3
- Capper D, Weissert S, Balss J, Habel A, Meyer J, Jager D, et al. Characterization of R132h Mutation-Specific Idh1 Antibody Binding in Brain Tumors. *Brain Pathol* (2010) 20(1):245–54. doi: 10.1111/j.1750-3639.2009.00352.x
- Watanabe T, Nobusawa S, Kleihues P, Ohgaki H. Idh1 Mutations Are Early Events in the Development of Astrocytomas and Oligodendrogliomas. *Am J Pathol* (2009) 174(4):1149–53. doi: 10.2353/ajpath.2009.080958

- Schumacher T, Bunse L, Pusch S, Sahm F, Wiestler B, Quandt J, et al. A Vaccine Targeting Mutant Idh1 Induces Antitumour Immunity. *Nature* (2014) 512(7514):324–7. doi: 10.1038/nature13387
- Platten M, Bunse L, Wick A, Bunse T, Le Cornet L, Harting I, et al. A Vaccine Targeting Mutant Idh1 in Newly Diagnosed Glioma. *Nature* (2021) 592 (7854):463–8. doi: 10.1038/s41586-021-03363-z
- Rohle D, Popovici-Muller J, Palaskas N, Turcan S, Grommes C, Campos C, et al. An Inhibitor of Mutant Idh1 Delays Growth and Promotes Differentiation of Glioma Cells. *Science* (2013) 340(6132):626–30. doi: 10.1126/science.1236062
- Kadiyala P, Carney SV, Gauss JC, Garcia-Fabiani MB, Haase S, Alghamri MS, et al. Inhibition of 2-Hydroxyglutarate Elicits Metabolic Reprogramming and Mutant Idh1 Glioma Immunity in Mice. *J Clin Invest* (2021) 131(4):e139542. doi: 10.1172/JCI139542
- Alghamri MS, McClellan BL, Avvari RP, Thalla R, Carney S, Hartlage MS, et al. G-Csf Secreted by Mutant Idh1 Glioma Stem Cells Abolishes Myeloid Cell Immunosuppression and Enhances the Efficacy of Immunotherapy. *Sci Adv* (2021) 7(40):eabh3243. doi: 10.1126/sciadv.abh3243
- Xu W, Yang H, Liu Y, Yang Y, Wang P, Kim SH, et al. Oncometabolite 2-Hydroxyglutarate Is a Competitive Inhibitor of Alpha-Ketoglutarate-Dependent Dioxygenases. *Cancer Cell* (2011) 19(1):17–30. doi: 10.1016/ j.ccr.2010.12.014

Conflict of Interest: The authors declare that the research was conducted in the absence of any commercial or financial relationships that could be construed as a potential conflict of interest.

Publisher's Note: All claims expressed in this article are solely those of the authors and do not necessarily represent those of their affiliated organizations, or those of the publisher, the editors and the reviewers. Any product that may be evaluated in this article, or claim that may be made by its manufacturer, is not guaranteed or endorsed by the publisher.

Copyright © 2022 Yan, Li, Liu and Yang. This is an open-access article distributed under the terms of the Creative Commons Attribution License (CC BY). The use, distribution or reproduction in other forums is permitted, provided the original author(s) and the copyright owner(s) are credited and that the original publication in this journal is cited, in accordance with accepted academic practice. No use, distribution or reproduction is permitted which does not comply with these terms.



Use of Single Cell Transcriptomic Techniques to Study the Role of High-Risk Human Papillomavirus Infection in Cervical Cancer

Lingzhang Meng^{1,2†}, Shengcai Chen^{3†}, Guiling Shi^{3†}, Siyuan He², Zechen Wang², Jiajia Shen², Jiajia Wang², Suren Rao Sooranna⁴, Jingjie Zhao^{5*} and Jian Song^{1,2,6*}

OPEN ACCESS

Edited by:

Xian Zeng, Fudan University, China

Reviewed by:

Zhirong Zhang, INSERM U964 Institut de Génétique et de Biologie Moléculaire et Cellulaire (IGBMC), France Jun Li, Shanghai Jiao Tong University, China Fu Wang, Xi'an Jiaotong University, China

*Correspondence:

Jian Song songj@uni-muenster.de Jingjie.zhao@ymun.edu.cn

[†]These authors have contributed equally to this work

Specialty section:

This article was submitted to Cancer Immunity and Immunotherapy, a section of the journal Frontiers in Immunology

Received: 29 March 2022 Accepted: 06 May 2022 Published: 13 June 2022

Citation:

Meng L, Chen S, Shi G, He S, Wang Z, Shen J, Wang J, Sooranna SR, Zhao J and Song J (2022) Use of Single Cell Transcriptomic Techniques to Study the Role of High-Risk Human Papillomavirus Infection in Cervical Cancer. Front. Immunol. 13:907599. doi: 10.3389/fimmu.2022.907599 ¹ Institute of Cardiovascular Sciences, Guangxi Academy of Medical Sciences, Nanning, China, ² Center for Systemic Inflammation Research (CSIR), Youjiang Medical University for Nationalities, Baise, China, ³ Department of Obstetrics and Gynecology, Affiliated Hospital of Youjiang Medical University for Nationalities, Baise, China, ⁴ Department of Metabolism, Digestion and Reproduction, Imperial College London, Chelsea & Westminster Hospital, London, United Kingdom, ⁵ Life Science and Clinical Research Center, Affiliated Hospital of Youjiang Medical University for Nationalities, Baise, China, ⁶ Department of Radiation Oncology, Renji Hospital, School of Medicine, Shanghai Jiao Tong University, Shanghai, China

High-risk human papillomavirus (hrHPV) infection has been associated with a higher probability of progression to cervical cancer. However, several extensive studies have reported that the presence of hrHPV can lead to a better prognosis, but the mechanism of how this occurs is unclear. In this study, microbiological analysis was used to identify HPV infection as a factor for the prognosis of patients with cervical squamous cell carcinoma (CSCC). Comparing the interactions of HPV⁺ and HPV⁻ malignant cells with immune cells as well as the trajectory of malignant cells either with or without HPV, we found that most of the HPV⁺ cells are well differentiated while HPV⁻ cells appear to be hypo-fractionated. Using transcriptomic and immunostaining data, we validated a set of unfavourable molecules in the HPV⁻ CSCC cells, including KRT16, ITGB1, CXCR1, VEGFA, CRCT1 and TNFRSF10B/DR5. This study provides a basis for the development of a rational post-operative follow-up programme and the development of an appropriate treatment plan for patients with cervical cancer.

Keywords: high-risk human papillomavirus, single cell transcriptomic, cervical cancer, tumor infiltrating macrophages, prognosis markers

INTRODUCTION

Persistent high-risk human papillomavirus (hrHPV) infection, particularly the subtypes HPV16 and HPV18 of alpha-HPV, is known to be associated with a higher likelihood of progression to cervical cancer and hrHPV testing has been considered as a routine test for screening for this disease (1). However, several studies using either PCR or sequencing methods to define the HPV infection and its subtypes have reported that mortality rates were significantly lower in the hrHPV⁺ when

Abbreviations: hrHPV, High-risk human papillomavirus; CSCC, Cervical squamous cell carcinoma; scRNA-seq, Single-cell RNA sequencing; CNVs, Copy number variations; UMAP, Uniform manifold approximation and projection; ROC, Receiver operating characteristic; PCA, Principal component analysis.

compared to hrHPV⁻ groups (2, 3). The fact that the presence of hrHPV can lead to a better prognosis in patients has also been observed in oropharyngeal cancer (4). To date the mechanisms involved are not clear and these need to be further explored.

In this study we analysed the clinical parameters of cervical cancer patients as well as their single-cell RNA sequencing (scRNA-seq) data in order to explore the relationships and mechanisms of hrHPV and progression of the cancer. This allowed us to determine the immune extent of cell infiltration as well as the related signaling pathways associated with HPV infection with a view to unravelling relevant potential treatment targets of the disease. This could provide a basis for developing a sound post-operative follow-up programme thus allowing the formulation of appropriate treatment plans for combatting CSCC in the future.

MATERIALS AND METHODS

Collection and Processing of the CSCC RNAseq Dataset

The RNA sequencing dataset and the clinically related data for patients with CSCC originated from the TCGA database (https:// portal.gdc.carcinoma.gov/) and consisted of 248 samples. The raw gene expression dataset was processed. Each probe ID received an annotation with respect to the gene from the corresponding platform annotation profile of the GDC website and the raw matrix data received the quantile normalization and log2 conversion. Samples with missing data were excluded. The scRNA-seq data from patients with cervical cancer originated from the gene expression omnibus database and were accessed through NCBI GSE168652 (5). Raw fastq data of scRNA-seq were processed using UMI-tools (6) and viruses present in the single cells were detected using the Viral-Track approach (7). In brief, the sequencing data containing the single cell index were mapped to the virus genome reference database and the status of the single cell was added to the expression matrix so as to correlate with the presence of HPV infection and the corresponding transcriptome. In order to distinguish between benign and malignant cells, inferCNV was used for the analysis of copy number variations (CNVs) in single cell transcriptomes (https://github.com/broadinstitute/inferCNV).

Building a Microbial Signature

Tumor microbiomes were obtained from the pan cancer microbiome of cBioportal and these were integrated with their respective clinical data (8). The association between the CSCC microbiome and overall survival time in patients from the cancer genome atlas (TCGA) program was studied. Univariate Cox regression analysis was carried out in order to identify the genes associated with survival of individuals (p value < 0.05). Subsequently, the significance of candidate genes was selected using variable importance by using a randomized survival forest (RSF) algorithm. A risk score model with the selected microbial signature was built using multi-variate Cox regression approaches. In addition, the Kaplan-Meier test was employed for a number of gene features and the p-values (log) were determined. Receiver operating characteristic (ROC) analysis was performed for 3- 5- and 10- year overall survival rates and area under the curves (AUCs) were determined for assessing the specificity and sensitivity of the microbial signature.

Microbiome Analysis

Based on the results generated by sample sequencing of the operational taxonomic unit (OTU), the phyloseq R package was used to calculate the alpha diversity distance matrices. Microbiome analysis was otherwise performed using the http://microbiomeanalyst.ca website. Beta diversity analysis is a comparative analysis between groups of species diversity among different ecosystems or microbial communities and can be used to obtain potential similarities or differences in community composition among differently grouped samples.

Single Cell RNA Sequencing Analysis

Specific to the integrated analysis that can be obtained from single-cell data, the data from infected new coronavirus and bacterial pneumonia samples as well as non-pneumonia samples were normalized using the SCTransform method (9). These were then analyzed by conducting mutual principal component analysis (PCA). PCA analysis was further conducted for the integrated datasets, and cluster analysis was performed by using uniform manifold approximation and projection (UMAP). The cluster analysis of single-cell data was performed with Seurat's graph-based clustering method. The resolution of the FindClusters feature was set to 0.1. Subsequently, the clusters were visualized with the UMAP version 0.2.6.0 graph. The R software package Seurat, (version 2.3.4), was subsequently used for data analysis. During quality control, unique molecular modifier (UMI) counts of less than 500 and those with double multiples were removed. Furthermore, cells with >5% of mitochondrial genes and >50% of ribosomal genes were filtered out.

Functional Assay

The gene features were processed and then analyzed by the method from the WebGestalt webserver for the annotation of involved GO ontology and KEGG pathway (10). Cell-cell communication was analyzed with the CellphoneDB approach and some of the data were illustrated using the InterCellar method (11, 12). Pseudotime analysis was performed using Monocle (version 2.10.1).

Immunofluorescent Imaging

Biopsies were taken from six cervical patients with cervical cancer. After embedding with a frozen section compound (Leica, #3801480), biopsies were sectioned into 4-µm on a microtome (Leica CM1950). For immunofluorescent staining, the sections were fixed in pre-cooled methanol (-20°C) for 5 minutes, after washing twice with PBS. The sections were then blocked with PBS/5%BSA/Fc γ blocker at 4°C for 1 hour. Primary antibodies were incubated with sections at 4°C overnight. After washing twice with PBS, the sections were incubated with fluorescent-coupled secondary antibodies for 1 hour at room

temperature. After two further washes, the sections were mounted and imaged on an immunofluorescence microscope (Leica DMI3000B).

The antibodies/materials used for immunofluorescent imaging included: A488 mouse-anti-human CD206 (Invitrogen, #MA5-23656), PE mouse-anti-human CD163 (Invitrogen, #12-1639-42), A488 mouse-anti-human EpCam (Abcam, #ab237395), mouse-anti-human KRT16/Cytokeratin Pan Antibody Cocktail (Invitrogen, #MA5-13203), rabbit-antihuman CRCT1 (Invitrogen, #PA5-23539), A594 goat-antimouse IgG (Invitrogen, #A11032), A594, goat-anti-rabbit IgG (Affinity, #S0006), rabbit-anti-human DR5 (Invitrogen, # PA1-957), A647 donkey-anti-rabbit IgG (Invitrogen, #A32795) and DAPI (Invitrogen, #D21490).

Statistical Methods

Statistical analyses were carried out using R software (version 3.6.0). Kaplan-Meier tests and ROC analysis were performed as described previously (13, 14). In brief, the "survivor" and "survROC" software packages were utilized for both types of analyses (15). Optimal cut-off data points were calculated using the "survminer" package (16). Single-variate and multi-variate Cox regression correlations were used to assess the prognosis-correlated factors of interest. Hazard ratios and 95% confidence intervals are presented for all the prognosis-correlated factors. Analysis of differences between groups was performed using GraphPad Prism 8.0 software. Student t-test was used for comparison between two groups and P < 0.05 was considered as statistically significant.

RESULTS

Microbiome Analysis Grouped Alpha-HPV to Low-Risk CSCC Patients

The CSCC microbiomes were obtained from the pan cancer microbiome of cBioportal and then integrated with their respective clinical data. In order to screen for any crucial survival-related viruses, all the viral genomes from the CSCC samples were analysed using multi-variate Cox regression and compared to the TCGA dataset. The CSCC samples were subsequently divided into high and low risk cohorts (Supporting Data 1). Kaplan-Meier curves showed that the high-risk group survived for shorter periods when compared to the patients with the low risk viruses (Figure 1A). ROC curve analysis of the CSCC cases were then plotted and this showed AUCs of 0.999, 0.981 and 0.99 for 3-, 5- and 10-year survival, respectively (Figure 1B). Analysis of the community compositions of both CSCC high and low risk groups showed a similar range of viruses in patients with CSCC at the Class level (Supplementary Figure 1A). However, the beta diversity test showed a significant difference in the viruses between high and low risk individuals and those in the high-risk group had significantly lower virus diversity and abundance (Supplementary Figure 1B). Correlations between clinical risk and viruses associated with CSCC were investigated based on the

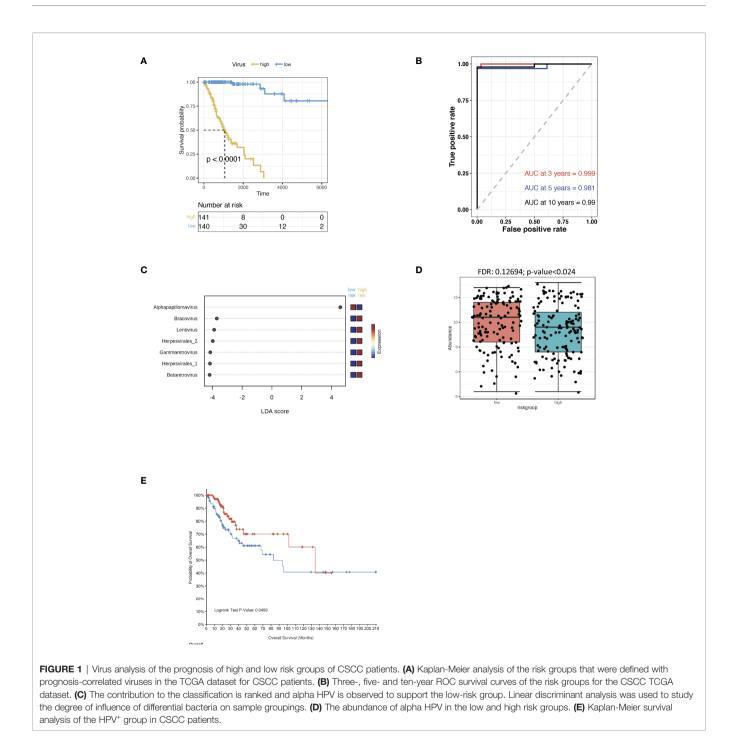
Spearman's correlation test and a significant positive correlation between the low-risk group and alpha-HPV was found (**Supplementary Figures 1C, D**). When correlated with the previous findings, linear discriminant analysis (LDA) classified alpha HPV to the low-risk patients (**Figure 1C**). Also, we found a higher abundance of alpha HPV in the low -risk group compared to that of the high-risk group (**Figure 1D**). The pan cancer microbiome of CSCC data also suggested that the HPV⁺ CSCC patients had a better prognosis compared to the HPV⁻ CSCC patients (**Figure 1E**).

Transcriptome Profiling of HPV–Infected Cells

Cervical cancer scRNA-seq data was used to study HPV infection responses *in vivo* so as to be able to study the transcriptome of different cells within the whole organism. During data mining, human cervical cancer cells were classified into 13 clusters (**Figure 2A**, **Supplementary Figures 2A**, **B**). HPV-infected cells could be identified by using the raw reads of cervical cancer cells together with the viral track approach (**Figure 2B**, **Supplementary Figure 2C**, **Supporting Data 2**). The infected cells could be separated from any uninfected ones in the main cell types by using the expression levels of HPV (**Figure 2C**). Approximately half of the cells from tumor tissues were found to be infected (**Figure 2D**). As indicated from the analysis, there was a significant level of viral gene expression not only in tumor cells but also in the macrophages and the levels found in the latter were significantly higher than the former (**Figures 2E, F**).

Identification of Malignant Cells Based on Their CNV Scores

We used infercnv to explore single-cell RNA-seq data from tumours, analysing them for large-scale chromosome copy number alterations (CNA), such as gains or deletions of whole chromosomes or large segments of chromosomes. We used a set of 'normal' cells from non-tumour tissues as a reference to analyse the changes in gene expression intensity at various locations on the tumour genome. The relative expression of genes on each chromosome is shown in the form of a heat map, and the tumour genome is either over- or under-expressed when compared to normal cells (Figure 3A). Using the infercnv approach, we identified the non-malignant and malignant cells present in the tumor tissue samples, and in these it was found that clusters 0 and 2 in the HPV⁻ cells displayed a higher malignant status when compared to the HPV⁺ cells (Figures 3B, C). The CNV scoring were found to be roughly correlated with the most markers of malignancy such as CDH1, EPCAM, CDKN2A and SERPINB3 (Figure 3D, Supplementary Figure 3A). As CNV scoring may represent the malignant cells more accurately compared with the malignant markers, we used the CNV-defined cells for the further analysis. By doing this, we were able to separate the HPV infected malignant cells from the non- malignant cells and these were then compared to the noninfected malignant cells with respect to the transcriptomic analysis (Supplementary Figures 3B-E). We found that keratin 16 was upregulated in most of the HPV⁻ tumor cells.

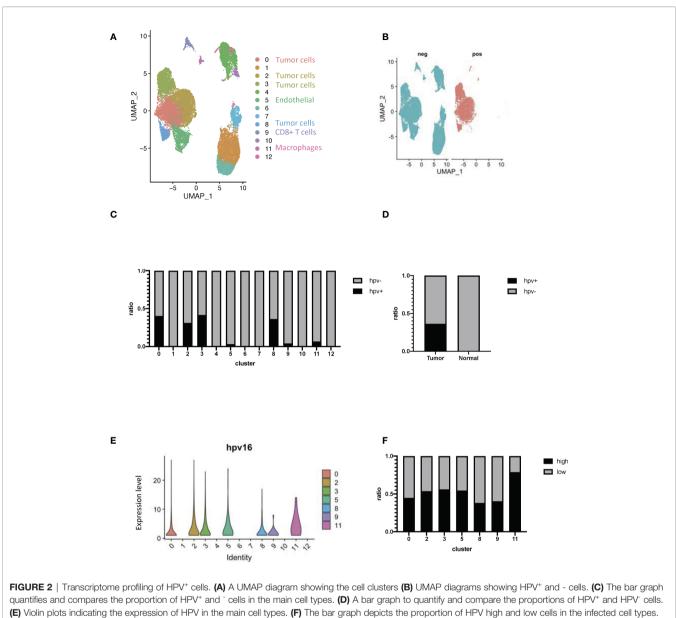


In addition, we validated the gene expression by immunostaining the tissue from HPV⁻ and HPV⁺ patients with both KRT16 and EPCAM antibodies (**Supporting Data 3**, **Figure 3E**).

Pseudotime Analysis of HPV Infected Tumor Cells

Each tumor cell could represent a step in time during the development of CSCC. Studying the transcriptome at the single-cell level allows us to identify genes in intermediate states

of biological processes, as well as genes in transition states between two different cellular fates. Using the pipeline of Monocle, HPV⁺ and HPV⁻ tumor cells can be sequenced and pseudotimes can be constructed based on the expression trends of the order of genes (**Figures 4A, B, Supplementary Figure 4A**, **Supporting Data 4**). 7 trajectory states have been identified and States 1 and 7 refer to the early phase of the pseudotime, and therefore correlate with cancer stemness (**Figures 4A, B**). HPV⁻ tumor cells displayed a high proportion of cancer stemness



HPV high refers to the cells with hpv16 counts of more than 1.

compared to HPV⁺ cells, while HPV⁺ cells and HPV expression were upregulated in the later states (**Figures 4C, D**). When correlated with the pseudotime states, differential gene expression analysis of State 1 revealed a set of malignant genes such as KRT16 and VEGFA (**Figure 4E**). GSEA functional analyses of DEGs in the HPV⁺ State 1 cells clearly indicated the virus induced signaling and reaction of innate immunity (**Figure 4F, Supplementary Figures 4B, D**), while GSEA functional analyses of State 1 correlated with the squamous cell metaplasia and tumorigenesis (**Figure 4G, Supplementary Figure 4C**).

Using a branched expression analysis modelling approach, we identified a set of genes that were regulated in a branch-dependent manner based on the trajectory analysis

(Supplementary Figure 4E), in which CRCT1 was upregulated in the HPV⁻ cells and appeared to play a significantly negative role in the survival prognosis of cervical cancer patients (Supplementary Figures 4F-H). In general, the cells in States 1 and 7 displayed a high CNV scores, which were correlated with cancer stemness and progression. Compared to HPV⁻ cells, HPV⁺ malignant cells were enriched in the intermediate phases, suggesting a crucial role of HPV infection in the progression of cervical cancer cells (Figure 4H).

Cell-Cell Communication Between Immune and HPV^{-Infected} Tumor Cells

In order to investigate the interactions of HPV^+ and HPV^- cells with immune cells in the tumor microenvironment, where tumor

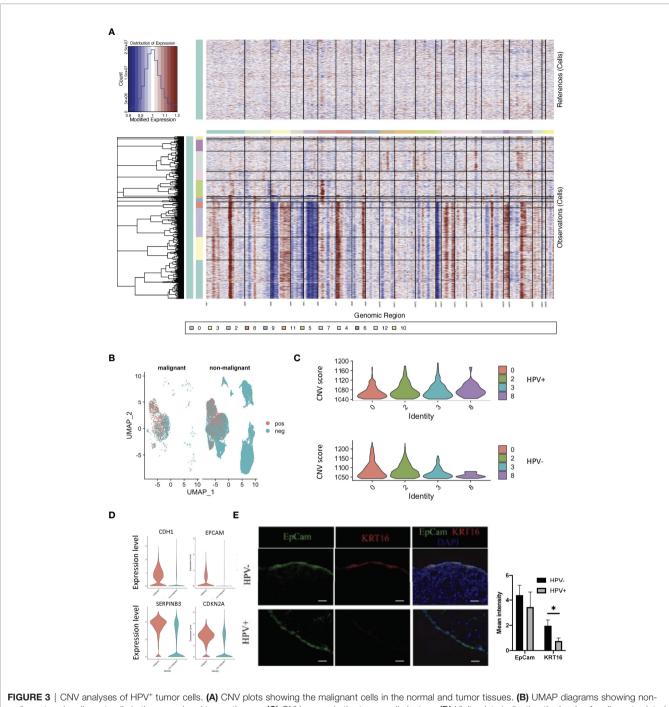
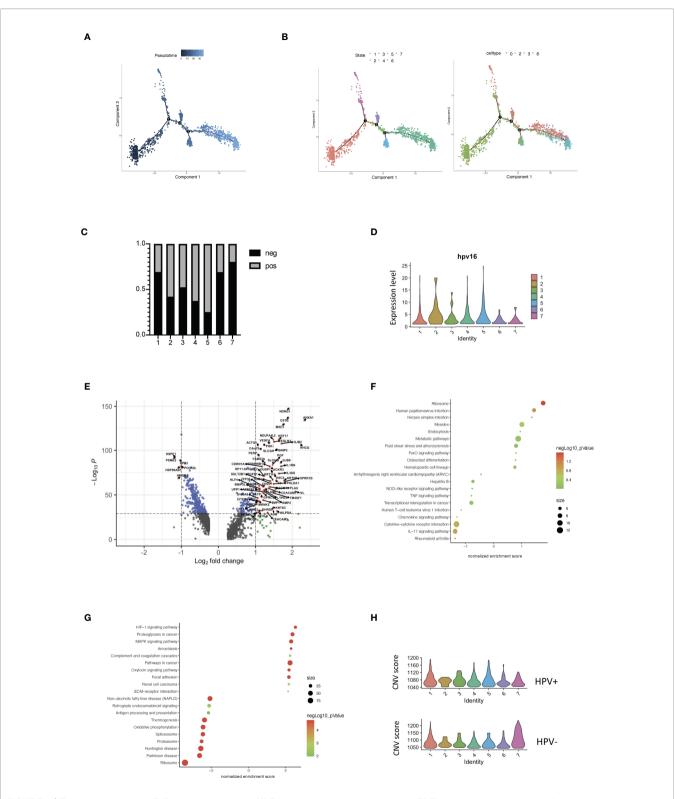


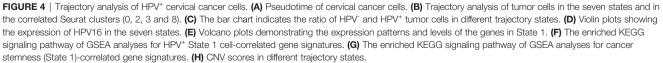
FIGURE 3 | CNV analyses of HPV⁺ tumor cells. (A) CNV plots showing the malignant cells in the normal and tumor tissues. (B) UMAP diagrams showing nonmalignant and malignant cells in the normal and tumor tissues. (C) CNV scores in the tumor cell clusters. (D) Violin plots indicating the levels of malignant-related gene expression in the non- malignant and malignant cells. (E) Representative immunostained photomicrographs of KRT16 in the tissues from HPV⁻ and HPV⁺ patients. EpCam staining refers to the squamous cell carcinoma. Scale bar indicates 50µm. The bar graphs show the mean fluorescent intensity of the indicated staining. * indicates p<0.05 of six samples.

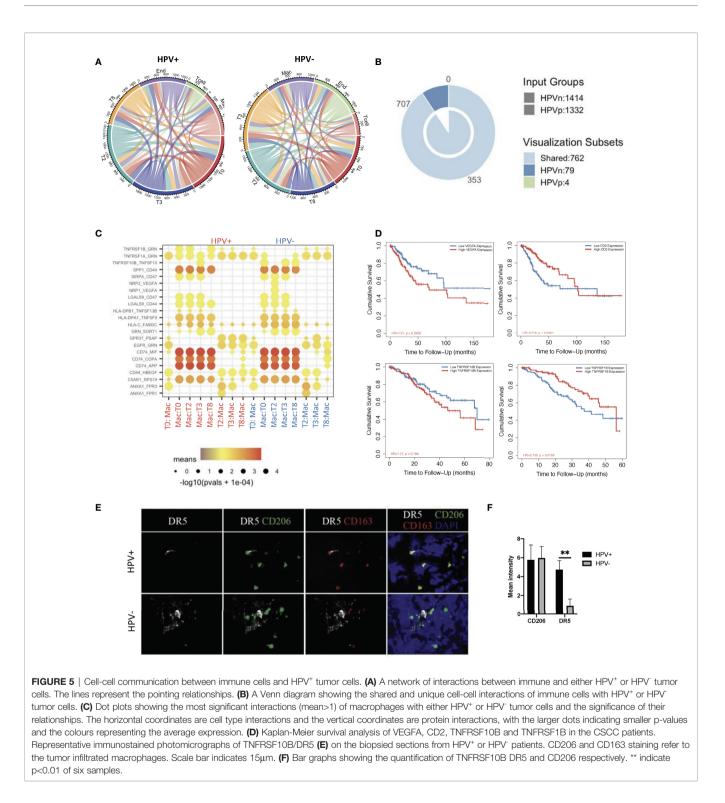
cells develop and immune cells interact very closely with them, we constructed an intercellular communication network by using the cellphoneDB method (12). The results showed that endothelial cells and macrophages had much more interactions with tumour cells when compared to T cells (**Figure 5A**, **Supporting Data 5**). Specifically, HPV⁻ tumor cells displayed

more unique cell-cell interactions when compared to HPV⁺ cells, and this is mainly due to the presence of the intergrin b1-extracellular matrix complex (**Figure 5B**, **Supporting Data 5**).

Of those unique cell-cell interactions of HPV⁻ cells, ITGB1 and CXCR1 were found to be associated with unfavourable prognosis of CSCC (Figure 5B, Supplementary







Figures 5A, B). In particular, tumour cell type 0 appeared to have a significantly higher amount of cellular communication with macrophages, which correlated with the high proportion of tumor infiltrated macrophages in CSCC (Figure 5A, **Supplementary Figure 5C**). Also, it was found that there was

a significantly enhanced VEGFA and TNFRSF10B/DR5 signaling association with macrophages interacting with HPV⁻ types 0 and 2 tumor cells, which was confirmed by tissue staining and appeared to play a significantly negative role in the prognosis of cervical cancer patients (**Figures 5C-F**). On the other hand,

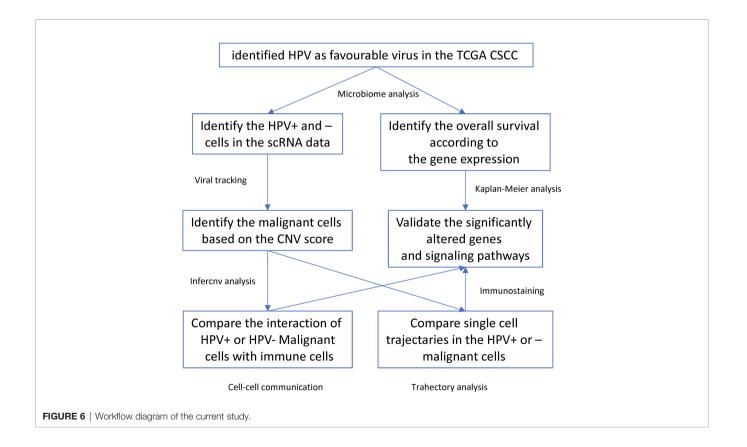
HPV⁺ tumor cells upregulated the favourable gene TNFRSF1B derived pathway (**Figures 5C, D**). Also, T cells interacting with various HPV⁺ of tumor cells had significantly upregulated CD2 signalling pathways (**Figure 5C, Supplementary Figure 5D**), while both HPV⁺ and – cells showed similar interactions with endothelial cells (**Supplementary Figure 5E**). Taken together, these data indicate a distinct scenario of HPV⁺ and HPV⁻ tumor cells in cervical cancer, which might explain the observation that mortality rates were lower in the hrHPV⁺ when compared to hrHPV⁻ CSCC patients.

DISCUSSION

HPV infection is a critical factor involved in the etiology and progression of cervical cancer. In this study, we used microbiological analysis to identify HPV as a favourable virus for the prognosis of CSCC patients. In addition, we used scRNA data and viral tracking methods to identify HPV infections and their subtypes. Then we identified malignant cells which together with the viral tracking methods allowed identification of DEGs by comparing HPV⁺ and HPV⁻ malignant cells. We also built a trajectory analysis for both HPV⁺ or HPV⁻ cells and identified the interactions between immune and malignant cells (**Figure 6**). We found that HPV⁺ cells upregulated the favourable genederived signaling, including CD2 and TNFRSF1B, whereas HPV⁻ cells upregulated the signaling that was derived by the CSCC unfavourable molecules such as ITGB1, CXCR1, VEGFA and

TNFRSF10B/DR5. Monoclonal antibody targeting of these molecules, such as Bevacizumab and Tigatuzumab (17, 18), have been developed and are currently under clinical trials for cancer patients other than CSCC, which suggests that they may be beneficial to the HPV⁻ CSCC patients in accordance with our study.

The fact that hrHPV negativity is associated with a good prognosis for tumors does not necessarily mean that hrHPV is not involved in the etiology of cancer development as the HPV⁻ cases may have been infected with the virus at an earlier timepoint before the cancer was diagnosed. HrHPV negativity is usually associated with advanced tumors, suggesting that these viruses may become undetectable at later stages of the carcinogenic process (19). Our data would suggest that hrHPV⁻ cells in tumor tissues are likely to indicate a loss of hrHPV expression in a subset of cells during carcinogenesis. However, the mechanism whereby this loss occurs is not fully understood. It is possible that hrHPV⁻ tumor cells may lose their internal mutational control and thus acquire genetic mutations associated with malignant growth and proliferation potential. In this scenario, the hrHPV⁺ tumor cells may be under better control of the viral protein by the immune system due to their expression and, therefore, this results in a relatively more positive prognosis of CSCC in these patients. In the present study we identified DEGs of hrHPV⁺ and hrHPV⁻ tumor cells in different clusters and states, as well as differential cellular communication and interactions of these cells with immune cells. However, due to limitations in the sequencing depth of scRNA-seq, we were



unable to investigate possible gene mutations in hrHPV⁻ tumor cells. In the future, we hope to remedy this failing by increasing the sequencing depth of single-cell sequencing with a view to obtaining a more comprehensive comparison between hrHPV⁺ and hrHPV⁻ tumor cells.

HPV infection is a major cause of cervical cancer and this study focuses on the correlation between HPV positivity and prognosis. In contrast to the single cause of cervical cancer, HNSCC is a cancer that arises as a result of exposure to carcinogens (e.g. alcohol and/or tobacco) or through malignant transformation due to HPV infection. Indeed, HPV-associated HNSCC has been found to exhibit unique biological and clinically relevant features, and the presence of the virus provides a survival advantage compared to its absence. However, because of the large number of cases of HPV unrelated tumours, it cannot be ruled out that the difference in prognosis between HPV⁺ and HPV⁻ cases is due to the fact that they have distinct etiologies, which differ in terms of pathogenesis. Therefore, a long-term follow-up of the presence of HPV in HNSCC patients is needed to establish the relevance of HPV changes in the disease.

In this study, the clinical and single-cell sequencing data of cervical cancer patients were analyzed in order to explore the relationships and mechanisms of hrHPV and cervical cancer progression. Our current data suggest that HPV⁻ cervical cancer cells can exhibit more cancer stemness properties, both with respect to analysis of the gene expression profile characteristics of the cancer and experimental validation. We also found that regulatory programs controlling stemness function are active in cancer, and continued research in this area will contribute to a better understanding of the mechanisms of the progression of HPV⁻ cervical cancer and help to combat treatment resistance in cancer patients.

The current study yielded information regarding the immune cell interactions and the related signaling pathways associated with HPV infection in cervical cancer patients. It is hoped that this will reveal potential targets for treatment regimens for CSCC patients. In addition, it may provide a basis for the development of a useful post-operative follow-up programme that will benefit the prognosis of future patients with CSCC.

DATA AVAILABILITY STATEMENT

The datasets presented in this study can be found in online repositories. The names of the repository/repositories and accession number(s) can be found in the article/ **Supplementary Material.**

ETHICS STATEMENT

The studies involving human participants were reviewed and approved by Ethical Committee of Youjiang Medical University for Nationalities. The patients/participants provided their written informed consent to participate in this study.

AUTHOR CONTRIBUTIONS

JS and JZ designed this study and performed the data analysis. LM, SC and GS performed partial data analysis and performed immunofluorescent imaging for this study. SC and GS performed clinical diagnosis and surgically isolated biopsies for this study. SH, ZW, JJS and JW performed partial data analysis for this study. SS helped to compose and review the manuscript for this study. LM, SC and GS contributed equally to this study. All authors contributed to the article and approved the submitted version.

FUNDING

This study was funded by grants from the National Science Foundation of China (#31970745), Guangxi Natural Science Foundation (#2020GXNSFAA259050), Youjiang Medical University for Nationalities (#yy2019bsky001), and Baise Development of Science & Technology Research Program (#20170505).

SUPPLEMENTARY MATERIAL

The Supplementary Material for this article can be found online at: https://www.frontiersin.org/articles/10.3389/fimmu.2022. 907599/full#supplementary-material

Supplementary Figure 1 | Virus analysis of the prognosis of high and low risk groups of CSCC patients. (A) Composition of the CSCC viruses at the class level in patients with high and low risks. (B) A two-dimensional scatter plot of the nonmetric multidimensional scale analysis of virus class levels in CSCC cancer patients.
 (C) Heatmap cluster analysis of the viruses in the high and low risk groups of CSCC patients. (D) The correlation coefficients which correlated with Herpesvirus.

Supplementary Figure 2 | Virus analysis of the high and low risk groups of CSCC prognosis. (A) Violin plots indicating the expression and distribution of marker genes.
 (B) A UMAP diagram showing the cell clusters in normal and tumor tissues in the CSCC patients (C) A bar graph showing the mapped reads of HPV in the CSCC scRNA data. (D) UMAP diagrams showing high and low dose of HPV expressing cells.

Supplementary Figure 3 | Gene expression analyses of HPV infected tumor cells. (A) Feature plots showing the malignance related genes in the non-malignant and malignant cells. (B–E) Volcano plots demonstrating the expression patterns and levels of the genes in non-malignant and malignant cell types.

Supplementary Figure 4 | Trajectory analysis of HPV infected cervical cancer cells. (A) Trajectory analysis of HPV⁻ (n) and HPV⁺ (p) tumor cells in different states. States 1 and 7 refer to the beginning and the end of the development. (B) Volcano plots demonstrating the expression patterns and levels of the genes in the HPV⁺ cells of State 1. (C) The enriched gene ontology of GSEA GO analysis for cancer stemness (State 1)-correlated gene signatures. (D) The enriched gene ontology of GSEA GO analysis for HPV⁺ State1 cell-correlated gene signatures. (E) BEAM (Branched expression analysis modelling) was used to find the genes that were regulated in a branch-dependent manner. A heatmap showing the temporal differential genes with the top 100 extracted. The horizontal axis of the heatmap refers to the proposed time. The genes shown are those that are highly expressed in the indicated clusters at the focus of the proposed time sort. (F) A dot plot showing the expression of CRCT1 in the seven states of HPV⁺ or HPV⁻ tumor cells. (G) Kaplan-Meier analysis of overall survival according to the gene expression of CRCT1 in CSCC patients from the TCGA dataset. (H) Representative immunostained photomicrographs of CRCT1 in the tissues obtained from HPV⁻ and HPV^+ patients. EpCam staining refers to the squamous cell carcinoma. Scale bar indicates $50 \mu m$. Bar graphs depicted the mean fluorescent intensity of the indicated staining. * indicates p<0.05 of six samples.

Supplementary Figure 5 | Cell-cell communication between immune cells and HPV infected tumor cells.Kaplan-Meier survival analysis of the HPV⁻ tumor cells using the interaction genes (A) ITGB1 and (B) CXCR1 in the CSCC patients. (C) A

REFERENCES

- Khan MJ, Castle PE, Lorincz AT, Wacholder S, Sherman M, Scott DR, et al. The Elevated 10-Year Risk of Cervical Precancer and Cancer in Women With Human Papillomavirus (HPV) Type 16 or 18 and the Possible Utility of Type-Specific HPV Testing in Clinical Practice. J Natl Cancer Inst (2005) 97:1072– 9. doi: 10.1093/jnci/dji187
- Lei J, Arroyo-Muhr LS, Lagheden C, Eklund C, Nordqvist Kleppe S, Elfstrom M, et al. Human Papillomavirus Infection Determines Prognosis in Cervical Cancer. J Clin Oncol (2022) 40(14):JCO2101930. doi: 10.1200/ JCO.21.01930
- Lei J, Ploner A, Lagheden C, Eklund C, Nordqvist Kleppe S, Andrae B, et al. High-Risk Human Papillomavirus Status and Prognosis in Invasive Cervical Cancer: A Nationwide Cohort Study. *PLos Med* (2018) 15:e1002666. doi: 10.1371/journal.pmed.1002666
- Lowy DR, Munger K. Prognostic Implications of HPV in Oropharyngeal Cancer. N Engl J Med (2010) 363:82–4. doi: 10.1056/NEJMe1003607
- Li C, Guo L, Li S, Hua K. Single-Cell Transcriptomics Reveals the Landscape of Intra-Tumoral Heterogeneity and Transcriptional Activities of ECs in CC. *Mol Ther Nucleic Acids* (2021) 24:682–94. doi: 10.1016/ j.omtn.2021.03.017
- Smith T, Heger A, Sudbery I. UMI-Tools: Modeling Sequencing Errors in Unique Molecular Identifiers to Improve Quantification Accuracy. *Genome Res* (2017) 27:491–9. doi: 10.1101/gr.209601.116
- Bost P, Giladi A, Liu Y, Bendjelal Y, Xu G, David E, et al. Host-Viral Infection Maps Reveal Signatures of Severe COVID-19 Patients. *Cell* (2020) 181:1475– 88.e12. doi: 10.1016/j.cell.2020.05.006
- Hoadley KA, Yau C, Hinoue T, Wolf DM, Lazar AJ, Drill E, et al. Cell-Of-Origin Patterns Dominate the Molecular Classification of 10,000 Tumors From 33 Types of Cancer. *Cell* (2018) 173:291–304.e6. doi: 10.1016/ j.cell.2018.03.022.
- 9. Stuart T, Butler A, Hoffman P, Hafemeister C, Papalexi E, Mauck III WM, et al. Comprehensive Integration of Single-Cell Data. *Cell* (2019) 177 (7):1888–902. doi: 10.1016/j.cell.2019.05.031
- Liao Y, Wang J, Jaehnig EJ, Shi Z, Zhang B. WebGestalt 2019: Gene Set Analysis Toolkit With Revamped UIs and APIs. *Nucleic Acids Res* (2019) 47: W199–205. doi: 10.1093/nar/gkz401
- Interlandi M, Kerl K, Dugas M. InterCellar Enables Interactive Analysis and Exploration of Cell-Cell Communication in Single-Cell Transcriptomic Data. *Commun Biol* (2022) 5:21. doi: 10.1038/s42003-021-02986-2
- Vento-Tormo R, Efremova M, Botting RA, Turco MY, Vento-Tormo M, Meyer KB, et al. Single-Cell Reconstruction of the Early Maternal-Fetal Interface in Humans. *Nature* (2018) 563:347–53. doi: 10.1038/s41586-018-0698-6
- Meng L, Qin H, Zhao J, He S, Wei Q, Wang Z, et al. Transcriptomic Signatures of Airway Epithelium Infected With SARS-CoV-2: A Balance Between Anti-

bar graph showing the CIBERSORT estimated infiltration of immune cell subsets of samples from HPV⁺ and HPV⁻ CSCC patients. Dot plots showing the most significant interactions (mean>1) of endothelial cells (**D**) and T cells (**E**) with either HPV⁺ or HPV⁻ tumor cells and the significance of their relationships. The horizontal coordinates are cell type interactions and the vertical coordinates are protein interactions, with the larger dots indicating smaller p-values and the colours representing the average expression.

Infection and Virus Load. Front Cell Dev Biol (2021) 9:735307. doi: 10.3389/ fcell.2021.735307

- 14. Wu Y, Meng L, Cai K, Zhao J, He S, Shen J, et al. A Tumor-Infiltration Cd8⁺T Cell-Based Gene Signature for Facilitating the Prognosis and Estimation of Immunization Responses in HPV Plus Head and Neck Squamous Cell Cancer. *Front Oncol* (2021) 11:749398. doi: 10.3389/fonc.2021.749398
- Therneau TM, Li H. Computing the Cox Model for Case Cohort Designs. Lifetime Data Anal (1999) 5:99–112. doi: 10.1023/A:1009691327335
- Zeng L, Fan X, Wang X, Deng H, Zhang K, Zhang X, et al. Bioinformatics Analysis Based on Multiple Databases Identifies Hub Genes Associated With Hepatocellular Carcinoma. *Curr Genomics* (2019) 20:349–61. doi: 10.2174/ 1389202920666191011092410
- Tewari KS, Sill MW, Penson RT, Huang H, Ramondetta LM, Landrum LM, et al. Bevacizumab for Advanced Cervical Cancer: Final Overall Survival and Adverse Event Analysis of a Randomised, Controlled, Open-Label, Phase 3 Trial (Gynecologic Oncology Group 240). *Lancet* (2017) 390:1654–63. doi: 10.1016/S0140-6736(17)31607-0
- Forero-Torres A, Infante JR, Waterhouse D, Wong L, Vickers S, Arrowsmith E, et al. Phase 2, Multicenter, Open-Label Study of Tigatuzumab (CS-1008), a Humanized Monoclonal Antibody Targeting Death Receptor 5, in Combination With Gemcitabine in Chemotherapy-Naive Patients With Unresectable or Metastatic Pancreatic Cancer. *Cancer Med* (2013) 2:925–32. doi: 10.1002/cam4.137
- Schiffman M, Kinney WK, Cheung LC, Gage JC, Fetterman B, Poitras NE, et al. Relative Performance of HPV and Cytology Components of Cotesting in Cervical Screening. J Natl Cancer Inst (2018) 110:501–8. doi: 10.1093/jnci/djx225

Conflict of Interest: The reviewer JL declared a shared affiliation with the author JS to the handling editor at time of review.

The remaining authors declare that this research was conducted in the absence of any commercial or financial relationships that could be construed as a potential conflict of interest.

Publisher's Note: All claims expressed in this article are solely those of the authors and do not necessarily represent those of their affiliated organizations, or those of the publisher, the editors and the reviewers. Any product that may be evaluated in this article, or claim that may be made by its manufacturer, is not guaranteed or endorsed by the publisher.

Copyright © 2022 Meng, Chen, Shi, He, Wang, Shen, Wang, Sooranna, Zhao and Song. This is an open-access article distributed under the terms of the Creative Commons Attribution License (CC BY). The use, distribution or reproduction in other forums is permitted, provided the original author(s) and the copyright owner(s) are credited and that the original publication in this journal is cited, in accordance with accepted academic practice. No use, distribution or reproduction is permitted which does not comply with these terms.



Different Immunoregulation Roles of Activin A Compared With TGF- β

Fanglin Li^{1,2}, Yiru Long^{1,2†}, Xiaolu Yu^{1,2†}, Yongliang Tong^{1,2†} and Likun Gong^{1,2,3*}

¹ State Key Laboratory of Drug Research, Shanghai Institute of Materia Medica, Chinese Academy of Sciences, Shanghai, China, ² University of Chinese Academy of Sciences, Beijing, China, ³ Zhongshan Institute for Drug Discovery, Shanghai Institute of Materia Medica, Chinese Academy of Sciences, Zhongshan, China

Activin A, a critical member of the transforming growth factor- β (TGF- β) superfamily, is a pluripotent factor involved in allergies, autoimmune diseases, cancers and other diseases with immune disorder. Similar to its family member, TGF- β , activin A also transmits signals through SMAD2/SMAD3, however, they bind to distinct receptors. Recent studies have uncovered that activin A plays a pivotal role in both innate and adaptive immune systems. Here we mainly focus its effects on activation, differentiation, proliferation and function of cells which are indispensable in the immune system and meanwhile make some comparisons with those of TGF- β .

OPEN ACCESS

Edited by:

Xuyao Zhang, Fudan University, China

Reviewed by: Francesco Elia Marino,

University of Pennsylvania, United States Yaprak Ozakman, Memorial Sloan Kettering Cancer Center, United States

> *Correspondence: Likun Gong Ikgong@simm.ac.cn

[†]These authors have contributed equally to this work

Specialty section:

This article was submitted to Cancer Immunity and Immunotherapy, a section of the journal Frontiers in Immunology

Received: 15 April 2022 Accepted: 23 May 2022 Published: 14 June 2022

Citation:

Li F, Long Y, Yu X, Tong Y and Gong L (2022) Different Immunoregulation Roles of Activin A Compared With TGF-β. Front. Immunol. 13:921366. doi: 10.3389/fimmu.2022.921366 Keywords: activin A, TGF- β , activin A signaling, macrophages, dendritic cells, B cells, T effector cells, regulatory T cells

INTRODUCTION

Activin A was initially defined as a factor which could induce the gonad to secrete folliclestimulating hormone (FSH) (1). Encoded by *inhibin* β A (*INHBA*), activin A is a homodimer of two inhibin β A subunits, and is referred to as the predominant member of activin branch of the transforming growth factor- β (TGF- β) superfamily (2). Theoretically, dimers composed of arbitrary two inhibin β subunits could exist, such as homodimer activin B and heterodimer activin AB (2), however, the vast majority of research has been carried out on activin A.

In the last few decades, activin A has been proven to be involved in a variety of biological processes apart from its original function, including hematopoiesis, tissue repair, angiogenesis and immune regulation (3, 4). In the aspect of immune regulation, activin A plays an important role in the development of diseases such as allergies, autoimmune diseases and cancers (5). However, how activin A modulates the immune system remains controversial and needs further exploration.

This review focuses on the effect of activin A signaling on the major components of the immune system. In view of the fact that it shares a classical downstream pathway with TGF- β , we choose to elaborate the difference between their functions throughout the paper.

ACTIVIN A SIGNALING PATHWAY

All the members of TGF- β superfamily transmit signal *via* a serine/threonine kinase receptor system which involves seven type-I and five type-II receptors (6). The formation of receptor complex needs at least one type-I and one type-II receptor. Even though each TGF- β superfamily member favors a certain receptor complex, promiscuity or overlap of ligand-receptor interactions exists since any one

of the 12 receptors binds to more than one ligand (6). The predominant receptors of activin A include activin receptor like kinase 4 (ALK4, type I) and activin receptor type IIB, activin receptor type IIA (ActRIIB, ActRIIA, type II) (2). The canonical downstream pathway of activin A is identical to that of TGF- β . Activin A first binds and promotes phosphorylation of type II receptors, and then recruits type I receptors to form phosphorylated heteropolymers. Activated receptor complex will phosphorylate mothers against decapentaplegic (SMAD) 2 and 3 at their carboxyl-terminal SSXS motif (6). Afterwards, SMAD4 is recruited to help form a transcriptional complex, which then translocates to the nucleus and affects transcription of genes Pax-6, FSH, p21 and follistatin (3, 7, 8). Apart from SMAD2/3, SMAD1/ 5/8 is also involved in the signaling of TGF- β superfamily members such as bone morphogenetic protein (BMP)s (9).

Some means can be used to intervene activin A signaling for the mechanism study. Activin A is strictly modulated by various molecules physiologically. Follistatin, a natural ligand of activin A, can bind to activin A with high affinity and is most commonly used to block the activity of activin A (10-13). Besides, a heterodimer comprised of inhibin α (INHA) and inhibin β (INHB) called inhibin, which also belongs to the activin family, is able to suppress activin A signaling by binding to activin A directly or competing for type II receptor (10). Antibodies designed for receptors are the major exogenous interventions. Notably, most of the TGF- β superfamily members bind to ActRIIB or ActRIIA while only a few ligands bind to ALK4 with high affinity, even excluding activin B and activin AB (14). In order to avoid nonspecific blockage as far as possible, it is better to use ALK4 inhibitor. For example, SB-431542 is the one that has been widely used in scientific research (11, 15-17).

In addition to the canonical receptor serine/threonine kinase-SMAD axis, activin A has also been shown to be involved in p38, ERK, PI3K, Wnt and other pathways (**Figure 1**) (18–21).

ACTIVIN A REGULATION OF THE INNATE IMMUNE SYSTEM

In general, innate immune cells including macrophages, dendritic cells (DCs) and natural killer (NK) cells are the sources of activin A (12, 22–24). Here, we describe the relationship between activin A and these cells, and make some comparison with those of TGF- β .

Monocytes/Macrophages

Although it has been demonstrated that tumor necrosis factor (TNF)-induced activation of RAW264.7, a macrophage cell line derived from BAB/14 mice, did not influence expression of activin A (22), an earlier study showed that *INHBA* could be up-regulated by LPS-induced human peripheral blood monocytes (23), suggesting that the activated monocytes/macrophages in specific conditions could be the source of activin A.

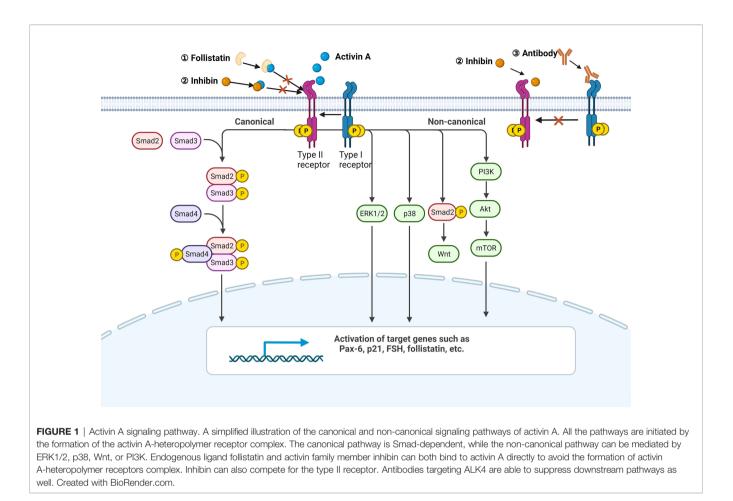
When macrophages are activated, secretion of pro-inflammatory cytokines including IL-1 β and IL-6 will be increased, and cell

surface markers like CD14 and CD80 will be up-regulated (25). It was reported that activin A could induce macrophages to release nitric oxide (NO), IL-1 β , IL-6 and TNF, and up-regulate the expression of CD80, CD86 and CD14 on the cell surface as well (22, 26, 27). However, the above studies all used resting macrophages as research subjects, while in immune disorders, macrophages are usually activated (25). In the latter case, the results are contrary to previous ones. Activin A inhibited production of NO by LPS-activated mouse peritoneal macrophages and also down-regulated the expression of CD14 (28). Moreover, activin A could significantly down-regulate the expression of CD80/CD86 and inhibit secretion of cytokines including IL-1 β , IL-6 and TNF- α by peripheral blood mononuclear cell (PBMC)-derived monocytes from acute Kawasaki disease patients (29).

For innate immunity, macrophages exert functions of phagocytosis and pinocytosis, while they play a role in presenting antigens to lymphocytes for adaptive immunity (25). Studies have shown that activin A can facilitate the pinocytic and phagocytic activities of both mouse peritoneal macrophages and RAW264.7 (26, 27). Change of the major histocompatibility complex (MHC) expression was uncertain in resting macrophages after being exposed to activin A (26, 27). Similarly, activin A plays a different role in LPS-activated mouse peritoneal macrophages by inhibiting phagocytosis and down-regulating expression of MHC-II (28). Lower percentage of MHC-II⁺ CD206⁺ cells in testicular leukocytes from Inha^{+/} C57BL/6 mice with elevated activin A supports the above phenomenon (30). Besides, whether activated or not, activin A did not affect the proliferation of macrophages (26-28). Overall, these lines of evidence suggest that activin A could facilitate activation and phagocytosis of resting macrophages and exert the opposite function in the activated macrophages. In contrast, TGF- β tends to serve as an immunosuppressive cytokine which suppresses activation and antigen presentation function of monocytes/macrophages (31). It is likely that activin A boosts priming of a macrophage response, while maintains the homeostasis when macrophages are over activated.

Several researches focused on whether activin A, could skew macrophage toward M2 type. It was reported that activin A could up-regulate M2 signature arginase-1 expression on RAW264.7 (32). Furthermore, kidney of mice exposed to androgen was found to release higher levels of activin A, which was accompanied with the polarization of renal macrophages to M2 type (33). Finally, compared with wildtype mice, the proportion of MHC-II⁻CD206⁺ cells in testicular leukocytes from Inha^{+/-} C57BL/6 mice was also declined (30). All of these results indicated that activin A is related to M2-biased macrophages polarization. Although it was shown that TGF- β secreted by mesenchymal stem cells (MSCs) induced M2-like polarization of macrophages, defining TGF- β as a contribution factor for promoting M2 polarization currently still lacks evidence (34).

In addition, activin A has been found to act in human monocyte chemotaxis (35) and participate in crosstalk between macrophages and tumor cells (15). *INHBA* was up-regulated in



melanoma-treated monocytes, and the exposure of activin A to human PBMC-derived monocytes and melanoma-treated monocytes, rather than wide type monocytes, could directly promote the transcription of protumoral cytokines such as CCL20, TNF and VEGFA, as well as immunosuppressive cytokines such as IDO-1 and PTGS2. Conditioned media of melanoma-treated monocytes could inhibit T cell proliferation and advance the invasion of melanoma cells. Administration of SB-431542 abolished these phenomena, while direct exposure to activin A showed no observable alterations. Such results suggested that melanoma cells could interact with monocytes through activin A to indirectly affect the tumor microenvironment (TME). Besides, activin A was enriched in tumor associated macrophages (TAM) of melanoma patients and its expression level in TAM was significantly associated with a worse prognosis for melanoma patients (15).

Dendritic Cells

Expression of both activin type I and type 2 receptors exists on the surface of dendritic cell and exogenous activin A can activate DC *via* SMAD2 or ERK1/2 signaling (36). After stimulation by CD40L/LPS, the mRNA levels of ALK4, ACTRIIA and ACTRIIB in human monocyte-derived DC (MoDC) changed with the extension of time, accompanied by increased secretion of activin A (12). While other members in the TGF- β superfamily, such as Nodal, TGF- β , BMP4, BMP7 and myostatin, remained unchanged during this process (12). These lines of evidence support that DCs are not only donors but also targets of activin A.

Blocking MoDC endogenous activin A after CD40L stimulation resulted in significant up-regulation of cytokines like IL-6 (12). As TGF- β is able to induce mouse antigen presenting cell (APC) to release BAFF (37), which can indirectly modulate immunoglobulin production of B cells, activin A could induce DCs and macrophages to secrete BAFF *via* ALK4/Smad3 pathway (36, 38). However, activin A was not found to impact on growth of DCs (38). Numerous studies have shown that TGF- β can inhibit maturation and antigen presentation function of DCs (39–42), while whether activin A plays a similar role to TGF- β is uncertain.

DCs require collaboration with other immune cells to function sophisticatedly. Although TGF- β is known to be an inhibitor of NK function (43), production of TGF- β by DCs was not found. It was confirmed that human NK cells expressed receptors of both activin A and TGF- β (44). Addition of activin A on the basis of IL-2 plus IL-12 stimulation to human NK cells gave rise to up-regulation of ALK4 together with downregulation of TGF-BRII and TGF-BRI mRNA (44). Strong upregulation of activin A and no change of TGF- β was observed in the NK-DC co-cultured system, and it was demonstrated that DC but not NK could contribute to production of activin A (11). Activin A elevation was blocked by neutralizing antibodies of various cytokines including granulocyte-macrophage colony stimulating factor (GM-CSF), TNF- α , interferon- γ (IFN- γ) and IL-1 β , which implied that cytokines exposure was responsible for the up-regulation of activin A in the co-cultured system (11). Given that activin A could not be released by NK and activin A blockage boosted NK cell IFN-y production prior to IL-12 plus Poly I:C stimulation in a co-cultured MoDC-NK system, activin A might be the mediator for MoDCs to regulate NK activity (44). Moreover, incubation of follistatin or SB-431542 in the co-cultured system significantly promoted secretion of IL-6, TNF- α and other DC-derived cytokines, while BMP inhibitors showed no effect (11). Additionally, activin A may serve as a regulator of DC maturation triggered by NK, since CD83 and CD86 were up-regulated following activin A inhibition in an NK-DC co-culture system (11).

Activin A also affected the effect of DCs on T cells. Different from TGF- β , which is known to exert immunosuppressive function by up-regulating regulatory T cells (Tregs) (45), activin A-stimulated DC mixed with T cells would not cause the up-regulation of CD25⁺Foxp3⁺ regulatory T cells (36). It was also shown that activin A could promote proliferation and inhibit apoptosis of T cells via BAFF and APRIL respectively (36). Whether these two factors are involved in differentiation and functions of T cells has not been reported. As tumor immunotherapy has become a hot spot in tumor research in recent years, the researchers fed activin A-treated DC back to B16/LLC tumor bearing mice to figure out whether activin A-treated DC could affect tumor progress in vivo (36). As a consequence, tumor progression was greatly inhibited and this function could be abolished by BAFF/APRIL knockdown (36). In vitro, activin A-treated DC also facilitated IFN-y production from mouse splenic T cells (36). Considering that exposing DC to TGF-β-induced Foxp3⁺ Treg could weaken DC's ability to stimulate naïve T cell immune responses (46), activin A induced-Foxp3⁻IL-10 producing Treg (Activin A-iTreg) was generated. Activin A-iTreg was able to inhibit DCs to prime Th2 response in vivo, presented by reduced release of IL-4 and IL-13 (47).

Natural Killer Cells

NK cells play roles as both activin A donors and activin A target cells in certain context. *INHBA*, *ACVR2B*, *SMAD2/3/4* were all shown to be expressed in mouse peripheral blood NK cells (24). Stimulation of these cells with IL-2 *in vitro* could promote the release of activin A in a dose-dependent manner (24).

It was reported that exogenous activin A or TGF- β both could inhibit IFN- γ production in human NK cells (44). Apart from IFN- γ , addition of activin A to NK cells stimulated with IL-12 plus Poly I:C also led to the down-regulation of cytokines including IL-6, TNF- α , GM-CSF and IL-1 β together with chemokines including MCP-1, IL-8 etc. (44). Moreover, IL-10 expression in NK cells was not altered after activin A administration, while IL-2 expression was up-regulated (24, 48).

Activin A was found to have no effect on the expression of perforin, granzyme A, granzyme B, IL-12RBI, and IL-12RBII in IL-2/IL-12 stimulated human NK cells. In contrast, TGF- β

significantly suppressed the secretion of granzyme B, IL-12RBI, and IL-12RBII (44). It was also pointed out that the lytic function of NK was not affected by activin A (44). Instead, activin A was considered to be an inhibitor of NK cell proliferation, as well as cytotoxicity by inhibiting the release of LDH with a decreased killing rate of YAC-1 cells (13, 24, 44).

Rautela, J. et al. compared the effects of activin A and TGF- β on NK cells (13). Despite activin A might inhibit proliferation, cytokine secretion and cytotoxicity of NK cells, its function always tended to be inferior to TGF- β (13). However, treating TGF- β RII-deleted mice with melanoma with follistatin could further reduce melanoma lung metastasis, indicating that activin A functioned independently from TGF- β (13).

ACTIVIN A REGULATION OF THE ADAPTIVE IMMUNE SYSTEM

The suppression effect of TGF- β for adaptive immunity has been widely reported. Whether activin A shows a similar function is the main topic in the following sections.

B Lymphocytes

B cells also serve as donors and targets of activin A (49). Pretreatment of naïve B cells with activin A before LPS stimulation resulted in enhanced proliferation and immunoglobulins (Ig) production ability of B cells. However, co-treatment of activin A and LPS did not affect B cell proliferation and Ig production, which implied that only resting B cells responded to activin A (49, 50). The potential reason accounting for this might be the down-regulation of activin A, TGF- β suppresses proliferation, Ig production and survival of B cells (49, 51).

Activin A, like TGF- β , promoted IgA secretion by B cells, according to Lee, H. J. et al. (50). Notably, this effect could not be reversed by TGF- β antibody (50). Activin A was reported to be involved in Th2-type responses, which are characterized by IgE production. Even though IgE production by B cells could not directly be increased by activin A *in vitro*, activin A neutralization *in vivo* significantly decreased IgE production in mice immunized with OVA (49). It was possible that activin A indirectly induced IgE production by B cells with the help of IL-4 released from other immune cells such as macrophages (49).

Increased secretion of activin A by inflammatory monocytes could subsequently activate APC to release BAFF (38). Small-molecule drug- P_4N was able to induce activin A production by monocytes, thereby promoting B cell proliferation and antibody production *via* activin A/BAFF pathway (52).

T Effector Lymphocytes

TGF- β is known to be an immune suppressive factor for inhibiting proliferation, survival, cytokine secretion and differentiation of T cells (53). Ogawa, K. et al. showed that activin A was unable to make a difference in proliferation of CD4⁺ CD25⁻ T cells (32). However, activin A significantly

reduced proliferation of human T cells and percentages of effector-producing CD4⁺ T cells, but greatly up-regulated IL-10⁺ CD4⁺ T cells (54). Blockade of TGF- β did not affect the function, demonstrating that activin A functions independently (54).

TGF- β can suppress the activity of CD8⁺ T cells (31), while the effects of activin A on CD8⁺ T cells are rarely explored. Similar to TGF- β blockade, knockdown (KD) of activin A induced CD8⁺ T cells priming during radiation therapy of 4T1 tumor-bearing mice, and combination of TGF- β blockade with activin A KD significantly augmented this effect (55, 56). Activin A could also inhibit the activity of CD8⁺ T cells in peripheral blood of acute Kawasaki disease patients (57).

Both activin A and TGF- β are involved in tumor immunology. In accordance with existing research and properties of TGF- β , activin A may also suppress tumor immune microenvironment. In contrast, Morianos, I. et al. provided evidence which might uncover activin A's role as an anti-tumor factor (58). Treatment of OVA-expressing Lewis Lung Carcinoma mice with activin A attenuated tumor progression and heightened the ratio of tumor-infiltrating effectors to regulatory CD4⁺ T cells (58). The expression of immune checkpoints including programmed cell death protein 1 (PD-1), lymphocyte-activation gene 3 (LAG-3), cytotoxic T-lymphocyte-associated protein 4 (CTLA-4) on tumorinfiltrating CD4⁺ T cells was reduced as well (58). Adoptive transferring of activin A-treated lung tumor-infiltrating CD4⁺ T cells into CD4 (-/-)-tumor-bearing mice could suppress tumor progression without CD4⁺ T cell exhaustion (58).. All of these results indicated that activin A might be a novel therapeutic molecule for lung cancer.

Multiple studies described activin A as a Th2 cytokine, as it mediates Th2-priming immune responses in allergic airway disease and some other diseases (4, 32, 59–61). When $CD4^+$ T cells differentiated into Th cells, the release of activin A was increased (32). The mRNA level of *INHBA* was more abundant in Th2 rather than Th1 cells (32). Compared with activated Th1 cells, activated Th2 cells secreted higher levels of activin A (32).

Activin A is also associated with Th17 pathogenicity. Experimental autoimmune encephalomyelitis (EAE) and relapsing-remitting multiple sclerosis (RRMS) are both kinds of autoimmune neuro-inflammatory disease driven by Th17. In EAE and RRMS mouse models, *INHBA* up-regulation was detected in serum and supernatant of spinal cord tissue of mice (62).

Th17 can be classified as pathogenic or non-pathogenic, and TGF- β 1 was considered to be dispensable for generation of pathogenic Th17 (63). Notably, activin A secretion increased markedly during the pathogenic Th17 instead of non-pathogenic Th17 differentiation (62). Neutralizing activin A *in vitro* in the process of CD4⁺ T cells differentiating into Th17 led to reduced Th17 generation, lower levels of *Il23r* and *Csf2* (considered as pathogenic Th17 genes), higher levels of *Il10* and *Cd51* (considered as non-pathogenic Th17 genes) (62). In line with this, an *in vivo* experiment discovered that T cell-derived activin A signaling was conducive to pathogenic Th17 cell-induced EAE rather than activin A signaling from

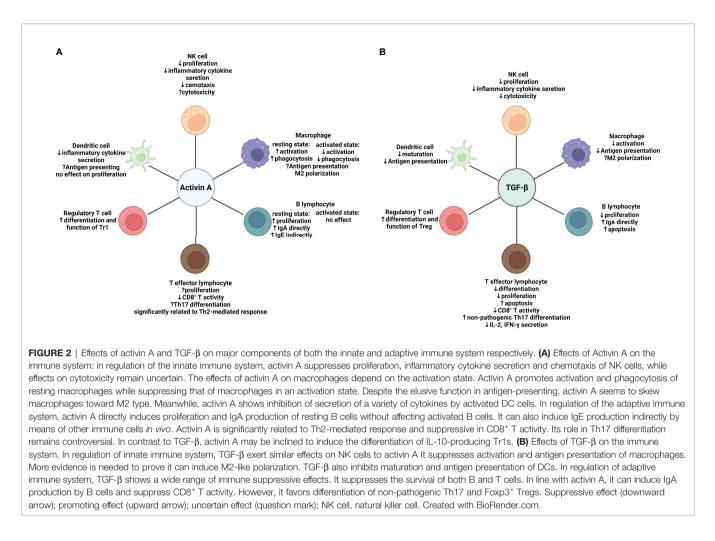
microenvironment (62). Activin A might confer Th17 pathogenicity by inducing ERK activation, while TGF-B might inhibit ERK signaling (62). TGF-B1 receptor ALK5 transduction into T cells elicited milder EAE compared with activin A receptor ALK4 transduction and increased Il10 expression could be observed, supporting that activin A and TGF-B1 favor pathogenic and non-pathogenic Th17 cell differentiation respectively (62). Despite this, role of activin A in Th17 cell differentiation remains controversial. RNAsequencing (RNA-seq) detected down-regulation of pathogenic Th17 signatures including Tbx21 and Batf in activin A treated Th17 cells, whereas non-pathogenic genes including Ahr, Maf and Ctla4 were enriched (64). Furthermore, reconstitution of Rag-1^{-/-} mice with activin A treated Th17 resulted in dampened EAE severity, indicating that activin A restrained pathogenic potential of Th17 cells (64). The reason for this contradiction may be the source of activin A. T cell-derived and exogenous activin A may have different functions in Th17 differentiation.

Regulatory T Lymphocytes

Regulatory T cells (Tregs) can be divided into three main groups: thymus regulatory T cells (tTregs), peripheral regulatory T cells (pTregs) and induced regulatory T cells (iTregs) (65). iTregs include Th3 and type 1 regulatory T (Tr1) and some other types (65). TGF- β is crucial in the differentiation of naïve CD4⁺ T cells into CD4⁺ CD25⁺ Foxp3⁺ T cells (66). Studies on activin A modulating Tregs are mainly carried out around allergic airway diseases. Activin A plays an important role in pathogenicity of allergic respiratory diseases (59). In asthma patients, serum activin A levels, rather than TGF- β levels, are significantly correlated with severity of asthma. *INHBA* mRNA expression in CD4⁺ T cells of asthma patients is also increased, while *TGF-\beta* is not (60).

It was demonstrated that the differentiation and function of Tr1 were promoted by activin A *via* transcription factor IRF4 (54). Adoptive transfer of activin A-induced Tr1 protected against asthma (54). Semitekolou, M. et al. unraveled that activin A could induce the generation of antigen-specific CD4⁺ IL-10⁺ Tregs to suppress Th2 immune response, thus resisting allergic airway disease (61). TGF- β assisted activin A to suppress Th2 immune response, however, it functioned by inducing another Treg group, CD4⁺ CD25⁺ Foxp3⁺ Tregs (61).

Activin A also impacts on Tregs in the TME. Tumor focal radiation therapy can lead to the up-regulation of Tregs in both mice and patients (67, 68). After radiation therapy or TGF- β blockade, secretion of activin A from breast cancer cells could be promoted (56). Both TGF- β and activin A contributed to generation of Tregs in 4T1 tumors, and they acted to complement each other in terms of the final effect (56). In comparison to TSA, which expressed lower levels of *INHBA*, 4T1 expressed higher levels of *INHBA*. 4T1-bearing mice presented significant up-regulation of Tregs in response to TGF- β blockade (56). What's more, in breast cancer patients, the expression of *INHBA* was positively correlated with tumor-



infiltrating Tregs signatures (56). All of above findings indicate that activin A may induce Tregs in breast tumor microenvironment after radiotherapy. Due to the complementary action between activin A and TGF- β , dual blockade of both molecules may reverse immune suppression driven by radiation therapy (69).

DISCUSSION AND PERSPECTIVES

In this review, we focus on modulation of activin A on the major components of the immune system (**Figure 2**). Although sharing similar canonical signaling pathway, activin A functions differently from TGF- β in certain contexts, which is possibly owing to spatio-temporal distribution of the receptors, crosstalk with other pathways, and expression of related signaling molecules. Although the role of activin A in antitumor immunity remains controversial, existing evidence has proved the potential of activin A as a novel target of tumor immune therapy. On the one hand, endogenous activin A may suppress anti-tumor immunity by inducing differentiation of Tr1, deactivating innate immune cells or inhibiting cytokine secretion from CD4⁺ T cells. On the other hand, surprisingly, adoptive transfer of exogenous activin A-treated DCs or CD4⁺ T cells prevents tumor cells from growing, which provides a brand new insight on functions of TGF- β superfamily (36, 58).

However, reports on the clinical management strategy of using activin A for cancer therapy remain rare. Multiple reasons give rise to challenges for targeting activin A in tumor immune therapy, for example: presence of similarities and compensatory mechanisms with other TGF- β superfamily members, involvement in other processes of tumor development: including tumor migration, invasion or angiogenesis and tissue or cell sources for targeting. Furthermore, limited targeting specificity may lead to adverse effects and uncertainty to what extent the benefits are due to the impact of targeting activin A. As a consequence, it is critical to find approaches to identify those functions mainly performed by activin A rather than other similar ligands. Based on the immune repressive role of endogenous activin A, we expect to validate activin A as an anti-tumor factor in a wider context. Considering activin A is a pleiotropic factor, precise cell or tissue targeting design is needed to avoid affecting basic physiological functions and to maximize therapeutic efficacy as well. In addition, patient collectives suitable for receiving activin A-targeting treatment, perhaps those with poor response to immune checkpoint blockade (ICB) or high expression of INHBA in tumor

microenvironment, should be clarified. Further studies will better be carried out around these aspects in order to filter out the clinical scenarios where cancer patients will receive the highest benefit with the least side effects from targeting activin A.

AUTHOR CONTRIBUTIONS

FL and LG conceived the topic. FL drafted the manuscript and prepared figures. Others reviewed the manuscript. All authors read and approved the final manuscript.

REFERENCES

- Gregory SJ, Kaiser UB. Regulation of Gonadotropins by Inhibin and Activin. Semin Reprod Med (2004) 22(3):253–67. doi: 10.1055/s-2004-831901
- Namwanje M, Brown CW. Activins and Inhibins: Roles in Development, Physiology, and Disease. *Cold Spring Harb Perspect Biol* (2016) 8(7):a021881. doi: 10.1101/cshperspect.a021881
- Kaneda H, Arao T, Matsumoto K, De Velasco MA, Tamura D, Aomatsu K, et al. Activin A Inhibits Vascular Endothelial Cell Growth and Suppresses Tumour Angiogenesis in Gastric Cancer. Br J Cancer (2011) 105(8):1210–7. doi: 10.1038/bjc.2011.348
- Kariyawasam HH, Semitekolou M, Robinson DS, Xanthou G. Activin-A: A Novel Critical Regulator of Allergic Asthma. *Clin Exp Allergy* (2011) 41 (11):1505–14. doi: 10.1111/j.1365-2222.2011.03784.x
- Chen W, Ten Dijke P. Immunoregulation by Members of the TGFbeta Superfamily. Nat Rev Immunol (2016) 16(12):723–40. doi: 10.1038/nri.2016.112
- Weiss A, Attisano L. The TGFbeta Superfamily Signaling Pathway. Wiley Interdiscip Rev Dev Biol (2013) 2(1):47–63. doi: 10.1002/wdev.86
- Pituello F, Yamada G, Gruss P. Activin A Inhibits Pax-6 Expression and Perturbs Cell Differentiation in the Developing Spinal Cord In Vitro. Proc Natl Acad Sci U.S.A. (1995) 92(15):6952–6. doi: 10.1073/pnas.92.15.6952
- Attardi B, Miklos J. Rapid Stimulatory Effect of Activin-A on Messenger RNA Encoding the Follicle-Stimulating Hormone Beta-Subunit in Rat Pituitary Cell Cultures. *Mol Endocrinol* (1990) 4(5):721–6. doi: 10.1210/mend-4-5-721
- Sconocchia T, Sconocchia G. Regulation of the Immune System in Health and Disease by Members of the Bone Morphogenetic Protein Family. Front Immunol (2021) 12:802346. doi: 10.3389/fimmu.2021.802346
- Harrison CA, Gray PC, Vale WW, Robertson DM. Antagonists of Activin Signaling: Mechanisms and Potential Biological Applications. *Trends Endocrinol Metab* (2005) 16(2):73–8. doi: 10.1016/j.tem.2005.01.003
- Seeger P, Bosisio D, Parolini S, Badolato R, Gismondi A, Santoni A, et al. Activin A as a Mediator of NK-Dendritic Cell Functional Interactions. *J Immunol* (2014) 192(3):1241–8. doi: 10.4049/jimmunol.1301487
- Robson NC, Phillips DJ, McAlpine T, Shin A, Svobodova S, Toy T, et al. Activin-A: A Novel Dendritic Cell-Derived Cytokine That Potently Attenuates CD40 Ligand-Specific Cytokine and Chemokine Production. *Blood* (2008) 111(5):2733–43. doi: 10.1182/blood-2007-03-080994
- Rautela J, Dagley LF, de Oliveira CC, Schuster IS, Hediyeh-Zadeh S, Delconte RB, et al. Therapeutic Blockade of Activin-A Improves NK Cell Function and Antitumor Immunity. *Sci Signal* (2019) 12(596):eaat7527. doi: 10.1126/ scisignal.aat7527
- Seeger P, Musso T, Sozzani S. The TGF-Beta Superfamily in Dendritic Cell Biology. *Cytokine Growth Factor Rev* (2015) 26(6):647–57. doi: 10.1016/ j.cytogfr.2015.06.002
- Gutierrez-Seijo A, Garcia-Martinez E, Barrio-Alonso C, Parra-Blanco V, Aviles-Izquierdo JA, Sanchez-Mateos P, et al. Activin A Sustains the Metastatic Phenotype of Tumor-Associated Macrophages and Is a Prognostic Marker in Human Cutaneous Melanoma. J Invest Dermatol (2021) 142(3):653–661.e2. doi: 10.1016/j.jid.2021.07.179
- Zheng J, Zhang T, Han S, Liu C, Liu M, Li S, et al. Activin A Improves the Neurological Outcome After Ischemic Stroke in Mice by Promoting

FUNDING

This work was supported by Foundation of Shanghai Science and Technology Committee (No.22S11902100), Zhongshan Municipal Bureau of Science and Technology (No. 2020SYF08) and the Department of Science and Technology of Guangdong Province (No. 2019B090904008 and No. 2021B0909050003).

ACKNOWLEDGMENTS

All the figures were created with BioRender.com.

Oligodendroglial ACVR1B-Mediated White Matter Remyelination. *Exp Neurol* (2021) 337:113574. doi: 10.1016/j.expneurol.2020.113574

- Chen B, Chang HM, Zhang Z, Cao Y, Leung PCK. ALK4-SMAD3/4 Mediates the Effects of Activin A on the Upregulation of PAI-1 in Human Granulosa Lutein Cells. *Mol Cell Endocrinol* (2020) 505:110731. doi: 10.1016/j.mce.2020.110731
- de Guise C, Lacerte A, Rafiei S, Reynaud R, Roy M, Brue T, et al. Activin Inhibits the Human Pit-1 Gene Promoter Through the P38 Kinase Pathway in a Smad-Independent Manner. *Endocrinology* (2006) 147(9):4351–62. doi: 10.1210/en.2006-0444
- Dean M, Davis DA, Burdette JE. Activin A Stimulates Migration of the Fallopian Tube Epithelium, an Origin of High-Grade Serous Ovarian Cancer, Through Non-Canonical Signaling. *Cancer Lett* (2017) 391:114–24. doi: 10.1016/j.canlet.2017.01.011
- Tamminen JA, Yin M, Ronty M, Sutinen E, Pasternack A, Ritvos O, et al. Overexpression of Activin-A and -B in Malignant Mesothelioma - Attenuated Smad3 Signaling Responses and ERK Activation Promote Cell Migration and Invasive Growth. *Exp Cell Res* (2015) 332(1):102–15. doi: 10.1016/ j.yexcr.2014.12.010
- Heinz M, Niederleithner HL, Puujalka E, Soler-Cardona A, Grusch M, Pehamberger H, et al. Activin A is Anti-Lymphangiogenic in a Melanoma Mouse Model. J Invest Dermatol (2015) 135(1):212–21. doi: 10.1038/jid.2014.328
- 22. Thomas AL, Castellanos K, Mancinelli G, Xia Y, Bauer J, Yazici C, et al. Activin A Modulates Inflammation in Acute Pancreatitis and Strongly Predicts Severe Disease Independent of Body Mass Index. *Clin Transl Gastroenterol* (2020) 11(5):e00152. doi: 10.14309/ctg.000000000000152
- Eramaa M, Hurme M, Stenman UH, Ritvos O. Activin A/erythroid Differentiation Factor Is Induced During Human Monocyte Activation. *J Exp Med* (1992) 176(5):1449–52. doi: 10.1084/jem.176.5.1449
- 24. Ma C, Liu Z, Shang S, Jiang L, Lv X, Qi Y, et al. Activin A Regulates Activities of Peripheral Blood Natural Killer Cells of Mouse in an Autocrine and Paracrine Manner. *Exp Cell Res* (2019) 374(1):114–21. doi: 10.1016/ j.yexcr.2018.11.013
- Shapouri-Moghaddam A, Mohammadian S, Vazini H, Taghadosi M, Esmaeili SA, Mardani F, et al. Macrophage Plasticity, Polarization, and Function in Health and Disease. J Cell Physiol (2018) 233(9):6425–40. doi: 10.1002/ jcp.26429
- Ge J, Wang Y, Feng Y, Liu H, Cui X, Chen F, et al. Direct Effects of Activin A on the Activation of Mouse Macrophage RAW264.7 Cells. *Cell Mol Immunol* (2009) 6(2):129–33. doi: 10.1038/cmi.2009.18
- Wang Y, Cui X, Tai G, Ge J, Li N, Chen F, et al. A Critical Role of Activin A in Maturation of Mouse Peritoneal Macrophages *In Vitro* and In Vivo. *Cell Mol Immunol* (2009) 6(5):387–92. doi: 10.1038/cmi.2009.50
- Zhou J, Tai G, Liu H, Ge J, Feng Y, Chen F, et al. Activin A Down-Regulates the Phagocytosis of Lipopolysaccharide-Activated Mouse Peritoneal Macrophages *In Vitro* and *In Vivo. Cell Immunol* (2009) 255(1-2):69–75. doi: 10.1016/j.cellimm.2008.11.001
- Wu Q, Yang Z, Huang Y, Wang L, Weng R, Yang J. Effect of Activin A on Activation Status of Monocytes in Acute-Phase Kawasaki Disease. *Clin Exp Med* (2021) 21(3):407–14. doi: 10.1007/s10238-021-00695-y
- Indumathy S, Pueschl D, Klein B, Fietz D, Bergmann M, Schuppe HC, et al. Testicular Immune Cell Populations and Macrophage Polarisation in Adult

Male Mice and the Influence of Altered Activin A Levels. J Reprod Immunol (2020) 142:103204. doi: 10.1016/j.jri.2020.103204

- Sanjabi S, Oh SA, Li MO. Regulation of the Immune Response by TGF-Beta: From Conception to Autoimmunity and Infection. *Cold Spring Harb Perspect Biol* (2017) 9(6):a022236. doi: 10.1101/cshperspect.a022236
- 32. Ogawa K, Funaba M, Chen Y, Tsujimoto M. Activin A Functions as a Th2 Cytokine in the Promotion of the Alternative Activation of Macrophages. J Immunol (2006) 177(10):6787–94. doi: 10.4049/jimmunol. 177.10.6787
- Hreha TN, Collins CA, Daugherty AL, Griffith JM, Hruska KA, Hunstad DA. Androgen-Influenced Polarization of Activin A-Producing Macrophages Accompanies Post-Pyelonephritic Renal Scarring. *Front Immunol* (2020) 11:1641. doi: 10.3389/fimmu.2020.01641
- 34. Liu F, Qiu H, Xue M, Zhang S, Zhang X, Xu J, et al. MSC-Secreted TGF-Beta Regulates Lipopolysaccharide-Stimulated Macrophage M2-Like Polarization via the Akt/FoxO1 Pathway. Stem Cell Res Ther (2019) 10(1):345. doi: 10.1186/s13287-019-1447-y
- Petraglia F, Sacerdote P, Cossarizza A, Angioni S, Genazzani AD, Franceschi C, et al. Inhibin and Activin Modulate Human Monocyte Chemotaxis and Human Lymphocyte Interferon-Gamma Production. J Clin Endocrinol Metab (1991) 72(2):496–502. doi: 10.1210/jcem-72-2-496
- 36. Shurin MR, Ma Y, Keskinov AA, Zhao R, Lokshin A, Agassandian M, et al. BAFF and APRIL From Activin A-Treated Dendritic Cells Upregulate the Antitumor Efficacy of Dendritic Cells In Vivo. *Cancer Res* (2016) 76 (17):4959–69. doi: 10.1158/0008-5472.CAN-15-2668
- Kim HA, Jeon SH, Seo GY, Park JB, Kim PH. TGF-Beta1 and IFN-Gamma Stimulate Mouse Macrophages to Express BAFF via Different Signaling Pathways. J Leukoc Biol (2008) 83(6):1431–9. doi: 10.1189/jlb.1007676
- Kim JH, Seo GY, Kim PH. Activin A Stimulates Mouse APCs to Express BAFF via ALK4-Smad3 Pathway. *Immune Netw* (2011) 11(4):196–202. doi: 10.4110/ in.2011.11.4.196
- Geissmann F, Revy P, Regnault A, Lepelletier Y, Dy M, Brousse N, et al. TGF-Beta 1 Prevents the Noncognate Maturation of Human Dendritic Langerhans Cells. J Immunol (1999) 162(8):4567–75.
- Dong Y, Tang L, Letterio JJ, Benveniste EN. The Smad3 Protein is Involved in TGF-Beta Inhibition of Class II Transactivator and Class II MHC Expression. *J Immunol* (2001) 167(1):311–9. doi: 10.4049/jimmunol.167.1.311
- Yang L, Huang J, Ren X, Gorska AE, Chytil A, Aakre M, et al. Abrogation of TGF Beta Signaling in Mammary Carcinomas Recruits Gr-1+CD11b+ Myeloid Cells That Promote Metastasis. *Cancer Cell* (2008) 13(1):23–35. doi: 10.1016/j.ccr.2007.12.004
- Kobie JJ, Wu RS, Kurt RA, Lou S, Adelman MK, Whitesell LJ, et al. Transforming Growth Factor Beta Inhibits the Antigen-Presenting Functions and Antitumor Activity of Dendritic Cell Vaccines. *Cancer Res* (2003) 63(8):1860–4.
- 43. Rook AH, Kehrl JH, Wakefield LM, Roberts AB, Sporn MB, Burlington DB, et al. Effects of Transforming Growth Factor Beta on the Functions of Natural Killer Cells: Depressed Cytolytic Activity and Blunting of Interferon Responsiveness. J Immunol (1986) 136(10):3916–20.
- Robson NC, Wei H, McAlpine T, Kirkpatrick N, Cebon J, Maraskovsky E. Activin-A Attenuates Several Human Natural Killer Cell Functions. *Blood* (2009) 113(14):3218–25. doi: 10.1182/blood-2008-07-166926
- 45. Li MO, Sanjabi S, Flavell RA. Transforming Growth Factor-Beta Controls Development, Homeostasis, and Tolerance of T Cells by Regulatory T Cell-Dependent and -Independent Mechanisms. *Immunity* (2006) 25(3):455–71. doi: 10.1016/j.immuni.2006.07.011
- Chattopadhyay G, Shevach EM. Antigen-Specific Induced T Regulatory Cells Impair Dendritic Cell Function via an IL-10/MARCH1-Dependent Mechanism. J Immunol (2013) 191(12):5875–84. doi: 10.4049/jimmunol. 1301693
- 47. Semitekolou M, Morianos I, Banos A, Konstantopoulos D, Adamou-Tzani M, Sparwasser T, et al. Dendritic Cells Conditioned by Activin A-Induced Regulatory T Cells Exhibit Enhanced Tolerogenic Properties and Protect Against Experimental Asthma. *J Allergy Clin Immunol* (2018) 141(2):671–684 e7. doi: 10.1016/j.jaci.2017.03.047
- Ma C, Qi Y, Liu H, Wu C, Cui X, Liu Z. Inhibitory Effect of Activin A on IL-9 Production by Mouse NK Cells Through Smad3 Signaling. *Biol Chem* (2020) 401(2):297–308. doi: 10.1515/hsz-2019-0245

- Ogawa K, Funaba M, Tsujimoto M. A Dual Role of Activin A in Regulating Immunoglobulin Production of B Cells. J Leukoc Biol (2008) 83(6):1451–8. doi: 10.1189/jlb.1007710
- Lee HJ, Kim PH. Further Characterization of Activin A-Induced IgA Response in Murine B Lymphocytes. *Immune Netw* (2009) 9(4):133–7. doi: 10.4110/in.2009.9.4.133
- Arsura M, Wu M, Sonenshein GE. TGF Beta 1 Inhibits NF-Kappa B/Rel Activity Inducing Apoptosis of B Cells: Transcriptional Activation of I Kappa B Alpha. *Immunity* (1996) 5(1):31–40. doi: 10.1016/s1074-7613(00)80307-6
- 52. Lin YL, Tsai NM, Hsieh CH, Ho SY, Chang J, Wu HY, et al. *In Vivo* Amelioration of Endogenous Antitumor Autoantibodies *via* Low-Dose P4N Through the LTA4H/activin A/BAFF Pathway. *Proc Natl Acad Sci USA* (2016) 113(48):E7798–807. doi: 10.1073/pnas.1604752113
- Gorelik L, Flavell RA. Transforming Growth Factor-Beta in T-Cell Biology. Nat Rev Immunol (2002) 2(1):46–53. doi: 10.1038/nri704
- 54. Tousa S, Semitekolou M, Morianos I, Banos A, Trochoutsou AI, Brodie TM, et al. Activin-A Co-Opts IRF4 and AhR Signaling to Induce Human Regulatory T Cells That Restrain Asthmatic Responses. *Proc Natl Acad Sci* U.S.A. (2017) 114(14):E2891–900. doi: 10.1073/pnas.1616942114
- Vanpouille-Box C, Diamond JM, Pilones KA, Zavadil J, Babb JS, Formenti SC, et al. TGFbeta Is a Master Regulator of Radiation Therapy-Induced Antitumor Immunity. *Cancer Res* (2015) 75(11):2232–42. doi: 10.1158/0008-5472.CAN-14-3511
- De Martino M, Daviaud C, Diamond JM, Kraynak J, Alard A, Formenti SC, et al. Activin A Promotes Regulatory T-Cell-Mediated Immunosuppression in Irradiated Breast Cancer. *Cancer Immunol Res* (2021) 9(1):89–102. doi: 10.1158/2326-6066.CIR-19-0305
- Wu Q, Weng R, Xu Y, Wang L, Huang Y, Yang J. Activin a Suppresses Peripheral CD8(+) T Lymphocyte Activity in Acute-Phase Kawasaki Disease. *BMC Immunol* (2021) 22(1):17. doi: 10.1186/s12865-021-00407-x
- Morianos I, Tsitsopoulou A, Potaris K, Valakos D, Fari O, Vatsellas G, et al. Activin-A Impedes the Establishment of CD4(+) T Cell Exhaustion and Enhances Anti-Tumor Immunity in the Lung. J Exp Clin Cancer Res (2021) 40 (1):295. doi: 10.1186/s13046-021-02092-5
- Hardy CL, O'Connor AE, Yao J, Sebire K, de Kretser DM, Rolland JM, et al. Follistatin is a Candidate Endogenous Negative Regulator of Activin A in Experimental Allergic Asthma. *Clin Exp Allergy* (2006) 36(7):941–50. doi: 10.1111/j.1365-2222.2006.02523.x
- 60. Karagiannidis C, Hense G, Martin C, Epstein M, Ruckert B, Mantel PY, et al. Activin A is an Acute Allergen-Responsive Cytokine and Provides a Link to TGF-Beta-Mediated Airway Remodeling in Asthma. J Allergy Clin Immunol (2006) 117(1):111–8. doi: 10.1016/j.jaci.2005.09.017
- Semitekolou M, Alissafi T, Aggelakopoulou M, Kourepini E, Kariyawasam HH, Kay AB, et al. Activin-A Induces Regulatory T Cells That Suppress T Helper Cell Immune Responses and Protect From Allergic Airway Disease. *J Exp Med* (2009) 206(8):1769–85. doi: 10.1084/jem.20082603
- Wu B, Zhang S, Guo Z, Bi Y, Zhou M, Li P, et al. The TGF-Beta Superfamily Cytokine Activin-A is Induced During Autoimmune Neuroinflammation and Drives Pathogenic Th17 Cell Differentiation. *Immunity* (2021) 54(2):308–323 e6. doi: 10.1016/j.immuni.2020.12.010
- Ghoreschi K, Laurence A, Yang XP, Hirahara K, O'Shea JJ. T Helper 17 Cell Heterogeneity and Pathogenicity in Autoimmune Disease. *Trends Immunol* (2011) 32(9):395–401. doi: 10.1016/j.it.2011.06.007
- 64. Morianos I, Trochoutsou AI, Papadopoulou G, Semitekolou M, Banos A, Konstantopoulos D, et al. Activin-A Limits Th17 Pathogenicity and Autoimmune Neuroinflammation via CD39 and CD73 Ectonucleotidases and Hif1-Alpha-Dependent Pathways. Proc Natl Acad Sci U.S.A. (2020) 117 (22):12269–80. doi: 10.1073/pnas.1918196117
- Shevach EM, Thornton AM. Ttregs, Ptregs, and Itregs: Similarities and Differences. Immunol Rev (2014) 259(1):88–102. doi: 10.1111/imr.12160
- Liu Y, Zhang P, Li J, Kulkarni AB, Perruche S, Chen W. A Critical Function for TGF-Beta Signaling in the Development of Natural CD4+CD25+Foxp3+ Regulatory T Cells. *Nat Immunol* (2008) 9(6):632–40. doi: 10.1038/ni.1607
- Schaue D, Xie MW, Ratikan JA, McBride WH. Regulatory T Cells in Radiotherapeutic Responses. Front Oncol (2012) 2:90. doi: 10.3389/ fonc.2012.00090
- Kachikwu EL, Iwamoto KS, Liao YP, DeMarco JJ, Agazaryan N, Economou JS, et al. Radiation Enhances Regulatory T Cell Representation. *Int J Radiat Oncol Biol Phys* (2011) 81(4):1128–35. doi: 10.1016/j.ijrobp.2010.09.034

 De Martino M, Daviaud C, Vanpouille-Box C. Activin A Backs-Up TGF-Ss to Promote Regulatory T Cells. Oncoimmunology (2021) 10(1):1883288. doi: 10.1080/2162402X.2021.1883288

Conflict of Interest: The authors declare that the research was conducted in the absence of any commercial or financial relationships that could be construed as a potential conflict of interest.

Publisher's Note: All claims expressed in this article are solely those of the authors and do not necessarily represent those of their affiliated organizations, or those of the publisher, the editors and the reviewers. Any product that may be evaluated in this article, or claim that may be made by its manufacturer, is not guaranteed or endorsed by the publisher.

Copyright © 2022 Li, Long, Yu, Tong and Gong. This is an open-access article distributed under the terms of the Creative Commons Attribution License (CC BY). The use, distribution or reproduction in other forums is permitted, provided the original author(s) and the copyright owner(s) are credited and that the original publication in this journal is cited, in accordance with accepted academic practice. No use, distribution or reproduction is permitted which does not comply with these terms.



OPEN ACCESS

Edited by: Xian Zeng,

Fudan University, China

Reviewed by:

Xiaopei Shen, Fujian Medical University, China Du Liping, Chongqing Eye Institute, China

*Correspondence:

Qinghua Lyu Lyuqh2020@163.com Jun Zhao doctorzhaojun@163.com

[†]These authors have contributed equally to this work and share first authorship

Specialty section:

This article was submitted to Cancer Immunity and Immunotherapy, a section of the journal Frontiers in Immunology

Received: 17 April 2022 Accepted: 10 May 2022 Published: 14 June 2022

Citation:

Ma X, Yu S, Zhao B, Bai W, Cui Y, Ni J, Lyu Q and Zhao J (2022) Development and Validation of a Novel Ferroptosis-Related LncRNA Signature for Predicting Prognosis and the Immune Landscape Features in Uveal Melanoma. Front. Immunol. 13:922315. doi: 10.3389/fimmu.2022.922315

Development and Validation of a Novel Ferroptosis-Related LncRNA Signature for Predicting Prognosis and the Immune Landscape Features in Uveal Melanoma

Xiaochen Ma^{1†}, Sejie Yu^{1†}, Bin Zhao², Wei Bai¹, Yubo Cui³, Jinglan Ni¹, Qinghua Lyu^{3*} and Jun Zhao^{3*}

¹ The Second Clinical Medical College, Jinan University, Shenzhen, China, ² Biomedical Research Institute, Shenzhen Peking University-The Hong Kong University of Science and Technology Medical Center, Shenzhen, China, ³ Department of Ophthalmology, Shenzhen People's Hospital, The Second Clinical Medical College of Jinan University & The First Affiliated Hospital of Southern University of Science and Technology, Shenzhen, China

Background: Ferroptosis is a newly iron-dependent mode of programmed cell death that is involved in a variety of malignancies. But no research has shown a link between ferroptosis-related long non-coding RNAs (FRLs) and uveal melanoma (UM). We aimed to develop a predictive model for UM and explore its potential function in relation to immune cell infiltration.

Methods: Identification of FRLs was performed using the Cancer Genome Atlas (TCGA) and FerrDb databases. To develop a prognostic FRLs signature, univariate Cox regression and least absolute shrinkage and selection operator (LASSO) were used in training cohort. Kaplan-Meier (K-M) and receiver operating characteristic (ROC) curve analyses were used to assess the reliability of the risk model. The immunological functions of FRLs signature were determined using gene set enrichment analysis (GSEA). Immunological cell infiltration and immune treatment were studied using the ESTIMATE, CIBERSORT, and ssGSEA algorithms. Finally, *in vitro* assays were carried out to confirm the biological roles of FRLs with known primer sequences (LINC00963, PPP1R14B.AS1, and ZNF667.AS1).

Results: A five-genes novel FRLs signature was identified. The mean risk score generated by this signature was used to create two risk groups. The high-risk score UM patients had

a lower overall survival rate. The area under the curve (AUC) of ROC and K-M analysis further validated the strong prediction capacity of the prognostic signature. Immune cells such as memory CD8 T cells, M1 macrophages, monocytes, and B cells showed a substantial difference between the two groups. GSEA enrichment results showed that the FRLs signature was linked to certain immune pathways. Moreover, UM patients with high-risk scores were highly susceptible to several chemotherapy drugs, such as cisplatin, imatinib, bortezomib, and pazopanib. Finally, the experimental validation confirmed that knockdown of three identified IncRNA (LINC00963, PPP1R14B.AS1, and ZNF667.AS1) suppressed the invasive ability of tumor cells *in vitro*.

Conclusion: The five-FRLs (AC104129.1, AC136475.3, LINC00963, PPP1R14B.AS1, and ZNF667.AS1) signature has effects on clinical survival prediction and selection of immunotherapies for UM patients.

Keywords: ferroptosis, IncRNA, immune microenvironment, uveal melanoma, bioinformatics, prognostic value

INTRODUCTION

Uveal melanoma (UM) is a rare subtype of melanoma that differs significantly from cutaneous and other types of melanoma in terms of biological and clinical characteristics, with extremely high mortality rates (1, 2). The mean incidence of UM in the USA was five per million (3, 4). Approximately half of UM patients will develop hepatic metastasis (5–8). Although various therapies, such as radiotherapy, local resection, immunotherapy, chemotherapy, and phototherapy, increase the possibility of preserving useful vision, the unsatisfied prognosis of UM has not improved appreciably (9, 10). In addition, recent investigations show that prospective diagnostic tools for UM are rare and limited, indicating the challenge of early diagnosis of UM (11). Therefore, novel predictive models and useful biomarkers for UM patients need to be found and used in clinical practice as soon as possible.

Dysfunction of anti-tumor immunity in tumor microenvironment is a hallmark of melanoma and re-balance of immunosuppressive microenvironment is crucial for melanoma treatment (12). Recently, several immune checkpoint blockage immunotherapies have been approved for the treatment of melanoma, which contributed to survival of UM patients and provided effective disease control in a fraction of patients (13). Recently clinical practices reported that programmed cell death 1(PD-1) inhibitors only achieved 3.6-4.7% of response rate in patients with UM, and blood biomarkers represented a hopeful mean to evaluate the efficacy of immunotherapy in UM (14, 15). These studies recapped the different characteristics of tumor immune microenvironment of UM and highlighted the importance of developing novel prognostic prediction tools for UM immunotherapy.

Recent years, ferroptosis, as a new category of regulated cell death, is triggered by intracellular iron and it participates in a variety of physiological activities, such as lipid peroxidation and iron metabolism (16–18). The abnormalities of ferroptosis have been associated with the development of hepatocellular, cervical, breast, lung, ovarian, prostate, colorectal, renal carcinomas, and melanoma

(17, 19–22). The tumor-suppressive effect of ferroptosis in carcinomatosis is crucial, including UM (23). Oleic acid prevented melanoma cells from entering ferroptosis, and enhanced lymphatic exposure protected melanoma cells against ferroptosis and boosted their ability to survive (24). Moreover, drugs-induced ferroptosis could potentially enhance anti-tumor immunity response by inhibiting the dedifferentiation of melanoma cells (25, 26). So, evaluation of ferroptosis-related genes (FRGs) or FRLs may provide new clues for diagnoses and prognosis prediction of UM.

Long noncoding RNAs (lncRNAs), as a form of non-coding RNA, play a pivotal role in cellular processes, such as metabolism, neurodegenerative dysfunction, cell cycle regulation, and neoplasia (27–29). LncRNAs are involved in essential carcinogenesis pathways in melanoma, such as the PI3K/Akt, NF-kappa B, and MAPK/ERK (30). Currently, fast-growing studies have explored the ferroptosis-related roles of lncRNAs in tumorigenesis (31). For examples, miR-9 promotes ferroptosis through targeting GOT1 in melanoma cells (32). The miR-137 inhibits necroptosis, and the knockdown of miR-137 boosted anticancer efficacy of erastin by enhancing ferroptosis both *in vitro* and *in vivo* (33). As a result, lncRNA might be examined as a possible target for novel RNA-based anti-UM treatments (34, 35).

Based on the above facts, we hypothesized that FRLs might benefit in the identification of high-risk UM patients and the development of customized treatment plans for them. Herein, we constructed a FRLs signature and confirmed its prognostic value for UM patients. Then, we evaluated the relationship between the immune infiltration landscape and FRLs signature. Finally, we conducted cell experiments to further verify the biological functions of three identified FRLs with known primer sequences.

MATERIALS AND METHODS

Collection and Sorting of Data

The RNA sequencing data in FPKM format and clinicopathological characteristics of UM patients (n=80) were downloaded from TCGA (https://portal.gdc.cancer.gov/). Our research only included

UM patients with known survival time and status. Additionally, patients with overall survival of fewer than 30 days in TCGA-UM were excluded to ensure the reliability of the study. The 'caret' R package randomly allocated all the selected patients (n=74) into the training and validation cohorts in a 1:1 ratio (36). The ensemble expression matrix was converted into a gene symbol expression matrix using Perl language. Log2 conversion of the data was performed.

Selection of Potential FRLs

In total, 382 FRGs were obtained from the FerrDb website (http://www.zhounan.org/ferrdb/index.html) database (37). Then, we determined the association between FRGs and lncRNAs by the 'limma' R package with Spearman correlation coefficient > 0.6 and p < 0.001 as the threshold (38).

Construction of a Prognostic FRLs Signature

Prognostic FRLs were screened using a univariate Cox regression analysis. Those FRLs with *p*-value < 0.01 were chosen for an overall survival-based LASSO regression analysis to reduce overfit and the number of FRLs by the 'glmnet' R package. The risk formula were calculated based on the FRLs expression levels and relevant regression coefficient as follows:

Risk score of FR – lncRNAs signature = \sum_{i} Coefficient(FR – lncRNAs_i)

 $* lncRNA Expression(FR - lncRNAs_i)$

Evaluation of Risk Model Prediction Ability

The predictive efficacy of the FRLs signature was assessed using K-M and ROC curve analyses by the 'survival' and 'survminer' R packages. The principal component analysis (PCA) and t-distributed stochastic neighbor embedding (t-SNE) analysis further examined the clustering ability of risk score. We also compared the prediction ability of the FRLs signature with additional clinical characteristics, such as gender, age, and tumor classification.

Construction of Ferroptosis-Related LncRNA-mRNA Network

The lncRNA-mRNA coexpression network was created to show the relationship between the FRLs and their related mRNAs using the 'ggalluvial' R package and Cytoscape software (version 3.9.0) (39).

Functional Analysis

Background biological enrichment analyses, such as the Kyoto Encyclopedia of Genes and Genomes (KEGG) pathways and GO biology functions, were examined using GSEA (Version 4.1.0) by 'ggplot2' R package. Gene sets items with normal p < 0.05 with FDR q < 0.25 were considered significant.

Comprehensive Analysis in the Immune Infiltration Response, Antitumor Drug Sensitivity, and Tumor Mutation Burden

The difference in immune cell infiltration, the stromal, tumor purity, immune, and ESTIMATE score between the two groups

was evaluated using the CIBERSORT and ESTIMATE algorithm (40). The immune function and cell subgroups were investigated using the ssGSEA. In addition, the immune checkpoint and m6A-related genes collected from prior publications were also investigated using 'limma' and 'ggplot2' R package. The IC50 of frequently used chemotherapeutic medicines was calculated by using R package 'pRRophetic.' (41). Tumor Mutation Burden (TMB) was also analyzed using the 'maftools' R package.

Cell Culture and siRNA Transfection

Human highly invasive UM cell line (C918) was purchased from Procell Life Science &Technology, Wuhan, China. C918 cells were cultivated in Roswell Park Memorial Institute medium. Small interfering and negative control RNA were used in knockdown experiments. After 48 hours transfection, cells were collected for RNA extraction or other functional assays. The sequences of siRNA utilized are listed in **Supplementary Table 1**.

RNA Collection and Quantitative Real Time-PCR

TRIzol (Invitrogen, Carlsbad, CA) was used to extract total RNA from cell samples. The reverse transcription of the RNA into complementary DNA was subsequently performed using a GoScript reverse transcription system (Promega). Quantitative Real Time-PCR (qRT-PCR) validated the transfection efficiency. The list of the primer sequences utilized is shown in **Supplementary Table 2**. The following were the qRT-PCR conditions: initial denaturation takes 5 minutes at 95°C, followed by 40 cycles of denaturation (15 sec at 95°C), annealing (30 sec 59°C), elongation (30 sec at 72°C), and ultimate extension (5 min at 72°C).

Cell Invasion Assays

Transwell assays were used to assess C918 cell invasion ability. 1.5×10^4 cells were placed in the top chamber. After a 24-hour incubation period, C918 cells shifted through the membrane were kept for 15 min in methanol and dyed with 10% crystal violet. For invasion assays, Matrigel (Basement Membrane Matrix) was placed into the top chambers 24 h before the trials. The number of C918 cells was counted in ten randomly chosen fields.

Cell Proliferation

The capacity of C918 cells to proliferate was assessed using the Cell Counting Kit-8 (CCK-8) assay (MCE). After 48 h transfection, C918 cells were seeded at a density of 3500 cells per well in 96-well plates in six repetitions. After 12 h, 24 h, 36 h, and 48 h, the C918 cells were incubated with 10% CCK-8 solution for 1 h at 37°C. A 450 nm wavelength was used to measure the absorbance of living cells.

Scratch Test

C918 cells were collected and implanted into a six-well plate, where they were grown until 80% fusion. Then the C918 cells were starved in a serum-free medium for 24 hours. The plate was scratched with a one-line design using a 1000 μ l pipette tip. Scratch healing was examined under the microscope and photographed after a 24-hour culture period.

Statistical Analysis

The R language software was used to conduct all statistical computations in this research. The Wilcoxon method was used for the two-sample tests. The Kruskal-Wallis test was utilized to assess differences in data among the multiple groups.

RESULTS

Acquisition of LncRNA Associated With Ferroptosis

The FRLs signature was constructed following the flowchart shown in **Figure 1**. We identified 14,057 lncRNAs and 240 FRGs from the TCGA-UM data. 535 FRLs were identified with the threshold of Pearson correlation coefficients > 0.6 and p < 0.001 (**Supplementary Table 3**).

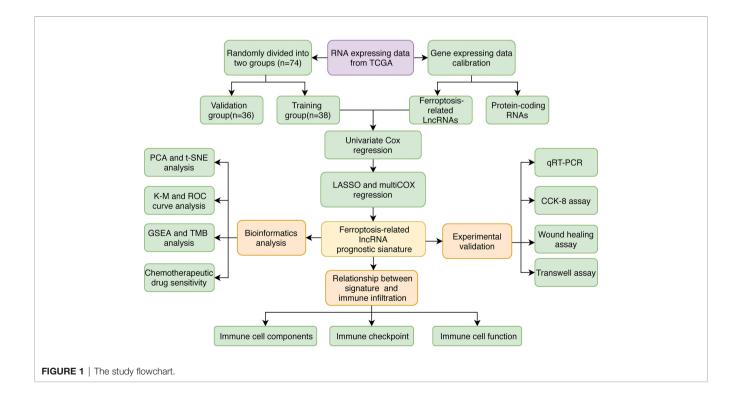
Development and Validation of Prognostic FRLs Signature

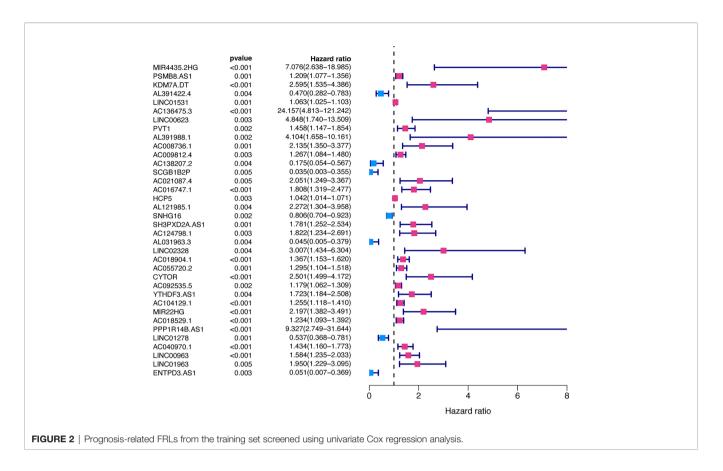
49 lncRNAs were uncovered after univariate Cox analysis with p < 0.01 filtering (**Figure 2**), five of which were determined using LASSO regression and finally included in the prognostic model (**Figures 3A, B**). The patients were divided into two groups (high-risk and low-risk) according to the median risk score, and the risk score was as follows: risk score = (4.9674 × AC136475.3) + (0.2274 × AC104129.1) + (1.4277 × PPP1R14B.AS1) + (-0.3151 × LINC00963) + (-0.6063 × ZNF667.AS1) (**Figure 3C**).

The predictive value of the five-FRLs signature was investigated. The K-M curves showed that patients with a high risk score had a considerably increased risk of mortality (Figures 4A-C). The areas under the ROC (AUC) values in the training and testing cohorts were 0.904 and 0.740 at 1 year, which showed high accuracy (Figures 4D-F). In addition, the survival status, survival times, and expression patterns of patients with UM are shown in Figures 5A-C. The ROC findings also revealed that the risk signature was a more relatively precise prognostic indicator than other clinical alternative prediction models for UM (Figures 5D-F). Patients with the elevated expression of the discovered FRLs, such as AC104129.1, AC136475.3, LINC00963, and PPP1R14B.AS1, showed a shorter overall life expectancy (p < 0.01) (Figures 6A–C). The lncRNA distribution of the two groups was shown in the PCA and t-SNE analyses (Figures 6D-F), and we obviously judged that the selected UM patients might be better discriminated between the two groups. Furthermore, univariate and multivariate Cox regression analysis showed that only the five FRLs signature could serve as an independent prognostic factor for UM patients (Figures 7A-C). Additionally, as the stages and T classification progressed, the risk score increased (p < 0.05) (Figures 7D-G). This finding implies that the FRL signature is strongly involved in the development and prognosis of UM. Sankey diagram depicted the link between FRLs and FRGs, as well as their risk types in UM (Figure 8A). The blue nodes represent genes, whereas the pink nodes indicate FRLs coexpressed with those genes (Figure 8B).

Functional Analysis

Immune-related GO terms and KEGG pathways were analyzed by GSEA. The high-risk group had an accumulation of immunerelated GO items (**Figure 8C**), including macrophage activation involved in immune response, immunological memory process,





lipopolysaccharide mediated signaling pathway, mature B cell differentiation, and innate immune response. In addition, the KEGG pathways proteasome, cytosolic DNA sensing, Toll-like receptor (TLR), leukocyte transendothelial migration, and Leishmania infection were also enriched in the high-risk group (**Figure 8D**). The details are presented in **Supplementary Table 4**. These results suggested that the newly identified FRLs signature was strongly associated with tumor immune function.

Differences in the Immune Cell Infiltration, Anti-Tumor Targeted Drug Sensitivity, and Tumor Mutation Burden

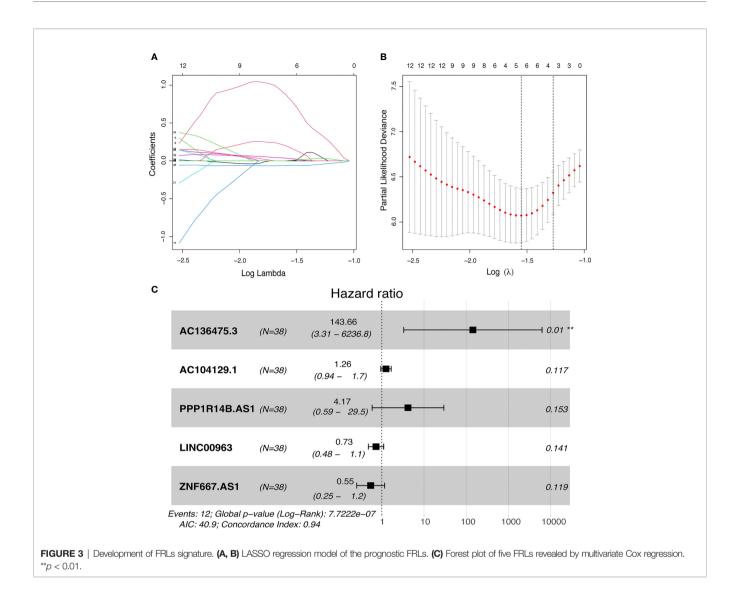
We used the CIBERSORT algorithm to examine the immune cell infiltration landscape in UM patients to comprehend more about the association between the FRLs signature and antitumor immune regulation. A heatmap was used to demonstrate the changes in immune cell infiltration between the two groups (**Figure 9A**). **Figure 9B** shows the percentage of each typical immune cell. We found that CD8 T cells, M1 macrophages, memory B cells, CD4 memory T cells, Monocytes, and resting mast cells were significantly different between the two groups. The different immune cell correlation was displayed in **Figure 9C. Figures 9D-G** showed that the immune, ESTIMATE, and stromal score were all considerably higher in the high-risk group. Almost all scores of immune cell proportion and immune-related functions differed substantially between the two groups (**Figures 10A, B**). As shown in **Figure 10C**, some validated effective checkpoint immunotherapy targets were overexpressed in the high-risk group, such as PDCD1 (PD-1) and CTLA4. Furthermore, the expression of m6A-related genes YTHDF1 and ALKBH5 was obviously higher in the high-risk group (**Figure 10D**). These revealed that the immune responses of the two groups differed, which might be applied to anti-tumor immunotherapy in UM.

We evaluated the estimated IC50 levels of some chemotherapy medicines between the two groups, and ten typical drugs are shown in **Figure 11A**. The results showed that cisplatin, imatinib, nilotinib, rapamycin, bortezomib, and pazopanib may be potential medications for treating UM patients in the high-risk group.

Although there was no statistically significant difference in TMB levels between the two groups (**Figures 11B–D**), we found that higher TMB had a tendency for lower overall survival rate (**Figures 11E–F**).

Experimental Validation Analysis

The roles of the five identified FRLs have not been reported in UM. In addition, the detailed primer sequences of AC104129.1 and AC136475.3 are unavailable in gene banks. Thus, to further explore the potential cell function of the other three lncRNAs (LINC00963, PPP1R14B.AS1, and ZNF667.AS1), we used the C918 cell line to construct the lncRNAs knockdown phenotypes. The transfection efficiency was confirmed by qRT–PCR (**Figure 12A**), and both siRNA fragments dramatically reduced

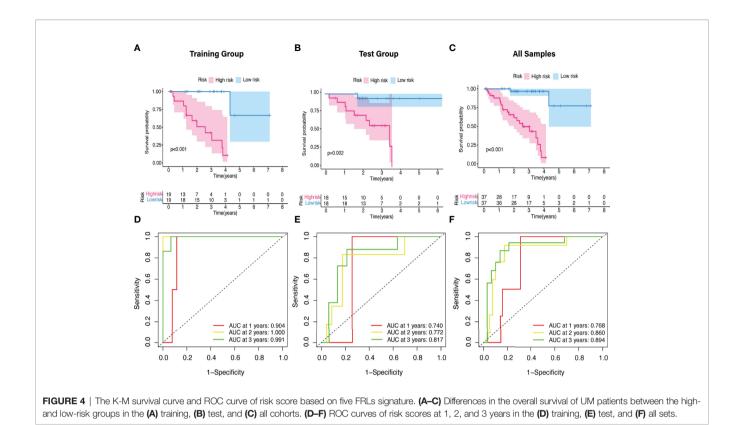


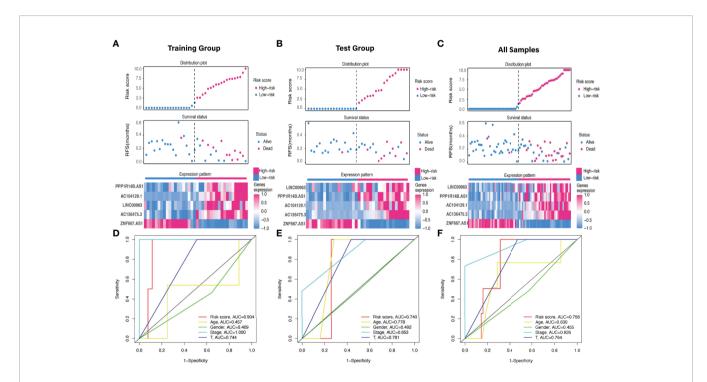
the expression of LINC00963, PPP1R14B.AS1, and ZNF667.AS1. Then, we performed a series of assays to study cell function change. CCK-8 assay results suggested that the down-regulation of PPP1R14B.AS1 inhibited the proliferation ability of C918, while the underexpression of ZNF667.AS1 enhanced the proliferation of C918 cells. The knockdown of LINC00963 in the C918 cells could not change the proliferation capacity (Figure 12B). Scratch test suggested that after culture for 24 h, scratches of the knock-down group healed slowly and the area of cell migration decreased, indicating that inhibition of LINC00963, PPP1R14B.AS1, and ZNF667.AS1 expression could reduce the migration ability of C918 cells (Figure 12C). Furthermore, knockdown of LINC00963, PPP1R14B.AS1, and ZNF667.AS1 attenuated the invasion ability of C918 cells via transwell assay (Figure 12D). These findings suggest that LINC00963, PPP1R14B.AS1, and ZNF667.AS1 serve as highrisk predictors in C918 cells, and their high expression promotes cancer growth in some way.

DISCUSSION

Patients with advanced stage UM have a death rate of more than 95% within 5 years (42), so discovering new and effective prognostic biomarkers is crucial for UM. Several studies have recently begun to mine the prognostic lncRNA value in tumors from public databases. For examples, a FRLs signature could be utilized to accurately predict the prognosis of glioma (43). BASP1-AS1 might be used as a biomarker to detect cutaneous malignant melanoma (44). However, to our knowledge, there is a scarcity of studies focusing on FRLs in UM. Many cellular processes, including ferroptosis, are regulated by lncRNAs in experimental studies. Several previously identified lncRNAs are related to shape, TNM stages, diagnosis, and progression of melanoma (45). Therefore, developing a FRLs signature may be useful in predicting UM prognosis and optimizing therapeutic methods.

In this study, we first obtained 240 FRGs and 535 FRLs in TCGA-UM data. Patients with UM were allocated to the







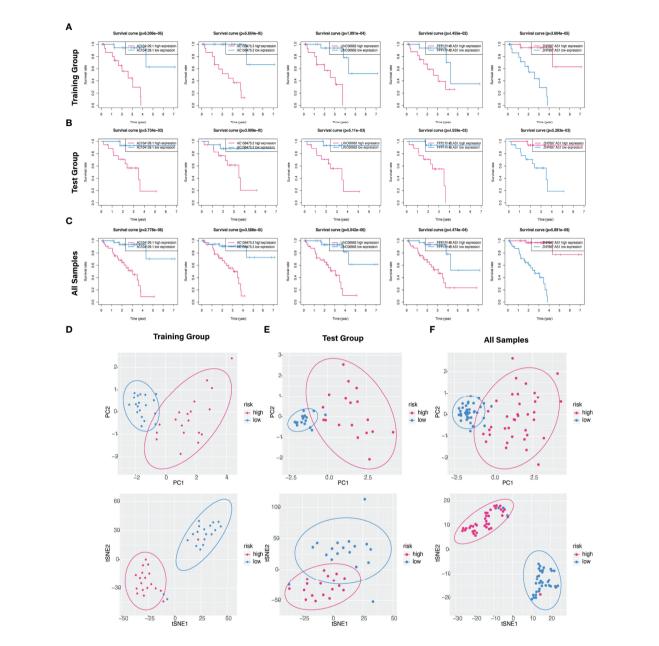
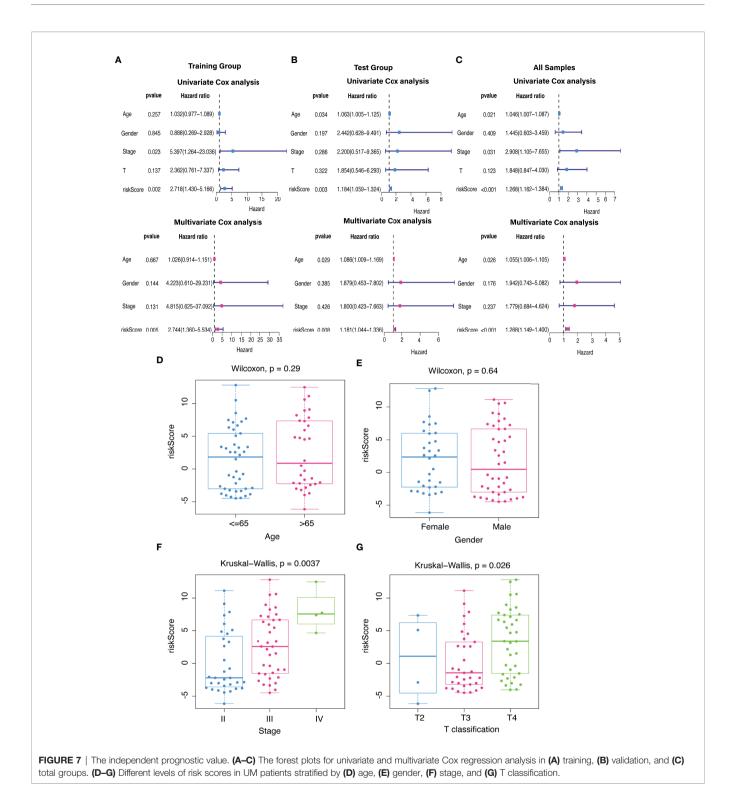


FIGURE 6 | Kaplan–Meier survival analysis of five hub FRLs and discrimination analysis of the risk score. (A–C) The K-M survival curve analysis of the five optimal FRLs signature (AC104129.1 AC136475.3, LINC00963, and PPP1R14B.AS1, and ZNF667.AS1) in the (A) training, (B) test, and (C) all cohorts. (D–F) PCA and t-SNE diagrams of genome-wide expression profiles of TCGA-UM in the (D) training, (E) validation, and (F) all groups, respectively.

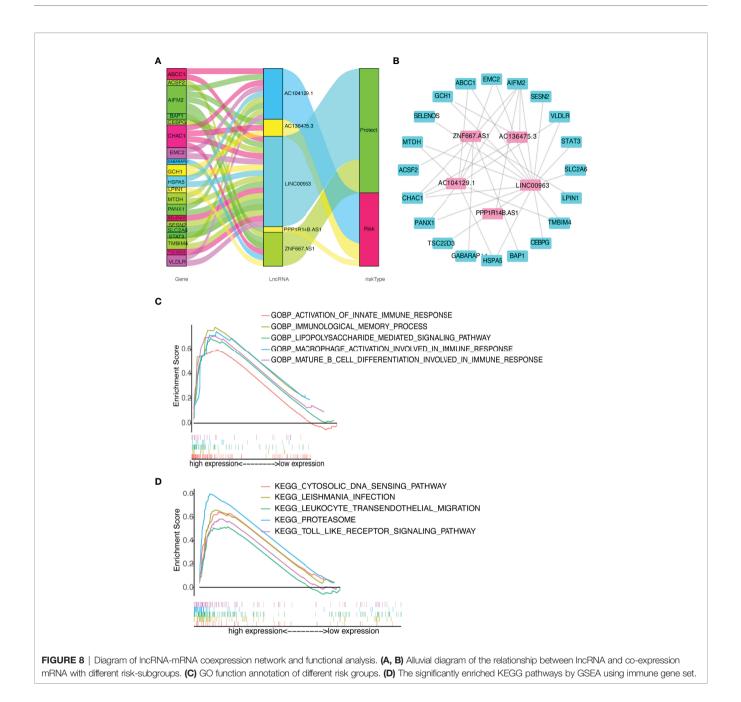
training and test groups in a 1:1 ratio. We first identified 49 prognostic FRLs using univariate Cox regression analysis. Then We obtained five FRLs signature using LASSO Cox regression. The following K-M survival analysis showed that UM patients with the high-risk score had a terrible prognosis, but those in the low-risk group had a better life expectancy, demonstrating strong prognostic potential of the newly discovered signature. Additionally, AUC analysis suggested stable performance in different risk-level UM patients. As a result, once the expression

levels of the five FRLs are identified, we can forecast the probability of mortality in patients with UM. We also found that risk score was significantly higher in advanced stage (IV) and T classification (IV), indicating that the FRLs signature has a significantly discriminable ability for UM patients. Then, we conducted a series of cell tests to verify the function of these discovered FRLs. These findings suggested that the FRL signature might be exploited as a viable UM prognostic biomarker.



Our FRLs signature included AC104129.1, AC136475.3, LINC00963, PPP1R14B.AS1, and ZNF667.AS1. The roles of the five FRLs have not been reported in UM. This research was the first to utilize the lncRNA AC104129.1 as a biomarker for cancer. Nevertheless, further research on AC104129.1 is needed to understand the deeper mechanisms in the future. The other

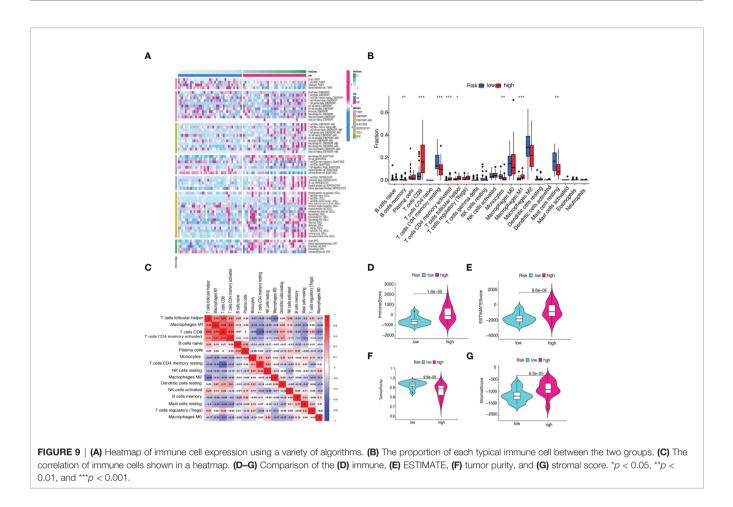
four lncRNAs have been reported as biomarkers for different carcinoma. For instance, AC136475.3 could be considered as a prognostic factor hepatocellular carcinoma (46). LINC00963 could serve as an oncogene by regulating biological processes, including survival, metastasis, and differentiation (47), was upregulated in prostate cancer (48), hepatocellular carcinoma (49),



osteosarcoma (50), and cutaneous squamous cell carcinoma (51, 52). PPP1R14B-AS1 was identified to be highly expressed in 12 malignancies in the TCGA database. The inhibition of PPP1R14B-AS1 can repress growth and migration in human hepatocellular carcinoma (53). ZNF667-AS1, as a tumor suppressor, could inhibit the viability, migration, and invasion of esophageal squamous cell carcinoma (54). In this study, the CCK-8 experiment revealed that the down-regulation of PPP1R14B.AS1 decreased C918 proliferation. In contrast, C918 cells proliferated more when ZNF667.AS1 was underexpressed. In addition, the knockdown of LINC00963 had no obvious effect on the proliferation of C918 cells. For the scratch migration and

transwell assay, the knockdown of the three identified FRLs (LINC00963, PPP1R14B.AS1, and ZNF667.AS1) could suppress migration and invasion in the C918 cell line, similar to the abovementioned findings.

Additionally, we investigated the correlation between the immune infiltration and the five-FRLs signature. We found that memory B cells, M1 macrophages, activated CD4 memory T cells, Monocytes, CD8 T cells, and resting mast cells were significantly different between the two groups. CD8 T cells have the capacity to promote ferroptosis *in vivo* (55, 56). In a recent case report, the accumulation of CD8 T cells was detected in hepatic metastases lesions in a patient with UM (57). In our



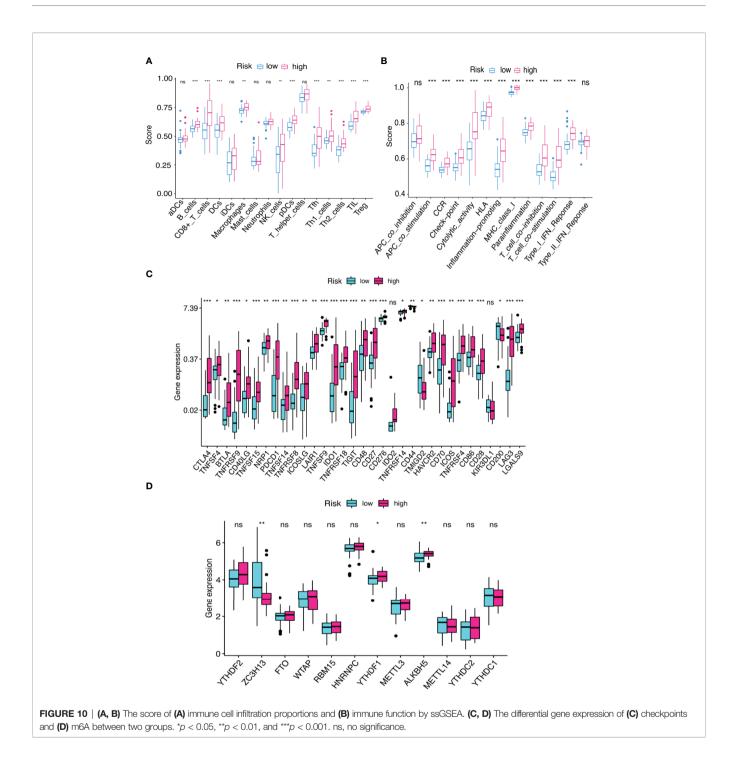
study, the percentage of CD8 T cells was greater in patients with a high risk score. Recent findings show that interferon-gamma produced by CD8 T cells has a tumor-suppressing impact when ferroptosis is activated, suggesting that the immune system may help to prevent carcinogenesis through ferroptosis (55). This could provide fresh insights into the association between ferroptosis and tumor immune microenvironment.

Immune checkpoint inhibitors (including PD-1, CTLA-4, PD-L1, and TIM-3) reduced the activation of immune cell, leading to immunosuppression of the tumor immune microenvironment (58, 59). Anti-PD-1 drugs, such as pembrolizumab, nivolumab, or atezolizumab, were already used to treat individuals with metastatic UM, displaying limited response rates and therapeutic effects in UM patients (14, 60, 61). Anti CTLA-4 drugs, such as tremelimumab and ipilimumab, were also used in patients with metastatic UM. A previous meta-analysis showed that immune checkpoint blockade immunotherapy was helpful for the treatment of UM patients in terms of long-term survival (62). In this study, the PD-1 expression was increased in the high-risk group. CD8 T cells could regulate endocytic recycling of PD-1 and exert synergistic effects with anti-PD-1 therapy in hepatocellular carcinoma (63), and inducing immunogenic ferroptosis

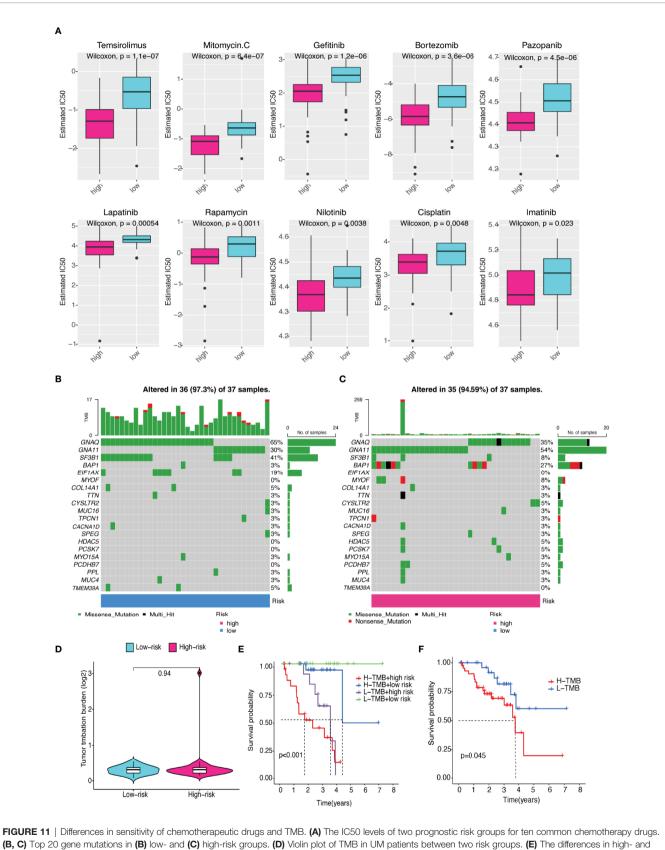
in cancer cells also potentiates anti-PD-1 therapy (64), highlighting a promising strategy for cancer immunotherapy.

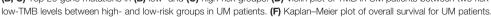
GSEA results showed that immune system hallmarks, such as immunological memory process, activation of innate immune response, mature B cell differentiation, lipopolysaccharide mediated pathway, and TLR, were considerably enriched in the high-risk score group. TLR is an essential protein molecule in innate immunity and a major regulator of ferroptosis (65–67), and the anti-tumor effectiveness of immunotherapy was aided by enhanced ferroptosis (55). TLR stimulation activated immunoinhibitory signaling pathways such as PD-1 expression (68), which indicates that new targets may be developed to improve therapeutic efficacy for UM.

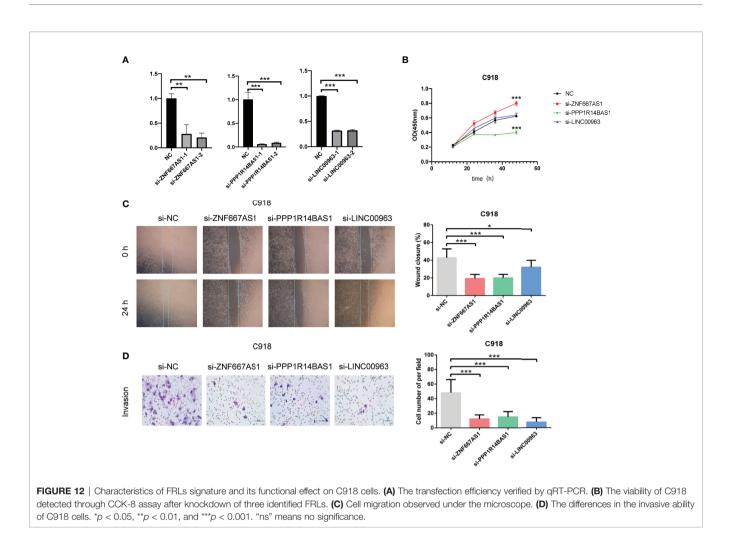
Predicting the drug sensitivity facilitated in avoiding ineffective use of drugs, revealed new applications for existing drugs, and increased the success rate of therapy (69). Chemotherapy may cause clinical benefits in UM, particularly in patients without bulky liver metastases. The combination of nivolumab and ipilimumab was found to be highly beneficial in metastatic UM (70). Chemotherapy regimens adapted from cutaneous melanoma, such as cisplatin, dacarbazine, and temozolomide, have been utilized in UM patients, and response rates vary between 0% and 15% (71, 72). A triple-



drug treatment regimen consisting of cisplatin, vinblastine, and dacarbazine also improved UM patient survival (73). Recent studies have shown that the inducing ferroptosis by blocking STAT3/Nrf2/GPx4 signaling makes osteosarcoma cells more sensitive to cisplatin (74). Our research demonstrated that patients in high-risk group were more susceptible to cisplatin, mitomycin C, gefitinib, bortezomib, pazopanib, lapatinib, rapamycin, and temsirolimus. This may provide novel therapeutic strategies targeting ferroptosis in UM patients. Admittedly, this study has some limitations. Firstly, the research only covered a limited number of patients owing to the low prevalence of UM, and some deviations might occur. Secondly, the stages N and M of UM patients were excluded because of the unavailable data. Therefore, it is unclear whether they are predictive factors. Lastly, the exact process through which these lncRNAs influence ferroptosis is uncertain. The association between these lncRNAs and FRGs has to be investigated further.







In summary, for the first time, we report and confirm a five-FRLs signature that could be used as a potential biomarker and treatment option for UM. Our results may contribute to predicting the prognosis and developing effective chemotherapy and immunotherapy for UM patients.

DATA AVAILABILITY STATEMENT

Publicly available datasets were analyzed in this study. This data can be found in TCGA (https://portal.gdc.cancer.gov/projects/TCGA-UVM). Further inquiries can be directed to the corresponding authors.

AUTHOR CONTRIBUTIONS

XM, JZ, and QL conceived and designed this study. XM, SY, WB, BZ, YC, JZ, QL, and JN downloaded and analyzed the raw data, performed bioinformatics, and wrote the manuscript. BZ, XM, SY, WB, YC, and JN performed the cell experiments. JZ and QL supervised the research and critically reviewed the paper. All of the writers contributed to the essay and gave their approval to the

final version. All authors contributed to the article and approved the submitted version.

FUNDING

This study received funding from the Science, Technology and Innovation Commission of Shenzhen Municipality under grant (No. JCYJ20210324113610029 and No. JCYJ20180228164400218).

ACKNOWLEDGMENTS

We are sincerely acknowledging the contributions from the TCGA.

SUPPLEMENTARY MATERIAL

The Supplementary Material for this article can be found online at: https://www.frontiersin.org/articles/10.3389/fimmu.2022. 922315/full#supplementary-material

REFERENCES

- Rodrigues M, de Koning L, Coupland SE, Jochemsen AG, Marais R, Stern M-H, et al. So Close, Yet So Far: Discrepancies Between Uveal and Other Melanomas. A Position Paper From Um Cure 2020. *Cancers* (2019) 11 (7):1032. doi: 10.3390/cancers11071032
- Talty R, Rosenberg M. The Role of Ferroptosis in Melanoma. Pigm Cell Melanom Res (2022) 35(1):18–25. doi: 10.1111/pcmr.13009
- Singh AD, Turell ME, Topham AK. Uveal Melanoma: Trends in Incidence, Treatment, and Survival. *Ophthalmology* (2011) 118(9):1881–5. doi: 10.1016/ j.ophtha.2011.01.040
- Ghazawi FM, Darwich R, Le M, Rahme E, Zubarev A, Moreau L, et al. Uveal Melanoma Incidence Trends in Canada: A National Comprehensive Population-Based Study. Br J Ophthalmol (2019) 103(12):1872-6. doi: 10.1136/bjophthalmol-2018-312966
- Amaro A, Gangemi R, Piaggio F, Angelini G, Barisione G, Ferrini S, et al. The Biology of Uveal Melanoma. *Cancer Metast. Rev* (2017) 36(1):109–40. doi: 10.1007/s10555-017-9663-3
- Lorenzo D, Maria Piulats J, Ochoa M, Arias L, Gutierrez C, Catala J, et al. Clinical Predictors of Survival in Metastatic Uveal Melanoma. *Japan J Ophthalmol* (2019) 63(2):197–209. doi: 10.1007/s10384-019-00656-9
- Wilson MA, Zhong J, Rosenbaum BE, Utter K, Moran U, Darvishian F, et al. Impact of Initial Stage on Metastatic Melanoma Survival. *Melanom. Res* (2019) 29(3):281–8. doi: 10.1097/cmr.00000000000526
- Branisteanu DC, Bogdanici CM, Branisteanu DE, Maranduca MA, Zemba M, Balta F, et al. Uveal Melanoma Diagnosis and Current Treatment Options (Review). *Exp Ther Med* (2021) 22(6):1428. doi: 10.3892/etm.2021.10863
- Damato B. Ocular Treatment of Choroidal Melanoma in Relation to the Prevention of Metastatic Death - a Personal View. *Prog Retina Eye Res* (2018) 66:187–99. doi: 10.1016/j.preteyeres.2018.03.004
- Wu M-Y, Lai T-T, Liao W-T, Li C-J. Clinicopathological and Prognostic Significance and Molecular Mechanisms Governing Uveal Melanoma. *Ther Adv Med Oncol* (2020) 12:1–12. doi: 10.1177/1758835920917566
- Bol KF, Donia M, Heegaard S, Kiilgaard JF, Svane IM. Genetic Biomarkers in Melanoma of the Ocular Region: What the Medical Oncologist Should Know. *Int J Mol Sci* (2020) 21(15):5231. doi: 10.3390/ijms21155231
- Iacono D, Vitale MG, Basile D, Pelizzari G, Cinausero M, Poletto E, et al. Immunotherapy for Older Patients With Melanoma: From Darkness to Light? *Pigm. Cell Melanom. Res* (2021) 34(3):550–63. doi: 10.1111/pcmr.12917
- Petrova V, Arkhypov I, Weber R, Groth C, Altevogt P, Utikal J, et al. Modern Aspects of Immunotherapy With Checkpoint Inhibitors in Melanoma. Int J Mol Sci (2020) 21(7):2367. doi: 10.3390/ijms21072367
- Algazi AP, Tsai KK, Shoushtari AN, Munhoz RR, Eroglu Z, Piulats JM, et al. Clinical Outcomes in Metastatic Uveal Melanoma Treated With Pd-1 and Pd-L1 Antibodies. *Cancer* (2016) 122(21):3344–53. doi: 10.1002/cncr.30258
- Heppt MV, Heinzerling L, Kaehler KC, Forschner A, Kirchberger MC, Loquai C, et al. Prognostic Factors and Outcomes in Metastatic Uveal Melanoma Treated With Programmed Cell Death-1 or Combined Pd-1/Cytotoxic T-Lymphocyte Antigen-4 Inhibition. *Eur J Cancer* (2017) 82:56–65. doi: 10.1016/j.ejca.2017.05.038
- Dixon SJ, Lemberg KM, Lamprecht MR, Skouta R, Zaitsev EM, Gleason CE, et al. Ferroptosis: An Iron-Dependent Form of Nonapoptotic Cell Death. *Cell* (2012) 149(5):1060–72. doi: 10.1016/j.cell.2012.03.042
- Stockwell BR, Angeli JPF, Bayir H, Bush AI, Conrad M, Dixon SJ, et al. Ferroptosis: A Regulated Cell Death Nexus Linking Metabolism, Redox Biology, and Disease. *Cell* (2017) 171(2):273–85. doi: 10.1016/j.cell.2017.09.021
- Yan H-f, Zou T, Tuo Q-z, Xu S, Li H, Belaidi AA, et al. Ferroptosis: Mechanisms and Links With Diseases. Signal Transduct Target Ther (2021) 6(1):49. doi: 10.1038/s41392-020-00428-9
- Tang R, Hua J, Xu J, Liang C, Meng Q, Liu J, et al. The Role of Ferroptosis Regulators in the Prognosis, Immune Activity and Gemcitabine Resistance of Pancreatic Cancer. Ann Trans Med (2020) 8(21):1347. doi: 10.21037/atm-20-2554a
- Wang H, Cheng Y, Mao C, Liu S, Xiao D, Huang J, et al. Emerging Mechanisms and Targeted Therapy of Ferroptosis in Cancer. *Mol Ther* (2021) 29(7):2185–208. doi: 10.1016/j.ymthe.2021.03.022
- Mou Y, Wang J, Wu J, He D, Zhang C, Duan C, et al. Ferroptosis, a New Form of Cell Death: Opportunities and Challenges in Cancer. J Hematol Oncol (2019) 12:34. doi: 10.1186/s13045-019-0720-y

- 22. Basit F, van Oppen LMPE, Schoeckel L, Bossenbroek HM, van Emst-de Vries SE, Hermeling JCW, et al. Mitochondrial Complex I Inhibition Triggers a Mitophagy-Dependent Ros Increase Leading to Necroptosis and Ferroptosis in Melanoma Cells. *Cell Death Dis* (2017) 8(3):e2716. doi: 10.1038/ cddis.2017.133
- Ashrafizadeh M, Mohammadinejad R, Tavakol S, Ahmadi Z, Roomiani S, Katebi M. Autophagy, Anoikis, Ferroptosis, Necroptosis, and Endoplasmic Reticulum Stress: Potential Applications in Melanoma Therapy. J Cell Physiol (2019) 234(11):19471–9. doi: 10.1002/jcp.28740
- Ubellacker JM, Tasdogan A, Ramesh V, Shen B, Mitchell EC, Martin-Sandoval MS, et al. Lymph Protects Metastasizing Melanoma Cells From Ferroptosis. *Nature* (2020) 585(7823):113-+. doi: 10.1038/s41586-020-2623-z
- Tsoi J, Robert L, Paraiso K, Galvan C, Sheu KM, Lay J, et al. Multi-Stage Differentiation Defines Melanoma Subtypes With Differential Vulnerability to Drug-Induced Iron-Dependent Oxidative Stress. *Cancer Cell* (2018) 33 (5):890-+. doi: 10.1016/j.ccell.2018.03.017
- Gagliardi M, Saverio V, Monzani R, Ferrari E, Piacentini M, Corazzari M. Ferroptosis: A New Unexpected Chance to Treat Metastatic Melanoma? *Cell Cycle* (2020) 19(19):2411–25. doi: 10.1080/15384101.2020.1806426
- Anastasiadou E, Jacob LS, Slack FJ. Non-Coding Rna Networks in Cancer. Nat Rev Cancer (2018) 18(1):5–18. doi: 10.1038/nrc.2017.99
- Durante G, Comito F, Lambertini M, Broseghini E, Dika E, Ferracin M. Non-Coding Rna Dysregulation in Skin Cancers. *Non-Cod Genome* (2021) 65 (4):641–55. doi: 10.1042/ebc20200048
- Bande M, Fernandez-Diaz D, Fernandez-Marta B, Rodriguez-Vidal C, Lago-Baameiro N, Silva-Rodriguez P, et al. The Role of Non-Coding Rnas in Uveal Melanoma. *Cancers* (2020) 12(10):2944. doi: 10.3390/cancers12102944
- Safa A, Gholipour M, Dinger ME, Taheri M, Ghafouri-Fard S. The Critical Roles of Lncrnas in the Pathogenesis of Melanoma. *Exp Mol Pathol* (2020) 117:104558. doi: 10.1016/j.yexmp.2020.104558
- Zhi Y, Gao L, Wang B, Ren W, Liang KX, Zhi K. Ferroptosis Holds Novel Promise in Treatment of Cancer Mediated by Non-Coding Rnas. Front Cell Dev Biol (2021) 9:686906. doi: 10.3389/fcell.2021.686906
- 32. Zhang K, Wu L, Zhang P, Luo M, Du J, Gao T, et al. Mir-9 Regulates Ferroptosis by Targeting Glutamic-Oxaloacetic Transaminase Got1 in Melanoma. *Mol Carcinogen*. (2018) 57(11):1566–76. doi: 10.1002/mc.22878
- Luo M, Wu L, Zhang K, Wang H, Zhang T, Gutierrez L, et al. Mir-137 Regulates Ferroptosis by Targeting Glutamine Transporter Slc1a5 in Melanoma. *Cell Death Differ* (2018) 25(8):1457–72. doi: 10.1038/s41418-017-0053-8
- Barbagallo C, Caltabiano R, Broggi G, Russo A, Puzzo L, Avitabile T, et al. Lncrna Linc00518 Acts as an Oncogene in Uveal Melanoma by Regulating an Rna-Based Network. *Cancers* (2020) 12(12):3867. doi: 10.3390/cancers12123867
- Wu X, Li X-F, Wu Q, Ma R-Q, Qian J, Zhang R. Lncrna Snhg15 Predicts Poor Prognosis in Uveal Melanoma and Its Potential Pathways. *Int J Ophthalmol* (2020) 13(8):1195–201. doi: 10.18240/ijo.2020.08.04
- Kuhn M. Building Predictive Models in R Using the Caret Package. J Stat Softw. (2008) 28(5):1–26. doi: 10.18637/jss.v028.i05
- Zhou N, Bao J. Ferrdb: A Manually Curated Resource for Regulators and Markers of Ferroptosis and Ferroptosis-Disease Associations. *Database J Biol Database Curation* (2020) 2020:baaa021. doi: 10.1093/database/baaa021
- Ritchie ME, Phipson B, Wu D, Hu Y, Law CW, Shi W, et al. Limma Powers Differential Expression Analyses for Rna-Sequencing and Microarray Studies. *Nucleic Acids Res* (2015) 43(7):e47. doi: 10.1093/nar/gkv007
- Shannon P, Markiel A, Ozier O, Baliga NS, Wang JT, Ramage D, et al. Cytoscape: A Software Environment for Integrated Models of Biomolecular Interaction Networks. *Genome Res* (2003) 13(11):2498–504. doi: 10.1101/gr.1239303
- Chen B, Khodadoust MS, Liu CL, Newman AM, Alizadeh AA. Profiling Tumor Infiltrating Immune Cells With Cibersort. *Methods Mol Biol (Clifton. NJ)* (2018) 1711:243–59. doi: 10.1007/978-1-4939-7493-1_12
- Geeleher P, Cox N, Huang RS. Prrophetic: An R Package for Prediction of Clinical Chemotherapeutic Response From Tumor Gene Expression Levels. *PloS One* (2014) 9(9):e107468. doi: 10.1371/journal.pone.0107468
- 42. Kujala E, Makitie T, Kivela T. Very Long-Term Prognosis of Patients With Malignant Uveal Melanoma. *Invest Ophthalmol Visual Sci* (2003) 44 (11):4651–9. doi: 10.1167/iovs.03-0538
- He Y, Ye Y, Tian W, Qiu H. A Novel Lncrna Panel Related to Ferroptosis, Tumor Progression, and Microenvironment Is a Robust Prognostic Indicator for Glioma Patients. Front Cell Dev Biol (2021) 9:788451. doi: 10.3389/fcell.2021.788451

- 44. Li Y, Gao Y, Niu X, Tang M, Li J, Song B, et al. Lncrna Basp1-As1 Interacts With Ybx1 to Regulate Notch Transcription and Drives the Malignancy of Melanoma. *Cancer Sci* (2021) 112(11):4526–42. doi: 10.1111/cas.15140
- Bian D, Shi W, Shao Y, Li P, Song G. Long Non-Coding Rna Gas5 Inhibits Tumorigenesis Via Mir-137 in Melanoma. Am J Trans Res (2017) 9(3):1509–20.
- 46. Ye J, Li H, Wei J, Luo Y, Liu H, Zhang J, et al. Risk Scoring System Based on Lncrna Expression for Predicting Survival in Hepatocellular Carcinoma With Cirrhosis. Asian Pacific. J Cancer Prevent.: APJCP (2020) 21(6):1787–95. doi: 10.31557/apjcp.2020.21.6.1787
- Xu S, Wang H, Pan H, Shi Y, Li T, Ge S, et al. Anril Lncrna Triggers Efficient Therapeutic Efficacy by Reprogramming the Aberrant Ink4-Hub in Melanoma. *Cancer Lett* (2016) 381(1):41–8. doi: 10.1016/j.canlet.2016.07.024
- Wang L, Han S, Jin G, Zhou X, Li M, Ying X, et al. Linc00963: A Novel, Long Non-Coding Rna Involved in the Transition of Prostate Cancer From Androgen-Dependence to Androgen-Independence. *Int J Oncol* (2014) 44 (6):2041–9. doi: 10.3892/ijo.2014.2363
- 49. Wu JH, Tian XY, An QM, Guan XY, Hao CY. Linc00963 Promotes Hepatocellular Carcinoma Progression by Activating Pi3k/Akt Pathway. *Eur Rev Med Pharmacol Sci* (2018) 22(6):1645–52. doi: 10.26355/ eurrev_201803_14574
- Zhou Y, Yin L, Li H, Liu L-H, Xiao T. The Lncrna Linc00963 Facilitates Osteosarcoma Proliferation and Invasion by Suppressing Mir-204-3p/Fn1 Axis. *Cancer Biol Ther* (2019) 20(8):1141–8. doi: 10.1080/15384047.2019.1598766
- Wang J, Li C, Xu L, Yang C, Zhang X. Mir-1193 Was Sponged by Linc00963 and Inhibited Cutaneous Squamous Cell Carcinoma Progression by Targeting Sox4. Pathol Res Pract (2019) 215(10):152600. doi: 10.1016/j.prp.2019.152600
- Jiao H, Jiang S, Wang H, Li Y, Zhang W. Upregulation of Linc00963 Facilitates Melanoma Progression Through Mir-608/Nacc1 Pathway and Predicts Poor Prognosis. *Biochem Biophys Res Commun* (2018) 504(1):34–9. doi: 10.1016/ j.bbrc.2018.08.115
- Yang Y, Zhang Y, Miao L, Liao W, Liao W. Lncrna Ppp1r14b-As1 Promotes Tumor Cell Proliferation and Migration Via the Enhancement of Mitochondrial Respiration. Front Genet (2020) 11:557614. doi: 10.3389/ fgene.2020.557614
- 54. Dong Z, Li S, Wu X, Niu Y, Liang X, Yang L, et al. Aberrant Hypermethylation-Mediated Downregulation of Antisense Lncrna Znf667-As1 and Its Sense Gene Znf667 Correlate With Progression and Prognosis of Esophageal Squamous Cell Carcinoma. *Cell Death Dis* (2019) 10:930. doi: 10.1038/s41419-019-2171-3
- Wang W, Green M, Choi JE, Gijon M, Kennedy PD, Johnson JK, et al. Cd8(+) T Cells Regulate Tumour Ferroptosis During Cancer Immunotherapy. *Nature* (2019) 569(7755):270. doi: 10.1038/s41586-019-1170-y
- Lang X, Green MD, Wang W, Yu J, Choi JE, Jiang L, et al. Radiotherapy and Immunotherapy Promote Tumoral Lipid Oxidation and Ferroptosis Via Synergistic Repression of Slc7a11. Cancer Discov (2019) 9(12):1673–85. doi: 10.1158/2159-8290.cd-19-0338
- 57. Johansson J, Siarov J, Kiffin R, Molne J, Mattsson J, Naredi P, et al. Presence of Tumor-Infiltrating Cd8(+) T Cells and Macrophages Correlates to Longer Overall Survival in Patients Undergoing Isolated Hepatic Perfusion for Uveal Melanoma Liver Metastasis. *Oncoimmunology* (2020) 9(1):e1854519. doi: 10.1080/2162402x.2020.1854519
- Pant A, Medikonda R, Lim M. Alternative Checkpoints as Targets for Immunotherapy. *Curr Oncol Rep* (2020) 22(12):126. doi: 10.1007/s11912-020-00983-y
- Tocheva AS, Mor A. Checkpoint Inhibitors: Applications for Autoimmunity. *Curr Allergy Asthma Rep* (2017) 17(10):72. doi: 10.1007/s11882-017-0740-z
- Kottschade LA, McWilliams RR, Markovic SN, Block MS, Bisneto JV, Pham AQ, et al. The Use of Pembrolizumab for the Treatment of Metastatic Uveal Melanoma. *Melanom Res* (2016) 26(3):300–3. doi: 10.1097/cmr.00000000000242
- Karydis I, Chan PY, Wheater M, Arriola E, Szlosarek PW, Ottensmeier CH. Clinical Activity and Safety of Pembrolizumab in Ipilimumab Pre-Treated Patients With Uveal Melanoma. *Oncoimmunology* (2016) 5(5):e1143997. doi: 10.1080/2162402x.2016.1143997
- 62. Zhao L, Xia W, Zhang Y, Zou P, Zhu Q, Zhang R. Efficacy and Safety of Immune Checkpoint Blockades in the Treatment of Ocular Melanoma: A Systematic Review and Meta-Analysis. *Front Oncol* (2021) 11:781162. doi: 10.3389/fonc.2021.781162

- 63. Wang X, He Q, Shen H, Xia A, Tian W, Yu W, et al. Tox Promotes the Exhaustion of Antitumor Cd8(+) T Cells by Preventing Pd1 Degradation in Hepatocellular Carcinoma. J Hepatol (2019) 71(4):731–41. doi: 10.1016/ j.jhep.2019.05.015
- 64. Fan F, Liu P, Bao R, Chen J, Zhou M, Mo Z, et al. A Dual Pi3k/Hdac Inhibitor Induces Immunogenic Ferroptosis to Potentiate Cancer Immune Checkpoint Therapy. *Cancer Res* (2021) 81(24):6233–45. doi: 10.1158/0008-5472.can-21-1547
- 65. Akira S, Takeda K. Toll-Like Receptor Signalling. Nat Rev Immunol (2004) 4 (7):499–511. doi: 10.1038/nri1391
- 66. Chen X, Xu S, Zhao C, Liu B. Role of Tlr4/Nadph Oxidase 4 Pathway in Promoting Cell Death Through Autophagy and Ferroptosis During Heart Failure. *Biochem Biophys Res Commun* (2019) 516(1):37–43. doi: 10.1016/ j.bbrc.2019.06.015
- 67. El-Khalik SRA, Ibrahim RR, Ghafar MTA, Shatat D, El-Deeb OS. Novel Insights Into the Slc7a11-Mediated Ferroptosis Signaling Pathways in Preeclampsia Patients: Identifying Pannexin 1 and Toll-Like Receptor 4 as Innovative Prospective Diagnostic Biomarkers. J Assist Reprod Genet (2022) 39:1115–24. doi: 10.1007/s10815-022-02443-x
- Sethi T, Kovach AE, Rubinstein SM, Lee L, Wang Y, Morgan DS, et al. Correlation of Toll-Like Receptor (Tlr) and Pd-1 Pathways in Central Nervous System Lymphoma: A Clinicopathological Study on Outcomes. *Blood* (2016) 128(22):929. doi: 10.1182/blood.V128.22.929.929
- Shen WX, Zeng X, Zhu F, Wang YL, Qin C, Tan Y, et al. Out-Of-the-Box Deep Learning Prediction of Pharmaceutical Properties by Broadly Learned Knowledge-Based Molecular Representations. *Nat Mach Intell* (2021) 3 (4):334-+. doi: 10.1038/s42256-021-00301-6
- Maria Piulats J, Espinosa E, de la Cruz-Merino L, Varela M, Alonso Carrion L, Martin-Algarra S, et al. Nivolumab Plus Ipilimumab for Treatment-Naive Metastatic Uveal Melanoma: An Open-Label, Multicenter, Phase Ii Trial by the Spanish Multidisciplinary Melanoma Group (Gem-1402). J Clin Oncol (2021) 39(6):586-+. doi: 10.1200/jco.20.00550
- Spagnolo F, Grosso M, Picasso V, Tornari E, Pesce M, Queirolo P. Treatment of Metastatic Uveal Melanoma With Intravenous Fotemustine. *Melanom Res* (2013) 23(3):196–8. doi: 10.1097/CMR.0b013e3283610586
- Augsburger JJ, Correa ZM, Shaikh AH. Effectiveness of Treatments for Metastatic Uveal Melanoma. Am J Ophthalmol (2009) 148(1):119–27. doi: 10.1016/j.ajo.2009.01.023
- 73. Schinzari G, Rossi E, Cassano A, Dadduzio V, Quirino M, Pagliara M, et al. Cisplatin, Dacarbazine and Vinblastine as First Line Chemotherapy for Liver Metastatic Uveal Melanoma in the Era of Immunotherapy: A Single Institution Phase Ii Study. *Melanom Res* (2017) 27(6):591–5. doi: 10.1097/ cmr.000000000000401
- Liu Q, Wang K. The Induction of Ferroptosis by Impairing Stat3/Nrf2/Gpx4 Signaling Enhances the Sensitivity of Osteosarcoma Cells to Cisplatin. Cell Biol Int (2019) 43(11):1245–56. doi: 10.1002/cbin.11121

Author Disclaimer: The authors' claims in this article are solely their own, and do not necessarily represent the opinions of their affiliated organizations, the publisher, editors, or reviewers.

Conflict of Interest: The authors declare that the research was conducted in the absence of any commercial or financial relationships that could be construed as a potential conflict of interest.

Publisher's Note: All claims expressed in this article are solely those of the authors and do not necessarily represent those of their affiliated organizations, or those of the publisher, the editors and the reviewers. Any product that may be evaluated in this article, or claim that may be made by its manufacturer, is not guaranteed or endorsed by the publisher.

Copyright © 2022 Ma, Yu, Zhao, Bai, Cui, Ni, Lyu and Zhao. This is an open-access article distributed under the terms of the Creative Commons Attribution License (CC BY). The use, distribution or reproduction in other forums is permitted, provided the original author(s) and the copyright owner(s) are credited and that the original publication in this journal is cited, in accordance with accepted academic practice. No use, distribution or reproduction is permitted which does not comply with these terms.



Orelabrutinib Combined With Lenalidomide and Immunochemotherapy for Relapsed/ Refractory Primary Central Nervous System Lymphoma: A Retrospective Analysis of Case Series

Chuanwei Yang^{1,2,3}, Yong Cui^{1,2}, Xiaohui Ren^{1,2}, Ming Li^{1,2}, Kefu Yu⁴, Shaoping Shen^{1,2}, Haihui Jiang^{1,2,5}, Mingxiao Li^{1,2}, Xiaokang Zhang^{1,2}, Xuzhe Zhao^{1,2}, Qinghui Zhu^{1,2} and Song Lin^{1,2,6*}

¹ Department of Neurosurgery, Beijing Tiantan Hospital, Capital Medical University, Beijing, China, ² Beijing Neurosurgical Institute, Capital Medical University, Beijing, China, ³ Department of Neurosurgery, Henan Provincial People's Hospital, People's Hospital of Zhengzhou University, Zhengzhou University, Henan, China, ⁴ Department of Pharmacy, Beijing Tiantan Hospital, Capital Medical University, Beijing, China, ⁵ Department of Neurosurgery, Peking University Third Hospital, Peking University, Beijing, China, ⁶ National Clinical Research Center for Neurological Diseases, Center of Brain Tumor, Beijing Key Laboratory of Brain Tumor, Beijing Institute for Brain Disorders, Beijing, China

Background: Relapsed/refractory (r/r) primary central nervous system lymphoma (PCNSL) is an intractable situation without sound treatment. Bruton's tyrosine kinase (BTK) represents an attractive drug target in PCNSL. Orelabrutinib is a new-generation BTK inhibitor with high cerebrospinal fluid (CSF) concentration. This study aimed to evaluate the efficacy and safety of orelabrutinib-containing combination therapy in patients with r/r PCNSL.

Methods: We retrospectively analyzed r/r PCNSL patients who received combination therapy with rituximab, high-dose methotrexate, temozolomide, orelabrutinib and lenalidomide, and further explored the relationship between the efficacy and genetic characteristics.

Results: A total of fifteen patients were included in this retrospective study. The overall response rate (ORR) was 86.7%, the complete remission (CR) rate was 73.3% and the disease control rate (DCR) was 93.3%. Among 13 responders, 9 patients are still receiving oral orelabrutinib and lenalidomide. The most common adverse event (AEs) was transaminase increase (66.7%). No grade 4 AE or drug-related death was reported. Genomic sequencing showed that patients who responded to orelabrutinib had abnormal NF- κ B activation, while those who had no response were mainly enriched with transcriptional misregulation. Patients who had mutations in TLR, BCR, or NF- κ B pathway achieved complete or partial response to the orelabrutinib-containing therapy.

OPEN ACCESS

Edited by:

Xian Zeng, Fudan University, China

Reviewed by:

Sonikpreet Aulakh, West Virginia University, United States Michele Merli, University of Insubria, Italy

> *Correspondence: Song Lin linsong2005@126.com

Specialty section:

This article was submitted to Cancer Immunity and Immunotherapy, a section of the journal Frontiers in Oncology

Received: 22 March 2022 Accepted: 09 May 2022 Published: 16 June 2022

Citation:

Yang C, Cui Y, Ren X, Li M, Yu K, Shen S, Jiang H, Li M, Zhang X, Zhao X, Zhu Q and Lin S (2022) Orelabrutinib Combined With Lenalidomide and Immunochemotherapy for Relapsed/ Refractory Primary Central Nervous System Lymphoma: A Retrospective Analysis of Case Series. Front. Oncol. 12:901797. doi: 10.3389/fonc.2022.901797

372

Moreover, the blood and cerebrospinal fluid circulating tumor DNA (ctDNA) were closely associated with tumor recurrence and treatment response and sustained tumor responses correlated with the clearance of ctDNA.

Conclusion: Orelabrutinib-containing regimen was effective and well-tolerated in patients with r/r PCNSL. Genome sequencing of tumor samples could help to screen patients who may respond to the orelabrutinib-containing regimen, and liquid biopsy may contribute to tracing tumor burden and monitoring treatment response.

Keywords: Orelabrutinib, safety, efficacy, relapsed/refractory, primary central nervous system lymphoma, genomic characteristics

INTRODUCTION

Primary central nervous system lymphoma (PCNSL) is a rare and aggressive subtype of non-Hodgkin's lymphoma, confining to the central nervous system (CNS) or eyes without systemic involvement. PCNSL incidence is approximately 5 per million and has been gradually increasing in recent decades (1). Approximately 95% of PCNSL pathology is represented by diffuse large B-cell lymphoma (DLBCL) (2). Compared to other extranodal DLBCL, PCNSL is associated with a relatively poor prognosis, with a 5-year survival rate of only 20%-30% (1). High-dose methotrexate (HD-MTX)-based chemotherapy has been recommended as the first-line treatment, however, about 30% of PCNSL cases are refractory to the HD-MTX-based chemotherapy, and up to 60% will eventually relapse (3-6). Moreover, about 25% of relapsed PCNSL cases fail to respond to the initial treatment (7). It was reported that the median survival for relapsed/refractory (r/r) PCNSL was only 8-18 months despite intensive treatment (3). Few effective treatment options and novel therapeutics exist for patients with refractory and early relapsed PCNSL, and thus a standard of care remains to be established. Although guidelines recommend whole-brain radiotherapy (WBRT) or autologous stem cell transplantation (ASCT), the usage is limited due to the late neurotoxicity associated with radiotherapy and the high mortality of myeloablative chemotherapy prior to ASCT. Notably, targeted therapy and immunochemotherapy may play an important role in this situation (8).

Compared to DLBCL without CNS, PCNSL has its unique genomic signature. Myeloid differentiation factor 88 (*MYD88*, 60%-80%) and *CD79B* (50%-60%) are more frequently mutated in PCNSL, and present not only in inactivated B cell-like-DLBCL (ABC-DLBCL) but also in germinal B cell-like-DLBCL (GCB-DLBCL) (9–11). *MYD88* L265P and *CD79B* Y196 are the two most common gain-of-function mutations in PCNSL, which are parts of toll-like receptors (TLR) and B-cell receptor (BCR) signaling pathways, respectively (10–12). The mutation of *MYD88* and *CD79B* was also used to classify DLBCL into a MCD subtype with a poor prognosis (13). Bruton tyrosine kinase (BTK) mediates the nuclear factor (NF)- κ B signaling pathway downstream of TLR and BCR. Activation of NF- κ B signaling continues to provide survival signals to tumor cells. Therefore, BTK plays an important role in

maintaining the malignant phenotype of PCNSL and is an attractive drug target in PCNSL.

The first-generation BTK inhibitor ibrutinib has shown antitumor activity in r/r PCNSL patients as a single agent or combination treatment (14, 15). Although ibrutinib revolutionized the treatment of B cell malignancies, its use has been limited by serious adverse events (AEs), such as fungal infections and atrial fibrillation resulting from off-target inhibition (15, 16). This has led to the development of highly selective BTK inhibitors with fewer off-target effects. Orelabrutinib, a new generation of BTK inhibitor, not only has higher blood-brain barrier permeability and higher bioavailability but also has excellent kinase selectivity and little off-target side effect (17). It has been approved by National Medical Products Administration for the treatment of mantle cell lymphoma and chronic lymphocytic leukemia. Results of several studies have demonstrated the anti-tumor activity and manageable safety profile of orelabrutinib (18, 19). Besides, tirabrutinib as a BTK inhibitor was approved for the treatment of PCNSL (20). More importantly, per-clinical data showed the synergistic effect of orelabrutinib as a partner for combination therapy (21). Therefore, we conducted a retrospective analysis of 15 patients with r/r PCNSL to evaluate the efficacy and safety of combination therapy with rituximab, high-dose methotrexate (HD-MTX), and temozolomide (RMT), as well as orelabrutinib and lenalidomide. Additionally, we also explored genetic differences between responders and non-responders to orelabrutinib and the changes in circulating tumor DNA (ctDNA) in blood and cerebrospinal fluid (CSF) before and during the treatment.

MATERIALS AND METHODS

Patients

Adult immunocompetent consecutive patients with r/r PCNSL who have received the combination therapy with RMT, orelabrutinib, and lenalidomide were retrospectively analyzed at the Department of Neurosurgery, Beijing Tiantan Hospital between October 2020 and February 2022. The diagnosis of the CNSL and diffuse large B-cell lymphoma subtype (non-germinal center B-cell-like [non-GCB], GCB, unknown) was made according to the Lymphoid Malignancies Guidelines 2021,

which were established by the Chinese Society of Clinical Oncology (22). Relapsed lymphoma was defined as lymphoma that relapsed after the complete response (CR) to prior treatment (23).

According to the NCCN Guidelines for Central Nervous System (CNS) Cancers, the diagnosis of PCNSL was made according to the following findings: 1) Diffuse large B-cell lymphoma (DLBCL) confirmed by stereotactic biopsy of brain lesions; 2) No invasion outside the CNS confirmed by physical examination (PET and CT examination, ophthalmic examination, and bone marrow aspiration and biopsy). Refractory lymphoma was diagnosed if any of the following criteria were met: the tumor shrank < 50% or progressive disease after 4 courses of chemotherapy; CR was achieved by standard chemotherapy but relapsed within 6 months; there were two or more relapses after CR; and relapse after hematopoietic stem cell transplantation (24). The inclusion criteria were as follows: age ≥ 18 years, a physician's diagnosis of r/r PCNSL, and receiving orelabrutinib combination regimens. Patients with mental disorders, unstable systemic disease, immunodeficiency, or pregnancy were excluded. This retrospective study was approved by the Medical Ethics Committee of the Beijing Tiantan Hospital (Ethics Approval No. YW2020-038-02) and was conducted in accordance with the principles of the Declaration of Helsinki.

Treatment Regimen

All patients had received the combination regimens, including rituximab, HD-MTX, temozolomide, orelabrutinib, and lenalidomide. Rituximab (dosed at 375 mg/m²) was administered intravenously (IV) on day 1, followed by HD-MTX (dosed at 3.5 g/ m²) over 4 hours on day 2. In order to reduce toxicity, approximately 24 hours after chemotherapy, leucovorin (50 mg) was injected intramuscularly every 6 hours until the MTX plasma concentration decreased to 0.05 µmol/L. Temozolomide was administered at a dose of 150 mg/m² once daily on days 4 to 8. The rituximab, HD-MTX, and temozolomide (RMT) regimen were administrated every 4 weeks. Oral orelabrutinib (150 mg once a day) and lenalidomide (25 mg once a day) along with prednisone (10 mg once a week) were administered until disease progression, death, or intolerable toxicity. The maximum duration of the RMT regimen was decided by the clinicians according to the patient's disease condition.

Assessment

Tumor responses were evaluated using magnetic resonance imaging (MRI), positron emission tomography (PET), CSF examination, ocular slit lamp, and bone marrow biopsy, according to the International PCNSL Collaborative Group (IPCG) guidelines (17). MRI evaluation was performed every cycle, and the time interval was gradually extended to 3-6 cycles after the patient reached a CR. Total tumor volume was the sum of volumes of lesions calculated by the largest longitudinal diameter multiplied by its perpendicular diameter on the MRI image. The efficacy endpoints were overall response rate (ORR), disease control rate (DCR), progression-free survival (PFS), and overall survival (OS). ORR was defined as the proportion of patients who achieved partial response (PR) and CR. DCR was defined as the proportion of patients who achieved PR, CR, and stable disease (SD). PFS was calculated from the initiation of treatment to the time of disease progression or death. OS was defined as the time from treatment to death due to any cause.

Safety and tolerability were evaluated through physical examination, vital signs, laboratory tests (including urinalysis, hematology, and blood chemistry), electrocardiography, and adverse events (AEs). AEs were collected and assessed following the Common Terminology Criteria for Adverse Events (CTCAE) version 5.0.

Sample Collection and Genomic Analysis

To explore the association between genomic characteristics and tumor response to orelabrutinib, we collected available baseline tumor biopsy samples from patients treated with orelabrutinib for genomic sequencing. Besides, all blood and CSF samples were collected before the RMT therapy and after 2 cycles of orelabrutinib and lenalidomide therapy. Archived blood samples were used for gene mutation assessments of *MYD88 L265P* and *CD79B Y196H* using the droplet digital polymerase chain reaction (ddPCR) or the next-generation sequencing (NGS).

Statistics Analysis

Statistical analyses and visualization were performed using R 4.0.0 and GraphPad Prism version 6.0 statistical software. Continuous variables were expressed as means (standard deviations) and medians (range); Categorical variables were expressed as numbers (proportions). The PFS and OS were estimated using the Kaplan-Meier method with 95% confidence intervals (CIs). A two-sided p<0.05 was considered statistically significant.

RESULTS

Patients' Characteristics

Between October 2020 and February 2022, a total of 15 eligible patients with r/r PCNSL (5 males, 10 females) were included in this retrospective study (Table 1), with a median age of 62 years (range, 33 to 78 years) and a median Karnofsky performance score of 60 (range, 40-90). Of these, 10 patients (66.7%) were relapsed disease and 5 (33.3%) were refractory to HD-MTXbased chemotherapy. Regarding the histological subtypes of PCNSL, there were 4 (26.7%) patients with GCB and 11 (73.3%) patients with non-GCB. Nine (60%) patients had tumors involving the deep brain, including the periventricular tissue, basal ganglia, corpus callosum, brainstem, and/or cerebellum. None of the patients received ASCT or radiotherapy before treatment, while 3 patients (P4, P5, and P6) received WBRT after treatment. Of all included patients, 5 had previously received orelabrutinib therapy; 4 (P1, P2, P3, and P15) of whom had a PR to orelabrutinib therapy and 1 (P4) had a progressed disease (PD). Seven of the 15 patients had previously received the RMT regimen. The median number of prior regimens was 2 (range, 1-5); and 3 patients (P1, P4, and P5) have received ≥ 3 prior lines. The median cycle of RMT therapy was 1 (range, 1-5). 9 patients received 1 cycle of RMT treatment

TABLE 1	Baseline	characteristics	of the	relapsed/	refractory	PCNSL	patients.
---------	----------	-----------------	--------	-----------	------------	-------	-----------

Characteristics	Patients (n = 15)
Age-years, median (range)	62 (33-78)
Median KPS score (range)	60 (40-90)
Sex, n (%)	
Male	5 (33.3)
Female	10 (66.7)
PCNSL subtype n (%)	
GCB	4 (26.7)
Non-GCB	11 (73.3)
Tumor location n (%)	
Superficial brain	6 (40)
Deep brain	9 (60)
Median number of prior regimens (range)	2 (1-5)
Median cycle of RMT salvage therapy (range)	1 (1-5)

PCNSL, primary central nervous system lymphoma; GCB, germinal B cell-like; RMT, rituximab, high-dose methotrexate, and temozolomide.

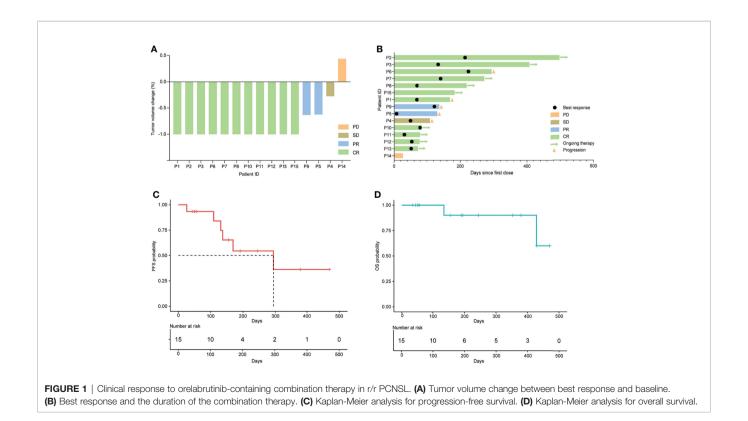
and 6 patients received ≥ 2 cycles. The median follow-up time was 219 days (range, 62-498).

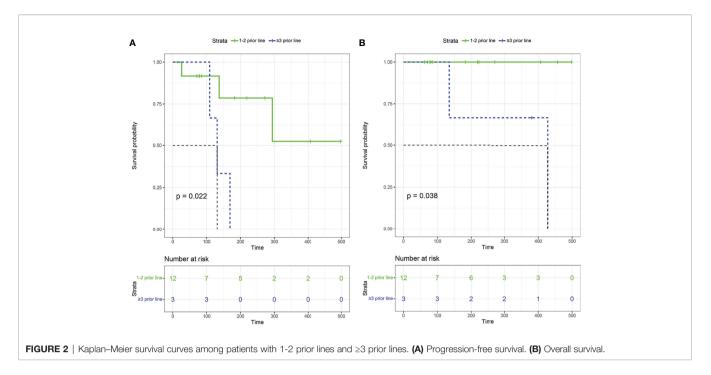
Efficacy

All the 15 eligible patients were included for efficacy analysis. The best responses were achieved, including 11 CR (11/15, 73.3%), 2 PR (2/15, 13.3%), 1 SD (1/15, 6.7%, P4) and 1 PD (1/15, 6.7%, P14), which resulted in an ORR of 86.7% (13/15) and DCR of 93.3% (14/15). The best changes in tumor diameter from baseline to the study closing date are shown in **Figure 1A**. Among these responders, 9 patients are still receiving orelabrutinib and lenalidomide therapy (**Figure 1B**). The median TTR was 23

days (range, 4-54 days), and the median time to best response was 66 days (range, 6-224 days). In addition, of 9 patients treated with 1 cycle of RMT, the best responses after this treatment regimen were 6 CR (66.7%), 1 PR (11.1%), 1 SD (11.1%), and 1 PD (11.1%), respectively; of 6 patients received \geq 2 cycles of RMT, 5 (83.3%) achieved a CR and 1 (16.7%) achieved a PR after this treatment regimen. The median PFS was 9.8 months (294 days, 95% CI: 137-NA) for the cohort (**Figure 1C**). Two patients (P4 and P5) died due to tumor progression. The median OS was not reached (**Figure 1D**). Patients who received 1-2 prior lines showed a longer PFS (p=0.022; **Figure 2A**) and OS (p=0.038; **Figure 2B**) than these received \geq 3 prior lines. The treatment regimens and disease progression of each patient were summarized in **Table S1**.

Three patients (P4, P5, and P6) received etoposide or programmed death (PD)-1 antibody due to the excessive tumor burden, and patient P4 also received chidamide (the selective inhibitor of histone deacetylase). The best response of these 3 patients was SD (P4), PR (P5), and CR (P6), respectively. Notably, 2 patients (P7 and P9) experienced the regimen adjustment by replacing the lenalidomide with temozolomide due to due to hypersensitivity to lenalidomide. As a result, P7 still achieved and maintained CR, and P9 achieved PR. None of the patients receiving prior orelabrutinib treatment, 4 achieved CR (P1, P2, P3, P15)and 1 (P4) achieved SD after orelabrutinibcontaining combination therapy (**Figure 3**). Of the 7 RMT prior treated patients, 4 achieved CR (P1, P7, P8, P12), 2 PR (P5, P9) and 1 PD (P14) (**Figure 3**).

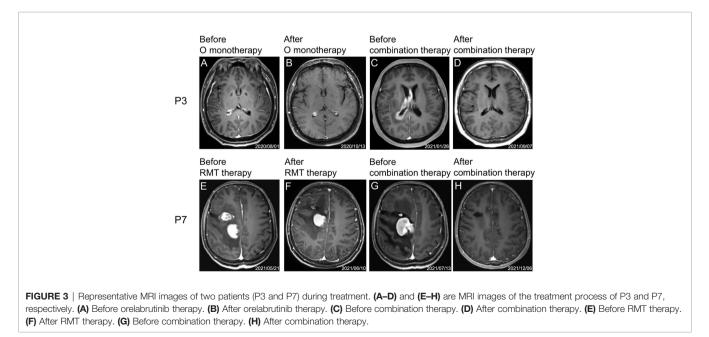


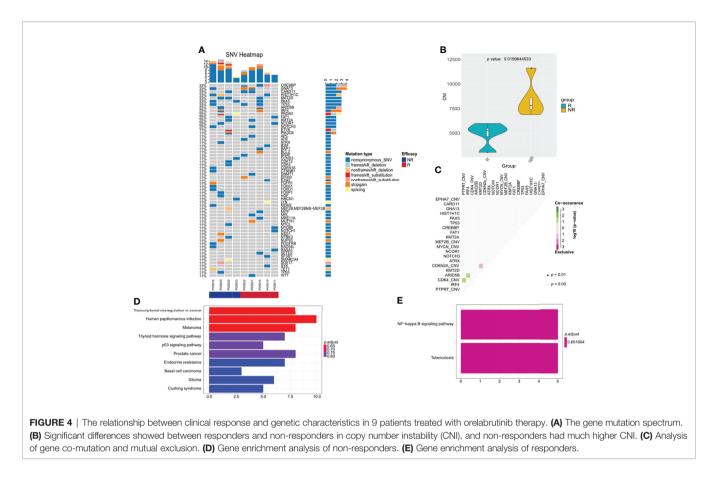


Clinical Response and Genomic Characteristics

Baseline tumor biopsy samples were available for 9 patients receiving orelabrutinib therapy. Of these, 5 patients were orelabrutinib-responders with the best response of PR, and 4 were non-responders with the best response of SD (1 patient) or PD (3 patients). We explored the association between treatment response and tumor gene mutation. As shown in **Figure 4A**, the most frequently mutated genes were *CREBBP*, *GNA13*, *CARD11*, *HIST1H1C*, *KMT2D*, *PAX5*, and *TP53* in this cohort. Additionally, patients who had *CARD11* mutation also

responded to orelabrutinib. There were no significant differences in efficacy between different ages, genders, pathological subtypes, or tumor sites. However, significant differences were observed in genomic traits between orelabrutinib-treated patients in different response groups; that is, non-responders had much higher copy number instability (CNI) score, indicating that non-responders had a higher degree of chromosomal instability (**Figure 4B**). Mutual exclusion analysis of gene co-mutation showed that *IRF4*, *ARID5B* and *CDK4*, *PTPRT* were co-occurrent mutations, while *CDKN2A*, *KMT2D* were exclusive mutations in this cohort (**Figure 4C**).





Gene enrichment analysis demonstrated that the mutated genes in non-responders were mainly enriched in transcriptional misregulation pathways (**Figure 4D**), while the mutated genes in responders were mainly enriched in NF- κ B abnormally activated pathways (**Figure 4E**). As shown in **Table 2**, patients who had gene mutations in the TLR pathway (*MYD88*), BCR pathway (*CD79B*, *CARD11*, *TNFAIP3*), NF- κ B pathway (*PIM1*, *IRF4*, *BTG2*), and cell cycle pathways (*TP53*, *CDKN2A*) achieved better response (CR or PR) to the orelabrutinib-containing combination therapy, while patients without the above gene mutations achieved a poor response. PCNSL that relies on the activation of the BCR or TLR signaling pathway to activate the NF- κ B signaling pathway has a better response to the orelabrutinib-containing combination therapy. The mechanism of action of BTK inhibitor orelabrutinib is summarized in **Figure 5**.

Disease Surveillance Through ctDNA

In the combination therapy, the ddPCR detection of *MYD88* and *CD79B* mutations was performed in 9 patients using blood samples and the NGS was performed in 1 patient using CSF. Among these patients, 3 patients (P7, P9, P15) showed *MYD88* or *CD79B* positive before the combination therapy and turned negative after two cycles of the combination therapy. Two patients (P7 and P9) showed no system involvement. P15 showed gastric involvement which was confirmed DLBCL two months later by biopsy. Additionally, one patient (P6) was detected as negative by blood ddPCR and negative CSF

cytology, but positive in the next-generation sequencing of CSF. However, the tumor relapses about two months later, and the blood ddPCR detection was still negative at that time. The mutational genes in CSF were consistent with that of his baseline tumor biopsy sample.

Safety

The overall incidence of AEs was summarized in **Table 3**. 10 patients (66.7%) experienced treatment-related AEs. Most common treatment-related AEs of any grade were transaminase increase (10/15, 66.7%), fatigue (6/15, 40%), and leukopenia (4/15, 26.7%). The reported grade 3 or worse AE was fatigue (6, 40%). Two patients (13.3%) had grade 3 hypersensitivity reactions and diarrhea to lenalidomide, respectively, and had resolution of symptoms after withdrawal of lenalidomide. No other patients required lenalidomide dose reduction. Most grade 2 or fewer toxicities were transaminase increase (66.7%), leukopenia (26.7%), and drowsiness (20%). No fungal infection was observed. Reported AEs were generally manageable and resolved soon after supportive treatment. No grade 4-5 toxicity was reported.

DISCUSSION

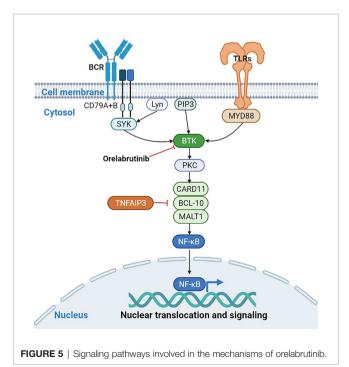
This study is the first report of orelabrutinib, lenalidomide plus immunochemotherapy in r/r PCNSL. In this study, the use of

ld	Disease	Status	Subtype	Response	TLR pathway	BCR pathway	NF-κB pathway	Cell cycle pathway
P1	PCNSL	Relapsed	non- GCB	CR	NA	NA	NA	NA
P2	PCNSL	Refractory	non- GCB	CR	WT	CD79B	PIM1	CDKN2A
P3	PCNSL	Relapsed	GCB	CR	WT	CD79B、 CARD11	WT	TP53
P4	PCNSL	Relapsed	non- GCB	SD	WT	WT	WT	WT
P5	PCNSL	Relapsed	GCB	PR	NA	NA	NA	NA
P6	PCNSL	Relapsed	GCB	CR	WT	TNFAIP3、	WT	TP53
P7	PCNSL	Relapsed	non- GCB	CR	MYD88	CD79B	PIM1IRF4	WT
P8	PCNSL	Relapsed	non- GCB	CR	WT	WT	BTG2	WT
P9	PCNSL	Refractory	non- GCB	PR	MYD88	CD79B	PIM1	CDKN2A
P10	PCNSL	Relapsed	non- GCB	PR	WT	CD79BCARD11	PIM1、BTG2、 IRF4	WT
P11	PCNSL	Refractory	non- GCB	PR	WT	WT	BTG2	WT
P12	PCNSL	Relapsed	non- GCB	PR	MYD88	CD79B	PIM1	WT
P13	PCNSL	Refractory	GCB	PR	NA	NA	NA	NA
P14	PCNSL	Refractory	non- GCB	PD	WT	WT	WT	TP53
P15	PCNSL	Relapsed	non- GCB	CR	MYD88	CD79B	PIM1、IRF4	TP53、CDKN2A

TABLE 2 | Gene mutations in pathways in pretreatment tumor tissue.

PCNSL, primary central nervous system lymphoma; GCB, germinal B cell-like; CR, complete remission; PR, partial remission; SD, stable disease; PD, progression disease; NA, not available; WT, wild-type; TLR, Toll-like receptor; BCR, B-cell receptor; NF- κB, nuclear factor-kappa B.

this combination regimen showed inspiring antitumor activity with ORR of 86.7% and DCR of 93.3%, as well as acceptable toxicity in r/r PCNSL patients. Our findings supported the clinical application of this combination regimen in r/r PCNSL,



which could provide a promising therapeutic strategy for this patient population.

The present study demonstrated an encouraging result in r/r PCNSL. The ORR achieved with orelabrutinib-containing regimen was 86.7%, which was comparable with other BTK inhibitor-containing regimens, such as results from ibrutinib (ORR, 52%) (25), temozomide/ibrutinib (ORR, 55%) (26), and the phase I/II study of tirabrutinib (ORR, 64%) (27). Nevertheless, a phase II showed that lenalidomide plus rituximab without orelabrutinib only induce an ORR of 35.6% (28). These results supported that various BTK inhibitors are potent therapeutic options against r/r PCNSL and especially adding orelabrutinib may provide additional benefit for this population. Actually, we observed a relative high ORR and DCR in this study. As a preliminary study reported, the favorable blood-brain barrier permeability of orelabrutinib could induce a high CSF concentration of 20.10 ± 14.70 ng/mL (29), which may partly explain the better response in these patients. Besides, the synergistic effects of BTK inhibitor and Combination of drugs may be another reason for better response, such as the combination of orelabrutinib and rituximab (21), BTK inhibitor and lenalidomide (30). The combination therapy eliminates tumor cells from multiple aspects by killing tumor cells directly with chemotherapy, blocking proliferation pathways with targeted therapy, and modulating the tumor microenvironment with immunotherapy. Besides, there were no treated-death or intolerable toxicity after combination therapy, which induced the better medication compliance.

TABLE 3	Adverse e	events of	Orelabrutinib-	containing	therapy.
---------	-----------	-----------	----------------	------------	----------

Adverse event	Grade 1	Grade 2	Grade 3	Total (%)
Hematological toxicities				
Leukopenia	3	1		4 (26.7%)
Neutropenia		1		1 (6.7%)
Purpura	1			1 (6.7%)
Non-hematological toxicities				
Transaminase increase	6	4		10 (66.7%)
Fatigue			6	6 (40%)
Drowsiness		3		3 (20%)
Diarrhea		1		1 (6.7%)
Constipation	1			1 (6.7%)

RMT, rituximab, high-dose methotrexate and temozolomide; OL, orelabrutinib and lenalidomide.

Most importantly, tumor load was reduced quickly through short-course RMT therapy combined with orelabrutinib and lenalidomide therapy, thus reducing the physical requirements for patients to tolerate intensive chemotherapy and achieving a certain short-term tumor remission effect and prolongating the survival of patients in this study. Overall, this novel combination regimen has a favorable tumor remission efficacy and survival.

Genetic signature analysis may contribute to individualized targeted therapy (31). As reported, patients with abnormal activation of NF-KB signaling achieved better efficacy (32), which supports our results of the orelabrutinib-containing regimens. Notably, BTK is a crucial regulator of BCR and TLR signaling, especially for PCNSL with NF-KB pathway activation. BTK inhibitors disrupt BCR downstream signaling and induce apoptosis (33, 34). The patients with mutations in all three pathways achieved a CR or PR after treatment, while the patients without mutations achieved a poor response, even PD. In addition, ctDNA monitor is equally important. The blood ctDNA of most patients was negative, and the positive results often indicated the possibility of PD or peripheral invasion. The negative ctDNA after combination therapy indicated that the patient responded to the treatment. Thus, we recommend simultaneous NGS of ctDNA in blood and cerebrospinal fluid. The main reasons are as follows: firstly, the positive rate of ctDNA in CSF is higher; secondly, the gene mutation spectrum detected by next-generation sequencing is broader; thirdly, the recurrence and invasion in and out of CNS can be monitored simultaneously. Moreover, we also found that the gene mutation profiles of CSF were high concordant with that of the tumor sample, which was consistent with the previous study (14).

In the present study, several intriguing cases were observed. Of the 7 RMT prior treated patients continued receiving orelabrutinib and immunochemotherapy therapy, and achieved 4 CR, 2 PR, and 1 PD, suggesting that this combination therapy might induce long-term immune-modulatory effects. For these patients with tumor progression after the RMT regimen, targeted therapy is likely to potentially reduce the burden of tumor and produce the long-term benefit, orelabrutinib has synergistic effects with the immunomodulator lenalidomide. Due to the sample size limitation, findings should be confirmed in future trials with larger data sets.

Regarding the safety analysis, our study demonstrated an acceptable safety profile for the orelabrutinib-containing

regimen in patients with r/r PCNSL. Here reported AEs (ie, transaminase increase, fatigue and leukopenia) were mild to moderate and manageable with supportive care. Besides, we found that most AEs were known and also uncommon, and the safety profile are generally similar to lenalidomide/rituximab regimen (35) or HD-MTX/temozolomide/rituximab regimen (36). This implicated that most of these AEs mostly resulted from the rituximab, HD-MTX, or temozolomide alone; and orelabrutinib did not increase the risk of toxicity. In addition, short-course RMT therapy may reduce toxicity in our study. As known, atrial fibrillation, bleeding and infectious complications are common AEs related to BKT inhibitors (37); however, these were not reported in our study, which may be attributed to the high target selectivity and low off-target reactivity of orelabrutinib (18). Besides, no unexpected AEs and grade 4 or more AEs and cardiotoxicity were observed in the present study. Taken together, the orelabrutinib-containing regimen is welltolerated and manageable in patients with r/r PCNSL.

This preliminary study had several limitations. First, the present results are based on limited sample size and non-randomized retrospective design, which may generate inevitable selection bias. Second, there is a lack of longitudinal CSF sequencing data to elucidate the role of ctDNA of CSF in the treatment monitor and prognosis assessment. Finally, long-term efficacy was not evaluated because of the limited observation period. Thus, strictly designed, large-scale, and high-quality clinical trials should be conducted to validate our findings.

CONCLUSIONS

In conclusion, the high response rate and good tolerance observed in this study suggested that orelabrutinib-containing regimens are a promising therapeutic option for r/r PCNSL. The results also indicated that gene sequencing of tumor specimens can help to screen the patient population responding to BTK inhibitor targeted therapy. The results provide preliminary evidence for the application of orelabrutinib-containing regimens in r/r PCNSL.

DATA AVAILABILITY STATEMENT

Due to institutional ethics restrictions, the dataset of the patients supporting the current study has not been deposited in a public repository, but is available from the corresponding authors upon request.

ETHICS STATEMENT

This retrospective study was approved by the Medical Ethics Committee of the Beijing Tiantan Hospital (Ethics Approval No. YW2020-038-02) and was conducted in accordance with the principles of the Declaration of Helsinki. All patients provided informed written consent prior to sample collection. The study was exempted informed consent and the protocol was approved by the Ethics Review Committee of Beijing Tiantan Hospital. Written informed consent was obtained from the individual(s) for the publication of any potentially identifiable images or data included in this article.

AUTHOR CONTRIBUTIONS

SL and CY conceived conceptualization, performed data analysis, and supervised the project. SL contributed to methodology. YC and XR provided the resources and contributed to project administration. ML, HHJ, KY, SS, MXL, XKZ, XZZ, and QZ

REFERENCES

- Ostrom QT, Gittleman H, Fulop J, Liu M, Blanda R, Kromer C, et al. CBTRUS Statistical Report: Primary Brain and Central Nervous System Tumors Diagnosed in the United States in 2008-2012. *Neuro-oncology* (2015) 17 Suppl 4(Suppl 4):iv1-iv62. doi: 10.1093/neuonc/nov189
- Batchelor TT. Primary Central Nervous System Lymphoma: A Curable Disease. *Hematol Oncol* (2019) 37 Suppl 1:15–8. doi: 10.1002/hon.2598
- Jahnke K, Thiel E, Martus P, Herrlinger U, Weller M, Fischer L, et al. Relapse of Primary Central Nervous System Lymphoma: Clinical Features, Outcome and Prognostic Factors. J Neuro-oncol (2006) 80(2):159–65. doi: 10.1007/ s11060-006-9165-6
- Ekenel M, Iwamoto FM, Ben-Porat LS, Panageas KS, Yahalom J, DeAngelis LM, et al. Primary Central Nervous System Lymphoma: The Role of Consolidation Treatment After a Complete Response to High-Dose Methotrexate-Based Chemotherapy. *Cancer* (2008) 113(5):1025–31. doi: 10.1002/cncr.23670
- Bergner N, Monsef I, Illerhaus G, Engert A, Skoetz N. Role of Chemotherapy Additional to High-Dose Methotrexate for Primary Central Nervous System Lymphoma (PCNSL). *Cochrane Database Systematic Rev* (2012) 11: Cd009355. doi: 10.1002/14651858.CD009355.pub2
- Langner-Lemercier S, Houillier C, Soussain C, Ghesquières H, Chinot O, Taillandier L, et al. Primary CNS Lymphoma at First Relapse/Progression: Characteristics, Management, and Outcome of 256 Patients From the French LOC Network. *Neuro-oncology* (2016) 18(9):1297–303. doi: 10.1093/neuonc/ now033
- Löw S, Han CH, Batchelor T. Primary Central Nervous System Lymphoma. *Ther Adv Neurol Diso* (2018) 11:1756286418793562. doi: 10.1177/ 1756286418793562
- Wirsching HG, Weller M, Balabanov S, Roth P. Targeted Therapies and Immune Checkpoint Inhibitors in Primary CNS Lymphoma. *Cancers* (2021) 13(12):3073. doi: 10.3390/cancers13123073
- Lionakis MS, Dunleavy K, Roschewski M, Widemann BC, Butman JA, Schmitz R, et al. Inhibition of B Cell Receptor Signaling by Ibrutinib in Primary CNS Lymphoma. *Cancer Cell* (2017) 31(6):833–43.e5. doi: 10.1016/ j.ccell.2017.04.012
- Grommes C, Pastore A, Palaskas N, Tang SS, Campos C, Schartz D, et al. Ibrutinib Unmasks Critical Role of Bruton Tyrosine Kinase in Primary CNS Lymphoma. *Cancer Discovery* (2017) 7(9):1018–29. doi: 10.1158/2159-8290.Cd-17-0613
- Fukumura K, Kawazu M, Kojima S, Ueno T, Sai E, Soda M, et al. Genomic Characterization of Primary Central Nervous System Lymphoma. *Acta Neuropathol* (2016) 131(6):865–75. doi: 10.1007/s00401-016-1536-2
- Braggio E, McPhail ER, Macon W, Lopes MB, Schiff D, Law M, et al. Primary Central Nervous System Lymphomas: A Validation Study of Array-Based Comparative Genomic Hybridization in Formalin-Fixed Paraffin-Embedded Tumor Specimens. *Clin Cancer Res* (2011) 17(13):4245–53. doi: 10.1158/ 1078-0432.Ccr-11-0395
- Schmitz R, Wright GW, Huang DW, Johnson CA, Phelan JD, Wang JQ, et al. Genetics and Pathogenesis of Diffuse Large B-Cell Lymphoma. *New Engl J Med* (2018) 378(15):1396–407. doi: 10.1056/NEJMoa1801445
- Chen F, Pang D, Guo H, Ou Q, Wu X, Jiang X, et al. Clinical Outcomes of Newly Diagnosed Primary CNS Lymphoma Treated With Ibrutinib-Based Combination Therapy: A Real-World Experience of Off-Label Ibrutinib Use. *Cancer Med* (2020) 9(22):8676–84. doi: 10.1002/cam4.3499

performed data curation. CY wrote original draft and involved in writing, reviewing, and editing. All authors contributed to the article and approved the submitted version.

SUPPLEMENTARY MATERIAL

The Supplementary Material for this article can be found online at: https://www.frontiersin.org/articles/10.3389/fonc.2022.901797/full#supplementary-material

- Pal Singh S, Dammeijer F, Hendriks RW. Role of Bruton's Tyrosine Kinase in B Cells and Malignancies. *Mol Cancer* (2018) 17(1):57. doi: 10.1186/s12943-018-0779-z
- Shaw ML. Second-Generation BTK Inhibitors Hit the Treatment Bullseye With Fewer Off-Target Effects. Am J Managed Care (2020) 26(7 Spec No.): Sp226–sp7. doi: 10.37765/ajmc.2020.88475
- Dhillon S. Orelabrutinib: First Approval. Drugs (2021) 81(4):503–7. doi: 10.1007/s40265-021-01482-5
- Wu JJ, Wang WH, Dong M, Ma SS, Zhang XD, Zhu LN, et al. Orelabrutinib-Bruton Tyrosine Kinase Inhibitor-Based Regimens in the Treatment of Central Nervous System Lymphoma: A Retrospective Study. *Invest New* Drugs (2022) 40(3):650–9. doi: 10.1007/s10637-022-01219-5
- Song Y, Song Y, Liu L, Zhang M, Li Z, Ji C, et al. Long-Term Safety and Efficacy of Orelabrutinib Monotherapy in Chinese Patients With Relapsed or Refractory Mantle Cell Lymphoma: A Multicenter, Open-Label, Phase II Study. *Blood* (2020) 136:1. doi: 10.1182/blood-2020-141781
- Dhillon S. Tirabrutinib: First Approval. Drugs (2020) 80(8):835–40. doi: 10.1007/s40265-020-01318-8
- Yu H, Wang X, Li J, Ye Y, Wang D, Fang W, et al. Addition of BTK Inhibitor Orelabrutinib to Rituximab Improved Anti-Tumor Effects in B Cell Lymphoma. *Mol Ther Oncol* (2021) 21:158–70. doi: 10.1016/j.omto.2021.03.015
- Zhu J, Ma J. Chinese Society of Clinical Oncology (CSCO) Diagnosis and Treatment Guidelines for Malignant Lymphoma 2021 (English Version). *Chin* J Cancer Res (2021) 33(3):289. doi: 10.21147/j.issn.1000-9604.2021.03.01
- Li M, Wang ZA. New advances in the treatment of relapsed/refractory diffuse large B-cell lymphoma. *Chinese J Gen Pract* (2015) 13(6):1000–1003. doi: CNKI:SUN:SYQY.0.2015-06-051
- Fridberg JW. The American society of hematology education program book. *Am Hematol* (2011) 498–505.
- 25. Soussain C, Choquet S, Blonski M, Leclercq D, Houillier C, Rezai K, et al. Ibrutinib Monotherapy for Relapse or Refractory Primary CNS Lymphoma and Primary Vitreoretinal Lymphoma: Final Analysis of the Phase II 'Proofof-Concept' iLOC Study by the Lymphoma Study Association (LYSA) and the French Oculo-Cerebral Lymphoma (LOC) Network. *Eur J Cancer (Oxford Engl 1990)* (2019) 117:121–30. doi: 10.1016/j.ejca.2019.05.024
- Renaud L, Bossard J-B, Terriou L, Cambier N, Chanteau G, Carpentier B, et al. Treatment With Temozolomide and Ibrutinib in Recurrent/Refractory Primary (PCNSL) and Secondary CNS Lymphoma (SCNSL). *Blood* (2020) 136:23–4. doi: 10.1182/blood-2020-138764
- Narita Y, Nagane M, Mishima K, Terui Y, Arakawa Y, Yonezawa H, et al. Phase I/II Study of Tirabrutinib, a Second-Generation Bruton's Tyrosine Kinase Inhibitor, in Relapsed/Refractory Primary Central Nervous System Lymphoma. *Neuro-oncology* (2021) 23(1):122–33. doi: 10.1093/neuonc/noaa145
- 28. Ghesquieres H, Chevrier M, Laadhari M, Chinot O, Choquet S, Moluçon-Chabrot C, et al. Lenalidomide in Combination With Intravenous Rituximab (REVRI) in Relapsed/Refractory Primary CNS Lymphoma or Primary Intraocular Lymphoma: A Multicenter Prospective 'Proof of Concept' Phase II Study of the French Oculo-Cerebral Lymphoma (LOC) Network and the Lymphoma Study Association (LYSA)†. Ann Oncol (2019) 30(4):621–8. doi: 10.1093/annonc/mdz032
- 29. Song Yuqin DL, Zhang B, Luo H, Zhao R. Preliminary Results of Orelabrutinib Concentrations in Peripheral Blood and Cerebrospinal Fluid in Patients With Relapsed/Refractory Primary or Secondary CNS Lymphoma. *CSCO, 24th Annual Meeting* (2021).

- Morabito F, Skafi M, Recchia AG, Kashkeesh A, Hindiyeh M, Sabatleen A, et al. Lenalidomide for the Treatment of Mantle Cell Lymphoma. *Expert Opin Pharmacother* (2019) 20(5):487–94. doi: 10.1080/14656566.2018.1561865
- Jackson SE, Chester JD. Personalised Cancer Medicine. Int J Cancer (2015) 137(2):262–6. doi: 10.1002/ijc.28940
- Kim HJ, Hawke N, Baldwin AS. NF-kappaB and IKK as Therapeutic Targets in Cancer. Cell Death Diff (2006) 13(5):738–47. doi: 10.1038/sj.cdd.4401877
- 33. Mohamed AJ, Yu L, Bäckesjö CM, Vargas L, Faryal R, Aints A, et al. Bruton's Tyrosine Kinase (Btk): Function, Regulation, and Transformation With Special Emphasis on the PH Domain. *Immunol Rev* (2009) 228(1):58–73. doi: 10.1111/j.1600-065X.2008.00741.x
- Davis RE, Ngo VN, Lenz G, Tolar P, Young RM, Romesser PB, et al. Chronic Active B-Cell-Receptor Signalling in Diffuse Large B-Cell Lymphoma. *Nature* (2010) 463(7277):88–92. doi: 10.1038/nature08638
- Martin P, Jung SH, Pitcher B, Bartlett NL, Blum KA, Shea T, et al. A Phase II Trial of Lenalidomide Plus Rituximab in Previously Untreated Follicular non-Hodgkin's Lymphoma (NHL): CALGB 50803 (Alliance). Ann Oncol (2017) 28 (11):2806–12. doi: 10.1093/annonc/mdx496
- 36. Chen C, Sun P, Cui J, Yan S, Chen H, Xia Y, et al. High-Dose Methotrexate Plus Temozolomide With or Without Rituximab in Patients With Untreated Primary Central Nervous System Lymphoma: A Retrospective Study From China. *Cancer Med* (2019) 8(4):1359–67. doi: 10.1002/cam4.1906

 Lewis KL, Chin CK, Manos K. Ibrutinib for Central Nervous System Lymphoma: The Australasian Lymphoma Alliance/MD Anderson Cancer Center Experience. Br J Haematol (2021) 192(6):1049–53. doi: 10.1111/ bjh.16946

Conflict of Interest: The authors declare that the research was conducted in the absence of any commercial or financial relationships that could be construed as a potential conflict of interest.

Publisher's Note: All claims expressed in this article are solely those of the authors and do not necessarily represent those of their affiliated organizations, or those of the publisher, the editors and the reviewers. Any product that may be evaluated in this article, or claim that may be made by its manufacturer, is not guaranteed or endorsed by the publisher.

Copyright © 2022 Yang, Cui, Ren, Li, Yu, Shen, Jiang, Li, Zhang, Zhao, Zhu and Lin. This is an open-access article distributed under the terms of the Creative Commons Attribution License (CC BY). The use, distribution or reproduction in other forums is permitted, provided the original author(s) and the copyright owner(s) are credited and that the original publication in this journal is cited, in accordance with accepted academic practice. No use, distribution or reproduction is permitted which does not comply with these terms.



Lighting a Fire: Gasdermin-Mediated Pyroptosis Remodels the Glioma Microenvironment and Promotes Immune Checkpoint Blockade Response

Yonghua Cai^{1†}, Ke Li^{1†}, Jie Lin¹, Xianqiu Liang¹, Wei Xu¹, Zhengming Zhan¹, Shuaishuai Xue¹, Yu Zeng¹, Peng Chai¹, Yangqi Mao¹, Zibin Song¹, Lei Han¹, Ye Song^{1,2*}, Xian Zhang^{1*} and Hai Wang^{1*}

¹ Department of Neurosurgery, Nanfang Hospital, Southern Medical University, Guangzhou, China, ² Department of Neurosurgery, Ganzhou People's Hospital, Ganzhou, China

Pyroptosis is a proinflammatory programmed cell death pathway mediated by gasdermins. Exploring the role of pyroptosis can provide new insights into tumor malignancy. The most recent studies on pyroptosis have focused on tumor cells. However, the effects of pyroptosis on the tumor microenvironment (TME), immunotherapeutic responses, and efficacy have been neglected, especially in case of glioma. In this study, four independent glioma cohorts comprising 1,339 samples and a pan-cancer cohort comprising 10,535 tumor samples were analyzed. The relationships among pyroptosis status, prognosis, microenvironment cellular components, and clinical and biological phenotypes were investigated through the identification of pyroptosis subtypes, construction of a gasdermin-related prognostic index (GPI), and evaluation of immunological characteristics in glioma. The Genomics of Drug Sensitivity in Cancer database and "pRRophetic" package in R were used to estimate temozolomide (TMZ) sensitivity. The "Submap" package and external immunotherapy cohorts were used to investigate and confirm the role of GPI in response to and efficacy of immunotherapy in glioma. Finally, potential small-molecule compounds related to GPI were identified using the connectivity map database and mode-of-action analysis. We identified three different pyroptosis subtypes: cluster 1 (C1) characterized by a higher GPI, while cluster 2 (C2) and cluster 3 (C3) characterized by a lower GPI. The high GPI of C1 was associated with glioma progression and worse prognoses, whereas the low GPI of subtype C2 and C3 was associated with better prognoses. However, patients with high GPIs were found to be more sensitive to TMZ and immune checkpoint blockade than those with low GPIs. Furthermore, gasdermin D may be a principal potential biomarker and play key roles in

OPEN ACCESS

Edited by: Xuyao Zhang, Fudan University, China

Reviewed by:

Qiushi Feng, China Pharmaceutical University, China Zeguo Sun, Icahn School of Medicine at Mount Sinai, United States

*Correspondence:

Hai Wang nfyyneurowh@163.com Xian Zhang zxa@smu.edu.cn Ye Song songye@smu.edu.cn

[†]These authors have contributed equally to this work

Specialty section:

This article was submitted to Cancer Immunity and Immunotherapy, a section of the journal Frontiers in Immunology

Received: 01 April 2022 Accepted: 11 May 2022 Published: 17 June 2022

Citation:

Cai Y, Li K, Lin J, Liang X, Xu W, Zhan Z, Xue S, Zeng Y, Chai P, Mao Y, Song Z, Han L, Song Y, Zhang X and Wang H (2022) Lighting a Fire: Gasdermin-Mediated Pyroptosis Remodels the Glioma Microenvironment and Promotes Immune Checkpoint Blockade Response. Front. Immunol. 13:910490. doi: 10.3389/fimmu.2022.910490

382

pyroptosis-inducible therapy combined with immunotherapy in glioma. This study provides a clinical, biological, and molecular landscape of pyroptosis and suggests that pyroptosis of glioma cells may perform the dual function of promoting both tumorigenesis and antitumor immunity.

Keywords: pyroptosis, immunity, immunotherapy, gasdermins, tumor immune microenvironment, glioma

INTRODUCTION

Diffuse glioma is the most common primary brain tumor, classified as World Health Organization (WHO) grades II, III, and IV (1, 2). Gliomas are highly heterogeneous tumors, ranging from low-grade glioma (LGG; WHO grade II) to high-grade glioma (HGG; WHO grades III and IV), depending on the malignancy of the tumor. Isocitrate dehydrogenase (*IDH*) mutations, chromosome arm 1p and 19q (1p/19q) codeletion, and O(6)-methylguanine-DNA methyltransferase (*MGMT*) promoter methylation are homogeneously present in gliomas (3). Patients with glioblastoma, the most malignant glioma, has a median overall survival (OS) of only 14–17 months, even when subjected to surgical resection combined with radiotherapy, temozolomide (TMZ) chemotherapy, and tumor-treating fields (4–6). Given the low survival outcomes, novel treatment strategies are urgently required to treat gliomas.

Pyroptosis, a gasdermin-mediated programmed cell death program, presents a novel paradigm for cancer treatment (7–9). The executors of pyroptosis, gasdermins, comprise a protein family encoded by six paralogous genes: gasdermin A (GSDMA), gasdermin B (GSDMB), gasdermin C (GSDMC), gasdermin D (GSDMD), gasdermin E (GSDME), and pejvakin (PJVK) (10). Gasdermins play extensive and complicated roles in cancers (11), such as esophageal and gastric tumors, non-small cell lung cancer, colorectal and breast cancers, bladder carcinoma, and melanoma (12-19). Unfortunately, only a few studies have investigated the role of pyroptosis in gliomas. A recent study showed that high GSDMD expression is associated with IDHwildtype and WHO grade IV gliomas as well as shorter OS and is a response marker for TMZ treatment in glioma (20). Chen et al. reported that kaempferol, a major flavonoid present in various edible plants, increased reactive oxygen species levels and further led to GSDME-mediated pyroptosis, thereby suppressing glioma cell proliferation (20). However, most recent studies on pyroptosis have mainly focused on tumor cells, and the contingent effects of pyroptosis in the tumor immune microenvironment (TIME) have been neglected. Hence, exploring the impact of pyroptosis on the microenvironment of gliomas will provide insights into malignant progression and may even help developing novel treatment strategies, especially for immunotherapy combined with pyroptosis-inducible therapy.

In this study, to explore the effects of pyroptosis on glioma in multiple dimensions, we comprehensively analyzed the transcriptional and genetic heterogeneity of pyroptosis executors, identified three pyroptosis subtypes (C1, C2, and C3), and developed a gasdermin-related prognostic index (GPI). Our results show that the pyroptosis subtype C1 and high GPI are associated with high malignancy of glioma but may improve the sensitivity and efficacy of TMZ and immune checkpoint blockade (ICB) treatment, highlighting the value of a combination of pyroptosis-inducible therapy with chemotherapy and/or immunotherapy for glioma. Collectively, the pyroptosis of glioma cells may be a double-edged sword that promotes both tumorigenesis and antitumor immunity.

MATERIALS AND METHODS

Data Sources and Processing

The RNA-sequencing datasets "TCGA-663", "CGGA-325", and "GSE43378" and the mRNA microarray dataset "CGGA-301", along with corresponding clinical information for glioma samples, were retrieved from The Cancer Genome Atlas (TCGA) (version 28.0, https://portal.gdc.cancer.gov/), Chinese Glioma Genome Atlas (CGGA) (2021 Feb, http://www.cgga.org. cn/index.jsp) (21), and Gene Expression Omnibus databases (2021 April, https://www.ncbi.nlm.nih.gov/geo). The mRNA transcription values were converted to thousands of millions of thousand-based (TPM) values and further normalized to log2 (TPM + 1) for downstream analysis. The main study was conducted using TCGA-663 and validated using CGGA-325. The CGGA-301 and GSE43378 datasets were used to validate the GPI for glioma prognosis. The baseline clinical characteristics of the glioma samples are summarized in Table 1. The glioma cell line expression matrix was obtained from Cancer Cell Line Encyclopedia (CCLE) (https://portals.broadinstitute.org/ccle/ about), and the unified and standardized TCGA pan-cancer dataset (n = 10535) was downloaded from the UCSC Xena database (https://xenabrowser.net/).

Online Databases and Tools

The cBioPortal (http://www.cbioportal.org) (22) was used to retrieve and visualize mutations and copy-number alterations (CNA) of gasdermins in the "Merged Cohort of LGG and GBM (TCGA, Cell 2016)." The Human Protein Atlas database (version 21.0, https://www.proteinatlas.org/) was used to explore the protein expression levels of gasdermins. STRING (https:// string-db.org/) (23) was used to identify gasdermin-related molecules, and Gene Ontology (GO) and Kyoto Encyclopedia of Genes and Genomes (KEGG) were used for term enrichment.

Identification of Pyroptosis Subtypes

Unsupervised cluster analysis was performed to identify the pyroptosisrelated subtypes in glioma using the "ConsensusClusterPlus" R package (24), based on the expression of pyroptosis-related molecules, using

TABLE 1	The baseline clinical	characteristics of	of the	alioma samples.

Characteristics	TCGA-663	CGGA-325	CGGA-301	GSE43378	Total	P value
N	663	325	301	50	1339	
Age						7.200E-06
<45	319 (23.86%)	191 (14.29%)	175 (13.09%)	14 (1.05%)	699 (52.28%)	
≥45	344 (25.73%)	134 (10.02%)	124 (9.27%)	36 (2.69%)	638 (47.72%)	
Gender						2.800E-01
Female	282 (21.06%)	122 (9.11%)	121 (9.04%)	16 (1.19%)	541 (40.40%)	
Male	381 (28.45%)	203 (15.16%)	180 (13.44%)	34 (2.54%)	798 (59.60%)	
Grade						8.400E-18
11	248 (18.52%)	103 (7.69%)	117 (8.74%)	5 (0.37%)	473 (35.32%)	
	261 (19.49%)	79 (5.90%)	57 (4.26%)	13 (0.97%)	410 (30.62%)	
IV	153 (11.43%)	139 (10.38%)	124 (9.26%)	32 (2.39%)	448 (33.46%)	
NA	1 (0.07%)	4 (0.30%)	3 (0.22%)	0 (0.0e+0%)	8 (0.60%)	
status						2.100E-29
Alive	415 (30.99%)	96 (7.17%)	112 (8.36%)	8 (0.60%)	631 (47.12%)	
Dead	247 (18.45%)	220 (16.43%)	187 (13.97%)	42 (3.14%)	696 (51.98%)	
NA	1 (0.07%)	9 (0.67%)	2 (0.15%)	0 (0.0e+0%)	12 (0.90%)	
OS						
Mean±SD	2.29±2.44	3.98±4.03	4.32±4.08	2.16±1.78	3.14±3.40	
Median [min-max]	1.55 [0.0E+0,17.60]	1.93 [0.05,13.18]	2.23 [0.06,13.22]	1.49 [0.05,8.27]	1.67 [0.0E+0,17.60]	

N, the number of glioma samples; NA, unknown; OS, overall survival.

agglomerative pam clustering with a 1-Pearson correlation distance and resampling 80% of the samples for 10 repetitions. The optimal number of clusters was determined using an empirical cumulative distribution function plot. Mutation data were downloaded from TCGA and visualized using the "maftools" R package (25) for identifying the somatic mutation landscape in distinct pyroptosis-related subtypes.

GPI and Nomogram Construction

We used the "glmnet" R package (26) to integrate survival time, survival status, and gene expression data for regression analysis using the Lasso-Cox method. In addition, we set up a 10-fold cross-validation to obtain the optimal model to yield the GPI equation with the coefficient multiplied by mRNA expression. The coefficient was derived by running "glmnet" on the entire TCGA-663 dataset with the optimal lambda value. A nomogram was created to predict the probability of OS based on the GPI combined with clinical characteristics through the "rms" R package and evaluated using a calibration plot, which compares nomogram-predicted probability with observed survival probability. Decision curve analysis (DCA) was used to evaluate the clinical application of the nomogram by assessing the net benefits of the prediction model at different threshold probabilities and concordance indices.

Gene Set Enrichment Analysis

We obtained the GSEA software (version 3.0) from the GSEA website (http://software.broadinstitute.org/gsea/index.jsp) (27) and downloaded the "h.all.v7.4.symbols.gmt" subset from the Molecular Signature Database (http://www.gseamsigdb.org/gsea/downloads.jsp) (28) to explore GPI-related pathways and molecular mechanisms based on gene expression profiles and GPI groups (high and low, separated by the median value). We adjusted the minimum gene set to 5 and the maximum gene set to 5000 and performed 1000 resamplings. P-value < 0.05 and FDR < 0.25 were considered statistically significant. Finally, the GSEA results were visualized using the "ggplot2" R package.

Evaluation of Immunological Characteristics

The "estimate" R package (29) was used to calculate the immune score and stromal score for each glioma sample. The "immunedeconv" R package (30) was utilized to estimate TME infiltrating cells for each glioma sample. The tumor mutation burden (TMB) score of each sample was calculated using the "tmb" function of the "maftools" R package (25). The microsatellite instability (MSI) score for each sample was obtained from a previous study (31). The stemness indices (mRNA expression-based stemness index, mRNAsi) for each sample were calculated using the OCLR algorithm developed by Malta et al. (32). The "deconvo_IPS" method of the "IOBR" R package (33) was used to assess the antigen processing cell (MHC), effector cell (EC), suppressor cell (SC), and checkpoint (CP) scores and immunophenoscore (IPS) of each tumor sample.

Correlation of GPI With TMZ Sensitivity

The TMZ sensitivity of each sample was estimated using Genomics of Drug Sensitivity in Cancer (GDSC, https://www. cancerrxgene.org/) (34), which is the largest publicly available pharmacogenomics database. The estimated half-maximal inhibitory concentration (IC_{50}) was calculated using ridge regression, and the prediction accuracy was determined using the "pRRophetic" R package (35). All parameters were set to default values with the removal of the batch effect of "combat" and "allSoldTumours" tissue types, and duplicate gene expression was summarized as the mean value.

Correlation of GPI With ICB Response

The potential ICB response was predicted using Submap (36)—a tool for comparing expression profiles—in GenePattern (https:// cloud.genepattern.org/gp). We used the Submap algorithm combined with human immunotherapy transcriptome data from Roh et al. (37) to further investigate the predictive value

of GPI in anti-PD1 and anti-CTLA4 immunotherapy response. Furthermore, several immunotherapy cohorts from Snyder et al. (38), Nathanson et al. (39), Mariathasan et al. (40), and Rose et al. (41) were used to validate the predictive value of GPI in the response to and efficacy of immunotherapy.

Candidate Small-Molecule Drugs Based on GPI

First, weighted co-expression gene modules identified and the module-trait relationships was determined using the "WGCNA" R package (42). The module with the correlation coefficient |> 0.5and P-value < 0.05 was considered as a meaningful module in this study. Second, only one module associated with immunity was identified using the STRING database (https://string-db.org/) (42). Then, differentially expressed genes (DEGs) were identified between the high- and low-GPI groups using the "limma" R package. Genes with P < 0.05 and |FC| > 1 were considered significant DEGs. The GO functional and KEGG pathway enrichment analyses of GPI- and immune-related DEGs were then performed using the "clusterProfiler" R package (43). Based on the upregulated and downregulated DEGs, candidate small-molecule drugs and mechanisms of action were predicted using the connectivity map (CMap, http://portals.broadinstitute.org/cmap/) database and CMap mode-of-action (MOA) analysis (44).

Statistical Analysis

All statistical analyses were conducted using R software (version 4.0.2), with a P-value < 0.05 (two-tailed) indicating significant differences. Unpaired t-tests were performed to compare two normally distributed variables. The Wilcoxon rank-sum test was performed to compare two non-normally distributed variables. The Kruskal-Wallis test (nonparametric method) or one-way analysis of variance (parametric method) was used for comparisons of three or more variables. Pearson and Spearman correlation coefficients were used to determine correlations between variables. The "survfit" function in the "Survminer" R package was used to evaluate prognostic differences between the two groups. Kaplan-Meier (KM) analysis was used to generate survival curves, and the log-rank test was performed to determine statistically significant differences. The receiver operating characteristic (ROC) curve was used to assess the prognosis prediction performance, and the area under the curve (AUC) was calculated using the "timeROC" R package.

RESULTS

Aberrant Expression, Genetic Alteration, and Prognostic Value of Gasdermins in Glioma

We comprehensively analyzed the molecular characteristics and prognostic significance of gasdermins—the executors of pyroptosis. The analysis of the data of glioma samples from

TCGA-693 showed that GSDMA and GSDMD were more highly expressed in grade IV than in grade II-III samples. Furthermore, GSDMB, GSDMC, and PJVK expression was lower in grade IV than in grade II-III samples, while GSDME expression showed no significant differences among grades (Figure 1A). As shown in Figure 1B, GSDMA, GSDMD, and GSDME expression was higher in IDH-wildtype than in IDH-mutant samples, while GSDMB, GSDMC, and PJVK expression was lower in IDHwildtype than in mutant samples. GSDMA, GSDMC, GSDMD, and GSDME expression was higher in 1p19q non-codel than in codel samples (Figure 1C), while PJVK expression was lower in 1p19q non-codel than in codel samples. Additionally, GSDMB expression showed no significant differences between the different 1p19q statuses. As shown in Figure 1D, GSDMA, GSDMD, and GSDME expression was lower in the MGMTpromoter methylated samples than in the unmethylated ones, while GSDMB, GSDMC, and PJVK expression was higher in MGMT-promoter methylated samples than in the unmethylated ones. Similar findings were observed for the CGGA-325 cohort (Figures S1A-D). Figure 1E shows that *IDH1* expression was positively related to GSDMA, GSDMD, and GSDME expression but negatively related to GSDMB, GSDMC, and PJVK expression. However, MGMT expression was positively related to GSDMA, GSDMC, and GSDMD expression but negatively related to GSDMB and GSDME expression. The analysis of glioma cell lines from CCLE showed that GSDMD and GSDME were more highly expressed in all glioma cell lines (including A-172, LN-229, T98G, U-251 MG, and U-87 MG) than GSDMB and PJVK, but GSDMA and GSDMC were poorly expressed in those glioma cell lines (Figure 1F). To explore the subcellular distribution of gasdermin expression in U-251 MG cells, we analyzed the results of immunofluorescence (ICC-IF) and confocal microscopy from the HPA database, and found that GSDMA was mainly located in the nucleoplasm, plasma membrane, and cytosol and GSDMB in the nucleoplasm and cytosol. As HPA did not contain U-251 MG-related ICC-IF results of GSDMB, we acquired the ICC-IF data of the U-2 OS cell line. We found that GSDMD was primarily located in the nucleoplasm, GSDME in the cytosol, and GSDMC and PJVK in the mitochondria (Figure 1G). To analyze the genetic characteristics of gasdermins, we explored the genetic alterations in 794 glioma samples with mutation and CNA data on the cBioPortal database. The results showed that gasdermins were altered in 48 (6%) of the 794 samples, but no gasdermin showed alternations of more than 3% (Figure S1E). Univariate and multivariate Cox regression analyses were performed to analyze the prognostic value of gasdermins in gliomas. The univariate Cox survival analysis indicated that GSDMA (P < 0.001), GSDMB (P < 0.001), GSDMC (P < 0.001), GSDMD (P < 0.001), and PJVK (P < 0.001) expression was strongly associated with clinical outcomes, but GSDME expression (P = 0.258) had no significant effect on survival (Figure 1H). Multivariate Cox survival analyses showed that GSDMC (P < 0.001), GSDMD (P < 0.001), and PJVK (P = 0.004) were independent prognostic factors for gliomas (Figure 1I). The immunohistochemistry (IHC) results from the HPA

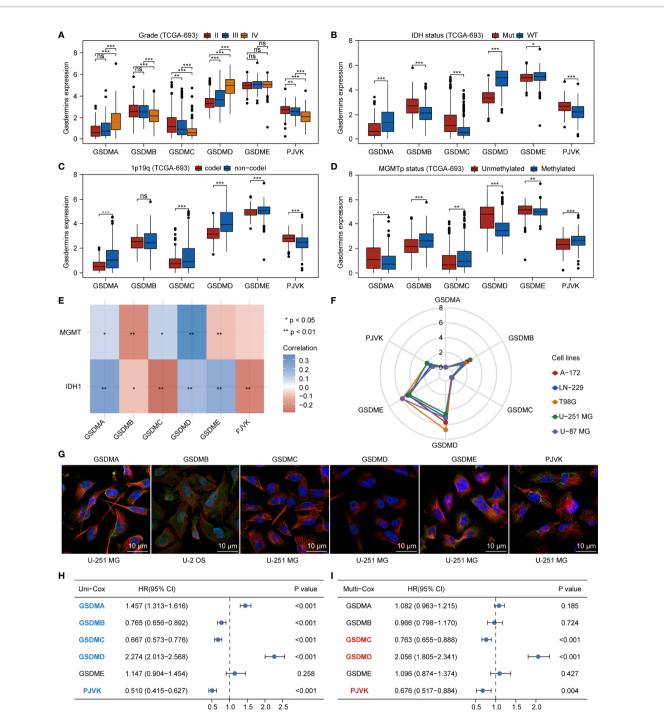
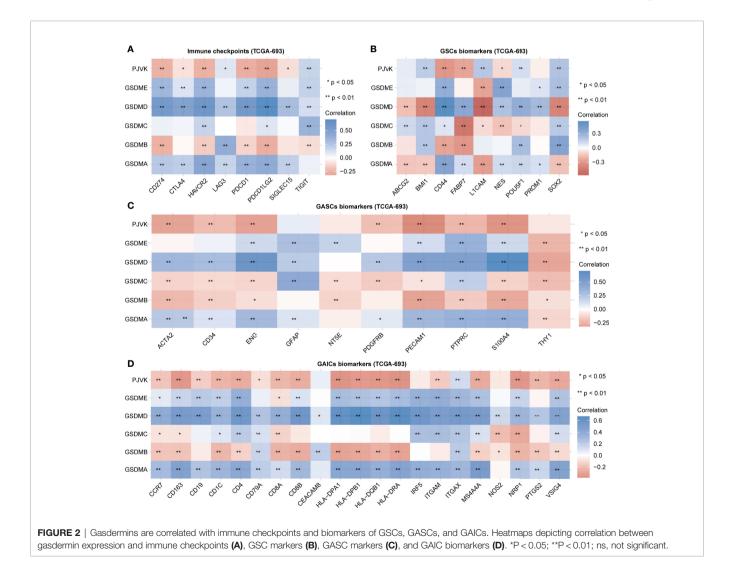


FIGURE 1 | Aberrant expression and prognostic value of gasdermins in glioma. Boxplots showing comparison of gasdermin expression in different grades (**A**), *IDH* mutation statuses (**B**), 1p19q codeletion statuses (**C**), and *MGMT*-promoter methylation statuses (**D**) of glioma samples. (**E**) Heatmap showing correlation between gasdermin expression and *IDH1* or *MGMT* expression. (**F**) Radar plot showing gasdermin expression in different glioma cell lines. (**G**) The results of immunofluorescence from HPA database showing the subcellular distribution of the gasdermin protein. (**H**, **I**) Forest plots showing the results of univariate and multivariate Cox regression analyses for gasdermins. *P<0.05; **P<0.01; ***P<0.001; ns, not significant.

database showed that GSDMC staining was not detected in normal brain, LGG, and HGG tissues, whereas GSDMD staining was not detected in normal brain tissues, was low in LGG tissues, and was medium in HGG tissues (**Figure S1F**). IHC staining data for PJVK were not available in the HPA database and therefore could not be assessed along these lines. These results suggest that gasdermins have potential target-treatment value for glioma.

Gasdermins are Correlated With Immune Checkpoints and Glioma Stem Cell, Glioma-Associated Stromal Cell, and Glioma-Associated Immune Cell Biomarkers

Initially, we explored the potential association between gasdermins and the major components of the glioma microenvironment. We extracted the transcript and expression values of eight immune checkpoints (CD274, CTLA4, HAVCR2, LAG3, PDCD1, PDCD1LG2, SIGLEC15, and TIGIT). **Figure 2A** shows that the expression of GSDMA, GSDMD, and GSDME was positively correlated with that of most immune checkpoints, while the expression of GSDMB and PJVK was negatively correlated with that of most immune checkpoints. The specific statistical data on the correlation between gasdermins and immune checkpoints are presented in **Table S1**. We summarized the data on nine glioma stem cell (GSC) biomarkers (ABCG2, BMI1, CD44, FABP7, L1CAM, NES, POU5F1, PROM1, and SOX2) from published studies (45–47). **Figure 2B** shows that all gasdermins were positively correlated with most GSC biomarkers; GSDMD was highly associated with all GSC markers. The specific statistical data on the correlation between gasdermins and GSC biomarkers are presented in Table S2. Next, we summarized the data on 10 glioma-associated stromal cell (GASC) biomarkers (ACTA2, CD34, ENG, GFAP, NT5E, PDGFRB, PECAM1, PTPRC, S100A4, and THY1) from a published study (48). Figure 2C shows that the expression of GSDMA, GSDMD, and GSDME was positively correlated with those of most GASC biomarkers, while those of GSDMB, GSDMC, and PJVK are negatively correlated. The specific statistical data for the correlation between gasdermins and GASC biomarkers are presented in Table S3. Finally, we summarized the data on 21 glioma-associated immune cell (GAIC) biomarkers (CCR7, CD163, CD19, CD1C, CD4, CD79A, CD8A, CD8B, CEACAM8, HLA-DPA1, HLA-DPB1, HLA-DQB1, HLA-DRA, IRF5, ITGAM, ITGAX, MS4A4A, NOS2, NRP1, PTGS2, and VSIG4) from existing studies (49, 50). Figure 2D shows that GSDMA, GSDMD, and GSDME expression was positively correlated with that of most GAIC biomarkers, while GSDMB and PJVK expression was negatively correlated. The specific statistical data for the correlation between gasdermins



and GAIC biomarkers are presented in **Table S4**. The CGGA-325 dataset showed similar results (**Figures S2A-D**). These results suggest that gasdermin-mediated pyroptosis has potential implications in tumor cell heterogeneity and the glioma immune microenvironment.

Three Glioma Pyroptosis Subtypes With Distinct TIME Features Identified *via* Gasdermin-Related Genes

We selected 54 gasdermin-related genes from the STRING database (Figure S3A and Table S5), most of which were pyroptosis-related molecules (9, 51, 52). GO functional enrichment analysis showed that the gasdermin-related genes were not only enriched in pyroptosis (GO:0070269) but also in positive regulation of T cell cytokine production (GO:0002726), cytokine production involved in the immune response (GO:0002367), positive regulation of interleukin-1 beta secretion (GO:0050718), regulation of T-helper 1 type immune response (GO:0002825), positive regulation of T-helper 1 cell cytokine production (GO:2000556), interleukin-18-mediated signaling pathway (GO:0035655), and positive regulation of Thelper 2 cell differentiation (GO:0045630) (Figure S3B and Table S6). These results imply that gasdermin-related genes are associated with the pyroptosis signaling pathway as well as with other immune system processes.

We further applied a consensus clustering method based on the expression profiles of the pyroptosis-related molecules and found that the optimal cluster number of glioma samples was three (K = 3) (**Figure 3A**). The division of the glioma samples of TCGA-693 into three pyroptosis subtypes (C1, C2, and C3) is shown in Figure 3B, and an overview of the pyroptosis-related molecule expression landscape in TCGA-693 is shown in Figure S4A. The glioma samples in C2 or C3 had better clinical outcomes than those in C1 (Figure 3C). Figure 3D shows the expression levels of aberrant gasdermins in different pyroptosis subtypes. GSDMA, GSDMD, and GSDME expression was higher in C1 than in C2 and C3; GSDMB expression was higher in C2 than in C1 and C3; and PJVK was expressed at a lower level in C1 than in C2 and C3. CGGA-325 showed similar results (Figures **S4B–E**). These results suggest that the three pyroptosis subtypes represent three major and different pyroptosis statuses with distinct OS in glioma.

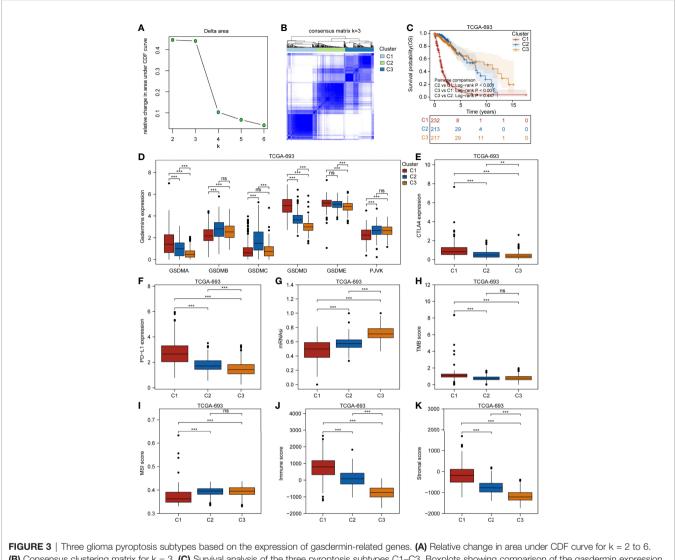
To explore the genetic alterations in different pyroptosis subtypes, we analyzed the top 10 mutated genes in TCGA glioma samples. As shown in **Figures S5A-C**, 191 samples had mutations with a frequency of 83.41% in C1, 194 samples with 93.72% in C2, and 202 samples with 94.39% in C3. Missense mutations were the most common in all three clusters. TP53 had the highest mutation frequency (31%), followed by *EGFR* (27%), *TTN* (25%), and *PTEN* (25%) in C1; *IDH1* had the highest mutation frequency (89%), followed by *TP53* (67%) and *ATRX* (49%) in C2; and *IDH1* had the highest mutation frequency (82%), followed by *CIC* (34%) and *TP53* (31%) in C3. These results imply that genetic features may influence the pyroptosis status in gliomas. To analyze the TIME characteristics of different pyroptosis subtypes, we compared PD-L1 expression, CTLA4 expression, mRNAsi score, TMB score, MSI score, immune score, stromal score, and infiltrating cells in the three glioma sample clusters. Figures 3E, F and Figures S5D, E show that PD-L1 and CTLA4 expression was higher in C1 than in C2 or C3. The mRNAsi score was higher for C3 than for C1 or C2 (Figure 3G). The TMB score was higher for C1 than for C2 or C3, while the MSI score was lower in C1 than in C2 or C3 (Figures 3H, I). Figures 3G-K and Figures S5F, G show that the immune and stromal scores were higher for C1 than for C2 and C3. Distinct proportions and subtypes of infiltrating immune and stromal cells existed between C1 and C3, while C2 likely had an intermediate state between the two (Figure 4A and Figures S6A, B). The percentage abundance of M2 macrophages, M1 macrophages, CD8⁺ T cells, astrocytes, and endothelial cells in C1 were significantly higher in C1 than those in C2 and C3, while the percentage abundance of plasma B cells and mesenchymal stem cells was lower in C1 than in C2 and C3 (Figure 4B). These results imply that different pyroptosis statuses may promote or suppress the formation of an immunosuppressive TME, further influencing the progression and prognosis of glioma.

Development and Validation of GPI for Glioma

Further, we developed GPI based on the gasdermins expression matrix using the Lasso-Cox method in TCGA-693 training set. **Figure 5A** shows the partial likelihood deviance versus log (λ), where λ is the tuning parameter. **Figure 5B** shows the optimal lambda (lambda.min = 0.0077) and the corresponding coefficients of the selected factors (GSDMC = -0.2321, GSDMD = 0.7436, PJVK = -0.4135). The formula for the final scoring model is as follows:

$$GPI = (-0.2321 \times GSDMC \ expression) + (0.7436 \times GSDMD \ expression) + (-0.4135 \times PJVK \ expression)$$

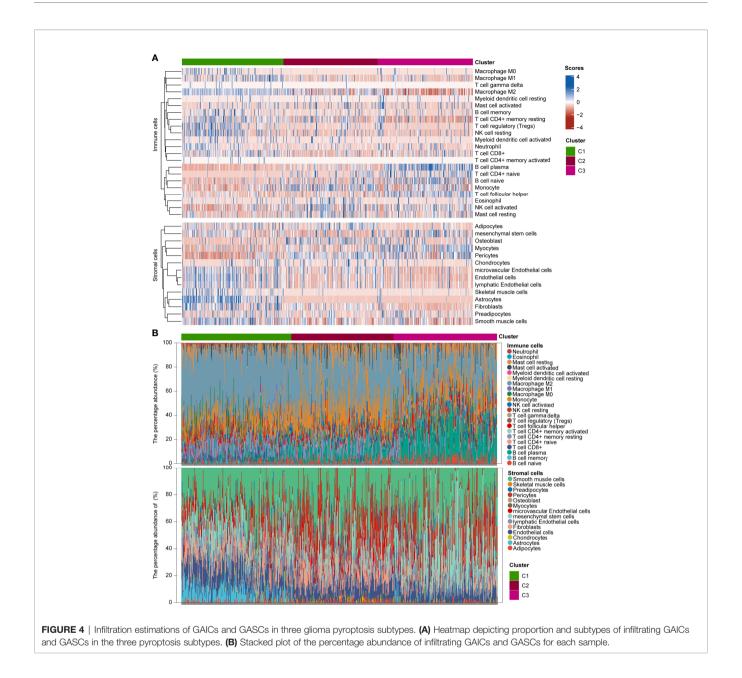
The dotted line represents the GPI ranging from low to high and divides the patients into low- and high-GPI groups (GPI-L and GPI-H, respectively) based on the median value (Figure 5C, upper). The alive-status samples were mainly distributed in the GPI-L group, whereas the dead-status samples in the GPI-H group (Figure 5C, middle). The heatmap of the expression profiles of the prognostic genes shows that GSDMC and PJVK were highly expressed in the GPI-L group, whereas GSDMD was highly expressed in the GPI-H group (Figure 5C, lower). Figure 5D shows that patients with higher GPIs had significantly worse prognoses than those with low GPI (logrank P < 0.001). The time-dependent ROC curve (Figure 5E) shows that GPI has a strong prognostic value for glioma and can help predict both short-term and long-term survival (1-year AUC = 0.816; 2-year AUC = 0.833; 3-year AUC = 0.850; 4year AUC = 0.806; 8-year AUC = 0.808). Three independent glioma cohorts ("CGGA-325", "CGGA-301", and "GSE43378") were used as validation sets to verify the predictive power of GPI. Figures S7A-C show that a high GPI significantly correlates with



(B) Consensus clustering matrix for k = 3. (C) Survival analysis of the three pyroptosis subtypes C1–C3. Boxplots showing comparison of the gasdermin expression (D), CTLA4 expression (E), PD-L1 expression (F), mRNAsi (G), TMB score (H), MSI score (I), immune score (J), and stromal score (K) in the three pyroptosis subtypes. **P < 0.01; ***P < 0.001; ns, not significant.

a worse prognosis in all three validation sets. The results in Figures S7D-F verify that the predictive accuracy of GPI is high in all independent validation sets ("CGGA-325," 1-year AUC = 0.683, 3-year AUC = 0.754, 5-year AUC = 0.786; "CGGA301," 1year AUC = 0.601, 3-year AUC = 0.633, 5-year AUC = 0.625; "GSE43378," 1-year AUC = 0.665, 3-year AUC = 0.836, 5-year AUC = 0.700); these results are consistent with those of TCGA-693 training set. In addition, we verified the prediction stability of GPI for gliomas in different clinical or molecular subgroups. Figures 6A-H show that the higher GPIs commonly correlated with shorter survival time, regardless of the LGG (log-rank P < 0.001), HGG (log-rank P < 0.001), IDH-wildtype (log-rank P = 0.01), IDH-mutant (log-rank P = 0.004), 1p19q codel (log-rank P = 0.056), 1p19q non-codel (log-rank P < 0.001), MGMTpromoter methylated (log-rank P < 0.001), and MGMTpromoter unmethylated (log-rank P < 0.001) groups. Similar results were observed for the CGGA-325 cohort (**Figures S7G-N**). These results demonstrate that GPI is generally stable and accurate for the prognosis of glioma.

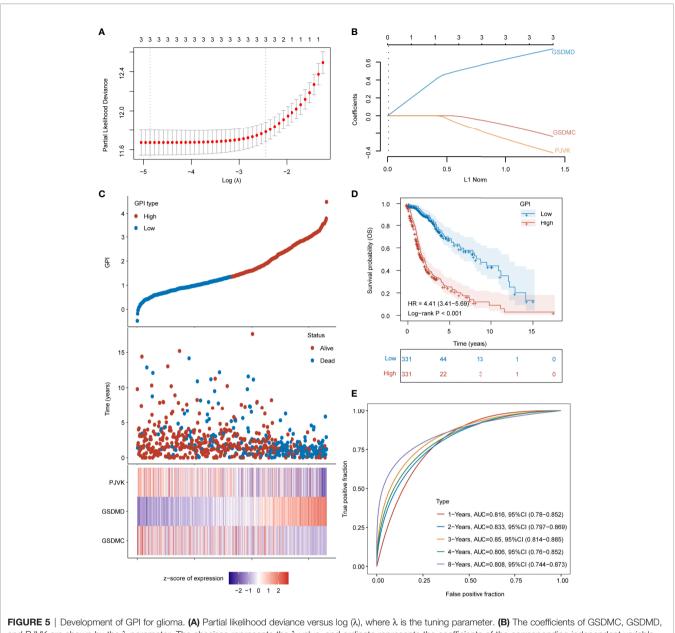
To further refine and optimize the prediction performance of GPI for glioma, we integrated GPI and clinical factors (including age, grade, *IDH* mutational status, 1p19q codel status, and *MGMT*-promoter methylation status) to construct an OS nomogram model (**Figure 6I**). **Figure 6J** shows that the nomogram calibration curves of 1-year (green line), 2-year (red line), and 5-year (purple line) OS are close to the ideal curve (dashed diagonal line), indicating that there is a good agreement between predicted and observed probabilities. Finally, we performed DCA to evaluate the clinical utility of GPI. **Figures 6K–N** show that the updated nomogram model integrating GPI and clinical characteristics provided a greater predictive net benefit than a single GPI for a wide range of



decision thresholds, including both short-term and long-term survival.

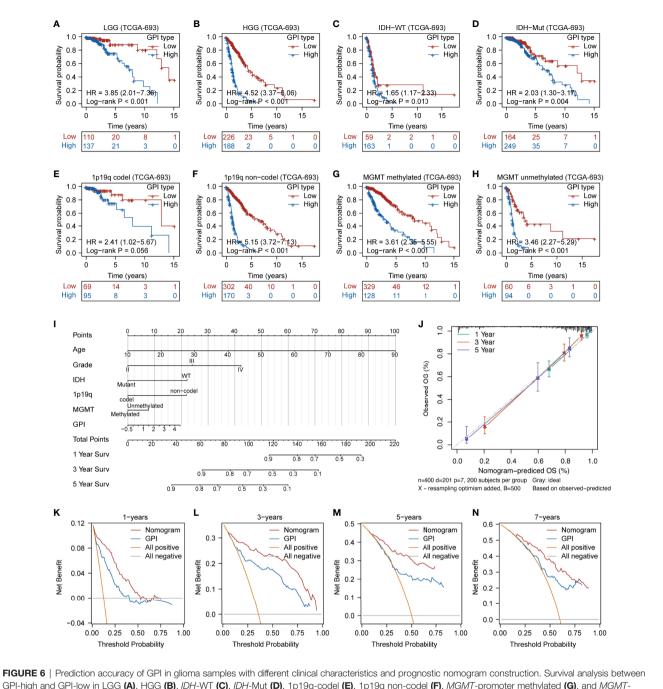
GPI Is Associated With Clinical Features and Immunity of Glioma Patients

Our findings demonstrate that different pyroptosis subtypes may exhibit different pyroptosis statuses. **Figure 7A** shows that the pyroptosis subtype C1 has the highest GPI, while the pyroptosis subtype C3 has the lowest GPI. These results indicate that, to some extent, GPI can be used as a quantitative attribute of the intrinsic pyroptosis status of glioma. To further explore the function of pyroptosis, we analyzed the correlation between GPI and different clinical features, molecular characteristics, and immune-related indices. **Figure 7B** shows that GPI progressively increases with the glioma grade. **Figures 7C–E** show that samples with *IDH*-wildtype, 1p19q non-codel, and *MGMT*-promoter unmethylated status had higher GPIs than those with *IDH*-Mut, 1p19q-codel, and *MGMT*-promoter methylated status. **Figures 7F–L** show that GPI was negatively correlated with mRNAsi (r = -0.490, P < 0.001) and MSI score (r = -0.330, P < 0.001) and positively correlated with immune score (r = 0.660, P < 0.001), stromal score (r = 0.700, P < 0.001), PD-L1 expression (r = 0.510, P < 0.001), CTLA4 expression (r = 0.150, P < 0.001), and TMB score (r = 0.390, P < 0.001). In addition, we analyzed the correlation between gasdermins (GSDMC, GSDMD, and PJVK) and GPI, mRNAsi, stromal score, immune score, PD-L1 and CTLA4 expression, TMB, and MSI. The results are shown in the form of a correlation



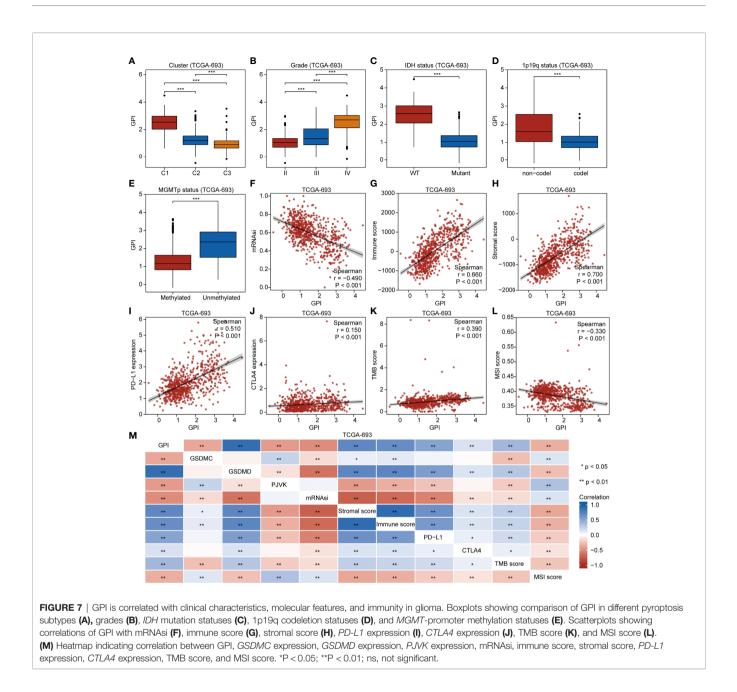
and PJVK are shown by the λ parameter. The abscissa represents the λ value, and ordinate represents the coefficients of the corresponding independent variable. (**C**, top) Scatterplot showing GPI from low to high; (**C**, middle) scatter plot distribution represents survival time and survival status of different samples with corresponding GPI; (**C**, bottom) heatmap showing GSDMC, GSDMD, and PJVK expression from GPI signature. (**D**) Survival analysis between GPI-high and GPI-low groups. (**E**) ROC curve of GPI for OS.

heatmap (**Figure 7M**), and the specific statistical data are summarized in **Table S7**. Similar findings were obtained from the CGGA-325 dataset (**Figures S8A–I**). To further determine which subsets of infiltrating cells are mainly affected by pyroptosis, we compared the infiltration degrees of immune and stromal cells between the GPI-H and GPI-L groups and calculated the correlation coefficients of GPI with the proportion of specific infiltrating cells. The upper panel of **Figure 8A** shows that the infiltration of memory B cells, CD8⁺ T cells, resting memory CD4⁺ T cells, activated memory CD4⁺ T cells, regulatory T cells, resting NK cells, M0 macrophages, M1 macrophages, M2 macrophages, activated myeloid dendritic cells, activated mast cells, and neutrophils was higher in the GPI-H group than in the GPI-L group, while that of naïve B cells, plasma B cells, naïve $CD4^+$ T cells, follicular helper T cells, activated NK cells, monocytes, and resting mast cells was lower. The lower panel of **Figure 8A** shows strong positive and negative correlations between GPI and each immune cell subtype, especially plasma B cells (r = -0.56), naïve CD4⁺ T cells (r = -0.47), resting memory CD4⁺ T cells (r = 0.33), regulatory T cells (r = 0.30), M1 macrophages (r = 0.31), and M2 macrophages (r = 0.40). The upper panel of **Figure 8B** shows that the infiltration of astrocytes,



GPI-high and GPI-low in LGG (A), HGG (B), *IDH*-WT (C), *IDH*-Mut (D), 1p19q-codel (E), 1p19q non-codel (F), *MGMT*-promoter methylated (G), and *MGMT*-promoter unmethylated (H) groups in glioma. (I) Nomogram was developed with the age, grade, *IDH* mutational status, 1p19q codeletion status, *MGMT*-promoter methylation status, and GPI. (J) Calibration plot for nomogram. (K–N) Decision curve analysis (DCA) of 1-, 3-, 5-, and 7-year overall survival for GPI and nomogram.

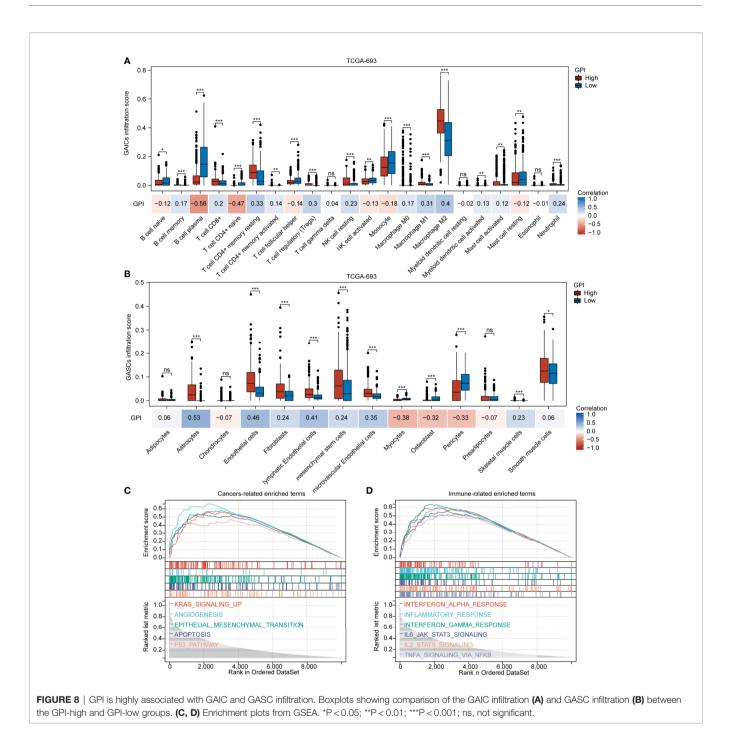
endothelial cells, fibroblasts, lymphatic endothelial cells, mesenchymal stem cells, microvascular endothelial cells, skeletal muscle cells, and smooth muscle cells was higher in the GPI-H group than in the GPI-L group, while that of myocytes, osteoblasts, and pericytes was lower. The lower panel of **Figure 8B** shows strong positive and negative correlations between GPI and each stromal cell subtype, especially astrocytes (r = 0.53), endothelial cells (r = 0.46), lymphatic endothelial cells (r = 0.41), microvascular endothelial cells (r = 0.35), myocytes (r = -0.38), osteoblasts (r = -0.32), and pericytes (r = -0.33). Similar results were obtained from the CGGA-325 dataset (**Figures S9A, B**). These results suggest that pyroptosis, as an immunogenic cell death mechanism, results in an imbalance in TIME by altering the proportion of immune cell and stromal cell infiltration.



To further explore the biological processes and pathways influenced by pyroptosis in gliomas, we performed GSEA. **Figure 8C** shows that several common cancer-related signaling pathways, including *KRAS* signaling up, angiogenesis, epithelial mesenchymal transition, apoptosis, and the *P53* pathway, were active in the GPI-H group. **Figure 8D** shows significant activation of many immune-related signaling pathways in the GPI-H group, including interferon alpha response, inflammatory response, interferon gamma response, *IL6/JAK/STAT3* signaling, *IL2/STAT5* signaling, and TNFA signaling *via NFKB*. However, GSEA did not identify any significantly enriched pathways in the GPI-L group. All GSEA results are presented in **Table S8**. These results imply that these cancer- and immune-related pathways may be involved in the regulation of pyroptosis and TIME balance in glioma.

Patients With High GPIs Are More Sensitive to TMZ and Anti-PD1 Therapy

So far, the correlations among pyroptosis subtypes, GPI, prognosis, and TIME in glioma have been demonstrated. Further studying the potential therapeutic value of pyroptosis is promising, especially in the context of chemoimmunotherapy. **Figure 9A** shows that the C1 had the lowest TMZ IC₅₀ among the three pyroptosis subtypes. **Figures 9B, C** show that the GPI-high group had a lower TMZ IC₅₀, and the GPI levels were negatively correlated with TMZ IC₅₀ (r = -0.360, P < 0.001),



indicating that patients with higher GPI were more sensitive to TMZ treatment. To explore the predictive value of GPI for ICB patients with high GPIs were more responsive to anti-PD1 one therapy (nominal P = 0.024; Bonferroni-corrected P = 0.003). To immunotherapy, we selected several external ICB show immunotherapy cohorts. **Figures 9E**, **F** show that the GPIs of GPI responders were higher than those of non-responders.

Figures 9G, H show that GPI has high accuracy in predicting patients' response to ICB (Snyder et al. cohort: GPI AUC = 0.812; Nathanson et al. cohort: GPI AUC = 0.841), and GSDMD may be one of the potential molecules influencing patient responses to immunotherapy (Snyder et al. cohort: GSDMD AUC = 0.812; Nathanson et al. cohort: GSDMD AUC = 0.909). **Figures 9I–L** show that the GPI-H group had a longer survival time than the GPI-L group. These results indicate that the high GPI may be associated with improved response to and efficacy of ICB therapy

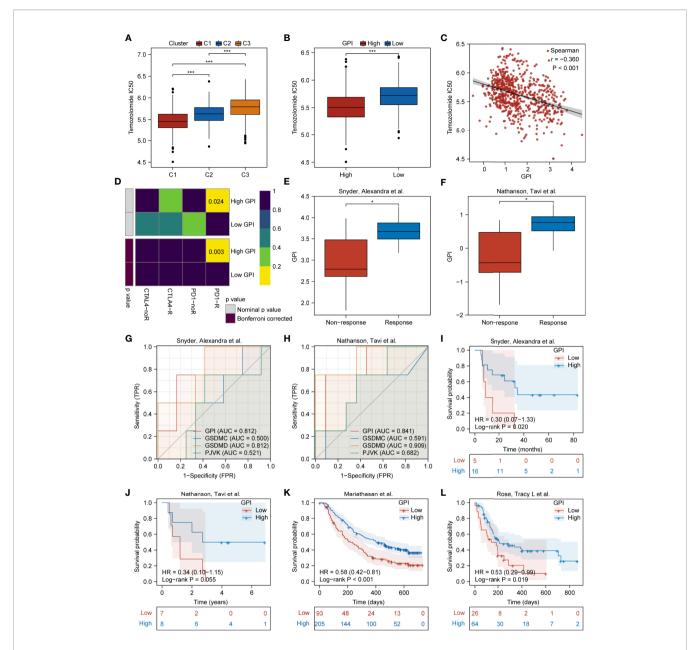
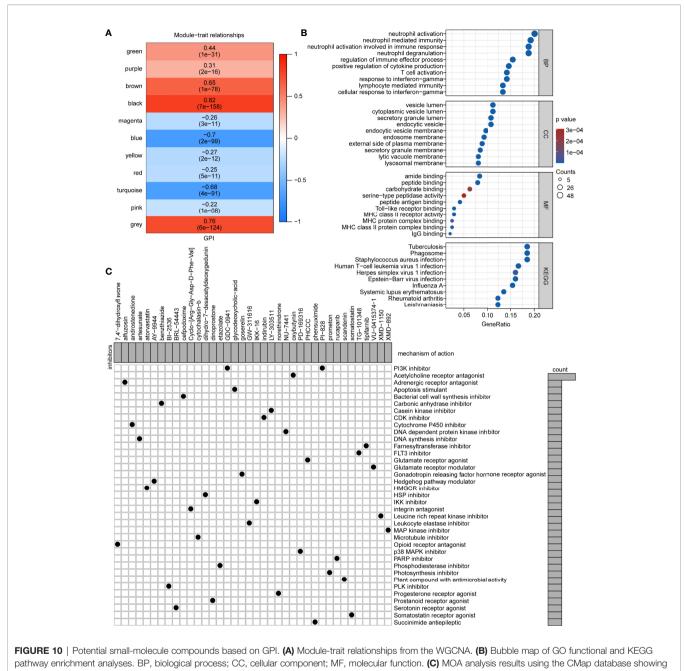


FIGURE 9 | Patients with high GPIs are more sensitive to TMZ and ICB therapy. Boxplots showing comparison of the TMZ IC₅₀ among the three pyroptosis subtypes (**A**) and between GPI-high and GPI-low groups (**B**). Scatterplots showing the correlation of TMZ IC₅₀ with GPI (**C**). (**D**) Submap analysis showing differences in sensitivity of GPI-high and GPI-low groups to anti-PD1 and anti-CTLA4 immunotherapy. (**E**, **F**) Boxplots showing comparison of the GPI level between responders and non-responders. (**G**, **H**) ROC curve of GPI for immunotherapy response. (**I–L**) Survival analysis between GPI-high and GPI-low groups in immunotherapy cohorts. *P < 0.05; ***P < 0.001; ns, not significant.

Potential Small-Molecule Compounds Based on GPI

To determine how pyroptosis can be activated or suppressed in tumor cells, we explored potential small molecules based on GPI. First, WGCNA was performed and 10 co-expression gene modules based on a soft threshold (power) of 11 (**Figures S10A, B**; namely, green, purple, brown, black, magenta, blue, yellow, red, turquoise, and pink, where gray module is considered a collection of genes that cannot be assigned to any module) were obtained (**Figure S10C** and **Table S9**). Among the 10 modules, brown (r = 0.65, P < 0.05), black (r = 0.82, P < 0.05), blue (r = -0.70, P < 0.05), and turquoise (r = -0.68, P < 0.05) were associated with GPI (**Figure 10A**). To further identify a module that correlated with immunity, we analyzed the main functions of these four GPI-related modules one by one in the STRING database and identified that the brown module genes were mainly related to immunity. We identified 767 upregulated and 973 downregulated DEGs between the GPI-H and GPI-L



small-molecule compounds with corresponding mechanisms of action.

groups *via* DEG analysis (**Figure S10D** and **Table S10**). The Venn diagram (**Figure S10E**) shows 249 upregulated genes and the only downregulated gene in the brown module (**Table S11**). The GO functional and KEGG pathway enrichment analyses for these genes showed that biological processes (BP) were mainly enriched in neutrophil activation, neutrophil-mediated immunity, neutrophil activation involved in immune response, neutrophil degranulation, regulation of immune effector process, positive regulation of cytokine production, T cell activation, response to interferon-gamma, lymphocyte-mediated immunity, and cellular response to interferon-gamma. The

cellular components (CCs) were mainly enriched in the vesicle lumen, endocytic vesicle, endosome membrane, secretory granule membrane, lysosomal membrane, among other processes. The molecular functions (MF) were mainly enriched in peptide antigen binding, Toll-like receptor binding, MHC class II receptor activity, MHC protein complex binding, and MHC class II protein complex binding. The KEGG pathways were mainly enriched in tuberculosis, phagosome, and human T cell leukemia virus 1 infection. (**Figure 10B** and **Table S12**). Finally, candidate small-molecule drugs and their mechanisms of action were predicted using the CMap database and MOA analysis based on the 249 upregulated genes in the brown module and the top 51 downregulated DEGs (**Table S13**). The results are summarized in **Table S14**, and the top 38 potential small-molecule compounds and their corresponding mechanisms of action are shown in **Figure 10C**. These results provide new insights into the mechanisms of triggering or inhibiting pyroptosis *via* drugs in glioma.

GSDMD Is Associated With Prognosis and Anticancer Immunity Pan-Cancers

Building on the previous analysis for the correlation of GPI with glioma pyroptosis subtypes, prognosis, and TIME features, we focused on GSDMD to provide further insights into future anticancer research (a complete list of cancer-type abbreviations is provided in Table S15). Figure S11A shows that the expression of GSDMD was significantly upregulated in 14 cancer types: GBM, LGG, UCEC, BRCA, KIRP, KIPAN, HNSC, KIRC, LIHC, SKCM, BLCA, PAAD, TGCT, and CHOL, while it was downregulated in 15 cancer types: LUAD, ESCA, STES, COAD, PRAD, STAD, LUSC, WT, THCA, OV, UCS, ALL, PCPG, ACC, and KICH. Figure S11B shows that in five cancer types (LGG, KIPAN, GBM, UVM, and ACC), high expression of GSDMD was associated with poor prognosis, while in three cancer types (KIRP, SKCM-M, and SKCM), its low expression correlated with poor prognosis. Figure S12 and Table S16 show that the expression of GSDMD was positively correlated with the majority of immunomodulators in OV, LGG, BLCA, LUSC, UVM, HNSC, KIPAN, STES, STAD, COAD, PRAD, SARC, PCPG, TGCT, KIRC, GBM, SKCM, LUAD, KICH, ESCA, CESC, THCA, and LAML and negatively correlated with those of THYM. Figure S13 and Table S17 show that GSDMD correlates positively with immune scores in GBM, LGG, CESC, LUAD, COAD, BRCA, ESCA, STES, SARC, KIPAN, STAD, PRAD, UCEC, HNSC, KIRC, LUSC, THYM, LIHC, MESO, SKCM-M, SKCM, OV, TGCT, PCPG, SKCM-P, UVM, UCS, BLCA, and KICH, whereas it was not negatively correlated with those of any cancer type. Figure S14 and Table S18 show that GSDMD expression was positively related to MHC score, EC score, and IPS in most cancers but negatively correlated with SC and CP scores, implying that GSDMC and GSDMD expression is correlated with immunogenicity in many cancers.

DISCUSSION

We systematically analyzed the transcriptional and genetic heterogeneity of pyroptosis executors, identified three pyroptosis subtypes, constructed a pyroptosis-related scoring system, and described the effects of pyroptosis on glioma in multiple dimensions. Here, we provide valuable information about the potential interrelationships among pyroptosis subtypes, GPI, clinical features, molecular characteristics, the immune microenvironment, and the immunotherapeutic response in glioma patients. Based on these interrelationships, our research may contribute to the development of appropriate novel therapeutic strategies for glioma.

Our study shows that GSDMC, GSDMD, and PJVK have transcriptional heterogeneity and are associated with glioma prognosis. Studies have demonstrated that GSDMC is highly expressed in metastatic melanoma (53) and that the knockdown of GSDMC inhibits the proliferation of colorectal cancer cells (54), while the expression of GSDMC is suppressed in esophageal and gastric cancers (13). Our results indicate that the expression of GSDMC decreased as the tumor grade increased and is a factor that indicates favorable prognosis. Thus, it is unclear whether GSDMC promotes or inhibits cancer development. GSDMD, one of the most important executors of pyroptosis, is widely expressed in various human tissues (10, 55). A previous study showed that GSDMD expression was negatively correlated with OS and increased after TMZ treatment in a time-dependent manner in glioma (20), which is consistent with our results. These results imply that GSDMD could be a novel prognostic biomarker as well as a marker of sensitivity to TMZ in glioma. Previous studies have demonstrated that all known mutations in PJVK are associated with deafness (56-58), but few studies have shown a link between PJVK and cancer. Here, we found that high PJVK expression correlates with favorable OS, indicating that further exploration of the role of PJVK in cancer development and treatment has broad prospects. Although GSDMA, GSDMB, and GSDME expression was not significantly correlated with glioma prognosis, it had significantly different levels in different clinical or molecular subtypes, suggesting that their potential value in glioma remains to be investigated. In conclusion, although all gasdermins may act as executors of pyroptosis in glioma, they play different roles and have different effects, possibly having opposite effects. The absence of a clear correlation between gasdermin expression and glioma prognosis likely reflects the complex role of pyroptosis in tumorigenesis. Thus, it may be better to assess the pyroptosis status than to explore individual executors.

Based on the pyroptosis-related genes, we defined three pyroptosis subtypes with significant differences in the clinical and TIME characteristics of glioma. Furthermore, we developed a GPI associated with prognosis and the infiltration of antitumor immune cells in glioma. Our study indicates that the pyroptosis subtype C1 is characterized by high GPI, while the subtype C2 and C3 are characterized by low GPI. Considering the expression of GSDMD-the primary executor of pyroptosis-the glioma pyroptosis subtype C1 and a high GPI may represent a potentially activated status of pyroptosis, while the glioma pyroptosis subtype C2 and C3 and a low GPI may represent a potentially suppressed status of pyroptosis. The pyroptosis subtype C1 and a high GPI were found to be associated with glioma progression and a worse prognosis, whereas the subtype C3 and a low GPI were found to be associated with glioma suppression and a better prognosis. These findings imply that although activating pyroptosis leads to cell death, it still promotes glioma malignancy. However, patients with high GPIs were also found to be more sensitive to TMZ and anti-PD1 therapy than those with low GPIs. These paradoxical results can be interpreted from several perspectives. On the one hand, pyroptosis, a lytic and proinflammatory type of regulated cell

death, is characterized by cell swelling, lysis, and the release of numerous proinflammatory factors, including IL-18, ATP, IL-1β, and HMGB1, which can promote tumor growth and progression (59-65). Chronic inflammation can increase the risk of cancers through multiple mechanisms involving not only the tumor but also tumor-infiltrating stromal cells and immune cells (66). On the other hand, the TME is composed of interstitial fluid, the extracellular matrix, and other components (tumor cells, immune cells, and stromal cells) (67), and the balance between tumor-promoting and tumor-suppressing factors in the TME regulates tumor growth (68). Therapyinduced acute inflammation boosts antitumor immunity by promoting antigen-presentation by recruiting immune cells (such as mature dendritic cells and macrophages) to the TME (11). Induction of tumor cell pyroptosis can create an opportunity to reverse the immune desert phenotype, turning a "cold" tumor into a "hot" tumor (11, 69, 70).

In this study, we found that gasdermins were significantly correlated with the biomarkers of GASCs, GAICs, and GSCs. The stromal score and immune score, calculated to predict the overall level of infiltrating stromal and immune cells, respectively, were both significantly increased in the pyroptosis subtype C1 and positively correlated with GPI. Specifically, for GASCs, the infiltration of astrocytes, endothelial cells, fibroblasts, lymphatic endothelial cells, mesenchymal stem cells, microvascular endothelial cells, and skeletal muscle cells significantly increased in C1 and was positively correlated with GPI. For GAICs, the infiltration of memory B cells, CD8⁺ T cells, resting memory CD4⁺ T cells, activated memory CD4⁺ T cells, regulatory T cells, resting NK cells, M0 macrophages, M1 macrophages, M2 macrophages, activated myeloid dendritic cells, activated mast cells, and neutrophils significantly increased in C1 and positively correlated with GPI. In addition, mRNAsi decreased in C1 and was negatively correlated with GPI. GASCs significantly enhance the proliferation and tumorigenicity of GSCs (71, 72) and promote glioma angiogenesis and growth in vitro and in vivo (73, 74). Multiple studies have shown that the infiltration of immunesuppressing cells (including lymphocytic B cells, M2 macrophages, myeloid dendritic cells, and regulatory T cells) enhances tumor growth and progression (75-80). A previous study demonstrated that high mRNAsi was present in GBM rather than in LGG and was associated with a poor prognosis, which is consistent with our results (32). Thus, the activation of pyroptosis may lead to an inhibitory immune microenvironment and affect the characteristics of GSCs, thereby promoting tumor progression, which could explain why subtype C1 and high GPI values were associated with aggressive phenotypes of glioma. However, studies have demonstrated that certain chemotherapeutic drugs, such as cisplatin and paclitaxel, effectively suppress tumor growth and metastasis by evoking the conversion from caspase 3-dependent apoptosis to pyroptosis (17, 81-83), which could explain why high activating levels of pyroptosis are associated with high TMZ sensitivity in glioma. Of note, Wang et al. showed that pyroptosis-inducible therapy increased the infiltration of CD8⁺ cells, CD4⁺ T cells, and NK cells in mammary tumor grafts, and the pyroptosis of less than 15% of tumor cells was sufficient to

clear all 4T1 experimental breast tumors (84). Furthermore, pyroptosis in 4T1 tumor cells induced the polarization of M1 macrophages (84). Zhang et al. also found that in the pyroptosisactivated TIME, CD8⁺ T and NK cells induced tumor cell pyroptosis through granzyme B, thus forming a positive feedback loop (18). Similarly, NK cells and CD8⁺ T cells have been recently shown to trigger tumor clearance via the GSDMBgranzyme A axis (12), and higher enrichment of NK and CD8⁺ T cells usually reflects better ICB efficacy (85). GSDMD is required for the antitumor function of CD8⁺ T cells (86), and GSDMD deficiency decreases the cytolytic capacity of CD8⁺ T cells (87). Thus, chemotherapy and immunotherapy may rapidly induce pyroptosis and boost antitumor immunity by increasing the recruitment and activation of CD8⁺ and NK cells in glioma, which could explain why the pyroptosis subtype C1 and high GPIs were associated with higher TMZ sensitivity and better anti-PD1 therapy response. Furthermore, we found that gasdermins were correlated with most of the immune checkpoints; the PD-L1 expression and TMB score were increased in C1 and positively correlated with GPI, while the MSI score showed the opposite trend. TMB and MSI scores and PD-L1 levels are important predictive biomarkers for ICB effectiveness (31, 88, 89), which help illustrate the potential predictive ability of GPI for ICB response. In addition, our results show significant differences in genetic alterations in tumor driver genes (IDH1, PTEN, TP53, and ATRX) among the pyroptosis subtypes C1, C2, and C3, and many cancer-promoting pathways and immune-related processes were greatly enriched in the GPI-H group. Whether the tumorpromoting or tumor-suppressing roles dominate, the role of pyroptosis likely depends on the specific genetic and epigenetic characteristics of the tumor, combined with differences in host inflammatory status and immunity (11). These results indicate that genetic features act as intrinsic factors, leading to differences in pyroptosis status via certain pathways, further remodeling the TIME to influence prognosis and therapy effectiveness in glioma. Further studies are required to verify this hypothesis.

This study has some limitations. This retrospective study used publicly available data and algorithms. We collected glioma samples for further analysis and verification. Overall, we explored the function of pyroptosis and developed a pyroptosisrelated index for glioma; however, there is a need to determine the mechanisms of certain oncogenes involved, on which we are conducting further research. The pan-cancer analysis suggests that GSDMD plays a potential role in immunotherapy. However, the specific mechanism of action requires further investigation. We hope that the pan-cancer exploration in our study will encourage further studies on this subject.

CONCLUSIONS

Taken together, the glioma pyroptosis subtype C1 and a high GPI were associated with malignant characteristics but may improve the sensitivity to and efficacy of TMZ and ICB treatment, highlighting the importance of a combination of pyroptosis-targeted therapy with chemotherapy and/or

immunotherapy for glioma. Thus, pyroptosis of glioma cells may perform the dual function of tumorigenesis and antitumor immunity.

DATA AVAILABILITY STATEMENT

Publicly available datasets were analyzed in this study. Those data can be found here: https://portal.gdc.cancer.gov/, http://www.cgga.org.cn/index.jsp, 924 https://www.ncbi.nlm.nih.gov/geo/query/acc.cgi?acc=GSE43378, https://portals.broadinstitute. org/ccle/about, and https://xenabrowser.net/.

AUTHOR CONTRIBUTIONS

Research design: HW, XZ, YS. Data analysis: YC, KL. Manuscript writing: YC, KL. Manuscript revision: YC, KL, JL, XL, WX, ZZ, SX, YZ, PC, YM, ZS, LH, HW, XZ, YS. All authors have read and approved the final manuscript.

REFERENCES

- Louis DN, Perry A, Wesseling P, Brat DJ, Cree IA, Figarella-Branger D, et al. The 2021 WHO Classification of Tumors of the Central Nervous System: A Summary. *Neuro Oncol* (2021) 23(8):1231–51. doi: 10.1093/neuonc/noab106
- Louis DN, Perry A, Reifenberger G, von Deimling A, Figarella-Branger D, Cavenee WK, et al. The 2016 World Health Organization Classification of Tumors of the Central Nervous System: A Summary. *Acta Neuropathol* (2016) 131(6):803–20. doi: 10.1007/s00401-016-1545-1
- Weller M, van den Bent M, Preusser M, Le Rhun E, Tonn J, Minniti G, et al. EANO Guidelines on the Diagnosis and Treatment of Diffuse Gliomas of Adulthood. *Nat Rev Clin Oncol* (2021) 18(3):170–86. doi: 10.1038/s41571-020-00447-z
- Molinaro A, Taylor J, Wiencke J, Wrensch M. Genetic and Molecular Epidemiology of Adult Diffuse Glioma. Nat Rev Neurology (2019) 15 (7):405–17. doi: 10.1038/s41582-019-0220-2
- Wen PY, Weller M, Lee EQ, Alexander BM, Barnholtz-Sloan JS, Barthel FP, et al. Glioblastoma in Adults: A Society for Neuro-Oncology (SNO) and European Society of Neuro-Oncology (EANO) Consensus Review on Current Management and Future Directions. *Neuro Oncol* (2020) 22(8):1073–113. doi: 10.1093/neuonc/noaa106
- Stupp R, Taillibert S, Kanner A, Read W, Steinberg D, Lhermitte B, et al. Effect of Tumor-Treating Fields Plus Maintenance Temozolomide vs Maintenance Temozolomide Alone on Survival in Patients With Glioblastoma: A Randomized Clinical Trial. *JAMA* (2017) 318(23):2306–16. doi: 10.1001/ jama.2017.18718
- Liu X, Xia S, Zhang Z, Wu H, Lieberman J. Channelling Inflammation: Gasdermins in Physiology and Disease. Nat Rev Drug Discov (2021) 20 (5):384–405. doi: 10.1038/s41573-021-00154-z
- Tan Y, Chen Q, Li X, Zeng Z, Xiong W, Li G, et al. Correction to: Pyroptosis: A New Paradigm of Cell Death for Fighting Against Cancer. J Exp Clin Cancer Res (2021) 40(1):219. doi: 10.1186/s13046-021-01959-x
- Shi J, Gao W, Shao F. Pyroptosis: Gasdermin-Mediated Programmed Necrotic Cell Death. *Trends Biochem Sci* (2017) 42(4):245–54. doi: 10.1016/ j.tibs.2016.10.004
- Broz P, Pelegrin P, Shao F. The Gasdermins, a Protein Family Executing Cell Death and Inflammation. *Nat Rev Immunol* (2020) 20(3):143–57. doi: 10. 1038/s41577-019-0228-2
- Zhang Z, Zhang Y, Lieberman J. Lighting a Fire: Can We Harness Pyroptosis to Ignite Antitumor Immunity? *Cancer Immunol Res* (2021) 9(1):2–7. doi: 10.1158/2326-6066.CIR-20-0525

FUNDING

The study was supported by the Science and Technology Program of Guangzhou, China (No. 201903010048); National Nature Science Fund of China (No. 81872064); the Natural Science Fund of Guangdong Province, China (No. 2020A1515010122 and 2021A1515012465). The funders had no role in study design, data collection, data analysis, decision to publish, or preparation of the manuscript.

ACKNOWLEDGMENTS

We thank Editage (www.editage.cn) for language polishing.

SUPPLEMENTARY MATERIAL

The Supplementary Material for this article can be found online at: https://www.frontiersin.org/articles/10.3389/fimmu.2022. 910490/full#supplementary-material

- Zhou Z, He H, Wang K, Shi X, Wang Y, Su Y, et al. Granzyme A From Cytotoxic Lymphocytes Cleaves GSDMB to Trigger Pyroptosis in Target Cells. Science (2020) 368(6494):eaaz7548. doi: 10.1126/science.aaz7548
- Saeki N, Usui T, Aoyagi K, Kim DH, Sato M, Mabuchi T, et al. Distinctive Expression and Function of Four GSDM Family Genes (GSDMA-D) in Normal and Malignant Upper Gastrointestinal Epithelium. *Genes Chromosomes Cancer* (2009) 48(3):261–71. doi: 10.1002/gcc.20636
- Wang WJ, Chen D, Jiang MZ, Xu B, Li XW, Chu Y, et al. Downregulation of Gasdermin D Promotes Gastric Cancer Proliferation by Regulating Cell Cycle-Related Proteins. J Dig Dis (2018) 19(2):74–83. doi: 10.1111/1751-2980.12576
- 15. Gao J, Qiu X, Xi G, Liu H, Zhang F, Lv T, et al. Downregulation of GSDMD Attenuates Tumor Proliferation *via* the Intrinsic Mitochondrial Apoptotic Pathway and Inhibition of EGFR/Akt Signaling and Predicts a Good Prognosis in Nonsmall Cell Lung Cancer. *Oncol Rep* (2018) 40(4):1971–84. doi: 10.3892/or.2018.6634
- Carl-McGrath S, Schneider-Stock R, Ebert M, Rocken C. Differential Expression and Localisation of Gasdermin-Like (GSDML), a Novel Member of the Cancer-Associated GSDMDC Protein Family, in Neoplastic and non-Neoplastic Gastric, Hepatic, and Colon Tissues. *Pathology* (2008) 40 (1):13–24. doi: 10.1080/00313020701716250
- Wang Y, Gao W, Shi X, Ding J, Liu W, He H, et al. Chemotherapy Drugs Induce Pyroptosis Through Caspase-3 Cleavage of a Gasdermin. *Nature* (2017) 547(7661):99–103. doi: 10.1038/nature22393
- Zhang Z, Zhang Y, Xia S, Kong Q, Li S, Liu X, et al. Gasdermin E Suppresses Tumour Growth by Activating Anti-Tumour Immunity. *Nature* (2020) 579 (7799):415–20. doi: 10.1038/s41586-020-2071-9
- Erkes DA, Cai W, Sanchez IM, Purwin TJ, Rogers C, Field CO, et al. Mutant BRAF and MEK Inhibitors Regulate the Tumor Immune Microenvironment via Pyroptosis. Cancer Discov (2020) 10(2):254–69. doi: 10.1158/2159-8290.CD-19-0672
- Liu J, Gao L, Zhu X, Geng R, Tao X, Xu H, et al. Gasdermin D Is a Novel Prognostic Biomarker and Relates to TMZ Response in Glioblastoma. *Cancers* (*Basel*) (2021) 13(22):5620 doi: 10.3390/cancers13225620
- Zhao Z, Zhang KN, Wang Q, Li G, Zeng F, Zhang Y, et al. Chinese Glioma Genome Atlas (CGGA): A Comprehensive Resource With Functional Genomic Data From Chinese Gliomas. *Genomics Proteomics Bioinf* (2021) 19(1):1–12. doi: 10.1101/2020.01.20.911982
- Cerami E, Gao J, Dogrusoz U, Gross BE, Sumer SO, Aksoy BA, et al. The Cbio Cancer Genomics Portal: An Open Platform for Exploring Multidimensional Cancer Genomics Data. *Cancer Discov* (2012) 2(5):401–4. doi: 10.1158/2159-8290.CD-12-0095

- 23. Szklarczyk D, Gable AL, Nastou KC, Lyon D, Kirsch R, Pyysalo S, et al. The STRING Database in 2021: Customizable Protein-Protein Networks, and Functional Characterization of User-Uploaded Gene/Measurement Sets. *Nucleic Acids Res* (2021) 49(D1):D605–D12. doi: 10.1093/nar/gkaa1074
- Wilkerson MD, Hayes DN. ConsensusClusterPlus: A Class Discovery Tool With Confidence Assessments and Item Tracking. *Bioinformatics* (2010) 26 (12):1572–3. doi: 10.1093/bioinformatics/btq170
- Mayakonda A, Lin DC, Assenov Y, Plass C, Koeffler HP. Maftools: Efficient and Comprehensive Analysis of Somatic Variants in Cancer. *Genome Res* (2018) 28(11):1747–56. doi: 10.1101/gr.239244.118
- Friedman J, Hastie T, Tibshirani R. Regularization Paths for Generalized Linear Models via Coordinate Descent. J Stat Software (2010) 33(1):1–22. doi: 10.18637/jss.v033.i01
- Subramanian A, Tamayo P, Mootha VK, Mukherjee S, Ebert BL, Gillette MA, et al. Gene Set Enrichment Analysis: A Knowledge-Based Approach for Interpreting Genome-Wide Expression Profiles. *Proc Natl Acad Sci USA* (2005) 102(43):15545–50. doi: 10.1073/pnas.0506580102
- Liberzon A, Subramanian A, Pinchback R, Thorvaldsdottir H, Tamayo P, Mesirov JP. Molecular Signatures Database (MSigDB) 3.0.*Bioinf* (2011) 27 (12):1739–40. doi: 10.1093/bioinformatics/btr260
- Yoshihara K, Shahmoradgoli M, Martinez E, Vegesna R, Kim H, Torres-Garcia W, et al. Inferring Tumour Purity and Stromal and Immune Cell Admixture From Expression Data. *Nat Commun* (2013) 4:2612. doi: 10.1038/ ncomms3612
- Sturm G, Finotello F, Petitprez F, Zhang JD, Baumbach J, Fridman WH, et al. Comprehensive Evaluation of Transcriptome-Based Cell-Type Quantification Methods for Immuno-Oncology. *Bioinformatics* (2019) 35(14):i436–i45. doi: 10.1093/bioinformatics/btz363
- Bonneville R, Krook MA, Kautto EA, Miya J, Wing MR, Chen HZ, et al. Landscape of Microsatellite Instability Across 39 Cancer Types. JCO Precis Oncol (2017) 1:PO.17.00073. doi: 10.1200/PO.17.00073
- Malta TM, Sokolov A, Gentles AJ, Burzykowski T, Poisson L, Weinstein JN, et al. Machine Learning Identifies Stemness Features Associated With Oncogenic Dedifferentiation. *Cell* (2018) 173(2):338–54.e15. doi: 10.1016/ j.cell.2018.03.034
- 33. Charoentong P, Finotello F, Angelova M, Mayer C, Efremova M, Rieder D, et al. Pan-Cancer Immunogenomic Analyses Reveal Genotype-Immunophenotype Relationships and Predictors of Response to Checkpoint Blockade. *Cell Rep* (2017) 18(1):248–62. doi: 10.1016/j.celrep.2016.12.019
- 34. Yang W, Soares J, Greninger P, Edelman EJ, Lightfoot H, Forbes S, et al. Genomics of Drug Sensitivity in Cancer (GDSC): A Resource for Therapeutic Biomarker Discovery in Cancer Cells. *Nucleic Acids Res* (2013) 41(Database issue):D955–61. doi: 10.1093/nar/gks1111
- Geeleher P, Cox N, Huang RS. Prrophetic: An R Package for Prediction of Clinical Chemotherapeutic Response From Tumor Gene Expression Levels. *PLoS One* (2014) 9(9):e107468. doi: 10.1371/journal.pone.0107468
- Hoshida Y, Brunet JP, Tamayo P, Golub TR, Mesirov JP. Subclass Mapping: Identifying Common Subtypes in Independent Disease Data Sets. *PLoS One* (2007) 2(11):e1195. doi: 10.1371/journal.pone.0001195
- 37. Roh W, Chen PL, Reuben A, Spencer CN, Prieto PA, Miller JP, et al. Integrated Molecular Analysis of Tumor Biopsies on Sequential CTLA-4 and PD-1 Blockade Reveals Markers of Response and Resistance. *Sci Transl Med* (2017) 9(379):eaah3560. doi: 10.1126/scitranslmed.aah3560
- Snyder A, Makarov V, Merghoub T, Yuan J, Zaretsky JM, Desrichard A, et al. Genetic Basis for Clinical Response to CTLA-4 Blockade in Melanoma. N Engl J Med (2014) 371(23):2189–99. doi: 10.1056/NEJMoa1406498
- Nathanson T, Ahuja A, Rubinsteyn A, Aksoy BA, Hellmann MD, Miao D, et al. Somatic Mutations and Neoepitope Homology in Melanomas Treated With CTLA-4 Blockade. *Cancer Immunol Res* (2017) 5(1):84–91. doi: 10.1158/ 2326-6066.CIR-16-0019
- Mariathasan S, Turley SJ, Nickles D, Castiglioni A, Yuen K, Wang Y, et al. TGFbeta Attenuates Tumour Response to PD-L1 Blockade by Contributing to Exclusion of T Cells. *Nature* (2018) 554(7693):544–8. doi: 10.1038/ nature25501
- 41. Rose TL, Weir WH, Mayhew GM, Shibata Y, Eulitt P, Uronis JM, et al. Fibroblast Growth Factor Receptor 3 Alterations and Response to Immune Checkpoint Inhibition in Metastatic Urothelial Cancer: A Real World

Experience. Br J Cancer (2021) 125(9):1251-60. doi: 10.1038/s41416-021-01488-6

- Langfelder P, Horvath S. WGCNA: An R Package for Weighted Correlation Network Analysis. BMC Bioinf (2008) 9:559. doi: 10.1186/1471-2105-9-559
- Yu G, Wang LG, Han Y, He QY. Clusterprofiler: An R Package for Comparing Biological Themes Among Gene Clusters. OMICS (2012) 16(5):284–7. doi: 10.1089/omi.2011.0118
- 44. Lamb J, Crawford ED, Peck D, Modell JW, Blat IC, Wrobel MJ, et al. The Connectivity Map: Using Gene-Expression Signatures to Connect Small Molecules, Genes, and Disease. *Science* (2006) 313(5795):1929–35. doi: 10.1126/science.1132939
- 45. Suva ML, Tirosh I. The Glioma Stem Cell Model in the Era of Single-Cell Genomics. *Cancer Cell* (2020) 37(5):630–6. doi: 10.1016/j.ccell.2020.04.001
- Van Meir EG, Hadjipanayis CG, Norden AD, Shu HK, Wen PY, Olson JJ. Exciting New Advances in Neuro-Oncology: The Avenue to a Cure for Malignant Glioma. CA Cancer J Clin (2010) 60(3):166–93. doi: 10.3322/ caac.20069
- Chen J, McKay RM, Parada LF. Malignant Glioma: Lessons From Genomics, Mouse Models, and Stem Cells. *Cell* (2012) 149(1):36–47. doi: 10.1016/ j.cell.2012.03.009
- Clavreul A, Menei P. Mesenchymal Stromal-Like Cells in the Glioma Microenvironment: What Are These Cells? *Cancers (Basel)* (2020) 12 (9):2628. doi: 10.3390/cancers12092628
- Domingues P, Gonzalez-Tablas M, Otero A, Pascual D, Miranda D, Ruiz L, et al. Tumor Infiltrating Immune Cells in Gliomas and Meningiomas. *Brain Behav Immun* (2016) 53:1–15. doi: 10.1016/j.bbi.2015.07.019
- Shu C, Li Q. Current Advances in PD-1/PD-L1 Axis-Related Tumour-Infiltrating Immune Cells and Therapeutic Regimens in Glioblastoma. Crit Rev Oncol Hematol (2020) 151:102965. doi: 10.1016/j.critrevonc.2020.102965
- 51. Tan Y, Chen Q, Li X, Zeng Z, Xiong W, Li G, et al. Pyroptosis: A New Paradigm of Cell Death for Fighting Against Cancer. J Exp Clin Cancer Res (2021) 40(1):153.doi: 10.1186/s13046-021-01959-x
- Yu P, Zhang X, Liu N, Tang L, Peng C, Chen X. Pyroptosis: Mechanisms and Diseases. Signal Transduct Target Ther (2021) 6(1):128. doi: 10.1038/s41392-021-00507-5
- 53. Watabe K, Ito A, Asada H, Endo Y, Kobayashi T, Nakamoto K, et al. Structure, Expression and Chromosome Mapping of MLZE, a Novel Gene Which Is Preferentially Expressed in Metastatic Melanoma Cells. *Jpn J Cancer Res* (2001) 92(2):140–51. doi: 10.1111/j.1349-7006.2001.tb01076.x
- 54. Miguchi M, Hinoi T, Shimomura M, Adachi T, Saito Y, Niitsu H, et al. Gasdermin C Is Upregulated by Inactivation of Transforming Growth Factor Beta Receptor Type II in the Presence of Mutated Apc, Promoting Colorectal Cancer Proliferation. *PLoS One* (2016) 11(11):e0166422. doi: 10.1371/ journal.pone.0166422
- Kovacs SB, Miao EA. Gasdermins: Effectors of Pyroptosis. Trends Cell Biol (2017) 27(9):673–84. doi: 10.1016/j.tcb.2017.05.005
- Collin RW, Kalay E, Oostrik J, Caylan R, Wollnik B, Arslan S, et al. Involvement of DFNB59 Mutations in Autosomal Recessive Nonsyndromic Hearing Impairment. *Hum Mutat* (2007) 28(7):718–23. doi: 10.1002/ humu.20510
- Mujtaba G, Bukhari I, Fatima A, Naz S. A P.C343S Missense Mutation in PJVK Causes Progressive Hearing Loss. *Gene* (2012) 504(1):98–101. doi: 10.1016/j.gene.2012.05.013
- Delmaghani S, del Castillo FJ, Michel V, Leibovici M, Aghaie A, Ron U, et al. Mutations in the Gene Encoding Pejvakin, a Newly Identified Protein of the Afferent Auditory Pathway, Cause DFNB59 Auditory Neuropathy. *Nat Genet* (2006) 38(7):770–8. doi: 10.1038/ng1829
- Silke J, Rickard JA, Gerlic M. The Diverse Role of RIP Kinases in Necroptosis and Inflammation. Nat Immunol (2015) 16(7):689–97. doi: 10.1038/ni.3206
- Degterev A, Hitomi J, Germscheid M, Ch'en IL, Korkina O, Teng X, et al. Identification of RIP1 Kinase as a Specific Cellular Target of Necrostatins. *Nat Chem Biol* (2008) 4(5):313–21. doi: 10.1038/nchembio.83
- He S, Wang L, Miao L, Wang T, Du F, Zhao L, et al. Receptor Interacting Protein Kinase-3 Determines Cellular Necrotic Response to TNF-Alpha. *Cell* (2009) 137(6):1100–11. doi: 10.1016/j.cell.2009.05.021
- 62. Zhang DW, Shao J, Lin J, Zhang N, Lu BJ, Lin SC, et al. RIP3, an Energy Metabolism Regulator That Switches TNF-Induced Cell Death From

Apoptosis to Necrosis. Science (2009) 325(5938):332-6. doi: 10.1126/ science.1172308

- Hu B, Elinav E, Huber S, Booth CJ, Strowig T, Jin C, et al. Inflammation-Induced Tumorigenesis in the Colon is Regulated by Caspase-1 and NLRC4. *Proc Natl Acad Sci USA* (2010) 107(50):21635–40. doi: 10.1073/ pnas.1016814108
- Janowski AM, Kolb R, Zhang W, Sutterwala FS. Beneficial and Detrimental Roles of NLRs in Carcinogenesis. *Front Immunol* (2013) 4:370. doi: 10.3389/ fimmu.2013.00370
- Dunn JH, Ellis LZ, Fujita M. Inflammasomes as Molecular Mediators of Inflammation and Cancer: Potential Role in Melanoma. *Cancer Lett* (2012) 314(1):24–33. doi: 10.1016/j.canlet.2011.10.001
- Grivennikov SI, Greten FR, Karin M. Immunity, Inflammation, and Cancer. Cell (2010) 140(6):883–99. doi: 10.1016/j.cell.2010.01.025
- Kozlova N, Grossman JE, Iwanicki MP, Muranen T. The Interplay of the Extracellular Matrix and Stromal Cells as a Drug Target in Stroma-Rich Cancers. *Trends Pharmacol Sci* (2020) 41(3):183–98. doi: 10.1016/ j.tips.2020.01.001
- Wu AA, Drake V, Huang HS, Chiu S, Zheng L. Reprogramming the Tumor Microenvironment: Tumor-Induced Immunosuppressive Factors Paralyze T Cells. Oncoimmunology (2015) 4(7):e1016700. doi: 10.1080/2162402X.2015.1016700
- Duan Q, Zhang H, Zheng J, Zhang L. Turning Cold Into Hot: Firing Up the Tumor Microenvironment. *Trends Cancer* (2020) 6(7):605–18. doi: 10.1016/ j.trecan.2020.02.022
- Kroemer G, Galluzzi L, Kepp O, Zitvogel L. Immunogenic Cell Death in Cancer Therapy. Annu Rev Immunol (2013) 31:51–72. doi: 10.1146/annurevimmunol-032712-100008
- Hossain A, Gumin J, Gao F, Figueroa J, Shinojima N, Takezaki T, et al. Mesenchymal Stem Cells Isolated From Human Gliomas Increase Proliferation and Maintain Stemness of Glioma Stem Cells Through the IL-6/Gp130/STAT3 Pathway. *Stem Cells* (2015) 33(8):2400–15. doi: 10.1002/ stem.2053
- Kong BH, Shin HD, Kim SH, Mok HS, Shim JK, Lee JH, et al. Increased *In Vivo* Angiogenic Effect of Glioma Stromal Mesenchymal Stem-Like Cells on Glioma Cancer Stem Cells From Patients With Glioblastoma. *Int J Oncol* (2013) 42(5):1754–62. doi: 10.3892/ijo.2013.1856
- Clavreul A, Etcheverry A, Chassevent A, Quillien V, Avril T, Jourdan ML, et al. Isolation of a New Cell Population in the Glioblastoma Microenvironment. *J Neurooncol* (2012) 106(3):493–504. doi: 10.1007/s11060-011-0701-7
- 74. Clavreul A, Guette C, Faguer R, Tetaud C, Boissard A, Lemaire L, et al. Glioblastoma-Associated Stromal Cells (GASCs) From Histologically Normal Surgical Margins Have a Myofibroblast Phenotype and Angiogenic Properties. *J Pathol* (2014) 233(1):74–88. doi: 10.1002/path.4332
- Deng Z, Rong Y, Teng Y, Zhuang X, Samykutty A, Mu J, et al. Exosomes miR-126a Released From MDSC Induced by DOX Treatment Promotes Lung Metastasis. Oncogene (2017) 36(5):639–51. doi: 10.1038/onc.2016.229
- Roghanian A, Fraser C, Kleyman M, Chen J. B Cells Promote Pancreatic Tumorigenesis. *Cancer Discov* (2016) 6(3):230–2. doi: 10.1158/2159-8290.CD-16-0100
- Shalapour S, Font-Burgada J, Di Caro G, Zhong Z, Sanchez-Lopez E, Dhar D, et al. Immunosuppressive Plasma Cells Impede T-Cell-Dependent Immunogenic Chemotherapy. *Nature* (2015) 521(7550):94–8. doi: 10.1038/ nature14395
- He H, Xu J, Warren CM, Duan D, Li X, Wu L, et al. Endothelial Cells Provide an Instructive Niche for the Differentiation and Functional Polarization of M2-Like Macrophages. *Blood.* (2012) 120(15):3152–62. doi: 10.1182/blood-2012-04-422758

- Corzo CA, Condamine T, Lu L, Cotter MJ, Youn JI, Cheng P, et al. HIF-1alpha Regulates Function and Differentiation of Myeloid-Derived Suppressor Cells in the Tumor Microenvironment. *J Exp Med* (2010) 207(11):2439–53. doi: 10.1084/jem.20100587
- Li L, Liu X, Sanders KL, Edwards JL, Ye J, Si F, et al. TLR8-Mediated Metabolic Control of Human Treg Function: A Mechanistic Target for Cancer Immunotherapy. *Cell Metab* (2019) 29(1):103–23.e5. doi: 10.1016/ j.cmet.2018.09.020
- Zhang CC, Li CG, Wang YF, Xu LH, He XH, Zeng QZ, et al. Chemotherapeutic Paclitaxel and Cisplatin Differentially Induce Pyroptosis in A549 Lung Cancer Cells via Caspase-3/GSDME Activation. Apoptosis (2019) 24(3-4):312–25. doi: 10.1007/s10495-019-01515-1
- Wang F, Liu W, Ning J, Wang J, Lang Y, Jin X, et al. Simvastatin Suppresses Proliferation and Migration in Non-Small Cell Lung Cancer via Pyroptosis. *Int J Biol Sci* (2018) 14(4):406–17. doi: 10.7150/ijbs.23542
- Rogers C, Fernandes-Alnemri T, Mayes L, Alnemri D, Cingolani G, Alnemri ES. Cleavage of DFNA5 by Caspase-3 During Apoptosis Mediates Progression to Secondary Necrotic/Pyroptotic Cell Death. *Nat Commun* (2017) 8:14128. doi: 10.1038/ncomms14128
- Wang Q, Wang Y, Ding J, Wang C, Zhou X, Gao W, et al. A Bioorthogonal System Reveals Antitumour Immune Function of Pyroptosis. *Nature*. (2020) 579(7799):421–6. doi: 10.1038/s41586-020-2079-1
- McLane LM, Abdel-Hakeem MS, Wherry EJ. CD8 T Cell Exhaustion During Chronic Viral Infection and Cancer. Annu Rev Immunol (2019) 37:457–95. doi: 10.1146/annurev-immunol-041015-055318
- 86. Xi G, Gao J, Wan B, Zhan P, Xu W, Lv T, et al. GSDMD Is Required for Effector CD8(+) T Cell Responses to Lung Cancer Cells. Int Immunopharmacol (2019) 74:105713. doi: 10.1016/j.intimp.2019.105713
- Young JD, Hengartner H, Podack ER, Cohn ZA. Purification and Characterization of a Cytolytic Pore-Forming Protein From Granules of Cloned Lymphocytes With Natural Killer Activity. *Cell* (1986) 44(6):849– 59. doi: 10.1016/0092-8674(86)90007-3
- Jiang P, Gu S, Pan D, Fu J, Sahu A, Hu X, et al. Signatures of T Cell Dysfunction and Exclusion Predict Cancer Immunotherapy Response. *Nat Med* (2018) 24(10):1550–8. doi: 10.1038/s41591-018-0136-1
- Chalmers ZR, Connelly CF, Fabrizio D, Gay L, Ali SM, Ennis R, et al. Analysis of 100,000 Human Cancer Genomes Reveals the Landscape of Tumor Mutational Burden. *Genome Med* (2017) 9(1):34. doi: 10.1186/s13073-017-0424-2

Conflict of Interest: The authors declare that the research was conducted in the absence of any commercial or financial relationships that could be construed as a potential conflict of interest.

Publisher's Note: All claims expressed in this article are solely those of the authors and do not necessarily represent those of their affiliated organizations, or those of the publisher, the editors and the reviewers. Any product that may be evaluated in this article, or claim that may be made by its manufacturer, is not guaranteed or endorsed by the publisher.

Copyright © 2022 Cai, Li, Lin, Liang, Xu, Zhan, Xue, Zeng, Chai, Mao, Song, Han, Song, Zhang and Wang. This is an open-access article distributed under the terms of the Creative Commons Attribution License (CC BY). The use, distribution or reproduction in other forums is permitted, provided the original author(s) and the copyright owner(s) are credited and that the original publication in this journal is cited, in accordance with accepted academic practice. No use, distribution or reproduction is permitted which does not comply with these terms.



A Novel PD-L1-Containing MSLN Targeting Vaccine for Lung Cancer Immunotherapy

Wuyi Zeng^{1†}, Jiayi Pan^{1†}, Zixuan Fang¹, Jiangtao Jia¹, Rong Zhang¹, Menghua He¹, Hanyu Zhong¹, Jiashan He¹, Xinyu Yang¹, Yi Shi¹, Bei Zhong¹, Jun Zeng¹, Bishi Fu^{1,2}, Maoping Huang^{1*} and Hui Liu^{1,2*}

¹ School of Basic Medical Sciences, The Sixth Affiliated Hospital of Guangzhou Medical University, Qingyuan People's Hospital, Guangzhou Medical University, Guangzhou, China, ² The State Key Laboratory of Respiratory Disease, Guangdong Provincial Key Laboratory of Allergy and Clinical Immunology, Guangzhou, China

OPEN ACCESS

Edited by:

Xuyao Zhang, Fudan University, China

Reviewed by:

Xi Lou, University of Alabama at Birmingham, United States Mingyue Li, Wistar Institute, United States

*Correspondence:

Hui Liu liuhui806@gzhmu.edu.cn Maoping Huang ping660815@126.com

⁺These authors have contributed equally to this work

Specialty section:

This article was submitted to Cancer Immunity and Immunotherapy, a section of the journal Frontiers in Immunology

Received: 21 April 2022 Accepted: 23 May 2022 Published: 20 June 2022

Citation:

Zeng W, Pan J, Fang Z, Jia J, Zhang R, He M, Zhong H, He J, Yang X, Shi Y, Zhong B, Zeng J, Fu B, Huang M and Liu H (2022) A Novel PD-L1-Containing MSLN Targeting Vaccine for Lung Cancer Immunotherapy. Front. Immunol. 13:925217. doi: 10.3389/fimmu.2022.925217 Therapeutic tumor vaccines have become an important breakthrough in the treatment of various solid tumors including lung cancer. Dendritic cells (DCs)-based tumor vaccines targeting tumor-associated antigens (TAAs) play a key role in immunotherapy and immunoprevention. However, the weak immunogenicity of TAAs and low immune response rates are a major challenge faced in the application of therapeutic tumor vaccines. Here, we tested whether targeting an attractive target Mesothelin (MSLN) and PD-L1 immune checkpoint molecule to DCs in vivo would elicit therapeutic antitumor cytotoxic T lymphocyte (CTL) response. We generated specific MSLN fragment combined with PD-L1 and GM-CSF peptide immunogen (MSLN-PDL1-GMCSF) based on the novel anti-PD-L1 vaccination strategy we recently developed for the cancer treatment and prevention. We found that DCs loaded with MSLN-PDL1-GMCSF vaccine elicited much stronger endogenous anti-PD-L1 antibody and T cell responses in immunized mice and that antigen specific CTLs had cytolytic activities against tumor cells expressing both MSLN and PD-L1. We demonstrated that vaccination with MSLN-PDL1-GMCSF potently inhibited the tumor growth of MSLN⁺ and PD-L1⁺ lung cancer cells, exhibiting a significant therapeutic anti-tumor potential. Furthermore, PD-1 blockade further improved the synergistic antitumor therapeutic efficacy of MSLN-PDL1-GMCSF vaccine in immunized mice. In summary, our data demonstrated for the first time that this PD-L1-containing MSLN therapeutic vaccine can induce persistent anti-PD-L1 antibody and CTL responses, providing an effective immunotherapeutic strategy for lung cancer immunotherapy by combining MSLN-PDL1-GMCSF vaccine and PD-1 blockade.

Keywords: dendritic cells, MSLN, PD-L1, immunotherapy, therapeutic vaccine

Abbreviations: ADCs, Antibody-drug conjugates; APCs, Antigen-presenting cells; BSA, Bovine Serum Albumin; CTL, Cytotoxic T lymphocyte; DC, Dendritic cell; ELISA, enzyme linked immunosorbent assay; FACS, Fluorescence-activated cell sorting; FBS, Fatal Bovine Serum; GM-CSF, Granulocyte macrophage colony stimulating factor; IFN, Interferon; IL, Interleukin; IPTG, Isopropyl-β-D-1-thiogalactoside; LLC, Lewis lung carcinoma; LPS, Lipopolysaccharide; McAb, Monoclonal antibody; MHC, Major histocompatibility complex; MOI, Multiplicity of infection; MSLN, Mesothelin; PD-1, Programmed death 1; PD-L1, Programmed death ligand 1; PMA, phorbol ester; qPCR, Real-time Quantitative polymerase chain reaction; SDS-PAGE, sodium dodecyl sulfate-polyacrylamide gel electrophoresis; TAAs, Tumor-associated antigens; Th1/Th2, T helper type 1/T helper type 2.

INTRODUCTION

Lung cancer is the most common malignant tumor with high morbidity and mortality in the world. Surgical treatment alone is no longer effective in further improving survival rates, and effective treatment of lung cancer remains a major challenge to be faced (1-3). Dendritic cells (DCs) are specialized antigen-presenting cells (APCs) that initiate and modulate innate and adaptive immunity (4, 5). DCs can present antigen through MHC I and MHC II molecules and activate CD4+T and CD8+T, which can activate specific anti-tumor immune response, so as to make tumor recede. Therefore, DC can be used to prepare therapeutic anti-tumor vaccine (6-8). Sipuleucel-T (Provenge), the first DCs-based cancer vaccine, which was approved by the US Food and Drug Administration (FDA) in 2010, was exploited for resistant prostate cancer (9). For the past two decades, DC therapy has been indicated to be able to induce anti-tumor immunity, which is safe and well-tolerated (10, 11). Programmed death 1 (PD-1) and programmed death ligand 1 (PD-L1) are the most well-studied immune checkpoints in recent years. Many tumor cells, including lung, ovarian, melanoma and pancreatic tumors, evade immune surveillance by upregulating PD-L1 expression (12, 13). The binding of PD-1 to PD-L1 leads to suppression of tumorspecific T cell immune responses (14). Currently, PD-1/PD-L1 monoclonal antibodies have been developed as immune checkpoint inhibitors for cancer therapy to remove the "brake" on the immune system and restore the ability of T cells to attack tumor cells (15). Nevertheless, treatment with anti-PD-1/PD-L1 antibodies has produced long-lasting and effective antitumor response in only a small percentage of patients (16-18). DCs or antigen-loaded DCs can directly induce antibody responses and promote antibody production of CD40-activated naive and memory B cells during stimulation of B cell responses (19). Moreover, our recent studies also found that DCs can activate both cellular and humoral immune responses (13). Therefore, identifying predictive biomarkers and designing rational PD-(L)1based combination therapies has become the focus of cancer immunotherapy.

Mesothelin (MSLN) is a glycosylphosphatidylinositol-linked membrane glycoprotein which is highly expressed in a variety of tumors and is also expressed in mesothelial cells of healthy individuals, but at low levels. Therefore, it can be considered as a promising target protein for tumor-targeted therapy (20-22). In the tumor environment, MSLN plays an important role in survival, proliferation, and migration/invasion of cancer cells as well as in drug resistance (23). Over the years, evidence has accumulated with regards to the importance of MSLN as a tumor-associated antigen (TAA) overexpressed in almost onethird of human cancers. For these reasons, various types of anti-MSLN therapies have been developed, including antibodies, antibody-drug conjugates (ADCs), immunotoxins, cancer vaccines, and chimeric antigen receptor (CAR)-T cell immunotherapies (24-26). Granulocyte macrophage colony stimulating factor (GM-CSF), produced mainly by macrophages and activated T cells, is a cytokine with multiple biological activities (27). GM-CSF is a key cytokine essential for the differentiation, proliferation, and recruitment of DCs and

promotes their capacity for antigen presentation, co-stimulatory molecule expression, and proinflammatory cytokine production. Therefore, it has been used as an adjuvant in several cancer vaccines to boost DC-mediated antitumor immunity (28–30). Preclinical studies have shown that GM-CSF not only has the capacity to increase antigen-induced immune responses, but it also can alter the Th1/Th2 cytokine balance. It appears that GM-CSF can stimulate both Th1 and Th2 type responses depending on immune cells and cytokines in the immediate local environment (31, 32). Therefore, GM-CSF acts an essential role as immune adjuvant played in tumor vaccine for enhancing effective immune response.

In this study, we generated a new therapeutic vaccine (MSLN-PDL1-GMCSF), with both autonomous induction of anti-PD-L1 antibody production and MSLN-specific targeting characteristics. We found that this MSLN-PDL1-GMCSF protein-loaded DCs vaccine induced an effective antigen-specific anti-tumor CTL response *in vivo*, and showed significant therapeutic effects in tumor-bearing mice. Furthermore, combination therapy with PD-1 blockade produced synergistic antitumor effects, which provides a new effective strategy for immunotherapy of solid tumors.

MATERIALS AND METHODS

Mice and Cell Lines

Six- to eight-week-old male C57BL/6 mice were purchased from Charles River Laboratories and bred at Guangzhou Medical University under specific pathogen-free (SPF) conditions. All animal procedures were approved by the Animal Ethics Committee of Guangzhou Medical University. The mice Lewis lung carcinoma (LLC) cell line was purchased from ATCC (American Type Culture Cell Bank). Cell lines were maintained in DMEM (Gibco) supplemented with 10% FBS (ExCell), 1% Penicillin-Streptomycin (Gibco). LLC stably expressing human MSLN and PD-L1 were maintained in DMEM supplemented with 2.5µg/ml puromycin (Solarbio).

Protein Production and Purification

To obtain the PDL1-GMCSF and MSLN-PDL1-GMCSF vaccines, the fusion gene of human MSLN extracellular domain, PD-L1 extracellular domain, T helper epitope and GM-CSF sequence was synthesized and cloned into pET21a expression vector to construct pET-21a-MSLN-PDL1-GMCSF and pET-21a-PDL1-GMCSF expression plasmids, respectively. Then the plasmids were transformed into BL21(DE3) expressing strain and induced to express in inclusion body form under IPTG (0.1 mM) condition. Next, the proteins were purified using Ni-NTA columns according to the instructions of the kit (Abbkine#KTP20010). The purified proteins solution was then subjected to gradient dialysis and endotoxin removal, and the entire proteins production process were analyzed by SDS-PAGE and Western blot. The prepared proteins were stored at -80°C for further studies. In addition, recombinant human PD-L1 protein was purchased from Abcam company.

Lentiviral-Transduced Tumor Cell Lines

Lentiviral vectors expressing MSLN and PD-L1 and carrying puromycin resistance genes were constructed using a threeplasmid system (psPAX2, PMD2.G, pHBLVTM) for lentiviral packaging. Mass de-endotoxin extraction of plasmids was performed using Qiagen extraction kit. 293T cells were transfected according to the instructions of LipoFiterTM reagent, and virus supernatants were collected twice at 48h and 72h after transfection. After virus resuspension, LLC cells were infected, and polybrene with a final concentration of 5µg/mL was added to improve infection rate. After 24 hours, the solution was changed, and the optimal MOI was 30. After 48 hours, fresh complete culture medium containing puromycin (5µg/mL) was added to screen stable LLC cell lines. The cells were collected for further Real-time Quantitative PCR (qPCR), Western blot and flow cytometry analysis.

Preparation of Dendritic Cells

C57BL/6 mouse bone marrow (BM)-derived dendritic cells (DCs) were prepared as we described previously (13). In brief, mouse BM was flushed from leg bones, and depleted of red cells with Red Cell Lysis Solution (Biosharp). Cells were cultured in RPMI-1640 supplemented with 10% FBS, recombinant mouse GM-CSF/ml (20ng/ml) and recombinant mouse IL-4 (10ng/ml; PeproTech). Every other day, the supernatant was replaced at half volume with fresh media containing adequate cytokines. On day 7, recombinant proteins (PDL1, PDL1-GMCSF, MSLN-PDL1-GMCSF;100µg/mL) or PBS was added, and then bacterial lipopolysaccharide (LPS; Sigma) was added at 1µg/mL after 4h of antigen loading for DC maturation. After 24h of culture, the expression of characteristic DC-specific markers (CD11c and CD80) as determined by FACS.

DC Immunization and Tumor Model

C57BL/6 mice were randomly divided into 5 groups (8 mice per group) as follows: 1) PBS control, 2) PDL1, 3) PDL1-GMCSF, 4) MSLN-PDL1-GMCSF, 5) MSLN-PDL1-GMCSF + anti-PD-1. $2x10^5$ LLC-MSLN-PDL1 cells at exponential growth stage were subcutaneously injected into the right side of the mouse. After 7 days, the mice were immunized with $1x10^6$ antigen-loaded dendritic cells *via* footpad injection, twice at one-week intervals. Tumor size was measured with a vernier caliper every three or five days. The tumor volume was calculated as follows: (longest diameter) × (shortest diameter)²×0.5. Images were taken every 7 days with a small animal live imager (IVIS Lumina XRMS Series III). The method of living image was as follows: mice were anesthetized generally and 150mg D-Luciferin was intraperitoneally injected into mice per kg, and then imaging analysis was performed after 10-15 minutes of injection.

Intracellular Staining (ICS) and Flow Cytometry Analysis

Spleens were isolated from immunized C57BL/6 mice 3 days after the last DC administration (n=3). Prepared splenocytes (1×10⁶ cells/well) were restimulated in 24-well plates with 5 μ g/mL freshly-prepared vaccine protein for 6 h in the presence of recombinant mouse IL-2 (20ng/ml; PeproTech). 50ng/mL PMA,

1ug/ml Ionomycin and 10 µg/mL Brefeldin A (Absin) was added to accumulate intracellular cytokines. After restimulation, the cells were firstly incubated with anti-mouse CD3, CD4 and CD8 antibodies for surface staining. Subsequently, intracellular staining for IL-2, IFN-y, Granzyme B and Perforin were performed after these cells were fixed and permeabilized. Fixable viability dye was used to gate out dead cells. Data were collected on FACS verse (BD Biosciences) and analyzed with Flow Jo software. The antibodies used in this study were including FITC anti-mouse CD3 (Thermo Fisher), PE antimouse CD4 (BD Biosciences), PerCP-CyTM5.5 anti-mouse CD8a (BD Biosciences), PE-Cy7 anti-mouse IL-2 (BD Biosciences); BV510 anti-mouse IFN-y (Biolegend); BV421 anti-mouse Granzyme B (Biolegend); APC anti-mouse Perforin (Biolegend); Fixable Viability Stain 780 (BD Biosciences); Fixation/Permeabilization Kit (BD Biosciences).

Antibody ELISA Assay

After immunization, serum of 3 mice in each group was collected for ELISA detection. ELISA plates were coated with recombinant PD-L1 proteins (500ng/mL) overnight at 4°C. The next day, the PD-L1-coated plates were blocked with BSA, and then added with serial dilutions of serum, and incubated at room temperature for 2h. After extensive washes, HRP-labeled antimouse IgG antibody (Bioss) was added and incubated at room temperature for 1 h. Then TMB was added to detect ELISA reactions. Optical density (OD) was read at 450 nm on a multiplate reader (Varioskan Flash, Thermo).

Hematoxylin-Eosin (HE) Staining

Mice livers and kidneys (n=3) were isolated from the above immune groups and fixed in 4% paraformaldehyde. After dewaxing treatment, stain sections with Hematoxylin solution for 3-5 min, rinse with tap water. Then treat the section with Hematoxylin Differentiation solution, rinse with tap water. Treat the section with Hematoxylin Scott Tap Bluing, rinse with tap water. 85% ethanol for 5 min; 95% ethanol for 5 min; then stain sections with Eosin dye for 5 min. Finally sealed with neutral gum for dehydration. Observe with microscope inspection, image acquisition and analysis.

Statistical Analysis

All analysis was performed using GraphPad Prism 8.0 statistical software. Two-way ANOVA and log-rank (Mantel-Cox) tests were used to analyze the tumor growth and mice survival data, respectively. All the other data were analyzed using unpaired two-tailed t tests. A value of p < 0.05 was considered statistically significant.

RESULTS

Production of Recombinant Protein Immunogens

A key problem in tumor immunotherapy is the weak immunogenicity and low immune response rate of tumor antigen (10). To generate new immunogens for cancer treatment and prevention, two specific PD-L1-containg

peptides fusion proteins PDL1-GMCSF and MSLN-PDL1-GMCSF were designed and synthesized based on the recent method of peptide assembly we developed (13) and cloned them into the pET21a expression vector. Plasmid construction map is shown in Supplementary Figure 1. Then, the plasmids were transformed into BL21 (DE3) (E. coli) to express the recombinant proteins PDL1-GMCSF and MSLN-PDL1-GMCSF, respectively. After culture fermentation and induction with IPTG, cells were collected, lysed, and examined by SDS-PAGE. As indicated by the black arrows (Figure 1A), the target proteins were expressed in pellet with expected molecular weights of 41.94 kDa (PDL1-GMCSF) and 65.41 kDa (MSLN-PDL1-GMCSF) upon induction. The His-tagged protein vaccine was then purified by Ni-NTA column under denaturing conditions, and the eluted fractions was further analyzed by Western blot using His antibody, which verified the accuracy of the target proteins (Figure 1B, arrows). To create a physiological consistency, the elution enriched portion of the purified protein was further dialysis and then analyzed by Western blot (Figure 1C). Additional quality control tests for endotoxin, mycoplasma and microorganisms were also performed. The purity of the recombinant proteins PDL1-GMCSF and MSLN-PDL1-GMCSF was >90% and the endotoxin was at an acceptable low level used for further studies.

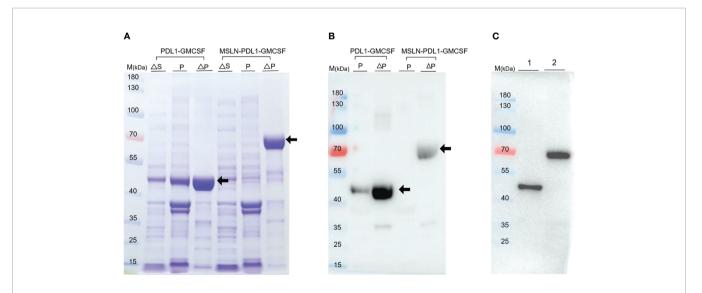
Maturation of DCs After Loading With Fusion Protein Vaccines

Mouse bone marrow-derived DCs were prepared as previously described (13). Approximately $2\sim 4\times 10^7$ bone marrow cells were obtained per mouse, cultured in an incubator containing 5% CO₂ at 37°C, denoted as Day 0. At this time, the cells were small in size, mostly round and without obvious protuberance. After 2

days culture in vitro, the cell volume increased, some cells were semi-adherent, and a few cell colonies were formed (Figure 2A). On day 4, a large number of cells grew in clusters (Figure 2B). After 6 days of culture, the immature BMDCs were obtained with the culture in the medium containing GM-CSF. Clusters of colonies of BMDCs were formed, and amounts of floating and semi-adherent BMDCs were seen. The cell volume was larger than before, with round or shuttle shape, and some cells were visible as spines (Figure 2C). After 24h stimulation with LPS $(1\mu g/mL)$, the number of cells increased, and a large number of DCs with typical morphology were released from the colonies with obvious dendritic protrusions (Figure 2D). In addition, in order to detect the maturity of BMDCs, on day 7 of culture, DCs were individually loaded with PDL1, PDL1-GMCSF, MSLN-PDL1-GMCSF protein and PBS. After 4h of antigen loading, LPS was added and stimulated overnight. Surface staining and subsequent flow cytometry analysis showed that the majority of DC cells used for immunization were induced to mature, with expression levels of co-stimulatory molecules CD11c and CD80 ranging from 68.7% to 71.7% (Figure 2E). The results show that the antigen uptake and DC maturation events have occurred during this culture and stimulation process.

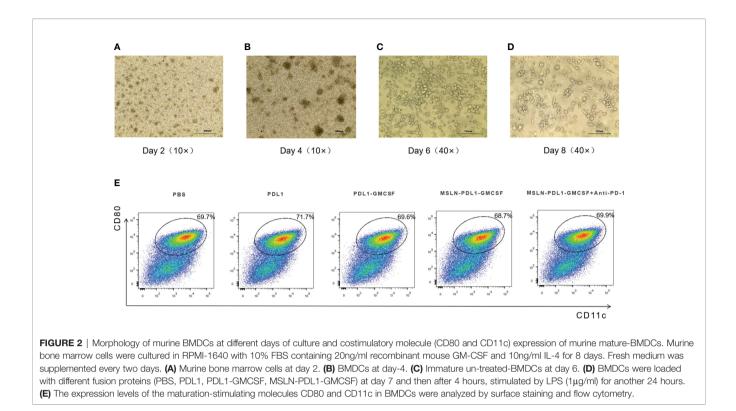
PD-L1-Containing MSLN Vaccine Induces Effective Th1 Cytokine Secretion and Elevated Anti-PD-L1 Antibody Production

To study whether this PD-L1-containing MSLN vaccine can induce efficient immune response, C57BL/6 mice were firstly immunized twice with 100 μ g/mL protein-loaded DCs and PBS-DCs weekly. On the third day after immunization with MSLN-PDL1-GMCSF protein-loaded DC vaccine, C57BL/6 mice were intraperitoneally injected with PD-1 monoclonal antibody



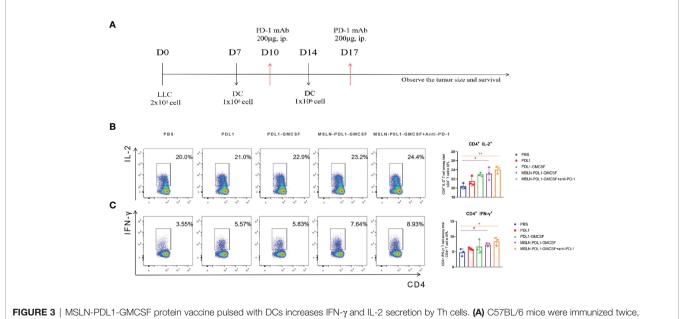


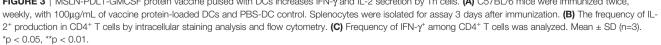
405



(McAb) (200 μ g/mouse) to carry out combination therapy (**Figure 3A**). Three days after the second immunization, spleens of immunized mice were isolated and digested into single-cell suspensions, which were then stimulated in 24-well plates with 50ng/mL PMA, 1ug/ml Ionomycin and 10 μ g/mL

Brefeldin A for 6 h. $CD4^+$ T cells producing IL-2 and IFN- γ were then determined and analyzed by intracellular staining and flow cytometry. As expected, the Th cells immunized with MSLN-PDL1-GMCSF protein vaccine generated a significantly higher percentage of IL-2 compared with cells immunized with PBS-





DCs (**Figure 3B**). Similarly, the frequency of IFN- γ producing T cells was induced by a 2.1-fold increase in total CD4⁺ cells, similar to IL-2 induction (Figure 3C). These results clearly demonstrated that MSLN-PDL1-GMCSF protein vaccine elicit enhanced IFN-y and IL-2 production and might generate good capability for CTL induction. Furthermore, to further study whether DCs-loaded with MSLN-PDL1-GMCSF can induce PD-L1-specific antibody responses, we used sera of immunized mice for anti-PD-L1 ELISA detection. As shown in Figure 4A, it showed that levels of anti-PD-L1 antibodies (IgG) in sera of MSLN-PDL1-GMCSF loaded DCs immunized mice slightly increased (p<0.05) compared to other two immunized groups, similar to our previous observation immunized with PDL1-Vax (13). Interestingly, when combined with PD-1 McAb treatment, the secretion of cytokines and anti-PD-L1 production were significantly increased determined by FACS and ELISA assay in this test. To further verify the possible adverse autoimmune pathology induced by immunization with protein-loaded DCs, HE staining was performed on sections of vital organs and tissues of immunized mice, and no significant pathological toxicity was observed in immunized mice (Figure 4B). Taken together, our data implies that this PD-L1-containing MSLN vaccine can induce effective Th1 responses and anti-PD-L1 antibody production, and it a relatively safe and effective tumor vaccine.

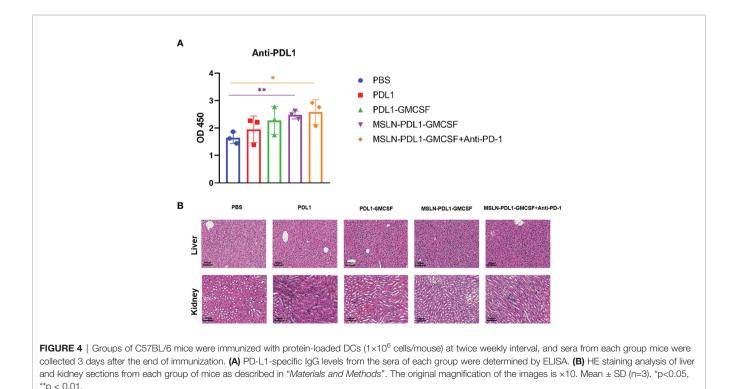
Vaccination Generates Significantly Enhanced Cytotoxic T Cell Response

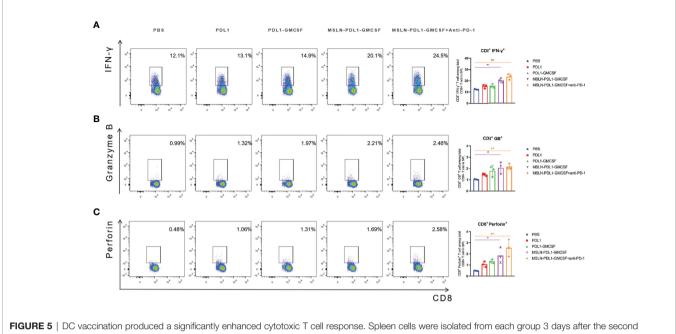
In human anti-tumor immune response, cellular immunity is the predominant form, and the production of CD8⁺ cytotoxic T lymphocyte cells (CTL) is the core of effective anti-tumor cell

immunity (33). Therefore, to study whether this MSLN-PDL1-GMCSF-loaded DC vaccine can induce an effective antigenspecific CTL response, C57BL/6 mice were immunized twice with fusion protein-loaded DCs and then spleen T cells were obtained 3 days after the second vaccination as described previously. The effector molecules IFN-y, Granzyme B, and perforin were then tested to evaluate the cytotoxic T cell response. As shown in Figure 5A, the increased expression level of IFN- γ was observed in CD8⁺ T cells using intracellular staining and FACS. MSLN-PDL1-GMCSF-DCs generated a significantly higher percentage of Granzyme B producing CD8⁺ T cells, with a 2.2-fold increase in the MSLN-PDL1-GMCSF-DCs group and had a 2.5-fold increase in the monoclonal antibody group compared to the PBS-DCs group (Figure 5B). The similar trend was observed for perforin secretion, which was increased by 3.5-fold in the MSLN-PDL1-GMCSF-DCs group and approximately 5.4-fold upregulation in the monoclonal antibody group (Figure 5C). These results suggest that DC-targeted MSLN-PDL1-GMCSF vaccine induces an efficient anti-tumor CTL response, which is even more significant in combination with PD-1 McAb.

Therapeutic Vaccination With DC Loading MSLN-PDL1-GMCSF Vaccine Significantly Inhibits Tumor Growth

In order to assess whether the fusion protein-loaded DC vaccine can generate therapeutic antitumor effects, 2×10^5 lung cancer cell lines LLC, which stably expressing MSLN and PD-L1, were injected subcutaneously on the right flank of C57BL/6 mice for better later treatment and monitoring. After tumor establishment, tumor-





inoculation of C57BL/6 mice, and incubated with RPMI-1640 containing 10%FBS for 6 hours, adding PMA (50ng/mL), Brefeldin A(10ug/ml) and lonomycin(1ug/ml). The cells were surface stained and intracellularly stained with FACS to analyze the expression of IFN- γ (A), granzyme B (B) and perform (C) in CD8⁺ T cells. Mean ± SD (n=3). *p < 0.05, **p < 0.01.

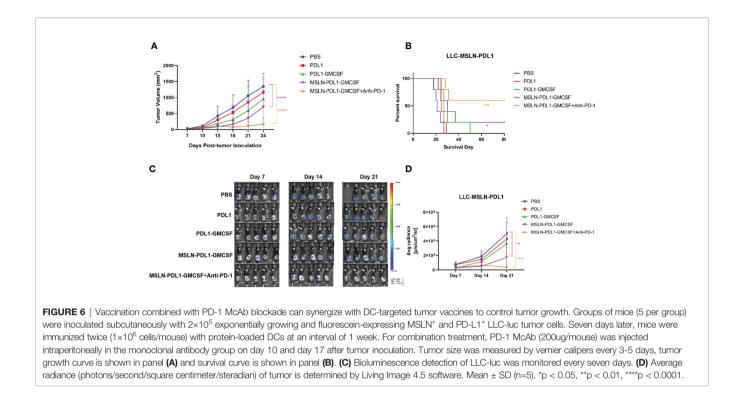
bearing mice were immunized with fusion protein-loaded DC vaccine via footpad injection on day 7 after tumor cell inoculation and booster immunization on day 14. Meanwhile, combination PD-1 monoclonal antibody treatment was administered on days 10 and 17. Tumor growth was monitored by vernier calipers every 3 days, and live imaging was performed every 7 days. As shown in Figure 6A, vaccination with MSLN-PDL1-GMCSF-DCs more efficiently delayed tumor growth compared to other groups. Interestingly, immunized mice in the PDL1 protein group and the PDL1-GMCSF vaccine group also showed some efficacy in inhibiting tumor growth. In addition, the survival of tumor-bearing mice was significantly improved by vaccination with MSLN-PDL1-GMCSF-DCs (Figure 6B). After injection of luciferase, in vivo bioluminescence showed that MSLN-PDL1-GMCSF-DCs combined with anti-PD-1 group greatly inhibited tumor growth in vivo (Figures 6C, D). Thus, these data suggest that this MSLN-PDL1-GMCSF vaccine could be a more potent therapeutic vaccine compared with conventional non-PD-L1 DC-targeting protein vaccines. Strikingly, Vaccination of PD-1 McAb can synergize with MSLN-PDL1-GMCSF-DCs vaccine to produce significantly enhanced antitumor effect, and 60% of treated mice survived for at least 80 days. Therefore, the combination of protein-loaded DC vaccine and PD-1 McAb blockade could be an effective therapeutic strategy against solid tumors.

DISCUSSION

In recent years, tumor vaccines designed based on DCs have been extensively studied. DC vaccines loaded with tumor antigens are

promising approaches for cancer immunotherapy due to their ability to present specific tumor antigen and activate specific T cells, stimulate B cells and form immune memory (5). Studies have shown that DC vaccines enhance antitumor immune responses and effectively control tumor growth in various mouse tumor models with good safety and tolerability (10, 34, 35). However, despite extensive efforts, tumor regression in DC vaccine-treated cancer patients is rare and limited progress has been made in cancer treatment (6). Therefore, new strategies and approaches are urgently needed to improve the efficacy of tumor vaccines and thus improve the poor efficacy in the clinic. A fusion protein targeting MSLN was found to promote tumor-specific T cell responses by increasing tumor antigen presentation and crosspresentation via DC in vitro and enhanced tumor cell immunogenicity in vivo (36). In this study, we designed a novel fusion peptide immunogen including human MSLN, PD-L1 immune checkpoint molecule, GM-CSF sequence and T helper epitope sequence assembly as therapeutic tumor vaccine (MSLN-PDL1-GMCSF). Our results showed that the novel PD-L1containing MSLN targeting vaccine was able to activate a MSLN and PD-L1-specific T cell immune responses in immunized mice, inhibit the growth of MSLN⁺ and PD-L1⁺ tumor cells. Meanwhile, cytokine GM-CSF component in the vaccine design as an adjuvant might elicit function in enhancing DC recruitment, activation and cross-presentation.

The immunosuppressive tumor microenvironment leading to inefficient antigen presentation is further complicated by the problem. The immune checkpoint molecule PD-1 is expressed on T cells and its binding with PD-L1 on tumor cells can downregulate T cell proliferation, reduce T cell cytokine secretion or



enhance T cell apoptosis (37-39). To date, there are five antibodies against PD-1 or PD-L1 that have been approved by the FDA and the European Medicines Agency for use in cancer immunotherapy (40). Clinical trials have shown that immune checkpoint regulation therapies have good potential, although in many cases the effect is limited, especially in solid tumors with low response rates, probably because the majority of cancer patients are resistant to PD-1/PD-L1 blockade (41). The induced anti-PD-L1 antibodies can kill PD-L1-expressing tumor cells through multiple mechanisms, including inhibition of PD-L1 interaction with PD-1 on CTLs, antibody-dependent cellular cytotoxicity (ADCC), and complement-dependent cytotoxicity (CDC) (13, 37, 42). Previous evidence supports that DCs can directly induce CTL and antibody responses, and DCs stimulating an antibody response is believed as a consequence of $CD4^+$ Th function (13, 43). In this study, we found that this novel PD-L1-containing MSLN vaccine can induce low-dose, durable anti-PD-L1 antibodies and elicit effective tumor-specific CTL responses in vivo. As shown in the Figure 6, compared with DC vaccine loaded with PD-L1 alone, the MSLN-PDL1-GMCSF vaccine inhibited the growth of lung cancer cells more effectively, and obtained a more pronounced survival benefit, which probably because blocking the PD-1 and PD-L1 restores the anti-tumor effect of T cells in the tumor microenvironment, thus reversing the "cold" state of the tumor.

Several clinical trials are underway to evaluate the efficacy of DC-based vaccines in combination with radiotherapy, chemotherapy, immune checkpoint inhibitors, and adoptive cell therapy for the treatment of various cancers (17, 34, 41). Teng, C. et al. demonstrated that blocking the PD-1/PD-L1 immune checkpoint during DC vaccination showed better therapeutic efficacy than DC vaccination alone in an

established mice model of *in-situ* liver tumor (15). However, in contrast to preclinical data, clinical data on the combination of immune checkpoint inhibitors and DCs vaccination are limited. Recent clinical data showed that 39 patients with metastatic melanoma who received ipilimumab plus DCs vaccine had an overall survival rate of only 38% (44). In this study, we further evaluated the therapeutic efficacy of this MSLN-PDL1-GMCSF vaccine in combination with PD-1 immune checkpoint inhibitors in an established mice model of lung cancer. The results showed that by inducing a stronger anti-tumor cytotoxic T-cell response, the combination of MSLN-PDL1-GMCSF vaccine and PD-1 antibody significantly prolonged overall survival, reduced tumor volume and increased tumor cell apoptosis compared to treatment alone. Thus, the combination therapy of this novel vaccine with PD-1 blockade may have great potential as a new treatment strategy for the treatment of other cancers, such as mesothelioma, pancreatic cancer, ovarian cancer and triple negative breast cancer with high expression of MSLN.

Nevertheless, we are aware of some limitations in this study. Firstly, more solid tumors with high expression of MSLN and PDL1 are needed to determine the overall anti-tumor effect of this novel vaccine in the future. Secondly, our next step is to optimize the MSLN epitope sequence to improve immunogenicity. Also, whether this PD-L1-containing MSLN vaccine can efficiently target *in vivo* needs to be determined. In addition, there are some potential clinical applications and challenges for this PD-L1-containing MSLN vaccine. Since the sequences of this novel fusion peptide immunogen (MSLN-PDL1-GMCSF) are originated from human, it is important to test this novel human MSLN-PDL1-GMCSF vaccine in cancer patients to determine whether anti-PD-L1 antibody and CTL responses can be induced and whether the PD-L1-containing MSLN vaccine is safe. Till now immunosuppression microenvironment remain a major challenge in developing effective immunotherapies, the combined therapies (CAR-T and chemotherapy, etc.) that modulate the tumor microenvironment were also needed to enhance the immune response and improve the efficacy of antitumor.

In summary, provided here for the first time is a novel PD-L1containing MSLN therapeutic vaccine with the ability to induce persistent anti-PD-L1 antibody and CTL responses. It provides a new effective immunotherapeutic strategy for various solid tumors expressing high MSLN and PD-L1 level by combining this MSLN-PDL1-GMCSF vaccine and PD-1 blockade. This work, together with our recent reported PDL1-Vax, lays out a new strategy to overcome the problem of immune tolerance, and promotes the development of drugs targeting MSLN as the relevant antigen, which have theoretical and application values in the development of tumor immunotherapy in human. The combination of therapeutic vaccination with PD-1 blockade therapy may prove to be critical for improving the management and clinical outcomes of patients who do not respond or whose disease eventually progresses.

DATA AVAILABILITY STATEMENT

The original contributions presented in the study are included in the article/**Supplementary Material**. Further inquiries can be directed to the corresponding authors.

ETHICS STATEMENT

The animal study was reviewed and approved by Guangzhou Medical University.

REFERENCES

- Siegel RL, Miller KD, Fuchs HE, Jemal A. Cancer Statistics, 2021. CA Cancer J Clin (2021) 71:7–33. doi: 10.3322/caac.21654
- Thai AA, Solomon BJ, Sequist LV, Gainor JF, Heist RS. Lung Cancer. Lancet (2021) 398:535–54. doi: 10.1016/S0140-6736(21)00312-3
- Ruiz-Cordero R, Devine WP. Targeted Therapy and Checkpoint Immunotherapy in Lung Cancer. Surg Pathol Clin (2020) 13:17–33. doi: 10.1016/j.path.2019.11.002
- Wculek SK, Cueto FJ, Mujal AM, Melero I, Krummel MF, Sancho D. Dendritic Cells in Cancer Immunology and Immunotherapy. *Nat Rev Immunol* (2020) 20:7–24. doi: 10.1038/s41577-019-0210-z
- Lee YS, Radford KJ. The Role of Dendritic Cells in Cancer. Int Rev Cell Mol Biol (2019) 348:123–78. doi: 10.1016/bs.ircmb.2019.07.006
- Patente TA, Pinho MP, Oliveira AA, Evangelista GCM, Bergami-Santos PC, Barbuto JAM. Human Dendritic Cells: Their Heterogeneity and Clinical Application Potential in Cancer Immunotherapy. *Front Immunol* (2019) 9:3176–6. doi: 10.3389/fimmu.2018.03176
- 7. Hayes C. Cellular Immunotherapies for Cancer. *Irish J Med Sci* (1971 -) (2021) 190:41–57. doi: 10.1007/s11845-020-02264-w
- Perez CR, De Palma M. Engineering Dendritic Cell Vaccines to Improve Cancer Immunotherapy. Nat Commun (2019) 10:5408. doi: 10.1038/s41467-019-13368-y

AUTHOR CONTRIBUTIONS

All authors listed have made a substantial, direct, and intellectual contribution to the work and approved it for publication.

FUNDING

This work was supported by the research funding the Grant No. 31770183 from the National Natural Science Foundation of China, by the High-level university foundation of the Grant No. JCXKJS2021B04 from Guangzhou Medical University, and supported by the funds under Grant Number 15001019002204 from the Sixth Affiliated Hospital of Guangzhou Medical University, Qingyuan People's Hospital. This work was also supported by Grant Number A2019144 from Medical Science and Technology Research Foundation of Guangdong Province.

ACKNOWLEDGMENTS

We would like to thank the members of SY Chen's laboratory in University of Southern California for providing technical assistance and helpful suggestions. We would like to thank WZ, JP, MH, ZF, and JJ for study support, RZ, MH, HZ, and JH for supporting flow cytometry analysis, XY, YS, BZ, JZ, and BF for mice experiment and Editage (www.editage.cn) for English language editing.

SUPPLEMENTARY MATERIAL

The Supplementary Material for this article can be found online at: https://www.frontiersin.org/articles/10.3389/fimmu.2022.925217/full#supplementary-material

- Wang S, Wang X, Zhou X, Lyerly HK, Morse MA, Ren J. DC-CIK as a Widely Applicable Cancer Immunotherapy. *Expert Opin Biol Ther* (2020) 20:601–7. doi: 10.1080/14712598.2020.1728250
- Sadeghzadeh M, Bornehdeli S, Mohahammadrezakhani H, Abolghasemi M, Poursaei E, Asadi M, et al. Dendritic Cell Therapy in Cancer Treatment; the State-of-the-Art. *Life Sci* (2020) 254:117580. doi: 10.1016/j.lfs.2020.117580
- Bol KF, Schreibelt G, Rabold K, Wculek SK, Schwarze JK, Dzionek A, et al. The Clinical Application of Cancer Immunotherapy Based on Naturally Circulating Dendritic Cells. J Immunother Cancer (2019) 7:109. doi: 10.1186/s40425-019-0580-6
- Wang G, Kang X, Chen KS, Jehng T, Jones L, Chen J, et al. An Engineered Oncolytic Virus Expressing PD-L1 Inhibitors Activates Tumor Neoantigen-Specific T Cell Responses. *Nat Commun* (2020) 11:1395. doi: 10.1038/s41467-020-15229-5
- Chen J, Liu H, Jehng T, Li Y, Chen Z, Lee K-D, et al. A Novel Anti-PD-L1 Vaccine for Cancer Immunotherapy and Immunoprevention. *Cancers* (2019) 11:1909. doi: 10.3390/cancers11121909
- Hassannia H, Ghasemi Chaleshtari M, Atyabi F, Nosouhian M, Masjedi A, Hojjat Farsangi M, et al. Blockage of Immune Checkpoint Molecules Increases T-Cell Priming Potential of Dendritic Cell Vaccine. *Immunology* (2020) 159:75–87. doi: 10.1111/imm.13126

- 15. Teng C-F, Wang T, Wu T-H, Lin J-H, Shih F-Y, Shyu W-C, et al. Combination Therapy With Dendritic Cell Vaccine and Programmed Death Ligand 1 Immune Checkpoint Inhibitor for Hepatocellular Carcinoma in an Orthotopic Mouse Model. *Ther Adv Med Oncol* (2020) 12:175883592092203. doi: 10.1177/1758835920922034
- Jiang Y, Chen M, Nie H, Yuan Y. PD-1 and PD-L1 in Cancer Immunotherapy: Clinical Implications and Future Considerations. *Hum Vaccin Immunother* (2019) 15:1111–22. doi: 10.1080/21645515.2019.1571892
- Huang M-Y, Jiang X-M, Wang B-L, Sun Y, Lu J-J. Combination Therapy With PD-1/PD-L1 Blockade in non-Small Cell Lung Cancer: Strategies and Mechanisms. *Pharmacol Ther* (2021) 219:107694. doi: 10.1016/ j.pharmthera.2020.107694
- Ai L, Xu A, Xu J. Roles of PD-1/PD-L1 Pathway: Signaling, Cancer, and Beyond. Adv Exp Med Biol (2020) 1248:33–59. doi: 10.1007/978-981-15-3266-5_3
- Huang NN, Han SB, Hwang IY, Kehrl JH. B Cells Productively Engage Soluble Antigen-Pulsed Dendritic Cells: Visualization of Live-Cell Dynamics of B Cell-Dendritic Cell Interactions. *J Immunol* (2005) 175:7125–34. doi: 10.4049/ jimmunol.175.11.7125
- Schoutrop E, El-Serafi I, Poiret T, Zhao Y, Gultekin O, He R, et al. Mesothelin-Specific CAR T Cells Target Ovarian Cancer. *Cancer Res* (2021) 81:3022–35. doi: 10.1158/0008-5472.CAN-20-2701
- Weidemann S, Gagelmann P, Gorbokon N, Lennartz M, Menz A, Luebke AM, et al. Mesothelin Expression in Human Tumors: A Tissue Microarray Study on 12,679 Tumors. *Biomedicines* (2021) 9:397. doi: 10.3390/biomedicines9040397
- Le K, Wang J, Zhang T, Guo Y, Chang H, Wang S, et al. Overexpression of Mesothelin in Pancreatic Ductal Adenocarcinoma (PDAC). *Int J Med Sci* (2020) 17:422–7. doi: 10.7150/ijms.39012
- Del Bano J, Florès-Florès R, Josselin E, Goubard A, Ganier L, Castellano R, et al. A Bispecific Antibody-Based Approach for Targeting Mesothelin in Triple Negative Breast Cancer. *Front Immunol* (2019) 10:1593. doi: 10.3389/ fimmu.2019.01593
- Klampatsa A, Dimou V, Albelda SM. Mesothelin-Targeted CAR-T Cell Therapy for Solid Tumors. *Expert Opin Biol Ther* (2021) 21:473–86. doi: 10.1080/14712598.2021.1843628
- Hagerty BL, Pegna GJ, Xu J, Tai C-H, Alewine C. Mesothelin-Targeted Recombinant Immunotoxins for Solid Tumors. *Biomolecules* (2020) 10:973. doi: 10.3390/biom10070973
- Lv J, Li P. Mesothelin as a Biomarker for Targeted Therapy. *Biomark Res* (2019) 7:18–8. doi: 10.1186/s40364-019-0169-8
- Dougan M, Dranoff G, Dougan SK. GM-CSF, IL-3, and IL-5 Family of Cytokines: Regulators of Inflammation. *Immunity* (2019) 50:796–811. doi: 10.1016/j.immuni.2019.03.022
- Mashima H, Zhang R, Kobayashi T, Hagiya Y, Tsukamoto H, Liu T, et al. Generation of GM-CSF-Producing Antigen-Presenting Cells That Induce a Cytotoxic T Cell-Mediated Antitumor Response. *OncoImmunology* (2020) 9:1814620. doi: 10.1080/2162402X.2020.1814620
- Lazarus HM, Ragsdale CE, Gale RP, Lyman GH. Sargramostim (Rhu GM-CSF) as Cancer Therapy (Systematic Review) and An Immunomodulator. A Drug Before Its Time? *Front Immunol* (2021) 12:706186. doi: 10.3389/ fimmu.2021.706186
- Yan W-L, Wu C-C, Shen K-Y, Liu S-J. Activation of GM-CSF and TLR2 Signaling Synergistically Enhances Antigen-Specific Antitumor Immunity and Modulates the Tumor Microenvironment. J Immunother Cancer (2021) 9: e002758. doi: 10.1136/jitc-2021-002758
- Dillman RO. An Update on GM-CSF and its Potential Role in Melanoma Management. *Melanoma Manag* (2020) 7:MMT49. doi: 10.2217/mmt-2020-0011
- Hilf N, Kuttruff-Coqui S, Frenzel K, Bukur V, Stevanović S, Gouttefangeas C, et al. Actively Personalized Vaccination Trial for Newly Diagnosed Glioblastoma. *Nature* (2019) 565:240–5. doi: 10.1038/s41586-018-0810-y

- 33. Guram K, Kim SS, Wu V, Sanders PD, Patel S, Schoenberger SP, et al. A Threshold Model for T-Cell Activation in the Era of Checkpoint Blockade Immunotherapy. *Front Immunol* (2019) 10:491. doi: 10.3389/ fimmu.2019.00491
- Nava S, Lisini D, Frigerio S, Bersano A. Dendritic Cells and Cancer Immunotherapy: The Adjuvant Effect. Int J Mol Sci (2021) 22:12339. doi: 10.3390/ijms222212339
- Mastelic-Gavillet B, Balint K, Boudousquie C, Gannon PO, Kandalaft LE. Personalized Dendritic Cell Vaccines—Recent Breakthroughs and Encouraging Clinical Results. *Front Immunol* (2019) 10:766. doi: 10.3389/ fimmu.2019.00766
- 36. Yuan J, Kashiwagi S, Reeves P, Nezivar J, Yang Y, Arrifin NH, et al. A Novel Mycobacterial Hsp70-Containing Fusion Protein Targeting Mesothelin Augments Antitumor Immunity and Prolongs Survival in Murine Models of Ovarian Cancer and Mesothelioma. J Hematol Oncol (2014) 7:15. doi: 10.1186/1756-8722-7-15
- Kadam P, Sharma S. PD-1 Immune Checkpoint Blockade Promotes Therapeutic Cancer Vaccine to Eradicate Lung Cancer. Vaccines (2020) 8:317. doi: 10.3390/vaccines8020317
- Khan M, Zhao Z, Arooj S, Fu Y, Liao G. Soluble PD-1: Predictive, Prognostic, and Therapeutic Value for Cancer Immunotherapy. *Front Immunol* (2020) 11:587460. doi: 10.3389/fimmu.2020.587460
- Topalian SL, Taube JM, Pardoll DM. Neoadjuvant Checkpoint Blockade for Cancer Immunotherapy. *Science* (2020) 367(6477):eaax0182. doi: 10.1126/ science.aax0182
- Córdova-Bahena L, Velasco-Velázquez MA. Anti-PD-1 And Anti-PD-L1 Antibodies as Immunotherapy Against Cancer: A Structural Perspective. *Rev Invest Clin* (2021) 73:008–16. doi: 10.24875/RIC.20000341
- Yap TA, Parkes EE, Peng W, Moyers JT, Curran MA, Tawbi HA. Development of Immunotherapy Combination Strategies in Cancer. *Cancer Discov* (2021) 11:1368–97. doi: 10.1158/2159-8290.CD-20-1209
- 42. Gou Q, Dong C, Xu H, Khan B, Jin J, Liu Q, et al. PD-L1 Degradation Pathway and Immunotherapy for Cancer. *Cell Death Dis* (2020) 11:955. doi: 10.1038/s41419-020-03140-2
- Ruprecht CR, Lanzavecchia A. Toll-Like Receptor Stimulation as a Third Signal Required for Activation of Human Naive B Cells. *Eur J Immunol* (2006) 36:810–6. doi: 10.1002/eji.200535744
- 44. Wilgenhof S, Corthals J, Van Nuffel AM, Benteyn D, Heirman C, Bonehill A, et al. Long-Term Clinical Outcome of Melanoma Patients Treated With Messenger RNA-Electroporated Dendritic Cell Therapy Following Complete Resection of Metastases. *Cancer Immunol Immunother* (2015) 64:381–8. doi: 10.1007/s00262-014-1642-8

Conflict of Interest: The authors declare that the research was conducted in the absence of any commercial or financial relationships that could be construed as a potential conflict of interest.

Publisher's Note: All claims expressed in this article are solely those of the authors and do not necessarily represent those of their affiliated organizations, or those of the publisher, the editors and the reviewers. Any product that may be evaluated in this article, or claim that may be made by its manufacturer, is not guaranteed or endorsed by the publisher.

Copyright © 2022 Zeng, Pan, Fang, Jia, Zhang, He, Zhong, He, Yang, Shi, Zhong, Zeng, Fu, Huang and Liu. This is an open-access article distributed under the terms of the Creative Commons Attribution License (CC BY). The use, distribution or reproduction in other forums is permitted, provided the original author(s) and the copyright owner(s) are credited and that the original publication in this journal is cited, in accordance with accepted academic practice. No use, distribution or reproduction is permitted which does not comply with these terms.



Discovering Innate Driver Variants for Risk Assessment of Early Colorectal Cancer Metastasis

Ruo-Fan Ding^{1†}, Yun Zhang^{1†}, Lv-Ying Wu^{1†}, Pan You^{2,3*}, Zan-Xi Fang³, Zhi-Yuan Li³, Zhong-Ying Zhang³ and Zhi-Liang Ji^{1*}

¹ State Key Laboratory of Cellular Stress Biology, National Institute for Data Science in Health and Medicine, School of Life Sciences, Xiamen University, Xiamen, China, ² Department of Clinical Laboratory, Xiamen Xianyue Hospital, Xiamen, China, ³ Department of Clinical Laboratory, Zhongshan Hospital, affiliated to Xiamen University, Xiamen, China

OPEN ACCESS

Edited by: Xian Zeng, Fudan University, China

Reviewed by:

Shixiang Wang, Sun Yat-sen University Cancer Center (SYSUCC), China Yuwei Liu, Jiangsu University, China Cao Dongsheng, Central South University, China

*Correspondence:

Zhi-Liang Ji appo@xmu.edu.cn Pan You panyou001@yahoo.com 'These authors have contributed equally to this work

Specialty section:

This article was submitted to Cancer Immunity and Immunotherapy, a section of the journal Frontiers in Oncology

Received: 17 March 2022 Accepted: 16 May 2022 Published: 20 June 2022

Citation:

Ding R-F, Zhang Y, Wu L-Y, You P, Fang Z-X, Li Z-Y, Zhang Z-Y and Ji Z-L (2022) Discovering Innate Driver Variants for Risk Assessment of Early Colorectal Cancer Metastasis. Front. Oncol. 12:898117. doi: 10.3389/fonc.2022.898117 Metastasis is the main fatal cause of colorectal cancer (CRC). Although enormous efforts have been made to date to identify biomarkers associated with metastasis, there is still a huge gap to translate these efforts into effective clinical applications due to the poor consistency of biomarkers in dealing with the genetic heterogeneity of CRCs. In this study, a small cohort of eight CRC patients was recruited, from whom we collected cancer, paracancer, and normal tissues simultaneously and performed whole-exome sequencing. Given the exomes, a novel statistical parameter LIP was introduced to quantitatively measure the local invasion power for every somatic and germline mutation, whereby we affirmed that the innate germline mutations instead of somatic mutations might serve as the major driving force in promoting local invasion. Furthermore, via bioinformatic analyses of big data derived from the public zone, we identified ten potential driver variants that likely urged the local invasion of tumor cells into nearby tissue. Of them, six corresponding genes were new to CRC metastasis. In addition, a metastasis resister variant was also identified. Based on these eleven variants, we constructed a logistic regression model for rapid risk assessment of early metastasis, which was also deployed as an online server, AmetaRisk (http://www.bio-add. org/AmetaRisk). In summary, we made a valuable attempt in this study to exome-wide explore the genetic driving force to local invasion, which provides new insights into the mechanistic understanding of metastasis. Furthermore, the risk assessment model can assist in prioritizing therapeutic regimens in clinics and discovering new drug targets, and thus substantially increase the survival rate of CRC patients.

Keywords: colorectal cancer, metastasis, local invasion, driver variants, machine learning

INTRODUCTION

Colorectal cancer (CRC) is one of the most frequent cancers worldwide and has the highest mortality after lung cancer (1, 2). The low survival rate and the high recurrence of CRC could be largely attributed to metastasis (3). About 20% of CRC patients already have metastases at diagnosis (4). Therefore, early assessment of metastasis risk can assist in prioritizing therapeutic regimen and thus substantially reduce the mortality of CRC patients.

Accumulating lines of evidence indicate that genetic factors may play a crucial role in CRC metastasis (5). However, CRC metastases are mechanistically heterogeneous, and the heterogeneity may answer for the poor prognosis in clinics. To date, the genomic basis of this variability has not been fully illustrated yet. With the goal of identifying driver genes/ mutations in metastasis, previous works performed comparative lesion sequencing of matched primary versus metastatic CRC in cohorts of different size, race, age, and metastatic sites (4, 6-9). Some studies attempted to seek a high genomic concordance between primary and metastatic CRCs (7, 9-11), in which the concordant genomic biomarkers were thus taken as effective indicators for both diagnostic and prognostic implications of CRCs (6). These biomarkers, for example, BRAF mutations, were applied to assess mortality of metastatic CRC (12). A recent meta-analysis on 61 clinical studies and 3,565 metastatic CRCs concluded that four highly concordant gene biomarkers (KRAS, NRAS, BRAF, and PIC3KA) might drive the metastatic spread (6). However, due to the interference of "background noise" produced by extensive heterogeneity of the tumor cell variations, biomarker discordance was also often observed. For instance, the discordance rates of KRAS mutations between primary CRC and its metastases could be as high as 22% (13). PIK3CA demonstrated a 6.8-fold higher odds of discordance between the primary and the metastatic sites (14). In addition, it was reported that 65% of somatic mutations originated from a common progenitor, in which 15% were tumor-specific and 19% were metastasis-specific (15). Alternatively, some studies paid more attention to the metastasis-specific alterations (5, 16). A previous study suggested that targeted therapy of colorectal liver metastases would be more effective on the basis of the genetic properties of metastasis rather than those of the primary tumor since there was a significant genetic difference (17). However, a phylogenetic analysis of pancancer metastases manifested that many genetic biomarkers or driver genes were common to all CRC metastases, and the driver gene mutations not shared by all metastases were unlikely to have functional consequences (8). After all, these efforts discovered a bundle of potential metastasis-associated genes that were recurrently mutated at the metastatic sites, including APC, TP53, KRAS, PIK3CA, and SMAD4 (Table 1). It should be noted that many of the metastasis-associated genes are also involved in CRC origin and progress (4).

In recent years, several prediction models were developed for tumor metastasis assessment. Some used conventional clinical pathological characteristics, such as age, race, gender, tumor site, and tumor size, to establish the Cox regression models (or the proportional hazards models) to assess metastasis and survival outcomes for CRC patients (18–20). Some applied nomograms to perform metastasis assessment on the basis of radiomics signatures (21–24). For instance, imaging descriptors derived from computed tomography (CT) were used as prognostic or predictive biomarkers for metastasis (25). With the widespread application of high-throughput sequencing technology, some research groups also mined multiple omics data for metastasis assessment. For examples, Kandimalla et al. constructed an 8-gene classifier based on gene expression profiles to predict lymph node metastasis in T1 CRC patients (26). Ozawa et al. used five microRNA signatures to predict lymph node invasion in T1 CRC cancers (27). Regretfully, despite the enormous efforts that have been made to identify biomarkers and build prediction models for CRC metastasis risk assessment, there is still a huge gap to translate these efforts into clinical applications due to the problem of poor consistency (28, 29). In particular, they are powerless on risk assessment of early CRC metastasis.

Tumor metastasis is an invasive action of tumor cells, which refers to the process of tumor cells spread to other parts of the body. In principle, metastasis usually progresses in four steps: local invasion, intravasation into the blood circulation system, extravasation into the surrounding tissues, and colonization and proliferation in new locations (30). Local invasion of tumor cells is the initial step of almost all types of metastases (31). Before the tumor cells detach from the primary lesion, they proliferate and spread to nearby tissues, and communicate with adjacent cells in response to the microenvironment changes (32). Therefore, instead of identifying concordant gene markers between the start point (primary tumor) and the end point (metastatic tumor), exploring the driving genetic force at the initial step (local invasion) may capture the true signals of early metastasis. Unfortunately, few studies have been ever undertaken to date to identify local invasion-associated genes in malignant cancers.

In this work, we attempted to mine driver genes/mutations in early CRC metastasis. For this purpose, we elaborately designed an experiment to profile genomic alternation landscapes of cancer, paracancer, and normal tissues simultaneously in a CRC cohort. Upon the genomic mutation profiles, a new statistical parameter was introduced to quantitatively evaluate the contribution of every mutation to local invasion. Subsequently, we identified metastasis driver mutations *via* mining multiple omics data derived from different CRC sources. Lastly, we developed a machine learning model for rapid assessment of early CRC metastasis.

DATA AND METHODS

The CRC Cohort

This study was approved by the Ethics Committee of the Xiamen Xianyue Hospital and was performed in accordance with the Helsinki Declaration. All patients provided written informed consent prior to inclusion in the study. A total of eight CRC inpatients from the Zhongshan Hospital, affiliated to Xiamen University, Fujian Province, China were recruited in this study. They were selected from more than 248 CRC inpatients on the basis of the following criteria: (1) the patients have no blood kinship by medical background review; (2) the patients were diagnosed with rectal differentiated adenocarcinoma of stage II or III; and (3) the patients received a similar chemotherapy regimen and the prognoses were benign. These eight patients were further divided into two groups: the NM group of four patients who had no metastasis till surgery excision, and the LM group of four patients who had local lymphatic metastasis but no

Gene	Description	Association
NRAS	N-RAS oncogene encoding a membrane protein	RAS signaling has been involved in the initiation of epithelial-to-mesenchymal transition (EMT) in CRC leading to tumor spreading (18).
BRAF	Encodes a protein belonging to the RAF family of serine/threonine protein kinases	BRAF mutation was related to CRC metastasis and distant metastasis in an Asian population (18
KRAS	Kirsten RAS oncogene homolog from the mammalian RAS gene family	KRAS mutation was associated with lymphatic and distant metastases in CRC patients (19).
PIK3CA	Phosphatidylinositol 3-kinase	PIK3CA mutation was associated with lung metastases in metastatic colorectal cancer (20).
NF1	Negative regulator of the RAS signal transduction pathway	Dysregulated NF1 expression promotes cell invasion, proliferation, and tumorigenesis (21).
PTEN	Encodes phosphatidylinositol-3,4,5-trisphosphate 3- phosphatase	Loss of PTEN expression contribute to CRC development and is associated with the migration aggressive capacity (22).
APC	Encodes a tumor suppressor protein that acts as an	APC mutation caused intestinal adenomas and combination with Trp53R270H mutation or
	antagonist of the Wnt signaling pathway	TGFBR2 deletion induced submucosal invasion (23).
TP53	Encodes a tumor suppressor protein containing	Combined inactivation of Mir34a and TP53 promotes azoxymethane-induced colorectal
	transcriptional activation, DNA binding, and oligomerization domains	carcinogenesis and tumor progression and metastasis by increasing levels of IL6R and PAI1 (24).
SMAD4	Encodes a member of the SMAD family of signal	Activation of BMP signaling in SMAD4-negative cells altered protein and messenger RNA levels of
	transduction proteins acts as a tumor suppressor and inhibits epithelial cell proliferation	markers of epithelial-mesenchymal transition and increased cell migration, invasion, and formation of invadopodia (25).
POLE	Encodes the catalytic subunit of DNA polymerase epsilon	POLE-mutated CRCs arose in the transverse colon and rectum, and showed increased tumor- infiltrating lymphocytes and immune cells at the tumor-stromal interface (26).
RHBDD1	Rhomboid Domain Containing 1	RHBDD1 regulated ser552 and ser675 phosphorylation of β -catenin to activate the Wnt signaling pathway resulted in the recovery of signaling pathway activity, migration, and invasion in CRC cel (27).
RNF183	Ring Finger Protein 183	RNF183 promotes proliferation and metastasis of CRC cells via activation of NF-kB-IL-8 axis (28)
LUZP1*	Encodes a protein that contains a leucine zipper motif	Expression of LUZP1 was specifically downregulated for liver metastasis of colon carcinoma (29).
ARHGEF17*	Rho Guanine Nucleotide Exchange Factor 17	ARHGEF17 was involved in Phospholipase C signaling, which contributed to the lung metastasis from colon cancer (30).
CCDC78*	Protein coding gene whose function unknown	CCDC78 gene silencing significantly suppressed the viability, migration, and invasion of colon cancer cells (31).
LBX2*	Putative transcription factor	LBX2 was correlated with advanced tumor stage (III or IV), vascular invasion, and lymphatic invasion in colorectal cancer (32).
WFDC10B*	Encodes a member of the WAP-type four-disulfide core (WFDC) domain family	Expression of WFDC10B significantly upregulated in the hepatic metastasis of colon carcinoma (33).
PLA2G4B*	Encodes a member of the cytosolic phospholipase A2 protein family	High expression of PLA2G4B can accelerate decomposition of cell membrane phospholipid proteins, enhance cellular membrane fluidity, then increase cell adhesion and migration (34, 35).

*Susceptible genes identified in this study.

distal metastasis. The medical details of the patients are briefly summarized in **Table 2**.

Experiment Design and Sample Collection

For every patient in the cohort, three tissue samples were collected from the tumor removal surgery under authorization in advance: the tumor sample was collected at the near edge of the tumor, and the paracancer and normal samples were taken 2 cm and 5 cm away from the tumor, respectively (**Figure 1A**). Overall, 24 tissue samples of eight patients were collected. The pathological status of tissue samples was determined by standard immunohistochemistry (IHC) examination. The tissue samples were frozen in liquid nitrogen soon after the surgical excision and kept at -80° C for long-term storage.

Mutation Profiling With the Whole-Exome Sequencing

The genomic DNAs of tissue samples were extracted using the EZ-10 Spin Column Blood Genomic DNA Purification Kit (Sangon Biotech Co, Ltd., Shanghai, China). The DNA

concentration was measured by a Qubit Fluorometer and diluted to 50–300 ng/µl. For each sample, 3–5 µg of DNA was applied for quality control, and its integrity was checked by the agarose electrophoresis. The whole exome was captured using the MGIEasy Exome Library Prep Kit (BGI, Shenzhen, China) and the library for sequencing was prepared according to the manufacturer's instruction. The whole-exome sequencing (WES) was performed by the Beijing Genome Institute (BGI, Shenzhen, China) using the BGISEQ-500 platform in a 100-base pair (bp) paired-end mode.

Exome Data Preprocessing, Variants Calling, and Variant Annotation

Before variant calling, quality control was conducted to the sequencing raw data using Trimmomatic (v.0.39; parameters: LEADING=20, TRAILING=20, SLIDINGWINDOW=5:20, MINLEN=80) (51). The clean reads were mapped to the human reference genome (GRCh38.p12) using the Burrows-Wheeler Aligner (BWA, v.0.7.17; parameters: mem -t 4 -M -R) (52). We used the Genome Analysis Toolkit (GATK, v.4.1.1.0) (53) and the Samtools (v.1.9) (54) for basic processing, duplicate

TABLE 2 | Detailed information of the CRC patients.

Sample ID	Gender	Age	Pathological Diagnosis	Medication	Prognosis	10-month prognosis
N1	Female	51	RAMD, T4aN0M0, IIB	Oxaliplatin, Tegafur	Benign	Benign
N2	Male	59	RAMD, pT4aN0M0, IIB	Oxaliplatin, Capecitabine	Benign	Benign
N3	Male	53	RAMD, T4aN0M0, IIB	Oxaliplatin, Capecitabine	Benign	Benign
N4	Male	60	RAMD, pT4aN0M0, IIB	Xeloda	Benign	Benign
L1	Male	54	RAMD, pT4aN1M0, IIIB	Oxaliplatin, Capecitabine	Benign	Benign
L2	Female	48	RAMD, pT4aN1aM0, IIIB	Oxaliplatin, Capecitabine	Benign	Not Available
L3	Male	47	RAMD, T4aN2M0, IIIC	Oxaliplatin, Capecitabine	Benign	Benign
L4	Male	54	RAMD, pT4aN2bM0, IIIC	Oxaliplatin, Capecitabine	Benign	Liver and lung metastase

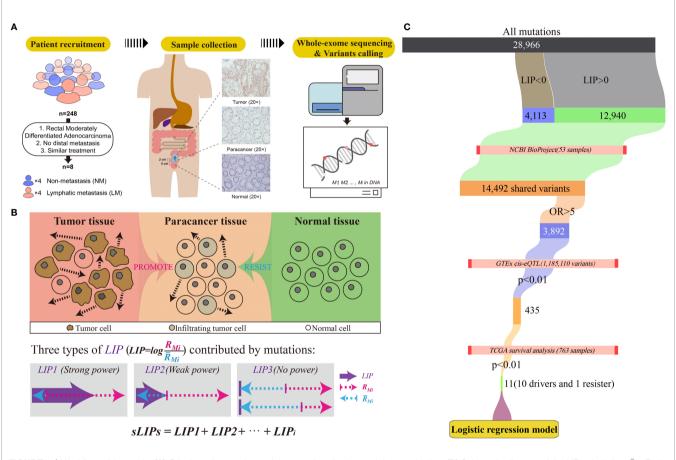


FIGURE 1 | Workflow of the study. (A) Criteria and procedures of the sample collection and tissue selection. (B) Schematic diagram of the LIP calculation. \bar{R}_{Mi} Rmi stands for the invasion promotion rate, and \bar{R}_{Mi} stands for the invasion resistance rate. (C) Schematic diagram of identification of germline driver mutations for early risk assessment of CRC metastasis.

marking, and base quality scores recalibrating (BQSR). Variant calling for germline mutations and somatic mutations was conducted using GATK HaplotypeCaller and Mutect2, respectively. The variants were further annotated with the ANNOVAR (v2019Oct24) (55).

Estimation of Tissue Purity and Ploidy

For every tumor and paracancer samples, the tissue purity and ploidy were estimated on the basis of genome-wide somatic mutation profiles with Sclust (v.1.1, -t tumor.bam -n normal.bam

-rc -minp 2 -maxp 3.5) (56), taking the corresponding normal tissue as the reference.

Calculation of Local Invasion Power

Every mutation likely plays dilemmatic roles in metastasis, promotion, or resistance. For a gene mutation, M_i if the driving potential outmatches the resisting potential, M_i is considered as the driver mutation to metastasis; otherwise, M_i is the resister mutation. To measure the summarized potential of

 M_i to local invasion, a novel parameter, namely, local invasion power (LIP), was introduced:

$$LIP_{i} = \log \frac{R_{Mi}}{\bar{R}_{Mi}}$$
(1)

where R_{Mi} and \overline{R}_{Mi} stand for the invasion promotion rate and the invasion resistance rate, respectively. The logarithm (log) took 2 as the base. R_{Mi} and \overline{R}_{Mi} were calculated by:

$$R_{Mi} = V_{MPi} / V_{MTi}$$
 (2)

$$\bar{R}_{Mi} = V_{MTi} / V_{MNi}$$
(3)

where V_{MTi} , V_{MPi} and V_{MNi} stand for the variant allele fraction (VAF) of variant M_i in tumor, paracancer, and normal tissues, respectively. They were determined by dividing reads of alternate allele M_i by total reads at this locus and further normalized by all reads count. LIP > 0 indicated that the variant M_i was prone to promoting invasion than resistance. A larger LIP suggested that the mutation had more power to drive local invasion.

Moreover, we assume that the tumor invasion is the accumulated consequence of all mutations. Some mutations likely promote tumor cells invading into nearby tissue (paracancer tissue), while some intend to resist the invasion. If the overall promotion effects at the paracancer tissue overwhelm the resistance effects, local invasion is prone to progress; otherwise, invasion unlikely happens (**Figure 1B**). We also assume that the impact of mutations on the invasion is linear. Accordingly, the invasion risk of whole mutation profiles can be simply determined by calculating the summation of LIPs (sLIPs):

$$sLIPs = \sum_{i=1}^{n} LIP_i \tag{4}$$

where n is the number of mutations involved in the analysis.

Identification of Metastasis Driver Variants

We identified potential metastasis driver variants by cascade bioinformatic analyses (Figure 1C): (1) By setting a threshold of LIP > 0, we obtained the list of invasion-promoting variants that were determined upon the CRC cohort of this study. (2) We estimated metastasis-variant association for the invasionpromoting variants by conducting the odds ratio (OR) analysis on the basis of external CRC datasets collected from the NCBI BioProject. The datasets were chosen by multiple criteria: (i) the CRC cohort consisted of both metastasis and non-metastasis cases; (ii) the mutation profiles were determined by WES; and (iii) the clinical information such as metastasis status was acquirable. Results show that three datasets met all criteria and were included in the OR analysis: PRJNA494574 (10 samples) (57), PRJNA514428 (24 samples) (58), and PRJNA246044 (19 samples) (41). Of these 53 CRC samples, 28 had either lymphatic metastasis or distal metastasis, and the remaining 25 did not observe metastasis by the time of experiment. The raw sequencing data of these datasets were downloaded and preprocessed, and germline variants were

called, following exactly the same operations as described above. For OR analysis, the contingency table was constructed and the OR values for every selected variants were calculated by:

$$OR = \frac{M_m N_n}{M_n N_m} \tag{5}$$

where M_m and M_n stand for the number of mutations and nonmutations (the wild type) at the selected allele in the metastasis group, respectively. N_m and N_n stand for the number of mutations and non-mutations at the selected allele in the non-metastasis group, respectively. As a result, a list of metastasis-associated variants with OR >5 was determined. (3) The genetic predisposition of metastasis-associated variants to patient survival was examined. For this, the gene expression level interfered by mutation was first determined according to the expression quantitative trait loci (eQTL) information derived from the Genotype-Tissue Expression (GTEx) (60). Only the significant (p < 0.01) variants to either sigmoid or transverse colons were included in the analysis, which were 1,185,110 variants in the GTEx. Having the information of mutations on gene expression levels, we then performed survival analysis subject to high or low gene expression on the basis of 763 CRC patients (including 571 colon and 192 rectum patients) from The Cancer Genome Atlas (TCGA) using the R packages survival (v3.2-3) and survminer (v0.4.8) with default parameters. As a result, we screened out eleven effective variants that could change the host gene expressions and subsequently affect the survival of patients (p < 0.01). These eleven effective variants included ten potential metastasis driver variants that may reduce the survival rate of CRC patients and one resister variant on the opposite.

Logistic Regression Model for Metastatic Risk Assessment

To aid risk assessment of early metastasis, we built a determinant classifier. The core component of classifier was a logistic regression model. The model was constructed on the basis of four exome datasets of this study and three independent CRC cohorts (NCBI BioProject: PRJNA514428, PRJNA246044, and PRJNA494574), covering a total 61 CRC patients. The datasets were split into a training set and a testing set in a combinational way (**Table 3**). The training set consisted of any three of four exome datasets, which were used for model construction and internal evaluation; the remaining dataset was taken as the testing set for external evaluation, which was independent of model construction.

The model took the mutation profiles of eleven metastasisassociated driver variants identified in this study as the input, and output the estimated probability of metastatic risk. In model construction, the input genetic mutation profile was converted into a one-dimension 11-feature binary vector **V**, corresponding to the eleven metastasis-associated variants, in which carrying the mutation was defined as 1, otherwise 0. TABLE 3 | Model construction and performance evaluation.

Dataset		Internal evaluation					External evaluation			
Training set	Testing set	AUC	Accuracy	Sensitivity	Specificity	AUC	Accuracy	Sensitivity	Specificity	
PRJNA246044, PRJNA494574, and this study	PRJNA514428	0.772	0.729	0.727	0.730	0.675	0.833	0.905	0.333	
PRJNA514428, PRJNA494574, and this study	PRJNA246044	0.834	0.738	0.750	0.700	0.793	0.842	0.736	0.600	
PRJNA514428, PRJNA246044, and this study	PRJNA494574	0.932	0.882	0.840	0.923	0.667	0.700	0.714	0.667	
PRJNA514428, PRJNA246044, PRJNA494574	This study	0.803	0.804	0.760	0.846	0.700	0.690	0.714	0.667	
Average		0.835	0.788	0.769	0.800	0.709	0.766	0.767	0.567	

$$\mathbf{V} = (V_1, V_2, ..., V_{11}) \tag{6}$$

Meanwhile, a weighted vector \mathbf{L} was prepared for \mathbf{V} , which contained the average LIPs of the eleven metastasis-associated variants determined on the basis of the training dataset.

$$L = (LIP_1, LIP_2, ..., LIP_{11})$$
(7)

Accordingly, we calculated the dot product of **V** and **L** (**V**·**L**) as the accumulated driving force of metastasis contributed by the eleven variants for the patient. For the metastasis issue (y = 1) . the probability of occurrence P (y = 1) can then be determined by the logistic regression:

$$P(y) = \frac{1}{1 + exp\left(\sum_{i=1}^{11} - w_i V_i L_i - b\right)}$$
(8)

where w_i is the regression coefficient for the variant and b is the intercept. The regression coefficient w_i and intercept b were estimated using the Maximum Likelihood Estimation (MLE) with the glm function of the R package stats (v3.6.0).

The model performance was evaluated by the conventional parameters of accuracy, sensitivity, and specificity, which were calculated with the R function confusionMatrix from the package Caret (v6.0-86) as follows:

$$Accuracy = \frac{TP + TN}{P + N} \tag{9}$$

$$Sensitivity = \frac{TP}{TP + FN}$$
(10)

$$Specificity = \frac{TN}{TN + FP}$$
(11)

where P and N stand for the positives and the negatives, respectively. The values of TP (true positives), TN (true negatives), FN (false negatives), and FP (false positives) were calculated on the basis of the confusion matrices of the classification model. The area under the receiver operating characteristic curve (AUC) was also determined with the R package pROC (v1.16.2). For evaluation of all models, the leave-one-out cross-validation (LOOCV) strategy was applied to attain unbiased estimation of training. For this purpose, the training dataset was divided 51-fold (corresponding to 51 patients), of which 50 were used for model construction and the remaining one was used for internal evaluation. The LOOCV process was repeated 51 times, and the average parameters were used to evaluate the model performance of the training set.

RESULTS

Determination of Local Invasion Power Based on Mutation Profiling

After quality control, WES of the 8-patient CRC cohort (24 tissue samples) produced an average on-target coverage of about 197×, indicating that the sequencing was substantially deep enough for reliable variant calling. Using the matched normal samples as reference, we determined the purities of tumor and paracancer tissue for every patient based on the genome-wide somatic mutation profiles. On average, the purity of tumor samples was significantly higher than that of matched paracancer samples (one-tailed paired *t*-test, p = 7.97e-4). The average purity of tumors and paracancer tissues was 0.52 and 0.33, respectively (**Figure 2A**). This result manifests that the genetic basis of paracancer tissues, though the cells have not yet exhibited a morphologically visible difference.

In the cohort, a total of 12,880 distinct and nonsynonymous somatic mutations were called, including 5,069 SNVs (singlenucleotide variants) and 8,275 indels (inserts and deletions). For every mutation, we calculated the LIP; meanwhile, we determined the summation of all mutation LIPs (namely, sLIP) for every cohort member. Regretfully, both the LIP distribution and sLIPs were unable to differentiate the lymphatic metastasis group (LM) from the non-metastasis group (NM) (**Figures 2B, C**). This finding challenges somatic mutations as the major driving force to local invasion.

Alternatively, we turned to seek clues from the germline mutations. Overall, 28,966 nonredundant nonsynonymous germline mutations were called in the cohort, including 619 nonsense SNVs, 25,169 missense SNVs, and 3,178 indels. In the same way, we calculated LIPs for every potential effective germline mutations and sLIPs for every cohort member. As illustrated in Figure 2B, the cohort members had different LIP distributions but a similar style, which the majority of LIPs valued at a narrow range. The different LIP distributions indicated different risk levels of local invasion; the larger LIP, the riskier. In general, the LM members had significantly larger LIPs than NM members (Figure 2C). The LM members all had a sLIP > 0; in contrast, the NM members all had a sLIP < 0. Furthermore, the sLIP value was positively correlated with the metastatic status of CRC (Figure 2D). For instance, patients L1 and L2 of the LM group were diagnosed as early stage of local lymphatic metastasis (N1), which had significantly lower sLIP values compared to that of patients L3 and L4 of metastasis stage N2. In particular, patient L4 who was diagnosed with liver and lung metastases 10 months after surgery had the largest sLIP value

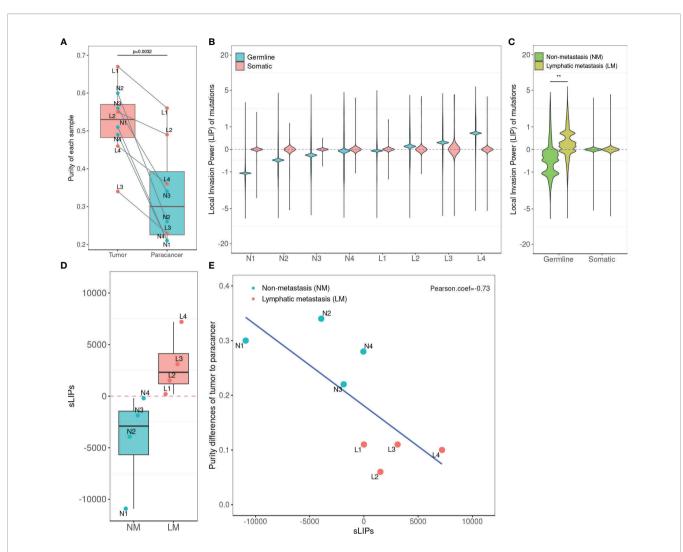


FIGURE 2 | Statistics of tumor purity in the 8-patient CRC cohort and the correlation with LIPs. (A) Purity of tumor and paracancer. The one-sided paired t-test was used to determine the difference between two groups. (B) Distribution of LIPs. The blue stands for the distribution determined on germline variants and the red stands for that on somatic variants. The *x*-axis is the subject name and the *y*-axis is the value of LIP. (C) The superimposed LIP distribution. Green stands for the non-metastasis group (NM) and yellow stands for the lymphatic metastasis group (LM). The Wilcoxon rank-sum test was used to determine the difference between the two groups. (D) The boxplot of sLIP comparison between the NM group and the LM group. (E) The Pearson correlation analysis between the sLIP and the tumor-to-paracancer purity change. **p < 0.01.

(7,204.88) in the cohort. In addition, we conducted a correlation analysis between the sLIP value and the tumor-to-paracancer purity change for every patient involved. A significant negative correlation was observed (Pearson coefficient = -0.732 and p = 0.039) (**Figure 2E**). These results suggest that the LIP value could properly reflect the contribution of mutation to the metastasis, and sLIP could serve as a good indicator of metastasis status.

Identification of Metastasis Driver Variants

As illustrated in **Figure 2C**, some variants (LIP > 0) contributed positively to metastasis. These variants were the potential driver variants that, to some extent, determined the incidence of metastasis. Hence, to identify the metastasis driver mutations consensus to most CRC cases, we conducted three-step

bioinformatic analyses (**Figure 1C**): (1) From the 8-patient cohort of this study, we extracted 13,089 distinct variants that promoted the metastasis (mean value of LIP > 0), of which 186 had mean LIP > 1. (2) Then, we affirmed the mutation-metastasis association by including 53 additional CRC cases (28 metastasis and 25 non-metastasis) from three independent cohort studies. Overall, 2,751 variants were found to be highly associated with metastasis with OR > 5, and 16 were also in the list of high metastasis-promoted variants. (3) Lastly, we examined the impact of mutations on gene expressions and thereby the penetration to metastasis *via* mining big data from the GTEx and the TCGA (763 CRC patients). In the end, we obtained ten potential driver variants to metastasis. These variants can enhance (six variants) or suppress (four variant) their parental gene expression, and all would consequently shorten the lifetime

of half survivals for an average of 31.5 months (Figure 3). There were nine SNVs (WFDC10B rs232729, LBX2 rs17009998, CCDC78 rs2071950, RGS3 rs10817493, MC1R rs885479, LUZP1 rs477830, RARS rs244903, STXBP4 rs1156287, and C6orf201 rs619483) and one insertion (ARHGEF17 rs113363731) (Table 4). Of these ten genes, five genes (WFDC10B, LBX2, CCDC78, LUZP1, and ARHGEF17) were previously reported to participate in nearby cell invasion, and lymphatic and distant CRC metastases (Table 1). Three genes (RARS, MC1R, and RGS3) were involved in tumor metastasis other than CRC (Table 4). For the remaining two genes (STXBP4 and C6orf201), their connections with metastasis have not been reported yet. However, STXBP4 can facilitate cell directional migration (61) and C6orf201 is related to the mesodermal commitment pathway (62). It is noteworthy that all these variants were common variants in the global population, owning an estimated allele frequency >10% in the ExAC database (63). Six of them even had a high frequency >60% of population. All these results suggested that the ten metastasis driver variants/ genes had a substantial population basis and could serve as good biomarkers in monitoring CRC metastasis. Other than the ten metastasis driver variants, we also detected one metastasis resister variant: PLA2G4B rs3816533 (**Table 4**). This variant was highly associated with (OR > 5) and resistant (LIP < -1) to CRC metastasis (**Figure 3K**). PLA2G4B encodes phospholipase 2A. The high expression of phospholipase 2A may accelerate decomposition of cell membrane phospholipid proteins, which enhance cellular membrane fluidity, a critical modulator of cell adhesion and migration (49). The change in cellular membrane fluidity may increase metastatic capacity (50). Notably, PLA2G4B was reported to be specifically upregulated in liver metastasis of colon carcinoma (44).

Logistic Regression Model for Early Metastatic Risk Assessment

In this study, we were also motivated to construct a logistic regression model for CRC metastatic risk assessment. The model

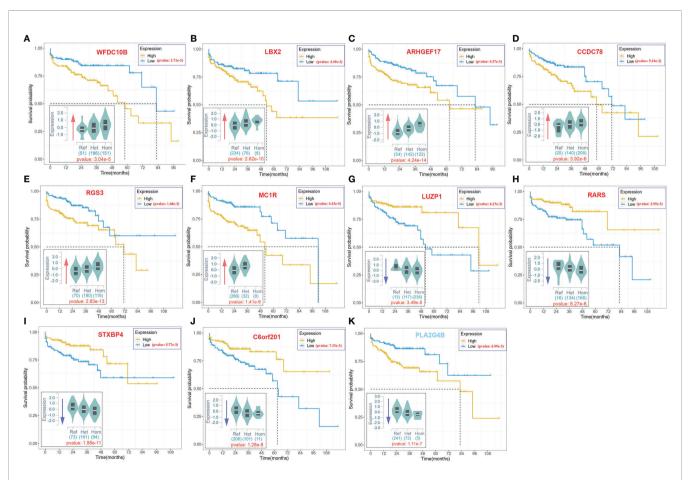


FIGURE 3 | The 10-year Kaplan–Meier survival analysis for ten metastasis driver mutations (gene symbol in red) and one resister mutation (gene symbol in blue). The violin figure at the bottom left corner in each subgraph stands for mutation effect on parental gene expression based on the cis-expression quantitative trait locus (cis-eQTL) analysis of the GTEx. The *x*-axis stands for the genotype of allele, and the *y*-axis stands for the normalized expression. The red arrow indicates upregulation of the host gene expression by the mutation. The blue arrow indicates downregulation of the host gene expression by the mutation. The blue arrow indicates downregulation of the cis-eQTL analysis. The significance of analysis is labeled in red.

dbSNP ID	Ref	Alt	Gene	Class*	Odds ratio	р (cis- eQTL)	p (Survival analysis)	Association with metastasis
rs232729	А	G	WFDC10B	MP	5.06	1.42E-09	2.71E-03	Expression of WFDC10B significantly upregulated in the hepatic metastasis of color carcinoma (33)
rs17009998	G	А	LBX2	MP	12.93	2.53E-23	4.49E-03	LBX2 was correlated with advanced tumor stage (III or IV), vascular invasion, and lymphatic invasion in colorectal cancer (32)
rs2071950	A	G	CCDC78	MP	+∞	1.98E-11	5.16E-03	CCDC78 gene silencing significantly suppressed the viability, migration, and invasion of colon cancer cells (31).
rs477830	С	Т	LUZP1	MP	+∞	3.49E-05	6.27E-03	Expression of LUZP1 was specifically downregulated for liver metastasis of colon carcinoma (29).
rs113363731	-	CTC	ARHGEF17	MP	+∞	9.55E-06	4.57E-03	Mutations on ARHGEF17 contributed to the lung metastasis from colon cancer (30).
rs244903	G	А	RARS	MP	9.05	2.83E-13	2.95E-03	ARS encodes the arginyl-tRNA synthetases involved in oral cancer cell invasiveness (61).
rs885479	G	А	MC1R	MP	9.36	1.41E-06	4.43E-05	MC1R is melanocortin 1 receptor gene directly connected with activation of cell division and metastasis in malignant melanoma (62).
rs10817493	С	G	RGS3	MP	+∞	8.27E-06	1.68E-03	Higher expression of RGS3 was associated with a larger tumor size, lymph node metastasis, and local invasion in gastric cancer (63).
rs1156287	G	А	STXBP4	MP	+∞	3.92E-06	5.77E-03	STXBP4 can facilitate cell directional migration, which plays a role in tumor metastasis with an unknown mechanism (64).
rs619483	G	С	C6orf201	MP	5.52	1.28E-08	7.33E-03	C6orf201 is related to the mesodermal commitment pathway (65).
rs3816533	С	Т	PLA2G4B	MR	5.59	1.11E-07	7.00E-3	High expression of PLA2G4B can accelerate decomposition of cell membrane phospholipid proteins, enhance cellular membrane fluidity, and then increase cell adhesion and migration (34, 35).

MP, metastasis promotion; MR, metastasis resistance.

was built on the basis of the eleven strong metastasis-associated variants (ten drivers and one resister) instead of the whole germline mutation profiles that would be much more costly in practice. The model performance was internally evaluated in a manner of LOOCV, which obtained an average result: accuracy = 0.788, specificity = 0.800, sensitivity = 0.769, and AUC = 0.839. Additional external evaluation also achieved a fairly good performance: accuracy = 0.766, specificity = 0.567, sensitivity = 0.767, and AUC = 0.709. These results affirm that the model is substantially effective for early metastatic assessment.

For user convenience, we also deployed the model as an online tool, AmetaRisk, for interactive risk assessment of CRC metastasis, which can be freely accessible at http://www.bio-add. org/AmetaRisk. The AmetaRisk was built upon an architecture of Linux + Tomcat + JSP. To initiate the assessment, the user is required to check the status (yes or no) of eleven metastasis driver/resister variants detected in the tissue samples, which can be determined on tumor, paracancer tissue, or peripheral blood. Upon submission of variant status profile, the server will return a probability value of metastatic risk, ranging from 0 to 1.0 (**Figure 4**). According to the probability value, the metastatic risk can be categorized into three status: high risk (0.75–1.0), moderate risk (0.50–0.75), and mild risk (<0.5).

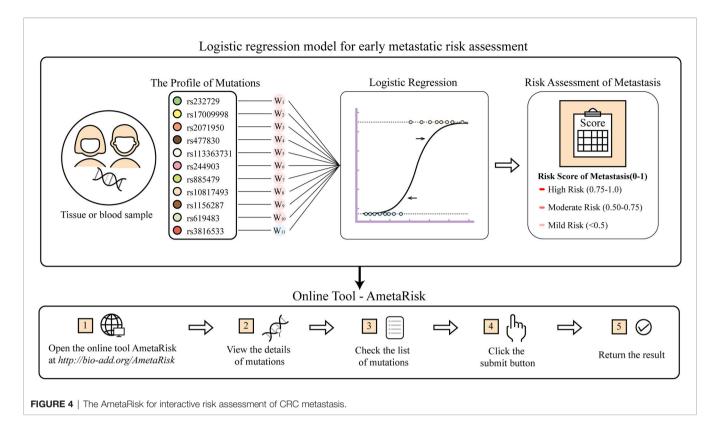
DISCUSSION

Early studies proposed that metastasis could progress *via* either a single lymphatic, hematogenous, or implantation route, or a combination of these (67). However, regardless of whichever route it may take, metastasis initiates through local invasion of tumor cells into nearby tissue (68, 69). The nearby tissue of

cancer, or so-called paracancer tissue, is usually taken as normal control in many cases, but this study as well as several previous studies challenge this opinion. Although the cell morphology of paracancer tissue exhibits a pattern similar to that of normal tissue by IHC examination, the intrinsic genetic profile could have substantially changed. As determined by WES in this study, the mutation profiles of cancer, paracancer, and normal tissues were significantly different from each other. The cancer metastasis may have progressed already before it can be detected in the clinic. This provides us a good opportunity to investigate the genetic basis underlying metastasis.

In this study, we introduced a new statistical parameter, LIP, to characterize the contribution of genetic mutation to metastasis. The LIP value was calculated on the basis of relative variant allele frequency (VAF), a surrogate measure of the proportion of DNA molecules in the tissue specimen carrying the variant (70). The VAF to some extent reflects tumor heterogeneity, which also manifests the infiltration degree of tumor cells into paracancer tissue. Surprisingly, LIPs based on somatic mutation profiles failed to differentiate patients with local lymphatic metastasis from non-metastatic patients, which challenged somatic mutations as the major driving force to local invasion. Instead, LIPs based on germline mutation profiles could reflect the different pathological status of CRC patients. In particular, sLIPs were negatively correlated with the tumor purity change between cancer and paracancer tissues. All the results suggested sLIPs as a potential indicator for metastasis.

However, using sLIP value directly to assess metastatic risk may not be a good solution; many mutations actually contributed little to metastasis (71). The tremendous background mutations will overwhelm the true signals and thus lead to inaccurate metastatic risk assessment. Therefore, we mined the driver/ resister variants that contributed most to the metastasis. Unlike



previous studies that sought highly concordant genomic variants between primary and metastatic CRCs or metastasis-specific variants (6), we aimed at variants that drove local spread of tumor cells into paracancer tissue. For this purpose, we examined variant contribution to local invasion, variant-metastasis association, and variant impact on parental gene expression and patient survival. As a result, ten driver variants and one resister variant were identified. Similar attempts have not been reported previously. Upon these potential metastasis driver variants, we constructed a logistic regression model for early metastatic risk assessment and further deployed it as an online tool, AmetaRisk. To the best of our knowledge, this model would be the first model that makes quantitative risk assessment at the very early stage of metastasis before it actually occurs.

Last but not the least, unlike many studies that took somatic mutations as pathogenic drivers or biomarkers (72), this study was grounded on the hypothesis that germline mutations (inherited from the last generation) might be responsible for the "born-to-bebad" characteristics of tumors, in which malignant progression has been determined long before visible invasion and metastasis were actually observed (73). Previous studies also identified several metastasis-associated germline variations, some of which were taken as prognosis markers of metastasis (74, 75). Many of them, such as KRAS, NRAS, BRAF, PIK3CA, and TP53, were also known as oncogenes. In **Table 1**, we summarized 18 potential metastasis driver genes/mutations identified to date. Comparing the gene list with the eleven driver/resister genes identified in this study, five genes (ARHGEF17, CCDC78, LBX2, LUZP1, and WFDC10B) were in common. These mutual genes have been reported to participate in the metastatic/invasive process. For instance, LBX2 is a transcription factor that is involved in diverse physiological processes and tumorigenesis. Upregulation of LBX2 in CRC may be associated with advanced tumor stage (III or IV), vascular invasion, and lymphatic invasion, which can be caused by the hypermethylation of LBX2 (59). ARHGEF17 (Rho Guanine Nucleotide Exchange Factor 17) contributes to the lung metastasis from colon cancer *via* participation in "phospholipase C signaling" (60).

We acknowledge that this study has several limitations. First of all, due to the difficulty of simultaneously collecting tumor, paracancer, and normal tissues, the study was demonstrated in a small cohort of eight patients. This may cause bias in LIP calculation and subsequent driver variant identification. Recently, WES studies of two larger CRC cohorts (146 patients and 618 patients, respectively) with a similar experiment design were reported (77, 78). Unfortunately, we were unable to acquire these datasets for mutation profile calling by all means. To complement the data gap, we strengthened the identification of metastasis driver variants by incorporating as many valid datasets derived from public databases such as NCBI, TCGA, and GTEx as possible. Moreover, this study focused on seeking inborn genetic bases of metastasis. However, both germline and somatic variants could together contribute to metastasis, as well as several other genetic features such as copy number variation (CNV) and structural variant (SV). Furthermore, this study used only eleven selected driver variants for metastatic risk assessment. The good part is that the variant selection largely reduces the tremendous background noise and enables achieving

good performance under the circumstance of the small dataset (cohort). The bad part is that the simplified model may miss some useful information for a better performance. To improve this work, experimental validation of metastasis driver variants and involvement of more highly metastasis-associated variants are thus desired.

CONCLUSION

In summary, we made a valuable attempt in this study to explore the genetic basis underlying CRC metastasis. Our efforts will provide new insights into the mechanistic understanding of early metastasis, as a complement to current metastasis hypotheses such as "seed and soil", "big-bang", and "tumor self-seeding". Moreover, we constructed a machine learning model for metastatic risk assessment at the early stage of local invasion. This model and its online tool, AmetaRisk, provide a rapid and economic way to assist in prioritizing a precise therapeutic regimen in advance and increasing the survival rate of CRC patients in clinics.

DATA AVAILABILITY STATEMENT

The datasets presented in this study can be found in online repositories. The names of the repository/repositories and

REFERENCES

- Abraham AD, Esquer H, Zhou Q, Tomlinson N, Hamill BD, Abbott JM, et al. Drug Design Targeting T-Cell Factor-Driven Epithelial-Mesenchymal Transition as a Therapeutic Strategy for Colorectal Cancer. J Med Chem (2019) 62(22):10182–203. doi: 10.1021/acs.jmedchem.9b01065
- Augestad KM, Merok MA, Ignatovic D. Tailored Treatment of Colorectal Cancer: Surgical, Molecular, and Genetic Considerations. *Clin Med Insights Oncol* (2017) 11:1179554917690766. doi: 10.1177/1179554917690766
- Fares J, Fares MY, Khachfe HH, Salhab HA, Fares Y. Molecular Principles of Metastasis: A Hallmark of Cancer Revisited. *Signal Transduct Tar Ther* (2020) 5(1):28. doi: 10.1038/s41392-020-0134-x
- Yaeger R, Chatila WK, Lipsyc MD, Hechtman JF, Cercek A, Sanchez-Vega F, et al. Clinical Sequencing Defines the Genomic Landscape of Metastatic Colorectal Cancer. *Cancer Cell* (2018) 33(1):125–36:e123. doi: 10.1016/ j.ccell.2017.12.004
- Testa U, Castelli G, Pelosi E. Genetic Alterations of Metastatic Colorectal Cancer. *Biomedicines* (2020) 8(10):414. doi: 10.3390/biomedicines8100414
- Bhullar DS, Barriuso J, Mullamitha S, Saunders MP, O'Dwyer ST, Aziz O. Biomarker Concordance Between Primary Colorectal Cancer and its Metastases. *EBioMedicine* (2019) 40:363–74. doi: 10.1016/j.ebiom.2019. 01.050
- Brannon AR, Vakiani E, Sylvester BE, Scott SN, McDermott G, Shah RH, et al. Comparative Sequencing Analysis Reveals High Genomic Concordance Between Matched Primary and Metastatic Colorectal Cancer Lesions. *Genome Biol* (2014) 15(8):454. doi: 10.1186/s13059-014-0454-7
- Reiter JG, Makohon-Moore AP, Gerold JM, Heyde A, Attiyeh MA, Kohutek ZA, et al. Minimal Functional Driver Gene Heterogeneity Among Untreated Metastases. *Science* (2018) 361(6406):1033–7. doi: 10.1126/ science.aat7171
- 9. Vakiani E, Janakiraman M, Shen R, Sinha R, Zeng Z, Shia J, et al. Comparative Genomic Analysis of Primary Versus Metastatic Colorectal Carcinomas. *J Clin Oncol* (2012) 30(24):2956–62. doi: 10.1200/JCO.2011.38.2994

accession number(s) can be found at: https://ngdc.cncb.ac.cn/gvm/ (accession number: GVM000184).

ETHICS STATEMENT

The studies involving human participants were reviewed and approved by the Ethics Committee of Xiamen Xianyue Hospital. The patients/participants provided their written informed consent to participate in this study.

AUTHOR CONTRIBUTIONS

Z-LJ and PY designed and supervised the study. PY, Z-XF, Z-YL, and Z-YZ collected the samples, performed the clinical diagnosis, and prepared the samples for sequencing. R-FD, YZ, and L-YW analyzed the data, and drafted and revised the manuscript. Z-LJ and PY commented on and revised the manuscript. All authors contributed to the article and approved the submitted version.

FUNDING

This work was supported by the National Key Research & Developmental Program of China (2018YFC1003601).

- Tan IB, Malik S, Ramnarayanan K, McPherson JR, Ho DL, Suzuki Y, et al. High-Depth Sequencing of Over 750 Genes Supports Linear Progression of Primary Tumors and Metastases in Most Patients With Liver-Limited Metastatic Colorectal Cancer. *Genome Biol* (2015) 16:32. doi: 10.1186/ s13059-015-0589-1
- Sutton PA, Jithesh PV, Jones RP, Evans JP, Vimalachandran D, Malik HZ, et al. Exome Sequencing of Synchronously Resected Primary Colorectal Tumours and Colorectal Liver Metastases to Inform Oncosurgical Management. *Eur J Surg Oncol* (2018) 44(1):115–21. doi: 10.1016/j.ejso.2017.10.211
- Rumpold H, Niedersuss-Beke D, Heiler C, Falch D, Wundsam HV, Metz-Gercek S, et al. Prediction of Mortality in Metastatic Colorectal Cancer in a Real-Life Population: A Multicenter Explorative Analysis. *BMC Cancer* (2020) 20(1):1149. doi: 10.1186/s12885-020-07656-w
- Siyar Ekinci A, Demirci U, Cakmak Oksuzoglu B, Ozturk A, Esbah O, Ozatli T, et al. and Metastatic Tumor in Patients With Metastatic Colorectal Carcinoma. J BUON (2015) 20(1):128–35.
- Kopetz S, Overman MJ, Chen K, Lucio-Eterovic AK, Kee BK, Fogelman DR, et al. Mutation and Copy Number Discordance in Primary Versus Metastatic Colorectal Cancer (mCRC). J Clin Oncol (2014) 32(15_suppl):3509. doi: 10.1200/jco.2014.32.15_suppl.3509
- Ishaque N, Abba ML, Hauser C, Patil N, Paramasivam N, Huebschmann D, et al. Whole Genome Sequencing Puts Forward Hypotheses on Metastasis Evolution and Therapy in Colorectal Cancer. *Nat Commun* (2018) 9(1):4782. doi: 10.1038/s41467-018-07041-z
- Xie T, Cho YB, Wang K, Huang D, Hong HK, Choi YL, et al. Patterns of Somatic Alterations Between Matched Primary and Metastatic Colorectal Tumors Characterized by Whole-Genome Sequencing. *Genomics* (2014) 104 (4):234–41. doi: 10.1016/j.ygeno.2014.07.012
- Vermaat JS, Nijman IJ, Koudijs MJ, Gerritse FL, Scherer SJ, Mokry M, et al. Primary Colorectal Cancers and Their Subsequent Hepatic Metastases are Genetically Different: Implications for Selection of Patients for Targeted Treatment. *Clin Cancer Res* (2012) 18(3):688–99. doi: 10.1158/1078-0432.CCR-11-1965

- Jiang H, Tang E, Xu D, Chen Y, Zhang Y, Tang M, et al. Development and Validation of Nomograms for Predicting Survival in Patients With non-Metastatic Colorectal Cancer. *Oncotarget* (2017) 8(18):29857–64. doi: 10.18632/oncotarget.16167
- Li Y, Liu W, Zhao L, Gungor C, Xu Y, Song X, et al. Nomograms Predicting Overall Survival and Cancer-Specific Survival for Synchronous Colorectal Liver-Limited Metastasis. J Cancer (2020) 11(21):6213–25. doi: 10.7150/jca.46155
- Mo S, Cai X, Zhou Z, Li Y, Hu X, Ma X, et al. Nomograms for Predicting Specific Distant Metastatic Sites and Overall Survival of Colorectal Cancer Patients: A Large Population-Based Real-World Study. *Clin Transl Med* (2020) 10(1):169–81. doi: 10.1002/ctm2.20
- Huang YQ, Liang CH, He L, Tian J, Liang CS, Chen X, et al. Development and Validation of a Radiomics Nomogram for Preoperative Prediction of Lymph Node Metastasis in Colorectal Cancer. J Clin Oncol (2016) 34(18):2157–64. doi: 10.1200/JCO.2015.65.9128
- Wu S, Zheng J, Li Y, Yu H, Shi S, Xie W, et al. A Radiomics Nomogram for the Preoperative Prediction of Lymph Node Metastasis in Bladder Cancer. *Clin Cancer Res* (2017) 23(22):6904–11. doi: 10.1158/1078-0432.CCR-17-1510
- Zhu J, Xu WG, Xiao H, Zhou Y. [Application of a Radiomics Model for Preding Lymph Node Metastasis in Non-Small Cell Lung Cancer]. Sichuan Da Xue Xue Bao Yi Xue Ban (2019) 50(3):373–8.
- 24. Zhou SC, Liu TT, Zhou J, Huang YX, Guo Y, Yu JH, et al. An Ultrasound Radiomics Nomogram for Preoperative Prediction of Central Neck Lymph Node Metastasis in Papillary Thyroid Carcinoma. *Front Oncol* (2020) 10:1591. doi: 10.3389/fonc.2020.01591
- Kuo MD, Jamshidi N. Behind the Numbers: Decoding Molecular Phenotypes With Radiogenomics–Guiding Principles and Technical Considerations. *Radiology* (2014) 270(2):320–5. doi: 10.1148/radiol.13132195
- Kandimalla R, Ozawa T, Gao F, Wang X, Goel A, Group TCCS. Gene Expression Signature in Surgical Tissues and Endoscopic Biopsies Identifies High-Risk T1 Colorectal Cancers. *Gastroenterology* (2019) 156(8):2338– 2341.e2333. doi: 10.1053/j.gastro.2019.02.027
- Ozawa T, Kandimalla R, Gao F, Nozawa H, Hata K, Nagata H, et al. A MicroRNA Signature Associated With Metastasis of T1 Colorectal Cancers to Lymph Nodes. *Gastroenterology* (2018) 154844-848(4):e847. doi: 10.1053/ j.gastro.2017.11.275
- Kamiyama H, Noda H, Konishi F, Rikiyama T. Molecular Biomarkers for the Detection of Metastatic Colorectal Cancer Cells. World J Gastroenterol (2014) 20(27):8928–38. doi: 10.3748/wjg.v20.i27.8928
- Lee MKC, Loree JM. Current and Emerging Biomarkers in Metastatic Colorectal Cancer. Curr Oncol (2019) 26(Suppl 1):S7–S15. doi: 10.3747/ co.26.5719
- Zhang Y, Fang N, You J, Zhou Q. [Advances in the Relationship Between Tumor Cell Metabolism and Tumor Metastasis]. *Zhongguo Fei Ai Za Zhi* (2014) 17(11):812–8. doi: 10.3779/j.issn.1009-3419.2014.11.07
- Lambert AW, Pattabiraman DR, Weinberg RA. Emerging Biological Principles of Metastasis. *Cell* (2017) 168(4):670-91. doi: 10.1016/ j.cell.2016.11.037
- Schwager SC, Taufalele PV, Reinhart-King CA. Cell-Cell Mechanical Communication in Cancer. Cell Mol Bioeng (2019) 12(1):1–14. doi: 10.1007/s12195-018-00564-x
- Huang D, Sun W, Zhou Y, Li P, Chen F, Chen H, et al Mutations of Key Driver Genes in Colorectal Cancer Progression and Metastasis. *Cancer Metastasis Rev* (2018) 37(1):173–87. doi: 10.1007/s10555-017-9726-5
- Maffeis V, Nicole L, Cappellesso R Ras, Cellular Plasticity, and Tumor Budding in Colorectal Cancer. *Front Oncol* (2019) 9:1255. Epub 2019/12/06. doi: 10.3389/fonc.2019.01255.
- Hou J, Zhang Y, Zhu Z Gene Heterogeneity in Metastasis of Colorectal Cancer to the Lung. Semin Cell Dev Biol (2017) 64:58–64. doi: 10.1016/ j.semcdb.2016.08.034
- 36. Fadhlullah SFB, Halim NBA, Yeo JYT, Ho RLY, Um P, Ang BT, et al Pathogenic Mutations in Neurofibromin Identifies a Leucine-Rich Domain Regulating Glioma Cell Invasiveness. Oncogene (2019) 38(27):5367–80. doi: 10.1038/s41388-019-0809-3
- Coronel-Hernandez J, Lopez-Urrutia E, Contreras-Romero C, Delgado-Waldo I, Figueroa-Gonzalez G, Campos-Parra AD, et al Cell Migration and Proliferation Are Regulated by Mir-26a in Colorectal Cancer Via the Pten-Akt Axis. *Cancer Cell Int* (2019) 19:80. doi: 10.1186/s12935-019-0802-5

- Sakai E, Nakayama M, Oshima H, Kouyama Y, Niida A, Fujii S, et al Combined Mutation of Apc, Kras, and Tgfbr2 Effectively Drives Metastasis of Intestinal Cancer. *Cancer Res* (2018) 78(5):1334–46. doi: 10.1158/0008-5472.CAN-17-3303
- Oner MG, Rokavec M, Kaller M, Bouznad N, Horst D, Kirchner T, et al Combined Inactivation of Tp53 and Mir34a Promotes Colorectal Cancer Development and Progression in Mice Via Increasing Levels of Il6r and Pail. *Gastroenterology* (2018) 155(6):1868–82. doi: 10.1053/gastro.2018.08.011.
- Voorneveld PW, Kodach LL, Jacobs RJ, Liv N, Zonnevylle AC Hoogenboom JP Loss of Smad4 Alters Bmp Signaling to Promote Colorectal Cancer Cell Metastasis Via Activation of Rho and Rock. *Gastroenterology* (2014) 147 (1):196–208.e13. doi: 10.1053/j.gastro.2014.03.052.
- 41. Forgo E, Gomez AJ, Steiner D, Zehnder J, Longacre TA Morphological, Immunophenotypical and Molecular Features of Hypermutation in Colorectal Carcinomas with Mutations in DNA Polymerase Epsilon (Pole). *Histopathology* (2020) 76(3):366–74. doi: 10.1111/his.13984.
- 42. Zhang M, Miao F, Huang R, Liu W, Zhao Y, Jiao T, et al Rhbdd1 Promotes Colorectal Cancer Metastasis through the Wnt Signaling Pathway and Its Downstream Target Zeb1. J Exp Clin Cancer Res (2018) 37(1):22. doi: 10.1186/ s13046-018-0687-5.
- Geng R, Tan X, Wu J, Pan Z, Yi M, Shi W, et al Rnf183 Promotes Proliferation and Metastasis of Colorectal Cancer Cells Via Activation of Nf-Kappab-Il-8 Axis. *Cell Death Dis* (2017) 8(8):e2994. doi: 10.1038/cddis.2017.400.
- 44. Liu J, Wang D, Zhang C, Zhang Z, Chen X, Lian J, et al. Identification of Liver Metastasis-Associated Genes in Human Colon Carcinoma by mRNA Profiling. *Chin J Cancer Res* (2018) 30(6):633–46. doi: 10.21147/j.issn.1000-9604.2018.06.08
- 45. Fang LT, Lee S, Choi H, Kim HK, Jew G, Kang HC, et al. Comprehensive Genomic Analyses of a Metastatic Colon Cancer to the Lung by Whole Exome Sequencing and Gene Expression Analysis. *Int J Oncol* (2014) 44(1):211–21. doi: 10.3892/ijo.2013.2150
- Huang Shi-Fang CY-F, Ying S, Lu Z, Shao-Hui T Screening of Differentially Expressed Genes in Colorectal Cancer Based on Tcga Database and Verification of Novel Gene Ccdc78. *Chin J Pathophysiol* (2020) 36(6):998– 1005. doi: 10.3969/j.issn.1000-4718.2020.06.006.
- Huang X, Yang Y, Yang C, Li H, Cheng H, Zheng Y. Overexpression of LBX2 Associated With Tumor Progression and Poor Prognosis in Colorectal Cancer. Oncol Lett (2020) 19(6):3751–60. doi: 10.3892/ol.2020.11489
- Lan H, Jin K, Xie B, Han N, Cui B, Cao F, et al Heterogeneity between Primary Colon Carcinoma and Paired Lymphatic and Hepatic Metastases. *Mol Med Rep* (2012) 6(5):1057-68. doi: 10.3892/mmr.2012.1051
- Matsuzaki T, Matsumoto S, Kasai T, Yoshizawa E, Okamoto S, Yoshikawa HY, et al. Defining Lineage-Specific Membrane Fluidity Signatures That Regulate Adhesion Kinetics. *Stem Cell Rep* (2018) 11(4):852–60. doi: 10.1016/j.stemcr.2018.08.010
- 50. Chang JT. EMT and Breast Cancer Metastasis Driven by Plasma Membrane Fluidity. AACR (2015).
- Bolger AM, Lohse M, Usadel B. Trimmomatic: A Flexible Trimmer for Illumina Sequence Data. *Bioinformatics* (2014) 30(15):2114-20. doi: 10.1093/bioinformatics/btu170
- Li H, Durbin R. Fast and Accurate Short Read Alignment With Burrows-Wheeler Transform. *Bioinformatics* (2009) 25(14):1754–60. doi: 10.1093/ bioinformatics/btp324
- McKenna A, Hanna M, Banks E, Sivachenko A, Cibulskis K, Kernytsky A, et al. The Genome Analysis Toolkit: A MapReduce Framework for Analyzing Next-Generation DNA Sequencing Data. *Genome Res* (2010) 20(9):1297–303. doi: 10.1101/gr.107524.110
- Li H, Handsaker B, Wysoker A, Fennell T, Ruan J, Homer N, et al. The Sequence Alignment/Map Format and SAMtools. *Bioinformatics* (2009) 25 (16):2078–9. doi: 10.1093/bioinformatics/btp352
- Wang K, Li M, Hakonarson H. ANNOVAR: Functional Annotation of Genetic Variants From High-Throughput Sequencing Data. *Nucleic Acids Res* (2010) 38(16):e164. doi: 10.1093/nar/gkq603
- Cun Y, Yang TP, Achter V, Lang U, Peifer M. Copy-Number Analysis and Inference of Subclonal Populations in Cancer Genomes Using Sclust. Nat Protoc (2018) 13(6):1488–501. doi: 10.1038/nprot.2018.033
- 57. Intarajak T, Udomchaiprasertkul W, Bunyoo C, Yimnoon J, Soonklang K, Wiriyaukaradecha K, et al. Genetic Aberration Analysis in Thai Colorectal

Adenoma and Early-Stage Adenocarcinoma Patients by Whole-Exome Sequencing. *Cancers (Basel)* (2019) 11(7):977. doi: 10.3390/cancers11070977

- Nikolaev SI, Sotiriou SK, Pateras IS, Santoni F, Sougioultzis S, Edgren H, et al. A Single-Nucleotide Substitution Mutator Phenotype Revealed by Exome Sequencing of Human Colon Adenomas. *Cancer Res* (2012) 72(23):6279–89. doi: 10.1158/0008-5472.CAN-12-3869
- Lim B, Mun J, Kim JH, Kim CW, Roh SA, Cho DH, et al. Genome-Wide Mutation Profiles of Colorectal Tumors and Associated Liver Metastases at the Exome and Transcriptome Levels. *Oncotarget* (2015) 6(26):22179–90. doi: 10.18632/oncotarget.4246
- GTEx Consortium. Genetic Effects on Gene Expression Across Human Tissues. Nature (2017) 550(7675):204–13. doi: 10.1038/nature24277
- Kanehisa M, Goto S. KEGG: Kyoto Encyclopedia of Genes and Genomes. Nucleic Acids Res (2000) 28(1):27–30. doi: 10.1093/nar/28.1.27
- Karczewski KJ, Weisburd B, Thomas B, Solomonson M, Ruderfer DM, Kavanagh D, et al. The ExAC Browser: Displaying Reference Data Information From Over 60 000 Exomes. *Nucleic Acids Res* (2017) 45(D1): D840–5. doi: 10.1093/nar/gkw971
- Matsuzaki T, Matsumoto S, Kasai T, Yoshizawa E, Okamoto S, Yoshikawa HY, et al. Defining Lineage-Specific Membrane Fluidity Signatures That Regulate Adhesion Kinetics. *Stem Cell Rep* (2018) 11(4):852-60. doi: 10.1016/j.stemcr.2018.08.010
- Lee CW, Chang KP, Chen YY, Liang Y, Hsueh C, Yu JS, et al Overexpressed Tryptophanyl-Trna Synthetase, an Angiostatic Protein, Enhances Oral Cancer Cell Invasiveness. *Oncotarget* (2015) 6(26):21979–92. doi: 10.18632/ oncotarget.4273.
- Rosenkranz AA, Slastnikova TA, Durymanov MO, Sobolev AS Malignant Melanoma and Melanocortin 1 Receptor. *Biochemistry (Mosc)* (2013) 78 (11):1228–37. doi: 10.1134/S0006297913110035.
- 66. Li W, Si X, Yang J, Zhang J, Yu K, Cao Y. Regulator of G-Protein Signalling 3 and Its Regulator Microrna-133a Mediate Cell Proliferation in Gastric Cancer. *Arab J Gastroenterol* (2020) 21(4):237-45. doi: 10.1016/jajg.2020.07.011.
- Wong SY, Hynes RO. Lymphatic or Hematogenous Dissemination: How Does a Metastatic Tumor Cell Decide? *Cell Cycle* (2006) 5(8):812–7. doi: 10.4161/ cc.5.8.2646
- van Zijl F, Krupitza G, Mikulits W. Initial Steps of Metastasis: Cell Invasion and Endothelial Transmigration. *Mutat Res* (2011) 728(1-2):23–34. doi: 10.1016/j.mrrev.2011.05.002
- Martin TA, Ye L, Sanders AJ, Lane J, Jiang WG. Cancer Invasion and Metastasis: Molecular and Cellular Perspective," in *Madame Curie Bioscience Database* [Internet]. Landes Biosci (2013). Austin (TX): Landes Biosci (2000-2013).
- Strom SP. Current Practices and Guidelines for Clinical Next-Generation Sequencing Oncology Testing. *Cancer Biol Med* (2016) 13(1):3–11. doi: 10.28092/j.issn.2095-3941.2016.0004

- Penney ME, Parfrey PS, Savas S, Yilmaz YE. A Genome-Wide Association Study Identifies Single Nucleotide Polymorphisms Associated With Time-to-Metastasis in Colorectal Cancer. *BMC Cancer* (2019) 19(1):133. doi: 10.1186/ s12885-019-5346-5
- Nemtsova MV, Kalinkin AI, Kuznetsova EB, Bure IV, Alekseeva EA, Bykov II, et al. Clinical Relevance of Somatic Mutations in Main Driver Genes Detected in Gastric Cancer Patients by Next-Generation DNA Sequencing. *Sci Rep* (2020) 10(1):504. doi: 10.1038/s41598-020-57544-3
- Sottoriva A, Kang H, Ma Z, Graham TA, Salomon MP, Zhao J, et al. A Big Bang Model of Human Colorectal Tumor Growth. *Nat Genet* (2015) 47 (3):209–16. doi: 10.1038/ng.3214
- Hsieh SM, Lintell NA, Hunter KW. Germline Polymorphisms are Potential Metastasis Risk and Prognosis Markers in Breast Cancer. *Breast Dis* (2006) 26:157–62. doi: 10.3233/bd-2007-26114
- Hunter K. Host Genetics Influence Tumour Metastasis. Nat Rev Cancer (2006) 6(2):141–6. doi: 10.1038/nrc1803
- Lee M, Crawford NP. Defining the Influence of Germline Variation on Metastasis Using Systems Genetics Approaches. Adv Cancer Res (2016) 132:73–109. doi: 10.1016/bs.acr.2016.07.003
- 77. Gong R, He Y, Liu XY, Wang HY, Sun LY, Yang XH, et al. Mutation Spectrum of Germline Cancer Susceptibility Genes Among Unselected Chinese Colorectal Cancer Patients. *Cancer Manag Res* (2019) 11:3721–39. doi: 10.2147/CMAR.S193985
- Li C, Sun YD, Yu GY, Cui JR, Lou Z, Zhang H, et al. Integrated Omics of Metastatic Colorectal Cancer. *Cancer Cell* (2020) 38(5):734–747.e739. doi: 10.1016/j.ccell.2020.08.002

Conflict of Interest: The authors declare that the research was conducted in the absence of any commercial or financial relationships that could be construed as a potential conflict of interest

Publisher's Note: All claims expressed in this article are solely those of the authors and do not necessarily represent those of their affiliated organizations, or those of the publisher, the editors and the reviewers. Any product that may be evaluated in this article, or claim that may be made by its manufacturer, is not guaranteed or endorsed by the publisher.

Copyright © 2022 Ding, Zhang, Wu, You, Fang, Li, Zhang and Ji. This is an openaccess article distributed under the terms of the Creative Commons Attribution License (CC BY). The use, distribution or reproduction in other forums is permitted, provided the original author(s) and the copyright owner(s) are credited and that the original publication in this journal is cited, in accordance with accepted academic practice. No use, distribution or reproduction is permitted which does not comply with these terms.



The Effect of Hypoxia-Induced Exosomes on Anti-Tumor Immunity and Its Implication for Immunotherapy

Wenwen Guo^{1†}, Tianyun Qiao^{2†}, Bingwei Dong^{1†}, Tian Li^{3*}, Qiang Liu^{1*} and Xiaofeng Xu^{1*}

¹ Clinical Research Center, Xianyang Central Hospital, Xianyang, China, ² Department of Thoracic Surgery, Tangdu Hospital, Fourth Military Medical University, Xi'an, China, ³ School of Basic Medicine, Fourth Military Medical University, Xi'an, China

OPEN ACCESS

Edited by:

Dianwen Ju, Fudan University, China

Reviewed by:

Jafar Rezaie, Urmia University of Medical Sciences, Iran Jessy Deshane, University of Alabama at Birmingham, United States

*Correspondence:

Xiaofeng Xu 1536238305@qq.com Qiang Liu drliuqiang1978@163.com Tian Li tian@fmmu.edu.cn [†]These authors have contributed equally to this work

Specialty section:

This article was submitted to Cancer Immunity and Immunotherapy, a section of the journal Frontiers in Immunology

Received: 08 April 2022 Accepted: 30 May 2022 Published: 22 June 2022

Citation:

Guo W, Qiao T, Dong B, Li T, Liu Q and Xu X (2022) The Effect of Hypoxia-Induced Exosomes on Anti-Turnor Immunity and Its Implication for Immunotherapy. Front. Immunol. 13:915985. doi: 10.3389/fimmu.2022.915985 Hypoxia is a critical feature of solid tumors and is considered to be a key factor in promoting tumorigenesis and progression. Beyond inducing metabolic reprogramming of tumor cells to adapt to the hypoxia tumor microenvironment (TME), hypoxia can also promote tumor growth by affecting the secretion of exosomes. Exosomes are nano-sized (30-150 nm in diameter) extracellular vesicles that can carry numerous substances including lipids, proteins, nucleic acids, and metabolites. Notably, hypoxia-induced exosomes alterations not only exist in tumor cells, but also in various TME cells including stromal cells and immune cells. Besides promoting tumor invasion, angiogenesis, and drug resistance, the secretion of these altered exosomes has recently been found to negatively regulate anti-tumor immune responses. In this review, we focus on the hypoxia-induced changes in exosome secretion and found it can contributes to immune evasion and cancer progression by recruiting protumor immune cells into TME, as well as inhibiting antitumor immune cells. Next, we also describe the recent advances of exosomes in immunotherapy and future direction. In conclusion, ongoing discoveries in this field have brought new insights into hypoxia exosome-led immunosuppression, enabling the development of exosome-based therapeutics and elucidating their potential in immunotherapy.

Keywords: hypoxia, exosomes, immunotherapy, tumor microenvironment, anti-tumor immunity

INTRODUCTION

The tumor microenvironment (TME) is a complex and highly heterogeneous environment, which is composed of blood vessels, immune cells, fibroblasts, extracellular matrix, signaling molecules (i.e., chemokines, cytokines, growth factors, etc.), and metabolic wastes (e.g., lactic acid) (1). Hypoxia (low oxygen concentration) is a major feature of the TME in most solid tumors and has been reported to be associated with tumor progression, therapy resistance, and poor clinical prognosis (2). Hypoxia is caused by the increased oxygen demand of rapid tumor tissue proliferation and insufficient oxygen supply due to tumor vascular defects. In general, tumors can improve oxygen supply by activating hypoxia-inducible factor (HIF) to promote tumor neo-angiogenesis (3).

Notably, hypoxia not only regulates tumor angiogenesis and metabolic reprogramming but also mediates tumor immune escape, invasion, and metastasis, as well as therapeutic drug resistance (4). Therefore, in the past decades, hypoxia TMEs have received extensive research attention and are regarded as an important target for tumor therapy. Drugs that improve tumor hypoxia, such as bevacizumab and topotecan, have been widely used in the clinical treatment of various tumors and significantly improve the prognosis of patients (5). Noteworthy, a growing number of new findings indicate that hypoxia can also affect tumor growth, invasion, and metastasis, as well as anti-tumor immunity by regulating the secretion of exosomes in the TME (6). Therefore, targeting hypoxia-induced exosomes may be the next key breakthrough in ameliorating the adverse effects of tumor hypoxia, as well as promoting the effect of tumor immunotherapy.

Exosomes are nanoscale bilayer vesicles released by various cell types (tumor cells, stromal cells, immune cells, etc.) upon fusion of multivesicular bodies with the plasma membrane (7). They carry various genetic information from parental cells and are deeply involved in the exchange of information between cells (8, 9). Therefore, the size and cargo of an exosome are directly determined by its cell of origin (10, 11). In addition, the size and cargo variables are also greatly affected by TME, such as hypoxia and acidic microenvironment (12). However, the exact mechanism of the association between exosomes and hypoxia during tumor progression needs further elucidation. Studies have shown that typical exosomes have a diameter of 30-150 nm and are usually cup-shaped (13). They all contain multiple types of proteins (such as Rab GTPases, annexin, heat shock proteins HSP60 and HSP905-7) and lipids (e.g., ceramides, cholesterol, and glycerophospholipids), nucleic acids (i.e., mRNAs, microRNAs, circRNAs, and long non-coding RNAs), and metabolites (14, 15). They are present in almost all body fluids, including blood, sweat, tears, urine, ascites, to cerebrospinal fluid. Exosomes were originally thought to be the "dumpster" of cells (16). This view remained unchanged until 1996 when Raposo et al. found that exosomes can affect the function of immune cells (17). However, subsequent studies on exosome functions have revealed their critical roles in intercellular communication, antigen presentation, cell differentiation, antitumor immune response, tumor cell migration, and invasion (15). Therefore, the exact mechanism of the association between exosomes and hypoxia during tumor progression needs further elucidation.

REGULATION OF HYPOXIA ON EXOSOMES

As mentioned above, the hypoxia TME can regulate processes such as exosome formation, loading, and release of cargo, which in turn affects intercellular communication at local and distant sites. Multiple studies have shown that tumor cells regulate the secretion of exosomes, as well as the size and distribution of exosomes through HIF-1 under hypoxia conditions (18). For instance, Li et al. found a marked increase in the number of miRNAs in exosomes secreted by oral squamous cell carcinoma (OSCC) cells under hypoxia conditions. Further mechanistic studies found that the up-regulation of miRNAs in exosomes, especially miRNA-21, was mediated by HIF-1 α and HIF-2 α , while closely related to tumor stage and lymph node metastasis in patients with OSCC (19). Similarly, Wang et al. exposed three human breast cancer cell lines to a hypoxia environment ($1\% O_2$), 24 h) and examined the changes in exosome secretion. Results showed that the number of exosomes was significantly increased under the regulation of the HIF-1 α -dependent small GTPase Rab22A (20). In addition, Huang et al. found that HIF-1 α can regulate the expression of miRNA-210 in a variety of tumors through hypoxia response elements (21). Noteworthy, other studies have also reported that miRNA-210 is also upregulated in multiple tumors and is therefore considered to be the most extensive miRNA in hypoxia-induced exosomes (22, 23). In ovarian cancer, HIF induces the release of exosomes with elevated levels of multiple miRNAs, such as miR-21-3p, miR-125b-5p, and miR-181d-5p. Further in vivo studies found that these hypoxia-induced exosomes can promote tumor proliferation and migration by inducing M2 polarization of macrophages (24). Notably, hypoxia-induced increased exosome secretion is not a phenomenon unique to tumor cells, as Zhang et al. observed HIF-1-mediated increased exosome production and secretion in renal proximal tubule cells under hypoxia (25). Recent studies have also shown that mesenchymal stem cells (MSCs) can also promote the secretion of miRNA-126 in exosomes through HIF-1 α in hypoxia (26).

Increasing evidences have shown that increased/altered exosomal protein content also responsible for tumorigenesis, invasion, and drug resistance. Notably, several studies further reported that exosomes released from hypoxia TME are more likely to cause tumor invasion and angiogenesis. Kore et al. qualitatively and quantitatively analyzed the protein content of exosomes secreted by hypoxia-treated glioblastoma cells. The results showed significantly elevated proteins levels such as thrombospondin-1 (TSP1), vascular endothelial growth factor (VEGF), and protein-lysine 6-oxidase (LOX), which have been well documented to be associated with tumor progression, angiogenesis, and treatment resistance (27). Moreover, Huang et al. found that exosomes secreted by colorectal cancer (CRC) cell under hypoxia conditions can promote the migration and invasion of normoxic CRC cell. Further quantitative analysis found that HIF1α-dependent Wnt4 was significantly elevated in these hypoxia-induced exosomes. Elevated Wnt4 in exosomes is thought to enhance the metastatic ability of normal CRC cell, which may provide a new target for CRC therapy (28). Besides proteins and nucleic acids, lipids and metabolites are also important components of exosomes, although much less information is available on their composition and effects. For instance, Schlaepfer et al. observed markedly elevated palmitic, stearic, and linoleic acids in exosomes secreted by hypoxia-treated prostate cancer cell (29). All these studies suggest that hypoxia can affect the secretion and release of various exosome contents.

HIF has been identified to induce exosome secretion by increasing the expression and activation of cell surface receptors

such as glucose transporter and transferrin receptor. Specifically, Luo et al. revealed that HIF-1 promotes aerobic glycolysis of tumor cells by up-regulating the expression of M2-type pyruvate kinase (PKM2) mRNA in the hypoxia TME (30). Furthermore, Wei et al. found that PKM2 regulates exosome release mainly by phosphorylating Ser95 of synaptosomeassociated protein 23 (SNAP-23), which is a major component of the synaptosome/SNARE complex. These finding suggests that PKM2 is not just a key enzyme in the process of aerobic glycolysis but promotes the release of exosomes under hypoxia conditions. Thus, it is not surprising that shikonin was found to reduce exosomes release by inhibiting glycolysis, whereas activation of glycolysis by tumor necrosis factor-alpha (TNF- α) increased the secretion of exosomes (31).

In addition to HIF, other signaling molecules and pathways, such as Rab-GTPase, NF- κ B, oxidative stress, and PI3K/Akt/ mTOR, are also involved in biogenesis and releasing of exosomes under hypoxia (32). For instance, signal transducer and activator of transcription 3 (STAT3) promotes exosome release by downregulating Rab7 and up-regulating Rab27a in ovarian cancer cells under hypoxia conditions (33). In addition, RAb5 has also been reported to regulate exosome release by regulating the transport of vesicles from the cell membrane to early endosomes and fusion with homotypic early endosomes (34). Moreover, the increase of reactive oxygen species under hypoxia can induce oxidative stress, which in turn promotes the release of exosomes. For example, Jurkat T cells secrete about 15 times more exosomes under oxidative stress conditions, while Raji cells secreted about 32 times more exosomes (35). Collectively, these findings confirm that the hypoxia TME can stimulate tumor cells to secrete more exosomes and thereby affect exosome cargo loading. However, the specific molecular mechanism by which hypoxia regulates exosome release is worth further exploration (**Figure 1**).

REGULATION OF THE IMMUNE SYSTEM BY HYPOXIA-INDUCED EXOSOMES

It is well known that exosomes are responsible for intercellular communication that can influence the development, maturation, and anti-tumor activity of immune cells by regulating their molecular signaling (36, 37). On the one hand, under normoxia, exosome secretions can directly activate immune

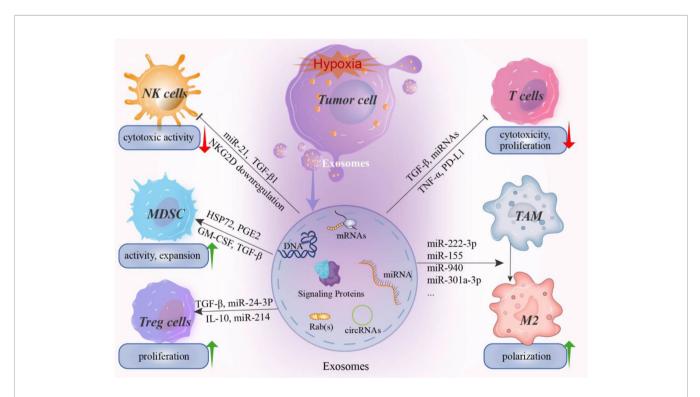


FIGURE 1 | The effect of hypoxia induced exosomes on immune system. Hypoxia in the tumor microenvironment can induce tumor cells to secrete a large number of exosomes, including miRNAs, mRNAs, signaling proteins, nucleotides, and immunomodulatory factors. These hypoxia-induced exosomes can mediate the immune evasion of tumor cells by affecting the activity of immune killer cells and promoting the proliferation and activation of immunosuppressive cells. For example, miR-21 and miR-29a in hypoxia-induced exosomes can inhibit the cytotoxicity of NK cell by downregulating the activating receptor NKG2D. In addition, the proliferation and activation of cytotoxic T cells were also inhibited by exosomes. In contrast, for MDSCs, Treg cells, and TAM, hypoxia-induced exosomes can promote the expansion and transformation of these cells. For example, various miRNAs have been reported to promote the M2 polarization of TAMs and thus promote the formation of an immunosuppressive microenvironment. NK cell, natural killer cell; MDSCs, myeloid-derived suppressor cells; Treg, regulatory T cell; TAM, Tumor-associated macrophages.

Hypoxia-Induced Exosomes in Oncology

effector cells in vivo and induce stronger immune responses. For example, HSP70 on the surface of exosomes can stimulate the activation of natural killer (NK) cells and macrophages, as well as induce stronger T cell responses (38). The exosomes released by mature dendritic cells (DCs) contain elevated levels of MHC I, MHC II, and co-stimulatory molecules, which showed a stronger effect on antigen presentation and immune stimulation (39). In addition, DC-derived exosomes can also express IL-15Ra and natural killer group 2D (NKG2D) ligands, which can promote the proliferation and activation of CD8⁺ T and NK cells respectively (40, 41). In view of the DC-derived exosomal immunogenicity and immune activation, numerous exosomebased anti-tumor vaccines have entered phase I and phase II clinical trials. On the other hand, tumor-derived exosomes, especially hypoxia-induced exosomes, are rich in a variety of immunomodulatory proteins and chemokines, including CSF-1, CCL2, FTH, FTL, IL-10, and TGF. These hypoxia-induced exosomes promoted the generation and infiltration of immunosuppressive T regulatory (Treg) cells, promoted the polarization of M2-macrophages, and inhibited the proliferation of T cells, collectively promote the immune evasion of tumors (42). In addition, studies have shown that programmed death protein ligand 1 (PD-L1) contained in tumor cell-derived exosomes can bind to programmed death protein 1 (PD-1) receptors on T cells to inhibit T cell activation, thereby promoting immune escape of tumors (43).

In general, recent studies on hypoxia-induced exosomes have found that inhibition of immune cells in the TME may be the main reason for the failure of anti-tumor immunity. Therefore, clarifying the regulatory role of exosomes on various immune cells in the hypoxia TME is particularly important for the development of more effective and precise immunotherapy methods (**Table 1**).

Macrophage

Tumor-associated macrophages (TAMs) can differentiate into either M1-type macrophages with pro-inflammatory effects or M2-type macrophages with anti-inflammatory effects, both of which are regulated by the TME (50). Furthermore, studies have shown that this polarization of macrophages can be affected by exosomes within the hypoxia TME. Specifically, exosomes derived from different parental cells will promote the polarization of macrophages into different subtypes. For example, the exosomes secreted by renal tubular epithelial cells under hypoxia can promote the polarization of M1 macrophages and induce high levels of inflammatory responses (51). On the other hand, hypoxia can alter miRNAs levels in tumor cellderived exosomes and leading to M2 polarization of macrophages (44). Similarly, Chen et al. found that hypoxia can stimulate M2 phenotype polarization by upregulating miR-940 expression in epithelial ovarian cancer (EOC)-derived exosomes, while the M2 subtype macrophages can in turn promote the proliferation and migration of EOC cells. In addition, hypoxia can also upregulate the expression of miR-21-3p, miR-125b-5p, and miR-181d-5p in exosomes via HIF to induce the M2-polarization of macrophages (24). In another study, Qian et al. found that compared with normoxic glioma cell exosomes, hypoxia glioma cell exosomes had a stronger ability to induce macrophage polarization to the M2 type. Meanwhile, the study also indicated that the miR-1246 level was significantly enriched in the exosomes of hypoxia glioma cells, which could activated the STAT3 pathway and inhibit the NF-KB signaling pathway, thereby promoting the polarization of M2 phenotype (52). Nevertheless, although exosomes secreted by tumor cells under hypoxia stress mostly induce M2 polarization of macrophages, strategies to convert TAMs to a predominantly M1 phenotype have been proposed for novel immunotherapy.

MDSC

Myeloid-derived suppressor cells (MDSCs) are highly heterogeneous immature cells derived from bone marrow that can inhibit the activation of T cells, promote M2 polarization of macrophages, and inhibit NK cytotoxicity (53). Numerous studies have demonstrated that the activation, expansion, and immunosuppression of MDSCs can be promoted by exosomes. However, whether exosomes under hypoxia conditions would

TABLE 1 | Hypoxia-induced exosomes involved in anti-tumor immunity.

Regulatory factors	Cancer types	Biological effect	Mechanism	Ret
Exosomal miR-940	Epithelial ovarian cancer	Suppress anti-tumor immune responses	Promotes M2 polarization of tumor-associated macrophages	(44)
Exosomal miR24-3p	Nasopharyngeal carcinoma	Suppress anti-tumor immune responses	Inhibit T-cell proliferation and differentiation, and the induction of Tregs	(45)
Exosomal TGF-β1	Hypoxic cancer	Suppress anti-tumor immune	TGF-β1 downregulates NKG2D and	()
and miR23a		responses	miR23a directly targets CD107a	(46)
Exosomal miRLet-7a	Melanoma	Suppress anti-tumor immune responses	Enhanced the oxidative phosphorylation in bone marrow-derived macrophages	(42)
Exosomal miR-10a and miR-21	Glioma	Suppress anti-tumor immune responses	Enhanced expansion and activation of myeloid-derived suppressor cells	(47)
Exosomal TGF- β	Breast cancer	Suppress anti-tumor immune responses	Inhibit T cell proliferation via TGF- β , IL-10 and PGE2	(48)
Exosomal HSP70	Oral squamous cell carcinoma	Suppress anti-tumor immune responses	Inhibit T cells through a miR-21/PTEN/PD-L1 regulation axis	(49)

have similar effects on the proliferation and immunosuppression of MDSCs remained to be elucidated. In this regard, researchers found that hypoxia can directly stimulate the expressions of HSP72 and toll-like receptor 2 (TLR2) in exosomes, which can directly participate in the regulation of MDSCs (54, 55). Specifically, Chalmin et al. found that HSP72 in exosomes can mediate the interaction between tumor cells and MDSCs by triggering STAT3 activation (56). Similarly, Xiang et al. found that exosomes released from cultured B16 tumor cells could induce the activation and expansion of MDSC in a TLR2dependent manner (57). All these results suggest that hypoxiainduced exosomes play a significant role in suppressing tumor immune surveillance by promoting the suppressive function of MDSC.

Although an immunosuppressive milieu mediated by MDSCs has been demonstrated in patients with glioma, the mechanisms of MDSC development and activation have not been elucidated. Guo et al. found that the expression of miR-10a and miR-21 was increased in glioma cells-derived exosomes under hypoxia conditions compared with normoxia (47). Furthermore, they also found that hypoxia-induced glioma cells can stimulate the differentiation of functional MDSCs by transferring exosomal miR-29a and miR-92a to MDSCs (58). Accumulating evidence supports that hypoxia can induce changes in miRNA expression in tumor-derived exosomes, thereby activating MDSCs and enhancing their function to promote tumor growth. This suggests that blocking the immunosuppressive effect of MDSCs may be an effective way to improve the efficacy of immunotherapy. Therefore, clarifying the exact effect of hypoxia on the immunosuppressive function of MDSCs may provide new insights for targeting exosomal secretion and its contents (especially miRNAs and proteins) for antitumor immunotherapy.

T Cell

T cells are considered to be the major cell subset in anti-tumor immunity. Treg cells are a specialized population of T cells thought to suppress anti-tumor immune responses (59). Studies have reported that miR-214 expression was significantly increased in tumor cell-derived exosomes under hypoxia TME (60). Yin et al. observed that exosomes from lung cancer cell lines can effectively transport miR-214 to CD4⁺ T cells, thereby promoting the expansion of Treg cell subsets and the secretion of IL-10 (61). A study by Mrizak et al. found that exosomes released from nasopharyngeal carcinoma cells under hypoxia conditions express the chemokine CCL20, leading to preferential recruitment of Treg cells to tumor sites. In addition, these hypoxia-induced exosomes were also able to induce Treg cell expansion and enhance their immunosuppressive effects (62). Collectively, these results suggest that hypoxia participates in Treg cell-mediated immunosuppression by modulating the cargo of exosomes.

On the other hand, hypoxia-induced exosomes can also promote tumor immune escape by directly inhibiting the activity of T cells. Rong et al. found that TGF- β can be delivered to T cells through breast cancer cell-derived exosomes, thereby

inhibiting T cell proliferation, while anti-TGF- β treatment reversed the immunosuppressive effects of the exosomes (48). In addition, HIF can also exert an immunosuppressive effect by upregulating the PD-L1 expression in exosomes. The study by Poggio et al. showed that tumor cells can release PD-L1-carrying exosomes under hypoxia conditions, which can function as an immune checkpoint by binding to PD-1 on the surface of activated T cells (63). In patients with gastric cancer, exosome-carried PD-L1 resulted in decreased CD4⁺ and CD8⁺ T cell infiltration and activity (64). Similarly, higher levels of PD-L1 were found in exosomes from patients with active disease and poor survival (65). Together, these studies suggest the inhibitory effect of hypoxiainduced exosomes on T cell-mediated anti-tumor immunity.

NK Cell

There is ample evidence that hypoxia-induced exosomes can evade immune surveillance by binding to NK cells. According to literature reports, the activation of NK cells in anti-tumor immunity is mediated by surface-active receptors, such as NKG2D and NKp44 (66). However, hypoxia-induced exosomes reportedly suppress host NK cell cytotoxicity by reducing NKG2D expression, thereby disrupting the host immune system and promoting the formation of a tumorpromoting microenvironment (67). For example, hypoxia TME can increase the levels of TGF-β1, miRNA-210, and miRNA-23a in exosomes secreted by tumor cells. Specifically, the uptake of hypoxia exosomes by NK cells can transfer TGF-β1 in exosomes to NK cells and inhibit the expression of its surface-activated receptor NKG2D, thereby inhibiting NK cell function. Subsequent miRNA analysis showed highly expressed miR-23a in hypoxia-induced exosomes, which can target the expression of CD107a in NK cells, thereby inhibiting the activation of NK cells (46). Similarly, Xia et al. also described that clear cell renal cancer triggers NK cell dysfunction in an exosome-dependent manner, and this inhibitory function also activates the TGF-B/SMAD signaling pathway through TGF- β 1 (68). In addition, the researchers found that exosomes isolated from the plasma of patients with melanoma contained a large amount of PD-L1, FasL, and TGF- β . These hypoxia-associated exosomes not only inhibited the activity of CD8⁺ T cells, but also down-regulated NKG2D expression in NK cells. In contrast, targeting these exosomes with monoclonal antibodies or pharmacological inhibitors can restore immune cell function (69).

EXOSOME-BASED ANTI-TUMOR IMMUNOTHERAPY

Tumor immunotherapy is a new anti-cancer strategy that kills tumor cells by activating immune cells or restoring exhausted immune cells. As an important regulator of the TME, exosomesbased therapies are considered a promising approach to promoting tumor immunotherapy. For example, exosomes secreted by tumor cells contain a vast number of tumorassociated antigens, such as MHC I and MHC II, that can be

Hypoxia-Induced Exosomes in Oncology

used as a tumor vaccine to promote anti-tumor immune responses (70). Hsu et al. found that dendritic cell (DC)derived exosomes can be loaded with a variety of polypeptide antigens (such as MHC I, MHC II) and co-stimulatory molecules that contribute to the initiation and activation of T cells, such as CD80, CD83, CD86, etc. (71). In a mouse model of pancreatic cancer, subcutaneous injection of exosome-loaded DC vaccine extended survival in mice, while combination therapy with chemotherapeutics such as of gemcitabine simultaneously reduced tumor MDSCs content and increased the activation of T cells (72). In addition, the use of DC cell-derived ovalbumin exosomes to stimulate CD4⁺ T cells can inhibit the differentiation and proliferation of Treg cells and promote the formation of memory CD8⁺ T cells. This represents another attractive exosome-based anti-tumor vaccine option (73). In addition, DC-derived exosomes contain NKG2D ligands. Therefore, Viaud et al. reported that DC vaccines can activate NK cells and release TNF (40). However, due to the cargo complexity of exosomes, exosome-based tumor vaccine strategies may also inhibit anti-tumor immunotherapy by inducing apoptosis of activated CD8⁺ T cells (74). For example, exosomes can impair the activation of T cells by IL-2 and promote the proliferation of Treg cells for immunosuppressive effects (75). Nevertheless, it is still possible to consider optimizing the use of exosome vaccines by modifying the exosomes and adjusting their dosage. For example, Samuel et al. used IFN-y to stimulate the secretion of exosomes from mature dendritic cells which increased the expression of co-stimulatory molecules in exosomes to enhance T cell activation (74).

CONCLUSION

In recent years, anti-tumor immunotherapy represented by immune checkpoint inhibitors has changed the treatment option for various tumor types. As mentioned earlier, the infiltration and activation of immune cells in the TME are closely related to successful immunotherapy. Therefore, understanding the impact of exosomes on the anti-tumor immune system can further enhance the effect of immunotherapy. In fact, hypoxia-induced exosomal features have been extensively studied and consensus has been reached. First, hypoxia-induced exosomes are not vesicles loaded with cellular waste, but key mediators of intercellular communication. Second, in the adverse TME such as hypoxia, high glucose and drug therapy, the cargo carried and delivered in exosomes is significantly altered, which in turn modulates immune cell function (76, 77). Third, exosomes secreted by immune cells such as DCs and chimeric antigen receptor T cells

REFERENCES

- Goliwas K, Deshane J, Elmets C, Athar M. Moving Immune Therapy Forward Targeting TME. *Physiol Rev* (2021) 101:417–25. doi: 10.1152/physrev.00008.2020
- Singleton D, Macann A, Wilson W. Therapeutic Targeting of the Hypoxic Tumour Microenvironment. Nat Rev Clin Oncol (2021) 18:751–72. doi: 10.1038/s41571-021-00539-4

(CAR T cells) can inhibit the growth, proliferation, and metastasis of tumor cells (78). Therefore, the preparation of exosome-based tumor vaccines to enhance tumor antigen presentation and modulate immune responses in the TME is a potential avenue for therapeutic development.

FURTHER PERSPECTIVE

While initial preclinical studies have shown promising results, clinical trials have failed to achieve comparable results. This suggests that there are still unresolved challenges with existing exosome treatments (79). For example, existing exosome therapeutics have low targeting efficiency and are easily engulfed by the immune system. In addition, the current exosome isolation methods are expensive, and large-scale exosome isolation technology still needs to be developed (80). Therefore, these problems would need to be solved before clinical application. Moreover, exosome-based immunotherapy is currently still in early clinical trials, and there are no specific international guidelines for the production and application of this novel therapeutic. Future studies should investigate the effects of hypoxia on the formation, release, and cargo components of exosomes, as well as the mechanism by which the hypoxia TME mediates the regulation of immune cell function by exosomes. These studies would not only provide insight into the poor response of cancer immunotherapy regimens in current clinical trials, but may also serve as a reference for exosome application in anti-cancer drug delivery to improve anti-tumor therapy precision.

AUTHOR CONTRIBUTIONS

WG and TQ drafted the manuscript and carried out the figures in manuscript.literature research of the review, figures and drafted the manuscript. BD performed literature analysis of the review and editing the final manuscript. TL, QL, and XX provided supervision and contributed to the conceptualization of the review. All authors read and approved the published version of the manuscript.

ACKNOWLEDGMENTS

We thank Bullet Edits Limited for the linguistic editing and proofreading of the manuscript (Anti-counterfeiting Code: 42868a05acb5ba0dae6b21af3085e8fc).

LaGory E, Giaccia A. The Ever-Expanding Role of HIF in Tumour and Stromal Biology. Nat Cell Biol (2016) 18:356-65. doi: 10.1038/ncb 3330

Riera-Domingo C, Audigé A, Granja S, Cheng W, Ho P, Baltazar F, et al. Immunity, Hypoxia, and Metabolism-The Ménage À Trois of Cancer: Implications for Immunotherapy. *Physiol Rev* (2020) 100:1–102. doi: 10.1152/physrev.00018.2019

- Muhsin M, Graham J, Kirkpatrick P. Bevacizumab. Nat Rev Drug Discovery (2004) 3:995–6. doi: 10.1038/nrd1601
- He G, Peng X, Wei S, Yang S, Li X, Huang M, et al. Exosomes in the Hypoxic TME: From Release, Uptake and Biofunctions to Clinical Applications. *Mol Cancer* (2022) 21:19. doi: 10.1186/s12943-021-01440-5
- Pegtel D, Gould S. Exosomes. Annu Rev Biochem (2019) 88:487–514. doi: 10.1146/annurev-biochem-013118-111902
- Rezaie J, Aslan C, Ahmadi M, Zolbanin N, Kashanchi F, Jafari R. The Versatile Role of Exosomes in Human Retroviral Infections: From Immunopathogenesis to Clinical Application. *Cell biosci* (2021) 11:19. doi: 10.1186/s13578-021-00537-0
- Vahabi A, Rezaie J, Hassanpour M, Panahi Y, Nemati M, Rasmi Y, et al. Tumor Cells-Derived Exosomal CircRNAs: Novel Cancer Drivers, Molecular Mechanisms, and Clinical Opportunities. *Biochem Pharmacol* (2022) 200:115038. doi: 10.1016/j.bcp.2022.115038
- Abramowicz A, Łabaj W, Mika J, Szołtysek K, Ślęzak-Prochazka I, Mielańczyk Ł., et al. MicroRNA Profile of Exosomes and Parental Cells is Differently Affected by Ionizing Radiation. *Radiat Res* (2020) 194:133–42. doi: 10.1667/ RADE-20-00007
- Attaran S, Bissell M. The Role of Tumor Microenvironment and Exosomes in Dormancy and Relapse. *Semin Cancer Biol* (2022) 78:35–44. doi: 10.1016/ j.semcancer.2021.09.008
- Yaghoubi S, Najminejad H, Dabaghian M, Karimi M, Abdollahpour-Alitappeh M, Rad F, et al. How Hypoxia Regulate Exosomes in Ischemic Diseases and Cancer Microenvironment? *IUBMB Life* (2020) 72:1286–305. doi: 10.1002/iub.2275
- Kalluri R, LeBleu V. The Biology Function and Biomedical Applications of Exosomes. Sci (New York N.Y.) (2020) 367:eaau6977. doi: 10.1126/ science.aau6977
- Dai J, Su Y, Zhong S, Cong L, Liu B, Yang J, et al. Exosomes: Key Players in Cancer and Potential Therapeutic Strategy. *Signal transduct targeted Ther* (2020) 5:145. doi: 10.1038/s41392-020-00261-0
- Rezaie J, Ahmadi M, Ravanbakhsh R, Mojarad B, Mahbubfam S, Shaban S, et al. Tumor-Derived Extracellular Vesicles: The Metastatic Organotropism Drivers. *Life Sci* (2022) 289:120216. doi: 10.1016/j.lfs.2021.120216
- Riau A, Ong H, Yam G, Mehta J. Sustained Delivery System for Stem Cell-Derived Exosomes. Front Pharmacol (2019) 10:1368. doi: 10.3389/ fphar.2019.01368
- Raposo G, Nijman H, Stoorvogel W, Liejendekker R, Harding C, Melief C, et al. B Lymphocytes Secrete Antigen-Presenting Vesicles. *J Exp Med* (1996) 183:1161–72. doi: 10.1084/jem.183.3.1161
- Xia X, Wang S, Ni B, Xing S, Cao H, Zhang Z, et al. Hypoxic Gastric Cancer-Derived Exosomes Promote Progression and Metastasis via MiR-301a-3p/ PHD3/HIF-1α Positive Feedback Loop. Oncogene (2020) 39:6231–44. doi: 10.1038/s41388-020-01425-6
- Li L, Li C, Wang S, Wang Z, Jiang J, Wang W, et al. Exosomes Derived From Hypoxic Oral Squamous Cell Carcinoma Cells Deliver miR-21 to Normoxic Cells to Elicit a Prometastatic Phenotype. *Cancer Res* (2016) 76:1770–80. doi: 10.1158/0008-5472.CAN-15-1625
- Wang T, Gilkes D, Takano N, Xiang L, Luo W, Bishop C, et al. Hypoxia-Inducible Factors and RAB22A Mediate Formation of Microvesicles That Stimulate Breast Cancer Invasion and Metastasis. Proc Natl Acad Sci United States America (2014) 111:E3234–42. doi: 10.1073/ pnas.1410041111
- Huang X, Ding L, Bennewith K, Tong R, Welford S, Ang K, et al. Hypoxia-Inducible Mir-210 Regulates Normoxic Gene Expression Involved in Tumor Initiation. *Mol Cell* (2009) 35:856–67. doi: 10.1016/j.molcel.2009.09.006
- Tadokoro H, Umezu T, Ohyashiki K, Hirano T, Ohyashiki J. Exosomes Derived From Hypoxic Leukemia Cells Enhance Tube Formation in Endothelial Cells. J Biol Chem (2013) 288:34343–51. doi: 10.1074/ jbc.M113.480822
- Zhang X, Sai B, Wang F, Wang L, Wang Y, Zheng L, et al. Hypoxic BMSC-Derived Exosomal miRNAs Promote Metastasis of Lung Cancer Cells via STAT3-Induced EMT. *Mol Cancer* (2019) 18:40. doi: 10.1186/s12943-019-0959-5
- Chen X, Zhou J, Li X, Wang X, Lin Y, Wang X. Exosomes Derived From Hypoxic Epithelial Ovarian Cancer Cells Deliver microRNAs to Macrophages and Elicit a Tumor-Promoted Phenotype. *Cancer Lett* (2018) 435:80–91. doi: 10.1016/j.canlet.2018.08.001

- Zhang W, Zhou X, Yao Q, Liu Y, Zhang H, Dong Z. HIF-1-Mediated Production of Exosomes During Hypoxia is Protective in Renal Tubular Cells. Am J Physiol Renal Physiol (2017) 313:F906–13. doi: 10.1152/ ajprenal.00178.2017
- 26. Liu W, Li L, Rong Y, Qian D, Chen J, Zhou Z, et al. Hypoxic Mesenchymal Stem Cell-Derived Exosomes Promote Bone Fracture Healing by the Transfer of miR-126. *Acta biomaterialia* (2020) 103:196–212. doi: 10.1016/ j.actbio.2019.12.020
- Kore R, Edmondson J, Jenkins S, Jamshidi-Parsian A, Dings R, Reyna N, et al. Hypoxia-Derived Exosomes Induce Putative Altered Pathways in Biosynthesis and Ion Regulatory Channels in Glioblastoma Cells. *Biochem biophys Rep* (2018) 14:104–13. doi: 10.1016/j.bbrep.2018.03.008
- Huang Z, Yang M, Li Y, Yang F, Feng Y. Exosomes Derived From Hypoxic Colorectal Cancer Cells Transfer Wnt4 to Normoxic Cells to Elicit a Prometastatic Phenotype. Int J Biol Sci (2018) 14:2094–102. doi: 10.7150/ijbs.28288
- Schlaepfer I, Nambiar D, Ramteke A, Kumar R, Dhar D, Agarwal C, et al. Hypoxia Induces Triglycerides Accumulation in Prostate Cancer Cells and Extracellular Vesicles Supporting Growth and Invasiveness Following Reoxygenation. Oncotarget (2015) 6:22836–56. doi: 10.18632/oncotarget.4479
- Luo W, Hu H, Chang R, Zhong J, Knabel M, O'Meally R, et al. Pyruvate Kinase M2 is a PHD3-Stimulated Coactivator for Hypoxia-Inducible Factor 1. *Cell* (2011) 145:732–44. doi: 10.1016/j.cell.2011.03.054
- Wei Y, Wang D, Jin F, Bian Z, Li L, Liang H, et al. Pyruvate Kinase Type M2 Promotes Tumour Cell Exosome Release via Phosphorylating Synaptosome-Associated Protein 23. Nat Commun (2017) 8:14041. doi: 10.1038/ ncomms14041
- Jafari R, Rahbarghazi R, Ahmadi M, Hassanpour M, Rezaie J. Hypoxic Exosomes Orchestrate Tumorigenesis: Molecular Mechanisms and Therapeutic Implications. J Trans Med (2020) 18:474. doi: 10.1186/s12967-020-02662-9
- 33. Dorayappan K, Wanner R, Wallbillich J, Saini U, Zingarelli R, Suarez A, et al. Hypoxia-Induced Exosomes Contribute to a More Aggressive and Chemoresistant Ovarian Cancer Phenotype: A Novel Mechanism Linking STAT3/Rab Proteins. Oncogene (2018) 37:3806–21. doi: 10.1038/s41388-018-0189-0
- 34. Panigrahi G, Praharaj P, Peak T, Long J, Singh R, Rhim J, et al. Hypoxia-Induced Exosome Secretion Promotes Survival of African-American and Caucasian Prostate Cancer Cells. *Sci Rep* (2018) 8:3853. doi: 10.1038/ s41598-018-22068-4
- Hedlund M, Nagaeva O, Kargl D, Baranov V, Mincheva-Nilsson L. Thermaland Oxidative Stress Causes Enhanced Release of NKG2D Ligand-Bearing Immunosuppressive Exosomes in Leukemia/Lymphoma T and B Cells. *PLoS* One (2011) 6:e16899. doi: 10.1371/journal.pone.0016899
- Yokoi A, Ochiya T. Exosomes and Extracellular Vesicles: Rethinking the Essential Values in Cancer Biology. Semin Cancer Biol (2021) 74:79–91. doi: 10.1016/j.semcancer.2021.03.032
- Vergani E, Daveri E, Vallacchi V, Bergamaschi L, Lalli L, Castelli C, et al. Extracellular Vesicles in Anti-Tumor Immunity. *Semin Cancer Biol* (2021). doi: 10.1016/j.semcancer.2021.09.004
- 38. Xie Y, Bai O, Zhang H, Yuan J, Zong S, Chibbar R, et al. Membrane-Bound HSP70-Engineered Myeloma Cell-Derived Exosomes Stimulate More Efficient CD8(+) CTL- and NK-Mediated Antitumour Immunity Than Exosomes Released From Heat-Shocked Tumour Cells Expressing Cytoplasmic HSP70. J Cell Mol Med (2010) 14:2655–66. doi: 10.1111/ j.1582-4934.2009.00851.x
- Wang Y, Xiang Y, Xin V, Wang X, Peng X, Liu X, et al. Dendritic Cell Biology and its Role in Tumor Immunotherapy. J Hematol Oncol (2020) 13:107. doi: 10.1186/s13045-020-00939-6
- Viaud S, Terme M, Flament C, Taieb J, André F, Novault S, et al. Dendritic Cell-Derived Exosomes Promote Natural Killer Cell Activation and Proliferation: A Role for NKG2D Ligands and IL-15ralpha. *PLoS One* (2009) 4:e4942. doi: 10.1371/journal.pone.0004942
- Hao S, Bai O, Yuan J, Qureshi M, Xiang J. Dendritic Cell-Derived Exosomes Stimulate Stronger CD8+ CTL Responses and Antitumor Immunity Than Tumor Cell-Derived Exosomes. *Cell Mol Immunol* (2006) 3:205–11.
- Park J, Dutta B, Tse S, Gupta N, Tan C, Low J, et al. Hypoxia-Induced Tumor Exosomes Promote M2-Like Macrophage Polarization of Infiltrating Myeloid Cells and microRNA-Mediated Metabolic Shift. *Oncogene* (2019) 38:5158–73. doi: 10.1038/s41388-019-0782-x

- Sun Y, Guo J, Yu L, Guo T, Wang J, Wang X, et al. PD-L1 Exosomes From Bone Marrow-Derived Cells of Tumor-Bearing Mice Inhibit Antitumor Immunity. *Cell Mol Immunol* (2021) 18:2402–9. doi: 10.1038/s41423-020-0487-7
- 44. Chen X, Ying X, Wang X, Wu X, Zhu Q, Wang X. Exosomes Derived From Hypoxic Epithelial Ovarian Cancer Deliver microRNA-940 to Induce Macrophage M2 Polarization. Oncol Rep (2017) 38:522–8. doi: 10.3892/ or.2017.5697
- 45. Ye S, Zhang H, Cai T, Liu Y, Ni J, He J, et al. Exosomal miR-24-3p Impedes T-Cell Function by Targeting FGF11 and Serves as a Potential Prognostic Biomarker for Nasopharyngeal Carcinoma. *J Pathol* (2016) 240:329–40. doi: 10.1002/path.4781
- 46. Berchem G, Noman M, Bosseler M, Paggetti J, Baconnais S, Le Cam E, et al. Hypoxic Tumor-Derived Microvesicles Negatively Regulate NK Cell Function by a Mechanism Involving TGF-β and Mir23a Transfer. *Oncoimmunology* (2016) 5:e1062968. doi: 10.1080/2162402X.2015.1062968
- 47. Guo X, Qiu W, Liu Q, Qian M, Wang S, Zhang Z, et al. Immunosuppressive Effects of Hypoxia-Induced Glioma Exosomes Through Myeloid-Derived Suppressor Cells via the miR-10a/Rora and miR-21/Pten Pathways. Oncogene (2018) 37:4239–59. doi: 10.1038/s41388-018-0261-9
- 48. Rong L, Li R, Li S, Luo R. Immunosuppression of Breast Cancer Cells Mediated by Transforming Growth Factor- β in Exosomes From Cancer Cells. Oncol Lett (2016) 11:500–4. doi: 10.3892/ol.2015.3841
- 49. Li L, Cao B, Liang X, Lu S, Luo H, Wang Z, et al. Microenvironmental Oxygen Pressure Orchestrates an Anti- and Pro-Tumoral γδ T Cell Equilibrium via Tumor-Derived Exosomes. Oncogene (2019) 38:2830–43. doi: 10.1038/ s41388-018-0627-z
- Chamseddine A, Assi T, Mir O, Chouaib S. Modulating Tumor-Associated Macrophages to Enhance the Efficacy of Immune Checkpoint Inhibitors: A TAM-Pting Approach. *Pharmacol Ther* (2022) 231:107986. doi: 10.1016/ j.pharmthera.2021.107986
- Ding C, Zheng J, Wang B, Li Y, Xiang H, Dou M, et al. Exosomal MicroRNA-374b-5p From Tubular Epithelial Cells Promoted M1 Macrophages Activation and Worsened Renal Ischemia/Reperfusion Injury. *Front Cell Dev Biol* (2020) 8:587693. doi: 10.3389/fcell.2020.587693
- Qian M, Wang S, Guo X, Wang J, Zhang Z, Qiu W, et al. Hypoxic Glioma-Derived Exosomes Deliver microRNA-1246 to Induce M2 Macrophage Polarization by Targeting TERF2IP via the STAT3 and NF-kb Pathways. Oncogene (2020) 39:428–42. doi: 10.1038/s41388-019-0996-y
- Tian X, Shen H, Li Z, Wang T, Wang S. Tumor-Derived Exosomes, Myeloid-Derived Suppressor Cells, and Tumor Microenvironment. J Hematol Oncol (2019) 12:84. doi: 10.1186/s13045-019-0772-z
- Hammerer-Lercher A, Mair J, Bonatti J, Watzka S, Puschendorf B, Dirnhofer S. Hypoxia Induces Heat Shock Protein Expression in Human Coronary Artery Bypass Grafts. *Cardiovasc Res* (2001) 50:115–24. doi: 10.1016/S0008-6363(01)00198-5
- Stridh L, Smith P, Naylor A, Wang X, Mallard C. Regulation of Toll-Like Receptor 1 and -2 in Neonatal Mice Brains After Hypoxia-Ischemia. *J Neuroinflamm* (2011) 8:45. doi: 10.1186/1742-2094-8-45
- Chalmin F, Ladoire S, Mignot G, Vincent J, Bruchard M, Remy-Martin J, et al. Membrane-Associated Hsp72 From Tumor-Derived Exosomes Mediates STAT3-Dependent Immunosuppressive Function of Mouse and Human Myeloid-Derived Suppressor Cells. J Clin Invest (2010) 120:457–71. doi: 10.1172/JCI40483
- 57. Xiang X, Liu Y, Zhuang X, Zhang S, Michalek S, Taylor D, et al. TLR2-Mediated Expansion of MDSCs is Dependent on the Source of Tumor Exosomes. Am J Pathol (2010) 177:1606–10. doi: 10.2353/ajpath. 2010.100245
- Guo X, Qiu W, Wang J, Liu Q, Qian M, Wang S, et al. Glioma Exosomes Mediate the Expansion and Function of Myeloid-Derived Suppressor Cells Through microRNA-29a/Hbp1 and microRNA-92a/Prkar1a Pathways. *Int J Cancer* (2019) 144:3111–26. doi: 10.1002/ijc.32052
- Sharabi A, Tsokos M, Ding Y, Malek T, Klatzmann D, Tsokos G. Regulatory T Cells in the Treatment of Disease. *Nat Rev Drug Discovery* (2018) 17:823–44. doi: 10.1038/nrd.2018.148
- 60. Yang K, Zhang J, Bao C. Exosomal Circeif3k From Cancer-Associated Fibroblast Promotes Colorectal Cancer (CRC) Progression via miR-214/ PD-L1 Axis. BMC Cancer (2021) 21:933. doi: 10.1186/s12885-021-08669-9

- Yin Y, Cai X, Chen X, Liang H, Zhang Y, Li J, et al. Tumor-Secreted miR-214 Induces Regulatory T Cells: A Major Link Between Immune Evasion and Tumor Growth. Cell Res (2014) 24:1164–80. doi: 10.1038/cr.2014.121
- Mrizak D, Martin N, Barjon C, Jimenez-Pailhes A, Mustapha R, Niki T, et al. Effect of Nasopharyngeal Carcinoma-Derived Exosomes on Human Regulatory T Cells. J Natl Cancer Inst (2015) 107:363. doi: 10.1093/ jnci/dju363
- Poggio M, Hu T, Pai C, Chu B, Belair C, Chang A, et al. Suppression of Exosomal PD-L1 Induces Systemic Anti-Tumor Immunity and Memory. *Cell* (2019) 177:414–27.e13. doi: 10.1016/j.cell.2019.02.016
- 64. Ricklefs F, Alayo Q, Krenzlin H, Mahmoud A, Speranza M, Nakashima H, et al. Immune Evasion Mediated by PD-L1 on Glioblastoma-Derived Extracellular Vesicles. *Sci Adv* (2018) 4:eaar2766. doi: 10.1126/sciadv.aar2766
- Theodoraki M, Yerneni S, Hoffmann T, Gooding W, Whiteside T. Clinical Significance of PD-L1 Exosomes in Plasma of Head and Neck Cancer Patients. *Clin Cancer research: an Off J Am Assoc Cancer Res* (2018) 24:896–905. doi: 10.1158/1078-0432.CCR-17-2664
- 66. Guo A, Jiao Y, Zhao Q, Huang H, Deng J, Zhang C, et al. Implications of the Accumulation of CXCR5 NK Cells in Lymph Nodes of HIV-1 Infected Patients. *EBioMedicine* (2022) 75:103794. doi: 10.1016/j.ebiom.2021.103794
- Mincheva-Nilsson L, Baranov V. Cancer Exosomes and NKG2D Receptor-Ligand Interactions: Impairing NKG2D-Mediated Cytotoxicity and Anti-Tumour Immune Surveillance. *Semin Cancer Biol* (2014) 28:24–30. doi: 10.1016/j.semcancer.2014.02.010
- Xia Y, Zhang Q, Zhen Q, Zhao Y, Liu N, Li T, et al. Negative Regulation of Tumor-Infiltrating NK Cell in Clear Cell Renal Cell Carcinoma Patients Through the Exosomal Pathway. *Oncotarget* (2017) 8:37783–95. doi: 10.18632/oncotarget.16354
- Sharma P, Diergaarde B, Ferrone S, Kirkwood J, Whiteside T. Melanoma Cell-Derived Exosomes in Plasma of Melanoma Patients Suppress Functions of Immune Effector Cells. *Sci Rep* (2020) 10:92. doi: 10.1038/s41598-019-56542-4
- Naseri M, Bozorgmehr M, Zöller M, Ranaei Pirmardan E, Madjd Z. Tumor-Derived Exosomes: The Next Generation of Promising Cell-Free Vaccines in Cancer Immunotherapy. *Oncoimmunology* (2020) 9:1779991. doi: 10.1080/ 2162402X.2020.1779991
- Hsu D, Paz P, Villaflor G, Rivas A, Mehta-Damani A, Angevin E, et al. Exosomes as a Tumor Vaccine: Enhancing Potency Through Direct Loading of Antigenic Peptides. J immunother (Hagerstown Md.: 1997) (2003) 26:440– 50. doi: 10.1097/00002371-200309000-00007
- Xiao L, Erb U, Zhao K, Hackert T, Zöller M. Efficacy of Vaccination With Tumor-Exosome Loaded Dendritic Cells Combined With Cytotoxic Drug Treatment in Pancreatic Cancer. *Oncoimmunology* (2017) 6:e1319044. doi: 10.1080/2162402X.2017.1319044
- Xie Y, Wang L, Freywald A, Qureshi M, Chen Y, Xiang J. A Novel T Cell-Based Vaccine Capable of Stimulating Long-Term Functional CTL Memory Against B16 Melanoma via CD40L Signaling. Cell Mol Immunol (2013) 10:72–7. doi: 10.1038/cmi.2012.37
- Samuel M, Gabrielsson S. Personalized Medicine and Back-Allogeneic Exosomes for Cancer Immunotherapy. J Internal Med (2021) 289:138–46. doi: 10.1111/joim.12963
- 75. Lu Z, Zuo B, Jing R, Gao X, Rao Q, Liu Z, et al. Dendritic Cell-Derived Exosomes Elicit Tumor Regression in Autochthonous Hepatocellular Carcinoma Mouse Models. J Hepatol (2017) 67:739–48. doi: 10.1016/ j.jhep.2017.05.019
- 76. Khaksar M, Sayyari M, Rezaie J, Pouyafar A, Montazersaheb S, Rahbarghazi R. High Glucose Condition Limited the Angiogenic/Cardiogenic Capacity of Murine Cardiac Progenitor Cells in *In Vitro* and *In Vivo* Milieu. *Cell Biochem Funct* (2018) 36:346–56. doi: 10.1002/cbf.3354
- 77. Soraya H, Sani N, Jabbari N, Rezaie J. Metformin Increases Exosome Biogenesis and Secretion in U87 MG Human Glioblastoma Cells: A Possible Mechanism of Therapeutic Resistance. Arch Med Res (2021) 52:151–62. doi: 10.1016/j.arcmed.2020.10.007
- Nikfarjam S, Rezaie J, Kashanchi F, Jafari R. Dexosomes as a Cell-Free Vaccine for Cancer Immunotherapy. J Exp Clin Cancer research: CR (2020) 39:258. doi: 10.1186/s13046-020-01781-x
- Cappello F, Fais S. Extracellular Vesicles in Cancer Pros and Cons: The Importance of the Evidence-Based Medicine. *Semin Cancer Biol* (2022). doi: 10.1016/j.semcancer.2022.01.011

 Srivastava A, Rathore S, Munshi A, Ramesh R. Organically Derived Exosomes as Carriers of Anticancer Drugs and Imaging Agents for Cancer Treatment. *Semin Cancer Biol* (2022). doi: 10.1016/j.semcancer.2022.02.020

Conflict of Interest: The authors declare that the research was conducted in the absence of any commercial or financial relationships that could be construed as a potential conflict of interest.

Publisher's Note: All claims expressed in this article are solely those of the authors and do not necessarily represent those of their affiliated organizations, or those of the publisher, the editors and the reviewers. Any product that may be evaluated in this article, or claim that may be made by its manufacturer, is not guaranteed or endorsed by the publisher.

Copyright © 2022 Guo, Qiao, Dong, Li, Liu and Xu. This is an open-access article distributed under the terms of the Creative Commons Attribution License (CC BY). The use, distribution or reproduction in other forums is permitted, provided the original author(s) and the copyright owner(s) are credited and that the original publication in this journal is cited, in accordance with accepted academic practice. No use, distribution or reproduction is permitted which does not comply with these terms.



IGFBP7 and the Tumor Immune Landscape: A Novel Target for Immunotherapy in Bladder Cancer

Xianyanling Yi^{1†}, Xiaonan Zheng^{1†}, Hang Xu^{1†}, Jin Li¹, Tianyi Zhang¹, Peng Ge², Dazhou Liao¹, Hong Li¹, Xiaoyan Lyu^{3,4*} and Jianzhong Ai^{1*}

¹ Department of Urology, Institute of Urology, West China Hospital, Sichuan University, Chengdu, China, ² Department of Endocrinology and Metabolism, West China Hospital of Sichuan University, Chengdu, China, ³ Department of Dermatology, West China Hospital, Sichuan University, Chengdu, China, ⁴ Laboratory of Dermatology, Clinical Institute of Inflammation and Immunology, Frontiers Science Center for Disease-related Molecular Network, West China Hospital, Sichuan University, Chengdu, China

OPEN ACCESS

Edited by:

Xian Zeng, Fudan University, China

Reviewed by:

Ping Lu, University of Massachusetts Medical School, United States Fan Shen, University of Alberta, Canada

*Correspondence:

Jianzhong Ai jianzhong.ai@scu.edu.cn Xiaoyan Lyu Ixiaoyan@scu.edu.cn

[†]These authors have contributed equally to this work and share first authorship

Specialty section:

This article was submitted to Cancer Immunity and Immunotherapy, a section of the journal Frontiers in Immunology

Received: 17 March 2022 Accepted: 26 May 2022 Published: 23 June 2022

Citation:

Yi X, Zheng X, Xu H, Li J, Zhang T, Ge P, Liao D, Li H, Lyu X and Ai J (2022) IGFBP7 and the Tumor Immune Landscape: A Novel Target for Immunotherapy in Bladder Cancer. Front. Immunol. 13:898493. doi: 10.3389/fimmu.2022.898493 Insulin-like growth factor binding protein-7 (IGFBP7) was recently reported to be a ligand of CD93, a potential target to normalize vasculature and attenuate immunotherapy. However, its role in the tumor microenvironment (TME) and immunotherapy response of bladder cancer (BLCA) remains unclear. We comprehensively evaluated the correlation between IGFBP7 and multiple immunological characteristics of BLCA across The Cancer Genome Atlas (TCGA) and two external cohorts. Importantly, the response of IGFBP7grouped BLCA patients to immunotherapy was predicted and validated by five real-word immunotherapy cohorts. Finally, we developed an IGFBP7-based immune risk model validated by five independent cohorts. IGFBP7 modulated the TME across pan-caners. In BLCA, high expression of IGFBP7 was correlated with more aggressive clinical features. IGFBP7 was positively associated with immunomodulators and promoted tumorinfiltrating lymphocyte trafficking into the tumor microenvironment. However, T cells recognition and tumor cell killing were lower in the high-IGFBP7 group. In addition, high expression of IGFBP7 displayed lower enrichment scores for most pro-immunotherapy pathways. Clinical data from IMvigor210 and GSE176307 indicated that IGFBP7 negatively correlated with the BLCA immunotherapy response. The same trend was also observed in a renal cell carcinoma (RCC) cohort and two melanoma cohorts. Notably, urothelial and luminal differentiation were less frequently observed in the high-IGFBP7 group, while neuroendocrine differentiation was more frequently observed. Mechanistically, high IGFBP7 was associated with an enriched hypoxia pathway and higher expression of key genes in ERBB therapy and antiangiogenic therapy. Furthermore, our IGFBP7-based immune risk model was able to predict the prognosis and response to immunotherapy with good accuracy (5-year AUC = 0.734). Overall, IGFBP7 plays a critical role in the immunoregulation and TME of BLCA and may serve as a novel potential target for combination treatment with immunotherapy for BLCA.

Keywords: IFGBP7, bladder cancer, immunotherapy, tumor microenvironment, molecular subtype, hypoxia, risk model

INTRODUCTION

Bladder cancer (BLCA) is one of the most common malignancies of the urinary system, with approximately 212,536 deaths each year from BLCA (1). Generally, the treatment strategies of BLCA include surgical resection, radiation therapy, chemotherapy and immunotherapy (2, 3). Some patients with local BLCA can be curable; however, the five-year survival rate of patients with metastatic bladder cancer is low (4). In recent years, significant advantages have been made in terms of immunotherapy and targeted therapies for bladder cancer (5). Immune checkpoint inhibitors (ICIs), as one of the most promising types in immunotherapy, are widely used in treating different kinds of cancers (6, 7). ICIs have also been reported to be relatively effective for BLCA (8, 9), which may be attributed to the high tumor mutation burden and abundant infiltration of immune cells within the tumor microenvironment (TME) of BLCA (10-12). Five ICIs have been approved for the treatment of locally advanced and metastatic BLCA by the FDA (13). However, the response to ICIs varies across BLCA patients, and only a minority of BLCA patients benefit from these agents (14, 15). To date, there is still a lack of novel drugs for the development of more effective therapeutic strategies.

Insulin-like growth factor binding protein-7 (IGFBP7) is a member of the IGFBP family, which binds insulin with high affinity and IGF with low affinity (16). IGFBP7 was originally identified in normal mammary epithelial cells and meningeal cells, and its expression pattern varies with tumor type (17). In some tumors, IGFBP7 exhibits tumor suppressor activity in certain cancer types via regulation of cell proliferation, apoptosis, cell adhesion epithelial mesenchymal transition (EMT) and angiogenesis (18-20). However, IGFBP7 acts as a cancerpromoting gene in esophageal adenocarcinoma and neck squamous cell carcinomas (21, 22). Recently, Sun et al. (23) found that IGFBP7, acting as a ligand of CD93, can disrupt normalizes tumor vasculature and increase immune infiltration through the CD93/IGFBP7 pathway. Moreover, a CD93-targeting monoclonal antibody (mAb) has been demonstrated to reduce tumor growth and enhance the effects of immunotherapy in pancreatic tumors or melanoma via the CD93/IGFBP7 pathway (24). Together, IGFBP7 may provide potential value for the immunotherapy of cancer, but the role of IGFBP7 in BLCA has not been elucidated.

In this study, IGFBP7 was highly correlated with the modulation of the TME in most cancers by pan-cancer analysis. We found that IGFBP7 was negatively associated with T cells recognition and tumor cell killing. In addition, IGFBP7 negatively correlated with the BLCA immunotherapy response, and IGFBP7 had the potential to predict the molecular subtype of BLCA. Anti-IGFBP7 therapy may be a suitable therapeutic candidate for BLCA, but more studies are required for further validation.

MATERIALS AND METHODS

Data Source and Preprocessing

The mRNA sequencing expression profiles and clinical information of bladder cancer patients were downloaded from

The Cancer Genome Atlas (TCGA) (http://cancergenome.nih. gov/). The abbreviations for various cancer types are listed in Table S1. The advanced urothelial cancer cohort (IMvigor210 cohort) (patients treated with atezolizumab) based on the Creative Commons 3.0 License was downloaded from a freely available data package (http://research-pub.gene.com/ IMvigor210CoreBiologies/) (25). Five BLCA datasets (GSE176307, GSE13507, GSE31684, GSE32894, GSE48277) and two melanoma datasets (GSE78220, GSE91061) were downloaded from the Gene Expression Omnibus (GEO) database (https://www.ncbi.nlm.nih.gov/geo/). Of these cohorts, GSE176307 (patients treated with pembrolizumab or atezolizumab), GSE78220 (patients treated with pembrolizumab and nivolumab) (26), and GSE91061 (patients treated with nivolumab) (27) were all treated with immunotherapy. In addition, another immunotherapy cohort of renal cell carcinoma (RCC) (PMID29301960) (patient treated with nivolumab) was obtained from Miao's study (28). The raw data are shown in Supplementary Material.

Pan-Cancer Analysis of IGFBP7

For the pan-cancer analysis, the R package "ggplot2" was used to identify the Spearman correlations between the expression of IGFBP7 and immunomodulators, which include immunostimulators, chemokines, major histocompatibility complex (MHC) and receptors (29). Correlations between the expression of IGFBP7 and immune checkpoints (CD274, CTLA4, HAVCR2, LAG3, PDCD1, PDCDLIG2, TIGIT, and SIGLEC15) were also computed. IGBP7 expression was measured in tumor-infiltrating immune cells (B cells, CD4+ T cells, CD8+ T cells, neutrophils, macrophages, and dendritic cells) by using TIMER 2.0 (http://timer.cistrome.org/) (30).

Association Between IGFBP7 Expression and Clinical Features

The patients were grouped based on different clinical features, including T stage (T1&T2 versus (vs) T3&T4), N stage (N0 vs N+), lymphovascular invasion (yes vs no), pathologic stage (stage I&II vs stage III&IV), histologic grade (low grade vs high grade) and histologic subtype (papillary vs non-papillary). According to the results of the normality test and homogeneity of variances, independent samples t tests were used to evaluate the differential expression of IGFBP7 between different groups.

The Effect of IGBP7 on Immunological Characteristics in BLCA

Coexpression was analyzed statistically by using the Spearman correlation coefficient to identify the expression differences of 122 immunostimulators between the high- and low-IGFBP7 groups (The patients in the same cohort were divided into high and low subgroups based on the median IGFBP7 expression value). Single-sample gene set enrichment analysis (ssGSEA) was used to quantify the relative abundance of 15 immune cell infiltrates (31). Subsequently, the infiltration of immune cells was compared between the high- and low-IGFBP7 groups using the Wilcoxon rank sum test. The R package "ComplexHeatmap" was used to visualize the expression of genes frequently expressed on the surfaces of immune cells (32). The cancer immunity cycle consists of the following seven steps: release of cancer cell antigens (Step 1), cancer antigen presentation (Step 2), priming and activation (Step 3), trafficking of immune cells to tumors (Step 4), infiltration of immune cells into tumors (Step 5), recognition of cancer cells by T cells (Step 6), and killing of cancer cells (Step 7). Tracking tumor immunophenotype (TIP, http://biocc.hrbmu.edu.cn/TIP/) was used to analyze and visualize the cancer immunity cycle (33). The status of anti-cancer immunity was compared according to IGFBP7 groups, and we plotted a heatmap with the R package ComplexHeatmap. Pan-cancer T cell-inflamed score can also define pre-existing cancer immunity, which includes eighteen genes (34). Moreover, 18 inhibitory immune checkpoints with therapeutic potential were selected, and then the correlations between them and IGFBP7 were assessed.

Prediction of Immunotherapeutic and Chemotherapy Drug Response

We compared the different expression levels of eight immune checkpoint-related genes between the high- and low-IGFBP7 groups. Eighteen immunotherapy-positive signatures were included in our study, and their enrichment scores were calculated using gene set variation analysis (GSVA). Comparisons for predicting the response to immunotherapy were performed between the high- and low-IGFBP7 groups. The TIDE algorithm was used to predict potential ICB responses in the high- and low-IGFBP7 groups (35). The immunotherapy response data for two BLCA cohorts (IMvigor210 and GSE176307), RCC cohort (PMID29301960) and two melanoma cohorts (GSE78220 and GSE91061) were collected. We evaluated IGFBP7 expression in the PR/CR group and SD/PD group. In addition, tumor mutation burden was compared in the high- and low-IGFBP7 groups. Moreover, we predicted IGFBP7-grouped chemotherapy and tyrosine kinase inhibitor drug responses based on the Genomics of Drug Sensitivity in Cancer (GDSC) database (https://www.cancerrxgene.org/) (36). The prediction process was implemented by the R package "pRRophetic", where the samples' half-maximal inhibitory concentration (IC50) was estimated by ridge regression and the prediction accuracy.

Enrichment Analysis of Various Therapeutic Signatures and BLCA Molecular Subtypes

By using consensus MIBC and BLCA subtyping R packages, the samples were assigned to different BLCA molecular subtypes, which included a combined consensus subtype and six published molecular classifications (University of North Carolina (UNC), Baylor, Cancer Genome Atlas (TCGA), MD Anderson Cancer Center (MDA), Lund and Cartes d'Identité des Tumeurs (CIT)) (37–42). Afterwards, we calculated the enrichment score of the 12 molecular subtype-specific signatures for the training and validation cohorts (37). A gene set enrichment analysis was performed computed by GSVA to evaluate various therapeutic

signatures in both the training cohort and validation cohort. The results are presented in the form of a heatmap, as well as bar graphs.

Identification of Gene Mutation Analysis and Drug-Related Genes of BLCA

To identify somatic mutations in patients with BLCA in the TCGA database, mutation data were retrieved from the TCGA database and visualized using the "maftools" package in R software. The waterfall plot shows the mutation data of the top 30 mutated genes. We further used the data of BLCA-related drug target genes obtained from the DrugBank database (https://go.drugbank.com/) to compare their expression in IGFBP7 groups (43).

Development of an IGFBP7-Based Immune Risk Model

We selected the dataset from TCGA as the training cohort. The DESeq2 R package was used to analyze the differentially expressed genes (DEGs) in the high- and low-IGFBP7 groups. Prognostic genes of TCGA-BLCA were screened with a P value < 0.05. Immunologic signature gene sets were downloaded from The Molecular Signatures Database (MSigDB) C7 dataset (https://www.gsea-msigdb.org/gsea/msigdb/index.jsp). Next, the three gene sets obtained were intersected and served as the candidate gene set. The least absolute shrinkage and selection operator (LASSO) Cox regression method using the "glmnet" and "survival" R packages was applied to select the optimal corresponding coefficients for risk model construction. Based on the following formula, the risk score for each patient was calculated.

RiskScore_i =
$$\sum_{j=1}^{n} exp_{ji} \times \beta_j$$

where *exp* means the gene expression value, *i* means each sample, *j* means each gene, and β means the coefficient in LASSO regression. A forest plot was used to explore the correlation between the genes and prognosis in BLCA. A Kaplan–Meier curve was drawn to compare the overall survival between the high-risk and low-risk groups. Receiver operating characteristic (ROC) curve analyses and decision curve analyses (DCA) were conducted to evaluate the model. For validation of the risk model, five independent cohorts (GSE13507, GSE31684, GSE32894, GSE48277, IMvigor210) were used. Furthermore, we explored the associations between the risk model and clinicopathological features, tumor microenvironment features, various therapeutic signatures, immune checkpoint genes, BLCA molecular subtype and BLCA-related drug target genes.

Statistical Analysis

All statistical data analyses were performed using R software, version 3.6.3. Continuous variables that conformed to the normal distribution were compared using independent t tests for comparisons between binary groups, while continuous variables with skewed distributions were compared with the Mann–Whitney U test. Categorical variables were compared by

using the chi-square test or Fisher's exact test. Spearman analysis was used for the correlation studies between quantitative variables. Survival curves were analyzed using the log-rank test (generated using the Kaplan–Meier method). All statistical tests were two-sided with a level of significance set as P < 0.05.

RESULT

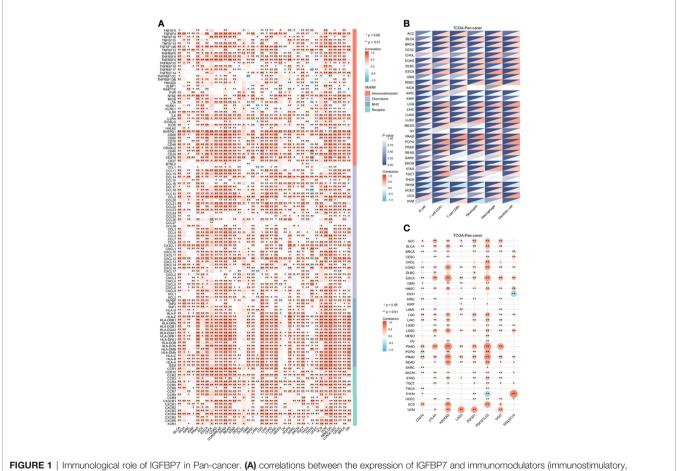
The Immunological Role of IGFBP7 in Pan-Cancer

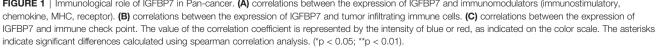
To determine the role of IGFBP7 in regulating the microenvironmental immunity of cancer, correlations between the expression of IGFBP7 and immunomodulators, immune checkpoints and tumor-infiltrating immune cells were performed. The results demonstrated that IGFBP7 was positively correlated with a majority of immunomodulators in the majority of cancers (**Figure 1A**). We also calculated the infiltration levels of TIICs in the TME using the ssGSEA algorithm. Except for KICH, KIRC, KIRP, SARC, TGCT,

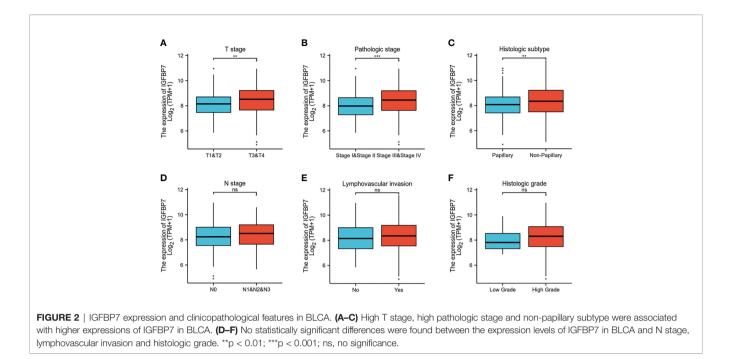
THCA, THYM and UVM, IGFBP7 exhibited a positive correlation with the majority of TIICs in most of the cancer types (**Figure 1B**). Additionally, we found that the expression of IGFBP7 was mutually exclusive to immune checkpoints in THCA, THYM, LAML, KIRC and KIRP. IGFBP7 was positively related to most immune checkpoints in other malignancies (**Figure 1C**). Overall, these findings indicated that IGFBP7 played a key role in regulating microenvironment immunity across most cancers.

Clinical Relevance of IGFBP7

The gene expression profiling data and clinical information of BLCA patients were downloaded from the TCGA database. The patients with BLCA were divided into different groups based on clinical parameters to analyze differences in gene expression. High expression of IGFBP7 was significantly related to advanced T stage, pathologic stage and poorly differentiated histologic subtype (**Figures 2A–C**). There were no statistically significant differences in the pattern of gene expression between N stage, lymphovascular invasion and histologic grade (**Figures 2D–F**).







The Immunological Role of IGFBP7 in the TME of BLCA

Based on the above pan-caner analyses, IGFBP7 showed a strong correlation with immunomodulators. We further examined the association between immunomodulators and the expression level of IGFBP7 (**Figure 3A**). This result indicated that IGFBP7 was significantly positively correlated with a majority of immunostimulators. Chemokines contributed to recruitment of CD8+ T cells, macrophages, TH17 cells, and antigen-presenting cells were also upregulated in the IGFBP7 high group. The results for major histocompatibility complex (MHC) and receptors demonstrated the same trend.

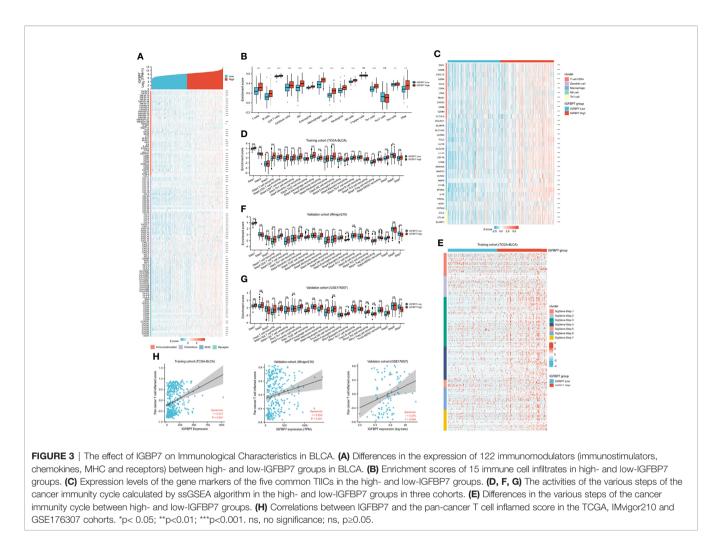
To further understand and characterize the microenvironment immunity with IGFBP7 expression, the profile of TME cell infiltration models was evaluated. We found that high expression of IGFBP7 prompted immune cell infiltration in the TME, with the exception of T helper cells and T17 cells (Figure 3B). The infiltration of regulatory T cells (Tregs), which have immunosuppressive effects, was also enhanced in the high-IGFBP7 group. Likewise, IGFBP7 was positively correlated with the effector genes of these TIICs (Figure 3C). Moreover, as a direct systematic performance of the functions of the chemokines and other immunomodulators, the activities of the cancer immunity cycle (Figure 3D), including the release of cancer cell antigens (Step 1), trafficking of immune cells to tumors (Step 4), and infiltration of immune cells into tumors (Step 5), were found to be upregulated in the IGFBP7 high group. Notably, the recognition of cancer cells by T cells (Step 6) was weakened by IGFBP7. These results were also presented by the heat-map graph (Figure 3E), and they are consistent with previous findings. Validation cohorts (Figures 3F, G) showed the same trend in some steps (Step 1, Step 4 and Step 5) of cancer immunity cycle. Although we did not observe that high expression of IGFBP7 could significantly weaken

the Step 6, in these two validation cohorts, the killing of cancer cells (Step 7) was downregulated in the IGFBP7 high group. Collectively, IGFBP7 shaped a hostile TME. The results of the correlation between IGFBP7 gene expression and the T-cell inflamed ssGSEA score indicated that IGFBP7 expression was significantly positively related to the pan-cancer T cell inflamed score in the training cohort and validation cohorts (IMvigor210 cohort and GSE176307) (**Figure 3H**). Furthermore, the inflamed TME exhibited higher immune checkpoint inhibitor expression levels (44). Consistently, IGFBP7 had positive correlations with the vast majority of inhibitory immune checkpoints (**Supplementary Figure S1**).

IGFBP7 Predicts Immunotherapy Response in BLCA

We compared the expression of several common immunotargets, including CD274, PDCD1, PDCD1LG2, CTLA4, HAVCR2, LAG3, TIGT and SIGLEC15, between the high- and low-IGFBP7 expression subgroups by using the training and validation cohorts, and the results showed that the expression of immunotargets was higher in the IGFBP7 high group (**Figures 4A–C**). As expected, a higher TIDE score occurred in the IGFBP7 high group (**Figure 4D**), which indicated that the IGFBP7 high group showed worse clinical efficacy to ICB therapy. In addition, IGFBP7 negatively correlated with the enrichment scores of most immunotherapy-positive gene signatures in the TCGA, IMvigor210 and GSE176307 cohorts (**Figures 4E–G**).

Subsequently, we collected immunotherapy response data for IMvigor210 and GSE176307 and evaluated IGFBP7 expression in the PR/CR group and SD/PD group. In line with the results of the response to ICB, IGFBP7 was shown to have lower expression in the PR/CR group than in the SD/PD group



(Figures 4H, I). The same trend occurred in three external cohorts (RCC cohort and two melanoma cohorts) (Figure 4J). However, there were no significant differences. The tumor mutation burden was significantly higher in the IGFBP7 low group (Figure 4I).

IGFBP7 Predicts the Response to Chemotherapy Drugs and Tyrosine Kinase Inhibitors in BLCA

We predicted the response to chemotherapy drugs and tyrosine kinase inhibitors for the high- and low-IGFBP7 groups based on the DrugBank database. The results indicated that patients with low expression of IGFBP7 were more sensitive to doxorubicin, gemcitabine, methotrexate, mitomycin C and paclitaxel (**Figure 5**). Nevertheless, a significantly higher response to cisplatin and sunitinib was observed in the IGFBP7 high group.

IGFBP7 Predicts Molecular Subtypes and Therapeutic Opportunities in BLCA

BLCA molecular typing was conducted in multiple research centers and named the UNC subtype, Baylor subtype, TCGA subtype, MDA subtype, Lund subtype, CIT subtype and consensus subtype. Despite these variations, all typing methods contain two fundamental subtypes: the basal subtype and the luminal subtype (45). The basal subtype has a poorer prognosis than the luminal subtype but is neo-adjuvant chemotherapy (NAC)-sensitive (46, 47). To further explore the expression patterns of IGFBP7 in BLCA, we evaluated the distribution of IGFBP7 in different molecular subtypes. In the training cohort, we found IGFBP7 to be negatively related to the luminal differentiation subtype of BLCA (Figure 6A). In addition, the enrichment scores for urothelial differentiation, the Ta pathway, luminal differentiation and mitochondria were greater in the low-IGFBP7 group. The enrichment scores for EMT differentiation, immune differentiation, smooth muscle, myofibroblast, interferon response and neuroendocrine differentiation were higher in the high-IGFBP7 group (Figure 6B). We validated these outcomes by using two external cohorts (Supplementary Figure S2A-D).

In addition, we performed enrichment analysis to evaluate various therapeutic signatures in different IGFBP7 groups. The difference in enrichment scores for various therapeutic signatures between the high- and low-IGFBP7 groups was significant (**Figure 6C, D**). Notably, the enrichment scores for hypoxia were lower in the low-IGFBP7 group, which was not the

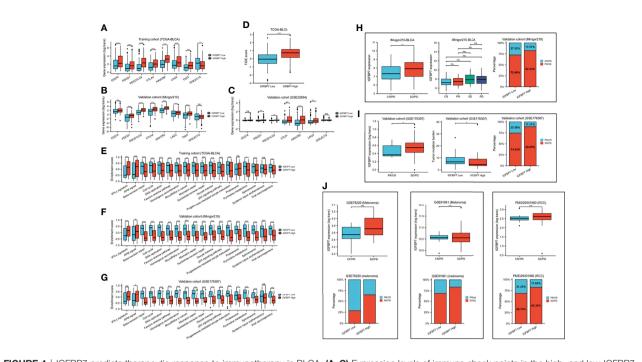


FIGURE 4 | IGFBP7 predicts therapeutic response to immunotherapy in BLCA. (A–C) Expression levels of immune check points in the high- and low-IGFBP7 groups in the TCGA, IMvigor210, GSE32894 cohorts. (D) ICB responses in the high- and low-IGFBP7 groups using TIDE algorithm. (E–G) The enrichment scores of several immune-related signatures in the high- and low-IGFBP7 groups. (H, I) Correlation between IGFBP7 and the clinical response of cancer immunotherapy in the IMvigor210 and GSE176307 cohort. (J) Correlation between IGFBP7 and the clinical response of cancer immunotherapy in the RCC cohort and two melanoma cohorts. CR: complete response; PR, partial response; PD, progressed disease; SD, stable disease. (CR/PR means patient who are CR or PR; SD/PD means patient who are SD or PD). *p<0.05; **p<0.01; ***p<0.001. ns, no significance; ns, p≥0.05.

same as other radiotherapy-predicted pathways. IMvigor210 and GSE176307 were used to validate our outcomes (**Supplementary Figures S2E-H**). Moreover, the results from the DrugBank database indicated a notably higher response to ERBB therapy and antiangiogenic therapy in the high-IGFBP7 group (**Figure 6E**; **Supplementary Figures S2I**, J). We further visualized the mutation data of TCGA-BLCA, and the top 30 mutated genes are displayed (**Supplementary Figure 3A**). Likewise, tumor mutation burden was calculated and

compared between the high- and low-IGFBP7 groups. There were no significant differences between the high- and low-IGFBP7 groups (**Supplementary Figure 3B**).

Development and Validation of the IGFBP7-Based Immune Risk Model

A Wayne diagram showed that 543 candidate genes were significantly related to prognosis (**Figure 7A**). Subsequently, the LASSO algorithm was used to identify the 23 best

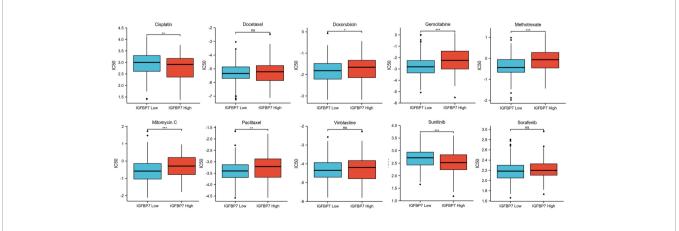
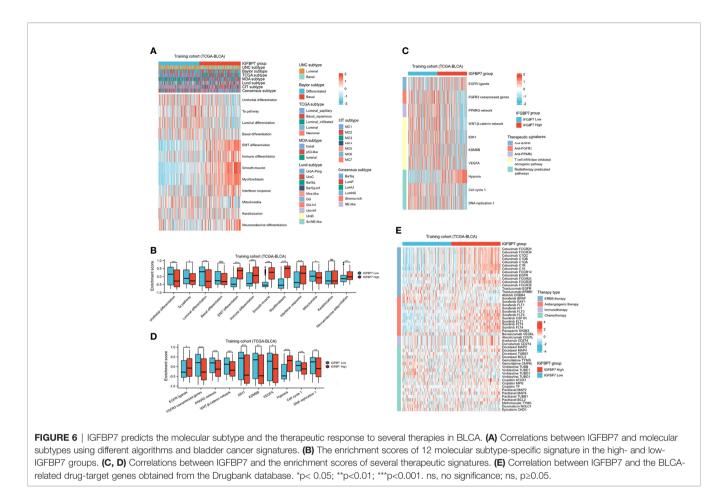


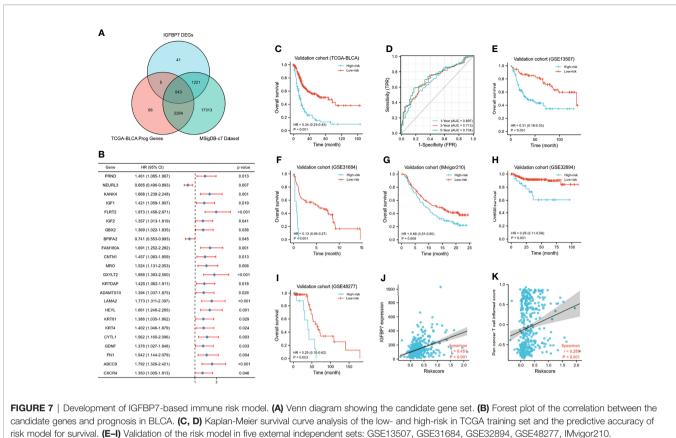
FIGURE 5 | IC50 of chemotherapy drugs and tyrosine kinase inhibitors in bladder cancer based on IGFBP7 expression. *p< 0.05; **p<0.01; ***,p<0.001. ns, no significance; ns, p≥0.05,



candidate genes. The forest plots illustrated univariate Cox analysis of the prognostic impact of the candidate gene set (Figure 7B). The risk score model was constructed based on the training cohort. ROC analysis was used to test our model, and the area under the ROC curve was above 0.697, which meant a moderate sensitivity and specificity for predicting the prognosis of BLCA (Figure 7D). Furthermore, we divided the patients into high- and low-risk groups based on their risk scores. As shown in Figure 7C, there was a significant difference in overall survival between the two groups. The risk model was then validated using another five sets of validation datasets (Figures 7E-I). Considering the clinical usefulness of the risk model, we drew a DCA curve. According to the DCA, when the threshold probability for a patient was within the approximate range of 20-100%, the risk model added more net benefit than the "all positive" or "all negative" strategies in the TCGA cohort (Figure 8A). A nomogram model was constructed for predicting the prognosis of BLCA by using clinical characteristics, including age, T stage, N stage and risk score. The nomogram plot in Figure 8B shows the weight of each variable based on the multivariate Cox analysis, and the straight line down to the endpoint scales could predict the probability of survival at 1, 3, and 5 years. In addition, as expected, patients with lymphovascular invasion, high

histologic grade, advanced pathologic stage and non-paillary subtype were more likely to obtain a higher risk score (Figures 8C-J).

Except for the value of predicting prognosis, our risk model significantly predicted the response to immunologic therapy. The expression of IGFBP7 and pan-cancer T cell inflamed score were both significantly positively correlated with the risk score (Figures 7J, K). Furthermore, the enrichment scores of most of the cancer immunity cycle steps were higher in the high-risk group (Supplementary Figure S4A). Similarly, the expression of a majority of immune checkpoints was higher in the high-risk group (Supplementary Figure S4B). The association between the risk score and different molecular subtypes was in line with previous findings. Patients with basal-type bladder cancer had a higher risk score and a worse prognosis (Supplementary Figures S4C, D). We also discovered that the enrichment scores of T cell infiltration inhibited oncogenic pathways were significantly higher in the highrisk group, while those in hypoxia were higher in the low-risk group (Supplementary Figures S4E, F). Finally, according to the heatmap, ERBB therapy, antiangiogenic therapy, immunotherapy and chemotherapy may be appropriate for BLCA with higher risk scores (Supplementary Figures S4G).



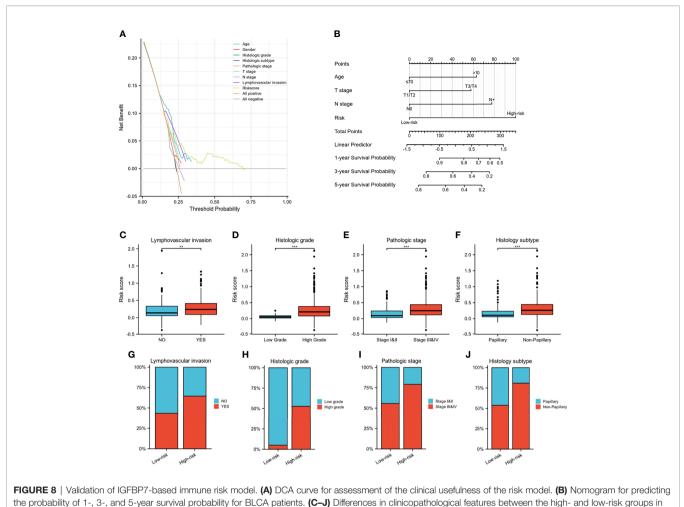
(J, K) Correlations between riskscore, expression of IGFBP7 and pan-cancer T cell inflamed score.

DISCUSSION

As one of the most common malignant tumors of the urinary system, BLCA lacks effective targeted treatment. With the great advances of immunotherapy in BLCA, its favorable safety and tolerability are progressively manifested. However, given that the overall response rates to immunotherapy are still low, more accurate and effective targets for immunotherapy are urgently needed. It is generally known that IGFBP7 plays a role in tumorigenesis via the IGF/insulin signaling pathway. IGFBP7 can block downstream signaling and impede cell growth, apoptosis and the TME. Previous studies indicated that IGFBP7 functions as a tumor suppressor in several tumors, including hepatocellular carcinoma, colorectal carcinoma, prostate cancer cells, and breast cancer (17, 48-50). Nevertheless, some differences in results were found in esophageal adenocarcinoma and neck squamous cell carcinomas (21, 22). The role of IGFBP7 in BLCA is still unclear, and more evidence is needed to explore the association between IGFBP7 and tumor immunologic features.

In this study, pan-cancer analysis indicated that IGFBP7 was positively correlated with immunomodulators, the infiltration levels of TIICs, and immune checkpoints in the majority of cancers. It is well known that the TME mediates immune escape and regulates the sensitivity of tumors to anticancer drugs. The TME is composed of various types of immune cells, including T cells, NK cells and dendritic cells, which are responsible for anticancer immunity (51). Regulatory T cells (Tregs) have immunosuppressive effects because they can promote evasion of the recognition of tumor antigens by antigen-presenting cells and T cells (52). More importantly, IGFBP7 showed a strong correlation with the TME in BLCA. We found that most immunostimulators and TIICs were significantly upregulated in the IGFBP7 high group. Additionally, the enrichment score of Tregs was also higher in the IGFBP7 high group. In the tumor immunity cycle, IGFBP7 enhanced the release of cancer cell antigens, trafficking of immune cells to tumors and infiltration of immune cells into tumors. Theoretically, high IGFBP7 expression may result in a better immune microenvironment. However, the recognition of cancer cells by T cells eventually weakened in TCGA cohort. Meanwhile, we did not observe that the killing of cancer cells was significantly downregulated by IGFBP7 in the TCGA cohort but was found in both the IMvigor 210 and GSE176307 cohorts.

Abnormal tumor blood vessels cause the formation of an immunosuppressive microenvironment, leading to immune escape. Several studies have demonstrated that IGFBP7 is typically overexpressed in tumor-associated endothelial cells relative to normal vascular endothelial cells (53–55). Sun et al. (23) demonstrated that IGFBP7 acted as a ligand of CD93 and disrupted normalizes tumor vasculature, including reducing pericyte and smooth muscle cell coverage on blood vessels and



the TCGA cohort. **p<0.01; ***p<0.001.

increasing vascular permeability and leakage by the CD93/ IGFBP7 pathway. Abnormal tumor vascular structure and function lead to interstitial hypertension and a hostile TME characterized by hypoxia and acidosis. These changes in the tumor microenvironment may influence immune cell function. Previous studies indicated that hypoxia and acidosis hindered the maturation of APCs and DCs, and immature DCs could not activate T cells effectively, although they can still present antigens (56, 57). Although immune infiltration can increase via the interaction of IGFBP7 and CD93, hypoxia drives the preferential recruitment of Tregs, which express negative costimulatory molecules and lead to inadequate costimulation for T-cell activation (58, 59). In the meantime, infiltrated TILs were inactive, and effector T cells were unable to recognize and kill the tumor cells. Therefore, as we demonstrate here, high expression of IGFBP7 did not seem to enhance the cancer immunity cycle but tended to diminish. Furthermore, we offer the following conjecture regarding why higher IGFBP7 expression is accompanied by more enriched TILs: the increases in tumor vascular permeability can result in leakage through the vessel wall, which allows the tumor cells and TILs to leave the tissue more easily. However, further studies are required to verify this conjecture. Overall, high expression of IGFBP7 increased TIICs, but the activities of the recognition of cancer cells by T cells and killing of cancer cells were decreased. These factors may shape the different responses to immune therapy between patients with high and low IGFBP7 expression.

In theory, the expression of immune checkpoints will be upregulated in an immunosuppressive microenvironment, and this was indeed the case. In our further analysis, we found that high IGFBP7 expression was correlated with a lower response to ICB. This result was consistent with the views of Sun et al (24). In addition, the enrichment scores of immunotherapy-positive signatures showed that most immunotherapy-positive signature enrichment scores were higher in the IGFBP7 low group. Clinical data indicated concordant findings. We found that IGFBP7 was significantly inversely correlated with the immunotherapeutic response in two BLCA cohorts (IMvigor210 and GSE176307). The same tendency was also found for two additional melanoma cohorts and the RCC cohort. Moreover, immunosuppressive oncogenic pathways, such as the FGFR3, PPARG, and β-catenin pathways, were found to suppress the infiltration of TIICs via a reduction in the expression of immunomodulators (60-62). IGFBP7 was

remarkably negatively correlated with these oncogenic pathways, which was consistent with our previous results. Notably, IGFBP7 expression was positively related to the enrichment scores of immunosuppressive pathways, including anti-EGFR and hypoxia therapy. In terms of chemotherapy drug response, the lower expression of IGFBP7 could make the cancer cells more sensitive to most chemotherapy drugs but resistant to cisplatin. Furthermore, IGFBP7 expression predicted the response to therapeutic options in BLCA, and it showed a notably higher response to ERBB therapy and antiangiogenic therapy in the high-IGFBP7 group.

Molecular subtype can help prognosticate and predict the response to immunotherapies, radiotherapy, neoadjuvant chemotherapy and several targeted therapies (37–39, 63). We found that high expression of IGFBP7 was less likely to be a luminal differentiation subtype, but the luminal subtype was related to a better prognosis. Moreover, the enrichment scores for urothelial differentiation, the Ta pathway, luminal differentiation and mitochondria were higher in the high-IGFBP7 group. All the results above were validated in independent cohorts. Eventually, we constructed a risk model to predict prognosis and the response to immunologic therapy. Our model was externally validated to show good robustness.

Given the above, IGFBP7 plays an important role in the regulation of the tumor microenvironment and impacts the immunotherapy response. We hypothesize that anti-IGFBP7 therapy holds great promise to improve the response to immune therapy, making it potentially an excellent drug target for combination treatment with immunotherapy for BLCA, which certainly necessitates further studies to verify our speculations.

DATA AVAILABILITY STATEMENT

The datasets presented in this study can be found in online repositories. The names of the repository/repositories and

REFERENCES

- Sung H, Ferlay J, Siegel RL, Laversanne M, Soerjomataram I, Jemal A, et al. Global Cancer Statistics 2020: GLOBOCAN Estimates of Incidence and Mortality Worldwide for 36 Cancers in 185 Countries. *CA: Cancer J Clin* (2021) 71(3):209–49. doi: 10.3322/caac.21660
- Antoni S, Ferlay J, Soerjomataram I, Znaor A, Jemal A, Bray F. Bladder Cancer Incidence and Mortality: A Global Overview and Recent Trends. *Eur Urol* (2017) 71(1):96–108. doi: 10.1016/j.eururo.2016.06.010
- Ghandour R, Singla N, Lotan Y. Treatment Options and Outcomes in Nonmetastatic Muscle Invasive Bladder Cancer. *Trends Cancer* (2019) 5 (7):426–39. doi: 10.1016/j.trecan.2019.05.011
- Dy GW, Gore JL, Forouzanfar MH, Naghavi M, Fitzmaurice C. Global Burden of Urologic Cancers, 1990-2013. Eur Urol (2017) 71(3):437–46. doi: 10.1016/j.eururo.2016.10.008
- Kamat AM, Hahn NM, Efstathiou JA, Lerner SP, Malmström PU, Choi W, et al. Bladder Cancer. *Lancet (London England)* (2016) 388(10061):2796–810. doi: 10.1016/s0140-6736(16)30512-8
- Bai R, Lv Z, Xu D, Cui J. Predictive Biomarkers for Cancer Immunotherapy With Immune Checkpoint Inhibitors. *biomark Res* (2020) 8:34. doi: 10.1186/ s40364-020-00209-0

accession number(s) can be found in the article/ Supplementary Material.

ETHICS STATEMENT

Our study did not require an ethical board approval because this article does not contain any studies with human participants or animals performed by any of the authors.

AUTHOR CONTRIBUTIONS

JA, XL and XY conceived the project and drafted the manuscript, XZ, HX, JL, DL, GP and TZ collected the public data and performed the bioinformatics analysis. HL and JA revised the manuscript. XL made great contributions during the revision of the manuscript. All authors contributed to the article and approved the submitted version.

FUNDING

This study was supported by grants from the National Natural Science Foundation of China (82070784,81702536) to J. A., a grant from Science & Technology Department of Sichuan Province, China (2022JDRC0040) to J. A., a grant from the National Natural Science Foundation of China (81871567) to X. L.

SUPPLEMENTARY MATERIAL

The Supplementary Material for this article can be found online at: https://www.frontiersin.org/articles/10.3389/fimmu.2022.898493/full#supplementary-material

- Darvin P, Toor SM, Sasidharan Nair V, Elkord E. Immune Checkpoint Inhibitors: Recent Progress and Potential Biomarkers. *Exp Mol Med* (2018) 50 (12):1–11. doi: 10.1038/s12276-018-0191-1
- Balar AV. Immune Checkpoint Blockade in Metastatic Urothelial Cancer. J Clin Oncol (2017) 35(19):2109–12. doi: 10.1200/jco.2017.72.8444
- Feld E, Harton J, Meropol NJ, Adamson BJS, Cohen A, Parikh RB, et al. Effectiveness of First-Line Immune Checkpoint Blockade Versus Carboplatin-Based Chemotherapy for Metastatic Urothelial Cancer. *Eur Urol* (2019) 76 (4):524–32. doi: 10.1016/j.eururo.2019.07.032
- Eruslanov E, Neuberger M, Daurkin I, Perrin GQ, Algood C, Dahm P, et al. Circulating and Tumor-Infiltrating Myeloid Cell Subsets in Patients With Bladder Cancer. Int J Cancer (2012) 130(5):1109–19. doi: 10.1002/ ijc.26123
- Michaud DS. Chronic Inflammation and Bladder Cancer. Urologic Oncol (2007) 25(3):260–8. doi: 10.1016/j.urolonc.2006.10.002
- Kandoth C, McLellan MD, Vandin F, Ye K, Niu B, Lu C, et al. Mutational Landscape and Significance Across 12 Major Cancer Types. *Nature* (2013) 502 (7471):333–9. doi: 10.1038/nature12634
- Twomey JD, Zhang B. Cancer Immunotherapy Update: FDA-Approved Checkpoint Inhibitors and Companion Diagnostics. AAPS J (2021) 23 (2):39. doi: 10.1208/s12248-021-00574-0

- Zou W, Wolchok JD, Chen L. PD-L1 (B7-H1) and PD-1 Pathway Blockade for Cancer Therapy: Mechanisms, Response Biomarkers, and Combinations. *Sci Trans Med* (2016) 8(328):328rv4. doi: 10.1126/scitranslmed.aad7118
- Sonpavde G, Dranitsaris G, Necchi A. Improving the Cost Efficiency of PD-1/ PD-L1 Inhibitors for Advanced Urothelial Carcinoma: A Major Role for Precision Medicine? *Eur Urol* (2018) 74(1):63–5. doi: 10.1016/j.eururo. 2018.03.015
- Oh Y, Nagalla SR, Yamanaka Y, Kim HS, Wilson E, Rosenfeld RG. Synthesis and Characterization of Insulin-Like Growth Factor-Binding Protein (IGFBP)-7. Recombinant Human Mac25 Protein Specifically Binds IGF-I and -II. J Biol Chem (1996) 271(48):30322–5. doi: 10.1074/jbc.271.48.30322
- Ruan W, Xu E, Xu F, Ma Y, Deng H, Huang Q, et al. IGFBP7 Plays a Potential Tumor Suppressor Role in Colorectal Carcinogenesis. *Cancer Biol Ther* (2007) 6(3):354–9. doi: 10.4161/cbt.6.3.3702
- Tamura K, Yoshie M, Hashimoto K, Tachikawa E. Inhibitory Effect of Insulin-Like Growth Factor-Binding Protein-7 (IGFBP7) on *In Vitro* Angiogenesis of Vascular Endothelial Cells in the Rat Corpus Luteum. *J Reprod Dev* (2014) 60 (6):447–53. doi: 10.1262/jrd.2014-069
- Li Y, Xi Y, Zhu G, Jia J, Huang H, Liu Y, et al. Downregulated IGFBP7 Facilitates Liver Metastasis by Modulating Epithelial–Mesenchymal Transition in Colon Cancer. Oncol Rep (2019) 42(5):1935–45. doi: 10.3892/ or.2019.7303
- Zhong Y, Lin Z, Lin X, Lu J, Wang N, Huang S, et al. IGFBP7 Contributes to Epithelial-Mesenchymal Transition of HPAEpiC Cells in Response to Radiation. J Cell Biochem (2019) 120(8):12500–7. doi: 10.1002/jcb.28516
- Smith E, Ruszkiewicz AR, Jamieson GG, Drew PA. IGFBP7 is Associated With Poor Prognosis in Oesophageal Adenocarcinoma and is Regulated by Promoter DNA Methylation. Br J Cancer (2014) 110(3):775-82. doi: 10.1038/bjc.2013.783
- 22. Sepiashvili L, Hui A, Ignatchenko V, Shi W, Su S, Xu W, et al. Potentially Novel Candidate Biomarkers for Head and Neck Squamous Cell Carcinoma Identified Using an Integrated Cell Line-Based Discovery Strategy. *Mol Cell Proteomics MCP* (2012) 11(11):1404–15. doi: 10.1074/mcp.M112.020933
- Sun Y, Chen W, Torphy RJ, Yao S, Zhu G, Lin R, et al. Blockade of the CD93 Pathway Normalizes Tumor Vasculature to Facilitate Drug Delivery and Immunotherapy. *Sci Trans Med* (2021) 13(604):eabc8922. doi: 10.1126/ scitranslmed.abc8922
- CD93 Blockade Stabilizes Tumor Vasculature to Improve Therapy Response. Cancer Discovery (2021) 11(10):2368. doi: 10.1158/2159-8290.Cd-rw2021-113
- Mariathasan S, Turley SJ, Nickles D, Castiglioni A, Yuen K, Wang Y, et al. Tgfβ Attenuates Tumour Response to PD-L1 Blockade by Contributing to Exclusion of T Cells. *Nature* (2018) 554(7693):544–8. doi: 10.1038/ nature25501
- Hugo W, Zaretsky JM, Sun L, Song C, Moreno BH, Hu-Lieskovan S, et al. Genomic and Transcriptomic Features of Response to Anti-PD-1 Therapy in Metastatic Melanoma. *Cell* (2016) 165(1):35–44. doi: 10.1016/j.cell. 2016.02.065
- Riaz N, Havel JJ, Makarov V, Desrichard A, Urba WJ, Sims JS, et al. Tumor and Microenvironment Evolution During Immunotherapy With Nivolumab. *Cell* (2017) 171(4):934–49.e16. doi: 10.1016/j.cell.2017.09.028
- Miao D, Margolis CA, Gao W, Voss MH, Li W, Martini DJ, et al. Genomic Correlates of Response to Immune Checkpoint Therapies in Clear Cell Renal Cell Carcinoma. *Sci (New York NY)* (2018) 359(6377):801–6. doi: 10.1126/ science.aan5951
- Charoentong P, Finotello F, Angelova M, Mayer C, Efremova M, Rieder D, et al. Pan-Cancer Immunogenomic Analyses Reveal Genotype-Immunophenotype Relationships and Predictors of Response to Checkpoint Blockade. *Cell Rep* (2017) 18(1):248–62. doi: 10.1016/j.celrep.2016.12.019
- Li T, Fu J, Zeng Z, Cohen D, Li J, Chen Q, et al. TIMER2.0 for Analysis of Tumor-Infiltrating Immune Cells. *Nucleic Acids Res* (2020) 48(W1):W509– w14. doi: 10.1093/nar/gkaa407
- Barbie DA, Tamayo P, Boehm JS, Kim SY, Moody SE, Dunn IF, et al. Systematic RNA Interference Reveals That Oncogenic KRAS-Driven Cancers Require TBK1. *Nature* (2009) 462(7269):108–12. doi: 10.1038/ nature08460
- Gu Z, Eils R, Schlesner M. Complex Heatmaps Reveal Patterns and Correlations in Multidimensional Genomic Data. *Bioinf (Oxford England)* (2016) 32(18):2847–9. doi: 10.1093/bioinformatics/btw313

- Xu L, Deng C, Pang B, Zhang X, Liu W, Liao G, et al. TIP: A Web Server for Resolving Tumor Immunophenotype Profiling. *Cancer Res* (2018) 78 (23):6575–80. doi: 10.1158/0008-5472.Can-18-0689
- Ayers M, Lunceford J, Nebozhyn M, Murphy E, Loboda A, Kaufman DR, et al. IFN-γ-Related mRNA Profile Predicts Clinical Response to PD-1 Blockade. J Clin Invest (2017) 127(8):2930–40. doi: 10.1172/jci91190
- 35. Jiang P, Gu S, Pan D, Fu J, Sahu A, Hu X, et al. Signatures of T Cell Dysfunction and Exclusion Predict Cancer Immunotherapy Response. *Nat Med* (2018) 24(10):1550–8. doi: 10.1038/s41591-018-0136-1
- 36. Yang W, Soares J, Greninger P, Edelman EJ, Lightfoot H, Forbes S, et al. Genomics of Drug Sensitivity in Cancer (GDSC): A Resource for Therapeutic Biomarker Discovery in Cancer Cells. *Nucleic Acids Res* (2013) 41(Database issue):D955–61. doi: 10.1093/nar/gks1111
- Kamoun A, de Reyniès A, Allory Y, Sjödahl G, Robertson AG, Seiler R, et al. A Consensus Molecular Classification of Muscle-Invasive Bladder Cancer. *Eur* Urol (2020) 77(4):420–33. doi: 10.1016/j.eururo.2019.09.006
- Robertson AG, Kim J, Al-Ahmadie H, Bellmunt J, Guo G, Cherniack AD, et al. Comprehensive Molecular Characterization of Muscle-Invasive Bladder Cancer. Cell (2018) 174(4):1033. doi: 10.1016/j.cell.2018.07.036
- Sjödahl G, Lauss M, Lövgren K, Chebil G, Gudjonsson S, Veerla S, et al. A Molecular Taxonomy for Urothelial Carcinoma. *Clin Cancer Res* (2012) 18 (12):3377–86. doi: 10.1158/1078-0432.Ccr-12-0077-t
- 40. Rebouissou S, Bernard-Pierrot I, de Reyniès A, Lepage ML, Krucker C, Chapeaublanc E, et al. EGFR as a Potential Therapeutic Target for a Subset of Muscle-Invasive Bladder Cancers Presenting a Basal-Like Phenotype. Sci Trans Med (2014) 6(244):244ra91. doi: 10.1126/scitranslmed.3008970
- Choi W, Porten S, Kim S, Willis D, Plimack ER, Hoffman-Censits J, et al. Identification of Distinct Basal and Luminal Subtypes of Muscle-Invasive Bladder Cancer With Different Sensitivities to Frontline Chemotherapy. *Cancer Cell* (2014) 25(2):152–65. doi: 10.1016/j.ccr.2014.01.009
- Mo Q, Nikolos F, Chen F, Tramel Z, Lee YC, Hayashi K, et al. Prognostic Power of a Tumor Differentiation Gene Signature for Bladder Urothelial Carcinomas. J Natl Cancer Institute (2018) 110(5):448–59. doi: 10.1093/jnci/ djx243
- Wishart DS, Feunang YD, Guo AC, Lo EJ, Marcu A, Grant JR, et al. DrugBank
 5.0: A Major Update to the DrugBank Database for 2018. Nucleic Acids Res (2018) 46(D1):D1074–d82. doi: 10.1093/nar/gkx1037
- 44. Gajewski TF, Corrales L, Williams J, Horton B, Sivan A, Spranger S. Cancer Immunotherapy Targets Based on Understanding the T Cell-Inflamed Versus Non-T Cell-Inflamed Tumor Microenvironment. Adv Exp Med Biol (2017) 1036:19–31. doi: 10.1007/978-3-319-67577-0_2
- McConkey DJ, Choi W. Molecular Subtypes of Bladder Cancer. Curr Oncol Rep (2018) 20(10):77. doi: 10.1007/s11912-018-0727-5
- 46. McConkey DJ, Choi W, Shen Y, Lee IL, Porten S, Matin SF, et al. A Prognostic Gene Expression Signature in the Molecular Classification of Chemotherapy-Naïve Urothelial Cancer is Predictive of Clinical Outcomes From Neoadjuvant Chemotherapy: A Phase 2 Trial of Dose-Dense Methotrexate, Vinblastine, Doxorubicin, and Cisplatin With Bevacizumab in Urothelial Cancer. Eur Urol (2016) 69(5):855–62. doi: 10.1016/j.eururo.2015.08.034
- 47. Seiler R, Ashab HAD, Erho N, van Rhijn BWG, Winters B, Douglas J, et al. Impact of Molecular Subtypes in Muscle-Invasive Bladder Cancer on Predicting Response and Survival After Neoadjuvant Chemotherapy. *Eur* Urol (2017) 72(4):544–54. doi: 10.1016/j.eururo.2017.03.030
- Akiel M, Guo C, Li X, Rajasekaran D, Mendoza RG, Robertson CL, et al. IGFBP7 Deletion Promotes Hepatocellular Carcinoma. *Cancer Res* (2017) 77 (15):4014–25. doi: 10.1158/0008-5472.Can-16-2885
- Hwa V, Tomasini-Sprenger C, Bermejo AL, Rosenfeld RG, Plymate SR. Characterization of Insulin-Like Growth Factor-Binding Protein-Related Protein-1 in Prostate Cells. J Clin Endocrinol Metab (1998) 83(12):4355–62. doi: 10.1210/jcem.83.12.5341
- 50. Landberg G, Ostlund H, Nielsen NH, Roos G, Emdin S, Burger AM, et al. Downregulation of the Potential Suppressor Gene IGFBP-Rp1 in Human Breast Cancer is Associated With Inactivation of the Retinoblastoma Protein, Cyclin E Overexpression and Increased Proliferation in Estrogen Receptor Negative Tumors. Oncogene (2001) 20(27):3497–505. doi: 10.1038/sj.onc. 1204471
- 51. Wessler S, Aberger F, Hartmann TN. The Sound of Tumor Cell-Microenvironment Communication - Composed by the Cancer Cluster

Salzburg Research Network. Cell communication Signaling CCS (2017) 15 (1):20. doi: 10.1186/s12964-017-0176-z

- 52. Corthay A. How do Regulatory T Cells Work? *Scandinavian J Immunol* (2009) 70(4):326–36. doi: 10.1111/j.1365-3083.2009.02308.x
- 53. Akaogi K, Okabe Y, Sato J, Nagashima Y, Yasumitsu H, Sugahara K, et al. Specific Accumulation of Tumor-Derived Adhesion Factor in Tumor Blood Vessels and in Capillary Tube-Like Structures of Cultured Vascular Endothelial Cells. *Proc Natl Acad Sci United States America* (1996) 93 (16):8384–9. doi: 10.1073/pnas.93.16.8384
- Pen A, Moreno MJ, Martin J, Stanimirovic DB. Molecular Markers of Extracellular Matrix Remodeling in Glioblastoma Vessels: Microarray Study of Laser-Captured Glioblastoma Vessels. *Glia* (2007) 55(6):559–72. doi: 10.1002/glia.20481
- St Croix B, Rago C, Velculescu V, Traverso G, Romans KE, Montgomery E, et al. Genes Expressed in Human Tumor Endothelium. *Sci (New York NY)* (2000) 289(5482):1197–202. doi: 10.1126/science.289.5482.1197
- Koebel CM, Vermi W, Swann JB, Zerafa N, Rodig SJ, Old LJ, et al. Adaptive Immunity Maintains Occult Cancer in an Equilibrium State. *Nature* (2007) 450(7171):903–7. doi: 10.1038/nature06309
- Yang M, Ma C, Liu S, Sun J, Shao Q, Gao W, et al. Hypoxia Skews Dendritic Cells to a T Helper Type 2-Stimulating Phenotype and Promotes Tumour Cell Migration by Dendritic Cell-Derived Osteopontin. *Immunology* (2009) 128(1 Suppl):e237–49. doi: 10.1111/j.1365-2567.2008.02954.x
- Peterson TE, Kirkpatrick ND, Huang Y, Farrar CT, Marijt KA, Kloepper J, et al. Dual Inhibition of Ang-2 and VEGF Receptors Normalizes Tumor Vasculature and Prolongs Survival in Glioblastoma by Altering Macrophages. *Proc Natl Acad Sci United States America* (2016) 113(16):4470–5. doi: 10. 1073/pnas.1525349113
- Facciabene A, Peng X, Hagemann IS, Balint K, Barchetti A, Wang LP, et al. Tumour Hypoxia Promotes Tolerance and Angiogenesis *via* CCL28 and T (reg) Cells. *Nature* (2011) 475(7355):226–30. doi: 10.1038/nature10169

- Korpal M, Puyang X, Jeremy Wu Z, Seiler R, Furman C, Oo HZ, et al. Evasion of Immunosurveillance by Genomic Alterations of Pparγ/Rxrα in Bladder Cancer. Nat Commun (2017) 8(1):103. doi: 10.1038/s41467-017-00147-w
- Spranger S, Bao R, Gajewski TF. Melanoma-Intrinsic β-Catenin Signalling Prevents Anti-Tumour Immunity. *Nature* (2015) 523(7559):231–5. doi: 10.1038/nature14404
- 62. Sweis RF, Spranger S, Bao R, Paner GP, Stadler WM, Steinberg G, et al. Molecular Drivers of the Non-T-Cell-Inflamed Tumor Microenvironment in Urothelial Bladder Cancer. *Cancer Immunol Res* (2016) 4(7):563–8. doi: 10.1158/2326-6066.Cir-15-0274
- Hu J, Yu A, Othmane B, Qiu D, Li H, Li C, et al. Siglec15 Shapes a non-Inflamed Tumor Microenvironment and Predicts the Molecular Subtype in Bladder Cancer. *Theranostics* (2021) 11(7):3089–108. doi: 10.7150/thno.53649

Conflict of Interests: The authors declare that the research was conducted in the absence of any commercial or financial relationships that could be construed as a potential conflict of interest.

Publisher's Note: All claims expressed in this article are solely those of the authors and do not necessarily represent those of their affiliated organizations, or those of the publisher, the editors and the reviewers. Any product that may be evaluated in this article, or claim that may be made by its manufacturer, is not guaranteed or endorsed by the publisher.

Copyright © 2022 Yi, Zheng, Xu, Li, Zhang, Ge, Liao, Li, Lyu and Ai. This is an openaccess article distributed under the terms of the Creative Commons Attribution License (CC BY). The use, distribution or reproduction in other forums is permitted, provided the original author(s) and the copyright owner(s) are credited and that the original publication in this journal is cited, in accordance with accepted academic practice. No use, distribution or reproduction is permitted which does not comply with these terms.



Risk of Adverse Events in Cancer Patients Receiving Nivolumab With Ipilimumab: A Meta-Analysis

Xin Zhao¹, Fengwei Gao¹, Jie Yang¹, Hua Fan², Qingyun Xie¹, Kangyi Jiang¹, Jie Gong¹, Benjian Gao¹, Qian Yang² and Zehua Lei^{1*}

¹ Department of Hepatobiliary Surgery, The People's Hospital of Leshan, Leshan, China, ² Department of Medical Oncology, The People's Hospital of Leshan, Leshan, China

OPEN ACCESS

Edited by:

Xian Zeng, Fudan University, China

Reviewed by:

Alessandro Morabito, G. Pascale National Cancer Institute Foundation (IRCCS), Italy Xi Lou, University of Alabama at Birmingham, United States Zeguo Sun, Icahn School of Medicine at Mount Sinai, United States

*Correspondence:

Zehua Lei leitsehua@126.com

Specialty section:

This article was submitted to Cancer Immunity and Immunotherapy, a section of the journal Frontiers in Oncology

Received: 16 February 2022 Accepted: 25 May 2022 Published: 23 June 2022

Citation:

Zhao X, Gao F, Yang J, Fan H, Xie Q, Jiang K, Gong J, Gao B, Yang Q and Lei Z (2022) Risk of Adverse Events in Cancer Patients Receiving Nivolumab With Ipilimumab: A Meta-Analysis. Front. Oncol. 12:877434. doi: 10.3389/fonc.2022.877434 **Background:** Combining two immune checkpoint inhibitors (ICIs) instead of using one can effectively improve the prognosis of advanced malignant tumors. At present, ipilimumab alongside nivolumab is the most widely used combinatorial regimen of ICIs. However, the risk of treatment-related adverse events is higher in combinatorial regimens than in single-drug regimens. Thus, this study aimed to evaluate the risks of common adverse events associated with the combinatorial regimen of ipilimumab and nivolumab by using meta-analysis.

Methods: We searched Pubmed, Medline, EMBASE, and Cochrane Library for reports published by 30 September 2021. A randomized controlled study was developed and analyzed using the statistical software R to determine the efficacy of the combinatorial treatment. Risk estimates (hazard ratios, RR) and 95% confidence intervals for various common serious adverse events were used.

Results: A total of 23 randomized control trials (n = 3970 patients) were included. Our meta-analysis indicated the risks of adverse events of any grade and grade \geq 3 as 90.42% (95%CI: 85.91% ~ 94.18%) and 46.46% (95%CI: 39.37% ~ 53.69%), respectively; the risks of treatment-related death and adverse events leading to discontinuation were estimated at 0.42% (95% CI, 0.18% ~ 0.72%) and 19.11% (95% CI, 14.99% ~ 24.38%), respectively. Classification of 19 common adverse events. The top 5 grade 1-2 adverse events were found to be fatigue (30.92%, 95% CI: 24.59% ~ 37.62%), pruritus (26.05%, 95%CI: 22.29% ~ 29.99%), diarrhea (23.58%, 95% CI: 20.62% ~ 26.96%), rash (19.90%, 95%CI: 15.75% ~ 25.15%), and nausea (17.19%, 95% CI:13.7% ~ 21.57%). The top 5 grade \geq 3 adverse events were identified as increased alanine aminotransferase(8.12%, 95% CI: 5.90% ~ 10.65%), increased lipase(7.62%, 95% CI: 4.88% ~ 10.89%), and colitis (6.39%, 95%CI: 3.98% ~ 10.25%), increased aspartate aminotransferase (6.30%, 95% CI: 4.61% ~ 8.22%), and diarrhea(5.72%, 95%CI: 3.50% ~ 8.44%). Subgroup analysis

447

revealed some differences in the adverse events between the N1-I3 and N3-I1 subgroups and between subgroups of different cancer types.

Conclusion: This study summarized the risks of common adverse events in the co-treatment of malignant-tumor patients with ipilimumab and nivolumab and identified the impacts of various initial administration schemes on the risks of such events, thereby providing an important reference for the toxicity of co-treatment with ipilimumab and nivolumab.

Systematic Review Registration: https://www.crd.york.ac.uk/prospero/, identifier: CRD42020181350.

Keywords: immune checkpoint inhibitors (ICI), ipilimumab, adverse events, nivolumab, meta-analysis

INTRODUCTION

According to the estimates of the World Cancer Center and the American Cancer Center, there were 9 million cancer-related deaths worldwide in 2020 and 600000 in the United States in 2021 (1, 2). Surgical treatment, radiotherapy, chemotherapy, and targeted drug treatment are the common treatment strategies for malignant tumors. However, these approaches have limited effects on some advanced malignant tumors. The in-depth studies on immune checkpoint inhibitors (ICIs) in recent years have provided a good prospect for the treatment of advanced malignant tumors (3, 4). ICIs are monoclonal antibodies that can activate the immune system to enhance antitumor immunity. The results of many large-scale multicenter randomized control trials (RCTs) have shown that immunotherapy can effectively prolong the survival of patients with advanced malignant tumors, and some immunotherapeutic drugs have become the first-line antitumor therapeutics (5, 6). At present, common ICIs include ipilimumab, tremelimumab, nivolumab, pembrolizumab, atezolizumab, and durvalumab. Studies have shown that the efficacy of single-drug therapies is limited, and thus combinatorial immunotherapy is gradually becoming the focus of cancer research worldwide (7, 8). Multi-phase clinical trials on combinatorial therapies involving immune-targeted therapy, chemoradiotherapy, or two ICIs have yielded gratifying results. Ipilimumab alongside nivolumab is the most common combination of two ICIs in cancer treatment and has been successfully applied to malignant tumors, such as advanced malignant melanoma and lung and kidney cancers (9). Combinatorial immunotherapy can have a good curative effect but lacks selectivity and specificity, inhibits both normal and abnormal immune responses, and is often accompanied by some adverse events. Although several meta-analysis studies have reported the risk of adverse events associated with some combinatorial immunotherapy regimens, the plausible combinations of immunotherapy drugs are extensive, and no such study has been reported on the combinatorial use of ipilimumab and nivolumab (10-12). Therefore, this study aimed to evaluate the risk of various common adverse events associated with the combinatorial use of ipilimumab and nivolumab, thereby providing an evidence-based basis for the management of such events in the clinic.

MATERIALS AND METHODS

Literature Review and Study Identification

This systematic review and meta-analysis was conducted according to the Preferred Reporting Items for Systematic Reviews and Meta Analyses (PRISMA) and Assessing the Methodological Quality of Systematic Reviews (AMSTAR) guidelines. This study was registered on Prospero (Registration number: CRD42020181350). Two independent researchers searched the PubMed, EMBASE, Cochrane Library, and MEDLINE databases for the relevant literature published between the beginning of database construction and September 30, 2021, and extracted the relevant data. The search keywords were "nivolumab", "ipilimumab", "CTLA-4", and "PD-1". We also manually checked the supplementary materials and list of references in each retrieved article to further identify any potential relevant RCT and searched the websites of the relevant regulatory agencies in the United States and Europe [The Federal Drug Administration and European Drug Administration, respectively]. We reported the basis of this systematic review and meta-analysis in accordance with Cochrane's recommendations on preferred reporting items for systematic review and meta-analysis.

Article Selection

We included only phase I–IV RCTs on ipilimumab and nivolumab combinatorial therapy of patients with malignant tumors. We excluded non-randomized trials, and studies with malignant-tumor patients, additional regimens (e.g., radiotherapy, chemotherapy, and targeted therapy), incomplete data on adverse events, or high bias in risk assessment. If two reports corresponded to the same study of a research group, we included only the most complete and up-to-date study. Two reviewers independently screened all titles, abstracts, and full texts to assess whether the corresponding studies qualified. Any disagreement among these reviewers was judged by a third researcher and finally resolved by consensus.

Data Extraction and Quality Assessment

Two researchers repeatedly extracted data according to the preset extraction table. Any inconsistency in extracted data between the two researchers was resolved *via* discussion with a third researcher. The extracted data included the study registration number, first author, publication year, trial stage, tumor type, number of cases, treatment scheme, and initial dose scheme of each included study. We defined adverse events ≥ 10 literatures as common adverse events. The extracted analysis data included the total number of adverse events of any grade, grade 1-2, and grade ≥ 3 , as well as adverse events leading to drug withdrawal and death. We evaluated the potential bias risk of each included RCT by using the bias-risk assessment tool of the Cochrane Center.

Statistical Analysis

The meta-analysis was performed using R statistical soft-ware (packages metafor and meta, R Foundation) (13). We used the R software to calculate the risk ratio and 95% confidence interval of each outcome index and to perform logarithmic, logit, antisinusoidal, and double anti-sinusoidal transformations on the analysis data to test the normal distribution of each transformation. For each set of data, we finally select the set of 4 transformed data that is closest to the normal distribution for meta-analysis. If there was significant heterogeneity ($I^2 > 50\%$), the random effect model was selected, otherwise, the fixed-effect model was used. For subgroup analysis, we sub-grouped the patients into N1-I3 subgroup (nivolumab 1 mg/kg + ipilimumab 3 mg/kg) and N3-I1 subgroup (nivolumab 3 mg/kg + ipilimumab 1 mg/kg), according to the different initial administration schemes. Finally, we used the Graphpad (version 9.2) software to draw the classification summary of results and used Egger's test to evaluate publication bias. The significance level of the bilateral test was set at p < 0.05.

RESULTS

Eligible Studies and Characteristics

We initially retrieved 1221 studies following the set retrieval strategy. Duplicate records were subsequently eliminated, leaving 832 studies after excluding trial protocol and non-cancerous disease site. Another 710 studies were excluded after reading the title and abstract, Including 584 non-randomized controlled studies(Non-RCTs), 59 were Comments, 43 were Combined chemoradiotherapy, 24 were Combined targeted therapy. Fulltext reading of the 122 studies led to the elimination of 99 articles. Amongst the 99 studies, 45 were not in the field of interest, 38 were review articles, 11 were conference abstracts, and 5 had insufficient data. The remaining 23 studies were included for meta-analysis (14-36), which included 32 single arms (see Figure 1 and Table 1) and a total of 3970 patients with malignant tumors. The tumor types included malignant melanoma, non-small cell lung cancer, advanced renal cell carcinoma, malignant pleural mesothelioma, malignant sarcoma, esophageal gastric junction cancer, colorectal cancer, malignant glioma, and urothelial, ovarian, and hepatocellular carcinomas. According to the number of reports, we analyzed 19 common adverse events, namely diet, pruritus, diarrhea, rash, nausea, hyperthyroidism, hyperthyroidism, discredited appetite,

pyrexia, headache, maculopapular rash, pneumonitis, adrenal insufficiency, colitis, vomiting, and increased aspartate aminotransferase (AST), increased alanine aminotransferase (ALT), increased amylase, and increased lipase.

Incidence of any adverse events and risk ratio of grade 3 or higher adverse events

Of the 23 studies analyzed, 19 reported adverse events of any grade, the mean incidence of any adverse events was 90.42% (95% CI, 85.91% ~ 94.18%, $I^2 = 93\%$) (see **Figure 2**). 22 reported adverse events of grade \geq 3, and the mean incidence of grade 3 or higher adverse events was 46.46% (95% CI, 39.37% ~ 53.69%, $I^2 = 91\%$) (see **Figure 3**). Subgroup analysis revealed that the mean incidence of any adverse event and that of a grade \geq 3 adverse event were 94.53% (95% CI, 91.18% ~ 97.21%, $I^2 = 71\%$) and 55.29% (95% CI, 46.73% ~ 63.86%, $I^2 = 85\%$) in the N1–I3 subgroup (see **Supplementary Material Figure S1**, **S2**), respectively, and 84.91% (95% CI, 80.02% ~ 90.10%, $I^2 = 90\%$) and 36.72% (95% CI, 30.51% ~ 43.39%, $I^2 = 81\%$) in the N3–I1 subgroup (see **Supplementary Material Figure S3**, **S4**).

Incidence of Treatment-Related Deaths and Treatment–Related Adverse Event Leading to Discontinuation

Of the 23 studies, 20 reported a total of 31 treatment-related deaths, with a mean incidence of 0.42%(95% CI, 0.18% ~ 0.72%, $I^2 = 0\%$) (see **Figure 4**). 20 reported the number of adverse events leading to discontinuation, with a mean incidence of 19.11% (95% CI, 14.99% ~ 24.38%, $I^2 = 93\%$) (see **Figure 5**). The mean incidence of treatment-related death and that of a treatment-related adverse event leading to discontinuation were 0.06% (95% CI, 0.00% ~ 0.44%, $I^2 = 0\%$) and 27.51% (95% CI, 21.45% ~ 35.29%, $I^2 = 83\%$) in the N1–I3 subgroup(see **Supplementary Material Figure S5-S6**), respectively, and 0.43% (95% CI, 0.14% ~ 0.83%, $I^2 = 0\%$) and 14.65% (95% CI, 11.54% ~ 18.04%, $I^2 = 75\%$) in the N3–I1 subgroup(see **Supplementary Material Figure S7-S8**).

Risk Ratio of Grade 1 and 2 Adverse Events

Among the 19 common adverse events analyzed, the risk of grade 1–2 adverse events was > 10%. The top 5 risks were fatigue(30.92%, 95% CI: 24.59% ~ 37.62%, $I^2 = 93\%$), pruritus (26.05%, 95% CI: 22.29% ~ 29.99%, $I^2 = 82\%$), diarrhea(23.58%, 95% CI: 20.62% ~ 26.96%, $I^2 = 88\%$), rash(19.90%, 95% CI: 15.75% ~ 25.15%, $I^2 = 88\%$), nausea (17.19%, 95% CI: 13.7% ~ 21.57%, $I^2 = 86\%$), the risks of other common adverse events are presented in **Figure 6**. Fatigue, pruritus, diarrhea, and rash were also among the top 5 risks in the N1–I3 and N3–I1 subgroups, which additionally included nausea and hypothyroidism, respectively. The risks of other common adverse events in each subgroup are presented in **Table 2**.

Risk Ratio of Grade 3 or Higher Adverse Events

Among the 19 common adverse events, the risk of a grade \geq 3 adverse event was > 5%. The top 5 risks were increased ALT

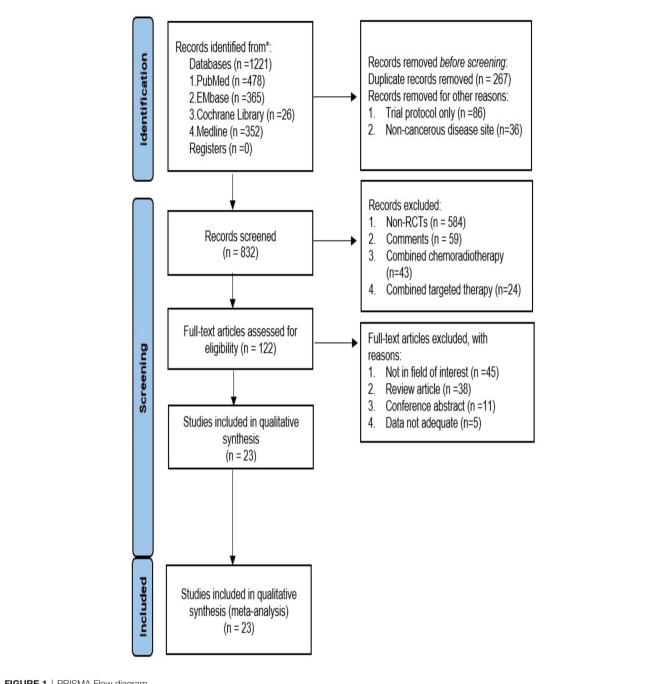


FIGURE 1 | PRISMA Flow diagram.

(8.12%, 95% CI: 5.90% \sim 10.65%, I 2 $^=$ 73%), increased lipase (7.62%, 95% CI: 4.88% ~ 10.89%, $I^2 = 77\%$), colitis (6.39%, 95% CI: 3.98% ~ 10.25%, I² = 80%), increased AST (6.30%, 95% CI: 4.61% ~ 8.22%, I 2 $^=$ 68%), diarrhea (5.72%, 95% CI: 3.50% ~ 8.44%, $I^2 = 83\%$), the risks of other common adverse events are presented in Figure 7. Sub-group analysis yielded the same adverse events as the top 5 risks in both N1-I3 and N3-I1 subgroups. The risks of other common adverse events are presented in Figure 7 and Table 3.

Subgroup Analysis of the Incidence of Adverse Events Based on Cancer Type

Based on the risk of any adverse events (Supplementary Material Figure S9), melanoma had the highest risk (95.87%, 95% CI: 92.93% ~ 98.12%, I2 = 72.4%), while colorectal cancer had the lowest risk (73.11%, 95% CI: 64.75% ~ 80.73%, I2 = 0%). Similarly, based on the risk of grade 3 and higher adverse events (Supplementary Material Figure S10), melanoma had the highest risk (58.13%, 95% CI: 47.67% ~ 70.88%, I2 = 92.3%),

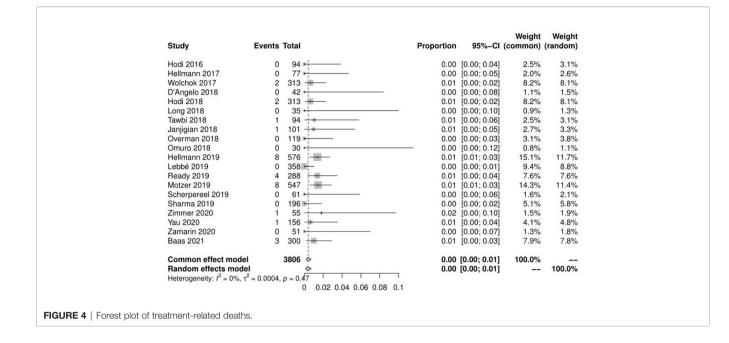
TABLE 1 | Characteristics of the included studies.

NCT number	Author	Year	Phase	No. of patients	Median age (years)	Male (%)	Cancer type	Follow-up (Median months)	Dose (I+N)
NCT01927419	Hodi	2016	П	94	NA	NA	Melanoma	24.5	3mg/kg+1mg/
NCT01454102	Hellmann	2017	I	77	68 (58~73)	25.00%	NCLC	12.8	kg 3mg/kg/+1mg/
					62 (57~73)	38.71%			kg 3mg/kg/+1mg/
NCT01472081	Hammers	2017	I	47	54 (26~68)	79.63%	RCC	22.3	kg 1mg/kg+3mg/
NCT01472081	Hammers	2017	I	47	56 (20~76)	64.29%	RCC		kg 3mg/kg+1mg/
NCT01844505	Wolchok	2017	Ш	313	NA	NA	Melanoma	36	kg 1mg/kg+3mg/
NCT02437279	Blank	2018	I	20	54 (40~58)	12.96%	Melanoma	25.6	kg 3mg/kg+1mg/
NCT02500797	D'Angelo	2018	Ш	42	57 (27~81)	19.00%	Sarcoma	13.6	kg 1mg/kg+3mg/
NCT02374242	Long	2018	Ш	35	59 (53–68)	83%	Melanoma	17	kg 3mg/kg+1mg/
NCT01844505	Hodi	2018	Ш	313	NA	NA	Melanoma	48	kg 3mg/kg+1mg/
NCT02320058	Tawbi	2018	Ш	94	59 (22~81)	65.00%	Melanoma	14	kg 3mg/kg+1mg/
NCT01928394	Janjigian	2018	1/11	49	53 (22~77)	34.00%	Esophagogastric cancer	24	kg 3mg/kg+1mg/
NCT01928394	Janjigian	2018	1/11	52	58 (19~81)	45.00%	Esophagogastric cancer	22	kg 1mg/kg+3mg/
NCT02060188	Overman	2018	Ш	119	58 (21~88)	70.00%	Colorectal Cancer	13.4	kg 1mg/kg+3mg/
NCT02017717	Omuro	2018	Ι	10	57 (37~68)	6.00%	Glioblastoma	NA	kg 3mg/kg+1mg/
NCT02017717	Omuro	2018	I	20	60 (27~73)	14.00%	Glioblastoma		kg 1mg/kg+3mg/
NCT02477826	Hellmann	2019	Ш	576	64 (26~87)	67.40%	NCLC	24	kg 1mg/kg/+3mg/
NCT02714218	Lebbé	2019	III/IV	180	58.5 (19~85)	58.30%	Melanoma	12	kg 1mg/kg+3mg/
NCT02714218	Lebbé	2019	III/IV	178	58.5 (26~85)	56.70%	Melanoma		kg 3mg/kg+1mg/
NCT02659059	Ready	2019	Ш	288	65 (39~91)	49.30%	NCLC	6	kg 1mg/kg+3mg/
NCT02231749	Motzer	2019		547	NA	NA	RCC	32.4	kg 1mg/kg+3mg/
NCT02977052	Rozeman	2019		30	64 (18~79)	19.00%	Melanoma	18	kg 3mg/kg+1mg/
NCT02977052	Rozeman	2019		30	54 (31~74)	14.00%	Melanoma	10	kg 1mg/kg+3mg/
NCT02716272				61	71.2 (48.1~88.1)	53.00%	Pleural mesothelioma	20.1	kg 1mg/kg+3mg/
NCT01928394	Sharma	2019	1/11	104	63 (39~83)	77.90%	Urothelial carcinoma	38.8	kg 1mg/kg+3mg/
NCT01928394				92				7.9	kg
	Sharma	2019	1/11		64 (38~83)	80.40%	Urothelial carcinoma		3mg/kg+1mg/ kg
NCT02523313	Zimmer	2020	11	55	52 (45~59)	55.00%	Melanoma	12.4	3mg/kg+1mg/ kg
NCT01658878	Yau	2020	1/11	49	NA	NA	HCC	30.7	3mg/kg+1mg/ kg
NCT01658878	Yau	2020	1/11	97			HCC		1mg/kg+3mg/ kg
NCT02498600	Zamarin	2020	Ш	51	62 (38~92)	NA	Ovarian Cancer	33	1mg/kg+3mg/ kg
NCT02899299	Baas	2021	III	300	69 (65~75)	77.00%	Malignant pleural mesothelioma	29.7	1mg/kg+3mg/ kg

NCLC, Non-small-cell lung cancer; RCC, Renal cell carcinoma; HCC, Hepatocellular Carcinoma; NA, Nae.

Study	Events	Total		Proportion	95%-CI	Weight (common)	
Hodi 2016	85	94	<u> </u>	0.90	[0.83; 0.96]	2.7%	5.3%
Hellmann 2017	59	77			[0.66; 0.86]		5.2%
Hammers 2017	88	94	<u> </u>		[0.87: 0.98]		5.3%
Wolchok 2017	300	313			[0.93; 0.98]		5.8%
Blank 2018	20	20			[0.83; 1.00]		3.7%
Hodi 2018	300	313			[0.93; 0.98]		5.8%
Long 2018	34	35			[0.85; 1.00]		4.4%
Tawbi 2018	91	94	·		[0.91; 0.99]		5.3%
Janjigian 2018	80	101	I		[0.70; 0.87]		5.3%
Overman 2018	87	119 -			[0.64; 0.81]		5.4%
Omuro 2018	30	30	1		[0.88; 1.00]		4.3%
Hellmann 2019	442	576			[0.73; 0.80]		5.9%
Lebbé 2019	321	358			[0.86; 0.93]		5.8%
Ready 2019	231	288	S		[0.75; 0.85]		5.7%
Motzer 2019	513	547			[0.91; 0.96]		5.9%
Scherpereel 201		61			[0.84; 0.98]		5.0%
Sharma 2019	162	196			[0.77; 0.88]		5.6%
Zimmer 2020	55	55	-		[0.94; 1.00]		4.9%
Yau 2020	119	156			[0.69; 0.83]		4.9%
1du 2020	119	150		0.76	[0.03, 0.03]	4.470	0.076
Common effect	model	3527	\$	0.89	[0.88; 0.90]	100.0%	
Random effects Heterogeneity: <i>I</i> ²	s model = 93%, τ ² = 0.0202	2, p < 0.6		0.90	[0.86; 0.94]		100.0%
			5 0.7 0.75 0.8 0.85 0.9 0.95				

Study	Events	Total	Proportion	95%-Cl
Hodi 2016	51	94	0.54	[0.44; 0.65]
Hellmann 2017	27	77	0.35	[0.25; 0.47]
Hammers 2017	47	94		[0.40; 0.60]
Wolchok 2017	184	313		[0.53; 0.64]
Blank 2018	18	20		[0.68; 0.99]
Hodi 2018	185	313	0.59	[0.53; 0.65]
Long 2018	22	35		[0.45; 0.79]
Tawbi 2018	56	94		[0.49; 0.70]
Janjigian 2018	37	101		[0.27; 0.47]
Overman 2018	38	119		[0.24; 0.41]
Omuro 2018	15	30		[0.31; 0.69]
Hellmann 2019	189	576	- 0.33	[0.29; 0.37]
Lebbé 2019	146	358	0.41	[0.36; 0.46]
Ready 2019	84	288	- 0.29	[0.24; 0.35]
Motzer 2019	255	547	0.47	[0.42; 0.51]
Rozeman 2019	18	60		[0.19; 0.43]
Scherpereel 2019	16	61 -		[0.16; 0.39]
Sharma 2019	68	196		[0.28; 0.42]
Zimmer 2020	45	55	0.82	[0.69; 0.91]
Yau 2020	55	156	0.35	[0.28; 0.43]
Zamarin 2020	34	51		[0.52; 0.79]
Baas 2021	91	300	- 0.30	[0.25; 0.36]
Common effect mod	el	3938	0.43	[0.41; 0.44]
Random effects mod Heterogeneity: $I^2 = 91\%$		0 - 0	0.46	[0.39; 0.54]
Heterogeneity. T = 9178	b, t = 0.4∠40	p < 0.	0.4 0.6 0.8	
			0.4 0.0 0.8	

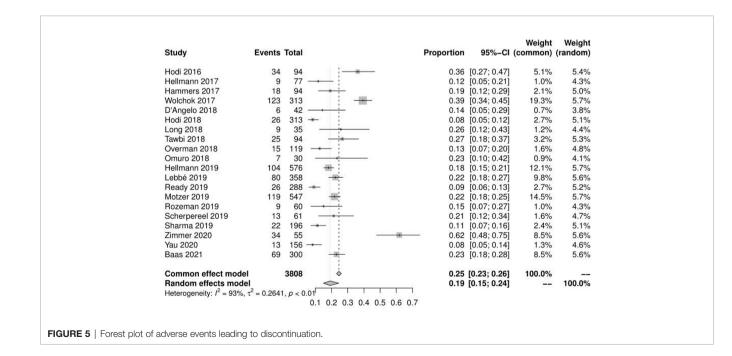


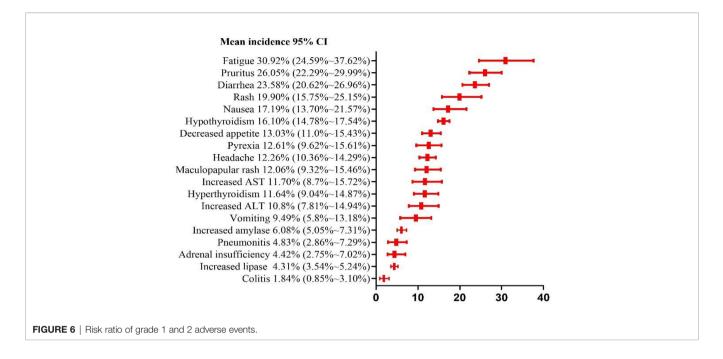
while pleural mesothelioma had the lowest risk (26.23%, 95% CI: 17.22% ~ 39.95%, I2 = 0%). Melanoma also had the highest risk (25.83%, 95% CI: 16.79) % ~ 39.75%, I2 = 94.2%) based on risk of any adverse event leading to discontinuation (**Supplementary Material Figure S11**), while glioblastoma had the lowest risk (23.33%, 95% CI: 12.20% ~ 44.64%, I2 = 0%). In contrast, glioblastoma had the highest risk (1.64%, 95% CI: 0.10% ~ 25.62%, I2 = 0%) based on the risk of treatment-related deaths (**Supplementary Material Figure S12**), while urothelial

carcinoma had the lowest risk (0.25%, 95% CI: 0.02% \sim 4.05%, I2 = 0%).

DISCUSSION

ICIs are monoclonal antibodies against regulatory immune checkpoint factors that inhibit T cell activation. These antibodies promote immune-mediated tumor-cell clearance by



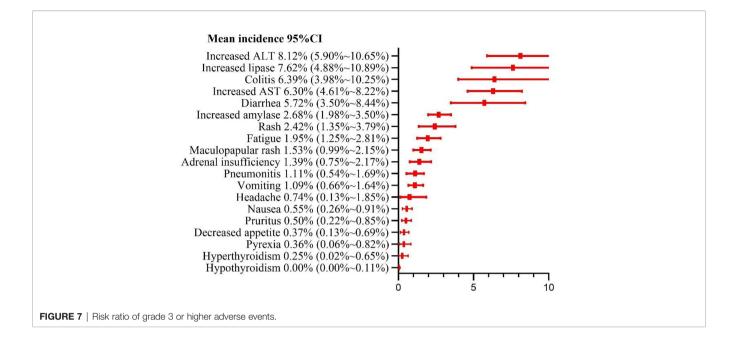


enhancing T cell-mediated anti-tumor immunity. At present, their targets mainly include CTLA-4 and PD-1/PD-L1, CTLA-4 regulates the activation of T cells by preventing the generation of T cell inhibitory signals (37, 38). let's first talk about the five common adverse events, and then describe whether the risk of grade \geq 3 is > 5%, so as to promote the further proliferation of T cells, thereby achieving the anti-tumor effect of PD-1. PD-L1 inhibits the signal transduction by blocking the interaction between T cells and antigen-presenting cells, promotes the proliferation of activated T cells, and then kills tumor cells (39, 40). However, activation of the immune system also impairs the

immune homeostasis in non-tumor tissues, resulting in a series of adverse reactions, mainly involving the skin, gastrointestinal tract, liver, lung, and endocrine glands (41, 42). In recent years, combinatorial immunotherapy has gradually become a research hotspot, and its antitumor effectiveness has been confirmed by multiple studies. However, combination of drugs seems to increase the risk of adverse events. The results of the metaanalyses by Yang et al. and Chen et al (43, 44). have shown that the antitumor effect of nivolumab and ipilimumab co-treatment was better than that of nivolumab or ipilimumab alone. The results of the meta-analysis by Xing et al. have shown that the

TABLE 2	Risk ratio of	f arade 1	and 2 adv	erse events f	or N3-I1and	N1-I3 subgroup

Subgroup	Mean incidence 95%Cl				
	N3-I1	N1-I3			
Fatigue	23.01% (17.63%~29.43%)	38.67% (31.17%~47.97%)			
Pruritus	22.34% (18.72%~25.96%)	30% (24.06%~35.95%)			
Diarrhea	18.95% (17.41%~20.54%)	27.18% (22.92%~31.64%)			
Rash	16.43% (13.77%~19.61%)	26.18% (18.66%~34.47%)			
Hypothyroidism	14.46% (11.49%~18.21%)	16.77% (14.75%~18.79%)			
Nausea	13.22% (9.82%~17.04%)	20.45% (15.10%~26.39%)			
Headache	12.67% (5.80%~21.40%)	13.54% (11.44%~15.96%)			
Pyrexia	11.21% (8.86%~14.19%)	13.59% (9.53%~17.64%)			
Decreased appetite	10.96% (9.56%~12.44%)	15.74% (13.83%~17.87%)			
Hyperthyroidism	8.45% (5.24%~12.34%)	13.92% (9.32%~10.29%)			
Maculopapular rash	8.20% (6.59%~9.80%)	15.04% (10.79%~20.58%)			
Increased ALT	7.94% (4.06%~12.97%)	11.61% (8.77%~14.75%)			
Increased AST	7.07% (3.69%~11.44%)	14.86% (11.67%~18.93%)			
Increased amylase	5.75% (2.23%~10.49%)	6.47% (5.17%~8.07%)			
Vomiting	5.12% (1.95%~9.37%)	13.06% (11.15%~15.24%)			
Adrenal insufficiency	5.09% (2.08%~9.33%)	3.68% (1.05%~7.83%)			
Increased lipase	3.24% (2.12%~4.54%)	5.16% (3.52%~7.5%)			
Pneumonitis	3.22% (1.94%~4.73%)	6.75% (4.74%~8.76%)			
Colitis	0.62% (0.11%~1.39%)	1.74% (0.27%~4%)			



risk of adverse events related to nivolumab and ipilimumab cotreatment was higher than that of the single-drug use (45). To the best of our knowledge, the study presented here is the largest and most comprehensive meta-analysis to evaluate the common adverse events of nivolumab and ipilimumab combination. The study by Xing et al. analyzed fewer studies than this study and did not include subgroup analysis of the initial medication regimen.

From the perspective of patient consultation, several results of this meta-analysis are crucial. Our results showed that approximately 9 of the 10 patients treated with nivolumab alongside ipilimumab had at least one adverse event, and 5 of the 10 patients had at least one grade \geq 3 adverse event. Among them, fatigue was the most common mild adverse event (30.92%), and increased ALT level was the most common grade \geq 3 adverse event (8.12%). Patients should also be informed that pruritus, diarrhea, and rash are also common adverse events but are remotely likely to manifest as serious complications. The fatality rate of any of these adverse events was very low (0.5%). The risk of drug withdrawal due to an adverse event was estimated at 42%. Approximately 1 of the 5 patients discontinued the treatment because of an adverse event.

TABLE 3 | Risk ratio of grade 3 and higher adverse events for N3-I1 and N1-I3 subgroup.

Subgroup	Mean incidence 95%CI				
	N3-I1	N1-I3			
Increased Lipase	6.14% (2.46%~11.32%)	9.13% (5.60%~13.41%)			
Increased ALT	3.99% (2.21%~6.27%)	11.02% (7.9%~14.58%)			
Increased AST	3.85% (2.22%~5.91%)	7.96% (5.44%~10.91%)			
Colitis	3.31% (0.83%~7.35%)	7.86% (4.58%~11.13%)			
Diarrhea	2.77% (2.17%~3.45%)	9.17% (6.06%~13.65%)			
Rash	1.94% (0.55%~1.89%)	2.32% (1.44%~3.34%)			
Increased Amylase	1.87% (0.21%~5.11%)	3.50% (2.57%~4.76%)			
Fatigue	1.30% (0.85%~1.83%)	2.21% (1.37%~3.20%)			
Adrenal insufficiency	1.27% (0.45%~2.35%)	1.14% (0.29%~2.36%)			
Pneumonitis	0.64% (0.07%~1.55%)	0.51% (0.00%~1.56%)			
Maculopapular rash	0.54% (0.09%~1.24%)	1.96% (1.05%~3.07%)			
Vomiting	0.46% (0.00%~2.39%)	1.21% (0.49%~2.15%)			
Headache	0.26% (0.00%~4.27%)	0.20% (0.00%~0.85%)			
Pruritus	0.21% (0.01%~0.60%)	0.43% (0.05%~1.05%)			
Nausea	0.10% (0.00%~0.41%)	1.08% (0.46%~1.87%)			
Decreased appetite	0.04% (0.00%~0.31%)	0.74% (0.34%~1.30%)			
Hyperthyroidism	0.00% (0.00%~0.12%)	0.49% (0.06%~1.17%)			
Hypothyroidism	0.00% (0.00%~0.08%)	0.00% (0.00%~0.13%)			
Pyrexia	0.00% (0.00%~0.39%)	0.29% (0.00%~0.91%)			

In this meta-analysis, fast, headache, decreased appetite, and pyrexia were found to be subjective symptoms. Of the remaining adverse events, diarrhea, nausea, vomiting, colitis, and increased AST, ALT, amylase, and lipase levels are related to the digestive system; rash, pruritus, and maculopapular rash are skin-related; hyperthyroidism and adult insufficiency are endocrine-related; and pneumonitis is mainly related to the respiratory system. Regarding the grade 1-2 adverse events, 13 had risks of > 10%, and 15 had > 5%. Fatigue (30.92%) had the highest risk, which was higher than the risk of adverse events reported in PD-1 (18.7%) and PD-L1 (26%) meta-analysis studies by Wang et al (42). Grade 1-2 adverse events often do not have serious consequences for patients but increase patient discomfort and weaken the eagerness of the patient for the treatment. Some grade 1–2 adverse events often develop into grade \geq 3 adverse events, such as colitis and pneumonitis, if not managed timely. We found that 5 grade \geq 3 events had risks of > 5%, and 12 had >1%. Among such events, increased ALT (8.12%) level was the most common. Increased ALT and AST levels are symptoms of hepatitis; increased lipase and amylase levels are symptoms of pancreatitis; hyperthyroidism and hyperthyroidism are symptoms of thyroiditis; diarrhea is a symptom of colitis. If autoimmune diseases are not identified early, they often cause severe health problems and can even be fatal. Pneumonia is the most common cause of treatment-related deaths in patients treated with immunosuppressants, and we estimated the incidence at 1.5% and 11%. In addition, our results show that the types of adverse events in the digestive system and their risks are significantly higher than those in other systems. Therefore, it is necessary to monitor the digestive system of the patients under treatment for such events to prevent development of severe problems in the digestive system.

In our study, we sub-grouped the patients according to their initial dosing regimen, namely N1-I3 and N3-I1 subgroups, and performed subgroup analysis. The N3-I1 subgroup had higher risks of adverse events of any grade, grade 1–2, and grade \geq 3 (both with and without classification) than the N1-I3 subgroup, consistent with the results of the meta-analysis by Xu et al (46). The risk of adverse events of any grade was not classified, and nearly 10% (94.53% vs. 84.51%) of the N3-I1 subgroup had a higher risk than the N1-I3 subgroup, whereas nearly 20% (55.29% vs. 36.72%) of the N3-I1 subgroup had a higher risk of adverse events of grade \geq 3 than the N1–I3 subgroup. Regarding the risk of classified grade 1 and grade 2 common adverse events, the most common risk in both N1-I3 and N3-I1 subgroups was fatigue (38.67% and 23.01%, respectively), whereas, regarding the classified grade \geq 3 common adverse events, the most common risks in the N1-I3 and N3-I1 subgroups were increased ALT (11.02%) and lipase (6.14%) levels, respectively. Therefore, initial medication schemes have a certain impact on the occurrence of adverse events. When deciding on the medication scheme, treatment effectiveness and cost should also be considered in addition to treatment safety. We should be more cautious about the impact of different initial medication regimens of N3-I1 and N1-I3 on adverse events, because we did not consider the impact of treatment period and sequence.

Our preliminary analysis of the incidence of adverse events in different types of tumors further revealed that melanoma had a higher overall risk of adverse events. However, the differences between different cancer types were not significant. A metaanalysis of PD-1 and PD-L1 by Wang et al. revealed a similar average incidence of adverse events across various cancer types (42). However, this conclusion could not be fully explained in our study, possibly because of the small sample size of some tumor types. Some studies postulate that there are certain differences in the risk of adverse events for different types of tumors (47, 48). Based on the dose subgroup analysis for different cancer types, choosing the best drug regimen can prevent the occurrence of some adverse events to a certain extent. Taking timely intervention measures to the occurrence of common adverse events can further reduce the occurrence of serious adverse events and deaths.

Nonetheless, this study was limited by several factors, some with high heterogeneity (I2> 90%). We did not conduct subgroup analysis by cancer type for different types of adverse events. We also did not further analyze race, age, gender, and smoking history, amongst other demographic and clinical factors, which may have led to deviations in the analysis results. The length of treatment cycles may also have impacted the results despite performing subgroup analyses based on different initial doses. The different follow-up times for each study may have also biased the results.

In conclusion, this study estimated the risks of common adverse events in the co-treatment of malignant-tumor patients with ipilimumab and nivolumab and identified the impacts of different initial administration schemes on the risks of such events. Accordingly, this study provides an important reference for the toxicity of co-treatment with ipilimumab and nivolumab.

DATA AVAILABILITY STATEMENT

The original contributions presented in the study are included in the article/**Supplementary Material**. Further inquiries can be directed to the corresponding author.

AUTHOR CONTRIBUTIONS

XZ, FG, and ZL conceived the study, had full access to all the data in the study, and take responsibility for the integrity of the data and the accuracy of the data analysis. XZ and FG designed the search strategy and discussed with JY, HF, and QX, BG, QY, and KJ performed study selection, data extraction and synthesis. XZ and FG drafted and led on the writing of the manuscript. All the other authors participated in the analysis and interpretation of the data, revised the manuscript critically for important intellectual content and re-drafted some of its section. All the authors read and approved the final version of the manuscript, and agreed to be accountable for all aspects of the work to ensure its accuracy and integrity.

SUPPLEMENTARY MATERIAL

The Supplementary Material for this article can be found online at: https://www.frontiersin.org/articles/10.3389/fonc.2022.877434/full#supplementary-material

Supplementary Figure 1 | Forest plot of any adverse events in N1-I3 subgroup.

Supplementary Figure 2 | Forest plot of grade 3 or higher adverse events in N1-I3 subgroup.

Supplementary Figure 3 | Forest plot of any adverse events in N3-I1 subgroup.

Supplementary Figure 4 | Forest plot of grade 3 or higher adverse events in N3-11 subgroup.

Supplementary Figure 5 | Forest plot of treatment-related deaths in N1-I3 subgroup.

REFERENCES

- Miller KD, Ortiz AP, Pinheiro PS, Bandi P, Minihan A, Fuchs HE, et al. Cancer Statistics for the US Hispanic/Latino Population, 2021. CA Cancer J Clin (2021) 71:466–87. doi: 10.3322/caac.21695
- Siegel RL, Miller KD, Fuchs HE, Jemal A. Cancer Statistics, 2021. CA Cancer J Clin (2021) 71:7–33. doi: 10.3322/caac.21654
- Hegde PS, Chen DS. Top 10 Challenges in Cancer Immunotherapy. *Immunity* (2020) 52:17–35. doi: 10.1016/j.immuni.2019.12.011
- Nakajima EC, Lipson EJ, Brahmer JR. Challenge of Rechallenge: When to Resume Immunotherapy Following an Immune-Related Adverse Event. J Clin Oncol (2019) 37:2714–8. doi: 10.1200/JCO.19.01623
- Owonikoko TK, Park K, Govindan R, Ready N, Reck M, Peters S, et al. Nivolumab and Ipilimumab as Maintenance Therapy in Extensive-Disease Small-Cell Lung Cancer: CheckMate 451. J Clin Oncol (2021) 39:1349–59. doi: 10.1200/JCO.20.02212
- Paz-Ares L, Ciuleanu TE, Cobo M, Schenker M, Zurawski B, Menezes J, et al. First-Line Nivolumab Plus Ipilimumab Combined With Two Cycles of Chemotherapy in Patients With Non-Small-Cell Lung Cancer (CheckMate 9LA): An International, Randomised, Open-Label, Phase 3 Trial. *Lancet* Oncol (2021) 22:198–211. doi: 10.1016/S1470-2045(20)30641-0
- Bhoori S, Mazzaferro V. Combined Immunotherapy and VEGF-Antagonist in Hepatocellular Carcinoma: A Step Forward. *Lancet Oncol* (2020) 21:740–1. doi: 10.1016/S1470-2045(20)30211-4
- Mayor S. Combined Immunotherapy Improves Survival in Metastatic Melanoma. BMJ (2015) 350:h2993. doi: 10.1136/bmj.h2993
- Di Federico A, Rizzo A, Ricci AD, Frega G, Palloni A, Tavolari S, et al. Nivolumab: An Investigational Agent for the Treatment of Biliary Tract Cancer. *Expert Opin Investig Drugs* (2021) 30:325–32. doi: 10.1080/ 13543784.2021.1863946
- Baxi S, Yang A, Gennarelli RL, Khan N, Wang Z, Boyce L, et al. Immune-Related Adverse Events for Anti-PD-1 and Anti-PD-L1 Drugs: Systematic Review and Meta-Analysis. *Bmj* (2018) 360:k793. doi: 10.1136/bmj.k793
- De Velasco G, Je Y, Bossé D, Ott PA, Moreira RB, et al. Comprehensive Meta-Analysis of Key Immune-Related Adverse Events From CTLA-4 and PD-1/ PD-L1 Inhibitors in Cancer Patients. *Cancer Immunol Res* (2017) 5:312–8. doi: 10.1158/2326-6066.CIR-16-0237
- Yan BY, Wasilewski G, Lacouture ME, Barker CA. Incidence of Dermatologic Adverse Events in Patients With Cancer Treated With Concurrent Immune Checkpoint Inhibitors and Radiation Therapy: A Systematic Review and Meta-Analysis. J Am Acad Dermatol (2021) 84:871–5. doi: 10.1016/ j.jaad.2020.10.071
- Shim S, Kim S-J. Intervention Meta-Analysis: Application and Practice Using R Software. *Epidemiol Health* (2019) 41:e2019008. doi: 10.4178/epih. e2019008
- Baas P, Scherpereel A, Nowak AK, Fujimoto N, Peters S, Tsao AS, et al. First-Line Nivolumab Plus Ipilimumab in Unresectable Malignant Pleural Mesothelioma (CheckMate 743): A Multicentre, Randomised, Open-Label, Phase 3 Trial. *Lancet* (2021) 397:375–86. doi: 10.1016/S0140-6736(20)32714-8

Supplementary Figure 6 | Forest plot of adverse events leading to discontinuation in N1-I3 subgroup.

Supplementary Figure 7 | Forest plot of treatment-related deaths in N3-I1 subgroup.

Supplementary Figure 8 | Forest plot of adverse events leading to discontinuation in N3-I1 subgroup.

Supplementary Figure 9 | Forest plot of any adverse events in different cancers.

Supplementary Figure 10 | Forest plot of grade 3 and higher adverse events in different cancers.

Supplementary Figure 11 | Forest plot of any adverse event leading to discontinuation in different cancers.

Supplementary Figure 12 | Forest plot of treatment-related deaths in different cancers.

- Blank CU, Rozeman EA, Fanchi LF, Sikorska K, van deWiel B, Kvistborg P, et al. Neoadjuvant Versus Adjuvant Ipilimumab Plus Nivolumab in Macroscopic Stage III Melanoma. *Nat Med* (2018) 24:1655–61. doi: 10.1038/s41591-018-0198-0
- D'Angelo SP, Mahoney MR, Van Tine BA, Atkins J, Milhem MM, Jahagirdar BN, et al. Nivolumab With or Without Ipilimumab Treatment for Metastatic Sarcoma (Alliance A091401): Two Open-Label, Non-Comparative, Randomised, Phase 2 Trials. *Lancet Oncol* (2018) 19:416–26. doi: 10.1016/ S1470-2045(18)30006-8
- Hammers HJ, Plimack ER, Infante JR, Rini BI, McDermott DF, Lewis LD, et al. Safety and Efficacy of Nivolumab in Combination With Ipilimumab in Metastatic Renal Cell Carcinoma: The CheckMate 016 Study. J Clin Oncol (2017) 35:3851–8. doi: 10.1200/JCO.2016.72.1985
- Hellmann MD, Paz-Ares L, Bernabe Caro R, Zurawski B, Kim SW, Carcereny Costa E, et al. Nivolumab Plus Ipilimumab in Advanced Non-Small-Cell Lung Cancer. N Engl J Med (2019) 381:2020–31. doi: 10.1056/ NEJMoa1910231
- Hellmann MD, Rizvi NA, Goldman JW, Gettinger SN, Borghaei H, Brahmer JR, et al. Nivolumab Plus Ipilimumab as First-Line Treatment for Advanced non-Small-Cell Lung Cancer (CheckMate 012): Results of an Open-Label, Phase 1, Multicohort Study. *Lancet Oncol* (2017) 18:31–41. doi: 10.1016/ S1470-2045(16)30624-6
- Hodi FS, Chesney J, Pavlick AC, Robert C, Grossmann KF, McDermott DF, et al. Combined Nivolumab and Ipilimumab Versus Ipilimumab Alone in Patients With Advanced Melanoma: 2-Year Overall Survival Outcomes in a Multicentre, Randomised, Controlled, Phase 2 Trial. *Lancet Oncol* (2016) 17:1558–68. doi: 10.1016/S1470-2045(16)30366-7
- Hodi FS, Chiarion-Sileni V, Gonzalez R, Grob JJ, Rutkowski P, Cowey CL, et al. Nivolumab Plus Ipilimumab or Nivolumab Alone Versus Ipilimumab Alone in Advanced Melanoma (CheckMate 067): 4-Year Outcomes of a Multicentre, Randomised, Phase 3 Trial. *Lancet Oncol* (2018) 19:1480–92. doi: 10.1016/S1470-2045(18)30700-9
- 22. Janjigian YY, Bendell J, Calvo E, Kim JW, Ascierto PA, Sharma P, et al. CheckMate-032 Study: Efficacy and Safety of Nivolumab and Nivolumab Plus Ipilimumab in Patients With Metastatic Esophagogastric Cancer. J Clin Oncol (2018) 36:2836–44. doi: 10.1200/JCO.2017.76.6212
- Lebbé C, Meyer N, Mortier L, Marquez-Rodas I, Robert C, Rutkowski P, et al. Evaluation of Two Dosing Regimens for Nivolumab in Combination With Ipilimumab in Patients With Advanced Melanoma: Results From the Phase IIIb/IV CheckMate 511 Trial. J Clin Oncol (2019) 37:867–75. doi: 10.1200/ JCO.18.01998
- Long GV, Atkinson V, Lo S, Sandhu S, Guminski AD, Brown MP, et al. Combination Nivolumab and Ipilimumab or Nivolumab Alone in Melanoma Brain Metastases: A Multicentre Randomised Phase 2 Study. *Lancet Oncol* (2018) 19:672–81. doi: 10.1016/S1470-2045(18)30139-6
- 25. Motzer RJ, Rini BI, McDermott DF, Arén Frontera O, Hammers HJ, Carducci MA, et al. Nivolumab Plus Ipilimumab Versus Sunitinib in First-Line Treatment for Advanced Renal Cell Carcinoma: Extended Follow-Up of

Efficacy and Safety Results From a Randomised, Controlled, Phase 3 Trial. Lancet Oncol (2019) 20:1370–85. doi: 10.1016/S1470-2045(19)30413-9

- 26. Omuro A, Vlahovic G, Lim M, Sahebjam S, Baehring J, Cloughesy T, et al. Nivolumab With or Without Ipilimumab in Patients With Recurrent Glioblastoma: Results From Exploratory Phase I Cohorts of CheckMate 143. Neuro Oncol (2018) 20:674–86. doi: 10.1093/neuonc/nox208
- Overman MJ, Lonardi S, Wong KYM, Lenz HJ, Gelsomino F, Aglietta M, et al. Durable Clinical Benefit With Nivolumab Plus Ipilimumab in DNA Mismatch Repair-Deficient/Microsatellite Instability-High Metastatic Colorectal Cancer. J Clin Oncol (2018) 36:773–9. doi: 10.1200/JCO.2017.76.9901
- Ready N, Hellmann MD, Awad MM, Otterson GA, Gutierrez M, Gainor JF, et al. First-Line Nivolumab Plus Ipilimumab in Advanced Non-Small-Cell Lung Cancer (CheckMate 568): Outcomes by Programmed Death Ligand 1 and Tumor Mutational Burden as Biomarkers. J Clin Oncol (2019) 37:992– 1000. doi: 10.1200/JCO.18.01042
- Rozeman EA, Menzies AM, van Akkooi ACJ, Adhikari C, Bierman C, van deWiel BA, et al. Identification of the Optimal Combination Dosing Schedule of Neoadjuvant Ipilimumab Plus Nivolumab in Macroscopic Stage III Melanoma (OpACIN-Neo): A Multicentre, Phase 2, Randomised, Controlled Trial. *Lancet Oncol* (2019) 20:948–60. doi: 10.1016/S1470-2045 (19)30151-2
- 30. Scherpereel A, Mazieres J, Greillier L, Lantuejoul S, Dô P, Bylicki O, et al. Nivolumab or Nivolumab Plus Ipilimumab in Patients With Relapsed Malignant Pleural Mesothelioma (IFCT-1501 MAPS2): A Multicentre, Open-Label, Randomised, non-Comparative, Phase 2 Trial. *Lancet Oncol* (2019) 20:239–53. doi: 10.1016/S1470-2045(18)30765-4
- 31. Sharma P, Siefker-Radtke A, de Braud F, Calvo E, Bono P, et al. Nivolumab Alone and With Ipilimumab in Previously Treated Metastatic Urothelial Carcinoma: CheckMate 032 Nivolumab 1 Mg/Kg Plus Ipilimumab 3 Mg/Kg Expansion Cohort Results. J Clin Oncol (2019) 37:1608–16. doi: 10.1200/ JCO.19.00538
- 32. Tawbi HA, Forsyth PA, Algazi A, Hamid O, Hodi FS, Moschos SJ, et al. Combined Nivolumab and Ipilimumab in Melanoma Metastatic to the Brain. N Engl J Med (2018) 379:722–30. doi: 10.1056/NEJMoa1805453
- 33. Wolchok JD, Chiarion-Sileni V, Gonzalez R, Rutkowski P, Grob JJ, Cowey CL, et al. Overall Survival With Combined Nivolumab and Ipilimumab in Advanced Melanoma. N Engl J Med (2017) 377:1345–56. doi: 10.1056/ NEJMoa1709684
- 34. Yau T, Kang YK, Kim TY, El-Khoueiry AB, Santoro A, Sangro B, et al. Efficacy and Safety of Nivolumab Plus Ipilimumab in Patients With Advanced Hepatocellular Carcinoma Previously Treated With Sorafenib: The CheckMate 040 Randomized Clinical Trial. JAMA Oncol (2020) 6:e204564. doi: 10.1001/jamaoncol.2020.4564
- 35. Zamarin D, Burger RA, Sill MW, Powell DJJr, Lankes HA, Feldman MD, et al. Randomized Phase II Trial of Nivolumab Versus Nivolumab and Ipilimumab for Recurrent or Persistent Ovarian Cancer: An NRG Oncology Study. J Clin Oncol (2020) 38:1814–23. doi: 10.1200/JCO.19.02059
- 36. Zimmer L, Livingstone E, Hassel JC, Fluck M, Eigentler T, Loquai C, et al. Adjuvant Nivolumab Plus Ipilimumab or Nivolumab Monotherapy Versus Placebo in Patients With Resected Stage IV Melanoma With No Evidence of Disease (IMMUNED): A Randomised, Double-Blind, Placebo-Controlled, Phase 2 Trial. *Lancet* (2020) 395:1558–68. doi: 10.1016/S0140-6736(20)30417-7
- Barrios DM, Do MH, Phillips GS, Postow MA, Akaike T, Nghiem P, et al. Immune Checkpoint Inhibitors to Treat Cutaneous Malignancies. J Am Acad Dermatol (2020) 83:1239–53. doi: 10.1016/j.jaad.2020.03.131
- de Miguel M, Calvo E. Clinical Challenges of Immune Checkpoint Inhibitors. Cancer Cell (2020) 38:326–33. doi: 10.1016/j.ccell.2020.07.004

- Dall'Olio FG, Marabelle A, Caramella C, Garcia C, Aldea M, Chaput N, et al. Tumour Burden and Efficacy of Immune-Checkpoint Inhibitors. *Nat Rev Clin* Oncol (2021) 19:75–90. doi: 10.1038/s41571-021-00564-3
- Doroshow DB, Bhalla S, Beasley MB, Sholl LM, Kerr KM, Gnjatic S, et al. PD-L1 as a Biomarker of Response to Immune-Checkpoint Inhibitors. *Nat Rev Clin Oncol* (2021) 18:345–62. doi: 10.1038/s41571-021-00473-5
- Nadelmann ER, Yeh JE, Chen ST. Management of Cutaneous Immune-Related Adverse Events in Patients With Cancer Treated With Immune Checkpoint Inhibitors: A Systematic Review. JAMA Oncol (2021) 8:130–8. doi: 10.1001/jamaoncol.2021.4318
- Wang Y, Zhou S, Yang F, Qi X, Wang X, Guan X, et al. Treatment-Related Adverse Events of PD-1 and PD-L1 Inhibitors in Clinical Trials: A Systematic Review and Meta-Analysis. *JAMA Oncol* (2019) 5:1008–19. doi: 10.1001/ jamaoncol.2019.0393
- Chen J, Li S, Yao Q, Du N, Fu X, Lou Y, et al. The Efficacy and Safety of Combined Immune Checkpoint Inhibitors (Nivolumab Plus Ipilimumab): A Systematic Review and Meta-Analysis. World J Surg Oncol (2020) 18:150. doi: 10.1186/s12957-020-01933-5
- 44. Yang Y, Jin G, Pang Y, Huang Y, Wang W, Zhang H, et al. Comparative Efficacy and Safety of Nivolumab and Nivolumab Plus Ipilimumab in Advanced Cancer: A Systematic Review and Meta-Analysis. *Front Pharmacol* (2020) 11:40. doi: 10.3389/fphar.2020.00040
- 45. Xing P, Zhang F, Wang G, Xu Y, Li C, Wang S, et al. Incidence Rates of Immune-Related Adverse Events and Their Correlation With Response in Advanced Solid Tumours Treated With NIVO or NIVO+IPI: A Systematic Review and Meta-Analysis. J Immunother Cancer (2019) 7:341. doi: 10.1186/ s40425-019-0779-6
- 46. Xu H, Tan P, Ai J, Zhang S, Zheng X, Liao X, et al. Antitumor Activity and Treatment-Related Toxicity Associated With Nivolumab Plus Ipilimumab in Advanced Malignancies: A Systematic Review and Meta-Analysis. Front Pharmacol (2019) 10:1300. doi: 10.3389/fphar.2019.01300
- Wang F, Yang S, Palmer N, Fox K, Kohane IS, Liao KP, et al. Real-World Data Analyses Unveiled the Immune-Related Adverse Effects of Immune Checkpoint Inhibitors Across Cancer Types. *NPJ Precis Oncol* (2021) 5(1):82. doi: 10.1038/ s41698-021-00223-x
- 48. Zhou X, Yao Z, Bai H, Duan J, Wang Z, Wang X, et al. Treatment-Related Adverse Events of PD-1 and PD-L1 Inhibitor-Based Combination Therapies in Clinical Trials: A Systematic Review and Meta-Analysis. *Lancet Oncol* (2021) 22:1265–74. doi: 10.1016/S1470-2045(21)00333-8

Conflict of Interest: The authors declare that the research was conducted in the absence of any commercial or financial relationships that could be construed as a potential conflict of interest.

Publisher's Note: All claims expressed in this article are solely those of the authors and do not necessarily represent those of their affiliated organizations, or those of the publisher, the editors and the reviewers. Any product that may be evaluated in this article, or claim that may be made by its manufacturer, is not guaranteed or endorsed by the publisher.

Copyright © 2022 Zhao, Gao, Yang, Fan, Xie, Jiang, Gong, Gao, Yang and Lei. This is an open-access article distributed under the terms of the Creative Commons Attribution License (CC BY). The use, distribution or reproduction in other forums is permitted, provided the original author(s) and the copyright owner(s) are credited and that the original publication in this journal is cited, in accordance with accepted academic practice. No use, distribution or reproduction is permitted which does not comply with these terms.



Emergence of the CD226 Axis in Cancer Immunotherapy

Michael Conner, Ken W. Hance, Sapna Yadavilli, James Smothers and Jeremy D. Waight *

Oncology R&D, GlaxoSmithKline, Collegeville, PA, United States

In recent years, a set of immune receptors that interact with members of the nectin/nectinlike (necl) family has garnered significant attention as possible points of manipulation in cancer. Central to this axis, CD226, TIGIT, and CD96 represent ligand (CD155)competitive co-stimulatory/inhibitory receptors, analogous to the CTLA-4/B7/CD28 tripartite. The identification of PVRIG (CD112R) and CD112 has introduced complexity and enabled additional nodes of therapeutic intervention. By virtue of the clinical progression of TIGIT antagonists and emergence of novel CD96- and PVRIG-based approaches, our overall understanding of the 'CD226 axis' in cancer immunotherapy is starting to take shape. However, several questions remain regarding the unique characteristics of, and mechanistic interplay between, each receptor-ligand pair. This review provides an overview of the CD226 axis in the context of cancer, with a focus on the status of immunotherapeutic strategies (TIGIT, CD96, and PVRIG) and their underlying biology (i.e., *cis/trans* interactions). We also integrate our emerging knowledge of the immune populations involved, key considerations for Fc gamma (γ) receptor biology in therapeutic activity, and a snapshot of the rapidly evolving clinical landscape.

OPEN ACCESS

Edited by:

Xian Zeng, Fudan University, China

Reviewed by:

Romain Roncagalli, INSERM U1104 Centre d'immunologie de Marseille-Luminy (CIML), France Andrey Shaw, Genentech, Inc., United States

*Correspondence:

Jeremy D. Waight jeremy.x.waight@gsk.com

Specialty section:

This article was submitted to Cancer Immunity and Immunotherapy, a section of the journal Frontiers in Immunology

Received: 06 April 2022 **Accepted:** 26 May 2022 **Published:** 24 June 2022

Citation:

Conner M, Hance KW, Yadavilli S, Smothers J and Waight JD (2022) Emergence of the CD226 Axis in Cancer Immunotherapy. Front. Immunol. 13:914406. doi: 10.3389/fimmu.2022.914406 Keywords: cancer immunotherapy, NK cells, T cells, Treg cells, antibodies, fc gamma receptors (Fc γ R)

INTRODUCTION

With the widespread clinical application of the 'first generation' of immune checkpoint inhibitors (ICI), namely antibody-mediated blockade of cytotoxic T lymphocyte-associated protein-4 (CTLA-4) and programmed cell death protein/ligand-1 (PD-[L]1), immunotherapy has become a mainstay approach for the treatment of cancer (1). However, despite a wealth of evidence supporting the use of anti-CTLA-4 and anti-PD-1/L1, many patients fail to derive meaningful benefit – highlighting the need for alternative and complementary immunotherapeutic interventions (2). In this regard, engagement of novel pathways, cell types, and combinations may provide therapeutic options for patients wherein the pre-existing host and tumor microenvironment factors do not favor current immunotherapeutic agents or where adaptive resistance has occurred (3).

For more than a decade, the CD226 axis have been characterized in the context of natural killer (NK) and T cell biology (4). At the core of this family, T cell immunoreceptor with Ig and ITIM domains (TIGIT) and CD96 (TACTILE) effectively compete with CD226 (DNAX Accessory Molecule-1 [DNAM-1] for binding to the necl protein CD155 (poliovirus receptor [PVR). This regulatory network is reminiscent of the interplay between cytotoxic T-lymphocyte-associated protein-4 (CTLA-4)/CD28 and B7 (CD80/CD86), where a common ligand (CD155) is shared

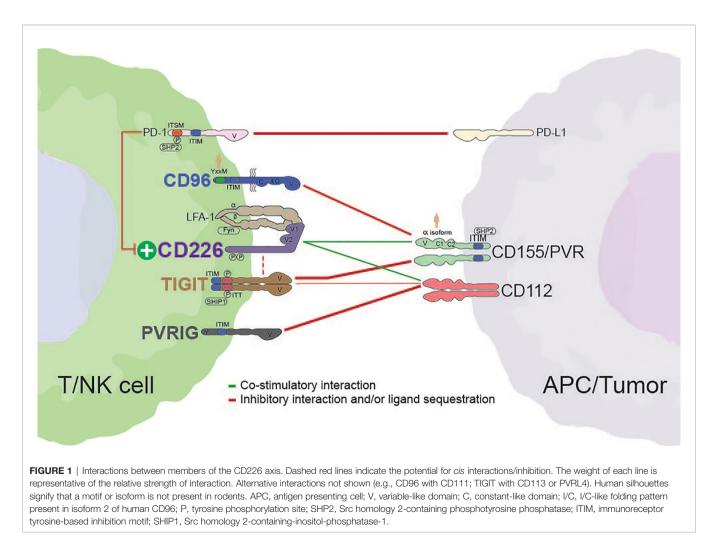
between costimulatory (CD226) and co-inhibitory receptors (CD96 and TIGIT) (**Figure 1**) (5). While a parallel with the CTLA-4 axis could provide some mechanistic insight to the CD226 axis, there are some important differences in cellular expression, potential for direct inhibitory receptor signaling, and the potential impact of soluble ligand (6, 7). Adding to this complexity, the recently described PVRIG has been shown to compete with CD226 binding to CD112, another ligand in this axis (**Figure 1**) (8–10).

The contiguous nature of the CD226 axis begs several questions. For example, are the family members redundant such that concurrent antagonism of multiple receptors is necessary to reveal their full functional potential, or are individual receptors dominant under distinct contexts? A thorough understanding of the dynamics of each ligandreceptor pair will be critical for the mechanistic deconvolution of a seemingly redundant family. These relationships may also inform the best approaches for successful therapeutic intervention (i.e., best indications to target individual or multiple receptors, mono- or bi-specific strategies, etc.). To help address this, we explore the structural characteristics, reported interactions, and expression patterns for each immune receptor in the CD226 axis (**Table 1**). We also discuss the potential for cell-intrinsic activity and present the available evidence supporting combinations with antibodies targeting the CD226 axis. In addition, given the importance of Fc-Fc gamma (γ) receptor co-engagement to CTLA-4 antibody function, and inherent similarities with the CTLA-4/B7/CD28 family, we briefly discuss the potential role of Fc γ Rs in promoting the functional activity of antibodies targeting the immune receptors in the CD226 axis (14–16). Finally, we provide a snapshot view of the current therapeutic landscape for the CD226 axis, surveying the available clinical data for each target and highlighting current indications, safety considerations, and combination strategies for each target.

THE CORE OF THE AXIS: CD226

Discovery, Structure, and Interactions

By virtue of its role in cytotoxic T cell maturation and platelet activation, CD226 was initially identified as T lineage-specific antigen (TLiSA1) and platelet and T cell antigen 1 (PTA1) shortly thereafter (17, 18). CD226, or DNAX accessory

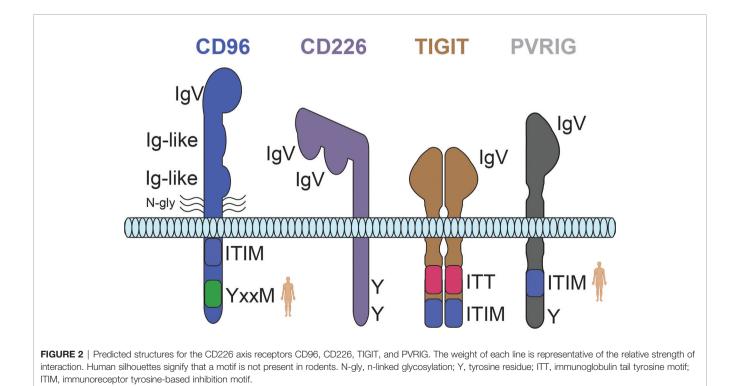


	TIGIT	CD96	PVRIG	CD226
CD4+ T cells: Naïve ^a	+/-	+/-	+/-*	++
CD4+ T cells: EM ^a	++	+++	+/-*	+++
CD4+ T cells: CM ^a	+	++	+/-*	+++
CD4+ T cells: TEMRA ^a	+/-	+/-	ND	++
CD4+ T cells: Treg ^a	++++	+/-	+/-*	++
CD4+ T cells: Tfh ^c	++	ND	ND	ND
CD8+ T cells: Naïve ^{a,b}	+/-	+	+/-	++
CD8+ T cells: EM ^{a,b}	++	+++	+++	+++
CD8+ T cells: CM ^{a,b}	+/-	++	+	+++
CD8+ T cells: TEMRA ^{a,b}	+++	+	+++	++
MAIT cells ^a	-	++	+*	+++
γδT cells ^a	+++	+/-	+*	+++
B cells ^a	+	+/-	_*	-
NK cells ^{a,b}	++	++	++	+++
NKT cells (CD56+ T cells) ^a	++	++	ND	+++
Myeloid ^a	-	-	_*	++

Analysis based on human PBMCs. Expression may vary depending on tissue type and indication (e.g., cancer). Symbols (+ and -) represent relative and qualitative expression of each receptor, wherein + is positive expression and – or -/+ is negative or minimal/variegated expression, respectively. ND, not determined. a (11); b (12); c (13); *RNA analysis only (Human Cell Atlas).

molecule 1 (DNAM-1), has since been thoroughly characterized as a T and NK cell co-stimulatory receptor responsible for orchestrating the signaling of shared ligands CD155 and CD112 (8, 19–22). Analogous to CD28 in the B7/CTLA-4 axis, CD226 has a reduced affinity for shared ligands CD155 and CD112 relative to the inhibitory receptors TIGIT, CD96, and PVRIG, thus creating a layer of immune regulation *via* competitive inhibition (9, 19, 23–26). Exemplifying its important role in immune homeostasis, CD226 genetic polymorphisms are associated with various immune pathologies (27–29). Similar correlations are lacking for TIGIT, CD96, and PVRIG, highlighting the central nature of CD226 in controlling immune activity within the family.

The extracellular region of CD226 forms a unique structure whereby its two IgV domains (domain [D]1 and D2) are linked in a side-by-side arrangement (**Figure 2**). As a result, while interactions are primarily mediated by a conserved 'lock-and-key' motif in D1, the second extracellular domain (D2) can also contribute to ligand binding (25, 26). The intracellular region of CD226 harbors a conserved tyrosine (Y)/asparagine (N) motif



(D/EIYV/MNY), which engages with multiple proteins, including growth factor receptor bound protein 2 (Grb2) (30). Site-directed mutagenesis of Y319 abrogates CD226-induced cellular cytotoxicity (30) (**Table 2**). This residue (Y319) has also been associated with regulation of CD226 expression *via* Casitas B-lineage lymphoma proto-oncogene-b (Cbl-b)-dependent ubiquitination/degradation following CD155 engagement (37). Additionally, although it appears to be contextual, co-localization with lymphocyte function-associated antigen 1 (LFA-1) during immune synapse formation has also been described (**Figure 1**) (30, 32).

Expression and Regulation

CD226 is broadly expressed on innate and adaptive immune populations and, like the associated inhibitory receptors within the axis, can be induced on peripheral human T cells following T cell receptor (TCR) activation (**Table 1**) (11, 38). Notably, the expression of CD226 on activated human T and intratumoral NK cells tracks closely to that of CD96 (11, 39). While coexpression could suggest some level of reactive regulation within the axis, it remains unclear if it is simply correlative or if it is biologically meaningful.

Another mechanism to temper immune activation could be the direct regulation of CD226 expression (i.e., by ligandinduced internalization/endocytosis or cleavage), as evidenced by its modulation in various disease settings including chronic viral infection and cancer (37, 40, 41). For example, in non-small cell lung cancer (NSCLC), CD226 expression is reduced on tumor-infiltrating NK cells relative to cells from normal adjacent tissues (NAT) and peripheral blood (42, 43). Moreover, CD226 has been shown to be sensitive to changes elicited by various therapeutics, such as chemotherapy (44).

While ligand-based interactions have primarily been implicated in driving the loss of cell surface CD226, recent work by Sun et al. also suggests that this effect could be mediated by soluble factors like transforming growth factor beta (TGF- β 1) (37, 39, 45, 46). It is unclear if this is a direct or indirect effect, however, TGF-\beta-dependent modulation of CD226 has the potential to skew axis signaling in the tumor microenvironment (TME), enhancing the potential for immune evasion. Additionally, increased soluble CD226, and related loss of cell-surface expression, has been observed in the sera of cancer patients, suggesting some level of protease-dependent biology (47). Regardless of mechanism, the reduction of CD226 on immune cells in tumor-bearing hosts and prevalence of other axis members, raises several questions. Most notably, how much CD226 expression is necessary to drive functional responses following blockade of inhibitory receptors in the axis, and is this something that needs to be monitored to predict responses? As clinical efforts progress, it will be of interest to interrogate the relevance of CD226 dynamics in therapeutic responses.

Functional and Therapeutic Implications

The importance of CD226 in shaping the overall immune response has been thoroughly described in the context of autoimmunity, cancer, and viral infections (48). CD226

orchestrates the net activity of innate (NK cells) and adaptive (T cells) immunity *via* interplay with CD155 and CD112 (8, 49). For example, high expression of cell-surface CD155 coupled with low human leukocyte antigen (HLA) expression increases the susceptibility of immature DCs to CD226-mediated killing by NK cells. This process bridges both innate and adaptive immunity by removing Th2-polarizing iDCs, thus skewing T helper cell polarization (50–52). CD226 has been shown to play a critical role in promoting broad T cell expansion, CD8⁺ T cell antitumor activity, and "adaptive" NK cell responses (37, 53–55).

A significant amount of information regarding the contribution of CD226 to immune responses has been gleaned from genetic- and biologics-based approaches in mice. In contrast to delayed tumor progression in TIGIT^{-/-} and CD96^{-/-}, CD226-deficient mice exhibit increased susceptibility to MCA-induced fibrosarcomas as well as metastatic lung colonization (e.g., LLC lung and RM-1 prostate tumors) (19, 20, 56–58). Moreover, genetic ablation or antibody-mediated blockade of CD226 has been shown to abrogate the antitumor activity observed in CD96-deficient mice and in mice treated with anti-TIGIT, anti-PD-(L)1, and/or GITR (19, 20, 59, 60). Tumors propagated in CD226-deficient mice also exhibit increased expression of CD155 and CD112, further highlighting the dynamics within the CD226 axis (54, 57).

Given its critical immunostimulatory role, agonist approaches for CD226 seem attractive as a means to generate antitumor responses. However, CD226 is also expressed on platelets and has been associated with their adhesion/activation, potentially complicating the desired pharmacology profile (18, 61). Thus far, only one agent for CD226, LY3435151 (anti-CD226 agonist antibody, Eli Lilly), has progressed to clinical testing (NCT04099277, **Table 3**). Nevertheless, shortly after initiation, the phase 1 study for LY3435151 was terminated. Although one can speculate as to the reason(s) for study termination, given the critical position of CD226 in CD155 and CD112 axes, it will be of great interest to understand the limitations surrounding CD226 as a target for cancer immunotherapy.

KEY LIGANDS IN THE AXIS: CD155 AND CD112

Discovery, Structure, and Interactions

Identified several decades before an association with relevant immune receptors, CD155 (poliovirus receptor [PVR], necl-5) and CD112 (PVRL2, nectin-2) represent structurally similar immunoglobulin superfamily (IgSF) adhesion glycoproteins (62–64). There are several isoforms of CD155 (α , β , γ , δ) and CD112 (short, CD112 α ; long, CD112 δ), each with slightly different structural characteristics and tissue distribution (8, 65, 66). While the α and δ isoforms of CD155 code for cell-surface expressed CD155, the β and γ isoforms lack transmembrane (TM) domains, resulting in a soluble/secreted proteins that are not present in rodents (7, 65, 67). The extracellular region of CD155 and CD112 is comprised of an N-terminal variable (V) domain and constant (C1-C2) domains (24, 68–70). Like CD226, the V domain contains conserved 'lock' (AX₆G) and 'key' (T[F/ Y]P) motifs that are critical for mediating homo- and heterophilic interactions (24, 25, 68). Appropriately, CD155 and CD112 are capable of *trans* interactions, which can facilitate sustained cell-to-cell contact and immunoregulation (71, 72). Contrary to many nectin proteins, CD155 fails to exhibit strong homophilic interactions (71, 73). Similar evidence suggests that CD112 functions as a monomer, but also exhibits proclivity for homodimerization (74).

Outside of their conserved binding motifs, CD155 and CD112 exhibit nuances in binding orientation depending on the partner. For example, both CD155 and CD112 have been suggested to form heterotetrameric structures with TIGIT, where TIGIT dimers are sandwiched between CD155 or CD112 monomers; while other CD155 (e.g., CD226 and CD96) and CD112 complexes (e.g., CD226) are thought to be more conventional monomeric interactions (Figure 1) (25, 68-70). Differential structural attributes of TIGIT, CD96, and CD226 provide a partial explanation for their relative affinity to cell surface CD155 (26, 75). However, this is likely more complex given the variegated glycosylation patterns of the axis proteins. As mentioned previously, this affinity gradient, which favors inhibitory receptor binding (i.e., TIGIT and CD96), is reminiscent of the archetype CTLA-4 axis, whereby CTLA-4 effectively outcompetes costimulatory receptor CD28 from binding to B7 (CD80/86) (5). In a similar fashion, the inhibitory receptor PVRIG demonstrates a greater affinity for CD112 relative to CD226 (9).

Expression and Regulation

Despite detectable levels on multiple cell types (e.g., myeloid and epithelial cells) under physiological conditions, CD155 and CD112 are often elevated in various solid and hematological malignancies, correlating with a worse overall survival (12, 76–83). These correlations are not ubiquitous, however, as lack of expression in hepatocellular carcinoma (HCC) has been shown to be prognostically unfavorable (84, 85). Indeed, akin to PD-L1, CD155 expression has also been shown to be predictive of response to ICI (e.g., anti-PD-1 and anti-PD-1/CTLA-4) (86). This underscores the need for a clear etiological understanding and cancer-immune interplay in each indication. Moreover, treatment status must be considered, as CD155 and CD112 can be induced downstream of a range of cellular insults or stimuli known to activate the DNA damage response (DDR) pathway (87–92).

In addition to relatively broad expression by human tumor tissue and stromal populations, CD155 and CD112 are expressed on myeloid cells, such as monocytes and various subsets of dendritic cells (DCs) (50, 93). Given the reported expression of CD155 on follicular DCs, a key component of B cell follicles/germinal centers (GC), the involvement of the CD226 axis in tertiary lymphoid structure (TLS) biology may warrant further exploration (93, 94). This is particularly attractive in light of recent correlations between TLS generation/presence and response to cancer immunotherapy (95–97). One area where CD155 and CD112 appear to diverge is in lymphocyte expression, whereby CD155 can be induced on highly activated T cells (87, 98, 99). While the functional consequences of CD155 on activated T cells remains to be determined, CD155 has been associated with thymic selection *via* lymphocyte retention, underscoring its adhesion properties and potential impact on T cells (100). The expression of CD155 on T cells may also introduce complexity into the mechanistic interpretation and be derivative of certain experimental models. For example, CD155 induction on T cells may complicate our understanding of how anti-CD96 antibodies mediate functional activity even under conditions of T cell isolation (i.e., agonist activity or blockade of CD96:CD155 T cell-to-T cell interactions).

As the name suggests, CD155 or poliovirus receptor (PVR) serves as a point of cellular entry for poliovirus and, similar to the described role for soluble intercellular adhesion molecule-1 (ICAM-1) in response to rhinovirus infection, soluble CD155 has been proposed to be a partial serum-based sink for poliovirus (65, 101). Interestingly, soluble CD155 and CD112, have also been described in the serum of cancer patients and are often correlated with disease stage (7, 66, 102, 103). However, the specific contribution of soluble CD155 and CD112 to disease progression remains to be determined. Despite the longstanding awareness of CD155 and CD112 expression in cancer, an understanding of their contribution to the regulation of immune function and migration was lacking until a connection with the CD226 was established (8-10, 70, 104, 105). Functional characteristics and therapeutic implications for each interaction will be discussed in the following sections.

TIGIT

Discovery, Interactions and Structure

Several years after the description of CD226 and its association with CD155, T cell immunoglobulin and ITIM domain (TIGIT; V-set and transmembrane domain-containing 3 [Vstm3]; V-set and Ig domain-containing 9 [Vsig9]; Washington University Cell Adhesion Molecule [WUCAM]) emerged as an important member of the CD226 axis (10, 23, 93). The discovery of TIGIT was aided by searching for predicted structural similarities with cell-surface immune receptors, like PD-1. After its initial identification as a receptor for CD155, an additional ligand (CD112) and a role for TIGIT in NK cell modulation was described (10).

The extracellular region of TIGIT is comprised of a single IgV, and, consistent with other receptor-ligand pairs in the axis, *trans* interactions are facilitated by a lock-and-key motif in the N-terminal domain (68) (**Figure 2**). The majority of TIGIT function is tied to CD155, with binding to CD112 representing a lower affinity interaction (~30-fold *via* surface plasmon resonance [SPR]) (106). TIGIT has also been shown to interact with CD113 (PVRL3) and nectin-4 (PVRL4); however, clear functional implications remain to be seen (23, 107). Primarily

facilitated by isoleucine (Ile) 42 (human; an analogous residue exists in mice) and the associated parallel interface, TIGIT exhibits a propensity for dimerization on the surface of cells (68). Accordingly, *cis* multimeric interactions with CD226 have also been reported, providing an additional means of CD226 regulation (36, 60).

The intracellular domain of TIGIT harbors an immunoreceptor tyrosine tail (ITT)-like phosphorylation motif and a conserved ITIM (LSYRSL) (106). While the role of each motif has been evaluated in mice and man, the relative contribution of ITT/ITIM to cell intrinsic TIGIT activity appears to be more contextual in humans (Table 2). Using a modified cytotoxicity system (YTS and 721.221 cells), Stanietsky et al. demonstrated that rescue of murine CD155-mediated NK cell suppression required mutation of both ITT and ITIM tyrosine residues (108). The same authors demonstrated that site-directed mutagenesis of only the ITIM (Y221) in human cells was able to abrogate CD155- and CD112-induced suppression of NK cell cytolytic activity (10). Further, a separate set of studies ascribed the ITT as the critical moiety for TIGIT-mediated inhibition of human NK cell IFNy production, granule polarization, cellular cytotoxicity (34, 35). Recently, Banta and colleagues demonstrated that the intracellular domain of TIGIT was largely dispensable for impairment of CD226 phosphorylation (36). Rather, as previously mentioned, cis multimeric interactions with CD226 and/or ligand competition were found to drive TIGIT inhibition of CD226 co-stimulation. While this work brings into question the relative contribution of intrinsic signaling to TIGIT function (Table 2), it will be necessary to understand if it is selective to the experimental system, specific to TIGIT/CD226, or a more ubiquitous phenomenon.

Apart from ligand sequestration, TIGIT has been credited with additional mechanisms of action, which may be extrinsic or intrinsic depending on cell type. For instance, Yu et al. utilized human T cell and monocyte-derived DC co-cultures to demonstrate that unabated TIGIT : CD155 ligation alters antigen presenting cell (APC) cytokine profiles, indirectly impairing T cell responses (23). While multiple studies have revealed similar cell-extrinsic function of TIGIT, T and NK cellintrinsic TIGIT signaling has also been described in both mice and man (22, 58, 108–112). For example, Joller et al. utilized an anti-mouse agonistic TIGIT antibody, in concert with TIGIT^{-/-} mice, to characterize intrinsic TIGIT signaling in CD4⁺ T cells (111). The authors found that components of the T cell receptor complex (e.g., TCRa and CD3E) were directly modulated following TIGIT engagement, adding another layer of immunoregulation to the mechanistic story of TIGIT.

Expression and Regulation

In the peripheral compartment, TIGIT is broadly represented on T and NK cell subsets, with noteworthy representation on regulatory T (Treg) cells, NKT cells, T follicular helper (Tfh) cells, and $\gamma\delta$ T cells (**Table 1**) (11, 13). Apart from prominent expression of TIGIT on Treg cells, expression patterns for CD226 axis members ostensibly diverge when it comes to memory T cell populations

(12). TIGIT and PVRIG are elevated on human terminally differentiated CD45RA+ TEMRA cells, whereas CD96 expression is mainly restricted to central memory (CM)/effector memory (EM) T cells (113, 114). It is intriguing to speculate about the functional effects that blockade of each immune receptor may have on peripheral or tumor/tissue-resident memory T cells. However, additional characterization, particularly on tumor-infiltrating immune populations, is required to determine if these expression patterns are indicative of any meaningful functional differentiation.

Consistent with its relatively high level of expression, TIGIT has been ascribed a role in the homeostasis and function of Treg cells. Indeed, TIGIT⁺ Treg cells have been shown to be highly immunosuppressive relative to their TIGIT⁻ counterparts, inhibiting T helper (Th)1 and Th17 responses *via* induction of fibrinogen-like 2 (Fgl2) (59, 113, 115). This observation may be particularly relevant in cancer due to the elevated expression of TIGIT on intratumoral Treg cells (58, 116). As such, cellular depletion represents a plausible therapeutic mechanism for Fc-enabled TIGIT antibodies in cancer patients (discussed later).

In addition to readily detectable baseline expression, TIGIT is also upregulated on T and NK cells following activation. As exhausted T cells (T_{EX}) are largely a product of tonic TCR stimulation, TIGIT has become a mainstay in several T cell 'exhaustion signatures' and has been implicated as a potential node for functional reversion of T_{EX} (117, 118). However, because T cell exhaustion is a complicated process that is encumbered by progressive stages of epigenetic modification, TIGIT blockade alone is likely insufficient for meaningful functional rescue of fully exhausted T cells (119). Perhaps one way to determine a functional role for TIGIT in this process is to longitudinally characterize the impact of TIGIT inhibition on the arc of T cell activation to terminal exhaustion. Adapting these observations to the TME may inform whether TIGIT blockade could effectively prevent exhaustion or simply accelerate it. Alternatively, one could consider TIGIT blockade in concert with epigenetic modulators as a potential strategy to unmask and concomitantly enhance the activity of T_{EX} (120). Regardless of potential functional implications, robust expression on T_{EX} is consistent with progressive TIGIT induction following immune activation.

TIGIT expression is detectable in a wide range of human cancers and is often tightly correlated with T cell transcripts (CD4 and CD8A) (11). While its expression profile is largely consistent between the periphery and TME, TIGIT is upregulated on various TIL populations and is often accompanied by the expression of other activation-induce immune receptors, such as CD244 (2B4), TIM-3, and PD-1 (121, 122). Similar to the expression of TIGIT on TEMRA cells in the periphery, terminally differentiated intratumoral CD8+ T cells also express elevated levels of TIGIT. One could hypothesize that these cells are derivative of TIGIT^{low} stem-like T cells residing within defined TME niches or in the periphery. Alternately, these could be newly infiltrating cytotoxic T cells that progressively acquire TIGIT during *in situ* differentiation or repeated TCR activation (123, 124).

Functional and Therapeutic Implications

No baseline developmental or immunological defects have been described in TIGIT (VSTM3)-deficient mice (C57BL/6 background) (125). However, the severity of induced autoimmune manifestations, such as myelin oligodendrocyte glycoprotein (MOG)-dependent encephalomyelitis (EAE) or graft-vs-host disease (GVHD) is increased relative to wildtype mice. In the context of cancer, TIGIT deficiency, or prophylactic antibody blockade, yields a modest level of protection against primary tumor growth in mice (19, 126-128). By contrast, TIGIT monotherapy is often ineffective in mice with established lesions (60). Therefore, combination with other ICI, such as anti-PD-(L)1, has been utilized to achieve more pronounced antitumor responses in a range of tumor models (60, 129, 130). In addition, the antitumor activity of murine anti-TIGIT antibodies has been tied to Fc-Fcy receptor co-engagement (15, 131). This dependency is noteworthy given the myriad of anti-TIGIT isotypes currently under clinical evaluation (discussed later).

While the focus has largely been on solid tumors, a role for TIGIT in hematological malignancies has also been described. TIGIT is most notably upregulated on CD8+ T cells in multiple myeloma (MM), in both mice and man (128, 132, 133). Akin to what has been suggested in solid tumors, repeat antigen exposure and associated progressive exhaustion have been implicated in the upregulation of TIGIT in this setting and is of particular interest in the context of relapsed/refractory (R/R) disease. Accordingly, inhibition of TIGIT (genetic- or antibody-based) results in T cell-dependent antitumor responses in several syngeneic models of MM and is currently being evaluated in clinical studies (e.g., NCT04045028 and NCT04150965) (128). TIGIT has also been implicated in other heme cancers, such as follicular lymphoma (FL) and acute myeloid leukemia (AML) (134–136).

CD96

Discovery, Interactions and Structure

CD96 (T-cell activation, increased late expression [TACTILE]) was first identified as an orphan receptor on AML and T-cell acute lymphoblastic leukemia (T-ALL) cell lines (137). A functional role for CD96 wasn't identified until half a decade later when the interaction between CD96 on NK cells and CD155 on tumor cells was described (105). Interestingly, this finding was influenced by observations involving NK cell expressed CD226 (8): The authors noted that, while the human NK cell line NK92 bound to the extracellular domain of CD155, the cells lacked detectable expression of CD226, thereby implicating a similarly structured receptor, CD96. This finding introduced a possible functional role for CD96 on immune cells and, with CD226, provided a framework for a novel immunoregulatory axis.

CD96 is comprised of three Ig-like extracellular domains and a flexible membrane-proximal stalk region containing multiple *O*-linked glycosylation sites (138) (**Figure 2**). Only the N-terminal domain (D1) contains a lock-and-key motif critical for binding

CD155. In addition to CD155 binding, CD96 has also recently been shown to interact with human CD111; however, a functional role for this interaction remains to be elucidated (70, 75). While much of the biophysical data generated suggest that CD96 functions as a monomer, the possibility of CD96 oligomerization (i.e., *cis* interactions) needs to be evaluated in more complex systems to better understand how CD96 behaves on cells. As an example, the anti-mouse CD96 clone 8B10 (D2 binder) exhibits partial tumor control in an experimental model of metastases, yet is not entirely dependent on the presence of CD155 (139). This leads one to question if *cis* interference has a contextual biological role for CD96, if there are other important *trans* interactions, or whether this is the result of technical limitations.

Three isoforms of CD96 have been identified in humans, with two membrane-tethered isoforms (a longer variant [1] and a shorter variant [2]) and a less studied soluble isoform (variant 3) (75, 138, 140). Due to a truncated exon 4, the V2 isoform lacks a stretch of amino acids (~18) in the second Ig domain, resulting in an abbreviated loop structure. While less is known about the soluble form (V3), the V2 isoform is reported to be the most widely expressed and exhibits the highest affinity for CD155. The first domain of CD96 is reported to contain the epitope(s) required for CD155 binding while the second domain supports the magnitude/strength of binding (138). The intracellular domain of CD96 contains multiple tyrosine residues, with a prototypical inhibitory motif (ITIM, IXYXXI) that is conserved across species (138). The presence of an ITIM, coupled with the capacity for direct cross-competition with CD226/CD155 binding, suggests that CD96 functions as an inhibitory receptor. However, the categorization of CD96 as an inhibitory receptor has been mired due to (i) limited knowledge of CD96 signaling, (ii) conflicting functional data (particularly with NK cells), and (iii) the existence of a YXXM motif (YHEM) in primate CD96 (Figure 1) (105). Recently, Chiang et al. ascribed costimulatory properties to both mouse and human CD96 (141). While certainly not the only description of CD96 as a costimulatory receptor, caution should be taken regarding the interpretation of data in certain experimental systems. Because CD155 can be induced on TCR-activated T cells and the primordial involvement of nectin/necl proteins in cell adhesion, it is important to understand if the functional effects elicited by anti-CD96 are simply the result of blocking CD155-CD96 trans interactions (87, 98, 99). In addition, while several costimulatory receptors (e.g., inducible T-cell co-stimulator [ICOS]) harbor a YXXM motif, defining anti-CD96 functional directionality based on its presence may be shortsighted, as CD96 lacks a YxxM in mice and inhibitory receptors like CTLA-4 also contain similar sequences without a clearly defined functional role (142, 143).

Expression and Regulation

CD96 is expressed at baseline by several T cell populations ($\alpha\beta$ and $\gamma\delta$), NK/NKT cells, and select B cell subsets in both mice and man (**Table 1**). The expression of CD96 on primary human immune cells is most evident on CD56+ NK cells and CD8+ T cells, with prominent representation on central and effector

memory T cells (11, 113). Interestingly, human bone marrowresident lymphoid tissue (lt) NK cells, which exhibit an overlapping transcriptional profile with tissue-resident memory CD8+ T cells, express both CD96 and TIGIT (144). Consistent with its alias (T-cell activation, increased late expression or 'TACTILE'), CD96 expression also increases following TCR- or cytokine-based activation (e.g., interleukin [IL]-18 for T cells and TGF- β for NK cells) (39, 145, 146). In a recent study, Lepletier et al. described a near-homogenous level of CD96 and CD226 coexpression on TCR-activated peripheral human CD8+ T cells (11).

CD96 is also highly represented on rodent and human T cells and NK cells within the TME. A marked correlation between CD96/TIGIT messenger(m) RNA levels and CD3E/CD8a/CD4, with similar observations at the protein level (i.e., T cells), can be seen across multiple tumor types (11). Relative to T cells, the correlation between CD96 and NK cell-related genes is more infrequent despite being strong for specific indications such as HCC, head and neck squamous cell carcinoma (HNSCC), stomach adenocarcinoma, and melanoma (11, 147). Relative expression of CD96 and TIGIT on HCC-derived NK cells was shown to be dependent on tissue sub-localization, with TIGIT evenly represented across NK cells in the normal liver and intra/ peritumoral space and CD96 more restricted to intratumoral NK cells (39, 148). CD96 expression in HCC is inversely correlated with several functional markers of NK cells, including T-bet (TBX21), perforin (PRF1), and granzyme B (GZMB) (39). Interestingly, TGF- β 1 has been implicated in the induction of CD96 and associated CD226 downregulation in HCC, establishing a connection between two immunosuppressive pathways (39). More recently, CD96 was found to be coexpressed with PD-1 on TCF1+ exhausted precursor T cells in cervical tumors, a characteristic that the authors tied to therapeutic insensitivity (149). CD96 expression has also been noted in various hematological malignancies, such as T-ALL, myelodysplastic syndrome (MDS), and leukemic stem cells (LSCs) in AML (137, 150, 151). However, the biological relevance of CD96 in heme malignancies and its potential as a therapeutic target remains to be determined.

Functional and Therapeutic Implications

Similar to TIGIT, CD96-deficient mice (C57BL/6 background) do not exhibit overt baseline immunological defects (19, 152). However, challenge of CD96^{-/-} mice with lipopolysaccharide (LPS) results in hyperinflammation characterized by enhanced IFNy production by NK cells. Augmented NK cell function in CD96^{-/-} mice is best exemplified by improved antimetastatic activity in B16F10 melanoma, RM-1 prostate cancer, and EO771 breast cancer models (127). Similar CD8+ T cell-dependent effects have been observed in CD96-defificent mice, albeit in the context of concomitant PD-1 (Pdcd1) knockout (114, 152). Notably, inflammatory responses and related antitumor activity in CD96^{-/-} mice are abrogated following genetic ablation of CD226, underscoring the level of axis interplay (19, 152). Similar improvements in antitumor responses have been observed in mice following therapeutic inhibition of CD96, alone or in combination with other immune checkpoint

inhibitors (114, 149). As an example, following neoadjuvant anti-PD-1 and gemcitabine, adjuvant therapy with anti-CD96 resulted in a significant survival benefit in pancreatic ductal adenocarcinoma (PDAC) tumor-bearing mice (153). Improvement in overall survival in this model was not solely driven by attenuation of primary tumor growth, but also by NK cell-dependent control of metastatic spread (153). Combination benefit of CD96 and PD-1 blockade has also been shown in other immunotherapy-insensitive models, such as the TC-1 (HPV+) tumor model (149).

Despite the wealth of information supporting an inhibitory role for CD96 in mice, functional data in humans is largely absent. Therefore, the progression of clinical-stage anti-CD96 antibodies, such as GSK6097608 will add important data to better understand mechanism of CD226 axis dynamics.

PVRIG

Discovery, Interactions and Structure

PVR-related Ig domain-containing (PVRIG) is the most recently discovered CD226 axis member (9). While much less is known about PVRIG, the sequestration of CD112 away from CD226 represents a regulatory mechanism similar to that utilized by TIGIT and CD96 co-inhibitory receptors (**Figure 1**) (9, 12). Alongside this potential for ligand competition, PVRIG has the capacity for intrinsic inhibitory signaling – which is likely facilitated by an ITIM-like motif found in the intracellular domain of PVRIG (9) (**Table 2**). Interestingly, this inhibitory domain is lacking in mice, suggesting that PVRIG function in mice is more dependent on ligand competition or is tied to an alternative mechanism that has yet to be described (**Figure 2**).

Expression and Regulation

Like TIGIT and CD96, PVRIG is expressed on various T and NK cell subsets and is upregulated on T cells following TCR stimulation (9). Elevated PVRIG expression has been described on exhausted T cells in human tumors, with noteworthy expression on TILs from ovarian, kidney, lung, endometrial, and breast cancers (12, 154). Similarly, antigen specific CD8+ T cells from virally infected mice exhibit similar upregulation of PVRIG as cells transition from activation to exhaustion (155). Despite lack of induction on *in vitro*-activated NK cells, increased PVRIG expression is observed on tumor-infiltrating NK cells (12). To date, little is known about regulation of PVRIG expression on different immune cell subsets.

Functional and Therapeutic Implications

Genetic- or biologics-based inhibition of PVRIG has been shown to impair tumor growth, particularly when combined with anti-PD-L1 (76, 155, 156). Notably, tumor-infiltrating CD8+ T cells and NK cells from PVRIG-deficient mice exhibit increased proinflammatory cytokine production, suggesting that PVRIG is involved in direct or indirect modulation of tumor-infiltrating T/NK cells (155, 156). In humans, *in vitro* blockade of PVRIG : CD112 binding results in enhanced TCR signaling and, when

TABLE 2	CD226 axis receptor ICD mutational studies and	d associated functional effects
TADLE Z	ODZZO axis receptor IOD mutational studies and	

Receptor	System (cell type)	Modifications	Finding(s)	Ref.
CD226 (human)	BW5147 (T cell line, mouse), human CD226 ectopic	S329F mutation; various truncations of intracellular domain	Prevention of protein kinase C (PKC) phosphorylation and subsequent cellular adhesion	(31)
CD226 (human)	Jurkat and NKL (T and NK cell lines, human)	WT in NKL cells. Mutation of S329F in Jurkat cells	S329F mutant failed to associate with LFA-1	(32)
CD226 (human)	Jurkat (T cell line, human) and COS-7 (fibroblast line, monkey)	Y322F	Fyn induced phosphorylation at Y322, abrogated by Y322F mutation.	(32)
CD226 (mouse)	Primary murine NK cells and YTS (human NK cell line)	Ectopic expression of mouse CD226 in YTS cells	Increased phosphorylation of Erk and Akt, as well as calcium flux and target cell lysis following CD226 engagement	(30)
CD226 (mouse)	YTS (NK cell line, human) and transgenic mice	Y319F, S326A	Y319F modification in CD226 attenuated mouse NK cell cytotoxicity and IFNg production	(30)
CD226 (mouse)	Synthetic peptide corresponding to 315-333 of mouse CD226	Synthesized with phosphorylation at Y319, D321Q	Phosphorylation of the amino acid corresponding to Y319 led to capture of Grb2. Mutation of the asparagine at +2 position led to loss of Grb2 binding	(30)
CD226 (human)	Jurkat (T cell line, human) or primary (T cells, human)	Y322A, S329A	Y322A modification, but not S329A, reduced downstream CD226 signaling after incubation with CHO-OKT3-PVR cells	(33)
TIGIT (human)	Jurkat (T cell line, human)	Y225A, Y231A	Y225A/Y231A dual mutation rescued CD69 expression on Jurkat cells following exposure to superantigen and CD155	(33)
TIGIT (human)	YTS (NK cell line, human)	Truncation (Y231stop); Y231A	Rescue of CD155-TIGIT induced inhibition of YTS (NK) mediated cytotoxicity following truncation or Y231A mutation in TIGIT	(10)
TIGIT (human)	YTS (NK cell line, human)	Y225A, Y231A	CD155 induced TIGIT phosphorylation. Pervanadate treatment-induced phosphorylation of TIGIT was prevented with Y225A or Y225A/Y231A, but not Y231A alone	(34)
TIGIT (human)	YTS (NK cell line, human)	Y225A, Y231A	TIGIT Y225 associates with Grb2, leading to downstream inhibitory function. Nominal rescue of cytotoxicity with Y231A mutation	(34)
TIGIT (human)	YTS (NK cell line, human)	Y225A, Y231A	Reduced association with β -arrestin 2 following mutation Y225A or Y225A/Y231A, but not Y231A alone	(35)
TIGIT (human)	Jurkat (T cell line, human)	ICD truncation, Y225F, Y231F	TIGIT intracellular domain is not required to prevent PVR-induced CD226 phosphorylation	(36)
TIGIT (human)	Cell-free liposome	ICD expressed on cell-free liposome	Lack of Shp2, Shp1, Zap70, Grb2, SHIP-1, or P50a recruitment following phosphorylation of TIGIT ICD by Fyn	(36)
CD96 PVRIG (human)	Undescribed HEK293T (kidney cell line, human) and MOLT4 (T cell line, human)	Undescribed Y233F, Y293F	Undescribed Y233F mutation reduced phosphorylation after pervanadate treatment. PVRIG associates with SHIP and Shp1/2 following pervanadate treatment	None (9)

combined with trastuzumab (anti-HER2) and anti-TIGIT, potentiates ADCC activity and IFN γ production by NK cells (9, 157).

CLINICAL LANDSCAPE

Overview

This current clinical landscape for the CD226 axis is heavily represented by TIGIT antibodies, with an increasing number of agents at various stages of clinical evaluation (158, 159). Two PVRIG antagonist antibodies (COM-701, Compugen; GSK4381562, GlaxoSmithKline [GSK]), a single CD96 antibody (GSK6097608; GSK/23andMe), and a recently discontinued CD226 agonist antibody (LY-3435151, Eli Lilly & Co) round out the rest of the agents under clinical testing (**Table 3**).

TIGIT

As peculiar as it may sound, given that several agents have progressed into late-stage studies, the clinical landscape for TIGIT is just starting to take shape. Recent positive signs from CITYSCAPE (NCT03563716), a first-line NSCLC (1L) phase 2 clinical trial exploring atezolizumab (anti-PD-L1)/tiragolumab (anti-TIGIT) versus atezolizumab/placebo, were on display at American Society of Clinical Oncology (ASCO) 2020 (160). The most striking observation was the large jump in overall response rate (ORR) in PD-L1^{high} patients (PD-L1 TPS > 50%; N=29 patients in each group) from 24% in the control arm (atezolizumab + placebo) to 66% with the combination. At first glance, this ORR compares favorably to similar ICI combinations (e.g., anti-PD-1/CTLA-4, Checkmate-227/NCT02477826) and is comparable to anti-PD-1 + chemotherapy (Keynote-189/ NCT02578680) in a similar NSCLC patient subset (N=202 patients) (161). These data have recently enabled a breakthrough therapy designation by the FDA for 1L PD-L1^{high} NSCLC. However, given the relatively small number of patients in CITYSCAPE, phase 3 studies from Roche and others will be critical for determining the robustness of the combination. Moreover, despite these promising results, both atezolizumab (18% [N=39 patients]) and the combination (16% [N=38 patients]) failed to elicit meaningful responses in PD-L1^{low} patients (TPS 1-49%) relative to historical use of anti-PD-1 or anti-PD-L1 + chemotherapy (e.g., Keynote-407/ NCT02775435 and Impower150/NCT02366143) (162, 163). This lack of overt activity across NSCLC patients may not be

TABLE 3 | Ongoing or discontinued (terminated) clinical trials evaluating CD226 axis-related antibody-based therapies in cancer patients.

Target	Agent	Isotype	Phase	Indication	Study	Details
FIGIT	Tiragolumab (Roche)	hlgG1	3	NSCLC	NCT04294810	PD-L1-selected
	0 ()	0			(SKYSCRAPER-01)	 + atezolizumab
			3	ES-SCLC	NCT04256421 NCT04665856	 + atezolizumab and chemo
			0	20 0020	(SKYSCRAPER-02/C)	
			3	NSCLC	NCT04513925	 + atezolizumab
			3	NGOLO		
					(SKYSCRAPER-03)	• + durvalumab
						 No progression on CRT
			3	LA Esophageal	NCT04543617	 + atezolizumab
					(SKYSCRAPER-07)	
			3	1L LA Esophageal	NCT04540211	 + atezolizumab and chemo
					(SKYSCRAPER-08)	
			2	Cervical	NCT04300647	 PD-L1+ patients
•	•••		2	Corvical	(SKYSCRAPER-04)	 + atezolizumab
			0			
			2	NSCLC	NCT03563716 (CITYSCAPE)	Chemo-naïve
						 + atezolizumab
			2	NSCLC	NCT05034055	• SBRT
					(SKYROCKET)	 + atezolizumab
			2	HNSCC	NCT04665843	• 1L PD-L1+
			-		(SKYSCRAPER-09)	 + atezolizumab
			2	Non-squam. NSCLC	NCT04958811	 + atezoizumab + bevacizumab
••			2	NULT-SQUALLE NOULE	110104300011	
			_			 + atezolizumab
			2	SCLC	NCT04308785	 + atezolizumab
						 No progression on CRT
			2	Melanoma	NCT05060003	 ctDNA+ following resection
						 + atezolizumab
			2	Non-squam. NSCLC	NCT04619797	 + atezolizumab and chemo
			-		(SKYSCRAPER-06)	
			0	Destal		•
			2	Rectal	NCT05009069	 + atezolizumab following
						neoadjuvant chemo
			2	HER2-G/GEJ	NCT04933227	 + atezolizumab and chemo
			2	NSCLC	NCT04832854	 + atezolizumab
						 +/- neoadjuvant chemo
			2	Melanoma	NCT03554083	 + atezolizumab and chemo
•			~	(stage III)	(NeoACTIVE)	
			0			• L popodi s cost at!
			2	HNSCC	NCT03708224	 + neoadjuvant atezolizumab
						 + tocilizumab
			2	Mixed	NCT04632992	 Platform study
					(MyTACTIC)	
			1b/2	GEJC	NCT05251948 (Morpheus-C-	 Platform study
					Gastric)	
			1b/2	HCC	NCT04524871	Platform study
			10/2	100		- nationni study
					(Morpheus-Liver)	
			1b/2	mUC	NCT03869190 (Morpheus-UC)	Platform study
						 Post-platinum fail
			1b/2	mPDAC	NCT03193190 (Morpheus-	 Platform study
					Pancreatic)	1L/2L cohorts
			1b/2	G/GEJ	NCT03281369	Platform study
			10/2			 1L/2L cohorts
			-		(Morpheus)	
••			1b	TNBC	NCT04584112	+ atezolizumab and chemo
			1	MM/NHL	NCT04045028	 R/R setting
						 + daratumumab and rituximab
			1	Mixed	NCT02794571	Dose-escalation
						 + atezolizumab and chemo
IGIT	Vibostolimab (Merck US)	hlgG1	3	NSCLC	NCT04738487	 PD-L1+
		ingor	0	1 JOLO		
			0		NOT04105070	+ pembrolizumab and chemo
			2	NSCLC	NCT04165070	 Treatment-naïve
					(Keynote-01A)	+ pembrolizumab and chemo
			2	R/R heme	NCT05005442	pembrolizumab co-formulation
				malignancies		
			2	NSCLC	NCT04725188	 Progression post-chemo/PD-1
			<u> </u>	NOOLO	10107120100	
						 pembrolizumab co-formulation
						chemo

(Continued)

Target	Agent	Isotype	Phase	Indication	Study	Details
			2	Mixed	NCT05007106	 pembrolizumab co-formulation +/chemo
			2	NSCLC	NCT04165070 (KEYMAKER-U01)	+ pembrolizumab and chemo
			1/2	Melanoma	NCT04305041	Platform study
					(KEYMAKER-U02A)	PD-1 refractory
					, , , , , , , , , , , , , , , , , , ,	 + pembrolizumab
			1/2	Castration-resistant	NCT02861573	 pembrolizumab co-formulation
				prostate	(KEYNOTE-365)	
			1/2	Melanoma	NCT04305054	Platform study
					(KEYMAKER-U02B)	1L patients
			1 /0		NOTO 1000100	 + pembrolizumab
			1/2	Melanoma	NCT04303169	Platform study
					(KEYMAKER-U02C)	Neoadjuvant Tx
			1	Mixed	NCT02964013	+ pembrolizumabDose-escalation
	•••	•••	1	IVIIAEU	(KEYNOTE-01A)	 + pembrolizumab and chemo
IGIT	Ociperlimab	hlgG1	3	NSCLC	NCT04746924	 + tislelizumab
GIT	(Beigene)	niger	0	NOOLO	10104740024	
•			3	LA NSCLC	NCT04866017	 + tislelizumab vs durvalumab
			0		NOT04040607	 + CRT + tislelizumab and BAT1706
			2 2	HCC NSCLC	NCT04948697	 + tislelizumab and BAT1706 + tislelizumab and chemo
	•••	•••	2	NSCLC	NCT05014815 NCT04952597	 + tislelizumab and CRT
	•••	•••	2	Esophageal	NCT04932397 NCT04732494	 + tislelizumab + tislelizumab
•			2	BTC	NCT05019677	• 1L
	•••		2	510		 + tislelizumab and chemo
			2	Cervical	NCT04693234	 + tislelizumab
			2	BTC	NCT05023109	Unresectable
						 + tislelizumab and chemo
			1	Mixed	NCT04047862	 + tislelizumab
IGIT	Domvanalimab	hgG1,	3	NSCLC	NCT04736173	 PD-L1+ patients
	AB154 (Arcus)	FcγR-null*				 1L setting
						 + zimberelimab and etrumadenan
			2	NSCLC	NCT04791839	Prior checkpoint blockade
			0			 + zimberelimab and AB928 DD I 1 - restincts
•			2	NSCLC	NCT04262856 (ARC-7)	 PD-L1+ patients 1L setting
					(ANU-7)	 1L setting + zimberelimab and AB928
			2	R/R melanoma	NCT05130177	 + zimberelimab + zimberelimab
			1	Mixed	NCT03628677	Dose-escalation
	•••			Winted	10100020011	 + zimberelimab
IGIT	BMS-986207 (BMS)	hgG1,	2	NSCLC (stage IV)	NCT05005273	 + nivolumab and ipilimumab
		FcγR-null*				
			1/2	Mixed	NCT04570839	Dose-escalation
						 + nivolumab and COM701
			1/2	Mixed	NCT02913313	 Dose-escalation
						 + nivolumab
					1070 / 50005	 + nivolumab and ipilimumab
•			1/2	MM	NCT04150965	R/R setting
IGIT	IBI939		4	Advanced lung cancer	NOTO4670056	+ chemotherapyDose-escalation
GH	(Innovent)	hlgG1*	1	Advanced lung cancer	NCT04672356	 Dose-escalation + sintilimab
	. ,		1	NSCLC	NCT04672369	 Dose-escalation
•			1		110101012000	 bose-escalation + sintilimab
			1	Mixed	NCT04353830	Dose-escalation
						 + sintilimab
TIGIT	Etigilimab	hlgG1	2	Ovarian/	NCT05026606	 + nivolumab
	(Oncomed)	U I	-	fallopian		
			1/2	Mixed	NCT04761198	 + nivolumab
			Term.	Mixed	NCT03119428	Dose-escalation

(Continued)

TABLE 3 | Continued

Farget	Agent	Isotype	Phase	Indication	Study	Details
TIGIT	ASP8374 ^{&} (Astellas)	hlgG4	1b	Mixed	NCT03260322	Dose-escalation
						 + pembrolizumab
			1	Mixed	NCT03945253	 Japanese patients
			1	Glioma	NCT04826393	 + cemiplimab
IGIT	EOS884448 (GSK/iTeos)	hlgG1	1/2	Mixed	NCT04335253 (IO-002)	Dose-escalation
			1/2	Mixed	NCT05060432 (TIG-006)	+ pembrolizumab+ inupadenant
IGIT	SGN-TGT	hlgG1 FcyR-	1	Mixed	NCT04254107	Dose-escalation
	(Seattle Genetics)	enhanced		Mixed		 Solid tumors and lymphomas + sasanlimab
IGIT	COM902 (Compugen)	hlgG4*	1	Mixed	NCT04354246	Dose-escalation
IGIT	M6223 (Merck KGaA)	hlgG1*	1	Mixed	NCT04457778	Dose-escalation+ bintrafusp alfa
IGIT	AB308 (Arcus)	hlgG1	1	Mixed	NCT04772989	Dose-escalation+ zimberelimab
IGIT	BAT6021 (Bio-Thera)	hlgG1 FcγR- enhanced*	1	Mixed	NCT05073484	Dose-escalation+ BAT1308
IGIT	JS006 (Junshi Bio)	hlgG4	1	Mixed	NCT05061628	Dose-escalation+ toripalimab
IGIT	AK127 (Akesobio)	?	1	Mixed	NCT05021120	Dose-escalation+ AK104
'IGIT x 'D-1	AZD2936 (AstraZeneca)	?	1/2	NSCLC	NCT04995523 (ARTEMIDE-01)	Bi-specific based on COM902
'IGIT x	AGEN1777 (Agenus/BMS)	?	1	Mixed	NCT05025085	 Bi-specific Dose-escalation + PD-1
VRIG	COM701 (Compugen)	hlgG4	1/2	Mixed	NCT04570839	 + nivolumab and BMS-986207
			1	Mixed	NCT03667716	 Dose-escalation + nivolumab
			1	Mixed	NCT04354246	 Dose-escalation + COM902
VRIG	GSK4381562 (Compugen)	hlgG1	1	Mixed	NCT05277051	 + Dose-escalation + dostarlimab
D226	(Eli Lilly)	Unknown	Term.	Mixed	NCT04099277 (terminated)	 Dose-escalation + pembrolizumab
D96	GSK6097608 (GSK/ 23andMe)	hlgG1	1	Mixed	NCT04446351	Dose-escalation+ dostarlimab

*to be confirmed; ⁸discontinued; LA, locally advanced; ES-SCLC, extensive-stage small cell lung cancer; mUC, metastatic urothelial carcinoma; mPDAC, metastatic pancreatic ductal adenocarcinoma; G/GEJ, gastric or gastroesophageal junction adenocarcinoma; GEJC, gastroesophageal junction carcinoma, TNBC, triple-negative breast cancer; R/R, relapsed/ refractory; MM/NHL, multiple myeloma/non-Hodgkin lymphoma; BTC, biliary tract carcinoma; FTIH, first time in human study; CRT, chemoradiotherapy. The "?" symbol in Table 3 symbolizes "undetermined".

all that surprising given the nature of TIGIT antibodies (i.e., activated T cell-orientation and combination dependence), however as clinical studies progress, it will be important to establish a mechanistic understanding for the reduced activity of the combination in these patients.

The safety profile of tiragolumab combined with atezolizumab was similar to that of atezolizumab alone. Immune-related adverse events (IRAEs) were more frequent with the combination (69% versus 47%) but these were primarily manageable grade 1 and 2 immune-mediated AEs. There were also a similar number of grade 3+ AEs in the two groups (48% versus 44%) suggesting that this ICI combination will be better tolerated than ICI/chemo combinations (Keynote-189/NCT02578680, pembrolizumab + chemo [67.2%]) (161). With respect to AEs that demonstrated a >5% difference between arms, infusion-related reactions (IRR), pruritus, rash, were more frequent with the combination whereas dyspnea, productive

cough, and hypercalcemia were more frequent with atezolizumab monotherapy.

Tiragolumab/atezolizumab combinations have since expanded into a suite of late-stage clinical trials dubbed the SKYSCRAPER trials. These trails are spread across indications, with SKYSCRAPER-01, -02, -03 and -06 in lung cancers, SKYSCRAPER-04 in PD-L1⁺ cervical cancer, and SKYSCRAPER-07, -08 and -09 in the ENT (esophageal or head and neck) sphere. Other indications including urothelial carcinoma, pancreatic cancer, and esophageal cancer are being explored *via* MORPHEUS umbrella studies (**Table 3**).

Other TIGIT molecules, including vibostolimab (MK-7684, Merck US) and ociperlimab (BGB-A1217, Beigene) are close behind with similar studies in NSCLC and a wave of studies in alternative indications (**Table 3**). Merck is also progressing vibostolimab and pembrolizumab as a co-formulation through phase 2 studies. This effort underscores the marriage between PD-1 or PD-L1 and TIGIT intervention strategies, however, time will tell if concurrent administration is sufficient or if dosing flexibility is required to enable optimal responses. Other agents, including Arcus (domvanalimab) and BMS (BMS-986207) are entering phase 2 and 3 studies. As opposed to the number of Fcenabled TIGIT antibodies like tiragolumab and vibostolimab, agents like domvanalimab and BMS-986207 have attenuated Fc regions. Adding to this diversity, Fc-enhanced (SGN-TGT and BAT6021) as well as bi-specific (AZD2936 and AGEN1777) TIGIT antibodies have recently entered clinical development (**Table 3**). Given the non-clinical data suggesting the importance of Fc-Fc γ R co-engagement for anti-TIGIT function, the divergence in Fc biology between clinical molecules will be something to consider as studies read out.

Outside of solid tumor indications, TIGIT is also being evaluated in heme malignancies, such as MM and non-Hodgkin lymphoma (B-NHL) (**Table 3**). As discussed previously, TIGIT has been mechanistically linked to T cell exhaustion in MM and has shown promise as a therapeutic target in non-clinical models (128, 164). It will be interesting to see how well these findings translate to the clinical space, and if this is unique to TIGIT or if the therapeutic potential extends to other CD226 axis members.

PVRIG and CD96

As of Q2 2022, COM701 (IgG4) and GSK4381562 (IgG1) are the only two PVRIG molecules under clinical evaluation. Notably, COM701 demonstrated some early signs of activity, with a preliminary single-agent disease control rate (DCR) of 69% (165). Compugen also initiated a phase 1/2 study evaluating the triple combination of COM701, anti-PD-1 (nivolumab), and BMS-96820 (anti-TIGIT) in ovarian, endometrial, and select PVRL2^{high} cancers. Clinical studies for CD96 are even more nascent, with a single molecule (GSK6097608, IgG1) in dose escalation as a monotherapy and in combination with anti-PD-1 (**Table 3**).

CONSIDERATIONS FOR THE CD226 AXIS

Stronger Together? Targeting Multiple CD226 Axis Members

Given the nuances in expression profiles and potential for promiscuity within the CD226 axis, it is intriguing to consider the possibility for compensatory regulation between different axis members, particularly under therapeutic pressure (**Figure 1** and **Table 1**). These characteristics also highlight the potential of therapeutic collaboration in order to prevent inhibitory exigencies and/or increase coverage of various immune subsets and regulatory nodes within the axis (12). Several lines of nonclinical evidence directly or indirectly support co-inhibition of CD226 axis members. For example, antibody-mediated blockade of PVRIG has been shown to both induce rapid receptor internalization and increase TIGIT expression on antigenspecific CD8+ T cells (12). Similar dynamics have been observed with the ligands in the axis (83, 166). Moreover, genetic- or biologics-based co-blockade of TIGIT and CD96 has been shown to improve tumor control while co-blockade of TIGIT and PVRIG has also been shown to promote NK cell function (152, 157).

A PD-(L)1 Partnership

Although difficult to accurately assess due to the potential concomitant impact on TCR and CD28 activity, PD-1 signaling has been described to attenuate CD226 activity *via* SHP2-mediated dephosphorylation (20, 167) (**Figure 1**). This suggests that any CD226 signaling mediated by anti-TIGIT-, CD96- or PVRIG-based ligand redirection has the potential to be undercut by PD-(L)1 activity. Therefore, it is logical that CD226 axis therapeutics may need to be considered in the context of PD-(L)1 pathway blockade in order to reveal their full functional potential. Thus far, the available non-clinical data are consistent with this hypothesis. However, it will be interesting to see how the clinical space evolves, and whether or not PD-(L)1 blockade will become a prerequisite for the efficacy of all of the CD226 axis-based strategies.

Potential Utility of Fc-FcγR Co-Engagement

Given the relative breadth of non-clinical studies, it is not surprising that much of the data describing a potential role for Fc biology in the efficacy of antibodies targeting CD226 axis members has been restricted to TIGIT (15, 16, 114). An underlying point of contention has been the potential for antibody-mediated cellular depletion, and whether this is beneficial or detrimental, either due to safety concerns or impairment of efficacy (60, 130, 168-170). TIGIT is highly expressed on both peripheral and tumor infiltrating Treg cells. While selective depletion of Treg cells in the TME could relieve a suppressive barrier and promote antitumor responses, depletion of Treg cells in other tissues could impair peripheral tolerance and result in autoimmune manifestations, as seen in patients treated with mogamulizumab, an afucosylated antibody targeting CCR4expressingTreg cells (11, 58, 171, 172). One could postulate that TIGIT+ effector/cytotoxic T cells would also be a target for depletion, which may attenuate the desired therapeutic effect. Thus, if these concerns were overwhelming, pursuing an Fcattenuated TIGIT antibody would appear logical. However, given that TIGIT expression is elevated on terminally exhausted T cells, one could also posit that depleting these cells in the TME would permit the establishment of more functional T cell populations, leading to a net beneficial effect. Multiple factors, including differential cellular thresholds for target opsonization, antibody affinity, presence of effector cells mediating depletion, and FcyR polymorphisms need to be considered (14, 173, 174). Moreover, while safety concerns have been allayed with the clinical progression of Fc-competent antibodies, various non-clinical studies have demonstrated a benefit and, in some cases, a requirement for intact Fc biology to facilitate anti-TIGIT function (15, 60, 114, 169). Although the exact mechanism(s) responsible for improved anti-TIGIT activity remains to be determined, it has been suggested that Fc-FcyR co-engagement drives myeloid activation and/or T cell-APC immune synapse

quality (15, 131, 169). Clinical efficacy and safety data for recently developed Fc-enhanced TIGIT antibodies should also provide visibility on potential advantages or disadvantages associated with this format. Ultimately, the clinic will be the proving ground for the seemingly disparate Fc variants under evaluation; that is, to determine if pure antagonism, effector biology, or a mixture of mechanisms are required for optimal patient responses.

Limited Fc-based characterization has been conducted for rodent/human PVRIG or human CD96 antibodies (139). However, it is important to consider that the optimal therapeutic potential for each target must integrate a thorough understanding of Fc biology. Finally, given the breadth of TIGIT antibodies with distinct Fc regions currently under clinical evaluation (**Table 3**), broader mechanistic insights into anti-TIGIT biology and whether these characteristics extend to other members of the CD226 axis, may begin to surface in the coming years.

CLOSING REMARKS

In an effort to provide a framework for our evolving understanding of the CD226 axis in cancer, we discuss available non-clinical data and give an overview of the current clinical landscape. However, despite an understanding of the differential functional characteristics and expression profiles of each axis member, many questions remain regarding the mechanistic dynamics and contextual roles for

REFERENCES

- Wei SC, Duffy CR, Allison JP. Fundamental Mechanisms of Immune Checkpoint Blockade Therapy. *Cancer Discovery* (2018) 8:1069–86. doi: 10.1158/2159-8290.CD-18-0367
- Andrews LP, Yano H, Vignali DAA. Inhibitory Receptors and Ligands Beyond PD-1, PD-L1 and CTLA-4: Breakthroughs or Backups. Nat Immunol (2019) 20:1425–34. doi: 10.1038/s41590-019-0512-0
- Sharma P, Hu-Lieskovan S, Wargo JA, Ribas A. Primary, Adaptive, and Acquired Resistance to Cancer Immunotherapy. *Cell* (2017) 168:707–23. doi: 10.1016/j.cell.2017.01.017
- de Andrade LF, Smyth MJ, Martinet L. DNAM-1 Control of Natural Killer Cells Functions Through Nectin and Nectin-Like Proteins. *Immunol Cell Biol* (2014) 92:237–44. doi: 10.1038/icb.2013.95
- Wei SC, Levine JH, Cogdill AP, Zhao Y, Anang NAS, Andrews MC. Distinct Cellular Mechanisms Underlie Anti-CTLA-4and Anti-PD-1 Checkpoint Blockade. *Cell* (2017) 170:1120–33.e1117.doi:10.1016/j.cell.2017.07.024
- Sanchez-Correa B, Valhondo I, Hassouneh F, Lopez-Sejas N, Pera A, Bergua JM. DNAM-1 and the TIGIT/PVRIG/TACTILE Axis: Novel Immune Checkpoints for Natural Killer Cell-Based Cancer Immunotherapy. *Cancers (Basel)* (2019) 11(6):877. doi: 10.3390/cancers11060877
- Okumura G, Iguchi-Manaka A, Murata R, Yamashita-Kanemaru Y, Shibuya A, Shibuya K. Tumor-Derived Soluble CD155 Inhibits DNAM-1-Mediated Antitumor Activity of Natural Killer Cells. J Exp Med (2020) 217(4): e20191290. doi: 10.1084/jem.20191290
- Bottino C, Castriconi R, Pende D, Rivera P, Nanni M, Carnemolla B. Identification of PVR (CD155) and Nectin-2 (CD112) as Cell Surface Ligands for the Human DNAM-1 (CD226) Activating Molecule. J Exp Med (2003) 198:557–67. doi: 10.1084/jem.20030788
- Zhu Y, Paniccia A, Schulick AC, Chen W, Koenig MR, Byers JT. Identification of CD112R as a Novel Checkpoint for Human T Cells. *J Exp Med* (2016) 213:167–76. doi: 10.1084/jem.20150785

each receptor. Some examples include (i) the functional implications of the variegated receptor expression (particularly with memory or stem-like memory T cell populations and regulatory T cells), (ii) the cell-intrinsic impact of individual receptor signaling, (iii) the functional consequence of ligand/receptor dynamics in different tissues (e.g., TME versus peripheral blood), (iv) the *trans/cis* interactions critical for activity, and (v) the contribution of Fc γ R biology to the function of antibodies for each receptor. As clinical programs advance and interest expands, some of these questions may begin to be addressed. Overall, it will be intriguing to see how therapeutic strategies for each receptor evolves and what mechanistic learnings precipitate from an increased amount of activity around the targets.

AUTHOR CONTRIBUTIONS

MC and JW generated the original draft manuscript. JW, KH, SY, and JS reviewed, edited, and added content. All authors contributed to the article and approved the submitted version.

ACKNOWLEDGMENTS

We would like to thank Iris Roth, Julia Cuende, Rachael Easton, and Gregory Driessens for their thoughtful review.

- Stanietsky N, Simic H, Arapovic J, Toporik A, Levy O, Novik A. The Interaction of TIGIT With PVR and PVRL2 Inhibits Human NK Cell Cytotoxicity. *Proc Natl Acad Sci U S A* (2009) 106:17858–63. doi: 10.1073/ pnas.0903474106
- Lepletier A, Lutzky VP, Mittal D, Stannard K, Watkins TS, Ratnatunga CN. The Immune Checkpoint CD96 Defines a Distinct Lymphocyte Phenotype and is Highly Expressed on Tumor-Infiltrating T Cells. *Immunol Cell Biol* (2019) 97:152–64. doi: 10.1111/imcb.12205
- Whelan S, Ophir E, Kotturi MF, Levy O, Ganguly S, Leung L. PVRIG and PVRL2 Are Induced in Cancer and Inhibit CD8(+) T-Cell Function. *Cancer Immunol Res* (2019) 7:257–68. doi: 10.1158/2326-6066.CIR-18-0442
- Wing JB, Kitagawa Y, Locci M, Hume H, Tay C, Morita T. A Distinct Subpopulation of CD25(-) T-Follicular Regulatory Cells Localizes in the Germinal Centers. *Proc Natl Acad Sci USA* (2017) 114:E6400–9. doi: 10.1073/pnas.1705551114
- Arce Vargas F, Furness AJS, Litchfield K, Joshi K, Rosenthal R, Ghorani E. Fc Effector Function Contributes to the Activity of Human Anti-CTLA-4 Antibodies. *Cancer Cell* (2018) 33:649–663 e644. doi: 10.1016/ j.ccell.2018.02.010
- Waight JD, Chand D, Dietrich S, Gombos R, Horn T, Gonzalez AM. Selective FcgammaR Co-Engagement on APCs Modulates the Activity of Therapeutic Antibodies Targeting T Cell Antigens. *Cancer Cell* (2018) 33:1033–1047 e1035. doi: 10.1016/j.ccell.2018.05.005
- Preillon J, et al. Restoration of T-Cell Effector Function, Depletion of Tregs, and Direct Killing of Tumor Cells: The Multiple Mechanisms of Action of a-TIGIT Antagonist Antibodies. *Mol Cancer Ther* (2021) 20:121–31. doi: 10.1158/1535-7163.MCT-20-0464
- Burns GF, Triglia T, Werkmeister JA, Begley CG, Boyd AW. TLiSA1, a Human T Lineage-Specific Activation Antigen Involved in the Differentiation of Cytotoxic T Lymphocytes and Anomalous Killer Cells From Their Precursors. J Exp Med (1985) 161:1063–78. doi: 10.1084/ jem.161.5.1063

- Scott JL, Dunn SM, Jin B, Hillam AJ, Walton S, Berndt MC. Characterization of a Novel Membrane Glycoprotein Involved in Platelet Activation. J Biol Chem (1989) 264:13475–82. doi: 10.1016/S0021-9258(18)80021-7
- Chan CJ, Martinet L, Gilfillan S, Souza-Fonseca-Guimaraes F, Chow MT, Town L. The Receptors CD96 and CD226 Oppose Each Other in the Regulation of Natural Killer Cell Functions. *Nat Immunol* (2014) 15:431–8. doi: 10.1038/ni.2850
- Wang B, Zhang W, Jankovic V, Golubov J, Poon P, Oswald EM. Combination Cancer Immunotherapy Targeting PD-1 and GITR can Rescue CD8(+) T Cell Dysfunction and Maintain Memory Phenotype. *Sci Immunol* (2018) 3(29):eaat7061. doi: 10.1126/sciimmunol.aat7061
- Tahara-Hanaoka S, Shibuya K, Onoda Y, Zhang H, Yamazaki S, Miyamoto A. Functional Characterization of DNAM-1 (CD226) Interaction With its Ligands PVR (CD155) and Nectin-2 (PRR-2/Cd112). *Int Immunol* (2004) 16:533–8. doi: 10.1093/intimm/dxh059
- Lozano E, Dominguez-Villar M, Kuchroo V, Hafler DA. The TIGIT/CD226 Axis Regulates Human T Cell Function. J Immunol (2012) 188:3869–75. doi: 10.4049/jimmunol.1103627
- Yu X, Harden K, Gonzalez LC, Francesco M, Chiang E, Irving B. The Surface Protein TIGIT Suppresses T Cell Activation by Promoting the Generation of Mature Immunoregulatory Dendritic Cells. *Nat Immunol* (2009) 10:48–57. doi: 10.1038/ni.1674
- Liu J, Qian X, Chen Z, Xu X, Gao F, Zhang S. Crystal Structure of Cell Adhesion Molecule Nectin-2/CD112 and its Binding to Immune Receptor DNAM-1/Cd226. J Immunol (2012) 188:5511–20. doi: 10.4049/ jimmunol.1200324
- Wang H, Qi J, Zhang S, Li Y, Tan S, Gao GF. Binding Mode of the Side-by-Side Two-IgV Molecule CD226/DNAM-1 to its Ligand CD155/Necl-5. Proc Natl Acad Sci USA (2019) 116:988–96. doi: 10.1073/pnas.1815716116
- Deuss FA, Watson GM, Goodall KJ, Leece I., Chatterjee S, Fu Z. Structural Basis for the Recognition of Nectin-Like Protein-5 by the Human-Activating Immune Receptor, DNAM-1. J Biol Chem (2019) 294:12534–46. doi: 10.1074/jbc.RA119.009261
- Liu G, Hu Y, Jin S, Jiang Q. Genetic Variant Rs763361 Regulates Multiple Sclerosis CD226 Gene Expression. *Proc Natl Acad Sci USA* (2017) 114:E906– 7. doi: 10.1073/pnas.1618520114
- Maiti AK, Kim-Howard X, Viswanathan P, Guillen L, Qian X, Rojas-Villarraga A. Non-Synonymous Variant (Gly307Ser) in CD226 is Associated With Susceptibility to Multiple Autoimmune Diseases. *Rheumatol (Oxford)* (2010) 49:1239–44. doi: 10.1093/rheumatology/kep470
- Hafler JP, Maier LM, Cooper JD, Plagnol V, Hinks A, Simmonds MJ. CD226 Gly307Ser Association With Multiple Autoimmune Diseases. *Genes Immun* (2009) 10:5–10. doi: 10.1038/gene.2008.82
- Zhang Z, Wu N, Lu Y, Davidson D, Colonna M, Veillette A. DNAM-1 Controls NK Cell Activation via an ITT-like motif. J Exp Med (2015) 212:2165–82. doi: 10.1084/jem.20150792
- Shibuya A, Lanier LL, Phillips JH. Protein Kinase C Is Involved in the Regulation of Both Signaling and Adhesion Mediated by DNAX Accessory Molecule-1 Receptor. J Immunol (1998) 161:1671–6.
- Shibuya K, Lanier LL, Phillips JH, Ochs HD, Shimizu K, Nakayama E. Physical and Functional Association of LFA-1 With DNAM-1 Adhesion Molecule. *Immunity* (1999) 11:615–23. doi: 10.1016/s1074-7613(00)80136-3
- 33. Jin HS, Ko M, Choi DS, Kim JH, Lee DH, Kang SH. CD226(hi)CD8(+) T Cells Are a Prerequisite for Anti-TIGIT Immunotherapy. *Cancer Immunol Res* (2020) 8:912–25. doi: 10.1158/2326-6066.CIR-19-0877
- 34. Liu S, Zhang H, Li M, Hu D, Li C, Ge B. Recruitment of Grb2 and SHIP1 by the ITT-Like Motif of TIGIT Suppresses Granule Polarization and Cytotoxicity of NK Cells. *Cell Death Differ* (2013) 20:456–64. doi: 10.1038/ cdd.2012.141
- 35. Li M, Xia P, Du Y, Liu S, Huang G, Chen J. T-Cell Immunoglobulin and ITIM Domain (TIGIT) Receptor/Poliovirus Receptor (PVR) Ligand Engagement Suppresses Interferon-Gamma Production of Natural Killer Cells. via beta-arrestin 2-mediated negative Signaling J Biol Chem (2014) 289:17647–57. doi: 10.1074/jbc.M114.572420
- Banta KL, Xu X, Chitre AS, Au-Yeung A, Takahashi C, O'Gorman WE. Mechanistic Convergence of the TIGIT and PD-1 Inhibitory Pathways Necessitates Co-Blockade to Optimize Anti-Tumor CD8(+) T Cell Responses. *Immunity* (2022) 55:512–526 e519. doi: 10.1016/j.immuni.2022.02.005

- 37. Braun M, Aguilera AR, Sundarrajan A, Corvino D, Stannard K, Krumeich S. CD155 on Tumor Cells Drives Resistance to Immunotherapy by Inducing the Degradation of the Activating Receptor CD226 in CD8(+) T Cells. *Immunity* (2020) 53:805–823 e815. doi: 10.1016/j.immuni. 2020.09.010
- Vo AV, Takenaka E, Shibuya A, Shibuya K. Expression of DNAM-1 (CD226) on Inflammatory Monocytes. *Mol Immunol* (2016) 69:70–6. doi: 10.1016/j.molimm.2015.11.009
- Sun H, Huang Q, Huang M, Wen H, Lin R, Zheng M. Human CD96 Correlates to Natural Killer Cell Exhaustion and Predicts the Prognosis of Human Hepatocellular Carcinoma. *Hepatology* (2019) 70:168–83. doi: 10.1002/hep.30347
- Cifaldi L, Doria M, Cotugno N, Zicari S, Cancrini C, Palma P. DNAM-1 Activating Receptor and Its Ligands: How Do Viruses Affect the NK Cell-Mediated Immune Surveillance During the Various Phases of Infection? Int J Mol Sci (2019) 20(15):3715. doi: 10.3390/ijms20153715
- Chauvin JM, Ka M, Pagliano O, Menna C, Ding Q, DeBlasio R. IL15 Stimulation With TIGIT Blockade Reverses CD155-Mediated NK-Cell Dysfunction in Melanoma. *Clin Cancer Res* (2020) 26:5520–33. doi: 10.1158/1078-0432.CCR-20-0575
- Platonova S, Cherfils-Vicini J, Damotte D, Crozet L, Vieillard V, Validire P. Profound Coordinated Alterations of Intratumoral NK Cell Phenotype and Function in Lung Carcinoma. *Cancer Res* (2011) 71:5412–22. doi: 10.1158/ 0008-5472.CAN-10-4179
- Gillard-Bocquet M, Caer C, Cagnard N, Crozet L, Perez M, Fridman WH. Lung Tumor Microenvironment Induces Specific Gene Expression Signature in Intratumoral NK Cells. *Front Immunol* (2013) 4:19. doi: 10.3389/ fimmu.2013.00019
- 44. Niu C, Jin H, Li M, Zhu S, Zhou L, Jin F. Low-Dose Bortezomib Increases the Expression of NKG2D and DNAM-1 Ligands and Enhances Induced NK and Gammadelta T Cell-Mediated Lysis in Multiple Myeloma. *Oncotarget* (2017) 8:5954–64. doi: 10.18632/oncotarget.13979
- Carlsten M, Norell H, Bryceson YT, Poschke I, Schedvins K, Ljunggren HG. Primary Human Tumor Cells Expressing CD155 Impair Tumor Targeting by Down-Regulating DNAM-1 on NK Cells. *J Immunol* (2009) 183:4921–30. doi: 10.4049/jimmunol.0901226
- Sanchez-Correa B, Gayoso I., Bergua JM, Casado JG, Morgado S, Solana R, et al. Decreased Expression of DNAM-1 on NK Cells From Acute Myeloid Leukemia Patients. *Immunol Cell Biol* (2012) 90:109–15. doi: 10.1038/ icb.2011.15
- 47. Xu Z, Zhang T, Zhuang R, Zhang Y, Jia W, Song C. Increased Levels of Soluble CD226 in Sera Accompanied by Decreased Membrane CD226 Expression on Peripheral Blood Mononuclear Cells From Cancer Patients. *BMC Immunol* (2009) 10:34. doi: 10.1186/1471-2172-10-34
- Huang Z, Qi G, Miller JS, Zheng SG. CD226: An Emerging Role in Immunologic Diseases. Front Cell Dev Biol (2020) 8:564. doi: 10.3389/ fcell.2020.00564
- Pauken KE, Wherry EJ. TIGIT and CD226: Tipping the Balance Between Costimulatory and Coinhibitory Molecules to Augment the Cancer Immunotherapy Toolkit. *Cancer Cell* (2014) 26:785–7. doi: 10.1016/ j.ccell.2014.11.016
- Pende D, Castriconi R, Romagnani P, Spaggiari GM, Marcenaro S, Dondero A. Expression of the DNAM-1 Ligands, Nectin-2 (CD112) and Poliovirus Receptor (CD155), On Dendritic Cells: Relevance for Natural Killer-Dendritic Cell Interaction. *Blood* (2006) 107:2030–6. doi: 10.1182/blood-2005-07-2696
- Walwyn-Brown K, Guldevall K, Saeed M, Pende D, Onfelt B, MacDonald AS, et al. Human NK Cells Lyse Th2-Polarizing Dendritic Cells via NKp30 and DNAM-1. J Immunol (2018) 201:2028–41. doi: 10.4049/ jimmunol.1800475
- 52. Seth S, Georgoudaki AM, Chambers BJ, Qiu Q., Kremmer E, Maier MK. Heterogeneous Expression of the Adhesion Receptor CD226 on Murine NK and T Cells and its Function in NK-Mediated Killing of Immature Dendritic Cells. J Leukoc Biol (2009) 86:91–101. doi: 10.1189/jlb.1208745
- Sun JC, Beilke JN, Lanier LL. Adaptive Immune Features of Natural Killer Cells. Nature (2009) 457:557–61. doi: 10.1038/nature07665
- 54. Gilfillan S, Chan CJ, Cella M, Haynes NM, Rapaport AS, Boles KS. DNAM-1 Promotes Activation of Cytotoxic Lymphocytes by Nonprofessional

Antigen-Presenting Cells and Tumors. J Exp Med (2008) 205:2965-73. doi: 10.1084/jem.20081752

- Nabekura T, Kanaya M, Shibuya A, Fu G, Gascoigne NR, Lanier LL. Costimulatory Molecule DNAM-1 Is Essential for Optimal Differentiation of Memory Natural Killer Cells During Mouse Cytomegalovirus Infection. *Immunity* (2014) 40:225–34. doi: 10.1016/j.immuni.2013.12.011
- 56. Du X, de Almeida P, Manieri N, de AlmeidaNagata D, Wu TD, Harden Bowles K. CD226 Regulates Natural Killer Cell Antitumor Responses via phosphorylation-mediated inactivation of transcription factor FOXO1. Proc Natl Acad Sci USA (2018) 115:E11731–40. doi: 10.1073/pnas.1814052115
- Iguchi-Manaka A, Kai H., Yamashita Y., Shibata K., Tahara-Hanaoka S., Honda S., Accelerated Tumor Growth in Mice Deficient in DNAM-1 Receptor. J Exp Med (2008) 205:2959–64. doi: 10.1084/jem.20081611
- Kurtulus S, Sakuishi K, Ngiow SF, Joller N, Tan DJ, Teng MW. TIGIT Predominantly Regulates the Immune Response via regulatory T cells. J Clin Invest (2015) 125:4053–62. doi: 10.1172/JCI81187
- 59. Weulersse M, Asrir A, Pichler AC, Lemaitre L, Braun M, Carrie N. Eomes-Dependent Loss of the Co-Activating Receptor CD226 Restrains CD8(+) T Cell Anti-Tumor Functions and Limits the Efficacy of Cancer Immunotherapy. *Immunity* (2020) 53:824–39.e810. doi: 10.1016/ j.immuni.2020.09.006
- 60. Johnston RJ, Comps-Agrar L, Hackney J, Yu X, Huseni M, Yang Y. The Immunoreceptor TIGIT Regulates Antitumor and Antiviral CD8(+) T Cell Effector Function. *Cancer Cell* (2014) 26:923–37. doi: 10.1016/ j.ccell.2014.10.018
- Kojima H, Kanada H, Shimizu S, Kasama E, Shibuya K, Nakauchi H. CD226 Mediates Platelet and Megakaryocytic Cell Adhesion to Vascular Endothelial Cells. J Biol Chem (2003) 278:36748–53. doi: 10.1074/jbc.M300702200
- Mendelsohn CL, Wimmer E, Racaniello VR. Cellular Receptor for Poliovirus: Molecular Cloning, Nucleotide Sequence, and Expression of a New Member of the Immunoglobulin Superfamily. *Cell* (1989) 56:855–65. doi: 10.1016/0092-8674(89)90690-9
- 63. Eberle F, Dubreuil P, Mattei MG, Devilard E, Lopez M. The Human PRR2 Gene, Related to the Human Poliovirus Receptor Gene (PVR), is the True Homolog of the Murine MPH Gene. *Gene* (1995) 159:267–72. doi: 10.1016/ 0378-1119(95)00180-e
- 64. Lopez M, Aoubala M, Jordier F, Isnardon D, Gomez S, Dubreuil P. The Human Poliovirus Receptor Related 2 Protein is a New Hematopoietic/ Endothelial Homophilic Adhesion Molecule. *Blood* (1998) 92:4602–11. doi: 10.1182/blood.V92.12.4602
- Baury B, Masson D, McDermott BM Jr., Jarry A., Blottiere HM, Blanchardie P. Identification of Secreted CD155 Isoforms. *Biochem Biophys Res Commun* (2003) 309:175–82. doi: 10.1016/s0006-291x(03)01560-2
- 66. Iguchi-Manaka A, Okumura G, Kojima H, Cho Y, Hirochika R, Bando H. Increased Soluble CD155 in the Serum of Cancer Patients. *PloS One* (2016) 11:e0152982. doi: 10.1371/journal.pone.0152982
- Ravens I, Seth S, Forster R, Bernhardt G. Characterization and Identification of Tage4 as the Murine Orthologue of Human Poliovirus Receptor/CD155. *Biochem Biophys Res Commun* (2003) 312:1364–71. doi: 10.1016/j.bbrc.2003.11.067
- 68. Stengel KF, Harden-Bowles K, Yu X, Rouge L, Yin J, Comps-Agrar L. Structure of TIGIT Immunoreceptor Bound to Poliovirus Receptor Reveals a Cell-Cell Adhesion and Signaling Mechanism That Requires Cis-Trans Receptor Clustering. *Proc Natl Acad Sci USA* (2012) 109:5399–404. doi: 10.1073/pnas.1120606109
- Deuss FA, Gully BS, Rossjohn J, Berry R. Recognition of Nectin-2 by the Natural Killer Cell Receptor T Cell Immunoglobulin and ITIM Domain (TIGIT). J Biol Chem (2017) 292:11413–22. doi: 10.1074/jbc.M117. 786483
- Deuss FA, Watson GM, Fu Z, Rossjohn J, Berry R. Structural Basis for CD96 Immune Receptor Recognition of Nectin-Like Protein-5, Cd155. *Structure* (2019) 27:219–28.e213. doi: 10.1016/j.str.2018.10.023
- Ikeda W, Kakunaga S, Itoh S, Shingai T, Takekuni K, Satoh K. Tage4/Nectin-Like Molecule-5 Heterophilically Trans-Interacts With Cell Adhesion Molecule Nectin-3 and Enhances Cell Migration. J Biol Chem (2003) 278:28167–72. doi: 10.1074/jbc.M303586200
- Devilard E, Xerri L, Dubreuil P, Lopez M, Reymond N. Nectin-3 (CD113) Interacts With Nectin-2 (CD112) to Promote Lymphocyte Transendothelial Migration. *PloS One* (2013) 8:e77424. doi: 10.1371/journal.pone.0077424

- Harrison OJ, Vendome J, Brasch J, Jin X, Hong S, Katsamba PS. Nectin Ectodomain Structures Reveal a Canonical Adhesive Interface. *Nat Struct Mol Biol* (2012) 19:906–15. doi: 10.1038/nsmb.2366
- 74. Samanta D, Ramagopal UA, Rubinstein R, Vigdorovich V, Nathenson SG, Almo SC. Structure of Nectin-2 Reveals Determinants of Homophilic and Heterophilic Interactions That Control Cell-Cell Adhesion. *Proc Natl Acad Sci U S A* (2012) 109:14836–40. doi: 10.1073/pnas.1212912109
- Holmes VM, Maluquer deMotes C, Richards PT, Roldan J, Bhargava AK, Orange JS. Interaction Between Nectin-1 and the Human Natural Killer Cell Receptor CD96. *PloS One* (2019) 14:e0212443. doi: 10.1371/ journal.pone.0212443
- 76. Stamm H, Klingler F, Grossjohann EM, Muschhammer J, Vettorazzi E, Heuser M. Immune Checkpoints PVR and PVRL2 are Prognostic Markers in AML and Their Blockade Represents a New Therapeutic Option. Oncogene (2018) 37:5269–80. doi: 10.1038/s41388-018-0288-y
- 77. Huang DW, Huang M, Lin XS, Huang Q. CD155 Expression and its Correlation With Clinicopathologic Characteristics, Angiogenesis, and Prognosis in Human Cholangiocarcinoma. Onco Targets Ther (2017) 10:3817–25. doi: 10.2147/OTT.S141476
- Nakai R, Maniwa Y, Tanaka Y, Nishio W, Yoshimura M, Okita Y. Overexpression of Necl-5 Correlates With Unfavorable Prognosis in Patients With Lung Adenocarcinoma. *Cancer Sci* (2010) 101:1326–30. doi: 10.1111/j.1349-7006.2010.01530.x
- Nishiwada S, Sho M, Yasuda S, Shimada K, Yamato I, Akahori T. Clinical Significance of CD155 Expression in Human Pancreatic Cancer. *Anticancer Res* (2015) 35:2287–97.
- Bevelacqua V, Bevelacqua Y, Candido S, Skarmoutsou E, Amoroso A, Guarneri C. Nectin Like-5 Overexpression Correlates With the Malignant Phenotype in Cutaneous Melanoma. *Oncotarget* (2012) 3:882–92. doi: 10.18632/oncotarget.594
- Sloan KE, Eustace BK, Stewart JK, Zehetmeier C, Torella C, Simeone M. CD155/PVR Plays a Key Role in Cell Motility During Tumor Cell Invasion and Migration. *BMC Cancer* (2004) 4:73. doi: 10.1186/1471-2407-4-73
- Masson D, Jarry A, Baury B, Blanchardie P, Laboisse C, Lustenberger P, et al. Overexpression of the CD155 Gene in Human Colorectal Carcinoma. *Gut* (2001) 49:236–40. doi: 10.1136/gut.49.2.236
- Nagumo Y, Iguchi-Manaka A, Yamashita-Kanemaru Y, Abe F, Bernhardt G, Shibuya A, et al. Increased CD112 Expression in Methylcholanthrene-Induced Tumors in CD155-Deficient Mice. *PloS One* (2014) 9:e112415. doi: 10.1371/journal.pone.0112415
- Qu P, Huang X, Zhou X, Lu Z, Liu F, Shi Z. Loss of CD155 Expression Predicts Poor Prognosis in Hepatocellular Carcinoma. *Histopathology* (2015) 66:706–14. doi: 10.1111/his.12584
- Huang X, Qu P, Chen Y, Zhou X, Wu Y, Liu F. Low Expression of CD112 is Associated With Poor Overall Survival in Patients With Hepatocellular Carcinoma. *Hum Pathol* (2014) 45:1944-50. doi: 10.1016/ j.humpath.2014.06.001
- Lepletier A, Madore J, O'Donnell JS, Johnston RL, Li XY, McDonald E. Tumor CD155 Expression Is Associated With Resistance to Anti-PD1 Immunotherapy in Metastatic Melanoma. *Clin Cancer Res* (2020) 26:3671–81. doi: 10.1158/1078-0432.CCR-19-3925
- Ardolino M, Zingoni A, Cerboni C, Cecere F, Soriani A, Iannitto ML, et al. DNAM-1 Ligand Expression on Ag-Stimulated T Lymphocytes Is Mediated by ROS-Dependent Activation of DNA-Damage Response: Relevance for NK-T Cell Interaction. *Blood* (2011) 117:4778–86. doi: 10.1182/blood-2010-08-300954
- 88. Soriani A, Zingoni A, Cerboni C, Iannitto ML, Ricciardi MR, Di Gialleonardo V. ATM-ATR-Dependent Up-Regulation of DNAM-1 and NKG2D Ligands on Multiple Myeloma Cells by Therapeutic Agents Results in Enhanced NK-Cell Susceptibility and Is Associated With a Senescent Phenotype. *Blood* (2009) 113:3503–11. doi: 10.1182/blood-2008-08-173914
- Gao J, Zheng Q, Shao Y, Wang W, Zhao C. CD155 Downregulation Synergizes With Adriamycin to Induce Breast Cancer Cell Apoptosis. *Apoptosis* (2018) 23:512–20. doi: 10.1007/s10495-018-1473-8
- 90. Fionda C, Abruzzese MP, Zingoni A, Soriani A, Ricci B, Molfetta R. Nitric Oxide Donors Increase PVR/CD155 DNAM-1 Ligand Expression in Multiple Myeloma Cells: Role of DNA Damage Response Activation. *BMC Cancer* (2015) 15:17. doi: 10.1186/s12885-015-1023-5

- Cerboni C, Fionda C, Soriani A, Zingoni A, Doria M, Cippitelli M, et al. The DNA Damage Response: A Common Pathway in the Regulation of NKG2D and DNAM-1 Ligand Expression in Normal, Infected, and Cancer Cells. *Front Immunol* (2014) 4:508. doi: 10.3389/fimmu.2013.00508
- Tang ML, Khan MK, Croxford JL, Tan KW, Angeli V, Gasser S. The DNA Damage Response Induces Antigen Presenting Cell-Like Functions in Fibroblasts. *Eur J Immunol* (2014) 44:1108–18. doi: 10.1002/eji.201343781
- Boles KS, Vermi W, Facchetti F, Fuchs A, Wilson TJ, Diacovo TG. A Novel Molecular Interaction for the Adhesion of Follicular CD4 T Cells to Follicular DC. Eur J Immunol (2009) 39:695–703. doi: 10.1002/eji.200839116
- Heesters BA, Myers RC, Carroll MC. Follicular Dendritic Cells: Dynamic Antigen Libraries. Nat Rev Immunol (2014) 14:495–504. doi: 10.1038/nri3689
- Helmink BA, Reddy SM, Gao J, Zhang S, Basar R, Thakur R. B Cells and Tertiary Lymphoid Structures Promote Immunotherapy Response. *Nature* (2020) 577:549–55. doi: 10.1038/s41586-019-1922-8
- 96. Petitprez F, de Reynies A, Keung EZ, Chen TW, Sun CM, Calderaro J. B Cells are Associated With Survival and Immunotherapy Response in Sarcoma. *Nature* (2020) 577:556–60. doi: 10.1038/s41586-019-1906-8
- Cabrita R, Lauss M, Sanna A, Donia M, Skaarup Larsen M, Mitra S. Author Correction: Tertiary Lymphoid Structures Improve Immunotherapy and Survival in Melanoma. *Nature* (2020) 580:E1. doi: 10.1038/s41586-020-2155-6
- Maier MK, Seth S, Czeloth N, Qiu Q, Ravens I, Kremmer E. The Adhesion Receptor CD155 Determines the Magnitude of Humoral Immune Responses Against Orally Ingested Antigens. *Eur J Immunol* (2007) 37:2214–25. doi: 10.1002/eji.200737072
- 99. Davis ZB, Sowrirajan B, Cogswell A, Ward JP, Planelles V, Barker E. CD155 on HIV-Infected Cells Is Not Modulated by HIV-1 Vpu and Nef But Synergizes With NKG2D Ligands to Trigger NK Cell Lysis of Autologous Primary HIV-Infected Cells. *AIDS Res Hum Retroviruses* (2017) 33:93–100. doi: 10.1089/AID.2015.0375
- 100. Qiu Q, Ravens I, Seth S, Rathinasamy A, Maier MK, Davalos-Misslitz A. CD155 is Involved in Negative Selection and is Required to Retain Terminally Maturing CD8 T Cells in Thymus. *J Immunol* (2010) 184:1681–9. doi: 10.4049/jimmunol.0900062
- Marlin SD, Staunton DE, Springer TA, Stratowa C., Sommergruber W, Merluzzi VJ. A Soluble Form of Intercellular Adhesion Molecule-1 Inhibits Rhinovirus Infection. *Nature* (1990) 344:70–2. doi: 10.1038/344070a0
- 102. Iguchi-Manaka A, Okumura G, Ichioka E, Kiyomatsu H, Ikeda T, Bando H. High Expression of Soluble CD155 in Estrogen Receptor-Negative Breast Cancer. Breast Cancer (2020) 27:92–9. doi: 10.1007/s12282-019-00999-8
- 103. Karabulut M, Gunaldi M, Alis H, Afsar CU, Karabulut S, Serilmez M. Serum Nectin-2 Levels are Diagnostic and Prognostic in Patients With Colorectal Carcinoma. *Clin Transl Oncol* (2016) 18:160–71. doi: 10.1007/s12094-015-1348-1
- 104. Shibuya A, Campbell D, Hannum C, Yssel H, Franz-Bacon K, McClanahan T.. DNAM-1, A Novel Adhesion Molecule Involved in the Cytolytic Function of T Lymphocytes. *Immunity* (1996) 4:573–81. doi: 10.1016/ s1074-7613(00)70060-4
- 105. Fuchs A, Cella M, Giurisato E, Shaw AS, Colonna M. Cutting Edge: CD96 (Tactile) Promotes NK Cell-Target Cell Adhesion by Interacting With the Poliovirus Receptor (CD155). J Immunol (2004) 172:3994–8. doi: 10.4049/ jimmunol.172.7.3994
- 106. Samanta D, Guo H, Rubinstein R, Ramagopal UA, Almo SC. Structural, Mutational and Biophysical Studies Reveal a Canonical Mode of Molecular Recognition Between Immune Receptor TIGIT and Nectin-2. *Mol Immunol* (2017) 81:151–9. doi: 10.1016/j.molimm.2016.12.003
- 107. Reches A, Ophir Y, Stein N, Kol I., Isaacson B, Charpak Amikam Y. Nectin4 Is a Novel TIGIT Ligand Which Combines Checkpoint Inhibition and Tumor Specificity. J Immunother Cancer (2020) 8(29):e000266. doi: 10.1136/jitc-2019-000266
- 108. Stanietsky N, Rovis TL, Glasner A, Seidel E, Tsukerman P, Yamin R. Mouse TIGIT Inhibits NK-Cell Cytotoxicity Upon Interaction With PVR. Eur J Immunol (2013) 43:2138–50. doi: 10.1002/eji.201243072
- 109. Chen X, Lu PH, Liu L, Fang ZM, Duan W, Liu ZL. TIGIT Negatively Regulates Inflammation by Altering Macrophage Phenotype. *Immunobiology* (2016) 221:48–55. doi: 10.1016/j.imbio.2015.08.003

- 110. Schorer M, Rakebrandt N, Lambert K, Hunziker A, Pallmer K, Oxenius A. TIGIT Limits Immune Pathology During Viral Infections. *Nat Commun* (2020) 11:1288. doi: 10.1038/s41467-020-15025-1
- 111. Joller N, Hafler JP, Brynedal B, Kassam N, Spoerl S, Levin SD. Cutting Edge: TIGIT has T Cell-Intrinsic Inhibitory Functions. J Immunol (2011) 186:1338–42. doi: 10.4049/jimmunol.1003081
- 112. Lucca LE, Axisa PP, Singer ER, Nolan NM, Dominguez-Villar M, Hafler DA. TIGIT Signaling Restores Suppressor Function of Th1 Tregs. JCI Insight (2019) 4(3):e124427. doi: 10.1172/jci.insight.124427
- 113. Fuhrman CA, Yeh WI, Seay HR, Saikumar Lakshmi P, Chopra G, Zhang L. Divergent Phenotypes of Human Regulatory T Cells Expressing the Receptors TIGIT and CD226. J Immunol (2015) 195:145–55. doi: 10.4049/ jimmunol.1402381
- 114. Mittal D, Lepletier A, Madore J, Aguilera AR, Stannard K, Blake SJ. CD96 Is an Immune Checkpoint That Regulates CD8(+) T-Cell Antitumor Function. *Cancer Immunol Res* (2019) 7:559–71. doi: 10.1158/2326-6066.CIR-18-0637
- 115. Joller N, Lozano E, Burkett PR, Patel B, Xiao S, Zhu C. Treg Cells Expressing the Coinhibitory Molecule TIGIT Selectively Inhibit Proinflammatory Th1 and Th17 Cell Responses. *Immunity* (2014) 40:569–81. doi: 10.1016/ j.immuni.2014.02.012
- 116. Ge Z, Zhou G, Campos Carrascosa L, Gausvik E, Boor PPC, Noordam L. TIGIT and PD1 Co-Blockade Restores Ex Vivo Functions of Human Tumor-Infiltrating CD8(+) T Cells in Hepatocellular Carcinoma. *Cell Mol Gastroenterol Hepatol* (2021) 12:443–64. doi: 10.1016/j.jcmgh.2021.03.003
- 117. Chew GM, Fujita T, Webb GM, Burwitz BJ, Wu HL, Reed JS. TIGIT Marks Exhausted T Cells, Correlates With Disease Progression, and Serves as a Target for Immune Restoration in HIV and SIV Infection. *PloS Pathog* (2016) 12:e1005349. doi: 10.1371/journal.ppat.1005349
- 118. Bengsch B, Ohtani T, Khan O, Setty M, Manne S, O'Brien S. Epigenomic-Guided Mass Cytometry Profiling Reveals Disease-Specific Features of Exhausted CD8 T Cells. *Immunity* (2018) 48:1029–1045 e1025. doi: 10.1016/j.immuni.2018.04.026
- 119. Beltra JC, Manne S, Abdel-Hakeem MS, Kurachi M, Giles JR, Chen Z. Developmental Relationships of Four Exhausted CD8(+) T Cell Subsets Reveals Underlying Transcriptional and Epigenetic Landscape Control Mechanisms. *Immunity* (2020) 52:825–41.e828. doi: 10.1016/ j.immuni.2020.04.014
- 120. McGoverne I, Dunn J, Batham J, Tu WJ, Chrisp J, Rao S. Epitherapy and Immune Checkpoint Blockade: Using Epigenetic Reinvigoration of Exhausted and Dysfunctional T Cells to Reimburse Immunotherapy Response. BMC Immunol (2020) 21:22. doi: 10.1186/s12865-020-00353-0
- 121. Li X, Wang R, Fan P, Yao X, Qin L, Peng Y. A Comprehensive Analysis of Key Immune Checkpoint Receptors on Tumor-Infiltrating T Cells From Multiple Types of Cancer. *Front Oncol* (2019) 9:1066. doi: 10.3389/ fonc.2019.01066
- 122. Kurtulus S, Madi A, Escobar G, Klapholz M, Nyman J, Christian E. Checkpoint Blockade Immunotherapy Induces Dynamic Changes in PD-1 (-)CD8(+) Tumor-Infiltrating T Cells. *Immunity* (2019) 50:181–94.e186. doi: 10.1016/j.immuni.2018.11.014
- 123. Jansen CS, Prokhnevska N, Master VA, Sanda MG, Carlisle JW, Bilen MA. An Intra-Tumoral Niche Maintains and Differentiates Stem-Like CD8 T Cells. *Nature* (2019) 576:465–70. doi: 10.1038/s41586-019-1836-5
- 124. Galletti G, De Simone G, Mazza EMC, Puccio S, Mezzanotte C, Bi TM. Two Subsets of Stem-Like CD8(+) Memory T Cell Progenitors With Distinct Fate Commitments in Humans. *Nat Immunol* (2020) 21(12):1552–62. doi: 10.1038/s41590-020-0791-5
- 125. Levin SD, Taft DW, Brandt CS, Bucher C, Howard ED, Chadwick EM. Vstm3 is a Member of the CD28 Family and an Important Modulator of T-Cell Function. *Eur J Immunol* (2011) 41:902–15. doi: 10.1002/eji.201041136
- 126. Zhang Q, Bi J, Zheng X, Chen Y, Wang H, Wu W. Blockade of the Checkpoint Receptor TIGIT Prevents NK Cell Exhaustion and Elicits Potent Anti-Tumor Immunity. Nat Immunol (2018) 19:723-32. doi: 10.1038/s41590-018-0132-0
- 127. Blake SJ, Stannard K, Liu J, Allen S, Yong MC, Mittal D. Suppression of Metastases Using a New Lymphocyte Checkpoint Target for Cancer Immunotherapy. *Cancer Discovery* (2016) 6:446–59. doi: 10.1158/2159-8290.CD-15-0944

- 128. Guillerey C, Harjunpaa H, Carrie N, Kassem S, Teo T, Miles K. TIGIT Immune Checkpoint Blockade Restores CD8(+) T-Cell Immunity Against Multiple Myeloma. *Blood* (2018) 132:1689–94. doi: 10.1182/blood-2018-01-825265
- 129. Hung AL, Maxwell R, Theodros D, Belcaid Z, Mathios D, Luksik AS. TIGIT and PD-1 Dual Checkpoint Blockade Enhances Antitumor Immunity and Survival in GBM. Oncoimmunology (2018) 7:e1466769. doi: 10.1080/ 2162402X.2018.1466769
- 130. Dixon KO, Schorer M, Nevin J, Etminan Y, Amoozgar Z, Kondo T. Functional Anti-TIGIT Antibodies Regulate Development of Autoimmunity and Antitumor Immunity. J Immunol (2018) 200:3000–7. doi: 10.4049/jimmunol.1700407
- 131. Han JH, Cai M, Grein J, Perera S, Wang H, Bigler M. Effective Anti-Tumor Response by TIGIT Blockade Associated With FcgammaR Engagement and Myeloid Cell Activation. *Front Immunol* (2020) 11:573405. doi: 10.3389/ fmmu.2020.573405
- 132. Lozano E, Mena MP, Diaz T, Martin-Antonio B, Leon S, Rodriguez-Lobato LG. Nectin-2 Expression on Malignant Plasma Cells Is Associated With Better Response to TIGIT Blockade in Multiple Myeloma. *Clin Cancer Res* (2020) 26:4688–98. doi: 10.1158/1078-0432.CCR-19-3673
- 133. Minnie SA, Kuns RD, Gartlan KH, Zhang P, Wilkinson AN, Samson L. Myeloma Escape After Stem Cell Transplantation is a Consequence of T-Cell Exhaustion and is Prevented by TIGIT Blockade. *Blood* (2018) 132:1675–88. doi: 10.1182/blood-2018-01-825240
- 134. Josefsson SE, Beiske K, Blaker YN, Forsund MS, Holte H, Ostenstad B. TIGIT and PD-1 Mark Intratumoral T Cells With Reduced Effector Function in B-Cell Non-Hodgkin Lymphoma. *Cancer Immunol Res* (2019) 7:355–62. doi: 10.1158/2326-6066.CIR-18-0351
- 135. Josefsson SE, Huse K, Kolstad A, Beiske K, Pende D, Steen CB. T Cells Expressing Checkpoint Receptor TIGIT Are Enriched in Follicular Lymphoma Tumors and Characterized by Reversible Suppression of T-Cell Receptor Signaling. *Clin Cancer Res* (2018) 24:870–81. doi: 10.1158/ 1078-0432.CCR-17-2337
- 136. Kong Y, Zhu L, Schell TD, Zhang J, Claxton DF, Ehmann WC. T-Cell Immunoglobulin and ITIM Domain (TIGIT) Associates With CD8+ T-Cell Exhaustion and Poor Clinical Outcome in AML Patients. *Clin Cancer Res* (2016) 22:3057–66. doi: 10.1158/1078-0432.CCR-15-2626
- 137. Gramatzki M, Ludwig WD, Burger R, Moos P, Rohwer P, Grunert C. Antibodies TC-12 ("Unique") and TH-111 (CD96) Characterize T-Cell Acute Lymphoblastic Leukemia and a Subgroup of Acute Myeloid Leukemia. *Exp Hematol* (1998) 26:1209–14.
- 138. Meyer D, Seth S, Albrecht J, Maier MK, du Pasquier L, Ravens I. CD96 Interaction With CD155 via its first Ig-like domain is modulated by alternative splicing or mutations in distal Ig-like domains. J Biol Chem (2009) 284:2235–44. doi: 10.1074/jbc.M807698200
- 139. Roman Aguilera A, Lutzky VP, Mittal D, Li XY, Stannard K, Takeda K. CD96 Targeted Antibodies Need Not Block CD96-CD155 Interactions to Promote NK Cell Anti-Metastatic Activity. Oncoimmunology (2018) 7:e1424677. doi: 10.1080/2162402X.2018.1424677
- 140. Gong J, Zhu C, Zhuang R, Song C, Li Q, Xu Z. Establishment of an Enzyme-Linked Immunosorbent Assay System for Determining Soluble CD96 and its Application in the Measurement of Scd96 in Patients With Viral Hepatitis B and Hepatic Cirrhosis. *Clin Exp Immunol* (2009) 155:207–15. doi: 10.1111/ j.1365-2249.2008.03829.x
- 141. Chiang EY, de Almeida PE, de AlmeidaNagata DE, Bowles KH, Du X, Chitre AS. CD96 Functions as a Co-Stimulatory Receptor to Enhance CD8(+) T Cell Activation and Effector Responses. *Eur J Immunol* (2020) 50:891–902. doi: 10.1002/eji.201948405
- Rudd CE, Schneider H. Unifying Concepts in CD28, ICOS and CTLA4 Co-Receptor Signalling. Nat Rev Immunol (2003) 3:544–56. doi: 10.1038/nri1131
- 143. Kirchgessner H, Dietrich J, Scherer J, Isomaki P, Korinek V, Hilgert I. The Transmembrane Adaptor Protein TRIM Regulates T Cell Receptor (TCR) Expression and TCR-Mediated Signaling *via* an association with the TCR zeta chain. J Exp Med (2001) 193:1269–84. doi: 10.1084/jem.193.11.1269
- 144. Melsen JE, Lugthart G, Vervat C, Kielbasa SM, van derZeeuw SAJ, Buermans HPJ. Human Bone Marrow-Resident Natural Killer Cells Have a Unique Transcriptional Profile and Resemble Resident Memory CD8(+) T Cells. *Front Immunol* (2018) 9:1829. doi: 10.3389/fimmu.2018.01829

- 145. Eriksson EM, Keh CE, Deeks SG, Martin JN, Hecht FM, Nixon DF. Differential Expression of CD96 Surface Molecule Represents CD8(+) T Cells With Dissimilar Effector Function During HIV-1 Infection. *PloS One* (2012) 7:e51696. doi: 10.1371/journal.pone.0051696
- 146. Cluxton CD, Spillane C, O'Toole SA, Sheils O, Gardiner CM, O'Leary JJ. Suppression of Natural Killer Cell NKG2D and CD226 Anti-Tumour Cascades by Platelet Cloaked Cancer Cells: Implications for the Metastatic Cascade. *PloS One* (2019) 14:e0211538. doi: 10.1371/ journal.pone.0211538
- 147. Wu M, Mei F, Liu W, Jiang J. Comprehensive Characterization of Tumor Infiltrating Natural Killer Cells and Clinical Significance in Hepatocellular Carcinoma Based on Gene Expression Profiles. *BioMed Pharmacother* (2020) 121:109637. doi: 10.1016/j.biopha.2019.109637
- 148. Sun H, Liu L, Huang Q, Liu H, Huang M, Wang J.. Accumulation of Tumor-Infiltrating CD49a(+) NK Cells Correlates With Poor Prognosis for Human Hepatocellular Carcinoma. *Cancer Immunol Res* (2019) 7:1535–46. doi: 10.1158/2326-6066.CIR-18-0757
- 149. Wang Y, Wang C, Qiu J, Qu X, Peng J, Lu C. Targeting CD96 Overcomes PD-1 Blockade Resistance by Enhancing CD8+ TIL Function in Cervical Cancer. J Immunother Cancer (2022) 10(3):e003667. doi: 10.1136/jitc-2021-003667
- 150. Hosen N, Park CY, Tatsumi N, Oji Y, Sugiyama H, Gramatzki M. CD96 is a Leukemic Stem Cell-Specific Marker in Human Acute Myeloid Leukemia. Proc Natl Acad Sci U.S.A. (2007) 104:11008–13. doi: 10.1073/ pnas.0704271104
- 151. Zhang W, Shao Z, Fu R, Wang H, Li L, Liu H. Expressions of CD96 and CD123 in Bone Marrow Cells of Patients With Myelodysplastic Syndromes. *Clin Lab* (2015) 61:1429–34. doi: 10.7754/clin.lab.2015.141240
- 152. Harjunpaa H, Blake SJ, Ahern E, Allen S, Liu J, Yan J. Deficiency of Host CD96 and PD-1 or TIGIT Enhances Tumor Immunity Without Significantly Compromising Immune Homeostasis. *Oncoimmunology* (2018) 7:e1445949. doi: 10.1080/2162402X.2018.1445949
- 153. Brooks J, Fleischmann-Mundt B, Woller N, Niemann J, Ribback S, Peters K. Perioperative, Spatiotemporally Coordinated Activation of T and NK Cells Prevents Recurrence of Pancreatic Cancer. *Cancer Res* (2018) 78:475–88. doi: 10.1158/0008-5472.CAN-17-2415
- 154. Hudson WH, Gensheimer J, Hashimoto M, Wieland A, Valanparambil RM, Li P. Proliferating Transitory T Cells With an Effector-Like Transcriptional Signature Emerge From PD-1(+) Stem-Like CD8(+) T Cells During Chronic Infection. *Immunity* (2019) 51:1043–1058 e1044. doi: 10.1016/ j.immuni.2019.11.002
- 155. Murter B, Pan X, Ophir E, Alteber Z, Azulay M, Sen R. Mouse PVRIG Has CD8(+) T Cell-Specific Coinhibitory Functions and Dampens Antitumor Immunity. *Cancer Immunol Res* (2019) 7:244–56. doi: 10.1158/2326-6066.CIR-18-0460
- 156. Li Y, Zhang Y, Cao G, Zheng X, Sun C, Wei H. Blockade of Checkpoint Receptor PVRIG Unleashes Anti-Tumor Immunity of NK Cells in Murine and Human Solid Tumors. J Hematol Oncol (2021) 14:100. doi: 10.1186/ s13045-021-01112-3
- 157. Xu F, Sunderland A, Zhou Y, Schulick RD, Edil BH, Zhu Y. Blockade of CD112R and TIGIT Signaling Sensitizes Human Natural Killer Cell Functions. *Cancer Immunol Immunother* (2017) 66:1367–75. doi: 10.1007/ s00262-017-2031-x
- Harjunpaa H, Guillerey C. TIGIT as an Emerging Immune Checkpoint. *Clin Exp Immunol* (2020) 200:108–19. doi: 10.1111/cei.13407
- 159. Chen X, Song X, Li K, Zhang T. FcgammaR-Binding Is an Important Functional Attribute for Immune Checkpoint Antibodies in Cancer Immunotherapy. *Front Immunol* (2019) 10:292. doi: 10.3389/ fmmu.2019.00292
- 160. Rodriguez-Abreu D, Johnson ML, Hussein MA, Cobo M, Patel AJ, Secen NM. Primary Analysis of a Randomized, Double-Blind, Phase II Study of the Anti-TIGIT Antibody Tiragolumab (Tira) Plus Atezolizumab (Atezo) Versus Placebo Plus Atezo as First-Line (1L) Treatment in Patients With PD-L1-Selected NSCLC (CITYSCAPE). J Clin Onco (2020) 38:9503–3. doi: 10.1200/JCO.2020.38.15_suppl.9503
- 161. Gandhi L, Rodriguez-Abreu D, Gadgeel S, Esteban E, Felip E, De Angelis F. Pembrolizumab Plus Chemotherapy in Metastatic Non-Small-Cell Lung Cancer. N Engl J Med (2018) 378:2078–92. doi: 10.1056/NEJMoa1801005

- Paz-Ares L, Luft A, Vicente D, Tafreshi A, Gumus M, Mazieres J. Pembrolizumab Plus Chemotherapy for Squamous Non-Small-Cell Lung Cancer. N Engl J Med (2018) 379:2040–51. doi: 10.1056/NEJMoa1810865
- 163. Socinski MA, Jotte RM, Cappuzzo F, Orlandi F, Stroyakovskiy D, Nogami N. Atezolizumab for First-Line Treatment of Metastatic Nonsquamous NSCLC. N Engl J Med (2018) 378:2288–301. doi: 10.1056/ NEJMoa1716948
- 164. Li W, Blessin NC, Simon R, Kluth M, Fischer K, Hube-Magg C. Expression of the Immune Checkpoint Receptor TIGIT in Hodgkin's Lymphoma. BMC Cancer (2018) 18:1209. doi: 10.1186/s12885-018-5111-1
- 165. Sullivan R, Rasco D, Lim E, Sharma M, Shepard D, Patnaik A. Abstract CT031: COM701 Demonstrates Preliminary Antitumor Activity as Monotherapy and in Combination With Nivolumab in Patients With Advanced Solid Tumors. J Cancer Res (2020) 80:CT031–1. doi: 10.1158/ 1538-7445.AM2020-CT031
- 166. Li XY, Das I, Lepletier A, Addala V, Bald T, Stannard K. CD155 Loss Enhances Tumor Suppression. via combined Host tumor-intrinsic mechanisms J Clin Invest (2018) 128:2613–25. doi: 10.1172/JCI98769
- 167. Celis-Gutierrez J, Blattmann P, Zhai Y, Jarmuzynski N, Ruminski K, Gregoire C. Quantitative Interactomics in Primary T Cells Provides a Rationale for Concomitant PD-1 and BTLA Coinhibitor Blockade in Cancer Immunotherapy. *Cell Rep* (2019) 27:3315–30.e3317. doi: 10.1016/ j.celrep.2019.05.041
- 168. Smith A, Zeng W, Grogan B, Haass J, Blackmarr A, Peterson S, et al. Abstract 4986: TIGIT Directed Human Antibody Modulates T-Regulatory and Effector Cell Function. J Cancer Res (2019) 79:4986–6. doi: 10.1158/1538-7445.AM2019-4986
- 169. Chand D, Waight JD, Paltrinieri E, Dietrich S, Bushell M, Costa M. Abstract 2390: FcgR Co-Engagement by Anti-TIGIT Monoclonal Antibodies Enhances T Cell Functionality and Antitumor Immune Responses. J Cancer Res (2019) 79:2390–0. doi: 10.1158/1538-7445.AM2019-2390
- 170. Argast GM, Cancilla B, Cattaruzza F, Yeung P, Scolan E, Harris R. Abstract 5627: Anti-TIGIT Biomarker Study: Inhibition of TIGIT Induces Loss of Tregs

From Tumors and Requires Effector Function for Tumor Growth Inhibition. J Cancer Res (2018) 78:5627–7. doi: 10.1158/1538-7445.AM2018-5627

- 171. Sakaguchi S, Yamaguchi T, Nomura T, Ono M. Regulatory T Cells and Immune Tolerance. *Cell* (2008) 133:775–87. doi: 10.1016/j.cell.2008. 05.009
- 172. Ishitsuka K, Yurimoto S, Tsuji Y, Iwabuchi M, Takahashi T, Tobinai K. Safety and Effectiveness of Mogamulizumab in Relapsed or Refractory Adult T-Cell Leukemia-Lymphoma. *Eur J Haematol* (2019) 102:407–15. doi: 10.1111/ejh.13220
- 173. Bulliard Y, Jolicoeur R, Windman M, Rue SM, Ettenberg S, Knee DA. Activating Fc Gamma Receptors Contribute to the Antitumor Activities of Immunoregulatory Receptor-Targeting Antibodies. J Exp Med (2013) 210:1685–93. doi: 10.1084/jem.20130573
- 174. Velders MP, van Rhijn CM, Oskam E, Fleuren GJ, Warnaar SO, Litvinov SV. The Impact of Antigen Density and Antibody Affinity on Antibody-Dependent Cellular Cytotoxicity: Relevance for Immunotherapy of Carcinomas. Br J Cancer (1998) 78:478–83. doi: 10.1038/bjc.1998.518

Conflict of Interest: All authors are employees of GlaxoSmithKline.

Publisher's Note: All claims expressed in this article are solely those of the authors and do not necessarily represent those of their affiliated organizations, or those of the publisher, the editors and the reviewers. Any product that may be evaluated in this article, or claim that may be made by its manufacturer, is not guaranteed or endorsed by the publisher.

Copyright © 2022 Conner, Hance, Yadavilli, Smothers and Waight. This is an openaccess article distributed under the terms of the Creative Commons Attribution License (CC BY). The use, distribution or reproduction in other forums is permitted, provided the original author(s) and the copyright owner(s) are credited and that the original publication in this journal is cited, in accordance with accepted academic practice. No use, distribution or reproduction is permitted which does not comply with these terms.



Mapping the Tumor Microenvironment in TNBC and Deep Exploration for M1 Macrophages-Associated Prognostic Genes

Baojin Xu^{1,2,3}, Hefen Sun^{1,2}, Xiaoqing Song^{1,2}, Qiqi Liu^{1,2} and Wei Jin^{1,2*}

¹ Key Laboratory of Breast Cancer in Shanghai, Fudan University Shanghai Cancer Center, Shanghai, China, ² Department of Oncology, Shanghai Medical College, Fudan University, Shanghai, China, ³ Department of Breast Surgery, Liaoning Cancer Hospital and Institute, Cancer Hospital of China Medical University, Shenyang, China

OPEN ACCESS

Edited by:

Yubin Li, University of Pennsylvania, United States

Reviewed by:

Zhe-Sheng Chen, St. John's University, United States Daming Gao, Chinese Academy of Sciences (CAS), China Qifeng Yang, Shandong University, China

> ***Correspondence:** Wei Jin weijin7207@126.com

Specialty section:

This article was submitted to Cancer Immunity and Immunotherapy, a section of the journal Frontiers in Immunology

Received: 19 April 2022 **Accepted:** 01 June 2022 **Published:** 30 June 2022

Citation:

Xu B, Sun H, Song X, Liu Q and Jin W (2022) Mapping the Tumor Microenvironment in TNBC and Deep Exploration for M1 Macrophages-Associated Prognostic Genes. Front. Immunol. 13:923481. doi: 10.3389/fimmu.2022.923481 Triple negative breast cancer (TNBC) remains the worst molecular subtype due to high heterogeneity and lack of effective therapeutic targets. Here we investigated the tumor and immune microenvironment heterogeneity of TNBC using scRNA-seq and bulk RNA-seq data from public databases and our cohort. Macrophage subpopulations accounted for a high proportion of tumor immune microenvironment (TIME), and M1 macrophages were associated with better clinical outcomes. Furthermore, three maker genes including IFI35, PSMB9, and SAMD9L showed a close connection with M1 macrophages. Specifically, IFI35 was positively associated with macrophage activation, chemotaxis, and migration. Also, patients with high IFI35 expression had a better prognosis. *In vitro* studies subsequently demonstrated that IFI35 was upregulated during the M1 subtype differentiation of macrophages. In summary, our data suggested that IFI35 maybe a promising novel target that helps to reshape macrophage polarization towards the M1 subtype for anti-tumor effects.

Keywords: triple negative breast cancer, tumor immune microenvironment, macrophages, IFI35, ScRNA-seq analysis, bulk-RNA sequencing

Significance: This study defines IFI35 as a potential therapeutic target to remodel the polarization of macrophages towards the M1 subtype in patients with TNBC.

INTRODUCTION

Triple negative breast cancer (TNBC) accounts for 10-15% of all breast cancer cases, and lacks effective therapeutic targets due to the paucity of ER, PR, and Her2 expression (1). Recently, advances in immunotherapy such as anti-PD1, anti-PDL1, and anti-CTLA4 have dramatically ameliorated outcomes in patients with a series of solid tumors, which also brings new hope for TNBC. Currently, PD-1/PD-L1 inhibitor therapy has been approved by the U.S. Food and Drug

Administration (FDA) for treating TNBC, but few patients received durable clinical responses as a result of the limitation of immunosuppressive tumor microenvironment (TME) (2). With an in-depth understanding of the tumor immune microenvironment (TIME), the most abundant macrophage subpopulation in TIME ignited our interest.

Generally speaking, macrophages can be polarized into classically activated macrophages and alternatively activated macrophages, termed M1 and M2 subsets, respectively (3, 4). On the one hand, M1 macrophages, stimulated by cytokines such as interferon gamma (IFN- γ) and lipopolysaccharide (LPS), act as phagocytic cells and antigen-presenting cells and release tumor necrosis factor-α (TNF-α), interleukin-1α (IL-1α), IL-1 β , and IFN- γ , which further exert tumoricidal activity. Phenotypically, they express costimulatory molecules including CD80, CD86, and MHC II. On the other hand, in response to other cytokines such as interleukin-4 (IL-4) and IL-13, macrophages are polarized into M2 subtype that produces anti-inflammatory factors such as arginase 1, IL-10, and TGFβ, participating in angiogenesis and forming immunosuppressive microenvironment to lead to tumor growth, progression and metastasis. M2 macrophages are phenotypically characterized by CD206 and CD163 expression. At present, mounting evidence has indicated that macrophage infiltration in most tumors is dominated by the M2 subtype and is associated with tumor progression and poor patient prognosis (5-7). In TNBC, peripheral blood monocytes recruited into tumor microenvironment, in response to specific stimuli, undergo M2 activation that promotes tumor progression via several mechanisms including the secretion of inhibitory cytokines, the reduction of cytotoxic T lymphocytes, and the promotion of regulatory T cells (8, 9). Application of specific gene knockout technology and antibody against M2 macrophages infiltration improve the efficacy of immunotherapy (10, 11). In fact, tumorassociated macrophages (TAMs) in the TIME cannot be simply referred to as the M1/M2 dichotomy, they actually exist in the form of a mixture and change dynamically in response to different environment milieu, consequently enabling them potential targets for cancer immunotherapy.

Interferon induced protein 35 (IFI35) was first identified in HeLa cells treated with IFN- γ . It exists in the extracellular region, cytoplasm and nucleus, but does not co-localized with any organelle (12, 13). To date, a series of studies demonstrated that IFI35 can bind to Nmi or BTas after viral infection, thereby activating type I interferon antiviral response (14). While others also revealed that it negatively regulate RIG-I-mediated antiviral signaling through the ubiquitination pathway (15, 16). In addition, extracellular IFI35 and Nmi, as two damageassociated molecular patterns (DAMPs), activated NF-KB pathway via Toll-like receptor 4 (TLR4) from macrophages, leading to the exacerbation of inflammation-related diseases such as lupus nephritis, sepsis and multiple sclerosis (17-19). Yu et al. also identify IFI35 as a marker associated with SARS-CoV-2 or influenza virus-induced syndromes. IFI35 knockout mice and IFI35 neutralizing antibodies reduce inflammationrelated lung injury (20). However, there are still very few studies on IFI35 in tumor biology, among which mainly focused on enhanced radiosensitivity of lung adenocarcinoma and colorectal cancer (21, 22). Thus, exploration for the relationship between IFI35 and macrophages polarization is an attractive direction for cancer immunotherapy.

Herein, we integrated single-cell RNA sequencing (scRNAseq) and bulk-RNA sequencing data of TNBC to analyze the heterogeneity of the tumor and TIME. The results indicated that TAMs were highly enriched in the TIME, which reflected the potential value for remodeling TAMs. To further indentify the key genes associated with macrophages polarization, a weighted gene co-expression network analysis (WGCNA) was constructed, and correlation and survival analyzed were performed. As a result, three marker genes involved in macrophage polarization toward M1 phenotype, including IFI35, were uncovered. Ultimately, we analyzed the connection between IFI35 and M1 macrophages from two levels of cell lines and tissue samples.

MATERIALS AND METHODS

Study Cohort

Our study included single-cell and bulk-RNA sequencing multiomics data, in which a total of 360 TNBC patients from Fudan University Shanghai Cancer Center (FUSCC) and 158 TNBC patients from TCGA cohort were analyzed, with more detailed information previously described (23). The scRNAseq data about 5 TNBC patients was downloaded from European Genome-phenome Archive with the study ID EGAS00001005061 (24).

Single-Cell RNA-Seq Analysis

In the process of data processing, the 'Seurat' package was used and UMAP method was applied for non-linear dimensional reduction (25). Then, the combination of the 'singleR" package and canonical marker annotated cell clusters (26). The copy number variations from malignant epithelial cells were inferred by the 'inferCNV' package. The 'Monocle 3 alpha' package was applied to infer pseudotime cell trajectory of immune cells (27).

Bulk-RNA Sequencing Analysis

In the bulk-RNA sequencing data from FUSCC and TCGA TNBC cohorts, immune cell infiltration was estimated by the 'CIBERSORT' package (28). The mutational landscape between the low and high M1 macrophages infiltration group was visualized by the 'maftools' package (29). Weighted gene co-expression network analysis (WGCNA) was constructed, in which a power of 5 was set as soft-threshold parameter (30). The module with the highest score for M1 infiltration was identified, in which top 30 genes with high connectivity were shown.

Correlation and Survival Analysis

Pearson's coefficient analysis was performed to explore correlation, and the 'Survival' package was applied to complete

survival analysis. A value of p < 0.05 was considered to indicate a statistically significant difference.

GSEA Enrichment Analysis

Three classical macrophage-associated gene sets were downloaded from the Molecular Signatures Database (MSigDB) (http://www.gsea-msigdb.org/gsea/msigdb/index.jsp), including GOBP_Macrophage_Activation, GOBP_Macrophage_Chemotaxis, and GOBP_Macrophage_Migration. The enrichment analysis was performed by GSEA software (version 4.1.0).

Cell Culture

Human monocyte cell line THP-1 was purchased from Chinese Academy of Science Cell Bank (Shanghai, China; catalog no. TCHu 57). THP-1 was cultured in complete RPMI 1640 containing 10% FBS (Gibco), and 1% PenStrep and induced into M0 macrophages in the presence of 100 ng/ mL PMA (Peprotech; catalog no. 1652981) for 8 hours. To obtain M1 macrophages, M0 macrophages were then treated with 100ng/ml LPS (Sigma-Aldrich; catalog no. L2630) and 20ng/ml IFN-γ (Peprotech; catalog no. 300-02). While, M2 macrophages were induced by the combination of 20ng/ml IL-4 (Peprotech; catalog no. 200-04) and 20ng/ml IL-13 (Peprotech; catalog no. 200-13). All cells were found to be negative for Mycoplasma upon repeated testing every month using MycoBlue Mycoplasma Detector (Vazyme; catalog no. D101) and were maintained in 37°C with a humidified atmosphere of 5% CO₂ in air.

RT-PCR

Total RNA was extracted by using Trizol reagent (Invitrogen; catalog no. 15596026). cDNA were synthesized from 500ng of total RNA using PrimeScriptTM RT reagent Kit (Takara; catalog no. RR037A) and RT-qPCR was performed by ChamQ Universal SYBR qPCR Master Mix (Vazyme; catalog no. Q711) using QuantStudioTM 6 Flex Real-Time PCR System (Thermofisher Scientific; catalog no. 4485691) according to the manufacturer's protocols. Gene expression was normalized relative to GAPDH. Data were analyzed by applying the $2-\Delta\Delta C_T$ calculation method. For a detailed list of RT-qPCR primer sequences, see **Supplementary Table S1**.

Immunoblotting

Cells were washed with PBS and lysed using RIPA cell lysis and extraction buffer (Thermofisher Scientific; catalog no. 89901) supplemented with HaltTM Protease and Phosphatase Inhibitor Cocktail (Thermofisher Scientific; catalog no. 78440). Total protein concentration was determined using PierceTM BCA Protein Assay Kit (Thermofisher Scientific; catalog no. 23225). Proteins were separated by gradient SDS-PAGE and transferred to PVDF membranes. Blots were blocked in PBS containing 5% milk powder and 0.1% Tween, and then incubated overnight at 4°C with primary antibodies; anti-IFI35 (1:1000, Abcam; catalog no. ab233415) and anti- β -Actin (1:5000, Proteintech; catalog no. HRP-60008). After washing, appropriate HRP-conjugated secondary antibody (SAB; catalog no. L3012) was incubated for 1 hours at room temperature. Chemoluminescence was detected by Pierce ECL Western Blotting Substrate (Thermofisher Scientific; catalog no. 32209) and captured on ChemiDocTM XRS+ System (Bio-Rad; catalog no. 1708265).

Immunofluorescence

Cells were washed with PBS and fixed using 4% paraformaldehyde. Subsequently, cells were permeabilized using 0.5% Triton X-100 for 5 min, and blocked by protein block (Abcam; catalog no. ab64226). Then, cells were incubated overnight at 4°C with primary antibody anti-IFI35 (1:100, Abcam; catalog no. ab233415) followed by appropriate biotinylated secondary antibody (1:500, Abcam; catalog no. ab150077). Finally, cells were mounted with mounting medium with DAPI (Beyotime Biotechnology; catalog no. P0131) and images were captured on inverted microscope (Leica; catalog no. DMI6000B).

Double-Labeling Immunohistochemistry

The paraffin-embedded TNBC specimens were sectioned in 4µm thickness. After removal of paraffin with xylenes and a graded series of alcohols, tissue sections were subjected to antigen retrieval by EDTA (Beyotime Biotechnology; catalog no. P0085) in a high temperature and pressure environment for 5 min, and then were blocked by peroxidase and alkaline phosphatase endogenous blocking solution (Vector; catalog no. SP-6000) for 15 min and protein block (Abcam; catalog no. ab64226) for 1 h, respectively. After washing with PBS buffer, the sections were incubated with primary antibody mix containing mouse anti-CD86 (1:50, Abcam; catalog no. ab220188) and rabbit anti-IFI35 (1:100, Abcam; catalog no. ab233415) overnight at 4°C. The following day, the sections were incubated for 30 min in HRP-conjugated goat-anti-mouse secondary antibody (1:500, Jackson ImmunoResearch; catalog no. 115-035-003), followed by a 1-min incubation period with peroxidase substrate (Vector; catalog no. SK-4105). After washing in in distilled water, they were then incubated with AP-conjugated horse-anti-rabbit secondary antibody (Cell Signaling Technology; catalog no. 18653) for 30 min, followed by a 20-min incubation period with alkaline phosphatase substrate (Vector; catalog no. SK-5105). Between each step the specimens were rinsed three times with TBS buffer. Nuclei were counterstained with hematoxylin. Finally, the sections were coverslipped using aqueous mounting medium (Abcam; catalog no. ab64230) and images were captured on microscope (Olympus; catalog no. BX43). All tissue samples included were approval by the Ethics Committee of Fudan University Shanghai Cancer Center (050432-4-1805C).

Statistical Analysis

All data were analyzed by GraphPad Prism Version 9 software. Normal distribution of all data were first tested. Comparisons between two groups were made by using an unpaired two-tailed Student's t-test. For scRNA-seq and bulk-RNA data, all statistical analysis were performed with RStudio (version 1.4.1106). All *p*values are two-sided, and statistical significance was evaluated at the 0.05 level.

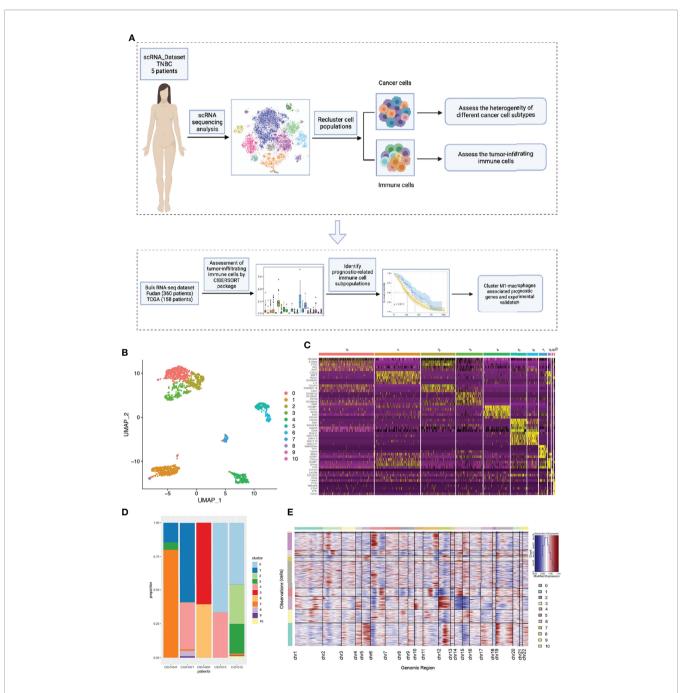
RESULTS

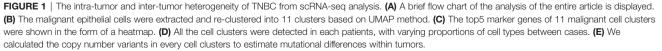
Intra-Tumor and Inter-Tumor Heterogeneity of TNBC

As shown in the flowchart (**Figure 1A**), we first explored the intra- and inter-tumor heterogeneity of TNBC based on scRNA-seq analysis. Using the 'SingleR' package and canonical marker,

we successfully annotated 12 cell clusters, including multiple immune cell clusters, epithelial cells, stromal cells, endothelial cells, and tissue stem cells (**Supplementary Figure S1**).

To further explore tumor heterogeneity, epithelial cells were divided into a total of 11 malignant cell subtypes (Figure 1B). Interestingly, we found that tumor cells had extensive and obvious heterogeneity, even within the same tumor type.





When elucidating the characteristics of different subtypes, top five marker genes were shown in Figure 1C. In order to more effectively prove the existence of heterogeneity within and between tumors, the composition ratio of different cell subgroups in each patient's tumor was depicted (Figure 1D). It is not difficult to find that cluster 7 accounted for more than 75% and constituted the main tumor population in patient CID44041, while this subtype was rarely found in other patients' tumors. In addition, patient CID44971 predominantly possessed cluster 1, patient CID44991 cluster 5, and patients CID4513 and CID4515 cluster 0. Thus, varying proportions of cell subpopulations between cases were demonstrated, indicating the existence of intra-tumor and inter-tumor heterogeneity. As we all know, copy number variations (CNVs) in tumor cells are widespread. Therefore, we further explored the genomic copy number alterations in various tumor cell subtypes using inferCNV (Figure 1E). Cluster 4 showed high CNVs on chromosome 12, whereas cluster 2 had higher CNVs on chromosome 6. It can be seen that the heterogeneity within the tumor is not only reflected in the constituent components, but also in the form of genetic mutations.

Complexity and Heterogeneity of the Tumor Immune Microenvironment

In addition to research on tumor heterogeneity, TIME has gradually become an area of significant research interest in recent years (31). To investigate the complexity and variability of the TIME, we identified eight immune cell clusters using canonical markers, which included B cells, CD4⁺ T helper cells, CD4⁺ Treg cells, cytotoxic CD8⁺ T cells, NK cells, neutrophils, and M1 and M2 macrophages (Figure 2A). As shown in Figure 2B, marker genes were identified in different cell clusters using the combined method of SingleR and canonical markers. Specifically, CD8A and CD8B were enriched in cvtotoxic CD8⁺ T cells, who mainly exerted antitumor immune killing. Other helper immune cells also play an important role in eliminating tumor cells, including B cells (CD79A), CD4⁺ T helper cells (IL7R and CCR7), NK cells (GNLY and KLRD1), M1 macrophages (CD86), and neutrophils (S100A8). In contrast, tumor cells in the TIME also recruited and induced immune cells to transform into a tumor-promoting phenotype. In our study, the classical immunosuppressive cells consisted of CD4⁺ Treg

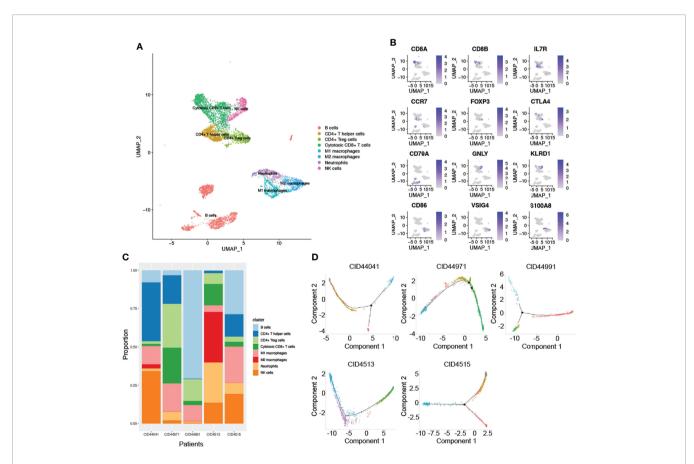


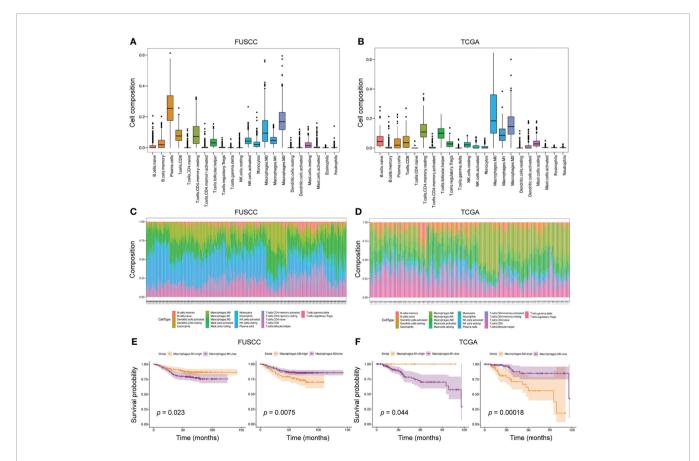
FIGURE 2 | The complex composition of the tumor immune microenvironment. (A) Combining singleR and canonical marker, we successfully annotated 8 immune cell clusters, including B cells, CD4⁺ T helper cells, CD4⁺ Treg cells, cytotoxic CD8⁺ T cells, NK cells, neutrophils, M1 and M2 macrophages. (B) Representative marker genes were shown using non-linear dimensional reduction (B cells: CD79A, CD4⁺ T helper cells: IL7R and CCR7, NK cells: GNLY and KLRD1, M1 macrophages: CD86, neutrophils: S100A8, CD4⁺ Treg cells: FOXP3 and CTLA4, and M2 macrophages: CD163 and VSIG4). (C) All annotated immune cell clusters were estimated in each patients, with varying proportions of cell types between cases. (D) Pseudotime analysis was used to construct the trajectory of immune cells differentiation.

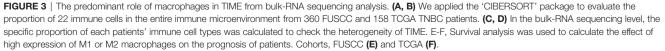
cells (FOXP3 and CTLA4), and M2 macrophages (CD163 and VSIG4). To effectively explore the heterogeneity of TIME, we further estimated the proportion ratio of each immune cell subpopulation in every patient (**Figure 2C**). The results showed that there was obvious heterogeneity in the immune cell composition among different patients with TNBC. In addition, differentiation trajectory of immune cells was constructed by pseudotime that is a measure of how much progress an individual cell has made during cell differentiation (**Figure 2D**). Based on this differentiation trajectory, it illustrated that myeloid and lymphoid immune cells were differentiated separately, and the differentiation trajectory of immune cells was variable. Collectively, all these results demonstrated the complexity and heterogeneity of the TIME.

Significance of Macrophages in the Tumor Immune Microenvironment

Due to the limited sample size of the scRNA-seq analysis only representing a small number of patients, we applied bulk-RNA sequencing from FUSCC and TCGA TNBC cohorts to further dissect the TIME. In this scenario, the 'CIBERSORT' package was used to assess the infiltration of various immune cells from 360 FUSCC and 158 TCGA patients with TNBC(**Figures 3A, B**). Consistent with the scRNA-seq results, macrophages accounted for a very high proportion of all 22 immune cells. This result once again emphasized the essential role of macrophages in the TIME. Through calculating the proportion of each patient's immune cells, we found that the heterogeneity between tumors was widespread in the TIME (**Figures 3C, D**).

To further explore the impact of different immune cell infiltrations on the prognosis of patients, we divided patients into high and low infiltration groups of 22 immune cell types according to the immune cell infiltration score estimated by the 'CIBERSORT' package. Then, survival analysis between the two groups was performed. In the FUSCC cohort, five immune cell subtypes were associated with patients' prognosis, including resting CD4⁺ memory T cells, resting dendritic cells, and M0, M1, and M2 macrophages. However, the TCGA cohort identified seven immune cell subpopulations related to prognostic outcomes, such as activated CD4+ memory T cells, resting NK cells, monocytes, neutrophils, and M0, M1, and M2 macrophages (**Figures 3E, F** and **Supplementary Figures S2A, B**). When comparing the results of the two cohorts, we found that higher M1 macrophages infiltration





483

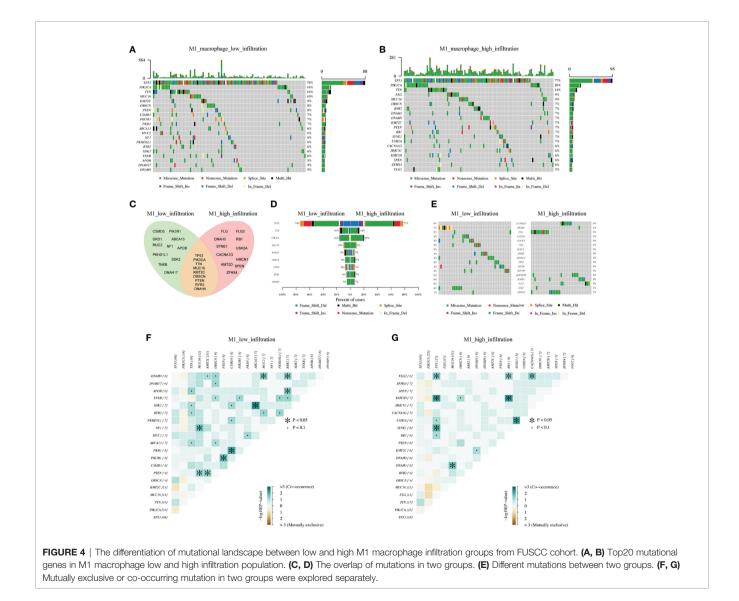
was associated with better prognosis (p = 0.023 and 0.044, respectively), whereas higher M2 macrophages infiltration exhibited shortened survival (p = 0.0075 and 0.00018, respectively). Collectively, macrophage subpopulations accounted for a high proportion of TIME, and were related to patients' prognosis.

Mutational Landscape Between High and Low Macrophage Infiltration

Generally speaking, macrophages can be induced into M1 antitumor or M2 pro-tumor phenotypes. Meanwhile, macrophages in the TIME are not completely dichotomous but follow a dynamic evolution process. As such, we focused on the M1 macrophages, which cause an inflammatory response and present tumor cells to cytotoxic $CD8^+$ T cells, eliciting antitumor immunity.

On this background, we analyzed the mutational landscape between M1 high and low macrophage infiltration groups.

The top 20 mutational genes were first identified (Figures 4A, **B**), among which the most prominent variants were TP53 (found in 74% or 77% of tumors), followed by PIK3CA (16% or 20%), and TTN (16% or 14%). When comparing the top 20 mutational genes from the two groups, we found that only nine genes were mutated in common, which included TP53, PIK3CA, TTN, MUC16, KMT2C, OBSCN, PTEN, RYR2, and DNAH9 (Figures 4C, D). As shown in Figure 4, E we also pointed out differentially mutational genes. In addition, mutually exclusive or co-occurring mutation of top 20 genes were detected (Figures 4F, G). The results indicated that PTEN and MUC16 were obviously co-mutated in the M1 low infiltration cohort, but not in the M1 high infiltration cohort. Also, we analyzed the mutational landscape of TCGA cohort (Supplementary Figure S3) and M2 infiltration groups (data not shown). Together, these data demonstrated that in TNBC, different mutational landscapes existed between the M1 high and low infiltration patient cohorts.



484

Key Marker Genes Associated With M1 Macrophages Infiltration

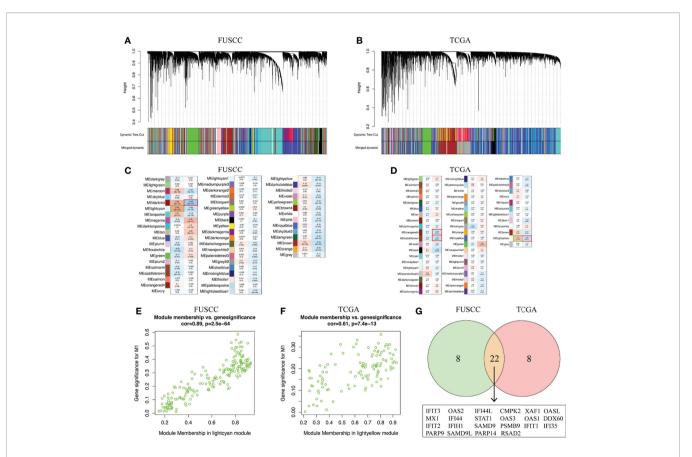
The above results confirmed that it is possible that the discrepancy in the mutational pattern of tumor cells leads to genetic variation, ultimately shaping the inconsistent macrophage infiltration microenvironment. So which genes are involved in this process?

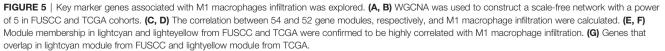
To identify the key marker genes associated with M1 or M2 macrophages infiltration, WGCNA was used to construct a scalefree network (Figures 5A, B). A total of 54 and 52 gene modules were identified from the FUSCC and TCGA TNBC cohorts, among which lightcyan module was associated with higher M1 macrophages infiltration in FUSCC (r = 0.44, $p = 4e^{-18}$, **Figure 5C**), and lightlyellow in TCGA (r = 0.3, $p = 1e^{-4}$, Figure 5D). We further calculated the correlation between module membership and gene significance for M1 macrophages. Both of two modules showed a high correlation with M1 macrophages (cor = 0.89, $p = 2.5e^{-64}$; cor = 0.61, $p = 7.4e^{-13}$; Figures 5E, F). Among these two modules, intramodule connectivity of each genes were estimated, and the top 30 hub genes with the highest degrees were identified. Interestingly, when taking the intersection of top30 hub genes from two modules, we surprisingly found 22 genes were

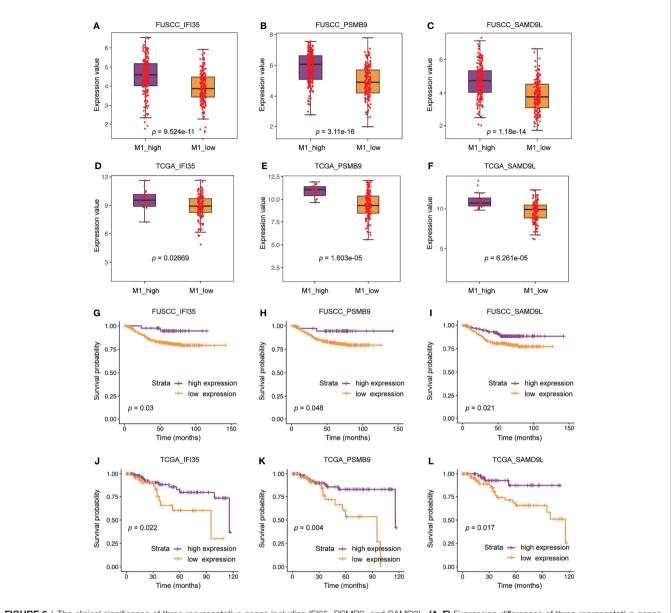
coincident, including IFIT3, IFI35, OAS2, PSMB9, SAMD9L, and so on (**Figure 5G**). Besides we did not find any consistent gene sets in the analysis of the M2 infiltrated groups (**Supplementary Table S2**). Therefore, these 22 genes were likely to be involved in the polarization of M1 macrophages in the TIME.

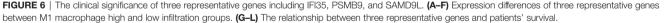
Three Typical Genes Associated With M1 Infiltration Were Associated With Better Prognosis

We further compared the difference in expression of 22 genes between the M1 high and low macrophage infiltration groups. All these genes were higher expression in M1 high macrophage infiltration group from the FUSCC and TCGA datasets (IFI35: $p = 9.524e^{-11}$ or 0.02669; PSMB9: $p = 3.11e^{-16}$ or $1.603e^{-5}$; SAMD9L: $p = 1.18e^{-14}$ or $6.261e^{-5}$; **Figures 6A–F**, data not all shown). To assess the relevance of these genes to the patient's prognosis, survival analysis were used. The results showed that only three representative genes, including IFI35, PSMB9, and SAMD9L, had reached a consistent conclusion in the FUSCC and TCGA cohorts (**Figures 6G–L**). Interestingly, higher expression of IFI35, PSMB9, and SAMD9L was associated with better prognosis (IFI35: p = 0.03 or 0.022; PSMB9: p = 0.048 or 0.004; SAMD9L:







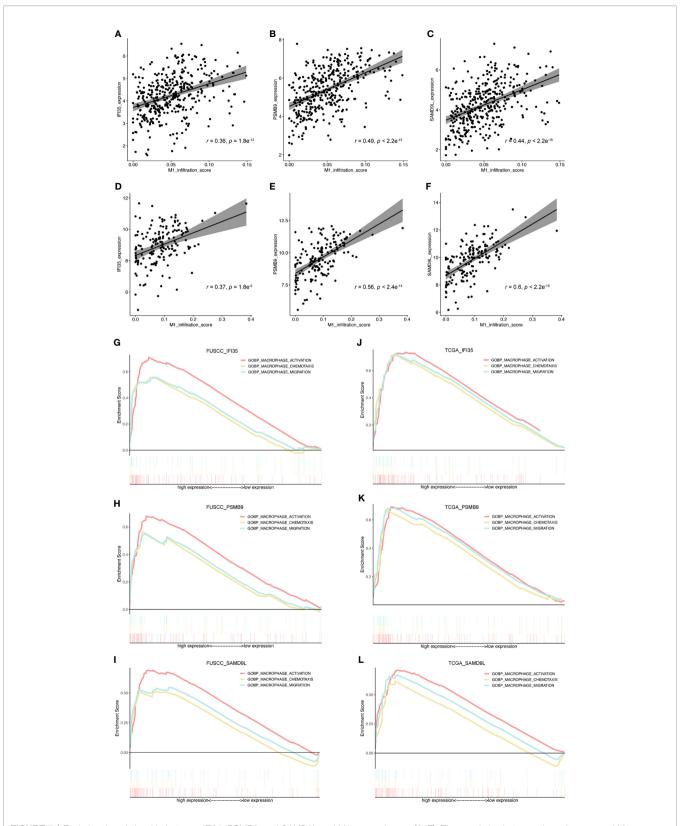


p = 0.021 or 0.017), which was consistent with the previous conclusion that patients with higher M1 macrophages had a prolonged survival.

Exploring the Relationship Between IFI35, PSMB9, and SAMD9L and M1 Macrophages

To further evaluate the connection between IFI35, PSMB9, and SAMD9L and the polarization of macrophages toward the M1 phenotype, we also calculated the correlation between these three genes and M1 macrophage infiltration score. As a result, all the genes were positively correlated with M1 macrophage infiltration (**Figures 7A–F**), in which the correlation coefficient of IFI35 was 0.36 and 0.37 ($p = 1.8e^{-12}$ and $1.8e^{-6}$, respectively),

PSMB9 0.49 and 0.56 ($p = 2.2e^{-16}$ and $2.4e^{-14}$, respectively), and SAMD9L 0.44 and 0.6 ($p = 2.2e^{-16}$ and $2.2e^{-16}$, respectively). Moreover, we extracted three classical macrophage activation, chemotaxis and migration gene sets from the GSEA datasets and analyzed the relationship between them and IFI35, PSMB9, and SAMD9L expression (**Figures 7G–L**). Compared with low IFI35 expression, higher IFI35 expression was positively associated with macrophages activation (FUSCC: NES = 2.26, p-val <0.001, q-val <0.001; TCGA: NES = 2.01, p-val <0.001, qval <0.001), chemotaxis (FUSCC: NES = 1.9, p-val <0.001, q-val <0.001; TCGA: NES = 1.94, p-val <0.001, q-val <0.001), and migration (FUSCC: NES = 1.98, p-val <0.001, q-val <0.001; TCGA: NES = 1.89, p-val <0.001, q-val <0.001). In addition,





PSMB9 and SAMD9L also led to the same conclusion with more detailed data shown in **Supplementary Table S3**. A previous study used an *in vivo* macrophage activation model to predict macrophage programs, and 49 gene modules were identified (32). Therefore, we further explored whether higher expression of IFI35, PSMB9, and SAMD9L was associated with these modules. The standard of higher NES, the lower *p*-val and *q*-val (NES > 1, *p*-val < 0.05, *q*-val < 0.25) were considered significant. As expected, approximately 50% of the gene sets were enriched in high expression of these three genes (FUSCC, IFI35: 23/49; PSMB9: 20/49; SAMD9L: 25/49; TCGA, IFI35: 31/ 49, PSMB9: 34/49, SAMD9L: 21/49; **Supplementary Tables S4A, B**). Taken together, we revealed that three genes that were closely associated with macrophage polarization toward the M1 subtype.

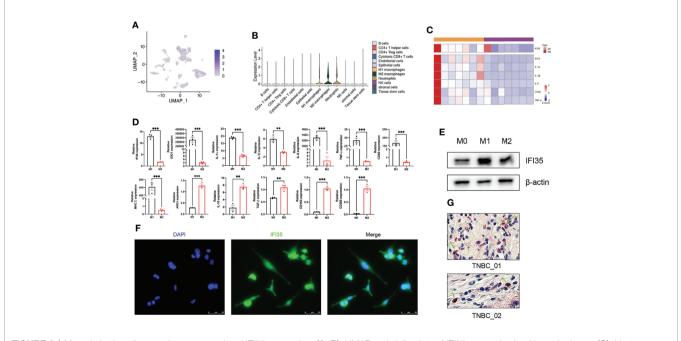
M1 Polarization of Macrophages Upregulated IFI35 Expression

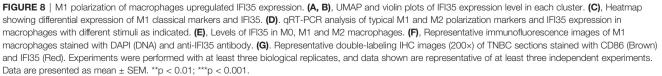
To confirm the results of our bioinformatics analysis, we selected one of the three marker genes for further verification. As we all know, tumor tissue is composed of tumor cells, immune cells, and stromal cells. Therefore, we explored the types of cells in which IFI35 was expressed based on scRNA-seq data. The results indicated that IFI35 was mainly dominated by myeloid-derived cells, including neutrophils, and M1 and M2 macrophages (**Figures 8A, B**). In transcriptome analysis of human M0, M1, and M2 macrophages, M1 macrophages showed higher IFI35 expression than M2 macrophages

(Figure 8C) (33). In response to different stimuli, M0 macrophages were successfully induced into M1 (LPS and IFN- γ) and M2 (IL-4 and IL-13) macrophages based on a series of M1 typical markers, including IDO1, IL-1 α , IL-1 β , IL-6, TNF-α, CD80, and MHC II, as well as M2 ones such as ARG1, IL-10, CD163 and CD206 (Figure 8D). Obviously, IFI35 was upregulated at both the RNA and protein levels (p < 0.001, Figures 8D, E). Meanwhile, we also demonstrated that IFI35 was expressed in the cytoplasm and nucleus of M1 macrophages, which showed cellular elongation in cell morphology (Figure 8F). This conclusion was consistent with the previous study that IFI35 can be transported from the cytoplasm to the nucleus in the activated state (13). Histologically, we found that M1 macrophages with high CD86 expression showed IFI35 expression, which directly reflected the close connection between IFI35 and M1-subtype macrophages (Figure 8G).

DISCUSSION

With the approval of immune checkpoint inhibitors (ICBs) represented by PD-1/PD-L1, anti-tumor therapy has entered a new era of immunotherapy (34). Macrophages, the most abundant immune cell subgroup in the TIME, have received extensive attention. Mounting evidence has revealed that TAMs in TIME-shaped pro-tumor immune responses and were associated with worse clinical outcome in breast cancer,





melanoma, lung cancer, and so on (35). Therefore, three methods of TAMs targeting emerged as required so far. Due to the dependence of TAMs on CSF1/CSF1R signaling, targeting CSF1R has become an effective way to deplete macrophages and improve patients' outcomes (36, 37). In addition, the CCL2-CCR2 axis plays an essential role in the recruitment of classical monocytes to tumor sites. Thus, inhibition of TAMs recruitment by targeting CCL2 or CCR2 has successfully reduced tumor burden in melanoma, breast cancer, and so on. However, the depletion of macrophages also brings a series of side effects that damage tissue homeostasis. Therefore, reprogramming of TAMs has become a more promising treatment strategy. Specifically, it mainly include toll-like receptor agonist, CD40 agonists, PI3Ky inhibitors, inhibition of microRNA activity, anti-CD47 antibodies, and anti-MARCO antibody therapy (38-40). Certain efficacies have been documented. Thus, the exploration for new molecular targets regulating TAMs repolarization is an attractive direction for cancer immunotherapy.

This study not only revealed the intra- and inter-tumor heterogeneity in TNBC, more importantly, demonstrated the complexity of the TIME and explored an abundance of macrophages using the scRNA-seq data of five patients, and two bulk-RNA sequencing datasets consisting of 158 patients from TCGA and 360 patients from our cohort. From multiple perspectives, it has been fully demonstrated that macrophages were the most abundant immune cell subset in the TIME, and the infiltration of M1 macrophages were associated with a better prognosis. This suggested that awakening the function of M1 macrophages from the overall macrophage population in TNBC would bring prolonged survival. Additionally, three representative genes including IFI35, PSMB9, and SAMD9L showed positive correlation with M1 macrophages. Thus, we speculated that these genes may participate in macrophage polarization toward the M1 subtype.

IFI35 has been widely studied in inflammation-related diseases (IRDs) and antiviral immunity since its discovery in 1993 (12). In IRDs, a large number of studies have pointed out that IFI35 was a marker of inflammation. Specifically, it promoted the progression of nephritis by activating the JAK-STAT1 signaling pathway, and served as a DAMP to activate NF-KB pathway, leading to the exacerbation of neuroinflammation (18). However, it seemed to be a double-edged sword. On the one hand, IFI35 can bind with Nmi or BTas after virus infection, thereby activating type I interferon antiviral response (14). On the other hand, it also negatively regulate RIG-I-mediated antiviral signaling *via* K48-linked ubiquitination (15). Then, what role does IFI35 play in the local inflammatory microenvironment after tumor formation, pro-tumor or anti-tumor role, is worthy of our further study.

To date, in the field of tumor biology, only a few studies revealed that IFI35 promoted the radiosensitivity of lung adenocarcinoma and colorectal cancer (21, 22). Herein, we explored the positive correlation between IFI35 expression and M1 infiltration in TNBC from bioinformatics analysis. Since IFI35 is an interferon-inducible protein, and interferon can induce M1-subtype polarization of macrophages, we speculated that IFI35 is upregulated with M1 subtype differentiation of macrophages. From two levels of the cell line and tissue sections of TNBC, we confirmed this hypothesis (**Figure 8**). Given the anti-tumor function of M1 macrophages and the better prognosis of patients with high IFI35 expression (**Figures 6G, J**), it suggested that IFI35 plays a pro-inflammatory and anti-tumor role in the TIME. However, the exact role of IFI35 in macrophages requires further validation in knockout mice, which is the focus of our next study.

In summary, this study has uncovered the essential role of macrophages. For the first time, the link between IFI35 and M1 macrophages in TNBC was elucidated, and the anti-tumor role of IFI35 was confirmed. Thus, IFI35 may be a promising novel target that helps to reshape macrophage polarization for antitumor effects.

DATA AVAILABILITY STATEMENT

Publicly available datasets were analyzed in this study. This data can be found here: the raw data were obtained from publicly available datasets (European Genome-phenome Archive with the study ID EGAS00001005061, TCGA) and our FUSCC datasets have been uploaded to the National Omics Data Encyclopedia (OEP000155).

ETHICS STATEMENT

The studies involving human participants were reviewed and approved by the Ethics Committee of Fudan University Shanghai Cancer Center (050432-4-1805C). The patients/participants provided their written informed consent to participate in this study.

AUTHOR CONTRIBUTIONS

WJ and BX designed this project. BX, XS, and QL completed the relevant experiment. BX and XS completed the process of analysis. BX completed the draft. HS and WJ reviewed this manuscript. All authors contributed to the article and approved the submitted version.

FUNDING

This work was supported by the grant from National Natural Science Foundation of China (81972727).

ACKNOWLEDGMENTS

The analysis of single cell sequencing was supported by Bioinformatics platform of Institutes of biomedical sciences, Fudan university.

SUPPLEMENTARY MATERIAL

The Supplementary Material for this article can be found online at: https://www.frontiersin.org/articles/10.3389/fimmu.2022.923481/ full#supplementary-material

Supplementary Figure 1 | 12 cell clusters were annotated, which included multiple immune cell clusters, epithelial cells, stromal cells, endothelial cells, and tissue stern cells.

REFERENCES

- Bianchini G, De Angelis C, Licata L, Gianni L. Treatment Landscape of Triple-Negative Breast Cancer - Expanded Options, Evolving Needs. *Nat Rev Clin Oncol* (2022) 19:91–113. doi: 10.1038/s41571-021-00565-2
- Brahmer JR, Tykodi SS, Chow LQ, Hwu WJ, Topalian SL, Hwu P, et al. Safety and Activity of Anti-PD-L1 Antibody in Patients With Advanced Cancer. N Engl J Med (2012) 366:2455–65. doi: 10.1056/NEJMoa1200694
- DeNardo DG, Ruffell B. Macrophages as Regulators of Tumour Immunity and Immunotherapy. Nat Rev Immunol (2019) 19:369–82. doi: 10.1038/ s41577-019-0127-6
- Cassetta L, Pollard JW. Targeting Macrophages: Therapeutic Approaches in Cancer. Nat Rev Drug Discov (2018) 17:887–904. doi: 10.1038/nrd.2018.169
- Hezaveh K, Shinde RS, Klötgen A, Halaby MJ, Lamorte S, Ciudad MT, et al. Tryptophan-Derived Microbial Metabolites Activate the Aryl Hydrocarbon Receptor in Tumor-Associated Macrophages to Suppress Anti-Tumor Immunity. *Immunity* (2022) 55:324–40 e8. doi: 10.1016/j.immuni. 2022.01.006
- Ma C, He D, Tian P, Wang Y, He Y, Wu Q, et al. miR-182 Targeting Reprograms Tumor-Associated Macrophages and Limits Breast Cancer Progression. *Proc Natl Acad Sci USA* (2022) 119:e2114006119. doi: 10.1073/ pnas.2114006119
- Nishida-Aoki N, Gujral TS. Polypharmacologic Reprogramming of Tumor-Associated Macrophages Toward an Inflammatory Phenotype. *Cancer Res* (2022) 82:433–46. doi: 10.1158/0008-5472.CAN-21-1428
- Santoni M, Romagnoli E, Saladino T, Foghini L, Guarino S, Capponi M, et al. Triple Negative Breast Cancer: Key Role of Tumor-Associated Macrophages in Regulating the Activity of Anti-PD-1/PD-L1 Agents. *Biochim Biophys Acta Rev Cancer* (2018) 1869:78–84. doi: 10.1016/j.bbcan.2017.10.007
- Sami E, Paul BT, Koziol JA, ElShamy WM. The Immunosuppressive Microenvironment in BRCA1-IRIS-Overexpressing TNBC Tumors Is Induced by Bidirectional Interaction With Tumor-Associated Macrophages. *Cancer Res* (2020) 80:1102–17. doi: 10.1158/0008-5472.CAN-19-2374
- Wang X, Tokheim C, Gu SS, Wang B, Tang Q, Li Y, et al. In Vivo CRISPR Screens Identify The E3 Ligase Cop1 as A Modulator of Macrophage Infiltration and Cancer Immunotherapy Target. *Cell* (2021) 184:5357– 74.e22. doi: 10.1016/j.cell.2021.09.006
- Ashraf Y, Mansouri H, Laurent-Matha V, Alcaraz LB, Roger P, Guiu S, et al. Immunotherapy of Triple-Negative Breast Cancer With Cathepsin D-Targeting Antibodies. J Immunother Cancer (2019) 7:29. doi: 10.1186/ s40425-019-0498-z
- Bange FC, Vogel U, Flohr T, Kiekenbeck M, Denecke B, Böttger EC. IFP 35 is an Interferon-Induced Leucine Zipper Protein That Undergoes Interferon-Regulated Cellular Redistribution. J Biol Chem (1994) 269:1091–8. doi: 10.1016/S0021-9258(17)42225-3
- Meyerdierks A, Denecke B, Rohde M, Taparowsky EJ, Böttger EC. A Cytoplasmic Structure Resembling Large Protein Aggregates Induced by Interferons. J Histochem Cytochem (1999) 47:169–82. doi: 10.1177/ 002215549904700206
- 14. Tan J, Qiao W, Wang J, Xu F, Li Y, Zhou J, et al. IFP35 Is Involved in the Antiviral Function of Interferon by Association With the Viral Tas Transactivator of Bovine Foamy Virus. J Virol (2008) 82:4275–83. doi: 10.1128/JVI.02249-07
- Yang H, Winkler W, Wu X. Interferon Inducer IFI35 Regulates RIG-I-Mediated Innate Antiviral Response Through Mutual Antagonism With Influenza Protein NS1. J Virol (2021) 95:e00283-21. doi: 10.1128/ JVI.00283-21

Supplementary Figure 2 | Survival analysis of immune cell subsets related to patients' prognosis. Cohorts, FUSCC (A) and TCGA (B).

Supplementary Figure 3 | The differentiation of mutational landscape between low and high M1 macrophage infiltration groups from TCGA cohort. (A, B), Top20 mutational genes in M1 macrophage low and high infiltration population. (C, D), The overlap of mutations in two groups. (E), Different mutations between two groups. (F, G), Mutually exclusive or co-occurring mutation in two groups were explored separately.

- Zhou P, Ma L, Rao Z, Li Y, Zheng H, He Q, et al. Duck Tembusu Virus Infection Promotes the Expression of Duck Interferon-Induced Protein 35 to Counteract RIG-I Antiviral Signaling in Duck Embryo Fibroblasts. Front Immunol (2021) 12:711517. doi: 10.3389/fimmu.2021.711517
- Xiahou Z, Wang X, Shen J, Zhu X, Xu F, Hu R, et al. NMI and IFP35 Serve as Proinflammatory DAMPs During Cellular Infection and Injury. *Nat Commun* (2017) 8:950. doi: 10.1038/s41467-017-00930-9
- Jing X, Yao Y, Wu D, Hong H, Feng X, Xu N, et al. IFP35 Family Proteins Promote Neuroinflammation and Multiple Sclerosis. Proc Natl Acad Sci USA (2021) 118:e2102642118. doi: 10.1073/pnas.2102642118
- Zhang LH, Jiang SZ, Guo X, Xiao B, Li Q, Chen JY, et al. MiR-146b-5p Targets IFI35 to Inhibit Inflammatory Response and Apoptosis via JAK1/STAT1 Signalling in Lipopolysaccharide-Induced Glomerular Cells. Autoimmunity (2021) 54:430–8. doi: 10.1080/08916934.2020.1864730
- Yu Y, Xu N, Cheng Q, Deng F, Liu M, Zhu A, et al. IFP35 as a Promising Biomarker and Therapeutic Target for the Syndromes Induced by SARS-CoV-2 or Influenza Virus. *Cell Rep* (2021) 37:110126. doi: 10.1016/ j.celrep.2021.110126
- Wang J, Han Q, Liu H, Luo H, Li L, Liu A, et al. Identification of Radiotherapy-Associated Genes in Lung Adenocarcinoma by an Integrated Bioinformatics Analysis Approach. *Front Mol Biosci* (2021) 8:624575. doi: 10.3389/fmolb.2021.624575
- Hu Y, Wang B, Yi K, Lei Q, Wang G, Xu X. IFI35 is Involved in the Regulation of the Radiosensitivity of Colorectal Cancer Cells. *Cancer Cell Int* (2021) 21:290. doi: 10.1186/s12935-021-01997-7
- 23. Jiang YZ, Ma D, Suo C, Shi J, Xue M, Hu X, et al. Genomic and Transcriptomic Landscape of Triple-Negative Breast Cancers: Subtypes and Treatment Strategies. *Cancer Cell* (2019) 35:428–40 e5. doi: 10.1016/ j.ccell.2019.02.001
- 24. Wu SZ, Roden DL, Wang C, Holliday H, Harvey K, Cazet AS, et al. Stromal Cell Diversity Associated With Immune Evasion in Human Triple-Negative Breast Cancer. *EMBO J* (2020) 39:e104063. doi: 10.15252/embj.2019104063
- Hao Y, Hao S, Andersen-Nissen E, Mauck WM3rd, Zheng S, Butler A, et al. Integrated Analysis of Multimodal Single-Cell Data. *Cell* (2021) 184:3573–87 e29. doi: 10.1016/j.cell.2021.04.048
- Aran D, Looney AP, Liu L, Wu E, Fong V, Hsu A, et al. Reference-Based Analysis of Lung Single-Cell Sequencing Reveals a Transitional Profibrotic Macrophage. *Nat Immunol* (2019) 20:163–72. doi: 10.1038/s41590-018-0276-y
- Qiu X, Mao Q, Tang Y, Wang L, Chawla R, Pliner HA, et al. Reversed Graph Embedding Resolves Complex Single-Cell Trajectories. *Nat Methods* (2017) 14:979–82. doi: 10.1038/nmeth.4402
- Newman AM, Steen CB, Liu CL, Gentles AJ, Chaudhuri AA, Scherer F, et al. Determining Cell Type Abundance and Expression From Bulk Tissues With Digital Cytometry. *Nat Biotechnol* (2019) 37:773–82. doi: 10.1038/s41587-019-0114-2
- Mayakonda A, Lin DC, Assenov Y, Plass C, Koeffler HP. Maftools: Efficient and Comprehensive Analysis of Somatic Variants in Cancer. *Genome Res* (2018) 28:1747–56. doi: 10.1101/gr.239244.118
- Langfelder P, Horvath S. WGCNA: An R Package for Weighted Correlation Network Analysis. BMC Bioinf (2008) 9:559. doi: 10.1186/ 1471-2105-9-559
- Waldschmidt JM, Kloeber JA, Anand P, Frede J, Kokkalis A, Dimitrova V, et al. Single-Cell Profiling Reveals Metabolic Reprogramming as a Resistance Mechanism in BRAF-Mutated Multiple Myeloma. *Clin Cancer Res* (2021) 27:6432–44. doi: 10.1158/1078-0432.CCR-21-2040

- Xue J, Schmidt SV, Sander J, Draffehn A, Krebs W, Quester I, et al. Transcriptome-Based Network Analysis Reveals a Spectrum Model of Human Macrophage Activation. *Immunity* (2014) 40:274–88. doi: 10.1016/ j.immuni.2014.01.006
- Beyer M, Mallmann MR, Xue J, Staratschek-Jox A, Vorholt D, Krebs W, et al. High-Resolution Transcriptome of Human Macrophages. *PloS One* (2012) 7: e45466. doi: 10.1371/journal.pone.0045466
- 34. Kraehenbuehl L, Weng CH, Eghbali S, Wolchok JD, Merghoub T. Enhancing Immunotherapy in Cancer by Targeting Emerging Immunomodulatory Pathways. Nat Rev Clin Oncol (2022) 19:37–50. doi: 10.1038/s41571-021-00552-7
- Pathria P, Louis TL, Varner JA. Targeting Tumor-Associated Macrophages in Cancer. Trends Immunol (2019) 40:310-27. doi: 10.1016/j.it.2019.02.003
- Anderson NR, Minutolo NG, Gill S, Klichinsky M. Macrophage-Based Approaches for Cancer Immunotherapy. *Cancer Res* (2021) 81:1201–8. doi: 10.1158/0008-5472.CAN-20-2990
- Güç E, Pollard JW. Redefining Macrophage and Neutrophil Biology in the Metastatic Cascade. *Immunity* (2021) 54:885–902. doi: 10.1016/ j.immuni.2021.03.022
- Bennett SR, Carbone FR, Karamalis F, Flavell RA, Miller JF, Heath WR. Help for Cytotoxic-T-Cell Responses is Mediated by CD40 Signalling. *Nature* (1998) 393:478–80. doi: 10.1038/30996

- Advani R, Flinn I, Popplewell L, Forero A, Bartlett NL, Ghosh N, et al. CD47 Blockade by Hu5F9-G4 and Rituximab in Non-Hodgkin's Lymphoma. N Engl J Med (2018) 379:1711–21. doi: 10.1056/NEJMoa1807315
- La Fleur L, Botling J, He F, Pelicano C, Zhou C, He C, et al. Targeting MARCO and IL37R on Immunosuppressive Macrophages in Lung Cancer Blocks Regulatory T Cells and Supports Cytotoxic Lymphocyte Function. *Cancer Res* (2021) 81:956–67. doi: 10.1158/0008-5472.CAN-20-1885

Conflict of Interest: The authors declare that they have no competing interests.

Publisher's Note: All claims expressed in this article are solely those of the authors and do not necessarily represent those of their affiliated organizations, or those of the publisher, the editors and the reviewers. Any product that may be evaluated in this article, or claim that may be made by its manufacturer, is not guaranteed or endorsed by the publisher.

Copyright © 2022 Xu, Sun, Song, Liu and Jin. This is an open-access article distributed under the terms of the Creative Commons Attribution License (CC BY). The use, distribution or reproduction in other forums is permitted, provided the original author(s) and the copyright owner(s) are credited and that the original publication in this journal is cited, in accordance with accepted academic practice. No use, distribution or reproduction is permitted which does not comply with these terms.

491



Pan-Cancer and Single-Cell Analysis Reveals CENPL as a Cancer Prognosis and Immune Infiltration-Related Biomarker

Ziyang Feng^{1,2}, Yu Chen¹, Changjing Cai^{1,2}, Jun Tan³, Ping Liu^{1,2}, Yihong Chen^{1,2}, Hong Shen^{1,2,4}, Shan Zeng^{1,2*} and Ying Han^{1,2*}

¹ Department of Oncology, Xiangya Hospital, Central South University, Changsha, China, ² Key Laboratory for Molecular Radiation Oncology of Hunan Province, Xiangya Hospital, Central South University, Changsha, China, ³ Department of Neurosurgery, Xiangya Hospital, Central South University, Changsha, China, ⁴ National Clinical Research Center for Geriatric Disorders, Xiangya Hospital, Central South University, Changsha, China

OPEN ACCESS

Edited by: Xuyao Zhang, Fudan University, China

Reviewed by:

Changwu Wu, Leipzig University, Germany Yuewen Gong, University of Manitoba. Canada

*Correspondence:

Shan Zeng zengshan2000@csu.edu.cn Ying Han yinghan@csu.edu.cn

Specialty section:

This article was submitted to Cancer Immunity and Immunotherapy, a section of the journal Frontiers in Immunology

Received: 09 April 2022 Accepted: 24 May 2022 Published: 30 June 2022

Citation:

Feng Z, Chen Y, Cai C, Tan J, Liu P, Chen Y, Shen H, Zeng S and Han Y (2022) Pan-Cancer and Single-Cell Analysis Reveals CENPL as a Cancer Prognosis and Immune Infiltration-Related Biomarker. Front. Immunol. 13:916594. doi: 10.3389/fimmu.2022.916594 **Background:** Centromere protein L (CENPL) is an important member of the centromere protein (CENP) family. However, the correlation between CENPL expression and cancer development and immune infiltration has rarely been studied. Here, we studied the role of CENPL in pan-cancer and further verified the results in lung adenocarcinoma (LUAD) through *in vitro* experiments.

Methods: The CENPL expression level was studied with TIMER 2.0 and Oncomine databases. The potential value of CENPL as a diagnostic and prognostic biomarker in pan-cancer was evaluated with the TCGA database and GEPIA. The CENPL mutation character was analyzed using the cBioPortal database. The LinkedOmics and CancerSEA databases were used to carry out the function analysis of CENPL. The role of CENPL in immune infiltration was studied using the TIMER and TISIDB websites. Moreover, the expression of CENPL was detected through RT-qPCR and Western blotting. Immunohistochemistry was used to evaluate the infiltration level of CD8⁺ T cells. Cell proliferation was detected by EdU and CCK8. A flow cytometer was used to analyze the influence of CENPL in cell cycle and apoptosis.

Results: CENPL was increased in most of the cancers. The upregulation and mutation of CENPL were associated with a poorer prognosis in many cancers. The results showed a significant positive correlation between CENPL and myeloid-derived suppressor cell (MDSC) infiltration and a negative correlation between CENPL and T-cell NK infiltration in most of the cancers. CENPL regulated cell proliferation and cell cycle, and was negatively correlated with the inflammation level of LUAD. The *in vitro* experiments suggested that CENPL was increased in LUAD tissue and cell lines. There was a negative correlation between CENPL expression and CD8⁺ T-cell infiltration. The knockdown of CENPL significantly suppressed the expression of CDK2 and CCNE2, and induced G0/G1 arrest and apoptosis of LUAD.

Conclusions: CENPL may function as a potential biomarker and oncogene in pancancer, especially LUAD. Furthermore, CENPL was associated with immune cell infiltration in pan-cancer, providing a potential immune therapy target for tumor treatment.

Keywords: pan-cancer, CENPL, immune infiltration, LUAD, G0/G1 arrest, apoptosis

INTRODUCTION

Nowadays, cancer has become a major threat to public health. Although huge improvements have been made in cancer treatment, including immunotherapy, target therapy, and radiotherapy, patients' 5-year overall survival (OS) remains unsatisfactory (1). In recent years, immunotherapy has made huge success in cancer treatment. For example, the immune checkpoint inhibitor has achieved great success in the clinic (2–4). Moreover, with the rapid development of the TCGA database and the GEO database, it is more convenient to further analyze the correlation and impact of a single gene on cancer prognosis and immune infiltration. Thus, it is necessary to find a novel diagnostic and prognostic biomarker for cancer. Furthermore, the huge success of immunotherapy makes the immune-related biomarker even more important.

Centromere protein L (CENPL) is a member of the centromere protein (CENP) family and plays significant roles in mediating cell division (5, 6). CENPs are important members of the centromere and kinetochore, which determine the separation of chromosomes during mitosis and meiosis. Many CENPs have been currently identified, including CENPA, CENPH, CENPI, and CENPU (7– 11). Among them, CENPA plays a significant role in cancer. For example, the upregulation of the CENPA/Myc/Bcl2 axis significantly enhances the sensitivity of retinoblastoma cells to cisplatin (12). Furthermore, CENPA may function as a prognostic biomarker in lung adenocarcinoma (LUAD) (13). However, the role of CENPL in cancer remains fragmentary.

Thus, we conducted a comprehensive analysis and assessed the potential value of CENPL in cancer diagnosis and prognosis. Moreover, we also performed enrichment analysis of CENPL coexpression genes and studied its association with immune infiltration. Furthermore, we verified our bioinformatics results through *in vitro* experiments. All in all, our results show that CENPL can function as an oncogene and immune infiltrationrelated biomarker in pan-cancer, especially LUAD.

MATERIALS AND METHODS

Data Collection

TCGA transcriptome RNA-seq data were downloaded using the Broad Institute platform (https://gdac.broadinstitute.org/).

Analysis of CENPL mRNA Expression

The Oncomine database (oncomine.org) and the TIMER 2.0 database (timer.cistrome.org) were used to evaluate the mRNA expression level of CENPL. At first, we searched "CENPL" in the Oncomine database, and the p-values < 0.05 and folding change < 1.5 were considered significant. Next, in the TIMER 2.0

database, the "Gene_DE" module was used to analyze the mRNA expression level of CENPL. The association between CENPL and cancer stage was analyzed with the "Stage plots" module of GEPIA (gepia2.cancer-pku.cn/#index).

Diagnostic and Prognostic Analysis

The potential value of CENPL in cancer diagnosis was detected with ROC curve with the data from the TCGA database. AUC > 0.85 was thought as a high diagnostic value. The potential value of CENPL in cancer prognosis was analyzed via OS and disease-free survival (DFS) from the GEPIA database.

Mutation Character Analysis

The mutation character of CENPL in different cancers was analyzed with the cBioPortal tool (http://www.cbioportal.org/). "TCGA Pan Cancer Atlas Studies" was selected as the cohort. Then, we entered "CENPL" in the "Query" module. CENPL alteration sites, types, and numbers can be found in the "cancer type summary" and "mutation" module. The correlation between CENPL mutation and the clinical prognosis was obtained from the "comparison/survival" module.

The Function and Enrichment Analysis

Gene co-expression analysis of CENPL was performed using LinkedOmics (www.linkedomics.org/login.php). The "HiSeq RNA" platform and "TCGA_LUAD" cohort were selected for the analysis. Pearson test was used to detect the correlation between CENPL and the co-expression genes.

The correlation between CENPL and 14 cancer functional states was analyzed using single-cell sequence data from the "correlation plot" module of the CancerSEA website (biocc. hrbmu.edu.cn/CancerSEA/home.jsp).

Immune Infiltration Analysis

The "GENE" module of the TIMER database was used to evaluate the infiltration level of immune cells in 32 cancer types. TISIDB (cis.hku.hk/TISIDB/index.php) was used to analyze the correlation between CENPL and major histocompatibility complexes (MHCs) and chemokine receptors.

Cell Culture

Beas2B (normal pulmonary epithelial cell), PC9, H1975, A549, and H1437 (human lung cancer cell lines) were derived from the Institutes of Biomedical Sciences. Cells were cultured at 37°C with 10% FBS and 1% penicillin/streptomycin in RPMI-1640.

Specimen Collection

LUAD tissues were collected from Xiangya Hospital. The specimen was stored at -80° C immediately after the surgery. All the patients received a LUAD diagnosis with the results of the

histopathological examination. The studies were approved by Ethics Committees of Xiangya Hospital. The patients' clinicopathological information can be found in **Table 1**.

Real-Time Quantitative PCR

The RNA was separated with Trizol reagent, and PrimeScriptTM Kit was used to perform the reverse transcription. SYBR Green assay was used to carry out the RT-qPCR reaction. The primers were as

follows: CENPL: F: CTGGCTGGTTCTGCTGTGTA; R: GGCA GCCATCCAGGAAAGAT. GAPDH: F: TGTGGGCATCAA TGGATTTGG; R: ACACCATGTATTCCGGGTCAAT. 2–ΔΔCt values were calculated to perform the quantitative analysis.

Western Blotting

The total protein was extracted using RIPA buffer with phosphatase inhibitor and protease inhibitor. After separating

Patient Aae Gender History History Location Differentiaion T classifica-N classifica-M classifica-TNM Living status **CENPL** rela-NO. (**y**) of of in lung tion tion tion stage and time tive expressmokina alcohol (days) sion 1 60 Female No Right Moderately 2 0 IIIA Living/2024 2.757631102 No 1a upper 2 55 Male 0 0 IA Living/1759 2.697716191 No Right Poorly 1 No upper 3 66 Male Yes No Right Poorly 1b 0 0 IA Living/1457 0.244443329 lower 4 41 Female No No Left lower Well 2a 0 0 IA Living/1291 0.11338954 5 67 Male Yes No Right 2 2 0 IIIA Dead/1266 0.121970052 upper 6 65 Male Yes No Left upper Poorly 2a 0 0 IA Living/1268 2.671662348 7 60 Male Yes No Left upper Moderately 2 2 0 IIIA Dead/748 0.625218754 8 59 Female Left upper 2 0 0 IΒ Living/1126 0.650366834 Well 9 58 Female No No Right 1b 2 0 IIIA Living/1643 4.910346156 upper 10 53 Male Yes 2c 0 0 IIA Dead/615 0.789007838 Yes Right Poorly lower 0 0 11 69 Male Yes Yes Right Poorly 3 IIB Living/1285 0.135412198 upper 12 Well-2 0 7.193870084 63 Male Yes Yes Right 1c IIIA Living/1399 upper Moderately 13 36 Male No Left upper 2 0 IIIA Living/1338 0.152539373 No 1c / 14 45 Female No Right / 0 0 1 IV Living/62 3.995745298 lower 2 0 IIIA 15 61 Male Yes Right Dead/1491 0.088769722 No Poorly 1 lower 53 2 0 0 IR Living/1674 16 Male Yes Left lower Moderately 6.459017468 17 53 Male Yes Left upper Moderately-2 0 IIIA Living/409 2.946329291 No 1b Poorly 18 66 Male Yes Left upper 2 0 0 IR Dead/1113 Yes 0.732881534 1 19 73 Male Yes Yes Right Poorly 1 0 0 IA Living/1552 1.334120069 upper 0 0 Living/1491 20 60 Male Yes No Left lower Well-1 IA 0.908902748 Moderately 21 59 Male / No Left upper Moderately-2 0 0 IΒ Dead/1583 2.164688313 Poorly 22 35 Female No No Right Well 4 2 0 IIIB Living/891 0.357811515 lower 23 74 Male Yes Yes Right Moderately-4 0 0 IIIA Living/335 0.618514161 lower Poorly 24 58 Female / No Right Moderately 2 0 0 IΒ Living/624 1.528012423 upper 25 52 Male Right Poorly 2 0 IIIA Dead/1552 0.023937207 Yes No 1 lower 26 60 Male Right 0 0 IA Living/1430 0.14419824 No Yes Moderately 1 upper 27 32 Female No No Left lower Moderately 3 3 0 IIIC Dead/1399 0.016709341 28 42 Male Moderately-0 0 IA Dead/1369 11.53368936 Yes Yes Right 1 upper Poorly 29 60 Female No Yes Right Poorly 2 2 0 IIIA Living/1004 1.344631759 lower

TABLE 1 | Clinicopathological parameters of LUAD cohort in Xiangya Hospital.

by SDS-PAGE, the protein was transferred onto polyvinylidene fluoride membranes under 250 mA for 100 min. Five percent skim milk was used to block the membrane. Next, the membrane was incubated with primary antibodies at 4°C for 12 h. Subsequently, the membrane was incubated with the secondary antibody at 37°C for 60 min. After washing 3 times with TBST, the signal was detected using the ChemiDocXRS+ System. Finally, Image Lab software was used for the quantitative analysis of protein.

Immunohistochemistry Procedure

Tumor tissue sections were deparaffinized using xylene and rehydrated with ethanol. Next, these sections were boiled by microwaving with citrate for 10 min. After eliminating endogenous peroxidase activity with 3% H2O2, the slides were incubated with anti-CD8 antibody (ab101500, Abcam) at 1:100 overnight at 4°C. Next, the slides were incubated using secondary antibody at 25°C for 60 min. After staining with DAB and hematoxylin, the CD8+ T cells were calculated using a microscope.

Cell Proliferation Assays

A total of 4,000 cells were seeded into 96-well plates. Subsequently, 10 μ l of the CCK-8 was mixed to every well. The absorbance at 450 nm was measured after 2.5 h.

EdU Assay

A total of 3,000 cells were seeded into 96-well plates. Next, the cells were maintained with 20 μ M EdU for 3 h and fixed with 4% paraformaldehyde. Subsequently, the cells were treated with 100 μ l of Apollo solution for 30 min. After washing with 0.5% Triton X-100 and staining with DAPI solution, the image was captured with a microscope.

Cell Cycle Test

A total of 100,000 cells were seeded in each well of 6-well plates. The cells were collected and treated with 1 ml of DNA Staining solution and 10 μ l of Permeabilization solution for 30 min. Subsequently, the sample was detected using a flow cytometer right away.

Apoptosis Test

A total of 100,000 cells were seeded into 6-well plates. Next, the cells were collected (including the cells in medium) and treated with 5 μ l of Annexin V-APC and 10 μ l of 7-AAD for 5 min. Subsequently, the sample was detected using a flow cytometer right away.

Statistical Analysis

The differences among groups were detected using t-test. The correlation analysis was evaluated with Spearman's test. The analysis was performed with SPSS 17.0 and p-value < 0.05 was considered significant.

RESULTS

CENPL Was Upregulated in Multiple Human Cancers

At first, Oncomine was used to study the expression level of CENPL. The results obtained show that CENPL was upregulated in breast cancer, lung cancer, colorectal cancer, gastric cancer, liver cancer, cervical cancer, and ovarian cancer (Figure 1A). By contrast, CENPL was downregulated in the brain and CNS cancer and leukemia (Figure 1A). To further explore the expression level of CENPL, we analyzed CENPL expression in the TCGA datasets using the TIMER 2.0 database. The results obtained show that CENPL was upregulated in most of the cancers (Figure 1B), including bladder urothelial carcinoma (BLCA), breast invasive cancer (BRCA), cervical and endocervical cancer (CESC), cholangiocarcinoma (CHOL), colon adenocarcinoma (COAD), esophageal carcinoma (ESCA), glioblastoma multiforme (GBM), head and neck squamous cell carcinoma (HNSC), kidney renal clear cell carcinoma (KIRC), liver hepatocellular carcinoma (LIHC), lung adenocarcinoma (LUAD), lung squamous cell carcinoma (LUSC), stomach adenocarcinoma (STAD), and uterine corpus endometrial carcinoma (UCEC). CENPL was upregulated in metastatic tumor of skin cutaneous melanoma compared with primary tumor. However, CENPL was downregulated in thyroid carcinoma (THCA).

Next, we analyzed the association between CENPL and the stages of pan-cancers in the GEPIA2 website. CENPL was associated with the stage of kidney renal papillary cell carcinoma (KIRP), adrenocortical carcinoma (ACC), LIHC, kidney chromophobe (KICH), LUAD, and testicular germ cell tumors (TGCT) (**Figures 1C-H**).

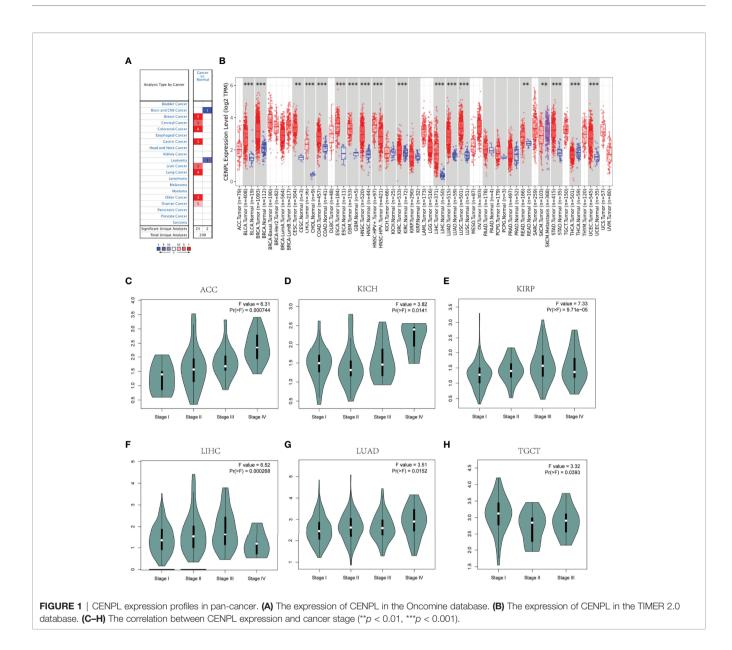
The Diagnostic and Prognostic Value of CENPL in Pan-Cancer

Then we analyzed the diagnostic value of CENPL in various cancers using the ROC curve. As shown in **Figures 2A–M**, CENPL may act as a perfect diagnostic marker in BLCA (AUC = 0.914), BRCA (AUC = 0.955), CAOD (AUC = 0.858), ESCA (AUC = 0.975), GBM (AUC = 0.999), glioma (GBMLGG; AUC = 0.887), HNSC (AUC = 0.922), LIHC (AUC = 0.952), LUAD (AUC = 0.952), LUSC (AUC = 0.993), STAD (AUC = 0.921), stomach and esophageal carcinoma (STES; AUC = 0.938), and UCEC (AUC = 0.968).

Furthermore, increased expression of CENPL was linked to poor OS in LGG (p = 5.4e-07), ACC (p = 3e-06), MESO (p = 0.00025), PAAD (p = 00049), LIHC (p = 0.0024), and LUAD (p = 0.009) (**Figures 3A–F**). By contrast, increased expression of CENPL was linked to better OS in THYM (p = 0.0085) (**Figure 3G**). DFS results suggested that higher CENPL expression was correlated with poorer prognosis in LGG (p = 7.5e-06), ACC (p = 0.00011), PAAD (p = 0.0017), LUAD (p = 0.0088), BLCA (p = 0.019), and KICH (p = 0.029) (**Figures 3H–M**).

The Characteristics of CENPL Mutations in the TCGA Pan-Cancer Cohort

Next, we analyzed the CENPL alteration status of the TCGA cohorts. As shown in **Figure 4A**, there were 42 kinds of cancers

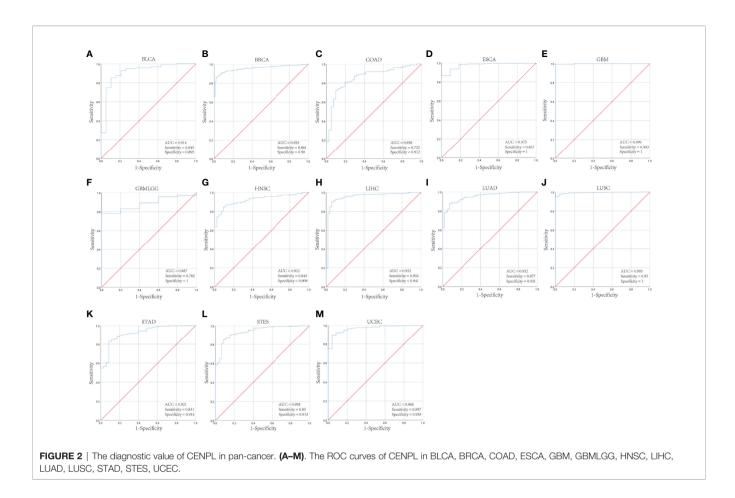


with CENPL alteration and uterine mixed endometrial carcinoma had the highest frequency of 14.29%. The CENPL alteration sites, types, and numbers are further presented in **Figure 4B**. Then, we further analyzed the correlation between CENPL mutation and the clinical prognosis. The data of **Figures 4C-F** suggested that patients that had breast invasive carcinoma with CENPL mutation had worse prognosis in DFS (p = 0.0334), DSS (p =3.717e-3), and PFS (p = 7.430e-3), but not OS (p = 0.0693).

CENPL Is Related to Immune Infiltration in Pan-Cancer

TIMER 2.0 was used to explore the potential role of CENPL in immune cell infiltration. The results suggested a significant positive correlation between myeloid-derived suppressor cell (MDSC) infiltration level and CENPL expression in most of the tumors (**Figure 5A**); the top 6 tumors were ACC (rho =

0.736, p = 1.16e-13), LIHC (rho = 0.626, p = 6.67e-39), MESO (rho = 0.573, p = 9.80e-09), UCEC (rho = 0.559, p = 1.74e-25), LUAD (rho = 0.545, p = 2.00e-39), and ESCA (rho = 0.45, p = 2.36e-10) (Figure 5B). Interestingly, the results suggested a negative association between the infiltration level of T-cell NK and CENPL expression in most of the tumors (Figure 5C); the top 6 tumors were UVM (rho = -0.724, p = 1.02e-13), PRAD (rho = -0.451, p = 3.14e-22), THYM (rho = -0.432, p = 1.42e-06), BRCA-Basal (rho = -0.372, p = 4.23e-07), DLBC (rho = -0.372, p = 1.66e-02), and SKCM-Primary (rho = -0.372, p = 1.18e-04) (Figure 5D). Finally, we studied the role of CENPL in immune cell infiltration of LUAD. There was a negative association between CENPL and the infiltration level of B cells (rho = -0.128, p = 4.41e-03), CD4+ T cells (rho = -0.092, p = -0.092)4.03e-02), CD8+ T cells (rho = -0.162, p = 3.07e-04), and T-cell NK (rho = -0.227, p = 3.48e-07) (Figure 5E).



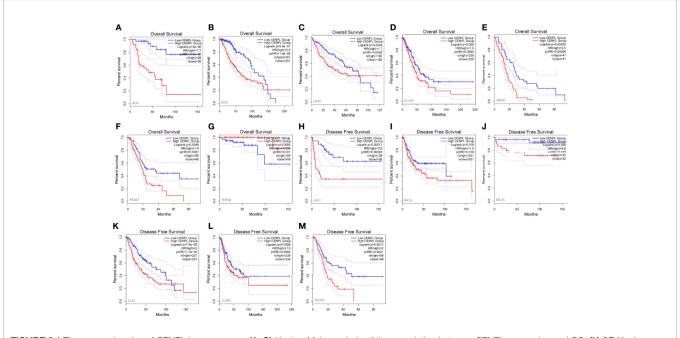
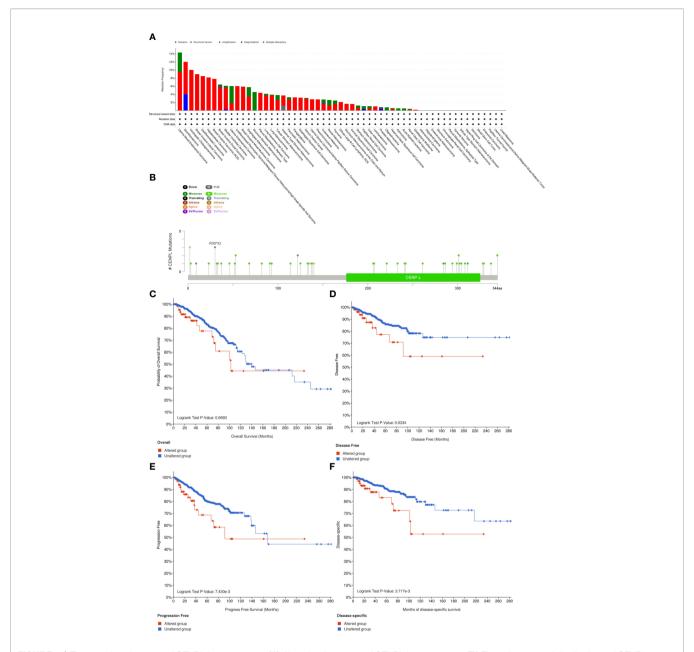
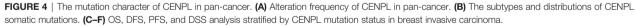


FIGURE 3 | The prognosis value of CENPL in pan-cancer. (A–G) Kaplan–Meier analysis of the association between CENPL expression and OS. (H–M) Kaplan–Meier analysis of the association between CENPL expression and DFS.





Next, we further analyzed the association between CENPL and MHCs and chemokine receptors in the TISIDB database. Our results suggested that the CENPL expression is negatively associated with most of the MHCs (**Figure 6A**). As for LUAD, the top 6 MHCs were HLA-MA (rho = -0.346, p = 6.76e-16), HLA-DOA (rho = -0.343, p = 1.27e-15), HLA-DPB1 (rho = -0.317, p = 1.94e-13), HLA-DQB1 (rho = -0.298, p = 5.46e-12), HLA-DRB1 (rho = -0.298, p = 2.48e-11), and HLA-DPA1 (rho = -0.252, p = 7.42e-09). **Figure 6B** shows the correlations between CENPL expression and 18 kinds of chemokine receptors. The results suggested that CENPL was negatively associated with

many chemokine receptors in LUAD; the top 6 were CX3CR1 (rho = -0.417, p < 2.2e-16), CCR (rho = -0.398, p < 2.2e-16), CXCR5 (rho = -0.246, p = 1.69e-08), CCR7 (rho = -0.311, p = 5.71e-13), CCR4 (rho = -0.217, p = 6.86e-07), and CXCR2 (rho = -0.194, p = 9.75e-06).

The Function Analysis of CENPL in LUAD

Then, we chose LUAD to further explore CENPL's biological function in LinkedOmics database. **Figure 7A** suggests the positively and negatively related genes with CENPL. The top 50 genes are shown in **Figures 7B, C**. Moreover, GO analysis

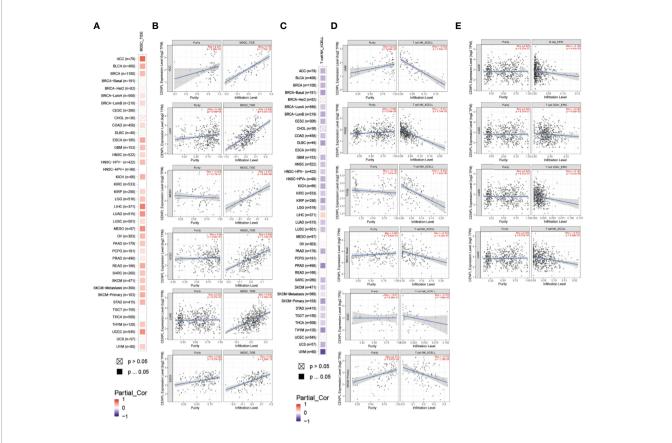


FIGURE 5 | The association between CENPL expression and immune cell infiltration. (A, B) CENPL expression is positively associated with MDSC infiltration in pancancer. (C, D) CENPL expression is negatively associated with NKT cell infiltration in pan-cancer. (E) CENPL expression is negatively associated with the infiltration level of B cells, CD4⁺ T cells, CD8⁺ T cells, and NKT cells.

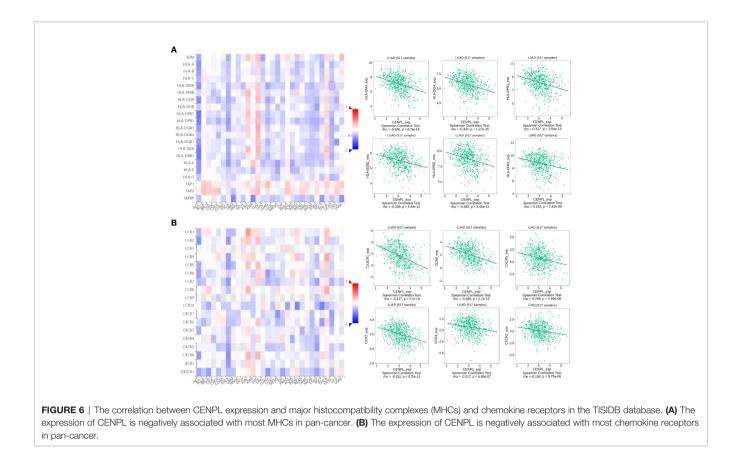
(Biological function) demonstrated that CENPL mainly joins in chromosome segregation, DNA replication, cell cycle checkpoint, DNA recombination, double-strand break repair, tRNA metabolic process, spindle organization, ribonucleoprotein complex biogenesis, etc. (**Figure 7D**). KEGG analysis illustrated enrichment in cell cycle, spliceosome, DNA replication, proteasome, RNA transport, ribosome, Fanconi anemia pathway, etc. (**Figure 7E**). Biological pathway analysis showed that CENPL may participate in cell cycle, mitotic, DNA replication, mitotic M-M/G1 phase, mitotic prometaphase, M phase, aurora B signaling, FOXM1 transcription factor network, G2/M checkpoints, G2/M DNA damage checkpoints, and cell cycle checkpoints (**Figure 7F**).

Next, we further analyzed the correlation between CENPL and 14 cancer functional states using single-cell sequence data of CancerSEA. CENPL was positively associated with cell cycle in most of the tumors (**Figure 8A**). Interestingly, CENPL was negatively associated with the inflammation status of most of the tumors, and LUAD was the top 1 (**Figure 8A**). As for LUAD, there is a significant positive correlation between CENPL expression and cell cycle (cor = 0.56), proliferation (cor = 0.56), DNA repair (cor = 0.55), and DNA damage (cor = 0.49), and a negative correlation with quiescence (cor = -0.43) and inflammation (cor = -0.4) (**Figure 8B–G**).

Knockdown of CENPL Induced Apoptosis and G0/G1 Arrest of LUAD

Next, we further confirm our bioinformatics results through *in vitro* experiments. CENPLs were significantly upregulated in LUAD tissues (**Figures 9A, E**) (C: cancer P: paracancerous non-cancer). Furthermore, CENPL was significantly upregulated in lung cancer cell lines as well (**Figures 9B, F**).

The biological pathway analysis in Figure 7 shows that CENPL was significantly correlated with the cell cycle in LUAD. Thus, we further detected the association between CENPL and CDK family, CDKI family, and Cyclin family expression in GEPIA2.0. The results obtained show that CENPL was positively associated with the expression of CCNA2 (R = 0.77), CCNB1 (R = 0.67), CCNB2 (R = 0.7), CCNE2 (R = 0.73), CCNF (R = 0.61), CDK1 (R = 0.67), CDK2 (R = 0.65), and CDKN3 (R = 0.72) (Figure 9H). Next, we designed 3 siRNA to knock down CENPL in A549 and H1437 cells. The knockdown efficiency is shown in Figures 9C, D, G. We found out that the knockdown of CENPL significantly decreased the expression of CDK1, CDK2, CCNA2, and CCNE2 at the mRNA level and decreased the expression of CDK2 and CCNE2 at the protein level (Figures 10A-D). Moreover, the results of immunohistochemistry indicated that CENPL was negatively



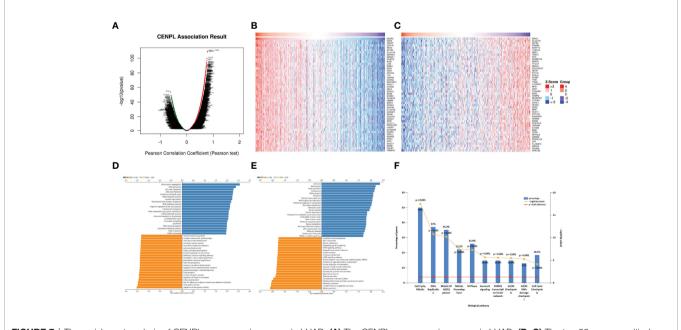
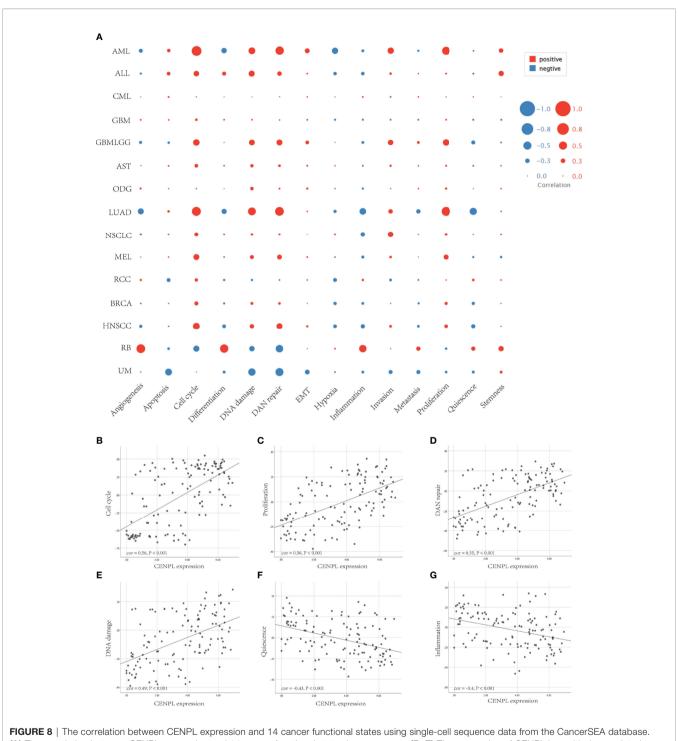


FIGURE 7 | The enrichment analysis of CENPL co-expression genes in LUAD. (A) The CENPL co-expression genes in LUAD. (B, C) The top 50 genes positively and negatively correlated to CENPL. (D, E) GO and KEGG analysis of CENPL co-expression genes in the LUAD cohort. (F) The biological pathway analysis of CENPL co-expression genes in the LUAD cohort.



(A) The correlation between CENPL expression and 14 cancer functional states using single-cell sequence data from the CancerSEA database. (A) The correlation between CENPL expression and 14 cancer functional states in pan-cancer. (B–E) The expression of CENPL is positively correlated to the cell cycle, proliferation, DNA repair, and DNA damage of LUAD. (F, G) The expression of CENPL is negatively correlated to the quiescence and inflammation of LUAD.

associated with the CD8+ T-cell infiltration (Figures 10E, F). Next, we further detected the influence of CENPL in cell proliferation, cell cycle, and apoptosis. The results of EdU (Figures 11A, B) and CCK8 (Figures 11C, D) suggest that the knockdown of CENPL suppressed the proliferation of LUAD cells. The knockdown of CENPL significantly induced G0/G1 arrest (**Figures 11E–G**) and apoptosis (**Figures 11H–J**) of A549 and H1437 cells.

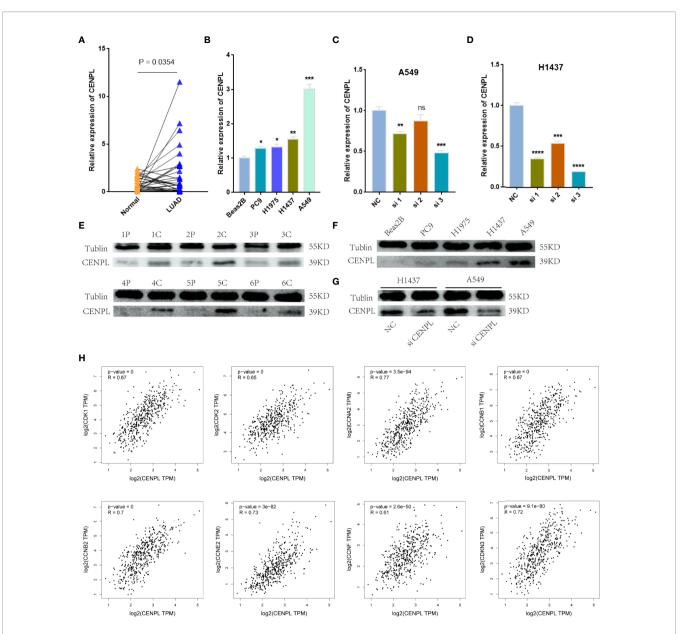
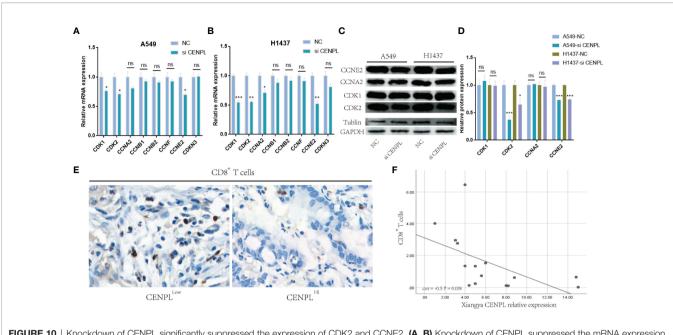
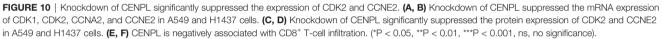


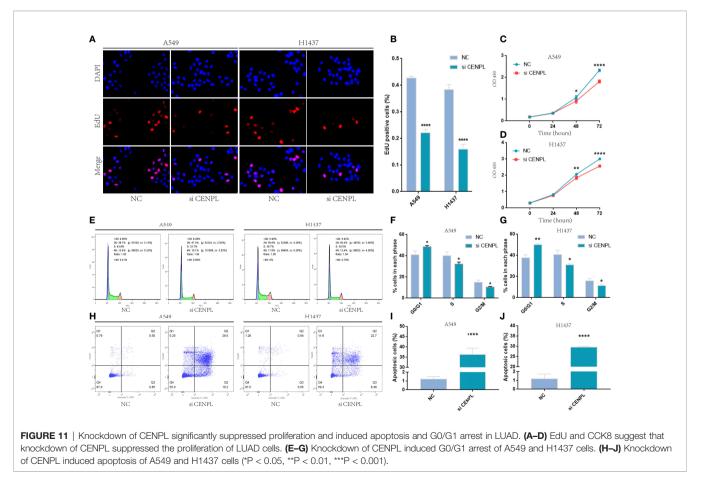
FIGURE 9 | Validation of CENPL expression. (**A**, **B**) CENPL mRNA expression in LUAD tissues and cell lines. (**C**, **D**) The knockdown efficiency of CENPL mRNA in A549 and H1437 cells. (**E**, **F**) CENPL protein expression in LUAD tissues and cell lines. (**G**) The knockdown efficiency of CENPL protein in A549 and H1437 cells. (**H**) The correlation between CENPL expression and CDK1, CDK2, CCNA2, CCNB1, CCNB2, CCNE2, CCNF, and CDKN3 in the GEPIA2.0 database (*p < 0.05, **p < 0.01, ***p < 0.001, ***p < 0.001, ms: no significance).

DISCUSSION

We found that CENPL was significantly upregulated and was correlated with the clinical stage in several cancers, and the ROC curve analysis showed that CENPL may function as a diagnostic biomarker. The prognostic analysis showed that increased CENPL was related to poorer OS in LGG, LIHC, LUAD, ACC, MESO, and PAAD. The mutation analysis showed that CENPL mutation was associated with worse OS, DFS, DSS, and PFS in breast invasive carcinoma. Among them, we found out that CENPL was significantly upregulated and correlated with the stage of LUAD. Thus, we chose LUAD to verify our bioinformatics result. In the *in vitro* experiments, CENPL was significantly upregulated in LUAD tissues and cell lines. In terms of the mechanism, the GO and KEGG analyses suggest that CENPL was correlated with cell cycle and DNA replication, and the single-cell sequence data also suggest that CENPL was positively associated with the proliferation, DNA damage, DNA repair, and cell cycle. Correlation analysis suggested a positive correlation between CENPL and CDK1, CDK2, CCNA2, CCNB1, CCNB2, CCNE2, CCNF, and CDKN3. Meanwhile, our *in vitro* experiments suggest that the knockdown of CENPL may







significantly suppress the proliferation abilities of A549 and H1437 cells, and induced G0/G1 arrest and apoptosis. Furthermore, CDK2 and CCNE2 were significantly downregulated after the knockdown of CENPL.

CDK2 is a member of the CDK family and plays significant roles in cell cycle and proliferation regulation (14, 15). Houguang Liu had reported that the knockout of CDK2 may induce G0/G1 arrest and apoptosis in melanocytes (16). Moreover, Jie Yang had also reported that the downregulation of CCNE2 significantly suppressed cell proliferation and induced G0/G1 arrest (17). Thus, our studies show that the knockdown of CENPL may significantly decrease the expression of CDK2 and CCNE2, and induce G0/G1 arrest and apoptosis of A549 and H1437 cells. CENPL may function as a potential biomarker and therapy target of LUAD.

Tumor microenvironment (TME) plays important roles in cancer recurrence and drug resistance (18-20). The immune cells of TME are associated with the effect of immunotherapy, including CD4+ T cells, CD8+ T cells, MDSCs, and NKT cells (21-26). Our results suggested a positive correlation between CENPL expression and MDSC infiltration and a negative correlation between CENPL and T-cell NK infiltration in most of the cancers. As for LUAD, the obtained results show that there was a negative association between CENPL and CD8+ T cells, CD4+ T cells, T-cell NK, B cells, and myeloid dendritic cell infiltration. Furthermore, the single-cell sequence data also suggest that CENPL was negatively correlated with the inflammation level of LUAD. Our in vitro experiments showed a negative correlation between CENPL and CD8+ T-cell infiltration in LUAD. Thus, CENPL is related to the infiltration level of immune cells and may function as a potential immune therapyrelated biomarker in LUAD.

However, some limitations still exist in our study. Although our results indicated that CENPL was associated with the immune cell infiltration of LUAD, the mechanisms are still unclear and further investigation is necessary.

CONCLUSION

CENPL may function as a potential biomarker and oncogene in pan-cancer, especially LUAD. Moreover, CENPL was associated

REFERENCES

- Siegel RL, Miller KD. Cancer Statistics, 2021. CA Cancer J Clin (2021) 71:7– 33. doi: 10.3322/caac.21654
- Forde PM, Chaft JE, Smith KN, Anagnostou V, Cottrell TR, Hellmann MD. Neoadjuvant PD-1 Blockade in Resectable Lung Cancer. N Engl J Med (2018) 378:1976–86. doi: 10.1056/NEJMoa1716078
- Herbst RS, Giaccone G, de Marinis F, Reinmuth N, Vergnenegre A, Barrios CH, et al. Atezolizumab for First-Line Treatment of PD-L1-Selected Patients With NSCLC. N Engl J Med (2020) 383:1328–39. doi: 10.1056/ NEJMoa1917346
- Gao J, Navai N, Alhalabi O. Neoadjuvant PD-L1 Plus CTLA-4 Blockade in Patients With Cisplatin-Ineligible Operable High-Risk Urothelial Carcinoma. *Nat Med* (2020) 26:1845–51. doi: 10.1038/s41591-020-1086-y
- Mellone BG, Zhang W, Karpen GH. Frodos Found: Behold the CENP-A "Ring" Bearers. Cell (2009) 137:409–12. doi: 10.1016/j.cell.2009.04.035

with immune cell infiltration in pan-cancer, providing a potential immune therapy target for tumor treatment.

DATA AVAILABILITY STATEMENT

The original contributions presented in the study are included in the article/supplementary material. Further inquiries can be directed to the corresponding authors.

ETHICS STATEMENT

The studies involving human participants were reviewed and approved by Ethics Committees of the Xiangya Hospital. The patients/participants provided their written informed consent to participate in this study.

AUTHOR CONTRIBUTIONS

SZ and YH designed this study. ZF performed the experiments and drafted the manuscript. SZ, HS, and YH supervised the study. YC, CC, JT, PL, and YHC collected the clinical samples. All authors contributed to the article and approved the submitted version.

FUNDING

This study was supported by grants from the National Key R & D Program of China (No. 2018YFC1313300), the National Natural Science Foundation of China (Nos. 81372629, 81772627, 81874073, 81974384, and 82173342), key projects from the Nature Science Foundation of Hunan Province (Nos. 2021JJ31092 and 2021JJ31048), projects from Beijing CSCO Clinical Oncology Research Foundation (Nos. Y-HR2019-0182 and Y-2019Genecast-043), and the Fundamental Research Funds of Central South University (2020zzts273 and 2019zzts797).

- Srivastava S, Foltz DR. Posttranslational Modifications of CENP-A: Marks of Distinction. *Chromosoma* (2018) 127:279–90. doi: 10.1007/s00412-018-0665-x
- Sharma AB, Dimitrov S, Hamiche A, Van Dyck E. Centromeric and Ectopic Assembly of CENP-A Chromatin in Health and Cancer: Old Marks and New Tracks. Nucleic Acids Res (2019) 47:1051–69. doi: 10.1093/nar/gky1298
- Zhang T, Zhou Y, Li L, Wang ZB, Shen W, Schatten H, et al. CenpH Regulates Meiotic G2/M Transition by Modulating the APC/CCdh1-Cyclin B1 Pathway in Oocytes. *Development* (2017) 144:305–12. doi: 10.1242/dev.141135
- Wang J, Liu X, Chu HJ, Li N, Huang LY, Chen J. Centromere Protein I (CENP-I) Is Upregulated in Gastric Cancer, Predicts Poor Prognosis, and Promotes Tumor Cell Proliferation and Migration. *Technol Cancer Res Treat* (2021) 20:15330338211045510. doi: 10.1177/15330338211045510
- Shao C, Wang Y, Duan H, Ding P, Zhang Y, Ning J, et al. Mitosis-Related Gene CENP-U as a Potential Biomarker in Malignancy. Ann Transl Med (2021) 9:1744. doi: 10.21037/atm-21-6516

- Foltz DR, Jansen LE, Black BE, Bailey AO, Yates JR, Cleveland DW3. The Human CENP-A Centromeric Nucleosome-Associated Complex. *Nat Cell Biol* (2006) 8:458–69. doi: 10.1038/ncb1397
- Li Z, Zhang L, Liu D, Yang Z, Xuan D, Zhang Y. Knockdown of NRMT Enhances Sensitivity of Retinoblastoma Cells to Cisplatin Through Upregulation of the CENPA/Myc/Bcl2 Axis. *Cell Death Discov* (2022) 8:14. doi: 10.1038/s41420-021-00622-w
- Zhou H, Bian T, Qian L, Zhao C, Zhang W, Zheng M, et al. Prognostic Model of Lung Adenocarcinoma Constructed by the CENPA Complex Genes is Closely Related to Immune Infiltration. *Pathol Res Pract* (2021) 228:153680. doi: 10.1016/j.prp.2021.153680
- Hinds PW. A Confederacy of Kinases: Cdk2 and Cdk4 Conspire to Control Embryonic Cell Proliferation. *Mol Cell* (2006) 22:432–3. doi: 10.1016/ j.molcel.2006.05.006
- Hinds PW. Cdk2 Dethroned as Master of S Phase Entry. Cancer Cell (2003) 3:305–7. doi: 10.1016/S1535-6108(03)00084-9
- Liu H, Li Z, Huo S, Wei Q, Ge L. Induction of G0/G1 Phase Arrest and Apoptosis by CRISPR/Cas9-Mediated Knockout of CDK2 in A375 Melanocytes. *Mol Clin Oncol* (2020) 12:9–14. doi: 10.3892/mco.2019.1952
- Yang J, Dong Z. Antibiotic Tigecycline Inhibits Cell Proliferation, Migration and Invasion via Down-Regulating CCNE2 in Pancreatic Ductal Adenocarcinoma. J Cell Mol Med (2020) 24:4245–60. doi: 10.1111/ jcmm.15086
- Oliver AJ, Lau PKH, Unsworth AS, Loi S, Darcy PK, Kershaw MH, et al. Tissue-Dependent Tumor Microenvironments and Their Impact on Immunotherapy Responses. *Front Immunol* (2018) 9:70. doi: 10.3389/ fimmu.2018.00070
- Meurette O, Mehlen P. Notch Signaling in the Tumor Microenvironment. Cancer Cell (2018) 34:536–48. doi: 10.1016/j.ccell.2018.07.009
- Hinshaw DC, Shevde LA. The Tumor Microenvironment Innately Modulates Cancer Progression. *Cancer Res* (2019) 79:4557-66. doi: 10.1158/0008-5472
- Farhood B, Najafi M, Mortezaee K. CD8(+) Cytotoxic T Lymphocytes in Cancer Immunotherapy: A Review. J Cell Physiol (2019) 234:8509–21. doi: 10.1002/jcp.27782

- Raskov H, Orhan A, Christensen JP, Gögenur I. Cytotoxic CD8(+) T Cells in Cancer and Cancer Immunotherapy. Br J Cancer (2021) 124:359–67. doi: 10.1038/s41416-020-01048-4
- Borst J, Ahrends T, Bąbała N, Melief CJM, Kastenmüller W. CD4(+) T Cell Help in Cancer Immunology and Immunotherapy. *Nat Rev Immunol* (2018) 18:635–47. doi: 10.1038/s41577-018-0044-0
- Li T, Liu T, Zhu W, Xie S, Zhao Z, Feng B, et al. Targeting MDSC for Immune-Checkpoint Blockade in Cancer Immunotherapy: Current Progress and New Prospects. *Clin Med Insights Oncol* (2021) 15:11795549211035540. doi: 10.1177/ 11795549211035540
- Li R, Salehi-Rad R, Crosson W, Momcilovic M, Lim RJ. Inhibition of Granulocytic Myeloid-Derived Suppressor Cells Overcomes Resistance to Immune Checkpoint Inhibition in LKB1-Deficient Non-Small Cell Lung Cancer. *Cancer Res* (2021) 81:3295–308. doi: 10.1158/0008-5472.CAN-20-3564
- Paul S, Chhatar S, Mishra A, Lal G. Natural Killer T Cell Activation Increases iNOS(+)CD206(-) M1 Macrophage and Controls the Growth of Solid Tumor. *J Immunother Cancer* (2019) 7:208. doi: 10.1186/s40425-019-0697-7

Conflict of Interest: The authors declare that the research was conducted in the absence of any commercial or financial relationships that could be construed as a potential conflict of interest.

Publisher's Note: All claims expressed in this article are solely those of the authors and do not necessarily represent those of their affiliated organizations, or those of the publisher, the editors and the reviewers. Any product that may be evaluated in this article, or claim that may be made by its manufacturer, is not guaranteed or endorsed by the publisher.

Copyright © 2022 Feng, Chen, Cai, Tan, Liu, Chen, Shen, Zeng and Han. This is an open-access article distributed under the terms of the Creative Commons Attribution License (CC BY). The use, distribution or reproduction in other forums is permitted, provided the original author(s) and the copyright owner(s) are credited and that the original publication in this journal is cited, in accordance with accepted academic practice. No use, distribution or reproduction is permitted which does not comply with these terms.



Recent Progress and Future Perspectives of Immunotherapy in Advanced Gastric Cancer

Xin Jin^{1,2}, Zhaorui Liu¹, Dongxiao Yang^{1*}, Kai Yin^{1*} and Xusheng Chang^{1*}

¹ Department of Gastrointestinal Surgery, Changhai Hospital, Naval Medical University, Shanghai, China, ² Key Laboratory of Natural Medicines of the Changbai Mountain, Ministry of Education, Yanbian University, Yanji, China

As one of the most common forms of solid tumours, gastric carcinoma has been revealed as the third leading cause of death worldwide. The symptom of gastric cancer is usually not obvious and thus difficult to detect at earlier stages. Therefore, gastric cancer is already in the advanced stage once detected in patients, which has a poor prognosis due to ineffective therapies and multiple resistance. Recent advance in understanding the microenvironment of cancer has significantly promoted the development of immunotherapy for advanced gastric cancer. Immunotherapy can induce immune responses in gastric cancer patients thus leads to the destruction of cancer cells. In comparison of traditional therapy, immunotherapy has demonstrated robust efficacy and tolerable toxicity. Therefore, this novel strategy for treatment of advanced gastric cancer has gain increasingly popularity. In this review, we summarize recent progress of immunotherapy in advanced gastric cancer, such as immune check point inhibitors, adoptive cell therapy, VEGF inhibitors, cancer vaccines and CAR-T cell therapy. We highlight immunotherapies involved in clinical applications and discuss the existing challenges of current immunotherapies and promising strategies to overcome these limitations.

Keywords: advanced gastric cancer, immunotherapy, immune checkpoint inhibitor, adoptive cell therapy, cancer vaccine, CAR-T cell therapy

1. INTRODUCTION

Gastric cancer is the third leading cause of cancer-related death (1). Due to the delay in diagnosis and lack of effective therapies, patients with advanced gastric cancer suffer from poor prognosis and a short lifespan of approximately one year (2). The commonly used therapies of advanced gastric cancer are radiotherapy, chemotherapy and targeted therapy. Agents such as imatinib, larotrectinib, entrectinib and regorafenib are widely used for treatment of advanced gastric cancer (3, 4). However, multi-drug resistance and tumour relapse have largely limited the effectiveness of these traditional therapies.

In the recent years, immunotherapy has become a novel therapy to treat advanced gastric cancer and has quickly drawn the attention of researchers around the world owing to its amazing antitumour efficacy (5, 6). A better understanding of the tumour microenvironment has greatly facilitated the development of immunotherapies in advance gastric cancer (7). The most widely

OPEN ACCESS

Edited by:

Xuyao Zhang, Fudan University, China

Reviewed by: Shuai Wang,

Harvard Medical School, United States Lijie Zhao, University of Michigan, United States

*Correspondence:

Dongxiao Yang dongxiaoyang2@gmail.com Kai Yin kyin67@smmu.edu.cn Xusheng Chang cxs20051014@163.com

Specialty section:

This article was submitted to Cancer Immunity and Immunotherapy, a section of the journal Frontiers in Immunology

Received: 20 May 2022 **Accepted:** 06 June 2022 **Published:** 01 July 2022

Citation:

Jin X, Liu Z, Yang D, Yin K and Chang X (2022) Recent Progress and Future Perspectives of Immunotherapy in Advanced Gastric Cancer. Front. Immunol. 13:948647. doi: 10.3389/fimmu.2022.948647

506

applied immunotherapies against advanced gastric cancer including immune checkpoint inhibitors (ICIs), adoptive cell therapy, cancer vaccine, vascular endothelial growth factor A (VEGFA) antibody and chimeric antigen receptor (CAR) T therapy, etc (8–10). Studies have shown that ICIs such as anti-PD-1/PD-L1 antibodies could effectively kill cancer cells *via* activation of the immune response (11). Clinical trials of ICIs have displayed efficacy and safety for cancer patients (12, 13). Notably, several ICIs such as pembrolizumab, avelumab, sintilimab, tislelizumab and ipilimumab have been approved for clinical application in combination with targeted therapy for treatment of advanced gastric tumour (14, 15).

In this review, we describe state-of-the-art development of immunotherapy for treatment of advanced gastric cancer, highlighting recent advances of ICIs, adoptive cell therapy, cancer vaccine and CAR-T cell therapy. In addition, we discuss the current challenges of immunotherapies, as well as potential strategies to overcome these limitations, such as combination of immunotherapy and targeted therapy.

2. IMMUNOTHERAPY FOR ADVANCED GASTRIC CANCER

Over the past few years, a better understanding of the immune mechanism of gastric cancer has greatly facilitated the development of novel immunotherapies. ICIs could effectively interrupt the immune checkpoint interactions, leading to the destruction of tumour cells *via* activation of host's immune system (16). The ongoing clinical trials of ICIs in advanced gastric cancer have been listed in **Table 1**. Other approaches such as adoptive cell therapy, VEGF inhibitors, cancer vaccines and CART cell therapy have also demonstrated potent anti-tumour activities (11, 17). These

 TABLE 1 | Representative clinical trials of ICIs in advanced gastric cancer.

achievements in immunotherapy have marked a new era for advanced gastric cancer treatment (Figure 1).

2.1 Immune Checkpoint Inhibitors

In 2011, ipilimumab became the world-first approved ICIs to treat melanoma (18). Since then, immune therapies have revolutionized the strategies for advanced gastric cancer treatment. There are mainly three types of ICIs, anti-PD1/PD-L1 and anti-CTLA4 antibodies (19). Activated immune cells such as T cells can express PD-1. PD-L1, the ligand of PD-1, binds to PD-1 thus resulted in immune cell apoptosis and immune suppression. PD-L1 is overexpressed in advanced gastric cancer, leading to the evasion of tumour cells from immune response (20). On the other hand, CTLA-4 protein can interact with B7-1/B7-2 with high affinity, leading to CD28 signalling pathway inhibition, which plays a critical role in T cell activation (21). Inhibitors targeting these immune checkpoints have been generated and studied in pre-clinical and clinical trials.

2.1.1 PD-1 Inhibitors

PD-1 inhibitor nivolumab is a monoclonal antibody that have gained the approval of FDA in the year 2014 for advanced gastric tumour treatment (22). The effects of nivolumab against advanced gastric cancer were examined *via* phase III clinical trials conducted over 40 countries in Asian (13). The initial results showed that nivolumab could significantly increase the survival rate of patients compared to the placebo. Nivolumab treatment in gastric tumour patients have demonstrated 12-month overall survival rates of 26.2% in contrast to that of 10.9% survival rates by placebo treatment, suggesting a promising cure for this poor prognosis population. Notably, nivolumab has been approved for clinical application as a novel approach to treat advanced and recurrent gastric cancer (22, 23).

Agent	Phase	Target	Conditions	NCT number	Other identifier
Ipilimumab	11	CTLA-4	Adenocarcinoma of the Stomach	NCT03647969	AIOSTO-0417
Nivolumab		PD-1	GastroEsophageal Cancer		
Ipilimumab	III	CTLA-4	Gastric Cancer	NCT02872116	CheckMate-649
Nivolumab		PD-1	Gastroesophageal Junction Cancer		
Atezolizumab	11	PD-L1	Gastric Cancer	NCT03421288	DANTE
			Gastroesophageal Junction Adenocarcinoma		
Durvalumab	11	PD-L1	Advanced solid tumors (including gastric cancer)	NCT04157985	/
Avelumab			, , ,		
Nivolumab	111	PD-1	Gastroesophageal Junction Cancer	NCT02743494	CheckMate-577
Pembrolizumab	III	PD-1	Gastric Cancer	NCT03221426	KEYNOTE-585
			Gastroesophageal Junction Cancer		
Nivolumab	11	PD-1	Gastric Cancer	NCT03662659	CA224-060
Relatlimab		LAG-3	Cancer of the Stomach		
			Esophagogastric Junction		
Pembrolizumab Trastuzumab	111	PD-1	Gastric Neoplasms	NCT03615326	KEYNOTE-811
		HER-2	Gastroesophageal Junction Adenocarcinoma		
Nivolumab	11	PD-1	Unresectable advanced or recurrent gastric cancer	NCT02267343	ATTRACTION-2
Pembrolizumab	111	PD-1	Advanced gastric	NCT02370498	KEYNOTE-061
			gastroesophageal junction adenocarcinoma		
Pembrolizumab	III	PD-1	Advanced gastric or gastroesophageal junction adenocarcinoma	NCT02494583	KEYNOTE-062
Pembrolizumab	III	PD-1	Gastric Neoplasms	NCT03019588	KEYNOTE-063
			Gastroesophageal Junction Adenocarcinoma		

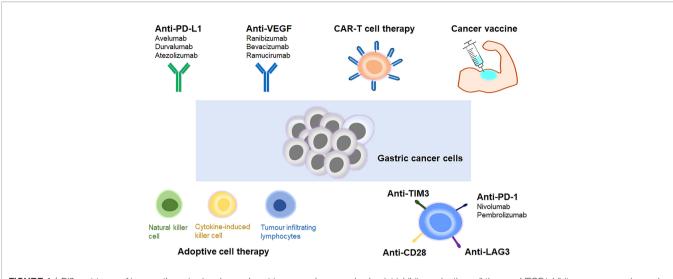


FIGURE 1 | Different types of immunotherapies in advanced gastric cancer. Immune checkpoint inhibitor, adoptive cell therapy, VEGF inhibitor, cancer vaccine and CAR-T cell therapy are the main types of immunotherapies for treatment of advanced gastric cancer.

Pembrolizumab is another promising inhibitor targeting PD-1. The efficacy of pembrolizumab has been assessed in the phase II trials among advanced gastric cancer (24). Treatment with pembrolizumab in advanced gastric cancer patients has demonstrated 11-month overall survival rates of 45.8%. In addition to its high anti-tumour activity, pembrolizumab has also shown moderate side effects. These advantages of pembrolizumab have prompted its approval for treatment of advanced gastric tumour in 2017 (25). Clinical trials of pembrolizumab in 592 patients with non-operable advanced gastric cancer have been conducted to determine the efficacy of pembrolizumab in comparison to paclitaxel (26). However, pembrolizumab alone didn't demonstrate significantly improved survival rates compared to paclitaxel in patients. When pembrolizumab combined with paclitaxel, enhanced antitumour effect and better toleration was detected (27). Tislelizumab has also been assessed for its anti-tumour effect against advanced gastric cancer, providing hope for the evolution of PD-1-based immunotherapy in advanced gastric tumour (28).

2.1.2 PD-L1 Inhibitors

PD-L1 is overexpressed on various cancer cells and plays a crucial role in T cell inhibition (29). The well-known PD-L1 inhibitors include avelumab, durvalumab and atezolizumab (30). Avelumab is an anti-PD-L1 mAb which has demonstrated well toleration in the phase III trial among patients with advanced gastric cancer (31). Avelumab among patients from Japan have exhibited high overall response rates and survival rates. In addition, the efficacy of avelumab against advanced gastric cancer is enhanced in combination with other therapeutics. However, a phase I trial in advanced gastric cancer showed that atezolizumab was effective in one case out of 171 patients (10). The response rates in this clinical trial are closely related to PD-L1 expression. The mechanism of how PD-L1 inhibitors contribute to advanced gastric cancer may be that PD-L1 inhibition could activate DC cells, T lymphocytes and natural kill cells, thus leading to the destruction of gastric tumour (32).

2.1.3 CTLA-4 Inhibitors

CTLA-4 plays important roles in human immune system. CTLA-4 is homologous to CD28, but it can interact with B7-1/B7-2 with higher affinity (21). Therefore, CTLA-4 can regulate or even inhibit CD28 signalling. CTLA-4 inhibitors tremelimumab and ipilimumab have been evaluated in clinical trials of advanced gastric cancer (10). Evaluation of ipilimumab was performed in a phase II trial among advanced gastric cancer patients (33). However, this study was terminated because ipilimumab didn't demonstrate significant improved survival rate compared with first line targeted agents. A clinical study of tremelimumab on 12 patients with non-operable advanced gastric cancer demonstrated moderate response rate, compared with a combined therapy using both tremelimumab and other anti-cancer agents. Of note, combined therapies targeting CTLA-4 and PD-1 have shown enhanced anti-tumour immunity (34). Combination therapy of ipilimumab and nivolumab has been approved to treat advanced gastric cancer. However, the efficacy of CTLA-4 inhibitor as a monotherapy in advanced gastric cancer remains to be further investigated.

2.2 Adoptive Cell Therapy

Gastric cancer cells can express specific neoantigens of high immunogenicity, thus leading to the activation of human immune system. In this way, cancer cells can be recognized and destroyed. However, cancer cells can generate suppressive factors including lymphocyte-activation gene 3 (LAG-3), TGF- β , prostaglandin E2 and IL-10 that inhibit immune response, thus escaping detection and clearance by the immune system (35). For patients whose immune systems fail to detect and response to cancer cells, adoptive cell therapy has been proved as effective strategies to treat advanced gastric cancer (36). Adoptive cell therapy utilizes various immune cells including tumour infiltrating lymphocytes (TILs), lymphokine-activated killer cells and cytokine-induced killer (CIK) cells to induce effective immunity to clear cancer cells (2, 37). CIK cells are derived from peripheral blood lymphocytes in the presence of CD3 monoclonal antibodies, IL-2 and IFN- γ (38). The CIK cell population consists of CD3⁺CD56⁻ T cell and CD3⁺CD56⁺ T cell, with high anti-tumour activity and proliferation activity (39). Moreover, CIK cells could generate cytokines and chemokines for the regulation and elevation of immune response. A preclinical study using CIK cells demonstrated strong anti-tumour activity of CIK (40). In addition, clinical trials of combined therapy using CIK cells and targeted therapy have shown increased effect against advanced gastric cancer (41).

TILs immunotherapy has been widely applied in advanced gastric cancer. In particular, TILs derived from gastric cancer in patients have been exposed to tumour specific antigens thus are extremely advantageous in immunotherapy. Clinical trials of adoptive cell therapy among gastric cancer patients have shown that combined therapies based on tumour-associated lymphocytes could increase the survival rate to 50% in comparation with using traditional therapy alone (42, 43). Furthermore, in recent years, expanded allogenic natural kill cells has also been used as a novel immunotherapy for treatment of advanced gastric cancer (44). Natural kill cells possess high anti-tumour activity and antibody-dependent cytotoxicity. However, the clinical application of natural kill cells in cancer treatment is severely limited by the lack of strategies to obtain a large amounts of functional natural kill cells (45). Further studies will be taken to investigate novel methods to generate sufficient natural kill cells for cancer immunotherapy.

2.3 Anti-Angiogenic Therapy

Vascular endothelial growth factor A (VEGFA) play essential roles in the development of gastric cancer via its involvement in the formation of new blood vessels, a process termed as angiogenesis (46). VEGFA functions in the modulation of cancer immune response, which could result in escape of tumour cells from the surveillance of the immune system (47). In addition, VEGF can promote the transfer of Treg cells to the sites of tumour. Clinical studies of combined therapies using VEGFA inhibitors and immune check point inhibitors among patients with advanced gastric cancer have shown promising effects, with enhanced anti-tumour effect and reduced toxicity. For instance, bevacizumab and ramucirumab can significantly prevent angiogenesis (48). Clinical studies of combined therapies using bevacizumab and ICIs such as atezolizumab, ramucirumab, durvalumab in advanced gastric cancer patients have shown favourable efficacy (48). These studies suggest that combined therapy using VEGFA inhibitors and ICIs targeting PD-1 or PD-L1 may shed light on the development of effective treatment in advanced gastric cancer.

2.4 Cancer Vaccines

Another novel immunotherapy in advanced gastric cancer is the application of cancer vaccines, which can activate immune responses against tumour cells in vivo (49, 50). Proteins and peptides are commonly used antigens to trigger immune responses. The most well-studied cancer vaccines are mRNA vaccines, which carries the genetic information of antigen and can translate it into protein rapidly to induce immune response, thus leading to the destruction of cancer cells (51). Studies have revealed that mRNA cancer vaccines showed strong efficacy and moderate side effects compared to traditional chemotherapy or targeted therapy (52). Moreover, combination of cancer vaccines and chemotherapies such as cisplatin and 5-fluorouracil have exhibited significantly enhanced cytotoxicity against tumour cells in preliminary clinical trials (53). A clinical study of HLA-A24 and HLA-A2 peptides examined the peripheral blood mononuclear cells in gastric cancer patients (54). Results showed that 50% of the patients treated with cancer vaccines had increased humoral and cellular response against vaccinated peptides.

2.5 CAR-T Cell Therapy

CAR-T cell is specifically designed for the expression of synthetic receptors that can induce T cells to detect specific cancer antigen, leading to the destruction of tumour cells *via* the host's immunity (55). Biomarkers such as claudin 18.2 (CLDN 18.2), human epidermal growth factor receptor 2 (HER2), mucin 1, natural-killer receptor group 2 (NKG2D), epithelial cell adhesion molecule (EpCAM), mesothelin (MSLN) and carcinoembryonic antigen (CEA) play important roles in the diagnosis and function of gastric cancer (56). Studies have shown that CAR-T therapy can effectively target the above biomarkers for treatment of advanced gastric cancer (**Table 2**) (57).

HER2 is a surface antigen overexpressed in gastric cancer cells. HER2-postive gastric cancer usually exhibit multi-drug resistance that inhibit the anti-tumour activity of traditional agents. The development of drug resistance severely hampered the treatment of advanced gastric cancer (57). Of note, CAR-T therapy is an effective strategy to overcome the multiple resistance in advanced gastric cancer patients. Notably, studies of HER2 CAR-T therapy demonstrate high affinity for advanced gastric cancer. Clinical studies of CLDN18.2 CAR-T cells in CLDN18.2-positive patients-derived tumour models have demonstrated high anti-tumour activity (58). CA 72-4 is a surface glycoprotein highly expressed in advanced gastric cancer. CAR-T therapy targeting CA 72-4 has shown potent effect in tumour elimination (59). Therefore, CA 72-4 may be a potential target for advanced gastric cancer treatment. Notably, clinical studies in patients showed that CAR-T therapy in combination with other therapeutics displayed enhanced anti-tumour effects (57).

TABLE 2 | Representative clinical studies of CAR-T cell therapies in advanced gastric cancer.

Agent	Phase	Target	Conditions	NCT number
CAR-CLDN18.2 T cells	I	CLDN18.2	CLDN 18.2 positive advanced gastric adenocarcinoma	NCT03159819
CT041	lb	CLDN18.2	Claudin18.2-positive adenocarcinoma gastroesophageal junction	NCT03874897
CT041	Ι	CLDN18.2	Gastric Cancer	NCT04404595

In addition, CAR-T cells targeting B7-H3 and CDH17 have made achievements in cancer treatment. Clinical studies have shown that B7-H3 is overexpressed in the tumour tissues of advanced gastric cancer patients and B7-H3 is strongly correlated to the advancement of gastric cancer. Anti-tumour effect of B7-H3 specific CAR-T cells has been evaluated in patients with advanced gastric cancer and demonstrated significant cytotoxicity against gastric tumour cells (60). CDH17 is a biomarker of gastrointestinal adenocarcinomas and plays key roles in CA2+-dependent adhesion switch and Wnt signalling. Recent progress in CAR-T cells targeting CDH17 has shed light on this novel immunotherapy as a potential safe and effective treatment for advanced gastric cancer. Pre-clinical studies using gastrointestinal carcinoma xenografts in mouse models have demonstrated that CDH17CART therapy has strong potency against advanced gastric cancer with no obvious toxicity to normal gastrointestinal epithelial cells (61).

3. CHALLENGES AND POTENTIAL STRATEGIES

Development of immunotherapy in advanced gastric cancer has demonstrated great advantages over traditional therapies. However, there still exists various challenges that have severely limited the clinical application of immunotherapy in advanced gastric cancer, for instance, the side effects and toxicity of ICIs, cancer vaccines and CAR-T therapies.

ICIs can lead to autoimmune toxicities in cancer patients (62, 63). For example, the side effects of nivolumab including fatigue, pruritus and rash. Pembrolizumab treatment in advanced gastric cancer can lead to thyroid-related complications. In addition, ICIs can lead to high risk of transplant loss in patients with organ transplants. Although the side effects of PD-1/PD-L1 and CTLA-4 inhibitors are similar, PD-L1 inhibition can lead to more severe immune adverse events due to the loss of PD-L1 ability to bind to B7 (64). However, these side effects of immune checkpoint inhibition can be effectively prevented by immunosuppressive agents such as corticosteroids without impairing the clinical benefits of immunotherapy in advanced gastric cancer. Furthermore, combination of ICIs and targeted therapy display synergistic effects on advanced gastric cancer.

VEGF has been established as a crucial target for treatment of advanced gastric cancer. However, due to the wide expression of VEGF, side effects of VEGF inhibitors are commonly seen in clinic, including hypothyroidism, coagulation disorders, gastrointestinal perforations, hypertension, proteinuria, neurotoxicity (65).

Although cancer vaccine has shown favourable benefits in phase I and phase II trials against advanced gastric cancer, its clinical efficacy is low because of regulation and suppression from the host immune system. Novel strategies to overcome this limitation involve the development of combined therapies, for example, combination of cancer vaccine and immune modulator to avoid immune suppression, use of conventional chemotherapy in addition to cancer vaccine to enhance anti-tumour activity but reduce cytotoxicity (66).

Despite the amazing efficacy of CAR-T therapy against advanced gastric cancer, this novel treatment also exhibits strong toxicity that could be fatal (57, 67). The most commonly seen side effects of CAR-T therapy are known as cytokine release syndrome and CAR-T therapy-related encephalopathy syndrome that includes fevers, chills, nausea, headache, cardiac toxicity and neurotoxicity. Development of CAR-T cells with shorter lifespan or "on-switch" may effectively overcome the limitations of current CAR-T therapy, reduce the toxicity, and facilitate the wide clinical application of this novel immunotherapy in advanced gastric cancer (68).

4. CONCLUSION

Over the past decades, cancer immunotherapy has emerged as promising therapeutics for various cancers. Development of ICIs has been a breakthrough for advanced gastric cancer and demonstrated anti-tumour effect in patients. However, the toxicity and efficacy of immune checkpoint inhibition have largely limited its broad clinical application. Other immunotherapies including adoptive cell therapy, cancer vaccines and CAR-T cell therapy also showed anti-tumour activity in gastric cancer patients. Clinical trials of immunotherapy in combination with targeted therapy have shown enhanced anti-tumour activity and survival rate compared with using immunotherapy alone. Despite the advantages of immunotherapy in advanced gastric cancer, challenges such as moderate clinical efficacy and immune evasion blocks the broad application of immunotherapy in advanced gastric cancer. New strategies to overcome these challenges will involve combination of CAR-T therapy and ICIs, utilizing of immune modulators to avoid immune suppression. We believe that developing novel immunotherapy may shed lights on the treatment of advanced gastric cancer.

AUTHOR CONTRIBUTIONS

DY, KY, and XC conceived the topic, revised and proofread the manuscript. XJ and ZL drafted the paper and prepared the figure and table. All authors approved the submitted version.

FUNDING

This study was supported by the Shanghai Science and Technology Funds (21Y11913100).

REFERENCES

- Ferlay J, Colombet M, Soerjomataram I, Mathers C, Parkin DM, Pineros M, et al. Estimating the Global Cancer Incidence and Mortality in 2018: GLOBOCAN Sources and Methods. *Int J Cancer* (2019) 144(8):1941–53. doi: 10.1002/ijc.31937
- Hogner A, Moehler M. Immunotherapy in Gastric Cancer. Curr Oncol (2022) 29(3):1559–74. doi: 10.3390/curroncol29030131
- Sasako M, Sakuramoto S, Katai H, Kinoshita T, Furukawa H, Yamaguchi T, et al. Five-Year Outcomes of a Randomized Phase III Trial Comparing Adjuvant Chemotherapy With S-1 Versus Surgery Alone in Stage II or III Gastric Cancer. *J Clin Oncol* (2011) 29(33):4387–93. doi: 10.1200/JCO.2011.36.5908
- Ajani JA, Lee J, Sano T, Janjigian YY, Fan D, Song S. Gastric Adenocarcinoma. Nat Rev Dis Primers (2017) 3:17036. doi: 10.1038/nrdp.2017.36
- Mellman I, Coukos G, Dranoff G. Cancer Immunotherapy Comes of Age. Nature (2011) 480(7378):480–9. doi: 10.1038/nature10673
- Kono K. Advances in Cancer Immunotherapy for Gastroenterological Malignancy. Ann Gastroenterol Surg (2018) 2(4):244–5. doi: 10.1002/ ags3.12184
- Uppal A, Dehal A, Chang SC, Barrak D, Naeini Y, Jalas JR, et al. The Immune Microenvironment Impacts Survival in Western Patients With Gastric Adenocarcinoma. J Gastrointest Surg (2020) 24(1):28–38. doi: 10.1007/ s11605-019-04403-w
- Sharma P, Allison JP. Immune Checkpoint Targeting in Cancer Therapy: Toward Combination Strategies With Curative Potential. *Cell* (2015) 161 (2):205–14. doi: 10.1016/j.cell.2015.03.030
- Sharma P, Allison JP. The Future of Immune Checkpoint Therapy. Science (2015) 348(6230):56–61. doi: 10.1126/science.aaa8172
- Xie J, Fu L, Jin L. Immunotherapy of Gastric Cancer: Past, Future Perspective and Challenges. *Pathol Res Pract* (2021) 218:153322. doi: 10.1016/j.prp.2020.153322
- Kono K, Nakajima S, Mimura K. Current Status of Immune Checkpoint Inhibitors for Gastric Cancer. Gastric Cancer (2020) 23(4):565–78. doi: 10.1007/s10120-020-01090-4
- Muro K, Chung HC, Shankaran V, Geva R, Catenacci D, Gupta S, et al. Pembrolizumab for Patients With PD-L1-Positive Advanced Gastric Cancer (KEYNOTE-012): A Multicentre, Open-Label, Phase 1b Trial. *Lancet Oncol* (2016) 17(6):717–26. doi: 10.1016/S1470-2045(16)00175-3
- Kang YK, Boku N, Satoh T, Ryu MH, Chao Y, Kato K, et al. Nivolumab in Patients With Advanced Gastric or Gastro-Oesophageal Junction Cancer Refractory to, or Intolerant of, at Least Two Previous Chemotherapy Regimens (ONO-4538-12, ATTRACTION-2): A Randomised, Double-Blind, Placebo-Controlled, Phase 3 Trial. *Lancet* (2017) 390(10111):2461– 71. doi: 10.1016/S0140-6736(17)31827-5
- 14. Janjigian YY, Kawazoe A, Yanez P, Li N, Lonardi S, Kolesnik O, et al. The KEYNOTE-811 Trial of Dual PD-1 and HER2 Blockade in HER2-Positive Gastric Cancer. *Nature* (2021) 600(7890):727–30. doi: 10.1038/s41586-021-04161-3
- Takei S, Kawazoe A, Shitara K. The New Era of Immunotherapy in Gastric Cancer. Cancers (2022) 14(4):1054. doi: 10.3390/cancers14041054
- Postow MA, Callahan MK, Wolchok JD. Immune Checkpoint Blockade in Cancer Therapy. J Clin Oncol (2015) 33(17):1974–82. doi: 10.1200/JCO.2014.59.4358
- Coutzac C, Pernot S, Chaput N, Zaanan A. Immunotherapy in Advanced Gastric Cancer, is it the Future? *Crit Rev Oncol Hematol* (2019) 133:25–32. doi: 10.1016/j.critrevonc.2018.10.007
- Robert C, Thomas L, Bondarenko I, O'Day S, Weber J, Garbe C, et al. Ipilimumab Plus Dacarbazine for Previously Untreated Metastatic Melanoma. N Engl J Med (2011) 364(26):2517–26. doi: 10.1056/NEJMoa1104621
- Bagchi S, Yuan R, Engleman EG. Immune Checkpoint Inhibitors for the Treatment of Cancer: Clinical Impact and Mechanisms of Response and Resistance. *Annu Rev Pathol* (2021) 16:223–49. doi: 10.1146/annurev-pathol-042020-042741
- Jacob JA. Cancer Immunotherapy Researchers Focus on Refining Checkpoint Blockade Therapies. JAMA (2015) 314(20):2117–9. doi: 10.1001/jama.2015.10795
- Dong H, Strome SE, Salomao DR, Tamura H, Hirano F, Flies DB, et al. Tumor-Associated B7-H1 Promotes T-Cell Apoptosis: A Potential Mechanism of Immune Evasion. Nat Med (2002) 8(8):793–800. doi: 10.1038/nm730
- 22. Kato K, Satoh T, Muro K, Yoshikawa T, Tamura T, Hamamoto Y, et al. A Subanalysis of Japanese Patients in a Randomized, Double-Blind, Placebo-

Controlled, Phase 3 Trial of Nivolumab for Patients With Advanced Gastric or Gastro-Esophageal Junction Cancer Refractory to, or Intolerant of, at Least Two Previous Chemotherapy Regimens (ONO-4538-12, ATTRACTION-2). *Gastric Cancer* (2019) 22(2):344–54. doi: 10.1016/S0140-6736(17)31827-5

- 23. Doi T, Iwasa S, Muro K, Satoh T, Hironaka S, Esaki T, et al. Phase 1 Trial of Avelumab (Anti-PD-L1) in Japanese Patients With Advanced Solid Tumors, Including Dose Expansion in Patients With Gastric or Gastroesophageal Junction Cancer: The JAVELIN Solid Tumor JPN Trial. *Gastric Cancer* (2019) 22(4):817–27. doi: 10.1007/s10120-018-0903-1
- 24. Marabelle A, Le DT, Ascierto PA, Di Giacomo AM, De Jesus-Acosta A, Delord JP, et al. Efficacy of Pembrolizumab in Patients With Noncolorectal High Microsatellite Instability/Mismatch Repair-Deficient Cancer: Results From the Phase II KEYNOTE-158 Study. J Clin Oncol (2020) 38(1):1–10. doi: 10.1200/JCO.19.02105
- 25. Fuchs CS, Doi T, Jang RW, Muro K, Satoh T, Machado M, et al. Safety and Efficacy of Pembrolizumab Monotherapy in Patients With Previously Treated Advanced Gastric and Gastroesophageal Junction Cancer: Phase 2 Clinical KEYNOTE-059 Trial. JAMA Oncol (2018) 4(5):e180013. doi: 10.1001/ jamaoncol.2018.0013
- 26. Shitara K, Ozguroglu M, Bang YJ, Di Bartolomeo M, Mandala M, Ryu MH, et al. Pembrolizumab Versus Paclitaxel for Previously Treated, Advanced Gastric or Gastro-Oesophageal Junction Cancer (KEYNOTE-061): A Randomised, Open-Label, Controlled, Phase 3 Trial. *Lancet* (2018) 392 (10142):123–33. doi: 10.1016/S0140-6736(18)31257-1
- 27. Shitara K, Van Cutsem E, Bang YJ, Fuchs C, Wyrwicz L, Lee KW, et al. Efficacy and Safety of Pembrolizumab or Pembrolizumab Plus Chemotherapy vs Chemotherapy Alone for Patients With First-Line, Advanced Gastric Cancer: The KEYNOTE-062 Phase 3 Randomized Clinical Trial. *JAMA Oncol* (2020) 6(10):1571–80. doi: 10.1001/jamaoncol.2020.3370
- Zayac A, Almhanna K. Esophageal, Gastric Cancer and Immunotherapy: Small Steps in the Right Direction? *Transl Gastroenterol Hepatol* (2020) 5:9. doi: 10.21037/tgh.2019.09.05
- Topalian SL, Drake CG, Pardoll DM. Immune Checkpoint Blockade: A Common Denominator Approach to Cancer Therapy. *Cancer Cell* (2015) 27(4):450–61. doi: 10.1016/j.ccell.2015.03.001
- Doroshow DB, Bhalla S, Beasley MB, Sholl LM, Kerr KM, Gnjatic S, et al. PD-L1 as a Biomarker of Response to Immune-Checkpoint Inhibitors. *Nat Rev Clin Oncol* (2021) 18(6):345–62. doi: 10.1038/s41571-021-00473-5
- 31. Bang YJ, Ruiz EY, Van Cutsem E, Lee KW, Wyrwicz L, Schenker M, et al. Randomised Trial of Avelumab Versus Physician's Choice of Chemotherapy as Third-Line Treatment of Patients With Advanced Gastric or Gastro-Oesophageal Junction Cancer: Primary Analysis of JAVELIN Gastric 300. Ann Oncol (2018) 29(10):2052–60. doi: 10.1093/annonc/mdy264
- Refolo MG, Lotesoriere C, Messa C, Caruso MG, D'Alessandro R. Integrated Immune Gene Expression Signature and Molecular Classification in Gastric Cancer: New Insights. J Leukoc Biol (2020) 108(2):633–46. doi: 10.1002/ JLB.4MR0120-221R
- Bang YJ, Cho JY, Kim YH, Kim JW, Di Bartolomeo M, Ajani JA, et al. Efficacy of Sequential Ipilimumab Monotherapy Versus Best Supportive Care for Unresectable Locally Advanced/Metastatic Gastric or Gastroesophageal Junction Cancer. *Clin Cancer Res* (2017) 23(19):5671–8. doi: 10.1158/1078-0432.CCR-17-0025
- 34. Kelly RJ, Lee J, Bang YJ, Almhanna K, Blum-Murphy M, Catenacci DVT, et al. Safety and Efficacy of Durvalumab and Tremelimumab Alone or in Combination in Patients With Advanced Gastric and Gastroesophageal Junction Adenocarcinoma. *Clin Cancer Res* (2020) 26(4):846–54. doi: 10.1158/1078-0432.CCR-19-2443
- Gao X, Mi Y, Guo N, Xu H, Xu L, Gou X, et al. Cytokine-Induced Killer Cells As Pharmacological Tools for Cancer Immunotherapy. *Front Immunol* (2017) 8:774. doi: 10.3389/fimmu.2017.00774
- Moreno V, Hernandez T, de Miguel M, Doger B, Calvo E. Adoptive Cell Therapy for Solid Tumors: Chimeric Antigen Receptor T Cells and Beyond. *Curr Opin Pharmacol* (2021) 59:70–84. doi: 10.1016/j.coph.2021.05.004
- Jafferji MS, Yang JC. Adoptive T-Cell Therapy for Solid Malignancies. Surg Oncol Clin N Am (2019) 28(3):465–79. doi: 10.1016/j.soc.2019.02.012
- 38. Elia AR, Circosta P, Sangiolo D, Bonini C, Gammaitoni L, Mastaglio S, et al. Cytokine-Induced Killer Cells Engineered With Exogenous T-Cell Receptors Directed Against Melanoma Antigens: Enhanced Efficacy of Effector Cells

Endowed With a Double Mechanism of Tumor Recognition. *Hum Gene Ther* (2015) 26(4):220–31. doi: 10.1089/hum.2014.112

- Zanon C, Stocchero M, Albiero E, Castegnaro S, Chieregato K, Madeo D, et al. Multivariate Statistical Data Analysis as a Tool to Analyze Ex Vivo Expansion Dynamics of Cytokine-Induced Killer Cells. *Cytometry B Clin Cytom* (2014) 86(4):257–62. doi: 10.1002/cyto.b.21124
- Zhang L, Zhao G, Hou Y, Zhang J, Hu J, Zhang K. The Experimental Study on the Treatment of Cytokine-Induced Killer Cells Combined With EGFR Monoclonal Antibody Against Gastric Cancer. *Cancer Biother Radiopharm* (2014) 29(3):99–107. doi: 10.1089/cbr.2012.1381
- Jiang JT, Shen YP, Wu CP, Zhu YB, Wei WX, Chen LJ, et al. Increasing the Frequency of CIK Cells Adoptive Immunotherapy may Decrease Risk of Death in Gastric Cancer Patients. World J Gastroenterol (2010) 16(48):6155– 62. doi: 10.3748/wjg.v16.i48.6155
- 42. Yoshida M, Ohtsu A, Boku N, Miyata Y, Shirao K, Shimada Y, et al. Long-Term Survival and Prognostic Factors in Patients With Metastatic Gastric Cancers Treated With Chemotherapy in the Japan Clinical Oncology Group (JCOG) Study. Jpn J Clin Oncol (2004) 34(11):654–9. doi: 10.1093/jjco/hyh120
- Shen X, Zhou J, Hathcock KS, Robbins P, Powell DJJr., Rosenberg SA, et al. Persistence of Tumor Infiltrating Lymphocytes in Adoptive Immunotherapy Correlates With Telomere Length. *J Immunother* (2007) 30(1):123–9. doi: 10.1097/01.cji.0000211321.07654.b8
- Cao B, Liu M, Huang J, Zhou J, Li J, Lian H, et al. Development of Mesothelin-Specific CAR NK-92 Cells for the Treatment of Gastric Cancer. *Int J Biol Sci* (2021) 17(14):3850–61. doi: 10.7150/ijbs.64630
- 45. Ishikawa T, Okayama T, Sakamoto N, Ideno M, Oka K, Enoki T, et al. Phase I Clinical Trial of Adoptive Transfer of Expanded Natural Killer Cells in Combination With IgG1 Antibody in Patients With Gastric or Colorectal Cancer. Int J Cancer (2018) 142(12):2599–609. doi: 10.1002/ijc.31285
- 46. Gabrilovich DI, Chen HL, Girgis KR, Cunningham HT, Meny GM, Nadaf S, et al. Production of Vascular Endothelial Growth Factor by Human Tumors Inhibits the Functional Maturation of Dendritic Cells. *Nat Med* (1996) 2 (10):1096–103. doi: 10.1038/nm1096-1096
- 47. Liang L, Hui K, Hu C, Wen Y, Yang S, Zhu P, et al. Autophagy Inhibition Potentiates the Anti-Angiogenic Property of Multikinase Inhibitor Anlotinib Through JAK2/STAT3/VEGFA Signaling in non-Small Cell Lung Cancer Cells. J Exp Clin Cancer Res (2019) 38(1):71. doi: 10.1186/s13046-019-1093-3
- Herbst RS, Arkenau HT, Santana-Davila R, Calvo E, Paz-Ares L, Cassier PA, et al. Ramucirumab Plus Pembrolizumab in Patients With Previously Treated Advanced non-Small-Cell Lung Cancer, Gastro-Oesophageal Cancer, or Urothelial Carcinomas (JVDF): A Multicohort, non-Randomised, Open-Label, Phase 1a/B Trial. *Lancet Oncol* (2019) 20(8):1109–23. doi: 10.1016/ S1470-2045(19)30458-9
- Wu H, Fu M, Liu J, Chong W, Fang Z, Du F, et al. The Role and Application of Small Extracellular Vesicles in Gastric Cancer. *Mol Cancer* (2021) 20(1):71. doi: 10.1186/s12943-021-01365-z
- Kole C, Charalampakis N, Tsakatikas S, Kouris NI, Papaxoinis G, Karamouzis MV, et al. Immunotherapy for Gastric Cancer: A 2021 Update. *Immunotherapy* (2022) 14(1):41–64. doi: 10.2217/imt-2021-0103
- Cafri G, Gartner JJ, Zaks T, Hopson K, Levin N, Paria BC, et al. mRNA Vaccine-Induced Neoantigen-Specific T Cell Immunity in Patients With Gastrointestinal Cancer. J Clin Invest (2020) 130(11):5976–88. doi: 10.1172/ JCI134915
- Pardi N, Hogan MJ, Weissman D. Recent Advances in mRNA Vaccine Technology. Curr Opin Immunol (2020) 65:14–20. doi: 10.1016/ j.coi.2020.01.008
- 53. Ajani JA, Hecht JR, Ho L, Baker J, Oortgiesen M, Eduljee A, et al. An Open-Label, Multinational, Multicenter Study of G17DT Vaccination Combined With Cisplatin and 5-Fluorouracil in Patients With Untreated, Advanced Gastric or Gastroesophageal Cancer: The GC4 Study. *Cancer* (2006) 106 (9):1908–16. doi: 10.1002/cncr.21814
- 54. Sato Y, Shomura H, Maeda Y, Mine T, Une Y, Akasaka Y, et al. Immunological Evaluation of Peptide Vaccination for Patients With Gastric Cancer Based on Pre-Existing Cellular Response to Peptide. *Cancer Sci* (2003) 94(9):802–8. doi: 10.1111/j.1349-7006.2003.tb01522.x

- 55. Lv J, Zhao R, Wu D, Zheng D, Wu Z, Shi J, et al. Mesothelin Is a Target of Chimeric Antigen Receptor T Cells for Treating Gastric Cancer. J Hematol Oncol (2019) 12(1):18. doi: 10.1186/s13045-019-0704-y
- Caruso HG, Heimberger AB, Cooper LJN. Steering CAR T Cells to Distinguish Friend From Foe. Oncoimmunology (2019) 8(10):e1271857. doi: 10.1080/2162402X.2016.1271857
- Bebnowska D, Grywalska E, Niedzwiedzka-Rystwej P, Sosnowska-Pasiarska B, Smok-Kalwat J, Pasiarski M, et al. CAR-T Cell Therapy-An Overview of Targets in Gastric Cancer. J Clin Med (2020) 9(6):1894. doi: 10.3390/jcm9061894
- Song Y, Tong C, Wang Y, Gao Y, Dai H, Guo Y, et al. Effective and Persistent Antitumor Activity of HER2-Directed CAR-T Cells Against Gastric Cancer Cells In Vitro and Xenotransplanted Tumors In Vivo. Protein Cell (2018) 9(10):867–78. doi: 10.1007/s13238-017-0384-8
- Zhang Q, Zhang Z, Peng M, Fu S, Xue Z, Zhang R. CAR-T Cell Therapy in Gastrointestinal Tumors and Hepatic Carcinoma: From Bench to Bedside. Oncoimmunology (2016) 5(12):e1251539. doi: 10.1080/2162402X.2016. 1251539
- Sun F, Yu X, Ju R, Wang Z, Wang Y. Antitumor Responses in Gastric Cancer by Targeting B7H3 via Chimeric Antigen Receptor T Cells. Cancer Cell Int (2022) 22(1):50. doi: 10.1186/s12935-022-02471-8
- Feng Z, He X, Zhang X, Wu Y, Xing B, Knowles A, et al. Potent Suppression of Neuroendocrine Tumors and Gastrointestinal Cancers by CDH17CAR T Cells Without Toxicity to Normal Tissues. *Nat Cancer* (2022) 3(5):581–94. doi: 10.1038/s43018-022-00344-7
- 62. Bajwa R, Cheema A, Khan T, Amirpour A, Paul A, Chaughtai S, et al. Adverse Effects of Immune Checkpoint Inhibitors (Programmed Death-1 Inhibitors and Cytotoxic T-Lymphocyte-Associated Protein-4 Inhibitors): Results of a Retrospective Study. J Clin Med Res (2019) 11(4):225–36. doi: 10.14740/jocmr3750
- Ramos-Casals M, Brahmer JR, Callahan MK, Flores-Chavez A, Keegan N, Khamashta MA, et al. Immune-Related Adverse Events of Checkpoint Inhibitors. Nat Rev Dis Primers (2020) 6(1):38. doi: 10.1038/s41572-020-0160-6
- Butte MJ, Keir ME, Phamduy TB, Sharpe AH, Freeman GJ. Programmed Death-1 Ligand 1 Interacts Specifically With the B7-1 Costimulatory Molecule to Inhibit T Cell Responses. *Immunity* (2007) 27(1):111–22. doi: 10.1016/ j.immuni.2007.05.016
- Fukumura D, Kloepper J, Amoozgar Z, Duda DG, Jain RK. Enhancing Cancer Immunotherapy Using Antiangiogenics: Opportunities and Challenges. Nat Rev Clin Oncol (2018) 15(5):325–40. doi: 10.1038/nrclinonc.2018.29
- 66. Smith JP, Cao H, Chen W, Mahmood K, Phillips T, Sutton L, et al. Gastrin Vaccine Alone and in Combination With an Immune Checkpoint Antibody Inhibits Growth and Metastases of Gastric Cancer. *Front Oncol* (2021) 11:788875. doi: 10.3389/fonc.2021.788875
- Bonifant CL, Jackson HJ, Brentjens RJ, Curran KJ. Toxicity and Management in CAR T-Cell Therapy. *Mol Ther Oncolytics* (2016) 3:16011. doi: 10.1038/ mto.2016.11
- Sterner RC, Sterner RM. CAR-T Cell Therapy: Current Limitations and Potential Strategies. *Blood Cancer J* (2021) 11(4):69. doi: 10.1038/s41408-021-00459-7

Conflict of Interest: The authors declare that the research was conducted in the absence of any commercial or financial relationships that could be construed as a potential conflict of interest.

Publisher's Note: All claims expressed in this article are solely those of the authors and do not necessarily represent those of their affiliated organizations, or those of the publisher, the editors and the reviewers. Any product that may be evaluated in this article, or claim that may be made by its manufacturer, is not guaranteed or endorsed by the publisher.

Copyright © 2022 Jin, Liu, Yang, Yin and Chang. This is an open-access article distributed under the terms of the Creative Commons Attribution License (CC BY). The use, distribution or reproduction in other forums is permitted, provided the original author(s) and the copyright owner(s) are credited and that the original publication in this journal is cited, in accordance with accepted academic practice. No use, distribution or reproduction is permitted which does not comply with these terms.



Case Report: A Programmed Cell Death-1 Inhibitor-Related Abdominal Fibroinflammatory Reaction Affecting Multiple Organs in A Non-Small-Cell Lung Cancer Patient

An-Tian Chen¹, Yue-Quan Shi², Bei Tan³, Liang Zhu⁴, Ya-Ping Luo⁵, Wei Zhong², Meng-Zhao Wang² and Yan Xu^{2*}

¹ Department of Cardiology, Peking Union Medical College Hospital, Chinese Academy of Medical Sciences and Peking Union Medical College, Beijing, China, ² Department of Respiratory and Critical Care Medicine, Peking Union Medical College Hospital, Chinese Academy of Medical Sciences and Peking Union Medical College, Beijing, China, ³ Department of Gastroenterology, Peking Union Medical College Hospital, Chinese Academy of Medical Science and Peking Union Medical College, Beijing, China, ⁴ Department of Radiology, Peking Union Medical College Hospital, Chinese Academy of Medical Science and Peking Union Medical College, Beijing, China, ⁵ Department of Nuclear Medicine, Peking Union Medical College Hospital, Chinese Academy of Medical Science and Peking Union Medical College, Beijing, China

OPEN ACCESS

Edited by:

Xian Zeng, Fudan University, China

Reviewed by:

Elisabetta Razzuoli, Experimental Zooprophylactic Institute for Piedmont, Italy Yan Zhang, Sichuan University, China Minglei Zhuo, Peking University, China

> *Correspondence: Yan Xu maraxu@163.com

Specialty section:

This article was submitted to Cancer Immunity and Immunotherapy, a section of the journal Frontiers in Immunology

Received: 13 February 2022 Accepted: 06 June 2022 Published: 01 July 2022

Citation:

Chen AT, Shi YQ, Tan B, Zhu L, Luo YP, Zhong W, Wang MZ and Xu Y (2022) Case Report: A Programmed Cell Death-1 Inhibitor-Related Abdominal Fibroinflammatory Reaction Affecting Multiple Organs in A Non-Small-Cell Lung Cancer Patient. Front. Immunol. 13:874932. doi: 10.3389/fimmu.2022.874932 Immunotherapy utilizing programmed cell death-1 (PD-1)/PD-L1 inhibitors has been regarded as a rising hope for tumor patients, and their effects have been demonstrated in many clinical trials. However, immune-related adverse events also occur in patients and can sometimes have severe consequences. Pembrolizumab (Keytruda) is a humanized monoclonal anti-PD-1 antibody that has been approved by the US Food and Drug Administration for non-small-cell lung cancer. Here, we report a rare case of an abdominal fibroinflammatory reaction that affected multiple organs during anti-PD-1 immunotherapy using pembrolizumab in a non-small-cell lung cancer patient. The patient's case demonstrates that immunotherapy-related abdominal fibroinflammatory reactions need to be considered, especially for patients with a history of pre-existing conditions in the abdomen. Glucocorticoids may be useful as a treatment when a diagnosis is confirmed.

Keywords: pembrolizumab, non-small-cell lung cancer, immune-related adverse events, fibroinflammatory reaction, immunothearpy

INTRODUCTION

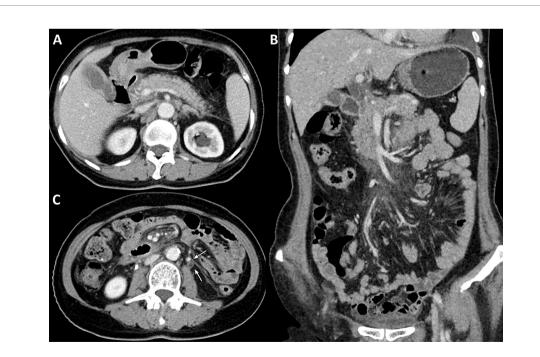
Immunotherapy has developed into a treatment option for patients with non-small-cell lung cancer (NSCLC) (1) and is regarded as a successful trend in NSCLC treatment (2). However, every successful therapy has deficiencies, and immune-related adverse events (irAEs) are observed during immunotherapy treatments. In patients using pembrolizumab, up to 60% suffered from adverse events, and less than 10% had grade 3/4 toxicities (3). IrAEs can occur in different organs with a variety of clinical manifestations. Some irAEs have phenotypes that mimic inflammatory diseases, including inflammatory arthritis, myositis, and vasculitis. Although rare, immune checkpoint inhibitor (ICI)-related fibroinflammatory diseases have been reported. Programmed cell death-1

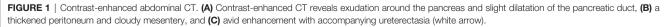
(PD-1) inhibitor-related sclerosing cholangitis has been reported to have clinical features of biliary dilation, diffuse thickening of the extrahepatic biliary tract with or without multiple strictures of the intrahepatic biliary tract, and normal serum immunoglobulin G4 (IgG4) (4). Systemic sclerosis, characterized by progressive fibrosis of the skin and internal organs, has been reported following treatment using ICIs (5). Retroperitoneal fibrosis, a rare disease characterized by fibrotic tissue in the retroperitoneum (6), rarely occurs secondary to anti-PD-1 therapy in patients with malignant tumors (7, 8). This phenomenon requires further insights and discovery. Here, we report a rare condition of an abdominal fibroinflammatory reaction affecting multiple organs following immunotherapy with pembrolizumab.

CASE DESCRIPTION

A 66-year-old female non-smoker presented with shortness of breath in May 2019 and was admitted to a local hospital. Chest CT revealed a spiculated mass in the left upper lobe, multiple pulmonary nodules, mediastinal lymphadenopathy, and pericardial effusion. Lung adenocarcinoma was diagnosed through a bronchoscopic biopsy. Molecular testing detected a p.L858R mutation in epidermal growth factor (EGFR) exon 21. Multiple metastases were confirmed in the lung, liver, pericardium, bone, brain, and distant lymph nodes. The tumor stage reached cT4N3M1c (stage IV B). She was prescribed gefitinib and had a progression-free period of 7 months. She was then switched to osimertinib treatment because EGFR exon 20 p.T790M (+) was detected in the progressive pleural fluid. However, four months later, the disease was characterized by progressive bone and brain metastases. The patient's past history indicated that she had suffered intestinal obstruction without clear cause, and the abdominal surgery was compelled to perform at age 13, while the intestinal obstruction recurred twice around 2003 and 2006.

The patient received four cycles of pemetrexed, carboplatin, bevacizumab, and pembrolizumab starting in August 2020. Two cycles of pemetrexed and pembrolizumab were administered as maintenance therapy. Stable disease (SD) was achieved and persisted after 2 cycles ICIs combined treatment. Four months after the first use of pembrolizumab, the patient experienced abdominal pain caused by right ureterectasia. A double-I stent was used to relieve her symptoms. One month later, the patient experienced recurrent abdominal pain. Laboratory tests showed that her total bilirubin rose from 8.9 µmol/L to 54.2 µmol/L (normal: 5.1-22.2 µmol/L), direct bilirubin rose from 3 μ mol/L to 45.9 μ mol/L (normal: $\leq 6.8 \mu$ mol/L), alanine serum aminotransferase rose from 103 to 162 U/L (normal: 7-40 U/L), aspartate serum aminotransferase rose from 92 to 446 U/L (normal: 13-35 U/L), and gamma-glutamyl transpeptidase rose from 488 to 1,350 U/L (normal: 7-45 U/L). Laboratory testing also revealed elevated serum amylase (132 U/L, normal: 35-115 U/L) and lipase (746 U/L, normal: 2-53 U/L). Contrast-enhanced CT revealed exudation around the pancreas, slight dilatation of the pancreatic duct (Figure 1A), a thickened peritoneum, and cloudy mesentery (Figure 1B), which are encountered often in abdominal inflammatory reactions such as acute pancreatitis or lupus. An unexpected finding, however, was that the left ureter was thickened and showed avid enhancement (Figure 1C) accompanied by





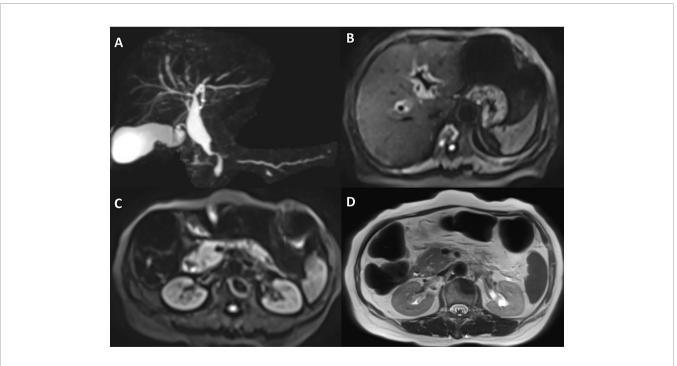
ureterectasia (Figure 1A). Magnetic resonance cholangiopancreatography (MRCP) showed narrowing of the distal bile duct and dilatation of the extrahepatic bile duct beyond the pancreatic portion. Instead of proportional dilatation in continuation with the extrahepatic bile duct, the intrahepatic duct showed multiple strictures (Figure 2A). The narrowed segments of the biliary tracts were thickened symmetrically, and diffusion was significantly restricted on diffusion-weighted imaging (Figure 2B). Segmental stenosis of the main pancreatic duct was noted in the pancreatic head, with slight dilation of the upstream pancreatic duct, which did not exceed 3 mm (Figure 2A). The entire pancreas demonstrated diffuse high signal on diffusion-weighted imaging (Figure 2C). A thickened mesentery and peritoneal fascia were also observed (Figure 2D). However, there was no evidence of pancreatic metastases or peritoneal seeding. In addition, obstruction of the common bile duct was confirmed, but endoscopic retrograde cholangiopancreatography failed because of severe stenosis. Percutaneous transhepatic cholangiography and drainage and biliary stent implantation was performed for obstructive cholangitis considering her continuously elevated bilirubin level. ^{18F}FDG positron emission tomography-computed tomography (PET-CT) (Figure 3) detected left renal perirenal fascial thickening with abnormal metabolic elevation and inflammatory changes in the bile duct and pancreas, without evidence of abdominal tumor-metastasis. Laboratory tests showed that the IgG4 level was within normal limits (IgG4: 475 mg/L, normal: 80-1400 mg/L), anti-nuclear antibodies were positive with a low titer of 1/80, and anti-neutrophil cytoplasmic antibodies were negative. Meanwhile, cytokines analysis showed that

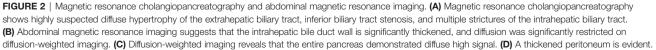
the interleukin 6 (IL-6) (IL-6: 8.4 pg/mL, normal: <5.9 pg/mL)and tumor necrosis factor-alpha (TNF α) (TNF α 8.9 pg/mL, normal: <8.1 pg/mL) were slightly elevated, while IL-8 and IL-10 were within normal limits.

Overall, the patient suffered from bile system disease, bilateral ureteral obstruction, chronic pancreatitis, and a thickened peritoneum and bilateral perirenal fascia. An abdominal fibroinflammatory reaction was highly suspected, which may have been caused by ICI treatment. The patient was treated with glucocorticoids (methylprednisolone 40mg daily, 0.8mg/kg), and her symptoms were well-controlled without aggravation. The patient was followed up for 6 months, and an enhanced abdominal CT revealed that there was less inflammatory reaction of the pancreas (**Figure 4A**), and the thickness of the renal fascia and peritoneum maintained without further thickening (**Figure 4B**). More importantly, her ureterectasia on the left side was partly relieved (**Figure 4B**), and a double-J stent was not needed.

DISCUSSION

Our patient presented with bilateral ureterectasia, bile system disease, chronic pancreatitis, and a thickened peritoneum, mesentery, and bilateral perirenal fascia. After excluding other possible causes, the ICI treatment history, imaging, and steroidsensitive response suggested an abdominal fibroinflammatory reaction elicited by the anti-PD-1 therapy.





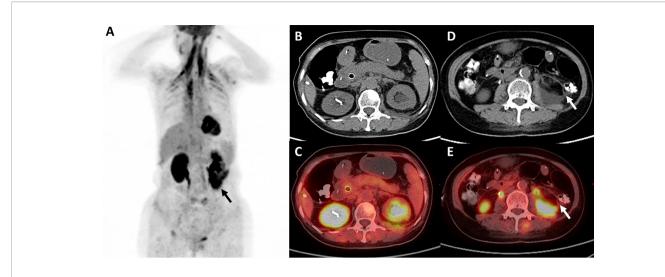
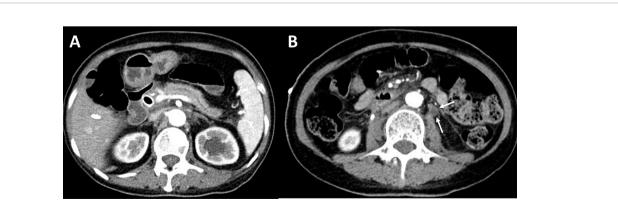
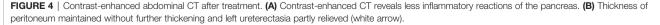


FIGURE 3 | ^{18F}FDG positron emission tomography-computed tomography. (A, D, E) ^{18F}FDG PET-CT reveals left renal perirenal fascial thickening with abnormal metabolic elevation (black arrow and white arrow), and (B, C) inflammatory change in the pancreas.

Immunotherapy-related events can be diagnosed only through comprehensive analysis and the elimination of other possible causes. First, it was the discovery of the thickening and hypermetabolic foci of the abdominal peritoneum and multiple organs that helped identify an extensive fibroinflammatory reaction in different organs and tissues. The thickened peritoneum detected in the radiological findings on abdominal CT also suggested an abdominal inflammatory reaction. The abdominal MRI and MRCP imaging patterns highly resembled sclerosing cholangitis and autoimmune pancreatitis (9, 10). Second, the diagnosis of the tumor made it necessary to exclude abdominal changes caused by metastasis. The results of ^{18F}FDG PET-CT and MRI did not support abdominal tumor-metastasis-related conditions. Third, the clinical manifestations in this patient were consistent with IgG4related disease, which is an immune-mediated fibroinflammatory disease, but it did not meet the diagnostic criteria for IgG4-related disease because a normal serum IgG4 concentration was detected. Fourth, immunotherapy-related sclerosing cholangitis, chronic pancreatitis, or retroperitoneal fibrosis can occur after immunotherapy, which may be an unusual adverse reaction and an exclusionary diagnosis. Ultimately, the diagnosis of an immunotherapy-related abdominal fibroinflammatory reaction was confirmed when the patient's symptoms were well-controlled after steroid treatment.

Fibroinflammatory disorders can occur in a spectrum of diseases. Retroperitoneal fibrosis is a rare disease characterized by chronic inflammation and profound fibrosis in the peri-aortic and peri-iliac organs or tissues (11). Chronic pancreatitis is characterized by a pathological fibroinflammatory syndrome of the pancreas (12). Sclerosing cholangitis is characterized by inflammation and fibrosis of the bile ducts and the liver (13). The IgG4-related disease is a systemic fibroinflammatory condition that affects multiple organs (14). Scleroderma occurs because of vascular disorders and fibrosis due to genetic and molecular changes (15). Until now, sclerosing cholangitis, retroperitoneal fibrosis, and chronic pancreatitis have been reported to be induced by ICI treatment; however, rare cases of extensive fibroinflammatory disorders in specific individuals have been reported.





The mechanism of fibroinflammatory reaction as an irAE is not fully understood, but there are potential mechanisms. Fibroinflammatory disorders are caused by a combination of genetic and environmental factors. Retroperitoneal fibrosis secondary to immunotherapy may be caused by the rejuvenation of antigen presentation by antigen-presenting cells (16). The mechanism underlying sclerosing cholangitis is still not fully understood. Tissues of pancreatitis and sclerosing cholangitis tissues share dominantly CD8+ cells in a CD3+ T cells infiltrate pathologically (17). Scleroderma can also be induced by immunotherapy. T cells are thought to respond more actively after ICI treatment, which results in not only the desired treatment effects but also the production of self-reactive T cells (18). Previously existing skin damage, such as that caused by ultraviolet light, could lead to exposure of self-antigens and thereby enhance T cell generation (19).

Underlying mechanism of fibroinflammatory reaction should be further explored. When stimulated by certain antigens, B cells proliferate; some differentiate into plasma cells, and IgG is produced. However, in some cases, IgG4 production is preferred (20). The IgG4 subclass of antibodies is expressed in alternative Th2 environments characterized by high levels of IL-10 (21). Furthermore, when an enhanced Th2 signal is observed, cytokines related to Th2 signaling, such as IL-10 and IL-13 are found to be elevated (22). It is known that Th2-skewed responses favor fibrocyte differentiation. Therefore, Th2 contributes to fibrotic effects. In the treatment of malignant tumors, Th2 cells may have anti-tumor potential by modulating the tumor microenvironment (23). PD-1 blockade is believed to inhibit Th2 response (24). However, the Th2 pathway exhibits an enhancement during follow-up with increasing levels of cytokines such as IL-4 and IL-5 (25). In addition, Th2 pathways may be implicated in patients with irAEs (25). For example, the serum level of IL-6 is increased in nivolumab-associated psoriasiform dermatitis, which indicates the involvement of Th2 pathways (26). It may also induce chronic pancreatitis since IL-6 is associated with exocrine pancreatic diseases including chronic pancreatitis and its serum level in chronic pancreatitis patients was found with a remarkable elevation compared to control subjects (27). Thus, it is reasonable to propose a possible mechanism of abdominal fibroinflammatory reaction as an irAE in immunotherapy. Although Th2 pathways are often suppressed in immunotherapy, related pathways might recover during followup and cause irAEs such as psoriasiform dermatitis.

Similarly, in this case, considering the patient's history of recurrent intestinal obstruction and an abdominal operation, the exudation of abdominal inflammatory lesions might have been aggravated after ICI treatment. To be specific, past abdominal inflammatory injuries expose self-antigen, which will enhance functions of T cells. At the same time, treatment effects of immunotherapy as well as APCs rejuvenated by antigen presentation would promote T cells. Activation of CD4/CD8 will start and lead to generation of follicular helper T (Tfh) cells, which could promote plasmablast differentiation (28). In fact, PD-1, which is surface receptor on Tfh cells, is responsible for negatively regulation (29). Thus, it is reasonable to suggest such process in activating plasma cells and T cells and progressively causing fibroinflammatory disorders. In summary, a pre-existing inflammatory state in the abdomen may accelerate the entire process and lead to an abdominal fibroinflammatory reaction being eventually triggered by immunotherapy.

There are some limitations. The patient did not have PD-L1 IHC test before or after osimertinib treatment, thus we do not know the PD-L1 expression situation and whether there was any change or not. Also, though abdominal fibroinflammatory reaction was obvious and typical in radiological examinations, it was hard to performed abdominal inflammatory lesions biopsy for pathological examinations.

In summary, we reported a rare condition of an abdominal fibroinflammatory reaction that affected multiple organs following immunotherapy with pembrolizumab, which is barely known and unfamiliar in clinical practice. Immunotherapy-related abdominal fibroinflammatory reactions need to be considered, especially for patients with a history of celiac disease. Glucocorticoids may be useful as a treatment when a diagnosis is reached.

DATA AVAILABILITY STATEMENT

The original contributions presented in this study are included in the article/supplementary material. Further inquiries can be directed to the corresponding author.

ETHICS STATEMENT

Written informed consent was obtained from the individual(s) for the publication of any potentially identifiable images or data included in this article.

AUTHOR CONTRIBUTIONS

ATC wrote the manuscript. YX designed the study and revised the manuscript. All authors contributed to the manuscript and approved the submitted version.

FUNDING

This study was supported by the Youth Program of the National Natural Science Foundation of China (to YX) (grant number: 82003309) and by CAMS Innovation Fund for Medical Sciences (CIFMS) (to YX) (grant number: 2021-I2M-C&T-B-014).

ACKNOWLEDGMENTS

We thank the patient and her family members for providing her information for this study.

REFERENCES

- Chiang AC, Herbst RS. Frontline Immunotherapy for NSCLC the Tale of the Tail. Nat Rev Clin Oncol (2020) 17(2):73–4. doi: 10.1038/s41571-019-0317-y
- Osmani L, Askin F, Gabrielson E, Li QK. Current WHO Guidelines and the Critical Role of Immunohistochemical Markers in the Subclassification of non-Small Cell Lung Carcinoma (NSCLC): Moving From Targeted Therapy to Immunotherapy. *Semin Cancer Biol* (2018) 52(Pt 1):103–9. doi: 10.1016/ j.semcancer.2017.11.019
- Kwok G, Yau TCC, Chiu JW, Tse E, Kwong Y-L. Pembrolizumab (Keytruda). *Hum Vaccines Immunother* (2016) 12(11):2777-89. doi: 10.1080/ 21645515.2016.1199310
- Onoyama T, Takeda Y, Yamashita T, Hamamoto W, Sakamoto Y, Koda H, et al. Programmed Cell Death-1 Inhibitor-Related Sclerosing Cholangitis: A Systematic Review. World J Gastroenterol (2020) 26(3):353–65. doi: 10.3748/ wjg.v26.i3.353
- Terrier B, Humbert S, Preta L-H, Delage L, Razanamahery J, Laurent-Roussel S, et al. Risk of Scleroderma According to the Type of Immune Checkpoint Inhibitors. *Autoimmun Rev* (2020) 19(8):102596. doi: 10.1016/ j.autrev.2020.102596
- Pipitone N, Vaglio A, Salvarani C. Retroperitoneal Fibrosis. Best Pract Res Clin Rheumatol (2012) 26(4):439–48. doi: 10.1016/j.berh.2012.07.004
- Daoussis D, Kraniotis P, Kalofonou F, Kalofonos H. Anti-PD-1 Associated Retroperitoneal Fibrosis. *Rheumatol (Oxf Engl)* (2021) 60(9):e329–e330. doi: 10.1093/rheumatology/keab264
- Moreau A, Giraudet AL, Mognetti T, Kryza D. Retroperitoneal Fibrosis in on-Going Anti-PD-1 Immunotherapy Detected With [(18)F]-FDG PET/CT. *Eur J Nucl Med Mol Imaging* (2019) 46(8):1758–9. doi: 10.1007/s00259-019-04352-1
- Ohara H, Okazaki K, Tsubouchi H, Inui K, Kawa S, Kamisawa T, et al. Clinical Diagnostic Criteria of IgG4-Related Sclerosing Cholangitis 2012. J Hepato-Biliary-Pancreat Sci (2012) 19(5):536–42. doi: 10.1007/s00534-012-0521-y
- Negrelli R, Manfredi R, Pedrinolla B, Boninsegna E, Ventriglia A, Mehrabi S, et al. Pancreatic Duct Abnormalities in Focal Autoimmune Pancreatitis: MR/ MRCP Imaging Findings. *Eur Radiol* (2015) 25(2):359–67. doi: 10.1007/ s00330-014-3371-y
- Raglianti V, Rossi GM, Vaglio A. Idiopathic Retroperitoneal Fibrosis: An Update for Nephrologists. *Nephrol Dial Transplant* (2020) 36(10):1773–1781. doi: 10.1093/ndt/gfaa083
- Kleeff J, Whitcomb DC, Shimosegawa T, Esposito I, Lerch MM, Gress T, et al. Chronic Pancreatitis. Nat Rev Dis Primers (2017) 3:17060. doi: 10.1038/ nrdp.2017.60
- Dyson JK, Beuers U, Jones DEJ, Lohse AW, Hudson M. Primary Sclerosing Cholangitis. *Lancet (Lond Engl)* (2018) 391(10139):2547–59. doi: 10.1016/ S0140-6736(18)30300-3
- Maritati F, Peyronel F, Vaglio A. IgG4-Related Disease: A Clinical Perspective. *Rheumatol (Oxf Engl)* (2020) 59(Suppl 3):iii123–31. doi: 10.1093/ rheumatology/kez667
- Gabrielli A, Avvedimento EV, Krieg T. Scleroderma. N Engl J Med (2009) 360 (19):1989–2003. doi: 10.1056/NEJMra0806188
- Fenaroli P, Maritati F, Vaglio A. Into Clinical Practice: Diagnosis and Therapy of Retroperitoneal Fibrosis. *Curr Rheumatol Rep* (2021) 23(3):18. doi: 10.1007/s11926-020-00966-9
- Suda T, Kobayashi M, Kurokawa K, Matsushita E. Simultaneous Occurrence of Autoimmune Pancreatitis and Sclerosing Cholangitis as Immune-Related Adverse Events of Pembrolizumab. *BMJ Case Rep* (2021) 14(6):e243360. doi: 10.1136/bcr-2021-243360
- Yoest JM. Clinical Features, Predictive Correlates, and Pathophysiology of Immune-Related Adverse Events in Immune Checkpoint Inhibitor Treatments in Cancer: A Short Review. *ImmunoTargets Ther* (2017) 6:73. doi: 10.2147/ITT.S126227

- Root-Bernstein R, Fairweather D. Unresolved Issues in Theories of Autoimmune Disease Using Myocarditis as a Framework. J Theor Biol (2015) 375:101–23. doi: 10.1016/j.jtbi.2014.11.022
- Zen Y, Fujii T, Harada K, Kawano M, Yamada K, Takahira M, et al. Th2 and Regulatory Immune Reactions are Increased in Immunoglobin G4-Related Sclerosing Pancreatitis and Cholangitis. *Hepatology* (2007) 45(6):1538–46. doi: 10.1002/hep.21697
- Jordakieva G, Bianchini R, Reichhold D, Piehslinger J, Groschopf A, Jensen SA, et al. IgG4 Induces Tolerogenic M2-Like Macrophages and Correlates With Disease Progression in Colon Cancer. *Oncoimmunology* (2021) 10 (1):1880687. doi: 10.1080/2162402X.2021.1880687
- Nicastro M, Vescovini R, Maritati F, Palmisano A, Urban ML, Incerti M, et al. Fibrocytes in Chronic Periaortitis: A Novel Mechanism Linking Inflammation and Fibrosis. Arthritis Rheumatol (2019) 71(11):1913–22. doi: 10.1002/ art.41024
- Schreiber S, Hammers CM, Kaasch AJ, Schraven B, Dudeck A, Kahlfuss S. Metabolic Interdependency of Th2 Cell-Mediated Type 2 Immunity and the Tumor Microenvironment. *Front Immunol* (2021) 12:632581. doi: 10.3389/ fimmu.2021.632581
- 24. Dulos J, Carven GJ, van Boxtel SJ, Evers S, Driessen-Engels LJA, Hobo W, et al. PD-1 Blockade Augments Th1 and Th17 and Suppresses Th2 Responses in Peripheral Blood From Patients With Prostate and Advanced Melanoma Cancer. J Immunother (2012) 35(2):169–78. doi: 10.1097/CJI.0b013e318247a4e7
- 25. Gérard A, Doyen J, Cremoni M, Bailly L, Zorzi K, Ruetsch-Chelli C, et al. Baseline and Early Functional Immune Response is Associated With Subsequent Clinical Outcomes of PD-1 Inhibition Therapy in Metastatic Melanoma Patients. J Immunother Cancer (2021) 9(6):e002512. doi: 10.1136/ jitc-2021-002512
- 26. Tanaka R, Okiyama N, Okune M, Ishitsuka Y, Watanabe R, Furuta J, et al. Serum Level of Interleukin-6 is Increased in Nivolumab-Associated Psoriasiform Dermatitis and Tumor Necrosis Factor-α is a Biomarker of Nivolumab Recativity. J Dermatol Sci (2017) 86(1):71–3. doi: 10.1016/ j.jdermsci.2016.12.019
- Lesina M, Wörmann SM, Neuhöfer P, Song L, Algül H. Interleukin-6 in Inflammatory and Malignant Diseases of the Pancreas. *Semin Immunol* (2014) 26(1):80–7. doi: 10.1016/j.smim.2014.01.002
- Akiyama M, Suzuki K, Yasuoka H, Kaneko Y, Yamaoka K, Takeuchi T. Follicular Helper T Cells in the Pathogenesis of IgG4-Related Disease. *Rheumatol (Oxf)* (2018) 57(2):236–45. doi: 10.1093/rheumatology/kex171
- Jogdand GM, Mohanty S, Devadas S. Regulators of Tfh Cell Differentiation. Front Immunol (2016) 7:520. doi: 10.3389/fimmu.2016.00520

Conflict of Interest: The authors declare that the research was conducted in the absence of any commercial or financial relationships that could be construed as a potential conflict of interest.

Publisher's Note: All claims expressed in this article are solely those of the authors and do not necessarily represent those of their affiliated organizations, or those of the publisher, the editors and the reviewers. Any product that may be evaluated in this article, or claim that may be made by its manufacturer, is not guaranteed or endorsed by the publisher.

Copyright © 2022 Chen, Shi, Tan, Zhu, Luo, Zhong, Wang and Xu. This is an openaccess article distributed under the terms of the Creative Commons Attribution License (CC BY). The use, distribution or reproduction in other forums is permitted, provided the original author(s) and the copyright owner(s) are credited and that the original publication in this journal is cited, in accordance with accepted academic practice. No use, distribution or reproduction is permitted which does not comply with these terms.

Frontiers in Immunology

Explores novel approaches and diagnoses to treat immune disorders.

The official journal of the International Union of Immunological Societies (IUIS) and the most cited in its field, leading the way for research across basic, translational and clinical immunology.

Discover the latest Research Topics



Frontiers

Avenue du Tribunal-Fédéral 34 1005 Lausanne, Switzerland frontiersin.org

Contact us

+41 (0)21 510 17 00 frontiersin.org/about/contact



